NASA Conference Publication 3042



# Two-Dimensional Intercomparison of Stratospheric Models

*Proceedings of a workshop held in*
*Virginia Beach, Virginia*
*September 11-16, 1988*

NASA

*NASA Conference Publication 3042*

# Two-Dimensional Intercomparison of Stratospheric Models

*Edited by*
Charles H. Jackman
*NASA Goddard Space Flight Center*
*Greenbelt, Maryland*

Robert K. Seals, Jr.
*NASA Langley Research Center*
*Hampton, Virginia*

Michael J. Prather
*NASA Goddard Institute for Space Studies*
*New York, New York*

Proceedings of a workshop sponsored by the National Aeronautics and Space Administration, Washington, D.C., Upper Atmosphere Theory and Data Analysis Program held in Virginia Beach, Virginia September 11–16, 1988

National Aeronautics and Space Administration
Office of Management
Scientific and Technical Information Division

**1989**

# TABLE OF CONTENTS

# CHAPTER 1

# INTRODUCTION, CORRESPONDENCE, AND PARTICIPANTS

# CHAPTER 1

## Section 1.1 Introduction

### Section 1.1.1 History

In September of 1988 a group of atmospheric scientists convened at Virginia Beach,Virginia to continue a process begun over a decade ago: intercomparison of stratospheric models. The modeling of stratospheric ozone has been fostered by both political and scientific needs to assess the impacts of human activity on atmospheric chemistry - in particular, the release of odd-nitrogen ($NO_x$) by aircraft and the increasing levels of chlorofluorocarbons (CFCs).

The responsibility of making predictions of future ozone levels, as well as the scientific curiosity of those involved, has led to a series of model intercomparisons. The earliest such efforts generally included little more than a collation of ozone perturbations predicted from the available 1-D photochemical models, using ostensibly the same scenario for CFCs and other trace gases. While trying to understand the range of predictions for ozone perturbations, it became clear that the models were not performing the same calculation. We uncovered many differences models, some obvious and others hidden: the fundamental chemical kinetic model, the method of averaging sunlight and reaction rates over the day, the choice of eddy diffusion coefficients and boundary conditions, and even some outright errors.

One of the first attempts at a formal intercomparison was made in the late 70's in which a group of scientists with 1-D photochemical models planned to perform specified calculations with detailed comparisons of photolysis rates and chemical budgets. In spite of the planning (a standard atmosphere and composition was specified, and a set of tables detailing the chemical rates and transports was to be filled in for each model calculation), the comparison was frustrated by basic differences in the simulations, so that different results could not be uniquely ascribed to a probable cause.

Current stratospheric science has progressed from highly averaged 1-D models to multi-dimensional, 2-D and 3-D models, which now include latitudinal and seasonal simulations of stratospheric ozone with more realistic transport (advection in 2 or 3 dimensions as well as diffusion). This extended dimensionality makes intercomparison even more difficult, since the range of predicted variables has increased by more than a factor of ten and the multi-dimensional models now have different formulations for transport in addition to chemistry.

The first major 2-D model intercomparison was organized by Paul Guthrie and held in January 1987 at Fort Myers Beach, Florida. The sponsor and a major force behind the intercomparison was NASA's Upper Atmosphere Theory and Data Analysis Program. The planning for this workshop recognized the complexity of multi-dimensional comparisons. The organizers defined a protocol of numerical experiments and established the Upper Atmosphere Data Pilot (UADP) under the management of Robert Seals at Langley Research Center as the principle vehicle for data-model as well as model -model comparisons. The major issues of protocol and the willingness to contribute one's proprietary model output to a community database were raised and effectively resolved at this meeting. This workshop created the basic agreements regarding the database and generated community support for further intercomparisons. The report of the chairman is included as Chapter 2 of this document.

### Section 1.1.2 Goals

The primary objective of these model intercomparisons has been to understand the fundamental differences among the stratospheric models, and in particular, their predictions of stratospheric ozone. When two models use the same atmospheric scenario and give different predictions of ozone perturbations, we need at least to explain or to understand these differences, and perhaps eventually, to make a critical judgment as to which model is better able to predict the future atmosphere.

An equally important objective of the intercomparisons is to promote basic improvements in the treatment of chemistry and transport in all of the models through the collective scientific effort of the community. As part of the workshop, "new and improved" versions of the models are presented and argued to be better than previous models. We may then recognize and implement improvements to our methods of calculating (or parameterizing) the chemistry and physics of the stratosphere.

There are several aspects of any intercomparison that we wish to downplay. For one, the comparison is not a beauty contest; there is no winner for "best" model. On the other hand, some chemical processes or transports may be better represented in certain models than in others. Similarly this is not a search for faults in the models, although once again, some errors may be uncovered during the intercomparison.

### Section 1.1.3 Today

The 2-D Intercomparison Workshop of 1988 at Virginia Beach was a major international meeting. Representatives from most of the multi-dimensional modeling groups in the world contributed to the planning and execution of the workshop; see the list of models and participants in Tables 3-1 and Section 1.3. A decision was made to limit participation to the number of scientists that could work effectively around a single large table in the conference room.

The title of the workshop was chosen carefully. The focus of the intercomparisons was on 2-D or 3-D models. The 2-D models are mature and formed the backbone of most comparisons; the 3-D models are in their developmental stages and usually lacked a sufficient number of annual-cycle simulations or had incomplete chemistry; occasionally, 1-D models were used for photochemical tests (without transport).

The intercomparison of 1988 was the most prepared for of such workshops and the most comprehensive in scope. Contributing research groups placed model output with the database in a "blind" mode, generally not knowing the results from other groups. The extensive list of set numerical experiments was developed and refined over the year preceeding the workshop through a series of meetings and telephone conferences among participants. There were four basic types of set experiments:

(1) photolysis and heating rates with given $O_3$ and temperature
(2) mechanistic tracer studies with prescribed chemistry;
(3) current atmosphere;
(4) future perturbations to $O_3$, temperature and circulation.

The detailed set of calculations and the proposed agenda for the meeting are given in Section 1.2 on Correspondence. The ambitious nature of the project put great stress on the interactive capability of the database, requiring the re-gridding and printing - during the workshop - of several hundred 2-D contour maps.

The different results from the models are documented here in the writeups from the discussion leaders and in the accompanying figures (1,640 in all). The cause of the different results from the models may not always be identified in these discussions, which often point to the fundamentally different formulation or atmospheric physics that goes into each of the chemical transport models. These differences are often a matter of physical parameterization or chemical constants, and there is no easy way to say who is right or which model is better.

This document records the findings of the 2-D Intercomparison Workshop of 1988. This report is a technical document, not a tutorial on stratospheric modeling. The report is meant to provide a detailed record for those scientists participating in the workshop, in addition to other modeling groups, and to those wishing to examine fundamental differences in photochemistry and transport among the models. A separate interpretation and assessment of the results is needed for the larger scientific community and will most likely be part of NASA's report to Congress and the EPA in 1990. Intercomparison of stratospheric models is a gradual process, in which we continue to learn from each workshop.

The scientifically useful lifetime of this admittedly long report is expected to be several years since many of these experiments will probably not be redone (with full participation) in future intercomparisons. Intercomparison is a continuing need for the atmospheric modeling community. Practical considerations - and the need to digest results from this workshop - limit the next such stratospheric chemistry comparison to 1990.

## Section 1.2 Correspondence Leading up to the September 1988

### Two-Dimensional Intercomparison Workshop

The following pages are correspondence generated in preparation of the September 1988 Two-dimensional Intercomparison Workshop held in Virginia Beach, VA. This correspondence section includes three letters from Michael Prather and one from Charles Jackman about the intercomparison meeting. The first letter from Michael Prather, dated December 28, 1987, initially informs all participants of the upcoming meeting and asks for inputs. In Michael Prather's second letter, dated February 29, 1988, he indicates which topics will be covered in the intercomparisons and which model experiments need to be run by each modeling group. The third letter from Michael Prather, dated May 18, 1988, clarifies which participants will be in charge of the various topics and finalizes the model experiments to be intercompared. Finally, the letter and template from Charles Jackman, dated June 3, 1988, asks for information from individual models to investigate the issue of the 3 mbar ozone budget. The letters from Michael Prather dated December 28 and February 29 were sent to all participants, however, the copies sent to Charles Jackman are being used as examples in the report.

NASA

National Aeronautics and
Space Administration

Washington, D.C.
20546

28 December 1987

Reply to Attn of:

M. Prather /EEU

Re: 2-D Model Intercomparison 1988

Dr. Charles H. Jackman
Code 616
Goddard Space Flight Center
Greenbelt, MD 20771

Dear Charley,

The Upper Atmosphere Research Program is coordinating a major intercomparison of stratospheric models for 1988. The goal of this and previous intercomparisons has been an improved understanding of stratospheric chemistry and dynamics. The UARP has a responsibility to assess changes in the stratospheric ozone and to report to Congress and to the Administrator of the EPA. The most recent intercomparisons sponsored by NASA and other agencies occurred in Chapter 12 of NASA/WMO 1985 and in the 2-D workshop chaired by Paul Guthrie in January 1987. The focus continues to be on 2-D models, which currently represent the best capability for assessing stratospheric change. Note that some of the proposed numerical experiments can be performed with 1-D or 3-D models, and contributions are welcomed. I have enclosed a 1st draft of "all possibly useful and well defined" numerical experiments for the 1988 Intercomparison. This list needs to be expanded and clarified before we make decisions as to what to do first.

Participating groups will be assigned one or more of the tasks selected for the intercomparison. It will be their responsibility to put together the results from all participants for that specific experiment, to present the comparison of different models, and to direct the discussion that examines the causes of the differences (if any). Results from the 2-D models will be put into the stratospheric database at Langley, which is under the direction of Bob Seals. Those contributing will have access to the database with the following restriction: all data are available for intercomparison, but no data are quotable without permission of the individual contributors.

Please reply **as soon as possible, no later than January 15,** with your criticisms, clarifications and **additions** to this overstuffed stocking of experiments. I will immediately send out a 2nd draft with the complete list so that you all may select and place priorities on the experiments for the first meeting. I would expect that by June 1988 all of those calculations designated for this 1988 Intercomparison can be completed and the results exchanged with those coordinating the specific tasks. The meeting would be held probably in late August. Participation in the 1988 Intercomparison is essential to the vitality and continued growth of the Upper Atmosphere Theory Program and should be of scientific benefit to those involved.

Yours,

Michael

Michael Prather, Acting Program Manager,
Upper Atmosphere Theory & Data Analysis
NASA/HQ/EEU: 202/453-1681 NASA/GISS: 212/678-5625
NASAMAIL or GSFCMAIL: mprather

*(1st DRAFT of 1988 Intercomparison: 2-D stratospheric models)*

**Part 2. Transport** (2-D, 3-D)

**Use the "BEST" circulation from your Model in the following:**

*Circulation Diagnostics.*

■d Present Q(net) or w* from your best circulation (lat × ht × month)

*Tropospheric Source.* Fix the mixing ratio of X at 1 ppb near the surface (all layers below 700 mb). Apply the following loss frequency,

$$\begin{aligned} L(p) &= 0 && \text{for } p > 100 \text{ mb}, \\ &= 3.E\text{-}6/p^2 \text{ sec}^{-1}, && \text{for } 1 \text{ mb} < p < 100 \text{ mb}, \\ &= 3.E\text{-}6 \text{ sec}^{-1}, && \text{for } p < 1 \text{ mb}, \end{aligned}$$

initialize with a uniform mixing ratio of 1 ppb and integrate through several annual cycles until steady-state is reached.
(? Include a seasonal dependence on L(p) ?)

■e Find steady-state distributions, budgets, ...
Compare constant mixing ratio surfaces vs. isentropes.

*Stratospheric Source.* Fix the mixing ratio of Z to be 8 ppmv for all p < 10 mb, and 0.010 ppmv for all p > 850 mb.

■f Calculate a "Dobson" map for Z (column (10-1000mb) vs. latitude × month).
■g Do budget analysis on the flux into troposphere.

*Time Dependent Source.* Put $5 \times 10^{12}$ kg of species Y (at.wt.=29) in the lower troposphere (>700mb).

■h Calculate the time-dependent growth of Y at 40 km (tropics & high lat),
assuming no loss of Y, and
assuming photolysis of Y as in L(p) above.

**Analytic, Specified Circulation.** Given the following analytic stream function or diabatic heating rates (Q) and the following $K_{yy}$ and $K_{zz}$: (? Ko et al, 1985)

■x Redo the experiments e,f,g,h from above (?)

(From your comments, this experiment has some interest but is difficult to implement. Any suggestions? Leave for second intercomparison meeting mid-89?)

**Part 3. Current Atmosphere: 1980.** (2-D, ?3-D)

This part is a straight comparison of your best "1980" atmosphere from the 1987 assessment, see table below. Critical issues are

- ■i $O_3$ at 40 km, full chemical budgets/rates/families: 0° & 45°N, March & June
- ■j Dobson maps of $O_3$ plus columns of $HNO_3$, HCl, HF(where possible), $NO_2$ (all months, all latitudes)
- ■k $NO_y$ & $Cl_x$ levels, (March & June, all latitudes & height)
- ■l ratios: $NO/NO_2$, $NO_2/HNO_3$, $NO_x/NO_y$, Cl/ClO, $ClO/Cl_x$, ClO/HCl, $ClNO_3$/HCl, $OH/HO_2$ (March & June, 3/10/30 mbar (40/32/24 km), all latitudes)
- ■m lifetimes of $N_2O$, CFCs and other halocarbons
- ■(n) ("aerosol" chemistry / Antarctic ozone --no suggestions at this point)
- ■(o) accuracy of simplifying assumptions (up to individual modelers to test)

**Part 4. Assessment Runs: 1980 -> 20xx.** (2-D)

This part is the same or similar to the 2nd part of the 1987 Assessment. It turns everything "on" and examines a pair of calculations based on Table 13-1 of NASA/WMO 1986: a 1980 standard with 2.48 ppb $Cl_x$ and a mid-21st century simulation with 8.2 ppb $Cl_x$. Mixing ratios are used as lower (tropospheric) boundary conditions in order to minimize differences in models due to varied lifetimes for the CFCs. Calculations of the individual effects (e.g., $Cl_x$ alone, with/without $CO_2$ or $CH_4$) are welcome in general, but it may not be possible to perform an adequate intercomparison (perhaps in future intercomparisons)

We will examine *perturbations* to

- ■p $O_3$ Dobson maps
- ■q $O_3$ latitude × height contours (March & June)
- ■r lifetimes of $N_2O$, CFCs and other halocarbons
- ■s $NO_x$
- ■t The Self-Consistent 2-D Circulation: perturbations to transport.
  ***A catalog of the methodologies and theories behind the circulation feedbacks applied in the newest 2-D models.*** VERY IMPORTANT

**TABLE. Reference Atmospheres**

| | | "1980" | "20xx" |
|---|---|---|---|
| $CO_2$* | | *340 ppm* | *680 ppm* |
| $N_2O$ | | 300 ppb | 360 ppb |
| $CH_4$ | | 1.6 ppm | 3.2 ppm |
| $H_2O$ (at tropopause)* | | 3.0 ppm | unchanged |
| CO | | 100 ppb | unchanged |
| $CH_3Cl$ | | 700 ppt | unchanged |
| $CH_3CCl_3$ | | 100 ppt | unchanged |
| $CCl_4$ | | 100 ppt | unchanged |
| $CFCl_3$ | (CFC-11) | 170 ppt | 800 ppt |
| $CF_2Cl_2$ | (CFC-12) | 285 ppt | 2200 ppt |
| $CH_3Br$ | (only $Br_x$)* | 20 ppt | 40 ppt |

* to be included where possible/applicable

**DISTRIBUTION**

2-D models

Guy Brasseur
Julius Chang
David Crisp
Paul Crutzen
Anne Douglass
Don Fisher
Rolando Garcia
Lesley Gray
Paul Guthrie
Matt Hitchman
Ivar Isaksen
Charley Jackman
Malcolm Ko
John Pyle
Mark Schoeberl
Susan Solomon
Frode Stordal
Nien Dak Sze
K.K. Tung
Don Wuebbles
Yuk Yung
Rich Zurek

(3-D models etc.)

Byron Boville
Daniel Carriolle
William Grose
Jerry Mahlman
Michael Prather
Richard Rood
Robert Seals
Robert Watson

PLEASE SEND E-MAIL TO ME SO I CAN COLLECT RETURN ADDRESSES
[mprather/NASA] TELEMAIL/USA or [mprather/GSFCMAIL] GSFC/USA

NASA

National Aeronautics and
Space Administration

Washington, D.C.
20546

Reply to Attn of

M. Prather /EEU

18 May 1988

Dear Colleagues,

The enclosed schedule of intercomparisons and assignments has been made on the basis of replies, telephone conversations and an informal meeting of those present at the Polar Ozone Workshop last week. I hope that we can accomplish this ambitious list for the first Intercomparison this Fall. The date has been definitely selected as the week of **11-16 September 1988, at Virginia Beach, Virginia.** Participation in this Intercomparison 1988 is critical to the Upper Atmosphere Research Program, and your work will lead directly into one or more chapters for the 1990 "blue book" series (NASA/WMO, 1989).

The rules of this intercomparison are as stated in previous correspondence: participants will be assigned a task selected for the intercomparison. It will be their responsibility to put together the results from all participants for that specific experiment, to present the comparison of different models, and to direct the discussion that examines the causes of the differences (if any). This requirement will force us to have used the database effectively before we meet. A chair has been assigned to each of the 5 parts of the intercomparison; it is their duty to coordinate efforts and presentation within that section.

Results from the models **must be put into the database by the first week in August.** Please use the current (JPL 87-41!), best working version of your model; please do not plan on last minute improvements to the model for *this* intercomparison. This is a working meeting: only those groups contributing to the database or directly involved in the intercomparison should plan on attending. If you are not on the attendance list (enclosed), it is due to your replies or lack thereof. Expenses for the meeting should be absorbed by existing grants; foreign participants may be required to cover their own costs. Those participants requiring support must notify this office by June 1.

If there are any misunderstandings please reply immediately so that a list of errata and clarifications can be sent by June 1. Please contact me if you have any questions.

Yours,

Michael Prather

Michael Prather, Acting Program Manager,
Upper Atmosphere Theory & Data Analysis
NASA/HQ/EEU: 202/453-1681 NASA/GISS: 212/678-5625

*(11-16 Sept 1988, 2-D Intercomparison of stratospheric models)*

**Part 0. Database Grid for Archives** Chair: Robert Seals/Langley

■A Establish a standard grid (latitude x height x time) for archival storage and intercomparison using the 2-D database at Langley under Bob Seals. The database will be responsible for converting each model's grid onto the standard grid:

| | | |
|---|---|---|
| time: | instant "snapshots" for the middle of each month (note if 1st of month, or if monthly averages) | [12] |
| latitude: | grid = 90°S(5°)90°N | [37] |
| height: | range $z^*$ = 0 km (2km) 60 km<br>coordinate $z^*$ = 16 $\log_{10}(1000/p)$ km | [31] |

**All model data sent to the database should include a full grid for the quantities requested (latitude x height/pressure x 12 months) unless otherwise directed. Please submit 9-track tapes in accord with previous specifications or possibly other media such as electronic file transfer or PC-disks (1.2 Mb / 360 Kb, 5.25"), please check with R. Seals. Each group must submit an exact definition of your model grid and appropriate documentation in a text format (1 page).** The total amount of data requested for this intercomparison is modest, of order 4 Mbytes per model represented (assuming formatted output).

**Part 1. Photochemistry & Radiation** Chair: John Pyle/Cambridge

Fix the atmosphere (T & $O_3$):
Use January mean $O_3$ (SBUV) and T (NMC) from McPeters's analysis (copies enclosed, use your own best interpolator for your grid).
Assume clear sky (no clouds), a ground albedo of 30%, solar flux from WMO 1985.

■B (Brasseur) Compare UV photolysis rates:

Calculate latitude x height cross-sections of J-values (/sec) for *one day* (January 1). Report 24-hour averages, except for J(NO) use local noon.

$J(O_2)$, $J(O_3\text{-total})$, $J(O_3 \rightarrow O^1D)$, J(NO),
$J(NO_2)$, $J(HNO_3)$, $J(N_2O)$, J(CFC-11), J(CFC-12), $J(ClNO_3)$

[The database will integrate loss rates for Jan 1 for the distributions:
$f(N_2O) = 300 \times (p/100\ mb)^{0.7}$ ppb, for p < 100 mb;
f(NO) = (100 mb/p) ppb for p > 10 mb, = 10 ppb above;
$f(CFC\text{-}11) = 200 \times (p/100\ mb)^{2.2}$ ppt, for p < 100 mb;
$f(CFC\text{-}12) = 300 \times (p/100\ mb)^{0.7}$ ppt, for p < 100 mb.]

■C (Kiehl) Compare heating rates:

Calculate heating ($Q_{uv}$) and cooling ($Q_{IR}$) rates for 340 & 680 ppm of $CO_2$ (lat x ht x 12 months):
use ground albedo = 0.30 (visible) & 0.05 (IR),
a clear sky (no clouds & aerosols),
and $f(H_2O) = 3 \times 10^{-2}\ (p/1000\ mb)^4$ for p > 100 mb, $= 3 \times 10^{-6}$ above.

*(11-16 Sept 1988, 2-D Intercomparison of stratospheric models)*

**Part 2. Transport** Chair: Paul Guthrie/GSFC

**Using the "BEST" circulation from your Model (your alternate circulations are also welcome) compute the following diagnostics and 3 experiments:**

■D (Garcia) Circulation diagnostics:

Compare $Q_{net}$ (lat x ht x 12 months) and note (but do not archive) the type of diffusion ($K_{yy}$ or appropriate quantity).

■E (Yung) Tropospheric source (X):

Fix the mixing ratio of X at 1 ppb near the surface (all layers below 700 mb). Apply the following loss frequency and integrate through several annual cycles until steady-state is reached. Report mixing ratios (lat x ht x 12 months) and integrated annual loss. Compare steady-state distributions and lifetime.

$$\begin{aligned} L(p) &= 0 && \text{for } p > 100 \text{ mb}, \\ &= 3.E\text{-}6/p^2 \text{ sec}^{-1}, && \text{for } 1 \text{ mb} < p < 100 \text{ mb}, \\ &= 3.E\text{-}6 \text{ sec}^{-1}, && \text{for } p < 1 \text{ mb}, \end{aligned}$$

■F (Gray) Time-dependent source (Y):

Put $5x10^{12}$ kg of species Y (at.wt.=29, yields global average of 1 ppm) in the lower troposphere (>700mb). Assume that there is no loss for Y. Begin January 1 and calculate 5 successive years. Record distribution (lat x ht) every 1/2 yr (Jan 1 and July 1) along with total mass.

■G (Tung) Stratospheric source (Z):

Fix the mixing ratio of Z to be 8 ppmv for all p < 10 mb, and 0.010 ppmv for all p > 850 mb. Run the calculation to steady state. Calculate a "Dobson" map (latitude x 12 months) for the total column abundance of Z.

**Part 3. Current Atmosphere: 1980.** Chair: Malcolm Ko/AER

This part is a straight intercomparison of your best "1980" atmosphere from the 1987 assessment, see table below. **It is imperative that your steady-state simulation of the "current" atmosphere use these boundary conditions!** (Otherwise, the *intercomparison* will be impaired.)

■H (Prather) Models versus Observations

A short time will be allocated to *individual* modelling groups to present their own comparison with data for the current atmosphere.

Generally, the intercomparison of chemical constituents will involve archiving of the standard grids (lat x ht x 12 months) of the **noontime** abundance of each listed species listed below. Special topics include column abundances (lat x 12 months); the ozone budget at 40 km (special template by Charley Jackman in next mailing); and the lifetimes of the CFCs and $N_2O$.

$O_3$, O, OH, $HO_2$, $H_2O_2$, $H_2CO$

$NO_y$ = total odd-nitrogen = $HNO_3$+NO+$NO_2$+$NO_3$+$N_2O_5$+$HNO_2$+$HNO_4$+$ClNO_3$
$NO_x$ (=NO+$NO_2$), NO, $NO_2$, $N_2O_5$, $HNO_3$, $HNO_4$

$Cl_x$ = total inorganic chlorine = Cl+$Cl_2$+ClO+HCl+HOCl+$ClNO_3$+$(ClO)_2$
Cl, ClO, HCl, HOCl, $ClNO_3$

$Br_x$ = total inorganic bromine = Br+BrO+HBr+HOBr+$BrNO_3$
BrO

$N_2O$, $CH_4$, $H_2O$, $CFCl_3$, $CF_2Cl_2$, $CCl_4$, $CH_3CCl_3$

■I (Jackman) The 40 km ozone "problem"

The $O_3$/odd-oxygen budget at 40 km (defined as 3 mb): full chemical budgets / rates / families; 0° & ±45°; March & June.

■J (Isaksen) Integrated columns of $O_3$, $HNO_3$, HCl, HF, $NO_2$.

■K (Ko) $NO_y$ & $Cl_x$ levels

■L (Douglass) $NO/NO_2$, $NO_2/HNO_3$, $NO_x/NO_y$, etc.

■M (Pyle) $Cl/ClO$, $ClO/Cl_x$, $ClO/HCl$, $ClNO_3/HCl$, etc.

■N (Guthrie) $O/O_3$, $OH/HO_2$, $H_2O_2$, $H_2CO$, etc.

■O (Fisher) Distribution & lifetimes of $N_2O$, $CH_4$, CFCs, $CCl_4$ & $CH_3CCl_3$

**Part 4. Assessment Runs: 1980 -> 20xx.** Chair: Don Wuebbles/LLNL

The perturbation simulations are the same or similar to the 2nd part of the 1987 Assessment and examine a pair of atmospheres ("1980" and "20xx") defined in the table below, including 3 typical scenarios: A = all trace gases; B = $CO_2$ alone; C = CFCs alone; D = chemistry alone ($CH_4$, $N_2O$, CFCs). Mixing ratios are used as lower (tropospheric) boundary conditions in order to minimize differences in models due to varied lifetimes; *if you are going to do these calculations please do not deviate from these tabulated values without notifying Don or myself.* There is not time in this first meeting for a complete intercomparison of the perturbation calculations. Therefore we have elected to have individuals present their results and to focus the intercomparison on changes in the circulation: $Q_{net}$.

■P (Prather) Perturbations to ozone

Time will be allocated to *individual* modelling groups to present their own predictions of ozone future. A list of such perturbations should include:

$O_3$ Dobson maps,
$O_3$ latitude x height contours (March & June),
lifetimes of $N_2O$, CFCs and other halocarbons,
$NO_y$ values.

■Q (Hitchman) Comparison of perturbed circulations and temperatures

Groups performing any of the perturbations (A, B, C or D) are asked to archive in the database the resulting circulation changes ($Q_{net}$ and T for 1980 and 20xx: lat x ht x 12 months). Please remember also to supply documentation to the database describing just *how* the 2-D/3-D circulation is calculated "consistently".

**TABLE. Reference Atmospheres**

| | Tropospheric Mixing Ratios | | SCENARIO: | | | |
|---|---|---|---|---|---|---|
| | "1980" | "20xx" | A | B | C | D |
| | ------ | ------ | - | - | - | - |
| $CO_2$* | 340 ppm | 680 ppm | ■ | ■ | | |
| $N_2O$ | 300 ppb | 360 ppb | ■ | | | ■ |
| $CH_4$ | 1.6 ppm | 3.2 ppm | ■ | | | ■ |
| $H_2O$ (at tropopause)* | 3.0 ppm | unchanged | | | | |
| CO | 100 ppb | unchanged | | | | |
| $CH_3Cl$ | 700 ppt | unchanged | | | | |
| $CH_3CCl_3$ | 100 ppt | unchanged | | | | |
| $CCl_4$ | 100 ppt | unchanged | | | | |
| $CFCl_3$ (CFC-11) | 170 ppt | 800 ppt | ■ | | ■ | ■ |
| $CF_2Cl_2$ (CFC-12) | 285 ppt | 2200 ppt | ■ | | ■ | ■ |
| $CH_3Br$ (only $Br_x$)* | 20 ppt | 40 ppt* | ■ | | | |

* to be included where possible/applicable

ATTENDANCE

**2-D Model Participants**

| | | |
|---|---|---|
| Christoph Bruhl<br>Paul Crutzen | MPI | 011/49-6131-305458 |
| Don Fisher | DuPont | 302/695-4276 |
| Rolando Garcia<br>Susan Solomon | NOCAR | 303/497-1446<br>FTS/320-3483 |
| Matt Hitchman<br>Guy Brasseur | NCAR | 303/497-1000 |
| Ivar Isaksen<br>Frode Stordal | Oslo | 011/472-455822<br>011/472-455821 |
| Paul Guthrie | GSFC1 | 301/286-5830 |
| Charley Jackman<br>Anne Douglass | GSFC2 | 301/286-8399<br>301/286-2337 |
| Yukio Makino | Japan | 011/81-298-51-7111 |
| John Pyle<br>Lesley Gray | Cambridge | 011/44-223-337733/x6473<br>011/44-235-21900/x6524 |
| Malcolm Ko<br>Nien Dak Sze | AER | 617/547-6207 |
| K.K. Tung | Clarkson | 315/268-3865 |
| Don Wuebbles<br>Peter Connell | LLNL | 415/422-1845 |
| Yuk Yung<br>David Crisp | Cal.Tech. | 818/356-6940<br>FTS/792 |

**Additional Invitees**

| | | |
|---|---|---|
| Daniel Carriolle | CNRM | 011/33-6107-9090 or 6107-9381 |
| Richard Eckman | LaRC | FTS/928-2218 |
| William Grose | LaRC | FTS/928-4788 |
| Jeff Kiehl | NCAR | 303/497-1350 |
| Jerry Mahlman | GFDL | 609/452-6502 |
| Alan Plumb | MIT | 617/253-6281 |
| Michael Prather | GISS | 212/678-5625 |
| Richard Rood | GSFC | 301/286-8203 |
| Mark Schoeberl | GSFC | 301/286-5819 |
| Robert Seals | LaRC | FTS/928-2576 |
| Robert Watson | HQ | 202/453-1681 |
| Rich Zurek | JPL | FTS/792-3725 |

2-D Intercomparison of Stratospheric Models:

DATA SET TEMPERATURES (K) for z = 0, 2, 4, 90 km tot=46 (8E10.3)
(from 2-D GSFC MODEL, JACKMAN & McPETERS, 1987)
/= month
/ /= latitude

| | | | | | | | | |
|---|---|---|---|---|---|---|---|---|
| T | JAN85S | | | | | | | |
| | 266.3 | 254.1 | 243.4 | 234.8 | 226.0 | 226.2 | 230.6 | 232.3 |
| | 233.5 | 234.4 | 234.9 | 235.4 | 235.9 | 238.5 | 241.8 | 244.8 |
| | 248.2 | 253.5 | 259.5 | 265.7 | 272.3 | 278.9 | 285.1 | 288.9 |
| | 291.1 | 293.3 | 291.6 | 286.7 | 282.6 | 278.1 | 271.7 | 265.1 |
| | 257.9 | 253.3 | 247.8 | 240.2 | 233.0 | 224.7 | 215.1 | 205.0 |
| | 194.4 | 183.0 | 175.0 | 170.0 | 164.7 | 159.3 | | |
| T | JAN75S | | | | | | | |
| | 269.7 | 258.8 | 248.0 | 237.7 | 227.7 | 225.3 | 229.2 | 231.0 |
| | 232.1 | 233.0 | 233.5 | 234.0 | 234.7 | 237.5 | 240.9 | 244.1 |
| | 247.6 | 252.6 | 258.0 | 263.8 | 270.1 | 276.5 | 282.3 | 286.1 |
| | 288.4 | 290.6 | 288.7 | 283.8 | 279.9 | 275.4 | 268.6 | 261.6 |
| | 254.0 | 250.6 | 244.8 | 237.0 | 229.6 | 221.0 | 211.6 | 201.6 |
| | 191.2 | 179.8 | 173.5 | 168.5 | 163.3 | 158.0 | | |
| T | JAN65S | | | | | | | |
| | 275.1 | 264.4 | 253.2 | 241.3 | 230.1 | 225.4 | 227.8 | 229.2 |
| | 230.1 | 230.8 | 231.1 | 231.6 | 232.2 | 234.9 | 238.4 | 241.7 |
| | 245.2 | 250.3 | 255.9 | 261.6 | 267.6 | 273.6 | 279.0 | 282.3 |
| | 284.3 | 286.0 | 283.5 | 279.2 | 276.0 | 271.1 | 262.6 | 254.1 |
| | 245.6 | 242.7 | 237.7 | 229.9 | 222.1 | 213.3 | 204.2 | 194.7 |
| | 184.6 | 174.9 | 170.5 | 165.6 | 160.6 | 156.0 | | |
| T | JAN55S | | | | | | | |
| | 278.7 | 268.5 | 257.7 | 245.6 | 233.4 | 225.6 | 224.9 | 225.5 |
| | 225.7 | 226.1 | 226.5 | 227.4 | 228.6 | 231.7 | 235.3 | 238.7 |
| | 242.5 | 247.9 | 253.6 | 259.3 | 264.9 | 270.7 | 275.3 | 277.6 |
| | 279.2 | 280.0 | 277.1 | 273.8 | 271.4 | 265.4 | 256.8 | 248.2 |
| | 240.4 | 235.5 | 229.4 | 220.9 | 212.8 | 204.9 | 196.7 | 188.2 |
| | 179.1 | 173.4 | 169.1 | 164.8 | 160.3 | 156.6 | | |
| T | JAN45S | | | | | | | |
| | 286.7 | 276.7 | 266.1 | 254.0 | 240.1 | 227.7 | 220.5 | 218.5 |
| | 217.7 | 217.8 | 219.3 | 221.9 | 224.4 | 228.3 | 232.2 | 236.1 |
| | 240.1 | 245.6 | 251.1 | 256.6 | 262.1 | 267.7 | 271.7 | 273.3 |
| | 274.3 | 274.2 | 271.5 | 269.0 | 267.0 | 259.0 | 250.0 | 240.4 |
| | 234.2 | 229.9 | 222.4 | 213.8 | 207.0 | 200.6 | 193.9 | 187.1 |
| | 180.3 | 177.1 | 173.8 | 170.4 | 167.1 | 164.1 | | |
| T | JAN35S | | | | | | | |
| | 293.5 | 283.6 | 273.1 | 260.9 | 246.5 | 232.9 | 220.8 | 213.0 |
| | 209.2 | 208.9 | 212.5 | 216.7 | 220.6 | 224.9 | 229.1 | 233.2 |
| | 237.6 | 242.9 | 248.0 | 253.7 | 259.3 | 265.0 | 268.5 | 269.8 |
| | 270.9 | 270.2 | 267.5 | 265.7 | 262.6 | 254.3 | 246.1 | 237.6 |
| | 234.0 | 228.9 | 221.1 | 213.4 | 207.9 | 202.9 | 197.6 | 192.3 |
| | 187.6 | 185.6 | 183.3 | 181.0 | 178.7 | 176.2 | | |
| T | JAN25S | | | | | | | |
| | 298.2 | 288.1 | 277.3 | 264.9 | 251.1 | 237.2 | 223.4 | 211.0 |
| | 203.2 | 201.6 | 207.4 | 213.0 | 217.9 | 222.4 | 226.7 | 231.0 |
| | 235.4 | 240.4 | 245.2 | 251.0 | 256.7 | 262.4 | 265.8 | 267.5 |
| | 269.0 | 267.7 | 264.9 | 263.1 | 259.0 | 251.3 | 243.6 | 236.8 |
| | 234.6 | 230.6 | 222.3 | 215.4 | 210.9 | 206.6 | 202.2 | 197.6 |
| | 194.0 | 192.7 | 191.2 | 189.7 | 188.2 | 186.8 | | |
| T | JAN15S | | | | | | | |
| | 299.1 | 289.1 | 278.6 | 266.8 | 253.4 | 239.2 | 224.2 | 209.9 |
| | 199.6 | 197.4 | 204.3 | 210.9 | 216.3 | 220.8 | 225.1 | 229.4 |
| | 233.9 | 238.5 | 243.3 | 249.0 | 254.9 | 260.5 | 263.9 | 265.9 |
| | 267.6 | 265.8 | 262.9 | 261.0 | 256.2 | 249.1 | 241.8 | 236.5 |

```
  235.1   229.9   220.9   214.6   210.7   206.9   202.9   198.9
  196.3   195.4   194.4   193.3   192.3   191.9
T  JAN 5S
  299.9   289.5   278.8   267.2   253.9   239.7   224.6   209.4
  198.2   195.8   203.1   209.9   215.5   220.1   224.5   228.9
  233.3   237.8   242.6   248.3   254.1   259.5   262.9   265.1
  266.9   264.7   261.8   259.7   254.3   247.0   239.4   234.4
  232.7   226.4   216.4   210.8   208.0   205.2   202.4   199.4
  197.6   196.5   195.2   193.8   192.6   191.9
T  JAN 5N
  299.9   289.5   278.6   267.2   254.1   239.3   224.0   209.3
  199.6   196.7   203.9   211.1   216.8   220.9   224.8   228.7
  233.1   238.3   243.4   248.9   254.5   259.8   262.9   264.6
  266.0   264.3   261.6   259.8   254.7   247.4   239.8   234.7
  231.4   223.8   213.7   208.2   206.1   204.1   202.1   200.1
  198.4   196.7   194.9   193.2   191.5   189.8
T  JAN15N
  298.2   288.1   277.5   265.7   252.2   237.9   223.3   209.7
  200.6   197.3   204.2   211.3   216.9   220.9   224.9   228.7
  233.0   238.2   243.1   248.6   254.1   259.3   262.3   264.0
  265.3   263.8   261.5   260.3   255.0   247.5   239.7   234.1
  230.8   223.7   214.2   209.0   206.6   204.3   202.0   199.7
  197.7   195.8   194.0   191.9   190.1   188.6
T  JAN25N
  292.1   282.3   271.9   259.9   246.5   233.1   221.0   211.4
  205.3   202.0   206.9   212.6   217.2   220.8   224.5   228.0
  232.2   237.2   242.1   247.3   252.5   257.2   259.9   261.6
  263.0   262.1   260.9   260.6   254.7   246.7   238.3   233.9
  231.8   225.5   217.5   212.6   209.4   206.3   203.2   199.9
  197.8   196.3   194.6   193.0   191.3   189.2
T  JAN35N
  284.7   274.1   262.8   250.0   236.1   224.4   218.3   215.4
  213.1   211.6   213.0   215.6   218.3   221.3   224.2   227.1
  230.7   235.3   239.7   244.3   249.0   253.2   255.9   257.9
  259.5   259.6   259.7   260.4   253.8   246.2   238.0   235.0
  233.3   227.8   221.6   217.2   213.7   210.0   206.3   202.4
  200.6   199.5   198.4   197.3   196.3   195.5
T  JAN45N
  273.7   264.7   254.4   241.5   228.2   219.1   217.5   217.8
  217.3   216.9   216.9   217.5   218.5   220.5   222.5   224.6
  227.9   232.3   236.6   240.9   245.1   249.0   251.9   254.5
  256.5   257.4   259.1   259.3   251.3   243.7   235.8   234.6
  232.6   229.9   225.1   221.5   218.0   214.4   210.8   206.9
  205.8   205.1   204.3   203.6   202.9   201.8
T  JAN55N
  266.6   258.6   249.0   236.1   223.7   216.2   216.0   216.4
  216.0   215.2   214.7   214.5   214.9   216.8   218.5   220.3
  224.4   229.1   233.8   238.4   243.1   247.1   250.6   254.1
  256.1   257.1   259.6   256.7   248.3   240.1   234.6   234.0
  232.0   230.1   227.5   224.1   220.9   217.5   214.2   211.0
  210.5   209.9   209.4   208.8   208.3   207.9
T  JAN65N
  259.8   253.8   245.1   232.2   220.3   213.7   213.1   212.3
  210.8   209.1   208.2   208.0   209.0   211.2   213.2   216.0
  221.5   226.8   232.6   238.2   243.6   248.4   252.8   256.4
  257.5   258.6   260.2   253.2   244.8   236.0   232.7   230.9
  228.6   226.8   224.0   221.6   219.1   216.5   213.9   212.5
  212.2   211.8   211.3   210.9   210.4   209.9
T  JAN75N
  257.4   250.5   241.4   229.0   217.5   211.3   209.8   208.0
```

```
      205.6     202.8     201.6     201.6     203.7     206.4     209.0     213.2
      219.4     225.6     232.3     238.9     245.1     250.6     255.8     258.7
      258.9     260.4     259.4     251.0     243.2     235.3     231.1     227.9
      223.2     218.6     217.1     216.0     214.9     213.8     212.6     212.4
      212.0     211.7     211.5     211.2     210.7     209.7
T     JAN85N
      252.2     246.8     238.5     226.3     215.7     210.2     208.2     205.9
      202.9     199.7     198.6     198.4     200.6     203.2     205.8     210.8
      217.5     224.4     231.8     238.9     245.4     251.4     257.1     259.0
      259.2     261.0     258.1     250.1     242.8     236.0     230.9     225.0
      218.6     214.7     214.2     213.8     213.3     212.9     212.5     212.3
      211.9     211.7     211.4     211.1     210.4     209.1
```

2-D Intercomparison of Stratospheric Models:

DATA SET OZONE (#/cm**3) for z = 0, 2, 4, 62 km tot=32 (8E10.3)
(from 2-D GSFC MODEL, McPETERS et al, 1984, JGR)

/= column (#/cm**2)
/ /= O3 density scale 60-62 km, use
/ / O3[z+2] = O3[z] * (O3[62]/O3[60]) for z > 62 km

```
O3  JAN85S 8.526E+18    -4.793
 1.641E+12 1.529E+12 1.136E+12 1.136E+12 1.454E+12 1.519E+12 1.610E+12 2.216E+12
 2.808E+12 3.537E+12 4.235E+12 4.208E+12 3.611E+12 2.942E+12 2.223E+12 1.620E+12
 1.353E+12 1.218E+12 1.043E+12 7.891E+11 5.571E+11 3.923E+11 2.354E+11 1.495E+11
 9.715E+10 6.236E+10 4.185E+10 2.890E+10 1.863E+10 1.262E+10 8.349E+09 5.501E+09
O3  JAN75S 8.594E+18    -4.792
 1.623E+12 1.520E+12 1.137E+12 1.110E+12 1.452E+12 1.554E+12 1.628E+12 2.225E+12
 2.845E+12 3.573E+12 4.305E+12 4.288E+12 3.671E+12 2.965E+12 2.242E+12 1.629E+12
 1.355E+12 1.224E+12 1.050E+12 7.885E+11 5.522E+11 3.870E+11 2.303E+11 1.469E+11
 9.493E+10 6.093E+10 4.094E+10 2.788E+10 1.804E+10 1.218E+10 8.025E+09 5.287E+09
O3  JAN65S 8.940E+18    -4.763
 1.462E+12 1.371E+12 1.025E+12 9.998E+11 1.365E+12 1.508E+12 1.588E+12 2.153E+12
 2.783E+12 3.541E+12 4.368E+12 4.492E+12 4.055E+12 3.390E+12 2.639E+12 1.994E+12
 1.640E+12 1.422E+12 1.164E+12 8.347E+11 5.740E+11 3.931E+11 2.336E+11 1.508E+11
 9.729E+10 6.290E+10 4.273E+10 2.853E+10 1.829E+10 1.236E+10 8.124E+09 5.339E+09
O3  JAN55S 8.990E+18    -4.681
 1.290E+12 1.217E+12 9.168E+11 8.654E+11 1.184E+12 1.341E+12 1.431E+12 1.923E+12
 2.483E+12 3.257E+12 4.182E+12 4.514E+12 4.289E+12 3.794E+12 3.090E+12 2.427E+12
 1.975E+12 1.622E+12 1.277E+12 8.786E+11 5.936E+11 3.884E+11 2.292E+11 1.496E+11
 9.577E+10 6.185E+10 4.201E+10 2.707E+10 1.743E+10 1.167E+10 7.613E+09 4.966E+09
O3  JAN45S 8.264E+18    -4.628
 1.013E+12 9.580E+11 7.311E+11 6.680E+11 8.670E+11 9.680E+11 1.017E+12 1.358E+12
 1.810E+12 2.520E+12 3.528E+12 4.100E+12 4.232E+12 3.992E+12 3.413E+12 2.799E+12
 2.245E+12 1.768E+12 1.336E+12 8.827E+11 5.983E+11 3.785E+11 2.268E+11 1.474E+11
 9.317E+10 6.036E+10 4.096E+10 2.553E+10 1.681E+10 1.107E+10 7.187E+09 4.665E+09
O3  JAN35S 7.580E+18    -4.549
 7.871E+11 7.471E+11 5.772E+11 5.111E+11 6.185E+11 6.729E+11 6.902E+11 8.951E+11
 1.246E+12 1.834E+12 2.891E+12 3.657E+12 4.114E+12 4.112E+12 3.672E+12 3.102E+12
 2.457E+12 1.881E+12 1.367E+12 8.813E+11 5.942E+11 3.629E+11 2.232E+11 1.442E+11
 9.044E+10 5.884E+10 3.911E+10 2.410E+10 1.608E+10 1.036E+10 6.676E+09 4.301E+09
O3  JAN25S 7.059E+18    -4.464
 6.545E+11 6.230E+11 4.839E+11 4.141E+11 4.666E+11 4.876E+11 4.885E+11 5.999E+11
 8.367E+11 1.298E+12 2.369E+12 3.304E+12 3.989E+12 4.180E+12 3.813E+12 3.285E+12
 2.571E+12 1.945E+12 1.381E+12 8.841E+11 5.942E+11 3.551E+11 2.194E+11 1.386E+11
 8.593E+10 5.644E+10 3.693E+10 2.290E+10 1.509E+10 9.642E+09 6.160E+09 3.935E+09
O3  JAN15S 6.684E+18    -4.416
 5.588E+11 5.319E+11 4.155E+11 3.491E+11 3.510E+11 3.353E+11 3.130E+11 3.670E+11
 5.014E+11 8.645E+11 1.950E+12 3.079E+12 3.930E+12 4.241E+12 3.962E+12 3.447E+12
 2.675E+12 2.012E+12 1.409E+12 8.924E+11 5.956E+11 3.459E+11 2.135E+11 1.322E+11
 8.118E+10 5.341E+10 3.418E+10 2.130E+10 1.386E+10 8.814E+09 5.604E+09 3.563E+09
O3  JAN 5S 6.332E+18    -4.418
 4.879E+11 4.639E+11 3.625E+11 2.988E+11 2.632E+11 2.251E+11 1.926E+11 2.185E+11
 2.855E+11 5.664E+11 1.616E+12 2.899E+12 3.825E+12 4.243E+12 3.998E+12 3.497E+12
 2.697E+12 2.005E+12 1.393E+12 8.816E+11 5.854E+11 3.386E+11 2.101E+11 1.287E+11
 7.860E+10 5.188E+10 3.279E+10 2.056E+10 1.335E+10 8.492E+09 5.400E+09 3.434E+09
O3  JAN 5N 6.209E+18    -4.407
 4.580E+11 4.355E+11 3.404E+11 2.819E+11 2.531E+11 2.170E+11 1.871E+11 2.183E+11
 2.925E+11 5.713E+11 1.591E+12 2.821E+12 3.703E+12 4.138E+12 3.904E+12 3.438E+12
 2.671E+12 1.971E+12 1.386E+12 8.842E+11 5.926E+11 3.455E+11 2.148E+11 1.324E+11
 8.065E+10 5.282E+10 3.347E+10 2.092E+10 1.357E+10 8.618E+09 5.474E+09 3.477E+09
O3  JAN15N 6.417E+18    -4.354
 4.717E+11 4.485E+11 3.492E+11 3.000E+11 3.228E+11 3.212E+11 3.130E+11 3.975E+11
```

```
 5.762E+11 9.924E+11 2.028E+12 3.029E+12 3.753E+12 3.992E+12 3.717E+12 3.221E+12
 2.521E+12 1.880E+12 1.334E+12 8.638E+11 5.829E+11 3.421E+11 2.129E+11 1.315E+11
 7.926E+10 5.135E+10 3.235E+10 2.017E+10 1.304E+10 8.237E+09 5.203E+09 3.286E+09
O3  JAN25N 7.019E+18    -4.240
 5.409E+11 5.146E+11 3.962E+11 3.550E+11 4.780E+11 5.607E+11 6.177E+11 8.501E+11
 1.224E+12 1.869E+12 2.879E+12 3.588E+12 3.930E+12 3.851E+12 3.382E+12 2.823E+12
 2.237E+12 1.711E+12 1.241E+12 8.356E+11 5.738E+11 3.431E+11 2.181E+11 1.334E+11
 7.882E+10 5.077E+10 3.123E+10 1.933E+10 1.230E+10 7.677E+09 4.790E+09 2.989E+09
O3  JAN35N 8.472E+18    -4.091
 6.506E+11 6.177E+11 4.646E+11 4.624E+11 7.855E+11 1.072E+12 1.315E+12 1.883E+12
 2.515E+12 3.387E+12 4.253E+12 4.498E+12 4.317E+12 3.820E+12 3.154E+12 2.507E+12
 1.989E+12 1.544E+12 1.141E+12 8.104E+11 5.592E+11 3.493E+11 2.297E+11 1.408E+11
 8.268E+10 5.308E+10 3.142E+10 1.949E+10 1.210E+10 7.420E+09 4.551E+09 2.791E+09
O3  JAN45N 9.645E+18    -3.995
 7.280E+11 6.880E+11 5.007E+11 5.633E+11 1.099E+12 1.599E+12 2.068E+12 2.968E+12
 3.793E+12 4.723E+12 5.293E+12 5.098E+12 4.417E+12 3.643E+12 2.857E+12 2.222E+12
 1.756E+12 1.370E+12 1.024E+12 7.493E+11 5.224E+11 3.362E+11 2.242E+11 1.362E+11
 8.114E+10 5.180E+10 2.977E+10 1.879E+10 1.139E+10 6.903E+09 4.184E+09 2.536E+09
O3  JAN55N 9.807E+18    -3.975
 7.848E+11 7.364E+11 5.253E+11 6.445E+11 1.295E+12 1.891E+12 2.474E+12 3.561E+12
 4.442E+12 5.376E+12 5.752E+12 5.142E+12 4.124E+12 3.182E+12 2.348E+12 1.812E+12
 1.462E+12 1.152E+12 8.639E+11 6.458E+11 4.356E+11 2.913E+11 1.905E+11 1.132E+11
 7.022E+10 4.358E+10 2.584E+10 1.627E+10 9.836E+09 5.947E+09 3.596E+09 2.174E+09
O3  JAN65N 9.726E+18    -4.047
 8.107E+11 7.572E+11 5.354E+11 7.010E+11 1.397E+12 2.002E+12 2.654E+12 3.883E+12
 4.852E+12 5.834E+12 6.004E+12 5.022E+12 3.828E+12 2.794E+12 1.995E+12 1.556E+12
 1.244E+12 9.610E+11 7.151E+11 5.184E+11 3.459E+11 2.355E+11 1.507E+11 9.090E+10
 5.911E+10 3.535E+10 2.222E+10 1.368E+10 8.349E+09 5.093E+09 3.107E+09 1.896E+09
O3  JAN75N 9.648E+18    -4.012
 8.264E+11 7.714E+11 5.440E+11 7.434E+11 1.445E+12 2.046E+12 2.730E+12 4.020E+12
 5.011E+12 5.999E+12 6.014E+12 4.858E+12 3.664E+12 2.610E+12 1.871E+12 1.482E+12
 1.173E+12 8.869E+11 6.560E+11 4.592E+11 3.052E+11 2.058E+11 1.274E+11 7.832E+10
 5.044E+10 2.985E+10 1.900E+10 1.154E+10 7.010E+09 4.258E+09 2.587E+09 1.571E+09
O3  JAN85N 9.637E+18    -3.985
 8.394E+11 7.801E+11 5.470E+11 7.729E+11 1.475E+12 2.082E+12 2.798E+12 4.118E+12
 5.134E+12 6.131E+12 5.996E+12 4.771E+12 3.576E+12 2.522E+12 1.835E+12 1.453E+12
 1.132E+12 8.418E+11 6.176E+11 4.213E+11 2.808E+11 1.850E+11 1.126E+11 7.080E+10
 4.427E+10 2.637E+10 1.669E+10 1.010E+10 6.116E+09 3.703E+09 2.242E+09 1.357E+09
```

DATE: JUNE 3, 1988

SUBJECT: INTERCOMPARISON OF OZONE BUDGETS AT 3 MBAR

TO: TWO-DIMENSIONAL MODELLERS

FROM: CHARLES JACKMAN

I have been charged with investigating the critical issue I in the upcoming 2-D Model Intercomparison. This issue concerns $O_3$ at 40 km (3 mbar) full chemical budgets/rates/families at 0° and 45°N for March and June. Most of the model results that I am requesting have a direct impact on $O_3$ at 3 mbar. Some of the model results requested have only a minor or indirect impact on $O_3$, however, I would like to be as complete as possible in this model analysis.

I have tried to send this letter to at least one member of each 2-D modelling group as well as several other participants.

COULD YOU PLEASE SEND THE FOLLOWING INFORMATION BY AUGUST 1, 1988 TO:

CHARLES JACKMAN
CODE 616
NASA/GODDARD SPACE FLIGHT CENTER
GREENBELT, MD 20771

DESIRED INFORMATION FROM EACH 2D MODEL:

o DO 1980 CURRENT ATMOSPHERE MODEL EXPERIMENT (2.48 PPBV $Cl_x$) USING JPL 87-41 (SEE THE TABLE IN INTERCOMPARISON LETTER DATED MAY 18, 1988 FROM MICHAEL PRATHER).

o GIVE OUTPUT FROM MARCH 21 (EQUINOX) AND JUNE 21 (SOLSTICE)

o GIVE OUTPUT AT 3 MBAR (IF NEED BE, IT IS YOUR RESPONSIBILITY TO INTERPOLATE!) FOR 45°S, 0°, AND 45°N

A) PHOTOLYSIS INFORMATION (24 HOUR AVERAGE) AT 3 MBAR IN $S^{-1}$:

1) $J(O_3) \rightarrow O(^1D) + O_2$
2) $J(O_3) \rightarrow O(^3P) + O_2$
3) $J(NO)$
4) $J(NO_2)$
5) $J(HNO_3)$
6) $J(N_2O_5)$
7) $J(ClONO_2)$

CONTINUATION OF NEEDED INFORMATION BY AUGUST 1, 1988 TO SEND TO:

CHARLES JACKMAN
CODE 616
NASA/GODDARD SPACE FLIGHT CENTER
GREENBELT, MD 20771

B) PRODUCTION OR LOSS INFORMATION AT 3 MBAR IN $CM^{-3}$ FOR A 24 HOUR TIME PERIOD (PLEASE NOTE THAT THIS IS THE INTEGRAL OVER THE PRODUCTION OR LOSS RATE FOR 24 HOURS!):

8) $J(O_2)$ $[O_2]$

9) $J(O_3 \rightarrow O(^1D))$ $[O_3]$

10) $J(O_3 \rightarrow O(^3P))$ $[O_3]$

11) $J(NO)$ $[NO]$

12) $J(NO_3 \rightarrow NO)$ $[NO_3]$

13) $k(O_3+O)$ $[O_3]$ $[O]$

14) $k(NO_2+O)$ $[NO_2]$ $[O]$

15) $k(HO_2+O_3)$ $[HO_2]$ $[O_3]$

16) $k(HO_2+O)$ $[HO_2]$ $[O]$

17) $k(OH+O)$ $[OH]$ $[O]$

18) $k(OH+O_3)$ $[OH]$ $[O_3]$

19) $k(H+O_3)$ $[H]$ $[O_3]$

20) $k(OH+HO_2)$ $[OH]$ $[HO_2]$

21) $k(HO_2+HO_2)$ $[HO_2]$ $[HO_2]$

22) $k(ClO+O)$ $[ClO]$ $[O]$

23) $k(O(^1D)+H_2O)$ $[O(^1D)]$ $[H_2O]$

24) $k(O(^1D)+N_2O)$ $[O(^1D)]$ $[N_2O]$

25) $k(N+NO)$ $[N]$ $[NO]$

CONTINUATION OF NEEDED INFORMATION BY AUGUST 1, 1988 TO SEND TO:

CHARLES JACKMAN
CODE 616
NASA/GODDARD SPACE FLIGHT CENTER
GREENBELT, MD 20771

C) THE DAYTIME AVERAGE VALUES FOR THE FOLLOWING SPECIES AT 3 MBAR IN $CM^{-3}$:

1) $O_3$
2) $O_2$
3) O
4) $O(^1D)$
5) $NO_2$
6) NO
7) N
8) $HNO_3$
9) $NO_3$
10) $N_2O_5$
11) $HO_2NO_2$
12) $N_2O$
13) H
14) OH
15) $HO_2$
16) $H_2O$
17) $H_2O_2$
18) Cl
19) ClO
20) HCl
21) HOCl
22) $ClONO_2$
23) $CH_4$
24) CO
25) M

D) TEMPERATURE AT 3 MBAR IN °K

26) T

E) THE FOLLOWING COLUMN DENSITIES ABOVE 3 MBAR IN $CM^{-2}$:

27) $O_3$ COLUMN
28) $O_2$ COLUMN

For our mutual convenience I am providing tabular forms on which to include your model information. Thanks for your help in compiling this data.

Charley Jackman

TWO-DIMENSIONAL MODEL INFORMATION

INVESTIGATORS ON MODEL _____

INSTITUTION MODELLERS AFFILIATED WITH _____

A) PHOTOLYSIS INFORMATION (24 HOUR AVERAGE) AT 3 MBAR IN $S^{-1}$:

| | MARCH | | | JUNE | | |
|---|---|---|---|---|---|---|
| | 45°S | 0° | 45°N | 45°S | 0° | 45°N |
| 1) $J(O_3 \rightarrow O(^1D))$ | | | | | | |
| 2) $J(O_3) \rightarrow O(^3P))$ | | | | | | |
| 3) $J(NO)$ | | | | | | |
| 4) $J(NO_2)$ | | | | | | |
| 5) $J(HNO_3)$ | | | | | | |
| 6) $J(N_2O_5)$ | | | | | | |
| 7) $J(ClONO_2)$ | | | | | | |

B) RATE INFORMATION AT 3 MBAR IN $CM^{-3}$ FOR A 24 HOUR TIME PERIOD:

| | MARCH | | | JUNE | | |
|---|---|---|---|---|---|---|
| | 45°S | 0° | 45°N | 45°S | 0° | 45°N |
| 8) $J(O_2)$ $[O_2]$ | | | | | | |
| 9) $J(O_3 \rightarrow O(^1D))$ $[O_3]$ | | | | | | |

CONTINUATION OF B) RATE INFORMATION AT 3 MBAR IN $CM^{-3}$ FOR A 24 HOUR TIME PERIOD:

| | MARCH | | | JUNE | | |
|---|---|---|---|---|---|---|
| | 45°S | 0° | 45°N | 45°S | 0° | 45°N |
| 10) $J(O_3 \rightarrow O(^3P))$ $[O_3]$ | | | | | | |
| 11) J(NO) [NO] | | | | | | |
| 12) $J(NO_3 \rightarrow NO)$ $[NO_3]$ | | | | | | |
| 13) $k(O_3+O)$ $[O_3]$ [O] | | | | | | |
| 14) $k(NO_2+O)$ $[NO_2]$ [O] | | | | | | |
| 15) $k(HO_2+O_3)$ $[HO_2]$ $[O_3]$ | | | | | | |
| 16) $k(HO_2+O)$ $[HO_2]$ [O] | | | | | | |
| 17) k(OH+O) [OH] [O] | | | | | | |
| 18) $k(OH+O_3)$ [OH] $[O_3]$ | | | | | | |
| 19) $k(H+O_3)$ [H] $[O_3]$ | | | | | | |
| 20) $k(OH+HO_2)$ [OH] $[HO_2]$ | | | | | | |
| 21) $k(HO_2+HO_2)$ $[HO_2]$ $[HO_2]$ | | | | | | |
| 22) k(ClO+O) [ClO] [O] | | | | | | |
| 23) $k(O(^1D)+H_2O)$ $[O(^1D)]$ $[H_2O]$ | | | | | | |
| 24) $k(O(^1D)+N_2O)$ $[O(^1D)]$ $[N_2O]$ | | | | | | |
| 25) k(N+NO) [N] [NO] | | | | | | |

C) THE DAYTIME AVERAGE VALUES FOR THE FOLLOWING SPECIES AT 3 MBAR IN $CM^{-3}$:

| | MARCH | | | JUNE | | |
|---|---|---|---|---|---|---|
| | 45°S | 0° | 45°N | 45°S | 0° | 45°N |
| 1) $O_3$ | | | | | | |
| 2) $O_2$ | | | | | | |
| 3) O | | | | | | |
| 4) $O(^1D)$ | | | | | | |
| 5) $NO_2$ | | | | | | |
| 6) NO | | | | | | |
| 7) N | | | | | | |
| 8) $HNO_3$ | | | | | | |
| 9) $NO_3$ | | | | | | |
| 10) $N_2O_5$ | | | | | | |
| 11) $HO_2NO_2$ | | | | | | |
| 12) $N_2O$ | | | | | | |
| 13) H | | | | | | |
| 14) OH | | | | | | |
| 15) $HO_2$ | | | | | | |
| 16) $H_2O$ | | | | | | |
| 17) $H_2O_2$ | | | | | | |

CONTINUATION OF C) THE DAYTIME AVERAGE VALUES FOR THE FOLLOWING SPECIES AT 3 MBAR IN $CM^{-3}$:

| | MARCH | | | JUNE | | |
|---|---|---|---|---|---|---|
| | 45°S | 0° | 45°N | 45°S | 0° | 45°N |
| 18) Cl | | | | | | |
| 19) ClO | | | | | | |
| 20) HCl | | | | | | |
| 21) HOCl | | | | | | |
| 22) $ClONO_2$ | | | | | | |
| 23) $CH_4$ | | | | | | |
| 24) CO | | | | | | |
| 25) M | | | | | | |

D) TEMPERATURE AT 3 MBAR IN °K

| | MARCH | | | JUNE | | |
|---|---|---|---|---|---|---|
| | 45°S | 0° | 45°N | 45°S | 0° | 45°N |
| 26) T | | | | | | |

E) THE FOLLOWING COLUMN DENSITIES ABOVE 3 MBAR IN $CM^{-2}$:

| | MARCH | | | JUNE | | |
|---|---|---|---|---|---|---|
| | 45°S | 0° | 45°N | 45°S | 0° | 45°N |
| 27) $O_3$ COLUMN | | | | | | |
| 28) $O_2$ COLUMN | | | | | | |

## Section 1.3 Participants' Names and Addresses


Dr. Guy Brasseur
Institute D'Aeronomie Spatiale
De Belgium
3, Avenue Circulaire
Brussels 1180
Belgium
Telephone: 32-2-3742728

Dr. Christoph Bruehl
Max Planck Institute for Chemistry
P.O. Box 3060
Mainz D-6500
Federal Republic of Germany
Telephone 011-49-6131-305434
FAX: 011-49-6131-305388

Dr. Peter S. Connell
L - 262
Lawrence Livermore
National Laboratory
P.O. Box 808
Livermore, CA 94550
Telephone: (415) 422-1811
FTS: 532-1811

Dr. David Crisp
MS-169-237
Jet Propulsion Laboratory
California Institue of Technology
Planetary Science Department
4800 Oak Grove Drive
Pasadena, CA 91109
Telephone: (818) 354-9617

Dr. Anne R. Douglass
Code 616
Goddard Space Flight Center
Greenbelt, MD 20771
Telephone: (301) 286-2337

Dr. Richard Eckman
MS-401B
NASA/Langley Research Center
Atmospheric Sciences Div.
Hampton, VA 23665 -5225
Telephone: (804) 864-5816
FTS: 928-5816

Dr. Don Fisher
E.I. DuPont De Nemour & Company, Inc.
DuPont Experimental Station
Wilmington, DE 19898
Telephone: (302) 695-4276

Dr. Alexander Frolov
Main Geophysical Observatory
Karbysheva 7
Leningrad 194018
U.S.S.R.

Dr. Rolando Garcia
National Center for Atmospheric
Research
P.O. Box 3000
Boulder, CO 80307
Telephone: (303) 497-1446

Dr. Lesley J. Gray
Rutherford Appleton Laboratory
Science and Engineering
Research Council
Chilton, Didcot OXON,
United Kingdom OX11 OXQ
Telephone: 011-144-235-21900 x6524

Dr. William L. Grose
MS-401B
NASA/Langley Research Center
Atmospheric Sciences Dept.
Hampton, VA 23665-5225
Telephone: (804)864-5820
FTS: 928-5820

Dr. Paul Guthrie
Code 616
NASA/Goddard Space Flight Center
Greenbelt, MD 20771
Telephone: (301) 286-5830

Dr. Matt Hitchman
University of Wisconsin-Madison
Department of Meteorology
1225 W. Dayton Street
Madison, WI 53706
Telephone: (608) 262-4653

Ms. Linda A. Hunt
MS-423
PRC
NASA Langley Research Center
Hampton, VA 23665-5225
Telephone: (804) 864-5856

Dr. Ivar Isaksen
University of Oslo
Institute of Geophysics
Box 1022
Blindern, Oslo 3
NORWAY
Telephone: 011-472-455822

Dr. Charles H. Jackman
Code 616
Goddard Space Flight Center
Greenbelt, MD 20771
Telephone: (301) 286-8399

Dr. Malcolm K. W. Ko
Atmospheric & Environmental Research, Inc.
840 Memorial Drive
Cambridge, MA 02139
Telephone: (617) 547-6207

Dr. V. Philushakin
Central Aerological Observatory
The State Committee of Meteorology & Hydrology
Pervomaijskya Street, 3
Moscow 141700
U.S.S.R.

Dr. Alan Plumb
Massachusetts Institute of Technology
Cambridge, MA 02139
Telephone: (617) 253-6281

Dr. Michael Prather
NASA Goddard Space Flight Center
Institute for Space Studies
2880 Broadway
New York, N.Y. 10025
Telephone: (212) 678-5625

Dr. Richard B. Rood
Code 616
Goddard Space Flight Center
Greenbelt, MD 20771
Telephone: 301-286-8203

Dr. Evgeny Rozanov
10H1
33 3rd Avenue South
New York, NY 10003

Dr. Anne De Rudder
Institut D'Aeronomie Spatiale De Belgique
3, Avenue Circulaire
Brussels, 1180
BELGIUM
Telephone: 32-2-3742728

Ms. Karen Sage
MS-423
PRC
NASA Langley Research Center
Hampton, VA 23665-5225
Telephone: (804) 596-3511

Dr. Toru Sasaki
Meteorological Research Institute
1-1 Nagamine
Tsukuba, Ibaraki
JAPAN 305
Telephone: 011-81-298-51-7111

Dr. Hans Schneider
Atmospheric and Environmental Research, Inc.
840 Memorial Drive
Cambridge, MA 02139
Telephone: (617) 547-6207

Dr. Robert Seals, Jr.
MS-401 A
NASA/Langley Research Center
Hampton, VA 23665-5225
Telephone: (804) 864-2696
FTS: 928-2696

Dr. Susan Solomon
R/E/AL8
NOAA
325 Broadway
Boulder, CO 80303
Telephone: (303) 320-3483
FTS: 320-3483

Dr. Frode Stordal
University of Oslo
Institute of Geophysics
Box 1022
Blindern, Oslo 3
NORWAY
Telephone: 011-472-455821

Dr. Nien Dak Sze
Atmospheric & Environmental
Research, Inc.
840 Memorial Drive
Cambridge, MA 02139
Telephone: (617) 547-6207

Dr. K.K. Tung
Department of Applied Mathematics
FS 20
University of Washington
Seattle, WA 98195
Telephone: (206) 545-3794

Dr. Robert Watson
EEU/NASA Headquarters
Washington, D.C. 20546
Telephone: (202) 453-1681

Ms. Debra Weisenstein
Atmospheric and Environmental Research,
Inc.
840 Memorial Drive
Cambridge, MA 02139
Telephone: (617) 547-6207

Dr. Donald Wuebbles
L-262
Lawrence Livermore National Laboratory
P.O. Box 808
Livermore, CA 94550
Telephone: (415) 422-1845
FTS: 536-1845

Prof. Yuk L. Yung
MS 170-25
California Institute of Technology
Division of Geological & Planetary
Sciences
Pasadena, CA 91125
Telephone: (818)356-6940

Dr. Evgeny Zhadin
The State Committee of Meteorology
and Hydrology
Central Aerological Observatory
Pervomaijskya Street, 3
Moscow 142700
U.S.S.R.

Dr. Richard W. Zurek
MS - 169-237
Jet Propulsion Laboratory
California Institute of Technology
4800 Oak Grove Drive
Pasadena, CA 91109
Telephone: (818) 354-3725
FTS: 792-3725
Telemail: RWZUREK

# PREFACE

The Two-Dimensional Intercomparison of Stratospheric Models Workshop, sponsored by the NASA Upper Atmosphere Theory and Data Analysis Program, was held in Virginia Beach, Virginia on September 11-16, 1988. The purpose of the international workshop was to intercompare stratospheric models. Approximately 35 scientists representing seven nations from university and government laboratories were invited to participate in the workshop. This report presents the results of sixteen different modeling groups for several model experiments. Some analyses of the similarities and differences of the various models' results are also included in this report.

Special thanks are extended to Mariellen M. Pemberton of International Development Energy Associates (at NASA/GSFC) for technical assistance in preparing the report and to Linda A. Hunt and Karen H. Sage of PRC (at NASA/LRC) for technical assistance in creating all figures presented in Chapter 6. We would also like to thank two scientists pariticipating in the workshop who contributed extra efforts for the completion of this document: Anne R. Douglass for special editing assistance and Malcolm K. W. Ko for special efforts in writing Chapter 3.

Charles H. Jackman,
Robert K. Seals, Jr.,
and Michael J. Prather - Editors

# CHAPTER 2

# REPORT ON THE 2-D MODEL INTERCOMPARISON WORKSHOP HELD JANUARY 11-16, 1987 IN FORT MYERS BEACH, FL

Paul D. Guthrie

## Section 2.1 Introduction

In our attempts to understand the processes which affect ozone in the stratosphere, and to predict future ozone levels, atmospheric scientists have developed and employed a variety of computer models. To oversimplify somewhat, they range from 1-D models with intricately detailed photochemistry but only the crudest representation of transport, to 3-D general circulation models with intricately detailed dynamics and no photochemistry at all. Each of these has its appropriate uses. Many investigators have felt that there was much to be gained from intermediate models incorporating an extensive treatment of photochemistry within a dynamical framework which at least recognizes that atmospheric motions are advective as well as diffusive, and that both chemistry and dynamics are subject to latitudinal and seasonal variations. Thus the 2-D, zonally averaged models have begun to play a larger role in the last several years, both in attempting to understand observed distributions of trace species and in attempting to assess the probable effects of anthropogenic perturbations.

There are many choices to be made in developing a model, from the basic transport representation to the sources of the required input data; it would be most surprising if all investigators made the same ones. It was the purpose of the 2-D model Intercomparison Workshop to permit many investigators to discuss the choices made and the behavior of the resulting models. Our goal was not to identify a best set of choices, but rather to identify areas in which the models are sensitive to the choices made, and to develop a sense of where these models as a class do well or poorly in simulating the observed atmosphere. The discussion in this report will be quite general. However, as described in Section 2.8, a database of model output fields has been established at NASA/Langley Research Center. Readers interested in specific results are encouraged to obtain them from the database as outlined in Section 2.8.

## Section 2.2 Description of 2-D Models

The basic structure of the models presented at this workshop is that of a grid point model in which each cell represents an average of conditions around a latitude circle. Transport between cells is by both advection and eddy diffusion, the details of which vary among models. Chemistry is treated as a local process in which the reaction rates depend on the temperature and solar rates during a day-night cycle in different ways. The time evolution of the concentrations of different molecular species is then followed by integrating the species continuity equations. The method of integration and the temporal resolution vary among models.

Early formulations of 2-D models expressed atmospheric transport processes in terms of prescribed zonal mean circulations and Fickian eddy diffusion (Prabakhara, 1963). The advection and eddy diffusion were treated as independent processes whose local values (wind velocities and diffusion coefficients) could be determined by observation of atmospheric motions and tracer distributions. Following the development of Lagrangian mean theory (Andrews and McIntyre, 1978) it became clear that the transports due to zonal mean and eddy motions should nearly cancel, and that the classical Eulerian framework used in early models placed severe demands on the accuracy of the calculation of the small residual from the combined transport effects.

More recent 2-D model transport formulations have been developed to be consistent with Lagrangian mean theory by incorporating the near cancellation of the zonal mean and eddy contributions and relating the residual transport directly to external forcing (i.e. diabatic heating and zonal momentum forcing). Perhaps the most widely employed such formulation at this time is the Residual Mean Circulation (RMC) form (WMO, 1986). As will be discussed below, however, this exchanges one data problem for another, since neither heating nor momentum forcing is directly observable. Both must be derived from temperature measurements and are highly sensitive to errors therein.

Another area in which the models differ greatly is the time scale at which various physical processes are resolved. For example, it is not clear a priori that photolysis rates must be recalculated for each

time step in the temporal integration. Because the computation of photolysis rates is relatively time consuming, it is tempting to recompute them only "as often as necessary" - an interval which is in practice determined subjectively by each investigator for the specific simulation at hand. The effects of the choice of this interval on the results of long integrations are still not well understood and the intervals chosen by different investigators span a wide range. Different numerical approaches also lead to varying degrees of model variability and sensitivity to uncertainties in input data.

## Section 2.3 Sensitivity of 2-D Models

In previous intercomparisons of 1-D photochemical models the procedure adopted was to standardize the inputs to the participating models and compare the outputs, which in 1-D are simply altitude profiles (usually in steady state) of trace gas mixing ratios. This direct approach was unworkable for intercomparison of 2-D models; there are simply too many differences of formulation to permit a definitive standardized input dataset. Instead we chose to ask each investigator to simulate the photochemistry of the recent atmosphere (circa 1980), the time for which we have the most extensive observations available. Other "standard experiments" focused on particular processes in the model will be undertaken for future intercomparisons.

In order to compare and interpret complex model experiments one needs measures of model sensitivity to the various parameterizations and processes. Among models of common transport formulation (e.g. RMC models) one can directly compare the wind fields and eddy diffusion coefficients fields with some confidence in interpreting their influence on constituent distributions. This is not the case when comparing RMC models to Classical Eulerian (CE) models; then one can only compare net transport fluxes and tracer distributions in assessing the model's transport properties. In comparing such distributions the transport effects are involved with chemistry effects in a way which depends on the local photochemical lifetime of the tracer. This lifetime, in turn, varies with location in the model grid and with season during the simulation. One must therefore be cautious in interpreting such intercomparisons.

Much of the discussion of transport treatments at the Workshop focused on the process of obtaining a residual mean circulation (although results obtained using a Classical Eulerian transport model were also shown and will be discussed below). In the past, and for many of the results presented here, models used temperatures from one source, heating rates from one or more other unrelated sources, and eddy mixing coefficients which were uniform in latitude and time. A conclusion of the Workshop was that this is not a justifiable approach. Within the RMC formulation, temperature, wind fields and eddy mixing are not independent, but should instead be treated in a coupled, self-consistent way, although there are probably several equally viable treatments. Plumb and Mahlman (1987) have shown that the RMC provides a reasonable approximation to the transport circulation in the stratosphere. Edmon et al. (1980) have shown that the RMC can be solved for in terms of the eddy forcing and diabatic heating. The eddy forcing can be written in terms of a potential vorticity flux, and this flux can be specified in terms of a horizontal diffusion coefficient ($K_{yy}$). Hence, the RMC, horizontal diffusion, and diabatic heating are mutually dependent. The closure problem arises from the need to specify at least two of these terms in order to derive the third. Usually the diabatic heating is calculated in the model, so either specification or parameterization of eddy diffusion determines the RMC. However, without additional information (from a 3-D model, a treatment of wave propagation through the mean flow, or some other source), it is not possible to compute a full self-consistent response of the transport properties and temperature distribution of the atmosphere to chemical perturbations within the 2-D formulation.

The present level of "coupling" of the advective and diffusive transport of 2-D models is to derive the self-consistent fields for the current atmosphere based on observations. (There are also 2-D models based on zonal averaging of GCM transport fields, but no results from such models were presented at the Workshop). The two approaches discussed at the Workshop were: i) to compute the RMC winds for observed temperature and constituent fields and use potential vorticity (derived from the associated

eddy motions) as a tracer in order to deduce the horizontal eddy coefficients (Newman et al. 1986) and ii) to specify the annual cycle of the zonal mean temperature and compute from this the heating and the associated RMC, and then compute the zonal momentum forcing required to balance the zonal momentum equation (Tung and Yang, 1988). Both approaches depend on temperature observations. It was the general consensus of the workshop participants that available temperature data have neither the accuracy (~1°K) nor the vertical resolution (~ 5 km or better) required using either approach.

The most general illustration of this problem was the notable lack of improvement in simulations of trace species distributions in a model based on contemporary temperature data as compared to the distributions in models based on older data. Several models based on distributions of net heating from Murgatroyd and Singleton (1961) [rescaled in various ways to merge with other datasets] were able to simulate long-lived trace species distributions fairly well, while the circulation derived by Rosenfield et. al. (1987) from NMC temperature data, using a modern heating code, was clearly too strong. Moreover, including the "self-consistent" eddy coefficients derived by Newman et. al. (1986) from the same data did not alleviate the problem.

## Section 2.4 Conclusions from an Intercomparison of the Species Distributions

### Section 2.4.1 Source gases

As noted above the circulation of Rosenfield et. al. (1987) [hereafter the NMC circulation] appears to be too strong, at least during some seasons. Specifically it transports air upward too rapidly in the tropics and downward too rapidly at high latitudes. This results in mixing ratios for $N_2O$ and $CH_4$ which are larger than those obtained from SAMS by as much as a factor of two at some seasons in the tropical stratosphere above 10 mbar (fig. 2-1). The slopes of the isopleths are also too steep, although this effect can be reduced by using the spatially variable self-consistent eddy coefficients. The frequently observed double-peaked distribution in these species could be simulated in one CE model (Gray and Pyle, 1987) by specifically imposing a semi-annually varying flux, and thus others were unable to reproduce this feature in long term simulations, although Solomon et al. (1986) had some success using circulations based on the specific temperatures as measured by LIMS during SAMS observations.

### Section 2.4.2 Odd Nitrogen

RMC models appear to require a source of odd nitrogen in the upper troposphere, perhaps attributable to lightning (Ko et al. 1986; Jackman et al. 1987). The alternative is to use much larger eddy-diffusion coefficients in the lower stratosphere (15-25 km) than those currently believed reasonable, [i.e. $K_{yy} > 10^{10}$ vs. an average value of ~3 x $10^9$]. This would reduce the latitude contrast in column $O_3$ and $HNO_3$ however. The odd nitrogen shortfall did not appear in the CE model of Gray and Pyle, in which the ratio of diffusion to advection in the lower stratosphere is substantially larger.

There is a general problem in all models with the seasonal behavior of $HNO_3$. In the models the mixing ratio maximum in the summer hemisphere is larger than that in the winter hemisphere, while in the LIMS measurements the opposite is observed (fig. 2-2). It has been suggested (Austin et al. 1986; Jackman et al. 1987) that this implies missing chemistry in the models. The effect of the missing chemistry would be to convert $N_2O_5$ into $HNO_3$ during the polar night, perhaps on the surface of aerosols or in cloud droplets.

### Section 2.4.3 Active Chlorine

All models show a latitude dependence of the partitioning of chlorine among HCl, ClO, $ClONO_2$ and HOCl. This is especially notable in the 35-45 km range, where active chlorine has its maximum impact as a catalyst for ozone and HCl is at minima. This maxima for $Cl_x$ loss of ozone occurs at

high latitudes in both hemispheres (see fig 2-3). As noted by Solomon et al. (1985) this latitudinal variation depends primarily on the methane distribution. The methane isopleth slopes, in turn, depend on the ratio of advection to diffusion in the model.

The major differences among model $Cl_x$ distributions occurred in polar night, and were caused by different schemes for treating polar night chemistry. These different schemes include computation of production and loss for night conditions, imposed nighttime photochemical equilibrium, and "freezing" the chemistry in polar night (i.e. no computation of changes in species concentrations). These differences probably also affect $NO_x$ in polar night. While the several schemes appear to give similar long-term behavior (e.g. annual cycles at mid-latitudes) they produce substantially different latitudinal gradients at the polar terminator. Such gradients in model distributions must be treated with caution.

### Section 2.4.4 Ozone

Peak ozone mixing ratios were similar in all models and consistent with available satellite data (i.e. 9-11 ppm at the maximum). The overall morphology, however, differed according to the transport used. The NMC circulation produced too much downward and poleward slope of the isopleths in the middle and lower stratosphere, as compared to observations.

There is still a general problem with modelled ozone mixing ratios above about 45 km altitude. The model values are consistently too low. This is a longstanding problem with both 1-D and 2-D models, and may derive from shortcomings in photolysis calculations, incorrect chemical kinetic data, incorrect temperatures or something not yet thought of. Jackman noted that, as a consequence, computed photolysis rates can be substantially different (up to 40% in some cases) from those obtained when observed ozone distributions are imposed.

## Section 2.5 Perturbation Assessments

Two groups (Oslo and AER) compared ozone depletion assessment calculations, in order to focus on depletion to date (i.e. trend detection in the current atmosphere). While the calculations agree that the earliest and greatest effect would be at high latitudes and at 40-45 km altitude, the estimates presented for maximum local ozone depletion to date differed by a factor of two. The differences do not appear in the computed column depletions. The major differences between the two calculations were the treatment of temperature changes due to increasing $CO_2$, and the distributions of $CH_4$ in the models. The latter appeared to be the major effect, influencing both the latitude dependence of ozone depletion in the upper stratosphere, and the projected increase in ozone in the tropical lower stratosphere. The $CH_4$ distributions, in turn, are sensitive to the transport characteristics of the models. The importance of temperature feedback was more difficult to assess, given the doubts previously expressed about the accuracy of available temperature data in the upper stratosphere. In any case the treatment of temperature feedback was purely photochemical; the importance of dynamical feedback remains unknown.

## Section 2.6 Coupled Models

In the context of this Workshop, coupled models are those which attempt to compute temperature, circulation and/or diffusion coefficients, radiative heating and photochemistry, all in an internally self-consistent manner. As noted above, this always requires some additional assumption about temperature or the momentum forcing in order to close the system of equations.

Tung presented preliminary calculations of the sensitivity of the ozone column to perturbations of the lower stratospheric net heating distribution. These suggested as much as a 4% change in column ozone for a 1% change in heating. Because this region is close to radiative equilibrium with large and nearly cancelling heating and cooling terms, the uncertainty in a model heating calculation is likely to be much larger than 1%. This suggests that a detailed comparison of the radiation codes used in models should be undertaken.

Hitchman showed results for a model in which the meridional diffusitivity and meridional circulation driven by Rossby waves were parameterized by including an equation for Rossby wave activity. The distribution of Rossby wave activity is determined by model zonal winds. The parameterized transport evolves with the zonal winds. This allows for studying feedbacks among temperature, wave driving and tracer distributions.

## Section 2.7 Summary

The assessment results are in qualitative agreement with each other (and with previous results) that there is a strong seasonal and latitudinal dependence in the $O_3$ response. Additional 2-D results will help us in interpretation of data and 1-D model results.

One conclusion of the workshop was that, within the RMC formulation, temperature, wind fields and eddy mixing are not independent, but should instead be treated in a coupled, self-consistent way. Despite the current efforts, a fully self-consistent treatment of the response of the transport properties and temperature distributions of the atmosphere to chemical perturbations within the 2-D formulation is not yet available. It is likely that one would have to depend on additional information from a 3-D model for treatment of wave propagation through mean flow and parameterization of the eddy forcing in order to formulate the approach.

We know that the models used to date have neglected processes (changes in temperature and circulation due to changes in ozone) which may well affect model predictions. Until we have gained more experience with depletion estimates in coupled models, we cannot reach reliable quantitative conclusions as to impact of the neglected feedback processes on the predicted depletion.

## Section 2.8 Upper Atmosphere Pilot Database

As a general facility for comparison of model species distributions to each other and to observed distributions (or intercomparison of observations) a remotely accessible database has been established at NASA's Langley Research Center. The participants in the Workshop have "deposited" their model outputs into this database where they are available for continuing intercomparison. Eventually, as additional model studies are published in the literature, the associated model species distributions will be made available in a publicly accessible section of the database. For the moment the publicly accessible portion contains only observational information. Non-Workshop-Participants who are interested in using the portion of the database containing model output are encouraged to contact the participating investigators.

This database is intended to be a community resource, and readers are encouraged to use it and suggest changes and improvements. For information, contact Dr. Robert Seals, Jr., MS401A, NASA/Langley Research Center, Hampton, VA 23665, (804) 864-2696. The data currently available is shown in Table 2-1.

**Table 2-1.**

Assorted balloon profiles
$N_2O$, $H_2O$, CO, $O_3$, $NO_2$, $HNO_3$, NO, COS, HF, HCl, $CH_4$

LIMS — November 78 - May 79
$H_2O$, $HNO_3$, $NO_2$, $O_3$

SAMS — January 79 - December 79
$CH_4$, $N_2O$

SBUV — October 78 - September 84
$O_3$

---

Workshop Models:

AER (Jan. 85; Apr. 85)
CNRM (Mar. 80; Dec. 80)
Dupont (Jan. 80; Apr. 80)
GSFC (Apr. 80; Jan. 81)
NOAA/NCAR (Mar. 84; Dec. 84)
CAMBRAL (Dec. 79; Apr. 80)

## Section 2.9 References


Andrews, D. G., and M. E. McIntyre, An exact theory of nonlinear waves on a Lagrangian mean flow, J. Fluid Mech., 89 , 609-646, 1978.

Austin, J., R. R. Garcia, J. M. Russell III, S. Solomon and A. F. Tuck, On the atmospheric photochemistry of nitric acid, J. Geophys. Res., 91, 5477-5485, 1986.

Edmon, H. J., Jr., B. J. Haskins and M. E. McIntyre, Eliasson - Palm cross sections for the troposphere, J. Atmos. Sci., 37, 2600-2616, 1980.

Gray, L. J., and J. A. Pyle, The semi-annual oscillation and equational tracer distributions, Q. J. R. Met. Soc., 112 , 387-407, 1986.

Jackman, C. H., P. D. Guthrie and J. A. Kaye, An intercomparison of nitrogen-containing species in Nimbus 7 LIMS and SAMS data, J. Geophys. Res., 92, 995-1008, 1987.

Ko, M. K. W., M. B. McElroy, D. K. Weisenstein and N. D. Sze, Lightning: A possible source of stratospheric odd nitrogen, J. Geophys. Res., 91, 5395-5404, 1986.

Murgatroyd, R. J. and F. Singleton, Possible meridional circulation in the stratosphere and mesosphere, Q. J. R. Met. Soc., 87, 125-235, 1961.

Newman, P. A., M. R. Schoeberl and R. A. Plumb, Horizontal mixing for two-dimensional chemical models calculated from National Meteorological Center Data, J. Geophys. Res., 91, 7919-7924, 1986.

Plumb, R. A. and J. D. Mahlman, The zonally-averaged transport characteristics of the GFDL general circulation/transport model ,J. Atmos. Sci., 44 , 298, 1987.

Prabhakara, C., Effects of non-photochemical processes on the meridional distribution and total amount of ozone in the atmosphere, Mon. Weather Rev., 91, 411-413, 1963.

Rosenfield, J. E., M. R. Schoeberl, and M. A. Geller, A computation of the stratospheric diabatic residual circulation using an accurate radiative transfer model, J. Atmos. Sci., 44, 859-876, 1987.

Solomon, S., R. R. Garcia and F. Stordal, Transport processes and ozone perturbations, J. Atmos. Sci., 90, 12,981-12,989, 1985.

Solomon, S., J. T. Kiehl, R. R. Garcia and W. Grose, Tracer transport by the diabatic circulation deduced from satellite observations, J. Atmos. Sci., 43, 1603-1617, 1986.

Tung, K.K., and H. Yang, Dynamical component of seasonal and year-to-year changes in Antartic and global ozone, J. Geophys. Res., 93, 12,537-12,559, 1988.

WMO, Atmospheric Ozone 1985, Rept. No. 16, Global Ozone Research and Monitoring Project, Geneva, 1986.

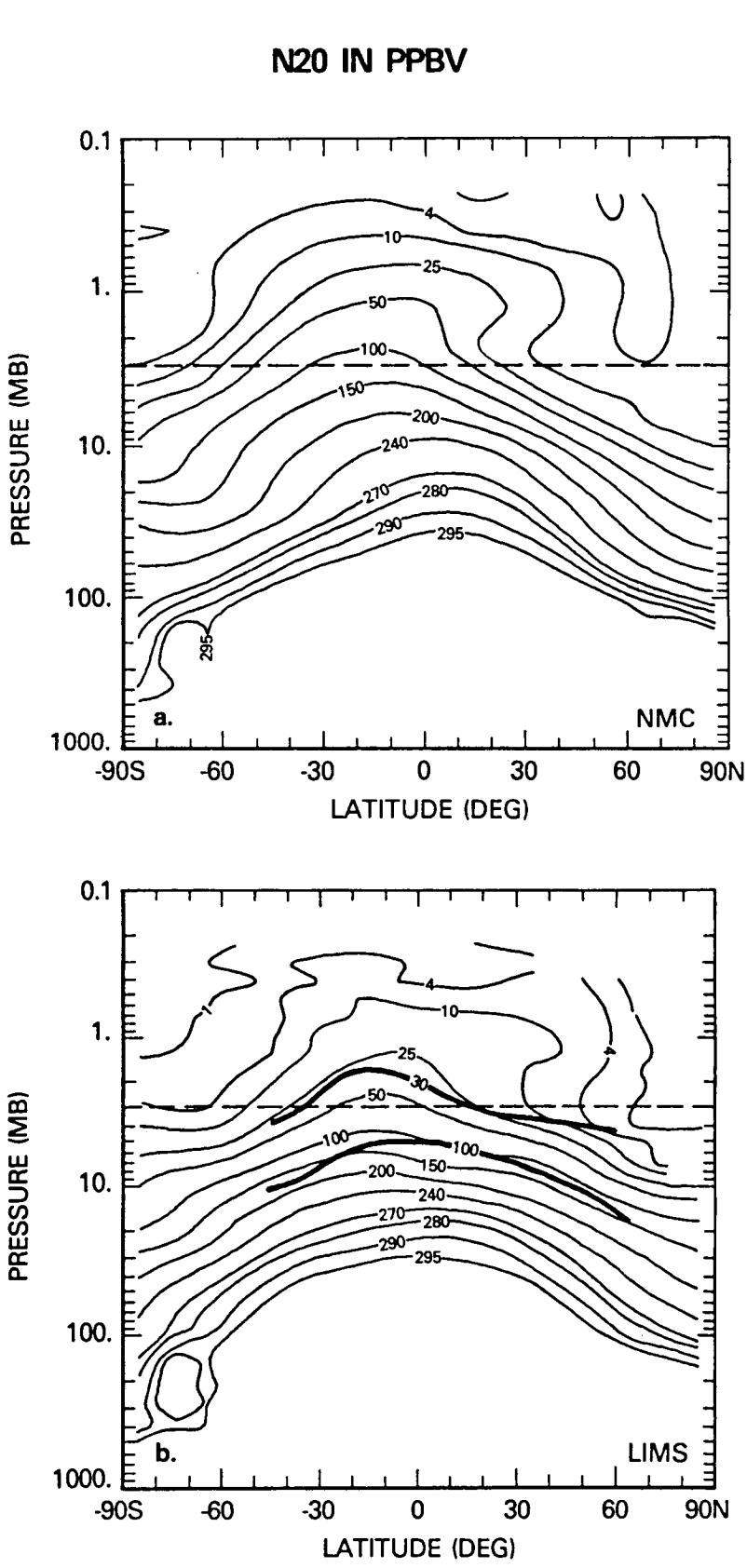


Figure 2-1. $N_2O$ distributions for January derived from the GSFC model using NMC-derived and LIMS-derived circulations. Heavy contours are SAMS observations. Dashed line highlights the 3 mbar level for comparison.

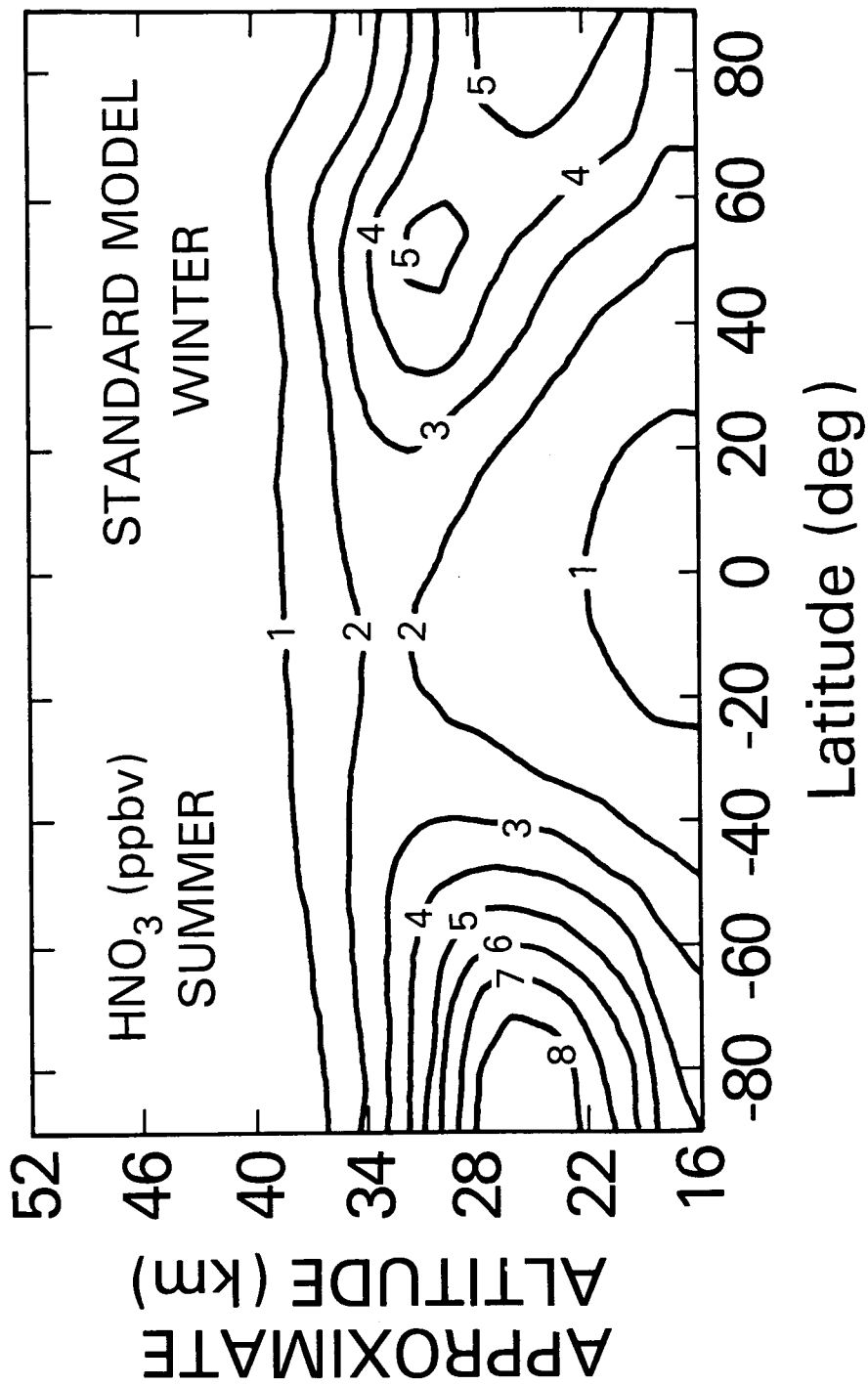


Figure 2-2. a) Calculated $HNO_3$ distribution at the end of December from the Garcia - Solomon model.

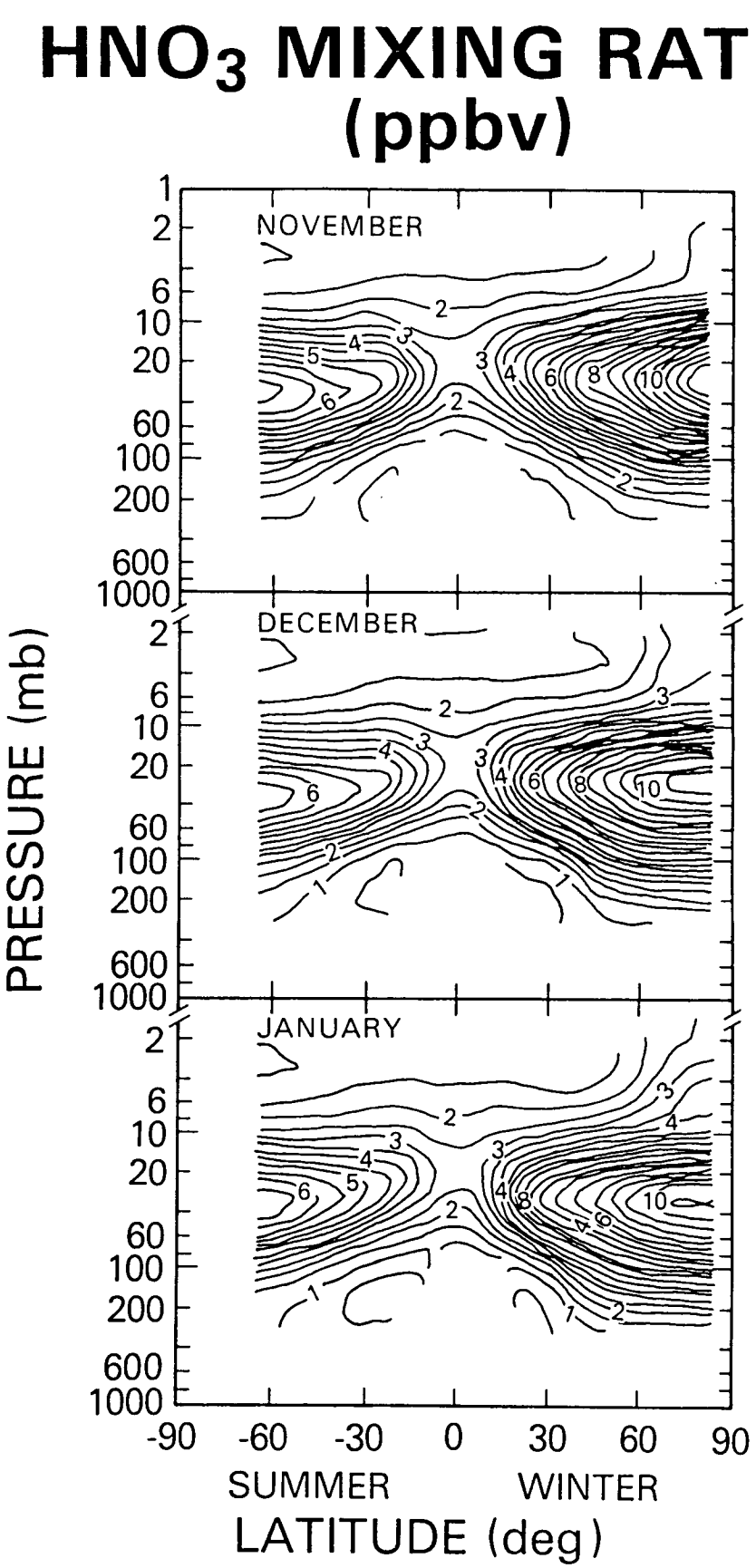


Figure 2-2. b) Monthly and zonally averaged $HNO_3$ distributions observed by LIMS.

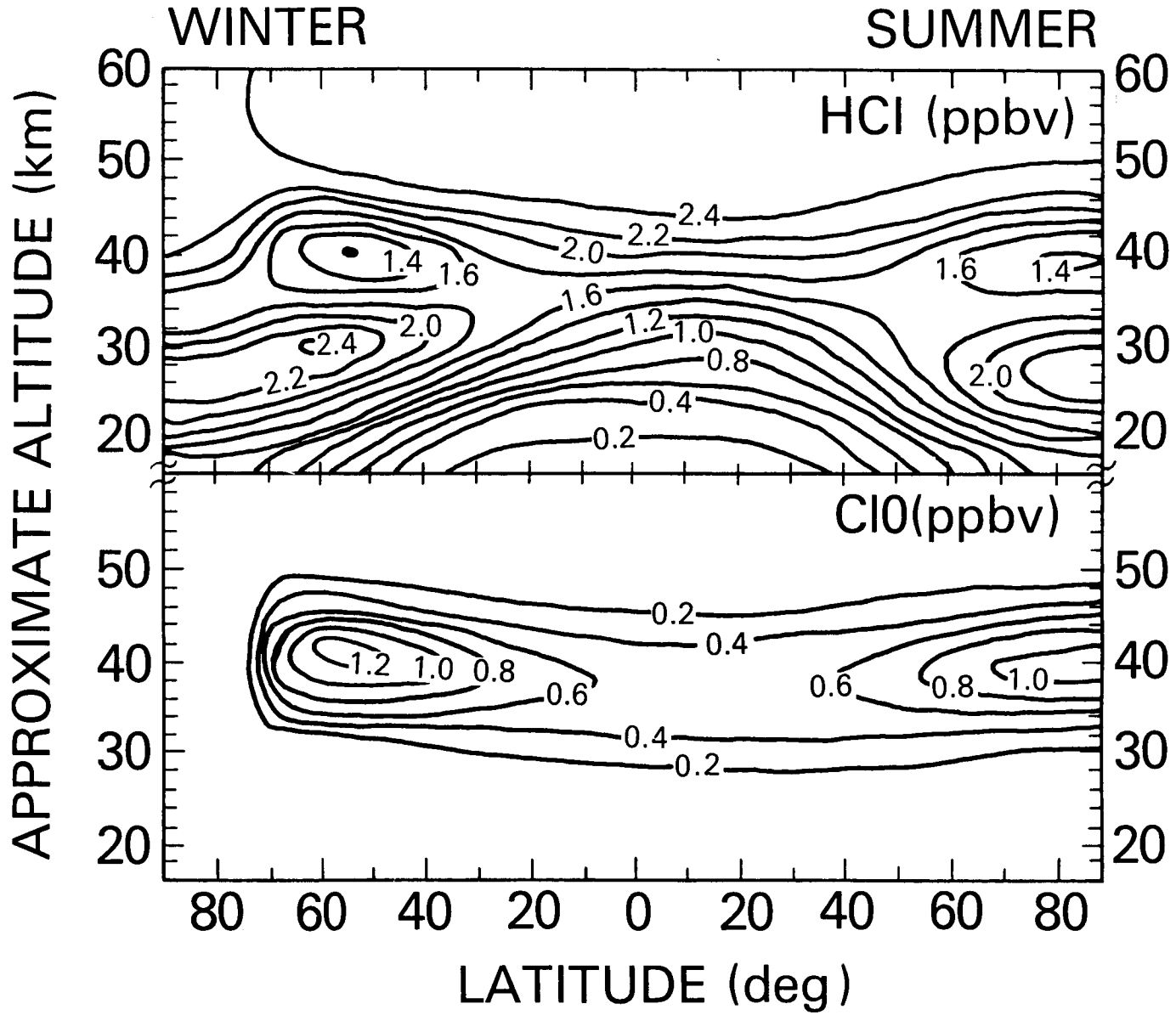


Figure 2-3. Contour plots of HCl and ClO near solstice (noon values derived from the Garcia-Solomon model).

# CHAPTER 3

# REPORT OF THE 1988

# 2-D INTERCOMPARISON WORKSHOP

## Section 3.1 Introduction

This report documents the findings of the participants of the September 11-16, 1988 2-D Intercomparison Workshop held in Virginia Beach, VA. The descriptions of the results of the various models for the several model experiments were done at this meeting. Several groups of investigators have updated their contributions to the model database since the meeting, therefore, the conclusions of this report should be taken as preliminary.

Table 3-1 shows the various modeling groups and their respective acronym or legend which is used to refer to modeling results of that group in the rest of this conference proceedings.

**Table 3-1.** Modeling groups involved and legends for figures.

| Legend | Modeling Group |
|---|---|
| AER - | Atmospheric and Environmental Research, Inc., Cambridge, MA (M.K.W. Ko, N.D. Sze, and D.K. Weisenstein) 2-D Chemistry Transport Model |
| AERI- | Atmospheric and Environmental Research, Inc., Cambridge, MA (M.K.W. Ko, H.R. Schneider, N.D. Sze, W.C. Wang, and D.K. Weisenstein) 2-D Interactive Model |
| CALJPL - | California Institute of Technology and Jet Propulsion Laboratory, Pasadena, CA (Y.L.Yung, D. Crisp, R.W. Zurek) 2-D Model |
| CAMBRAL- | Cambridge University and Rutherford Appleton Laboratory, Great Britain (J.A. Pyle, L.J. Gray, and R.S. Eckman) 2-D Model |
| CAO - | Central Aerological Observatory, U.S.S.R. (V. Philushakin, E. Zhadin) 2-D Model |
| CLKSON - | Clarkson University, Postdam, N.Y. (K.K. Tung, H. Yang, and E. Olaguer) 2-D Model |
| DUPONT - | E. I. Du Pont De Nemour & Company, Inc., Wilmington, DE (D. Fisher) 2-D Model |
| GISS - | Goddard Institute for Space Studies, New York, N.Y. (M.J. Prather, M.M. Garcia, and D. Rind) 1-D and 3-D Model |
| GSFC1 - | Goddard Space Flight Center, MD (P.D. Guthrie, C.H. Jackman, and T.L. Kucsera) 2-D Model |
| GSFC2 - | Goddard Space Flight Center, MD (C.H. Jackman, A.R. Douglass, R.S. Stolarski, and P.D. Guthrie) 2-D Model |
| LARC - | Langley Research Center, Hampton, VA (W.L. Grose, R.S. Eckman, R.E. Turner, and W.T. Blackshear) 3-D Model |
| LLNL - | Lawrence Livermore National Laboratory, Livermore, CA (D.J. Wuebbles, P.S. Connell, K.E. Grant, and R. Tarp) 2-D Model |

**Table 3-1 (continued)**

MPIC - Max Planck Institute for Chemistry, Mainz, Federal Republic of Germany (P. Crutzen and C. Bruehl) 2-D Model

MRI - Meteorological Research Institute, Japan (T. Sasaki and Y. Makino) 2-D Model

NOCAR - National Oceanic and Atmospheric Administration and the National Center for Atmospheric Research, Boulder, CO (S. Solomon, and R. Garcia) 2-D Model

OSLO - University of Oslo, Oslo, Norway (I. Isaksen and F. Stordal) 2-D Model

WISCAR - University of Wisconsin, Eau Claire, WI and National Center for Atmospheric Research, Boulder, CO (G. Brasseur, M. H. Hitchman, and A. DeRudder) 2-D Model

## Section 3.2 Photochemistry and Radiation

Charles Jackman

Since radiation drives the chemistry and dynamics of the atmosphere, it is important to understand the differences that arise in the various workshop models among the radiation fundamental quantities. The photodissociation coefficients are used in the computation of the dissociation of important molecules of the atmosphere. This dissociation leads to production of odd oxygen (mainly ozone in the stratosphere) and to radical production, which in turn lead to a whole host of photochemistry; some of which results in ozone destruction. The radiative heating and cooling of the atmosphere results in wind patterns with upward winds associated with atmospheric heating and downward winds associated with atmospheric cooling. A good simulation of the radiation and its multitude of effects in the atmosphere is necessary in order to model atmospheric problems correctly.

### Section 3.2.1 Photodissociation Coefficients

Guy Brasseur

An important quantity in the source terms of chemical compounds is the photodissociation frequency of atmospheric molecules J. The value

$$J(z,\chi) = \int_{\lambda} \sigma(\lambda)\ q(\lambda,z,\chi)\ d\lambda,$$

where $\sigma$ is the cross section of the molecule under consideration and $q(\lambda,z,\chi)$ the solar irradiance at altitude z for a solar zenith angle $\chi$. The determination of the irradiance field depends on the absorption of solar light by ozone and molecular oxygen, multiple scattering and albedo. Furthermore, most 2-D models use diurnal averages of the J-values, which have to be defined properly. The spectral integration is usually performed over defined spectral intervals (typically 500 $cm^{-1}$ width) except in the region of the Schumann-Runge bands where parameterizations of the averaged atmospheric transmissions over given wavelength intervals are usually determined following different methods (Nicolet and Peetermans, 1980; Allen and Frederick, 1982).

The comparison of the coefficients provided by the different groups shows several substantial differences. In the case of the $O_2$ photodissociation coefficient, variations of the order of a factor 2 are found among the different models in the upper stratosphere. Factor of 5 differences are seen for $J_{NO}$. This is an indication that the penetration of solar radiation in the Schumann-Runge region is treated differently in the various models. Substantial differences are also found for the photodissociation coefficients of F-11 and F-12. A possible reason for these discrepancies is the temperature dependence of the CFC-cross sections which is not taken into account in all models. A comparison of results dealing with species which are sensitive to wavelengths subject to scattering ($NO_2$, $HNO_3$, $ClONO_2$) suggests substantial differences due to the approximate treatment of multiple scattering. These are noticeable in the lower stratosphere and in the troposphere but also at higher altitude. In the case of $ClONO_2$, for example, differences of a factor 2 are observed at 40 km altitude. The photodissociation coefficient of $NO_2$ does not vary substantially with altitude but is highly dependent on the value adopted for surface albedo and on the treatment of multiple scattering. Differences between the calculated J's are of the order of 50% or less. In the case of $N_2O$, the differences between calculated J's reach a factor of 2 at 30 km.

Finally, in the case of ozone, there is a 30-50 percent discrepancy among models at 40 km altitude but the differences are larger in the lower stratosphere, where multiple scattering plays an important role.

Clearly, the differences among models are too large and need to be reduced by a more detailed comparison of the input (cross-section, solar irradiance), the calculation techniques and the results. The modelers involved in the Virginia Beach meeting will run a few simple and specific cases and compare these results in the near future.

## Section 3.2.2 Comparison of UV Heating and IR Cooling in Two-Dimensional Models

Susan Solomon

### UV Heating

Stratospheric heating is provided almost entirely by absorption of incoming solar radiation by ozone. At low altitudes, this is dominated by the Chappuis bands in the visible part of the spectrum, while at high altitudes (z>30 km) absorption in the ultraviolet through the Hartley bands becomes important. Further, weak absorption by $NO_2$ and other trace species makes a small (order 2 to 10%) contribution to the total heating in the lower stratosphere.

Table 3-2 displays calculated heating rates at particular points from some of the models for fixed $O_3$ and temperature on 1 January. The models are all in excellent agreement at 50°S, 20 km, where the estimated heating rate is 0.6 K/day. This suggests that the treatment of the Chappuis bands is comparable in all the models. However, the heating rates near the stratopause differ by as much as 35%, suggesting that there are large differences in the treatment of UV radiation or diurnal averaging. The difference in high altitude heating rates are strongly latitude dependent, suggesting that diurnal averaging plays an important role.

### IR Cooling

There are also substantial differences among models in terms of their calculated IR cooling. All of the models considered here include both $CO_2$ 15μm and $O_3$ 9.6μm cooling (see Table 3-3). Near the tropical tropopause, $O_3$ may contribute net heating through infrared emission (e.g. positive rather than negative tendency) depending on the vertical temperature structure in the troposphere and other parameters. Some models also include minor contributions from IR emission of $CH_4$, $CF_2Cl_2$, etc.

The minimum cooling rates calculated near the summer stratopause vary by more than 40%. It is somewhat surprising that such large variations are obtained here, since the cooling rate does not require diurnal averaging and since infrared cooling codes have already been extensively intercompared by climate studies and other assessments. Further work will be required to understand the origin of these differences.

It is also important to note that large differences in magnitude and even in sign are found for the net cooling near the tropical tropopause. The nature of the sign in this region is heavily dependent on 9.6μm $O_3$ cooling, suggesting substantial differences in the treatments used.

Only a few groups reported cooling rates for doubled $CO_2$ using the standardized atmosphere. From the point of view of assessment studies, the cooling in the extra-tropical lower stratosphere is of great importance, as it plays a major role in determining the total $O_3$ response to doubled $CO_2$. Although only a few models reported results for that particular study, those that did were in reasonable agreement.

**Table 3-2.** Heating Rates from Two-Dimensional Models (°K/d)

| Model Parameter | CLKSON | NOCAR | MPIC | AERI | CAMBRAL | OSLO | LLNL | CALJPL | WISCAR |
|---|---|---|---|---|---|---|---|---|---|
| Maximum heating near summer stratosphere | 20 | 20 | 20 | 21 | 15 | 17 | 14 | 16 | 12 |
| Equatorial maximum heating | 10 | 10 | 10 | 11 | 11 | 9 | 8.5 | 10 | 9.5 |
| Equator, 30 km | 2 | 2.5 | 2.4 | 3 | 3.5 | 2.5 | 2 | | 3 |
| 50°S, 20 km | 0.6 | 0.6 | 0.6 | 0.6 | 0.6 | | 0.6 | | 0.65 |

**Table 3-3.** IR Cooling Rates from Two-Dimensional Models (°K/d)

| Model Parameter | CLKSON | NOCAR | MPIC | AERI | CAMBRAL | OSLO | LLNL | CALJPL | WISCAR | GISS |
|---|---|---|---|---|---|---|---|---|---|---|
| Maximum cooling near summer stratosphere | -13 | -16 | -14 | -11 | -12 | -11 | -12 | -16 | -13 | -16 |
| As above, doubled $CO_2$ | | | -18 | -15 | -15 | | -15 | | | -19 |
| Tropical tropopause region, maximum value | +0.2 | +0.1 | +0.2 | -0.4 | +0.1 | +0.23 | +0.3 | +0.2 | +0.16 | +0.1 |
| Doubled $CO_2$, 50 mb, 60°S | | | -1.0 | -1.2 | -1.25 | | -1.2 | | | |
| Doubled $CO_2$, 50 mb, 60°N | | | -0.6 | -0.8 | -0.6 | | -0.5 | | | |

## Section 3.3 Transport

Paul Guthrie

The representation of transport of constituents by atmospheric motions plays a major role in determining the spatial and temporal distribution of ozone (and other species) in 2-D model simulations of the atmosphere. Transport affects ozone directly, by moving it among regions where its photochemical lifetime differs greatly, and indirectly, by determining the distributions of the precursors to the radicals which catalyze ozone destruction. As part of the Intercomparison we have sought to focus on the processes which drive the simulated air motions in our models, and on the direct effect of the resulting transport on specified artificial "tracer" distributions.

This section describes the results of four intercomparisons. The first is an examination of the net radiative heating produced by different models for specified distributions of ozone and temperature. This is directly relevant to the advective transport which dominates the models using a Residual Mean Circulation formulation; it is less relevant for models based on a Classical Eulerian formulation. Differences among models noted here arise from differences in methods of approximating the transfer of solar and terrestrial radiation through the atmosphere. The remaining three intercomparisons employ surrogates for different classes of atmospheric species. Tracer X has a tropospheric source and stratospheric sink, representing precursor species such as $N_2O$. Tracer Y is a conserved species and examines the evolution in time of the distribution of a purely inert substance subject only to model transport. Tracer Z has a stratospheric source and tropospheric sink representing an "ozone-like" species. By comparing the model simulations for these three tracer experiments we hope to gain insight into the sensitivity of simulated species distributions to the model treatments of transport without confusion due to different model treatments of chemistry. A comparison of tracer Z with the ozone simulation in each model is quite instructive in illustrating the effects of interactions of transport and chemistry on the ozone column density.

### Section 3.3.1 Residual Circulation Inferred from Heating Rates

Rolando Garcia

Transport in two-dimensional models is due to advection by the mean meridional circulation and mixing, usually parameterized as eddy diffusion. By examining the net diabatic heating rates, it is possible to obtain an estimate of the upward component of the residual circulation $\bar{w}^*$ The thermodynamic equation in the residual mean formulation for isobaric coordinates.

$$\frac{\partial \bar{T}}{\partial t} + \bar{v}\cdot\frac{\partial \bar{T}}{\partial y} + \bar{w}\cdot\frac{HN^2}{R} = \bar{Q}_{net} \qquad (1)$$

can be approximated as a balance between net diabatic heating and adiabatic effect due to vertical motions, i.e.

$$\bar{w}\cdot\frac{HN^2}{R} = \bar{Q}_{net} \qquad (2)$$

This approximation is most easily justified near solstice (when $\partial \bar{T} / \partial t \approx 0$ and in the middle and lower stratosphere (where horizontal nonlinear advection $\bar{v}^* \bar{T}_y$ can be neglected). In isentropic coordinates the analog of eq. (2) is the full thermodynamic equation, so mean vertical motions can always be deduced from net heating rates, provided the latter is available on isentropic surfaces.

In what follows $\bar{Q}_{net}$ is used as a diagnostic of the vertical component of the residual circulation for the various 2-D models included in this intercomparison. Different 2-D models can be classified according to whether $\bar{Q}_{net}$ is specified externally or computed interactively. Implicit in externally specified $\bar{Q}_{net}$ distributions is the effect of wave processes which drive the atmosphere away from radiative equilibrium. If $\bar{Q}_{net}$ is computed interactively, its value depends ultimately on the specification or parameterization of wave driving.

Table 3-4 lists the various models included in this intercomparison, together with the method used to obtain $\bar{Q}_{net}$. Models with specified $\bar{Q}_{net}$ are somewhat more common at present than models wherein $\bar{Q}_{net}$ is computed interactively. The CLKSON model is a special case in that the net heating rate is obtained from computed UV heating and IR cooling based on a specified temperature distribution. Table 3-4 also notes whether any attempt is made to parameterize wave driving and eddy diffusion in a self-consistent fashion. For example, the CLKSON model wave driving is estimated from the zonal momentum equation,

$$\overline{v'q'} = - f \bar{v}^* \qquad (3)$$

and $\overline{v'q'}$ is then parameterized as diffusion of mean potential vorticity,

$$K_{yy} = \frac{\overline{v'q'}}{q_y} \qquad (4)$$

It should also be noted that in models wherein the circulation is specified at the lower boundary (e.g., NOCAR), an integrated EP flux divergence in the interior is implied. Briefly, from the steady-state balance

$$- f \bar{v} = \frac{1}{\rho} \nabla \cdot F \qquad (5)$$

we can derive the relationship

$$\bar{\chi}^*(z_o) = \frac{1}{f\rho(z_o)} \int_{z_o}^{\infty} \nabla \cdot F \; dz \qquad (6)$$

which says that the stream function at $z_0$ depends on the EP flux divergence throughout the interior of the model above $z_0$.

Regardless of whether $\bar{Q}_{net}$ is specified or computed, it is desirable that eddy diffusivities used in 2-D models should be consistent with the wave driving. It is not totally clear at present what is the best method for obtaining such consistency. The CLKSON model (which considers all wave driving to be due to non-linear effects, and hence to imply mixing), is an example of an approach to this self-consistency criterion. The validity of this approach in regions where thermal dissipation might be

not conserved) remains to be investigated.

The role of mixing cannot be assessed from an examination of $\bar{Q}_{net}$. The following comparison focuses on overall patterns of $\bar{Q}_{net}$ and on its magnitude in certain key regions as a means of comparing advective transport in various 2-D models. Figures on pages 205-211 show $\bar{Q}_{net}$ for January for all models listed in Table 3-4. Qualitatively, the overall patterns in most models are strongly similar, with upwelling in the summer upper stratosphere and downwelling throughout the winter stratosphere. In the lower stratosphere, there is upwelling in the tropics and downwelling in both summer and winter hemispheres.

More detailed examination of figures on pages 205-211 reveals significant differences among the various models. These are especially noticeable in the summer upper stratosphere, where most models show strong upwelling, but some of the models have much weaker upwelling, or even downwelling. Table 3-5 shows summer, high latitude vertical velocities near the summer stratopause (70°S, 1 mb) to further quantify this point. Upwelling in this region of the atmosphere is important because it determines the temperature of the summer stratopause and hence the ozone concentration there.

Table 3-5 also compares vertical velocities at the tropical tropopause (0°, 100 mb) and the high latitude, winter lower stratosphere (70°N, 50 mb). These locations are chosen for the presumed importance of vertical advection there (flux of source gases from the troposphere and advective control of the total ozone column at high latitudes). The vertical velocities implied by $\bar{Q}_{net}$ at these locations are generally in good agreement among models, especially in winter high latitudes.

The results presented here are only a rough indication of transport differences among models. It should be emphasized once again that eddy transport is not taken into account by this comparison, and that there are significant differences in the definition or parameterization of eddy diffusion in the various models. Nevertheless, vertical motions should have important effects in the distribution of constituents (and ozone in particular) and the present comparison indicates that differences in vertical advection among models could be significant, especially near the summer stratopause.

**Table 3-4.** Description of $\bar{Q}_{net}$ in each Model

| Model | Formulation |
|---|---|
| AER | $\bar{Q}_{net}$ specified |
| AERI | $\bar{Q}_{net}$ computed. Wave driving from parameterized Raleigh friction and diffusion of potential vorticity. |
| CALJPL | $\bar{Q}_{net}$ specified from GFDL 3-D model. Eddy diffusion coefficients estimated from momentum balance. |
| CAMBRAL | $\bar{Q}_{net}$ computed; $\overline{u'v'}$ specified; $\overline{v'T'}$ parameterized in terms of $K_{yy}$, $K_{yz}$ and mean temperature gradients. |
| CLKSON | $\bar{Q}_{net}$ computed, from specified temperature field. Eddy diffusion estimated from momentum balance. |
| GSFC1 (interactive) | $\bar{Q}_{net}$ computed. |
| GSFC2 (fast) | $\bar{Q}_{net}$ specified. |
| MRI | $\bar{Q}_{net}$ specified. |
| NOCAR | $\bar{Q}_{net}$ computed. $\bar{\chi}^*$ specified at lower boundary. |
| WISCAR | $\bar{Q}_{net}$ computed. Wave driving and diffusion obtained from planetary wave calculation. |

**Table 3-5.** Vertical Velocities (cm/sec)

| Model | 0°,100 mb | 70°N, 50 mb | 70°S, 1 mb | Comments |
|---|---|---|---|---|
| AER | 0.3 | -0.6 | 1.2 | Strong summer-winter circulation |
| CALJPL | 0.0 | -0.5 | 0.5 | Strong summer-winter circulation |
| CLKSON | 0.5 | -0.5 | 1.5 | Strong summer-winter circulation |
| GSFC1 | 0.4 | -0.5 | 0.2 | Weak summer upwelling |
| GSFC2 | 0.2 | -0.5 | 0.5 | Strong summer-winter circulation |
| MRI | 0.4 | -0.4 | 1.0 | Weak downwelling in winter upper stratosphere |
| NOCAR | 0.2 | -0.5 | 1.8 | Strong summer-winter circulation |
| WISCAR | 0.1 | -0.4 | -0.3 | Weak summer upwelling (Downwelling above 3 mb at 70°S.) |

## Section 3.3.2 Tropospheric Source (X)

Yuk Yung

This experiment is designed to test three fundamental properties of the 2-D model:

(1) Advection
   (a) Equatorial upwelling
   (b) Pole-pole circulation

(2) Diffusion
   (a) $K_{yy}$
   (b) $K_{zz}$

(3) Lifetime of a chemical tracer.

From the morphology of the tracer distribution in various seasons we can deduce whether the advective and diffusive processes are strong or weak. {For a number of models the upper boundary is located near 60 km, therefore, the large discrepancies between the contour lines at the highest altitudes are not significant.} In Table 3-6 we provide a qualitative assessment of whether advection and diffusion in each model is strong or weak, and whether the pole-to-pole circulation is evident or not.

Table 3-7 summarizes the mixing ratio of X at the equator in June at 30 and 40 km. The values at 30 km in all models are dominated by the troposphere and are therefore very close to each other. The value at 40 km is an indication of the strength of the equatorial upwelling. Thus, AER has strong upwelling whereas WISCAR has less upwelling.

The mean lifetime of X is summarized in Table 3-8, along with the number of years the models were run. It takes about 10 years for the steady-state distribution of X to be established. The mean lifetime is about 110 years, with about 30% spread among the various groups. There seems to be a qualitative correlation between models with fast circulation and shorter lifetimes. The lifetime of X is determined by (a) transport through the tropopause and by (b) transport to the middle stratosphere. To obtain a quantitative indication of the above processes, these three mass integrals should be investigated:

(i) Total mass of X in model
(ii) Mass of X above 100 mb
(iii) Mass of X above 10 mb

**Table 3-6.** Qualitative Assessment of Advection and Diffusion in each Model

| Model | Advection | Diffusion | Pole-Pole Circulation |
|---|---|---|---|
| AER | Strong | Weak | None |
| GSFC2 | Average | Average | Strong |
| MRI | Weak | Strong | None |
| CALJPL | Strong | Average | Present |
| CLKSON | Average | Average | Present |
| WISCAR | Weak | Average | Weak (strong $K_{zz}$ effects at high altitudes) |
| OSLO | Average | Average | Weak |

**Table 3-7.** The Mixing Ratio of X at the Equator in June

| Model | 30 km | 40 km |
|---|---|---|
| AER | 7 (-10)* | 2 (-10) |
| GSFC2 | 7 (-10) | 3 (-11) |
| MRI | 7 (-10) | 3 (-11) |
| WISCAR | 6 (-10) | 4 (-11) |
| CALJPL | 7.5 (-10) | 3 (-10) |
| CLKSON | 7 (-10) | 1 (-10) |
| OSLO | 6 (-10) | 1 (-10) |

* 7( -10) means 7 x $10^{-10}$

**Table 3-8.** The Mean Lifetime of X

| Model | Mean Lifetime (years) | # of Years Run |
|---|---|---|
| AER | 103 | 15 |
| GSFC2 | 127 | 15 |
| CLKSON | 97 | 10 |
| WISCAR | 109 | 3 |
| CALJPL | 122 | 9 |
| OSLO | 120 | 40 |
| LLNL | 109 | 10 |

## Section 3.3.3 Time-dependent Source (Y)

Lesley Gray

### Experiment Description

$5x10^{10}$ kg of species Y (at. wt.=29 yields a global average of 1 ppmv) placed in the lower troposphere (>700 mb). No loss for species Y. Model experiment started January 1st and run for 5 years. This experiment highlights: (a) the speed with which each model achieves troposphere - stratosphere exchange, (b) the morphology of a passive tracer in the stratosphere, (c) the ability of each model to conserve mass.

### Results

Figures on pages 222-246 show latitude-height distributions every 1/2 year (January 1st, July 1st), from each model. A general pattern of ascent in equatorial regions is evident. There is some variation in the speed of troposphere-stratosphere exchange among the models (which is quantified more fully below). For example, the distributions after six months show that the MRI, AER and LLNL models achieve a rapid transfer compared with the GSFC2 and CLKSON models. Once a sufficient amount of tracer has reached the stratosphere, a seasonal cycle in distribution is displayed by the models, with the maximum mixing ratios generally displaced off the equator into the summer hemisphere. There is some variation among the models in the strength of this seasonality. For example, the GSFC2 model exhibits strong evidence of a summer to winter circulation; the MRI model, on the other hand, shows a weak seasonal dependence, with a distribution that is almost symmetric about the equator in both January and July. The complicated pattern displayed by the GSFC2 model, for example in July of year 2, is probably a result of small values for $K_{yy}$, therefore, the bulge in the southern hemisphere in the region 25-35 km is a remnant of the southern hemisphere's peak six months previously. The well-defined equatorial peak in, e.g. the AER model, compared with the much broader distribution in the MRI model, can be attributed to (a) stronger equatorial upwelling, (b) weaker $K_{yy}$ values or (c) a combination of both (a) and (b).

In Figure 3-1 the time-evolution of the 0.7 ppm contour at the equator is shown for each model. The time taken for the contour to traverse 10 km height intervals is tabulated in Table 3-9. From these time-estimates a value has been calculated for the annual-average-$\bar{w}$ that would be required to perform this transport. There is a large variation in the time taken to reach 20 km. This must be due to differences in the value of $K_{zz}$ employed in the troposphere or in the strength of the equatorial upwelling in the troposphere. Note that the two models with slowest ascent to 20 km (GSFC2 and CLKSON) also have significantly smaller tropospheric $K_{zz}$ values. Above 30 km, the AER, LLNL, and CLKSON models display rapid ascent while MRI has weak ascent. These observations are in good agreement with conclusions from the model intercomparison of net heating rates. For example, several of the models display a similar pattern of strong ascent below 20 km and above 30 km, with a region of weak ascent in the intervening region (20-30 km) coinciding with a region of reduced net heating rates between 20 and 30 km.

**Table 3-9.** Time taken for 0.7 ppm contour to traverse 10 km height intervals

| | 0-20 km | 20-30 km | 30-40 km | 40-50 km | Average Tropospheric 20-50 km | $K_{zz}$ |
|---|---|---|---|---|---|---|
| AER | 0.7 yrs. | 1.75 yrs. | 0.8 yrs. | 0.45 yrs. | 0.31 mm $s^{-1}$ | $\sim 10^5$ |
| GSFC2 | 2.0 yrs. | 1.0 yrs.<br>0.29 mm $s^{-1}$ | 1.1 yrs.<br>0.29 mm $s^{-1}$ | 0.9 yrs.<br>0.35 mm $s^{-1}$ | 0.31 mm $s^{-1}$ | $\sim 10^4$ |
| MRI | 0.5 yrs. | 1.5 yrs.<br>0.21 mm $s^{-1}$ | 3.0 yrs.<br>0.11 mm $s^{-1}$ | | 0.14 mm $s^{-1}$ | $\sim 10^5$ |
| LLNL | 0.5 yrs. | 1.8 yrs.<br>0.18 mm $s^{-1}$ | 0.9 yrs.<br>0.35 mm $s^{-1}$ | 0.5 yrs.<br>0.63 mm $s^{-1}$ | 0.34 mm $s^{-1}$ | $\sim 10^5$ |
| CLKSON | 1.5 yrs. | 1.35 yrs.<br>0.23 mm $s^{-1}$ | 0.9 yrs.<br>0.35 mm $s^{-1}$ | 0.5 yrs.<br>0.63 mm $s^{-1}$ | 0.34 mm $s^{-1}$ | 0 |

## Section 3.3.4 Stratospheric Source (Z)

K. K. Tung

The mixing ratio of Z for p<10 mb is specified at a large value (8 ppmv) in the stratosphere while its value is fixed near the lower boundary at a small value of 0.10 ppm for p>850 mb. The large value represents a stratospheric source, while the lower boundary acts as a tropospheric sink. At steady state (annually periodic), tracer Z in the region between p=850 mb and p=10 mb will equilibrate when the "production rate" (the amount of flux transported down from the source region) balances the "destruction rate" (the flux into the surface sink region).

In the absence of vertical transports, the column amount of Z should be approximately 60 Dobson units, uniform in latitude and in season, assuming that Z=0 in the middle layer: 850 mb > p > 10 mb. All models produce column amounts above 100 DU when the effect of transport is included even if one starts with the initial condition of Z=0 in the middle layer.

It is interesting to note that all models have 100 DU or more of Z over the equatorial region, where there is upwelling in most models. Apparently, the excess over 60 DU is caused either by vertical mixing down from the source region in models that have $K_{zz}$, and/or by high latitude downward advective transport from the source region followed by horizontal transports into the tropical region.

In the presence of transport below 10 mb, all models create an equatorial column minimum and high latitude maxima. Some models also produce seasonal behavior with high-latitude maximum in spring and minimum in fall, mirroring their respective simulations of column ozone presented in Section 3.4.2.

The AER model yields 120 DU in the equatorial region, while CALJPL, CLKSON, and GSFC2 produce values of Z about 40 DU higher in the same region. The present version of the AER model has a larger value of equatorial upwelling. The polar spring maximum for all 4 models are between 400 and 500 DU.

The LLNL model has 120 DU in the tropical region as in the AER model, but the high latitude maximum is a weaker 350 DU. Similar to the above mentioned models the seasonal behavior of spring maximum and fall minimum in high latitudes is clearly present in the LLNL model. However, LLNL appears to have larger amounts of Z in the southern hemisphere than in the northern hemisphere, in contrast to the behavior of its simulated column ozone.

The MRI model is distinctly different than all the other models in having a smaller global content (100 DU in the equatorial region and 300 DU over the poles) and a much weaker seasonal variation. The OSLO model has a low equatorial minimum of 100 DU, but the polar maxima are 400 DU. The seasonal behavior of spring maximum and fall minimum is present in the OSLO model in the Northern Hemisphere. In the Southern Hemisphere, however, the maximum occurs instead in winter. This behavior is consistent with its ozone simulation, and is probably caused by a discontinuity in its specified radiative heating rate near 25 km in the Southern Hemisphere winter.

The differences in the model results for Z are attributable to differences in model transport characteristics below 10 mb. The weak seasonal and latitudinal contrasts in the MRI model may be due to weak vertical circulation in that model near the 10 mb region. The AER model has a stronger vertical upwelling velocity in the equatorial region than most models. It tends to bring air depleted in Z by the surface sink to the region between 850 mb and 10 mb, resulting in a smaller value of Z in the equatorial region.

Although the Dobson map for Z resembles that for ozone simulated for each model, there is a significant difference between column Z and column ozone of some models. By design, the seasonal and latitudinal contrasts in tracer Z column can be attributed entirely to transports in the region below 10 mb. For ozone, however, seasonal variations in photochemical production and loss rates can also induce seasonal variation in the ozone column. In addition, transport above 10 mb affects the seasonal and latitudinal contrasts slightly. By comparing the Dobson maps for ozone and tracer Z, some ideas concerning the relative importance of these processes (vs. that of transport below 10 mb) can be discerned.

## Section 3.4 Current Atmosphere: 1980

Malcolm Ko

Since all models have some adjustable parameters in their formulations, the real test of the performance of a model is not how it simulates the latitudinal and seasonal behavior of just one single trace gas, but how successful it is in simulating the behaviors of all the trace gases in a self-consistent manner. For models that are designed to predict the future response of $O_3$, validation of the present day $O_3$ distributions should be a prerequisite. With a large data base from satellite observations detailing the behavior of $O_3$, it is not surprising that most model results for $O_3$ appear quite similar. However, it is also necessary to ascertain that the present day behavior is obtained by correctly simulating the appropriate mechanisms. This is why there is a need to compare the simulated behavior of other trace gases.

The behavior of the column abundance of $O_3$ is sensitive to the transport treatment in the lower stratosphere. Apart from the experiments in Section 3.2 specifically designed to test the transport, examination of the behavior of the column abundances of $HNO_3$, HCl, and $NO_2$ will be useful as a consistency check particularly since observations are available for validation. The behavior of the source gases such as $N_2O$, $CH_4$, $CCl_4$, $CH_3Cl$, and CFC's are sensitive to the transport treatment in the middle and upper stratosphere. Comparison of the calculated lifetimes of those gases that are removed in the stratosphere also provides a measure of the strength of the circulation.

In this comparison, an attempt is made to isolate the effect of photochemical treatment by comparing separately the total odd nitrogen ($NO_y$) and the partitioning of the nitrogen species (i.e., $NO/NO_2$, $NO_2/HNO_3$ ratios). The same is also done for total chlorine ($Cl_y$) and the partitioning of the chlorine species. Although no comparison was made on the water vapor content, a comparison of the hydroxyl radicals provided information on the $HO_x$ cycle.

Given the importance of the 40 km $O_3$ problem (that model calculated $O_3$ is smaller than observation), a special comparison was made on the species concentrations, photolysis rates, and reaction rates that would affect the concentration of $O_3$ at 40 km.

The simulated trace gas distribution from the models are presented in Chapter 6 of this report. These include:

- latitude and season plots of the column abundances of $O_3$, $HNO_3$, $NO_2$, and ClO
- latitude and altitude cross-sections of $NO_y$ and $Cl_y$,
- latitude and altitude cross-sections of $NO_x$, NO, $NO_2$, $HNO_3$, $N_2O_5$, $HNO_4$, the ratio of $NO/NO_2$, $HNO_3/NO_2$, and $NO_x/NO_y$
- latitude and altitude cross-sections of ClO, HCl, $ClNO_3$, HOCl, the ratio of Cl/ClO, $ClO/Cl_y$ and ClO/HCl
- latitude and altitude cross-sections of $O_3$, $HO_2$, $H_2O_2$, O, OH, the ratio of $O/O_3$ and $OH/HO_2$
- latitude and altitude cross-sections of $N_2O$, $CH_4$, F-11, F-12, $CCl_4$ and $CH_3CCl_3$.

There is no uniform criteria one can apply to all the model simulated results to quantify whether agreements among the models are good. Such a decision is based on subjective judgement and the sensitivity of the individual results on model parameters. The following discussion will concentrate more on the relevance of certain quantities selected for discussions rather than on detailed agreement and discrepancies among the models.

## Section 3.4.1 The 40 km Ozone "Problem"

Charles Jackman

The odd oxygen ($O_x$) budget including all losses and production was compared at the 3 mbar level for three latitudes (-45°S, 0°, and 45°N) at two months (March and June). The 3 mbar level was chosen for three major reasons: 1) models have a problem in predicting the ozone amount at this altitude (models predict ozone values at a smaller level than measured), 2) production should approximately equal the loss for $O_x$ at least at the equator, and 3) all four families ($O_x$, $HO_x$, $NO_x$, and $Cl_x$) are believed to be important for the loss of odd oxygen at this level. It was thought that by careful analysis of several models' output, additional insight into the ozone level problem would be possible.

Ten separate modelling groups took part in this intercomparison, some groups providing all the information at the three latitudes for both months, others providing information for a couple of latitudes, and still others providing limited information for a couple of latitudes. Since all ten modelling groups provided information at the equator for March, we focus on that point in this analysis.

We do, however, rely on other latitudes and June data to provide corroborative information as well. The ten groups included one 1-D model, eight 2-D models, and one 3-D model. The groups and acronyms used in the figures are given in Table 3-1.

The major items compared were the $O_x$ production and loss terms. The production for $O_x$ was defined to be $P(tot) = 2\, J_1(O_2)\, [O_2]$. The loss terms $L(tot) = L(O_x) + L(HO_x) + L(NO_x) + L(Cl_x)$ were all taken from Johnston and Podolske [1978] and were defined to be $L(O_x) = 2\, k_2\, [O_3]\, [O]$, $L(HO_x) = 2\, \{k_3\, [HO_2]\, [O] + k_4\, [HO_2]\, [O_3] + k_5\, [H]\, [O_3] + k_6\, [OH]\, [HO_2] + k_7\, [HO_2]\, [HO_2]\}$, $L(NO_x) = 2\, \{k_8\, [NO_2]\, [O] + J_9\, [NO_3]\}$, and $L(Cl_x) = 2\, k_{10}\, [ClO]\, [O]$. Table 3-10 presents results of the comparison of the various models at the equator in March.

The ratio of the highest model value to the lowest model value was relatively small for P(tot) and L(tot), being 1.44 and 1.42, respectively. The variance among the various families was larger, varying from 1.47 for $L(O_x)$ to 2.64 for $L(Cl_x)$.

P(tot) does approximately equal L(tot) at the equator at 3 mbar in March for the various models which indicates a relative consistency in a given model and among the various models when comparing these $O_x$ rates. The relative fraction of loss in a family is given in Figure 3-2 (a-d), where $L(O_x)/L(tot)$, $L(HO_x)/L(tot)$, $L(NO_x)/L(tot)$, and $L(Cl_x)/L(tot)$ are presented.

The $L(O_x)$ and $L(HO_x)$ are thought to be relatively consistent within the various models because of the good correlation that is apparent when $L(HO_x)$ is plotted as a function of $L(O_x)$ in Figure 3-3. Since $H_2O$, affecting only $L(HO_x)$, does not vary greatly among the models and $O_3$ and O influence both $L(O_x)$ and $L(HO_x)$, the good correspondence between $L(O_x)$ and $L(HO_x)$ was expected.

The $L(NO_x)$ is more complicated. Since $L(NO_x)$ depends on both $NO_2$ and O, and because both $NO_2$ and O have strong diurnal cycles with $NO_2$ being larger in the nighttime and O larger in the daytime, it is not clear what would happen in an intermodel comparison of $L(NO_x)$. We do find that $NO_x$ ($NO+NO_2$) is not well correlated with its major production of $2\, k_{11}\, [N_2O]\, [O(^1D)]$, but rather seems to asymptote for most models to values between 15 and 25 ppbv for larger $NO_x$ production rates (see Figure 3-4). $NO_x$ is very dependent on transport at 3 mbar and has an overall lifetime on the order of months (including both transport and chemistry). It is interesting that we find a variance in $N_2O$ of over a factor of five and a range in $NO_x$ of only about 50%.

The level of $NO_x$ appears to be fairly robust, which is a surprising result considering the large variation in the circulation from model to model. A qualitative explanation is found by considering the ramifications of a weak and a strong circulation on $NO_x$ behavior. A weak circulation will not move $N_2O$ and $NO_x$ upward or downward in the atmosphere very quickly, thus $N_2O$ will be kept at a fairly small level at 3 mbar whereas $NO_x$ will be allowed to increase to a moderately large (15-25 ppbv) equilibrium level. A strong circulation, on the other hand, will move $N_2O$ and $NO_x$ upward and downward in the atmosphere

very quickly, thus $N_2O$ will reach a relatively large level at 3 mbar whereas $NO_x$ will be constrained to an equilibrium level of 15-25 ppbv. The largest loss for $NO_x$ or odd nitrogen in the atmosphere is transformation to $HNO_3$, transport to the troposphere, and subsequent rainout as constituent $HNO_3$. The equilibrium level for $NO_x$ will be constrained by a balance between production through oxidation of $N_2O$ and loss through the rainout of tropospheric $HNO_3$. One of the major keys to this equilibrium balance is the strength of the transport of $NO_x$ away from its production region in the middle to upper stratosphere.

There is a fairly large disagreement in $L(Cl_x)$ among the models, most of the discrepancy arising from the large variation in the amount of $Cl_x$ at 3 mbar. The fractional loss due to $Cl_x$ then affects the relative fractions available to the other three families, $O_x$, $HO_x$, and $NO_x$.

Since $L(Cl_x)$, $L(NO_x)$, their relation to each other and to the losses from $L(O_x)$ and $L(HO_x)$ is complicated, we have taken a more detailed look at the results of five modeling groups which have fairly similar P(tot) values (variations only on the order of 5%), but which have a fairly large $O_3$ variation (on the order of 28%). The values of ten important rates and species are given in Table 3-11.

The most obvious correlation with ozone amount is an inverse correlation with $J(O_3\,tot)$, etc. The model with the smallest $J(O_3\,tot)$ [GSFC2] has the largest ozone and the model with the largest $J(O_3\,tot)$ [MRI] has the smallest ozone. Other correlations involving absolute amounts of $Cl_x$ and $L(Cl_x)$ are not so obvious, although there does seem to be some correspondence. The two models [AER and GSFC2] with the smallest amounts of $Cl_x$ have the smallest $L(Cl_x)$ values and the two models [LLNL and MRI] with the largest amounts of $Cl_x$ have the largest $L(Cl_x)$ values, however, this is only a very general relationship.

The reason for the relationship between $J(O_3\,tot)$ and amount of $O_3$ is more easily envisioned when P(tot) is set equal to L(tot) and $O_3$ is solved for, including only the major terms. Using that approximation, we derive the following relationship

$$[O_3] = \frac{J_1[O_2] - k_3[HO_2][O] - k_8[NO_2][O] - k_{10}[ClO][O]}{k_2[O]} \qquad (7)$$

Now [O] is dependent on $J(O_3\,tot)$ and $[O_3]$ through the equation

$$[O] = \frac{J(O_3\,tot)\,[O_3]}{k_{12}[O_2]\,[M]} \qquad (8)$$

Using (8), we can rewrite (7) as

$$[O_3] = \frac{J_1[O_2] - f\{HO_x, NO_x, Cl_x, J(O_3\,tot)\}}{g\{O_x, J(O_3\,tot)\}} \qquad (9)$$

where

$$f\{HO_x, NO_x, Cl_x, J(O_3\,tot)\} = \frac{J(O_3\,tot)[O_3](k_3[HO_2] + k_8[NO_2] + k_{10}[ClO])}{k_{12}[O_2]\,[M]} \qquad (10)$$

and $$g(O_x, J(O_3\ tot)\} = k_2\ J(O_3\ tot)\ [O_3] / k_{12}[O_2]\ [M] \quad (11)$$

Ignoring the fact that (9) is a transcendental equation for the moment, we find that $[O_3]$ will be inversely related to $J(O_3\ tot)$ because of the influence of f and g which are directly proportional to $J(O_3\ tot)$. The numerator in (9) has f subtracted from $J_1[O_2]$ and then that result is divided by the denominator g. Generally, larger values of $J(O_3\ tot)$ mean smaller levels of $[O_3]$.

This relationship between $J(O_3\ tot)$ and $[O_3]$ can be understood in another way. P(tot) is independent of the O at a given level and more or less fixed with the sun angle, whereas most terms in L(tot) are directly proportional to the amount of O at that level. The greater the $J(O_3\ tot)$, the greater the O, but since P(tot) is approximately equal to L(tot) at the equator and O is directly proportional to $O_3$ then the level of $O_3$ is forced to be smaller in order to maintain photochemical equilibrium.

All the modelling groups appear to be internally consistent, although a more constrained test of the $O_x$ budget at 3 mbar could verify and quantify this conclusion. The $L(O_x)$ and $L(HO_x)$ do not vary much from model to model because $O_3$ and $H_2O$ have relatively small variances among the models. The $L(NO_x)$ and $L(Cl_x)$ have quite a large model to model variance. Interfamily conversion and interference as well as substantial $NO_x$ and $Cl_x$ level differences among the models are believed to be the causes of this large model variance.

The level of $NO_x$ does not vary as much from model to model as does the $N_2O$ amount, indicating that $NO_x$ amounts are fairly robust. The $J(O_3\ tot)$ is the most important quantity for determining the absolute amount of $O_3$ at 3 mbar and has a variance of about 29%. We were surprised at the differences in $J(O_3\ tot)$ from model to model and encourage a more rigorous comparison of photolysis rates for a fixed atmosphere in order to investigate these differences. This more detailed photolysis intercomparison is planned as a follow-up to the two-dimensional intercomparison workshop.

**Table 3-10.** $O_x$ Production and Loss Rate Comparisons

| Rate | Mean | Highest Value/Lowest Value |
|---|---|---|
| P(tot) | 4.70(11) | 1.44 |
| $L(O_x)$ | 3.88(10) | 1.47 |
| $L(HO_x)$ | 6.29(10) | 1.59 |
| $L(NO_x)$ | 1.16(10) | 1.97 |
| $L(Cl_x)$ | 5.10(10) | 2.64 |
| L(tot) | 4.74(11) | 1.42 |

*4.70(11) means $4.70 \times 10^{11}$

**Table 3-11.** Comparison of Ten Rates and Species at 3 mbar, Equator, in March from Five Modeling Groups

| Group | P(tot) #cm$^{-3}$ day$^{-1}$ | L($O_x$) #cm$^{-3}$ day$^{-1}$ | L($HO_x$) #cm$^{-3}$ day$^{-1}$ | L($NO_x$) #cm$^{-3}$ day$^{-1}$ | L($Cl_x$) #cm$^{-3}$ day$^{-1}$ | J($O_3$tot) #sec$^{-1}$ | $O_3$ ppmv | $H_2O$ ppmv | $NO_x$ ppbv | $Cl_x$ ppbv |
|---|---|---|---|---|---|---|---|---|---|---|
| AER | 4.49(11) | 8.12(10) | 5.85(10) | 2.30(11) | 7.78(10) | 1.00(-3) | 5.82 | 4.50 | 17.8 | 2.23 |
| GSFC1 | 4.72(11) | 7.74(10) | 6.32(10) | 2.49(11) | 8.73(10) | 9.64(-4) | 5.83 | 4.88 | 18.9 | 2.36 |
| GSFC2 | 4.74(11) | 9.14(10) | 6.79(10) | 2.38(11) | 7.82(10) | 9.57(-4) | 6.04 | 5.03 | 18.2 | 2.01 |
| LLNL | 4.52(11) | 8.10(10) | 6.53(10) | 2.20(11) | 7.79(10) | 1.12(-3) | 4.85 | 4.95 | 23.0 | 2.26 |
| MRI | 4.61(11) | 6.53(10) | 7.03(10) | 1.80(11) | 1.26(11) | 1.17(-3) | 4.74 | 5.69 | 14.8 | 2.48 |

*4.49(11) means 4.49 x $10^{11}$

## Section 3.4.2 Integrated Columns of $O_3$, $HNO_3$, HCl, and HF and $NO_2$

Ivar Isaken

Except for HF, for which no columns were presented at the workshop, $O_3$, $HNO_3$, HCl and $NO_2$ columns were available from several groups. Ozone columns were available from nine (9) groups. The overall agreement among models (and with observed ozone columns) are good. This might not be surprising since total ozone columns in many cases are used to test the models, and some tuning is applied. The main feature of column ozone is reproduced in the Northern Hemisphere. Ozone maximum occurs at high latitudes during spring varying between February and May, and with a minimum in late summer and fall. Low latitude ozone levels show several variations which is in agreement with observations. The absolute values are also in fairly good agreement with observations, except for a couple of cases where ozone columns are on the high side (~10 - 20 %).

Southern Hemispheric ozone columns show considerable variations among the models. Several of the models do not predict ozone maximum at the right location and the time it is observed. Particularly, the observed low springtime values in the south polar region is not predicted in most of the models. $HNO_3$ is indicative of horizontal transport in the stratosphere. $HNO_3$ integrated columns were available for 6 models. There were marked differences among the models. Some differences were almost a factor two. All models show a marked increase toward the poles. Comparisons with observations indicate that the high column cases are closer to observations than the model estimates giving the smallest columns. However, there is one serious discrepancy between observations and all model devised columns. At high latitudes where observations show maximum values during winter, models predict a winter minimum, and a maximum during spring (1 model) or summer. One explanation which has been suggested is that models do not include heterogeneous conversion of $N_2O_5$ to $HNO_3$. This could be an important source for winter time $HNO_3$ as $N_2O_5$ is high during high latitude winter. The large differences among the models are not understood, and should be investigated.

Integrated $NO_2$ columns show marked variations with season and with latitudes. Maximum values occur at high latitudes during summer. At high latitude winter there is a drop in $NO_2$ columns poleward of approximately 60° which is in agreement with observations. Latitudinal gradients differ among the models, probably reflecting the efficiency of horizontal transport in the stratosphere. One model which calculates average diurnal values seems to give higher $NO_2$ columns than the other models. Using integrated diurnal average $NO_2$ values (one model) will probably lead to larger $NO_2$ columns than when noontime or daytime average values are used.

The integrated HCl columns show a large scatter. However, all models give pronounced latitudinal gradients. The differences in absolute levels are due to the effect of adopted surface level HCl. In most models, an arbitrary surface level is chosen. This leads to highly different contributions to the integrated HCl column which, in several cases, are significant. In order to make meaningful comparisons of stratospheric HCl columns, the tropospheric contribution has to be removed from the data.

In order to be able to make meaningful comparisons, the following suggestions are made: Integrated columns for HCl, $NO_2$ and $HNO_3$ are made for heights above 12 km to avoid any contribution from ground sources which leads to enhanced levels in the lower troposphere. $NO_2$ columns have to be calculated for the same time of day (noontime values) in all models.

The largest discrepancies among the models of integrated columns seem to be in $HNO_3$, which at high latitudes does not compare well with observed seasonal variations. Two groups have HF columns (not available at the workshop) which should be included in the comparisons.

## Section 3.4.3 $Cl_y$ and $NO_y$

Malcolm Ko

Through photochemical reactions in the atmosphere, chlorine atoms released by photodissociation of the chlorine-containing organic molecules are transformed into HCl, $ClNO_3$, ClO, Cl, $Cl_2$ and $Cl_2O_2$ referred to as odd chlorine species. The concentration of total odd chlorine, $[Cl_y]$, is defined as the sum of $[HCl] + [ClNO_3] + [ClO] + [Cl] + 2[Cl_2O_2] + .....$ Our current understanding is that while photochemical reactions can repartition the odd chlorine species, there is no reaction occurring in the atmosphere that could chemically convert odd chlorine species to an inert form. The only mechanism for removal of $Cl_y$ is by transport to the troposphere where the soluble species such as HCl could be removed by a physical process of rain-out and wash-out. In a steady state simulation of the atmosphere, the rate of $Cl_y$ removal should be equal to the production rate from the organic molecules. The total number of chlorine atoms bound up in the organic molecules and in the $Cl_y$ species should be a constant in the stratosphere.

The recommended boundary conditions for the organic chlorine species for the 1980 atmosphere simulation are summarized in Table 3-12.

**Table 3-12.** Boundary Conditions for the Organic Chlorine Species for 1980

| Species | Boundary condition (pptv) | Contributions to odd odd chlorine (pptv) |
|---|---|---|
| $CH_3Cl$ | 700 | 700 |
| $CH_3CCl_3$ | 100 | 300 |
| $CCl_4$ | 100 | 400 |
| $CFCl_3$ | 170 | 510 |
| $CF_2Cl_2$ | 285 | 570 |
| | Total odd chlorine | 2,480 |

If the mixing time in the troposphere is sufficiently fast, so that the mixing ratios of the organic molecules at the tropopause are the same as their boundary values, the $[Cl_y]$ in the upper stratosphere where most of the source gases have dissociated should approach a uniform value of 2.5 ppbv. Note that this should hold independent of the treatment (grouping or no grouping, method of partitioning of the $Cl_y$ species) in the models.

The calculated [$Cl_y$] in the upper stratosphere for the models are given in Table 3-13.

**Table 3-13.** Calculated [$Cl_y$] at 50 km

| Model | [$Cl_y$] at 50 km (ppbv) | Prescribed boundary condition |
|---|---|---|
| AER | 2.4 | yes |
| CAMBRAL* | 2.0 | * |
| CLKSON | 2.5 | no |
| GSFC1* | 2.4 | * |
| GSFC2 | 2.1 | yes |
| LLNL* | 2.4 | * |
| MRI | 2.5 | yes (no $CH_3Cl$)+ |
| NOCAR | 2.5 | no |
| OSLO | 2.3 | yes (no $CH_3Cl$)+ |
| WISCAR | 2.3 | yes (no $CH_3Cl$)+ |

*Data from these groups were not available on the database when the table was prepared. Values estimated from graphs.
+Values for $CH_3Cl$ not found in database

The low value for GSFC2 is due to a lower mixing ratio at the tropopause for $CH_3Cl$ because of slow mixing in the troposphere.

The calculated vertical and latitudinal behavior of $Cl_y$ is also useful as a diagnostic for the circulation. However, it should be noted that if one accepts the closure argument, the $Cl_y$ behavior is a result of the combined effects of the calculated scale heights and latitudinal behaviors of different source gases. A more meaningful diagnostic could be obtained by looking at the individual source gases. A rough estimate of the circulation can be obtained by examining the vertical and latitudinal distribution of $Cl_y$. The vertical distributions given at the equator in Table 3-14 provides a measure of the strength of the upwelling at the tropics.

**Table 3-14.** Vertical distribution of calculated [$Cl_y$] for January

| Model | Altitude(km) at which {$Cl_y$} is 90% of value in Table 3-13 | | Altitude at which {$Cl_y$} is 50% of value in Table 3-13 | |
|---|---|---|---|---|
| | Equator | 60° N | Equator | 60° N |
| AER | 36 | 26 | 25 | 18 |
| CAMBRAL* | 38 | 32 | 23 | 17 |
| CLKSON | 31 | 31 | 21 | 21 |
| GSFC1* | 36 | 30 | 25 | 20 |
| GSFC2 | 35 | 27 | 28 | 20 |
| LLNL* | 38 | 36 | 26 | 19 |
| MRI | 32 | 26 | 25 | 21 |
| NOCAR | 36 | 27 | 26 | 20 |
| OSLO | 31 | 26 | 25 | 18 |
| WISCAR | 36 | 30 | 27 | 24 |

*Data from these groups were not available on the database when the table was prepared. Values estimated from graphs.

Assuming that all models use similar boundary conditions on source gases, one can conclude from the Table 3-14 that the GSFC2 and WISCAR models have the strongest equatorial pumping in the lower stratosphere. In the upper stratosphere, the AER, GSFC2, NOCAR and WISCAR models have relatively strong pumping while those from the OSLO and MRI are considerably weaker.

The latitudinal contrast of [$Cl_y$] in the lower stratosphere provides a measure of the effectiveness of the competing effects of advection and eddy mixing in maintaining the slopes of the surfaces of constant mixing ratio. Table 3-15 shows that the CLKSON, MRI, CAMBRAL and WISCAR models have relatively small equator to pole contrast at 20 km.

**Table 3-15.**

Calculated ratio of {$Cl_y$} at 60°N to {$Cl_y$} at the Equator for January at 20 km and 30 km.

| Model | 20 km | 30 km |
|---|---|---|
| AER | 4.8 | 1.4 |
| CAMBRAL* | 3.5 | 1.1 |
| CLKSON | 1.0 | 1.0 |
| GSFC1* | 4.0 | 1.3 |
| GSFC2 | 4.5 | 1.5 |
| LLNL* | 2.8 | 1.3 |
| MRI | 3.2 | 1.2 |
| NOCAR | 6.2 | 1.4 |
| OSLO | 5.4 | 1.1 |
| WISCAR | 2.1 | 1.3 |

*Data from these groups were not available on the database when the table was prepared. Values estimated from graphs.

Let us now turn to the effect of calculated $Cl_y$ on $O_3$ and to what extent the difference in calculated $O_3$ could be explained in terms of the difference in calculated $Cl_y$. For the present day atmosphere, the effect of chlorine chemistry on the calculated column distribution of $O_3$ should be less than 10% at high latitudes. Table 3-16 shows that the calculated [$Cl_y$] at 25 km differ typically by about 20%. The effect on explaining differences in column $O_3$ for the present day atmosphere should be small. However, this may be relevant in explaining the different responses of ozone in different models to chlorine perturbations.

**Table 3-16.** Calculated [$Cl_y$] at 25 km (ppbv)

| Model | 60°N | Equator |
|---|---|---|
| AER | 2.1 | 1.2 |
| CAMBRAL* | 1.9 | 1.6 |
| CLKSON | 1.8 | 1.8 |
| GSFC1* | 1.8 | 1.1 |
| GSFC2 | 1.7 | 0.7 |
| LLNL* | 1.8 | 1.1 |
| MRI | 2.1 | 1.1 |
| NOCAR | 2.1 | 1.0 |
| OSLO | 2.0 | 1.2 |
| WISCAR | 1.36 | 0.76 |

*Data from these groups were not available on the database when the table was prepared. Values estimated from graphs

The impact of chlorine is more important at 40 km where the calculated $Cl_y$ differs by 10% (see Table 3-13).

The photochemical source for $NO_y$ in the stratosphere is from the reaction of $O(^1D)$ with $N_2O$. In addition to the physical removal in the troposphere, $NO_y$ is also removed by recombination of N and NO to form molecular $N_2$. The vertical distribution of N as well as the reaction rate constant of N reacting with NO are a strong function of altitude in the upper stratosphere where photochemical removal is most effective. Thus, $NO_y$ is more sensitive to transport in the upper stratosphere than $Cl_y$. In addition, the calculated [$NO_y$] at the stratopause is affected by treatment of the mesospheric source of $NO_y$, while [$NO_y$] in the equatorial lower stratosphere would depend on treatment of tropospheric lightning sources. All these complications make $NO_y$ less useful as a diagnostic for circulation. In this discussion, we will concentrate on the comparison of the calculated values and the effect on $O_3$.

Nearly all the models calculate a maximum in [$NO_y$] at about 40 km with the peak mixing ratio ranging from 18-23 ppbv.

**Table 3-17.** Calculated maximum [$NO_y$] and location of peak for January.

| Model | Altitude at which maximum occurs (km) | Mixing ratio at maximum (ppbv) |
|---|---|---|
| AER | 42 | 19 |
| CAMBRAL* | 42 | 18 |
| CLKSON* | 30 | 19 |
| GSFC1* | 35 | 22 |
| GSFC2 | 40 | 18 |
| LARC | 39 | 21 |
| LLNL* | 42 | 22 |
| MRI | 35 | 17.5 |
| NOCAR | 41 | 23 |
| OSLO | 37 | 21 |
| WISCAR* | 40 | 22 |

*Data from these groups were not available on the database when the table was prepared. Values estimated from graphs.

Different models also showed significant deviation at the upper boundary of the models around 50 km.

**Table 3-18.** Calculated [$NO_y$] around 50 km for January

| Model | Equator (ppbv) | High Latitudes (ppbv) |
|---|---|---|
| AER | 17 | 10 |
| CAMBRAL* | 12 | 12 |
| CLKSON* | 13 | 10 |
| GSFC1* | 12 | 8 |
| GSFC2 | 8 | 5-7 |
| LARC | 12 | 4 |
| LLNL* | 18 | 18 |
| MRI | 10 | 10 |
| NOCAR | 16 | 6-10 |
| OSLO | 14 | 14 |
| WISCAR* | 7 | 6 |

*Data from these groups were not available on the database when the table was prepared. Values estimated from graphs.

The calculated [$NO_y$] at 20 km at high latitudes should have a large impact on the calculated column abundance of $O_3$. Table 3-19 gives the calculated [$NO_y$] at 20 km for January for both the summer and the winter hemispheres.

**Table 3-19.** Calculated [$NO_y$] at 20 km

| Model | Summer 60° S (ppbv) | Equator (ppbv) | Winter 60°N (ppbv) |
|---|---|---|---|
| AER | 7 | 1.3 | 8 |
| CAMBRAL* | 10 | 2.0 | 10 |
| CLKSON* | 11 | 2.0 | 5 |
| GSFC1* | 5 | 1.0 | 6 |
| GSFC2 | 8 | 0.9 | 4 |
| LARC | 7 | 2.5 | -- |
| LLNL* | 10 | <2 | 10 |
| MRI | 9 | 0.5 | 5 |
| NOCAR | 8 | 1.8 | 8 |
| OSLO | 6 | 1.0 | 10 |
| WISCAR | 5.5 | <2 | 4 |

*Data from these groups were not available on the database when the table was prepared. Values estimated from graphs.

A large range of values (5-10 ppbv) is obtained among the models. In addition, some of the models (CLKSON, GSFC2, MRI, and OSLO) show large differences between the summer and the winter hemisphere.

## Section 3.4.4 $NO_y$ Species

Anne Douglass

Comparisons of dissociation rate calculations and transport experiments indicate that there are substantial differences among these models. In spite of these sources of variance, comparison of ratios of family members provides a measure of the overall consistency of the models. The interchange reactions among the odd nitrogen species ($NO_y$ = NO + $NO_2$ + $NO_3$ + $HNO_3$ + $HO_2NO_2$ + 2 $N_2O_5$ + $ClONO_2$+ $HNO_2$) are rapid compared to the net production and loss of $NO_y$. These interchange reactions are affected both directly and indirectly by model quantities including dissociation rates, the concentrations of species such as odd hydrogen species which are in photochemical equilibrium, and the concentrations of long lived (transported) species.

The ratio (NO + $NO_2$)/$NO_y$, whether daytime average or noontime concentrations are used to formulate the ratios, indicates the fraction of total $NO_y$ that participates in the catalytic cycles that destroy ozone. For January current atmosphere values, these ratios show remarkable agreement. For all models, the ratio is greater than 0.9 at 40 km. At 35 km, the high and low values of the ratio are all in the range 0.75 to 0.90. At 30 km, the model ratios are in the range 0.45 to 0.60. Above about 28 km, the ratio is smaller at the winter pole than at the summer pole. In the lower stratosphere there is some similarity among the major structures.

Similar agreement is seen for the ratio $HNO_3/NO_2$. Although the high latitude, lower stratospheric lifetime of $HNO_3$ is long, through much of the stratosphere its concentration is controlled by photochemical processes. The photochemical equilibrium ratio is given by

$$\frac{k_1\,[OH]\,[M]}{k_2\,[OH] + k_3\,[O] + J} \quad \text{approx.} = \quad \frac{k_1\,[OH]\,[M]}{J}$$

where $k_1$ is the rate for $NO_2$ + OH + M, $k_2$ for OH + $HNO_3$, $k_3$ for O + $HNO_3$ and J is the dissociation rate for $HNO_3$; J dominates the other two loss processes. The consistency of the values of this ratio among the models is a measure of the consistency of the ratio of the OH concentration to the dissociation rate for $HNO_3$.

## Section 3.4.5 $Cl_y$ in the Current Atmosphere

Richard Eckman

For the purposes of the intercomparison, the abundances of chlorine source gases in the present day atmosphere were fixed to yield a total inorganic chlorine level of 2.48 ppbv in the stratosphere. The uniform level of $Cl_y$ removes some of the uncertainty associated with the comparison of the models. Interchange between family members determines the efficiency at which the odd chlorine family destroys odd oxygen, primarily through reactions involving Cl with $O_3$ and ClO with O in the upper stratosphere. This intercomparison focused on several ratios of chlorine species and the absolute abundances of certain family members (ClO, $ClNO_3$, HOCl, and HCl) to ascertain the areas of disagreement among the models.

Cl and ClO rapidly interchange throughout much of the stratosphere and their relative abundance is

$$\frac{[Cl]}{[ClO]} = \frac{k_1[O] + k_2[NO] + J_{ClO}}{k_3[O_3] + k_4[NO]}$$

The dependence of the ratio on NO and the photodissociation of ClO are secondary to the reactions involving O and $O_3$. Hence, this ratio should reflect closely the ratio of oxygen and ozone examined in the next section.

Among the models examined in this study, a substantial degree of consistency is seen among the results of this ratio with discrepancies generally less than 20%, at least above 30 km. The comparison is impaired however by steep gradients in the ratio in the 40-50 km range.

HCl in the stratosphere acts as a reservoir for odd chlorine by effectively sequestering $Cl_y$ in a form that removes it from participating in odd oxygen destruction. HCl can be formed by reaction of Cl with $CH_4$ and also $HO_2$. In the lower stratosphere, reaction of Cl with $CH_2O$ can also be important. Lesser sources involve reactions with $H_2O_2$ and $H_2$. The primary source of destruction is by reaction with OH. The ratio of ClO to HCl will clearly show the importance of the differences in model-calculated $CH_4$, a long-lived gas, and the odd hydrogen family (through its dependence on OH and $HO_2$). Agreement among the models in the upper stratosphere (30-50 km) is, again, reasonable but with somewhat more spread than in the case of Cl/ClO. Indeed, the ratio is in a sense a convolution of both the Cl/HCl and Cl/ClO relative abundances. Therefore, discrepancies in the Cl/ClO ratio will be reflected in the ClO/HCl comparison. It is difficult to ascribe the differences to any one factor without a critical intercomparison of the other species mentioned above which was not possible during the time frame of the workshop.

Recent airborne measurements by Brune et al. (Polar Ozone Workshop Abstracts, NASA Conference Pub. 10014, 189-190, 1988) at northern high latitudes (~60°N) in the winter lower stratosphere reveal elevated levels of ClO in the 55 pptv range. Table 3-20 shows the ClO mixing ratio calculated by the models. These values are at least a factor of three below the measured value and thus cannot account for the enhancement in ClO.

**Table 3-20.** Calculated ClO at 50 mb, 60°N latitude

| Model | ClO (pptv) |
|---|---|
| NOCAR | 10 |
| AER | 20 |
| GSFC2 | 2-10 |
| MRI | 10 |
| DUPONT | 5 |
| LLNL | 16 |

## Section 3.4.6 $O_x$ and $HO_x$ Partitioning, $H_2O_2$, $CH_2O$

Paul Guthrie

### $O/O_3$

The odd-oxygen partitioning between atomic oxygen and ozone depends primarily on the model treatment of ozone photolysis. A comparison of the $O/O_3$ ratio among models thus gives us information about differences in the ways the models handle radiative transfer in the near UV, and about the ways the models compute photolysis rates, including seasonal variation and diurnal (or other temporal) averaging effects. Where ozone photolysis becomes small (i.e. at large optical depths), the ratio becomes sensitive to processes involving other chemical families (e.g. $NO_2$ photolysis)

The spread in model distributions of $O/O_3$ is perhaps somewhat surprising. The two GSFC models use essentially the same photolysis calculation, and as might be expected, have similar distributions of $O/O_3$. They differ more below 20 km where the differences in the treatment of other chemical families becomes more important. Using GSFC2 arbitrarily for comparison purposes, the overall span in $O/O_3$ values for all models is roughly plus 100% (AER) to minus 50% (WISCAR, LLNL) based on the December distributions.

There are substantial differences in the seasonality of the ratio. LLNL, WISCAR, and OSLO are the most strongly seasonal (steepest winter/summer slope), while CAMBRAL and LARC show minimal latitudinal variation, at least in December. Most models show a monotonic increase in the ratio at summer high latitudes for a constant altitude, but some (CAMBRAL, AER, LARC) have a tropical maximum at least at some altitudes.

There are also differences in the "shape" of the altitude variations of the ratio. For example, GSFC2, OSLO and MRI all have similar values at 20 and 30 km, but at 40 km MRI is perhaps a factor of three larger than GSFC2, while OSLO is perhaps 50% smaller than GSFC2.

### $O_3$

There are some notable differences in the $O_3$ distributions among the models. Differences in the curvature of isopleths (especially the upward-poleward extension in high latitudes in the winter hemisphere) appear to be related to the eddy diffusion coefficients used. There is a spread of ~20% between the peak mixing ratios obtained by various models. There is also a substantial difference in the mixing ratios obtained by the various models in the 10-20 km altitude region. This is presumably related to the relative strengths of the upward advection and downward diffusion in the lower stratosphere and the troposphere.

### $OH/HO_2$

Based solely on a comparison of the $OH/HO_2$ ratio among models, there is less disagreement for these species than for most others in this intercomparison. That is perhaps to be expected since transport plays essentially no role in determining this partitioning, at least in the middle and upper stratosphere. All models show a value of 1.0 for this ratio between 37 and 40 km. There is a slight offset (perhaps 1-2 km) in this between the models which compute temperature and those which specify it, consistent with the small temperature differences seen at these altitudes. The ratio decreases with decreasing altitude, reaching a minimum of about 0.1 somewhere between 20 and 30 km in most models, with the exception of LARC. Since the ratio becomes sensitive to the $CH_4$ concentration in this altitude range, and thus to the already established differences in transport among models, greater variance is probably to be expected in this region. The LARC exception is presumably due to the specification of the $CH_4$ distribution in that

model.

There is some indication that differences in chemical schemes may affect the $OH/HO_2$ ratio at 40 km near the polar terminator. One group of models (WISCAR, GSFC1, OSLO) shows substantial structure in the ratio in this region, while a second group (AER, NOCAR, GSFC2, LARC) shows much flatter contours. The NOCAR model has unique structure in the ratio at 16 km which is presumably a reflection of the lower boundary treatment.

$\underline{HO_2}$

There is a disagreement among models as to $HO_2$ distribution in the upper stratosphere and lower mesosphere. In CAMBRAL the mixing ratio slope decreases with altitude, in effect, creating a broad maximum at the model top. AER has an approximately constant slope to a maximum value of 450 pptv. The other models have constant or slightly increasing slope to maximum values of 550 pptv or greater. The different mixing ratio values at the model tops may simply reflect different maximum altitudes, but slope differences are probably related to differences in $HO_x$ production rates, given the similarity of $OH/HO_2$ ratios.

$\underline{H_2O_2, CH_2O}$

For $H_2O_2$ all models show a similar distribution in the stratosphere with a broad tropical maximum reaching a peak mixing ratio of about 0.2-0.4 ppbv (CAMBRAL is slightly below 0.2 and MRI is slightly above 0.4) at 30 km. There is a minimum at around 16 km which varies substantially among models, presumably due to differences in transport and tropospheric removal. GSFC1 appears to be somewhat anomalous in this, using a much faster removal rate for $H_2O_2$ than the other models. There is also some indication that the $H_2O_2$ distribution may not have converged completely in GSFC1.

The $CH_2O$ distributions are also similar with a tropical mixing ratio maximum at about 40 km and another at the ground. MRI has a notably smaller mixing ratio peak in the stratosphere than other models ($< 0.1$ ppbv) while LARC has the largest ($> .25$ ppbv). The other models show peak values of about .15 - .25 ppbv.

## Section 3.4.7 Distribution and Lifetimes of Source Gases

Malcolm Ko and Donald Fisher

Source gases with lifetimes longer than one year are uniformly distributed in the troposphere where mixing is very efficient. Gases transported to the stratosphere are removed by photochemical reactions. The calculated distributions of the source gases in the stratosphere is a good indication of the efficiency of transport to maintain the concentration against photochemical loss. The behavior of the simulated distributions of the trace gases from the different models are consistent with the strengths of their circulations as discussed in Section 3.3.2. Models with stronger circulations would have higher concentrations in the stratosphere. The lifetimes of the trace gases as calculated by some of the models are given in Table 3-21.

**Table 3-21.** Model Calculated Lifetimes (years) of Source Gases*

| Trace Gas | AER | GSFC2 | LLNL |
|---|---|---|---|
| $N_2O$ | 114 | 168 | 130 |
| $CCl_4$ | 40 | 52 | 52 |
| F-11 | 46 | 60 | 60 |
| F-12 | 95 | 132 | 121 |

* Some of the values given in this table are taken from simulations performed for the UNEP/WMO report and do not correspond exactly to the distributions given in Chapter 6. however the difference should be small.

The lifetimes for the trace gases given in Table 3-21 are determined by removal in the stratosphere. As expected, models with strong circulations that predict higher concentrations in the stratosphere give shorter lifetimes. Lifetimes for the species such as $CH_4$ and $CH_3CCl_3$ are determined by removal in the troposphere through reaction with OH. Calculated values from the models will depend on the treatment of tropospheric chemistry in predicting OH in the models.

## Section 3.5 Perturbed Atmospheres

Donald J. Wuebbles
Matthew H. Hitchman

For the workshop, each of the modeling groups was asked to examine their calculated effects on ozone from four steady-state scenarios for perturbed concentrations of CFCs, $CO_2$, and other trace gases. In each scenario, the change in ozone is determined relative to a "1980" atmosphere, as indicated in Table 3-22. The four perturbation scenarios, as defined in Table 3-22, are:

A = All trace gases perturbed (including approximately 8 ppbv $Cl_y$, 2 x $CO_2$, 2 x $CH_4$, 1.2 x $N_2O$);
B = 2 x $CO_2$ only;
C= CFC perturbation only; and
D = all gases perturbed except $CO_2$

Many of the groups brought results to the meeting and the calculated changes in stratospheric ozone and temperature were compared. However, there was insufficient time to make detailed comparison of the results, and at this time, many of the differences in the results from different models remain unresolved. In order to not mislead the reader, we have chosen not to present any of the individual graphs for the perturbation results in ozone of the different groups until a more detailed comparison of two-dimensional (and three-dimensional) model results for the perturbed atmosphere can be done at a later time. However, we will provide an overview of the results.

**Table 3-22.** Reference and perturbed atmospheres

| | Tropospheric Mixing Ratios | | Scenario | | | |
|---|---|---|---|---|---|---|
| | "1980" | "20xx" | A | B | C | D |
| $CO_2$* | 340 ppm | 680 ppm | • | • | | |
| $N_2O$ | 300 ppb | 360 ppb | • | | | • |
| $CH_4$ | 1.6 ppm | 3.2 ppm | • | | | • |
| $H_2O$(at tropopause)* | 3.0 ppm | unchanged | | | | |
| CO | 100 ppb | unchanged | | | | |
| $CH_3Cl$ | 700 ppt | unchanged | | | | |
| $CH_3CCl_3$ | 100 ppt | unchanged | | | | |
| $CCl_4$ | 100 ppt | unchanged | | | | |
| $CFCl_3$ | 170 ppt | 800 ppt | • | | • | • |
| $CF_2Cl_2$ | 285 ppt | 2200 ppt | • | | • | • |
| $CH_3Br$ | 20 ppt | 40 ppt | • | | | |

* To be included where possible/applicable.

Table 3-23 describes which modeling groups provided calculations for the perturbed atmosphere scenarios, and, in a rough sense, gives an indication of those models that determine interactive changes in temperature and /or circulation, as well as determining the chemical effects on ozone. There were five groups that both submitted perturbation results and that have the

capability for treating interactive temperature and/or circulation changes. For example, the LLNL model has fixed circulation and eddies for perturbation calculations, but allows the changes in net heating rates to affect stratospheric temperatures. Other models, such as NOCAR and WISCAR, are attempting to include fully interactive radiation, circulation, and wave-driven eddies in their calculations (the approaches used in different models to determine these interactions vary widely, reflecting the significant uncertainties in attempting to make current models fully interactive).

**Table 3-23.** Modeling groups represented in the perturbations calculations discussed, and their capability at the time of the workshop for determining interactive heating rates ($\Delta Q$), temperatures ($\Delta T$), and circulation ($\Delta \chi$) changes. The degree at which various models are "interactive" in determining these changes varies, and is not represented by this table.

| Model representatives | Interactive $\Delta Q$, $\Delta T$, $\Delta \chi$ | Ran perturbations |
|---|---|---|
| AER | No | Yes |
| DUPONT | No | Yes |
| GSFC2 | No | Yes |
| MRI | No | No |
| MPIC | No | No |
| OSLO | No | Yes |
| LLNL | $\Delta Q$, $\Delta T$ | Yes |
| CLKSON | $\Delta Q$, $\Delta \chi$ | No |
| CALJPL | $\Delta Q$, $\Delta \chi$ | No |
| AERI | $\Delta Q$, $\Delta T$, $\Delta \chi$ | Yes |
| CAMBRAL | $\Delta Q$, $\Delta T$, $\Delta \chi$ | No |
| NOCAR | $\Delta Q$, $\Delta T$, $\Delta \chi$ | Yes |
| WISCAR | $\Delta Q$, $\Delta T$, $\Delta \chi$ | Yes |
| GSFC1 | $\Delta Q$, $\Delta T$, $\Delta \chi$ | Yes |

As we will discuss below, there was a wide variation in the calculated changes in total ozone among models for the four cases. Tables 3-24 through 3-26 present the results from several of the models compared at the meeting for the calculated changes in total ozone in the tropics and at the poles for scenarios C, B, and A, respectively. For the CFC-only scenario, the models generally agreed well in their calculated changes in total ozone for the tropics. However, two models got much larger changes in ozone at the poles than the other three models. Very large differences were found among models for the doubled $CO_2$ scenario. Part of this difference, as seen in Table 3-25, is related to whether tropospheric temperatures were assumed to have changed for the perturbed atmosphere. The altitude at which lower stratospheric temperatures are first allowed to be perturbed in the model also appears to affect the change in total ozone determined. Given the significant differences in results among models for cases B and C, it is not surprising that there are substantial differences in the calculated changes in total ozone for case A, where all of the gases are perturbed together.

**Table 3-24.** Comparison of calculated change in total ozone from five models for scenario C ($Cl_y$ only perturbation). The models are listed randomly.

| Model | Δ Total $O_3$ (%) Tropics | Δ Total $O_3$ (%) Pole |
|---|---|---|
| A | -2 | - 6 |
| B | -3 | - 6 |
| C | -4 | -12 |
| D | -4 | - 6 |
| E | -4 | -16 |

**Table 3-25.** Calculated changes in total ozone for scenario B (2 x $CO_2$) from three models. Models are listed randomly. Also shown is whether tropospheric temperatures were assumed to be changed for this scenario.

| Model | ΔT in troposphere | ΔTotal $O_3$ (%) Tropics | Pole |
|---|---|---|---|
| F | No | +1.5 | + 5.6 |
| F | Yes | +1.2 | + 2.8 |
| G | No | +4.0 | +10.0 |
| H | No | +1.8 | + 7.5 |

**Table 3-26.** Calculated changes in total ozone for scenario A from three models. Models are listed randomly.

| Model | ΔTotal $O_3$ (%) Tropics | Pole |
|---|---|---|
| I | -0.4 | +2.0 |
| J | +3.0 | +7.0 |
| K | 0 | -2.5 |

In contrast, reasonably good agreement was found among models for the temperature perturbations calculated for the scenarios. Regarding the effects on dynamics, there is agreement between the AERI and WISCAR models regarding the feedback of gravity wave drag, wherein a weakened pole-to-pole circulation above 30 km occurs as a result of the latitudinal variations in projected temperature decreases in cases A-D. The WISCAR model reports a modest Rossby wave feedback in cases where $CO_2$ doubling alters lower stratospheric temperatures somewhat. Initial diagnosis suggests a delayed spring polar ozone maximum. Changes in temperature and net heating rates calculated for the four scenarios from available models are presented in the database summary of plots. A more detailed comparison of model results for perturbed atmospheres is to be done for the International Ozone Scientific Assessment report next year. That report will also

need to examine what effect including heterogeneous chemistry in these models, such as for the conversion of $N_2O_5$ to $HNO_3$ at winter polar latitudes or the reaction of chlorinated molecules on particle surfaces, has on perturbation calculations. Future comparisons of perturbed atmospheres in two- and three- dimensional models will require much more detailed analysis of the differing approaches used to treat radiative and dynamical, as well as chemical interactions. We need to determine how these interactions are affected in perturbed atmospheres.

## Section 3.6 References

Allen, M., and J. E. Frederick, Effective photodissociation cross sections for molecular oxygen and nitric oxide in the Schumann-Runge bands, J. Atmos. Sci., 39, 2066-2075, 1982.

Johnston, H. S., and J. Podolske, Interpretations of stratospheric photochemistry, Rev. Geophys. and Space Phy., 16, 491-519, 1978.

Nicolet, M., and W. Peetermans, Atmospheric absorption in the $O_2$ Schumann-Runge band spectral region and photodissociation in the stratosphere and mesosphere, Planet. Space Sci., 28, 85-103, 1980.

# TRACER EXPERIMENT Y

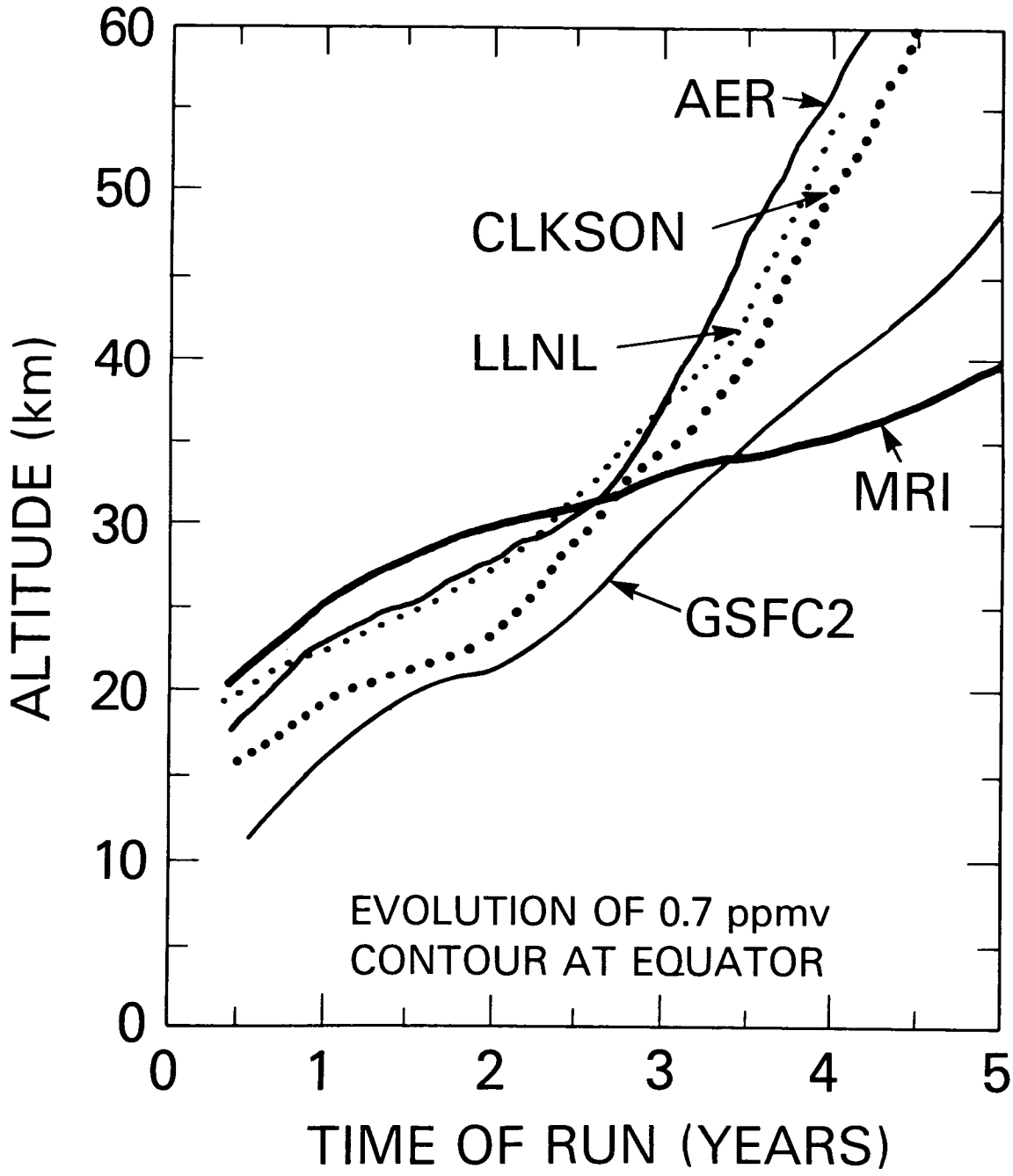


Figure 3-1. Time evolution of the 0.7 ppmv contour at the equator is shown for models AER, CLKSON, GSFC2, LLNL,and MRI.

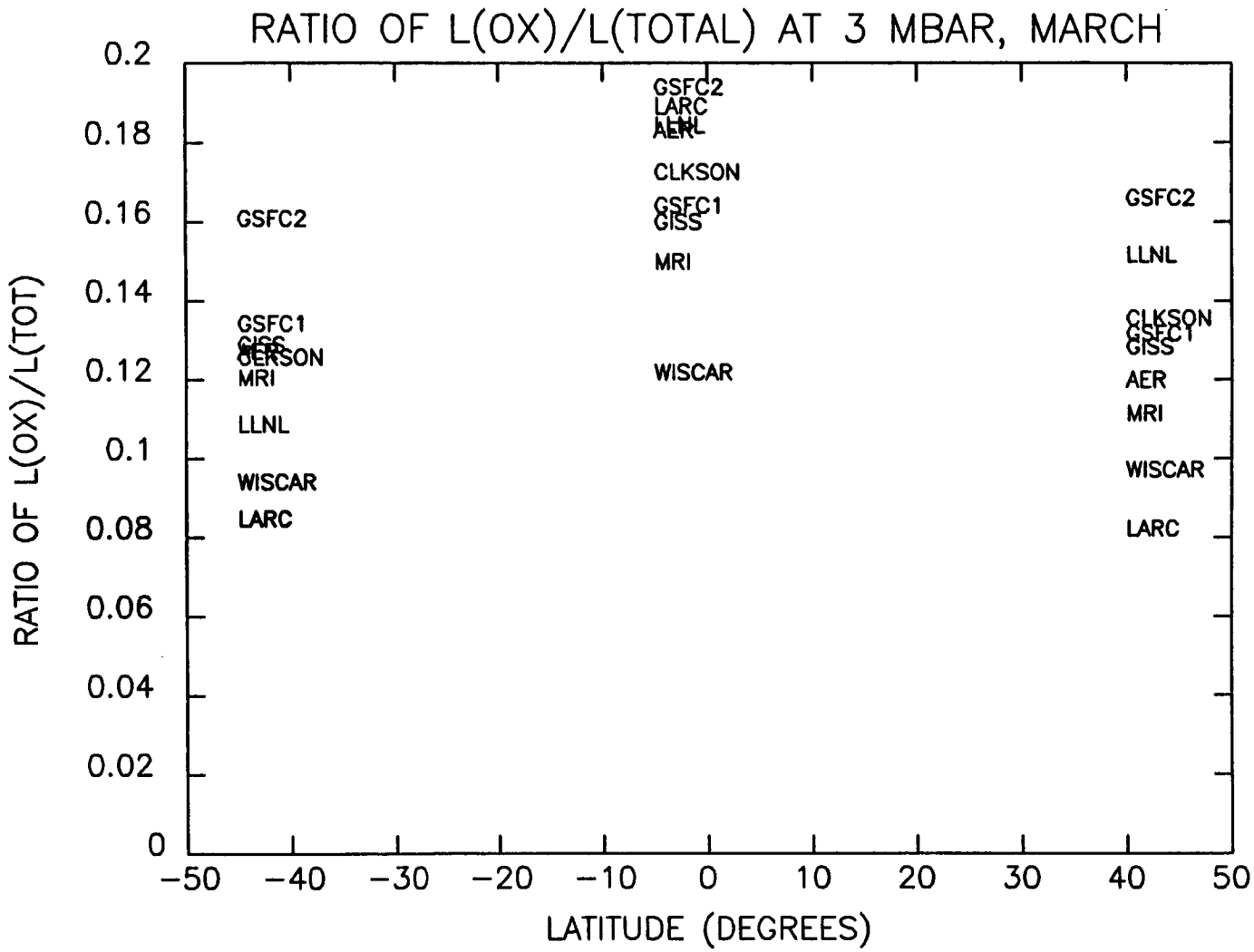


Figure 3-2. The relative fraction of odd oxygen (ozone) loss in a family at 3 mbar (40 km) for latitudes 45°S, 0°, and +45°N degrees is given for a) $L(O_x)/L(tot)$.

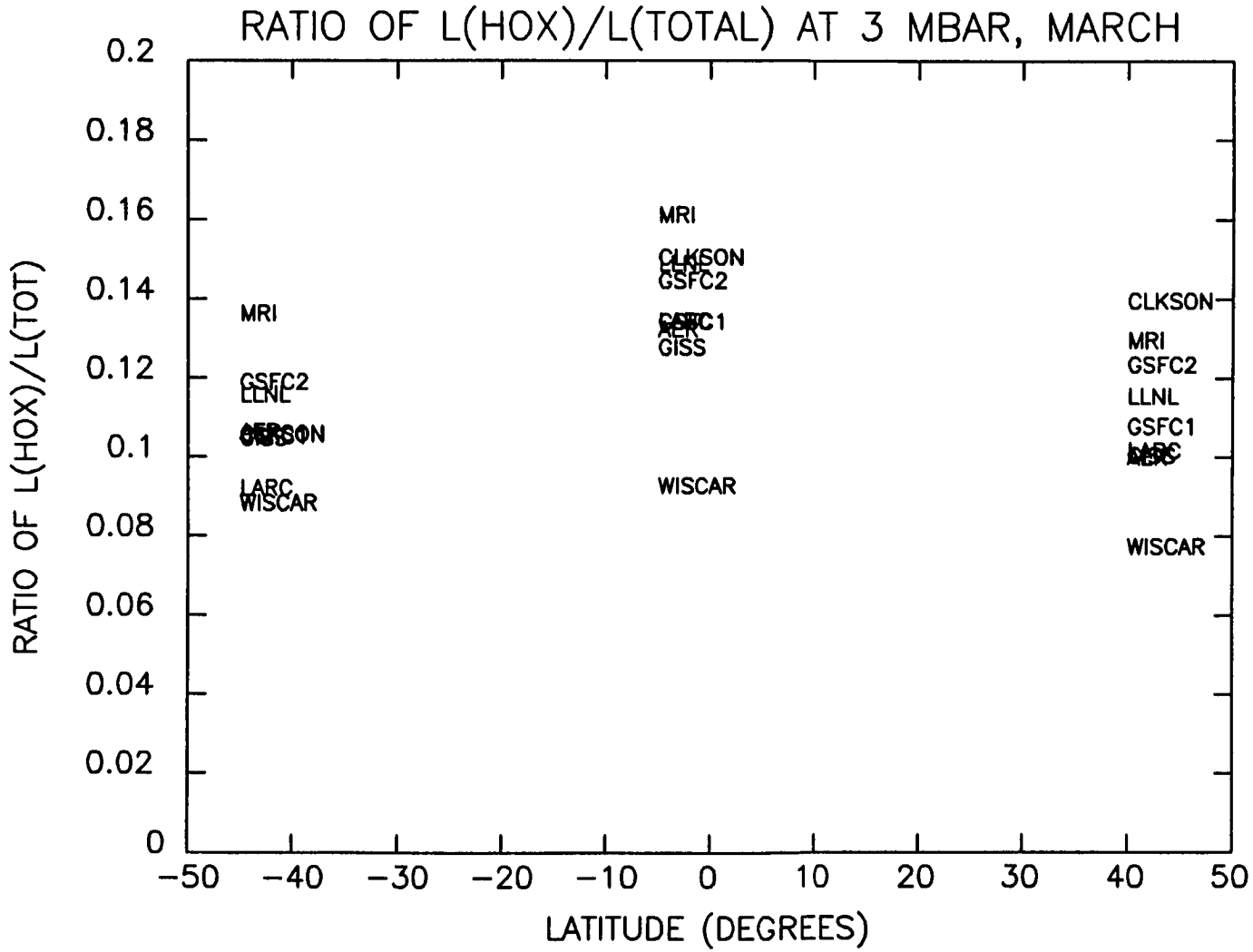


Figure 3-2. The relative fraction of odd oxygen (ozone) loss in a family at 3 mbar (40 km) for latitudes 45°S, 0°, and +45°N degrees is given for b) $L(HO_x)/L$ (tot).

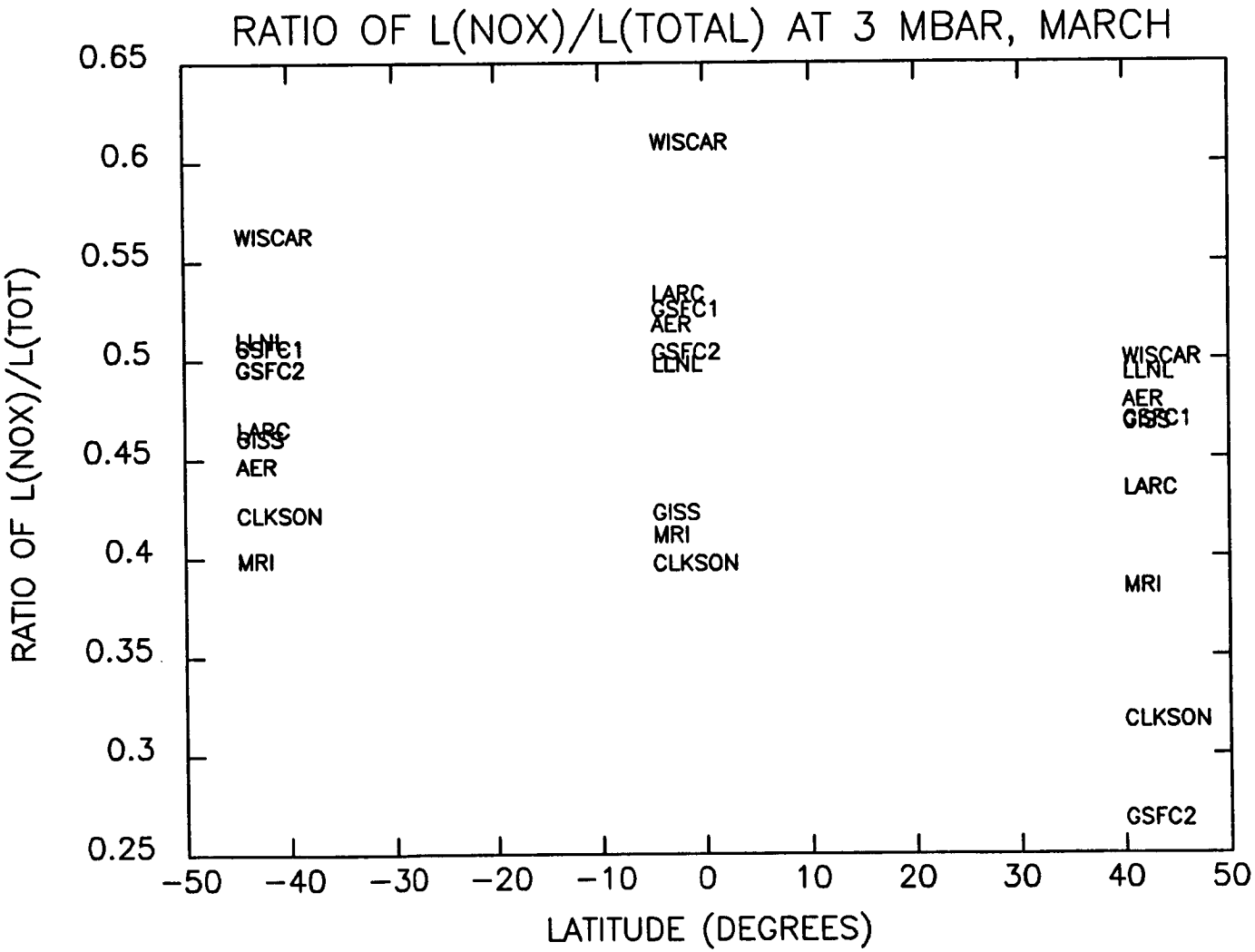


Figure 3-2. The relative fraction of odd oxygen (ozone) loss in a family at 3 mbar (40 km) for latitudes 45°S, 0°, and +45°N degrees is given for c) $L(NO_x)/L(tot)$.

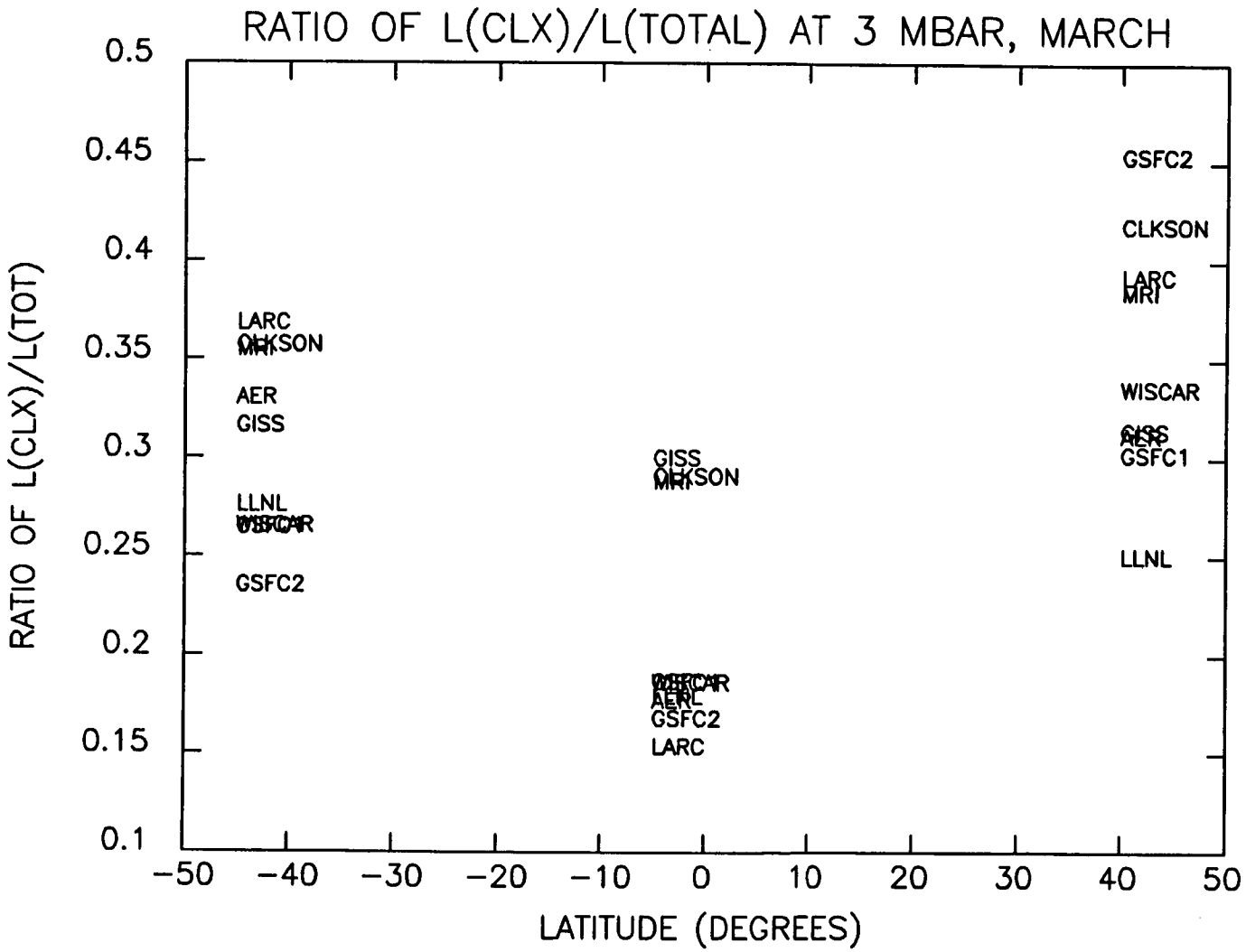


Figure 3-2. The relative fraction of odd oxygen (ozone) loss in a family at 3 mbar (40 km) for latitudes 45°S, 0°, and +45°N degrees is given for d) L ($Cl_x$)/L(tot).

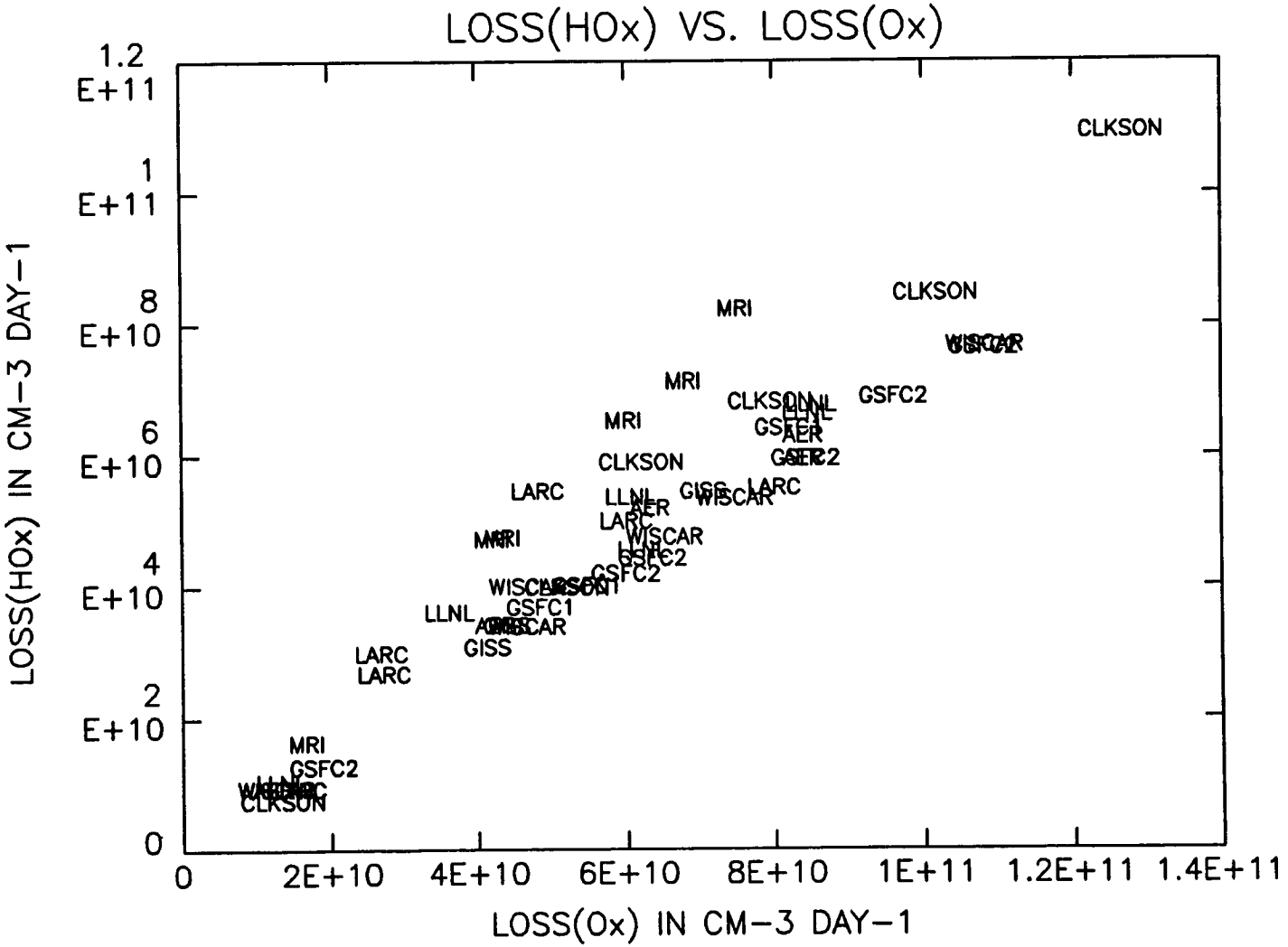


Figures 3-3. The loss of odd oxygen due to $O_x$, $L(O_x)$, as a function of the loss of the odd oxygen due to $HO_x$, $L(HO_x)$; all points given for level 3 mbar (40 km).

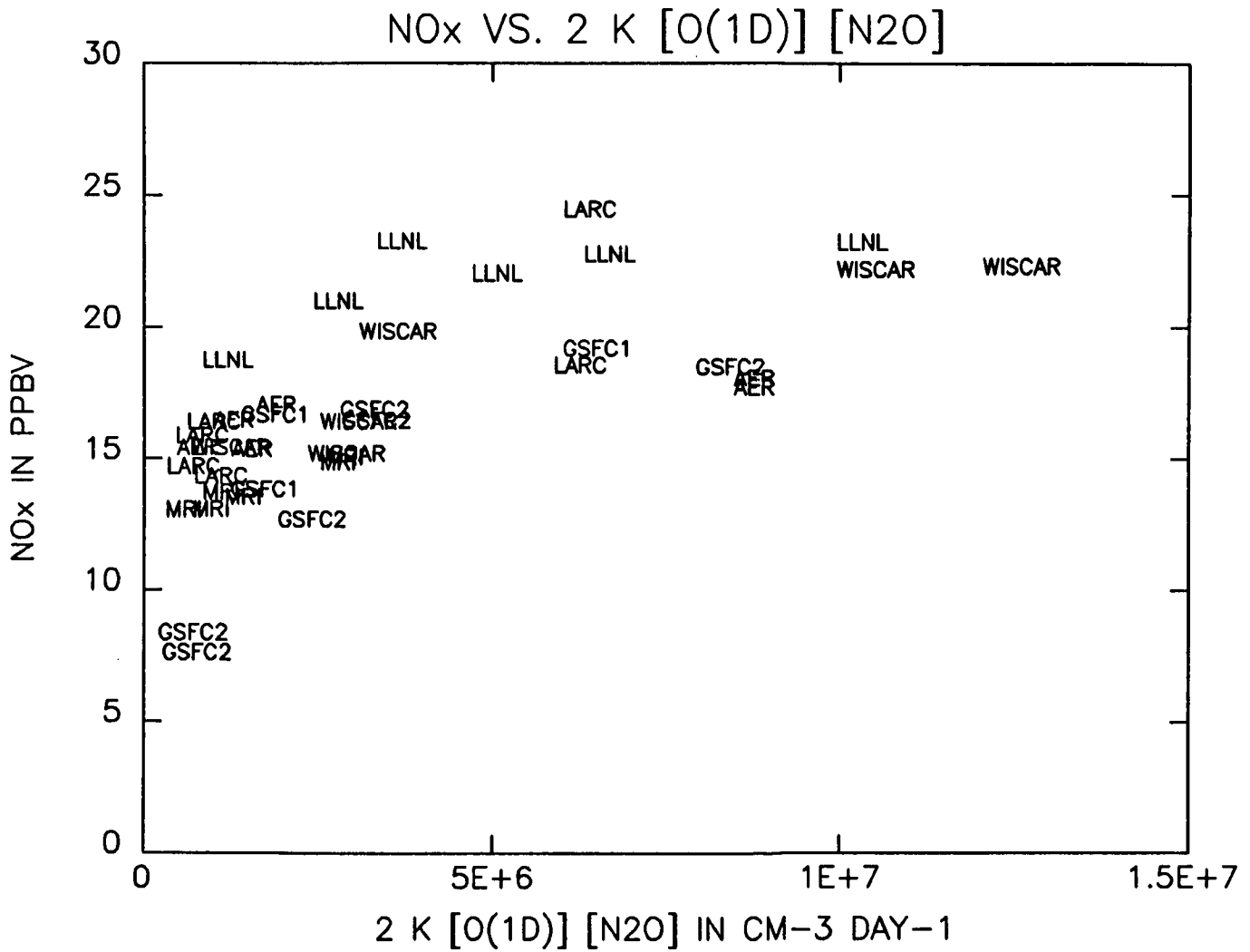


Figure 3-4. The production of odd nitrogen, 2 k[O($^1$D)][ $N_2O$], as a function of $NO_x$ at 3 mbar (40 km).

## Section 3.7 Appendix: Comparison Of Thermal Infrared Cooling Rates

Report was prepared after the September 11-16, 1988 2-D Workshop

Dave Crisp

### Objectives:

This test was designed to compare the thermal infrared cooling rate algorithms that are currently being used in 2-D chemical tracer transport models. Thermal cooling rates play an important role in these models since the advective component of the 2-D transport circulation is usually approximated by the diabatic circulation, which is derived from the difference between the solar heating rates and the thermal cooling rates. Accurate methods for finding thermal cooling rates are essential in this application because the solar heating and thermal cooling rates often differ by only a few percent. This is particularly true in the middle and lower stratosphere, where the trace gas distribution is largely determined by transport. At these levels, 10% errors in either the solar heating or thermal cooling will often produce 100 % errors in the computed diabatic circulation.

Earlier comparisons of radiative algorithms have revealed large differences in thermal cooling rates for identical input model atmospheres. To help determine the causes of these differences, thermal fluxes and cooling rates were computed separately for model atmospheres that included only $H_2O$, $CO_2$, or $O_3$, as well as for an atmosphere that included all three gases. Cooling rates obtained from an accurate line-by-line calculation were used as an absolute standard in these tests.

### Model Atmospheres Used:

Atmospheric pressures and temperatures from the McClatchey et al. (1971) "Midlatitude Summer" sounding were used for all tests in this comparison. $H_2O$ and $O_3$ mixing ratios were also derived from that source. Two different $CO_2$ mixing ratio profiles were used, including a "1980 atmosphere" (300 ppmv) and a "doubled $CO_2$" (600 ppmv) case. These quantities were specified at the middle of 123 layers between the surface and approximately 100 km.

### Standard Line-by-Line Cooling Rates:

Fluxes and cooling rates obtained from the GFDL line-by-line model (Fels and Schwarzkopf, 1981; Schwarzkopf and Fels, 1985) were used as the standard "exact" results in this comparison. These results were chosen because they were available, and because they were included and validated as part of the ICRCCM comparison study (Luther and Fouquart, 1984).

### Spectral Intervals:

Spectrally-resolved fluxes and heating/cooling rates were requested for the following spectral intervals to facilitate the diagnosis of differences among models:

| test | gas | interval ($cm^{-1}$) | bands included |
|---|---|---|---|
| 1) | $H_2O$: | 0 - 1650 | 6.3, rotation, continuum: ICRCCM case 20. |
| 2) | $CO_2$: | 450 - 900 | 15 micron band only: ICRCCM case 9 and 10. |
| 3) | $O_3$: | 0 - 1350 | 9.6 and 14 micron bands: ICRCCM case 23. |
| 4) | ALL: | 0 - 1650 | All bands of all gases: ICRCCM case 27. |

**The Models Used:**

Eight groups participated in the revised thermal cooling rate comparison:

| | |
|---|---|
| 1) GFDL | (S. B. Fels, M.D. Schwarzkopf, S. Freidenreich, GFDL/NOAA) |
| 2) Caltech | (D. Crisp, Jet Propulsion Laboratory/Caltech) |
| 3) Clarkson | (K.K. Tung, E. Olaguer, and H. Yang, Clarkson). |
| 4) Goddard | (J. Rosenfield, NASA Goddard Space Flight Center) |
| 5) LLNL | (K. Grant, Lawrence Livermore National Laboratory) |
| 6) Leningrad | (I. Karol, Main Geophysical Observatory, Leningrad) |
| 7) Mainz | (C. Bruehl, Max-Planck Institute for Chemistry, Mainz) |
| 8) Oslo | (F. Stordal, Institute for Geophysics, Oslo) |

No two groups used the same algorithm, and there are vast differences in computational efficiency and accuracy of the methods evaluated here. Each model is briefly outlined below.

**1. The GFDL Line-By-Line Model:**

Fels and Schwarzkopf (1981) describe the GFDL line-by-line model as a "substantially-modified version of a code provided by Drayson" (Drayson, 1967). This classical line-by-line model employs an explicit integration over the spectrum. The spectral resolution is variable, with finer spacing near line cores (< 0.001 $cm^{-1}$). A Voigt line shape is used. The sub-Lorentzian behavior of the far wings of $CO_2$ lines is modeled by cutting lines off 3 $cm^{-1}$ from the line center, and renormalizing the line-shape function. The far wings of $H_2O$ and $O_3$ lines are assumed to have Lorentzian profiles. These lines are cut off 10 $cm^{-1}$ from the line center. They use an explicit integration over optical path in the transmission calculation. Four-point Gaussian quadrature is used to perform the integration over zenith angle in the thermal flux equation. These procedures avoid errors produced by the commonly-used Curtis-Godsen and Diffusivity-Factor approximations, respectively.

The GFDL model atmospheres are divided into 123 (case 4), 108 (cases 2 and 3) or 52 (Case 1) levels. The model atmospheres used in cases 2 through 4 extend from the surface to 0.001 mbar (approximately 93 km). The model atmosphere used in case 1 ($H_2O$) extends from the surface to 10 mbar. Vertical levels are equally spaced in log(pressure), but different spacings are used at pressures above and below 100 mbar. At pressures greater than 100 mbar, the vertical resolution is approximately 1/2 km. At lower pressures, the vertical resolution is approximately 1 km. Much finer resolution is used to compute the transmission between nearby layers. Cooling rates were interpolated (or extrapolated) to the 123 level grid for this comparison. These line-by-line computations are based on the 1982 AFGL line catalog (Rothman et al. 1983). Further details of this model are documented in Fels and Schwarzkopf (1981) and Schwarzkopf and Fels (1985).

The GFDL line-by-line cooling rates were provided on a 1600 BPI magnetic tape by Stuart Freidenreich of GFDL. These cooling rates were resolved into 10 $cm^{-1}$ spectral intervals for 18 different model atmospheres. A more complete description of this tape is given in the appendix. Copies of the tape can be obtained from Stuart Freidenreich. The cases and spectral regions chosen here are listed above.

We have discovered two errors in the description of the GFDL $H_2O$ cooling rates that were distributed for this test. First, the GFDL $H_2O$ cooling rates extend only from the surface to 10 mbar. Cooling rates above this level were extrapolated, and not used in this intercomparison. Second, The GFDL model did not include $H_2O$ continuum absorption case 1. This accounts for the large discrepancies in the tropospheric $H_2O$ cooling rates reported by all groups.

## 2. Caltech:

The Caltech algorithm accounts for extinction by gases, clouds, and aerosols. A Voigt quasi-random model is used to find the line absorption by all gases in all spectral regions (see Wyatt et al. 1962 for a general description of these models). The principal approximation used in this narrow band model is that absorption line positions are uncorrelated within narrow spectral regions (5 $cm^{-1}$ for these runs). This simplification usually improves the computational speed by about a factor of 300 over the line-by-line model. Unlike the commonly-used Goody (1952) and Malkmus (1967) random models, the quasi-random model uses a Voigt line shape and an accurate description of the line strength distribution in each narrow spectral region. A direct integration over inhomogeneous optical paths is used to avoid errors introduced by the Curtis-Godsen approximation. The transmission calculation for each spectral interval explicitly accounts for absorption by the far wings of spectral lines with centers outside of that interval. The standard version of this model employs a diffusivity factor approximation instead of an explicit integration over zenith angle in the thermal flux calculation.

The method described by Roberts et al. (1976) is used to account for water vapor continuum absorption. The absorption by cloud and aerosol particles in partially-cloudy model atmospheres can also be included, but multiple scattering is ignored. Only clear (cloud and aerosol free) model atmospheres were used in this comparison. The 123-level ICRCCM model atmosphere was interpolated to a standard 75 layer grid (0 to 65 km) for these tests. Line parameters were obtained from the 1986 version of the AFGL line catalog (Rothman et al. 1987).

## 3. Clarkson:

The Clarkson model uses different broad-band formulations to find the absorption by $CO_2$, $H_2O$ and $O_3$. The $CO_2$ algorithm is based on an emissivity parameterization developed by Ou and Liou (1983). This model uses a polynomial fit to the Fels and Schwarzkopf (1981) line-by-line transmission data.

The ozone model is similar to the method originally described by Rosenfield et al. (1987). A single-interval Malkmus (1967) random model is used to find the transmission in the 9.6 micron band. Doppler and Voigt effects are included by a simple modification to the Lorentz halfwidth (Fels, 1979). A Curtis Matrix approach is used to find the cooling rates by this band. The integration over angle in the thermal flux equation is replaced by the diffusivity-factor approximation.

Water vapor absorption in the 6.3 micron and rotation bands is computed with a method similar to the broad-band model for $CO_2$ described by Ramanathan (1976). Within the $CO_2$ 15 micron band, water vapor absorption is found using a single-interval Goody (1952) random model. The method described by Roberts et al., (1976) is used to include the effects of water vapor continuum absorption at wavelengths between 8 and 12 microns. This model can also account for partially-overlapped black clouds. The 123-level ICRCCM grid was used in these calculations.

## 4. Goddard:

The Goddard model uses different algorithms for finding $CO_2$, $H_2O$ and $O_3$ transmission (Rosenfield et al., 1987; Rosenfield, 1989). The $CO_2$ broad-band transmission algorithm uses precomputed transmissions for a standard atmosphere temperature profile. The temperature dependence of the transmission is treated by a linear expansion method. The standard atmosphere transmission and the linear expansion coefficients are computed by line-by-line calculations at 0.002 $cm^{-1}$ resolution. The $CO_2$ mixing ratio is fixed at 330 ppmv. The line-by-line calculations, which employ a full Voigt profile and

explicit integration over zenith angle, are described in Chou and Kouvaris (1976). The cooling rates computed by this line-by-line code differ from those given in Schwarzkopf and Fels (1985), especially in the 10 mbar region. The Chou and Kouvaris calculations give about 0.4 K/day less cooling than the Schwarzkopf and Fels model. These differences have been attributed to different treatments of the line cutoff. When Chou and Kouvaris increase the limits of the line cutoff, their line-by-line calculations agree much better with those given in Fels and Schwarzkopf (1985).

The $O_3$ transmission algorithm has just been updated (Rosenfield, 1989). The new model divides the 9.6 micron band into band-center and band-wing components, and uses a model with the functional form of the Goody (1952) random model to find the transmission in each region. Band parameters for each region are derived by fitting line-by-line calculations which incorporate Voigt line shape effects.

The broad-band model of Chou (1984) is used to find transmission in water vapor bands. The method of Roberts et al. (1976) is used to include water vapor continuum absorption. Both the ozone and water vapor models use a method similar to the Curtis-Godsen approximation to compute transmission along inhomogeneous atmospheric optical paths. For the ozone model, a diffusivity factor approximation is used to parameterize the effects of integration over zenith angle in the thermal flux calculation. Line parameters for all gases were obtained from the 1982 version of the AFGL line catalog (Rothman et al. 1983). The 123-layer ICRCCM model atmosphere was interpolated to the standard Goddard grid, with 45 levels between the surface and 90 km.

## 5. LLNL:

The radiative transfer code used at Lawrence Livermore National laboratory is based on broad-band parameterizations for $CO_2$, $O_3$ and $H_2O$ that were originally compiled and documented by Harshvardhan et al. (1987). $CO_2$ transmission in the 15 micron is computed using a modified version of the broad-band model of Chou and Peng (1983). This algorithm uses a "far-wing" model at levels below the upper stratosphere, and a different parameterization at higher levels. A single-interval Malkmus (1967) random model (Rodgers, 1968) is used to find the transmission in the 9.6 micron ozone band. Water vapor absorption in the 6.3 micron and rotation bands is computed using the broad-band model (Chou, 1984). The method described by Roberts et al. (1976) is used to compute the water vapor continuum absorption. This algorithm can also account for the extinction by absorbing clouds in a partially-cloudy atmosphere.

## 6. Leningrad:

The radiative transfer model used at the Main Geophysical Laboratory in Leningrad is based on the Goody (1952) random model. The thermal infrared spectrum is divided into 17 spectral intervals. The band parameters in each interval are based on the 1975 AFGL line catalog. The Curtis-Godsen approximation is used to account for variations in the absorber amount, pressure and temperature along inhomogeneous atmospheric optical paths. The diffusivity factor approximation is used instead of an explicit integration over zenith angle in the thermal flux equation. Their model atmosphere uses 2 km vertical resolution between the surface and 60 km.

## 7. Mainz:

The model used at the Max Planck Institute for Chemistry is described in Bruehl and Crutzen (1988). $CO_2$ absorption is derived from a simplified version of the Kiehl and Ramanathan (1983) model. They divide the $CO_2$ 15 micron band into 52 sub-bands. The effects of partial overlap between these sub-bands is included only in the calculation of transmission to space (i.e. the flux at the top of the atmosphere). Total overlap is assumed for all other paths. The Ramanathan and Dickinson (1979) model is used to find $O_3$ transmission. This model has been modified to include contributions from hot and isotopic bands. $H_2O$ absorption in the rotation band is computed using the method of Ramanathan

(1976). The Roberts et al. (1976) model is used to find the $H_2O$ continuum absorption. Heating and cooling rates are computed directly from analytic derivatives of the absorption functions. This model uses 86 levels between the surface and 64 km. Cooling rates were reported only at levels in the stratosphere and lower mesosphere. An approximate method is used to include the effects of tropospheric clouds on the upwelling flux at the base of the model.

### 8. Oslo:

The Oslo model is described in Stordal (1988). The model for $CO_2$ and $O_3$ is based on the wide-band model described by Ramanathan (1976) and Kiehl and Ramanathan (1983). This model explicitly accounts for partially-overlapped hot and isotopic bands, as well as the fundamental band. The Ramanathan and Downey (1986) non-isothermal emissivity formulation is used for $H_2O$. A method similar to the Curtis-Godsen approximation is used to accommodate the effects of changes in the absorber amount, temperature and pressure along inhomogeneous atmospheric optical paths. A diffusivity approximation is used to parameterize the integration over angle in the thermal flux equation.

## RESULTS:

Contributions to the radiative cooling by $H_2O$, $CO_2$, and $O_3$ are shown along with the combined effects of all three gases in Figures 3-5(a - h). $H_2O$ is the principal absorber at tropospheric levels. The standard case chosen from the GFDL tape did not include continuum absorption. This accounts for most of the $H_2O$ cooling rate differences at levels near the surface. The remaining differences among the models are caused primarily by inadequate vertical resolution in the troposphere.

All three gases contribute significantly to the radiative forcing at levels between 50 and 250 mbar. At these levels, $CO_2$ and $H_2O$ cooling must balance the solar and thermal heating by $O_3$. Ozone thermal heating (negative cooling) is produced as upwelling thermal flux from the warm surface and is absorbed by the ozone layer in the cool lower stratosphere. At levels near the stratopause, $CO_2$ produces up to 80% of the cooling. $O_3$ is the next most important absorbing gas, producing about 25% as much cooling as $CO_2$ at these levels. $H_2O$ cooling rates rarely exceed 1 K/Day in the stratosphere. (Note: GFDL cooling rates for $H_2O$ were not available for pressures less than 10 mbar.)

At most stratospheric levels, cooling rates for doubled $CO_2$ (600 ppmv) are comparable to the combined cooling rates from $CO_2$, $H_2O$, and $O_3$ in the present atmosphere (300 ppmv $CO_2$). Differences between the cooling rates obtained by each model and the GFDL line-by-line model are shown in Figures 3-6 and 3-7. The largest cooling rate differences (K/Day) occur at levels near 1 mbar, where the cooling rates are largest. Most models underestimate the GFDL line-by-line cooling rates at these levels [Figure 3-6 (a - g)].

The largest relative differences (Figure 3-7) occur at levels where the GFDL cooling rates approach zero. The large $O_3$ cooling rate differences at levels near 10 mbar in Figure 3-7 are caused by very small differences in the altitude where the $O_3$ cooling rate crosses through zero. Such apparent errors are not a cause for concern in 2-D modeling.

### 1. Caltech:

The Caltech model never differs from the GFDL model by more than 0.7 K/Day, and the differences are always smaller than 0.02 K/day at levels in the middle and lower stratosphere. Errors in the total cooling rate never exceed 8% at stratospheric levels. $CO_2$ cooling rates are overestimated by almost 10% at levels near 5 mbar, but these errors are partially offset by a small underestimate of the $O_3$ cooling rates at this level. $CO_2$ cooling rate errors at levels between 1 and 10 mbar are primarily a consequence of the relatively course spectral resolution used in this comparison. These errors can be reduced by 60% if the

spectral resolution is increased from 5 $cm^{-1}$ to 1 $cm^{-1}$, but we cannot afford to run the model at this higher resolution on the existing MicroVAX computer. The diffusivity factor approximation contributes about 25% of the error for the present atmosphere (300 ppmv) and about 40% of the error for the doubled $CO_2$ case. The Caltech model underestimates the $H_2O$ and $O_3$ cooling rates by up to 10% (0.02 K/Day) at some stratospheric levels, but these errors rarely contribute more than 1% to the total error budget.

### 2. Clarkson:

The Clarkson model underestimates the cooling rates by approximately 20% throughout the stratosphere. Most of this disagreement is caused by an underestimate of the $CO_2$ cooling rates. Systematic errors of this magnitude were somewhat surprising, since the Clarkson $CO_2$ model is based on a polynomial fit to the GFDL line-by-line data (Fels and Schwarzkopf, 1981). These cooling rate differences are partially offset in the middle and lower stratosphere by 20 to 30% overestimates of the $H_2O$ cooling. Ozone cooling rates are overestimated at pressures greater than 1 mbar, and underestimated at lower pressures.

### 3. Goddard:

The Goddard model also underestimates the GFDL cooling at most stratospheric levels, but these models generally differ by more than 1 K/Day. The largest cooling rate differences (20%) occur in the lower stratosphere. $CO_2$ cooling rate differences of 10 to 20% account for most of the disagreement between the Goddard $CO_2$ model and GFDL. The Goddard broad-band model is based on the Chou Kouvaris line-by-line model, which also differs from the GFDL model by about this amount. This disagreement has been attributed primarily to differences between the treatments of the far wings of $CO_2$ lines. The new $O_3$ cooling rate model (Rosenfield 1989) performs very well, rarely producing errors larger than 5%. The $H_2O$ algorithm underestimates the cooling by this gas by 10 to 30% (0.1 K/Day) at levels in the middle and lower stratosphere. Errors in the total cooling rate by all three gases are somewhat larger than the sum of the errors contributed by each component because ozone cooling in the 14 micron band was neglected in the total cooling rate calculation. This weak ozone band contributes up to 0.22 K/Day at some stratospheric levels.

### 4. LLNL:

The LLNL model underestimates the total cooling by 10 to 40% at stratospheric levels. Much of this disagreement can be attributed to underestimates of the $CO_2$ cooling rates. These errors are partially offset at most levels by 20 to 40% overestimates of ozone cooling rates. Errors in the total cooling by all gases are much larger than the sum of the errors by each component because cooling by the 14 micron ozone band was neglected in the total cooling calculation.

### 5. Leningrad:

The Leningrad model underestimates the cooling by up to 30% (0.1 K/Day) in the lower stratosphere, overestimates the cooling by about 10% (1 K/Day) at the 3 mbar level, and underestimates the cooling by up to 40% (5 K/Day) at the 1 mbar level. Crisp et al. (1986) show that these differences are primarily a consequence of the shortcomings of the $CO_2$ line strength distribution and line shape assumed in the Goody random model.

### 6. Mainz:

The performance of the Mainz model is similar to that of the Leningrad model, even though they use very different algorithms. This model overestimates the cooling by 10 to 15% at levels between 2 and 100 mbar, and underestimates the cooling by up to 25% above this level. Most of this discrepancy can be attributed $CO_2$ cooling rate differences. Crisp et al. (1986) show that $CO_2$ cooling rate errors of this magnitude can be produced as a consequence of the neglect of Voigt line shape effects in the Kiehl and Ramanathan (1983) model. Further, $CO_2$ cooling is underestimated because of the assumption of total overlap between the $CO_2$ subbands.

### 7. Oslo:

The Oslo model underestimates the cooling by 10 to 40% throughout the stratosphere. Differences between this model and the Mainz model are somewhat surprising, since both are based on the Ramanathan (1976) algorithm. At pressures less than 5 mbar, much of the disagreement can be attributed to an underestimate of the $CO_2$ cooling rates. A large underestimate of the ozone cooling rates at pressures greater than 5 mbar accounts for most of the errors at those levels.

## CONCLUSIONS:

Several factors contribute to the errors encountered in this investigation. With the exception of the line-by-line model, all of the models employ simplifying assumptions that place fundamental limits on their accuracy and range of validity. For example, all 2-D modeling groups use the diffusivity factor approximation. This approximation produces little error in tropospheric $H_2O$ and $CO_2$ cooling rates, but can produce significant errors (>10%) in $CO_2$ and $O_3$ cooling rates at the stratopause. Much larger errors in $CO_2$ cooling rates (50%) are produced at these levels if Voigt line-shape effects are not accurately modeled. The Curtis-Godson approximation produces little error in $CO_2$ or $H_2O$ cooling rates, but can cause 5 to 10% $O_3$ cooling rate errors in the middle and lower stratosphere. The broad-band convolution of the transmission and the Plank function in the thermal flux equation can produce errors that range from 10 to 50% throughout the stratosphere. Such errors are largely avoided in narrow-band models, but these methods are too computationally expensive for use in applications where cooling rates must be recomputed often. All models suffer from fundamental uncertainties in shapes and strengths of spectral lines.

Thermal flux algorithms currently being used in 2-D tracer transport models produce cooling rates that differ by as much as 40% for the same input model atmosphere. Disagreements of this magnitude are important since the thermal cooling rates must be subtracted from the almost-equal solar heating rates to derive the net radiative heating rates and the 2-D model diabatic circulation. For much of the annual cycle, the net radiative heating rates are comparable in magnitude to the cooling rate differences described above.

Many of the models (Clarkson, Goddard, LLNL and Oslo) underestimate the cooling rates in the middle and lower stratosphere. The consequences of these errors for the net heating rates and the diabatic circulation will depend on their meridional structure, which was not tested here. Other models underestimate the cooling at levels near 1 mbar (Clarkson, Leningrad, Mainz and Oslo). Such errors pose potential problems for future interactive ozone assessment studies, since they could produce artificially-high temperatures and increased $O_3$ destruction at these levels. These concerns suggest that a great deal of work is needed to improve the performance of thermal cooling rate algorithms used in 2-D tracer transport models.

REFERENCES CITED:


Bruehl, C. and P.J. Crutzen, "Scenarios of possible changes in atmospheric temperatures and ozone concentrations due to man's activities, estimated from a one-dimensional coupled photochemical climate model," J. Climate Dynam., 2, 173-203, 1988.

Chou, M.D., "Broadband water vapor transmission functions for atmospheric IR flux computations," J. Atmos. Sci., 41, 1775-1778, 1984.

Chou, M.D. and A. Arking, "Computation of infrared cooling rates in the water vapor bands, J. Atmos. Sci., 37, 856-867, 1980.

Chou, M.D. and L. Kouvaris, "Monochromatic calculations of atmospheric radiative transfer due to molecular line absorption," J. Geophys. Res., 91, 4047-4055, 1986.

Chou, M.D. and L. Peng, "A parameterization of the absorption in the 15 micron $CO_2$ spectral region with applications to climate sensitivity studies," J. Atmos. Sci., 40, 2183-2192, 1983.

Crisp, D., S.B. Fels, and M.D. Schwarzkopf, "Approximate methods for finding $CO_2$ 15 micron band transmission in planetary atmospheres," J. Geophys. Res., 91, 11851-11866, 1986.

Drayson, S.R. "Atmospheric transmission in the $CO_2$ bands between 12 microns and 18 microns," Applied Optics, 5, 385-391, 1967.

Fels, S.B., "Simple strategies for inclusion of Voigt effects in infrared cooling rate calculations," Applied Optics , 18, 2634-2637, 1979.

Fels, S.B. and M.D. Schwarzkopf, "An efficient, accurate algorithm for calculation $CO_2$ 15 micron cooling rates," J. Geophys. Res., 86, 1205-1232, 1981.

Goody, R.M., "A statistical model for water-vapour absorption," Quart. J. Roy. Meteor. Soc., 78, band 165-169, 1952.

Harshvardhan, R. Davies, D.A. Randall, and T.G. Corsetti, "A fast radiation parameterization for atmospheric circulation models," J. Geophys. Res., 92, 1009-1016, 1987.

Kiehl, J.T., and V. Ramanathan, "$CO_2$ radiative parameterizations used in climate models: Comparison with narrow band models and with laboratory data," J. Geophys. Res., 88, 5191-5202, 1983.

Luther, F.M., and Y. Fouquart, "The intercomparison of radiation codes in climate models (ICRCCM) ," WMO Rep. WCP-93, 37 pp., World Meteorological Organization, Geneva, Switzerland, 1984.

McClatchey, R.A., R.W. Fenn, J.E.A. Selby, F.E. Voltz, and J. S. Garing, "Optical properties of the atmosphere (Revised)," Rep. AFCRL-71-0279, 85pp, Air Force Cambridge Research Laboratory, Bedford, MA, 1971.

Ou, S.S. and K.N. Liou, "Parameterization of carbon dioxide 15 micron band absorption and emission, " J. Geophys. Res., 88, 5203-5207, 1983.

Ramanathan, V. "Radiative transfer within the Earth's troposphere and stratosphere, a simplified radiative-convective model," J. Atmos. Sci., 33, 1330-1346, 1976.

Ramanathan, V. and R.E. Dickinson, "The role of stratospheric ozone in the zonal and seasonal ' radiative energy balance of the earth-troposphere system," J. Atmos. Sci., 36, 1084-1104, 1979.

Ramanathan, V. and P. Downey, "A non-isothermal emissivity and absorptivity formulation for water vapor, " J. Geophys. Res., 91, 8649-8666, 1986.

Roberts, R.E., J.E.A. Selby, and L.M. Biberman, "Infrared continuum absorption by atmospheric water vapor in the 8-12 micron window," Applied Optics, 15, 2085-2090, 1976.

Rodgers, C.D., "Some extensions and applications of the new random band model for molecular band transmission ," Quart. J. Roy. Meteor. Soc., 94, 99-102, 1968.

Rosenfield, J.E., M.R. Schoeberl, and M.A. Geller, "A computation of the stratospheric diabatic circulation with an accurate radiative transfer model," J. Atmos. Sci., 44, 859-876, 1987.

Rosenfield, J.E., "A simple parameterization of ozone infrared absorption for atmospheric heating rate calculations ," submitted to J. Geophys. Res., 1989.

Rothman, L.S., R.R. Gamache, A. Barbe, A. Goldman, J.R. Gillis, L.R. Brown, R.A. Toth, J.M. Flaud, and C. Camy-Peyret, "AFGL atmospheric line parameters compilation: 1982 edition," Applied Optics, 22, 2247-2256, 1983.

Rothman, L.S., R.R. Gamache, L.R. Brown, R.A. Toth, H.M. Pickett, R.L. Poynter, J.M. Flaud, C. Camy-Peyrey , A. Barbe, N. Husson, C.P. Rinsland, and M.A.H. Smith, "The HITRAN Database : 1986 edition," Applied Optics, 26, 4058-4096, 1987.

Schwarzkopf, M.D. and S.B. Fels, "Improvements to the algorithm for computing $CO_2$ transmissivities and cooling rates," J. Geophys. Res., 90, 10541-10550, 1985.

Stordal, F. "A wide band model for transfer of infrared radiation: Altitudinal, latitudinal and yearly variation of cooling rates in the troposphere and stratosphere," Institute Report Series, No. 68, Institutt for Geofysikk, Universitetet I Oslo, 1988.

Wyatt, P.J., V. R. Stull, and G.N. Plass, "Quasi-Random Model of band absorption," J. Opt. Soc. Amer., 32, 1209-1217, 1962.

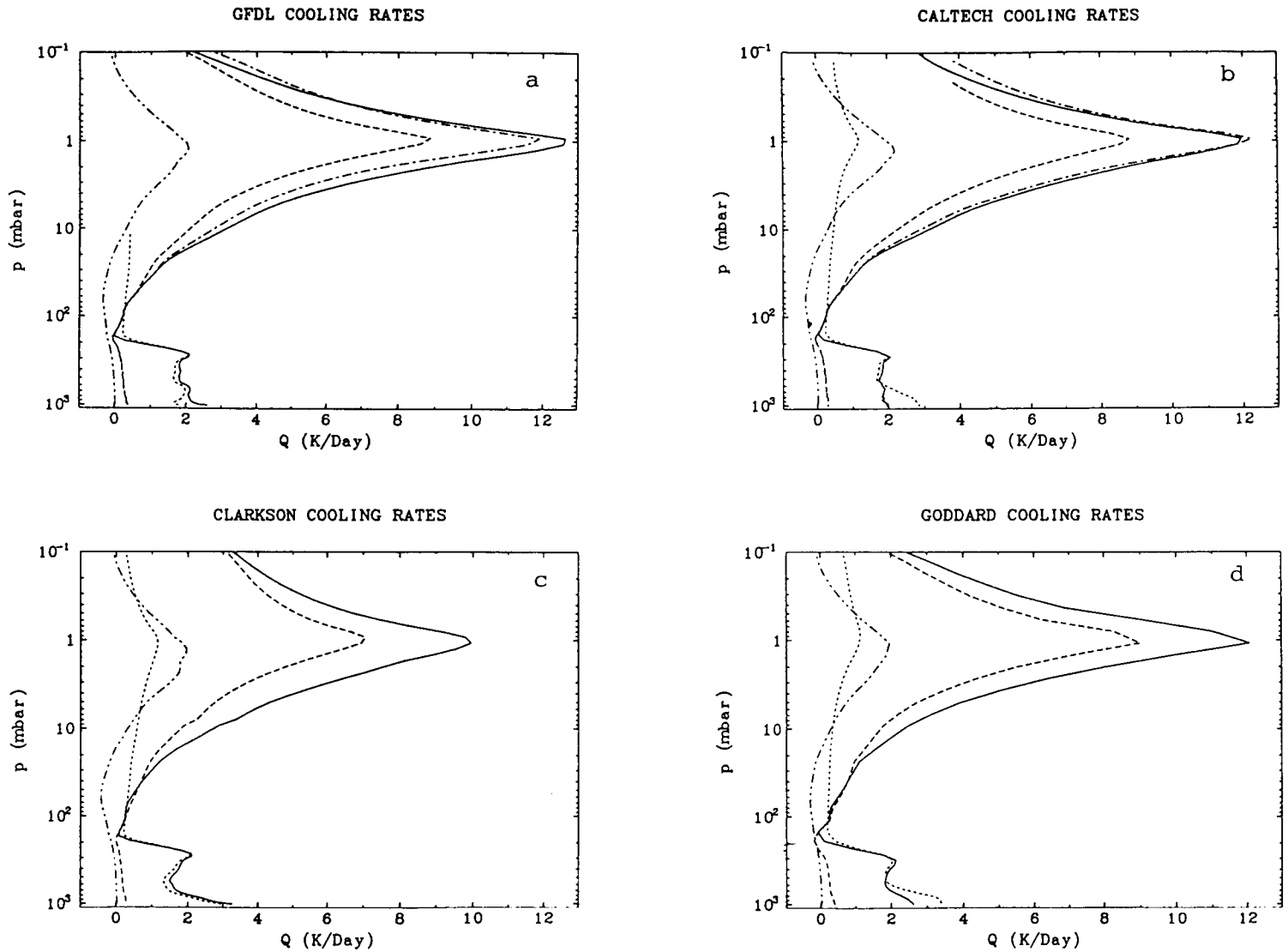


Figure 3-5. Cooling rates for $H_2O$ (dotted), $CO_2$ (long dash), doubled $CO_2$ (dash-dot) and $O_3$ (dash-dot-dot) are shown along with the total cooling rate by all gases (solid) for the: (a) GFDL, (b) Caltech, (c) Clarkson, (d) Goddard, (e) LLNL, (f) Leningrad, (g) Mainz, and (f) Oslo models. All models except the GFDL model include water vapor continuum absorption at tropospheric levels. Water vapor cooling rates for the GFDL model were available only for pressures greater than 10 mbar. No tropospheric cooling rates were given for the Mainz model.

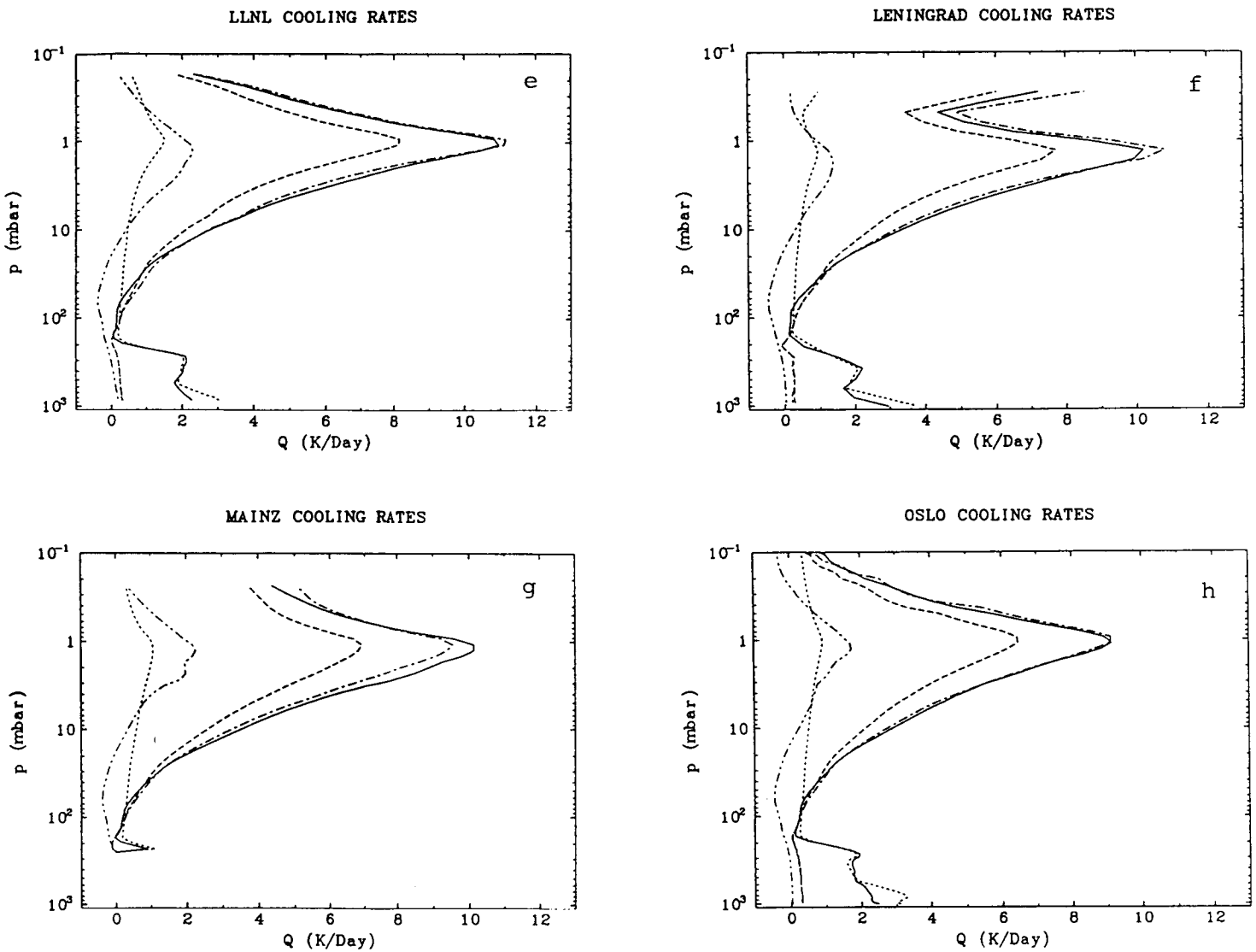


Figure 3-5 (continued). Cooling rates for $H_2O$ (dotted), $CO_2$ (long dash), doubled $CO_2$ (dash-dot) and $O_3$ (dash-dot-dot) are shown along with the total cooling rate by all gases (solid) for the: (a) GFDL, (b) Caltech, (c) Clarkson, (d) Goddard, (e) LLNL, (f) Leningrad, (g) Mainz, and (f) Oslo models. All models except the GFDL model include water vapor continuum absorption at tropospheric levels. Water vapor cooling rates for the GFDL model were available only for pressures greater than 10 mbar. No tropospheric cooling rates were given for the Mainz model.

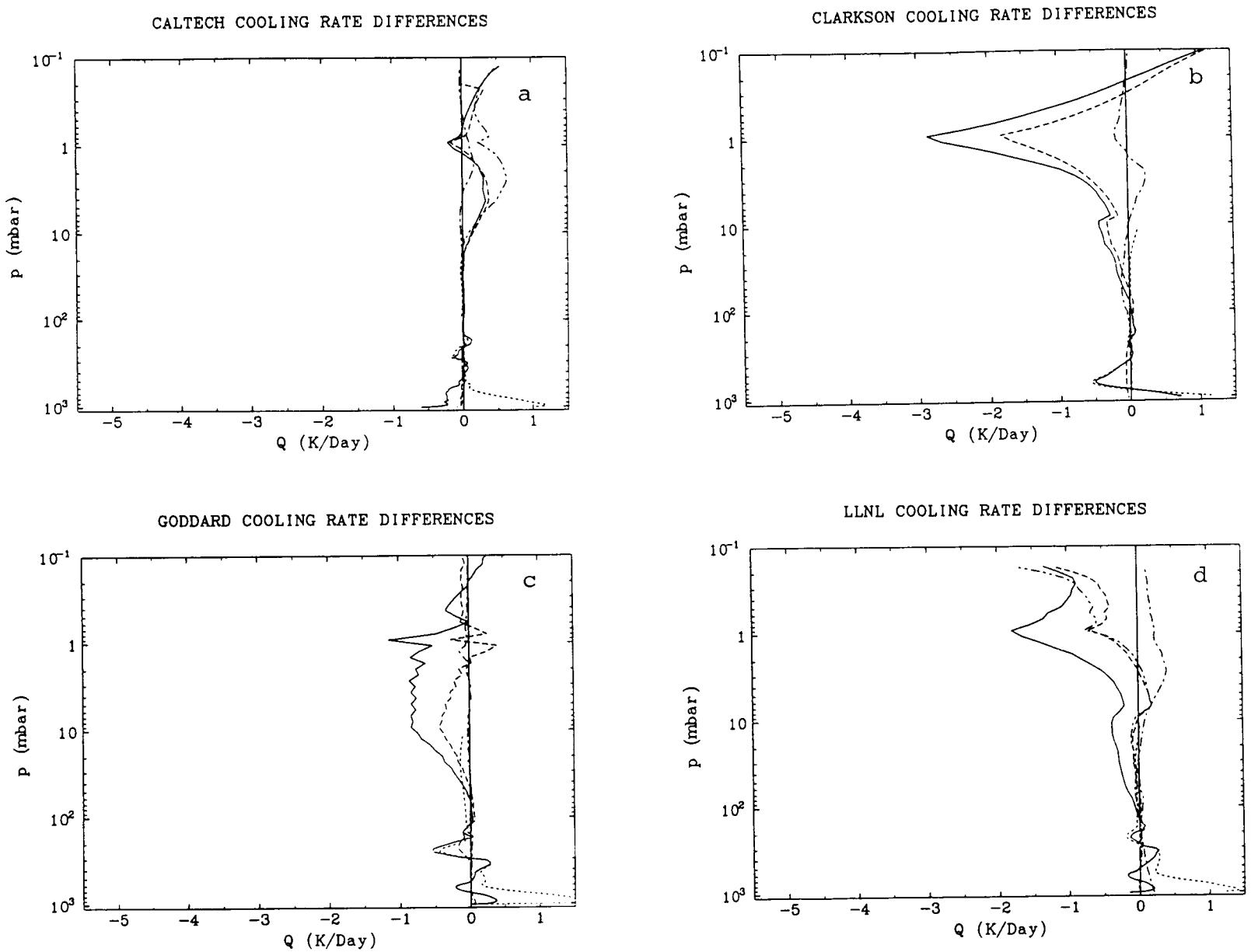


Figure 3-6. Differences between the cooling rates obtained from each model and those from the GFDL line-by-line model are shown for $H_2O$ (dotted), $CO_2$ (330 ppmv, long dash; 660 ppmv, dash-dot-dot), $O_3$ (dash-dot), and the total cooling rate by all three gases (solid).

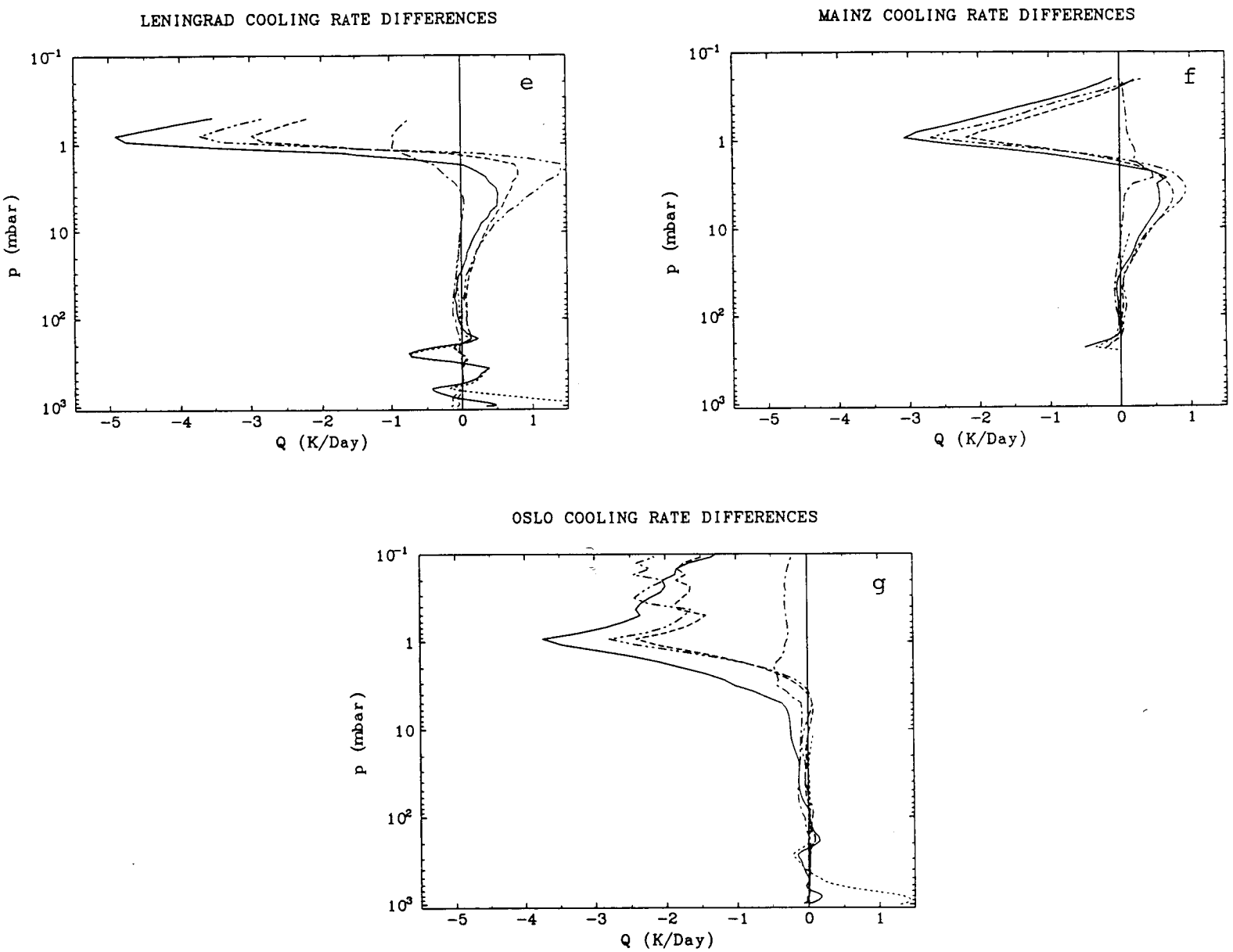


Figure 3-6 (continued). Differences between the cooling rates obtained from each model and those from the GFDL line-by-line model are shown for $H_2O$ (dotted), $CO_2$ (330 ppmv, long dash; 660 ppmv, dash-dot-dot), $O_3$ (dash-dot), and the total cooling rate by all three gases (solid).

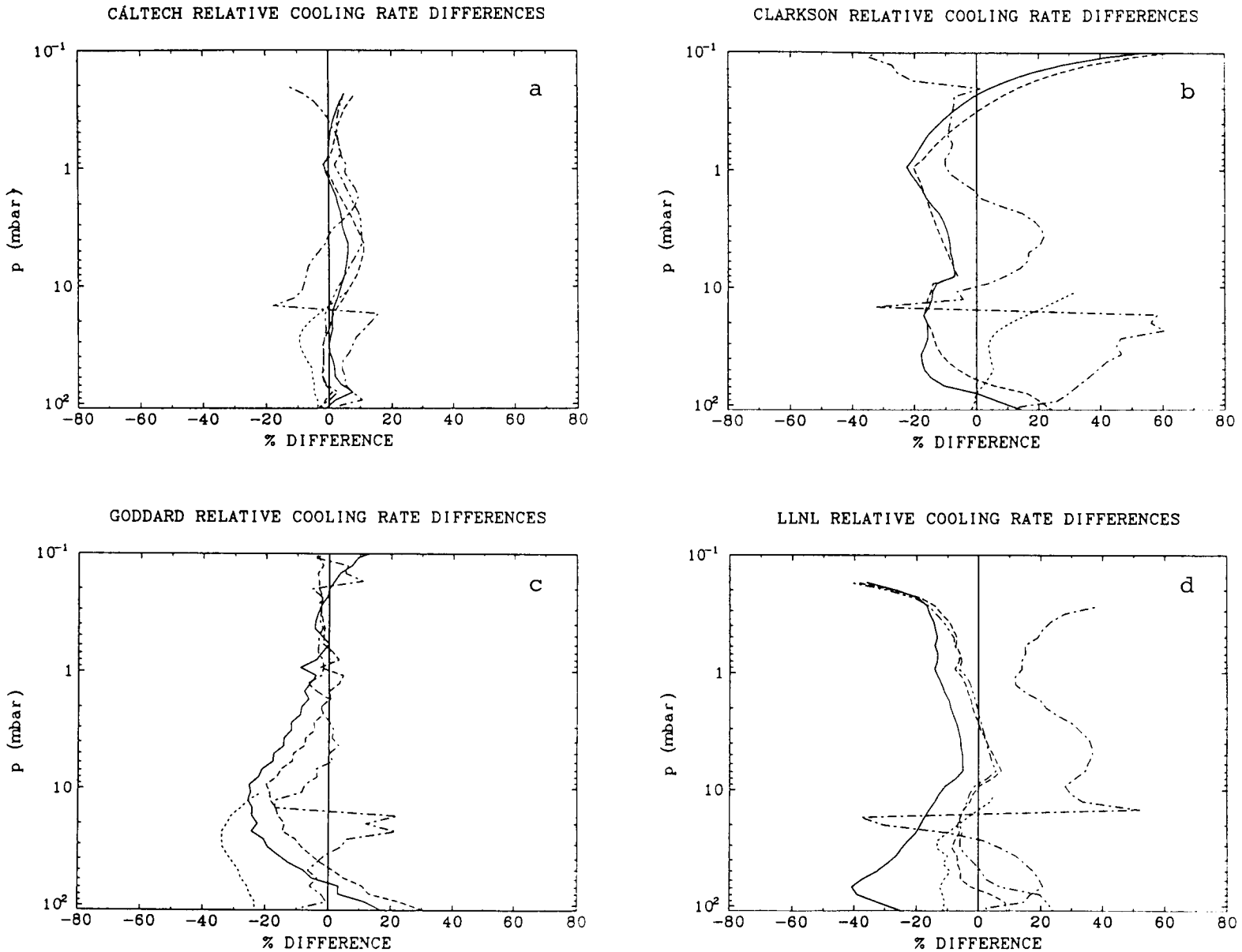


Figure 3-7. Relative differences (%) between the cooling rates obtained from each model and those from the GFDL line-by-line model are shown for $H_2O$ (dotted), $CO_2$ (330 ppmv, long dash; 660 ppmv, dash-dot-dot), $O_3$ (dash-dot), and the total cooling rate by all three gases (solid).

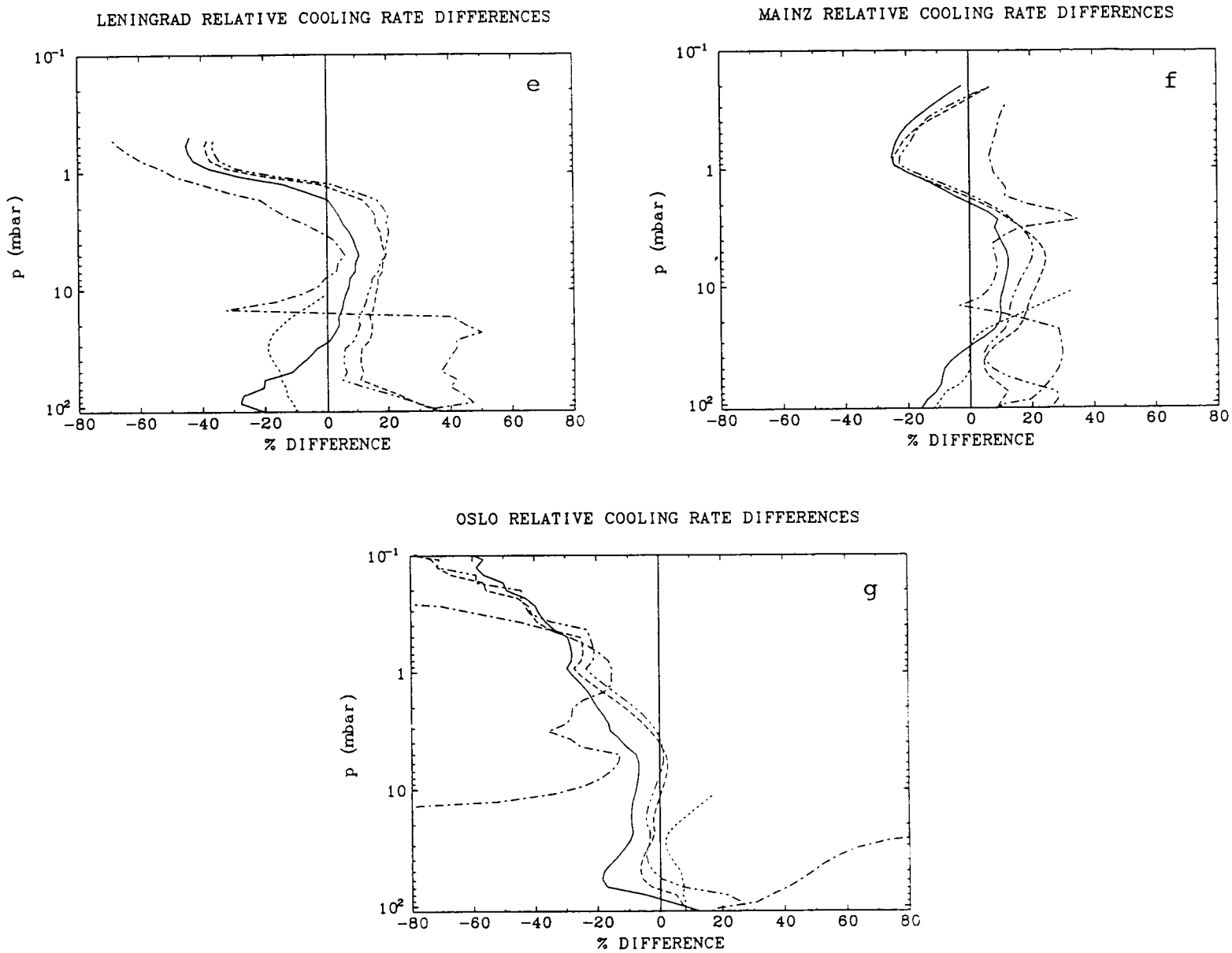


Figure 3-7 (continued). Relative differences (%) between the cooling rates obtained from each model and those from the GFDL line-by-line model are shown for $H_2O$ (dotted), $CO_2$ (330 ppmv, long dash; 660 ppmv, dash-dot-dot), $O_3$ (dash-dot), and the total cooling rate by all three gases (solid).

```
C*********************************************************************
C*                                                                   *
C* THIS TAPE WAS GENERATED AT:                                       *
C*                                                                   *
C*            GEOPHYSICAL FLUID DYNAMICS LABORATORY / NOAA           *
C*                        PRINCETON UNIVERSITY                       *
C*                            P.O. BOX 308                           *
C*                    PRINCETON, NEW JERSEY 08542                    *
C*                            (609) 452-6500                         *
C*                                                                   *
C* QUESTIONS OR SUGGESTIONS REGARDING ITS USAGE CAN BE DIRECTED TO:  *
C*                                                                   *
C*         STUART FREIDENREICH      ROOM 226     (609) 452-5279      *
C*         DAN SCHWARZKOPF          ROOM 246     (609) 452-6521      *
C*                                                                   *
C*********************************************************************
C* THIS IS A NON-LABEL, 9-TRACK, 1600 B.P.I. TAPE WRITTEN IN ASCII   *
C* FORMAT WITH A RECORD SIZE OF 80 AND BLOCK SIZE OF 4000.           *
C*********************************************************************
C*                                                                   *
C* THIS TAPE CONTAINS TWO MAIN SOURCES OF INFORMATION:               *
C*                                                                   *
C* 1.  TEMPERATURE AND MIXING RATIO (WATER VAPOR AND OZONE ONLY) DATA *
C*     AS A FUNCTION OF PRESSURE FOR VERTICAL GRIDS OF VARIOUS       *
C*     RESOLUTIONS AND ATMOSPHERIC STRUCTURES OF VARIOUS CLIMATIC    *
C*     REGIMES.                                                      *
C*                                                                   *
C* 2.  FLUX AND HEATING RATE DATA AS A FUNCTION OF FREQUENCY BAND AND*
C*     PRESSURE FOR ATMOSPHERES OF VARIOUS COMPOSITIONS, VERTICAL GRIDS*
C*     OF VARIOUS RESOLUTIONS AND ATMOSPHERIC STRUCTURES OF VARIOUS  *
C*     CLIMATIC REGIMES.                                             *
C*                                                                   *
C*********************************************************************
C*                                                                   *
C* THIS TAPE IS STRUCTURED AS FOLLOWS:                               *
C*                                                                   *
C* FILE 1 CONTAINS THE TAPE DOCUMENTATION AS WELL AS A PROGRAM TO BOTH *
C* READ THE TAPE AND WRITE OUT THE DATA FOR ONE CASE.                *
C*                                                                   *
C* FILES 2 TO 20 CONTAIN THE DATA FOR THE DIFFERENT CASES. THE       *
C* CHARACTERISTICS OF EACH FILE ARE DESCRIBED BELOW:                 *
C*                                                                   *
C*                                NUMBER OF      TYPE     FREQUENCY ICRCCM*
C*          ATMOSPHERIC             FLUX         OF       BAND      CASE *
C* FILE     CONSTITUENT(S)         LEVELS     ATMOSPHERE  REGION    NUMBER*
C*                                                                   *
C*   2    CO2(300PPMV)              108          MLS     0-3000CM-1    9  *
C*   3    H2O                        52          MLS     0-3000CM-1   20  *
C*   4    O3                        108          MLS     0-3000CM-1   23  *
C*   5    CO2(300PPMV)+H2O+H2O      123          MLS     0-3000CM-1   27  *
C*        CONTINUUM+O3                                                   *
C*   6    CO2(300PPMV)+H2O+O3+H2O 123            MLS     0-3000CM-1    -  *
C*        CONTINUUM+CH4(1.75PPMV)+                                       *
C*        N2O(0.28PPMV)                                                  *
C*   7    H2O+H2O CONTINUUM          52          MLS     0-3000CM-1   19  *
C*   8    H2O+H2O CONTINUUM          52           T      0-3000CM-1    -  *
C*   9    CO2(300PPMV)              108           T      0-2200CM-1    7  *
C*  10    CO2(600PPMV)              108          MLS     0-2200CM-1   10  *
C*  11    CO2(300PPMV)              108          MLW     0-2200CM-1   11  *
C*  12    CO2(300PPMV)              108          SAW     0-2200CM-1   15  *
C*  13    O3(1.25 X O3 IN           108          MLS     0-2200CM-1   24  *
C*        STRATOSPHERE)                                                  *
C*  14    O3(0.75 X O3 IN           108          MLS     0-2200CM-1   24  *
```

```
C*        STRATOSPHERE)                                                 *
C*  15    CO2(300PPMV)+H2O+H2O     123          T      0-2200CM-1   25  *
C*        CONTINUUM+O3                                                  *
C*  16    CO2(600PPMV)+H2O+H2O     123         MLS     0-2200CM-1   28  *
C*        CONTINUUM+O3                                                  *
C*  17    CO2(300PPMV)+H2O+H2O     123         MLW     0-2200CM-1   29  *
C*        CONTINUUM+O3                                                  *
C*  18    CO2(300PPMV)+H2O+H2O     123         SAW     0-2200CM-1   33  *
C*        CONTINUUM+O3                                                  *
C*  19    N2O(0.28PPMV)             52         MLS     0-3000CM-1   37  *
C*  20    H2O                      108         MLS     0-2200CM-1   20  *
C*                                                                      *
C*  KEY:    MLS - MIDDLE LATITUDE SUMMER      SAW - SUBARCTIC WINTER    *
C*          MLW - MIDDLE LATITUDE WINTER      T   - TROPICAL            *
C*                                                                      *
C**********************************************************************
C*                                                                      *
C*    I N P U T    D A T A :                                           *
C*                                                                      *
C*     ICASE - EXPERIMENT CASE NUMBER (1 - 19)                          *
C*    IFILE1 - UNIT NUMBER OF INPUT FILE (30)                           *
C*    IFILE2 - UNIT NUMBER OF OUTPUT FILE (40)                          *
C*    infile - NAME OF INPUT FILE (CHARACTER*(*))                       *
C*   outfile - NAME OF OUTPUT FILE (CHARACTER*(*))                      *
C*      FMIN - MINIMUM WAVENUMBER FOR OUTPUT (CM**-1)                   *
C*      FMAX - MAXIMUM WAVENUMBER FOR OUTPUT (CM**-1)                   *
C*     ITYPE - TYPE OF OUTPUT DESIRED:                                  *
C*             1) SPECTRALLY-DEPENDENT FLUXES AND HEATING RATES.        *
C*             2) SPECTRALLY-INTEGRATED FLUXES AND HEATING RATES        *
C*                                                                      *
C* THE DATA FOR EACH FILE ARE ORGANIZED AS FOLLOWS:                     *
C*                                                                      *
C* EXPNM           : CHARACTER STRING DEFINING THE EXPERIMENT           *
C*                                                                      *
C* THE PRESSURE, TEMPERATURE AND MIXING RATIO DATA ARE WRITTEN OUT AS:  *
C*                                                                      *
C*    PFLUX, TFLUX, PDATA, TDATA, RATH2O, RATO3                         *
C*                                                                      *
C* PFLUX(I=1,NLP)  : PRESSURE (IN MB) AT FLUX LEVELS                    *
C* TFLUX(I=1,NLP)  : TEMPERATURE (IN K) AT FLUX LEVELS                  *
C* PDATA(I=1,NL)   : PRESSURE (IN MB) AT DATA LEVELS                    *
C* TDATA(I=1,NL)   : TEMPERATURE (IN K) AT DATA LEVELS                  *
C* RATH2O(I=1,NL)  : MASS MIXING RATIO OF WATER VAPOR AT THE DATA LEVELS*
C* RATO3(I=1,NL)   : MASS MIXING RATIO OF OZONE AT THE DATA LEVELS      *
C* NL              : NUMBER OF DATA LEVELS OR NUMBER OF LAYERS          *
C* NLP             : NUMBER OF FLUX LEVELS (NL+1) (=52, 108, 123 )      *
C*                                                                      *
C* THE FLUX AND HEATING RATE DATA ARE WRITTEN OUT AS:                   *
C*                                                                      *
C*    FLX, UPFLUX, DNFLUX, HEAT                                         *
C*                                                                      *
C* FLX(I=1,NLP; N=1,NBANDS)     : NET FLUX AT FLUX LEVELS IN W/M2 FOR   *
C*                                EACH BAND                             *
C* UPFLUX(I=1,NLP; N=1,NBANDS)  : UPWARD FLUX AT FLUX LEVELS IN W/M2 FOR*
C*                                EACH BAND                             *
C* DNFLUX(I=1,NLP; N=1,NBANDS)  : DOWNWARD FLUX AT FLUX LEVELS IN W/M2  *
C*                                FOR EACH BAND                         *
C* HEAT(I=1,NL; N=1,NBANDS)     : HEATING RATE AT DATA LEVELS IN DEG/DAY*
C*                                FOR EACH BAND                         *
C*                                                                      *
C*    FLXTRP, FLXTRU, FLXTRD                                            *
C*                                                                      *
C* FLXTRP(N=1,NBANDS)           : NET FLUX AT TROPOPAUSE LEVEL IN W/M2  *
```

```
C*                                  FOR EACH BAND                          *
C* FLXTRU(N=1,NBANDS)            : UPWARD FLUX AT TROPOPAUSE LEVEL IN      *
C*                                  W/M2 FOR EACH BAND                     *
C* FLXTRD(N=1,NBANDS)            : DOWNWARD FLUX AT TROPOPAUSE LEVEL IN    *
C*                                  W/M2 FOR EACH BAND                     *
C*                                                                         *
C*    SUMFLX, SUMFLU, SUMFLD, SUMHT                                        *
C*                                                                         *
C* SUMFLX(I=1,NLP)               : SUM (OVER FREQUENCY) OF NET FLUX AT     *
C*                                  FLUX LEVELS IN W/M2                    *
C* SUMFLU(I=1,NLP)               : SUM (OVER FREQUENCY) OF UPWARD FLUX AT*
C*                                  FLUX LEVELS IN W/M2                    *
C* SUMFLD(I=1,NLP)               : SUM (OVER FREQUENCY) OF DOWNWARD FLUX   *
C*                                  AT FLUX LEVELS IN W/M2                 *
C* SUMHT(I=1,NL)                 : SUM (OVER FREQUENCY) OF HEATING RATE    *
C*                                  AT DATA LEVELS IN DEG/DAY              *
C*                                                                         *
C*    SUMTRP, SUMTRU, SUMTRD                                               *
C*                                                                         *
C* SUMTRP                        : SUM (OVER FREQUENCY) OF NET FLUX AT     *
C*                                  TROPOPAUSE LEVEL IN W/M2               *
C* SUMTRU                        : SUM (OVER FREQUENCY) OF UPWARD FLUX AT*
C*                                  TROPOPAUSE LEVEL IN W/M2               *
C* SUMTRD                        : SUM (OVER FREQUENCY) OF DOWNWARD FLUX   *
C*                                  AT TROPOPAUSE LEVEL IN W/M2            *
C* NBANDS                        : NUMBER OF FREQUENCY BANDS( = 220, 300)*
C*                                  (EACH BAND IS 10CM-1 WIDE)             *
C*                                                                         *
C*************************************************************************
C*                                                                         *
C* NOTES:                                                                  *
C*                                                                         *
C*   FLUXES WERE DETERMINED FROM LINE-BY-LINE CALCULATIONS USING THE       *
C*   AIR FORCE GEOPHYSICS LAB CATALOG OF LINES. CASES BASED ON             *
C*   FREQUENCY BANDS FROM 0-3000CM-1 USE THE 1982 VERSION, AND CASES       *
C*   BASED ON FREQUENCY BANDS FROM 0-2200CM-1 USE THE 1980 VERSION.        *
C*                                                                         *
C*   VERTICAL PROFILES OF TEMPERATURE AND MIXING RATIO OF WATER VAPOR      *
C*   AND OZONE ARE THE QUANTITIES DEPENDENT ON THE TYPE OF ATMOSPHERE      *
C*   SPECIFIED (MLS, SAW, ETC.).                                           *
C*                                                                         *
C*   TEMPERATURE PROFILES ARE FROM MCCLATCHY ET AL., 1971 AS MODIFIED      *
C*   BY THE "PTZ" PROCEDURE (FELS, 1986).                                  *
C*                                                                         *
C*   THE STANDARD CO2 VOLUME MIXING RATIOS USED ARE 300PPMV AND 600PPMV*
C*                                                                         *
C*   THE STANDARD N2O VOLUME MIXING RATIO USED IS 0.28PPMV.                *
C*                                                                         *
C*   THE STANDARD CH4 VOLUME MIXING RATIO USED IS 1.75PPMV.                *
C*                                                                         *
C*   TROPOPAUSE LEVEL IS AS DEFINED BY THE ICRCCM PROTOCOL.                *
C*                                                                         *
C*   DATA LEVELS ARE DEFINED HALFWAY BETWEEN FLUX LEVELS.                  *
C*                                                                         *
C*   MIXING RATIO VALUES OF WATER VAPOR AND OZONE ARE WRITTEN OUT AS       *
C*   ZERO'S IF NO SUCH DATA IS USED FOR A PARTICULAR CASE.                 *
C*                                                                         *
C*************************************************************************
C*                                                                         *
C* NOTES ON USAGE:                                                         *
C*                                                                         *
C*   USER DEFINES THE CASE NUMBER TO BE READ AND WRITTEN OUT AND THE       *
C*   UNIT NUMBERS FOR THE READ AND WRITE STATEMENTS IN A PARAMETER         *
```

```
C*    STATEMENT ( ICASE, IFILE1, IFILE2, RESPECTIVELY ).                *
C*                                                                       *
C*    USER MAY WISH TO MODIFY THE FORMAT FOR WRITING OUT THE DATA (E.G. *
C*    WRITING OUT ONLY SELECTED BANDS). NOTE HOWEVER THAT THE ARRAYS    *
C*    'FLX', 'UPFLUX', 'DNFLUX' AND 'HEAT' CAN ONLY BE READ AND WRITTEN *
C*    OUT IN THE SAME LOOP UNLESS THE ARRAYS ARE MADE TWO DIMENSIONAL   *
C*    WITH 'NBANDS' AS THE SECOND DIMENSION.                            *
C*                                                                      *
C*    THE PROGRAM CAN BE MODIFIED TO PROCESS MORE THAN ONE CASE IN A    *
C*    SINGLE RUN BY LOOPING OVER THE EXECUTABLE PORTION OF THE CODE AND *
C*    INCREMENTING THE UNIT NUMBERS IN THE READ AND WRITE STATEMENTS.   *
C*                                                                      *
C***********************************************************************
C
```

# CHAPTER 4

# MODEL DOCUMENTATION

**The following is a list of modeling groups along with a brief description of the respective models.**

## Section 4.1 AER 2-D Model

M.K.W. Ko, D. Weisenstein, N.D. Sze
Atmospheric and Environmental Research, Inc.
840 Memorial Drive
Cambridge, Massachusetts 02139
(617) 547-6207

# Description of the AER 2-D Photochemical Transport Model

## Model Domain and Resolution

The AER 2-D model domain extends from south pole to north pole and approximately from the ground to 55 km. Latitude ($\phi$) and the logarithm of the equilibrium pressure ($\zeta = \log(p_o/p_e)$, $p_o$ = 1000 mb) are used as coordinates. The equilibrium pressure, $p_e$, is a pressure-like variable which is a function of potential temperature ($\theta$) defined as

$$p_e = p_o\left[\frac{T_e}{\theta}\right]^{\frac{1}{k}}$$

where $T_e$ is latitudinally-averaged radiative equilibrium temperature, $k = R/c_p$. The model grid uses 19 latitudes and 17 heights. The latitudinal resolution is approximately 9.5 degrees. The vertical levels are constant in $\zeta$ with $\Delta\zeta = 0.5$, corresponding to approximately 3 km. The coordinates for the grid point (i,j) at the center of the box are defined in latitude and equilibrium pressure as follows:

$$\phi = \left[(i - 10)*\frac{180}{19}\right], \qquad i = 1,19$$

$$p_e = 1000*\exp(-.5*j + .25), \qquad j = 1,17$$

The grid boxes are centered one-half space away from model boundaries. Tracer concentrations are defined at grid box centers and fluxes are defined at grid box edges.

## Transport Treatment

Dynamical transport within the model is affected by the zonal-mean diabatic circulation, by quasi-horizontal diffusion along isentropic surfaces, and by vertical diffusion in the troposphere and upper stratosphere. The diabatic circulation was derived by combining the calculated heating rates from Murgatroyd and Singleton (1961) for the upper stratosphere and Dopplick (1979) for the lower stratosphere into a sum of hyperbolic secant functions which is continuous over the model domain. Tracer concentrations depend critically on the details of the circulation in the lower stratosphere, where heating rates are small (less than 1°/day) and poorly determined. Our diabatic heating rates resemble those derived by Rosenfeld et al. (1987) in both structure and magnitude. The vertical velocity is derived from the diabatic heating by:

$$w_e = - \rho g \frac{Q}{\Gamma}$$

where $w_e = dp_e/dt$, $\rho$ is the air density, g the gravitational acceleration, Q the diabatic heating rate, and $\Gamma$ the static stability parameter. To ensure mass continuity, $w_e$ has to be adjusted so that the global average of $w_e$ along a $p_e$ surface vanishes. This is approximately equivalent to adjustment of Q to ensure that the global average heating vanishes. Horizontal motions are derived from continuity:

$$\frac{1}{a \cos\phi} \frac{\partial}{\partial\phi} (v \cos\phi) + \frac{\partial w_e}{\partial p_e} = 0$$

where a is the earth's radius. The stream function, defined by:

$$\psi(p_e,\phi) = \int_{-90}^{\phi} w_e(p_e,\phi') \; a \cos\phi' \; d\phi$$

is determined for four seasons and interpolated every time step.

The horizontal eddy diffusion coefficient, $K_{yy}$, for the troposphere and lower stratosphere varies from $3x10^9$ cm²/sec at low latitudes to $6x10^9$ cm²/sec at mid-latitudes in fall and winter or $2x10^{10}$ cm²/sec at mid-latitudes in spring and summer. These values yield a good fit to observed ozone profiles in the lower stratosphere and are close to the magnitudes derived by Newman and Schoeberl (1986). The value of $K_{yy}$ in the stratosphere above 25 km is $3x10^9$ cm²/sec for all latitudes and seasons. This is based on the work of Kida (1983) and Tung (1984) in estimating an average horizontal diffusion coefficient for the stratosphere.

The vertical diffusion coefficient is $1 \times 10^5$ cm²/sec in the troposphere, $1 \times 10^3$ cm²/sec in the stratosphere below 40 km, and $1 \times 10^4$ cm²/sec above 40 km. The relatively large vertical diffusion coefficient in the troposphere simulates convective overturning and synoptic scale eddies. Stratospheric vertical diffusion was estimated by Kida (1983) to be $1 \times 10^3$ cm²/sec. Enhanced vertical mixing above 40 km is based on the work of Garcia and Solomon (1985) regarding gravity wave breaking.

Chemical Treatment

The chemistry scheme contains about 50 chemical species which interact through 130 reactions. Reactions for the oxygen, hydrogen, methyl, nitrogen, and chlorine families are included in all model calculations. Chemistry for bromine and fluorine species can be included as an option. Water vapor concentration is not calculated, but is parameterized in the stratosphere based on the Nimbus 7 observations of Remsberg et al. (1984). The tropospheric values of $H_2O$ vary seasonally depending on the parameterized value of relative humidity.

The chemical scheme employs the grouping technique to deal with chemicals having vastly different atmospheric lifetimes. Short-lived species are always in chemical equilibrium with their surroundings and their concentrations vary diurnally. Long-lived species vary only on the scale of weeks or months and therefore are affected by atmospheric motions.

The AER 2-D model does explicit diurnal calculations of the short-lived chemical species. An iterative newton scheme is used to solve for all the fast species simultaneously, making 10 steps for the daylight hours and 5 steps for the nighttime hours until 24-hour periodicity is reached. The fast species are computed for a given day while holding the sum of the odd chlorine species, the sum of the odd nitrogen species, and the concentrations of other slow species fixed. Production and loss rates for the slow species are then computed. These production and loss rates are used to compute the chemical source terms (production rate and loss frequency) in the advection equation for the next 10 days of model simulation.

The kinetic reaction rates and absorption cross sections are those given by NASA/JPL (1987). The solar fluxes are from WMO/NASA (1982). The spectral resolution is 5 nm or less over the wavelength range from 93 nm to 405 nm. Photolysis rates were computed with allowance for the effects of Rayleigh

## Section 4.2 CALJPL 2-D Model

Y.L. Yung, D. Crisp, and R.W.Zurek
California Institute of Technology and Jet Propulsion Laboratory

Model Domain and Resolution

Height: 0-80 km (variable), ~2 km resolution, log p coordinate
Latitude: Pole-to-Pole, $\Delta\theta$ = 10° (variable)

Transport Treatment: Modular Radiative-Dynamic-Chemical Model

Residual-mean stream function algorithm
Net Heating computed by independent radiation code
Mass continuity equation solved using Prather's method
Chemistry taken from 1-D Caltech model (45 species)

Radiation:

Complete "physical" radiative transfer model that uses distributions of T and $H_2O$, $CO_2$, $O_3$, $O_2$ $N_2O$, $NO_2$, and $CH_4$ amounts as inputs (Crisp et al., 1986)

Chemistry Treatment:

Family Groups (Initially)

Kinetics: Demore et al., 1986

1000Å - 8000Å, Wavelength interval = 50Å
Diurnal Averaging: same as 1-D (Allen et al., 1981)
Cross-sections: DeMore et al.(1986); Allen and Frederick (1982) for $O_2$ Schumann-Runge Bands; Froidevaux and Yung (1982) for Herzberg Continuum.
Multiple scattering and albedo treatment same as Froidevaux (1983)

Heterogeneous Removal:

Rainout for soluble species (as in 1-D CIT model)

scattering and cloud albedo using a radiative transfer model described by Sze (1976) and Sze et al. (1981).

Heterogeneous removal processes are used to remove $H_2O_2$, $CH_3OOH$, $CH_2O$, $NO_y$, $Cl_y$, $Br_x$, and $F_x$ in the lowest three layers of the model. Fixed first order loss rates, based on Wofsy (1976), are used to simulate washout and rainout with lifetimes of 5 days, 10 days, and 40 days for levels 1, 2, and 3, respectively.

Integration Algorithm

Concentrations of long-lived atmospheric species are integrated forward in time, with the change in mixing ratio per unit time given by:

$$\frac{\partial f}{\partial t} = -\frac{1}{a\cos\phi}\frac{\partial}{\partial\phi}(f v\cos\phi) - e^{\zeta}\frac{\partial}{\partial\zeta}(f we^{-\zeta}) + \frac{1}{a^2\cos\phi}\frac{\partial}{\partial\phi}\left[k_{yy}\cos\phi\frac{\partial f}{\partial\phi}\right]$$

$$+ e^{\zeta}\frac{\partial}{\partial\zeta}\left[k_{zz}e^{-\zeta}\frac{\partial f}{\partial\zeta}\right] + P - Lf$$

where f represents the zonal-mean volume mixing ratio of a trace atmospheric species, v is the horizontal transport velocity, w the vertical transport velocity ($w=d\zeta/dt=-w_e/p_e$), and $K_{yy}$ and $K_{zz}$ are the horizontal and vertical eddy mixing coefficients, respectively. Chemical production and loss is represented by the terms P and Lf, respectively.

The finite differencing scheme used is that developed by Smolarkiewicz (1984). It is a multi-dimensional iterative upstream scheme which removes much of the implicit diffusion of upwind differencing by adding a corrective step to each time step. Negative mixing ratios are not generated provided the time step is small enough. The scheme computes fluxes at grid box boundaries and transports mass only in the direction of fluid flow.

The time step used in the AER model is 12 hours, or 2 steps per day. This yields a CFL parameter of 0.02 or less over most of the model domain, with a maximum value of 0.3 near the upper boundary.

## Description of AERI, the Interactive Model

A description of the scheme for calculating the radiative and dynamical variables for the interactive model can be found in "An Evaluation of the Role of Eddy Diffusion in Stratospheric Interactive 2-D Models" by H.R. Schneider, M.K.W. Ko, N.D. Sze, G.Y. Shi, and W.C. Wang, in press, J. Atmos. Sci., 1989.

## Section 4.3 CAMBRAL 2-D Model

J.A. Pyle and R.S. Eckman[1]
Department of Physical Chemistry
University of Cambridge
Lensfield Road
Cambridge CB2 1EP
UK

Lesley Gray
Rutherford Appleton Laboratory
Chilton, Didcot
Oxon OX1 0QX
UK

### UK 2D Eulerian - Mean Circulation Model

Model domain

"pole-to-pole" $\Delta y = \pi/19$

0-60 km (chemistry) $\Delta z$ = 1/2 scale height (~3.5 km)
0-90 km (dynamics)

$\Delta t$ = 4 hours (diurnally averaged)

Dependent variables

Temperature, wind components, chemical constituents

Dynamics

Thermal wind balance is maintained. A second-order partial differential equation solved for the meridional stream function given the forcing by radiative and diabatic heating and eddy heat and momentum fluxes.

Eddy transport of heat and matter employs Reed and German's (1965) diffusion using Luther's (1973) monthly-averaged K's.

Eddy momentum transport derived from satellite data (Crane et al, 1980) above 50 mb and taken from Oort and Rasmussen (1971) below 50 mb.

Rayleigh friction employed to parameterize effect of breaking gravity waves in mesosphere. Friction coefficient is equal to zero below 50 km and rises to 1 day$^{-1}$ at ~85 km.

[1] Now at NASA Langley Research Center

Photochemistry

Family grouping as follows-

$O(^1D)$, O, $O_3$
N, NO, $NO_2$, $NO_3$, $ClONO_2$
$HO_2NO_2$
H, OH, $HO_2$
Cl, ClO, $ClONO_2$, HCl, HOCl
$CFCl_3$
$CF_2Cl_2$
$CCl_4$
$CH_3Cl$
$CH_3CCl_3$
$N_2O_5$
$CH_4$
$N_2O$
$HNO_3$
$H_2O_2$
$H_2O$

Constant volume mixing ratios above top boundary of photochemical scheme (~60 km).

Reaction rates from DeMore et al. (1987).

Tropospheric rainout rates: first-order removal rates for $HNO_3$, HCl, $HO_2NO_2$, and $H_2O_2$.

Radiation

Curtis matrix method for $CO_2$ 15μm band.

Cooling to space approximation for $O_3$ 9.6μm band.

Heating due to absorption of solar radiation by $O_2$ and $O_3$. Use solar fluxes from WMO (1981) and absorption cross sections based on WMO (1985) and DeMore et al. (1987).

Infrared cooling and solar heating calculated above 25 km.

Radiative equilibrium or fixed heating rates used from tropopause to 25 km.

Fixed heating rates in troposphere.

References

Harwood and Pyle, 1975, Q.J.R. Met. Soc., 101, 723.
Pyle, 1980, Pageoph, 118, 355.
Gray and Pyle, 1987, Q.J.R. Met. Soc., 113, 635.
Eckman, Haigh, and Pyle, 1987, Nature, 329, 616.

## Section 4.4 CAO 2-D Model

V. Philushakin and E. Zhadin
Central Aerological Observatory
U.S.S.R.

### The Model of Residual Circulation and the Planetary Waves of the Central Aerological Observatory (U.S.S.R.)

The 2-D residual circulation model of the stratosphere and mesosphere (16-80 km) is similar to the model of Solomon and Garcia (1983), but the IR cooling rates in the 15μ $CO_2$ and 9.6μ $O_3$ bands are calculated with parameterization of Fomichev and Shzed (1985). This parameterization takes into account the non-local dependence of the cooling rates upon a temperature profile.

The planetary wave's model calculates non-zonal dynamic and temperature disturbances for the fixed mean flow. The planetary wave sources are the orography and sea-surface temperature contrasts. The dissipation of stationary planetary waves is parameterized by Newtonian cooling and Rayleigh friction. The planetary wave's model (0-80 km) has a high resolution [~0.8° latitude step and ~2 km altitude step, $z=\ln(p_0/p)$]. The response of the atmosphere to the sea-surface temperature anomalies can be numerically evaluated by means of the model.

The model of the residual circulation takes into account the planetary wave forcing calculated in the planetary wave's model on the eddy heat and momentum transport by dissipative planetary waves. The eddy heat transport is parameterized in the diffusion form with coefficients which depend upon Newtonian cooling, zonal wind and planetary wave parameters. The dynamical planetary wave effect on the mean flow is calculated in the form of E-P divergence cross-sections. Chemical eddies are calculated as Pyle and Rogers (1980).

Now we create the interactive 3-D model with coupled dynamics and composition of the middle atmosphere. This model will take into account the feedbacks between circulation, thermal regime and composition in a self-consistent manner and will calculate the three-dimensional distribution of the wind, temperature and composition in the stratosphere and mesosphere. The aim of the Central Aerological Observatory 2-D and 3-D models is a numerical study of the anthropogenic and natural effect on ozone layer, the evaluation of stratospheric conditions in the future, and the problem of sudden stratospheric warmings, etc.

## Section 4.5 CLKSON 2-D Model

E. Olaguer, H. Yang, and K. K. Tung
Clarkson University[1]

# Documentation of a Coupled 2-D Model of Dynamics, Radiation and Chemistry in Isentropic Coordinates

Abstract

This is our most recent (Oct. 1988) version of model, with prognostic chemistry. Long-lived species such as $O_3$, $NO_y$, $CH_4$ and $N_2O$ are transported using 2-D circulation deduced from NMC temperature. The isentropic mixing coefficient is determined consistently from the same temperature data. The radiative code has recently been updated, and most of the feedback cycles have now been incorporated.

## 1. Dynamical Aspects of the Model

The dynamical transport formulation is as given in Tung (1982, 1986), Tung and Yang (1988), and Yang (1988). Briefly, the model is based on a self-consistent non-geostrophic formulation in isentropic coordinates in which the isentropic mixing coefficient is calculated from momentum equation using the same NMC temperature input as that used in the radiative calculations. The vertical coordinate is log (potential temperature) above 350K and log (potential temperature/surface potential temperature) below 350K. The lower surface is currently specified to be at p=1000 mb, but an actual (variable) surface pressure can be easily specified instead, if so desired.

No gravity wave cross-isentrope mixing is incorporated. This limits the applicability of the present version of the model to below the upper stratosphere. No vertical diffusion is included ($K_{zz}$=0) in the present version of the model, although it is recognized that some form of vertical diffusion should be necessary for the troposphere and perhaps also the equatorial lower stratosphere.

The horizontal domain of the model is from pole to pole in increments of 10 degrees of latitude. The vertical domain is from the ground to 8 pressure scale-heights (limited by the availability of NMC temperature data) in increments of about 2.3 km. Resolution is variable and can be increased but at the expense of a considerable increase in computation time.

The Prather scheme (Prather, 1986), as tested and implemented by the Caltech group (Shia et al., 1988) is recently incorporated in place of the scheme of Smolarkiewicz (1983) used in a previous version of the model.

## 2. The Radiative Transfer Code

The $CO_2$ IR code utilizes the parameterizaton developed by Ou and Liou (1983), who employed an empirical broadband emissivity formulation based on the detailed line-by-line calculation of Fels and Schwarzkopf (1981) for the $CO_2$ 15 micron band.

The $O_3$ IR scheme is similar to that of Rosenfield et al. (1987). The water vapor scheme consists of an emissivity formulation similar to that employed for $CO_2$ and is taken from Ramanathan (1976). The water vapor mixing ratio profile may either be specified externally or else take on default values which are determined in the same way as in Rosenfield et al. (1987).

[1]Present Affiliation: University of Washington

In the solar radiation part of the code, diurnally averaged heating rates due to solar absorption are computed by the same method employed in the MIT-GIT 3-D model (see Cunnold et al., 1975). Solar declination is not rigorously calculated based on orbital parameters. It is instead computed simply as $\sin \delta = 0.4\sin(2\pi t/365 \text{ days})$, where t=0 on March 21.

There are two versions of the code used to calculate solar absorption by ozone and molecular oxygen: fast and slow. The fast version employs the parameterization of Strobel (1978) as modified by Apruzese et al. (1983) for the absorption of solar radiation in the visible and ultraviolet regions by ozone and molecular oxygen. In addition to the absorption of the direct beam, we include the effects of multiple scattering by the lower atmosphere in the Chappius band. The resulting diffusive radiation is modeled by a pure ozone absorption region on top a reflecting layer with an effective albedo as given by Lacis and Hansen (1974). The ground albedo are taken from Sellers (1965) and are a function of latitude.

The "slow" version of the radiative code employs a more direct calculation of the energy absorption due to ozone and molecular oxygen, and includes the contribution to the atmospheric heating rate by nitrogen dioxide. Multiple scattering is taken into account in a manner similar to that in the "fast" version, except that it is applied to all spectral intervals with wavelengths greater than 3125 Angstroms.

The clear-sky treatment of water vapor absorption in the rear-infrared follows that of Lacis and Hansen (1974).

The treatment of radiation in a cloudy sky is also incorporated in the radiative transfer code.

In addition to radiative transfer, the model also includes the diabatic effects of precipitation in the troposphere. Latent heating is calculated using the approach of Jacqmin and Lindzen (1985) from rainfall data as tabulated by Schutz and Gates (1972a, b) for winter/summer.

## 3. Photochemistry

A 64-reaction photochemical package is adopted with $O_x$, $NO_x$, $HO_x$, and $ClO_x$ chemistry. The long lived species are advected (and diffused) by model calculated transports, while the short-lived species are calculated algebraically under the assumption of photochemical equilibrium. For the present calculation presented here, the transported species are $O_3$, $NO_y$, $CH_4$, and $N_2O$. The specified species are $H_2$, $O_2$, $N_2$, CO, $H_2O$, and $Cl_y$ (with an asymptotic value of 2.5 ppbv). All photochemical processes are assumed to take place only in daylight. The interaction involving the species $N_2O_5$ are ignored. The photodissociation rates are calculated at two solar hour angles as described in section 2 and then averaged. The daylight averaged concentrations of all the constituents are then derived and the 24-hour average odd oxygen generation rate computed by multiplying both the production and loss terms by the fractional length of day.

The required photochemical reaction rate constants, quantum yields, and absorption cross sections are from DeMore et al. (1987), with the exception of cross section for water vapor (from Baulch et al. 1982), ozone and molecular oxygen, which for the Herzberg continuum beyond 200 nm are taken from WMO (1986). The Schumann-Runge $O_2$ cross sections, on the other hand, are computed as recommended by Allen and Frederick (1982) for wavelengths below 200 nm. The ozone cross sections are those prescribed in WMO (1986) and include the temperature dependence between 260 and 350 nm. Also taken from WMO (1986) are the wave number intervals and photon fluxes used in the computation of the photodissociation rates. For wavelengths beyond 400 nm we use the coarser of the two recommended grids.

The photodissociation rates are calculated assuming that single scattering takes place above the tropopause and multiple scattering below. The Rayleigh single scattering cross sections are taken from WMO (1986). Lower atmosphere effective albedo is computed as in section 2. A Lambert surface is assumed to exist at the ground with the same effective albedo as that of the troposphere. The effects of multiple scattering are included only for wavelengths greater than 321.5 nm.

References:

Allen and Frederick (1982), JGR, 87, 2066.
Apruzese et al. (1982), JGR, 87, 8951.
Baulch et al. (1982), J. Phys. Chem. Ref. Data, 11, 327.
Cunnold et al. (1975), JAS, 32, 170.
DeMore et al. (1987), Chemical kinetics and photochemical data..., JPL 87-41.
Fels and Schwarzkopf (1981), JGR, 86, 1205.
Jacqmin and Lindzen (1985), JAS, 42, 724.
Lacis and Hansen (1974), JAS, 31, 118.
Ou and Liou (1983), JGR, 88, 5203.
Prather (1986), JGR, 91, 6671.
Ramanathan (1976), JAS, 33, 1330.
Rosenfield et al. (1987), JAS, 44, 859.
Sellers (1965), Physical Climatology, Univ. of Chicago Press, 272 pp.
Schutz and Gates (1972a), Supplemental Global Climatic Data: January, Rand Corp.
Schutz and Gates (1972b), Global Climatic Data for Surface, 800 mb, 400mb: July, Rand Corp.
Shia et al. (1988), submitted to JGR.
Smolarkiewicz (1983), Mon. Wea. Rev., 111, 479.
Strobel (1978), JGR, 83, 6225.
Tung (1982), JAS, 39, 2330.
Tung (1986), JAS, 43, 2600.
Tung and Yang (1988), JGR, in press.
Yang (1988), Numerical Simulation of Global and Antarctic Ozone..., Ph.D. thesis, MIT.
WMO (1986), Atmospheric Ozone 1985: Assessment..., World Meteorological Organization.

## Section 4.6 DUPONT 2-D Model

D. Fisher
E.I. DuPont De Nemours & Company, Inc.

### General

The present DuPont 2-D atmospheric model is an enhanced version of the model that was extensively described in the paper, Miller et al., Journal of Geophysical Research, Vol 86, p. 12039-12065 (1981). Enhancements have been made to the model as far as treatment of the vertical coordinate system and treatment of the chemistry. Modern recommendations for chemical rate constants are in place.

### Model Domain and Resolution

The DuPont 2-D model covers the domain of the entire earth, pole to pole with altitude domain from zero to approximately 56 km. There are ten latitude bins, all of equal areas, parameterized on the sine of latitudes with dimensions of 0.2 units. Therefore bin centers are at sin(phi) =-0.9, -0.7,...0.9. There are 18 altitude bins, specified in log-pressure units, each bin corresponding to approximately 3 kilometers.

### Transport Treatment Used

#### Formulation

The transport formulation contains both advective and diffusive terms, in a Lagrangian formulation. In this formulation the circulation is characterized by the sum of the Eulerian mean stream function and an appropriate average of the skew portion of the eddy diffusion tensor. In the Lagrangian formulation only the symmetric portion of the diffusion tensor is needed to define the diffusive transport.

#### Basis for Winds and Eddy Coefficients

The advective circulation field of Murgatroyd and Singleton (appropriately scaled) is used to approximate the Lagrangian mean flow. The scaling factor of 0.4 was used based on improved atmospheric heating rates determined by Dopplick, which in general are about 1/2 of those employed by Murgartroyd and Singleton in the lower half of the stratosphere.

Below the 15 km lower bound of the Murgatroyd and Singleton velocity field formulation, bounded by constant velocity contours, the vertical component of velocity is calculated using a weighted least squares interpolation procedure including a contour of zero velocity at ground level.

The eddy diffusion parameterization is basically that of Luther (1974) with minor modifications. The latitudinal eddy coefficient $K_{yy}$ has been increased below 10 km to provide a more realistic inter-hemispherical mixing time of 14 months in the troposphere. The vertical eddy coefficient, $K_{zz}$ which represents the most uncertain portion of the Luther parameterization has been replaced by that of Hunten (1975), for all seasons throughout the model stratosphere. This parameterization utilized a tropospheric value of 1.0E+05 (units = $cm^2/sec$) and stratospheric values of

$$K_{zz} = 500*\exp(.10597*Z)$$

Location of the tropopause and therefore definition of discontinuity in $K_{zz}$ varies with latitude.

## Chemistry Treatment Used

### Species Computed

The current model utilizes the following species:

Photochemical equilibrium: H, N

Family groups: $O_x$= [$O(^3P)$, $O(^1D)$, $O_3$]

Active: $H_2O$, $CH_4$, $H_2$, CO, $CH_2O$
$O_x$
NO, $NO_2$, $HNO_3$, $N_2O$, $NO_3$, $N_2O_5$, $HO_2NO_2$
HCl, ClO, Cl, $ClONO_2$, HOCl
$H_2O_2$, OH, $HO_2$
$CFCl_3$, $CF_2Cl_2$, $CCl_4$, $CH_3Cl$, $CH_3CCl_3$

($H_2O$ is only active above 20 km)

Inactive: $N_2$, $O_2$, $CO_2$

### Family Grouping (if any)

Calculations are done without major family groupings except odd oxygen ($O$,$O_3$).

### Diurnal Averaging Scheme

The 'two tank' diurnal averaging scheme is being used for diurnal averaging. The relative sizes of the day and night tanks depend on latitude and season.

## Photolysis Calculations

### Spectral Resolution

The spectrum is divided into 126 bins to cover wavelengths from 175.4 nm to 730. nm. Bin sizes vary over the spectrum from a coarse size of 10 nm at the high wavelengths to a normal size of 5.0 nm over the middle range. Over the Schumann-Runge portion of the spectrum, the bin size varies in order to capture the features of this region. Bin sizes in this region range from 1.0 to 2.5 nm. Treatment of the Schumann-Runge parallels that of Nicolet and Partimonies.

Source of Cross Section

The cross-sections are from various literature sources:

| Photo Reaction | Reference Source |
|---|---|
| Solar Flux | WMO/NASA 1986 |
| $O_2$ --> 2O | Nicolet (1980), Frederick and Hudson (1979) |
| $O_3$ --> $O_2$+O | Gelinas, Relative Quantum Fields from NASA 1049 |
| --> $O_2$+O($^1$D) | |
| $NO_2$ --> NO+ O | NASA 1010, NASA Modeling Workshop 1979 |
| $N_2O$ --> $N_2$+O($^1$D) | Selwyn et al (1977) |
| NO--> N + O | Frederick and Hudson (1979) |
| $HNO_3$ --> OH + $NO_2$ | Johnson and Graham |
| $H_2O_2$ --> 2OH | NASA Modeling Workshop, JPL 1982, CIAP |
| $N_2O_5$ --> $NO_2$ +$NO_3$ | Johnson and Graham, NASA 1010 |
| $NO_3$ --> NO +$O_2$ | |
| --> $NO_2$ + O | Magnotta and Johnson (1980) |
| HCl --> H + Cl | Inn (1976) |
| $CF_2Cl_2$ --> 2Cl | JPL 1982 |
| $CFCl_3$ --> 3Cl | JPL 1982 |
| $CCl_4$ --> 4Cl | Gelinas |
| $CHClF_2$ --> Cl | Watson |
| $CHCl_2F$ --> 2Cl | JPL 1982 |
| ClO --> Cl + O | Watson (1974) |
| $HO_2NO_2$ --> OH + $NO_3$ | Molina and Molina (1980) |
| $O_3$ Solar Heating | |
| $O_2$ Solar Heating | |
| $ClONO_2$ --> Cl + $NO_3$ | NASA 1979 Modeling Workshop |
| $CH_3Cl$ --> Cl | Robins (1976) |
| $CO_2$ --> CO + O | Hudson and Kieffer (CIAP) |
| $CH_3CCl_3$ --> 3 Cl | Van Laethem-Meuree et al. (1979) |
| $CH_2O$ --> H + HCO | JPL 1982, |
| --> $H_2$ + CO | Interpolated to 230 K |
| HOCl --> OH + Cl | NASA 1979 Reference Publication |
| $CH_3O_2H$ --> $CH_3O$ +OH | NASA 1979 Reference Publication |
| $CH_3O_2NO_2$ --> $CH_3O$ + $NO_3$ | Cox (1979) |

Radiative Transfer Approach

Radiative transfer includes multiple scattering with absorption parameterized based on secant columns of $O_2$ and $O_3$.

Multiple Scattering and Albedo Assumptions

Multiple scattering of solar radiation and ground albedo effects are included in the calculation of photolytic reaction rate constants. For the daytime reaction rates, appropriate averages are taken to account for latitude and season. A Rayleigh phase function is used in the calculations. Ground level albedo is taken as 0.25, independent of latitude and season.

Integration Algorithm Used
Method

The two-dimensional transport and conservation partial differential equations are solved using an appropriate method that removes the numerical dispersion characteristically associated with first order representations of advective transports and also minimized other (discretization) errors produced by the finite grid size. The time-dependent integration of the mass balance equation makes use of an implicit finite difference formula to ensure stability. The specific formulation uses the trapezoidal rule for the transport terms in the mass balance equation, and the backward Euler's approximation for the chemical production and loss terms. At each time step, the finite difference formula is solved for the mixing ratio of each species at each grid point by using a Newton-Raphson iteration scheme until convergence is achieved. The calculations are preformed on DuPont's CRAY-1 computer.

Time Step

For most runs, a time step of 1/60th of a season is used or about 18 hours.

Treatment of Negative Mixing Ratios

Negative mixing ratios are not encountered in normal runs.

Heterogeneous Removal Processes

Species Removed: The following species are removed via rainout below 10 km with a 5 day time constant.

| | |
|---|---|
| Cl | OH |
| ClO | $HO_2$ |
| $ClONO_2$ | $H_2O_2$ |
| HCl | $NO_2$ |
| $HNO_3$ | #$CH_3O_2$ |
| $CH_2O$ | #$CH_3O_2H$ |
| HOCl#$CH_3O_2NO_2$ | |
| $HO_2NO_2$ | |
| OClO | |

. # Normally set to zero.

Basis for Removal Rate

This rain-out time constant was derived by fitting a first order equation to the tropospheric water vapor data and evaluating the time constant. Also sensitivity analyses were run to determine that the net effect is not extremely sensitive to the precise value of this constant.

## Section 4.7 GISS 1-D and 3-D Models

M.J. Prather
Goddard Institute for Space Studies

GISS 1-D Photochemical Model

JPL 87 (cross-sections, kinetics, fluxes, temp dep of $O_3$ not $N_2O_5$)
- radiation code uses multi-stream scattering & spherical solar source

- S-R bands & NO by opacity distribution function (ODF: Fang et al, Harvard) updated to include temperature dependence of ODF

- calculations use the January mean profiles for $O_3$ and T as specified

- latitude grid is 85S (10 deg) 85N (18 latitudes)

-altitude grid is pressure-height $z^* = 16 \log_{10}(1000/p)$ begin 0 (2 km) 62 km (32 levels)

GISS: 3-D Chemical Tracer Model

Michael J. Prather (GISS)
Maria M. Garcia (Columbia U.)
David Rind (GISS)
2880 Broadway
New York, NY 10025

The chemical tracer model (CTM) uses the winds and convection from the GISS general circulation model (GCM) for the middle atmosphere. The GCM stores horizontal mass fluxes across the boundary of grid boxes and surface pressures at 4-hour intervals. The CTM is run from these history tapes. The coordinates of the CTM are the same as the GCM:

- Sigma coordinates in layers 1-9 (984 mb-100 mb)
- fixed-pressure in layers 10-23 (100 mb, 46 mb, 22 mb,...)
- 3 levels per decade in pressure
- 7.83 deg lat boundaries = (90S, 82.17S, 74.35S,... ,3.91S, 0, 3.91N, 7.8N...., 82.17N, 90N)
- 10 deg long
- Total 23 layers x 24 lat x 36 long.

The 3-D tracer continuity equation is solved by operator splitting: advection of tracer is done upstream with second-order moments. Diffusion and convective mixing only in the troposphere; chemistry every 4 hours (diurnal average only). Chemistry is limited to a single tracer with linearized production and loss. The photochemical model assumes observed ozone climatologies and temperature to calculate zonal and monthly averaged chemistry. Ozone chemistry is fully linearized, other gases ($N_2O$, $CFCl_3$, $CF_2Cl_2$) use linear loss frequencies from tables (24 lat x 13 alt x 12 months).

References

Prather, M.: Numerical advection by conservation of second-order moments, J. Geophys Res., 91, no. D6, 6671-6681, May 1986.

Prather, M.; McElroy, M. Wosfy, S.; Russell, G.; Rind, D.; Chemistry of the global troposphere: fluorocarbons as tracers of air motions, J. Geophys. Res., 92, no. D6, 6579-6613, June 1986.

Rind D.; Suozzo, R.; Balachandran, N.K.; Lacis A.; Russell G.; The GISS golobal climate-middle atmosphere model. Part I: model structure and climatology, J. Atmos. Sci., 45, 330-370, 1988.

-Part II: Model variability due to interactions between planetary waves, the mean circulation and gravity wave drag. J. Atmos. Sci., 45, 371-386, 1988.

## Section 4.8 GSFC1 2-D Model

P.D. Guthrie, C.H. Jackman and T.L. Kucsera
Goddard Space Flight Center

Domain, Resolution, and Timestep

85°S to 85°N, 10° latitude bands

Ground to ~60 km altitude with ~2 km vertical resolution
(log pressure coordinates)

Chemistry

35 species computed, all transported independently (no families)

Diurnal averaging based on square wave approximation, day/night ratios scaled to 1-D mid-latitude model.

Photolysis calculations -

Spectral resolution - 39 wavelength intervals
In Angstroms -1215.67, 1700-1724, 1724-1739, 1739-1754, 1754-1770, 1770-1786, 1786-1801, 1802-1818, 1818-1835, 1835-1852, 1852-1869, 1869-1887, 1887-1905, 1905-1923, 1923-1942, 1942-1961, 1961-1980, 1980-2000, 2000-2020, 2020-2105, 2105-2198, 2198-2299, 2299-2410, 2410-2532, 2532-2667, 2667-2817, 2817-2857, 2857-2985, 2985-3030, 3030-3077, 3077-3125, 3125-3175, 3175-3225, 3225-2275, 3375-3575, 3575-3775, 3775-3975, 3975-5475, 5475-7350

Source of cross sections used - World Meteorological Organization, Atmospheric Ozone 1985
Exception is $O_2$ - Allen and Frederick (1982) for Schumann Runge bands, Herman and Mentall (1982) for Herzberg continum.

Radiative transfer approach - Two-stream radiative transfer method of Herman (1979) which is based on the matrix operator method of Plass et al. (1973)

Multiple scattering and albedo assumptions - Two-stream approach with 0.3 assumed as albedo at ground for all wavelengths.

Integration Algorithm

Alternative direction forward time differences ("angled derivative").
Fourth order spatial differences centered in the interior shifting to one-sided at the boundaries.
Newton-Raphson interactive solution of species continuity equations.
Time step is one day, decreasing if needed.
Time step reduced if negative mixing ratios occur.

Heterogeneous Removal

"Solubles" removed at rate proportional to specified "Rain" profile ($HNO_3$, HCl, $H_2O_2$, NO, $CH_2O$, $CH_3OOH$)

Transport Treatment

Residual mean formulation

Base case winds, based on Rosenfield et al. heating calculations (in turn based on NMC temperature data, SBUV ozone, present-day $CO_2$)
Water vapor: 3.2 ppm above 20 mb, fixed relative humidity (Manabe and Wetherald) in troposphere

Base eddy coefficients

| | |
|---|---|
| Stratosphere | $K_{yy} = 2x10^9$ cm$^2$-s$^{-1}$ |
| | $K_{zz} = 2x10^3$ cm$^2$-s$^{-1}$ |
| Troposphere | $K_{yy} = 2x10^{10}$ cm$^2$-s$^{-1}$ |
| | $K_{zz} = 2x10^4$ cm$^2$-s$^{-1}$ |

transition zone between 500-100 mbar

## Section 4.9 GSFC2 2-D Model

C.H. Jackman, A.R. Douglass, R.S.Stolarski and P.D. Guthrie
Goddard Space Flight Center

### Summary of the NASA/GSFC Fast 2-D Model

GSFC2, a two-dimensional (2-D) residual circulation stratospheric model, was developed to be used as a tool for examining the sensitivity of model calculations to photochemical and dynamical inputs and assumptions and evaluating the response of stratospheric ozone to a wide range of possible scenarios for changes in trace gases. Photochemical inputs include the reaction rates, photodissociation cross sections, solar flux values, and solar cycle effects, including both solar flux variations and particle precipitation events. Dynamical inputs include the diffusion coefficients, the circulation, and their seasonal and inter-annual variability. Currently the model is non-interactive between ozone and dynamics; the dynamics are changed monthly and computed from observed temperature and ozone.

To be useful for such a wide range of applications, the model was designed to require minimal computer resources. Family chemistry approximations are used to reduce the number of species continuity equations that must be solved. The species continuity equations are solved through process splitting, that is by successive application of the advection, diffusion and photochemical operators. The advection is calculated using an efficient non-dispersive transport scheme developed by Prather (1986). The diffusion operators act on the transported fields. The photochemical production and loss are calculated using the previous timestep's values for species concentrations; this implicitly assumes that the timestep to timestep changes in species concentration are small. The main inputs to this model are summarized in the accompanying table on the following pages:

More detailed information about GSFC2 can be obtained by calling or writing:

C.H. Jackman
Code 616
NASA/GSFC
Greenbelt, MD 20771
phone (301) 286-8399
or FTS 888-8399

A.R. Douglass
Code 616
NASA/GSFC
Greenbelt, MD 20771
phone (301) 286-2337
or FTS 888-2337

Domain, Resolution, and Timestep

85°S to 85°N, 10° latitude bands
Ground to ~60 km altitude with ~2 km vertical resolution (log pressure coordinates)
One day timestep - 360 day model year
Photolysis rates computed every 10 days
Residual circulation, $K_{yy}$'s and $K_{zz}$'s computed every 30 days
Species are output in daytime average form

| Transported Families | Derived Species |
|---|---|
| $O_x$ | $O_3$, $O(^3P)$, $O(^1D)$ |
| Odd N | N, NO, $NO_2$, $NO_3$, $2N_2O_5$ $HNO_3$, $HO_2NO_2$, $ClONO_2$ |
| $Cl_x$ | Cl, ClO, HOCl, $ClONO_2$, HCl |

Transported Species

$N_2O$, $H_2$, $CH_4$, $CCl_4$, $CH_3Cl$, ClFCl, $CF_2Cl_2$, $CH_3CCl_3$, $CH_3OOH$, CO

Photochemical Species

H, OH, $HO_2$, $H_2O_2$, HCO, $CH_2O$, $CH_3O$, $CH_3O_2$

| Dissociation Rates | Reference or Explanation |
|---|---|
| Spectral Resolution | 39 wavelength intervals |
| Solar Flux | WMO (1986) |
| Diurnal Averaging | Look up table for diurnal average solar flux as function of optical depth, latitude, and solar declination.<br><br>Table produced by detailed diurnal cycle calculations using a 1D photochemical model (Herman 1979). |
| Multiple Scattering | Two-stream radiative transfer (Herman, 1979) |
| Albedo | 0.3 at ground for all wavelengths:<br>no clouds included |
| Cross Sections | JPL 87-41 |
| $O_2$, NO | Allen and Frederick (1982) |

Reaction Rates

From JPL 87-41

Heterogeneous Removal

$HNO_3$, $HO_2NO_2$, HCl, $H_2O_2$, and $CH_3OOH$ rained out in troposphere

| Dynamical Inputs | Reference or Explanation |
|---|---|
| Residual Circulation | Dunkerton (1978) |
| Heating Rates | Rosenfield et al. (1987), p<100mbar<br>Dopplick (1974, 1979), p>100 mbar |
| Temperature | NMC data, 4 year monthly average |

Diffusion

| | |
|---|---|
| $K_{yy}$, $K_{yz}$ | Stratosphere: Newman et al. (1988)<br>Troposphere: 1 x $10^{10}$ $cm^2$/sec at ground, decreasing with altitude to stratosphere value |
| $K_{zz}$ | Stratosphere: 2 x $10^3$ $cm^2$/sec<br>Troposphere: 1 x $10^4$ $cm^2$/sec at ground, decreasing with latitude to stratospheric value |

| Boundary Conditions | Value |
|---|---|
| Top | Zero flux for all transported families and species |
| Bottom | |
| $O_x$ | Deposition velocity - 0.1 cm/sec |
| Odd N | Fixed mixing ratio -100 pptv |
| $Cl_x$ | Zero flux |
| $N_2O$ | Fixed mixing ratio - 300 ppbv |
| $H_2$ | Fixed mixing ratio - 0.5 ppmv |
| $CH_4$ | Fixed mixing ratio -1.6 ppmv |
| $CCl_4$ | Fixed mixing ratio - 100 pptv |
| $CH_3Cl$ | Fixed mixing ratio - 700 pptv |
| $CFCl_3$ | Fixed mixing ratio - 170 pptv |
| $CF_2Cl_3$ | Fixed mixing ratio - 285 pptv |
| $CH_3CCl_3$ | Fixed mixing ratio -100 pptv |
| $CH_3OOH$ | Zero Flux |
| CO | Fixed mixing ratio -100 ppbv |

## Section 4.10 LARC 3-D Model

W. Grose, R. Eckman, R. Turner, and T. Blackshear
NASA Langley Research Center
Mail Stop 401B
Hampton, VA 23665-5225

### NASA Langley 3-D GCM/Chemistry Model

| | |
|---|---|
| Model Domain | pole-to-pole with 32 latitude bins at approximately 5 degree intervals<br>0-60 km with 12 height intervals<br>using sigma coordinates<br>time step = 30 minutes |
| Dependent variables | temperature, wind components, chemical constituents chemistry/transport done "off-line" |
| Dynamics | Spectral, primitive equation, general circulation model to zonal wave number 16 with triangular truncation |
| Chemistry | Family approach with six families/species explicitly integrated:<br>$O_x$, $NO_y$, $HNO_3$, $Cl_x$, $N_2O_5$, $H_2O_2$<br>39 species partitioned using 115 reactions |
| Radiation | Shortwave radiation: method of Lacis and Hansen (1974)<br>Longwave radiation: Newtonian approximation |
| References | Grose, W.L., J.E. Nealy, R.E. Turner, and W.T. Blackshear, Modeling the transport of chemically active constituents in the stratosphere, Proceedings of the NATO Erice Workshop, 1987.<br><br>Blackshear, W.T., W.L. Grose, and R.E. Turner, Simulating sudden stratospheric warming synopotic evolution, Quart. J. Roy. Met. Soc., 113, 815-846, 1987. |

## Section 4.11 LLNL 2-D Model

D.J. Wuebbles, P.S. Connell, K.E. Grant, and R. Tarp
Lawrence Livermore National Laboratory

The LLNL zonally-averaged two-dimensional chemical-radiative transport model currently determines the atmospheric distributions of 31 chemically active atmospheric trace constituents in the troposphere and stratosphere. The model domain extends from pole to pole, and from the ground to 0.56 mb (approximately 0 to 54 km). The sine of latitude is used as the horizontal coordinate because of its advantages in the transformed continuity equation, with uneven increments corresponding to about 10° in latitude used to provide adequate resolution, particularly towards the the poles. The vertical coordinate corresponds to the natural logarithm of pressure ($z^* = -H_o \ln(p/p_o)$, where $H_o$ is the assumed scale height of 7.2 km, and $p_o$ is the surface pressure, 1013 mb). The vertical resolution is $\ln(p/p_o) = 0.417$ or approximately 3 km.

Approximately 95 chemical and photochemical reactions are included in the model. Reaction rates, solar flux data, absorption cross-sections, and quantum yields are based on the latest NASA panel recommendations (JPL 87-41, 1987). Photodissociation rates, including the effects of multiple scattering, are computed as a function of time at each zone, with optical depths consistent with calculated species distributions.

The diabatic circulation for the ambient atmosphere is determined using net heating rates calculated in an internally consistent way with the derived species distributions. The technique for deriving the diabatic circulation is similar to that used by Solomon et al. (1986): the vertical velocity is determined from the zonally averaged residual Eulerian thermodynamic equation, while the horizontal velocity is determined using the equation for mass continuity.

The net heating rates are determined using accurate solar and infrared radiative models. The solar model includes absorption and scattering effects for $O_3$, $O_2$, and $NO_2$ at ultraviolet and visible wavelengths, and for $H_2O$, $CO_2$, and $O_2$ in the near infrared. The longwave emission and absorption by $O_3$, $CO_2$, and $H_2O$ are included in the infrared sub-model.

Temperatures for the ambient atmosphere vary continuously, over the annual cycle, based on the reference model of Barnett and Corney (1985). The derived diabatic circulation depends strongly on the temperature distribution; by using observed temperatures for the ambient atmosphere, a more accurate representation of the diabatic circulation can be derived. The model determined net radiative heating rates and resulting diabatic circulation compare well with those derived from LIMS data (Kiehl and Solomon, 1986; Rosenfield et al.; 1987; Solomon et al.; 1986).

For the perturbed atmosphere, a perturbation form of the thermodynamic equation is solved for the changes in stratospheric temperatures resulting from changes in the distributions of ozone and other radiatively active constituents. Using this approach, the diabatic circulation is assumed to be unchanged in the perturbed atmosphere from that calculated for the ambient.

Turbulent eddy transport is parameterized through diffusion coefficients $K_{yy}$ and $K_{zz}$. In the current version of the model, a value $K_{yy}$ of $2 \times 10^9$ cm$^2$ s$^{-1}$ is assumed at all stratospheric altitudes and latitudes, and values of $1 \times 10^{11}$ in the troposphere. Values of $K_{zz}$ are $1 \times 10^3$ cm$^2$ s$^{-1}$ in the lower stratosphere, increasing slowly with altitude based on gravity wave modeling studies.

The continuity equation for each individual species is solved using a variable time step, variable order, implicit technique for solving stiff numerical systems with strict error control. Advection terms are treated accurately using the two-dimensional transport algorithm of Smolarkiewicz (1984). The diurnal-averaged concentrations for each species at each zone are calculated at each time step. Accurate diurnal calculations are used to derive time-varying factors for each chemical and photochemical reaction included in the diurnal-averaged version of the model.

## Section 4.12 MPIC 2-D Model

C. Bruehl and P.J. Crutzen
Max Planck Institute for Chemistry, D-6500
Federal Republic of Germany

### 2-D Mainz Chemistry - Climate - Model

| | |
|---|---|
| Grid | 10° latitude, surface to 54 (60) km pressure grid, resolution about 2 km |
| Chemistry | families including $Br_x$, about 140 reactions, timestep 2 hrs. |
| Transport | Eulerian, large $K_{yy}$, $K_{yz}$ and $K_{zz}$, Circulation from Louis, 1974. In development: Circulation from our radiation code (diabatic). |
| Radiation | UV+ VIS Delta two-stream method, 176 spectral intervals, clouds included. Includes IR broadband-model of Ramanathan ($CO_2$ Kiehl, Ram., 1983). In present version the radiation is not used for calculation of temperatures or circulation. |
| References | Gidel et al (1983): J. Geophys Res. 88, 6622.<br>Bruehl, Crutzen (1988): Climate Dynamics, 2, 173. |
| Contact | Ch. Bruehl 49-6131-305434 Bitnet CHB@DGAIPP1S Fax - 305388 |

## Section 4.13 MRI 2-D Model

Toru Sasaki
Meterological Research Institute
1-1 Nagamine, Tsukuba, Ibaraki,
305 Japan

The present version of MRI 2-D photochemical model calculates the mixing ratio of minor constituents with prescribed temperature, circulation and eddy diffusion coefficients. The basic equation of the model is

$$\frac{\partial \bar{f}_x}{\partial t} + \frac{1}{a\cos\phi}\frac{\partial(\bar{f}_x\bar{v}\cos\phi)}{\partial\phi} + e^{\xi}\frac{\partial(e^{-\xi}\bar{f}_x\bar{w})}{\partial\xi} = \frac{\bar{Q}_x}{N} + \bar{F}_x$$

where $f_x$ is the mixing ratio of constituent x, $\phi$ is latitude, $\xi = -\ln(p/p_o)$ is altitude, v and w are northward and upward velocity of the circulation, respectively, $Q_x$ is photochemical production, $F_x$ is eddy diffusion transport, a is the earth radius and N is the number density of the air. The overbar _ denotes its diurnal or zonal mean.

Grid points are defined as follows. The latitudinal range is divided into 18 divisions of 10° width from the south pole to the north pole and the altitude range ( $\xi$ = 0 to 8) is divided into 16 divisions of $\Delta\xi$ = 0.5 height. So we get 18 x 16 cells in the model meridional plane. Mixing ratio, temperature, photochemical production, etc., are defined at the center point of each cell, v and w are defined at the center point of the vertical and horizontal wall, respectively, and eddy diffusion coefficients are defined at the cross point of the walls. So we can calculate mixing ratio of minor constituents from 85° S to 85° N and from $\xi$ = 0.25 to 7.75.

We include 38 species in the model, and the mixing ratio of 36 species are calculated. Some species, which are photochemically active and quickly converted into each other, are grouped as a family. Each of these families is treated as one constituent in the basic equation. The mixing ratio of each species of the family is determined on the photochemical equilibrium condition. The species and the families are as follows:

$O_x$ (=$O_3$+O+O($^1$D)),
$N_2O$, $NO_x$ (=N+NO+$NO_2$), $NO_3$, $N_2O_5$, $HNO_3$, $HNO_4$,
$H_2O$, $H_2$, $HO_x$ (=H+OH+$HO_2$) , $H_2O_2$,
$CH_4$, $CHO_{x1}$ (= $CH_3$+$CH_3O_2$), $CH_3O_2H$, $CHO_{x2}$ (=CHO+$CH_2O$ +CHO), CO, $CO_2$
$CF_2Cl_2$ , $CFCl_3$, $CCl_4$, $CH_3Cl$, $CH_3CCl_3$, $ClO_x$ (=Cl+ClO), HCl, HOCl, $ClONO_2$.

We set some boundary conditions in the model. The boundary mixing ratio is given at the surface ($\xi$ = 0), it affects the above atmosphere by diffusion. Some species are removed by rainout in the first and second layer with 10 days lifetime.

We consider 83 chemical reactions and 31 photodissociations in the model. The kinetic data and the absorption cross sections are from JPL 87-41. Solar flux at the top of the atmosphere and the absorption cross sections of $O_2$ and $O_3$ are from WMO (1986).

The data of temperature is from Louis (1975) and circulation is from Murgatroyd and Singleton (1961) multiplied by 0.5. The eddy diffusion coefficients are selected by trial and error to simulate ozone and other trace species well. In our model the components of the eddy diffusion coefficients are formulated by

$K_{yy} = K_{yy0}(\xi) + A(\xi) \cdot B(\phi) \cdot C(s)$

$K_{yz} = A(\xi) \cdot B(\phi) \cdot C(s) \cdot D(h)$

$K_{zz} = K_{zz0}(\xi) + A(\xi) \cdot B(\phi) \cdot C(s) \cdot D(h) \cdot D(h).$

$K_{yy0}(\xi)$ is set to be (50 --> 10) x$10^9$ $cm^2$ $sec^{-1}$ for $0 < \xi < 2$ and 2 x $10^9$ $cm^2$ $sec^{-1}$ for $\xi > 3$. $K_{zz0}(\xi)$ is set to be (150 --> 20) x $10^3$ $cm^2 sec^{-1}$ for $0 < \xi < 2$, (2-->6) x $10^3$ $cm^2 sec^{-1}$ for $3 < \xi < 5$, and 25 x $10^3$ $cm^2$ $sec^{-1}$ for $\xi > 6$. The other terms are seasonal contributions from planetary wave activity. A(x) is an altitudinal factor to be 1 for lower to middle stratosphere and to be 0 otherwise. $B(\phi)$ is a latitudinal factor set to be 1 for midlatitude and to be zero otherwise. C(s) is a seasonal function of wave activity parameter set to be 9x$10^9$ $cm^2$ $sec^{-1}$ for winter and 0 for summer. D(h) is declination set to be 8 x $10^{-4}$ for southern and -8 x $10^{-4}$ for northern hemisphere.

Our model year has 360 days. Prescribed seasonal data such as temperature, circulation and eddy diffusion coefficients are renewed by every 3 days by interpolation. For the assessment of diurnal change effects diurnal change of density and photodissociation rates are calculated by every 15 days. A time step of diurnal change calculation is 10 minutes. From these calculations we define diurnal change coefficients as,

$$e_{kl} = \overline{N_k \cdot N_l} \;/\; (\bar{N}_k \cdot \bar{N}_l)$$

$$e_j = \overline{J_j \cdot N_j} \;/\; (\bar{J}_j \cdot \bar{N}_j)$$

where $N_k$ is number density of the species k, $J_j$ is the j-th photodissociation rate as a function of local time. Using these coefficients we can easily obtain diurnal mean photochemical production by diurnal mean value of density and photodissociation rate, i.e.,

$$\bar{Q}_x = \pm \Sigma e_{kl} \cdot R_{kl} \cdot \bar{N}_k \cdot \bar{N}_l \pm \Sigma e_j \cdot \bar{J}_j \cdot \bar{N}_j$$

So we can predict the zonal mean mixing ratio of the next time step on the basis of the present zonal mean value.

A time step of the zonal mean calculation is 8 hours. When the photochemical lifetime gets less than a time step, numerical instability generates. To avoid the instability some relaxation method of the change rate is introduced. To assure mass conservation the excess or the lack caused by relaxation is compensated by its converted species.

This method enables us to execute the stable integration on any photochemical condition.

References

JPL 87-41 (W.B.DeMore et al.), Chemical Kinetics and Photochemical Data for Use in Stratospheric Modeling, Evaluation 8, JPL Pasadena, 1987.

Louis, J.J., Mean Meridional Circulation. The Natural Stratosphere of 1974, in CIAP Monograph, U.S. Dept. of Transportation, 6-23, 1975.

Murgatroyd, R.J., and F. Singleton, Possible Meridional Circulations in the Stratosphere, Quart. J. Roy. Meteorol. Soc., 87, 125-135, 1961.

W.M.O., Atmospheric Ozone 1985, Assessment of Our Understanding of the Proceedings Controlling Its Present Distribution and Change, Geneva, 1986.

## Section 4.14 NOCAR 2-D Model

R.R. Garcia, S. Solomon, and J.T.Kiehl
National Oceanic and Atmospheric Administration
National Center for Atmospheric Research

### Garcia - Solomon - Kiehl 2-D Model

The model used for stratospheric studies extends from 100 mb (about 16 km) to 0.04 mb (about 70 km), and from 89.5 S to 89.5 N.

Dynamics:

The transport is represented by the residual Eulerian circulation computed from the mean residual streamfunction $\chi^*$. The streamfunction equation includes nonlinear terms, and a specification of $\chi^*$ at the lower boundary. The temperature field is obtained from the thermodynamic equation given the residual Eulerian velocities $v^*$ and $w^*$. The mean zonal wind is evaluated from the temperature field assuming thermal wind balance. Rayleigh friction is prescribed as a function of height only. Eddy diffusion coefficients are non-interactive and are presented as indicated in the archived model results. See Garcia and Solomon (1983), Solomon et al. (1985) for details.

Photochemistry:

Continuity equations including transport terms are solved for the following species:

$O_x$ (=$O(^1D)$ + $O(^3P)$ + $O_3$)
$HO_x$ (=OH + $HO_2$ + H)
$NO_x$ (=NO + $NO_2$ + $NO_3$ + $2N_2O_5$)
$HNO_3$
$H_2O_2$
$ClO_x$ (=Cl +ClO +HOCl +$ClONO_2$)
HCl
$CF_2Cl_2$
$CFCl_3$
$CCl_4$
$CH_3Cl$
$H_2O$
$CH_4$
$N_2O$
$H_2$

The $O_x$, $HO_x$, $NO_x$, and $ClO_x$ chemical families are partitioned based on steady-state approximations when the time scale for partitioning is less than 10 minutes. Longer-lived individual members of these chemical families (e.g., $N_2O_5$ at high latitudes) are solved for individually, including transport terms, whenever their photochemical lifetimes exceed 10 minutes.

$CH_4$ oxidation chemistry is considered in detail, and includes the chemistry of relevant intermediates such as $H_2CO$, HCO, etc., as described by LeTexier et al. (1988).

Approximation number 4 of Cogley and Borucki (1976) is used to derive daytime averaged photolysis

rates. These values are applied to all photolysis reactions during the sunlit period of the day at any particular latitude. Photolysis rates are set to zero at night, so that this essentially corresponds to a "two-tank" approximation.

See also Garcia and Solomon (1983), Solomon and Garcia (1983; 1984), and Solomon et al. (1985).

Radiation:

Heating due to absorption of utlraviolet and visible radiation by ozone, molecular oxygen, and $NO_2$ is evaluated using the same wavelength intervals as those employed in the photolysis calculations. Near-infrared heating by $CO_2$ and water vapor employs the solar radiation code used in the NCAR Community Climate Model (Kiehl et al., 1987).

The longwave cooling rates due to $CO_2$, $O_3$, and $H_2O$ are obtained from the computed mixing ratios and temperature. Longwave radiative cooling is calculated with the radiation model from the NCAR CCM. The scheme is based on the broadband absorption method (see Kiehl et al., 1987). $CO_2$ and $O_3$ cooling include Voigt line effects as described by Kiehl and Briegleb (1988).

References:

Cogley, A. C. and W. J. Borucki, Exponential approximation for daily average solar heating and photolysis, J. Atmos. Sci., 33, 1347, 1976.

Garcia, R. R. and S. Solomon, A numerical model of the zonally average dynamical and chemical structure of the middle atmosphere, J. Geophys. Res., 88, 1379, 1983.

Kiehl, J. T. , R. J. Wolski, B. P. Briegleb, and V. Ramanathan, Documentation of radiation and cloud routines in the NCAR Community Climate Model (CCM1), NCAR Technical Note, NCAR/TN -288+IA, 1987.

Kiehl, J. T. and B. Briegleb, A new parameterization of the absorptance due to the 15um band system of carbon dioxide, submitted to J. Geophys. Res., 1988.

LeTexier, H., S. Solomon, and R. R. Garcia, The role of molecular hydrogen and methane oxidation in the water vapor budget of the stratosphere, Quart. J. Roy. Met. Soc., 114, 281, 1988.

Solomon, S. and R. R. Garcia, On the distribution of nitrogen dioxide in the high latitude stratosphere, J. Geophys. Res., 88, 5497, 1983.

Solomon, S. and R. R. Garcia, On the distribution of long-lived tracers and chlorine species in the middle atmosphere, J. Geophys. Res., 89, 11633, 1984.

Solomon, S., R. R. Garcia, and F. Stordal, Transport processes and ozone perturbations, J. Geophys. Res., 90, 12981, 1985.

## Section 4.15 OSLO 2-D Model

I.S.A. Isaksen and F. Stordal
University of Oslo
Institute of Geophysics
P.O. Box 1022 Blindern
0315 Oslo
NORWAY

* Brief:

A two dimensional transport-chemistry model of the troposphere and the stratosphere (0-50 km), covering latitudes from pole to pole, employing the diabatic circulation with small eddy diffusion coefficients in the stratosphere.

*Journal reference for model documentation:

Stordal, F., Isaksen, I.S. A. and Horntveth, K. 1985. A diabiatic circulation two-dimensional model with photochemistry: Simulations of ozone and long-lived tracers with surface sources, J. Geophys. Res., 90, 5757-5776.

Isaksen, I.S.A. and Stordal, F. 1986. Ozone perturbations by enhanced levels of CFCs, $N_2O$ and $CH_4$: a two-dimensional diabatic circulation study including uncertainty estimates. J. Geophys. Res., 91, 5245 -5263.

Stordal, F. and Isaksen, I.S.A. 1987. Ozone perturbations due to increase in $N_2O$, $CH_4$ and chlorocarbons: two-dimensional time dependent calculations, Tellus, 39B, 333-353.

*Units:

Gas concentrations given as volume mixing ratios
Heating rates given in K/day

*Time steps covered:

Mid-month data twelve months of year 1980.

## Section 4.16 WISCAR 2-D Model

G. Brasseur, M.H. Hitchman, and A. DeRudder
University of Wisconsin and
National Center for Atmospheric Research

This radiative-chemical-dynamical model was designed at the Belgian Institute for Space Aeronomy (BISA) by G. Brasseur, M. Dymek, and K.E.. Falise and further developed at NCAR. Two cooperative projects have been established for mutual benefit. A detailed radiative code has been provided by Drs. P. Crutzen and C. Bruhl of the Max Planck Institute for Chemistry in Mainz, Germany. A transport scheme is being developed by Dr. M. Pirre of the Laboratory for Physics and Chemistry of the Environment in Orleans, France. It will be expressed in isentropic coordinates but will retain the same chemical and radiative codes.

1. Model domain and resolution

0-85 km $\Delta$ = 1 km
pole-pole $\Delta = 5°$

2. Transport treatment

Entropy and chemical species are advected by a residual (transformed Eulerian) mean meridional circulation in log-pressure coordinates. The residual mean meridional stream-function is forced by spatial gradients in wave driving and in radiative heating or cooling (see Garcia and Solomon, 1983). Zonal winds are derived from the thermal wind law and a seasonally-varying surface boundary condition. The zonal wind distribution determines the distribution of wave driving and vertical eddy diffusivity due to gravity waves and of wave driving and meridional eddy diffusivity due to Rossby waves. These self-determined eddy diffusivities are used with the residual circulation and photochemical sources and sinks to determine distributions.

Two codes are available for radiative heating and cooling calculations: fast or accurate. For fast calculations IR transfer is approximated by a Newtonian relaxation toward a seasonally-varying climatological temperature cross-section, while the parameterization of Schoeberl and Strobel (1978) is used for isolation absorption by ozone. The detailed code was provided by Crutzen and Bruhl who adapted an earlier model of Ramanathan. IR transfer is calculated for carbon dioxide, ozone, water vapor, methane, nitrous oxide, and CFC-11 and CFC-12. Solar heating is calculated for ozone, nitrogen dioxide, water vapor, and carbon dioxide.

The model can be run with a variety of dynamical forcings. Most simply, momentum drag is parameterized by a Rayleigh friction and eddy diffusivities vary with altitude only. A more complex representation of the effects of small scale eddies is afforded by the breaking gravity wave parameterization of Lindzen (1981) and Holton (1982). A spectrum of phase speeds were chosen and parameters were tuned to yield residual circulations comparable to those inferred from LIMS observations (Hitchman and Leovy, 1986). A new parameterization of Rossby wave driving was introduced to provide a self-consistent determination of their torque on the zonal flow and dispersion of tracers (Hitchman and Brasseur, 1987). A conservation equation for Rossby wave action is solved, given climatologically-varying upward fluxes across the tropopause and a damping profile. The meridional eddy diffusivity and zonal torque are proportional to the flux convergence of wave action. A background value of $3 \times 10^5 m^2/s$ is added to the calculated meridional eddy diffusivity.

3. Chemistry Treatment

Approximately 40 species are included. The family grouping method is used. A discrimination is made between (1) long-lived species and families and (2) short-lived species. The source gases are: $N_2O$, $CCl_4$, $CFCl_3$, $CF_2Cl_2$, $CH_3CCl_3$, $CH_3Cl$, $CH_4$, $C_2H_2$, $C_2H_6$, $C_3H_8$, HCN, $CH_3CN$, $H_2O$, $H_2$, and $CO_2$. Transported families include $NO_y$ ($N+ NO + NO_2 + NO_3 + 2N_2O_5 + HNO_3 + HO_2NO_2 + ClONO_2$), $Cl_x$ ($Cl + ClO + HCl + HOCl + ClNO_2$), and $O_x$ ($O_3 + O(^3P) + O(^1D)$). Long-lived (transported) species are : CO, $HNO_3$, $N_2O_5$, and H. Short-lived species include: $O(^1D)$, $O(^3P)$, $O_3$; N, NO, $NO_2$, $NO_3$, $HNO_4$; Cl, ClO, HCl, $ClONO_2$, HOCl; OH, $HO_2$, and $CH_3O_2$. The reaction rate constants JPL (1985) compilation.

4. Photolysis Calculations

Photodissociation coefficients (J's) are calculated by spectral integration, using the 171 wavelength intervals specified by Ackerman (1971). These correspond to a resolution of 500 $cm^{-1}$ (wavenumber) between 117 and 308 nm, of 2.5 nm (wavelength) between 310 and 645 nm, and of 5 nm between 650 and 730 nm. The solar spectrum is specified according to Brasseur and Simon (1981). The cross sections are taken from the model used at BISA and are close to the values given in the JPL compilation.

Different routines for the calculation of the photodissociation coefficients are available in the code. The most comprehensive method includes multiple scattering and albedo, and is based on formalism of Fred Luther (private communication): six orders of scattering are considered together with absorption by $O_2$ and $O_3$. The surface albedo has to be specified. Penetration of solar ultraviolet in the Schumann-Runge bands is calculated by the parameterization of either Kockarts (1976) or of Nicolet and Peetermans (1980). For photolysis of NO in the $\delta$ (0-0) and $\delta$ (1-0) bands, the parameterization by Nicolet (1979) is used. The model can also be run using less detailed but faster codes for the calculation of the J's.

The diurnal average of the photodissociation coefficients is approximated by a 4 point integral between sunrise and sunset (see Cunnold et al., 1975). This procedure allows us to calculate an accurate mean J for different altitudes, latitudes and season with minimum computer costs.

5. Integration Algorithm

Centered space differences are used, together with an implicit 'alternating direction' method for time integration, yielding truncation errors of $O(\Delta x^2, \Delta t^2)$ (Carnahan et al., 1969). This method is absolutely stable, but underestimates time trends in proportion to $\Delta t$. With $\Delta t$ = 15 days inexpensive long integrations may be performed in which seasonal trends are adequately modeled. A shorter time step (e.g., 1 day) may be desirable for examining trends of a shorter time scale.

Negative mixing ratios are allowed but are rare and small and do not generally cause numerical instability.

6. Heterogeneous Removal Processes

Washout of $HNO_3$ and HCl is parameterized via specified altitude-dependent destruction rates in the troposphere.

7. Future Work

Ozone column amounts are somewhat sensitive to the details of how we specify the troposphere. We plan to carry out sensitivity studies and examine the lower boundary conditions carefully. We are also working with Dr. A.K. Smith of the University of Michigan to extend the domain to 120 km. Some thought needs to be given toward a representation of 'chemical eddies'. We will soon incorporate a vectorized detailed radiative code provided by Dr. J.T. Kiehl (another descendant of Ramanathan's code),

which should mitigate the cost of running the 'accurate' version. Finally, we are working on parameterizing the effects of Kelvin waves so that a self-consistent equatorial semiannual oscillation will occur in the model.

References

Ackerman, M., Mesospheric Models and Related Experiments, 149-159, 1972.

Brasseur, G., and P.C. Simon, J. Geophys. Res., 86, 7343, 1981.

Carnahan et al., Numerical Methods, 1969.

Cunnold et al., J. Atmos. Sci., 32, 170, 1975.

Garcia, R.R. and S. Solomon, J. Geophys. Res., 88, 1379, 1983.

Hitchman, M.H., and C.B. Leovy, J. Atmos. Sci., in press, 1986.

Hitchman, M.H., and G. Brasseur, Rossby wave action as an interactive tracer in a 2-D model: parameterization of wave driving and eddy diffusivity, in preparation.

Holton, J.R., J. Atmos.Sci., 40, 2497, 1982.

Kocharts, G., Planet Space Sci., 24, 589, 1976.

Lindzen, R.S., J. Geophys. Res., 86, 9707, 1981.

Nicolet, M., Geophys. Res. Letters, 6, 866, 1979.

Nicolet, M. and W. Peetermans, Planet. Space Sci., 28, 85, 1980.

Schoeberl, M.R., and D. F. Strobel, J. Atmos.Sci., 35, 577, 1978.

# CHAPTER 5

# INTRODUCTION AND DATA SUMMARY

# CHAPTER 5

# INTRODUCTION AND DATA SUMMARY

## Section 5.1 Introduction

### Section 5.1.1 Data Overview

For the Workshop Meeting in Virginia Beach, a subset of data representing most of the participating model groups was available for discussion and review. Chapter 3 presents the results of the intercomparisons of that subset of data. Subsequent to the Workshop, the various modeling groups had the opportunity to either update or add to the data sets discussed at the Workshop. Chapter 6 presents the overall revised data sets as of December 1988. The organization of Chapter 6 follows that of Chapter 3 with data from all the models (where available) grouped according to:

1. Photochemistry and Radiation
   - Photodissociation Coefficients
   - UV Heating and IR Cooling

2. Transport
   - Net Radiative Heating
   - Tropospheric Source Tracer Experiment
   - Time-dependent Source Conserved Tracer Experiment
   - Stratospheric Source Tracer Experiment
   - $O_3$ Column

3. Current Atmosphere
   - Integrated Columns of Trace Gases
   - $Cl_y$ and $NO_y$
   - Nitrogen Gases
   - Chlorine Gases
   - $O_x$ and $HO_x$ Gases
   - Source Gases

4. Perturbed Circulations and Temperatures

The data presented here provide a detailed summary of the two-dimensional picture of the atmosphere as seen by current atmospheric models. Chapter 6 is intended to serve as a comprehensive set of reference data depicting current capabilities.

**Section 5.1.2** Upper Atmosphere Data Base

The Upper Atmosphere Data Program (UADP) at NASA Langley Research Center has been established to serve as a working data base for information on stratospheric trace gases and related parameters. It includes data both from measurements and from model calculations. The UADP data base presently includes measurement data from satellite instruments such as LIMS, SAMS, SBUV, and ATMOS and the initial stages of a compilation of stratospheric balloon measurements. The recent focus, however, has been on assembling two-dimensional results from atmospheric model calculations, principally for use in intercomparison activities. Additional information on the UADP can be obtained from

Dr. Robert K. Seals, Jr.
MS 401A
NASA Langley Research Center
Hampton, Virginia 23665
(Telephone 804-864-2696)

The UADP served as the central focal point for assembly of data for the Model Workshop discussed in this report. A substantial amount of work was required with the principal activities involving the handling of data from the various model groups, incorporation of the desired data into the UADP data base on each model's particular grid, gridding of the model data onto a predefined intercomparison grid, data manipulation to derive sums and ratios, and display of the data in graphical form. For the Workshop itself, selected plots were generated for photodissociation coefficients, UV heating and IR cooling rates, net radiative heating, the three tracer experiments (X, Y, and Z), integrated gas columns, and January model outputs for a set of trace gases ($NO_y$, $NO_x$, $Cl_y$, $NO_x/NO_y$, $HNO_3/NO_2$, ClO/HCl, Cl/ClO, $OH/HO_2$, $H_2O_2$, $N_2O$, $CH_4$, and $CFCl_3$). This was done both using the UADP system prior to the Workshop and with workstations at the Workshop. The workstations utilized both electronic connection to the remote UADP computer and a self-contained approach utilizing optical disks. Subsequent to the Workshop a more complete data set, of both original and gridded data, has been incorporated in the UADP. The plots presented in Chapter 6 cover the complete range of intercomparisons.

Two principal areas of work in dealing with the model data sets were the decoding of data from the wide variety of formats used by the model groups submitting data and the transformation of data from each model's specific spatial grid to the predefined intercomparison grid. At the Workshop a standard data format for future transmittal of data to the UADP was established to address the first area. The issue of data gridding arises from the need to intercompare outputs from different models by taking sums,

differences, ratios, and the like. In order to do this, the data sets must be on a common grid. For the two-dimensional data sets addressed here the desired standard intercomparison grid was confirmed to be

Horizontal: 90° S to 90° N in latitude at increments of 5 degrees

Vertical: $z^* = 0$ to 60 km in increments of 2 km
where $z^* = 16 \log_{10}(1000/P)$
and P is the pressure in mbar

After considerable discussion at the Workshop, it was decided that the most desirable course for dealing with the gridding issue in the future would be for each group to submit data on the standard grid. The basic premise that data interpolation or gridding is best done by the data generating team was a deciding point in this decision. For the present Workshop data, the data gridding has been done at the UADP.

## **Section 5.2** Data Summary

Data presented in Chapter 6 represents results from sixteen model groups. The groups are designated by the following abbreviations:

AER - Atmospheric and Environmental Research, Inc.
CALJPL - California Institute of Technology; Jet Propulsion Laboratory
CAMBRAL - Cambridge University; Rutherford Appleton Laboratory, U.K.
CAO - Central Aerological Observatory, U.S.S.R
CLKSON - Clarkson University
DUPONT - E. I. DuPont De Nemours & Company, Inc.
GISS - NASA Goddard Institute for Space Studies
GSFC1 - NASA Goddard Space Flight Center
GSFC2 - NASA Goddard Space Flight Center (Fast 2D Model)
LARC - NASA Langley Research Center
LLNL - Lawrence Livermore National Laboratory
MPIC - Max Planck Institute for Chemistry, Germany
MRI - Meteorological Research Institute, Japan
NOCAR - NOAA; NCAR
OSLO - University of Oslo, Norway
WISCAR - University of Wisconsin; NCAR

Brief descriptions for each of these modeling activities can be found in Chapter 4 of this report. Data presented are noontime values for models AER, LARC, MRI, NOCAR, and OSLO. Daytime (daylight hours only) average values are presented for models CAMBRAL, CLKSON, GSFC1, and GSFC2. Finally, diurnal (24 hour) average values are given for models DUPONT, LLNL, and WISCAR.

Chapter 6 contains contour plots for the intercomparison parameters, either as pressure altitude ($z^*$) versus latitude for a particular month or as latitude versus month. An overall summary of the data plots is contained in Tables 5-1 and 5-2. Tables 5-1 and 5-2 are organized with the columns representing a particular model and the rows a particular parameter or group of parameters. Each entry in the tables corresponds to the page number(s) in Chapter 6 where the plot or plots can be found. Dash mark entries indicate that there is no plot for a parameter for a particular model. Table 5-3 provides a summary listing and page location for the tables in Chapter 6 which provide additional information on each parameter such as the parameter designation, a brief description, the units, and the contour levels for the corresponding plots. Each individual plot has a heading which gives the designation for the plotted parameter, the model abbreviation, and the month of the data (where appropriate). Tables 6-1a and 6-1b describe the plots for photochemistry and radiation parameters. Plots in this group are for one month, typically January. Tables 6-2a, 6-2b, 6-2c, and 6-2d cover the transport parameter plots. The net radiative heating and tracer X plots are generally for the four months of March, June, September, and December. Tracer Y plots are snapshots at six month intervals, and the ozone and tracer Z column plots cover a full twelve month period. Table 6-3a, 6-3b, 6-3c, 6-3d, 6-3e, and 6-3f describe the current (1980) atmosphere parameter plots. These plots are also generally for the four months of March, June, September, and December. Table 6-4 describes the perturbation atmosphere parameter plots which cover the same four months. The four perturbation scenarios are described in Chapter 3 and are designated by A, B, C, and D.

**Table 5-1.** Data Plot Summary - First Eight Models

| | Model | | | | | | | |
|---|---|---|---|---|---|---|---|---|
| | AER | CALJPL | CAMBRAL | CAO | CLKSON | DUPONT | GISS | GSFC1 |
| Photodissociation | 155-7 | 158-60 | 161-3 | --- | 164-5 | --- | 166-8 | 169-71 |
| Heating and Cooling Rates | 194 | --- | 195 | 196 | 197 | --- | 198 | --- |
| Net Heating | 205 | 206 | --- | --- | 207 | --- | --- | 208 |
| Tracer X | 213 | 214 | --- | --- | 215 | --- | 216 | --- |
| Tracer Y | 222-3 | 224-6 | 227-9 | --- | 230-2 | --- | 233-5 | --- |
| $O_3$ and Z Columns | 248 | 248 | --- | --- | 249 | --- | 249 | --- |
| $HNO_3$, HCl, $NO_2$, and ClO Columns | 254 | --- | --- | --- | 255 | --- | --- | --- |
| $NO_y$ | 263 | --- | 265 | --- | 267 | 269 | --- | 270 |
| $Cl_y$ | 264 | --- | 266 | --- | 268 | 269 | --- | 270 |
| $NO_x$ | 286 | --- | 294 | --- | 302 | 309 | --- | 313 |
| $NO_2$ | 287 | --- | 295 | --- | 303 | 310 | --- | 314 |
| $HNO_3$ | 288 | --- | 296 | --- | 304 | 310 | --- | 314 |
| $N_2O_5$ | 289 | --- | 297 | --- | --- | 311 | --- | 314 |
| $HO_2NO_2$ | 290 | --- | 298 | --- | 305 | 311 | --- | 314 |

Table 5-1. Data Plot Summary - First Eight Models (Continued)

| | Model | | | | | | | |
|---|---|---|---|---|---|---|---|---|
| | AER | CALJPL | CAMBRAL | CAO | CLKSON | DUPONT | GISS | GSFC1 |
| $NO/NO_2$ | 291 | --- | 299 | --- | 306 | 312 | --- | 313 |
| $HNO_3/NO_2$ | 292 | --- | 300 | --- | 307 | 312 | --- | 313 |
| $NO_x/NO_y$ | 293 | --- | 301 | --- | 308 | 309 | --- | 313 |
| ClO | 372 | --- | 379 | --- | 386 | 392 | --- | 396 |
| HCl | 373 | --- | 380 | --- | 387 | 393 | --- | 396 |
| $ClNO_3$ | 374 | --- | 381 | --- | 388 | 393 | --- | 396 |
| HOCl | 375 | --- | 382 | --- | --- | 392 | --- | 396 |
| Cl/ClO | 376 | --- | 383 | --- | 389 | 394 | --- | 397 |
| $ClO/Cl_y$ | 377 | --- | 384 | --- | 390 | 395 | --- | 397 |
| ClO/HCl | 378 | --- | 385 | --- | 391 | 395 | --- | 397 |
| $O_3$ | 448 | --- | 456 | --- | 463 | 468 | --- | 472 |
| $HO_2$ | 449 | --- | 457 | --- | 464 | 469 | --- | 472 |
| $H_2O_2$ | 450 | --- | 458 | --- | 465 | 469 | --- | 472 |
| $H_2CO$ | 451 | --- | --- | --- | --- | 468 | --- | 472 |
| O | 452 | --- | 459 | --- | --- | --- | --- | 473 |
| OH | 453 | --- | 460 | --- | --- | 470 | --- | 473 |
| $O/O_3$ | 454 | --- | 461 | --- | 466 | --- | --- | 474 |

Table 5-1. Data Plot Summary - First Eight Models (Continued)

| | Model | | | | | | | |
|---|---|---|---|---|---|---|---|---|
| | AER | CALJPL | CAMBRAL | CAO | CLKSON | DUPONT | GISS | GSFC1 |
| $OH/HO_2$ | 455 | --- | 462 | --- | 467 | 471 | --- | 474 |
| $N_2O$ | 527 | --- | 533 | --- | 539 | 541 | --- | 544 |
| $CH_4$ | 528 | --- | 534 | --- | 540 | 541 | --- | 544 |
| $CFCl_3$ | 529 | --- | 535 | --- | --- | 542 | --- | 545 |
| $CF_2Cl_2$ | 530 | --- | 536 | --- | --- | 542 | --- | 545 |
| $CCl_4$ | 531 | --- | 537 | --- | --- | 543 | --- | 545 |
| $CH_3CCl_3$ | 532 | --- | 538 | --- | --- | 543 | --- | 545 |
| DQ-A | --- | --- | --- | --- | --- | --- | --- | --- |
| DT-A | --- | --- | --- | --- | --- | --- | --- | --- |
| DQ-B | 582 | --- | --- | --- | --- | --- | --- | --- |
| DT-B | 583 | --- | --- | --- | --- | --- | --- | --- |
| DQ-C | 584 | --- | --- | --- | --- | --- | --- | --- |
| DT-C | 585 | --- | --- | --- | --- | --- | --- | --- |
| DQ-D | 586 | --- | --- | --- | --- | --- | --- | --- |
| DT-D | 587 | --- | --- | --- | --- | --- | --- | --- |

Table 5-2. Data Plot Summary - Second Eight Models

| | Model | | | | | | | |
|---|---|---|---|---|---|---|---|---|
| | GSFC2 | LARC | LLNL | MPIC | MRI | NOCAR | OSLO | WISCAR |
| Photodissociation | 172-4 | --- | 175-7 | 178-80 | 181-3 | 184-6 | 187-9 | 190-2 |
| Heating and Cooling Rates | --- | --- | 199 | 200 | --- | 201 | 202 | 203 |
| Net Heating | 209 | --- | --- | --- | 210 | --- | --- | 211 |
| Tracer X | 217 | --- | 218 | --- | 219 | --- | --- | 220 |
| Tracer Y | 236-8 | --- | 239-41 | --- | 242-4 | --- | --- | 245-6 |
| $O_3$ and Z Columns | 250 | 250 | 251 | --- | 251 | --- | 252 | 252 |
| $HNO_3$, HCl, $NO_2$, and ClO Columns | 256 | 257 | 258 | --- | 259 | --- | 260 | 261 |
| $NO_y$ | 271 | 273 | 275 | --- | 277 | 279 | 281 | 283 |
| $Cl_y$ | 272 | 274 | 276 | --- | 278 | 280 | 282 | 284 |
| $NO_x$ | 315 | 323 | 331 | --- | 339 | 347 | 355 | 363 |
| $NO_2$ | 316 | 324 | 332 | --- | 340 | 348 | 356 | 364 |
| $HNO_3$ | 317 | 325 | 333 | --- | 341 | 349 | 357 | 365 |
| $N_2O_5$ | 318 | 326 | 334 | --- | 342 | 350 | 358 | 366 |
| $HO_2NO_2$ | 319 | 327 | 335 | --- | 343 | 351 | 359 | 367 |

Table 5-2. Data Plot Summary - Second Eight Models (Continued)

| | Model | | | | | | | |
|---|---|---|---|---|---|---|---|---|
| | GSFC2 | LARC | LLNL | MPIC | MRI | NOCAR | OSLO | WISCAR |
| $NO/NO_2$ | 320 | 328 | 336 | --- | 344 | 352 | 360 | 368 |
| $HNO_3/NO_2$ | 321 | 329 | 337 | --- | 345 | 353 | 361 | 369 |
| $NO_x/NO_y$ | 322 | 330 | 338 | --- | 346 | 354 | 362 | 370 |
| ClO | 398 | 405 | 412 | --- | 419 | 426 | 433 | 440 |
| HCl | 399 | 406 | 413 | --- | 420 | 427 | 434 | 441 |
| $ClNO_3$ | 400 | 407 | 414 | --- | 421 | 428 | 435 | 442 |
| HOCl | 401 | 408 | 415 | --- | 422 | 429 | 436 | 443 |
| Cl/ClO | 402 | 409 | 416 | --- | 423 | 430 | 437 | 444 |
| $ClO/Cl_y$ | 403 | 410 | 417 | --- | 424 | 431 | 438 | 445 |
| ClO/HCl | 404 | 411 | 418 | --- | 425 | 432 | 439 | 446 |
| $O_3$ | 475 | 483 | 490 | --- | 498 | 504 | 512 | 520 |
| $HO_2$ | 476 | 484 | 491 | --- | 499 | 505 | 513 | 521 |
| $H_2O_2$ | 477 | --- | 492 | --- | 500 | 506 | 514 | --- |
| $H_2CO$ | 478 | 485 | 493 | --- | 501 | 507 | 515 | --- |
| O | 479 | 486 | 494 | --- | --- | 508 | 516 | 522 |
| OH | 480 | 487 | 495 | --- | --- | 509 | 517 | 523 |
| $O/O_3$ | 481 | 488 | 496 | --- | 502 | 510 | 518 | 524 |

**Table 5-2.** Data Plot Summary - Second Eight Models (Continued)

| | Model | | | | | | | |
|---|---|---|---|---|---|---|---|---|
| | GSFC2 | LARC | LLNL | MPIC | MRI | NOCAR | OSLO | WISCAR |
| $OH/HO_2$ | 482 | 489 | 497 | --- | 503 | 511 | 519 | 525 |
| $N_2O$ | 546 | --- | 552 | --- | 558 | 564 | 569 | 575 |
| $CH_4$ | 547 | --- | 553 | --- | 559 | 565 | 570 | 576 |
| $CFCl_3$ | 548 | --- | 554 | --- | 560 | 566 | 571 | 577 |
| $CF_2Cl_2$ | 549 | --- | 555 | --- | 561 | 567 | 572 | 578 |
| $CCl_4$ | 550 | --- | 556 | --- | 562 | 568 | 573 | 579 |
| $CH_3CCl_3$ | 551 | --- | 557 | --- | 563 | --- | 574 | 580 |
| DQ-A | --- | --- | --- | --- | --- | --- | --- | 588 |
| DT-A | --- | --- | --- | --- | --- | --- | --- | 589 |
| DQ-B | --- | --- | --- | --- | --- | --- | --- | 590 |
| DT-B | --- | --- | --- | --- | --- | --- | --- | 591 |
| DQ-C | --- | --- | --- | --- | --- | --- | --- | 592 |
| DT-C | --- | --- | --- | --- | --- | --- | --- | 593 |
| DQ-D | --- | --- | --- | --- | --- | --- | --- | 594 |
| DT-D | --- | --- | --- | --- | --- | --- | --- | 595 |

# CHAPTER 6

# UPPER ATMOSPHERE DATA PLOTS

Robert K. Seals, Jr.

**Table 5-3.** Plot Description Summary Locations

| Parameter Group | Descriptor Table | Table Page |
|---|---|---|
| Photodissociation Coefficients | Table 6-1a | 153-4 |
| Heating and Cooling Rates | Table 6-1b | 193 |
| Net Radiative Heating | Table 6-2a | 204 |
| Tracer X | Table 6-2b | 212 |
| Tracer Y | Table 6-2c | 221 |
| $O_3$ and Tracer Z Columns | Table 6-2d | 247 |
| Trace Gas Columns | Table 6-3a | 253 |
| $Cl_y$ and $NO_y$ | Table 6-3b | 262 |
| Nitrogen Gases | Table 6-3c | 285 |
| Chlorine Gases | Table 6-3d | 371 |
| $O_x$ and $HO_x$ Gases | Table 6-3e | 447 |
| Source Gases | Table 6-3f | 526 |
| Perturbed Circulations and Temperatures | Table 6-4 | 581 |

**Table 6-1a.** Photodissociation Coefficients

Fixed January atmosphere (Temperature and $O_3$)
Models Represented - AER, CALJPL, CAMBRAL, CLKSON, GISS, GSFC1, GSFC2, LLNL, MPIC, MRI, NOCAR, OSLO, WISCAR

| Parameter | Description | Units | Contour Levels |
|---|---|---|---|
| J $HNO_3$ | $HNO_3$ Photodissociation Coefficient | $sec^{-1}$ | 1.0E-07, 2.0E-07, 5.0E-07, 1.0E-06, 2.0E-06, 5.0E-06, 1.0E-05, 2.0E-05, 3.0E-05, 4.0E-05, 5.0E-05, 6.0E-05, 7.0E-05, 8.0E-05, 9.0E-05, 1.0E-04 |
| J NO | NO Photodissociation Coefficient | $sec^{-1}$ | 1.0E-10, 1.0E-09, 1.0E-08, 2.0E-08, 5.0E-08, 1.0E-07, 2.0E-07, 4.0E-07, 6.0E-07, 8.0E-07, 1.0E-06, 2.0E-06, 3.0E-06, 4.0E-06, 5.0E-06 |
| J $ClNO_3$ | $ClNO_3$ Photodissociation Coefficient | $sec^{-1}$ | 1.0E-05, 2.0E-05, 3.0E-05, 4.0E-05, 6.0E-05, 8.0E-05, 1.0E-04, 2.0E-04, 3.0E-04, 4.0E-04, 5.0E-04, 6.0E-04, 7.0E-04 |
| J $NO_2$ | $NO_2$ Photodissociation Coefficient | $sec^{-1}$ | 1.0E-04, 1.0E-03, 2.0E-03, 3.0E-03, 4.0E-03, 5.0E-03, 6.0E-03, 7.0E-03, 8.0E-03, 9.0E-03, 1.0E-02, 2.0E-02 |
| J $O_3$-TOT | $O_3$ Photodissociation Coefficient | $sec^{-1}$ | 1.0E-05, 1.0E-04, 2.0E-04, 3.0E-04, 4.0E-04, 5.0E-04, 6.0E-04, 7.0E-04, 8.0E-04, 9.0E-04, 1.0E-03, 2.0E-03, 3.0E-03, 4.0E-03, 5.0E-03, 6.0E-03, 7.0E-03, 8.0E-03 |
| J $O_3$-$^1D$ | $O_3$-$^1D$ Photodissociation Coefficient | $sec^{-1}$ | 1.0E-07, 1.0E-06, 2.0E-06, 5.0E-06, 1.0E-05, 2.0E-05, 5.0E-05, 1.0E-04, 2.0E-04, 5.0E-04, 1.0E-03, 2.0E-03, 3.0E-03, 4.0E-03, 5.0E-03, 6.0E-03 |

**Table 6-1a.** Photodissociation Coefficients (Continued)

Fixed January atmosphere (Temperature and $O_3$)
Models Represented - AER, CALJPL, CAMBRAL, CLKSON, GISS, GSFC1, GSFC2, LLNL, MPIC, MRI, NOCAR, OSLO, WISCAR

| Parameter | Description | Units | Contour Levels |
|---|---|---|---|
| J $O_2$ | $O_2$ Photodissociation Coefficient | $sec^{-1}$ | 1.0E-13, 1.0E-12, 2.0E-12, 5.0E-12, 1.0E-11, 2.0E-11, 5.0E-11, 1.0E-10, 2.0E-10, 3.0E-10, 4.0E-10, 5.0E-10, 6.0E-10, 7.0E-10, 8.0E-10, 9.0E-10, 1.0E-09 |
| J $CF_2Cl_2$ | $CF_2Cl_2$ (F-12) Photodissociation Coefficient | $sec^{-1}$ | 1.0E-09, 1.0E-08, 2.0E-08, 5.0E-08, 1.0E-07, 2.0E-07, 3.0E-07, 4.0E-07, 5.0E-07, 6.0E-07, 7.0E-07, 8.0E-07, 9.0E-07, 1.0E-06, 2.0E-06, 3.0E-06 |
| J $CFCl_3$ | $CFCl_3$ (F-11) Photodissociation Coefficient | $sec^{-1}$ | 1.0E-09, 1.0E-08, 1.0E-07, 2.0E-07, 5.0E-07, 1.0E-06, 2.0E-06, 3.0E-06, 4.0E-06, 5.0E-06, 6.0E-06, 7.0E-06, 8.0E-06, 9.0E-06, 1.0E-05 |
| J $N_2O$ | $N_2O$ Photodissociation Coefficient | $sec^{-1}$ | 1.0E-11, 1.0E-10, 1.0E-09, 2.0E-09, 5.0E-09, 1.0E-08, 2.0E-08, 4.0E-08, 6.0E-08, 8.0E-08, 1.0E-07, 2.0e-07, 3.0E-07, 4.0E-07, 5.0E-07, 6.0e-07, 7.0E-07 |

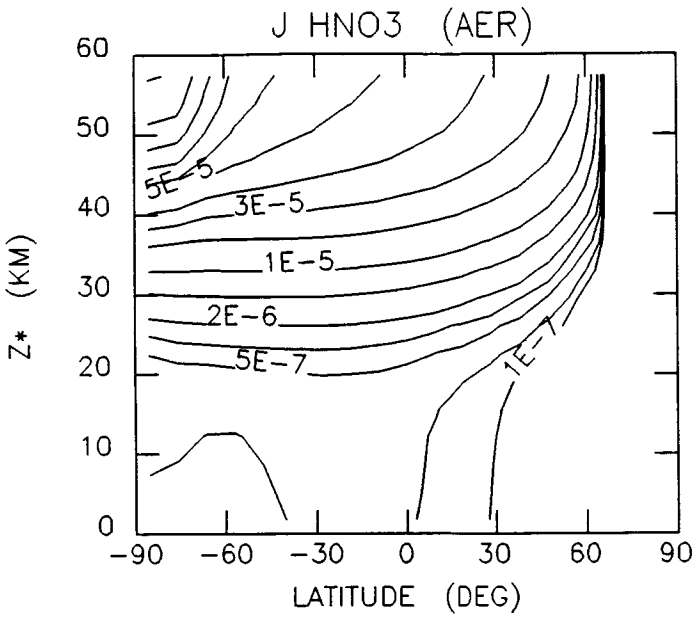
J HNO3 (AER)
Z* (KM)
LATITUDE (DEG)
5E-5
3E-5
1E-5
2E-6
5E-7
1E-7

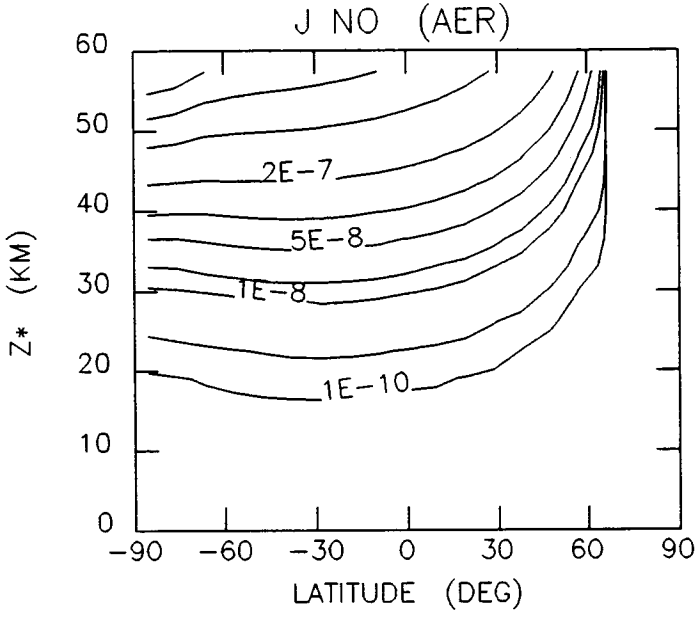
J NO (AER)
Z* (KM)
LATITUDE (DEG)
2E-7
5E-8
1E-8
1E-10

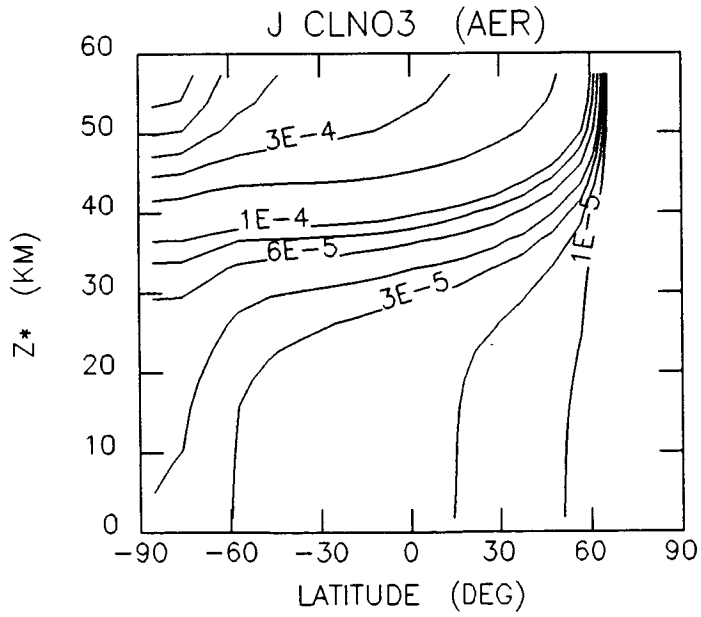
J CLNO3 (AER)
Z* (KM)
LATITUDE (DEG)
3E-4
1E-4
6E-5
3E-5
1E-5

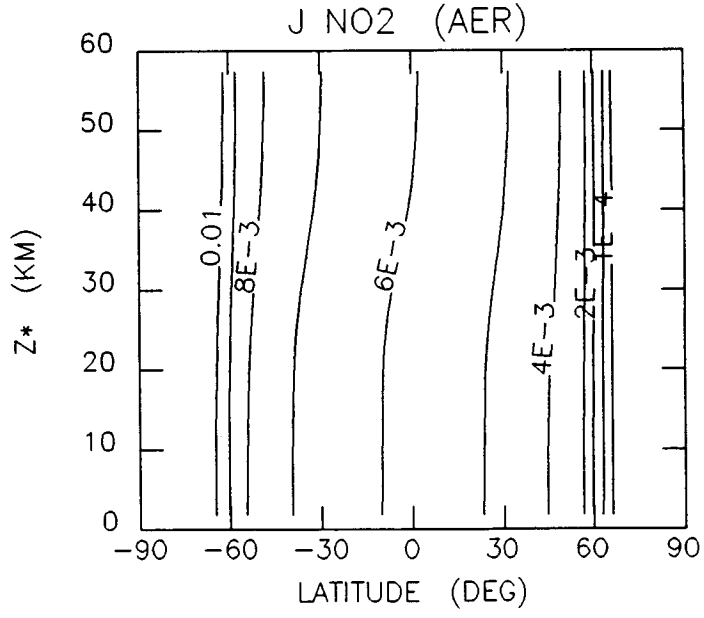
J NO2 (AER)
Z* (KM)
LATITUDE (DEG)
0.01
8E-3
6E-3
4E-3
2E-3
1E-4

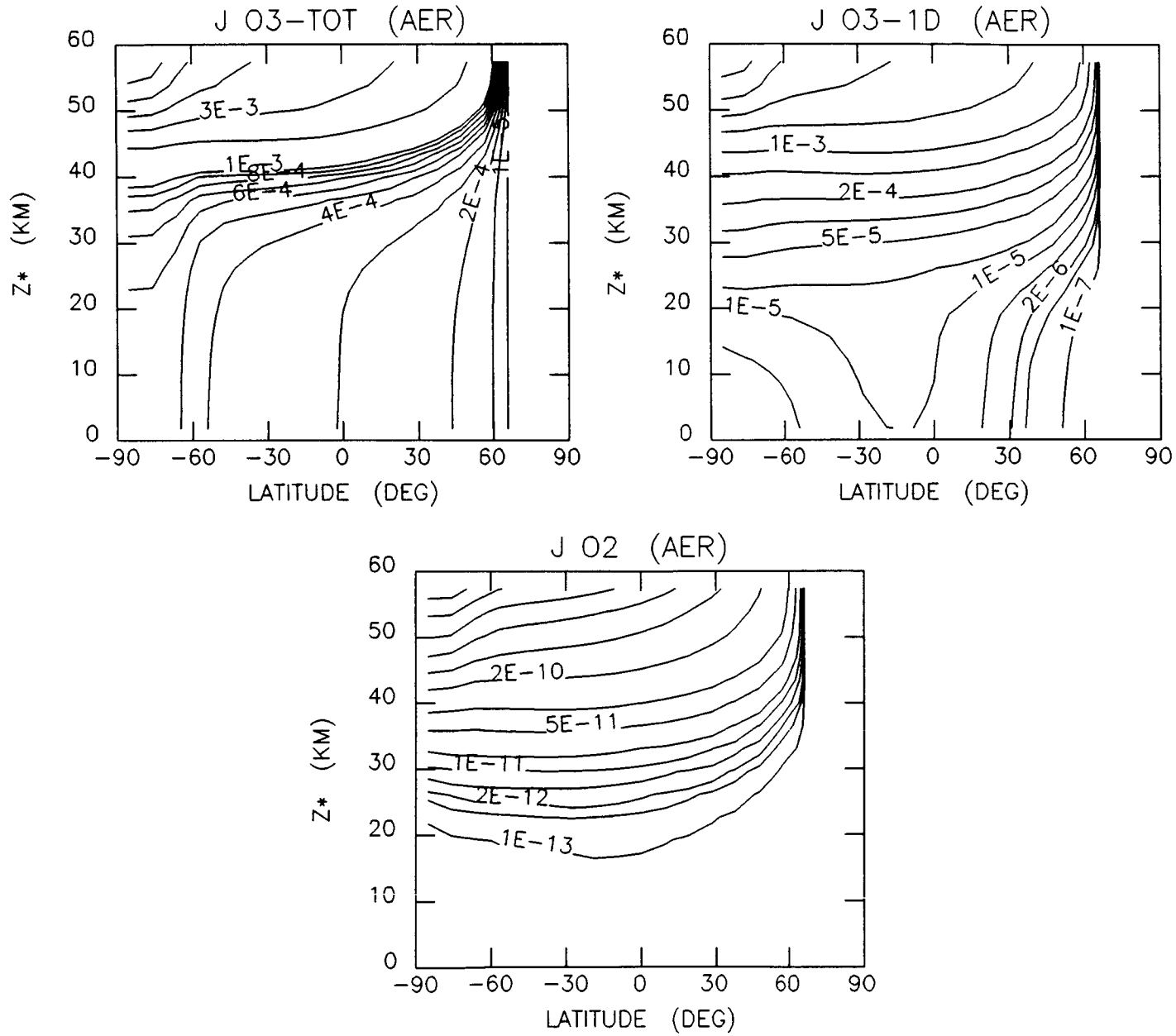
J O3−TOT (AER)
Z* (KM)
LATITUDE (DEG)
3E−3
1E−3
8E−4
6E−4
4E−4
2E−4
J O3−1D (AER)
Z* (KM)
LATITUDE (DEG)
1E−3
2E−4
5E−5
1E−5
1E−5
2E−6
1E−7
J O2 (AER)
Z* (KM)
LATITUDE (DEG)
2E−10
5E−11
1E−11
2E−12
1E−13

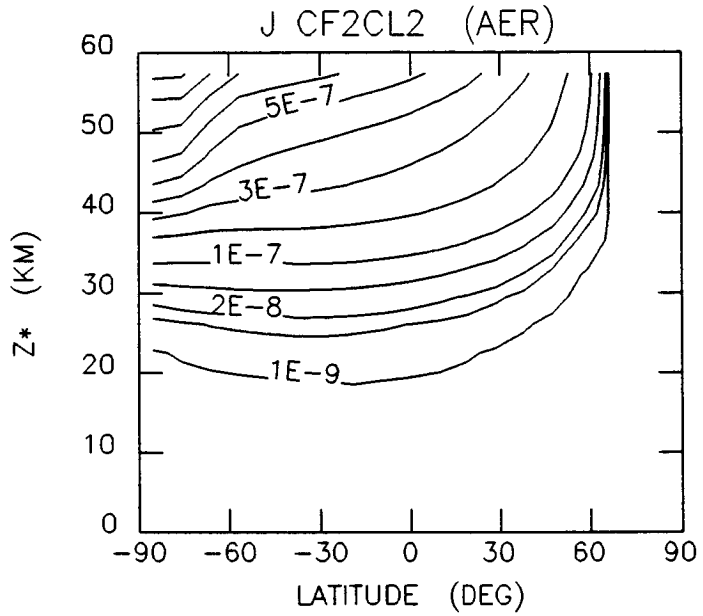
J CF2CL2 (AER)
Z* (KM)
LATITUDE (DEG)
5E-7
3E-7
1E-7
2E-8
1E-9

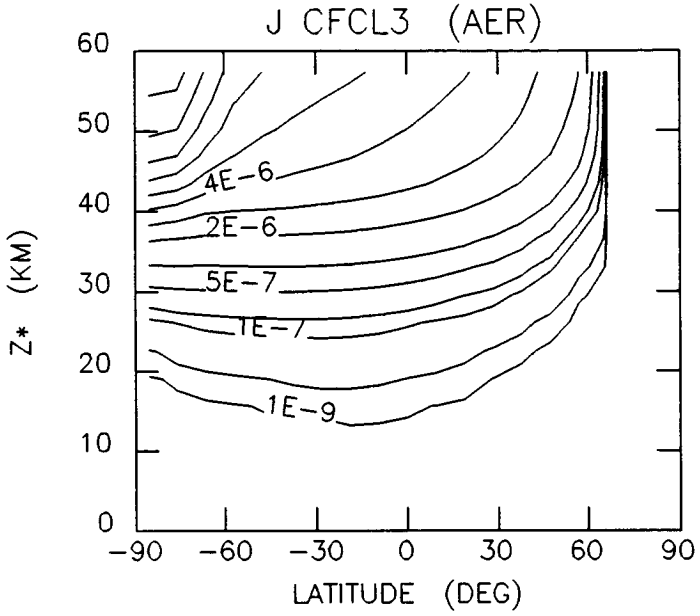
J CFCL3 (AER)
Z* (KM)
LATITUDE (DEG)
4E-6
2E-6
5E-7
1E-7
1E-9

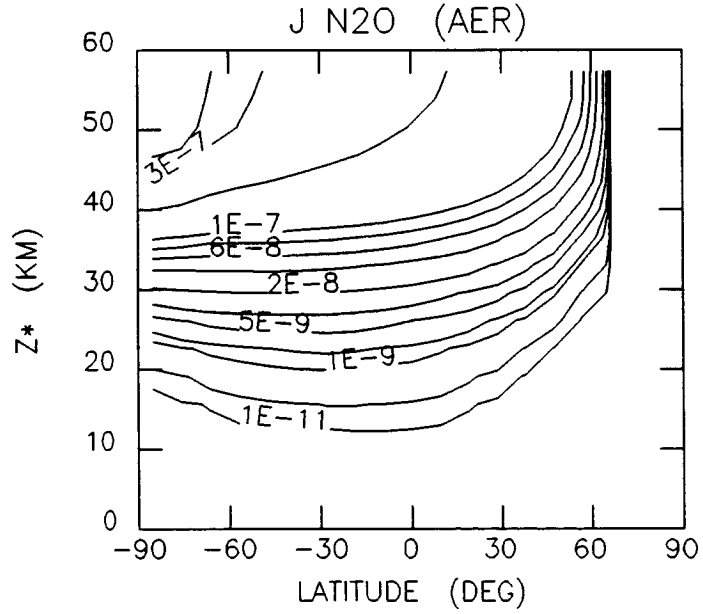
J N2O (AER)
Z* (KM)
LATITUDE (DEG)
3E-7
1E-7
6E-8
2E-8
5E-9
1E-9
1E-11

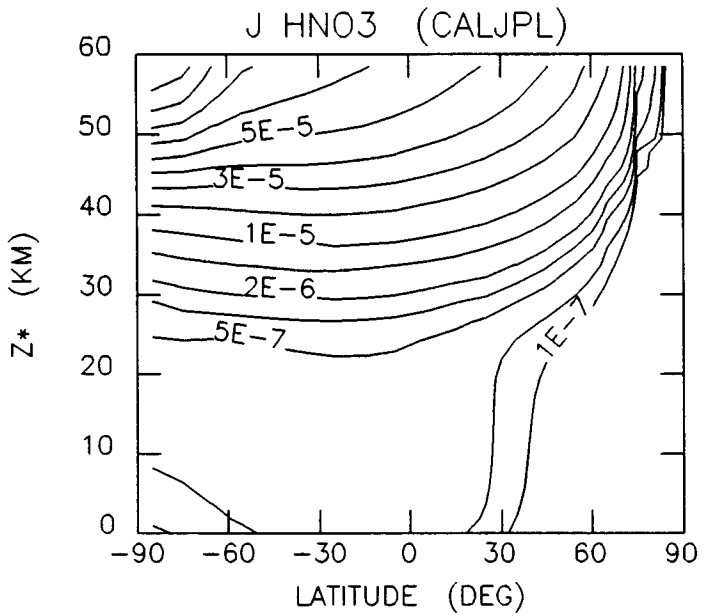
J HNO3 (CALJPL)
Z* (KM)
LATITUDE (DEG)
5E-5
3E-5
1E-5
2E-6
5E-7
1E-7

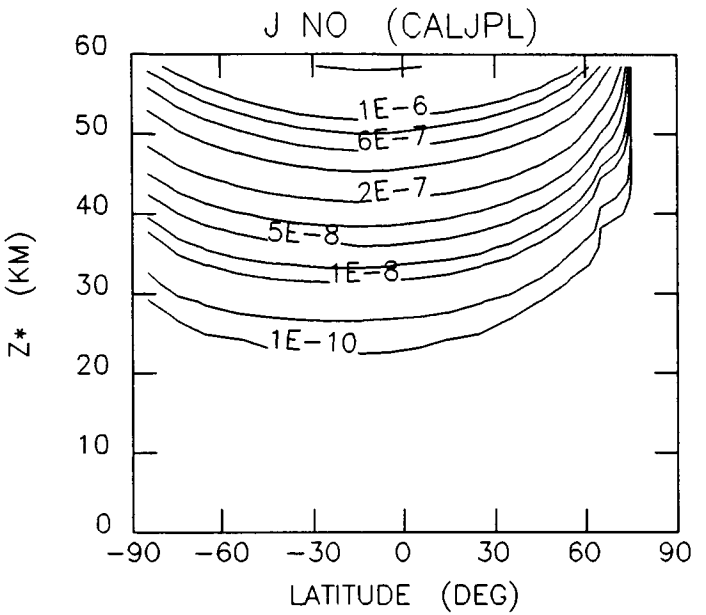
J NO (CALJPL)
Z* (KM)
LATITUDE (DEG)
1E-6
6E-7
2E-7
5E-8
1E-8
1E-10

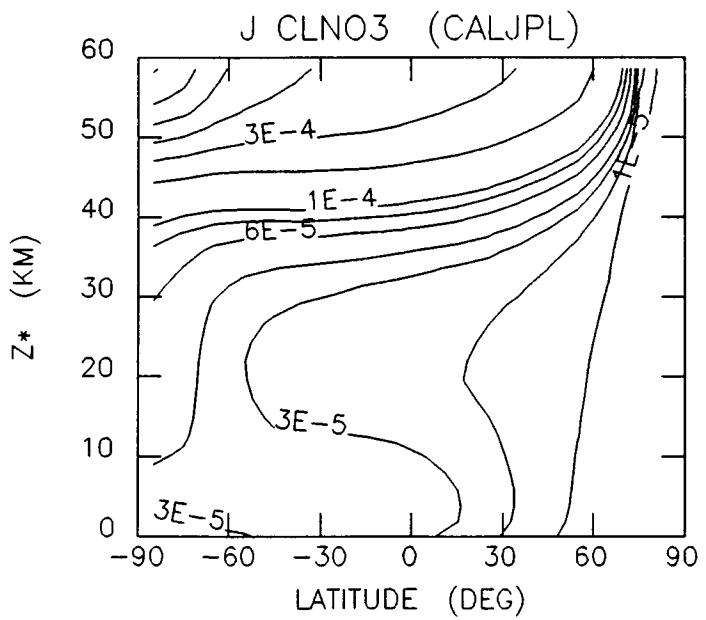
J CLNO3 (CALJPL)
Z* (KM)
LATITUDE (DEG)
3E-4
1E-4
6E-5
3E-5
3E-5

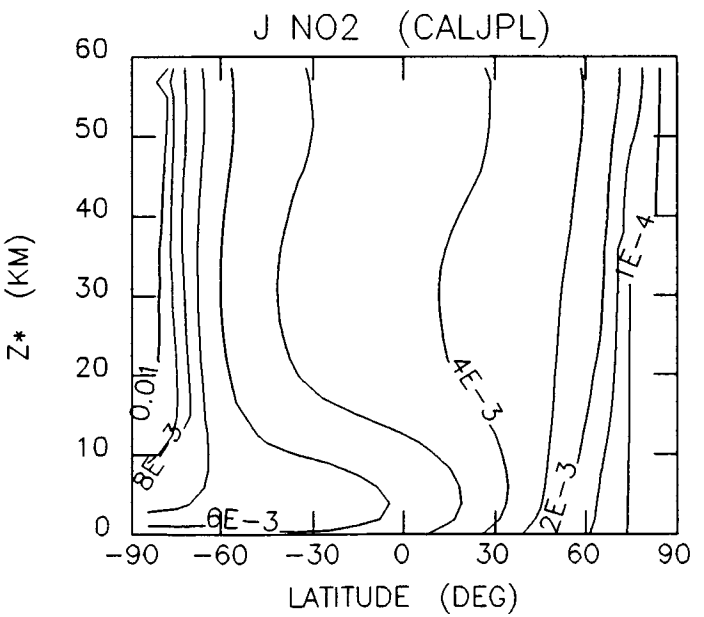
J NO2 (CALJPL)
Z* (KM)
LATITUDE (DEG)
0.011
8E-3
6E-3
4E-3
2E-3
1E-4

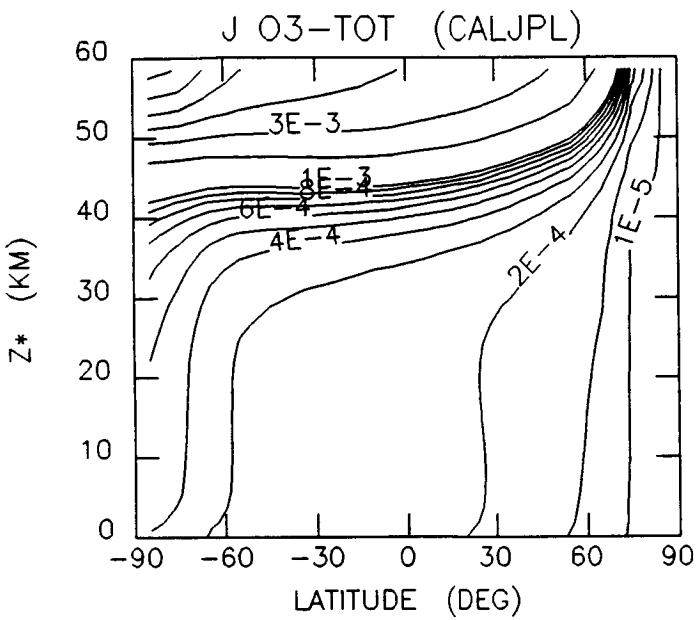
J O3−TOT (CALJPL)
Z* (KM)
LATITUDE (DEG)
3E−3
1E−3
8E−4
6E−4
4E−4
2E−4
1E−5

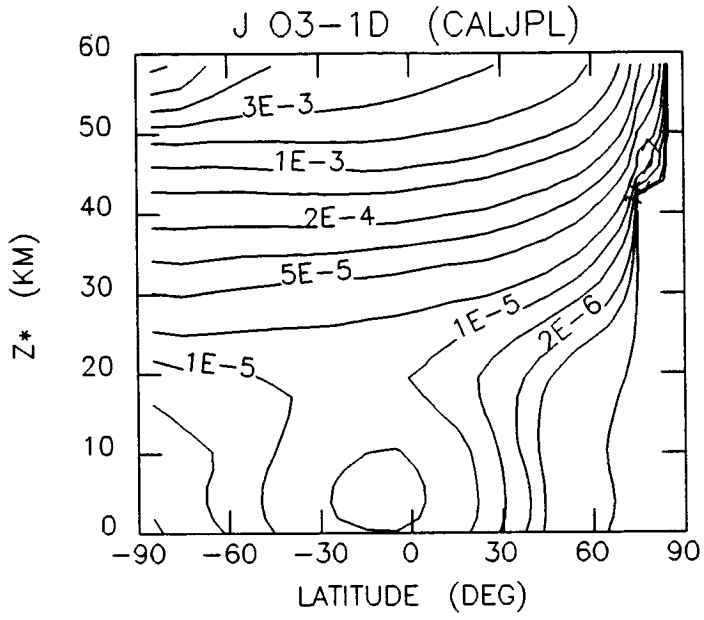
J O3−1D (CALJPL)
Z* (KM)
LATITUDE (DEG)
3E−3
1E−3
2E−4
5E−5
1E−5
1E−5
2E−6

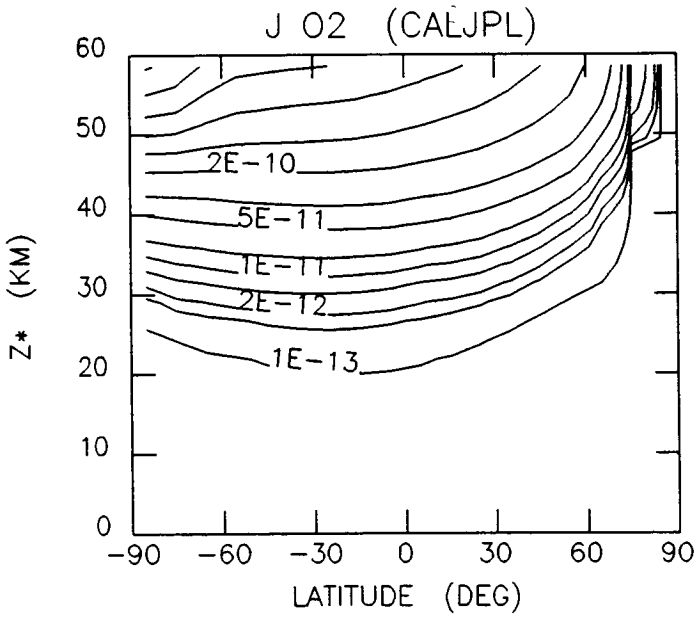
J O2 (CALJPL)
Z* (KM)
LATITUDE (DEG)
2E−10
5E−11
1E−11
2E−12
1E−13

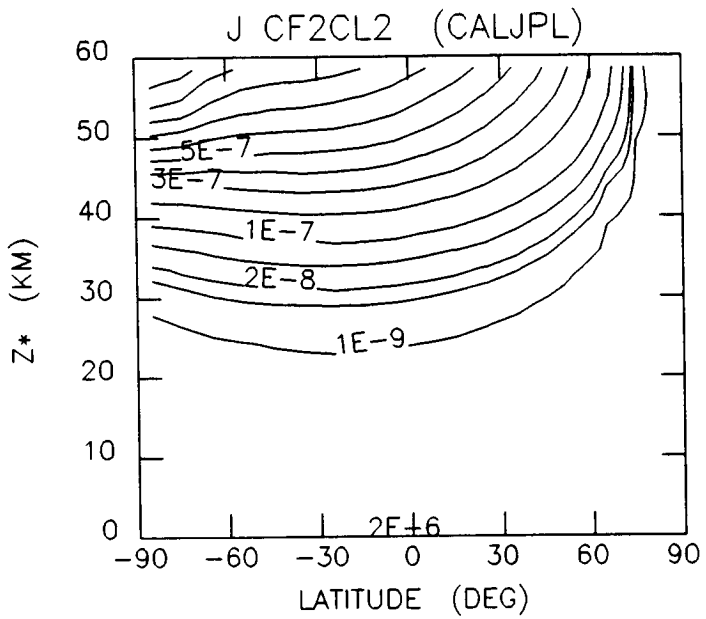
J CF2CL2 (CALJPL)
Z* (KM)
LATITUDE (DEG)
5E-7
3E-7
1E-7
2E-8
1E-9
2E+6

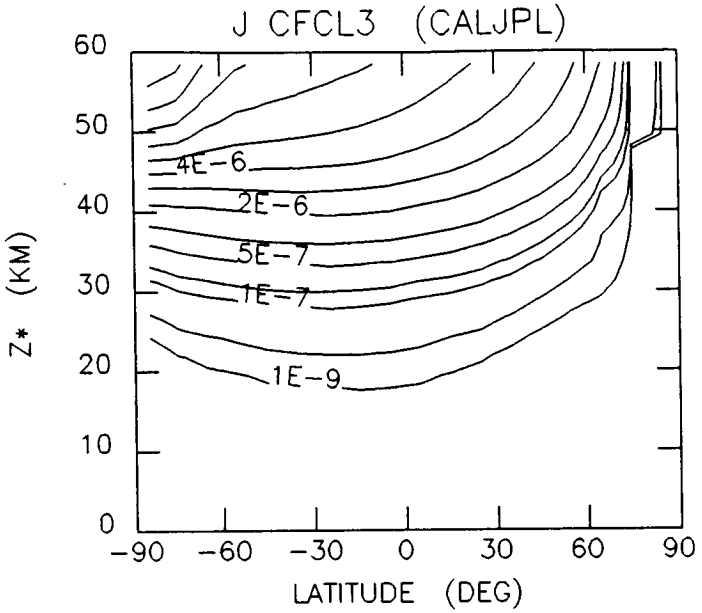
J CFCL3 (CALJPL)
Z* (KM)
LATITUDE (DEG)
4E-6
2E-6
5E-7
1E-7
1E-9

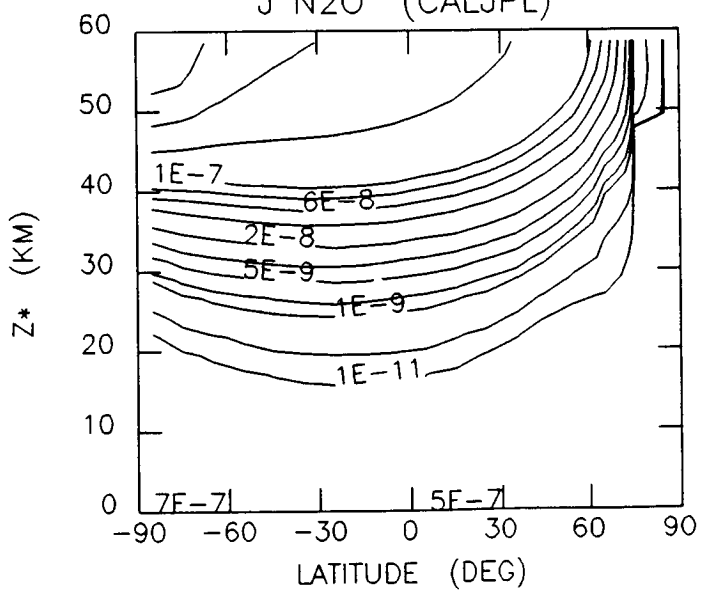
J N2O (CALJPL)
Z* (KM)
LATITUDE (DEG)
1E-7
6E-8
2E-8
5E-9
1E-9
1E-11
7E-7
5E-7

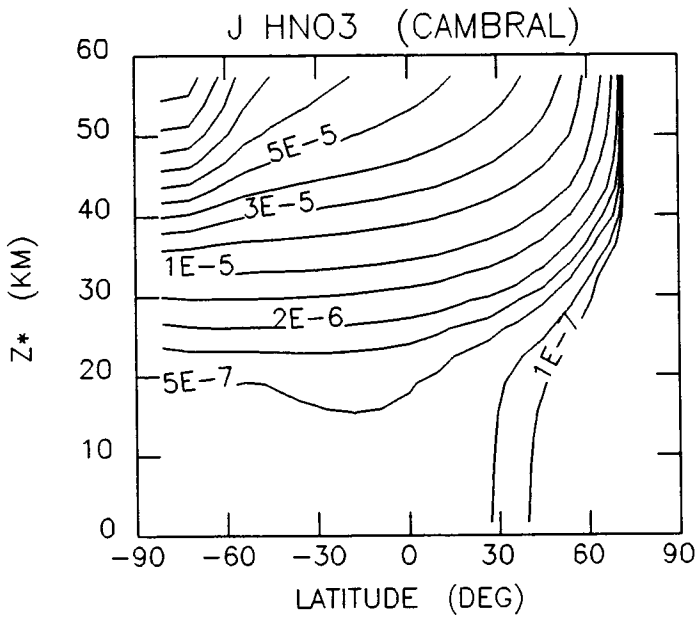
J HNO3 (CAMBRAL)
Z* (KM)
LATITUDE (DEG)
5E-5
3E-5
1E-5
2E-6
5E-7
1E-7

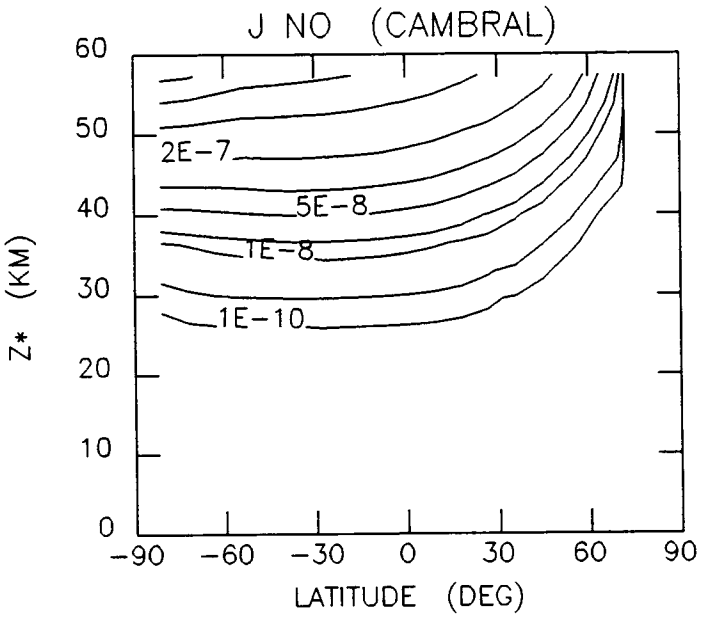
J NO (CAMBRAL)
Z* (KM)
LATITUDE (DEG)
2E-7
5E-8
1E-8
1E-10

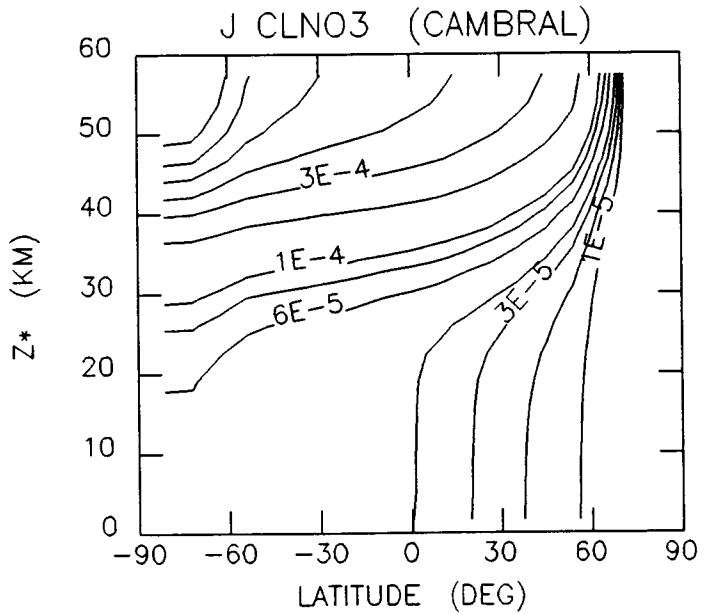
J CLNO3 (CAMBRAL)
Z* (KM)
LATITUDE (DEG)
3E-4
1E-4
6E-5
3E-5
1E-5

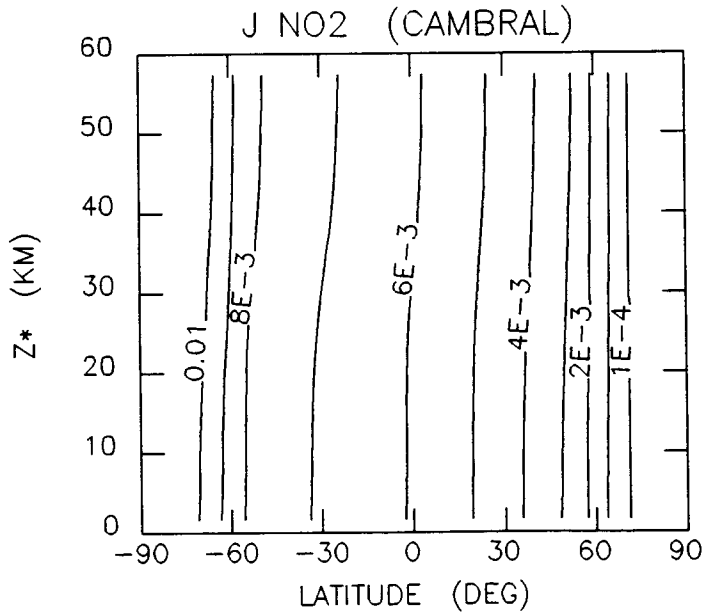
J NO2 (CAMBRAL)
Z* (KM)
LATITUDE (DEG)
0.01
8E-3
6E-3
4E-3
2E-3
1E-4

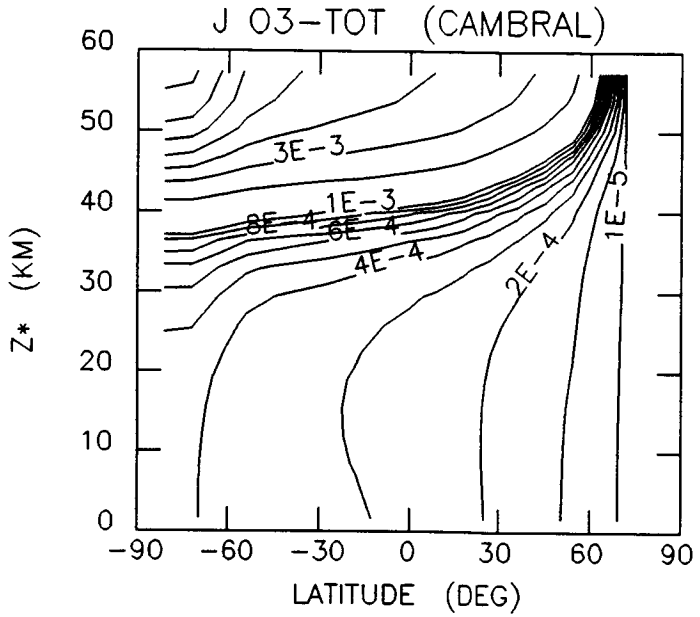
J O3−TOT (CAMBRAL)
Z* (KM)
LATITUDE (DEG)
3E−3
1E−3
8E−4
6E−4
4E−4
2E−4
1E−5

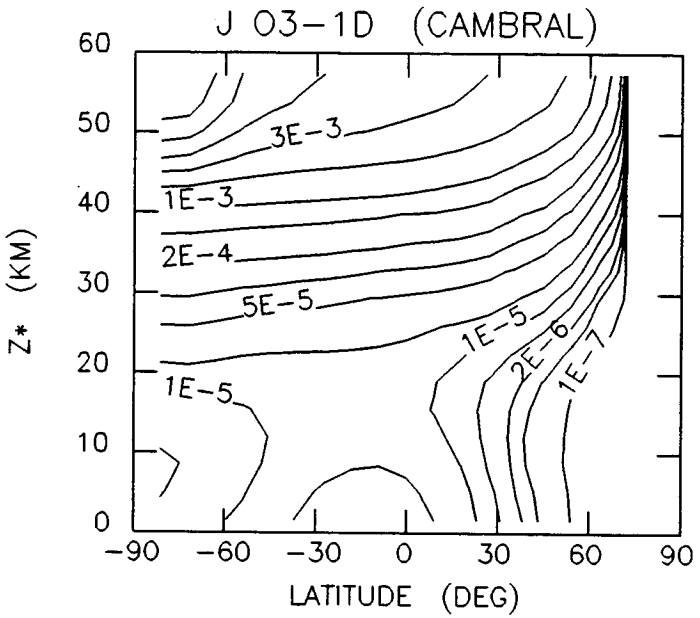
J O3−1D (CAMBRAL)
Z* (KM)
LATITUDE (DEG)
3E−3
1E−3
2E−4
5E−5
1E−5
2E−6
1E−7
1E−5

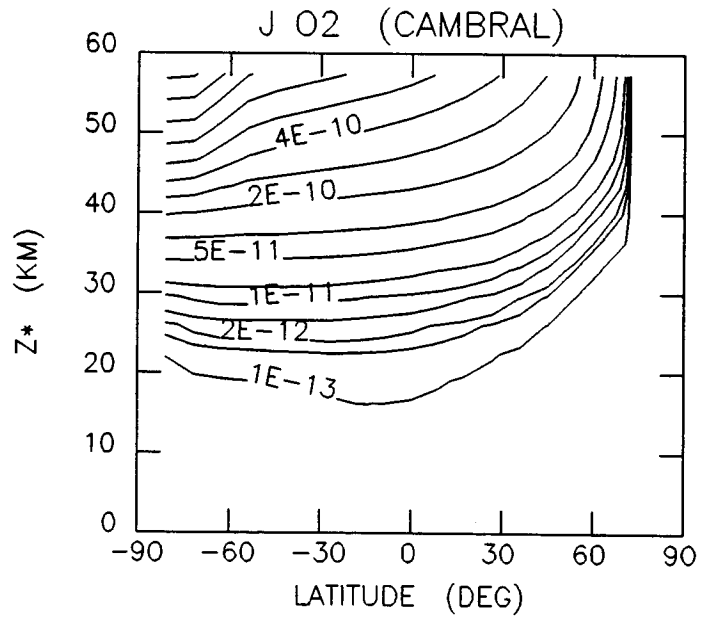
J O2 (CAMBRAL)
Z* (KM)
LATITUDE (DEG)
4E−10
2E−10
5E−11
1E−11
2E−12
1E−13

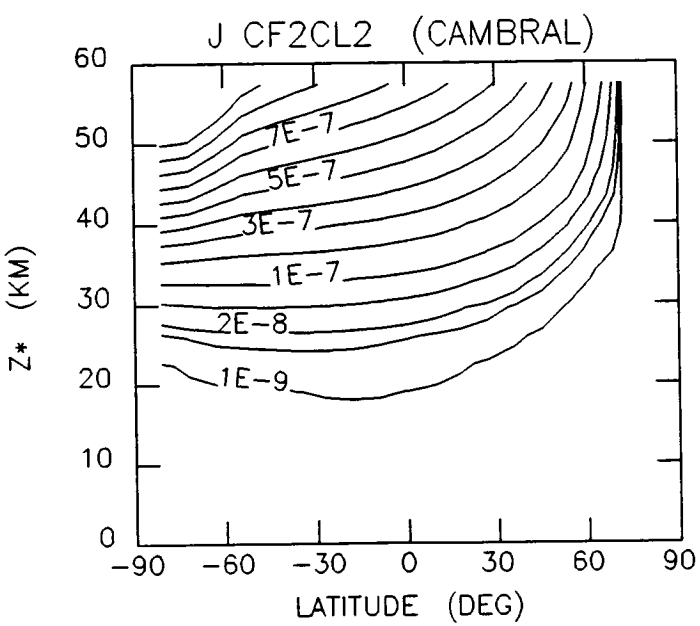
J CF2CL2 (CAMBRAL)
7E-7
5E-7
3E-7
1E-7
2E-8
1E-9
Z* (KM)
LATITUDE (DEG)

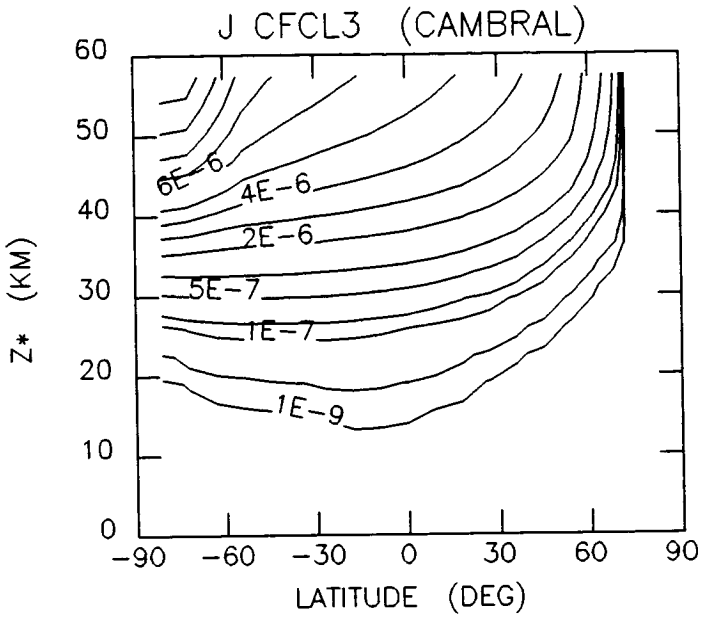
J CFCL3 (CAMBRAL)
6E-6
4E-6
2E-6
5E-7
1E-7
1E-9
Z* (KM)
LATITUDE (DEG)

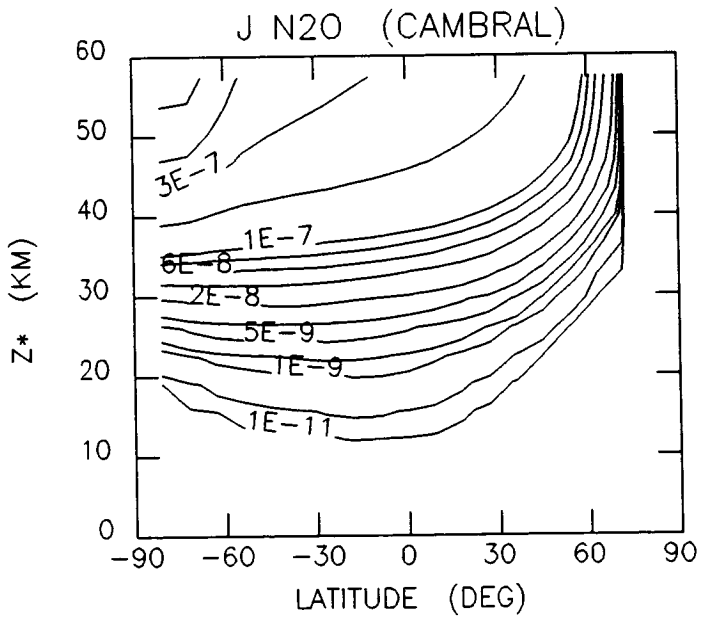
J N2O (CAMBRAL)
3E-7
1E-7
6E-8
2E-8
5E-9
1E-9
1E-11
Z* (KM)
LATITUDE (DEG)

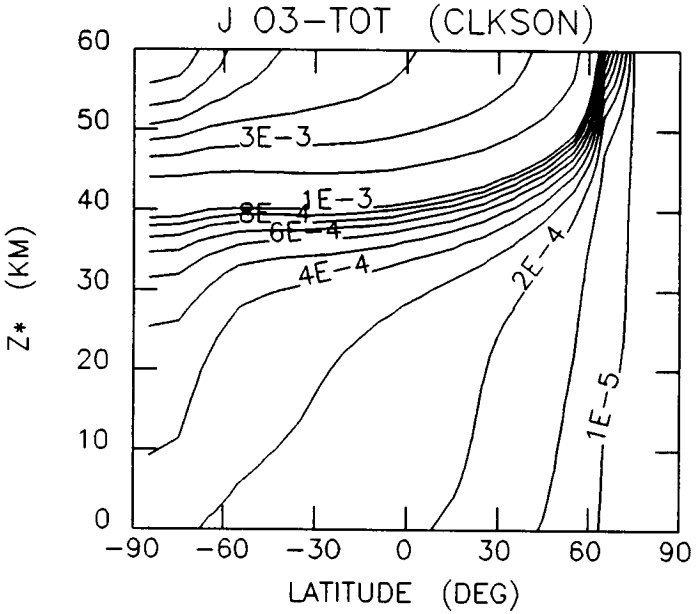
J O3−TOT (CLKSON)
Z* (KM)
LATITUDE (DEG)
3E−3
1E−3
8E−4
6E−4
4E−4
2E−4
1E−5

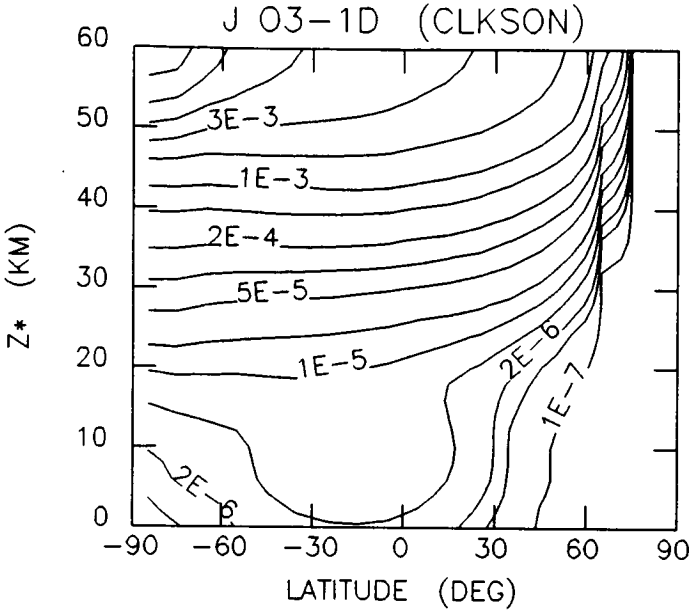
J O3−1D (CLKSON)
Z* (KM)
LATITUDE (DEG)
3E−3
1E−3
2E−4
5E−5
1E−5
2E−6
1E−7
2E−8

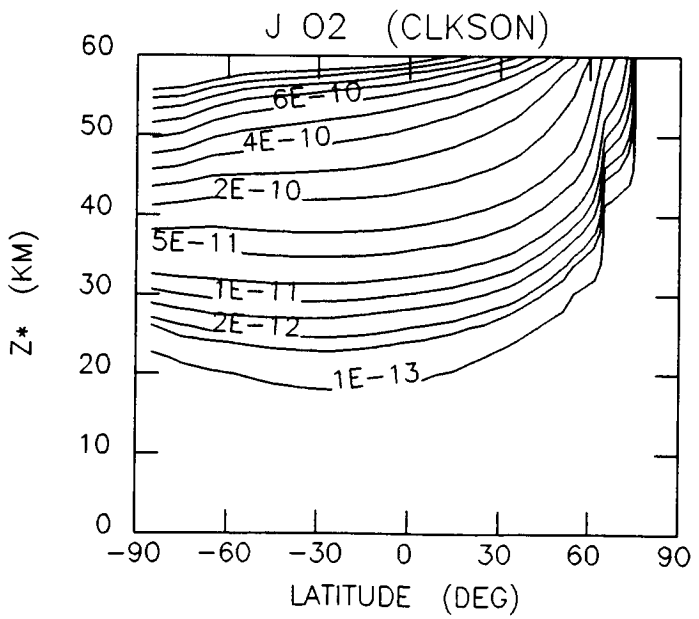
J O2 (CLKSON)
Z* (KM)
LATITUDE (DEG)
6E−10
4E−10
2E−10
5E−11
1E−11
2E−12
1E−13

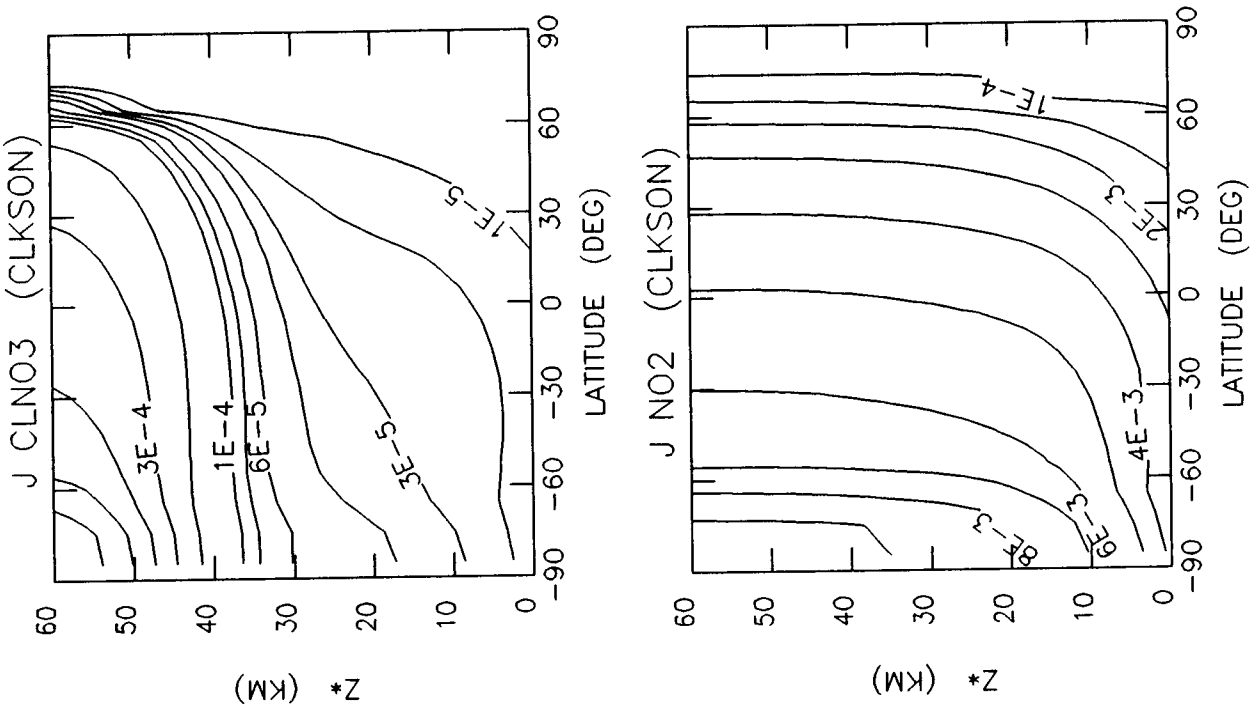
J CLNO3 (CLKSON)
3E-4
1E-4
6E-5
3E-5
1E-5
Z* (KM)
LATITUDE (DEG)
J NO2 (CLKSON)
1E-4
8E-3
6E-3
4E-3
Z* (KM)
LATITUDE (DEG)

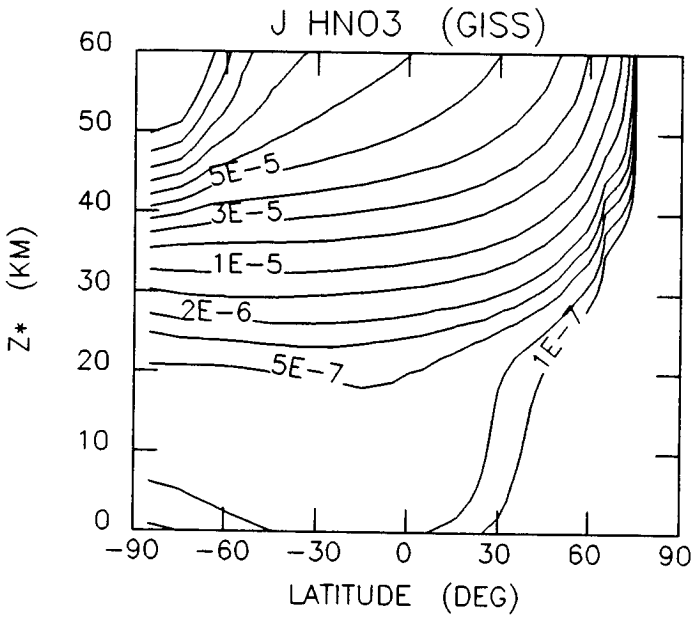
J HNO3 (GISS)
Z* (KM)
LATITUDE (DEG)
5E-5
3E-5
1E-5
2E-6
5E-7
1E-7

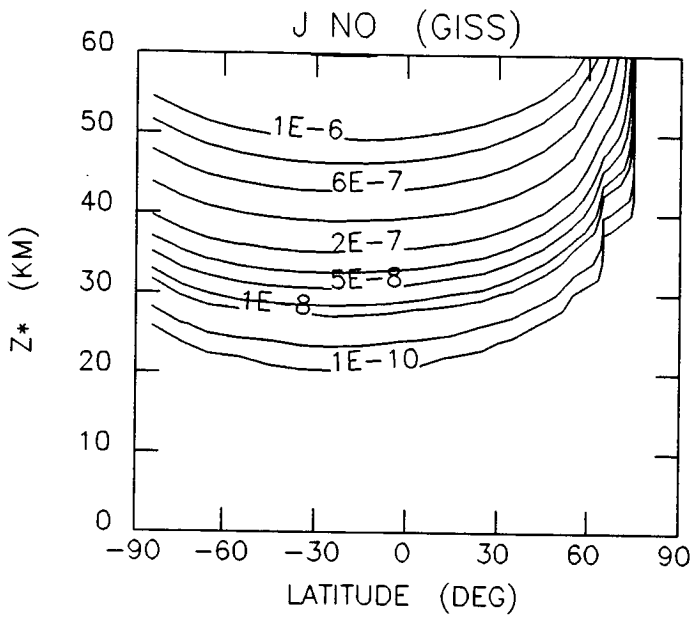
J NO (GISS)
Z* (KM)
LATITUDE (DEG)
1E-6
6E-7
2E-7
5E-8
1E-8
1E-10

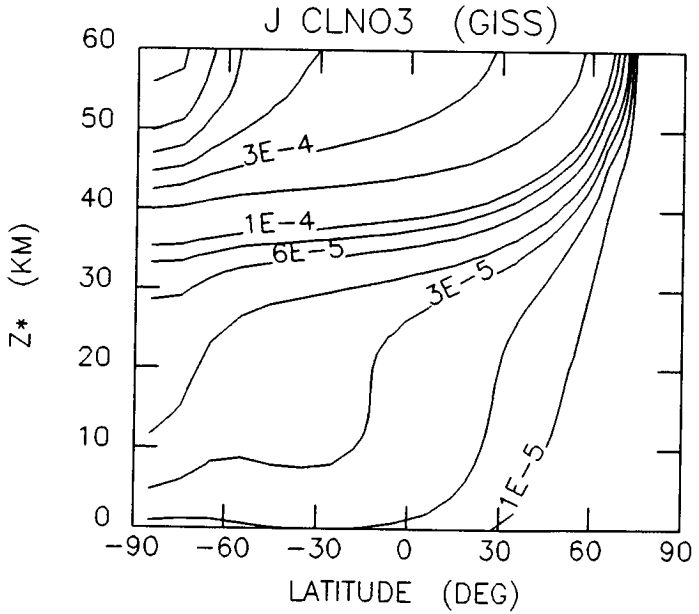
J CLNO3 (GISS)
Z* (KM)
LATITUDE (DEG)
3E-4
1E-4
6E-5
3E-5
1E-5

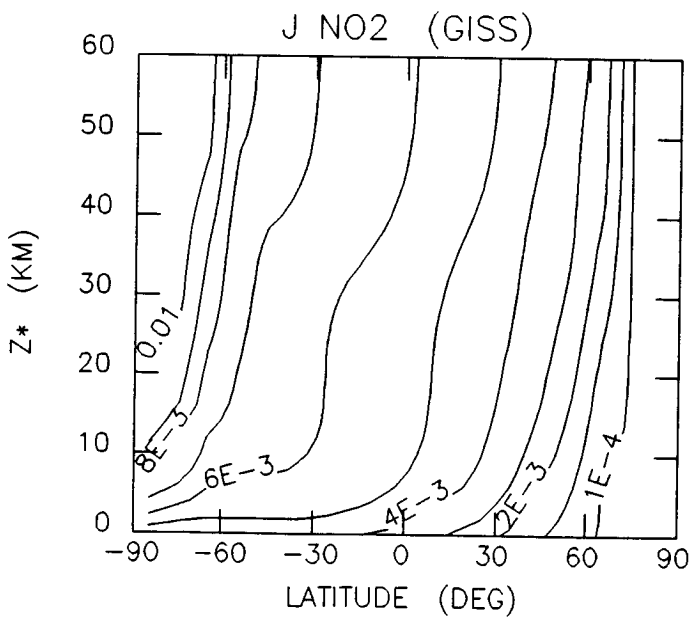
J NO2 (GISS)
Z* (KM)
LATITUDE (DEG)
0.01
8E-3
6E-3
4E-3
2E-3
1E-4

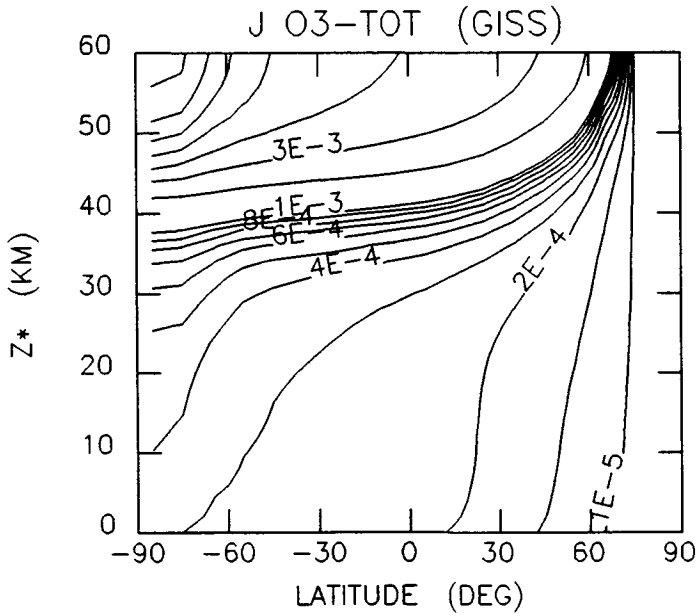
J O3-TOT (GISS)
Z* (KM)
LATITUDE (DEG)
3E-3
1E-3
8E-4
6E-4
4E-4
2E-4
1E-5

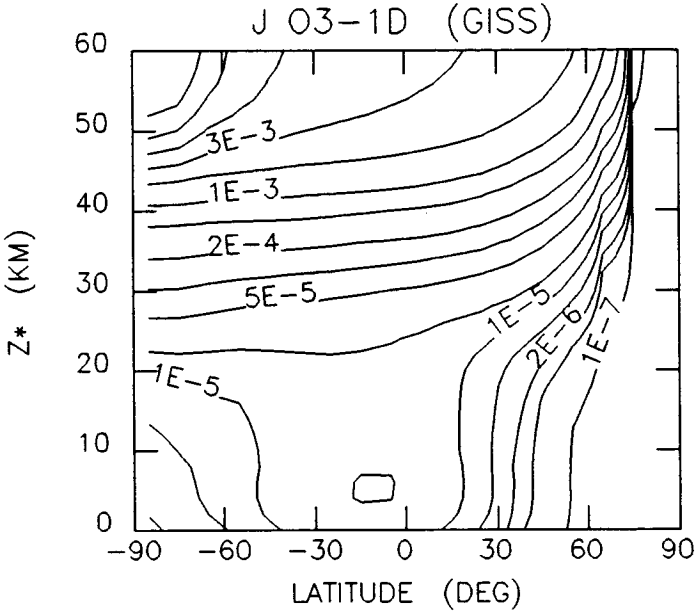
J O3-1D (GISS)
Z* (KM)
LATITUDE (DEG)
3E-3
1E-3
2E-4
5E-5
1E-5
1E-5
2E-6
1E-7

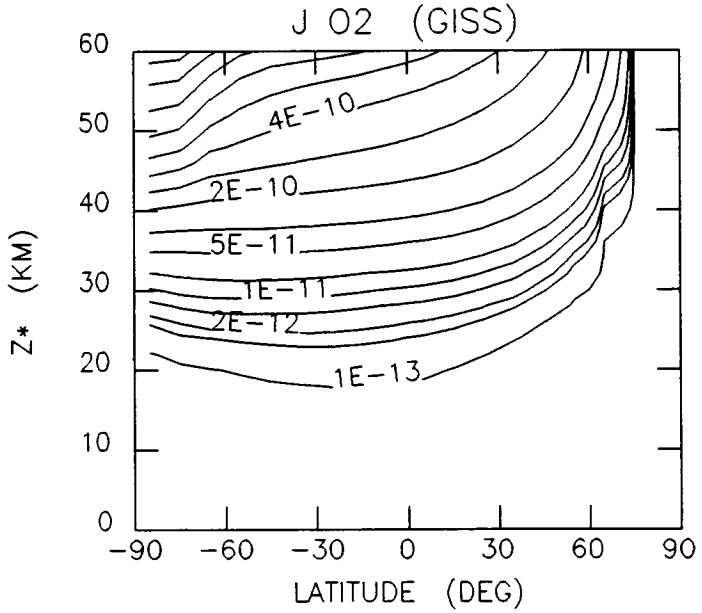
J O2 (GISS)
Z* (KM)
LATITUDE (DEG)
4E-10
2E-10
5E-11
1E-11
2E-12
1E-13

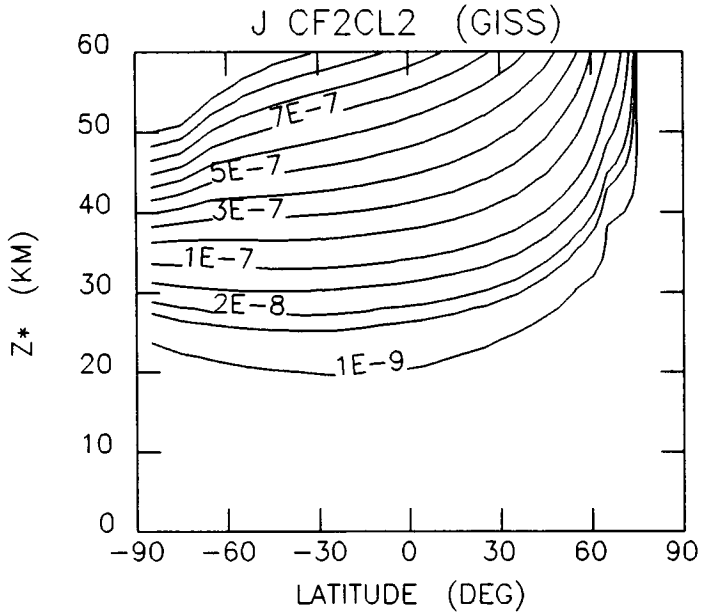
J CF2CL2 (GISS)
Z* (KM)
LATITUDE (DEG)
7E-7
5E-7
3E-7
1E-7
2E-8
1E-9

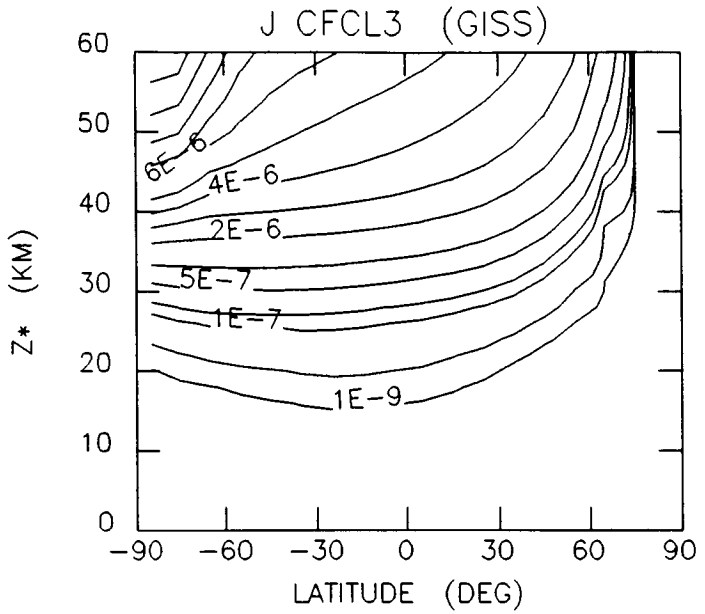
J CFCL3 (GISS)
Z* (KM)
LATITUDE (DEG)
6E-6
4E-6
2E-6
5E-7
1E-7
1E-9

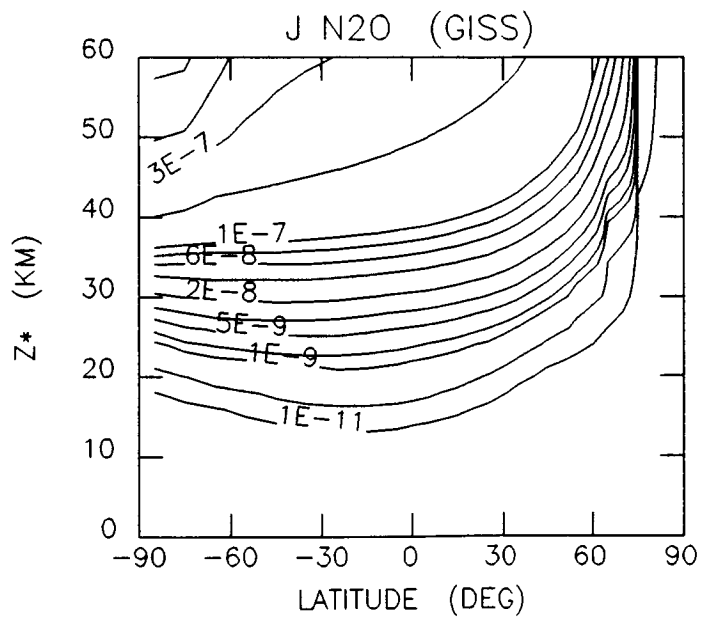
J N2O (GISS)
Z* (KM)
LATITUDE (DEG)
3E-7
1E-7
6E-8
2E-8
5E-9
1E-9
1E-11

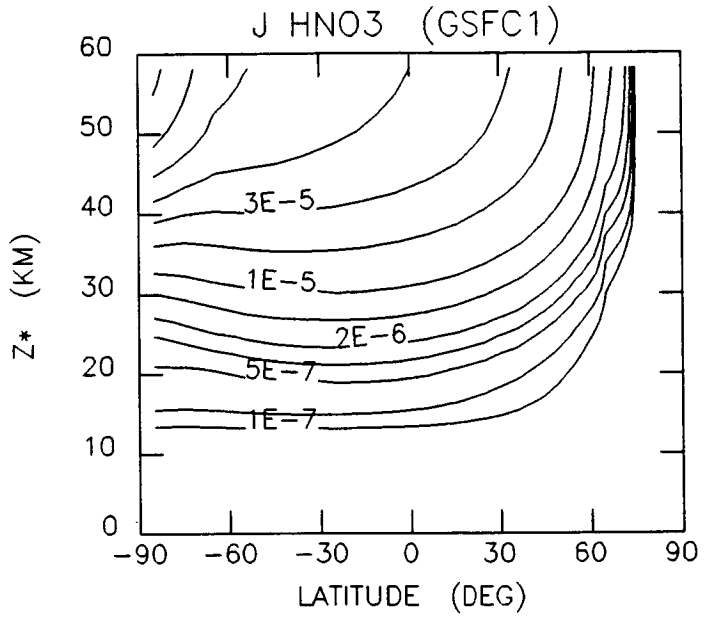
J HNO3 (GSFC1)
Z* (KM)
LATITUDE (DEG)
3E-5
1E-5
2E-6
5E-7
1E-7

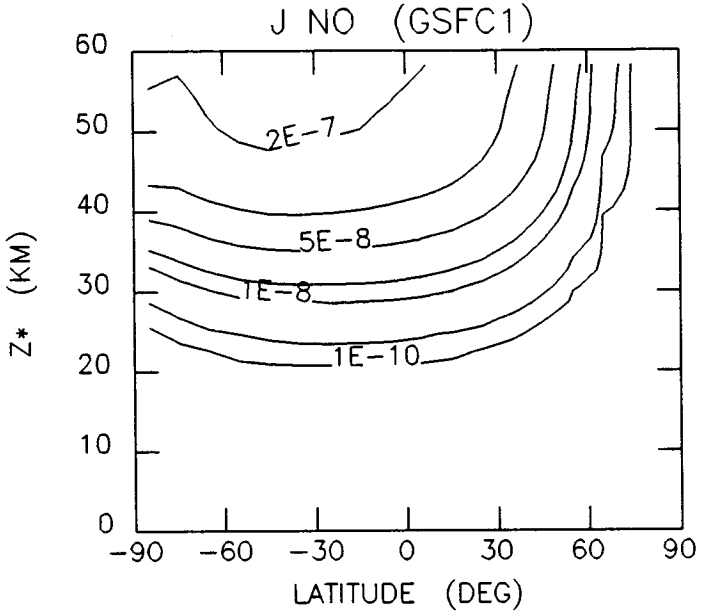
J NO (GSFC1)
Z* (KM)
LATITUDE (DEG)
2E-7
5E-8
1E-8
1E-10

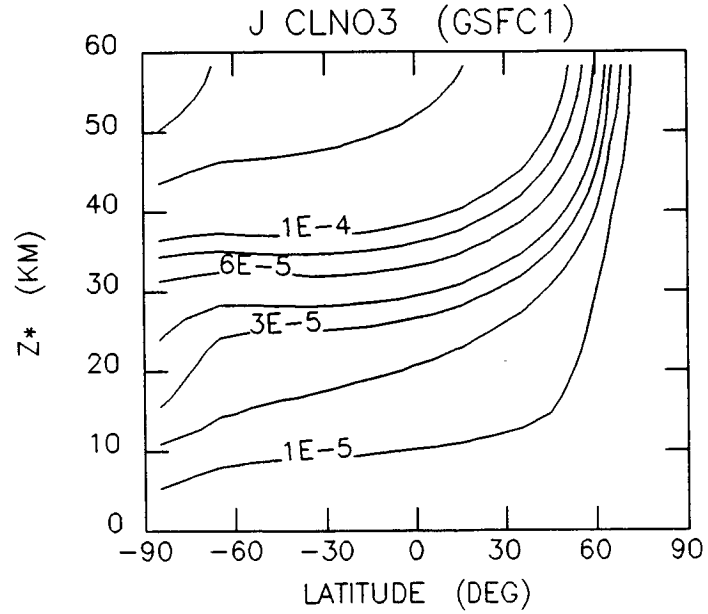
J CLNO3 (GSFC1)
Z* (KM)
LATITUDE (DEG)
1E-4
6E-5
3E-5
1E-5

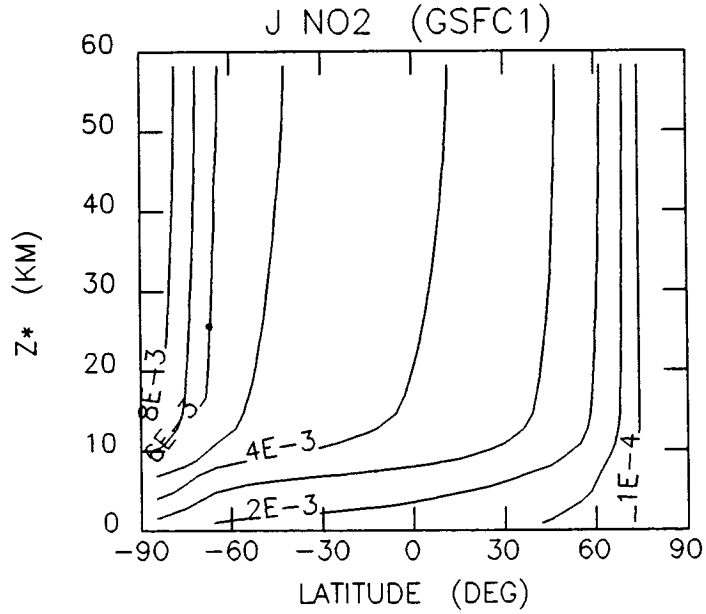
J NO2 (GSFC1)
Z* (KM)
LATITUDE (DEG)
8E-3
6E-3
4E-3
2E-3
1E-4

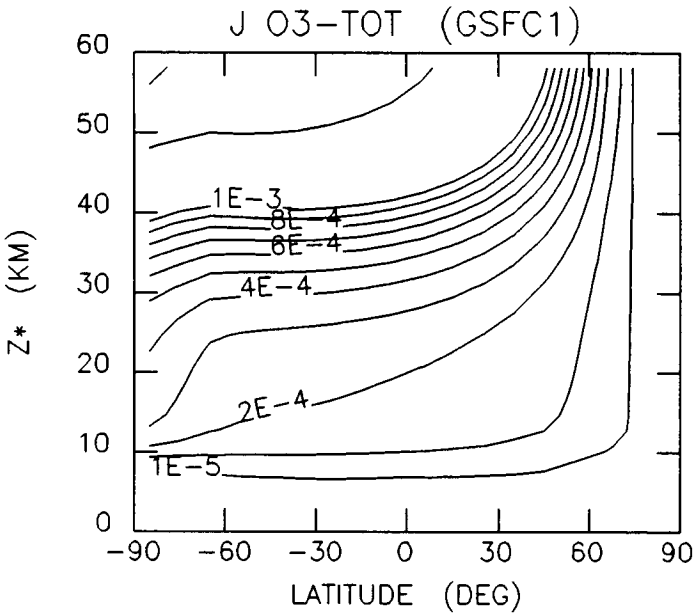
J O3-TOT (GSFC1)
Z* (KM)
LATITUDE (DEG)
1E-3
8E-4
6E-4
4E-4
2E-4
1E-5

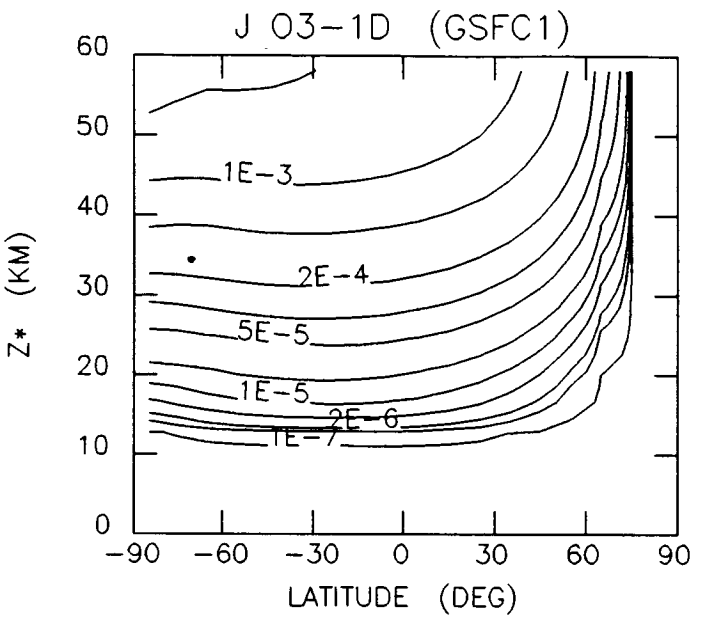
J O3-1D (GSFC1)
Z* (KM)
LATITUDE (DEG)
1E-3
2E-4
5E-5
1E-5
2E-6
1E-7

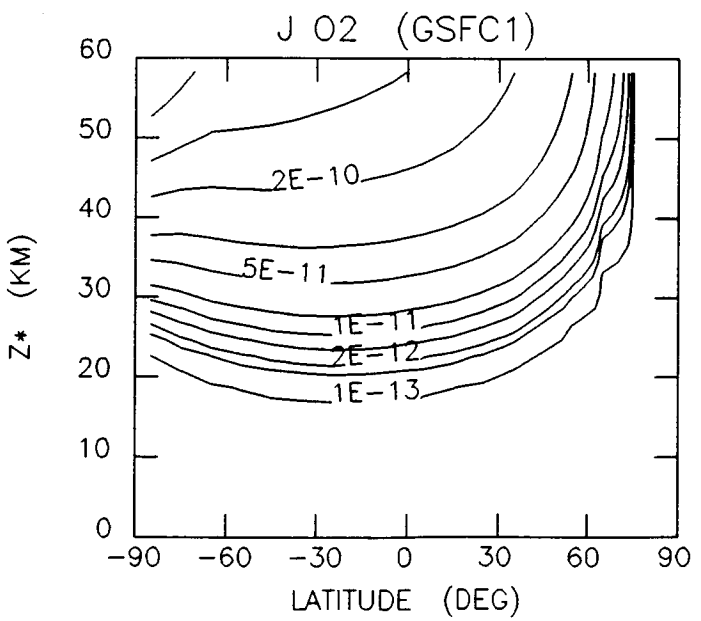
J O2 (GSFC1)
Z* (KM)
LATITUDE (DEG)
2E-10
5E-11
1E-11
2E-12
1E-13

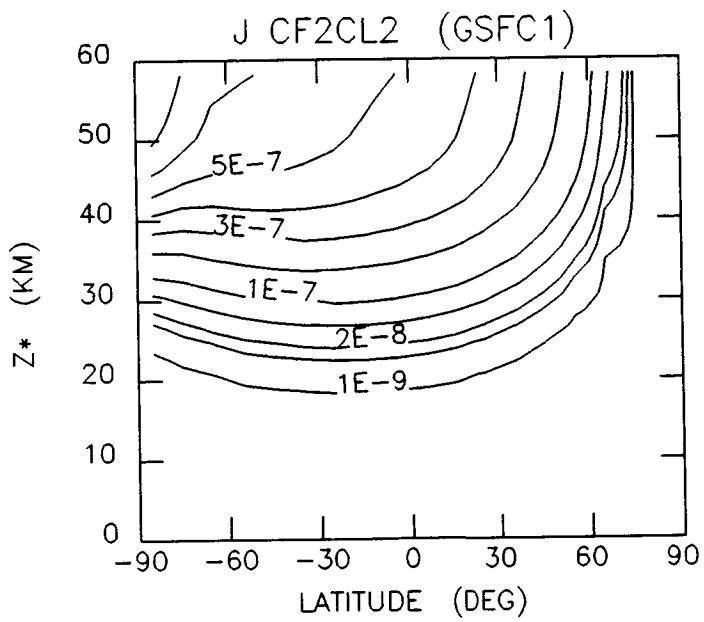
J CF2CL2 (GSFC1)
Z* (KM)
LATITUDE (DEG)
5E-7
3E-7
1E-7
2E-8
1E-9

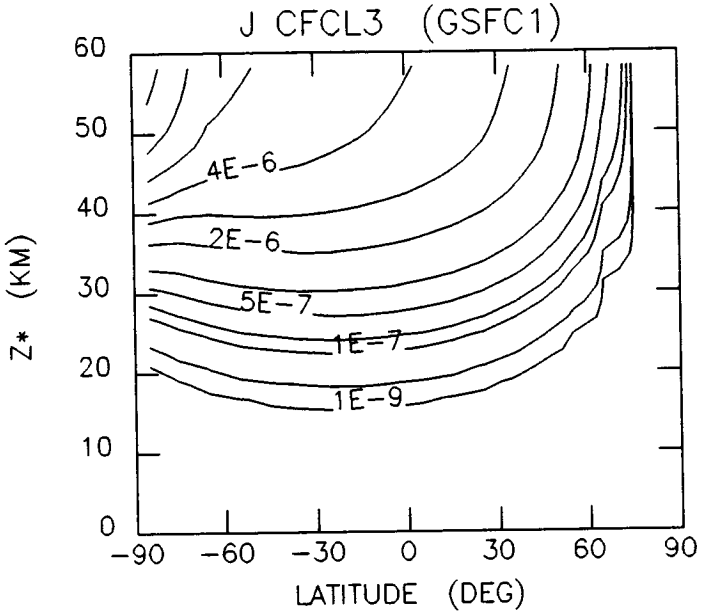
J CFCL3 (GSFC1)
Z* (KM)
LATITUDE (DEG)
4E-6
2E-6
5E-7
1E-7
1E-9

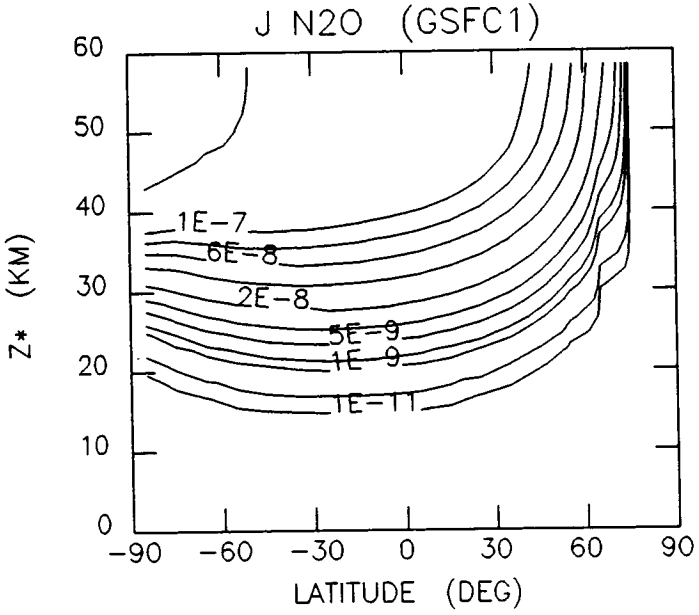
J N2O (GSFC1)
Z* (KM)
LATITUDE (DEG)
1E-7
6E-8
2E-8
5E-9
1E-9
1E-11

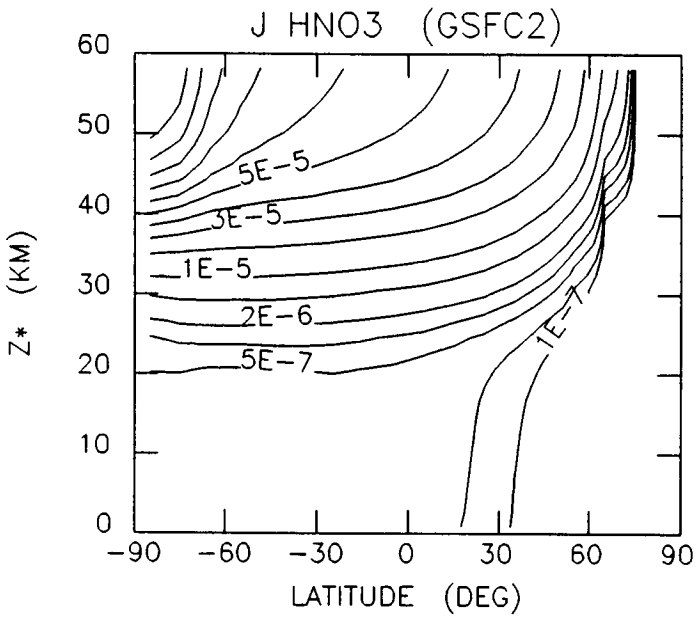
J HNO3 (GSFC2)
Z* (KM)
LATITUDE (DEG)
5E-5
3E-5
1E-5
2E-6
5E-7
1E-7

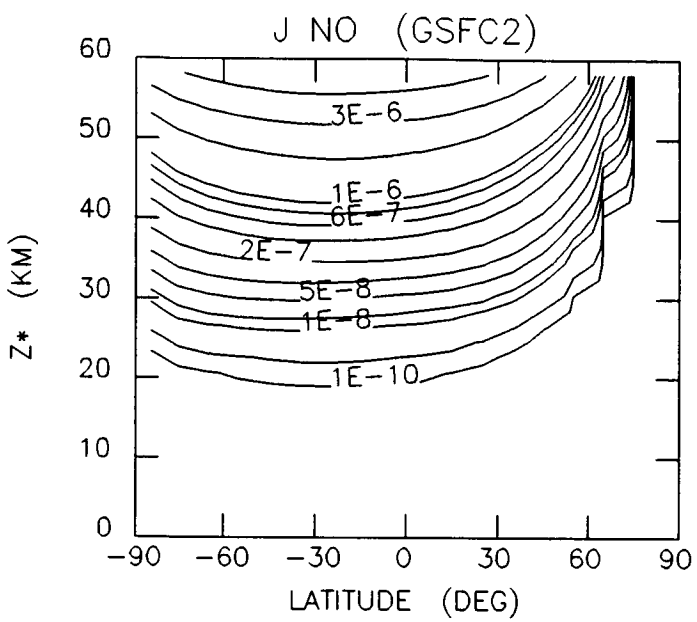
J NO (GSFC2)
Z* (KM)
LATITUDE (DEG)
3E-6
1E-6
6E-7
2E-7
5E-8
1E-8
1E-10

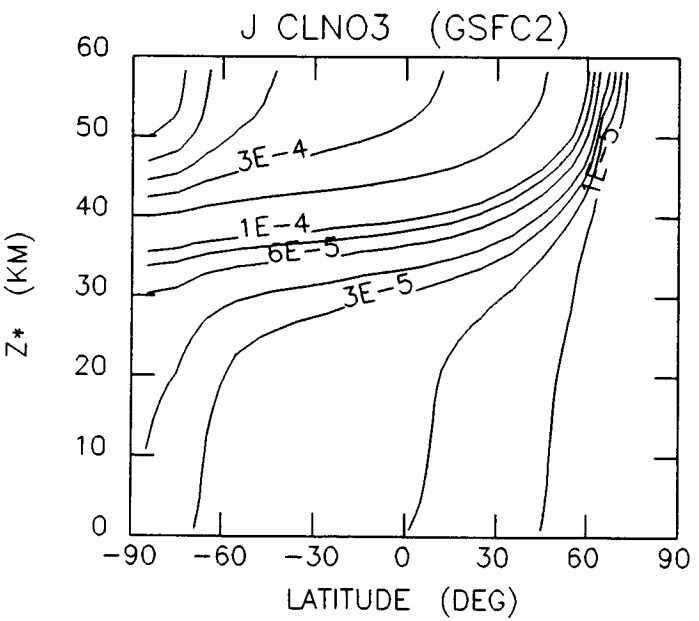
J CLNO3 (GSFC2)
Z* (KM)
LATITUDE (DEG)
3E-4
1E-4
6E-5
3E-5
1E-5

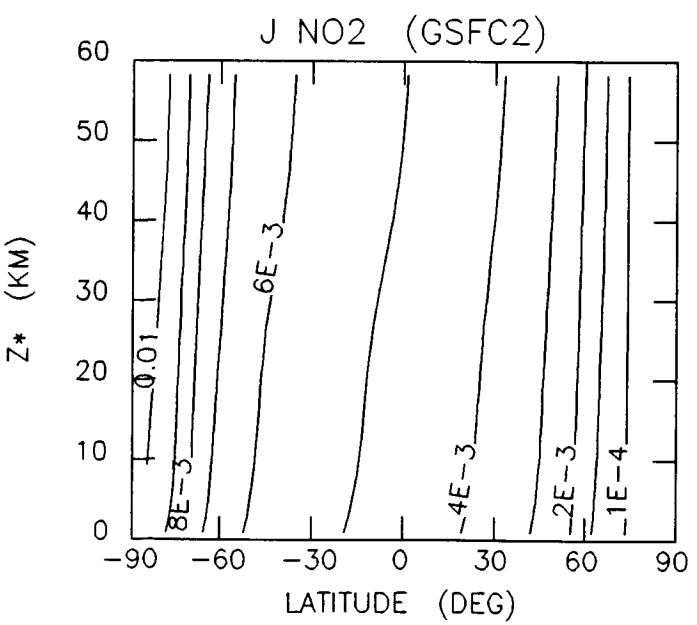
J NO2 (GSFC2)
Z* (KM)
LATITUDE (DEG)
0.01
8E-3
6E-3
4E-3
2E-3
1E-4

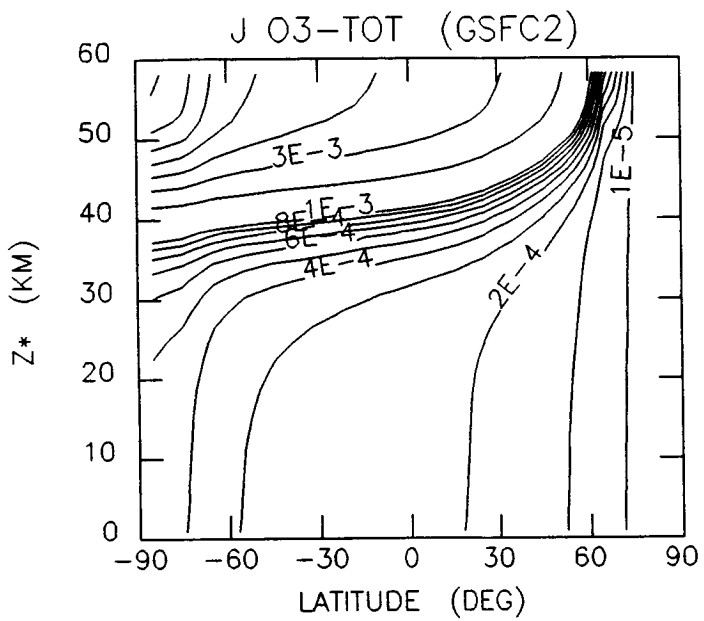
J O3-TOT (GSFC2)
Z* (KM)
LATITUDE (DEG)
3E-3
1E-3
8E-4
6E-4
4E-4
2E-4
1E-5

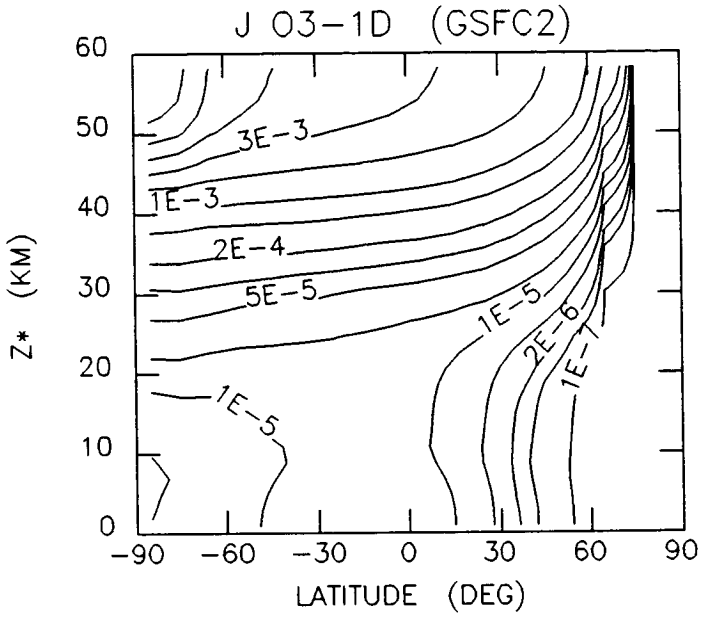
J O3-1D (GSFC2)
Z* (KM)
LATITUDE (DEG)
3E-3
1E-3
2E-4
5E-5
1E-5
2E-6
1E-7
1E-5

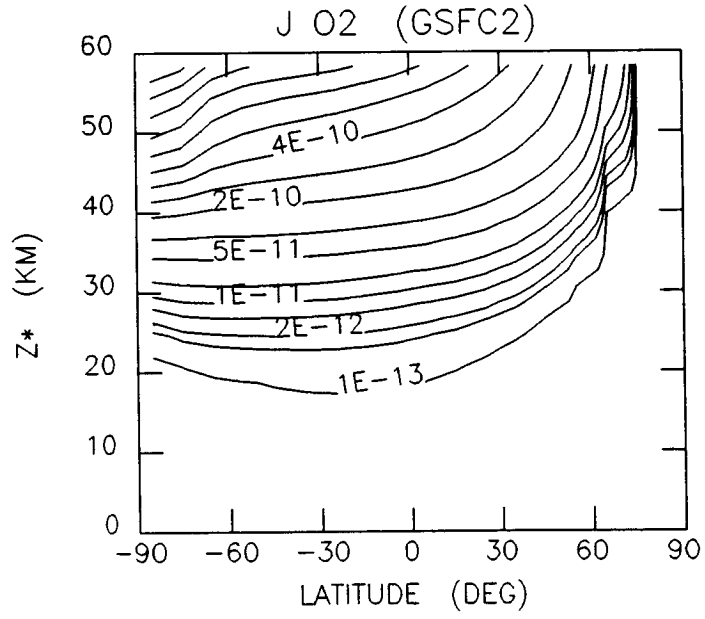
J O2 (GSFC2)
Z* (KM)
LATITUDE (DEG)
4E-10
2E-10
5E-11
1E-11
2E-12
1E-13

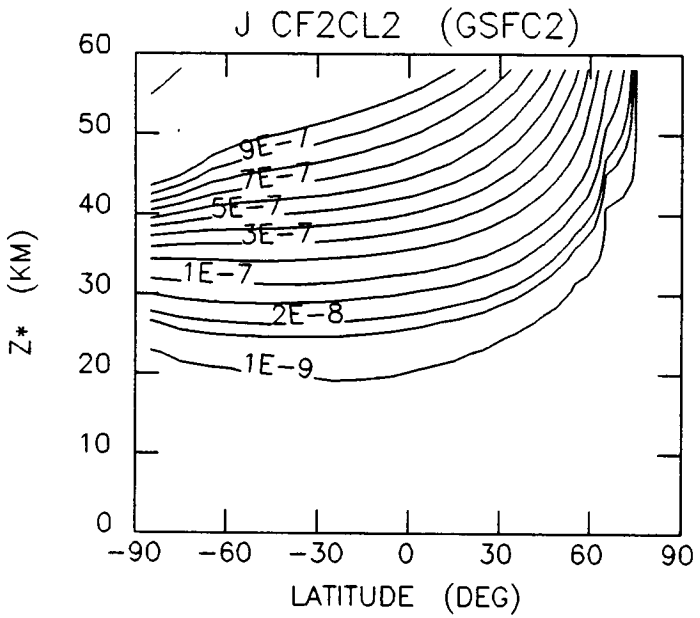
J CF2CL2 (GSFC2)
Z* (KM)
LATITUDE (DEG)
9E-7
7E-7
5E-7
3E-7
1E-7
2E-8
1E-9

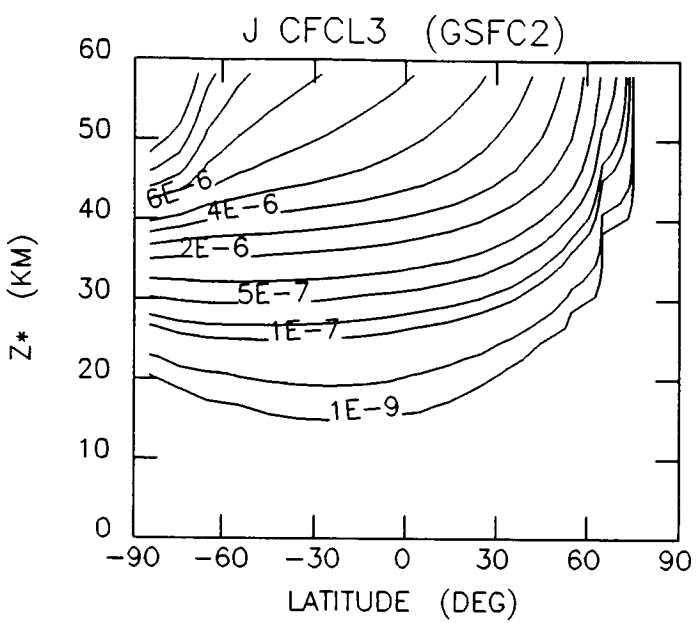
J CFCL3 (GSFC2)
Z* (KM)
LATITUDE (DEG)
6E-6
4E-6
2E-6
5E-7
1E-7
1E-9

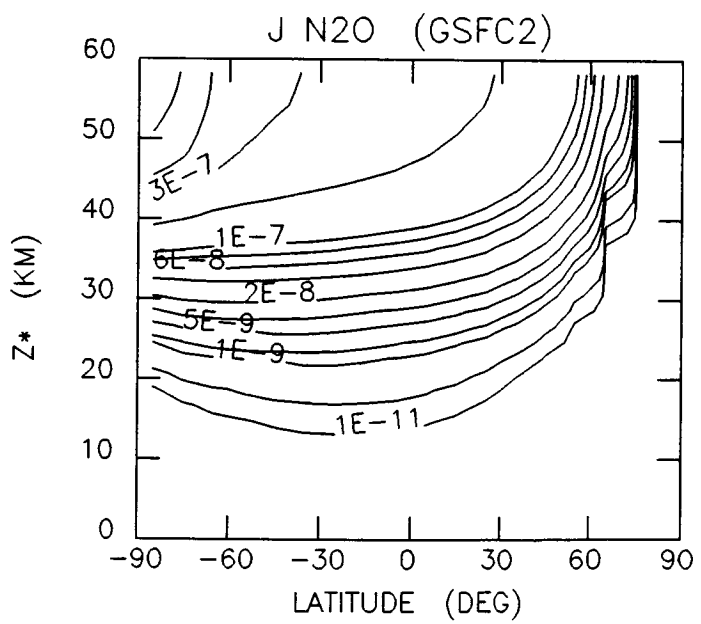
J N2O (GSFC2)
Z* (KM)
LATITUDE (DEG)
3E-7
1E-7
6E-8
2E-8
5E-9
1E-9
1E-11

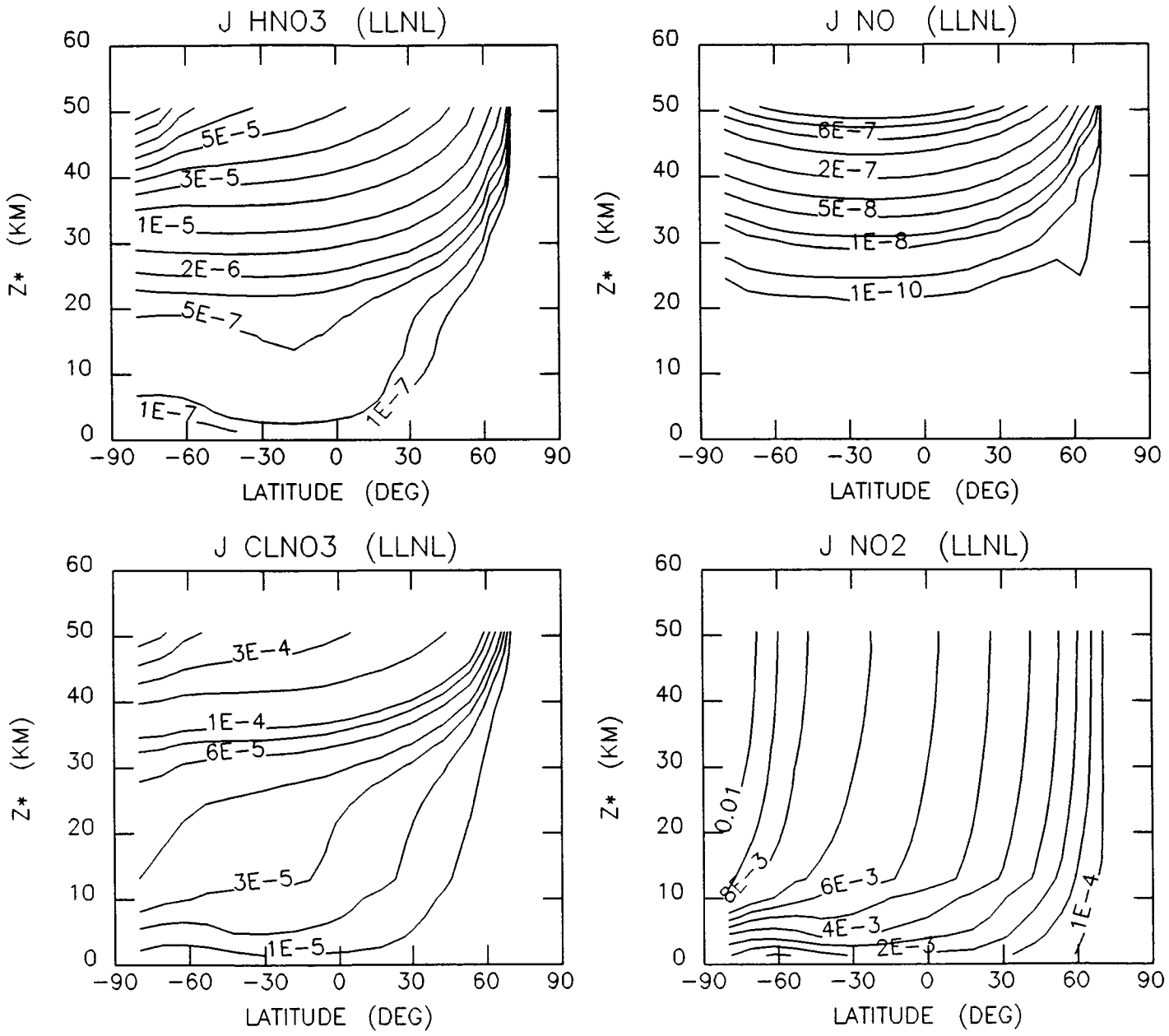
J HNO3 (LLNL)
5E-5
3E-5
1E-5
2E-6
5E-7
1E-7
1E-7
J NO (LLNL)
6E-7
2E-7
5E-8
1E-8
1E-10
J CLNO3 (LLNL)
3E-4
1E-4
6E-5
3E-5
1E-5
J NO2 (LLNL)
0.01
8E-3
6E-3
4E-3
2E-3
1E-4
Z* (KM)
LATITUDE (DEG)
0
10
20
30
40
50
60
-90
-60
-30
0
30
60
90

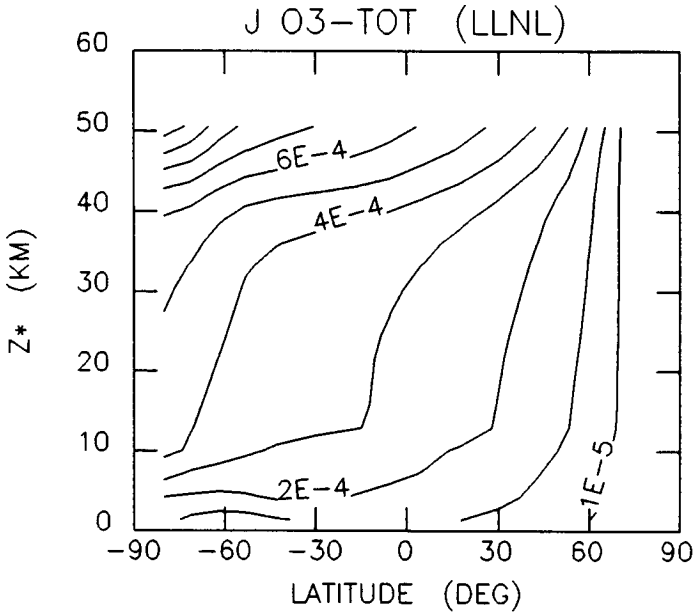
J O3−TOT (LLNL)
Z* (KM)
LATITUDE (DEG)
6E−4
4E−4
2E−4
1E−5

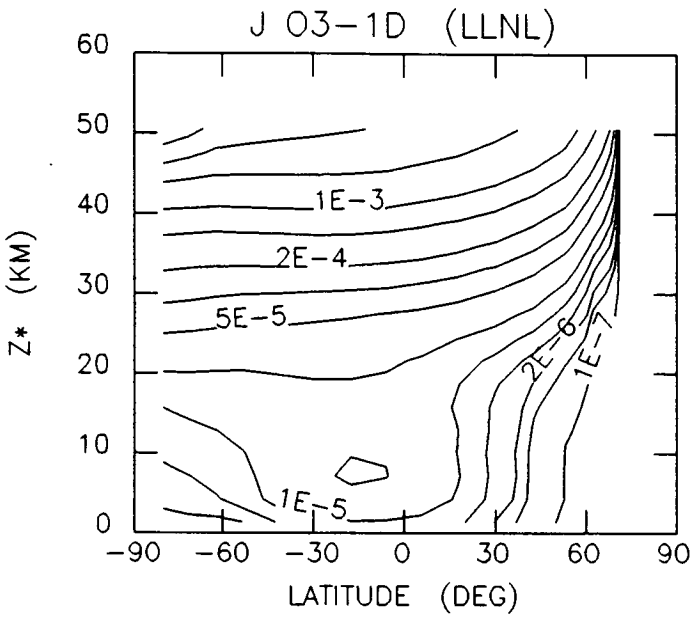
J O3−1D (LLNL)
Z* (KM)
LATITUDE (DEG)
1E−3
2E−4
5E−5
2E−6
1E−7
1E−5

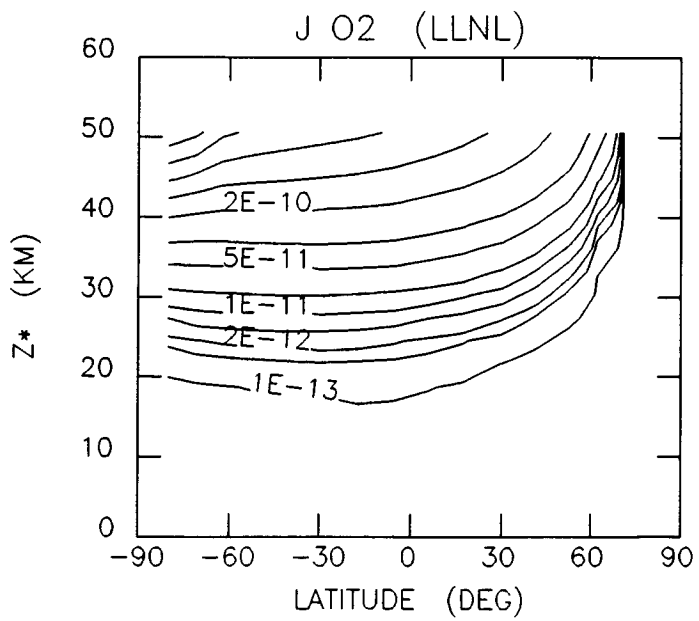
J O2 (LLNL)
Z* (KM)
LATITUDE (DEG)
2E−10
5E−11
1E−11
2E−12
1E−13

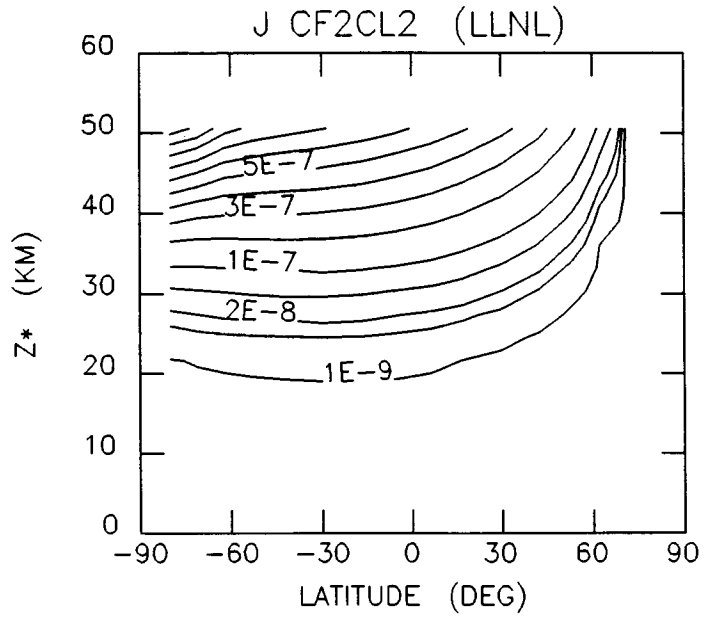
J CF2CL2 (LLNL)
Z* (KM)
LATITUDE (DEG)
5E-7
3E-7
1E-7
2E-8
1E-9

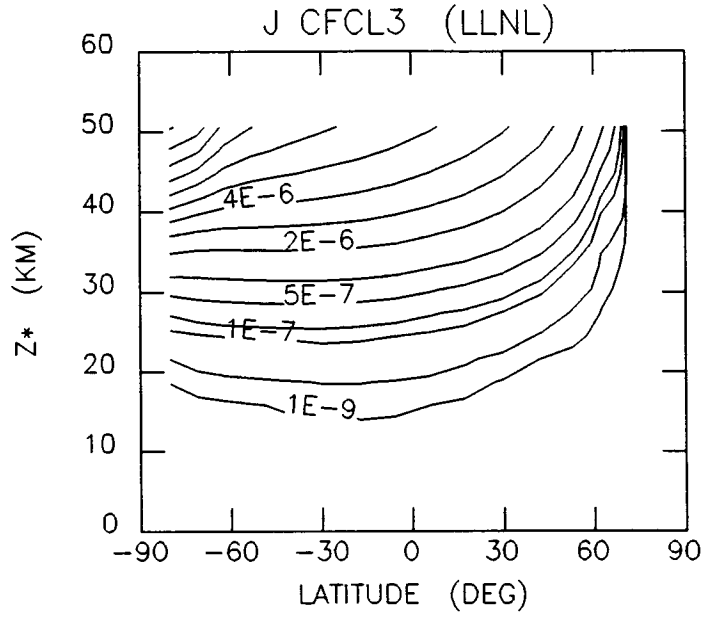
J CFCL3 (LLNL)
Z* (KM)
LATITUDE (DEG)
4E-6
2E-6
5E-7
1E-7
1E-9

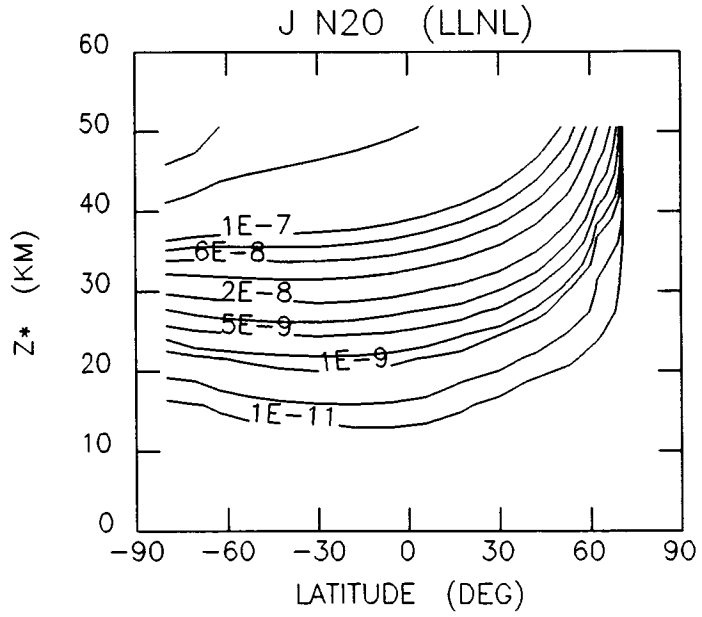
J N2O (LLNL)
Z* (KM)
LATITUDE (DEG)
1E-7
6E-8
2E-8
5E-9
1E-9
1E-11

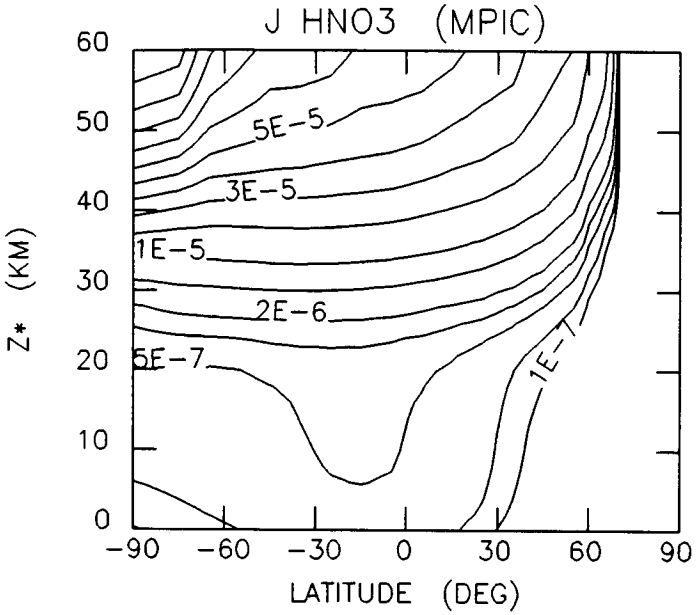
J HNO3 (MPIC)
5E-5
3E-5
1E-5
2E-6
5E-7
1E-7
Z* (KM)
LATITUDE (DEG)

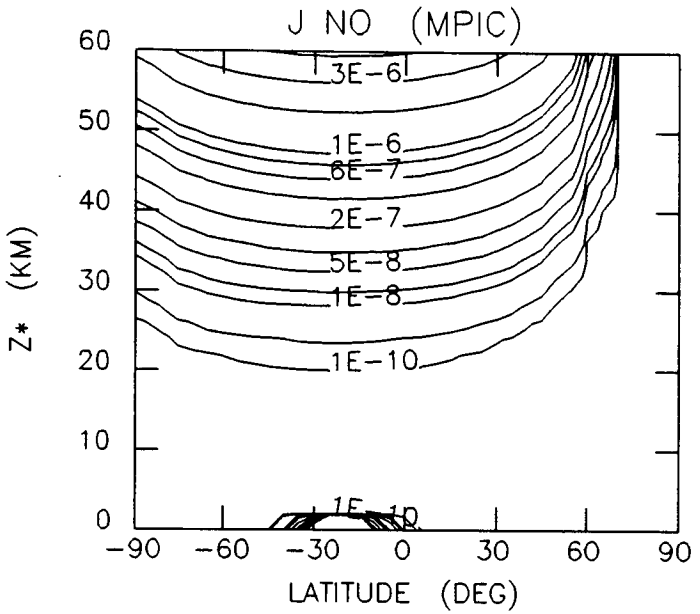
J NO (MPIC)
3E-6
1E-6
6E-7
2E-7
5E-8
1E-8
1E-10
Z* (KM)
LATITUDE (DEG)

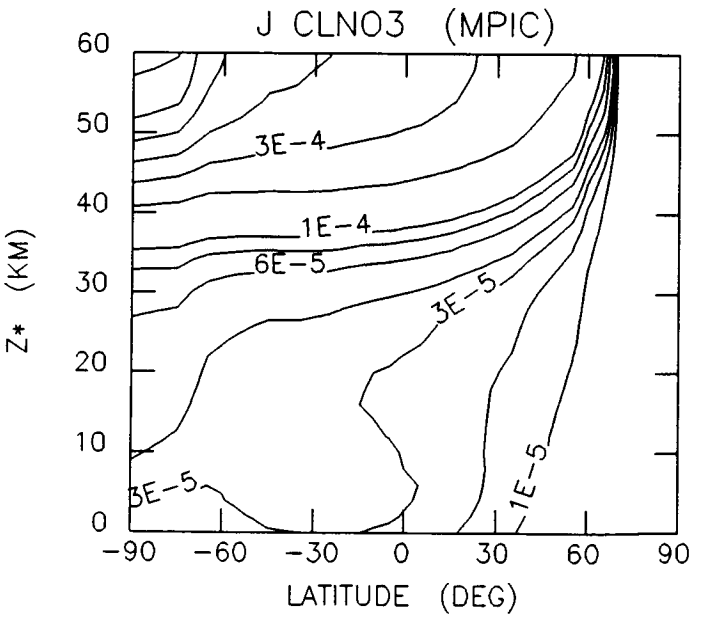
J CLNO3 (MPIC)
3E-4
1E-4
6E-5
3E-5
3E-5
1E-5
Z* (KM)
LATITUDE (DEG)

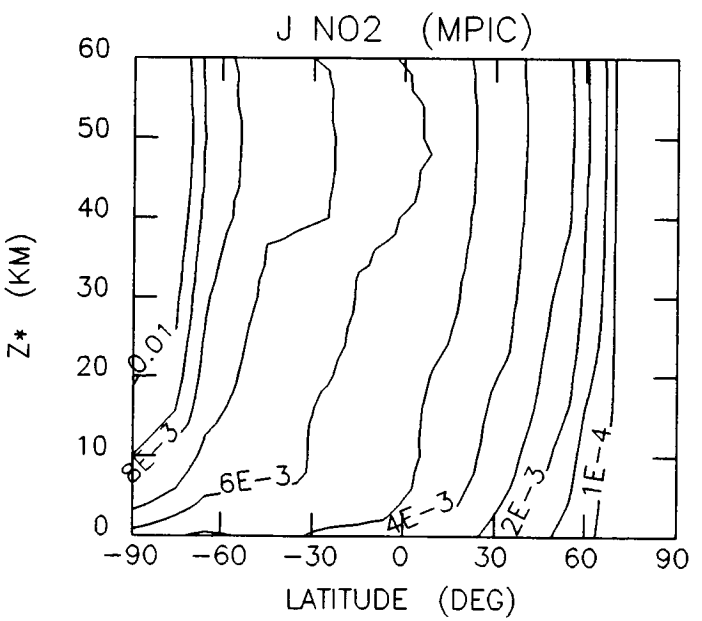
J NO2 (MPIC)
0.01
8E-3
6E-3
4E-3
2E-3
1E-4
Z* (KM)
LATITUDE (DEG)

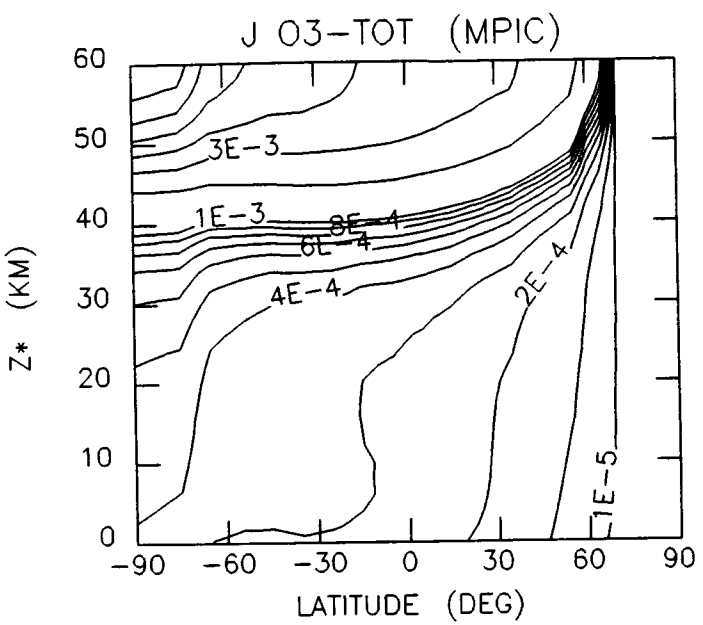
J O3-TOT (MPIC)
Z* (KM)
LATITUDE (DEG)
3E-3
1E-3
8E-4
6E-4
4E-4
2E-4
1E-5

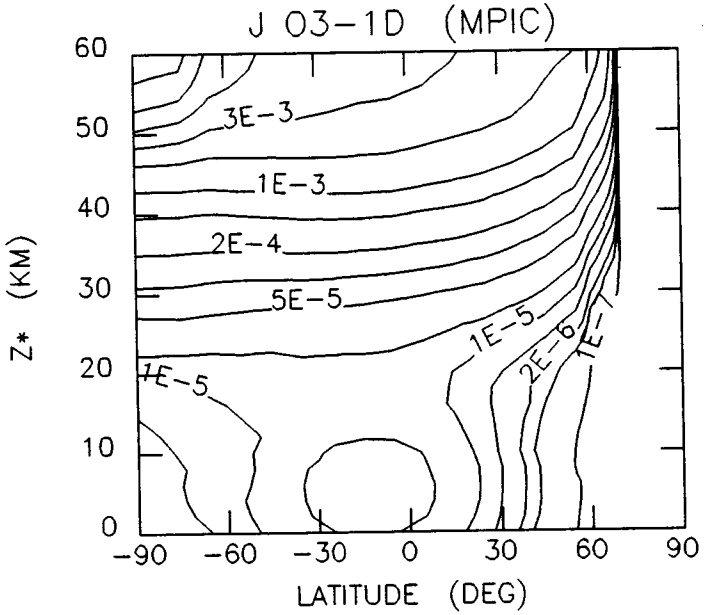
J O3-1D (MPIC)
Z* (KM)
LATITUDE (DEG)
3E-3
1E-3
2E-4
5E-5
1E-5
2E-6
1E-7

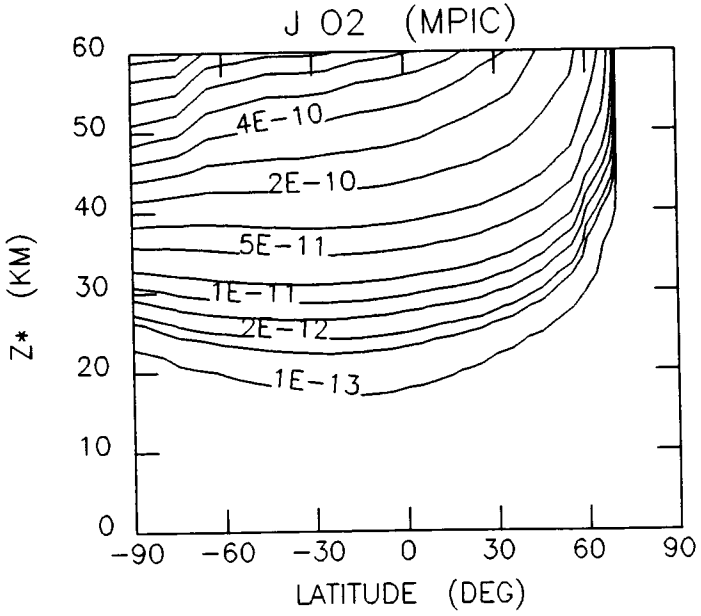
J O2 (MPIC)
Z* (KM)
LATITUDE (DEG)
4E-10
2E-10
5E-11
1E-11
2E-12
1E-13

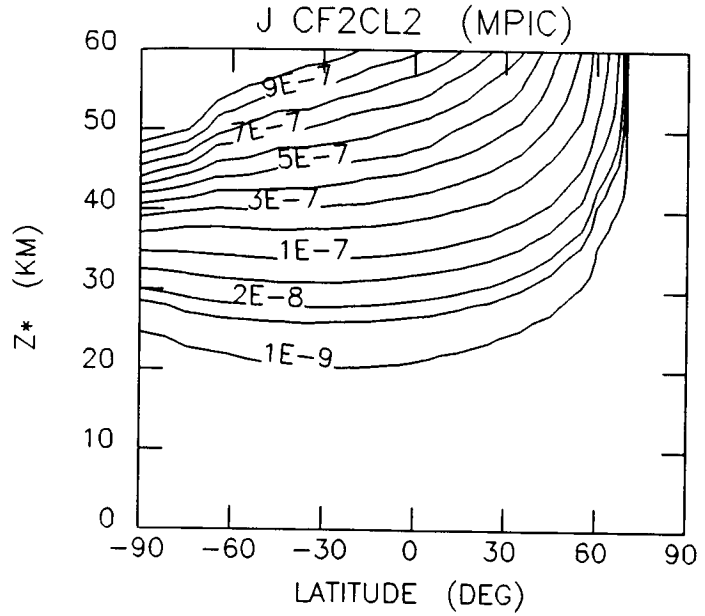
J CF2CL2 (MPIC)
Z* (KM)
LATITUDE (DEG)
9E-7
7E-7
5E-7
3E-7
1E-7
2E-8
1E-9

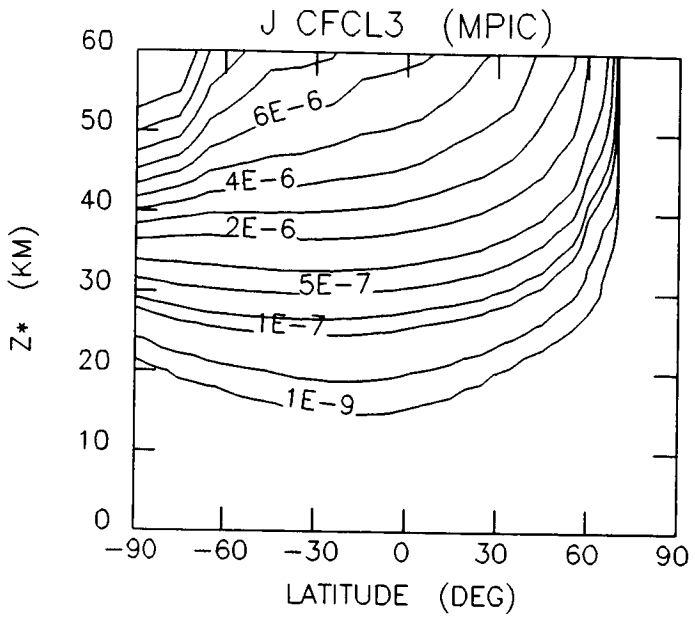
J CFCL3 (MPIC)
Z* (KM)
LATITUDE (DEG)
6E-6
4E-6
2E-6
5E-7
1E-7
1E-9

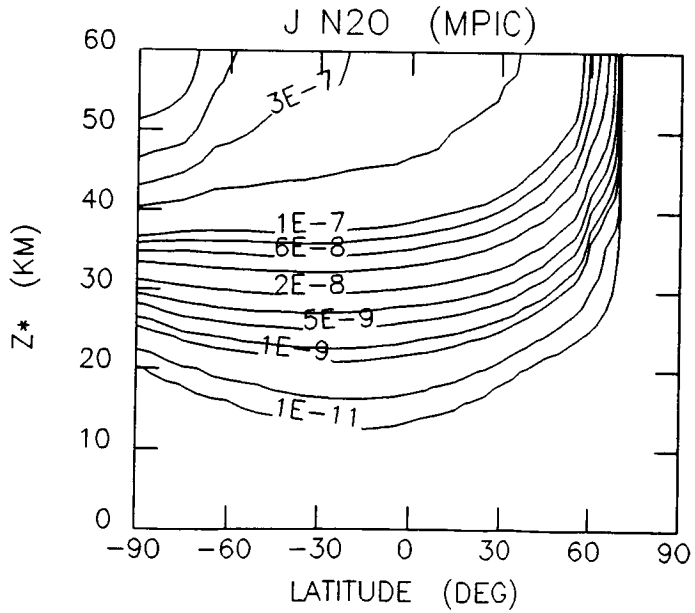
J N2O (MPIC)
Z* (KM)
LATITUDE (DEG)
3E-7
1E-7
6E-8
2E-8
5E-9
1E-9
1E-11

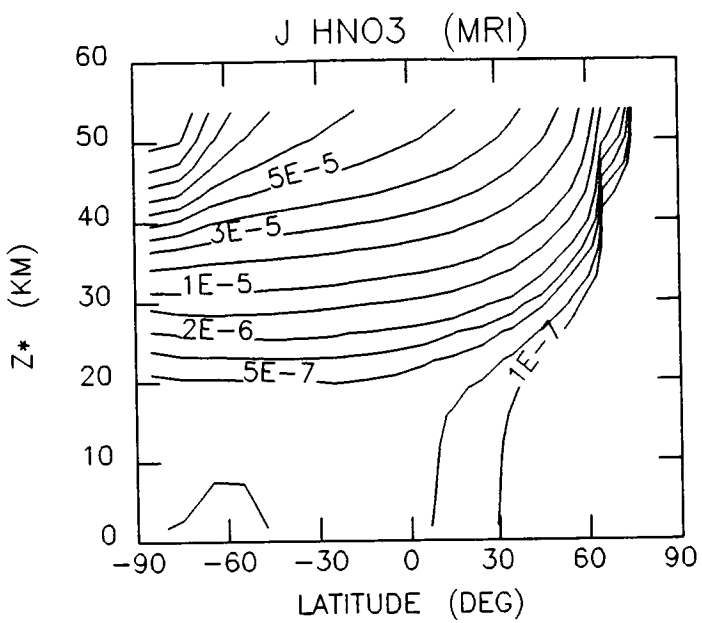
J HNO3 (MRI)
Z* (KM)
LATITUDE (DEG)
5E-5
3E-5
1E-5
2E-6
5E-7
1E-7

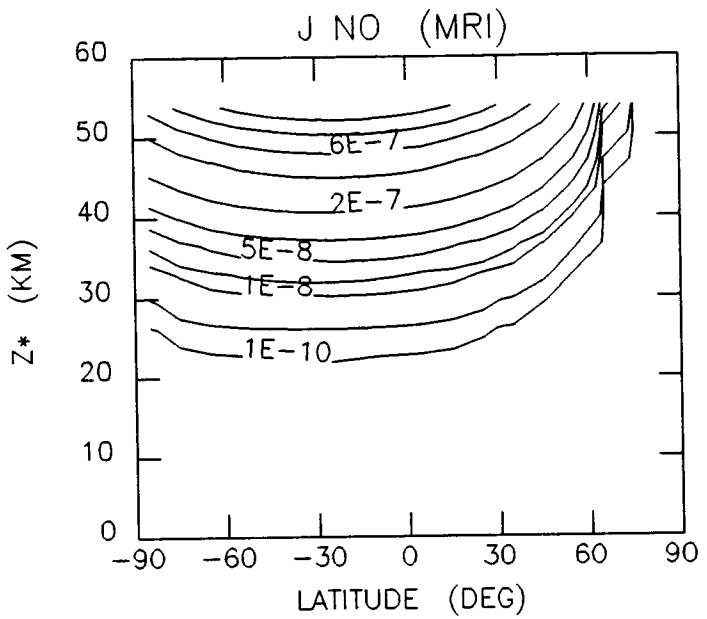
J NO (MRI)
Z* (KM)
LATITUDE (DEG)
6E-7
2E-7
5E-8
1E-8
1E-10

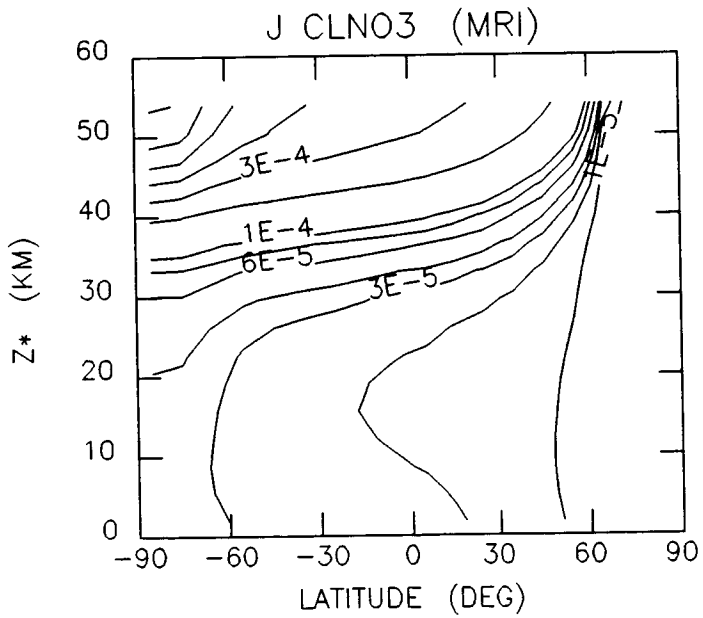
J CLNO3 (MRI)
Z* (KM)
LATITUDE (DEG)
3E-4
1E-4
6E-5
3E-5

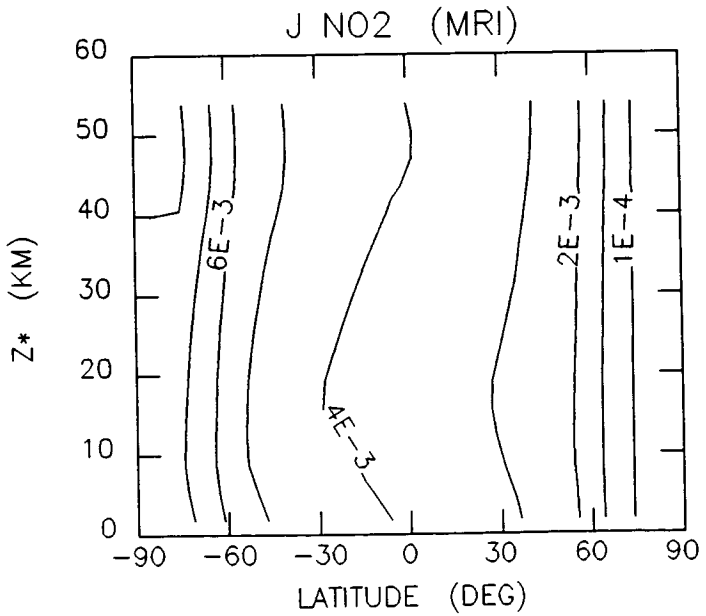
J NO2 (MRI)
Z* (KM)
LATITUDE (DEG)
6E-3
4E-3
2E-3
1E-4

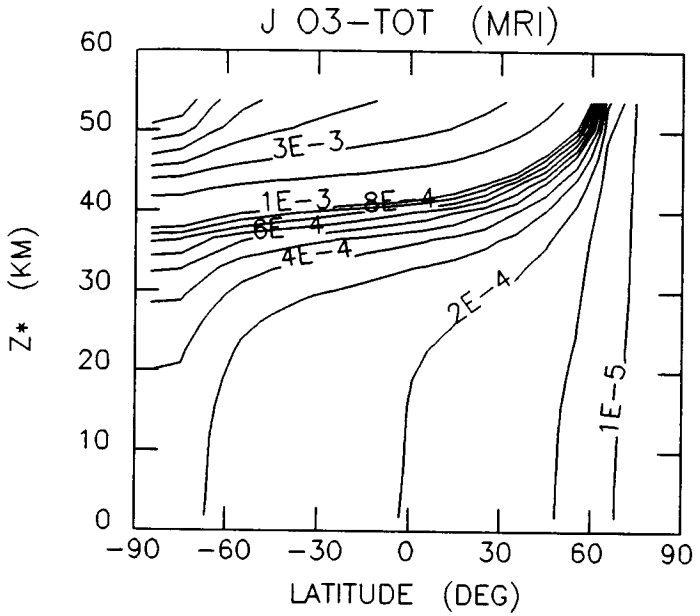
J O3−TOT (MRI)
Z* (KM)
LATITUDE (DEG)
3E−3
1E−3
8E−4
6E−4
4E−4
2E−4
1E−5

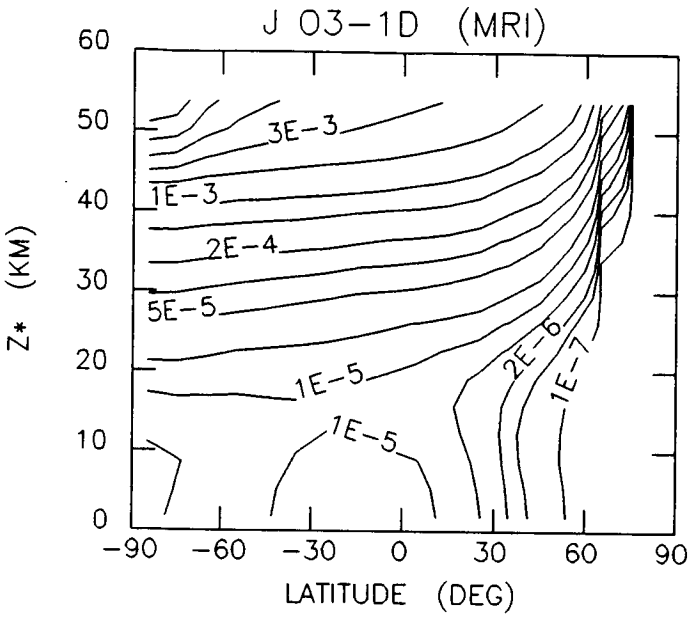
J O3−1D (MRI)
Z* (KM)
LATITUDE (DEG)
3E−3
1E−3
2E−4
5E−5
1E−5
1E−5
2E−6
1E−7

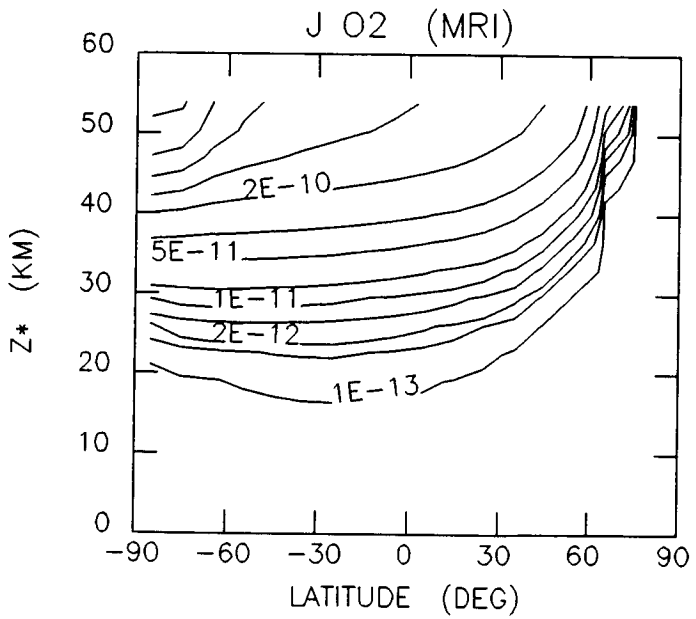
J O2 (MRI)
Z* (KM)
LATITUDE (DEG)
2E−10
5E−11
1E−11
2E−12
1E−13

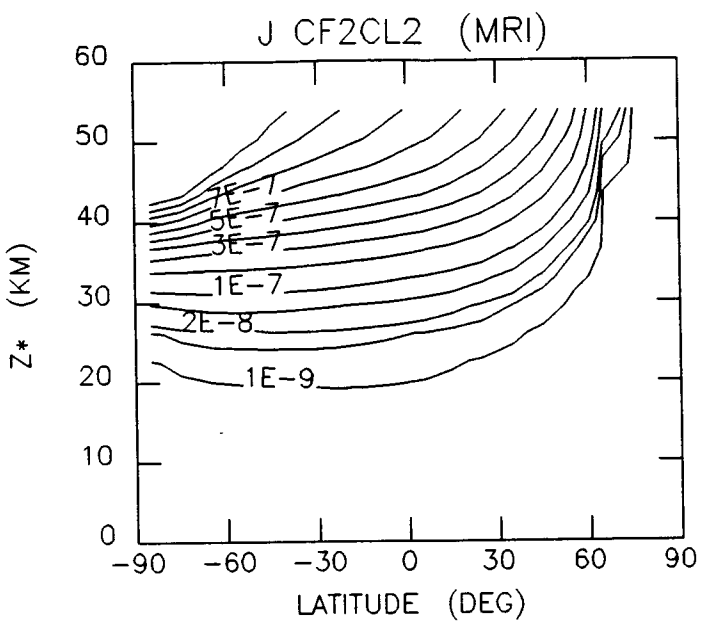
J CF2CL2 (MRI)
Z* (KM)
LATITUDE (DEG)
7E-7
5E-7
3E-7
1E-7
2E-8
1E-9

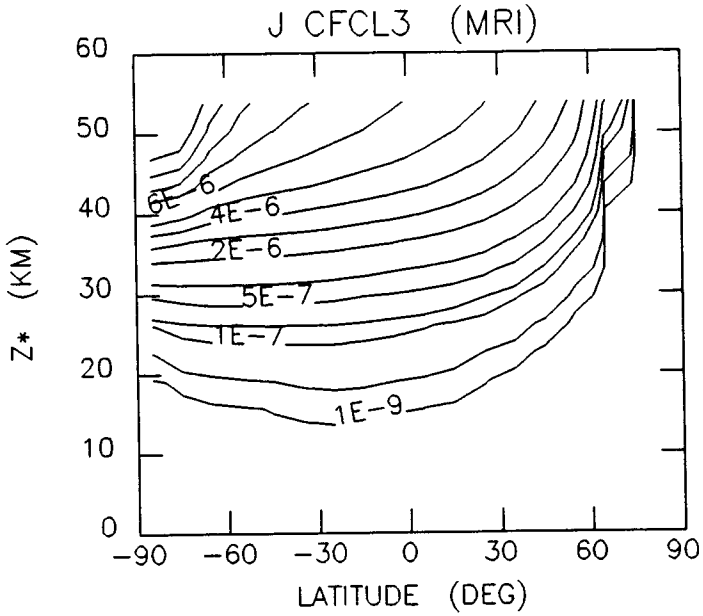
J CFCL3 (MRI)
Z* (KM)
LATITUDE (DEG)
6E-6
4E-6
2E-6
5E-7
1E-7
1E-9

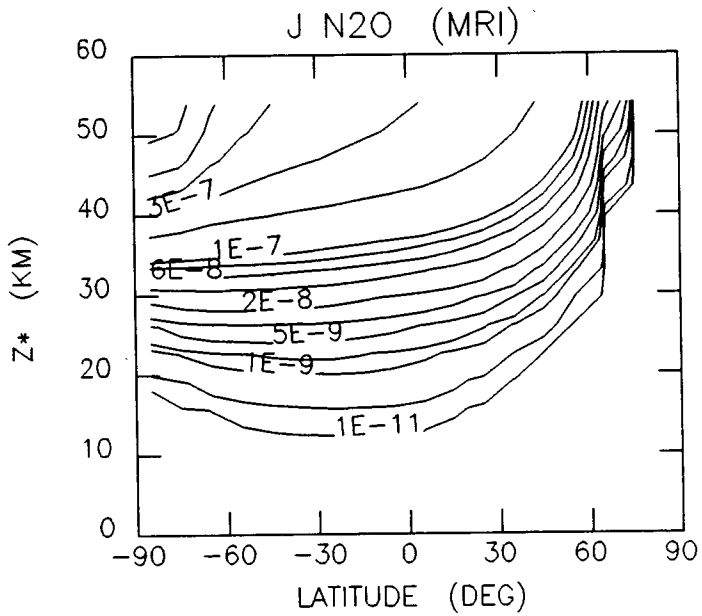
J N2O (MRI)
Z* (KM)
LATITUDE (DEG)
3E-7
1E-7
6E-8
2E-8
5E-9
1E-9
1E-11

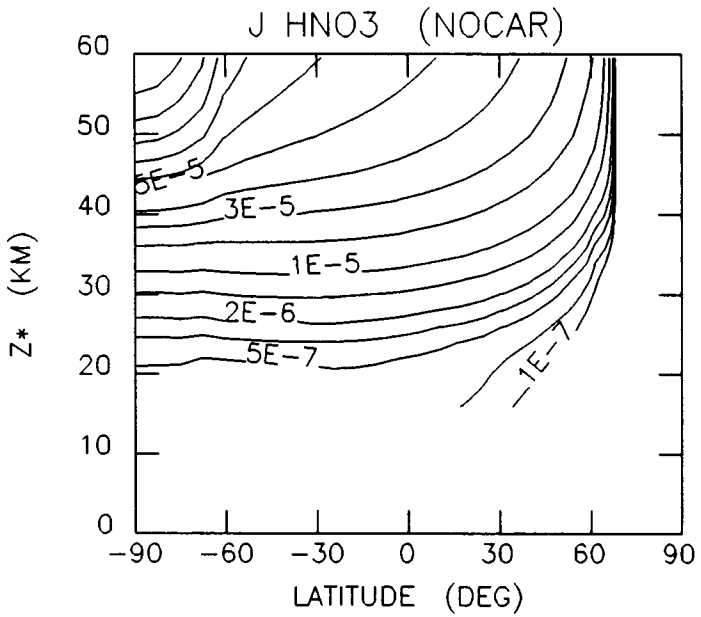
J HNO3 (NOCAR)
Z* (KM)
LATITUDE (DEG)
1
5E-5
3E-5
1E-5
2E-6
5E-7
1E-7

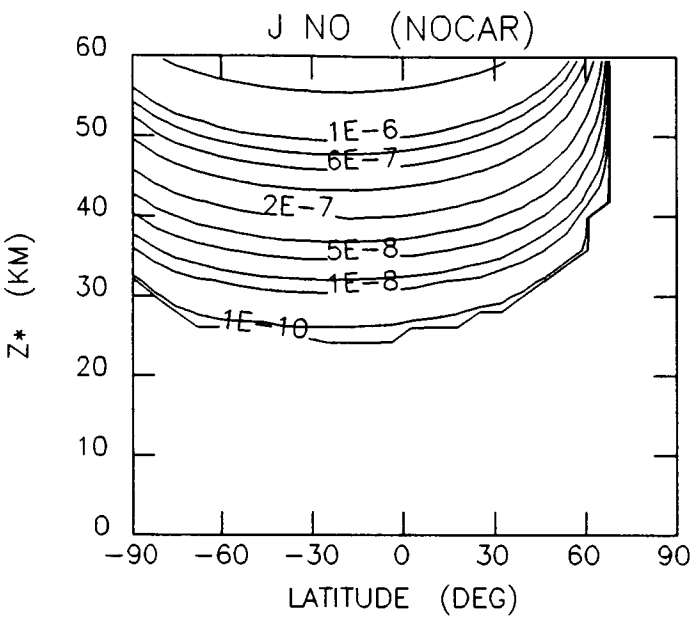
J NO (NOCAR)
Z* (KM)
LATITUDE (DEG)
1E-6
6E-7
2E-7
5E-8
1E-8
1E-10

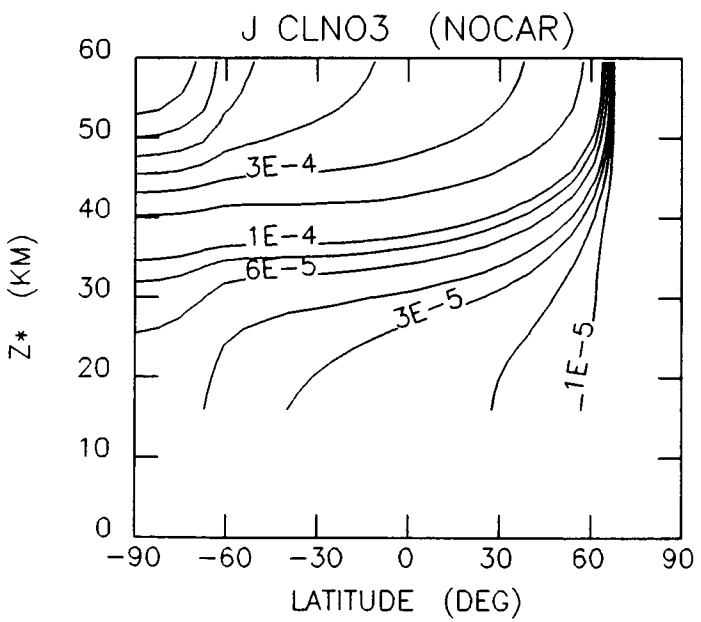
J CLNO3 (NOCAR)
Z* (KM)
LATITUDE (DEG)
3E-4
1E-4
6E-5
3E-5
1E-5

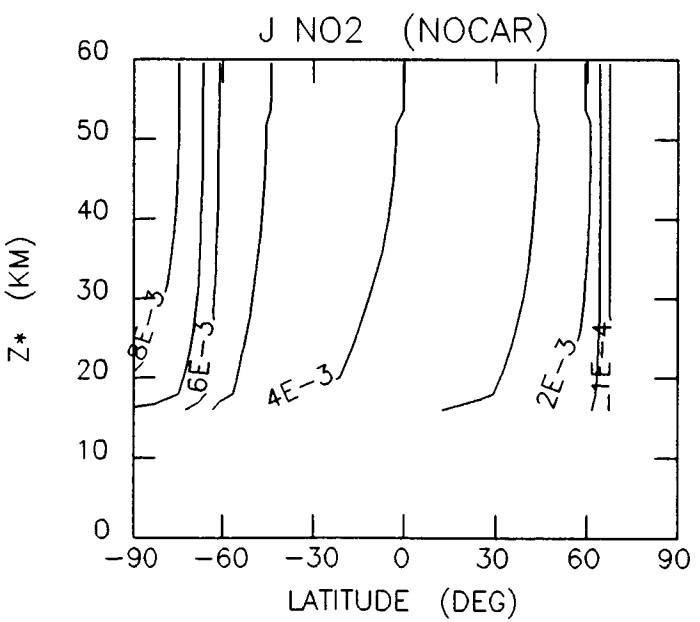
J NO2 (NOCAR)
Z* (KM)
LATITUDE (DEG)
8E-3
6E-3
4E-3
2E-3
1E-4

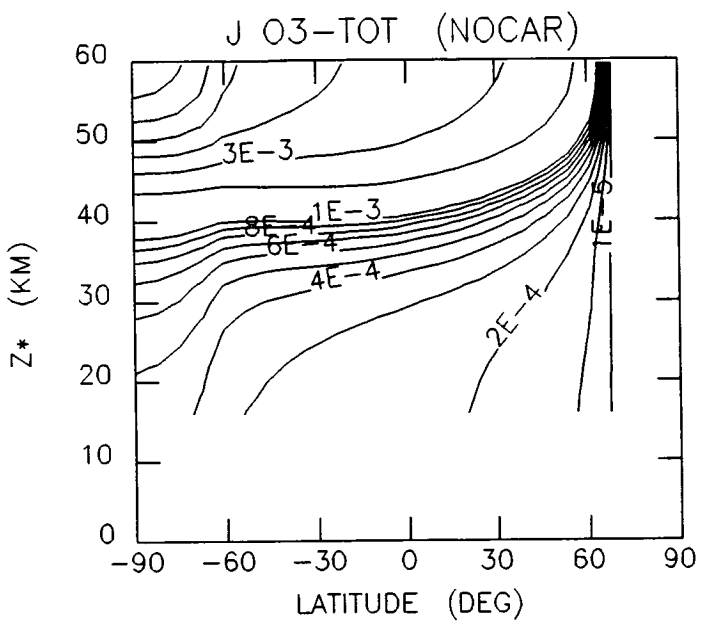
J O3-TOT (NOCAR)
Z* (KM)
LATITUDE (DEG)
3E-3
1E-3
8E-4
6E-4
4E-4
2E-4
1E-5

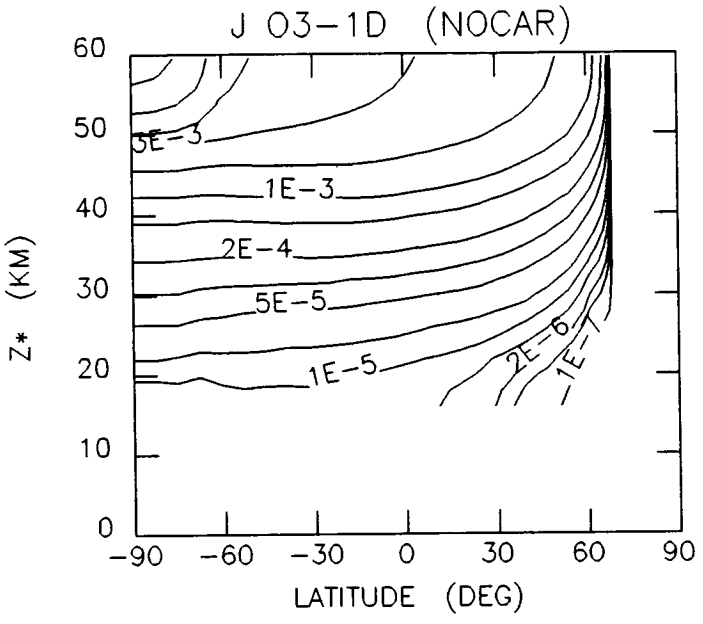
J O3-1D (NOCAR)
Z* (KM)
LATITUDE (DEG)
5E-3
1E-3
2E-4
5E-5
1E-5
2E-6
1E-7

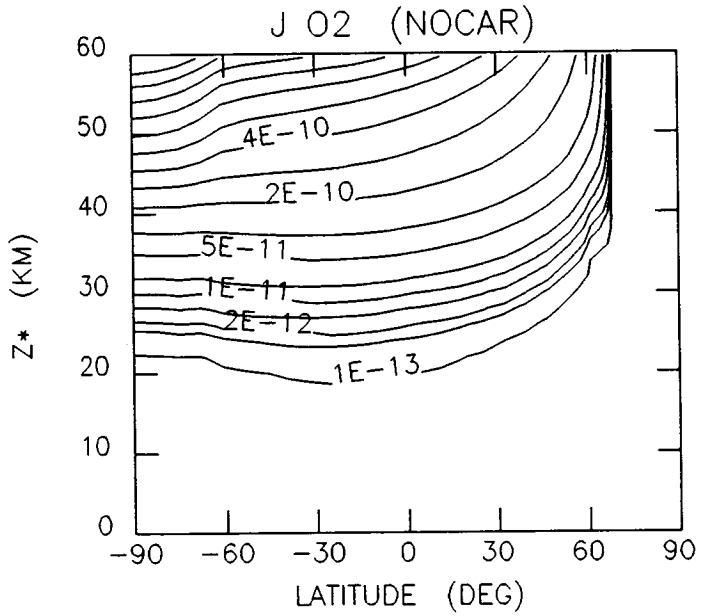
J O2 (NOCAR)
Z* (KM)
LATITUDE (DEG)
4E-10
2E-10
5E-11
1E-11
2E-12
1E-13

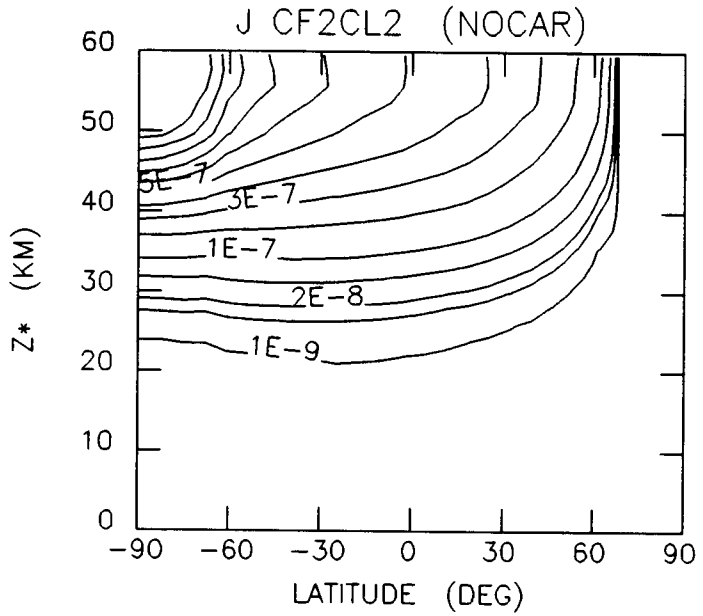
J CF2CL2 (NOCAR)
Z* (KM)
LATITUDE (DEG)
5E-7
3E-7
1E-7
2E-8
1E-9

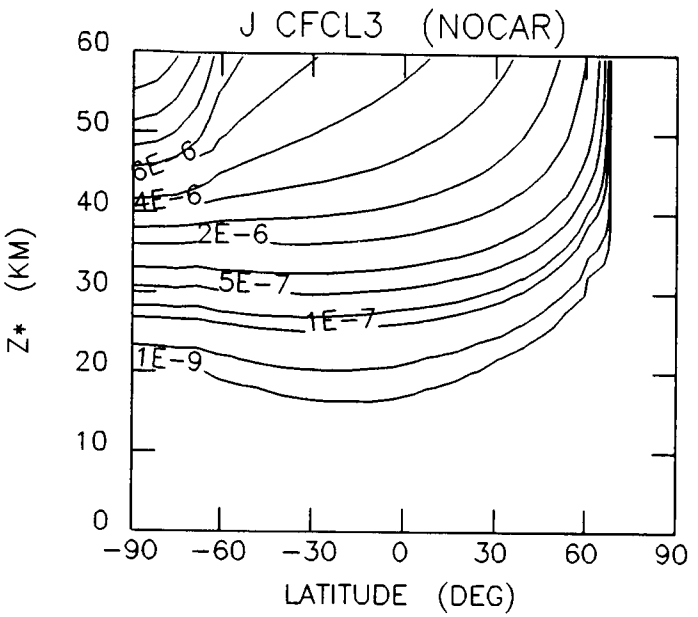
J CFCL3 (NOCAR)
Z* (KM)
LATITUDE (DEG)
6E-6
4E-6
2E-6
5E-7
1E-7
1E-9

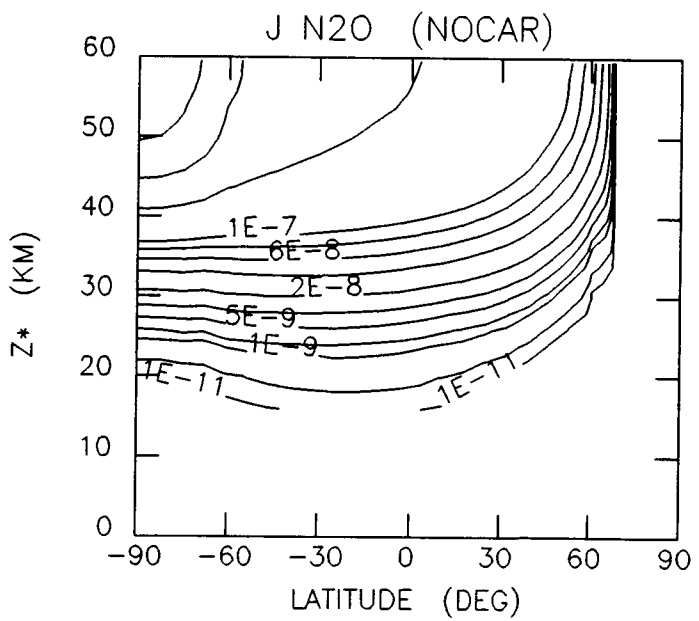
J N2O (NOCAR)
Z* (KM)
LATITUDE (DEG)
1E-7
6E-8
2E-8
5E-9
1E-9
1E-11
1E-11

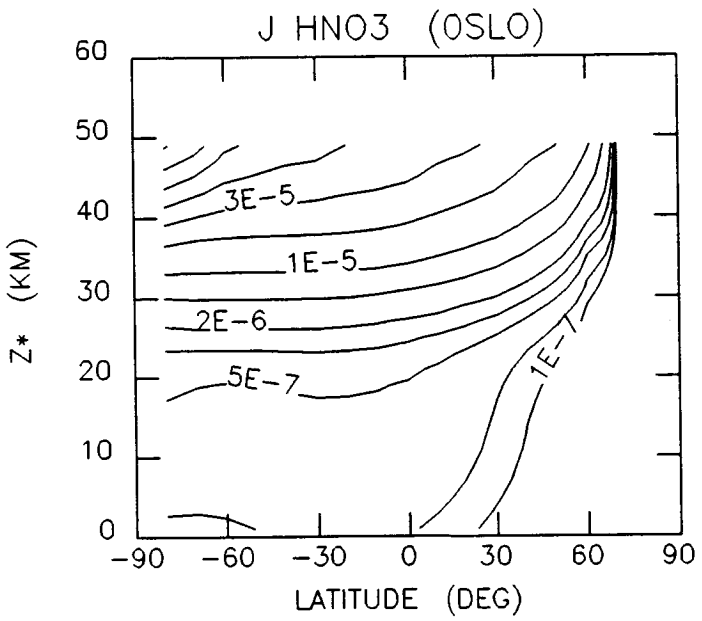
J HNO3 (OSLO)
Z* (KM)
LATITUDE (DEG)
3E-5
1E-5
2E-6
5E-7
1E-7

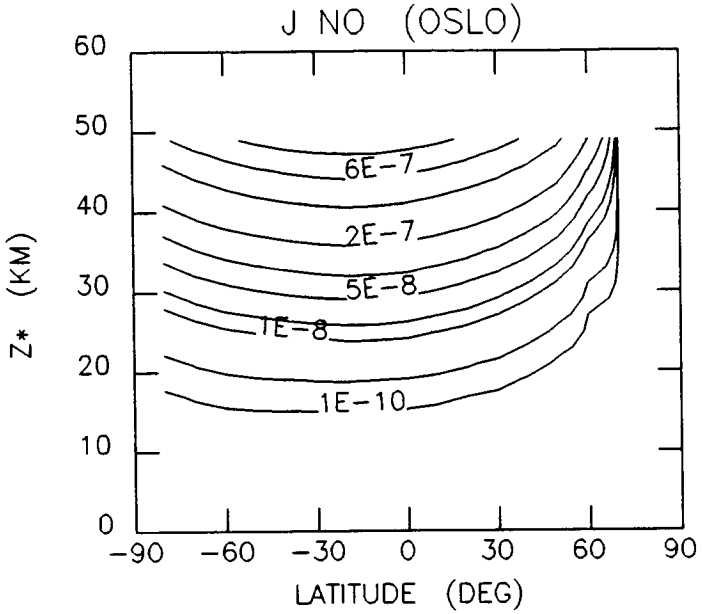
J NO (OSLO)
Z* (KM)
LATITUDE (DEG)
6E-7
2E-7
5E-8
1E-8
1E-10

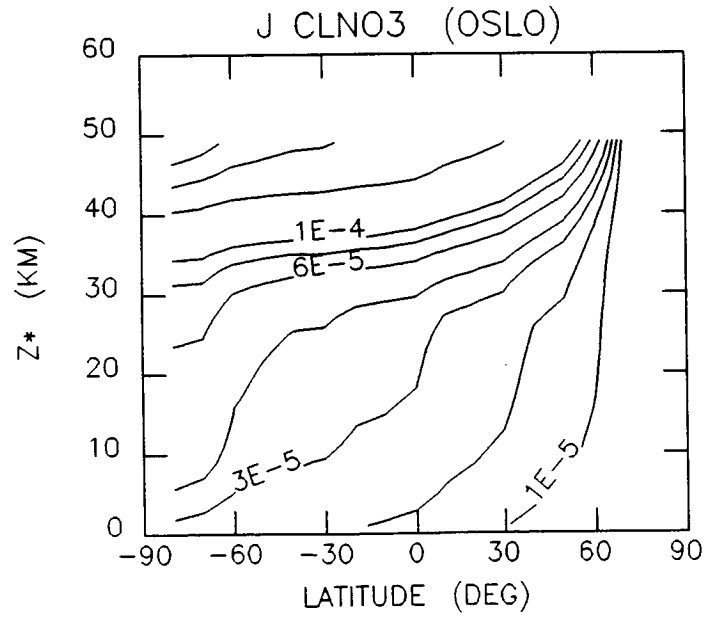
J CLNO3 (OSLO)
Z* (KM)
LATITUDE (DEG)
1E-4
6E-5
3E-5
1E-5

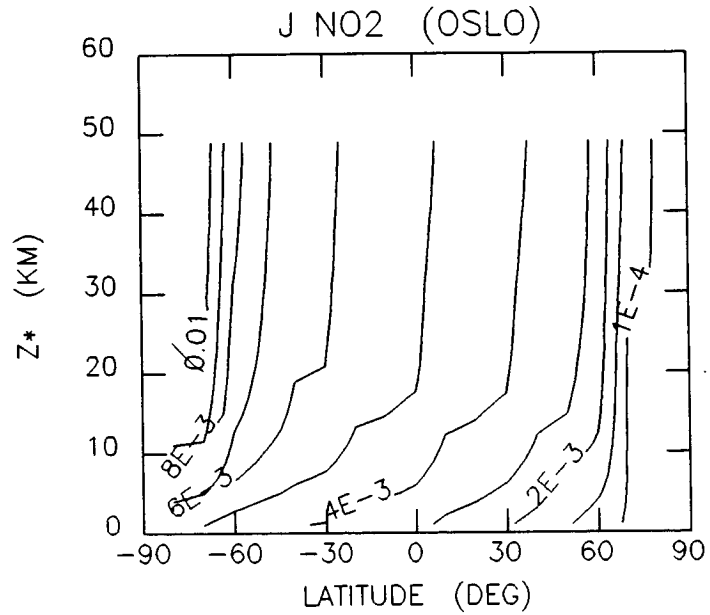
J NO2 (OSLO)
Z* (KM)
LATITUDE (DEG)
Ø.01
8E-3
6E-3
4E-3
2E-3
1E-4

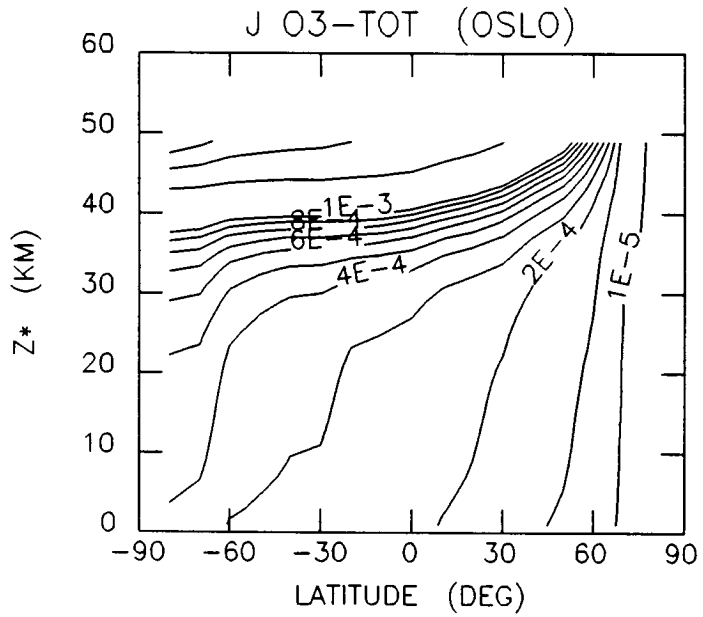
J 03-TOT (OSLO)
Z* (KM)
LATITUDE (DEG)
1E-3
8E-4
6E-4
4E-4
2E-4
1E-5

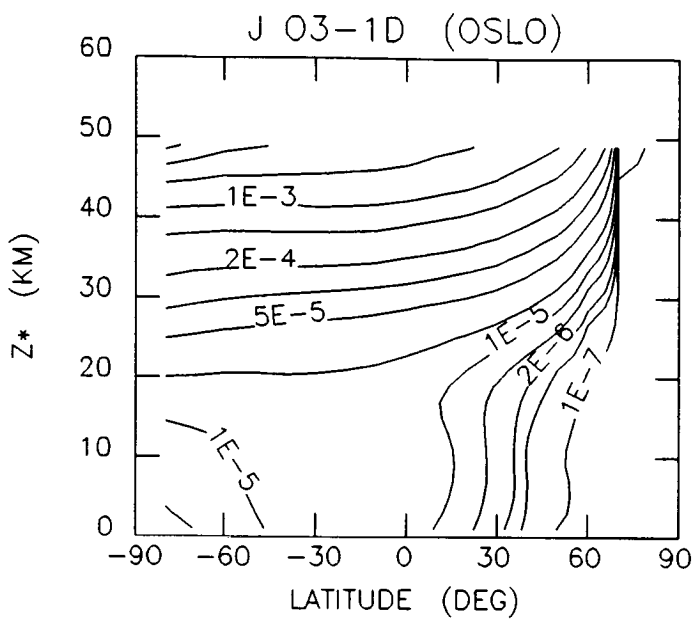
J 03-1D (OSLO)
Z* (KM)
LATITUDE (DEG)
1E-3
2E-4
5E-5
1E-5
2E-6
1E-7
1E-5

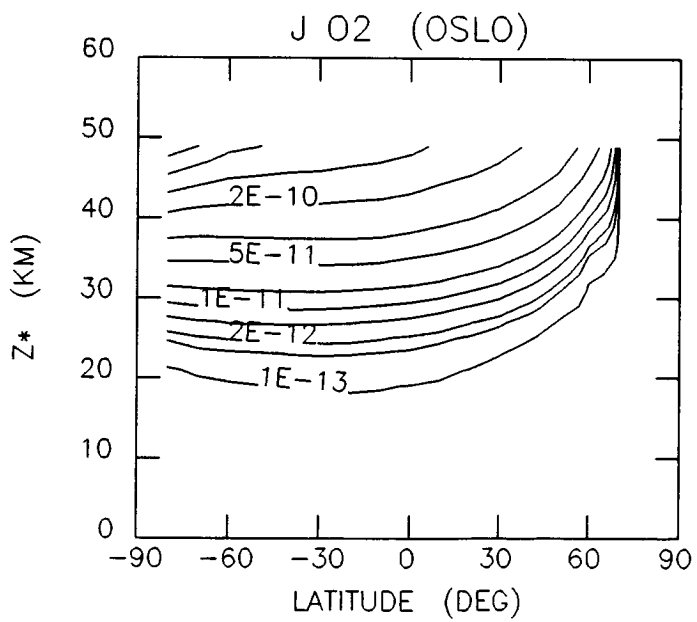
J 02 (OSLO)
Z* (KM)
LATITUDE (DEG)
2E-10
5E-11
1E-11
2E-12
1E-13

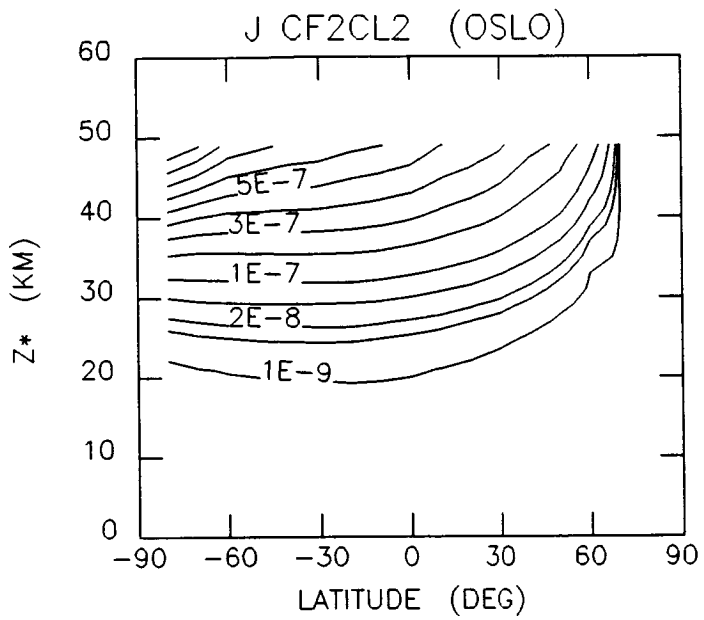
J CF2CL2 (OSLO)
Z* (KM)
LATITUDE (DEG)
5E-7
3E-7
1E-7
2E-8
1E-9

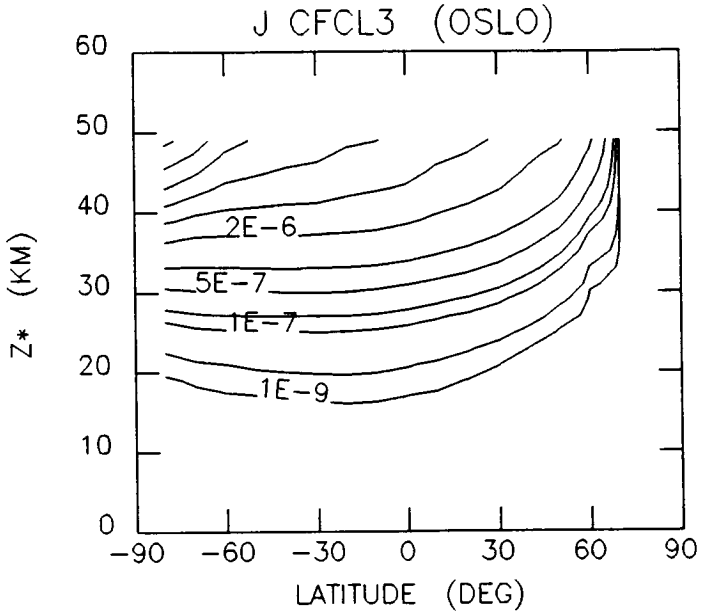
J CFCL3 (OSLO)
Z* (KM)
LATITUDE (DEG)
2E-6
5E-7
1E-7
1E-9

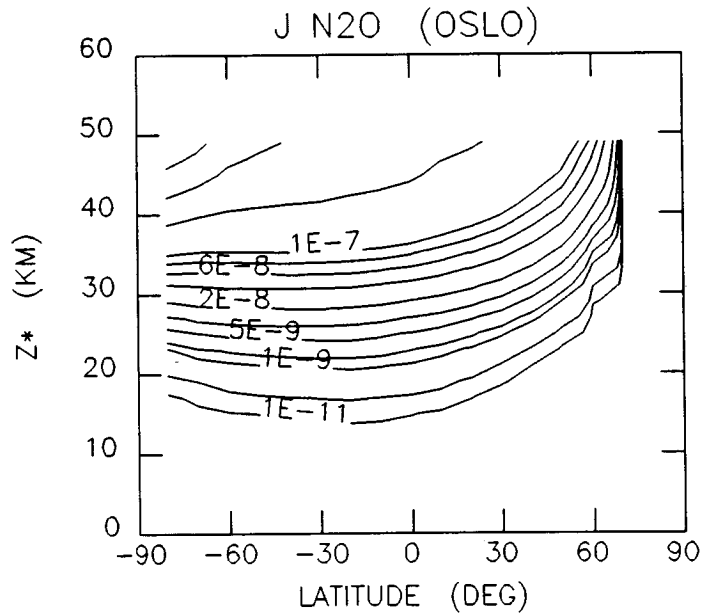
J N2O (OSLO)
Z* (KM)
LATITUDE (DEG)
1E-7
6E-8
2E-8
5E-9
1E-9
1E-11

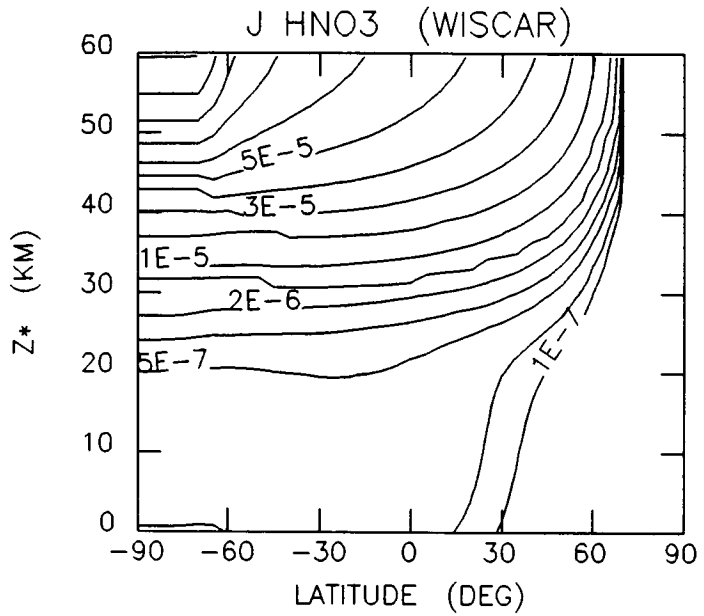
J HNO3 (WISCAR)
Z* (KM)
LATITUDE (DEG)
5E-5
3E-5
1E-5
2E-6
5E-7
1E-7

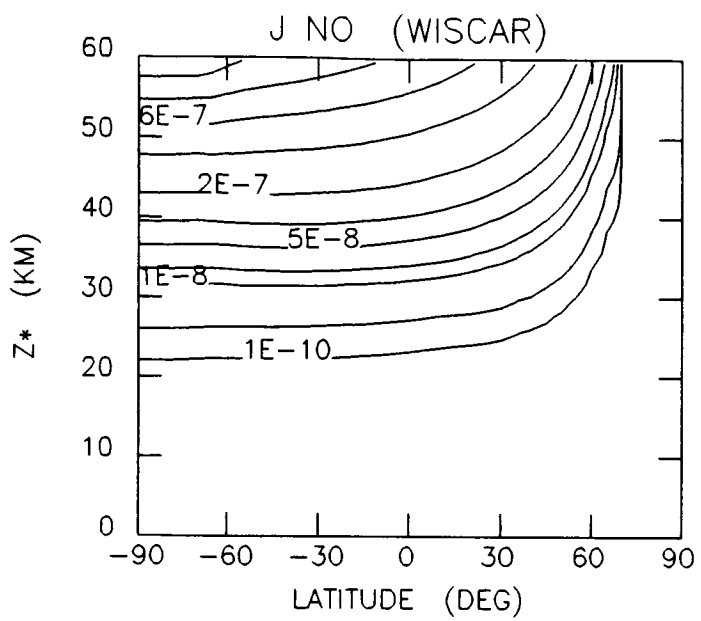
J NO (WISCAR)
Z* (KM)
LATITUDE (DEG)
6E-7
2E-7
5E-8
1E-8
1E-10

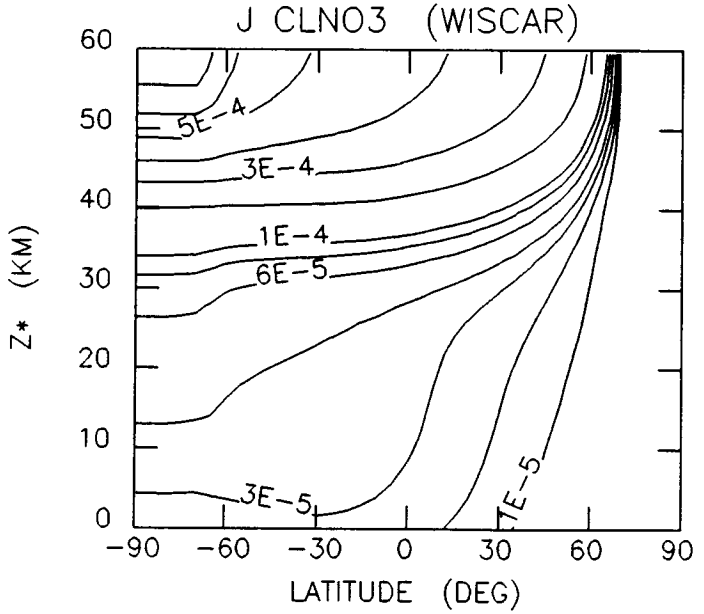
J CLNO3 (WISCAR)
Z* (KM)
LATITUDE (DEG)
5E-4
3E-4
1E-4
6E-5
3E-5
1E-5

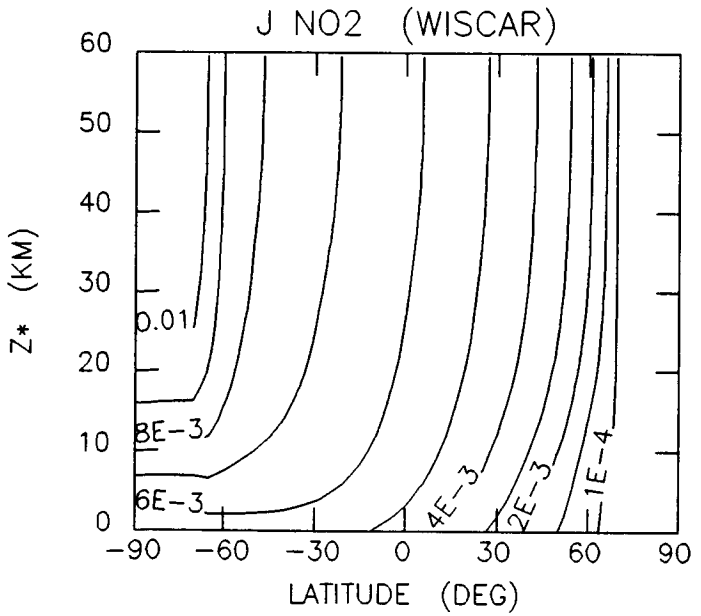
J NO2 (WISCAR)
Z* (KM)
LATITUDE (DEG)
0.01
8E-3
6E-3
4E-3
2E-3
1E-4

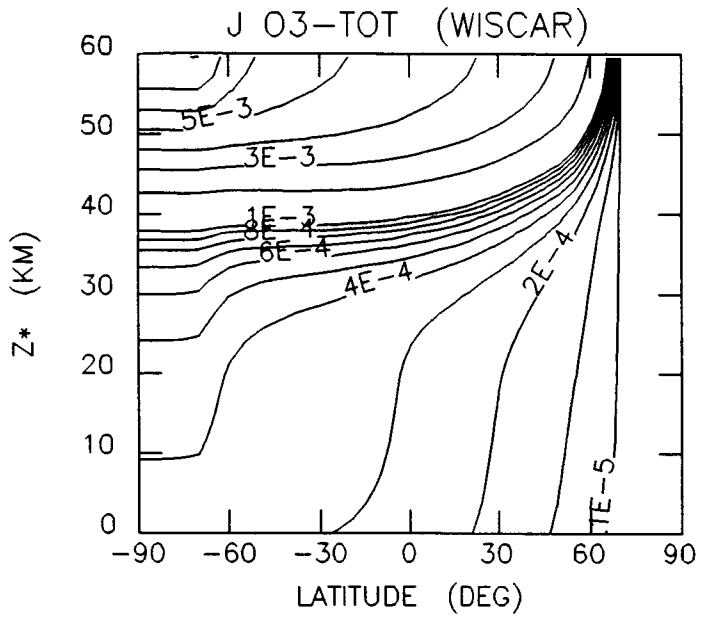
J O3−TOT (WISCAR)
Z* (KM)
LATITUDE (DEG)
5E−3
3E−3
1E−3
8E−4
6E−4
4E−4
2E−4
1E−5

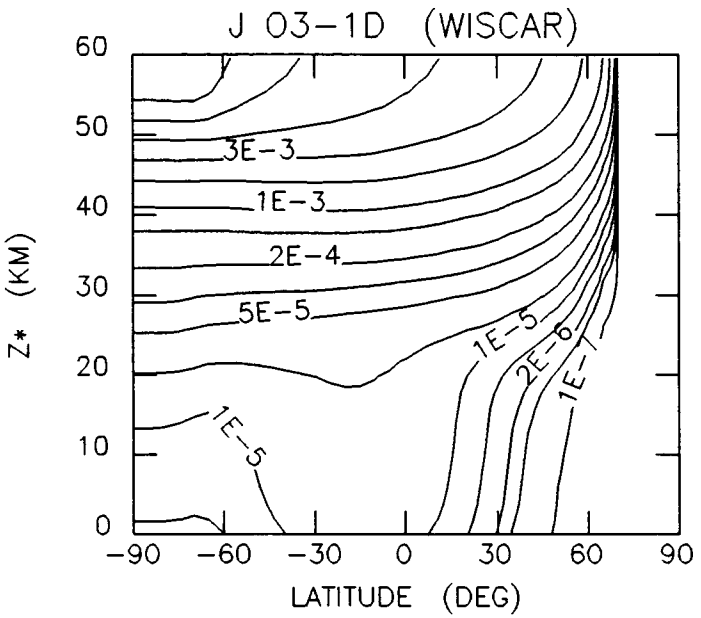
J O3−1D (WISCAR)
Z* (KM)
LATITUDE (DEG)
3E−3
1E−3
2E−4
5E−5
1E−5
1E−5
2E−6
1E−7

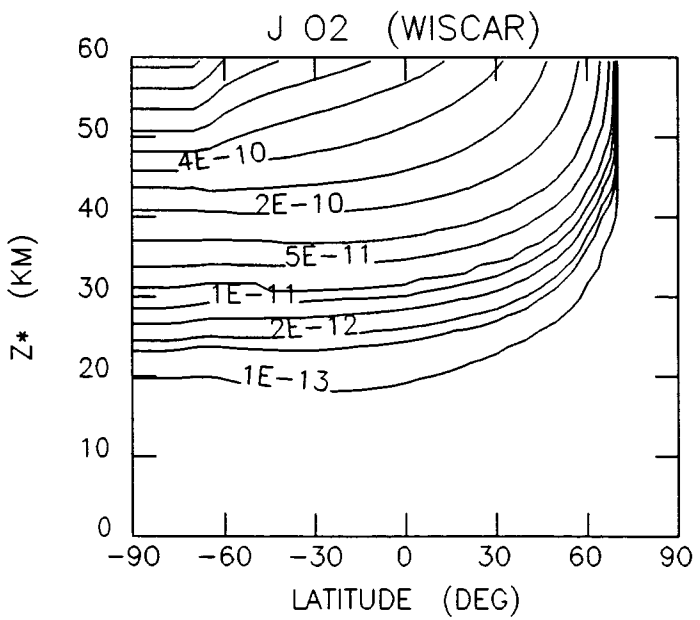
J O2 (WISCAR)
Z* (KM)
LATITUDE (DEG)
4E−10
2E−10
5E−11
1E−11
2E−12
1E−13

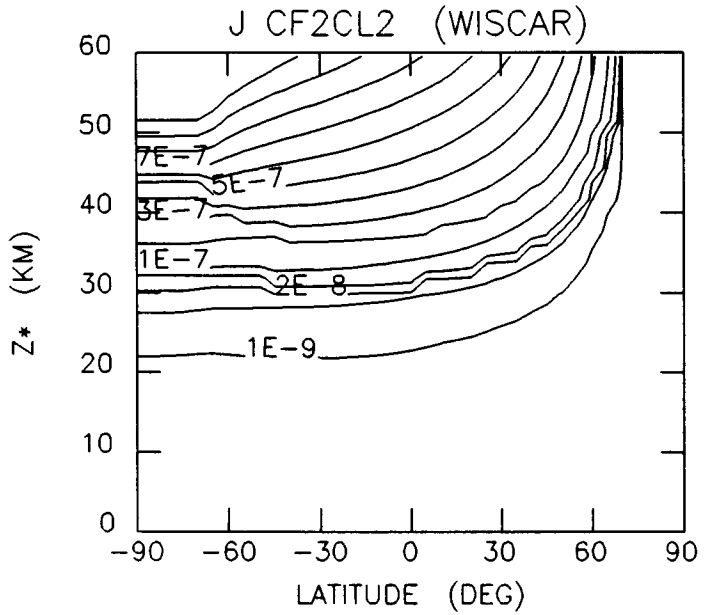
J CF2CL2 (WISCAR)
Z* (KM)
LATITUDE (DEG)
7E-7
5E-7
3E-7
1E-7
2E-8
1E-9

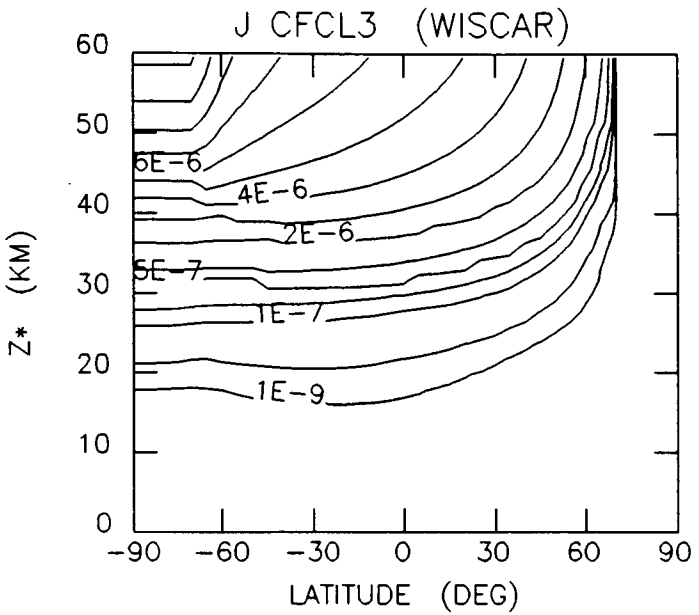
J CFCL3 (WISCAR)
Z* (KM)
LATITUDE (DEG)
6E-6
4E-6
2E-6
5E-7
1E-7
1E-9

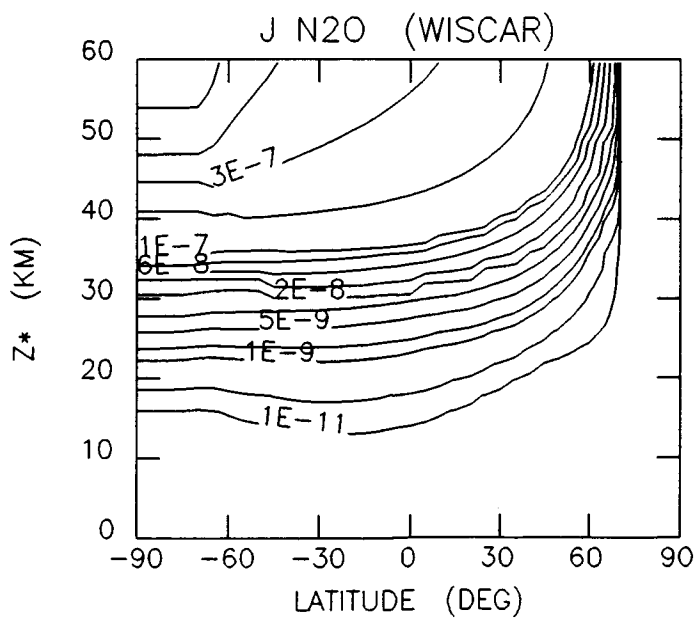
J N2O (WISCAR)
Z* (KM)
LATITUDE (DEG)
3E-7
1E-7
6E-8
2E-8
5E-9
1E-9
1E-11

**Table 6-1b.** Heating and Cooling Rates

Fixed January atmosphere (Temperature and $O_3$);
Normal (340 ppmv) and Doubled (680 ppmv) $CO_2$
Models Represented - AER, CAMBRAL, CAO, CLKSON, GISS, LLNL, MPIC, NOCAR, OSLO, WISCAR

| Parameter | Description | Units | Contour Levels |
|---|---|---|---|
| QIR1 | IR Cooling Rate | K/day | -24, -22, -20, -18, -16, -14, -12, -10, -9, -8, -7, -6, -5, -4, -3, -2, -1, -0.8, -0.6, -0.4, -0.2, 0, 0.2, 0.4, 0.6, 0.8, 1.0 |
| QIR2 | IR Cooling Rate for Doubled $CO_2$ | K/day | -22, -20, -18, -16, -14, -12, -10, -9, -8, -7, -6, -5, -4, -3, -2, -1, -0.8, -0.6, -0.4, -0.2, 0, 0.2, 0.4, 0.6, 0.8, 1.0 |
| QUV1 | UV Heating Rate | K/day | 0, 0.2, 0.4, 0.6, 0.8, 1, 2, 3, 4, 5, 6, 7, 8, 9, 10, 12, 14, 16, 18, 20, 22, 24 |
| QUV2 | UV Heating Rate for Doubled $CO_2$ | K/day | 0, 0.2, 0.4, 0.6, 0.8, 1, 2, 3, 4, 5, 6, 7, 8, 9, 10, 12, 14, 16, 18 |

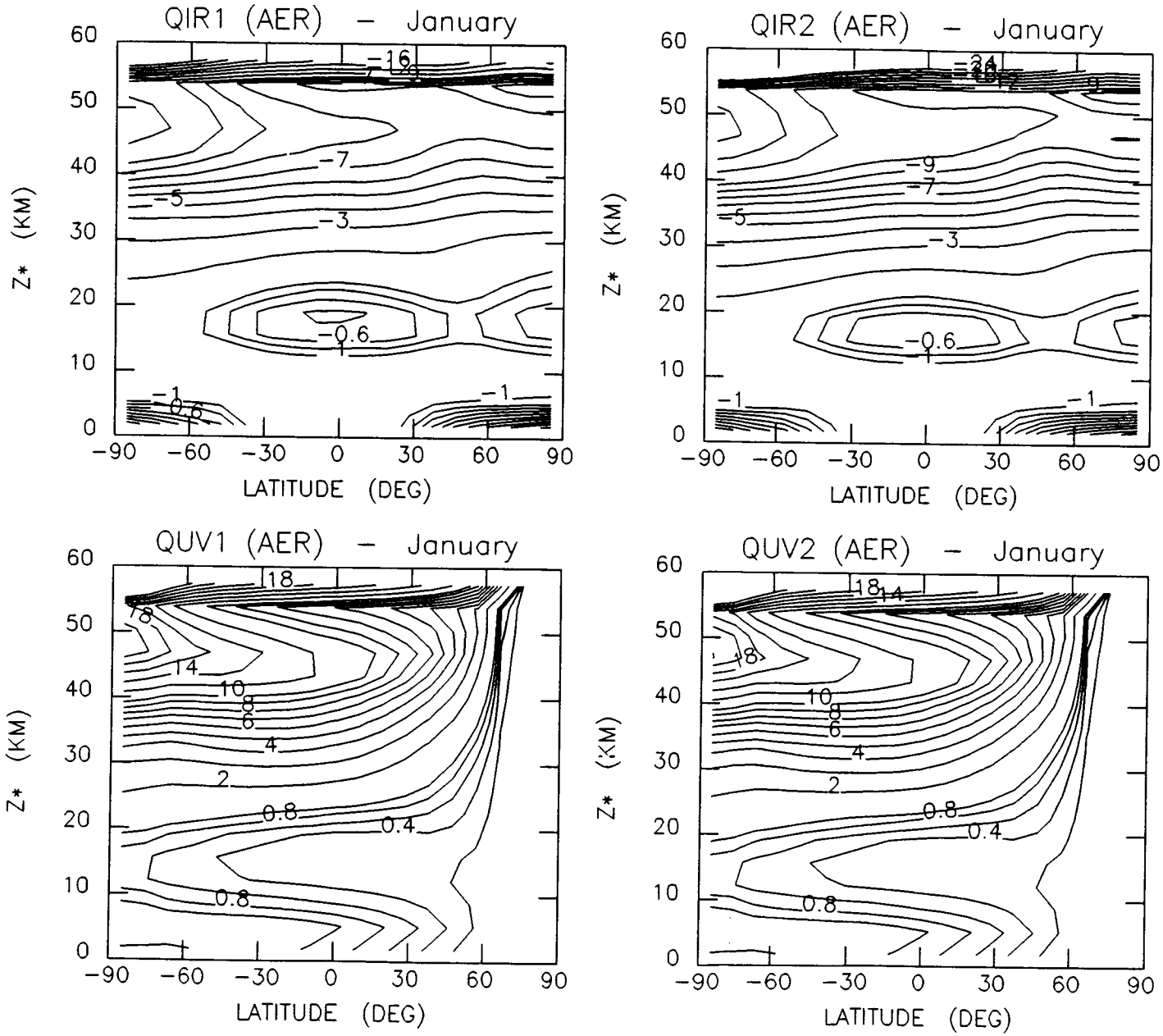
QIR1 (AER) – January
QIR2 (AER) – January
QUV1 (AER) – January
QUV2 (AER) – January
Z* (KM)
LATITUDE (DEG)
60
50
40
30
20
10
0
−90 −60 −30 0 30 60 90
−16
−7
−5
−3
−0.6
−1
−0.6
−9
−7
−5
−3
−0.6
−1
18
14
10
8
6
4
2
0.8
0.4
0.8

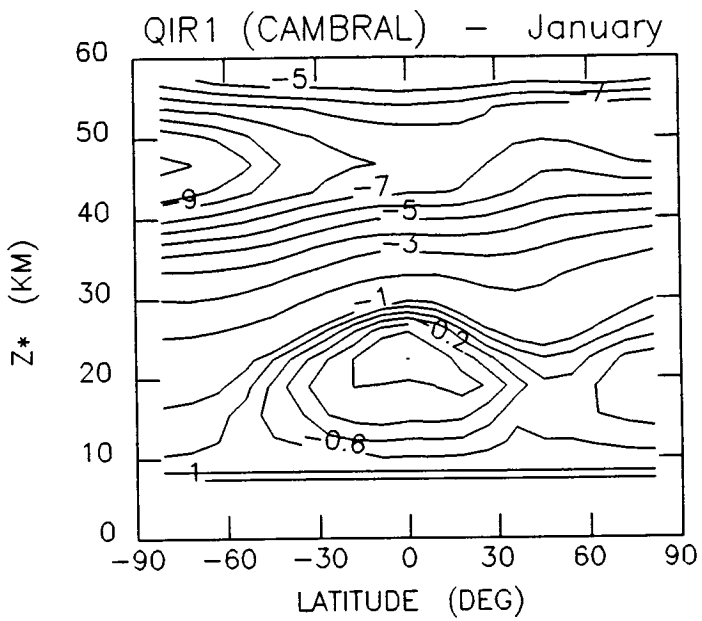
QIR1 (CAMBRAL) – January
Z* (KM)
LATITUDE (DEG)
-5
-7
-9
-7
-5
-3
-1
-0.2
-0.6
1

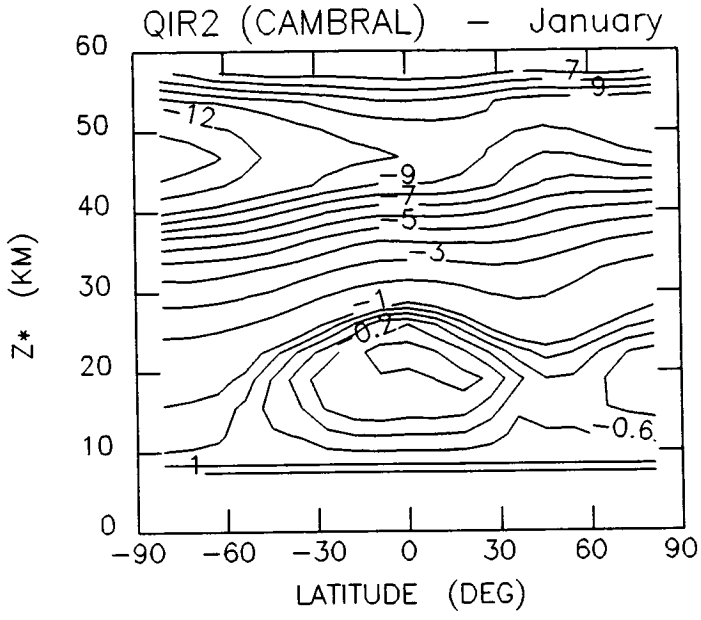
QIR2 (CAMBRAL) – January
Z* (KM)
LATITUDE (DEG)
-12
-9
-7
-5
-3
-1
-0.7
-0.6
1

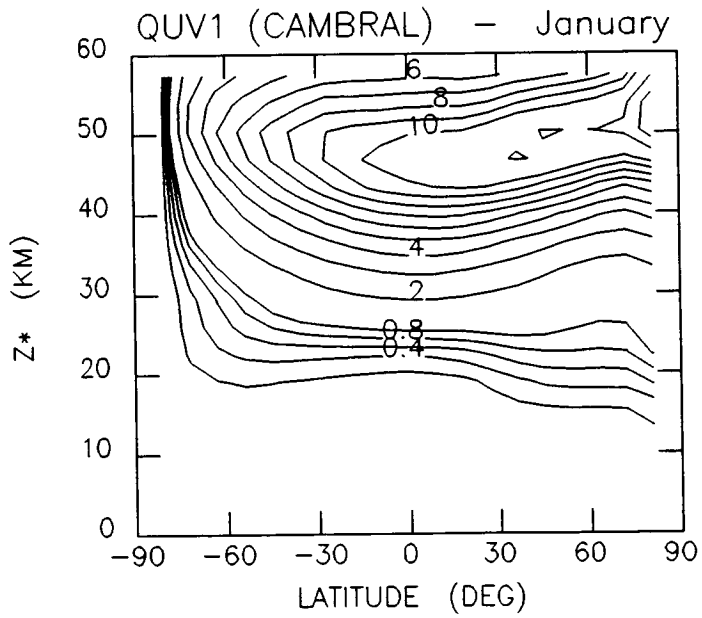
QUV1 (CAMBRAL) – January
Z* (KM)
LATITUDE (DEG)
6
8
10
4
2
0.8
0.4

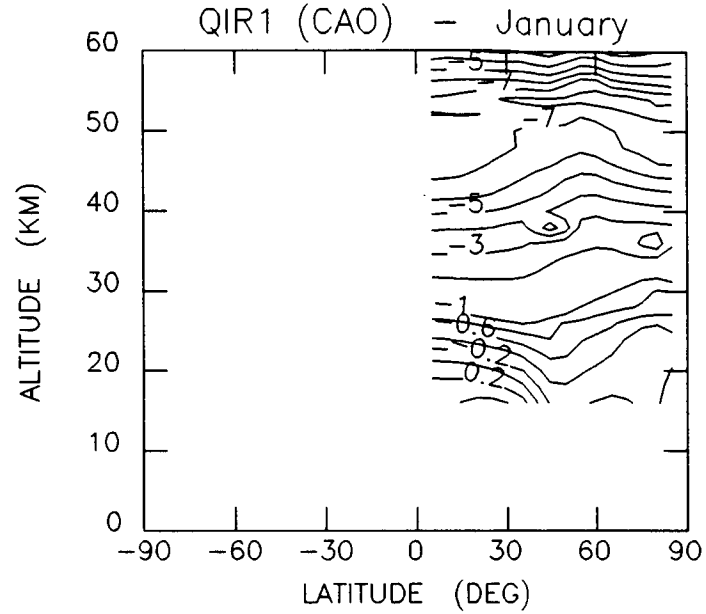
QIR1 (CAO) – January
ALTITUDE (KM)
LATITUDE (DEG)
60
50
40
30
20
10
0
-90
-60
-30
0
30
60
90
-5
-7
-7
-5
-3
-1
-0.6
-0.2
-0.2

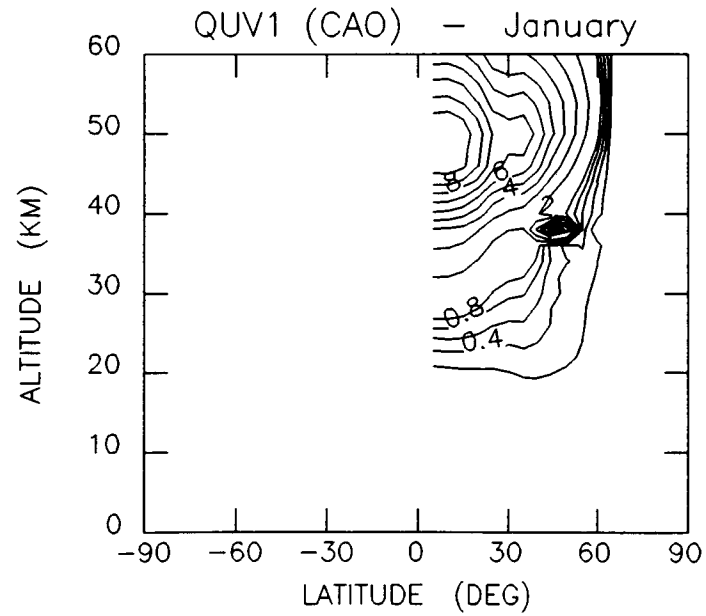
QUV1 (CAO) – January
ALTITUDE (KM)
LATITUDE (DEG)
60
50
40
30
20
10
0
-90
-60
-30
0
30
60
90
-0.8
-0.4
-0.8
-0.4
-2
-0.8
-0.4

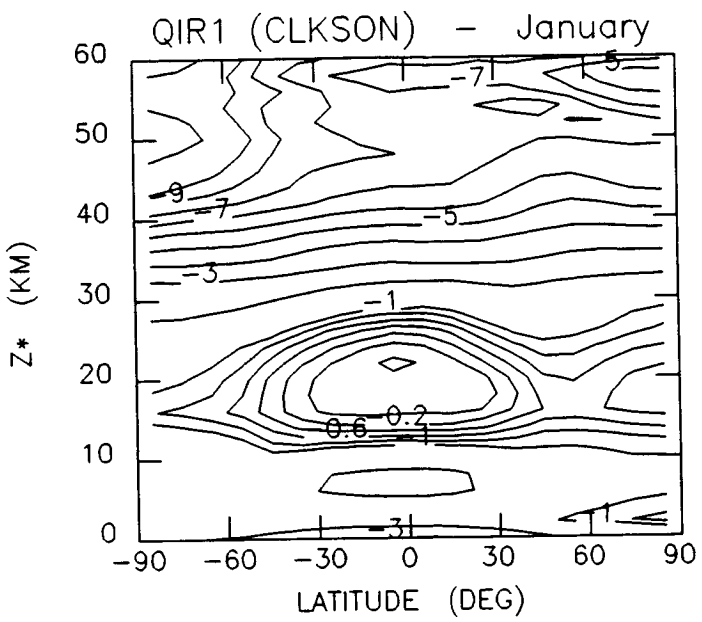
QIR1 (CLKSON) – January
Z* (KM)
LATITUDE (DEG)

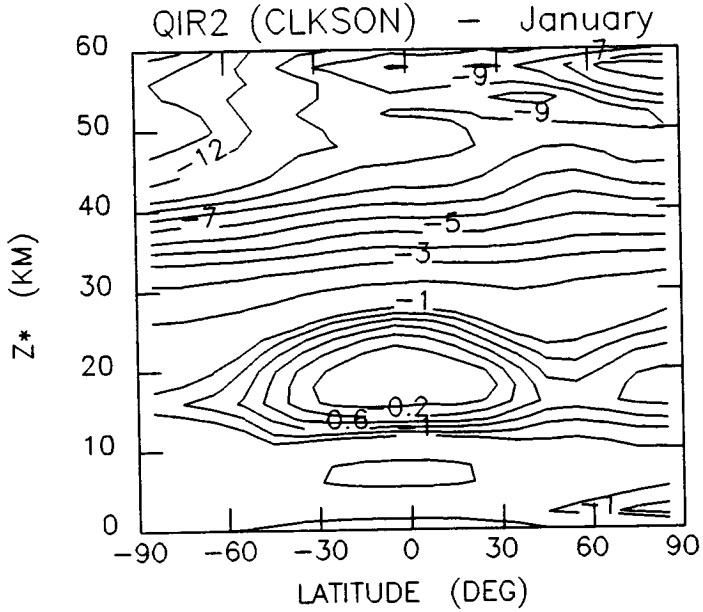
QIR2 (CLKSON) – January
Z* (KM)
LATITUDE (DEG)

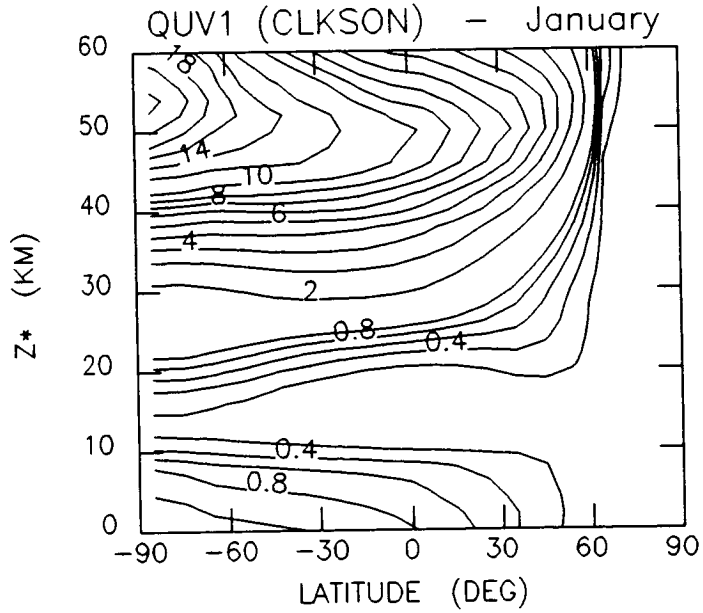
QUV1 (CLKSON) – January
Z* (KM)
LATITUDE (DEG)

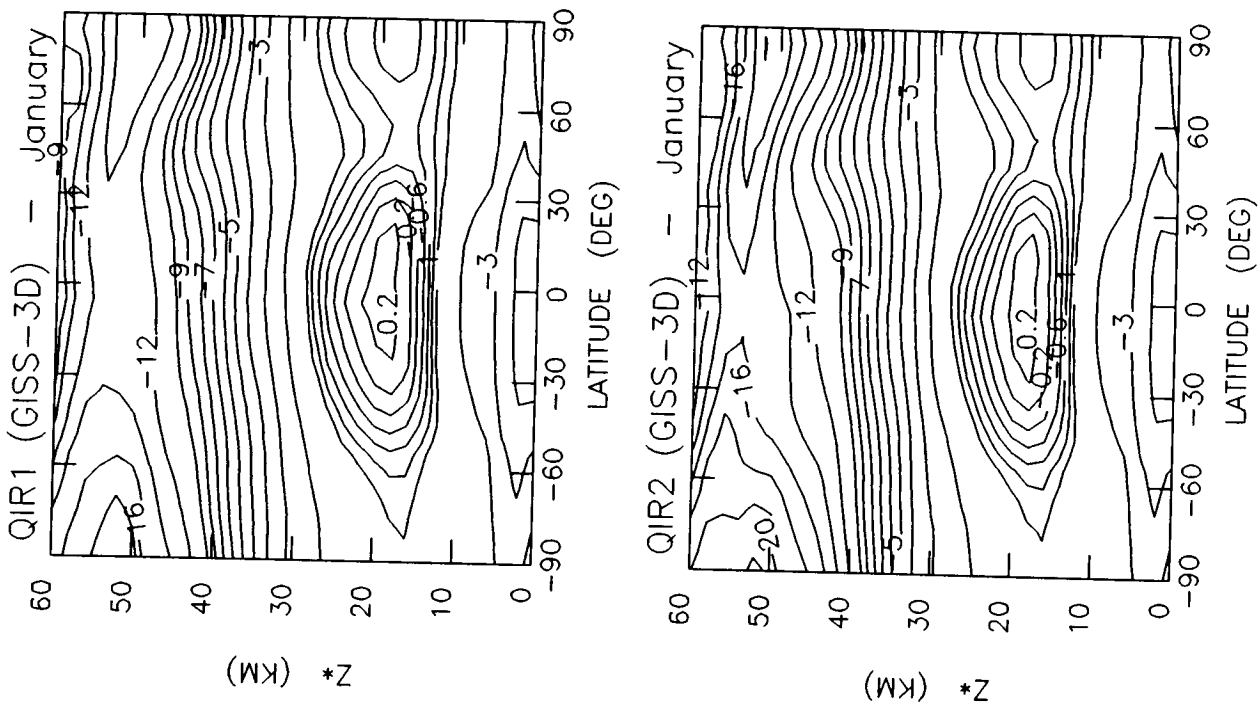
QIR1 (GISS-3D) - January
QIR2 (GISS-3D) - January
Z* (KM)
LATITUDE (DEG)
60
50
40
30
20
10
0
90
60
30
0
-30
-60
-90
-16
-12
-9
-7
-5
-3
0.2
-0.2
-0.6
20

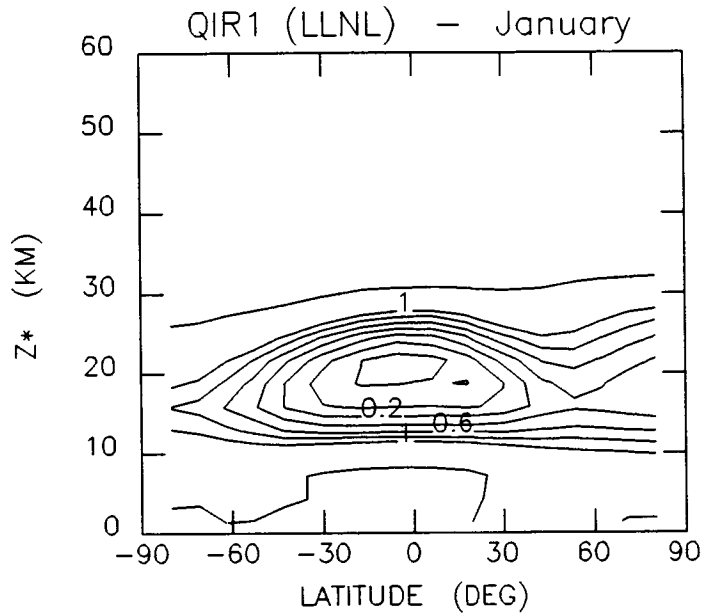
QIR1 (LLNL) – January
Z* (KM)
LATITUDE (DEG)
60
50
40
30
20
10
0
-90 -60 -30 0 30 60 90
1
0.2
0.6
1

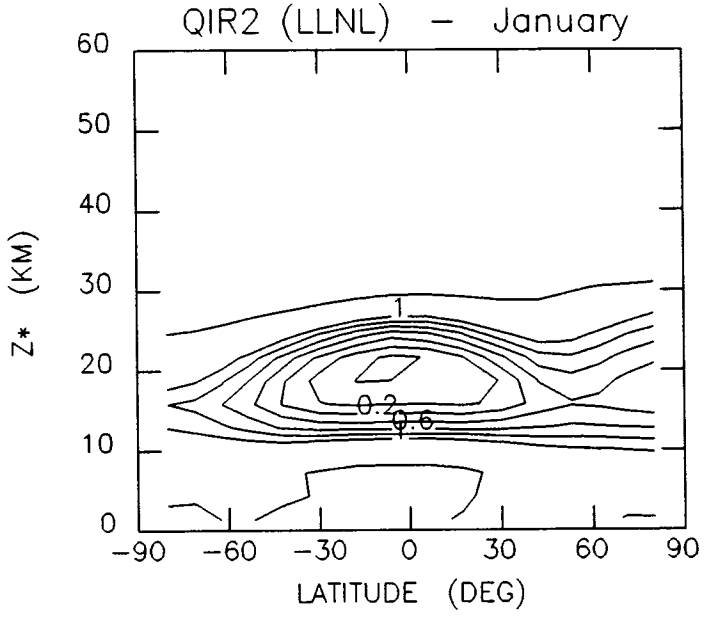
QIR2 (LLNL) – January
Z* (KM)
LATITUDE (DEG)
60
50
40
30
20
10
0
-90 -60 -30 0 30 60 90
1
0.2
0.6
1

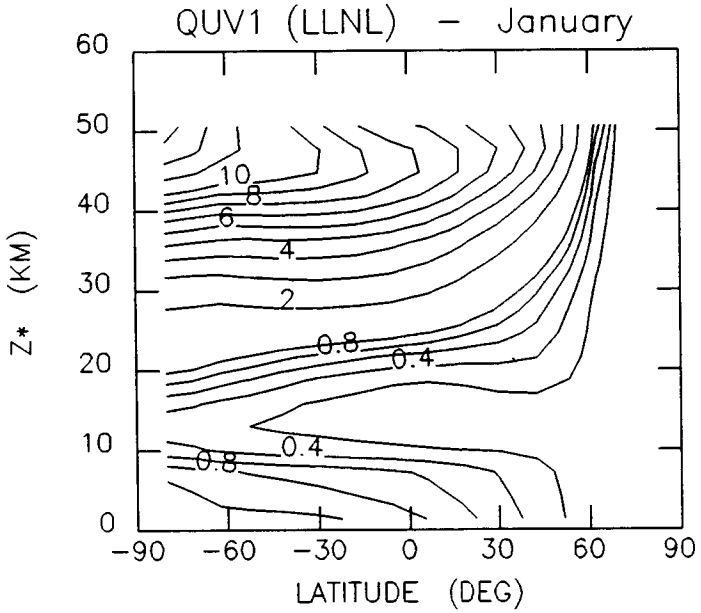
QUV1 (LLNL) – January
Z* (KM)
LATITUDE (DEG)
60
50
40
30
20
10
0
-90 -60 -30 0 30 60 90
10
8
6
4
2
0.8
0.4
0.4
0.8

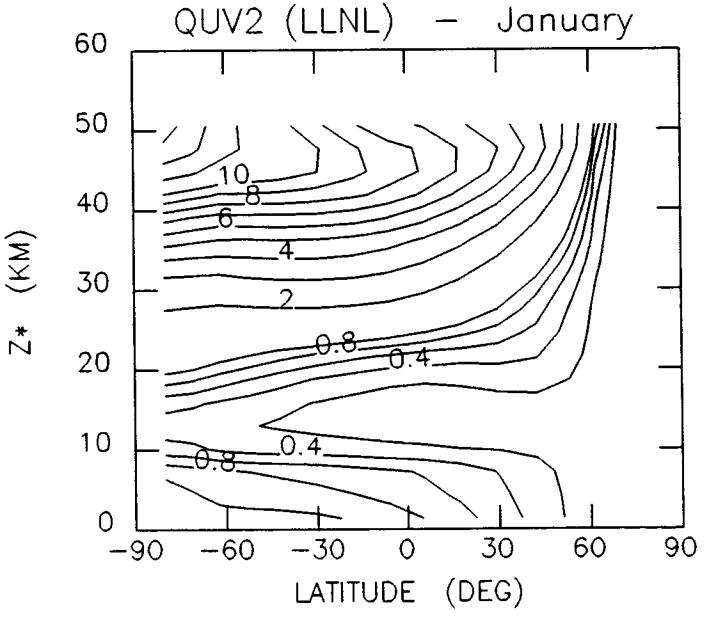
QUV2 (LLNL) – January
Z* (KM)
LATITUDE (DEG)
60
50
40
30
20
10
0
-90 -60 -30 0 30 60 90
10
8
6
4
2
0.8
0.4
0.4
0.8

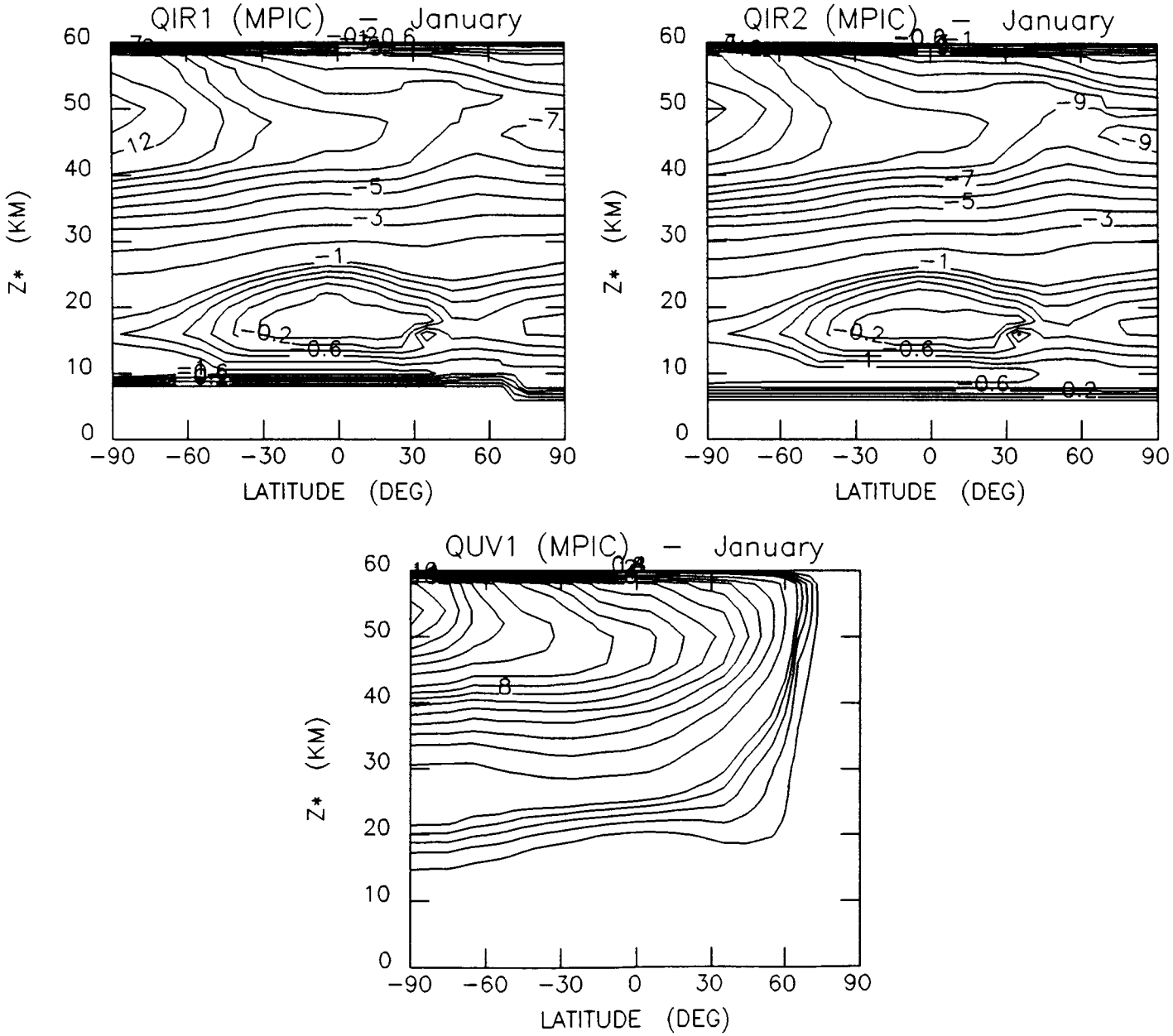
QIR1 (MPIC) – January
QIR2 (MPIC) – January
QUV1 (MPIC) – January
Z* (KM)
LATITUDE (DEG)
60
50
40
30
20
10
0
−90
−60
−30
0
30
60
90
12
−7
−5
−3
−1
−0.2
−0.6
−9
8

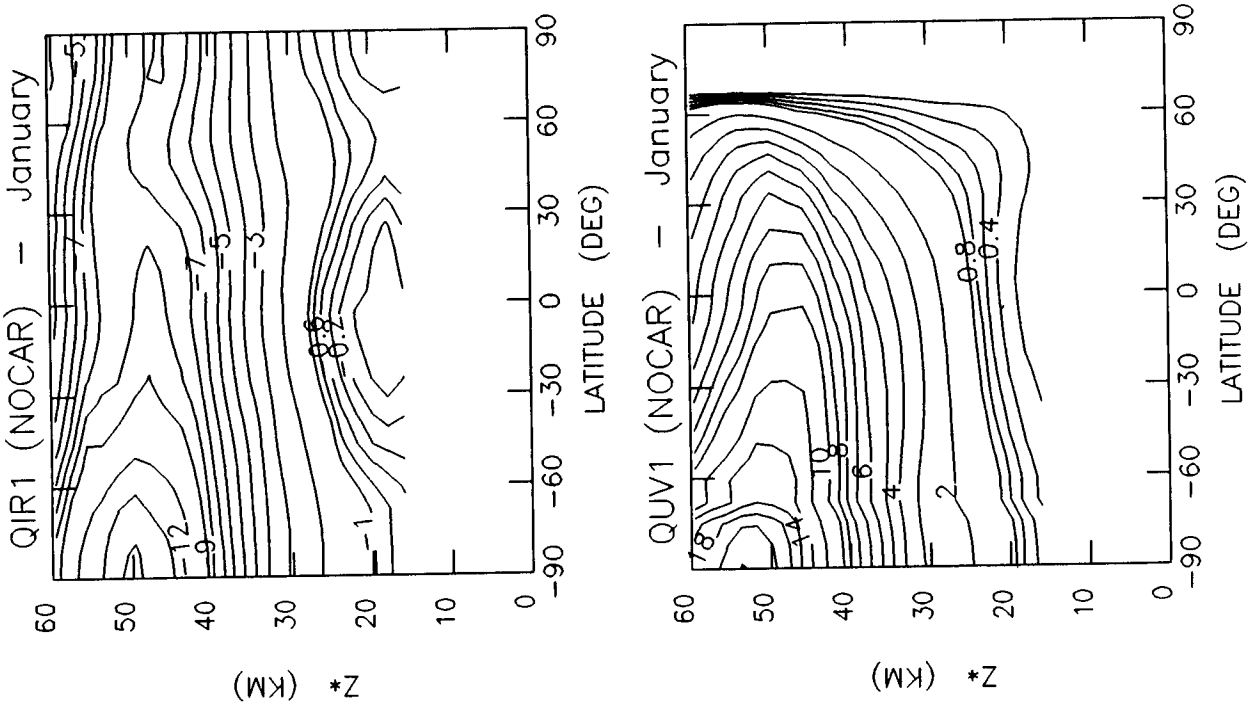
QIR1 (NOCAR) – January
QUV1 (NOCAR) – January
Z* (KM)
LATITUDE (DEG)
60
50
40
30
20
10
0
-90
-60
-30
0
30
60
90

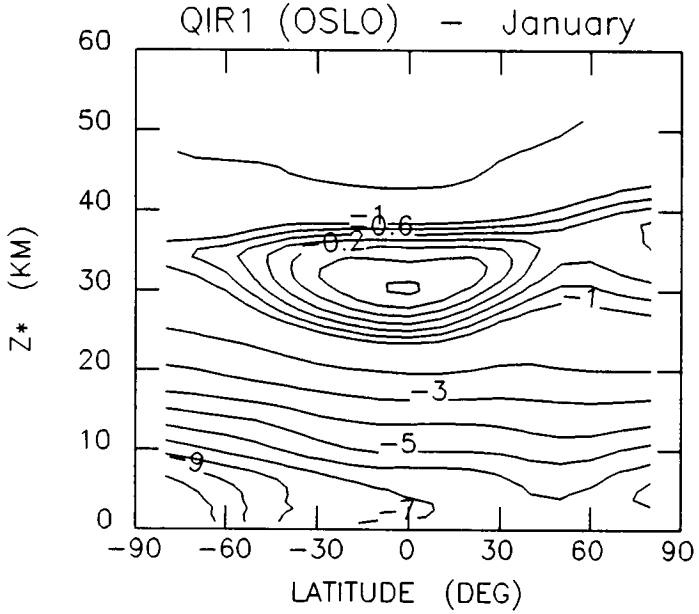
QIR1 (OSLO) – January
Z* (KM)
LATITUDE (DEG)
60
50
40
30
20
10
0
-90 -60 -30 0 30 60 90
-1
-0.6
-0.2
-1
-3
-5
-9
-7

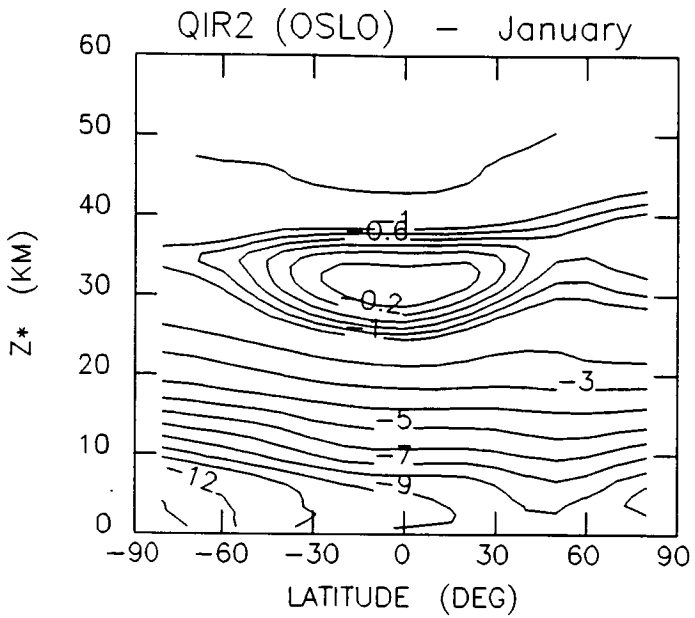
QIR2 (OSLO) – January
Z* (KM)
LATITUDE (DEG)
60
50
40
30
20
10
0
-90 -60 -30 0 30 60 90
-1
-0.6
-0.2
-1
-3
-5
-7
-9
-12

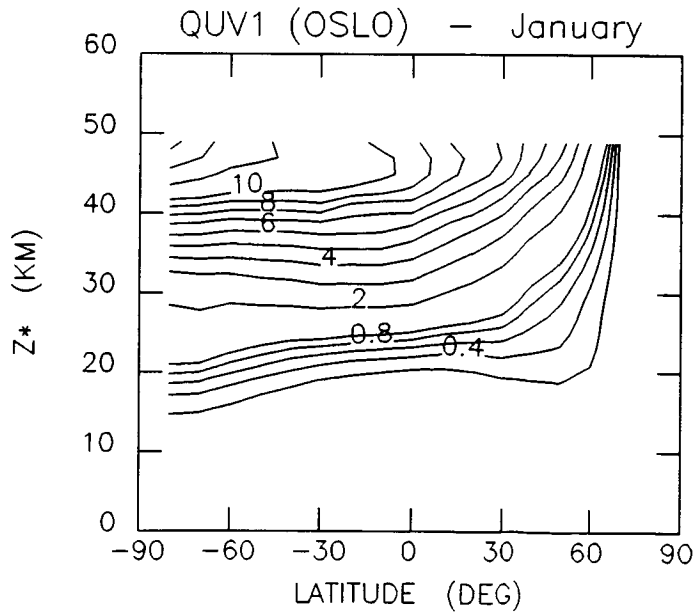
QUV1 (OSLO) – January
Z* (KM)
LATITUDE (DEG)
60
50
40
30
20
10
0
-90 -60 -30 0 30 60 90
10
8
6
4
2
0.8
0.4

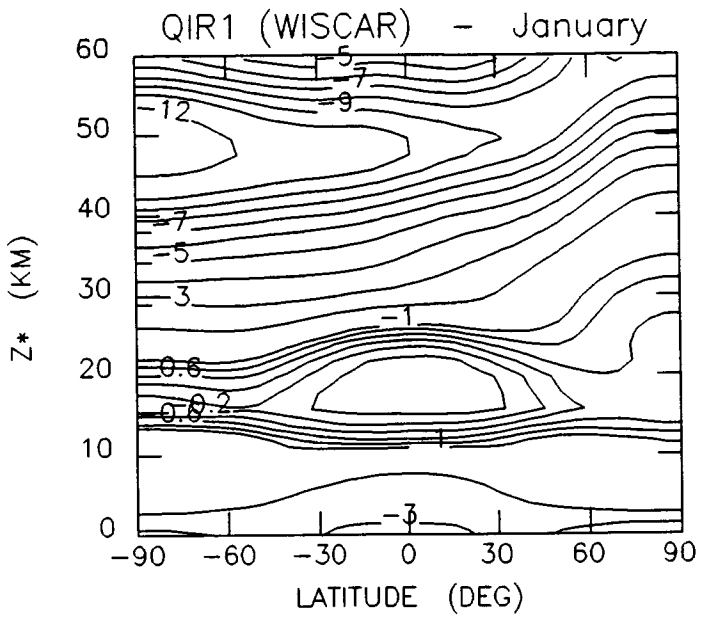
QIR1 (WISCAR) – January
Z* (KM)
LATITUDE (DEG)

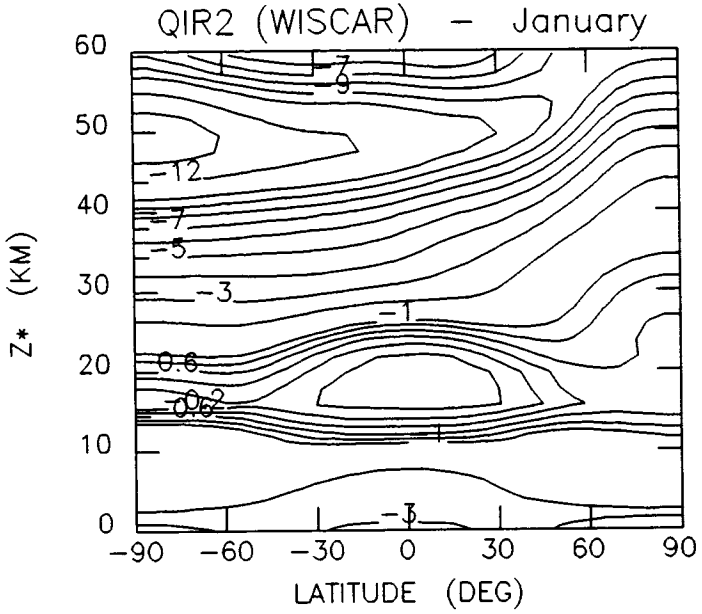
QIR2 (WISCAR) – January
Z* (KM)
LATITUDE (DEG)

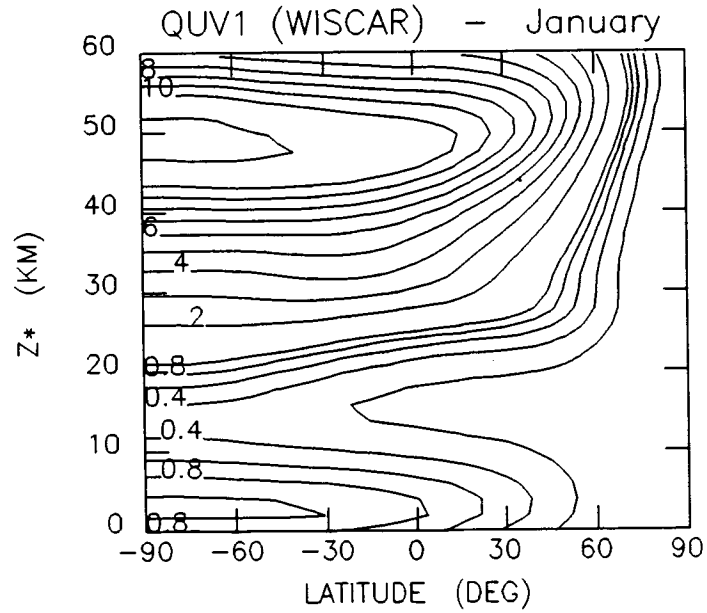
QUV1 (WISCAR) – January
Z* (KM)
LATITUDE (DEG)

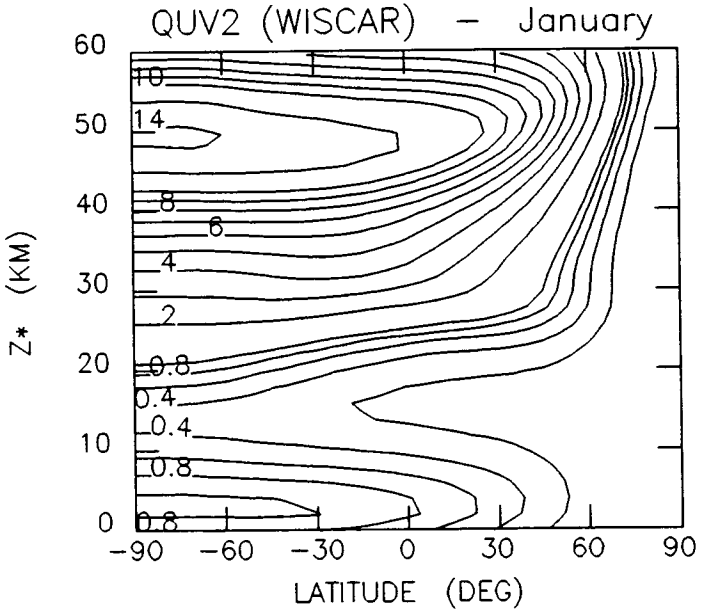
QUV2 (WISCAR) – January
Z* (KM)
LATITUDE (DEG)

**Table 6-2a.** Net Radiative Heating

March, June, September, and December; "Best" circulation
Models Represented - AER, CALJPL, CLKSON, GSFC1 (Jan. only), GSFC2, MRI, WISCAR

| Parameter | Description | Units | Contour Levels |
|---|---|---|---|
| QNET | Net Radiative Heating | K/day | -16, -14, -12, -10, -8, -6, -4, -2, -1, -0.5, 0, 0.5, 1, 2, 4 |

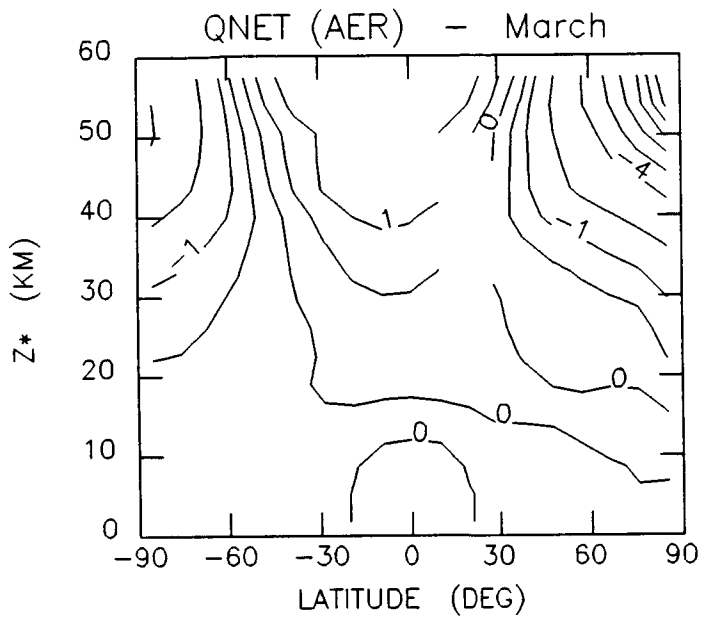
QNET (AER) – March
Z* (KM)
LATITUDE (DEG)

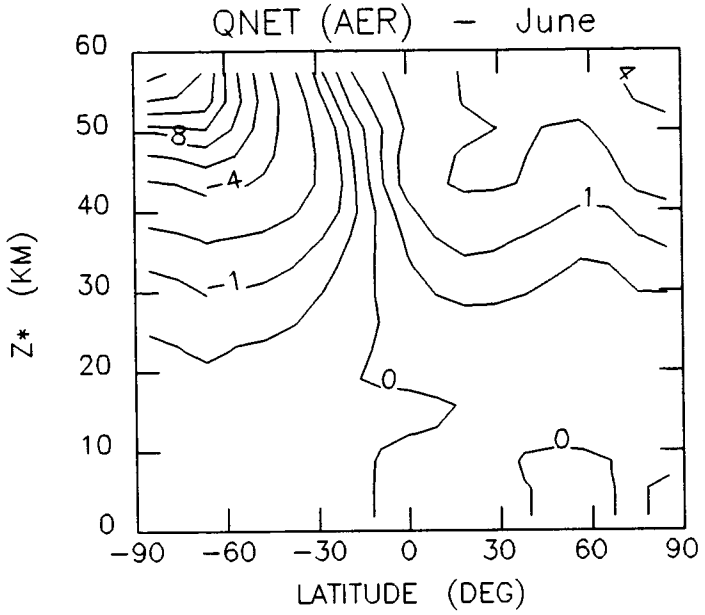
QNET (AER) – June
Z* (KM)
LATITUDE (DEG)

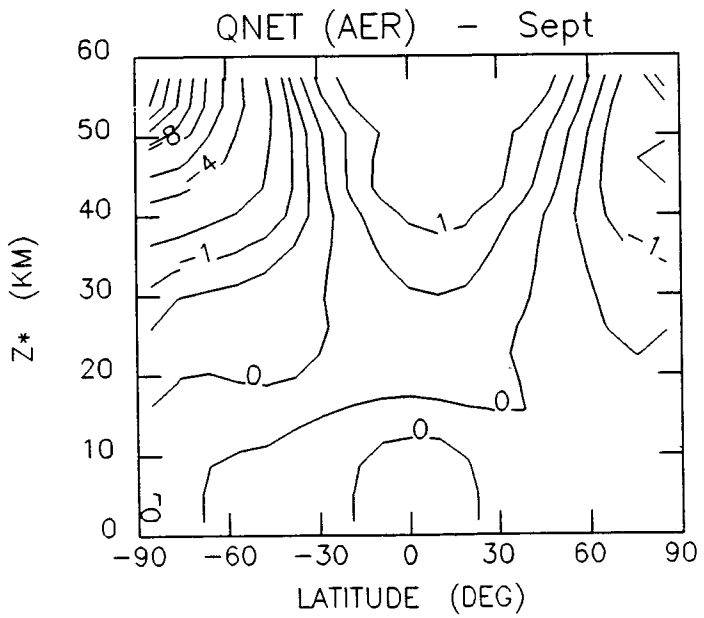
QNET (AER) – Sept
Z* (KM)
LATITUDE (DEG)

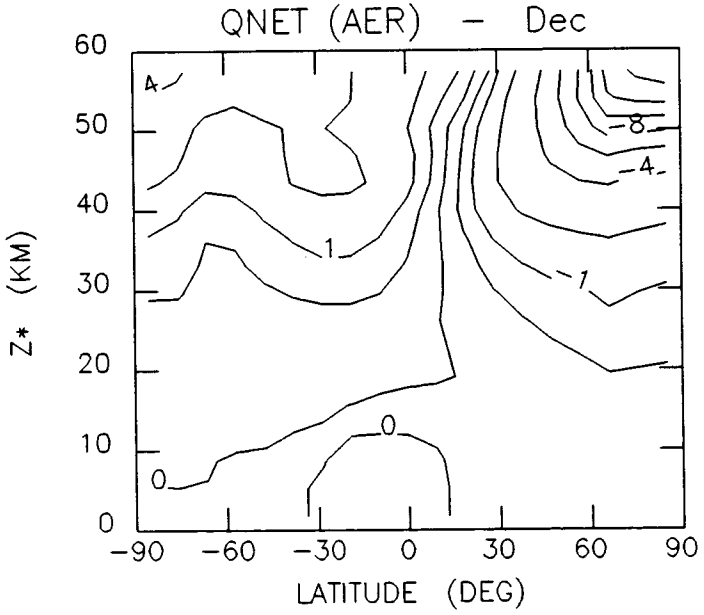
QNET (AER) – Dec
Z* (KM)
LATITUDE (DEG)

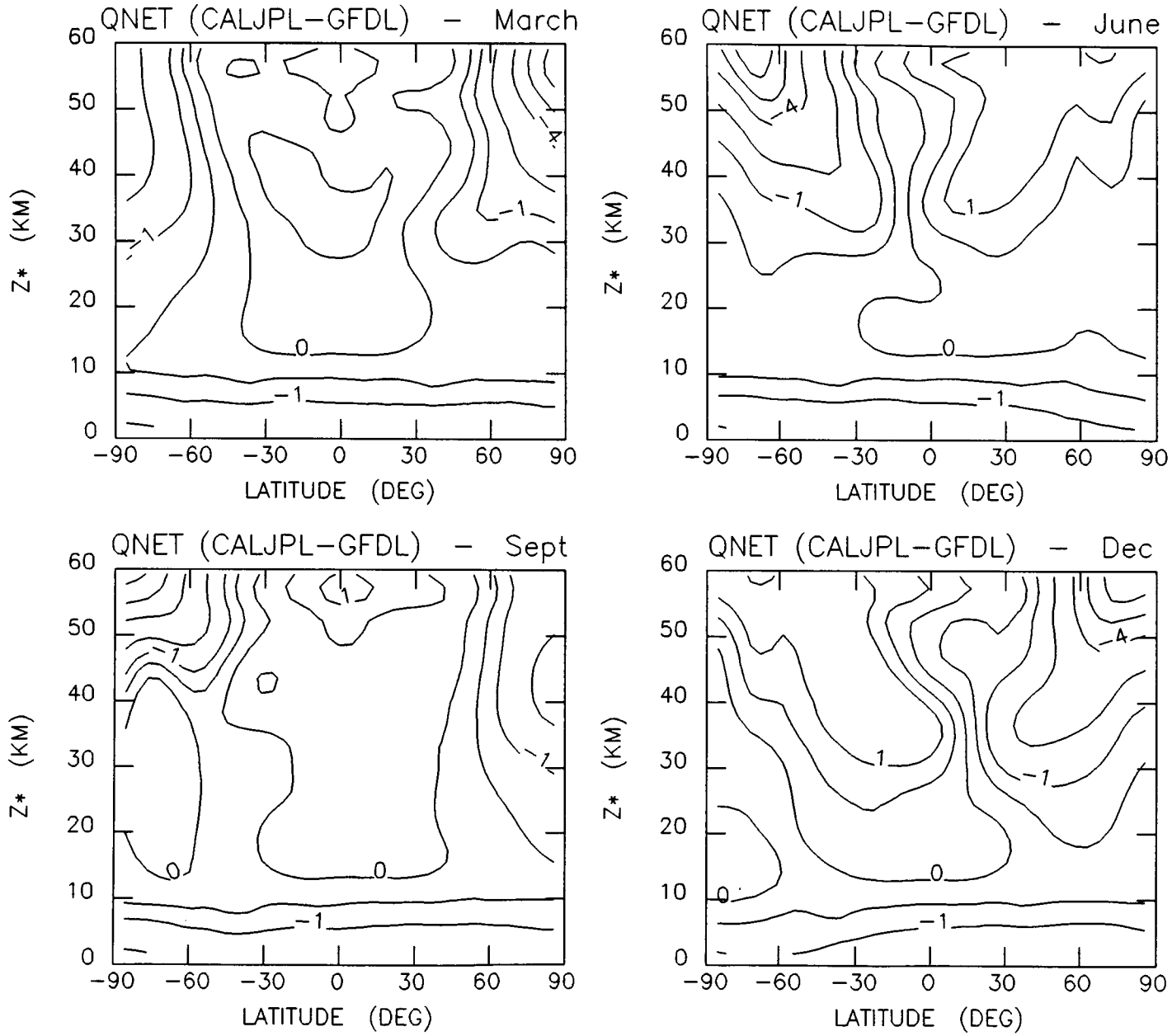
QNET (CALJPL−GFDL) − March
QNET (CALJPL−GFDL) − June
QNET (CALJPL−GFDL) − Sept
QNET (CALJPL−GFDL) − Dec
Z* (KM)
LATITUDE (DEG)
60
50
40
30
20
10
0
−90 −60 −30 0 30 60 90
4
1
0
−1

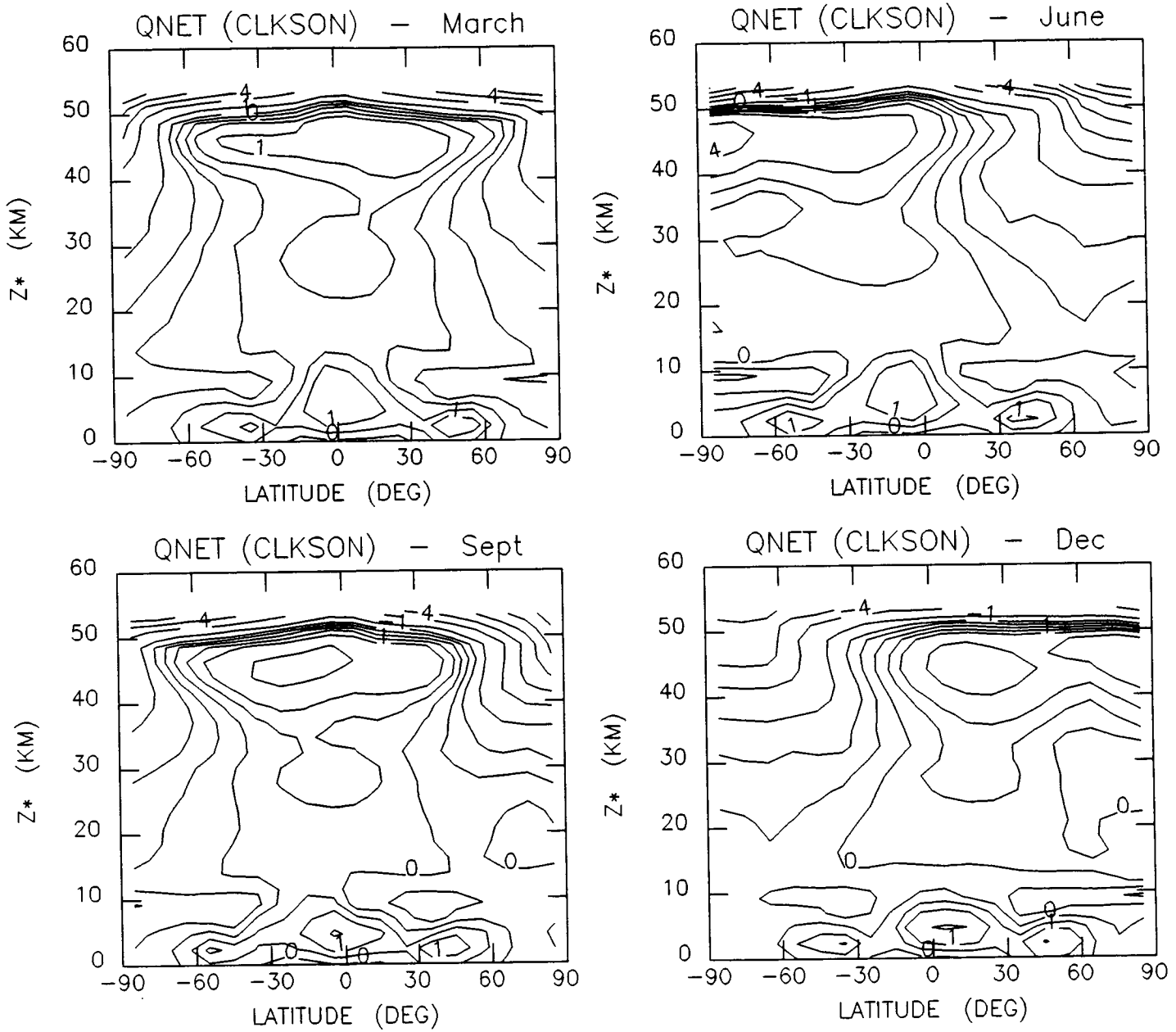
QNET (CLKSON) – March
QNET (CLKSON) – June
QNET (CLKSON) – Sept
QNET (CLKSON) – Dec
Z* (KM)
LATITUDE (DEG)
0
10
20
30
40
50
60
-90
-60
-30
0
30
60
90

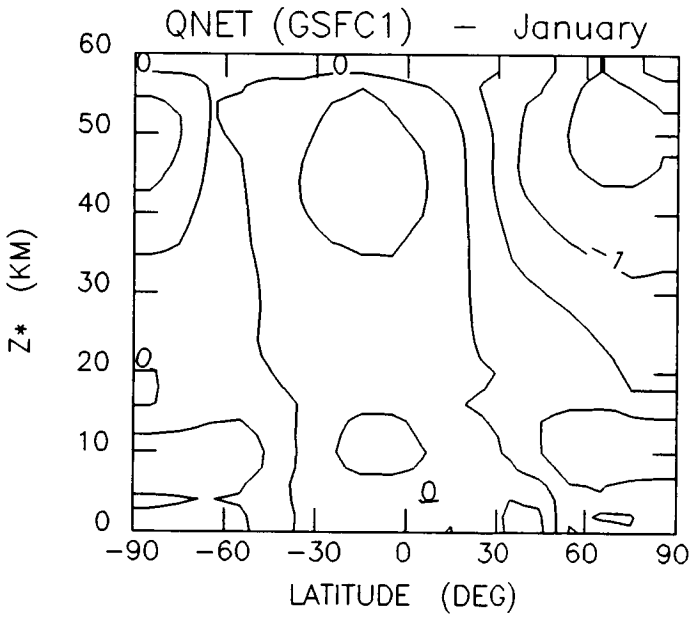
QNET (GSFC1) – January
Z* (KM)
60
50
40
30
20
10
0
0
0
0
0
1
0
-90
-60
-30
0
30
60
90
LATITUDE (DEG)

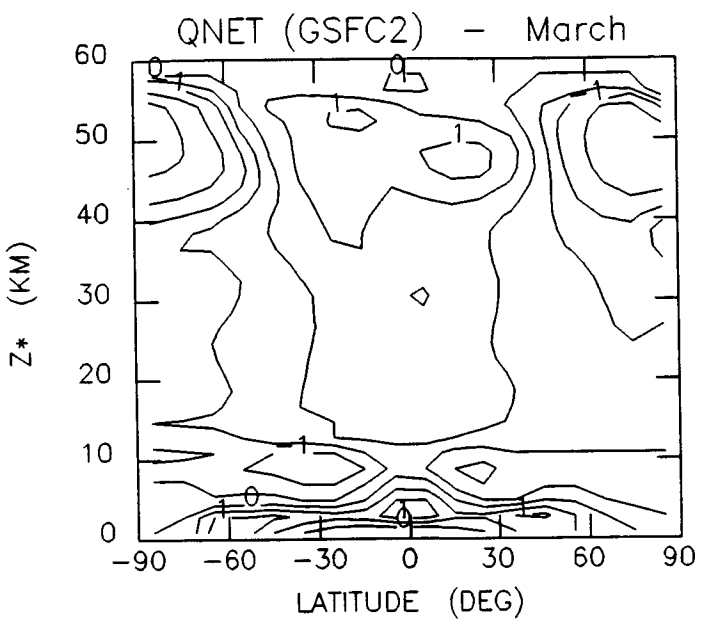
QNET (GSFC2) – March
Z* (KM)
LATITUDE (DEG)

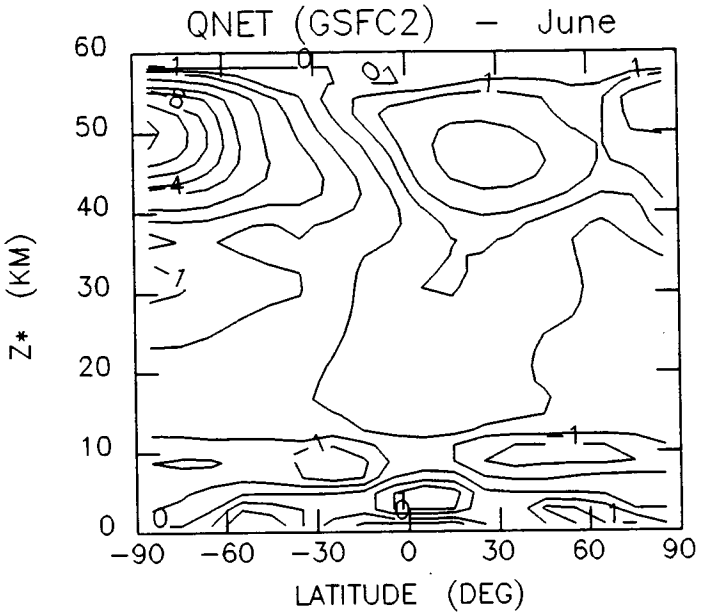
QNET (GSFC2) – June
Z* (KM)
LATITUDE (DEG)

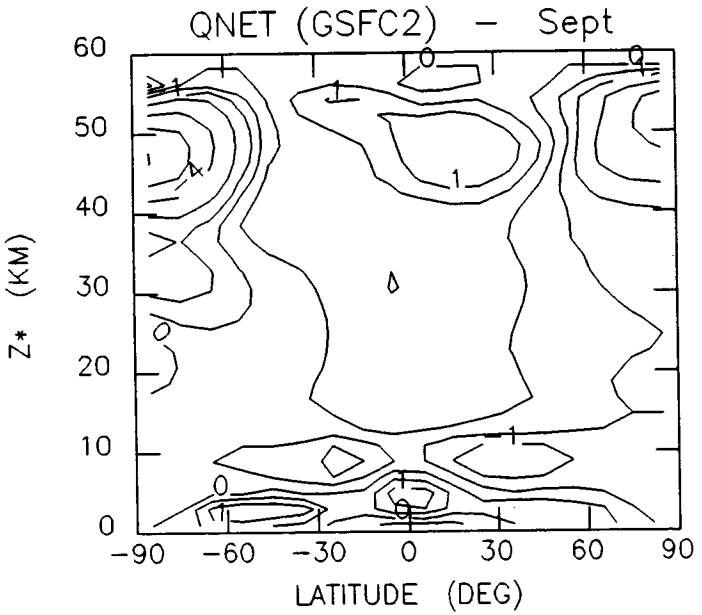
QNET (GSFC2) – Sept
Z* (KM)
LATITUDE (DEG)

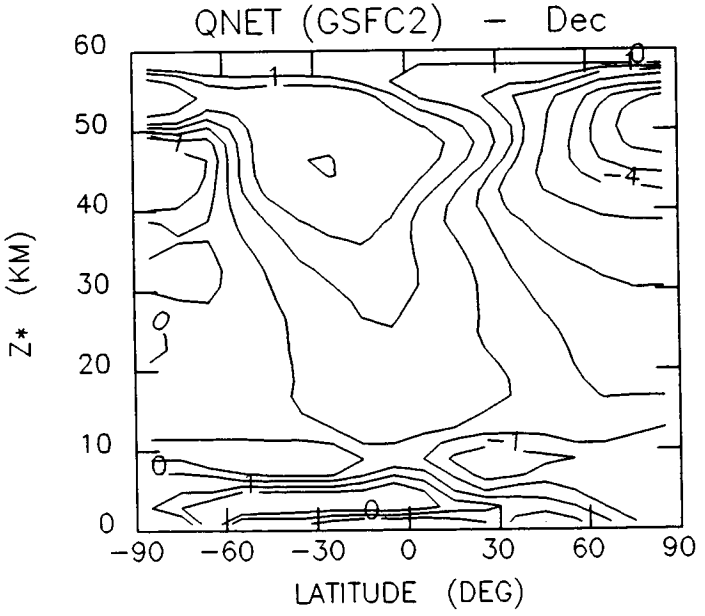
QNET (GSFC2) – Dec
Z* (KM)
LATITUDE (DEG)

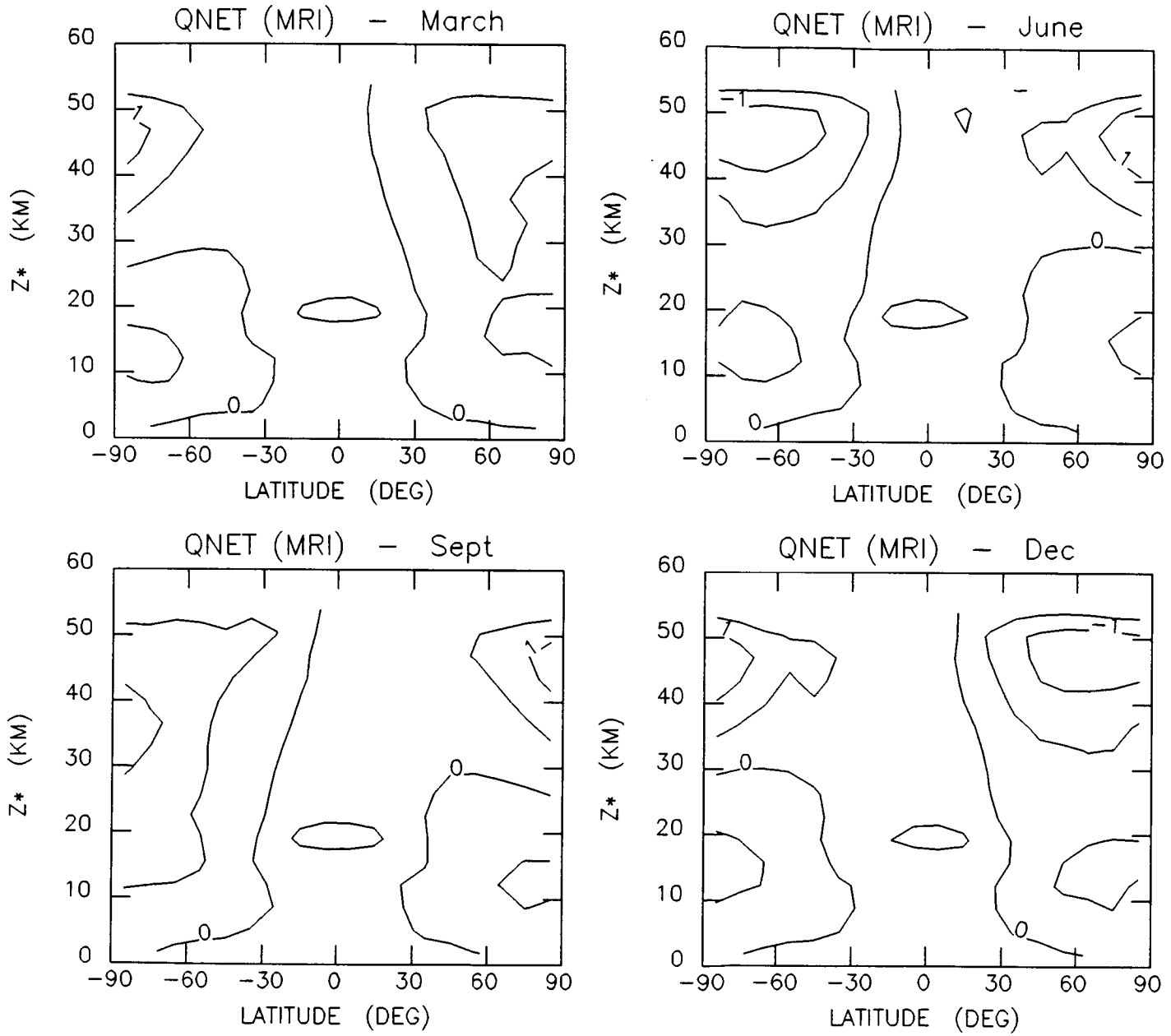
QNET (MRI) – March
QNET (MRI) – June
QNET (MRI) – Sept
QNET (MRI) – Dec
Z* (KM)
LATITUDE (DEG)
60
50
40
30
20
10
0
-90 -60 -30 0 30 60 90
0
-1
1

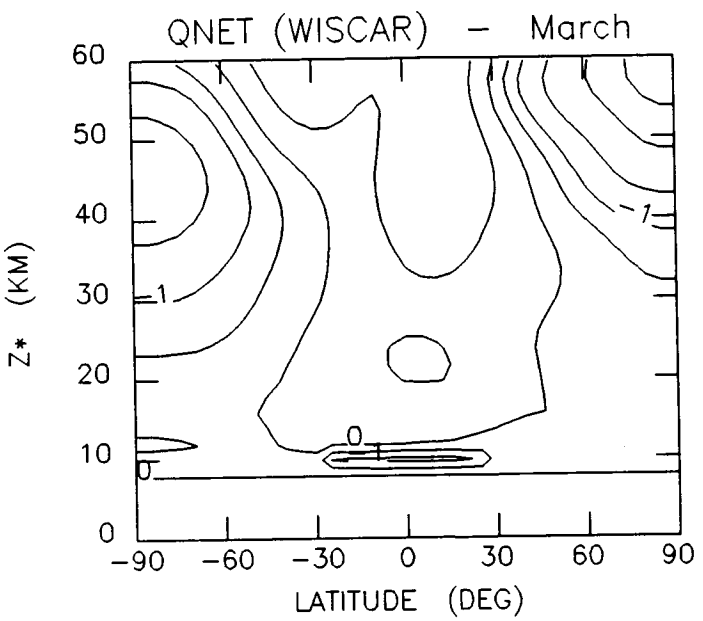
QNET (WISCAR) – March
Z* (KM)
LATITUDE (DEG)

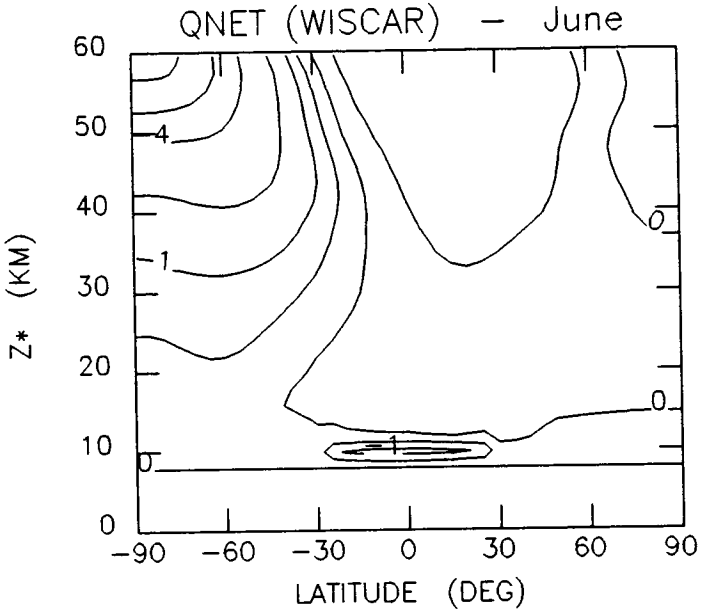
QNET (WISCAR) – June
Z* (KM)
LATITUDE (DEG)

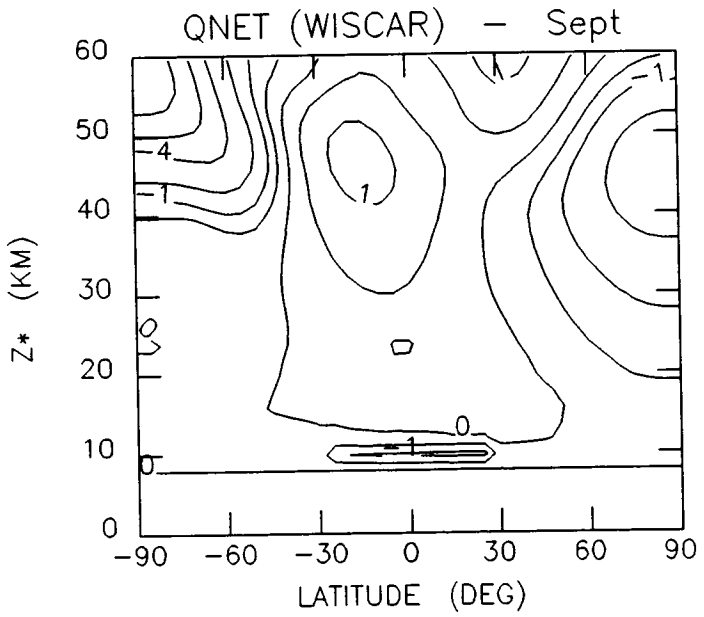
QNET (WISCAR) – Sept
Z* (KM)
LATITUDE (DEG)

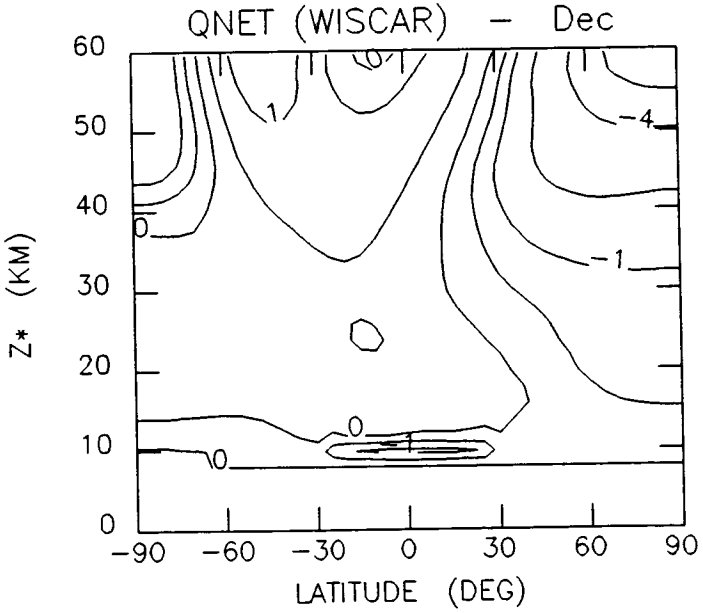
QNET (WISCAR) – Dec
Z* (KM)
LATITUDE (DEG)

**Table 6-2b.** Tropospheric Source Tracer Experiment

Steady-state for March, June, September, and December
Models Represented - AER, CALJPL, CLKSON, GISS-3D, GSFC2, LLNL, MRI, WISCAR

| Parameter | Description | Units | Contour Levels |
|---|---|---|---|
| X | Tropospheric Source Gas X | ppbv | 1.0E-04, 1.0E-03, 0.01, 0.0, 2, 0.05, 0.1, 0.2, 0.3, 0.4, 0.5, 0.6, 0.7, 0.8, 0.9, 1 |

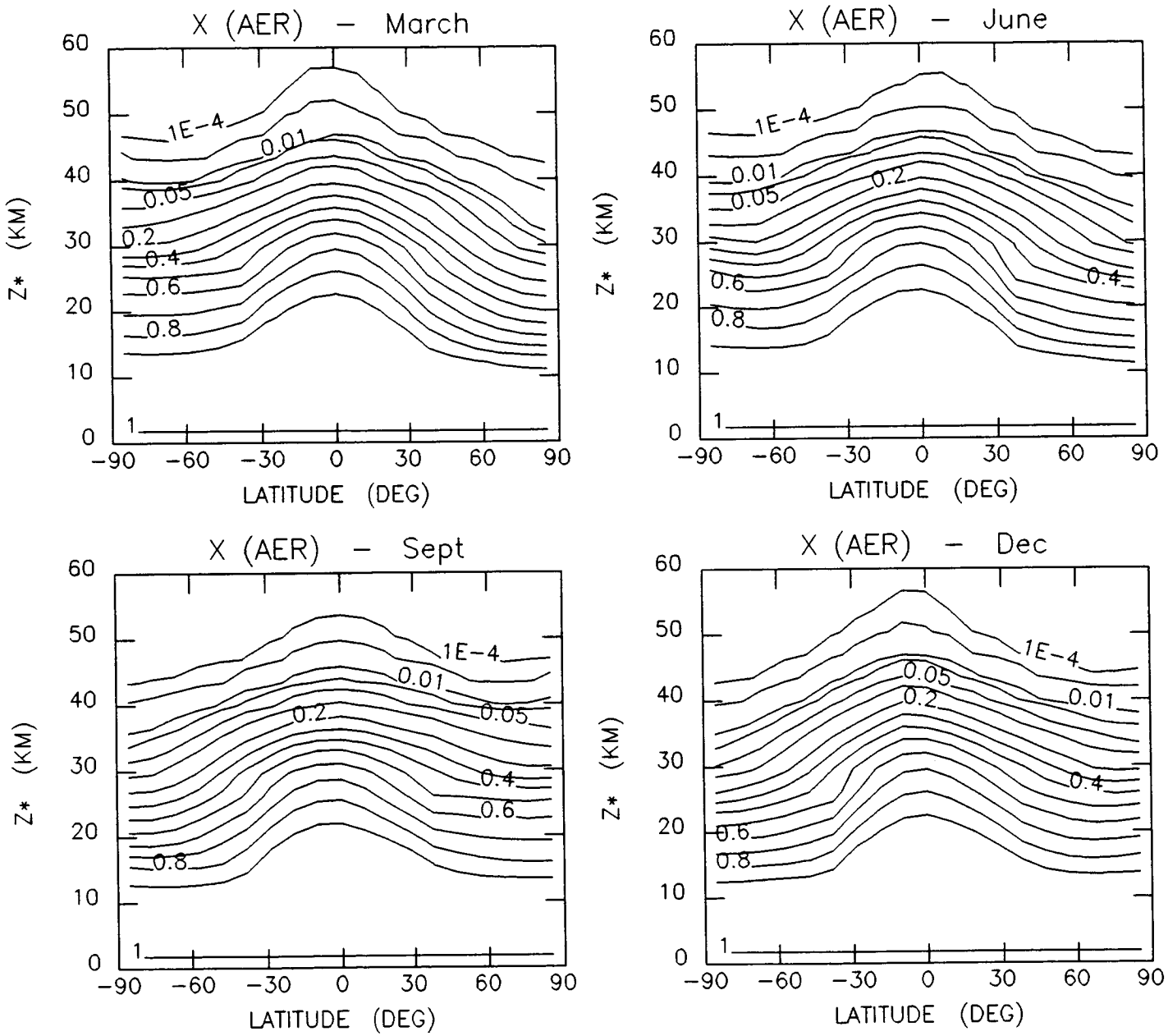
X (AER) – March
X (AER) – June
X (AER) – Sept
X (AER) – Dec
Z* (KM)
LATITUDE (DEG)
1E-4
0.01
0.05
0.2
0.4
0.6
0.8
1
0
10
20
30
40
50
60
-90
-60
-30
0
30
60
90

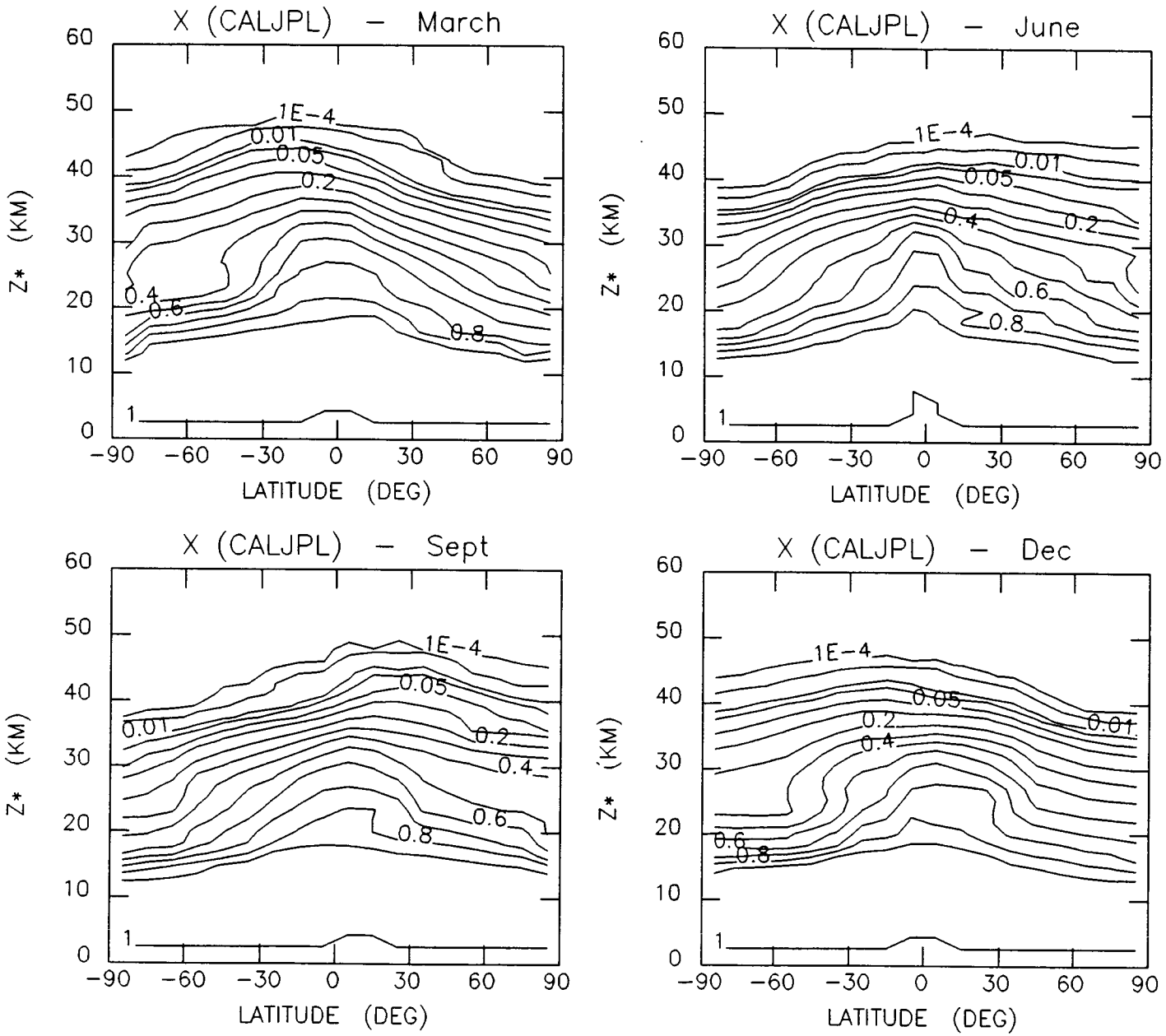
X (CALJPL) – March
X (CALJPL) – June
X (CALJPL) – Sept
X (CALJPL) – Dec
Z* (KM)
LATITUDE (DEG)
1E-4
0.01
0.05
0.2
0.4
0.6
0.8
1
0
10
20
30
40
50
60
-90
-60
-30
0
30
60
90

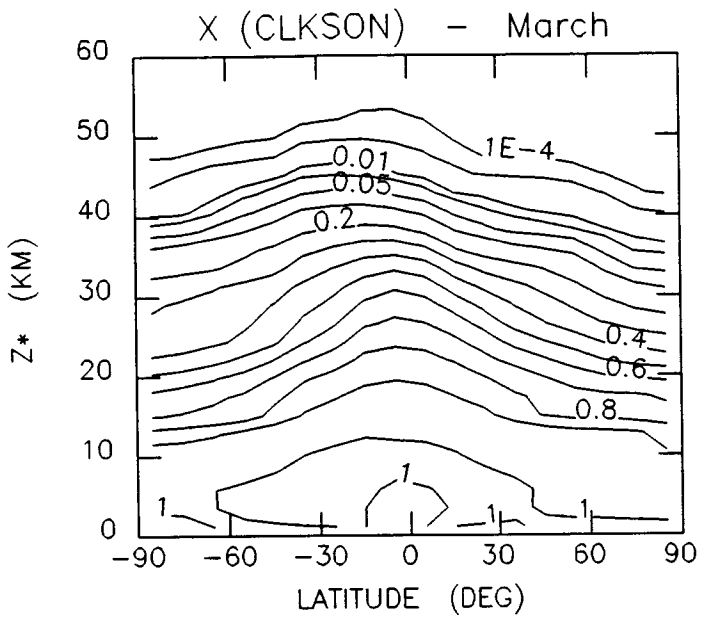
X (CLKSON) – March
Z* (KM)
LATITUDE (DEG)
1E-4
0.01
0.05
0.2
0.4
0.6
0.8
1

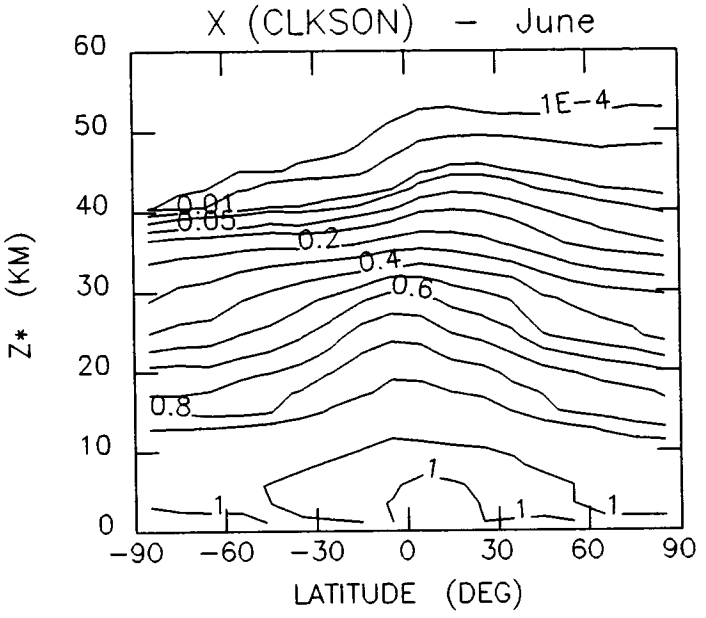
X (CLKSON) – June
Z* (KM)
LATITUDE (DEG)
1E-4
0.01
0.05
0.2
0.4
0.6
0.8
1

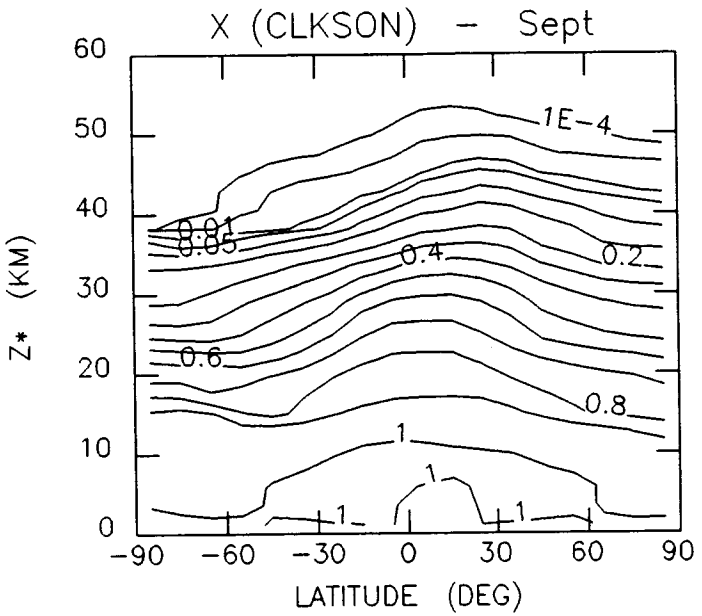
X (CLKSON) – Sept
Z* (KM)
LATITUDE (DEG)
1E-4
0.01
0.05
0.4
0.2
0.6
0.8
1

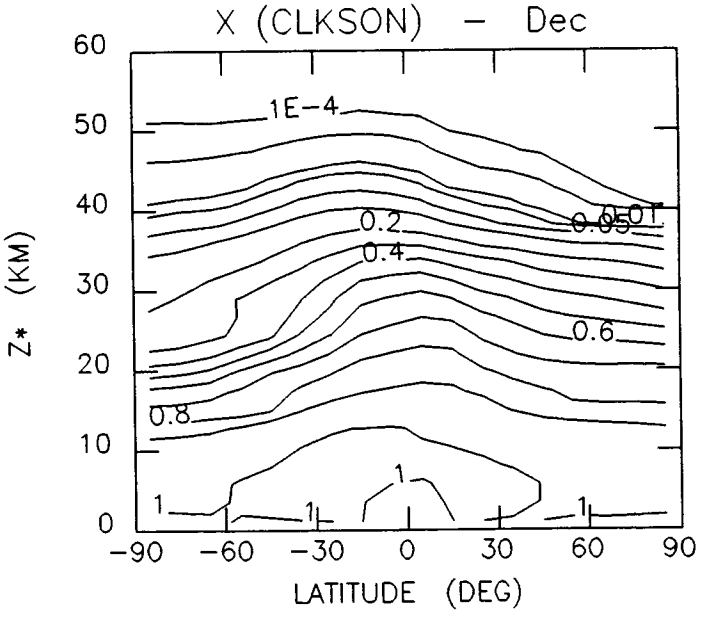
X (CLKSON) – Dec
Z* (KM)
LATITUDE (DEG)
1E-4
0.2
0.01
0.05
0.4
0.6
0.8
1

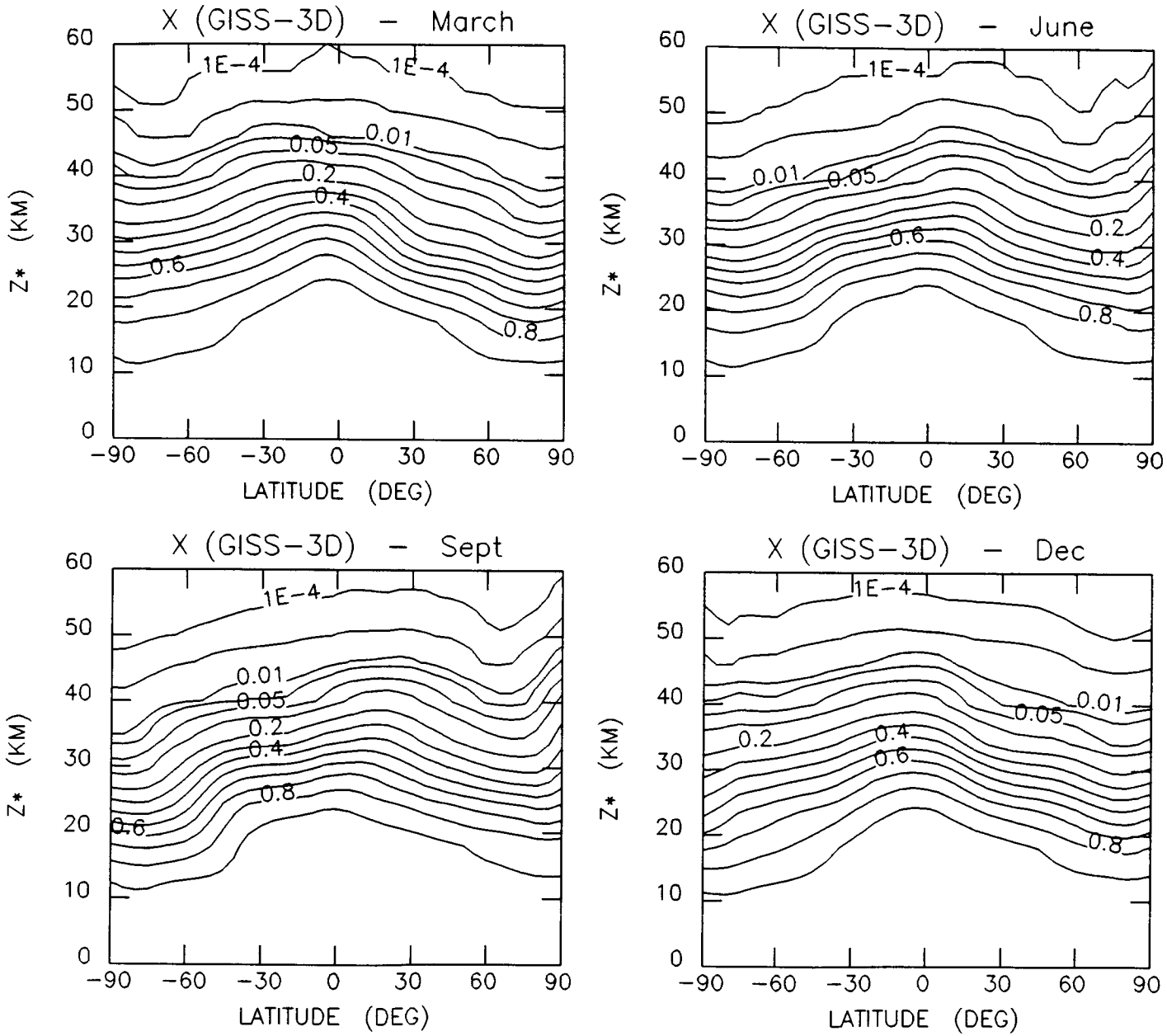
X (GISS-3D) - March
X (GISS-3D) - June
X (GISS-3D) - Sept
X (GISS-3D) - Dec
Z* (KM)
LATITUDE (DEG)
1E-4
0.01
0.05
0.2
0.4
0.6
0.8
0
10
20
30
40
50
60
-90
-60
-30
0
30
60
90

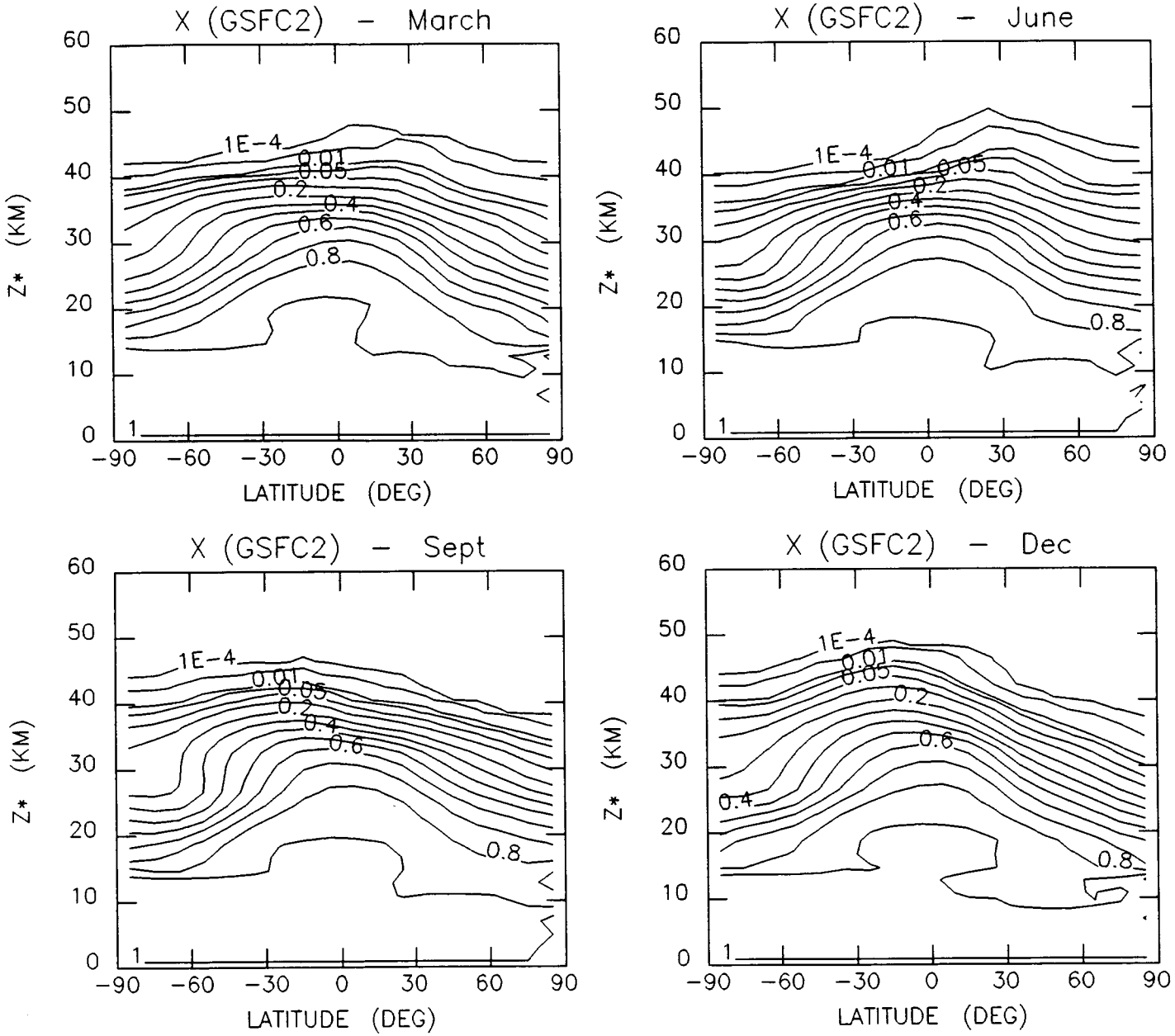
X (GSFC2) – March
X (GSFC2) – June
X (GSFC2) – Sept
X (GSFC2) – Dec
Z* (KM)
LATITUDE (DEG)
1E-4
0.01
0.05
0.2
0.4
0.6
0.8
1
0
10
20
30
40
50
60
-90
-60
-30
0
30
60
90

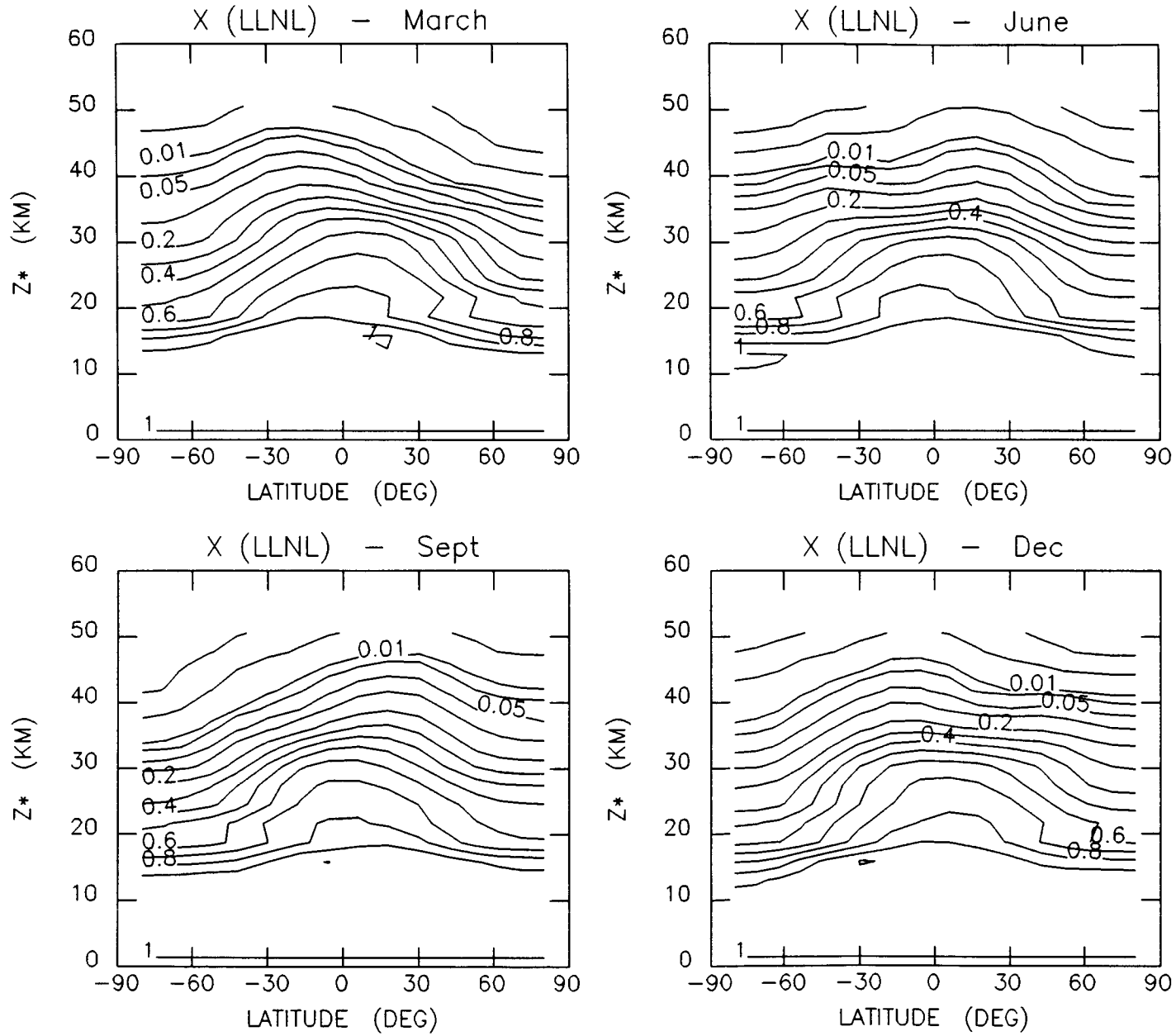
X (LLNL) – March
X (LLNL) – June
X (LLNL) – Sept
X (LLNL) – Dec
Z* (KM)
LATITUDE (DEG)
0
10
20
30
40
50
60
-90
-60
-30
0
30
60
90
0.01
0.05
0.2
0.4
0.6
0.8
1

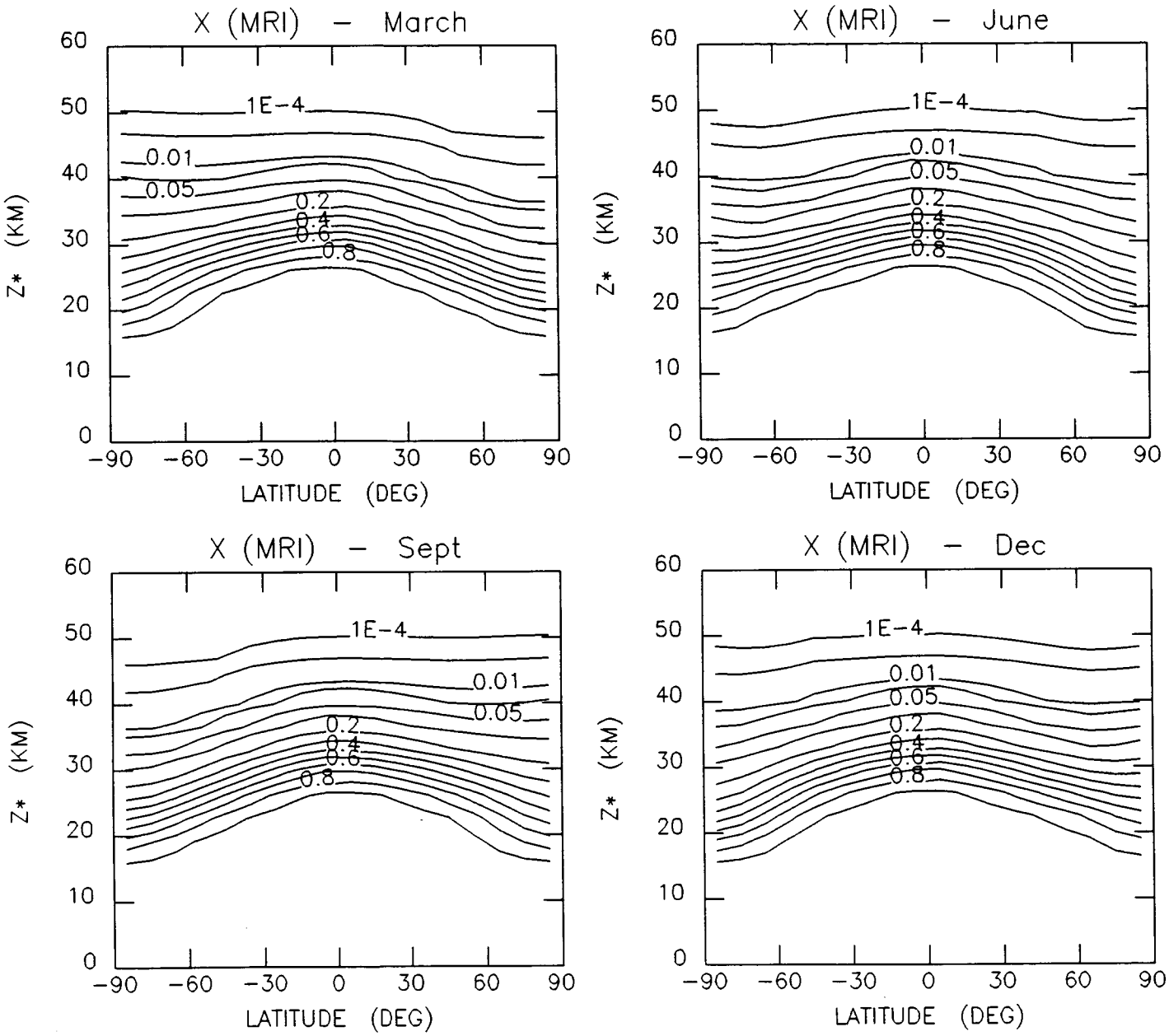
X (MRI) – March
X (MRI) – June
X (MRI) – Sept
X (MRI) – Dec
Z* (KM)
LATITUDE (DEG)
1E-4
0.01
0.05
0.2
0.4
0.6
0.8
0
10
20
30
40
50
60
-90
-60
-30
0
30
60
90

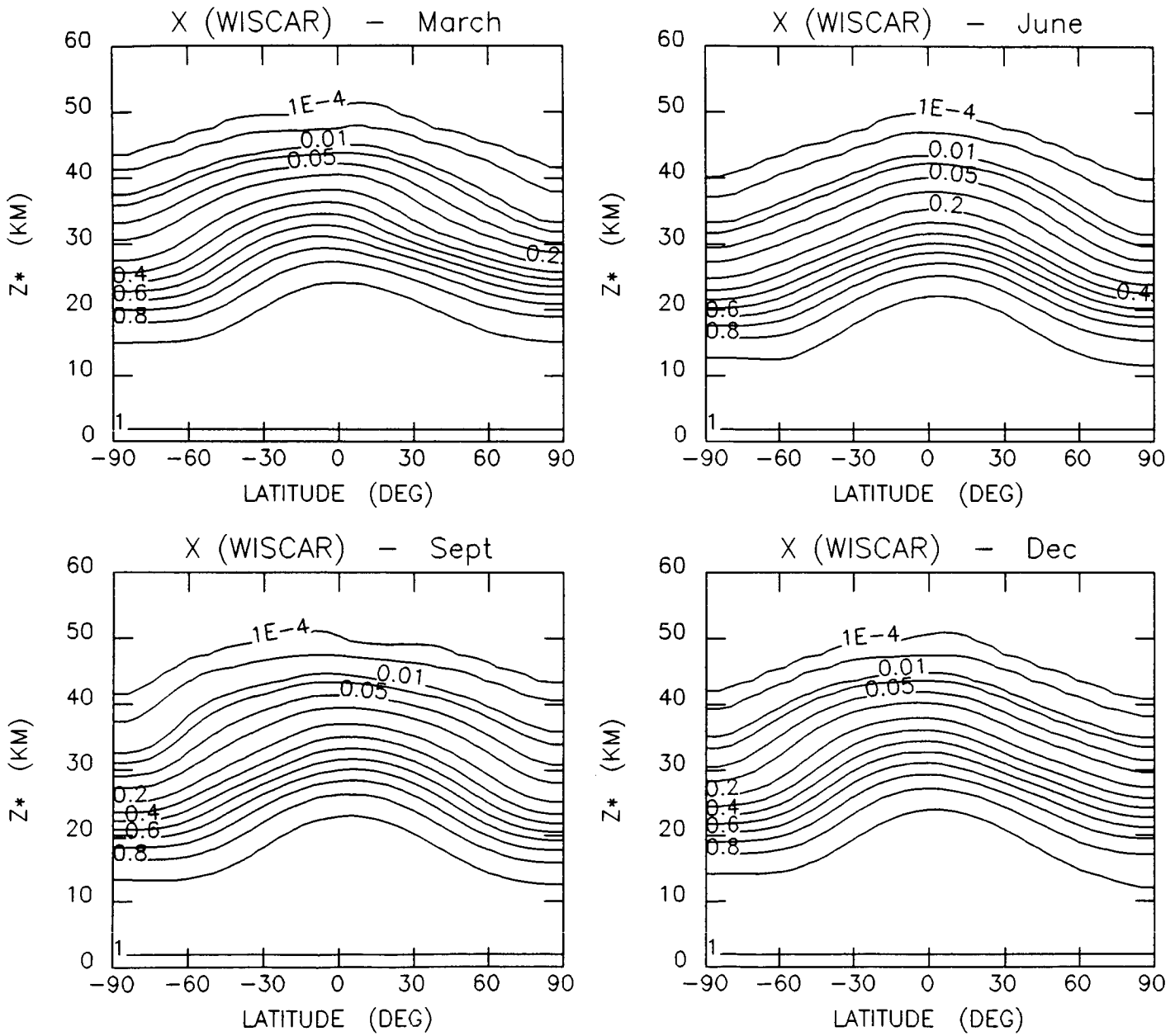
X (WISCAR) – March
X (WISCAR) – June
X (WISCAR) – Sept
X (WISCAR) – Dec
Z* (KM)
LATITUDE (DEG)
60
50
40
30
20
10
0
−90 −60 −30 0 30 60 90
1E−4
0.01
0.05
0.2
0.4
0.6
0.8
1

**Table 6-2c.** Time-Dependent Conserved Tracer Experiment

Initialized at January 1 of Year 0; 0.5 Year Increments
Models Represented - AER, CALJPL, CAMBRAL, CLKSON, GISS-3D, GSFC2, LLNL, MRI, WISCAR

| Parameter | Description | Units | Contour Levels |
|---|---|---|---|
| Y | Conserved Gas Y | ppmv | 1.0E-04, 1.0E-03, 0.01, 0.02, 0.05, 0.1, 0.2, 0.3, 0.4, 0.5, 0.6, 0.7, 0.8, 0.9, 1 |

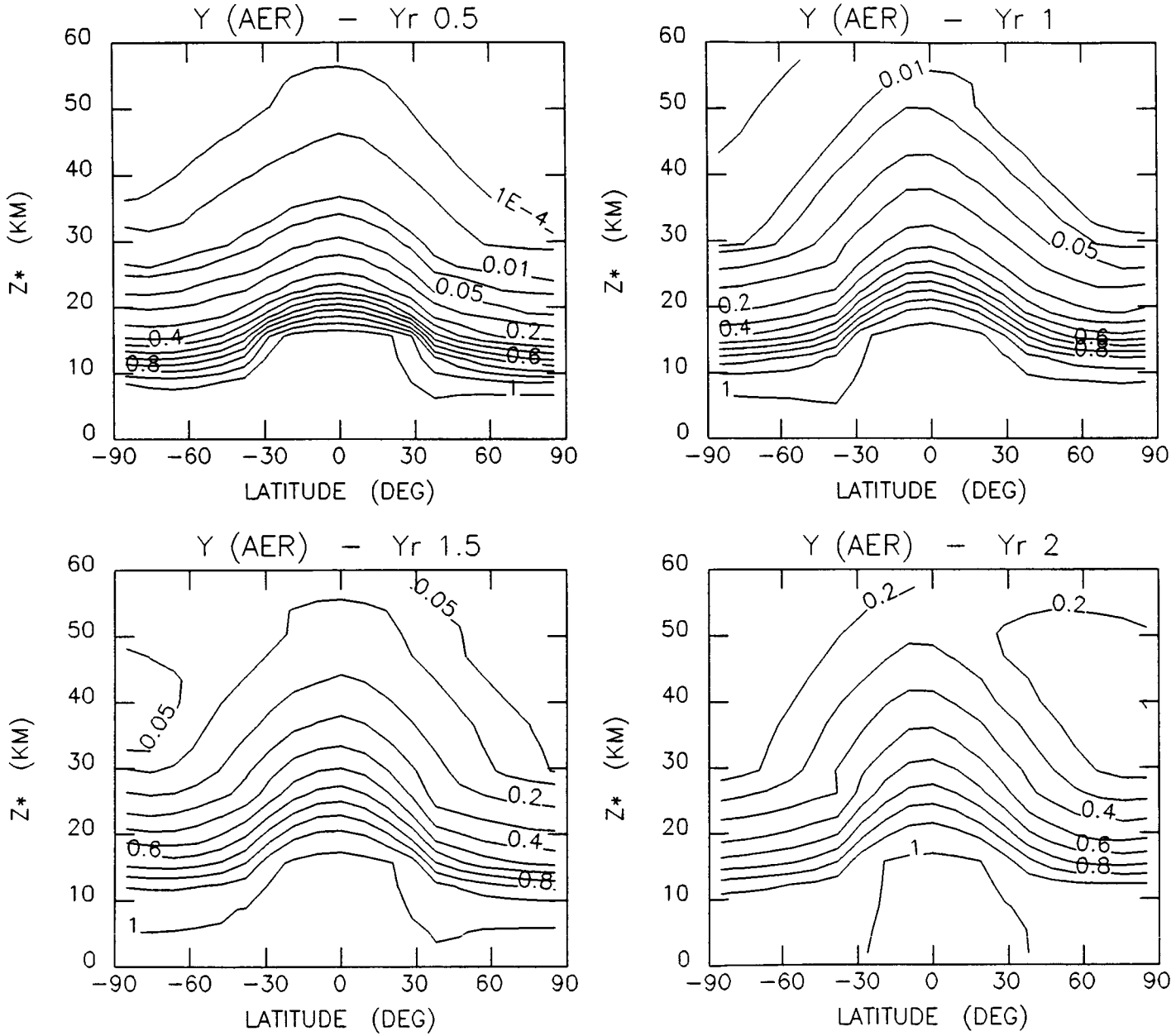
Y (AER) – Yr 0.5
Y (AER) – Yr 1
Y (AER) – Yr 1.5
Y (AER) – Yr 2
Z* (KM)
LATITUDE (DEG)
1E-4
0.01
0.05
0.2
0.4
0.6
0.8
1

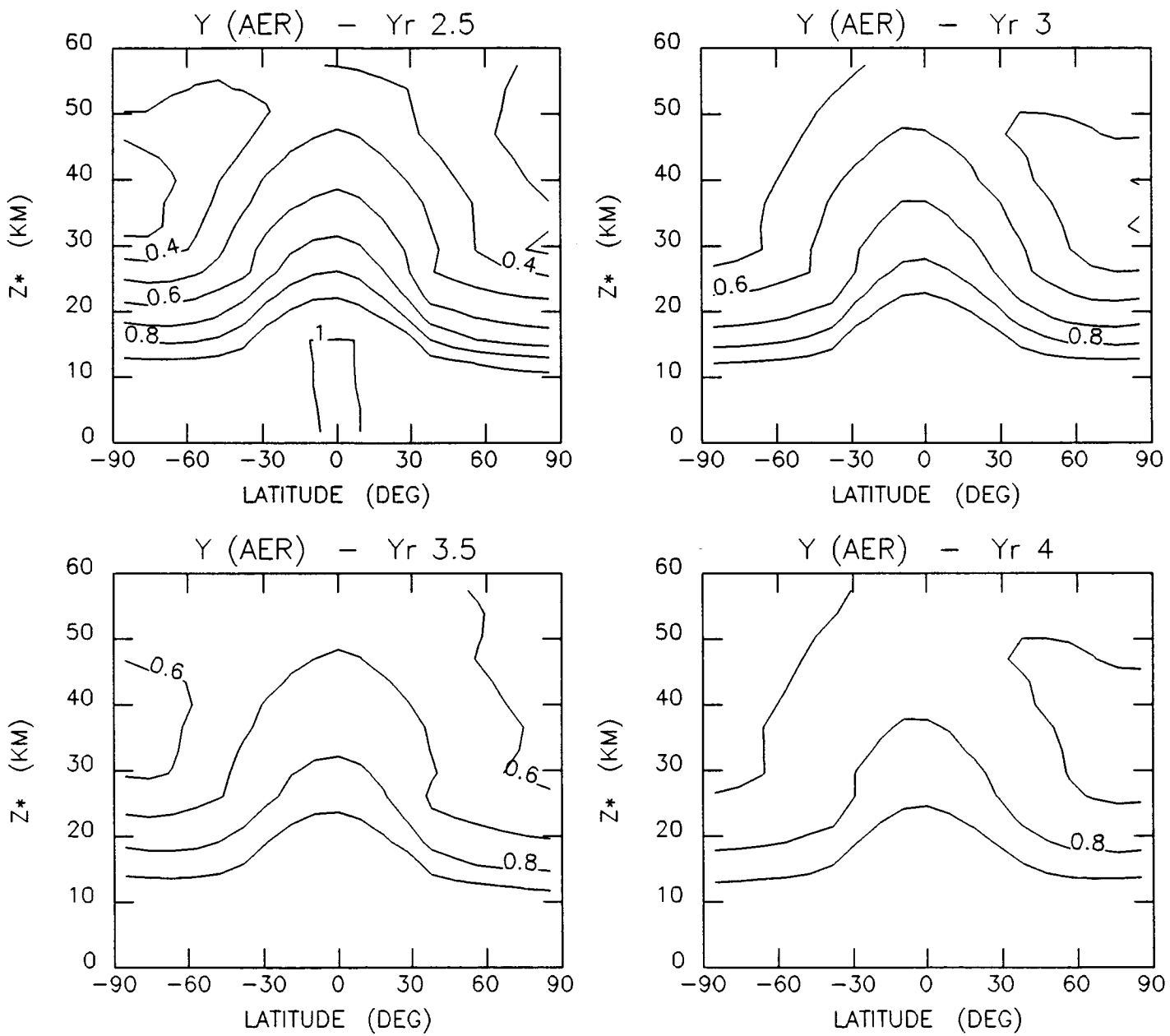
Y (AER) – Yr 2.5
Y (AER) – Yr 3
Y (AER) – Yr 3.5
Y (AER) – Yr 4
Z* (KM)
LATITUDE (DEG)
0
10
20
30
40
50
60
−90
−60
−30
0
30
60
90
0.4
0.6
0.8
1

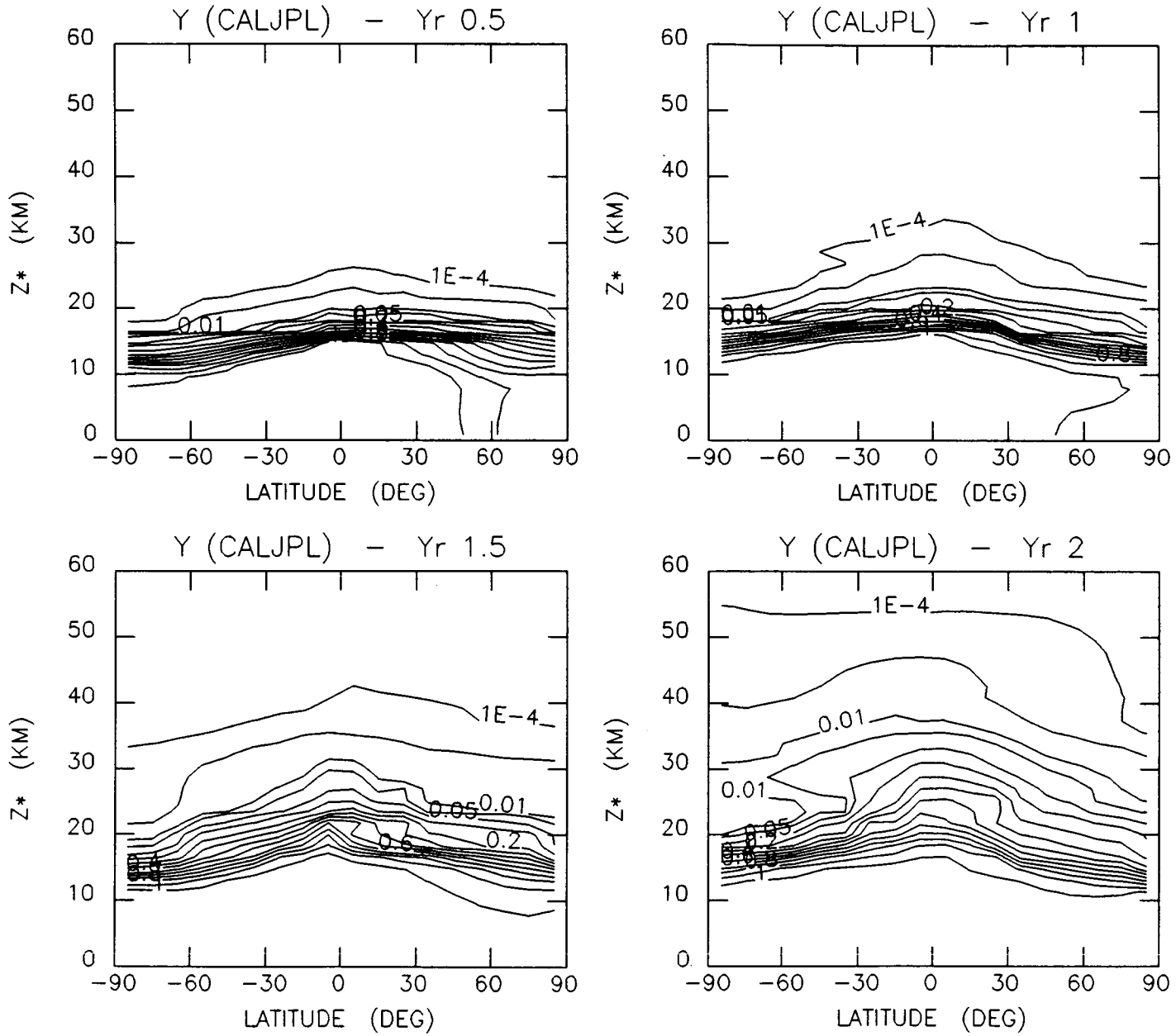
Y (CALJPL) – Yr 0.5
Y (CALJPL) – Yr 1
Y (CALJPL) – Yr 1.5
Y (CALJPL) – Yr 2
Z* (KM)
LATITUDE (DEG)
1E-4
0.01
0.05
0.2
0.5
60
50
40
30
20
10
0
−90
−60
−30
0
30
60
90

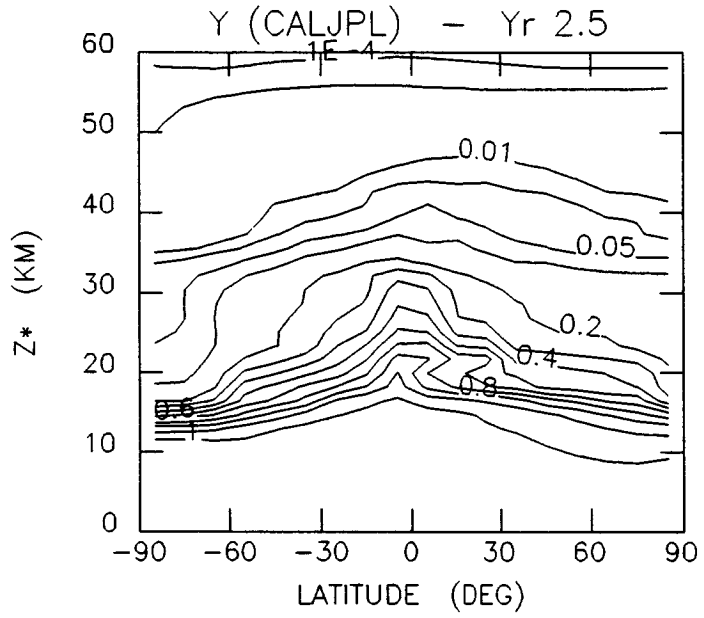
Y (CALJPL) – Yr 2.5
1E-4
0.01
0.05
0.2
0.4
0.6
0.8
1
Z* (KM)
LATITUDE (DEG)

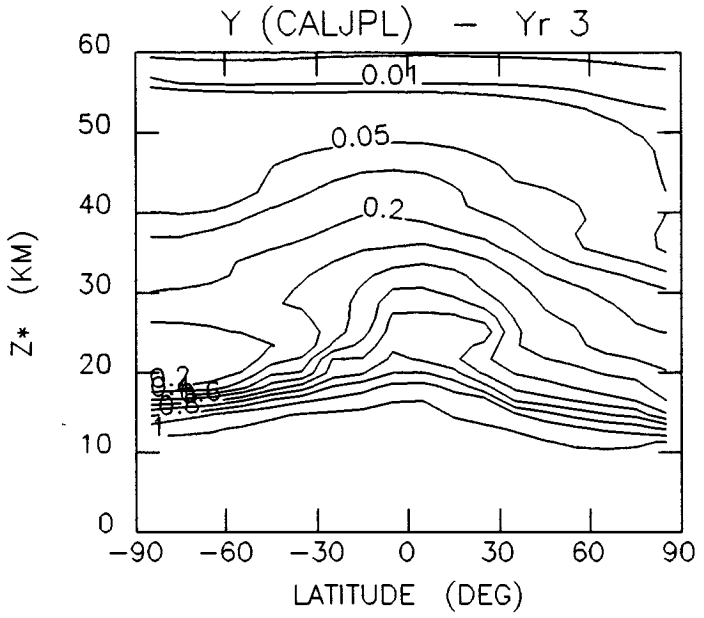
Y (CALJPL) – Yr 3
0.01
0.05
0.2
0.4
0.6
0.8
1
Z* (KM)
LATITUDE (DEG)

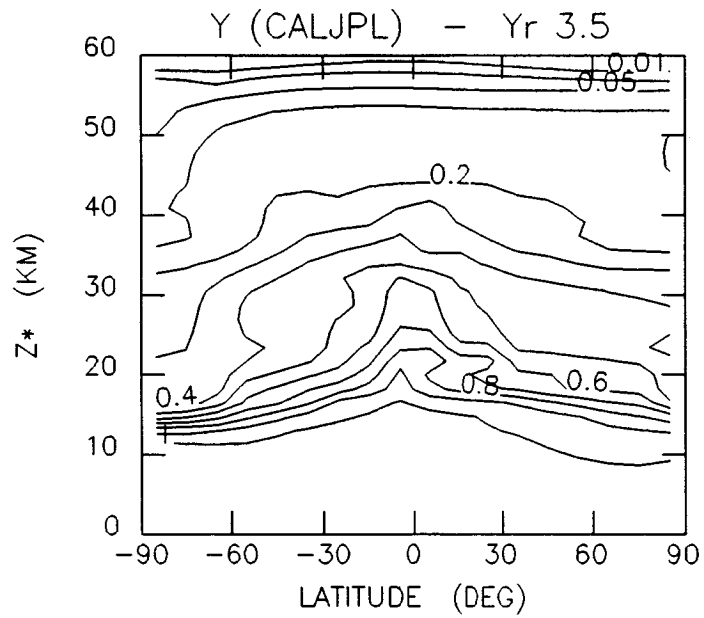
Y (CALJPL) – Yr 3.5
0.01
0.05
0.2
0.4
0.6
0.8
1
Z* (KM)
LATITUDE (DEG)

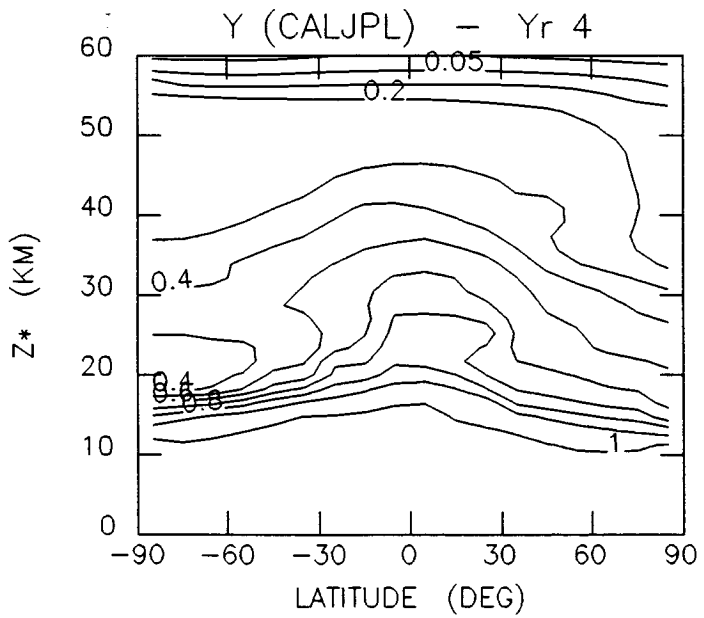
Y (CALJPL) – Yr 4
0.05
0.2
0.4
0.6
0.8
1
Z* (KM)
LATITUDE (DEG)

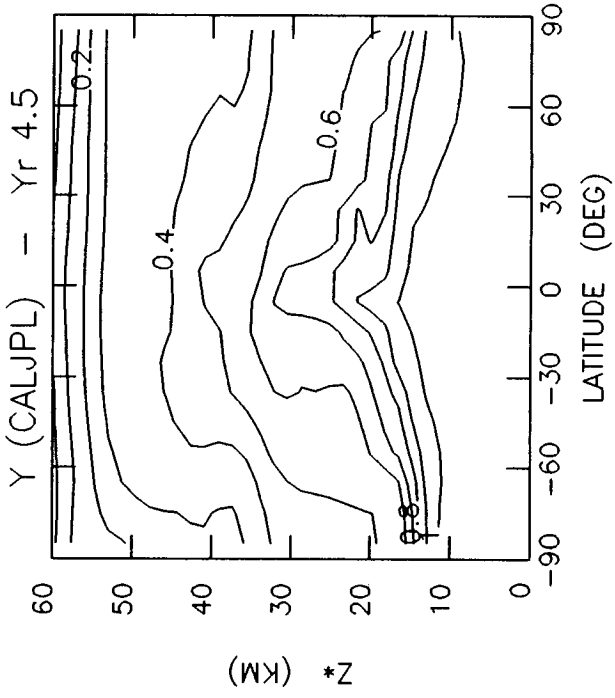
Y (CALJPL) - Yr 4.5
0.2
0.4
0.6
0.8
1.0
60
50
40
30
20
10
0
Z* (KM)
-90
-60
-30
0
30
60
90
LATITUDE (DEG)

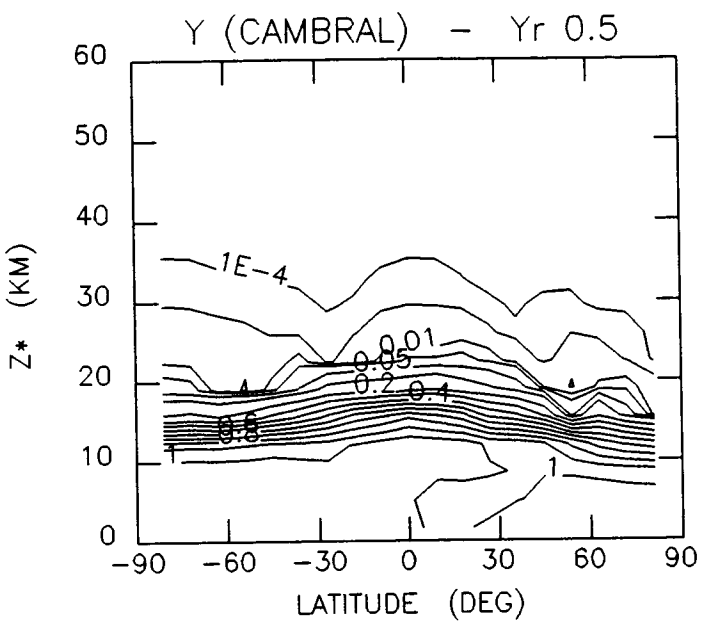
Y (CAMBRAL) - Yr 0.5
Z* (KM)
LATITUDE (DEG)
1E-4
0.01
0.05
0.2
0.4
0.6
0.8
1

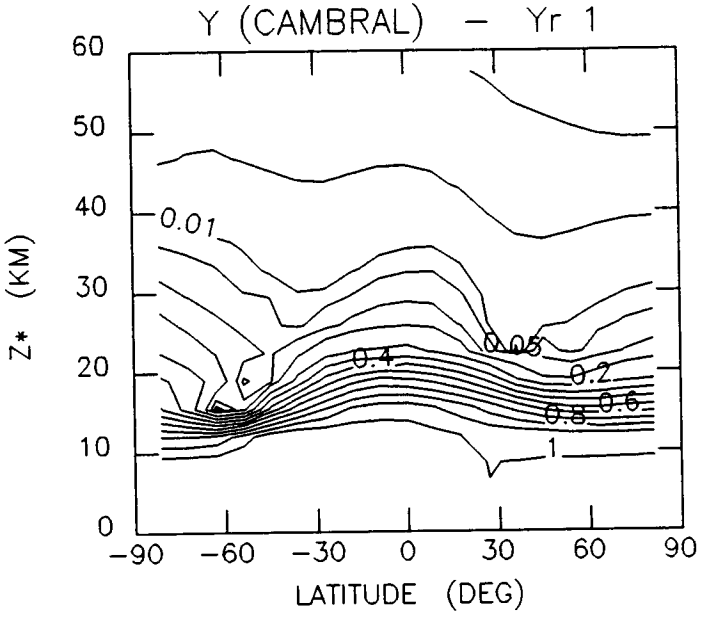
Y (CAMBRAL) - Yr 1
Z* (KM)
LATITUDE (DEG)
0.01
0.05
0.2
0.4
0.6
0.8
1

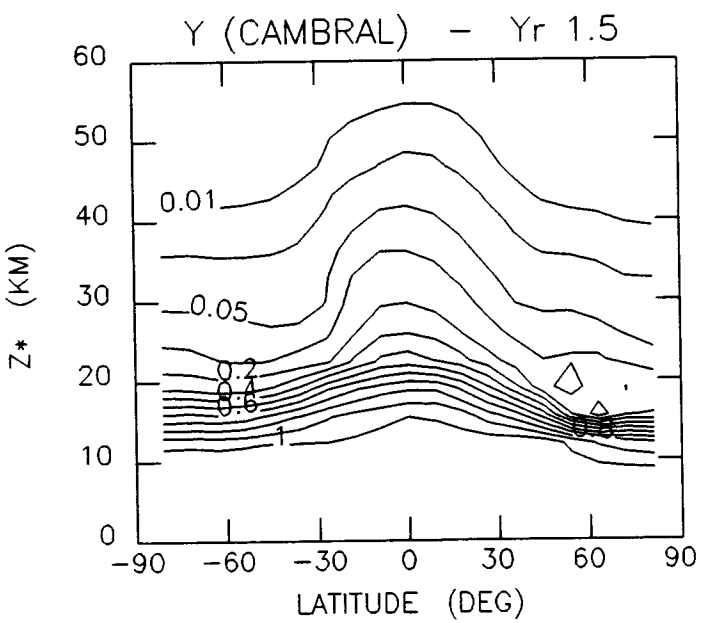
Y (CAMBRAL) - Yr 1.5
Z* (KM)
LATITUDE (DEG)
0.01
0.05
0.2
0.4
0.6
0.8
1

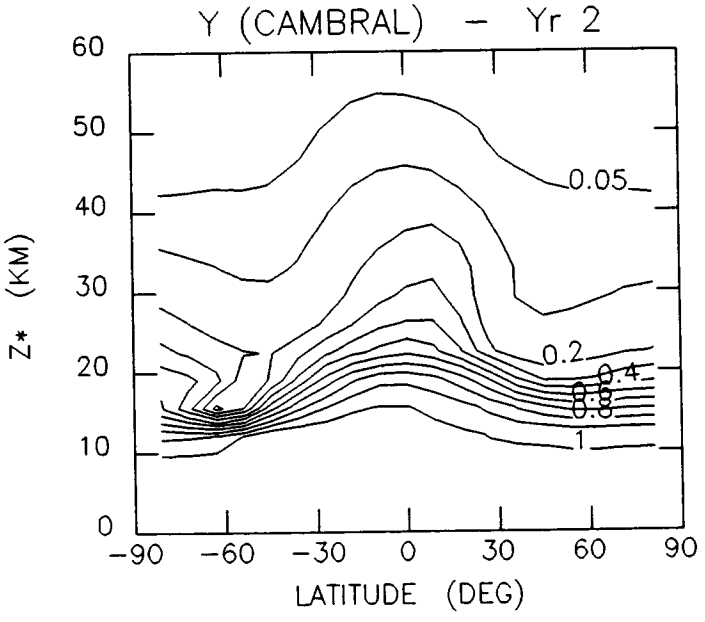
Y (CAMBRAL) - Yr 2
Z* (KM)
LATITUDE (DEG)
0.05
0.2
0.4
0.6
0.8
1

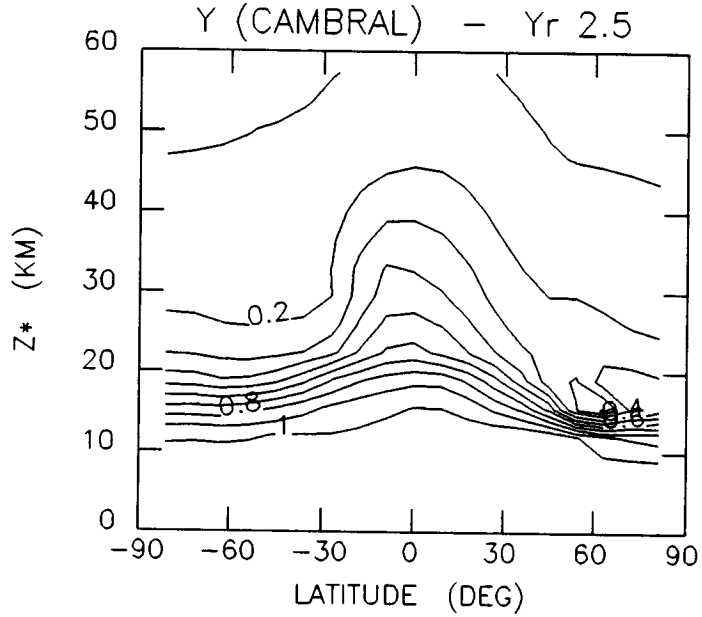
Y (CAMBRAL) – Yr 2.5
Z* (KM)
LATITUDE (DEG)
0.2
0.8
1
0.4
0.6

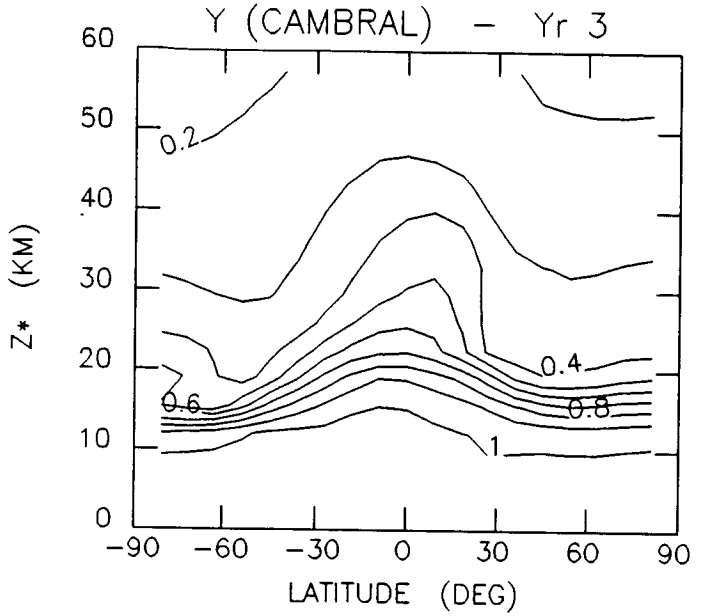
Y (CAMBRAL) – Yr 3
Z* (KM)
LATITUDE (DEG)
0.2
0.4
0.6
0.8
1

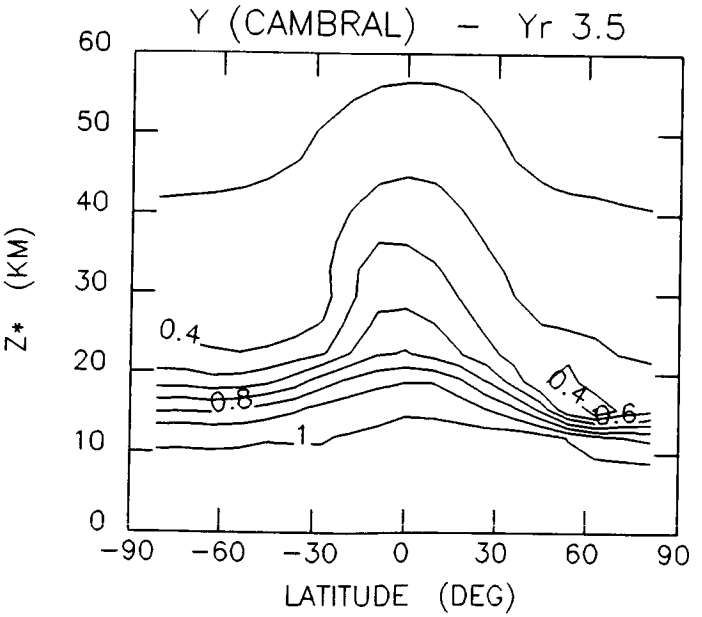
Y (CAMBRAL) – Yr 3.5
Z* (KM)
LATITUDE (DEG)
0.4
0.8
1
0.4
0.6

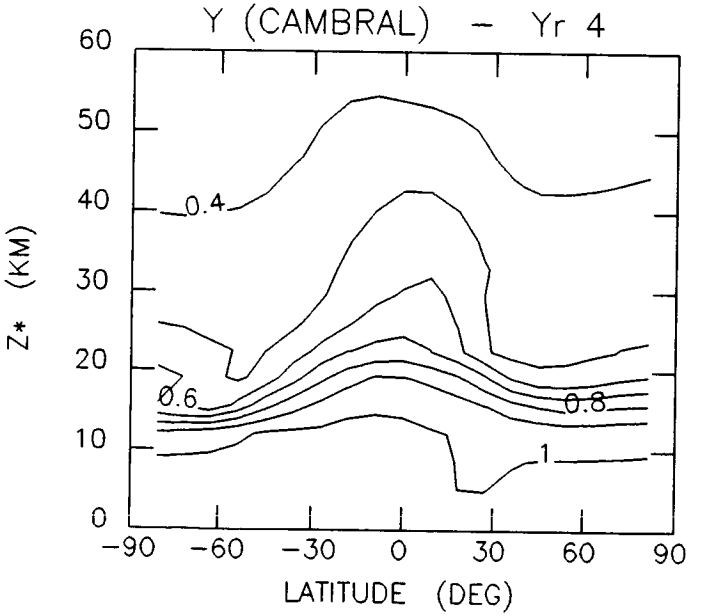
Y (CAMBRAL) – Yr 4
Z* (KM)
LATITUDE (DEG)
0.4
0.6
0.8
1

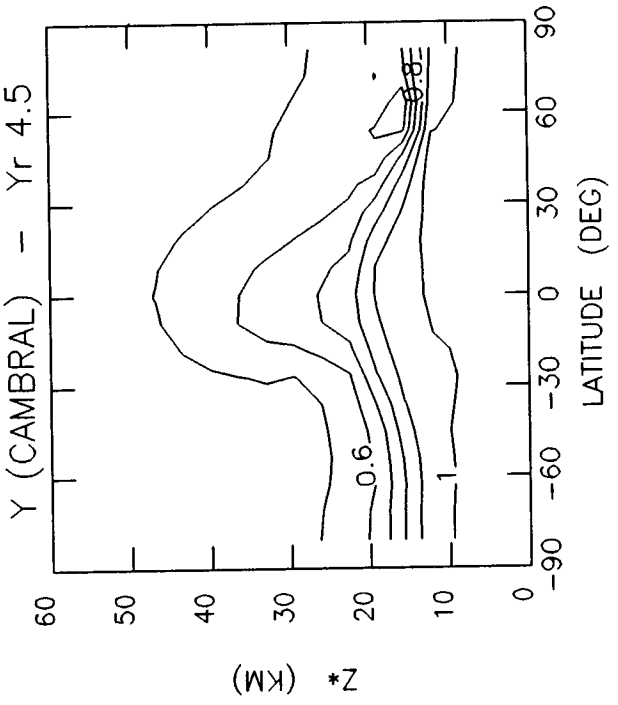
Y (CAMBRAL) - Yr 4.5
Z* (KM)
LATITUDE (DEG)
0.6
0.8
1
60
50
40
30
20
10
0
-90
-60
-30
0
30
60
90

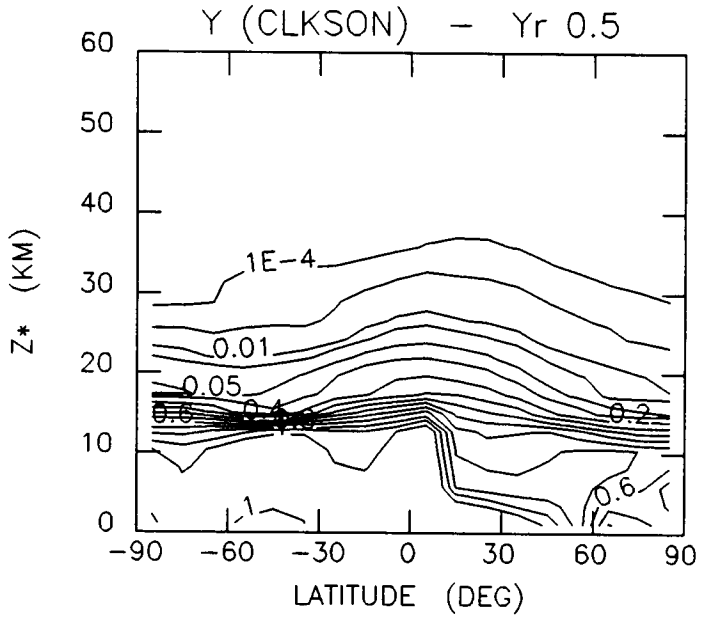
Y (CLKSON) – Yr 0.5
Z* (KM)
LATITUDE (DEG)
1E-4
0.01
0.05
0.4
0.2
0.6
1

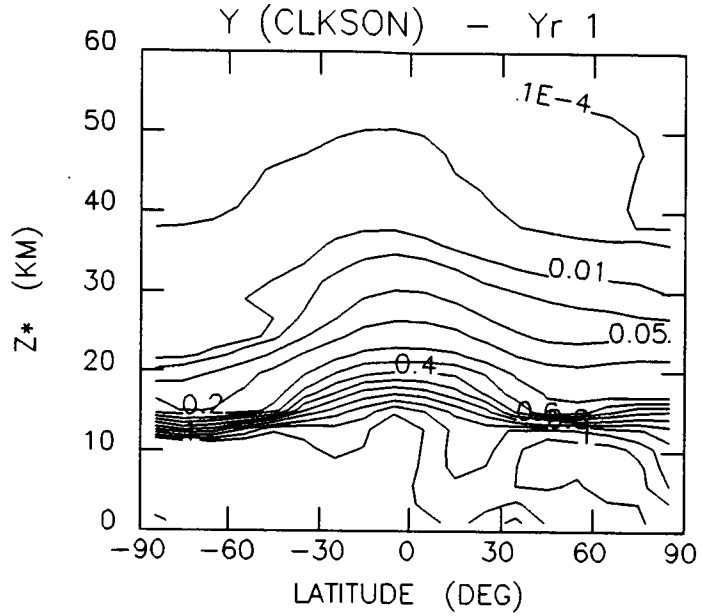
Y (CLKSON) – Yr 1
Z* (KM)
LATITUDE (DEG)
1E-4
0.01
0.05
0.4
0.2
0.6

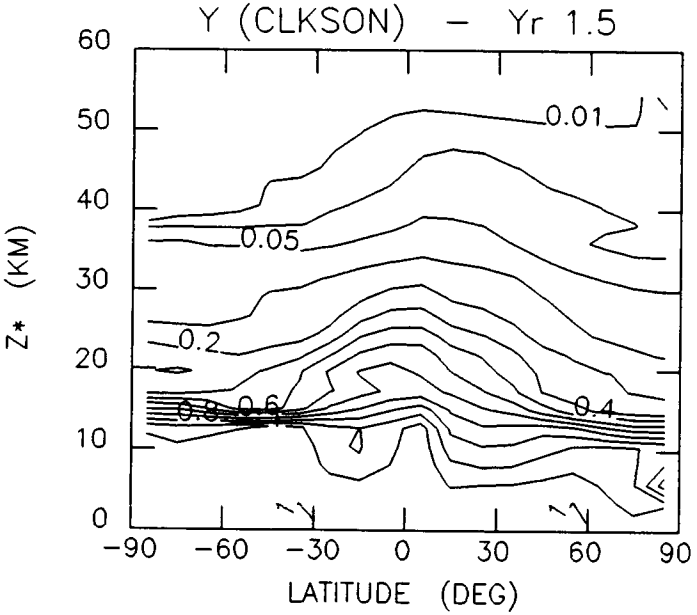
Y (CLKSON) – Yr 1.5
Z* (KM)
LATITUDE (DEG)
0.01
0.05
0.2
0.4
0.6

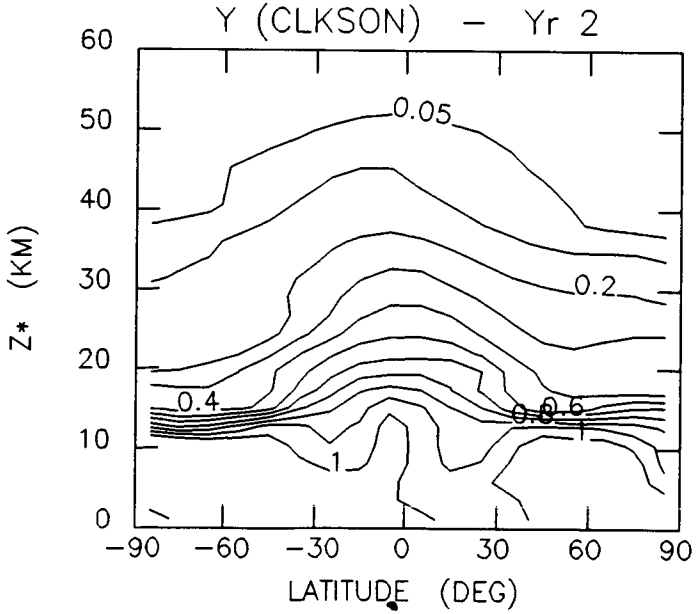
Y (CLKSON) – Yr 2
Z* (KM)
LATITUDE (DEG)
0.05
0.2
0.4
0.6
1

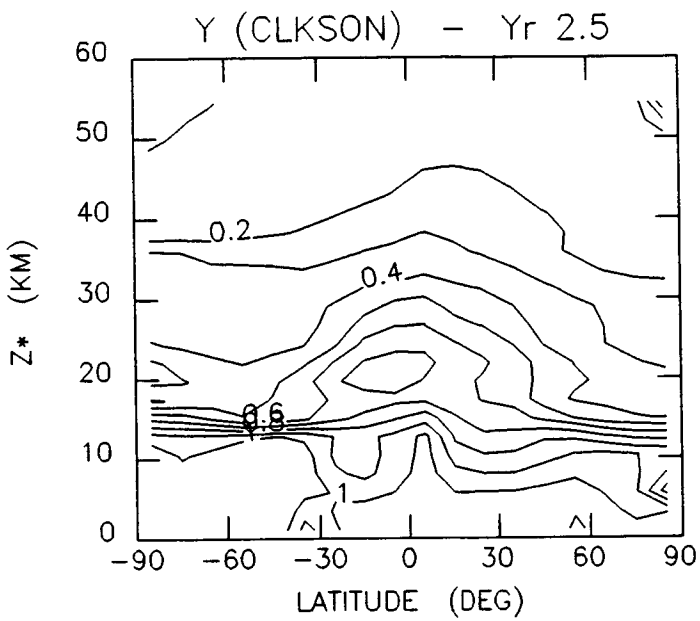
Y (CLKSON) – Yr 2.5
Z* (KM)
LATITUDE (DEG)
0.2
0.4
0.6
0.8
1

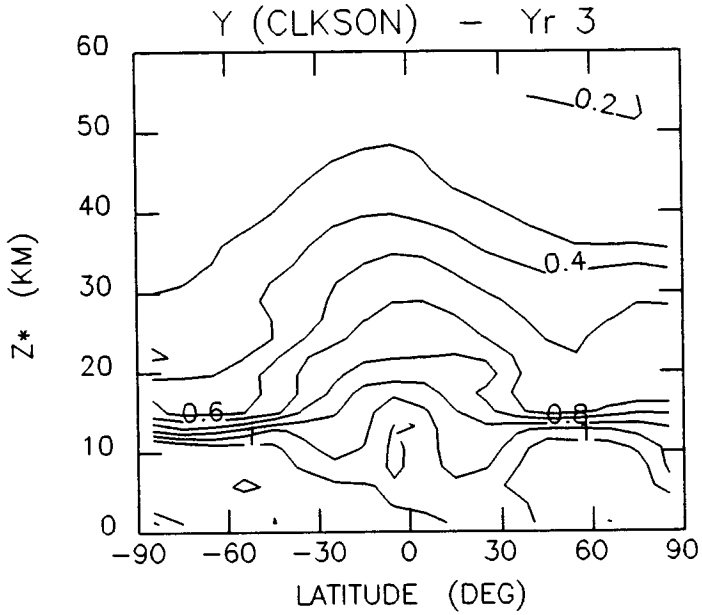
Y (CLKSON) – Yr 3
Z* (KM)
LATITUDE (DEG)
0.2
0.4
0.6
0.8

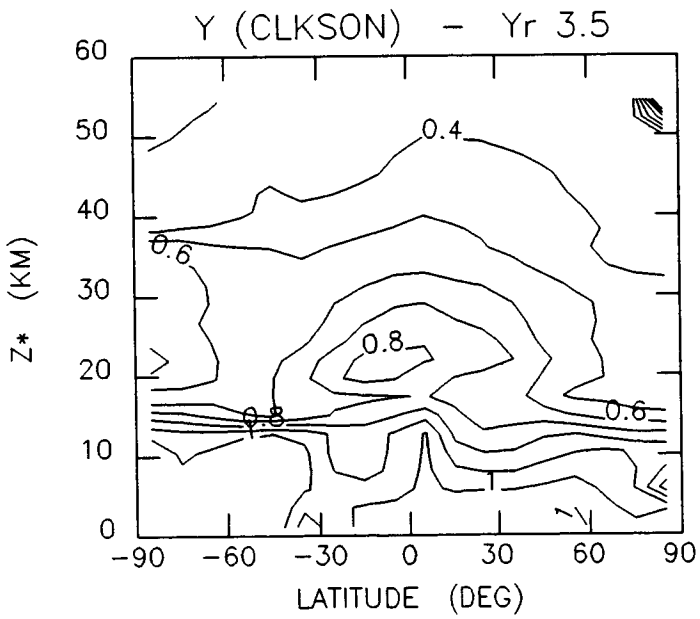
Y (CLKSON) – Yr 3.5
Z* (KM)
LATITUDE (DEG)
0.4
0.6
0.8
0.6
0.8

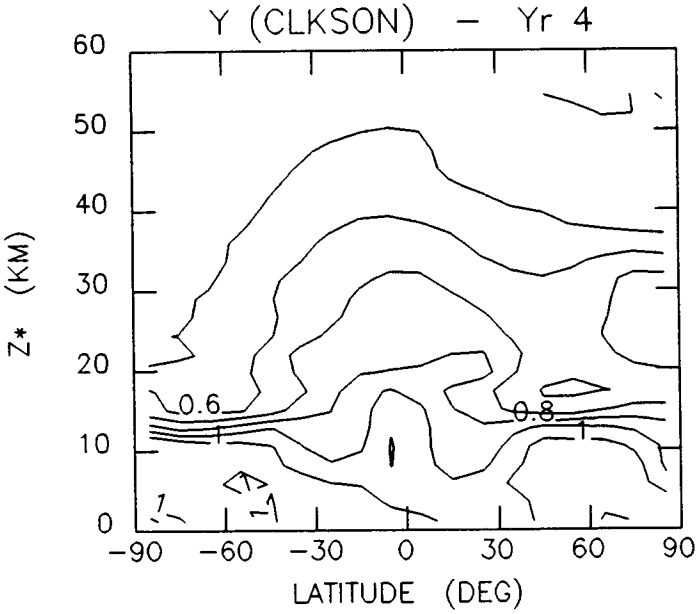
Y (CLKSON) – Yr 4
Z* (KM)
LATITUDE (DEG)
0.6
0.8
1

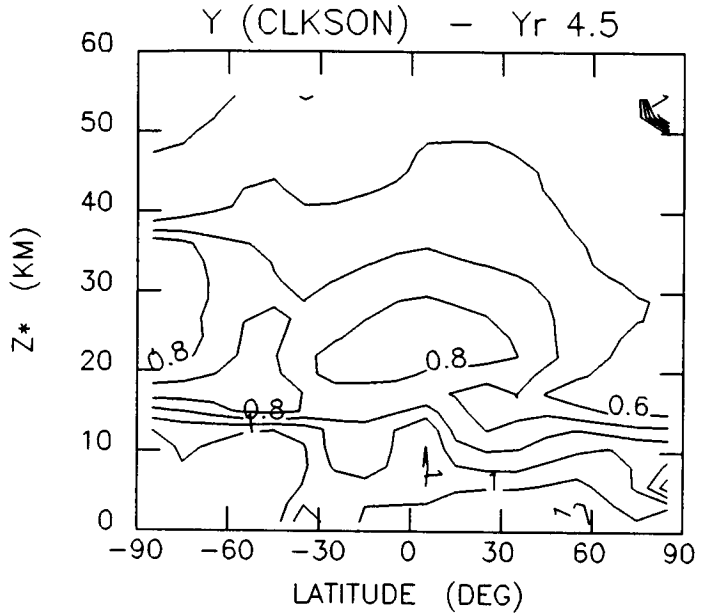
Y (CLKSON) – Yr 4.5
Z* (KM)
LATITUDE (DEG)
0.8
0.6

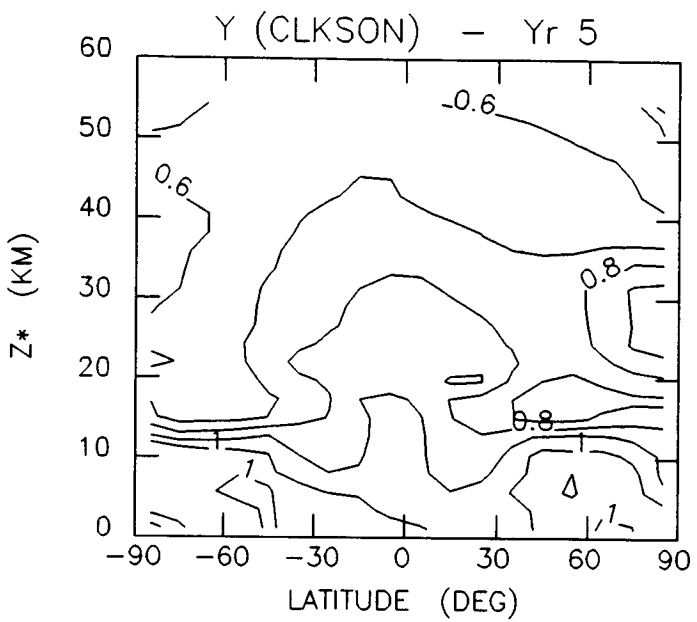
Y (CLKSON) – Yr 5
Z* (KM)
LATITUDE (DEG)
-0.6
0.6
0.8

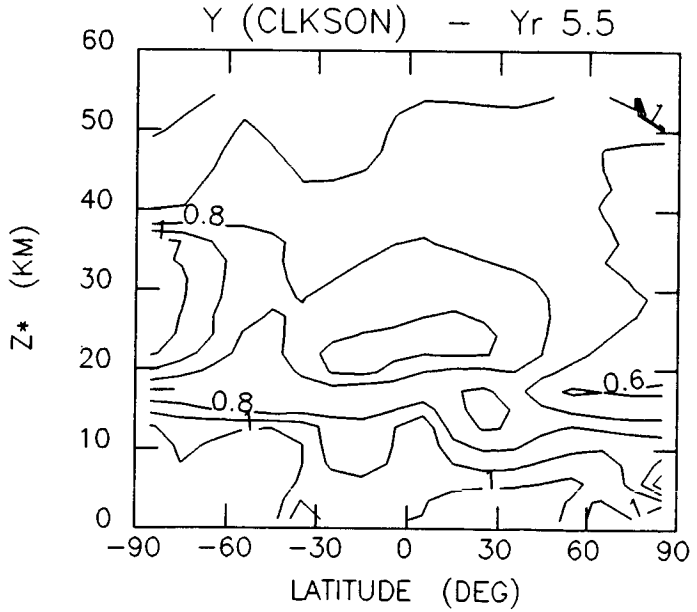
Y (CLKSON) – Yr 5.5
Z* (KM)
LATITUDE (DEG)
0.8
0.6

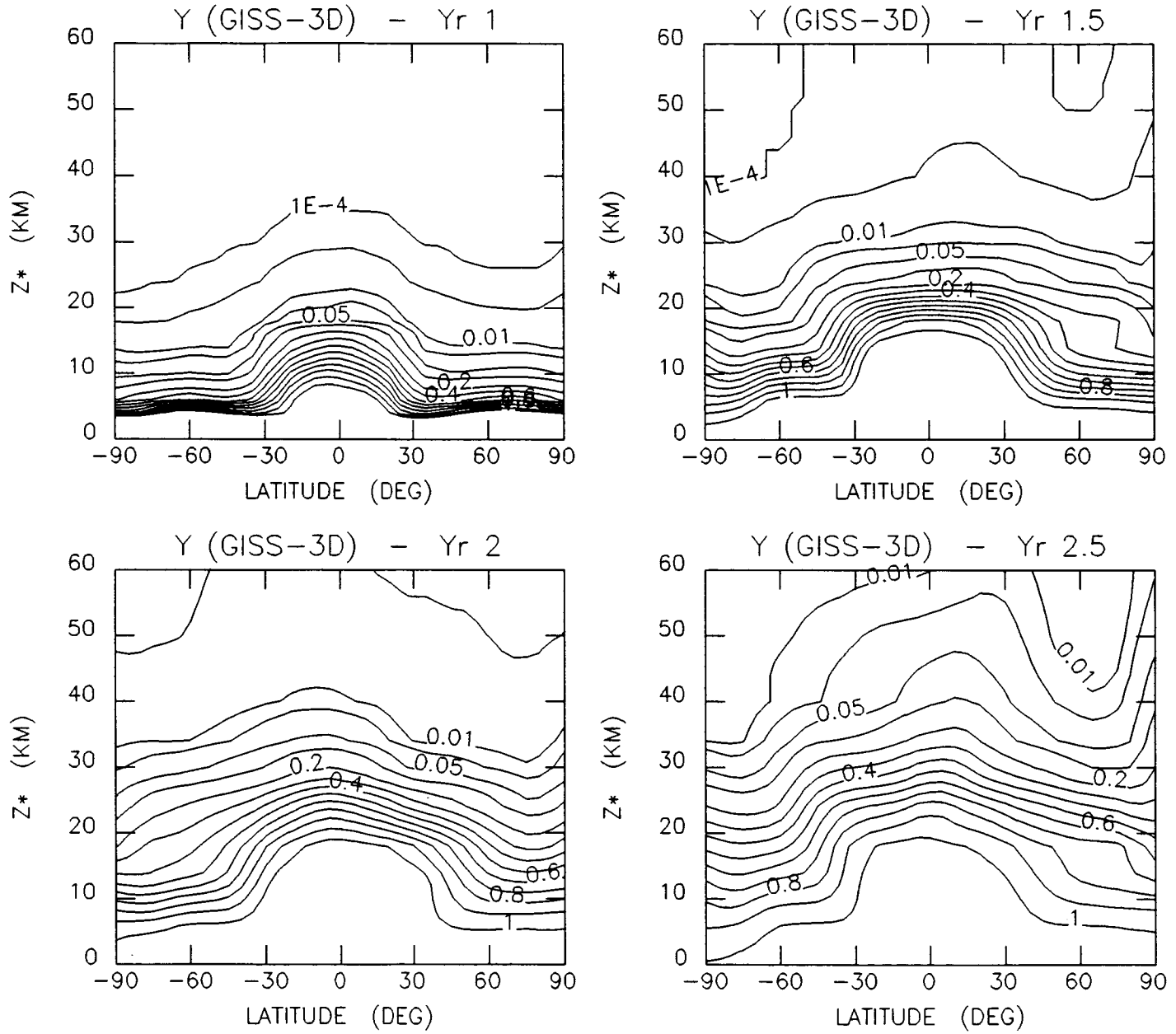
Y (GISS-3D) - Yr 1
Y (GISS-3D) - Yr 1.5
Y (GISS-3D) - Yr 2
Y (GISS-3D) - Yr 2.5
Z* (KM)
LATITUDE (DEG)
1E-4
0.01
0.05
0.2
0.4
0.6
0.8
1

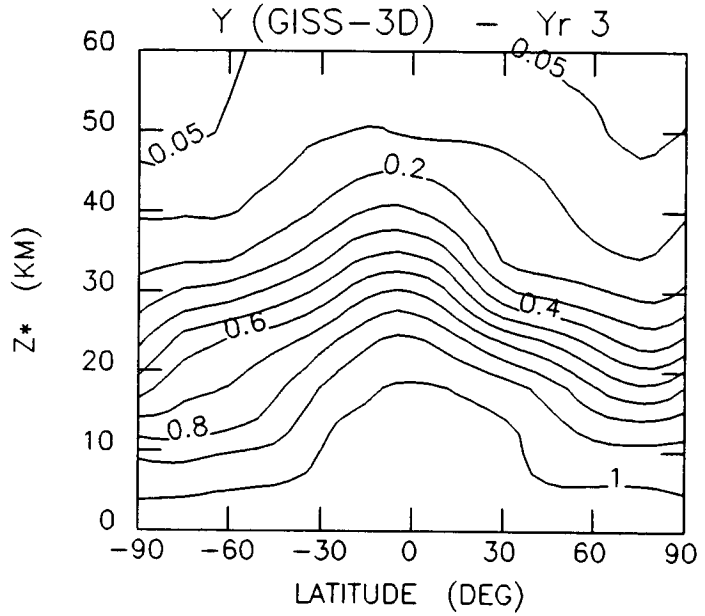
Y (GISS-3D) – Yr 3
Z* (KM)
LATITUDE (DEG)
0.05
0.2
0.4
0.6
0.8
1

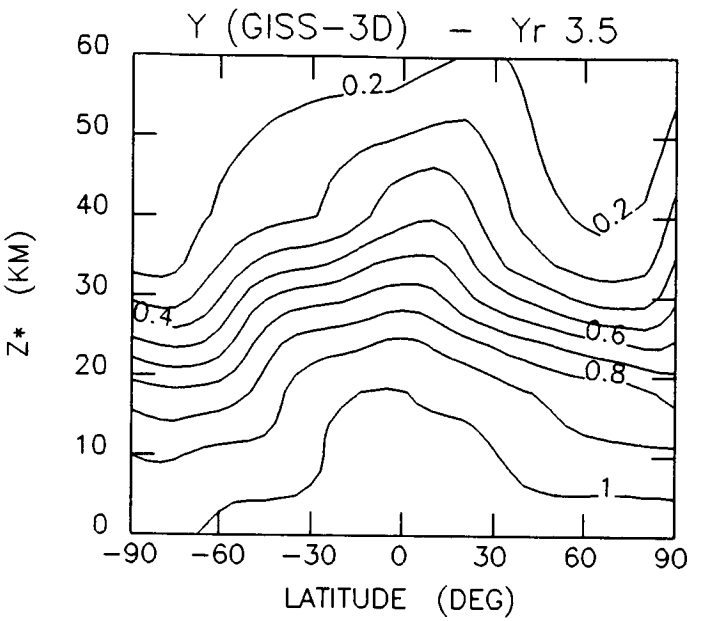
Y (GISS-3D) – Yr 3.5
Z* (KM)
LATITUDE (DEG)
0.2
0.4
0.6
0.8
1

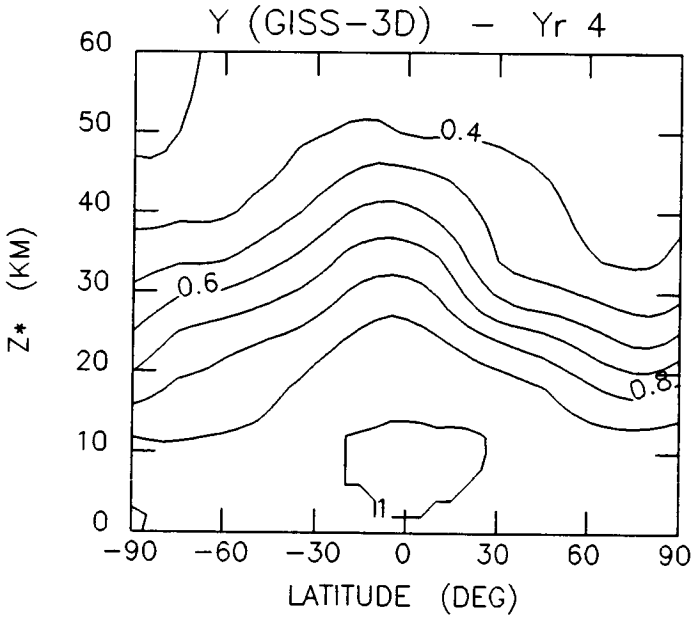
Y (GISS-3D) – Yr 4
Z* (KM)
LATITUDE (DEG)
0.4
0.6
0.8
1

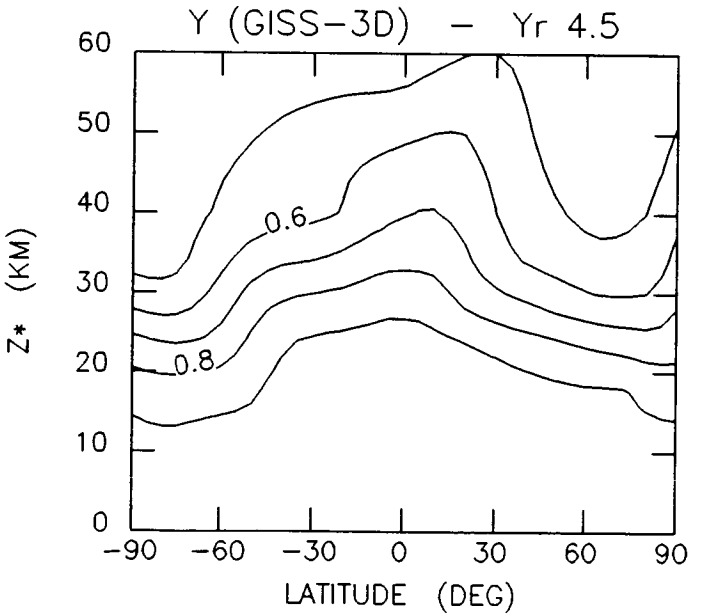
Y (GISS-3D) – Yr 4.5
Z* (KM)
LATITUDE (DEG)
0.6
0.8

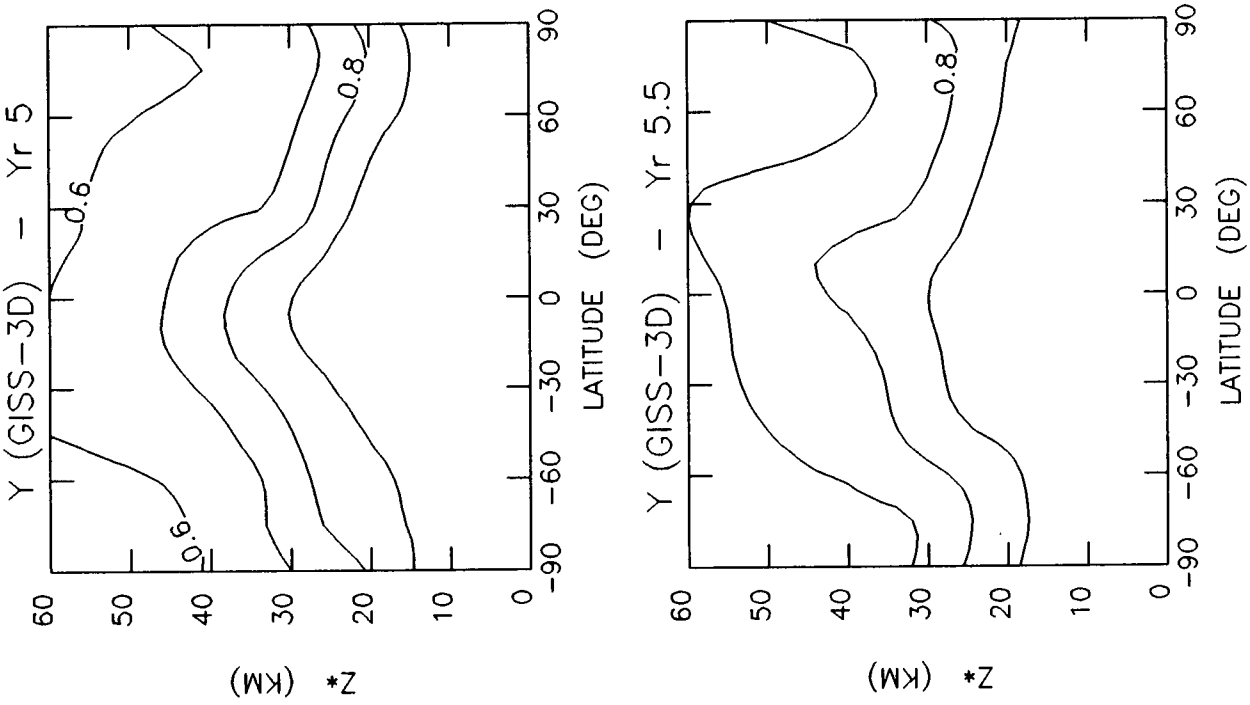
Y (GISS-3D) - Yr 5
0.6
0.6
0.8
Z* (KM)
LATITUDE (DEG)
60
50
40
30
20
10
0
-90
-60
-30
0
30
60
90
Y (GISS-3D) - Yr 5.5
0.8
Z* (KM)
LATITUDE (DEG)

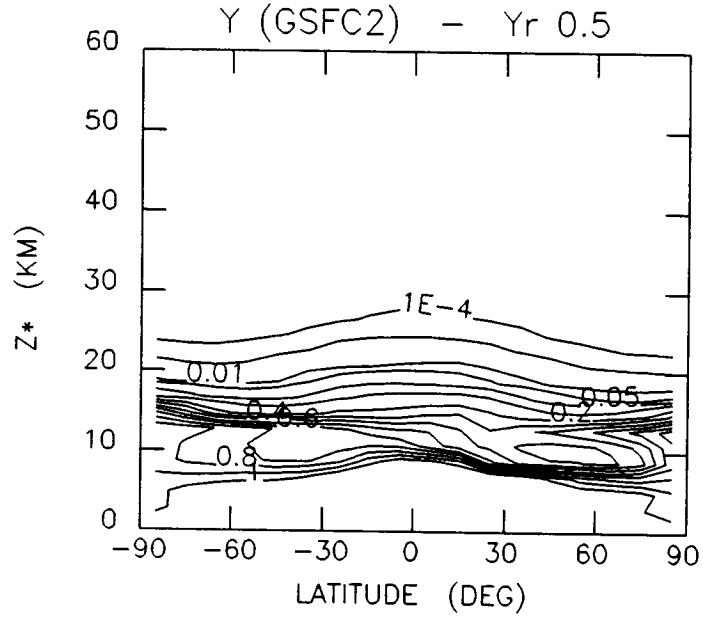
Y (GSFC2) – Yr 0.5
Z* (KM)
LATITUDE (DEG)
1E-4
0.01
0.05
0.2
0.4
0.6
0.8
1

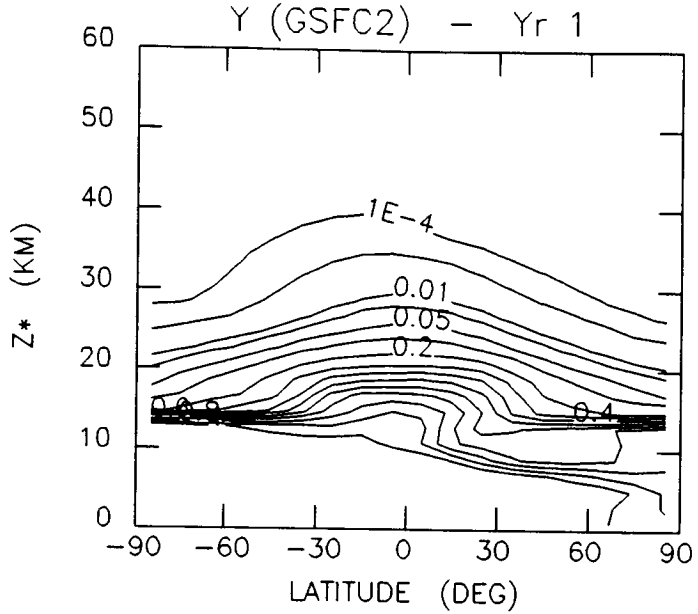
Y (GSFC2) – Yr 1
Z* (KM)
LATITUDE (DEG)
1E-4
0.01
0.05
0.2
0.4

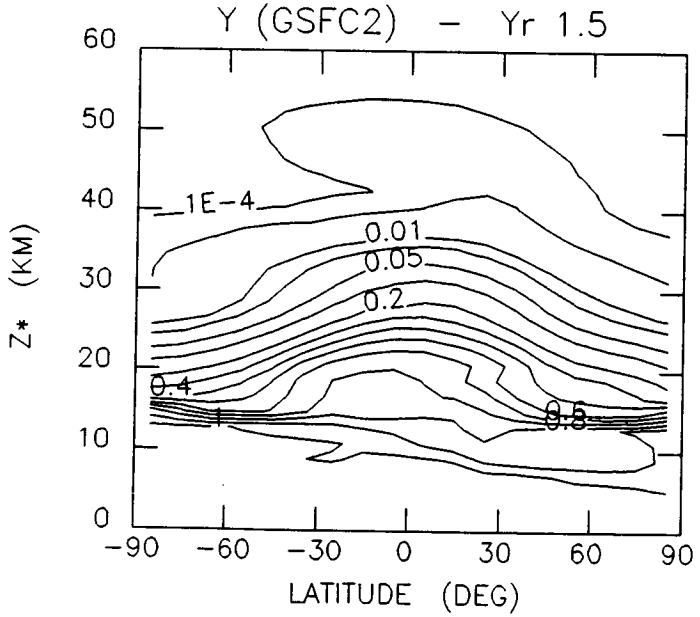
Y (GSFC2) – Yr 1.5
Z* (KM)
LATITUDE (DEG)
1E-4
0.01
0.05
0.2
0.4
0.6
0.8
1

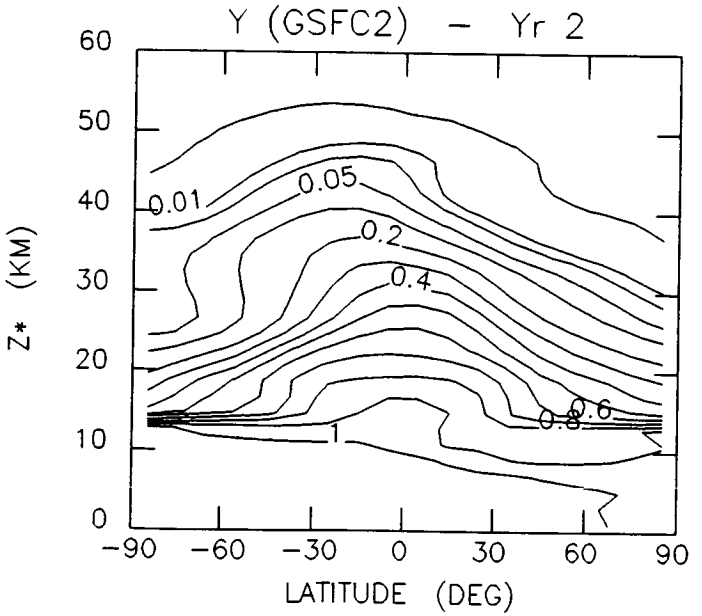
Y (GSFC2) – Yr 2
Z* (KM)
LATITUDE (DEG)
0.01
0.05
0.2
0.4
0.6
0.8
1

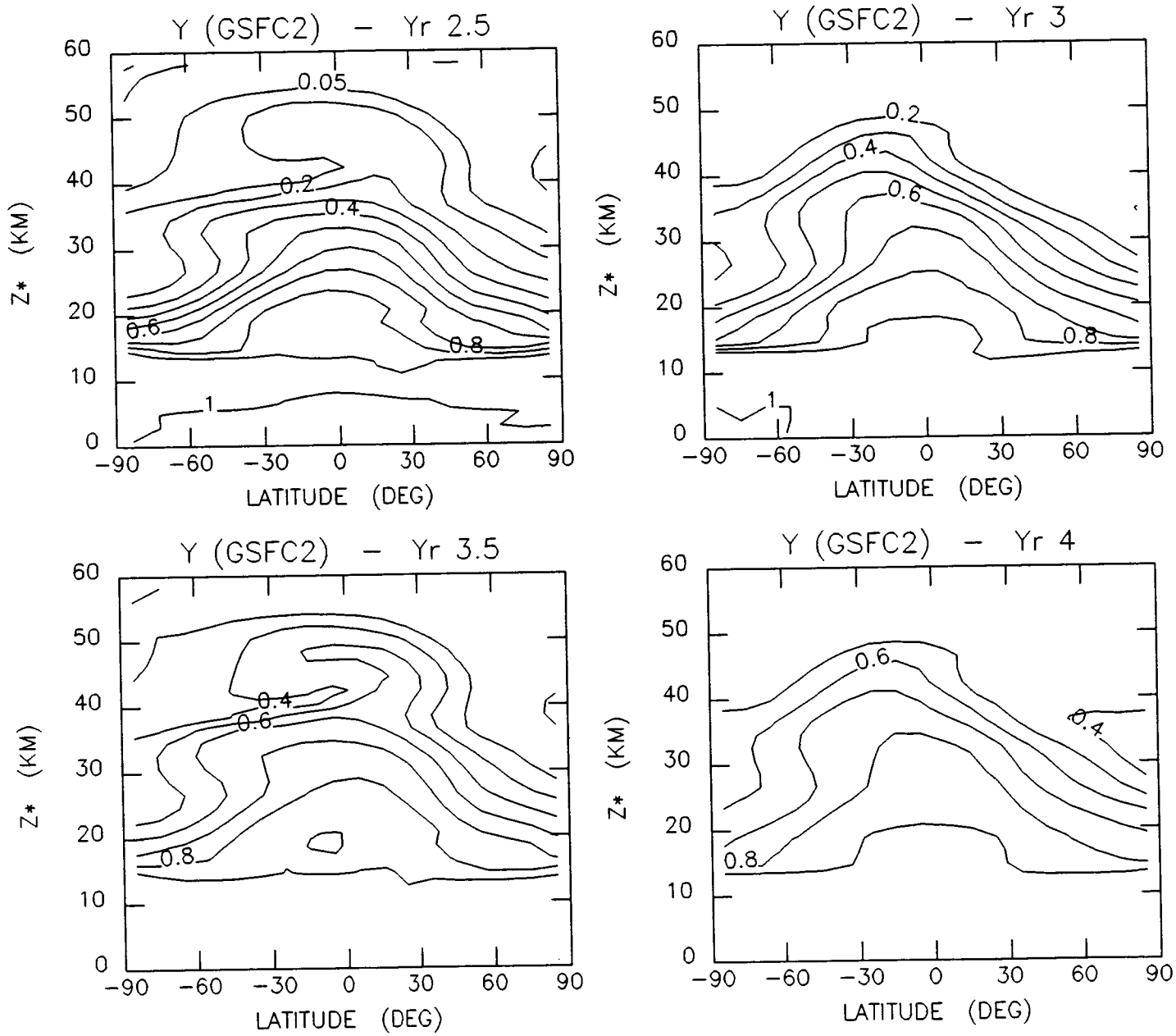
Y (GSFC2) – Yr 2.5
Z* (KM)
LATITUDE (DEG)
0.05
0.2
0.4
0.6
0.8
1
Y (GSFC2) – Yr 3
Z* (KM)
LATITUDE (DEG)
0.2
0.4
0.6
0.8
1
Y (GSFC2) – Yr 3.5
Z* (KM)
LATITUDE (DEG)
0.4
0.6
0.8
Y (GSFC2) – Yr 4
Z* (KM)
LATITUDE (DEG)
0.6
0.4
0.8

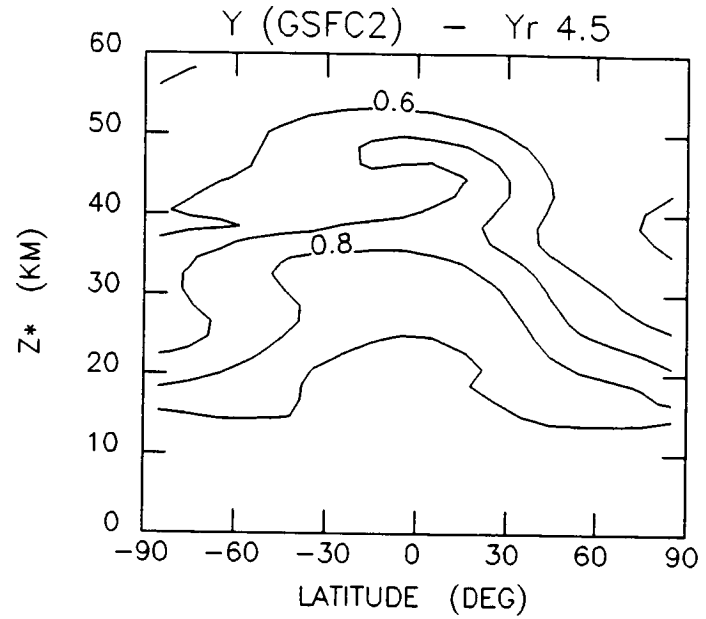
Y (GSFC2) – Yr 4.5
60
50
40
30
20
10
0
Z* (KM)
0.6
0.8
−90 −60 −30 0 30 60 90
LATITUDE (DEG)

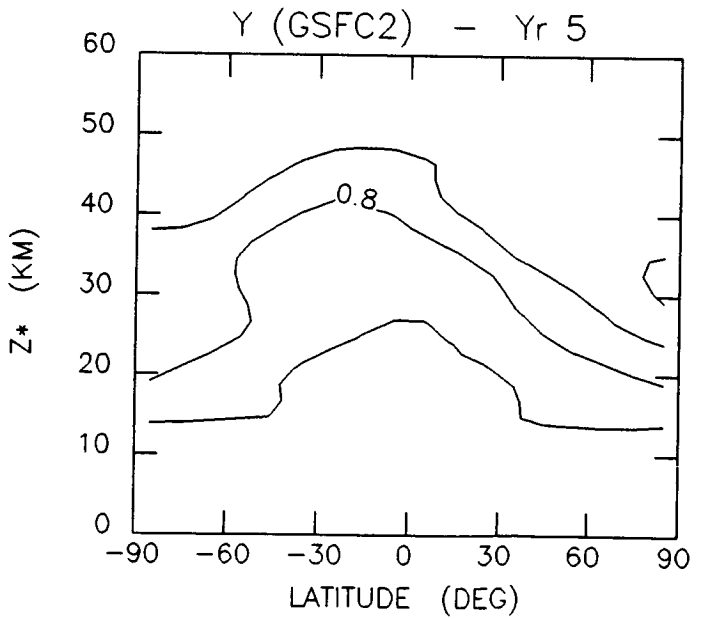
Y (GSFC2) – Yr 5
60
50
40
30
20
10
0
Z* (KM)
0.8
−90 −60 −30 0 30 60 90
LATITUDE (DEG)

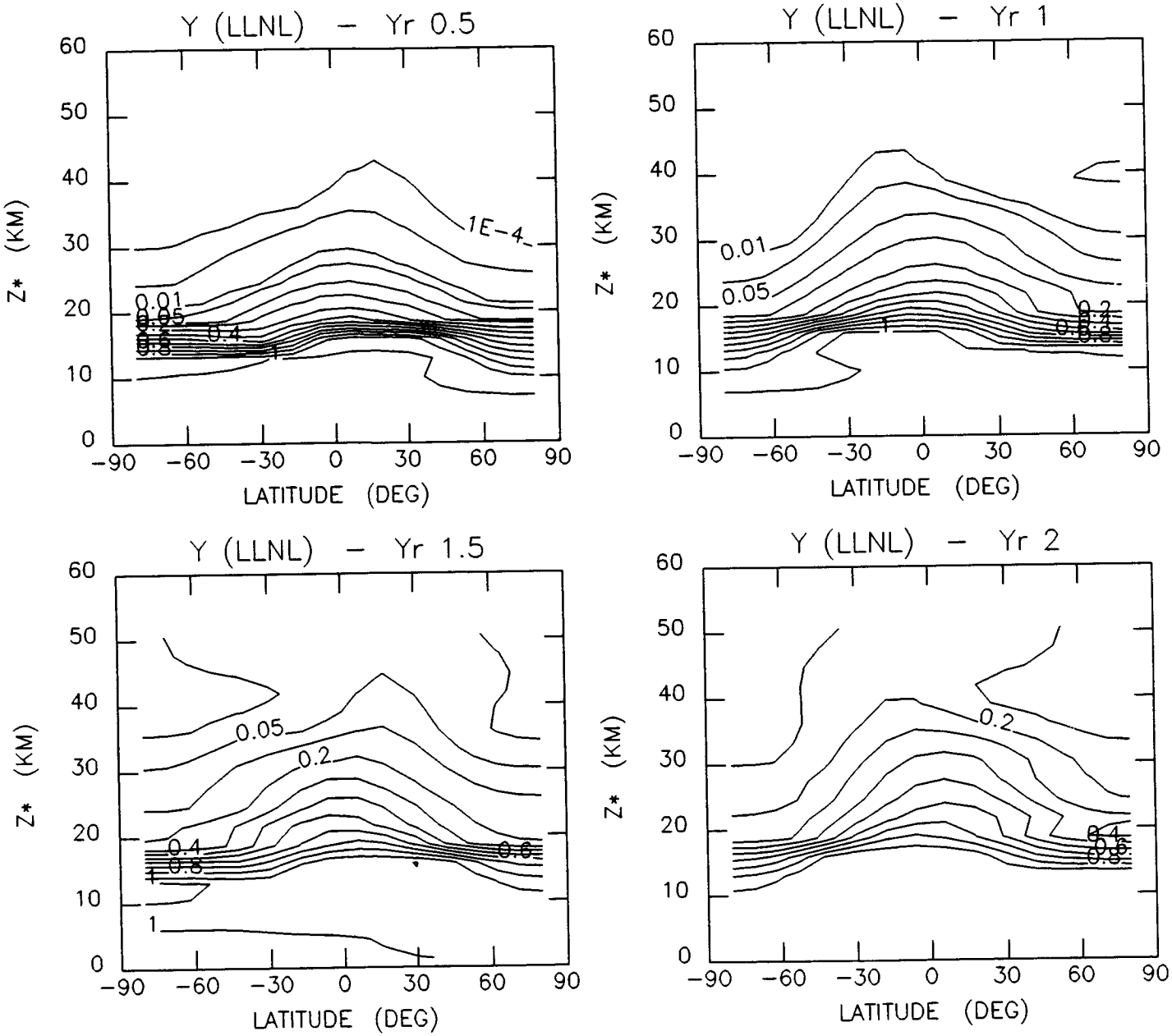
Y (LLNL) – Yr 0.5
Y (LLNL) – Yr 1
Y (LLNL) – Yr 1.5
Y (LLNL) – Yr 2
Z* (KM)
LATITUDE (DEG)
1E-4
0.01
0.05
0.2
0.4
0.6
0.8
1
0
10
20
30
40
50
60
-90
-60
-30
0
30
60
90

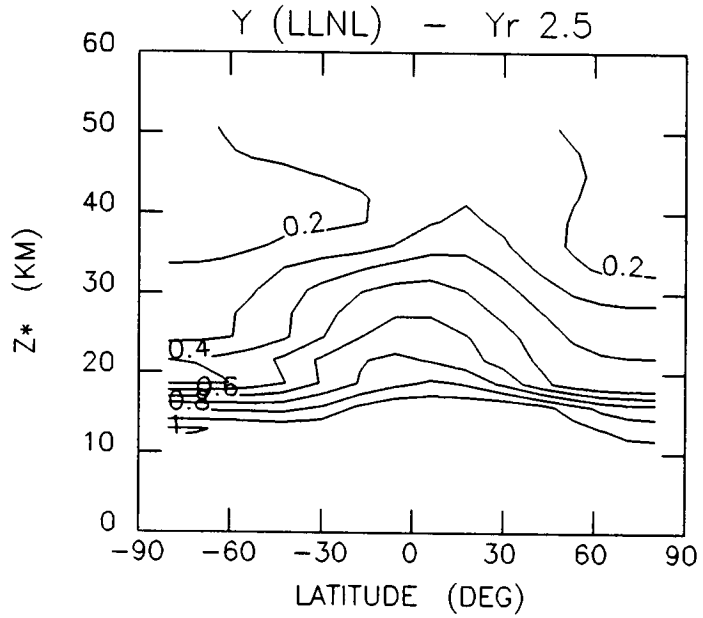
Y (LLNL) – Yr 2.5
Z* (KM)
LATITUDE (DEG)
0.2
0.4
0.6
0.8
1

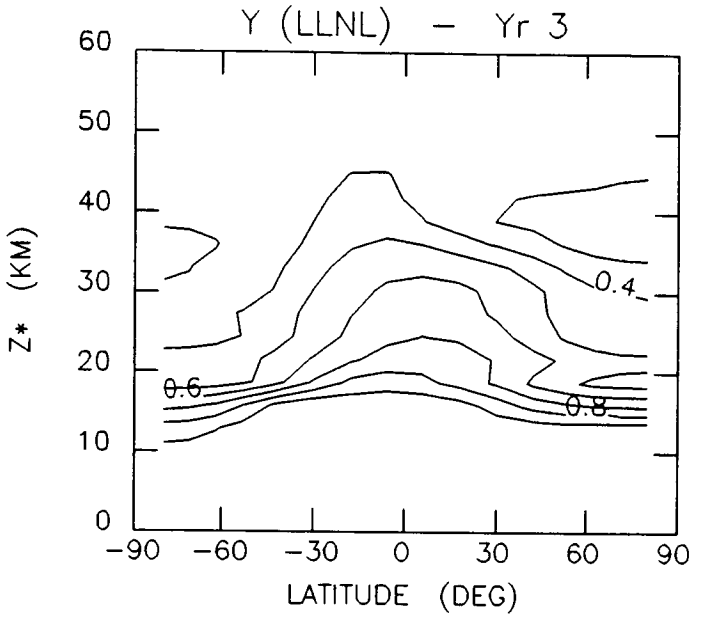
Y (LLNL) – Yr 3
Z* (KM)
LATITUDE (DEG)
0.4
0.6
0.8

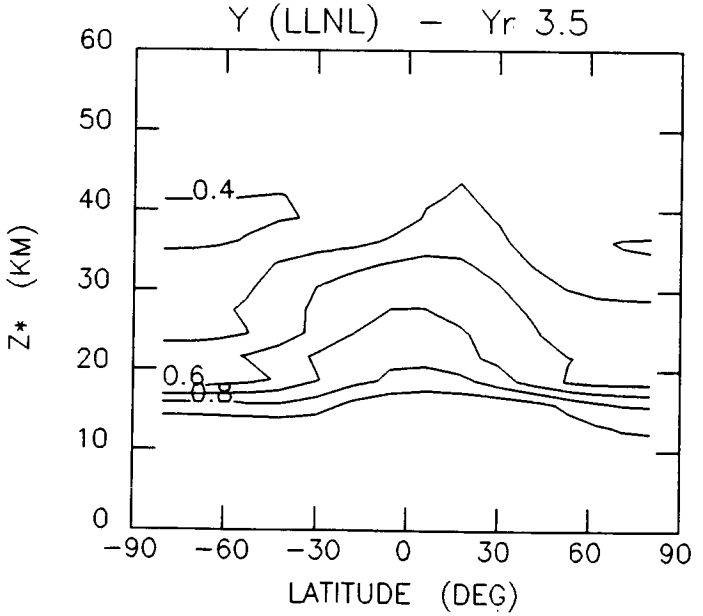
Y (LLNL) – Yr 3.5
Z* (KM)
LATITUDE (DEG)
0.4
0.6
0.8

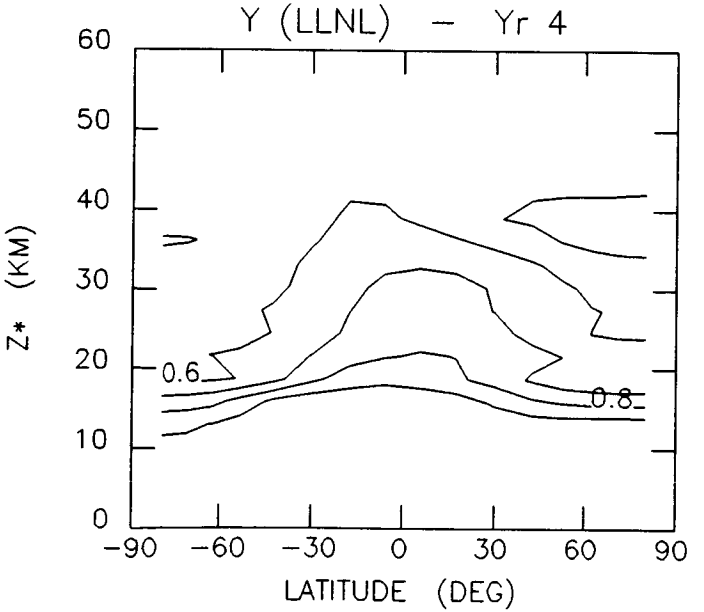
Y (LLNL) – Yr 4
Z* (KM)
LATITUDE (DEG)
0.6
0.8

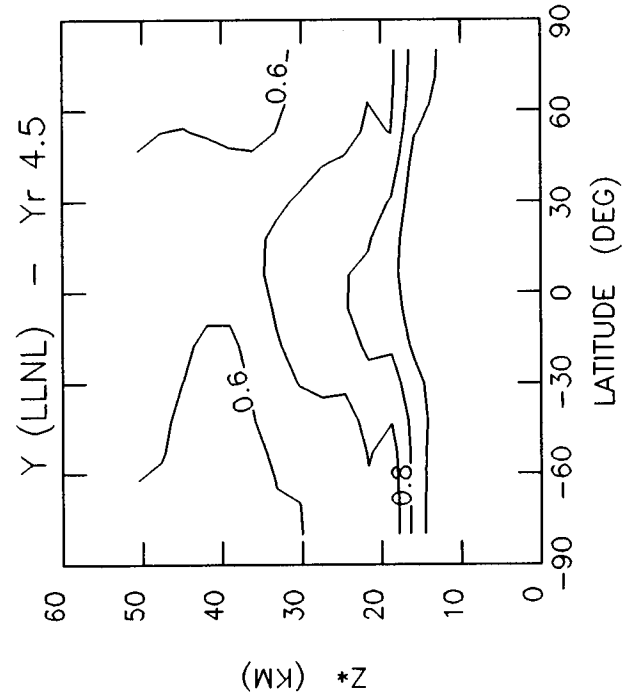
Y (LLNL) - Yr 4.5
0.6
0.6
0.8
Z* (KM)
60
50
40
30
20
10
0
-90
-60
-30
0
30
60
90
LATITUDE (DEG)

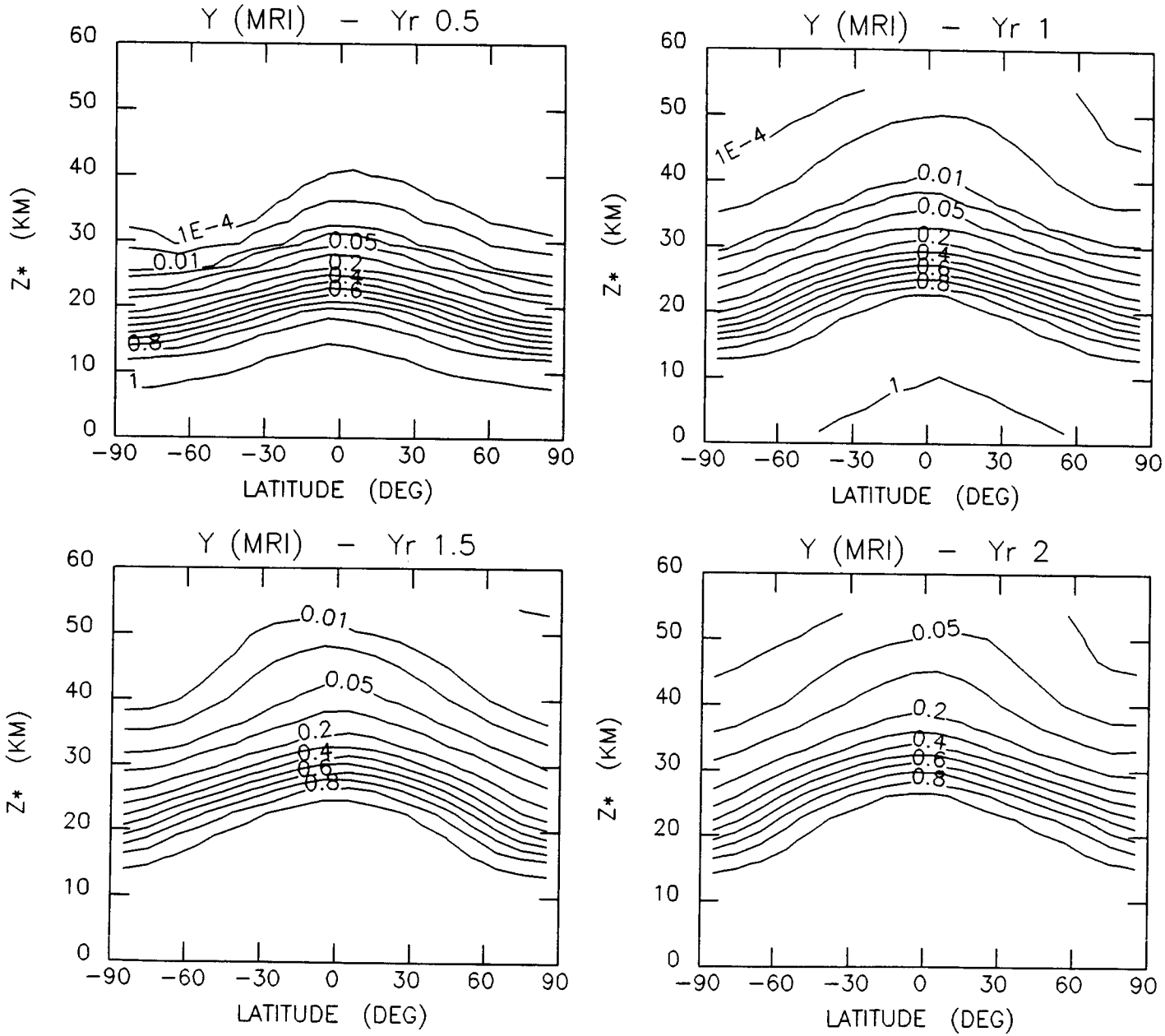
Y (MRI) – Yr 0.5
Y (MRI) – Yr 1
Y (MRI) – Yr 1.5
Y (MRI) – Yr 2
Z* (KM)
LATITUDE (DEG)
1E-4
0.01
0.05
0.2
0.4
0.6
0.8
1

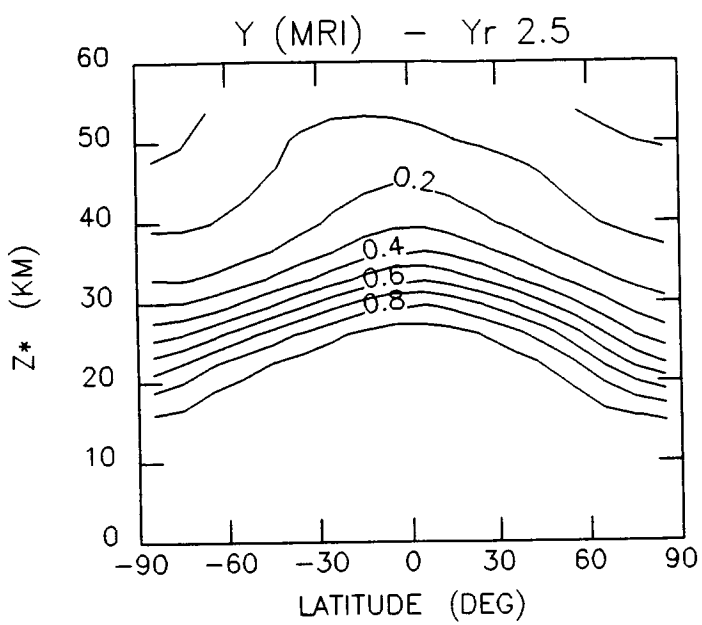
Y (MRI) – Yr 2.5
Z* (KM)
LATITUDE (DEG)
0.2
0.4
0.6
0.8

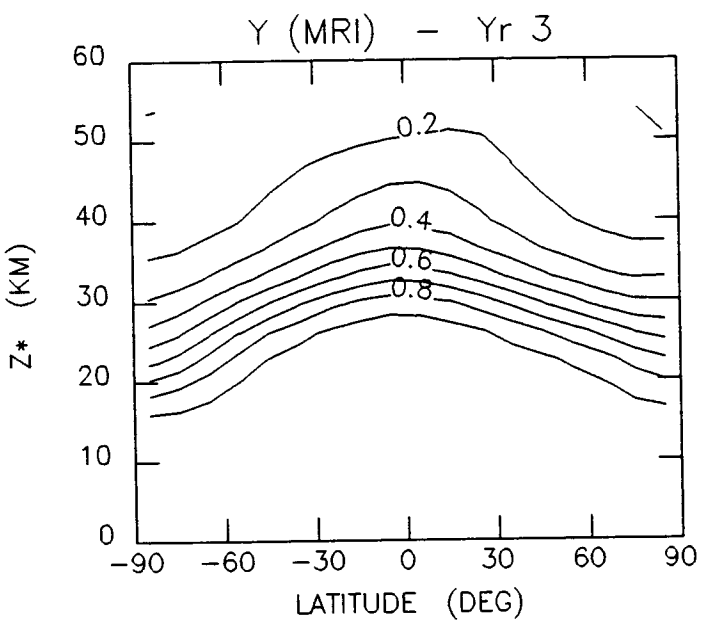
Y (MRI) – Yr 3
Z* (KM)
LATITUDE (DEG)
0.2
0.4
0.6
0.8

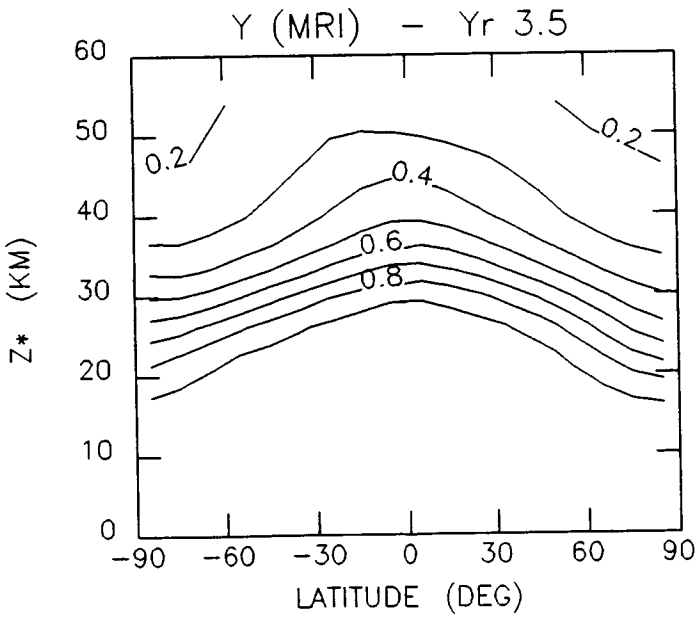
Y (MRI) – Yr 3.5
Z* (KM)
LATITUDE (DEG)
0.2
0.4
0.6
0.8

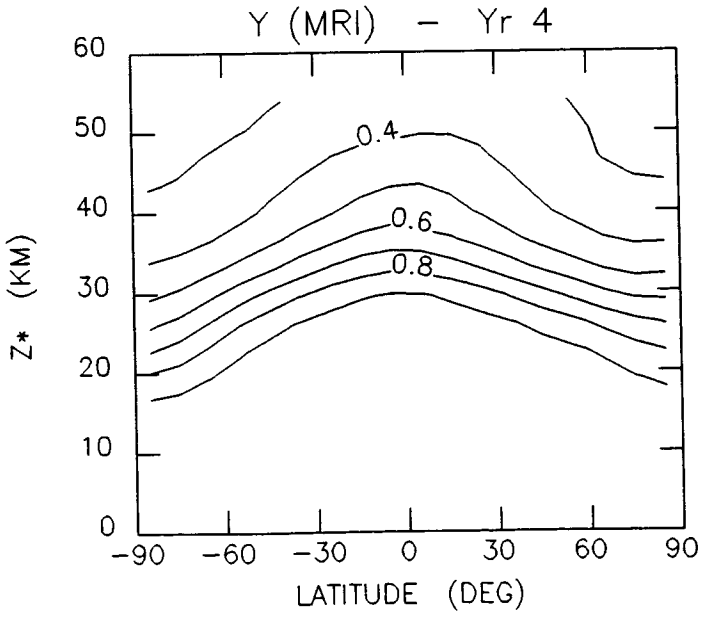
Y (MRI) – Yr 4
Z* (KM)
LATITUDE (DEG)
0.4
0.6
0.8

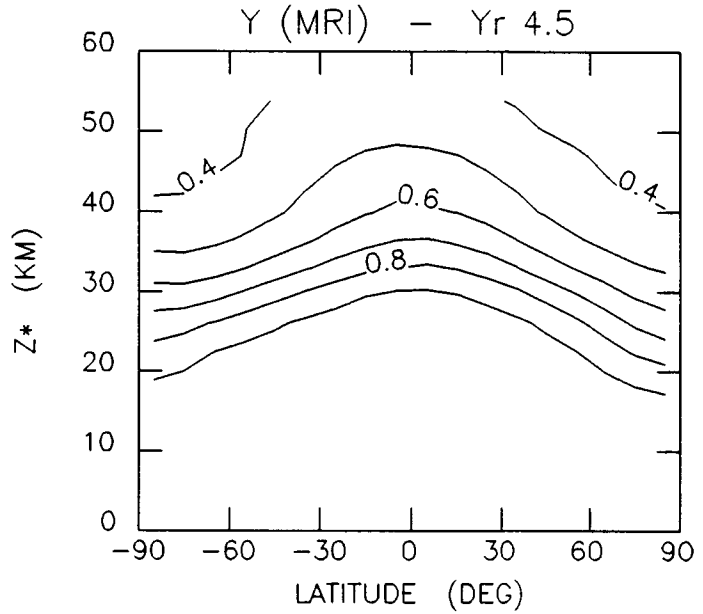
Y (MRI) – Yr 4.5
Z* (KM)
60
50
40
30
20
10
0
0.4
0.6
0.8
0.4
−90 −60 −30 0 30 60 90
LATITUDE (DEG)

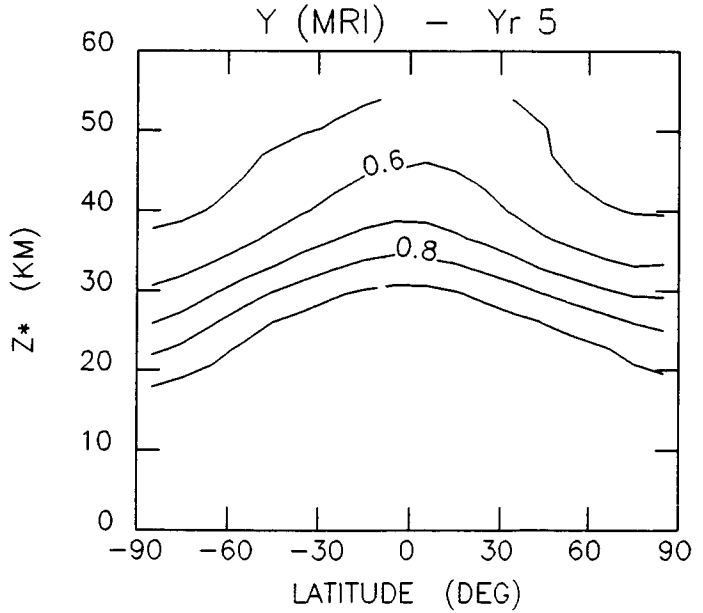
Y (MRI) – Yr 5
Z* (KM)
60
50
40
30
20
10
0
0.6
0.8
−90 −60 −30 0 30 60 90
LATITUDE (DEG)

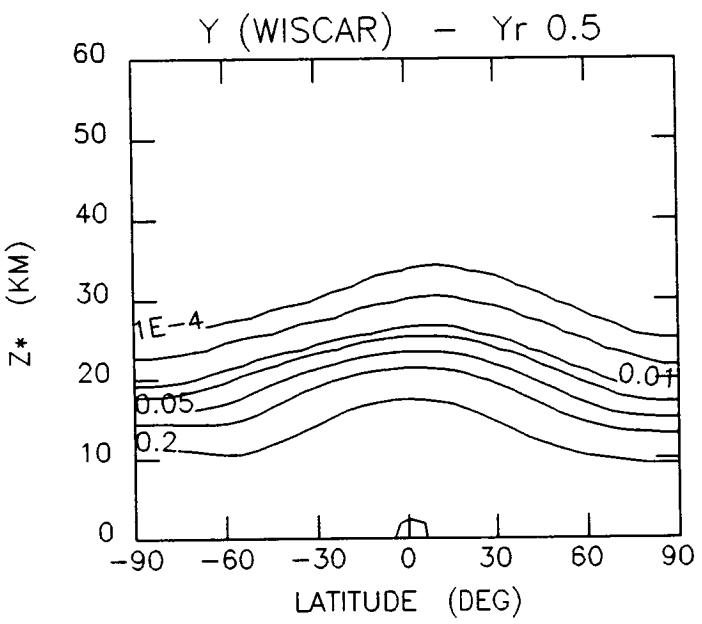
Y (WISCAR) – Yr 0.5
Z* (KM)
LATITUDE (DEG)
1E-4
0.01
0.05
0.2

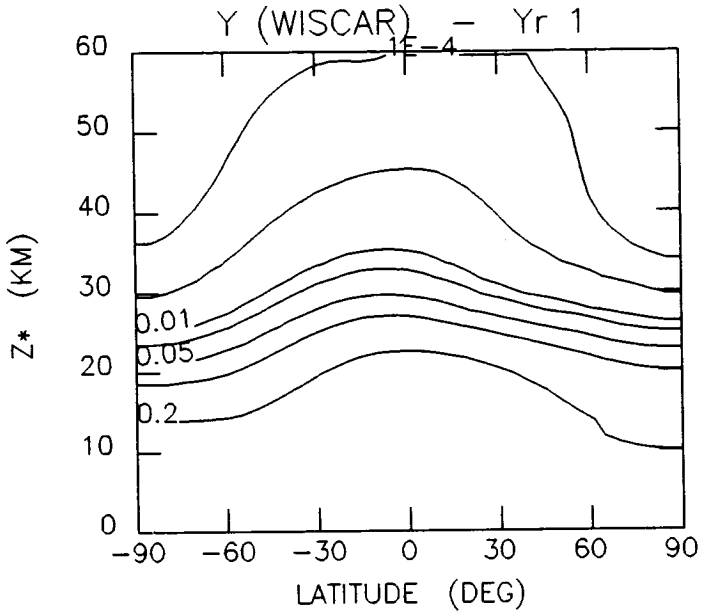
Y (WISCAR) – Yr 1
Z* (KM)
LATITUDE (DEG)
1E-4
0.01
0.05
0.2

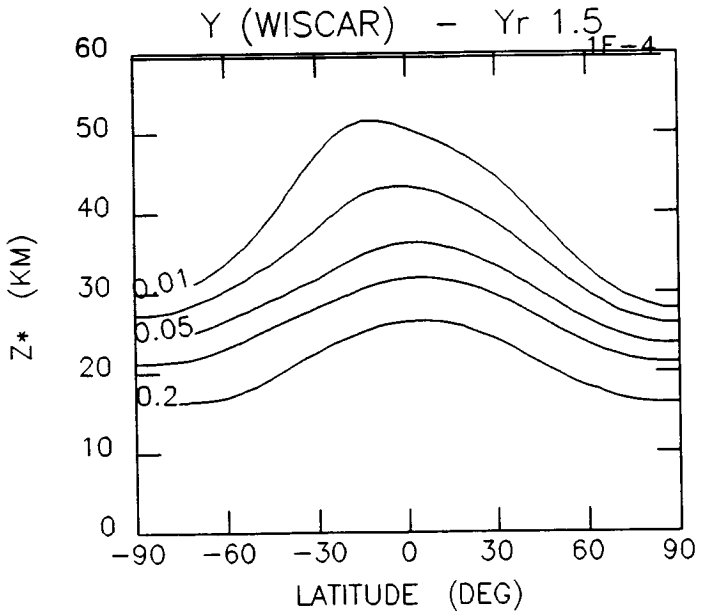
Y (WISCAR) – Yr 1.5
Z* (KM)
LATITUDE (DEG)
1E-4
0.01
0.05
0.2

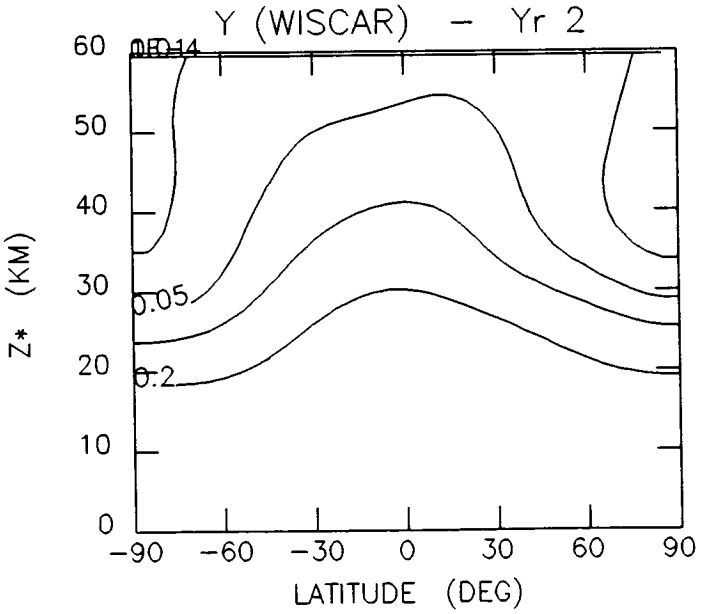
Y (WISCAR) – Yr 2
Z* (KM)
LATITUDE (DEG)
0.05
0.2

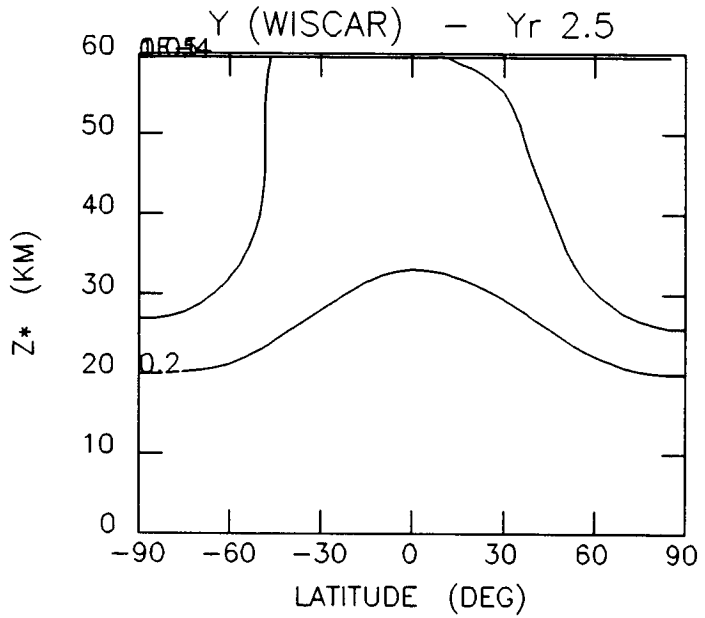
Y (WISCAR) – Yr 2.5
Z* (KM)
LATITUDE (DEG)
0.2

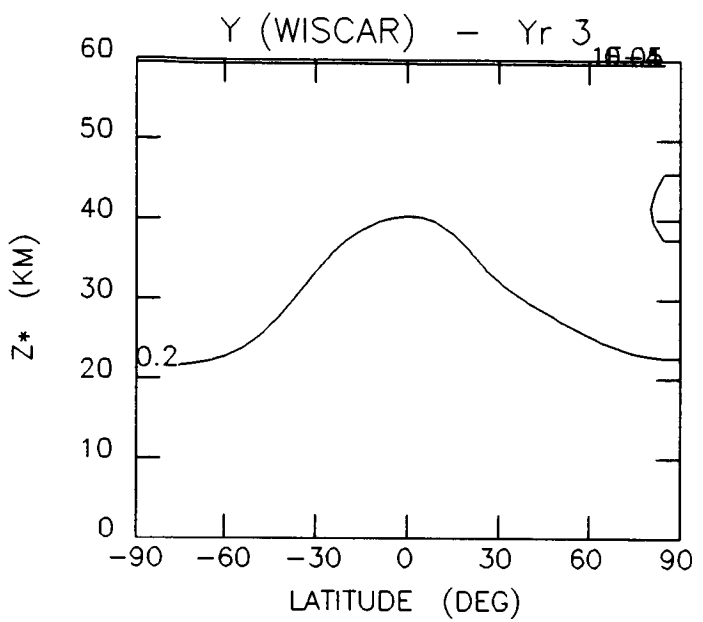
Y (WISCAR) – Yr 3
Z* (KM)
LATITUDE (DEG)
0.2

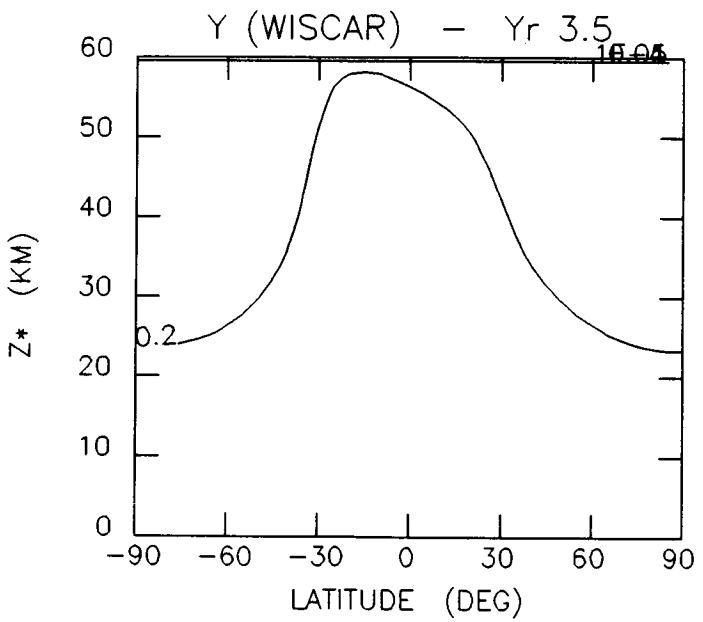
Y (WISCAR) – Yr 3.5
Z* (KM)
LATITUDE (DEG)
0.2

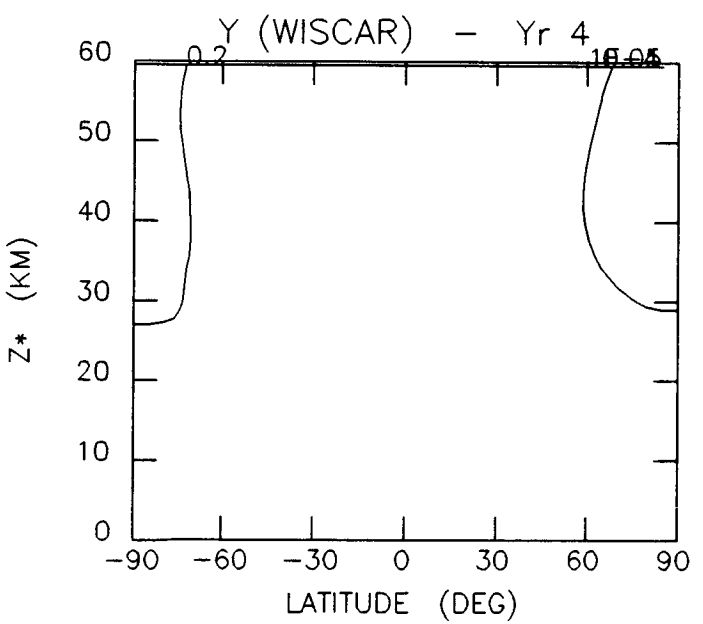
Y (WISCAR) – Yr 4
Z* (KM)
LATITUDE (DEG)
0.2

**Table 6-2d.** Stratospheric Source Tracer Experiment

Steady-state; Twelve months with January as month 1.
Integrated columns of tracer Z and of $O_3$ above $z^* = 0$; $z^* = 16 \log_{10}(1000/P)$.
Models Represented - AER, CALJPL, CLKSON, GISS-3D, GSFC2, LARC, LLNL, MRI, OSLO, WISCAR

| Parameter | Description | Units | Contour Levels |
|---|---|---|---|
| Z COLUMN | Integrated Column of Stratospheric Source Gas Z | Dobson Units | 100, 120, 140, 160, 180, 200, 250, 300, 350, 400, 500, 600 |
| $O_3$ COLUMN | Integrated Column of $O_3$ | Dobson Units | 200, 220, 240, 260, 280, 300, 320, 340, 360, 380, 400, 450, 500, 550, 600 |

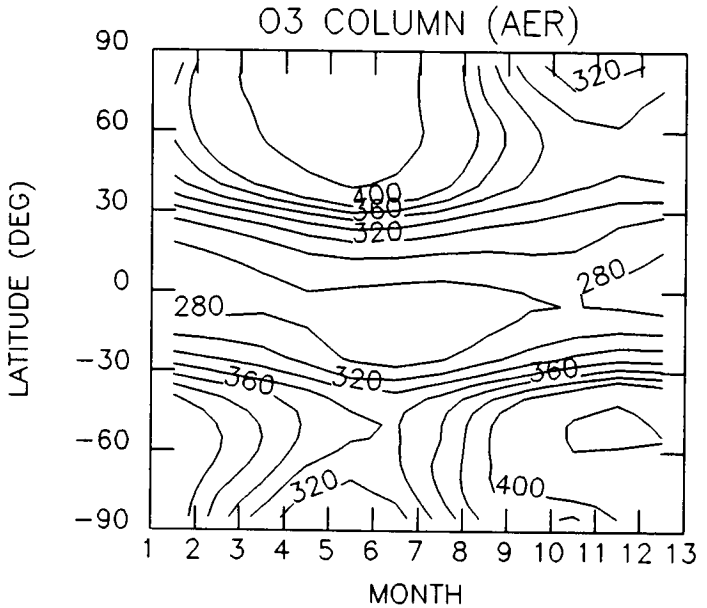
O3 COLUMN (AER)
LATITUDE (DEG)
90
60
30
0
-30
-60
-90
1 2 3 4 5 6 7 8 9 10 11 12 13
MONTH
320
400
360
320
280
280
360
320
360
320
400

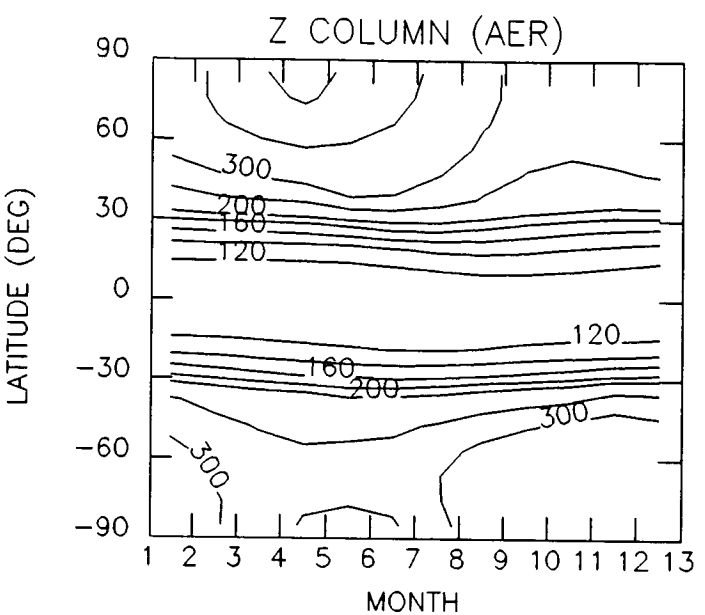
Z COLUMN (AER)
LATITUDE (DEG)
90
60
30
0
-30
-60
-90
1 2 3 4 5 6 7 8 9 10 11 12 13
MONTH
300
200
160
120
120
160
200
300
300

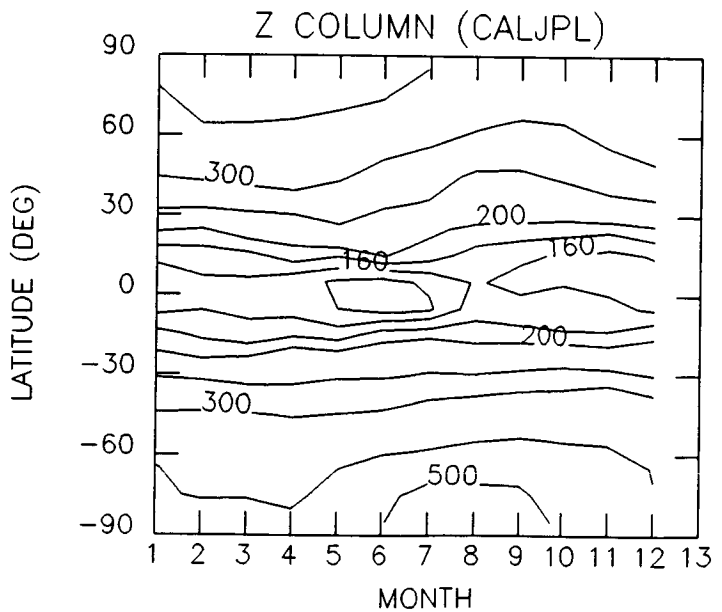
Z COLUMN (CALJPL)
LATITUDE (DEG)
90
60
30
0
-30
-60
-90
1 2 3 4 5 6 7 8 9 10 11 12 13
MONTH
300
200
160
160
200
300
500

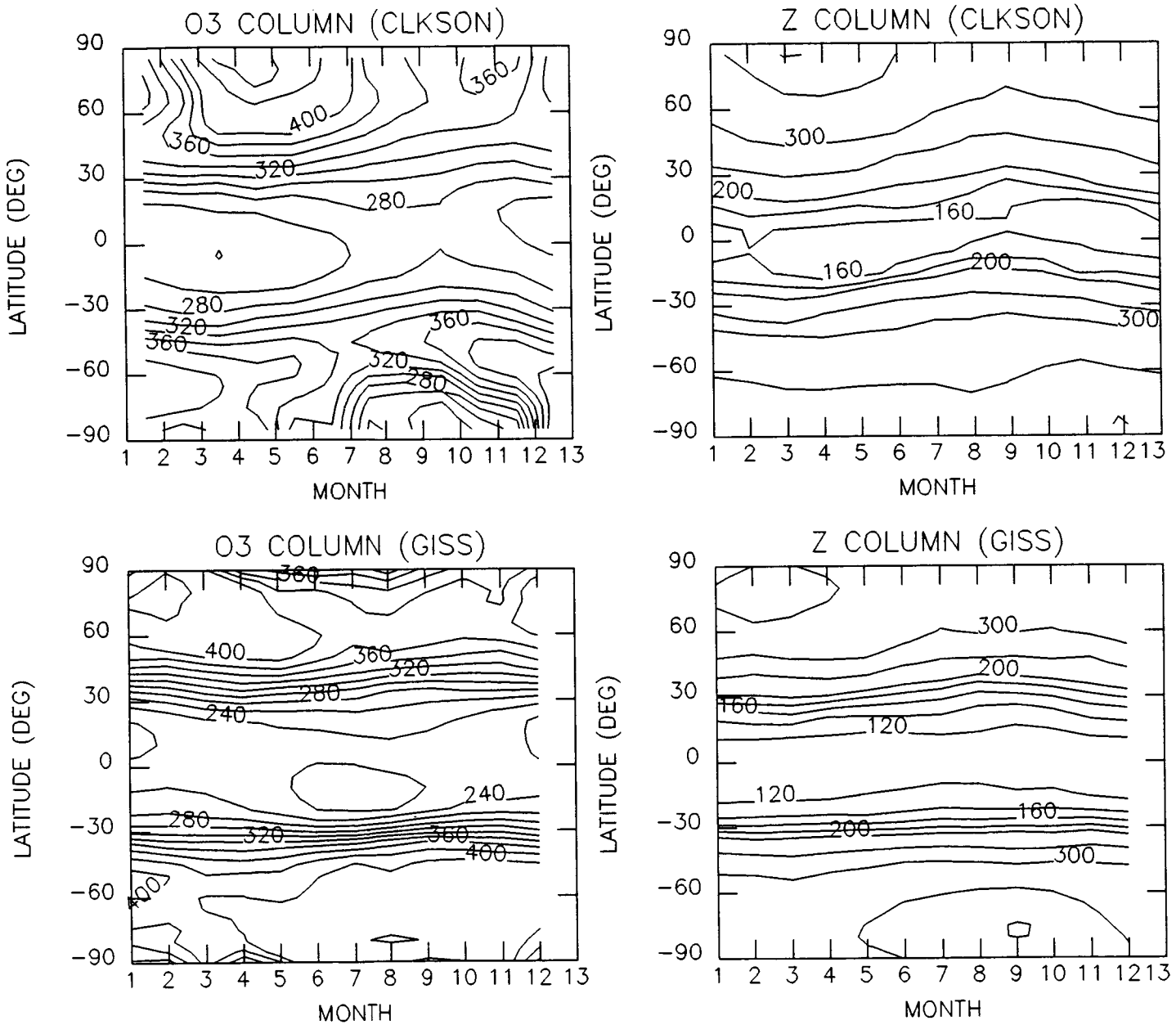
O3 COLUMN (CLKSON)
LATITUDE (DEG)
MONTH
Z COLUMN (CLKSON)
LATITUDE (DEG)
MONTH
O3 COLUMN (GISS)
LATITUDE (DEG)
MONTH
Z COLUMN (GISS)
LATITUDE (DEG)
MONTH

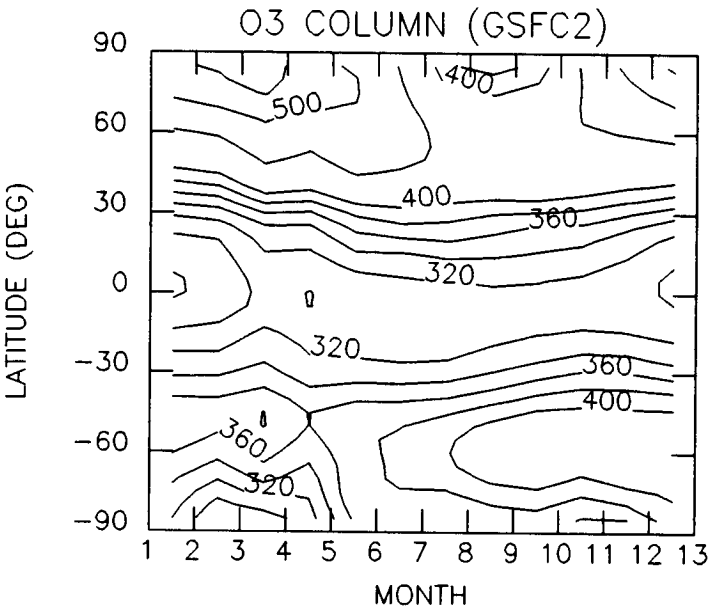
O3 COLUMN (GSFC2)
LATITUDE (DEG)
90
60
30
0
-30
-60
-90
500
400
400
360
320
320
360
400
360
320
1 2 3 4 5 6 7 8 9 10 11 12 13
MONTH

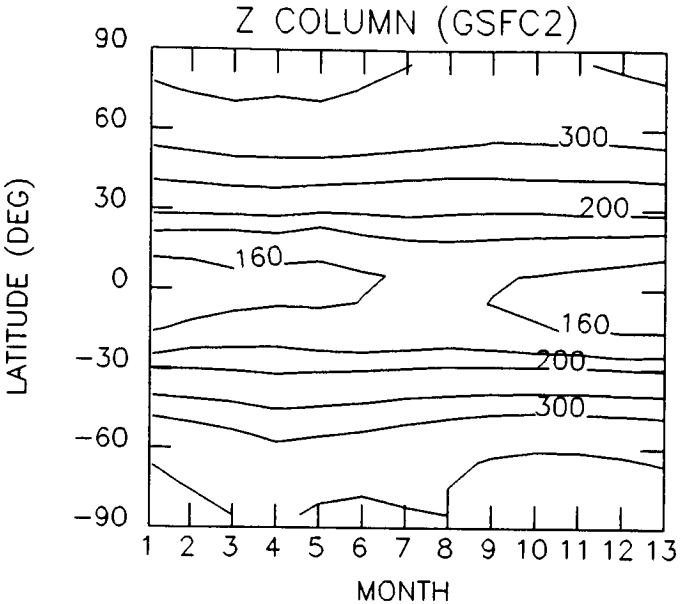
Z COLUMN (GSFC2)
LATITUDE (DEG)
90
60
30
0
-30
-60
-90
300
200
160
160
200
300
1 2 3 4 5 6 7 8 9 10 11 12 13
MONTH

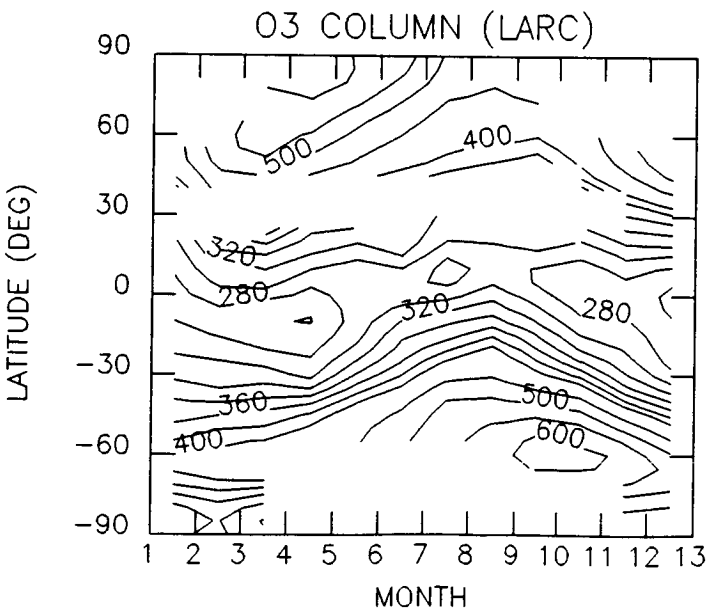
O3 COLUMN (LARC)
LATITUDE (DEG)
90
60
30
0
-30
-60
-90
500
400
320
280
320
280
360
500
400
600
1 2 3 4 5 6 7 8 9 10 11 12 13
MONTH

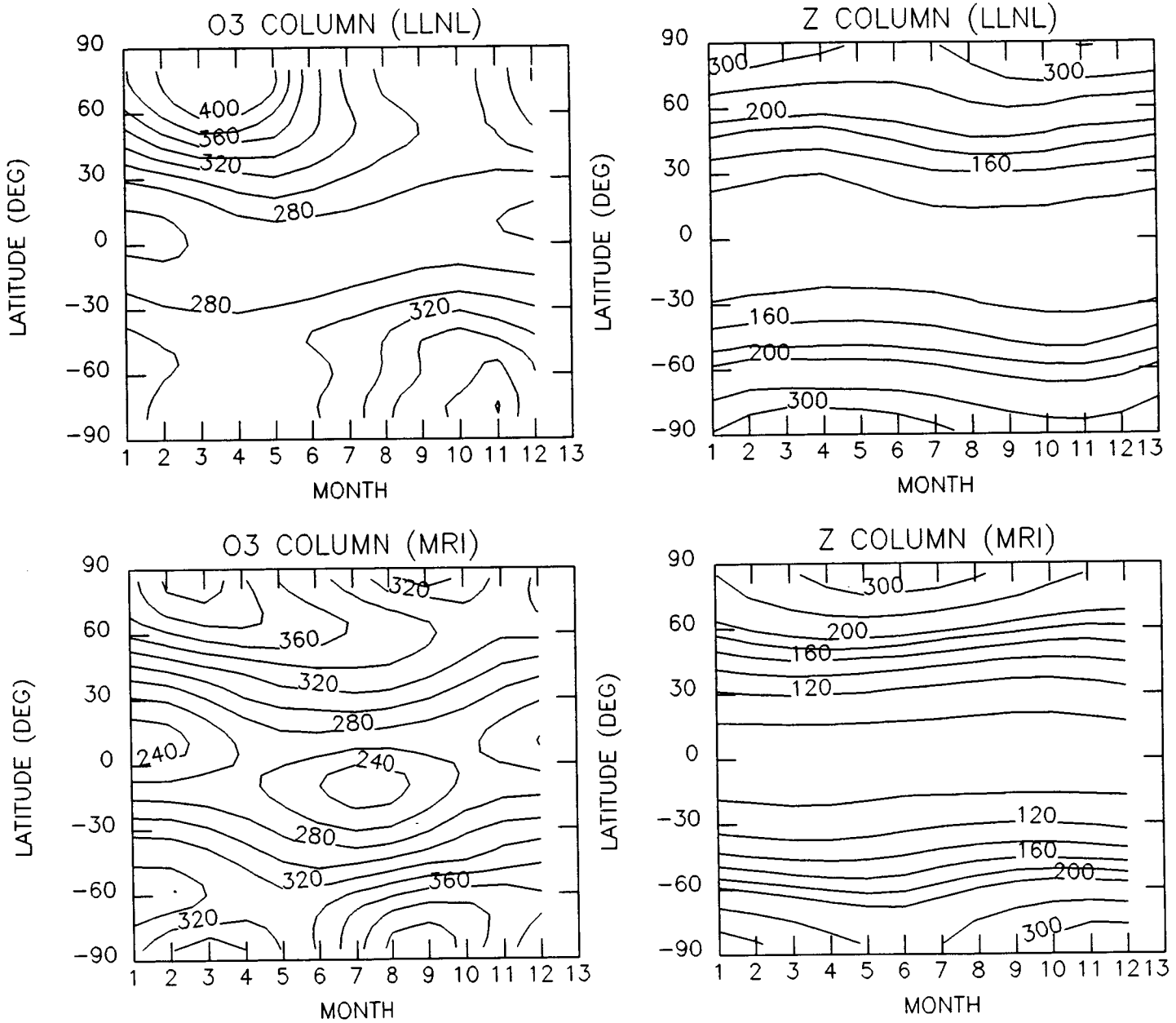
O3 COLUMN (LLNL)
Z COLUMN (LLNL)
O3 COLUMN (MRI)
Z COLUMN (MRI)
LATITUDE (DEG)
MONTH
90
60
30
0
-30
-60
-90
1 2 3 4 5 6 7 8 9 10 11 12 13
400
360
320
280
240
300
200
160
120

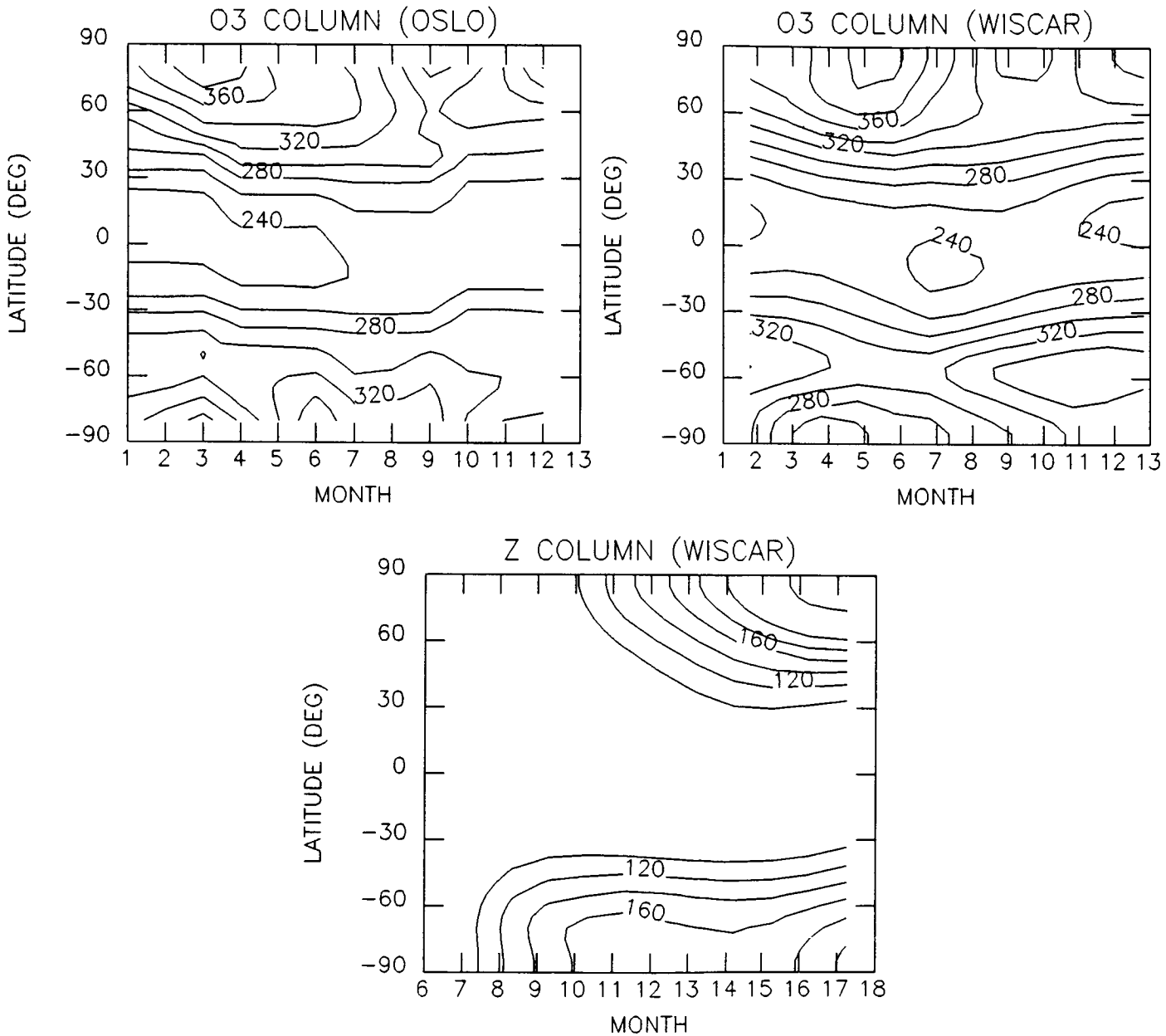
O3 COLUMN (OSLO)
LATITUDE (DEG)
90
60
30
0
-30
-60
-90
360
320
280
240
280
320
1 2 3 4 5 6 7 8 9 10 11 12 13
MONTH
O3 COLUMN (WISCAR)
LATITUDE (DEG)
360
320
280
240
240
280
320
320
280
1 2 3 4 5 6 7 8 9 10 11 12 13
MONTH
Z COLUMN (WISCAR)
LATITUDE (DEG)
160
120
120
160
6 7 8 9 10 11 12 13 14 15 16 17 18
MONTH

**Table 6-3a.** Current Atmosphere(1980): Integrated Trace Gas Columns

Steady-state; Twelve months with January as month 1
Integrated columns of $HNO_3$, HCl, and ClO above $z^* = 12$; integrated column of $NO_2$ above $z^* = 0$; $z^* = 16 \log_{10}(1000/P)$
Models Represented - AER, CLKSON, GSFC2, LARC, LLNL, MRI, OSLO, WISCAR

| Parameter | Description | Units | Contour Levels |
|---|---|---|---|
| $HNO_3$ COLUMN | Integrated Column of $HNO_3$ | 10E+15 Molecules/$cm^2$ | 2, 3, 4, 5, 6, 8, 10, 12, 14, 16, 18, 20, 22, 24 |
| HCl COLUMN | Integrated Column of HCl | 10E+15 Molecules/$cm^2$ | 0.5, 0.75, 1, 1.25, 1.5, 1.75, 2, 2.5, 3, 3.5, 4, 4.5, 5, 5.5, 6 |
| $NO_2$ COLUMN | Integrated Column of $NO_2$ | 10E+15 Molecules/$cm^2$ | 0, 0.5, 1, 1.5, 2, 2.5, 3, 4, 5, 6, 7, 8, 9, 10 |
| ClO COLUMN | Integrated Column of ClO | 10E+15 Molecules/$cm^2$ | 0, 0.02, 0.04, 0.06, 0.08, 0.1, 0.12, 0.14, 0.16, 0.18, 0.2, 0.3, 0.4, 0.5, 0.6, 0.7 |

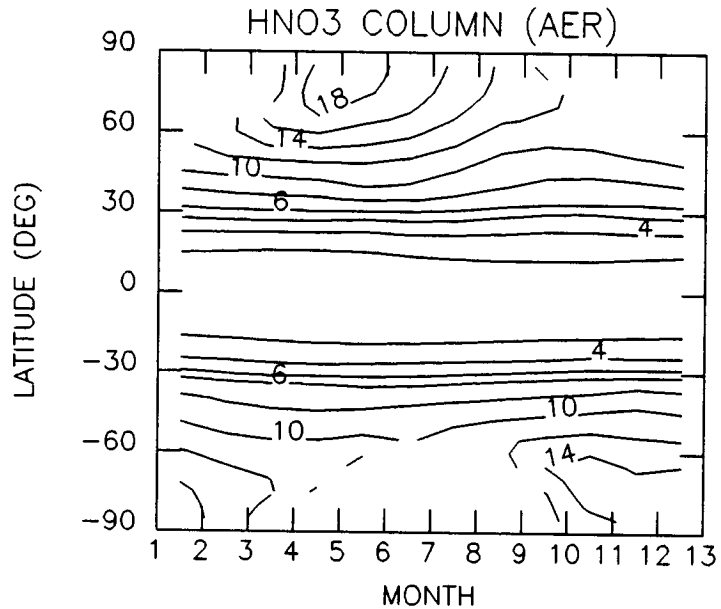
HNO3 COLUMN (AER)
LATITUDE (DEG)
90
60
30
0
-30
-60
-90
18
14
10
6
4
4
6
10
10
14
1 2 3 4 5 6 7 8 9 10 11 12 13
MONTH

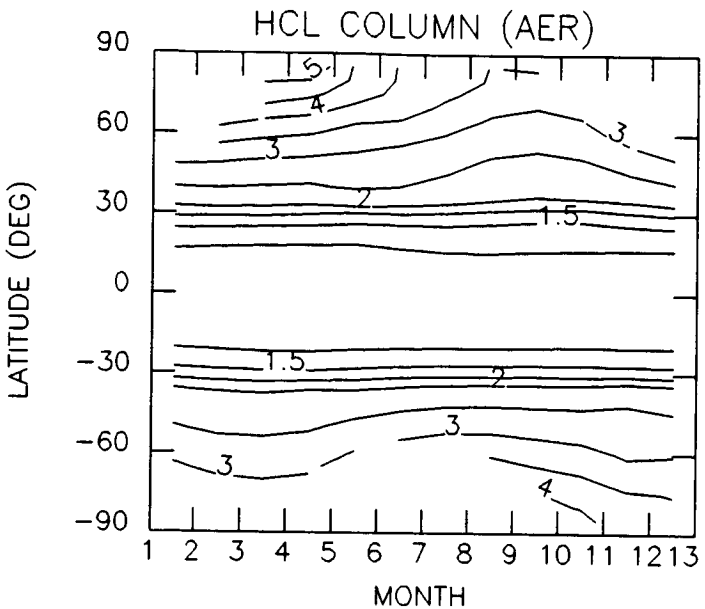
HCL COLUMN (AER)
LATITUDE (DEG)
90
60
30
0
-30
-60
-90
5
4
3
3
2
1.5
1.5
2
3
3
4
1 2 3 4 5 6 7 8 9 10 11 12 13
MONTH

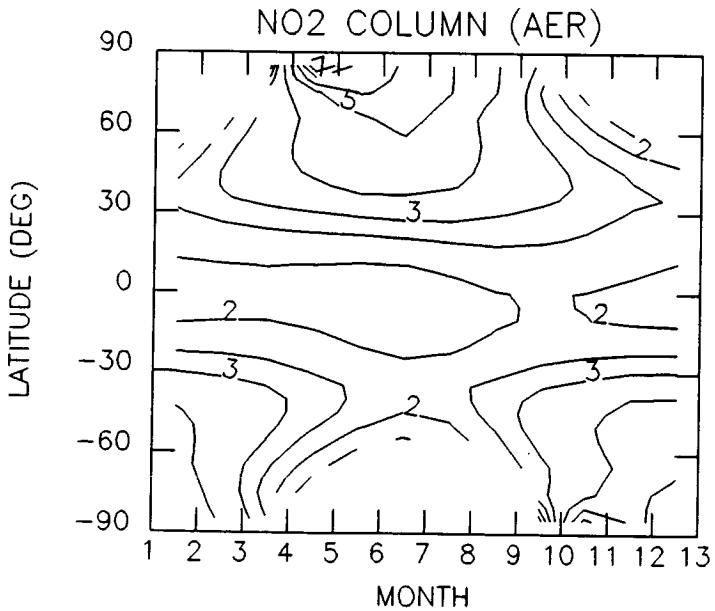
NO2 COLUMN (AER)
LATITUDE (DEG)
90
60
30
0
-30
-60
-90
7
5
2
3
2
2
3
3
2
1 2 3 4 5 6 7 8 9 10 11 12 13
MONTH

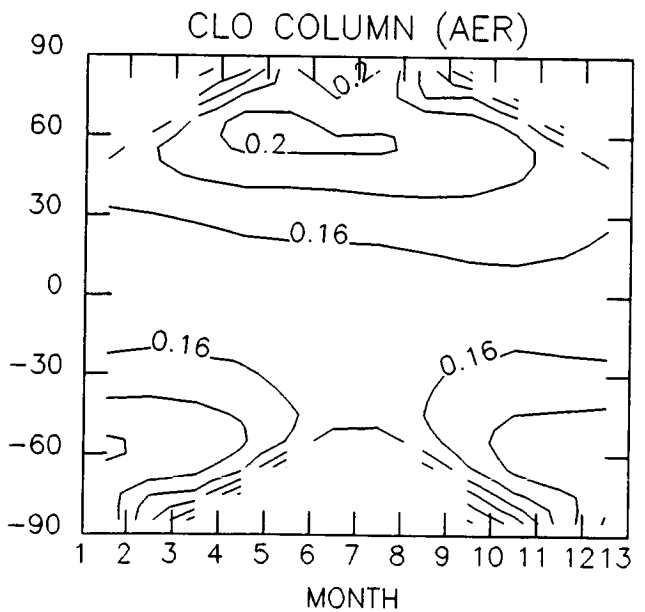
CLO COLUMN (AER)
LATITUDE (DEG)
90
60
30
0
-30
-60
-90
0.2
0.2
0.16
0.16
0.16
1 2 3 4 5 6 7 8 9 10 11 12 13
MONTH

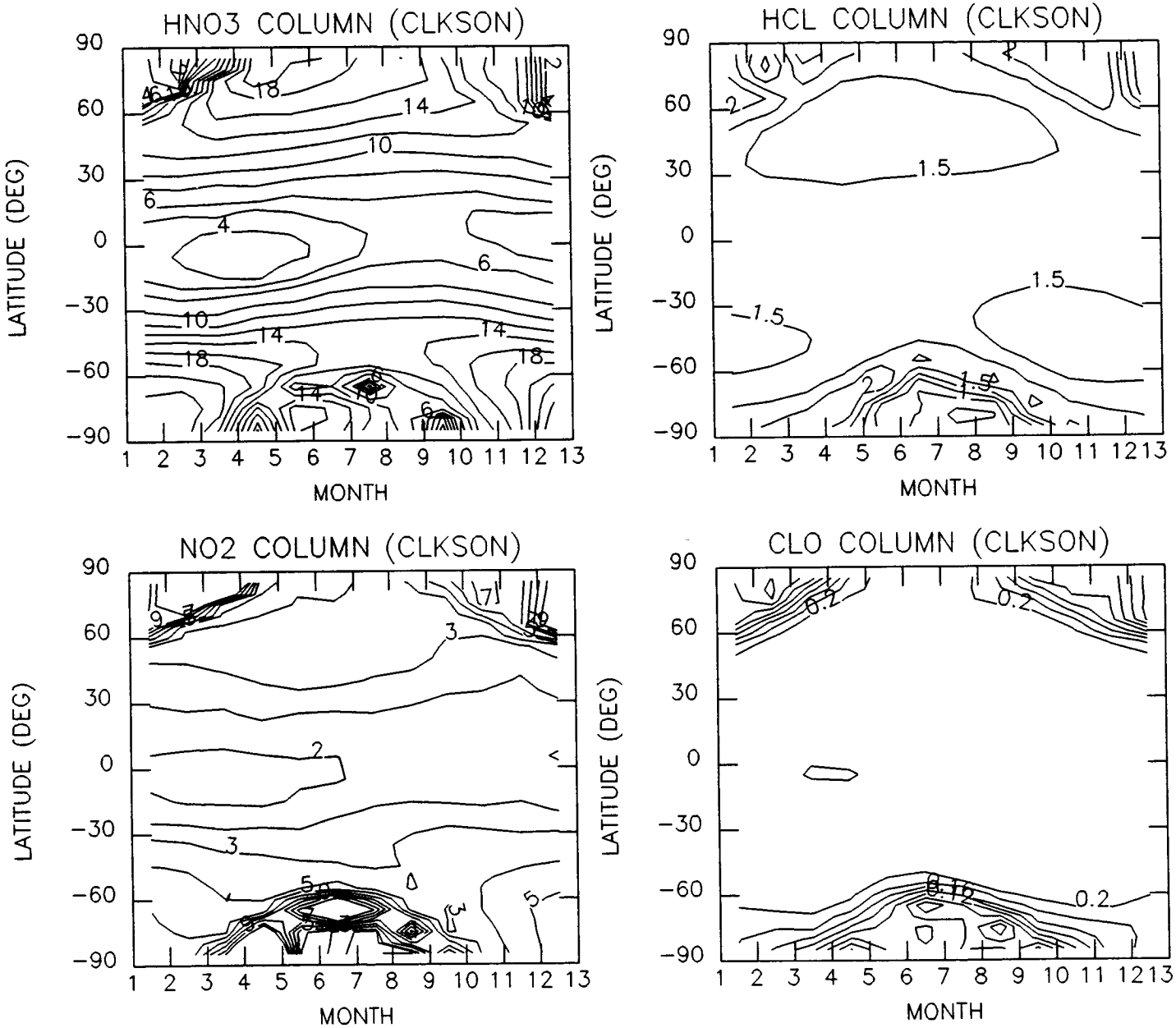
HNO3 COLUMN (CLKSON)
HCL COLUMN (CLKSON)
NO2 COLUMN (CLKSON)
CLO COLUMN (CLKSON)
LATITUDE (DEG)
MONTH
90
60
30
0
-30
-60
-90
1 2 3 4 5 6 7 8 9 10 11 12 13

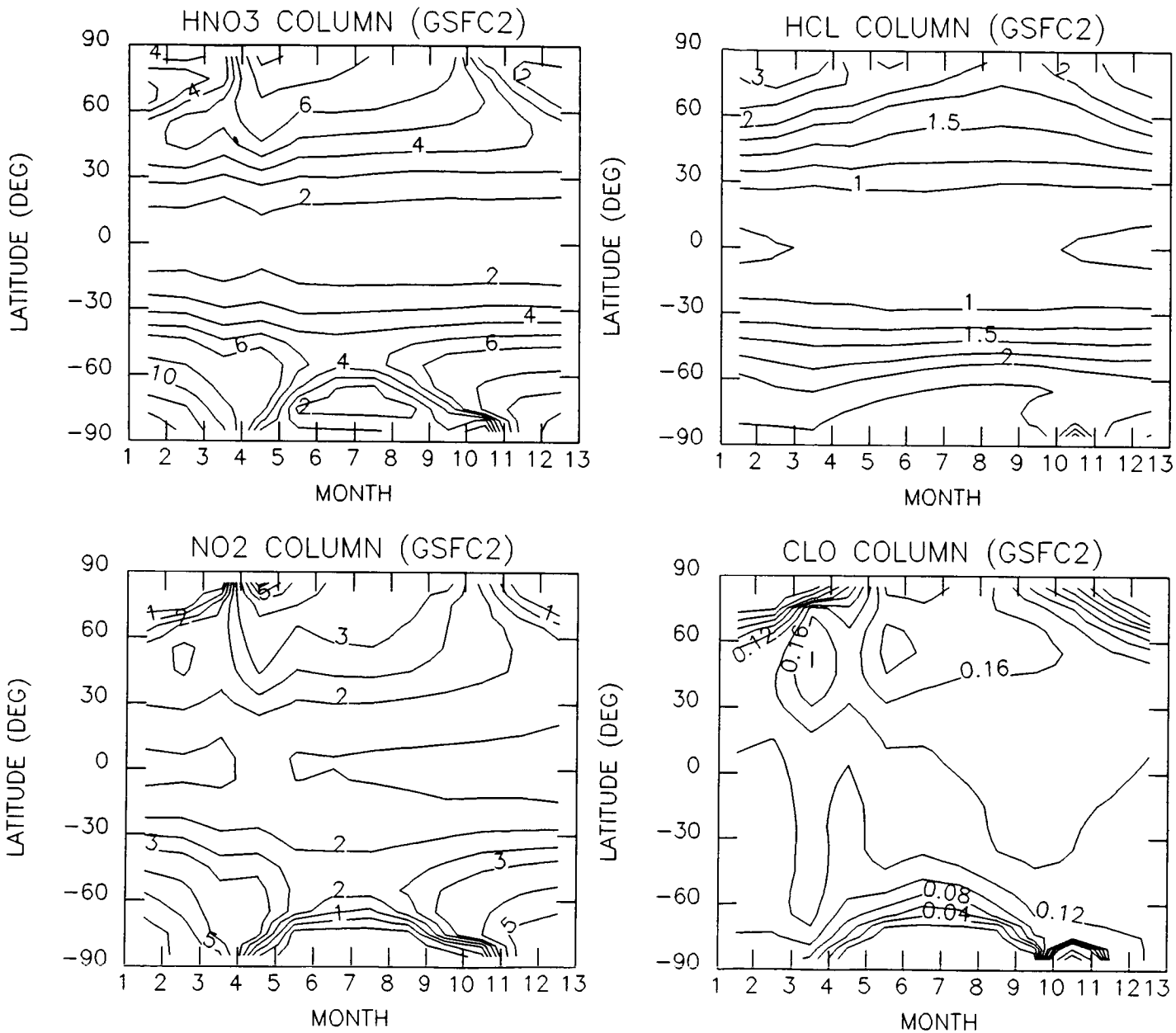
HNO3 COLUMN (GSFC2)
HCL COLUMN (GSFC2)
NO2 COLUMN (GSFC2)
CLO COLUMN (GSFC2)
LATITUDE (DEG)
MONTH
90
60
30
0
-30
-60
-90
1 2 3 4 5 6 7 8 9 10 11 12 13
0.16
0.12
0.08
0.04

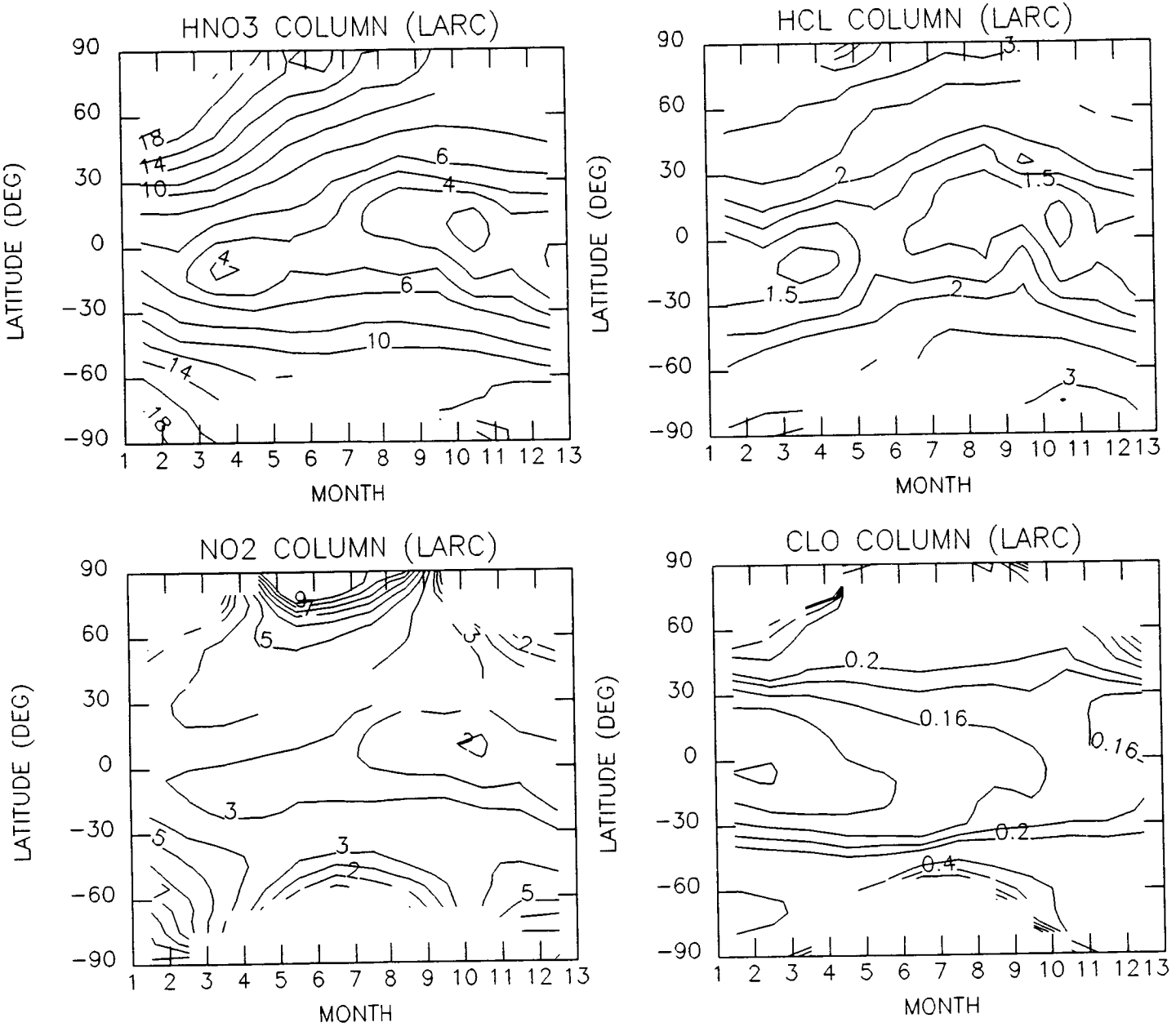
HNO3 COLUMN (LARC)
LATITUDE (DEG)
90
60
30
0
-30
-60
-90
18
14
10
6
4
4
6
10
14
18
1 2 3 4 5 6 7 8 9 10 11 12 13
MONTH
HCL COLUMN (LARC)
LATITUDE (DEG)
3
2
1.5
1.5
2
3
MONTH
NO2 COLUMN (LARC)
LATITUDE (DEG)
9
5
3
2
2
3
5
3
2
5
MONTH
CLO COLUMN (LARC)
LATITUDE (DEG)
0.2
0.16
0.16
0.2
0.4
MONTH

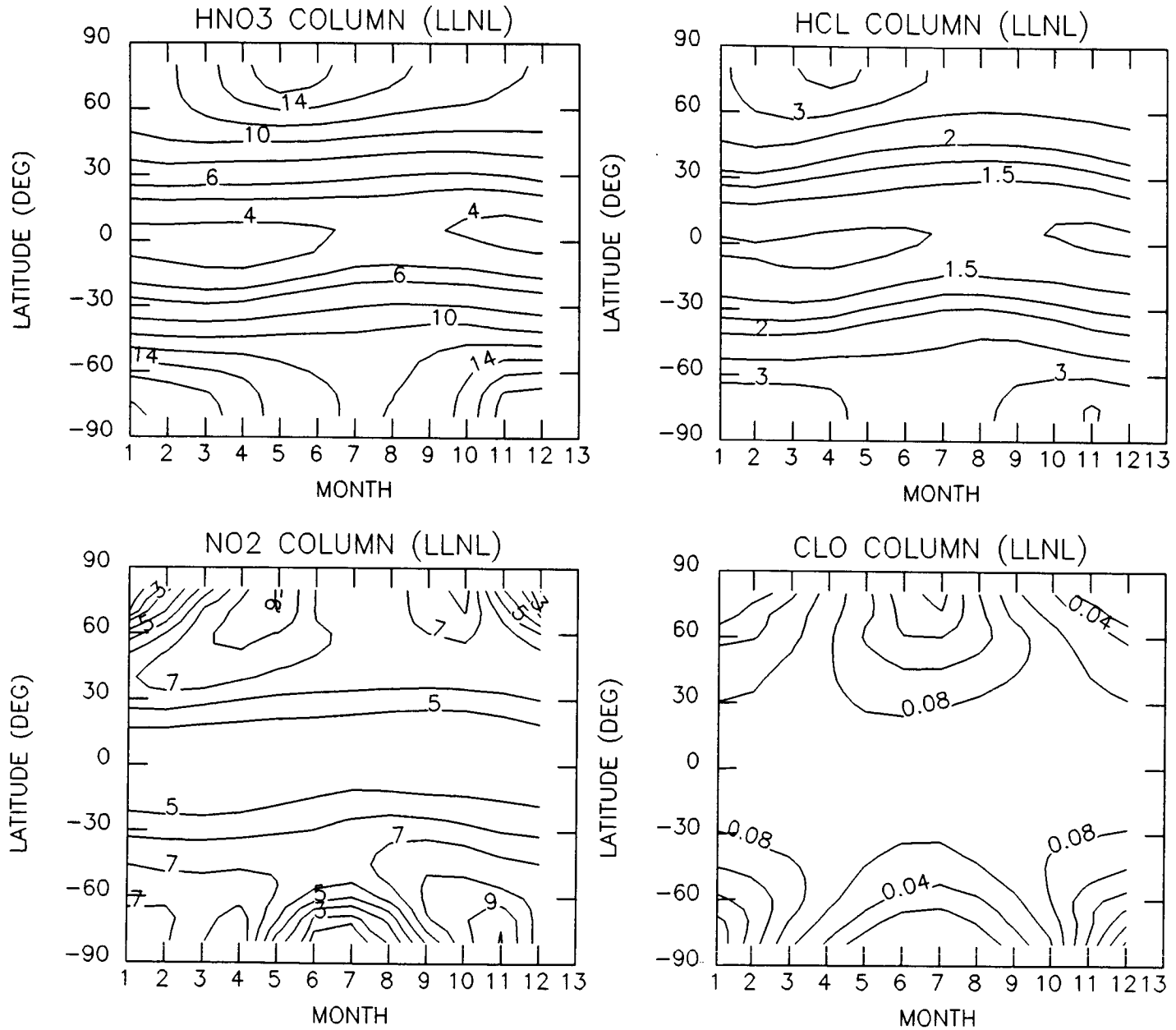
HNO3 COLUMN (LLNL)
HCL COLUMN (LLNL)
NO2 COLUMN (LLNL)
CLO COLUMN (LLNL)
LATITUDE (DEG)
MONTH
90
60
30
0
-30
-60
-90
1 2 3 4 5 6 7 8 9 10 11 12 13
14
10
6
4
3
2
1.5
0.08
0.04

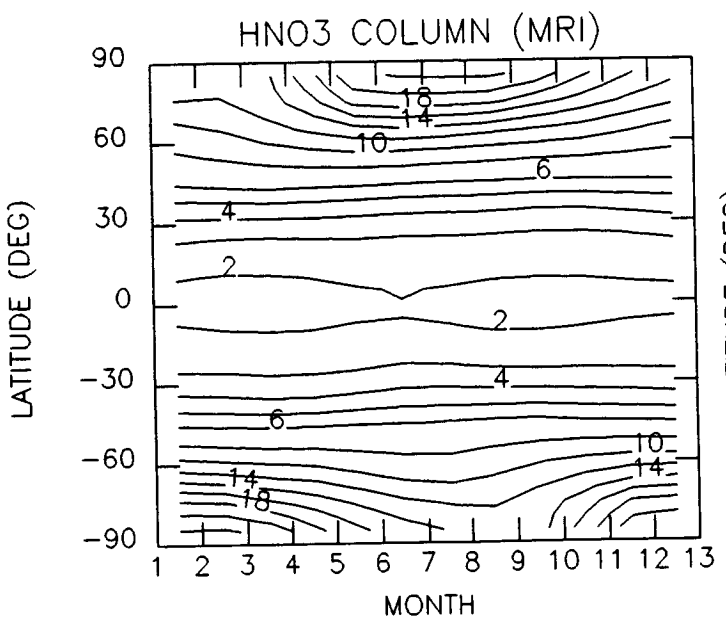
HNO3 COLUMN (MRI)
LATITUDE (DEG)
90
60
30
0
-30
-60
-90
1 2 3 4 5 6 7 8 9 10 11 12 13
MONTH
18
14
10
6
4
2
2
4
6
10
14
18

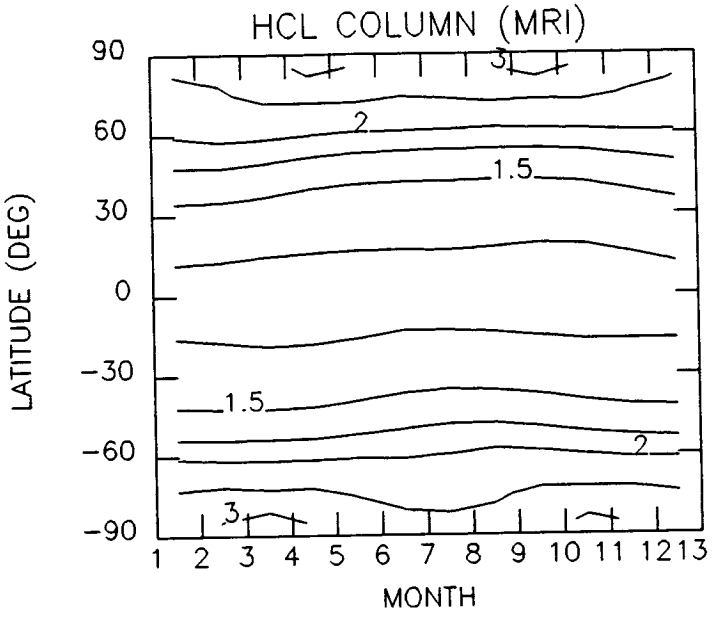
HCL COLUMN (MRI)
LATITUDE (DEG)
90
60
30
0
-30
-60
-90
1 2 3 4 5 6 7 8 9 10 11 12 13
MONTH
3
2
1.5
1.5
2
3

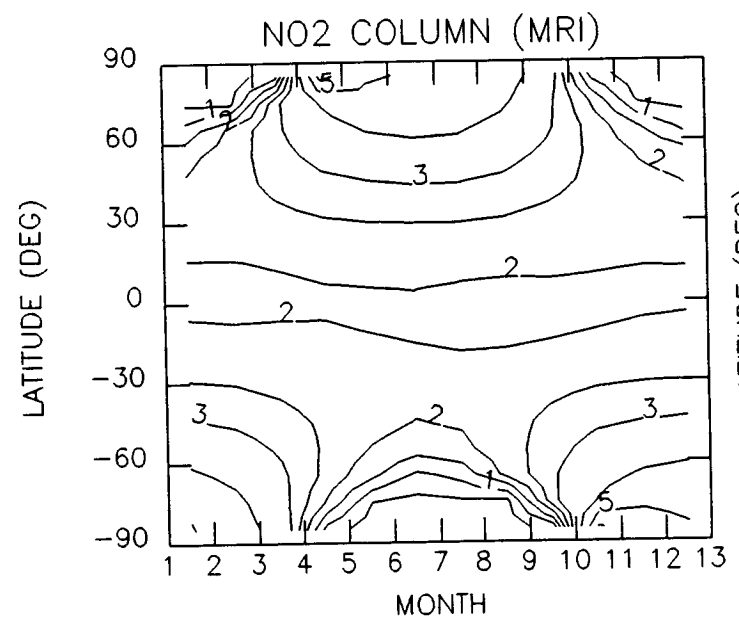
NO2 COLUMN (MRI)
LATITUDE (DEG)
90
60
30
0
-30
-60
-90
1 2 3 4 5 6 7 8 9 10 11 12 13
MONTH
5
1
1
3
2
2
2
3
2
3
1
5

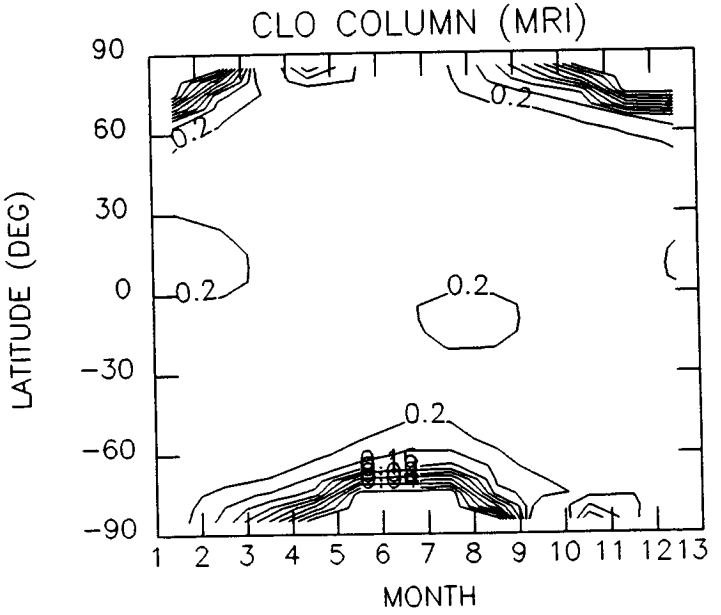
CLO COLUMN (MRI)
LATITUDE (DEG)
90
60
30
0
-30
-60
-90
1 2 3 4 5 6 7 8 9 10 11 12 13
MONTH
0.2
0.2
0.2
0.2
0.2

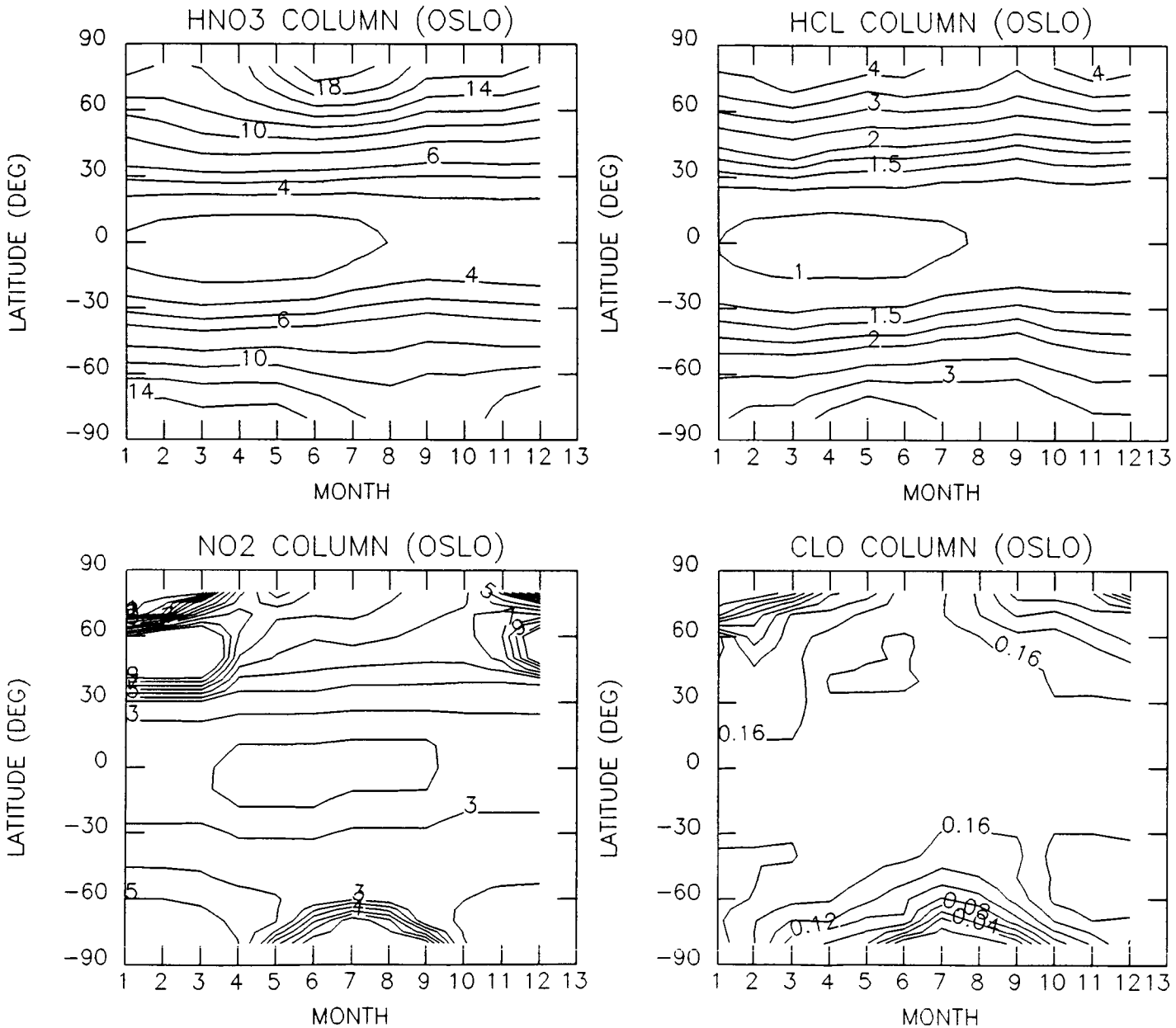
HNO3 COLUMN (OSLO)
HCL COLUMN (OSLO)
NO2 COLUMN (OSLO)
CLO COLUMN (OSLO)
LATITUDE (DEG)
MONTH
90
60
30
0
-30
-60
-90
1 2 3 4 5 6 7 8 9 10 11 12 13
18
14
10
6
4
1
1.5
2
3
0.16
0.12
0.08
0.04

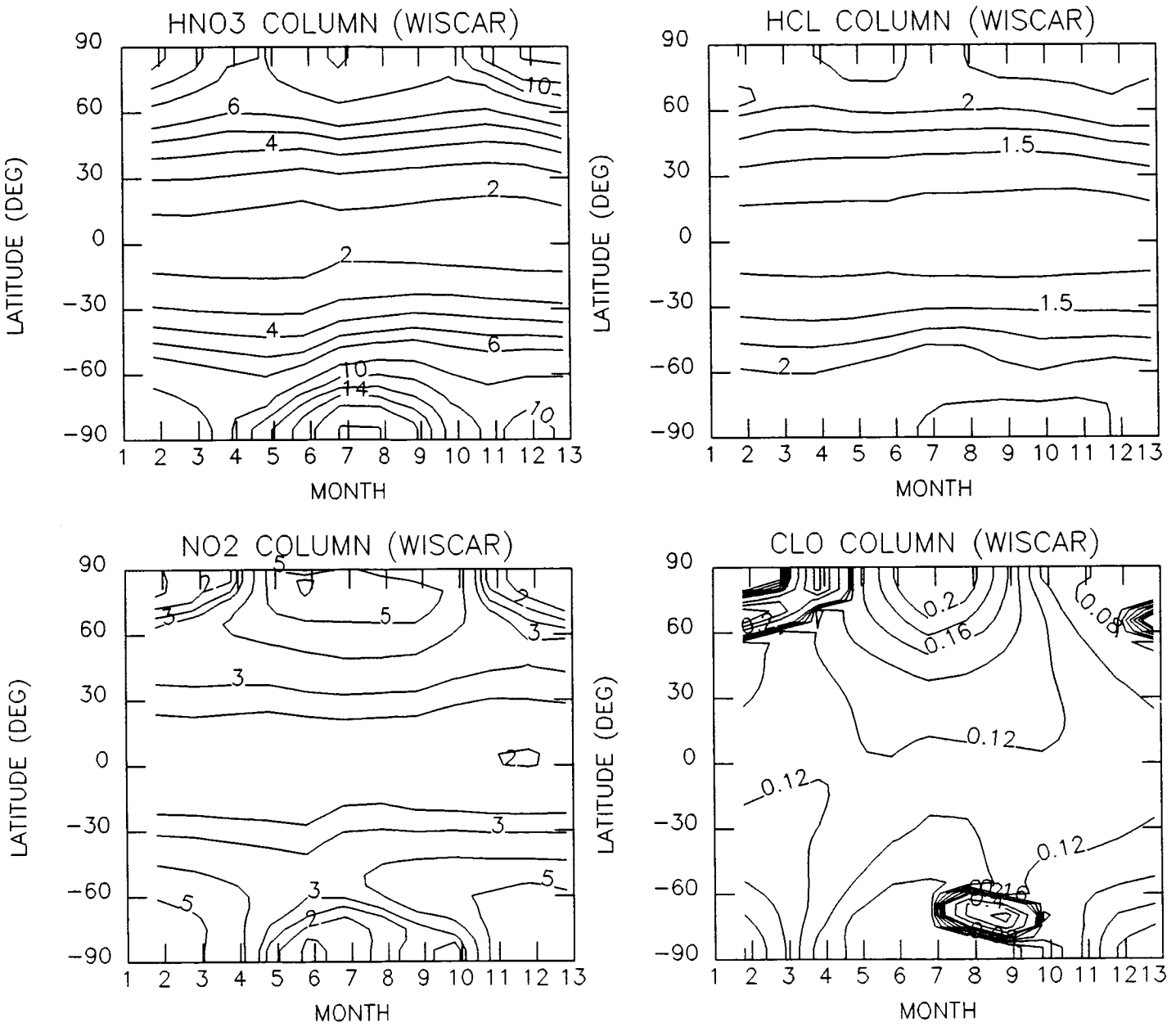
HNO3 COLUMN (WISCAR)
HCL COLUMN (WISCAR)
NO2 COLUMN (WISCAR)
CLO COLUMN (WISCAR)
LATITUDE (DEG)
MONTH
90
60
30
0
-30
-60
-90
1 2 3 4 5 6 7 8 9 10 11 12 13
10
6
4
2
14
1.5
0.2
0.16
0.12
0.08
0.04

**Table 6-3b.** Current Atmosphere (1980): $Cl_y$ and $NO_y$

March, June, September, and December
Models Represented - AER, CAMBRAL, CLKSON, DUPONT (Jan. & April), GSFC1 (Jan.), GSFC2, LARC, LLNL, MRI, NOCAR, OSLO, WISCAR

| Parameter | Description | Units | Contour Levels |
|---|---|---|---|
| $NO_y$ | Sum of Odd Nitrogen Gas Mixing Ratios | ppbv | 1, 2, 4, 6, 8, 10, 12, 14, 16, 18, 20, 22, 24, 26, 28, 30 |
| $Cl_y$ | Sum of Odd Chlorine Gas Mixing Ratios | ppbv | 0.1, 0.5, 1, 1.4, 1.8, 2, 2.2, 2.4, 2.6, 2.8, 3, 3.2, 3.4, 3.6, 3.8, 4 |

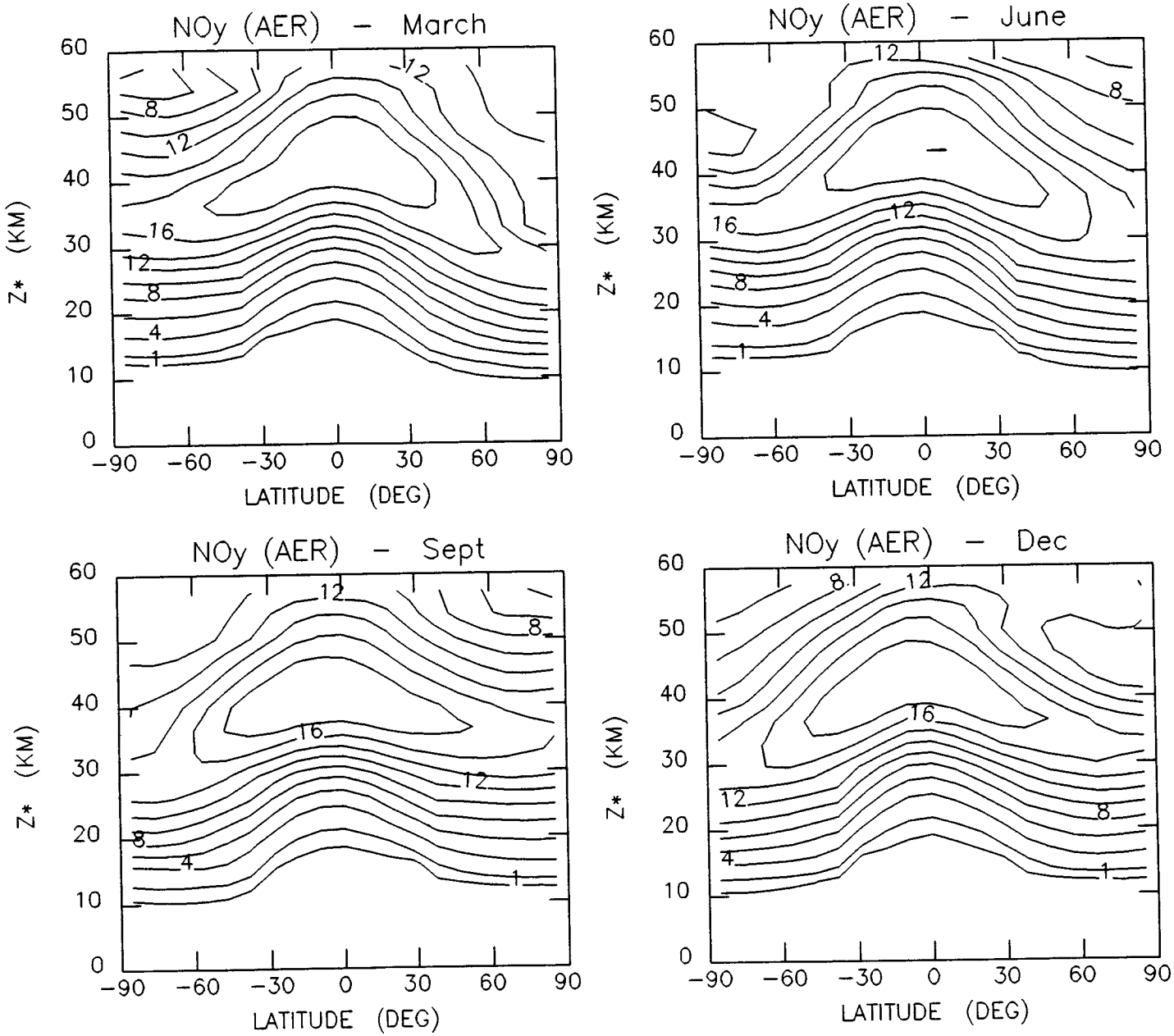
NOy (AER) – March
NOy (AER) – June
NOy (AER) – Sept
NOy (AER) – Dec
Z* (KM)
LATITUDE (DEG)
0
10
20
30
40
50
60
-90
-60
-30
0
30
60
90
1
4
8
12
16

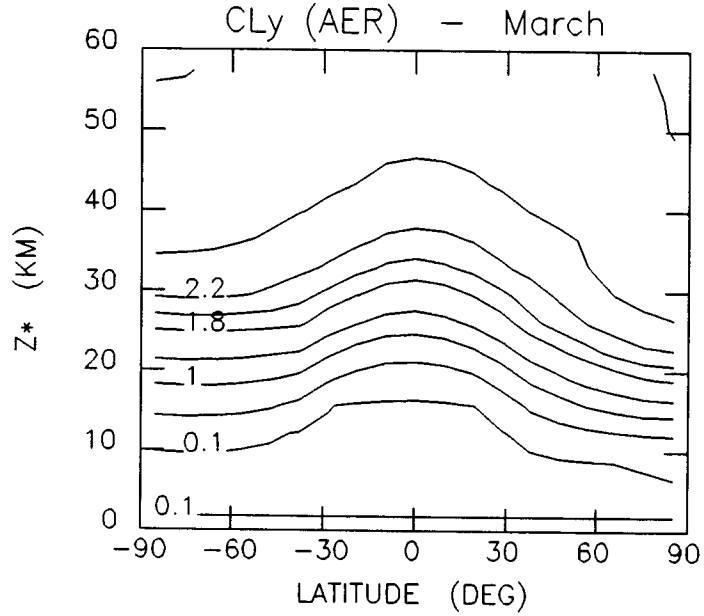
CLy (AER) – March
Z* (KM)
LATITUDE (DEG)
2.2
1.8
1
0.1
0.1

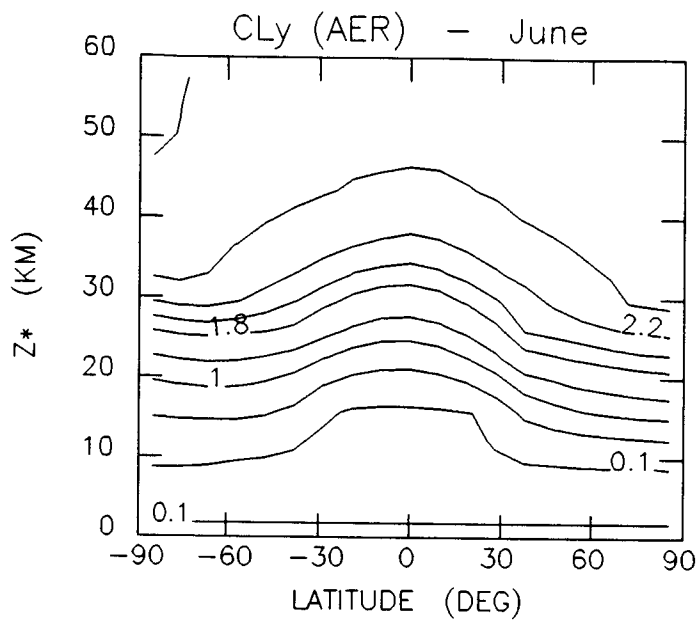
CLy (AER) – June
Z* (KM)
LATITUDE (DEG)
2.2
1.8
1
0.1
0.1

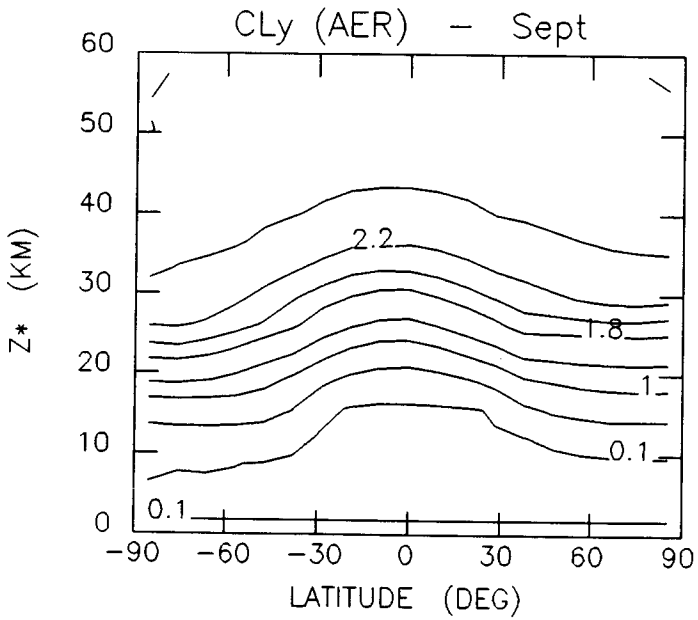
CLy (AER) – Sept
Z* (KM)
LATITUDE (DEG)
2.2
1.8
1
0.1
0.1

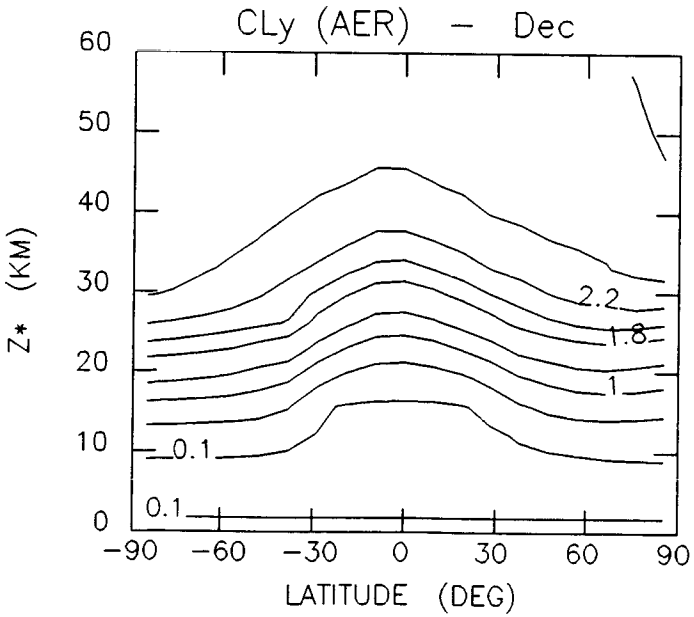
CLy (AER) – Dec
Z* (KM)
LATITUDE (DEG)
2.2
1.8
1
0.1
0.1

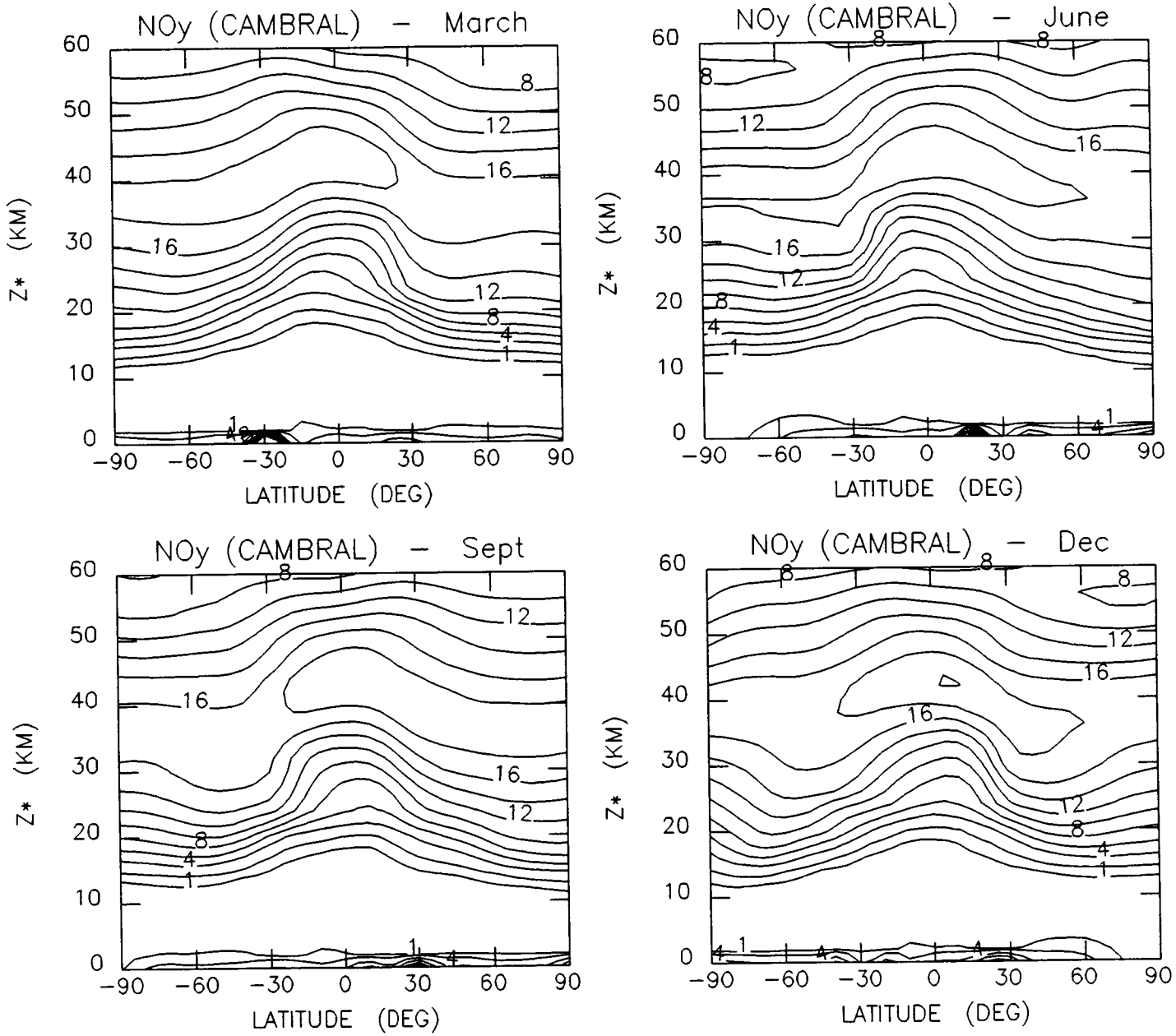
NOy (CAMBRAL) – March
NOy (CAMBRAL) – June
NOy (CAMBRAL) – Sept
NOy (CAMBRAL) – Dec
Z* (KM)
LATITUDE (DEG)
0
10
20
30
40
50
60
-90
-60
-30
0
30
60
90
1
4
8
12
16

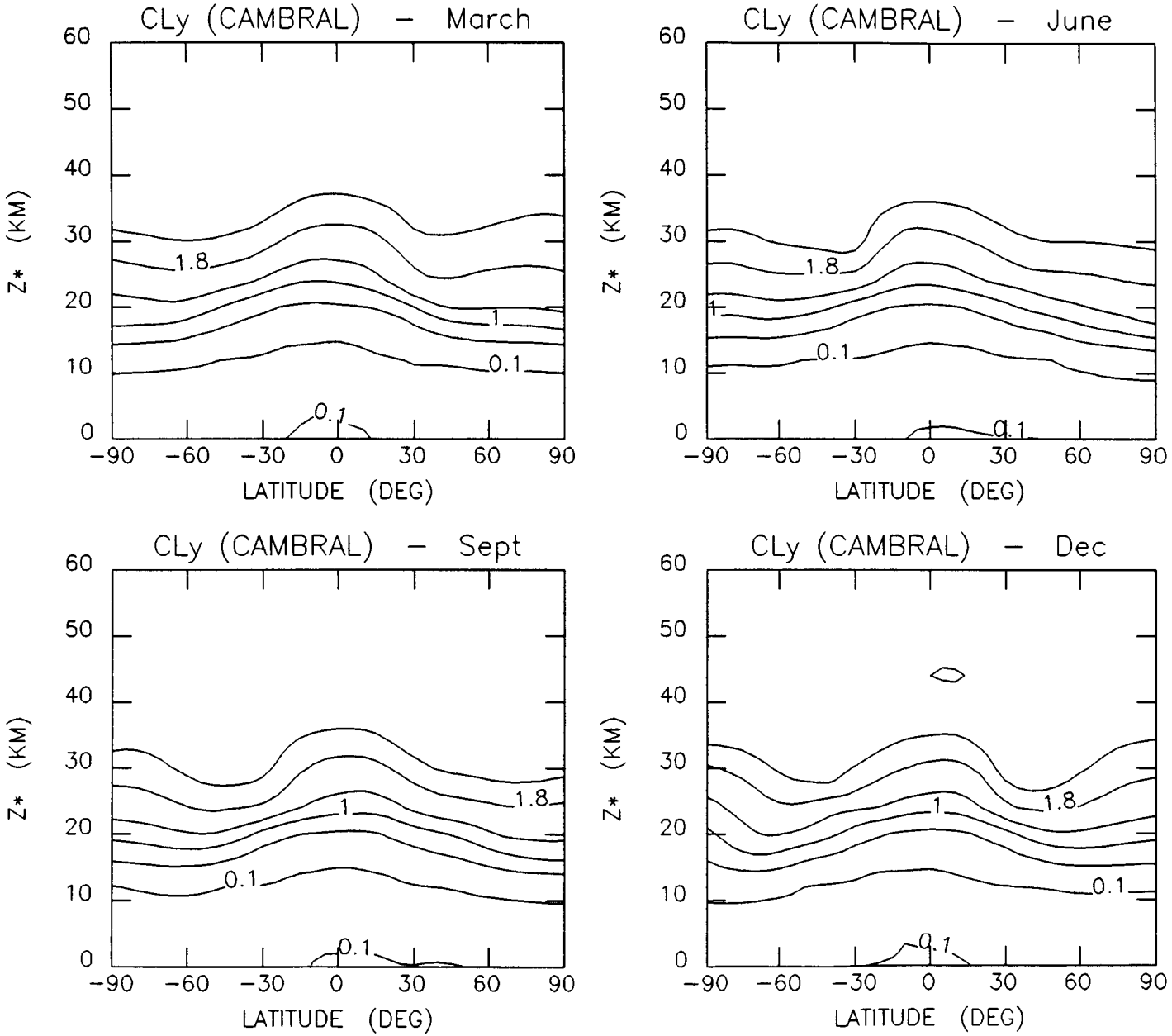
CLy (CAMBRAL) – March
CLy (CAMBRAL) – June
CLy (CAMBRAL) – Sept
CLy (CAMBRAL) – Dec
Z* (KM)
LATITUDE (DEG)
60
50
40
30
20
10
0
−90 −60 −30 0 30 60 90
1.8
1
0.1

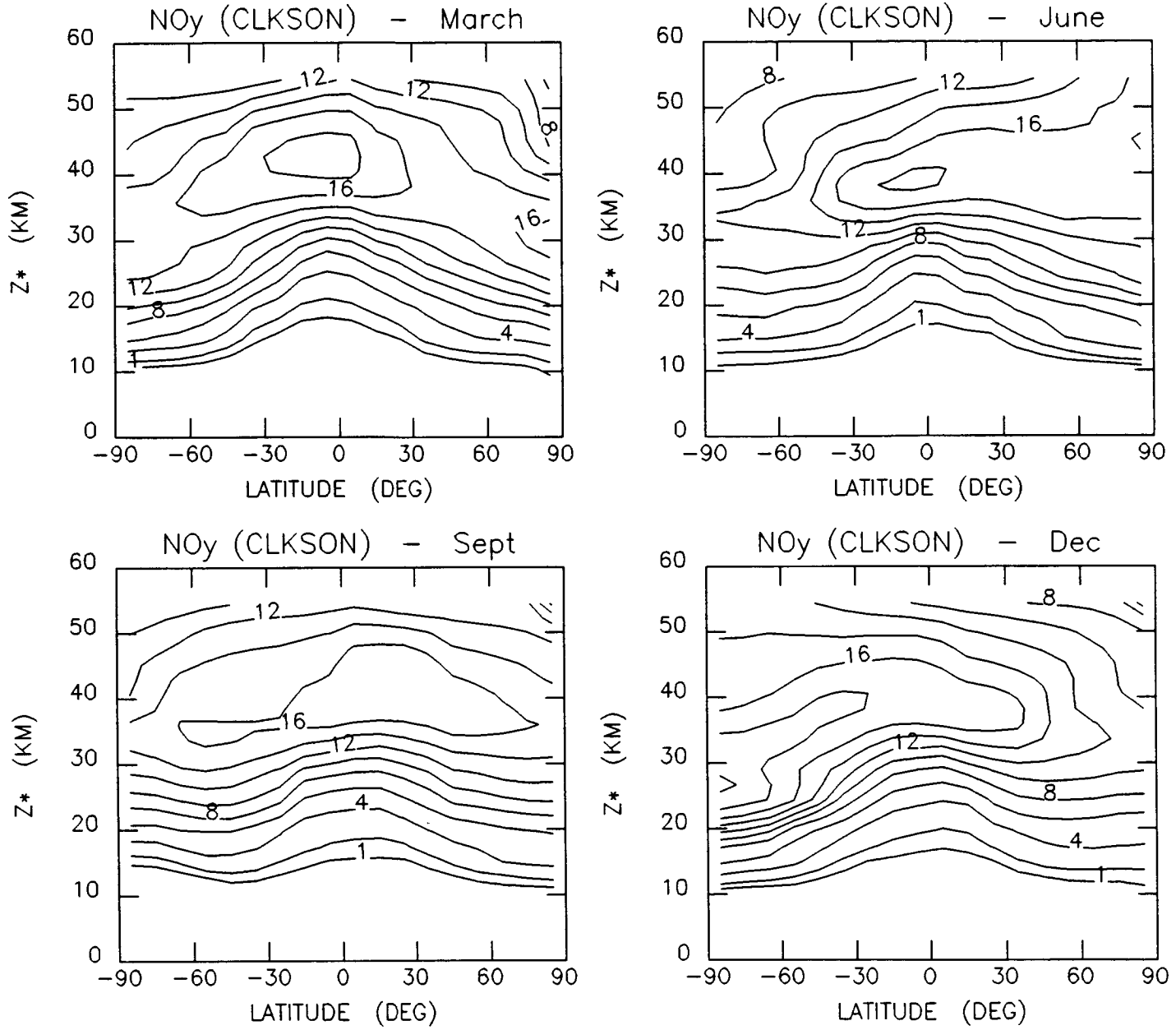
NOy (CLKSON) – March
NOy (CLKSON) – June
NOy (CLKSON) – Sept
NOy (CLKSON) – Dec
Z* (KM)
LATITUDE (DEG)
0
10
20
30
40
50
60
-90
-60
-30
0
30
60
90
1
4
8
12
16

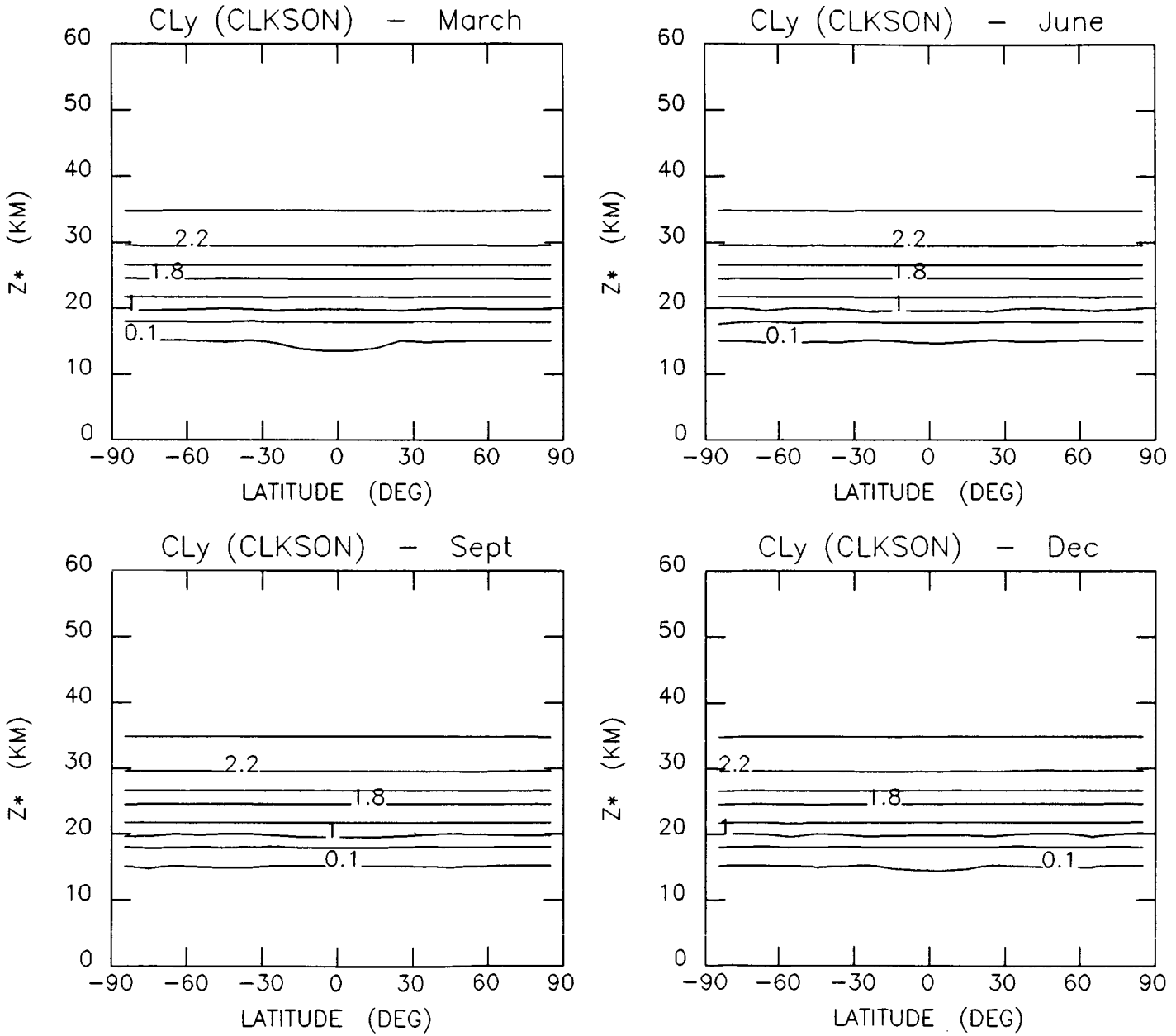
CLy (CLKSON) – March
CLy (CLKSON) – June
CLy (CLKSON) – Sept
CLy (CLKSON) – Dec
Z* (KM)
LATITUDE (DEG)
0
10
20
30
40
50
60
−90
−60
−30
0
30
60
90
2.2
1.8
1
0.1

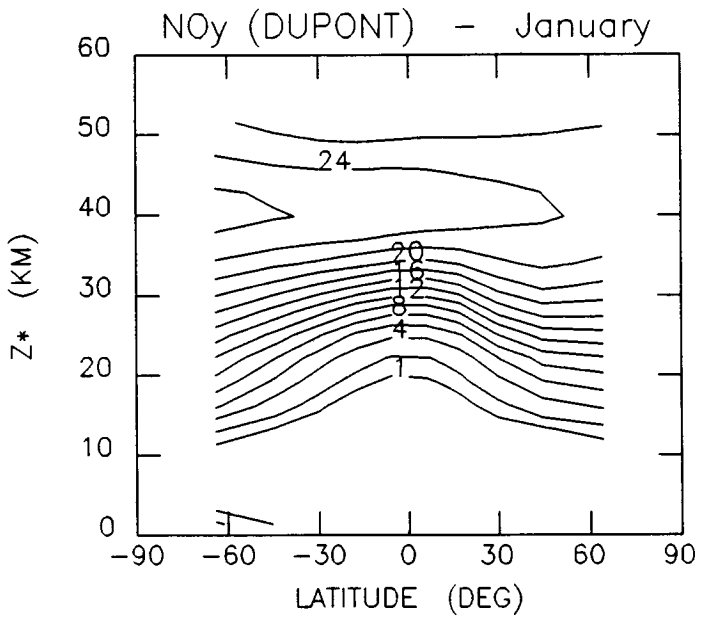
NOy (DUPONT) – January
Z* (KM)
LATITUDE (DEG)
24
20
16
12
8
4
1

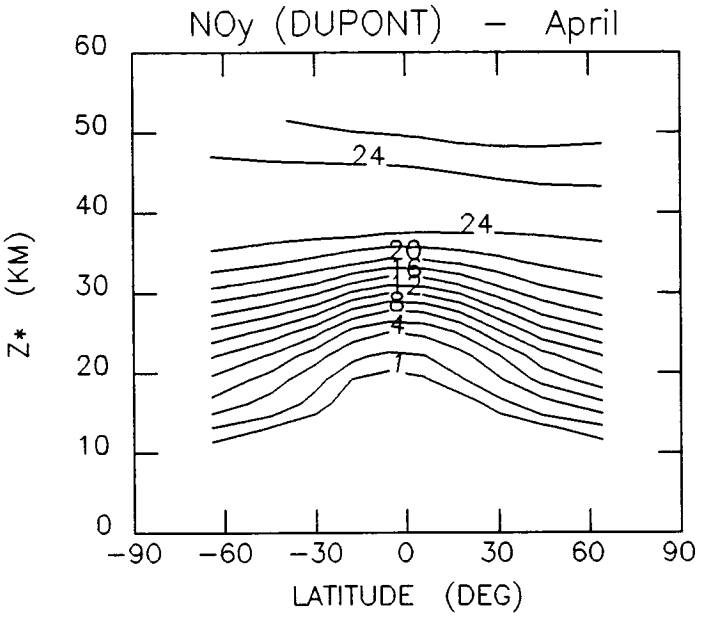
NOy (DUPONT) – April
Z* (KM)
LATITUDE (DEG)
24
24
20
16
12
8
4
1

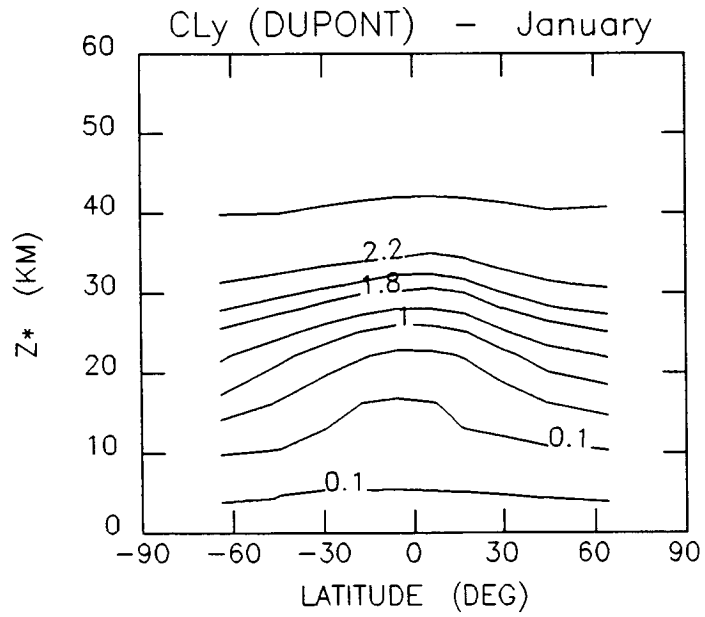
CLy (DUPONT) – January
Z* (KM)
LATITUDE (DEG)
2.2
1.8
1
0.1
0.1

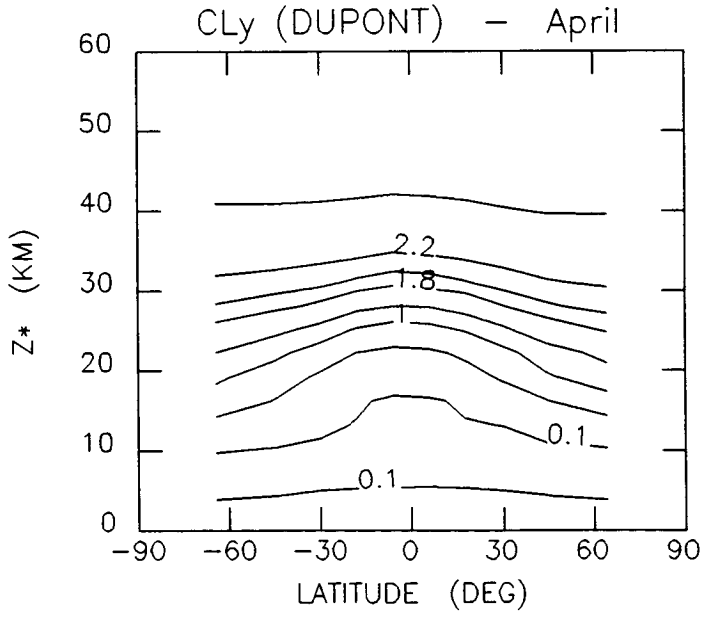
CLy (DUPONT) – April
Z* (KM)
LATITUDE (DEG)
2.2
1.8
1
0.1
0.1

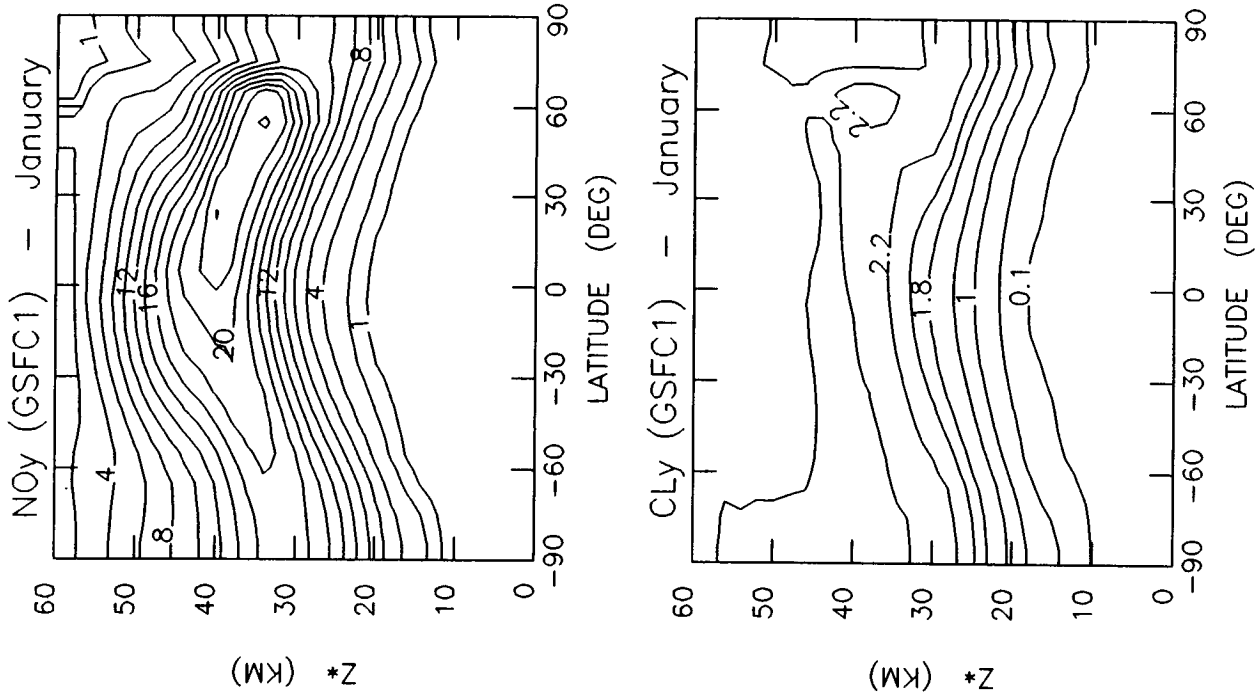
NOy (GSFC1) - January
CLy (GSFC1) - January
Z* (KM)
LATITUDE (DEG)
60
50
40
30
20
10
0
-90
-60
-30
0
30
60
90
1
4
8
12
16
20
2.2
1.8
0.1

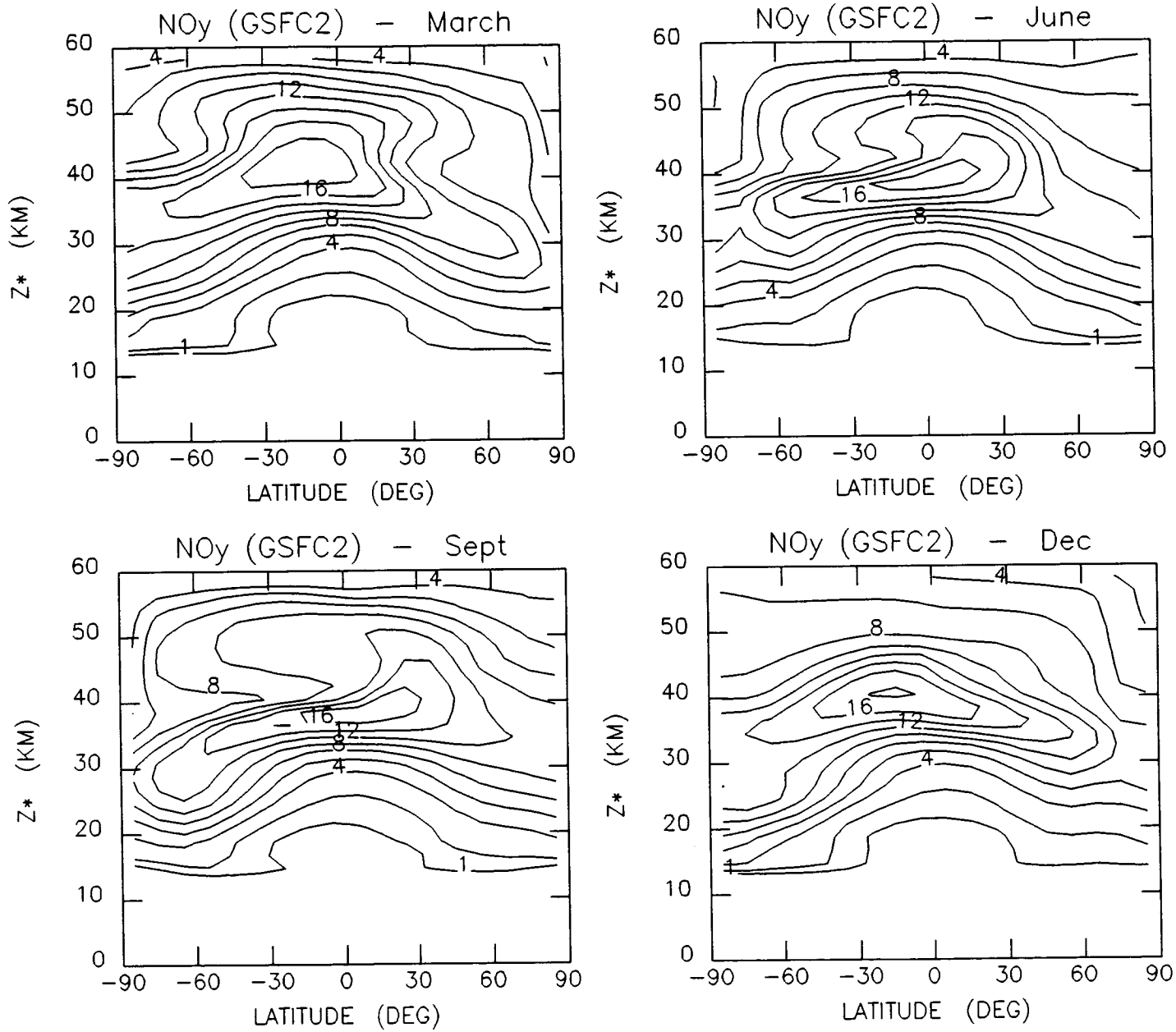
NOy (GSFC2) – March
NOy (GSFC2) – June
NOy (GSFC2) – Sept
NOy (GSFC2) – Dec
Z* (KM)
LATITUDE (DEG)
0
10
20
30
40
50
60
-90
-60
-30
0
30
60
90
1
4
8
12
16

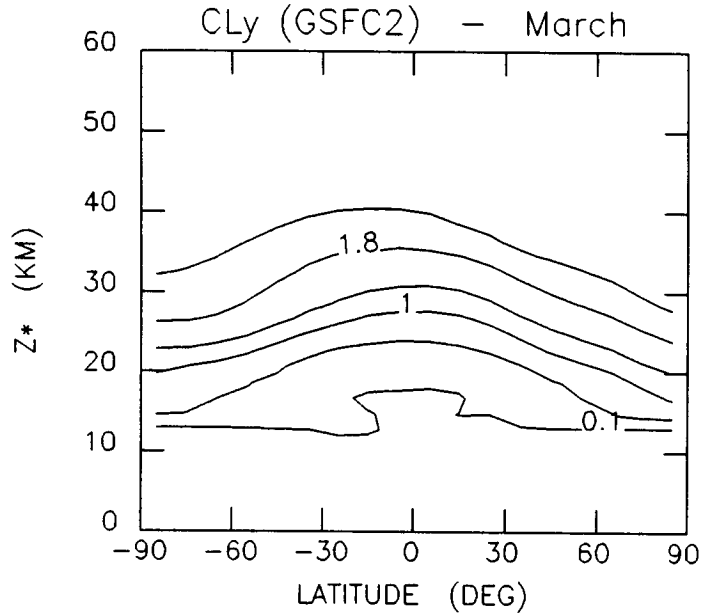
CLy (GSFC2) – March
Z* (KM)
LATITUDE (DEG)
1.8
1
0.1

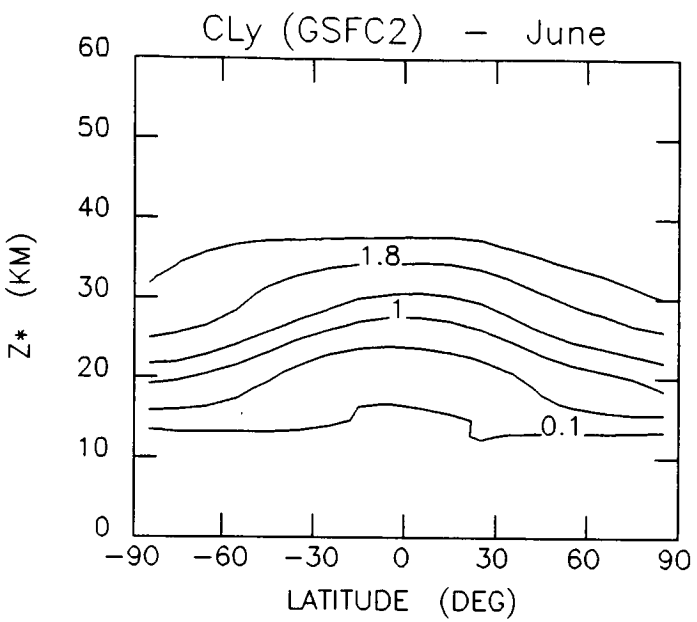
CLy (GSFC2) – June
Z* (KM)
LATITUDE (DEG)
1.8
1
0.1

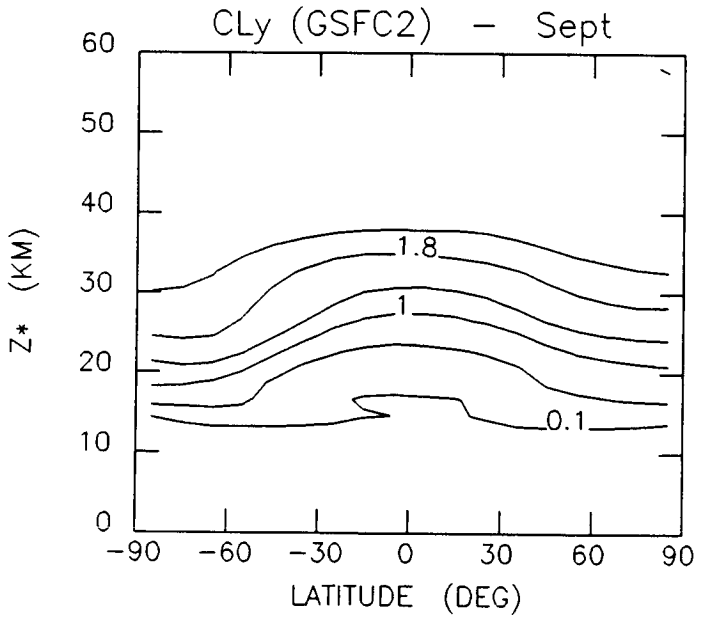
CLy (GSFC2) – Sept
Z* (KM)
LATITUDE (DEG)
1.8
1
0.1

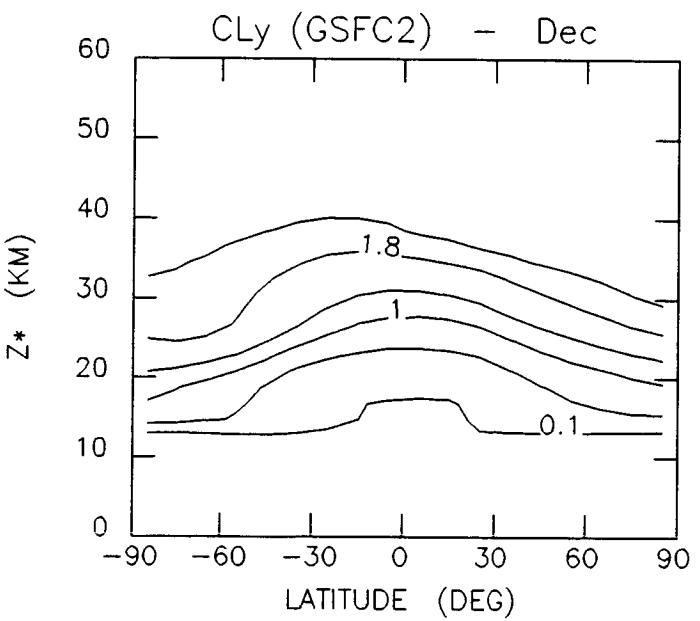
CLy (GSFC2) – Dec
Z* (KM)
LATITUDE (DEG)
1.8
1
0.1

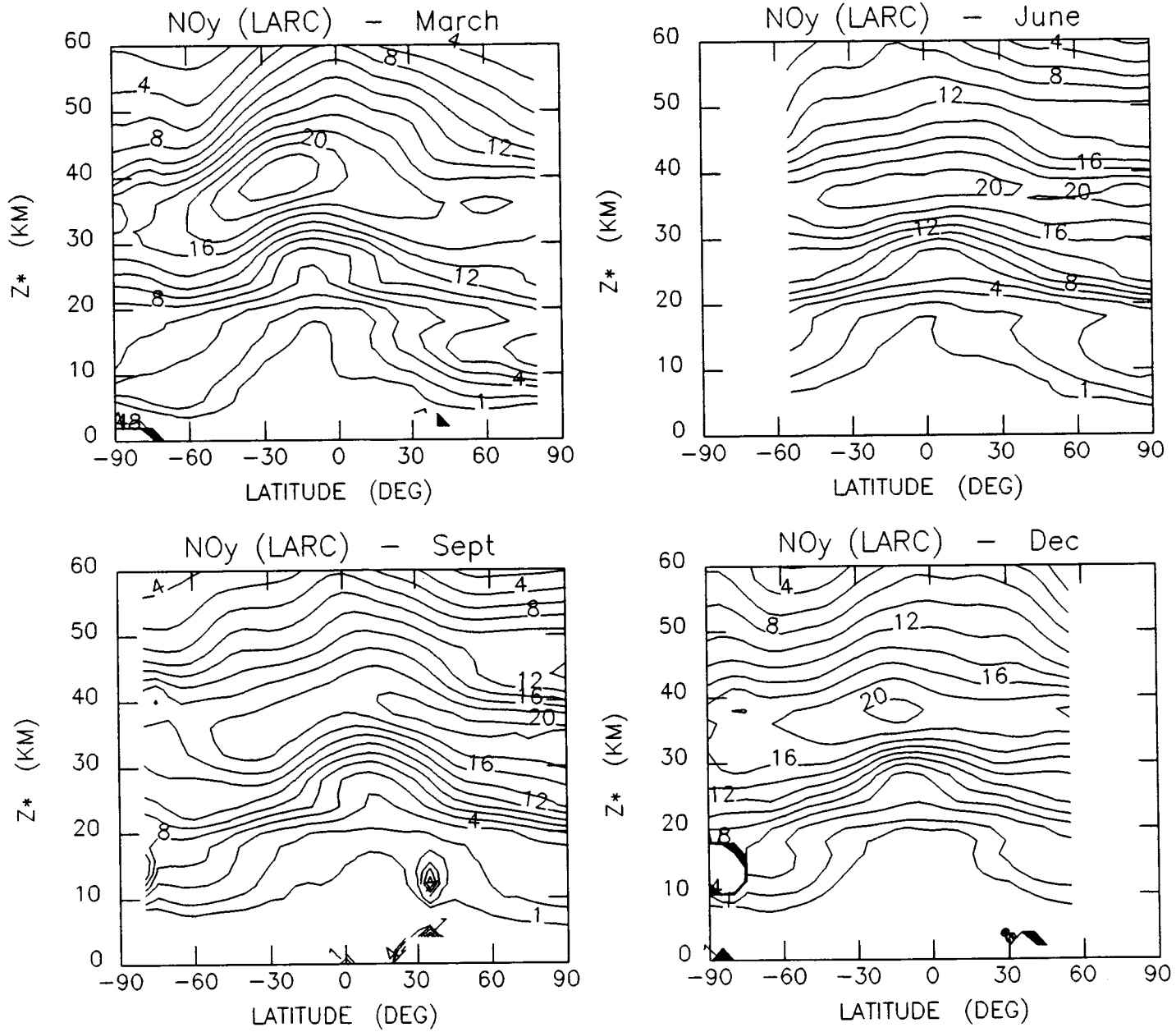
NOy (LARC) – March
NOy (LARC) – June
NOy (LARC) – Sept
NOy (LARC) – Dec
Z* (KM)
LATITUDE (DEG)
0
10
20
30
40
50
60
-90
-60
-30
0
30
60
90

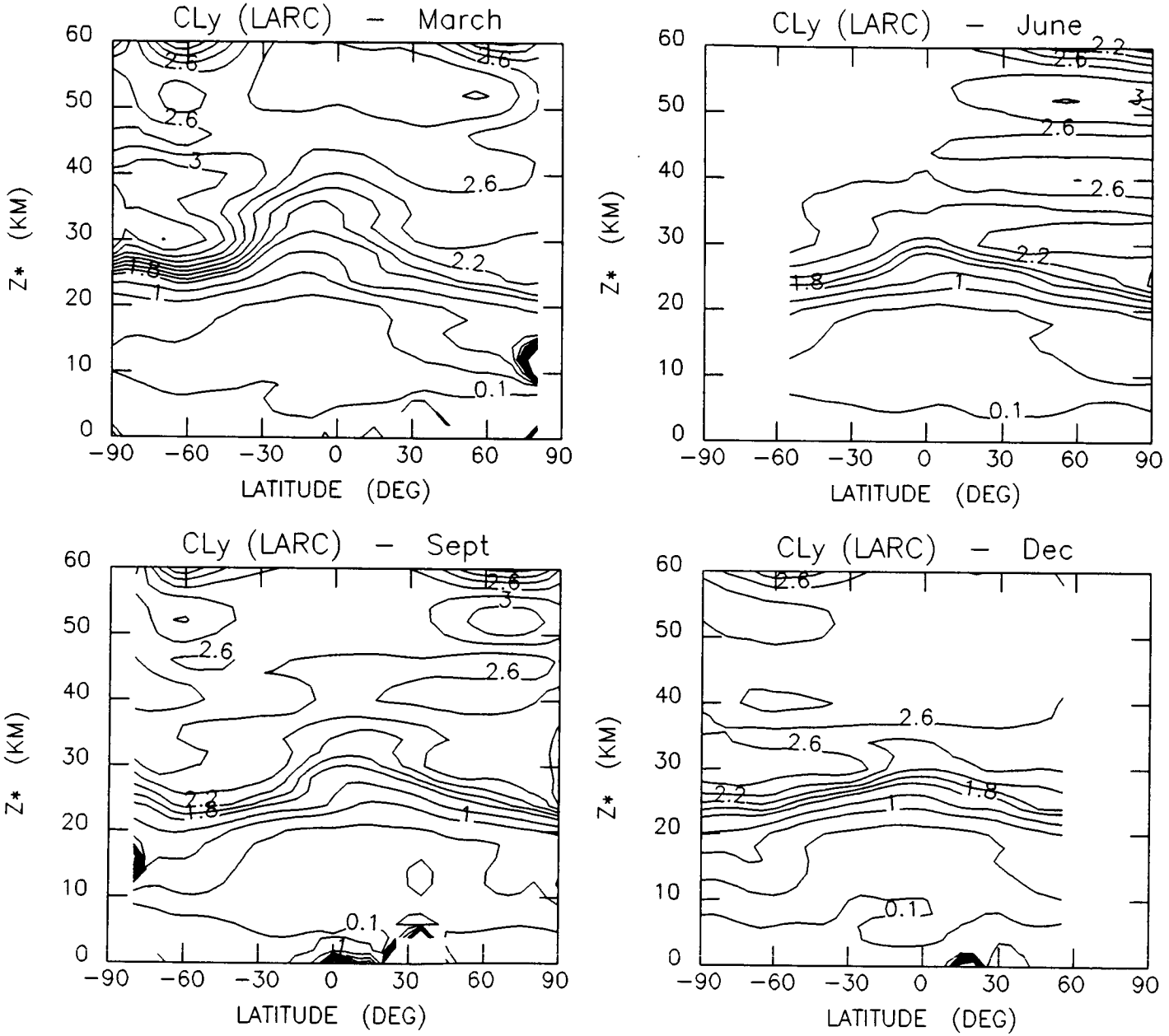
CLy (LARC) – March
CLy (LARC) – June
CLy (LARC) – Sept
CLy (LARC) – Dec
Z* (KM)
LATITUDE (DEG)
0
10
20
30
40
50
60
-90
-60
-30
0
30
60
90
0.1
1
1.8
2.2
2.6
3

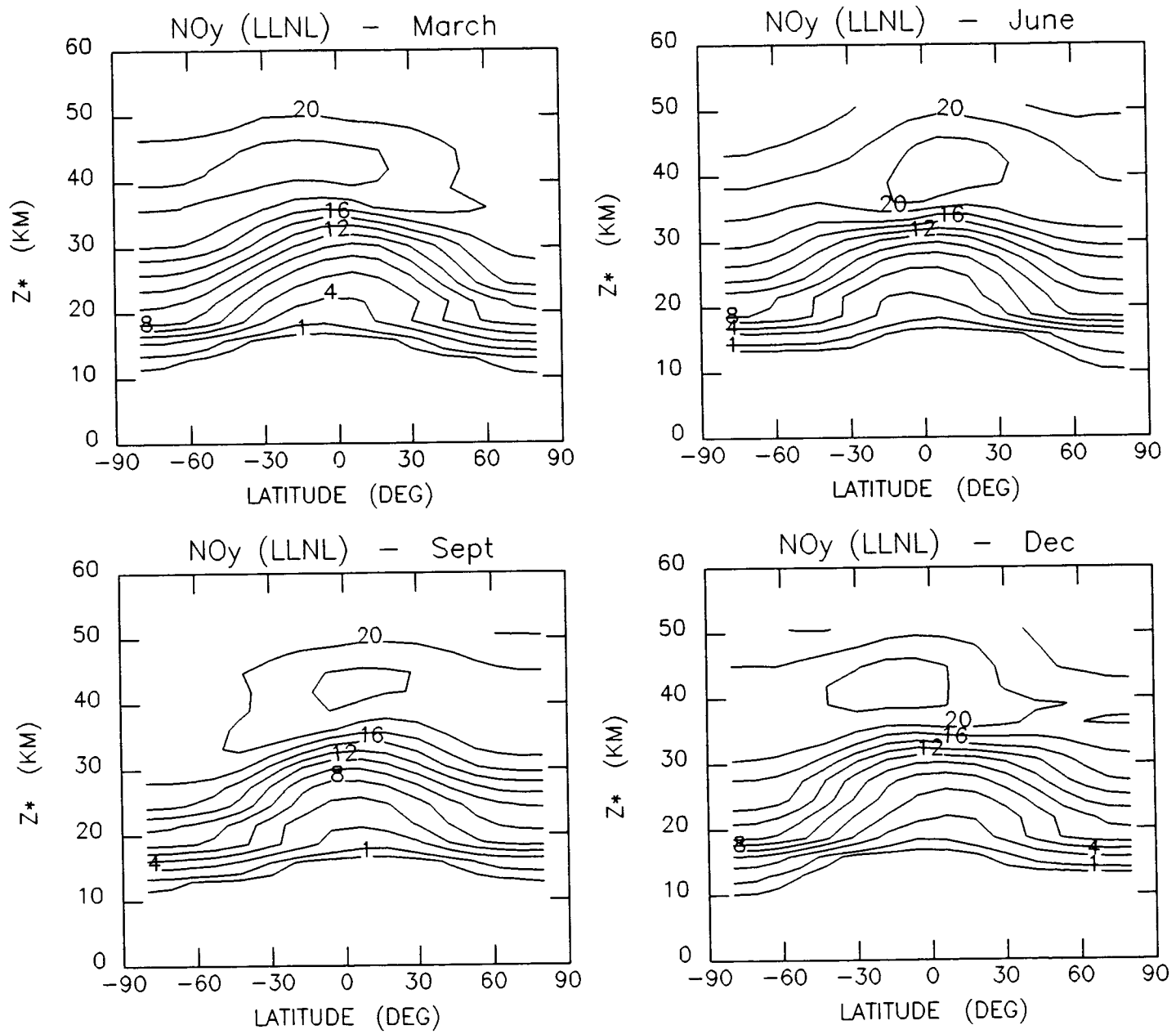
NOy (LLNL) – March
NOy (LLNL) – June
NOy (LLNL) – Sept
NOy (LLNL) – Dec
Z* (KM)
LATITUDE (DEG)
0
10
20
30
40
50
60
-90
-60
-30
0
30
60
90
20
16
12
8
4
1

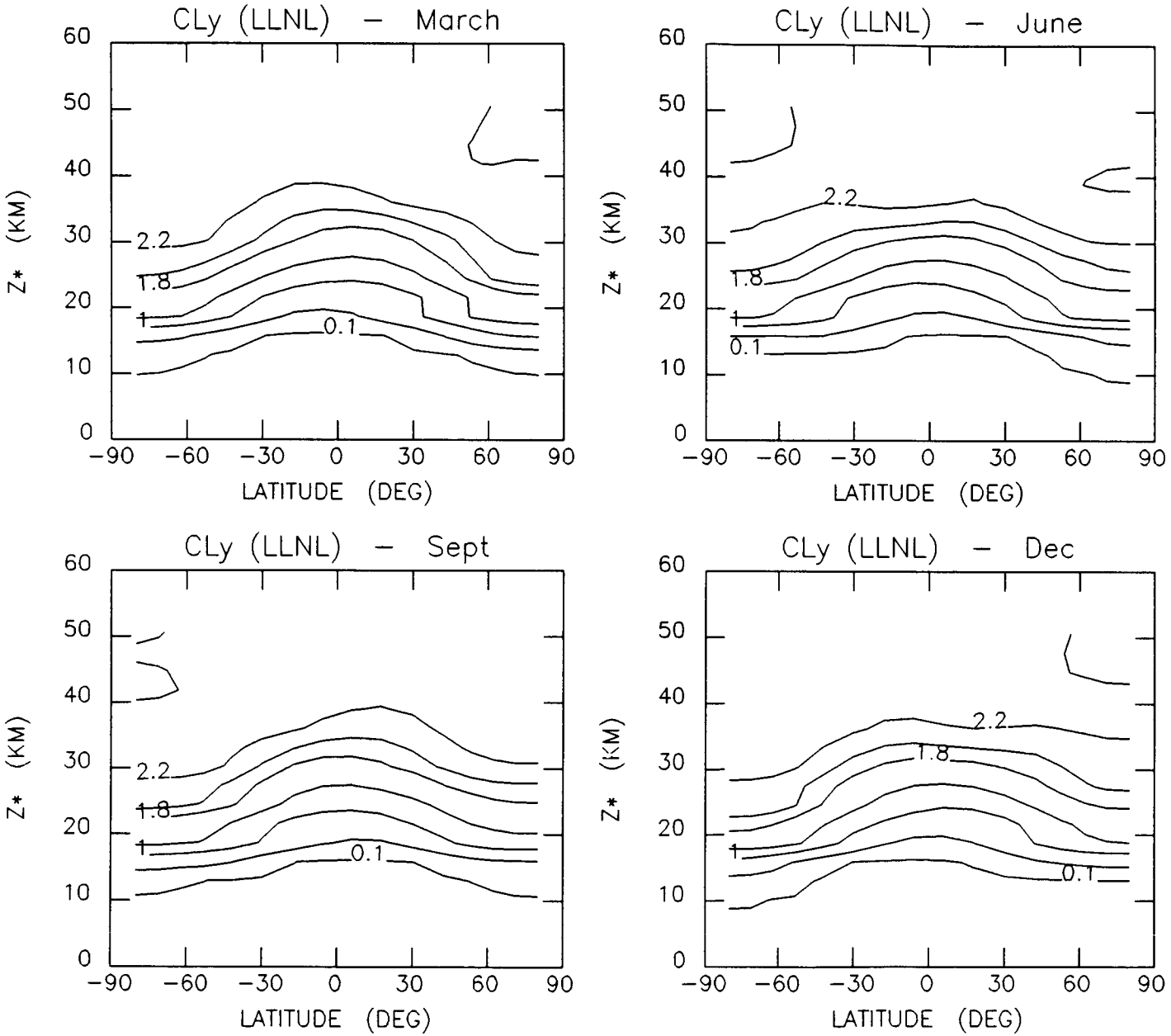
CLy (LLNL) – March
CLy (LLNL) – June
CLy (LLNL) – Sept
CLy (LLNL) – Dec
Z* (KM)
LATITUDE (DEG)
2.2
1.8
1
0.1
0
10
20
30
40
50
60
-90
-60
-30
0
30
60
90

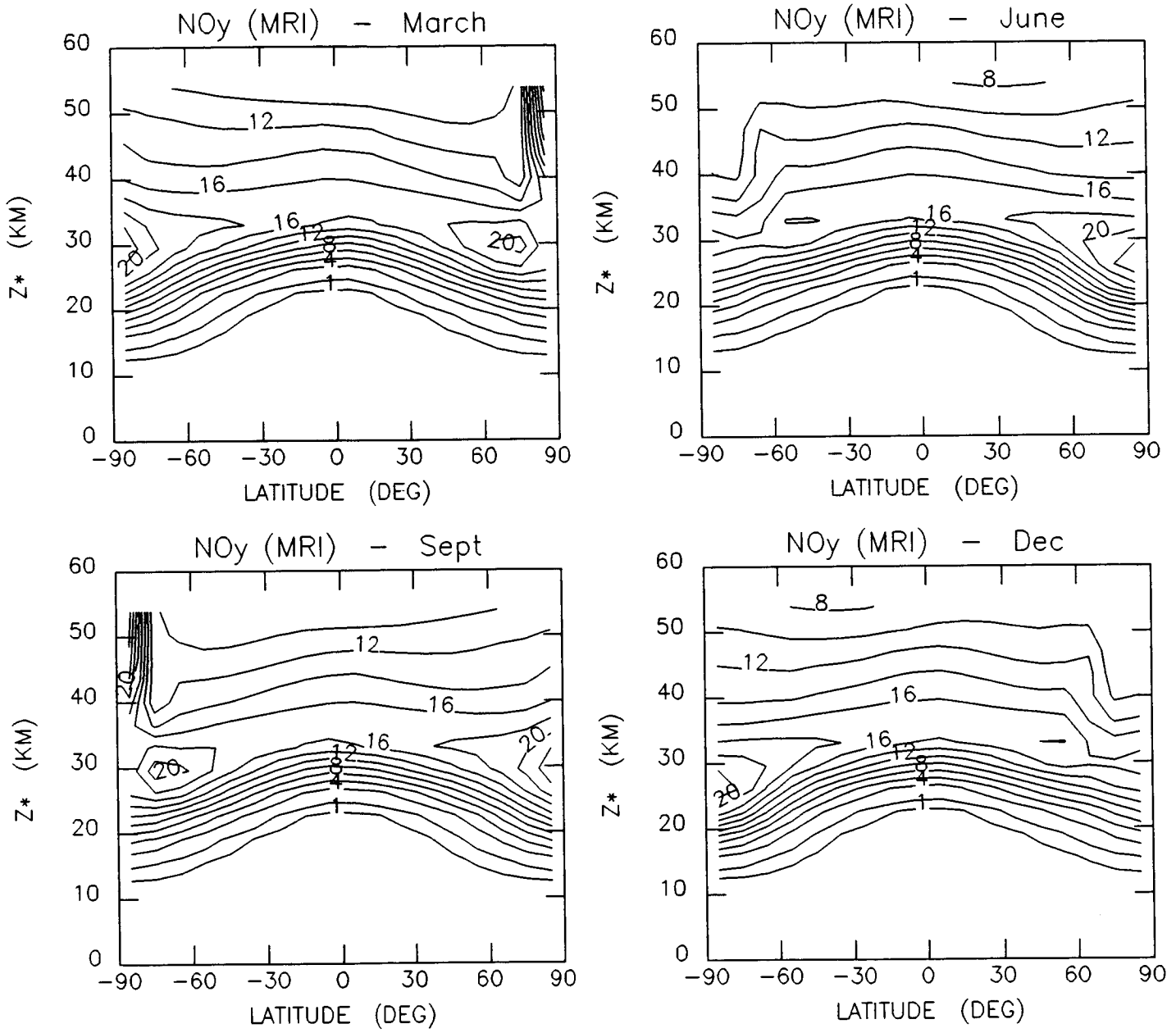
NOy (MRI) – March
NOy (MRI) – June
NOy (MRI) – Sept
NOy (MRI) – Dec
Z* (KM)
LATITUDE (DEG)
60
50
40
30
20
10
0
-90
-60
-30
0
30
60
90
1
4
8
12
16
20

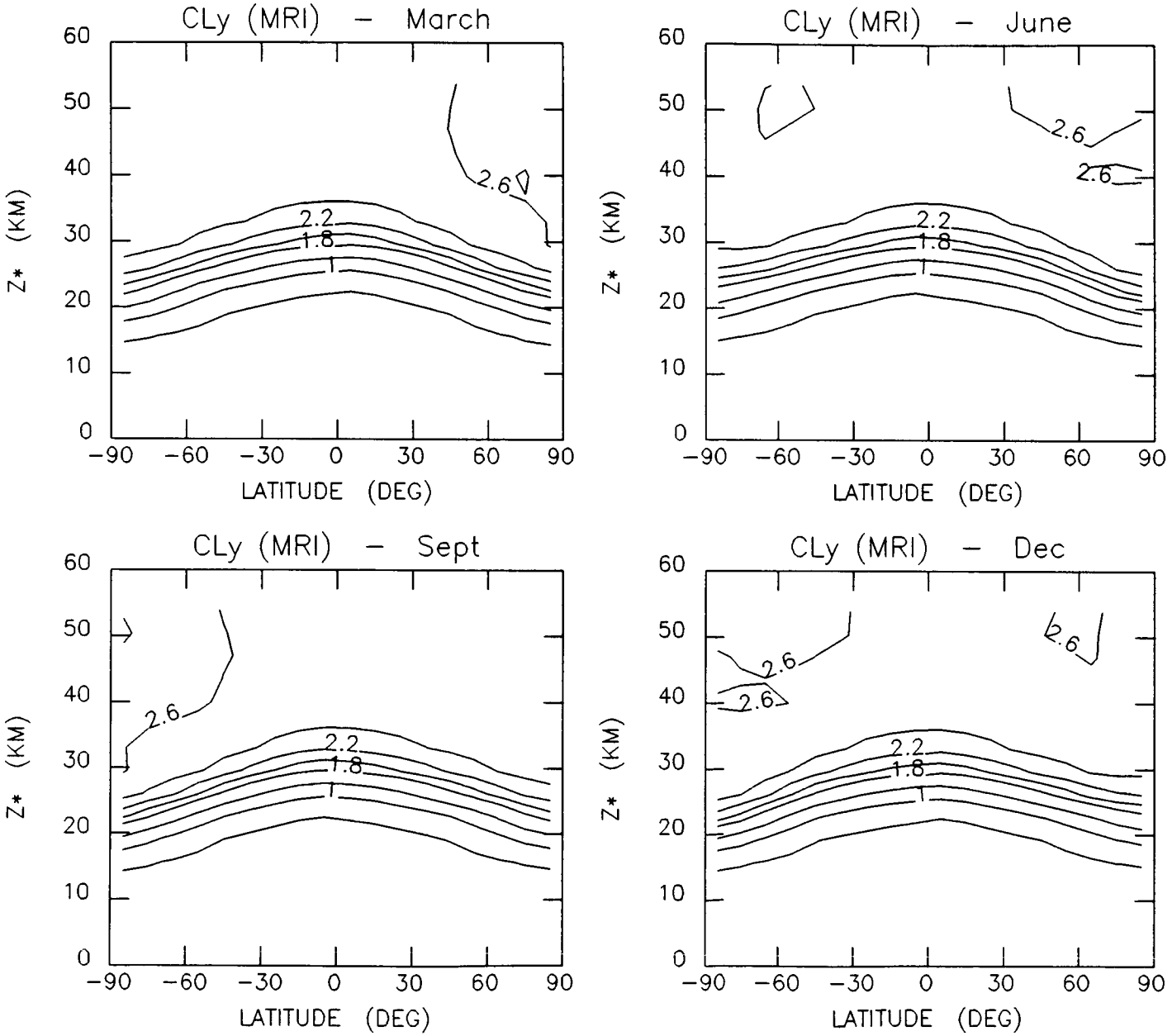
CLy (MRI) – March
CLy (MRI) – June
CLy (MRI) – Sept
CLy (MRI) – Dec
Z* (KM)
LATITUDE (DEG)
60
50
40
30
20
10
0
−90 −60 −30 0 30 60 90
2.6
2.2
1.8
1



17 - C

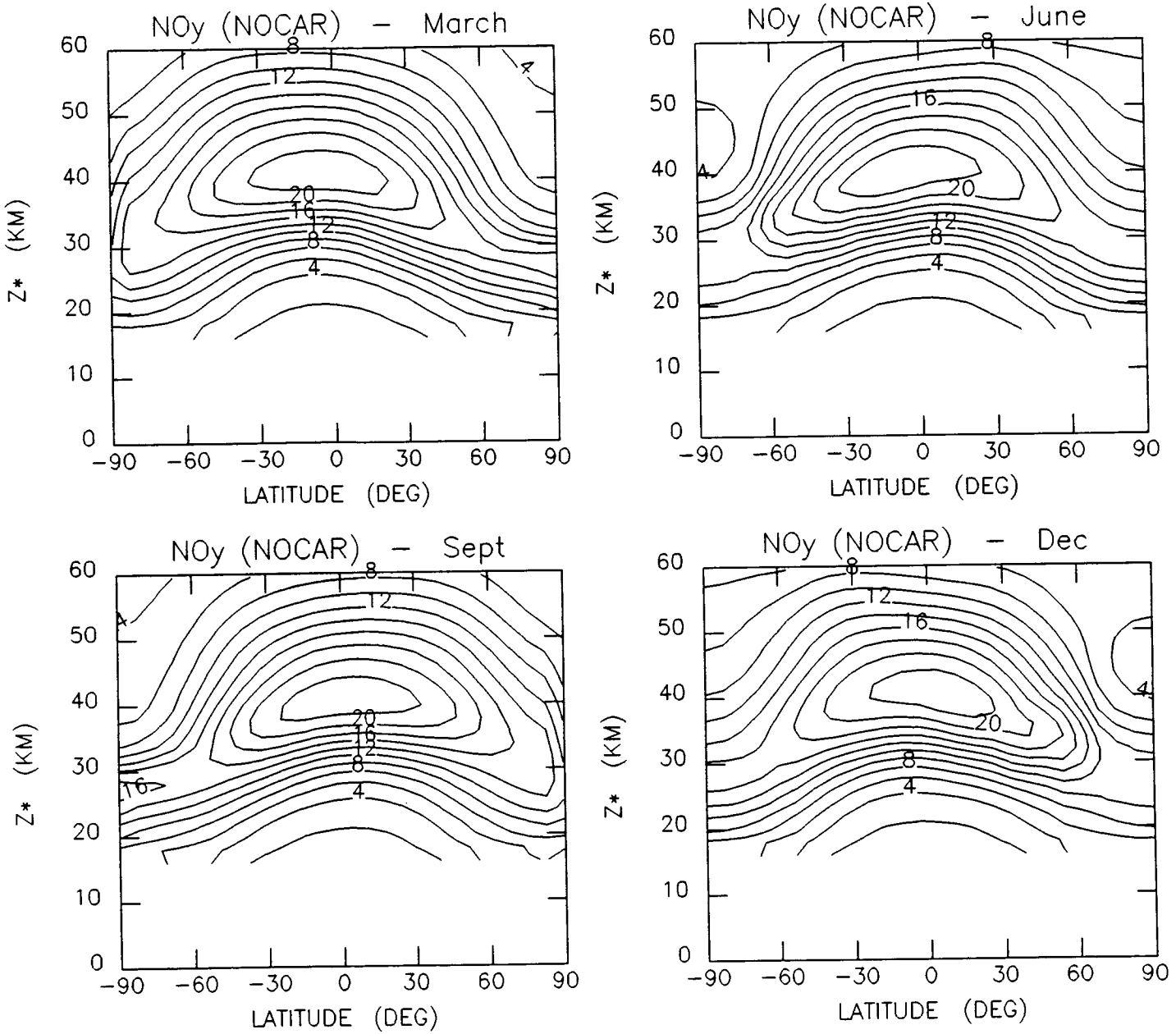
NOy (NOCAR) – March
NOy (NOCAR) – June
NOy (NOCAR) – Sept
NOy (NOCAR) – Dec
Z* (KM)
LATITUDE (DEG)
0
10
20
30
40
50
60
-90
-60
-30
0
30
60
90
4
8
12
16
20

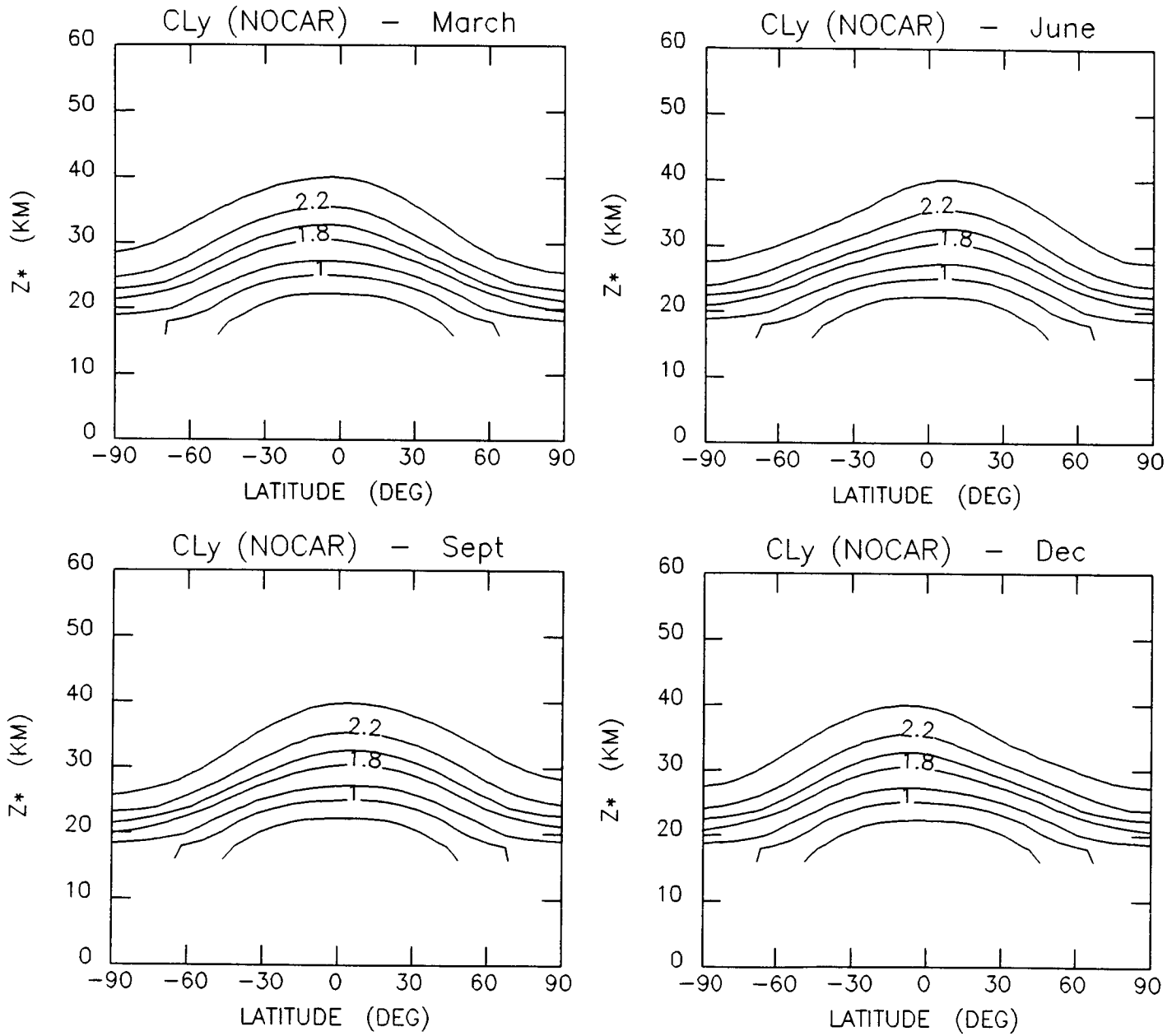
CLy (NOCAR) – March
CLy (NOCAR) – June
CLy (NOCAR) – Sept
CLy (NOCAR) – Dec
Z* (KM)
LATITUDE (DEG)
2.2
1.8
1
0
10
20
30
40
50
60
−90
−60
−30
0
30
60
90

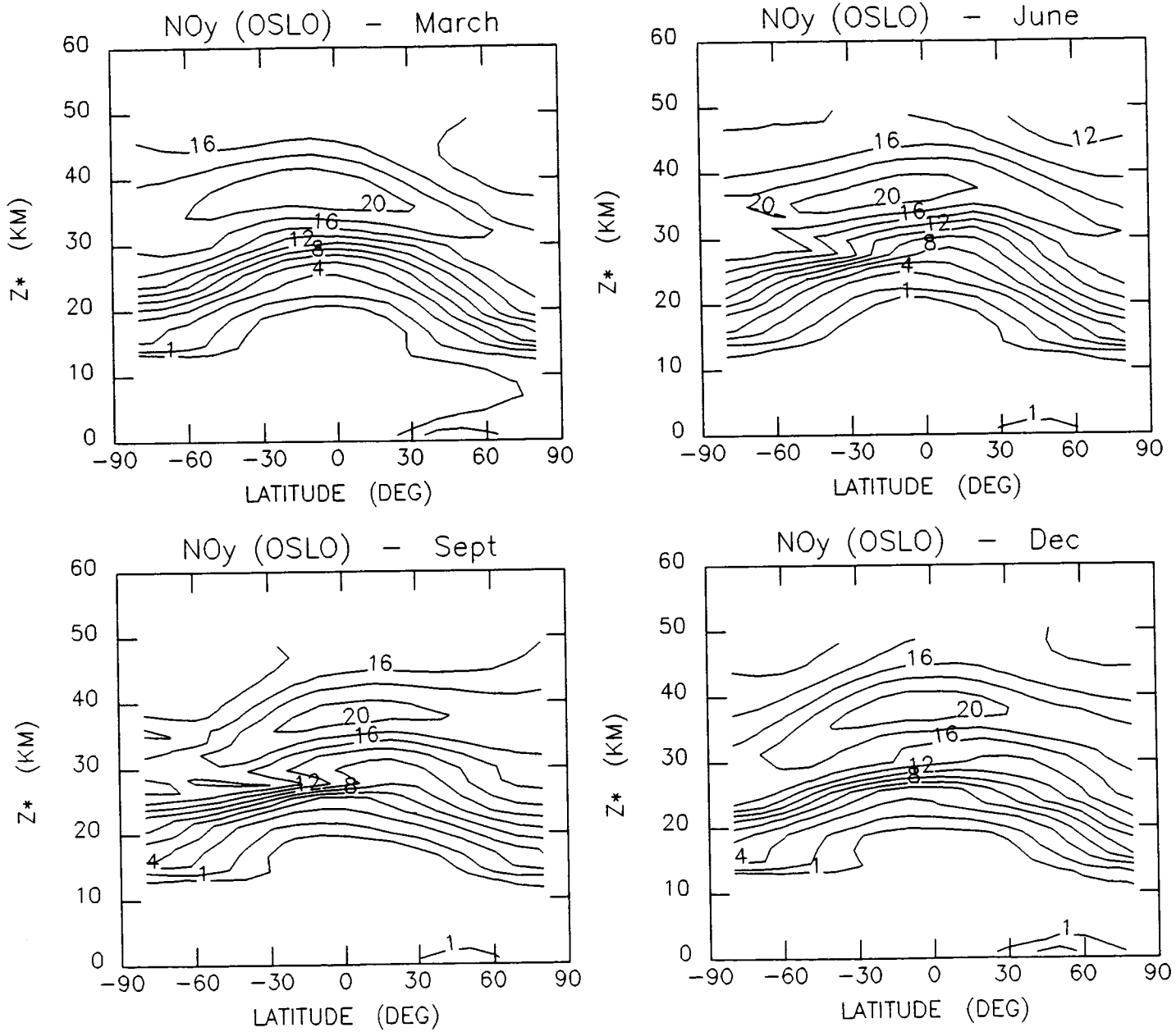
NOy (OSLO) – March
NOy (OSLO) – June
NOy (OSLO) – Sept
NOy (OSLO) – Dec
Z* (KM)
LATITUDE (DEG)
60
50
40
30
20
10
0
-90
-60
-30
0
30
60
90
16
20
12
8
4
1

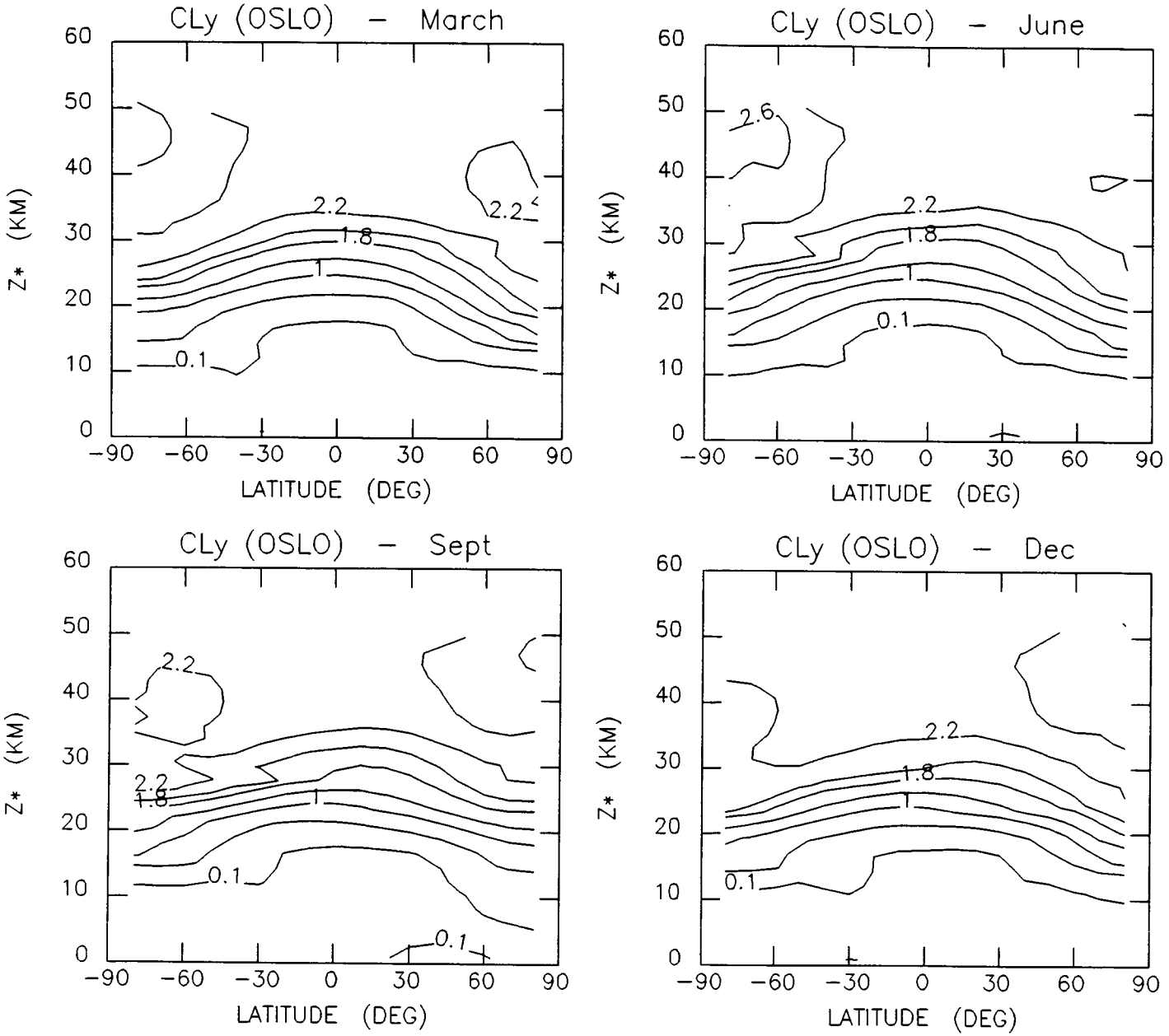
CLy (OSLO) – March
CLy (OSLO) – June
CLy (OSLO) – Sept
CLy (OSLO) – Dec
Z* (KM)
LATITUDE (DEG)
0
10
20
30
40
50
60
-90
-60
-30
0
30
60
90
0.1
1
1.8
2.2
2.6

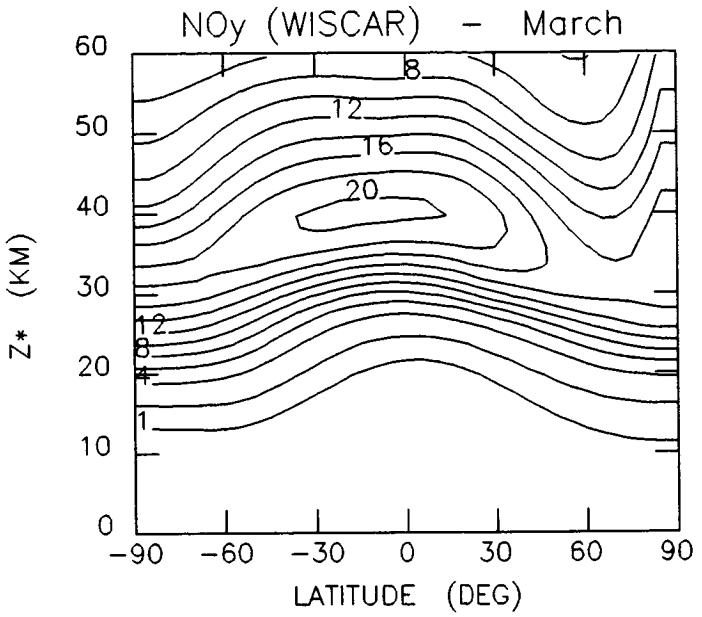
NOy (WISCAR) – March
Z* (KM)
LATITUDE (DEG)

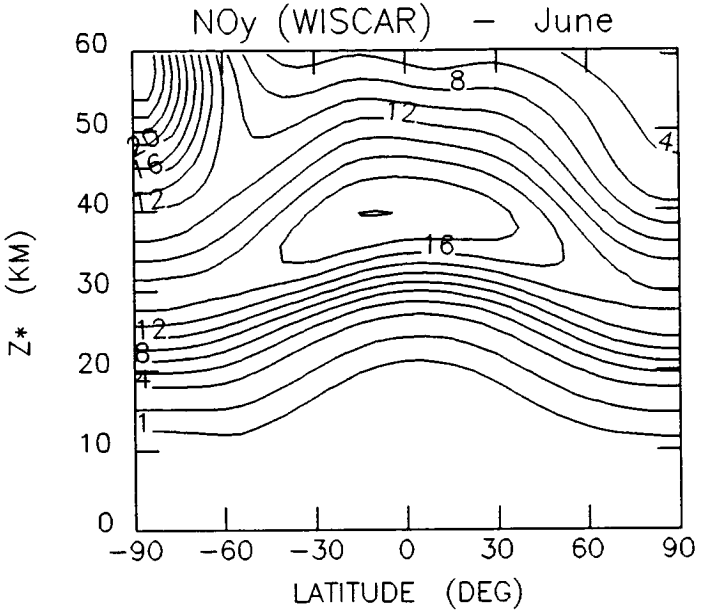
NOy (WISCAR) – June
Z* (KM)
LATITUDE (DEG)

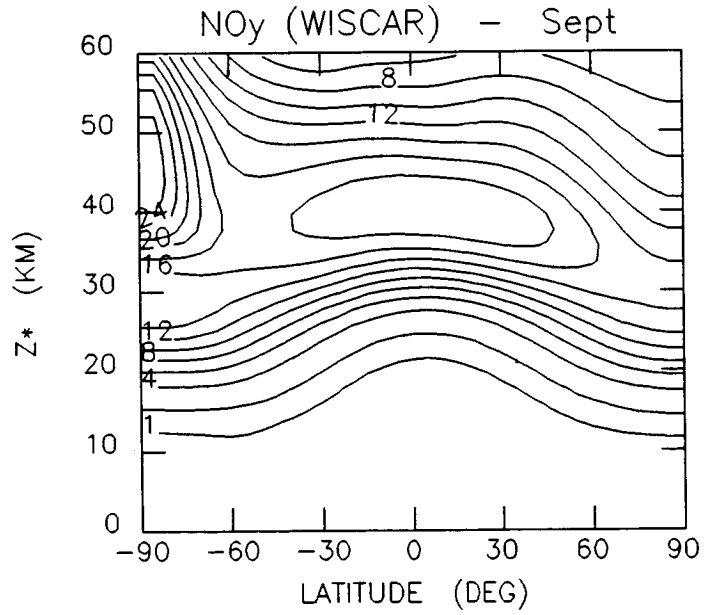
NOy (WISCAR) – Sept
Z* (KM)
LATITUDE (DEG)

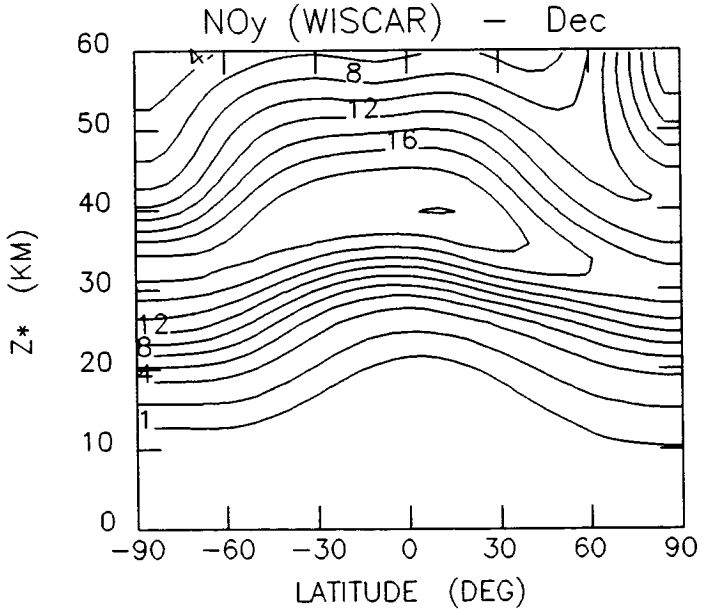
NOy (WISCAR) – Dec
Z* (KM)
LATITUDE (DEG)

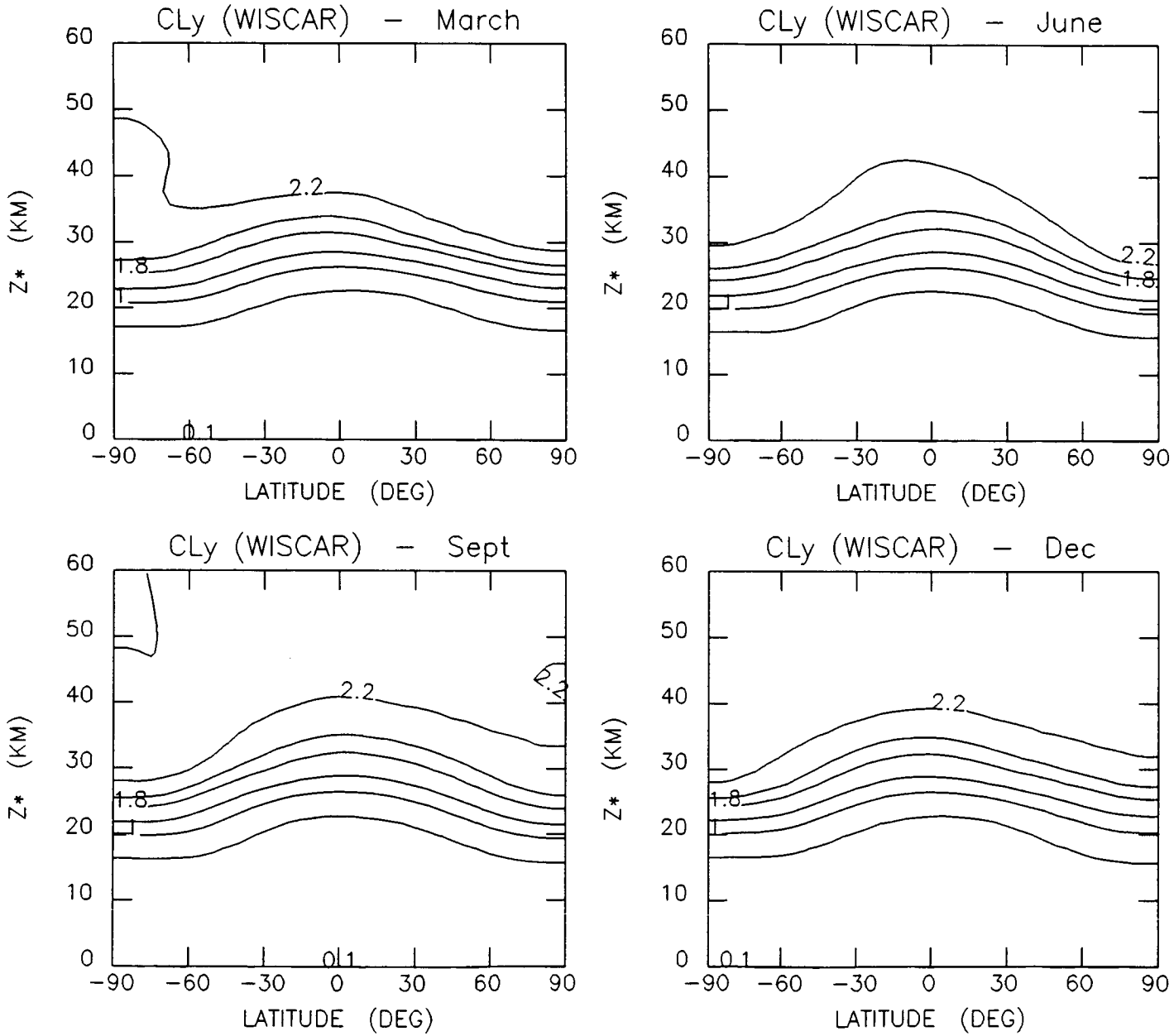
CLy (WISCAR) – March
CLy (WISCAR) – June
CLy (WISCAR) – Sept
CLy (WISCAR) – Dec
Z* (KM)
LATITUDE (DEG)
60
50
40
30
20
10
0
-90
-60
-30
0
30
60
90
2.2
1.8
1
0.1

**Table 6-3c.** Current Atmosphere (1980): Nitrogen Gases

March, June, September, and December
Models Represented - AER, CAMBRAL, CLKSON, DUPONT (Jan. & April), GSFC1 (Jan.), GSFC2, LARC, LLNL, MRI, NOCAR, OSLO, WISCAR

| Parameter | Description | Units | Contour Levels |
|---|---|---|---|
| $NO_x$ | Sum of NO, $NO_2$, and $NO_3$ Mixing Ratios | ppbv | 0.1, 0.2, 0.5, 1, 2, 4, 6, 8, 10, 12, 14, 16, 18, 20, 22, 24 |
| $NO_2$ | $NO_2$ Mixing Ratio | ppbv | 0.1, 0.2, 0.5, 1, 2, 4, 6, 8, 10, 12 |
| $HNO_3$ | $HNO_3$ Mixing Ratio | ppbv | 1.0E-03, 0.01, 0.1, 0.2, 0.5, 1, 2, 3, 4, 5, 6, 7, 8, 9, 10 |
| $N_2O_5$ | $N_2O_5$ Mixing Ratio | ppbv | 0.01, 0.1, 0.2, 0.5, 1, 1.5, 2, 2.5, 3, 3.5, 4, 4.5, 5 |
| $HO_2NO_2$ | $HO_2NO_2$ ($HNO_4$) Mixing Ratio | pptv | 1, 5, 10, 50, 100, 150, 200, 250, 300, 350, 400, 450, 500, 550, 600 |
| $NO/NO_2$ | Ratio of NO to $NO_2$ Mixing Ratios | --- | 0.1, 0.5, 1, 2, 5, 10, 20, 50, 100, 200, 500, 1000 |
| $HNO_3/NO_2$ | Ratio of $HNO_3$ to $NO_2$ Mixing Ratios | --- | 1.0E-03, 0.01, 0.1, 0.2, 0.5, 1, 2, 5, 10, 100, 1000 |
| $NO_x/NO_y$ | Ratio of $NO_x$ to $NO_y$ Mixing Ratios | --- | 1.0E-03, 0.01, 0.1, 0.15, 0.2, 0.25, 0.3, 0.4, 0.5, 0.6, 0.7, 0.8, 0.9, 1 |

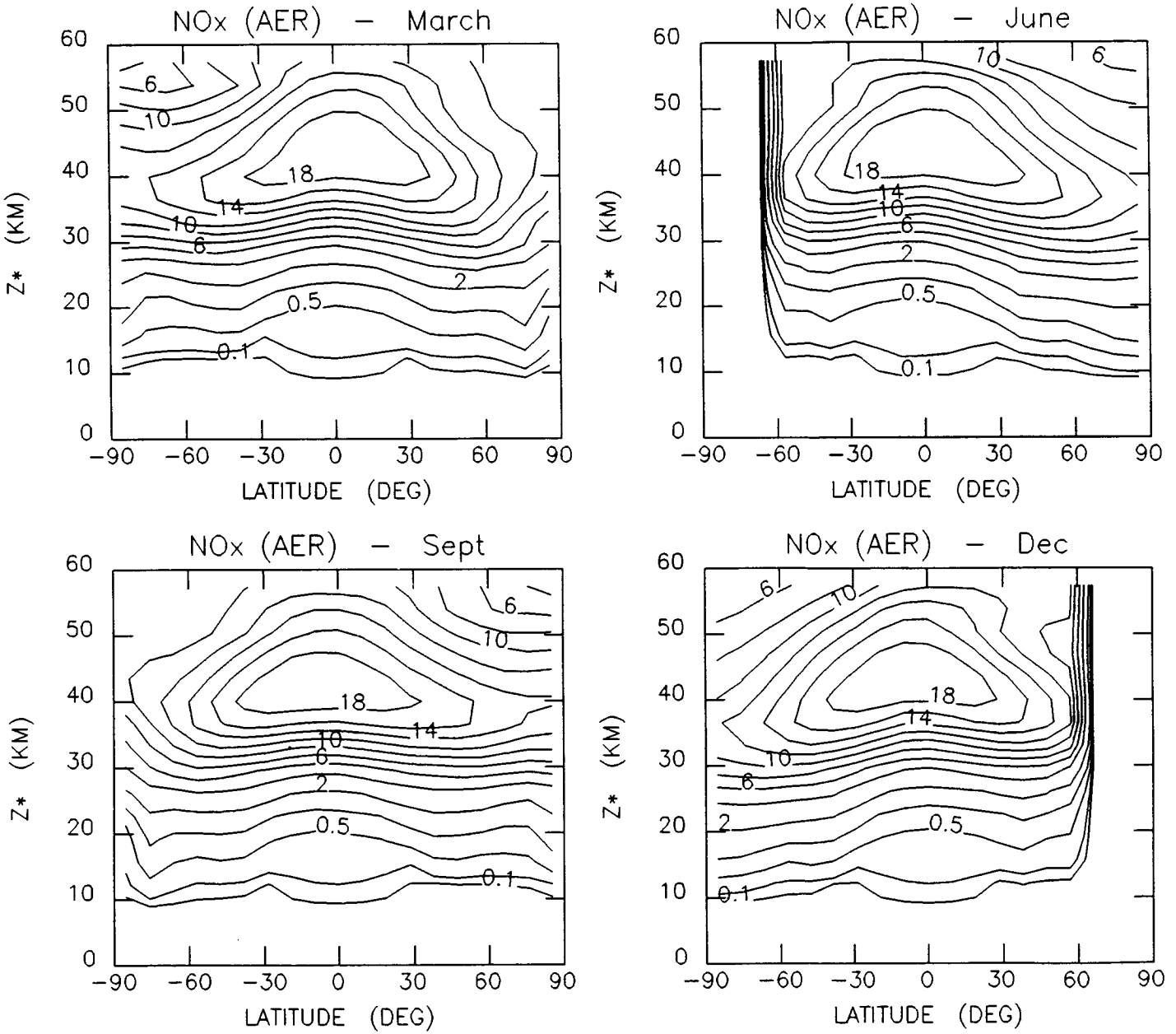
NOx (AER) – March
NOx (AER) – June
NOx (AER) – Sept
NOx (AER) – Dec
Z* (KM)
LATITUDE (DEG)
0
10
20
30
40
50
60
-90
-60
-30
0
30
60
90
6
10
18
14
2
0.5
0.1

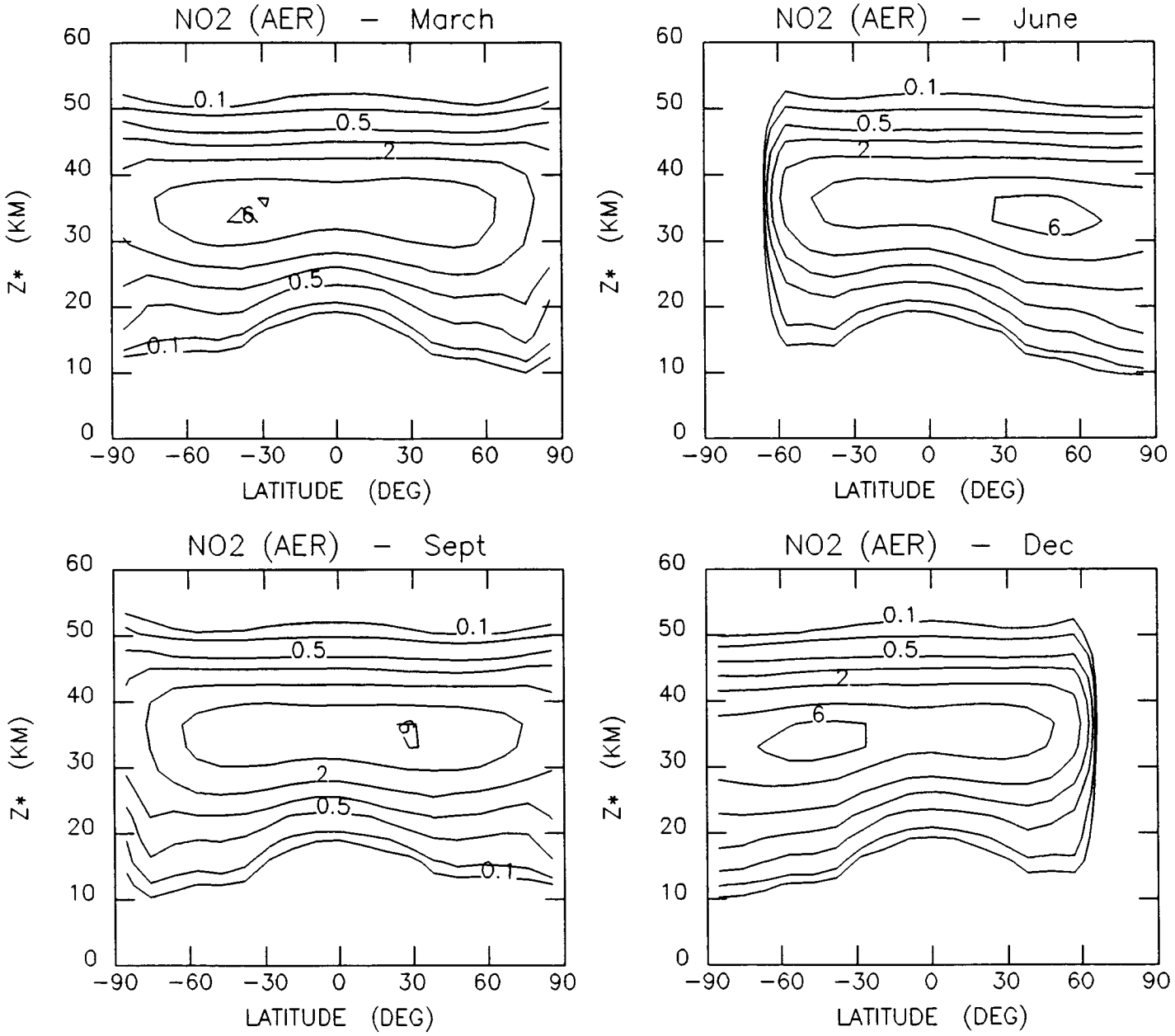
NO2 (AER) – March
NO2 (AER) – June
NO2 (AER) – Sept
NO2 (AER) – Dec
Z* (KM)
LATITUDE (DEG)
0
10
20
30
40
50
60
-90
-60
-30
0
30
60
90
0.1
0.5
2
6

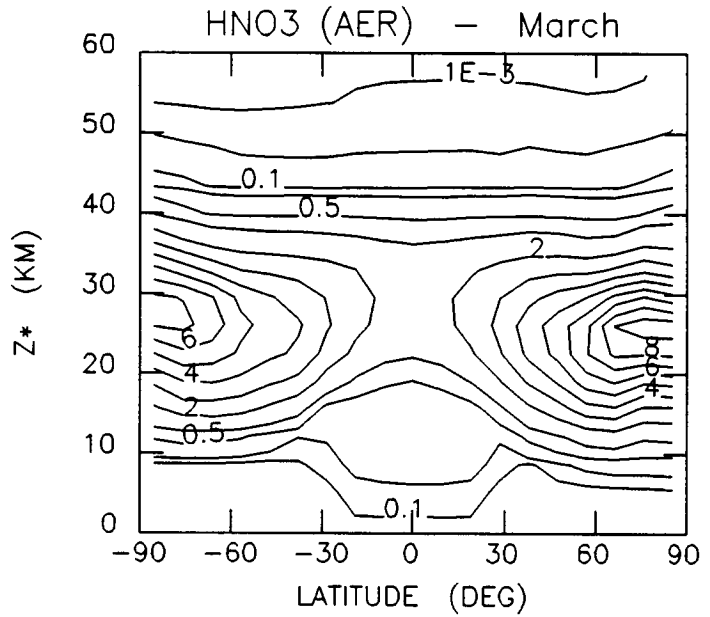
HNO3 (AER) – March
Z* (KM)
LATITUDE (DEG)
1E-3
0.1
0.5
2
4
6
8
60
50
40
30
20
10
0
−90 −60 −30 0 30 60 90

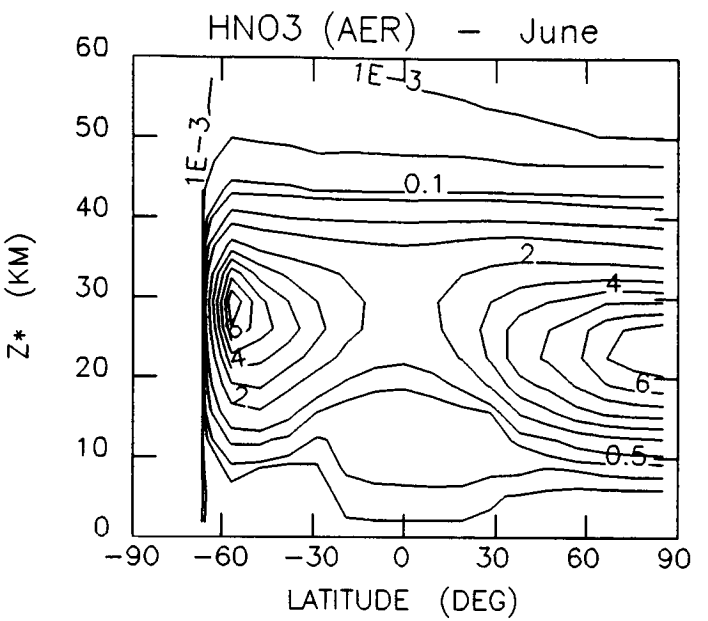
HNO3 (AER) – June
Z* (KM)
LATITUDE (DEG)
1E-3
0.1
0.5
2
4
6
60
50
40
30
20
10
0
−90 −60 −30 0 30 60 90

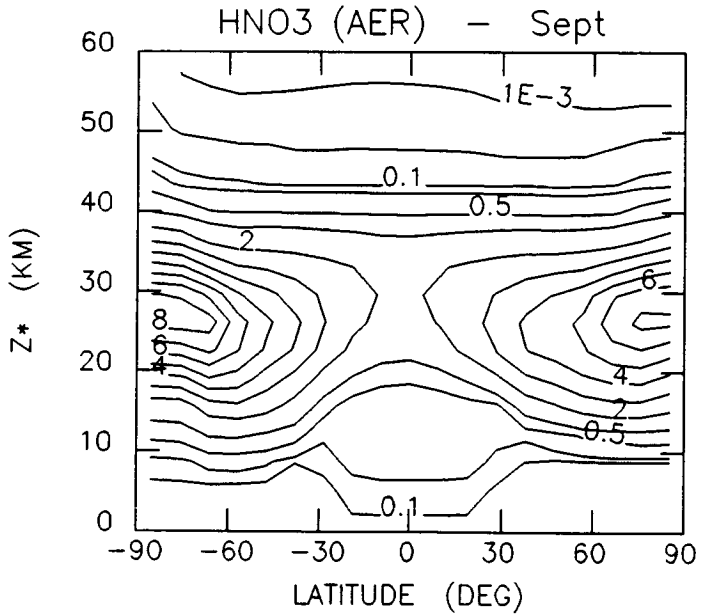
HNO3 (AER) – Sept
Z* (KM)
LATITUDE (DEG)
1E-3
0.1
0.5
2
4
6
8
60
50
40
30
20
10
0
−90 −60 −30 0 30 60 90

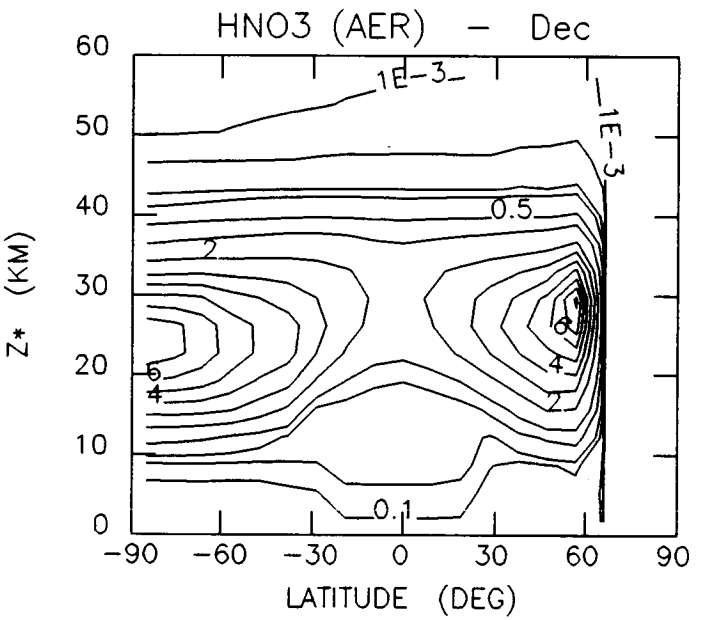
HNO3 (AER) – Dec
Z* (KM)
LATITUDE (DEG)
1E-3
0.1
0.5
2
4
6
60
50
40
30
20
10
0
−90 −60 −30 0 30 60 90

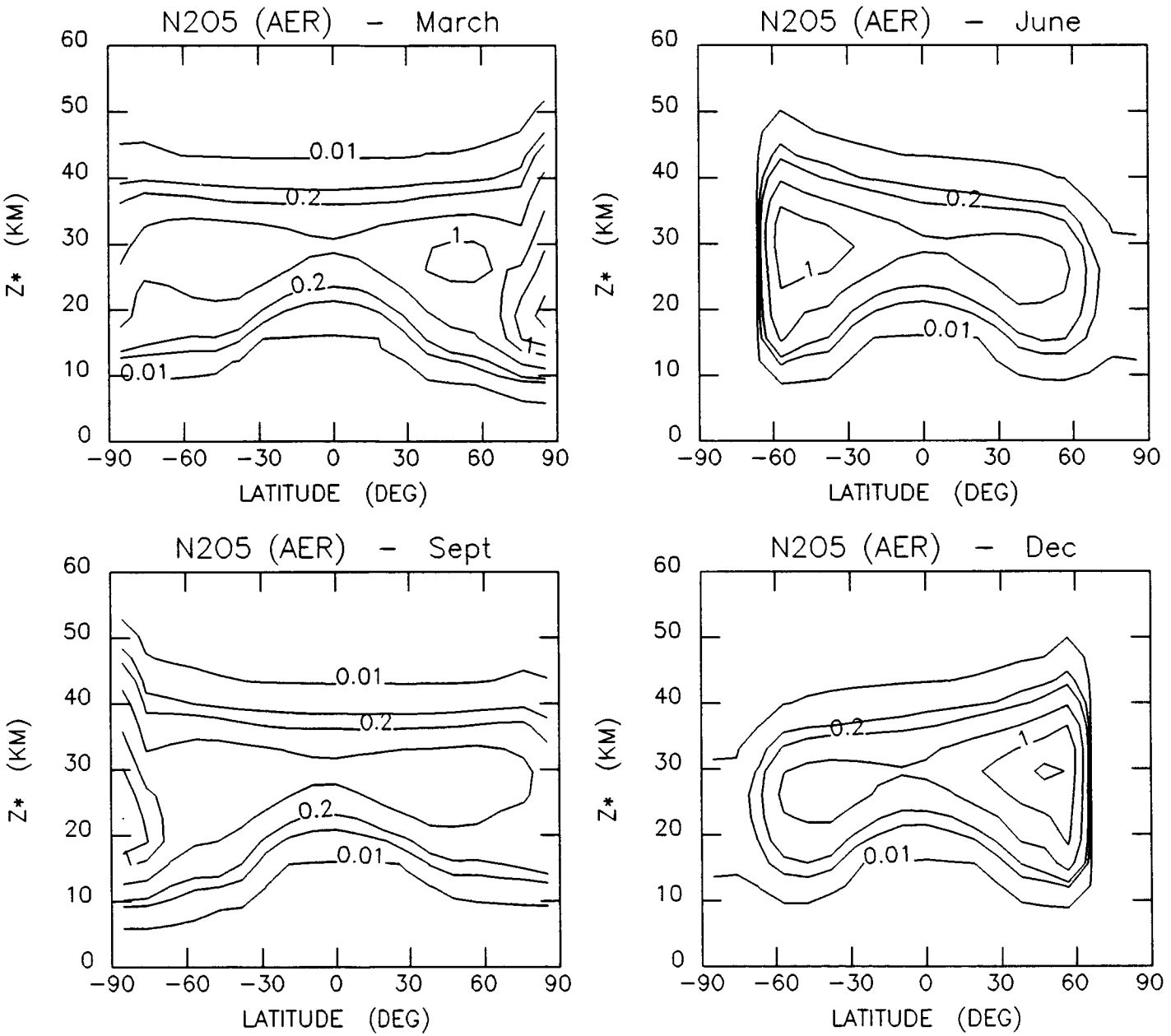
N2O5 (AER) - March
N2O5 (AER) - June
N2O5 (AER) - Sept
N2O5 (AER) - Dec
Z* (KM)
LATITUDE (DEG)
0.01
0.2
1
0
10
20
30
40
50
60
-90
-60
-30
0
30
60
90

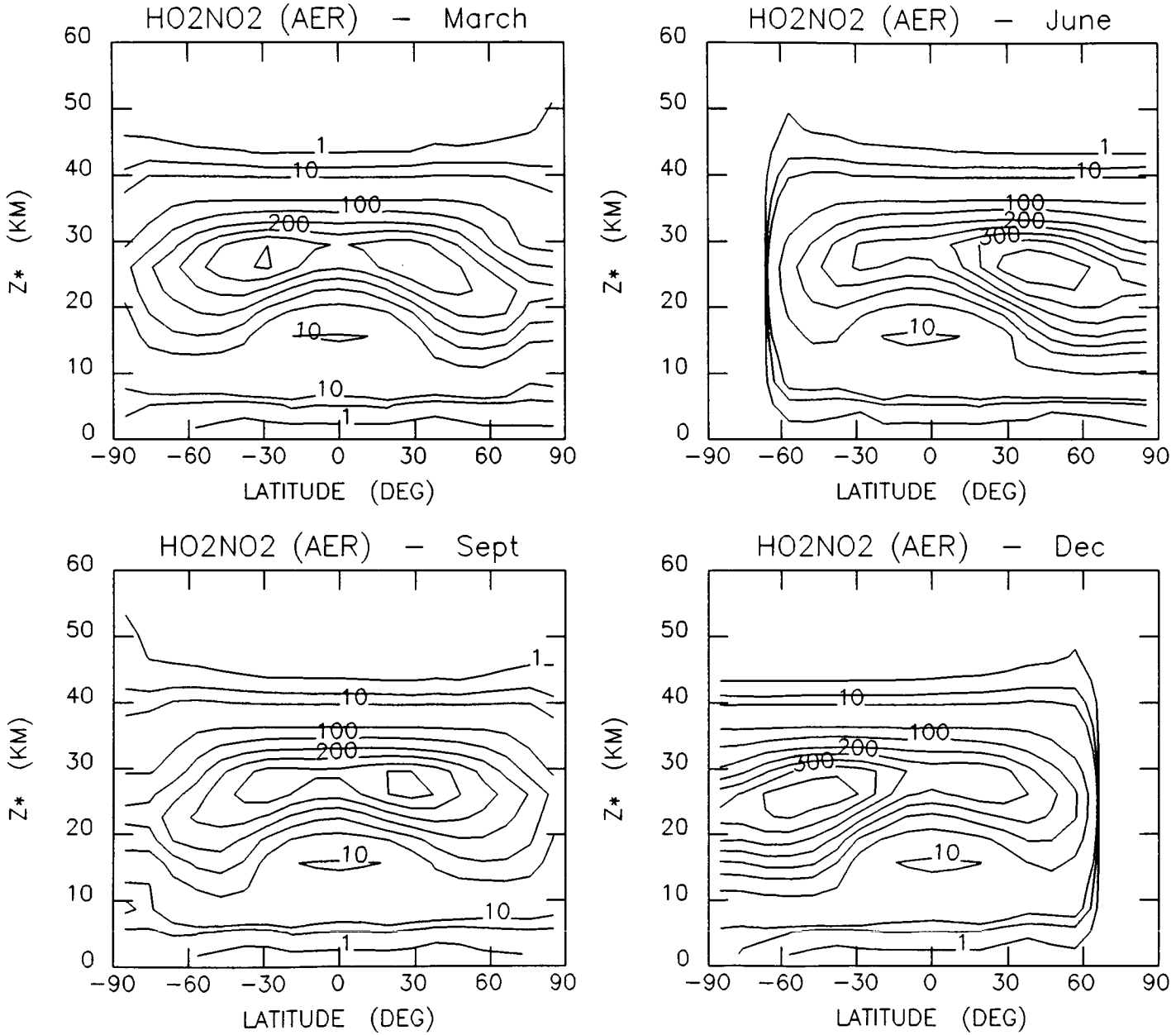
HO2NO2 (AER) – March
HO2NO2 (AER) – June
HO2NO2 (AER) – Sept
HO2NO2 (AER) – Dec
Z* (KM)
LATITUDE (DEG)
60
50
40
30
20
10
0
-90 -60 -30 0 30 60 90
1
10
100
200
300

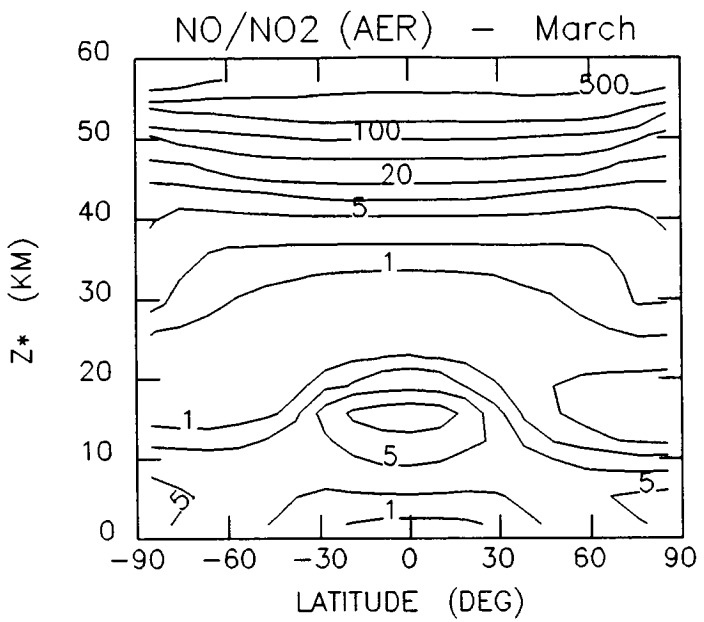
NO/NO2 (AER) – March
Z* (KM)
LATITUDE (DEG)
500
100
20
5
1

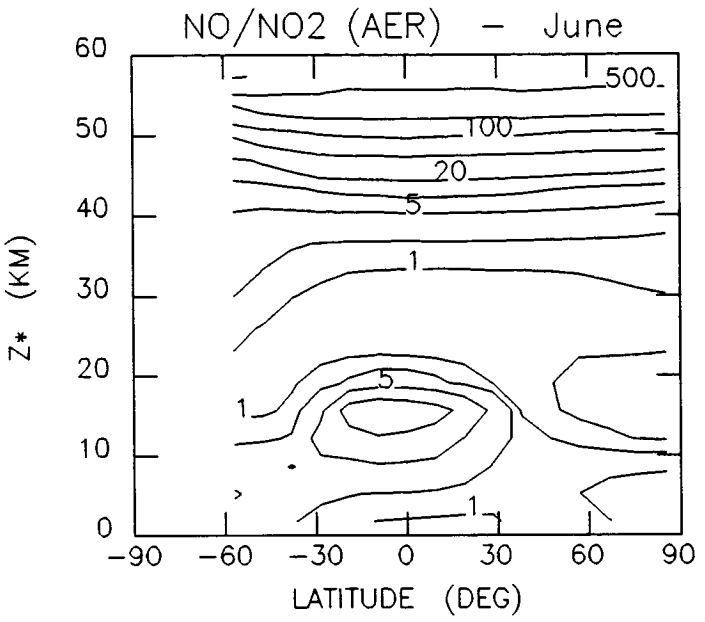
NO/NO2 (AER) – June
Z* (KM)
LATITUDE (DEG)
500
100
20
5
1

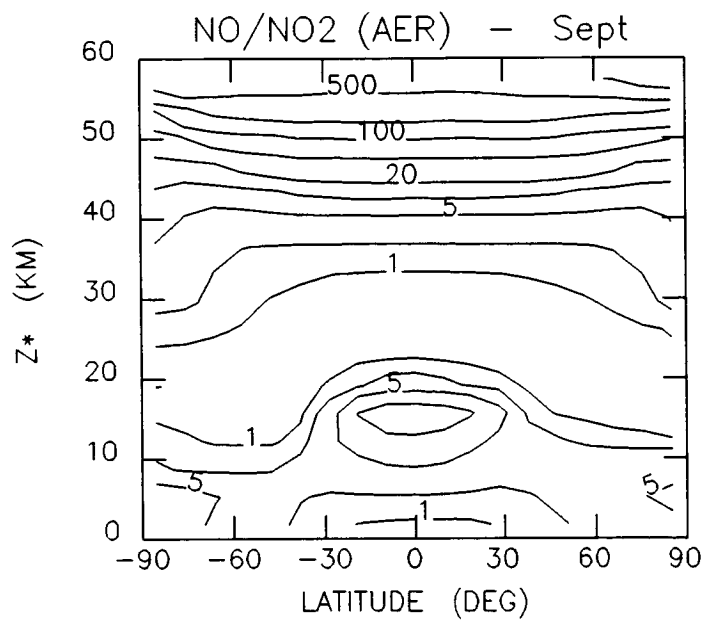
NO/NO2 (AER) – Sept
Z* (KM)
LATITUDE (DEG)
500
100
20
5
1

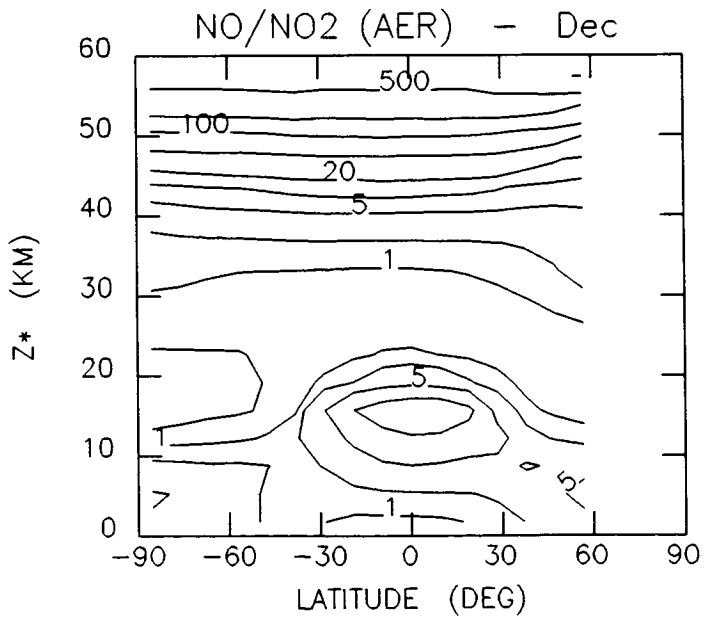
NO/NO2 (AER) – Dec
Z* (KM)
LATITUDE (DEG)
500
100
20
5
1

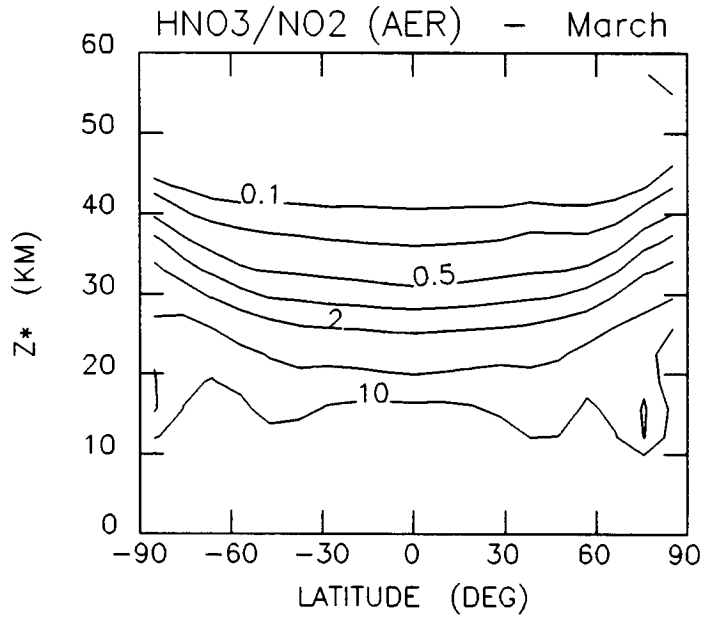
HNO3/NO2 (AER) – March
Z* (KM)
LATITUDE (DEG)
0.1
0.5
2
10

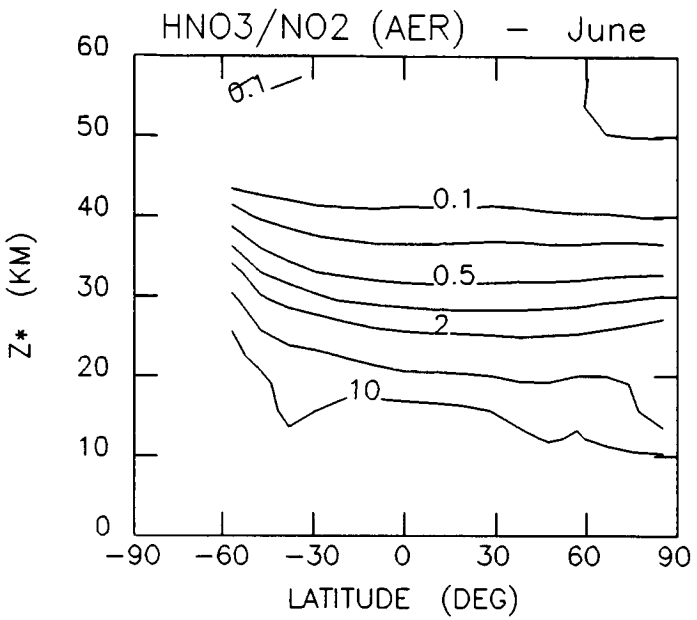
HNO3/NO2 (AER) – June
Z* (KM)
LATITUDE (DEG)
0.1
0.5
2
10

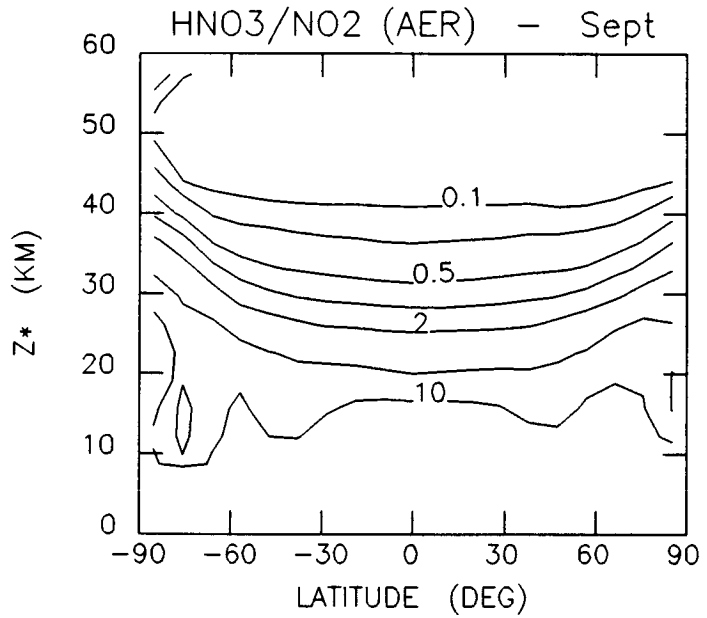
HNO3/NO2 (AER) – Sept
Z* (KM)
LATITUDE (DEG)
0.1
0.5
2
10

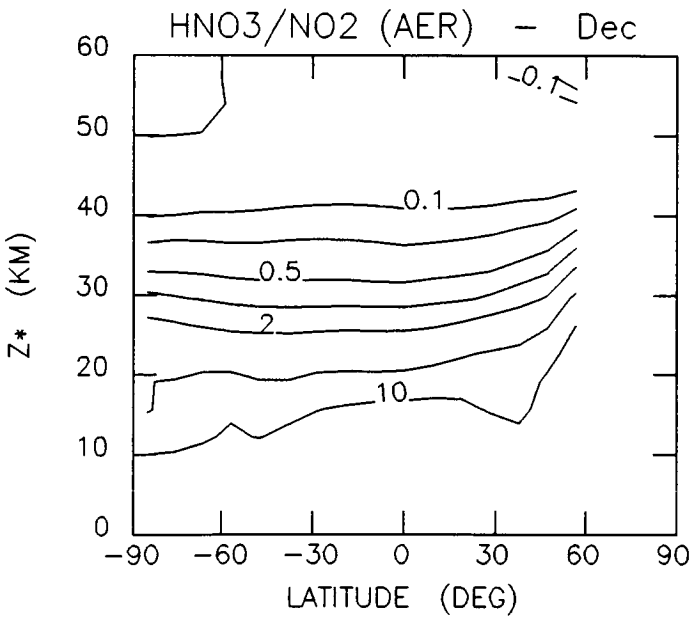
HNO3/NO2 (AER) – Dec
Z* (KM)
LATITUDE (DEG)
0.1
0.5
2
10

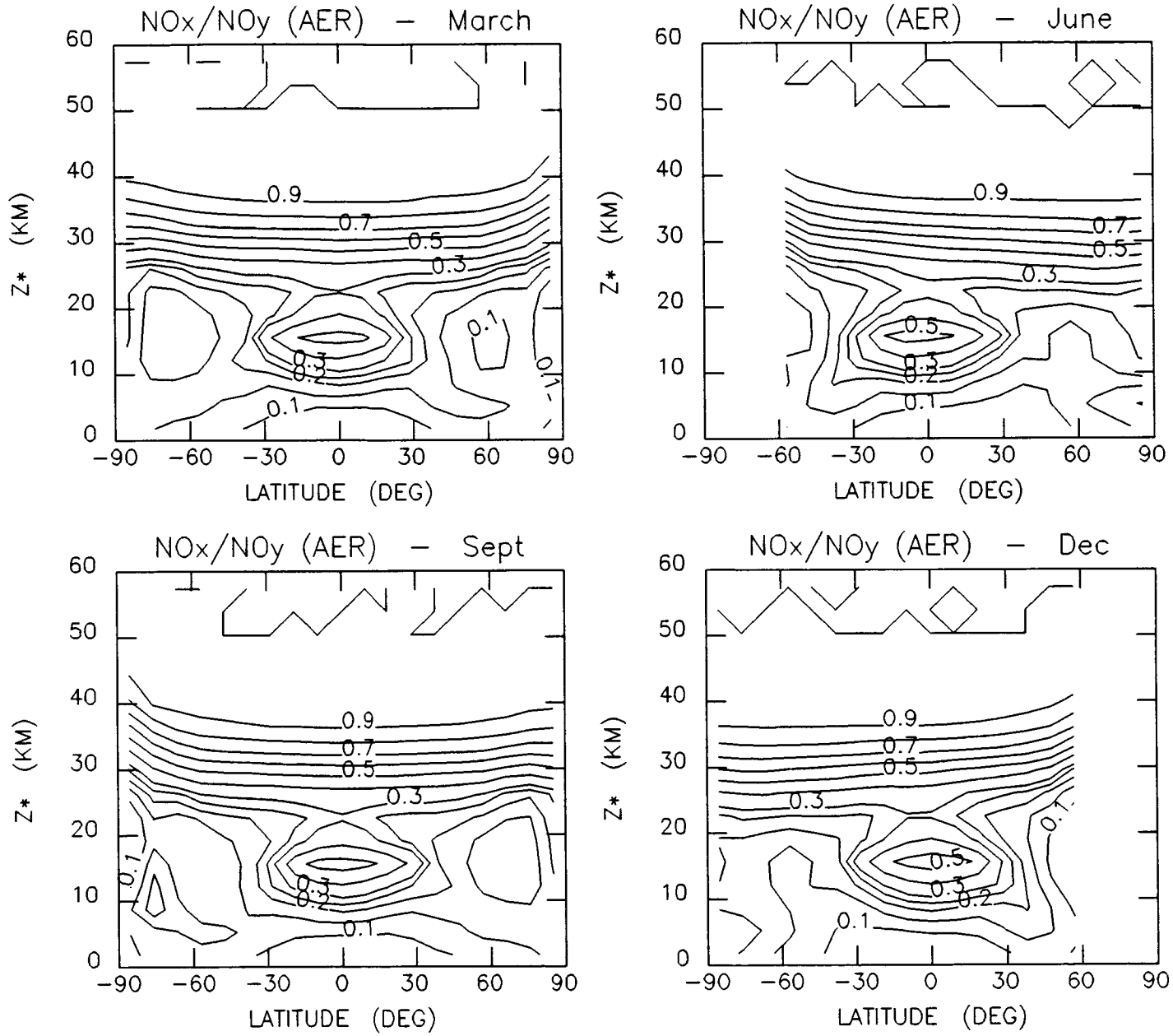
NOx/NOy (AER) – March
NOx/NOy (AER) – June
NOx/NOy (AER) – Sept
NOx/NOy (AER) – Dec
Z* (KM)
LATITUDE (DEG)
0
10
20
30
40
50
60
-90
-60
-30
0
30
60
90
0.9
0.7
0.5
0.3
0.2
0.1

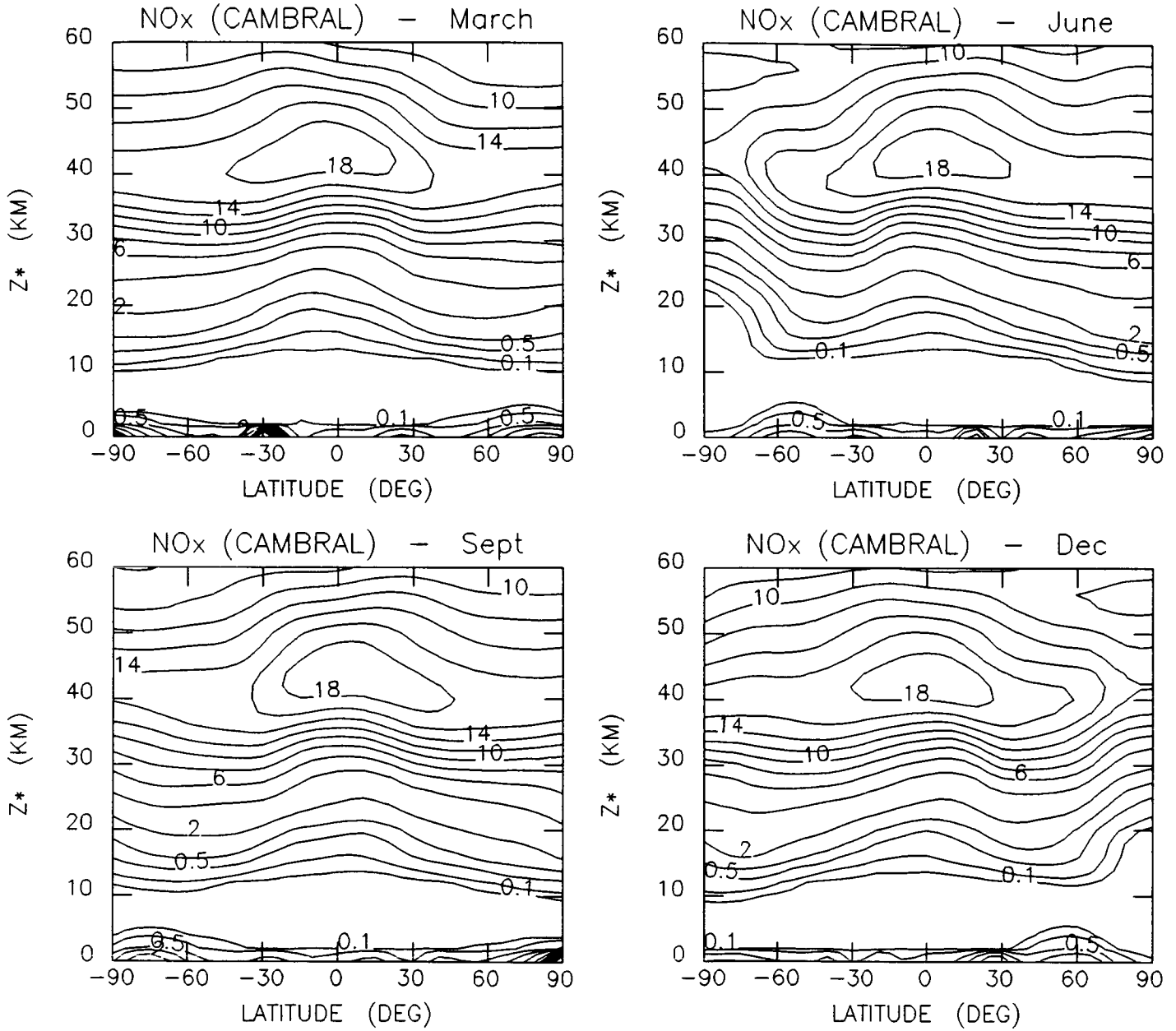
NOx (CAMBRAL) – March
NOx (CAMBRAL) – June
NOx (CAMBRAL) – Sept
NOx (CAMBRAL) – Dec
Z* (KM)
LATITUDE (DEG)
60
50
40
30
20
10
0
−90 −60 −30 0 30 60 90
0.1
0.5
2
6
10
14
18

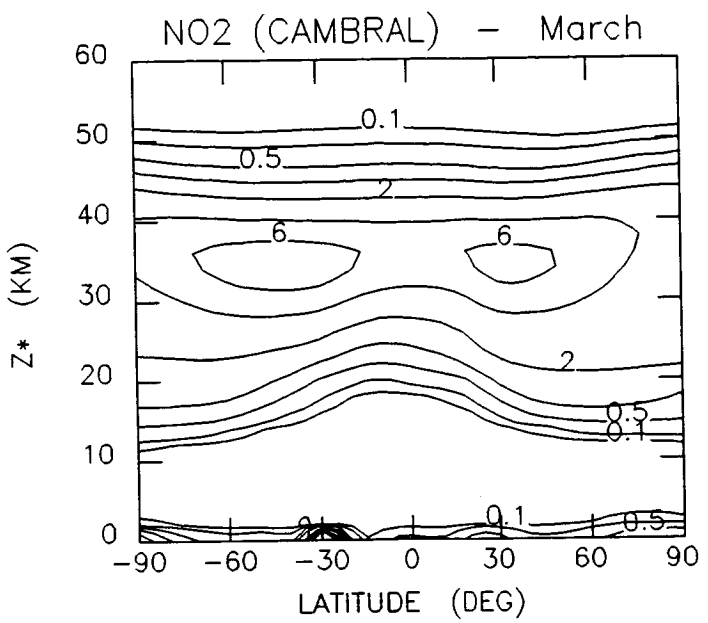
NO2 (CAMBRAL) – March
Z* (KM)
LATITUDE (DEG)
0.1
0.5
2
6

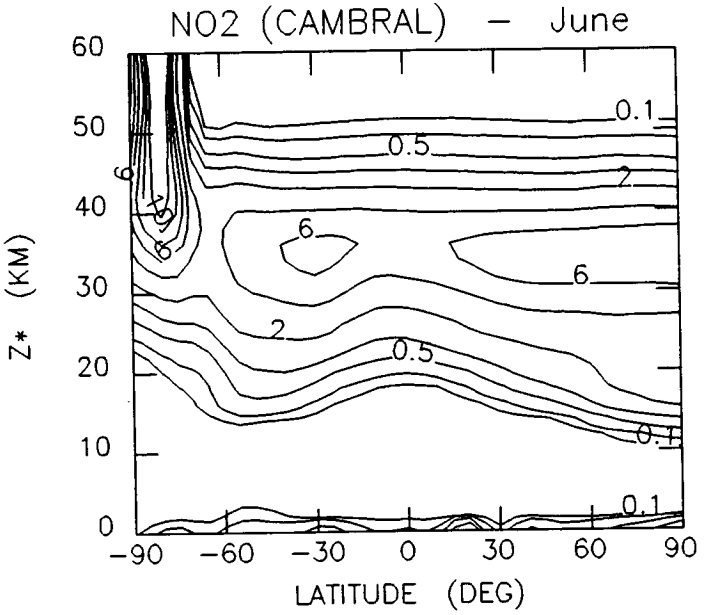
NO2 (CAMBRAL) – June
Z* (KM)
LATITUDE (DEG)
0.1
0.5
2
6

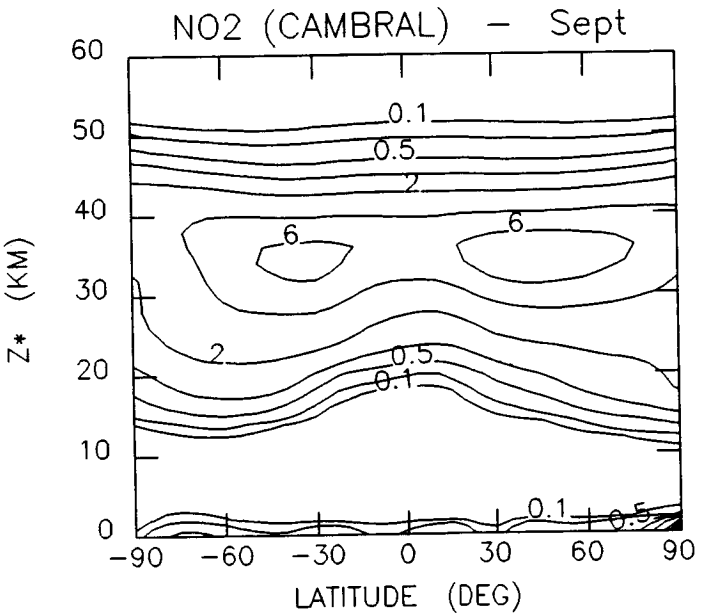
NO2 (CAMBRAL) – Sept
Z* (KM)
LATITUDE (DEG)
0.1
0.5
2
6

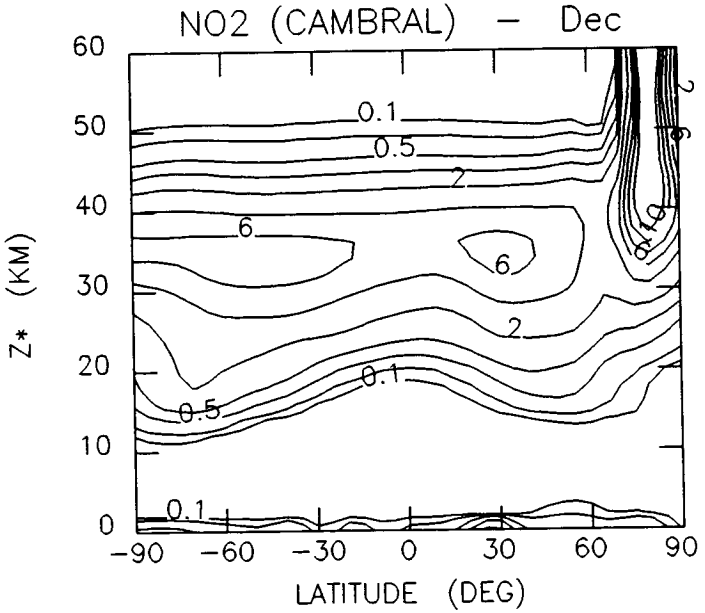
NO2 (CAMBRAL) – Dec
Z* (KM)
LATITUDE (DEG)
0.1
0.5
2
6

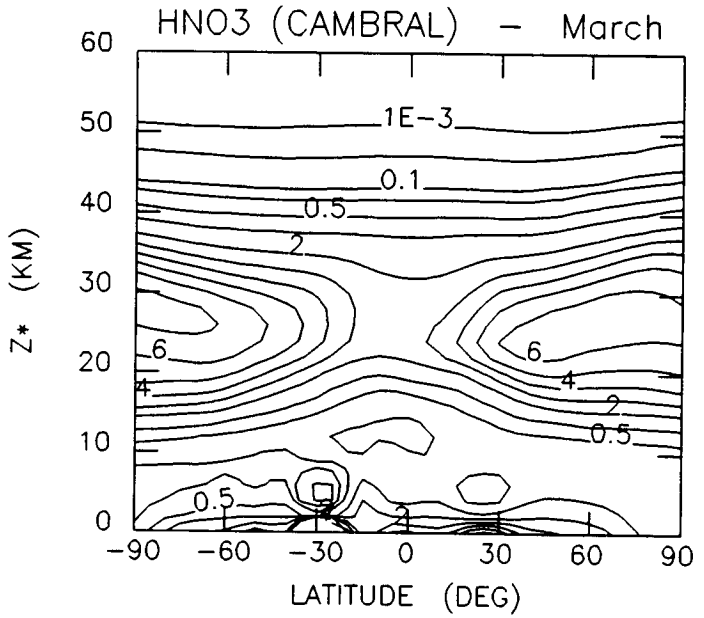
HNO3 (CAMBRAL) – March
Z* (KM)
LATITUDE (DEG)
1E-3
0.1
0.5
2
4
6
-90 -60 -30 0 30 60 90
0 10 20 30 40 50 60

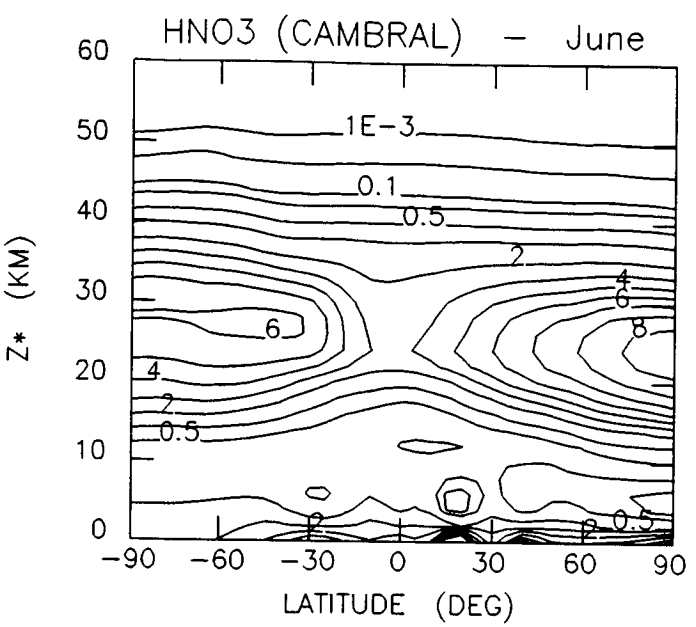
HNO3 (CAMBRAL) – June
Z* (KM)
LATITUDE (DEG)
1E-3
0.1
0.5
2
4
6
8
-90 -60 -30 0 30 60 90
0 10 20 30 40 50 60

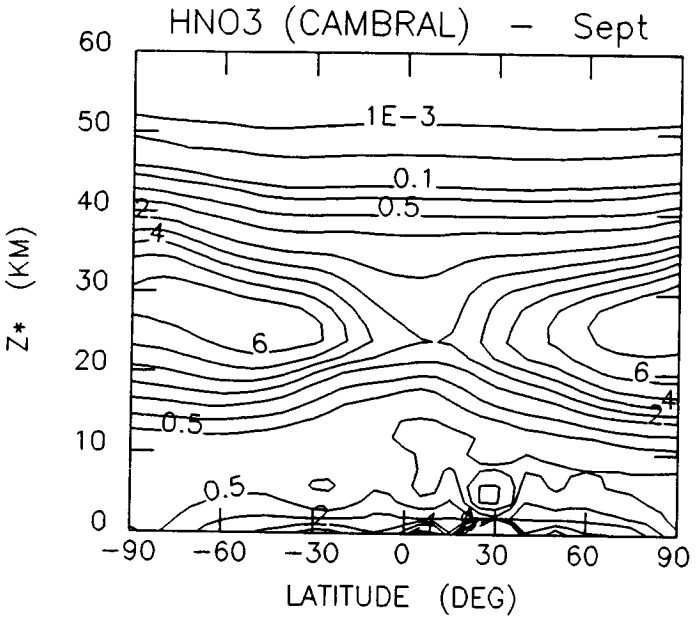
HNO3 (CAMBRAL) – Sept
Z* (KM)
LATITUDE (DEG)
1E-3
0.1
0.5
2
4
6
-90 -60 -30 0 30 60 90
0 10 20 30 40 50 60

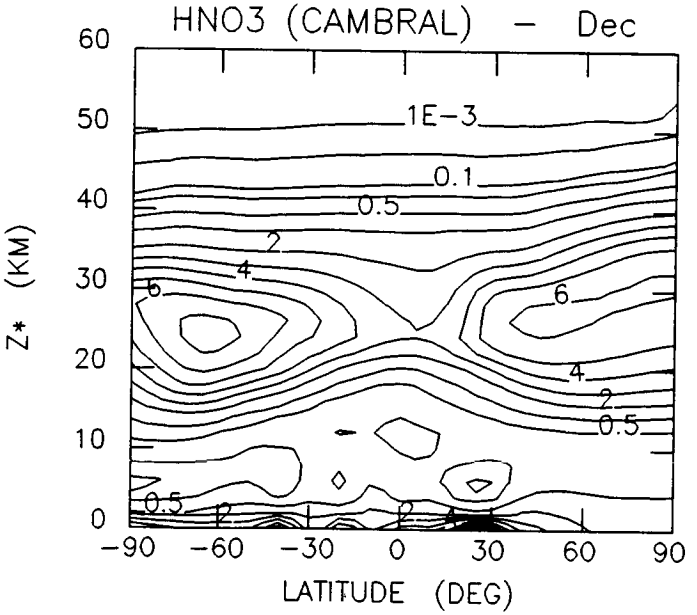
HNO3 (CAMBRAL) – Dec
Z* (KM)
LATITUDE (DEG)
1E-3
0.1
0.5
2
4
6
-90 -60 -30 0 30 60 90
0 10 20 30 40 50 60

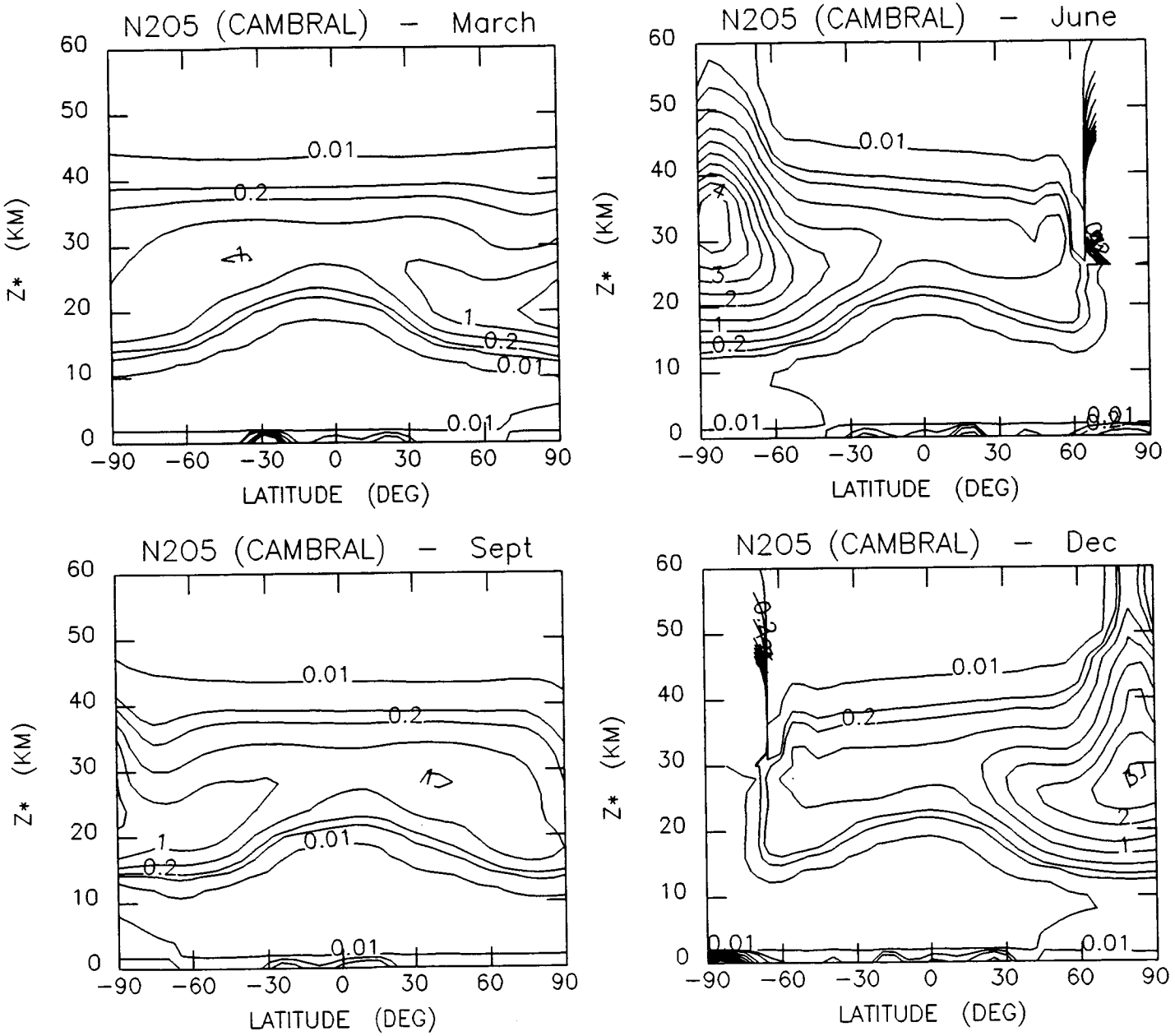
N2O5 (CAMBRAL) – March
N2O5 (CAMBRAL) – June
N2O5 (CAMBRAL) – Sept
N2O5 (CAMBRAL) – Dec
Z* (KM)
LATITUDE (DEG)
0.01
0.2
1
2
3
4
5
0
10
20
30
40
50
60
−90
−60
−30
0
30
60
90

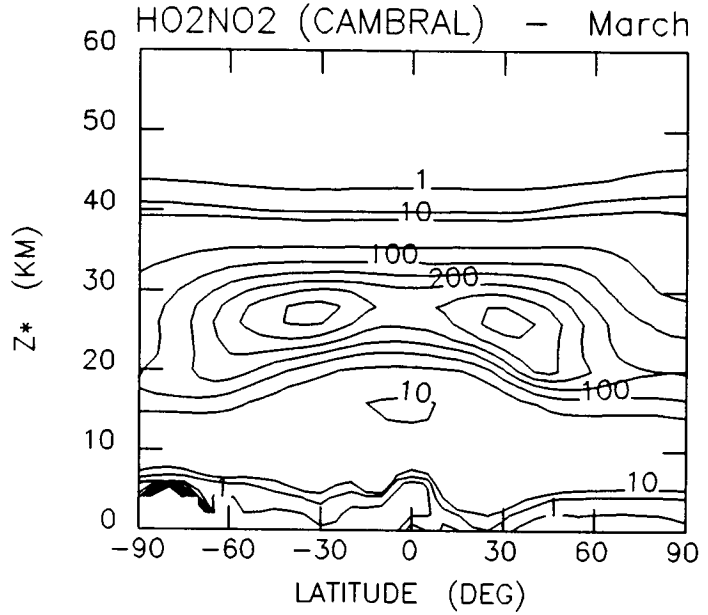
H02NO2 (CAMBRAL) – March
Z* (KM)
LATITUDE (DEG)
60
50
40
30
20
10
0
-90 -60 -30 0 30 60 90
1
10
100
200
10
100
10
1

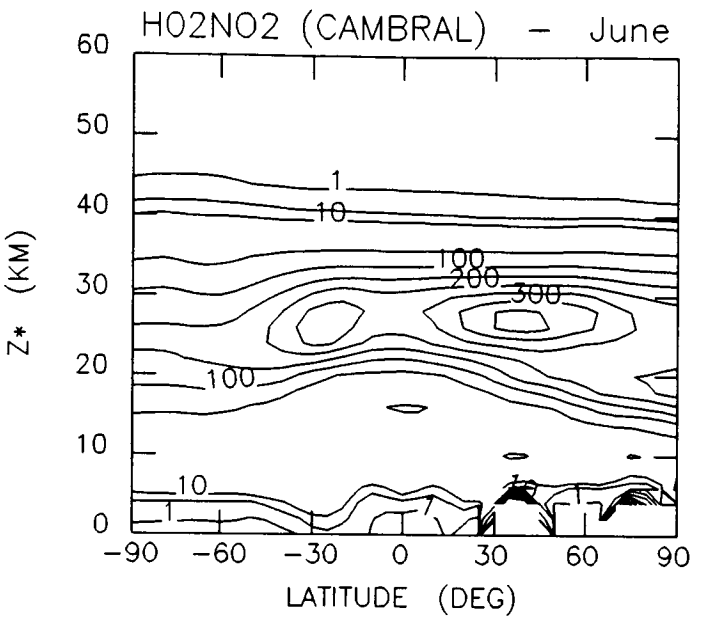
H02NO2 (CAMBRAL) – June
Z* (KM)
LATITUDE (DEG)
60
50
40
30
20
10
0
-90 -60 -30 0 30 60 90
1
10
100
200
300
100
10
1

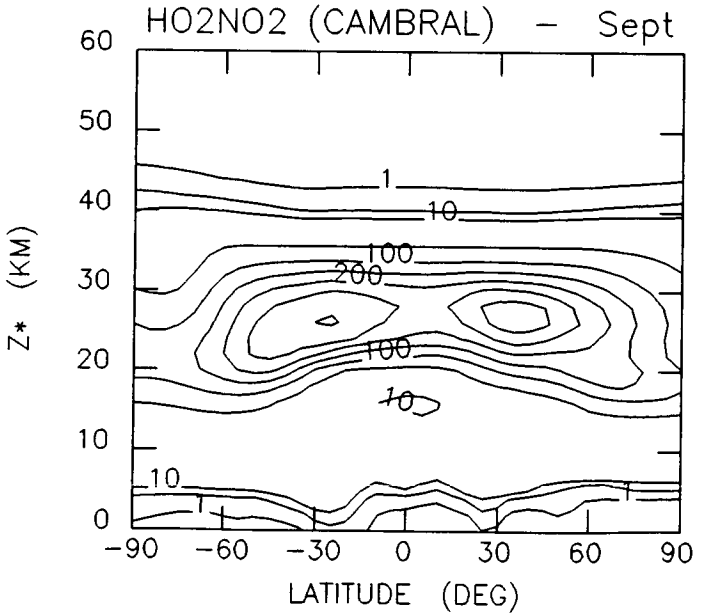
H02NO2 (CAMBRAL) – Sept
Z* (KM)
LATITUDE (DEG)
60
50
40
30
20
10
0
-90 -60 -30 0 30 60 90
1
10
100
200
100
10
10
1

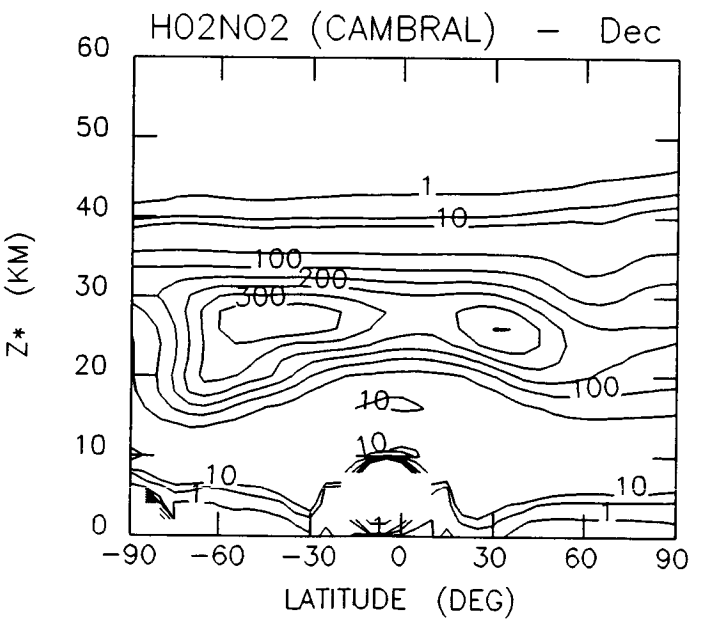
H02NO2 (CAMBRAL) – Dec
Z* (KM)
LATITUDE (DEG)
60
50
40
30
20
10
0
-90 -60 -30 0 30 60 90
1
10
100
200
300
100
10
10
10
10

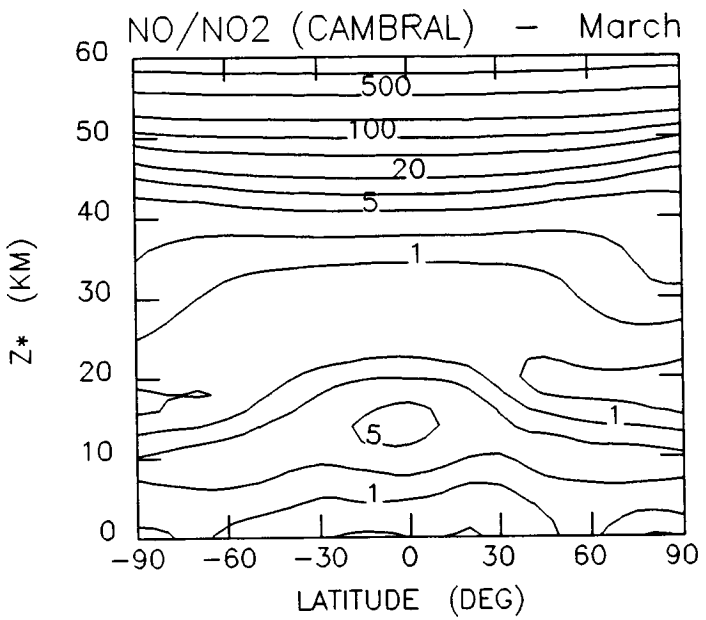
NO/NO2 (CAMBRAL) – March
Z* (KM)
LATITUDE (DEG)
500
100
20
5
1
5
1
1

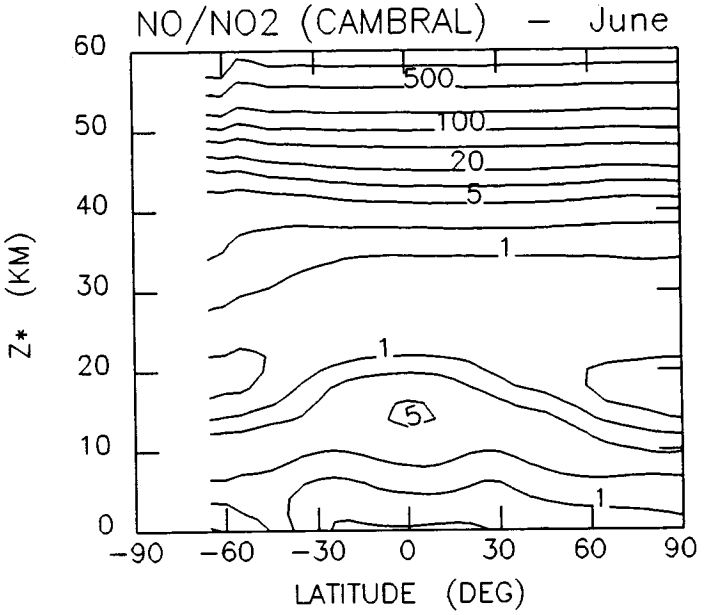
NO/NO2 (CAMBRAL) – June
Z* (KM)
LATITUDE (DEG)
500
100
20
5
1
1
5
1

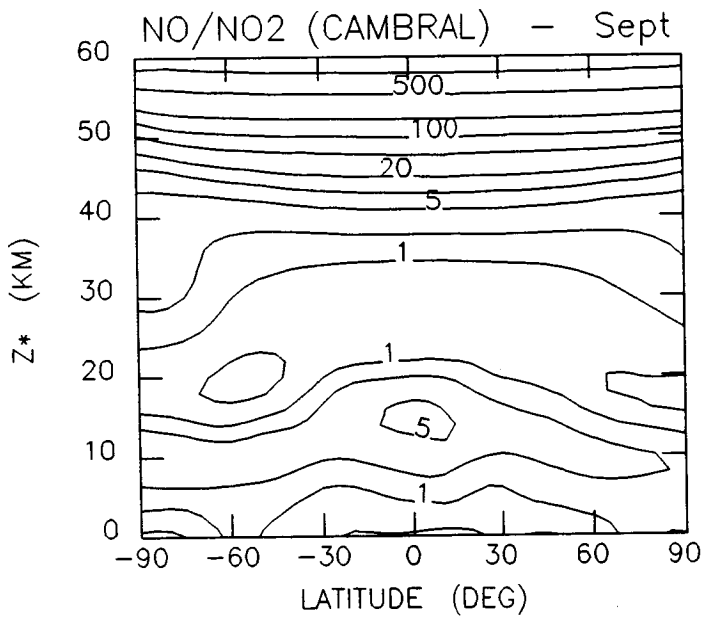
NO/NO2 (CAMBRAL) – Sept
Z* (KM)
LATITUDE (DEG)
500
100
20
5
1
1
5
1

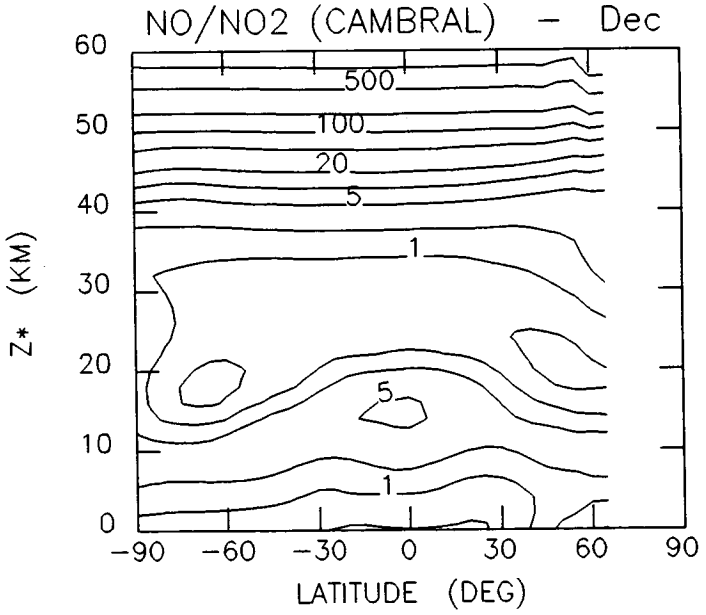
NO/NO2 (CAMBRAL) – Dec
Z* (KM)
LATITUDE (DEG)
500
100
20
5
1
5
1

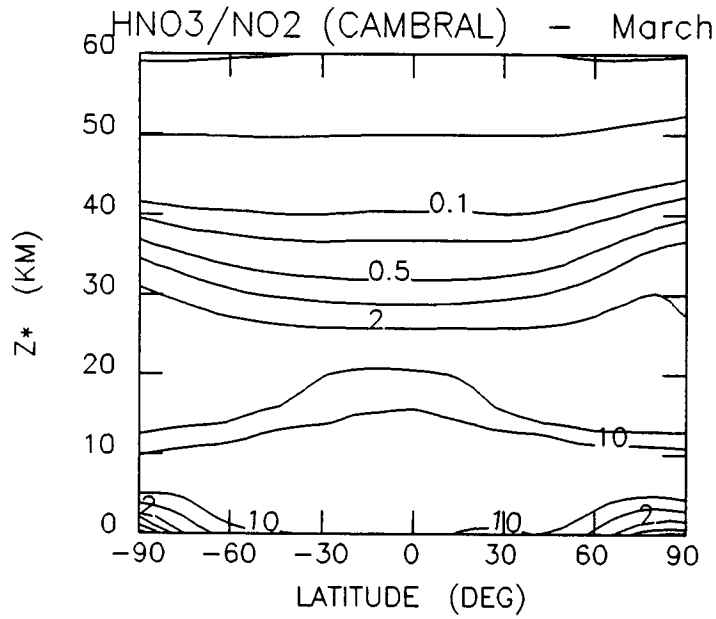
HNO3/NO2 (CAMBRAL) – March
Z* (KM)
LATITUDE (DEG)
0.1
0.5
2
10

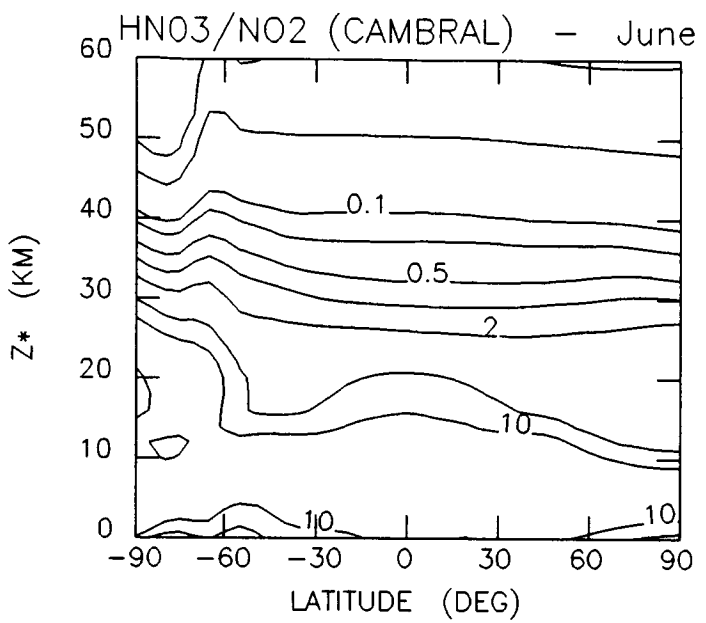
HNO3/NO2 (CAMBRAL) – June
Z* (KM)
LATITUDE (DEG)
0.1
0.5
2
10

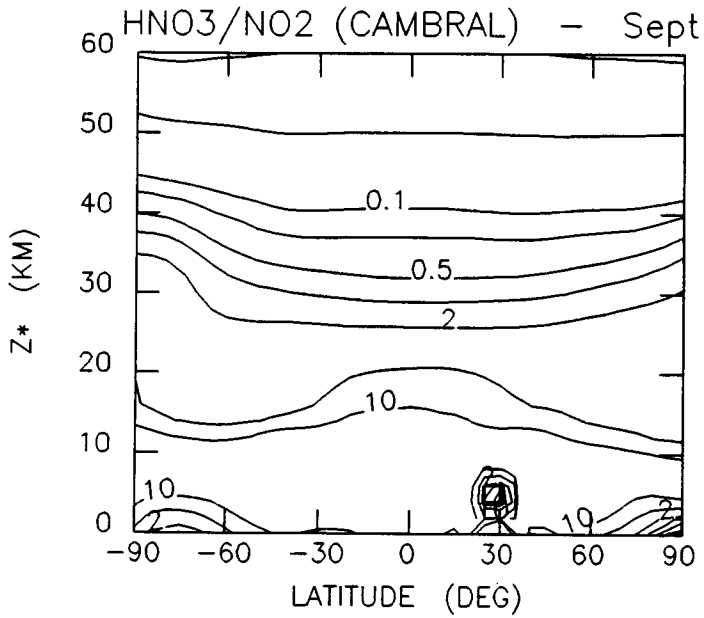
HNO3/NO2 (CAMBRAL) – Sept
Z* (KM)
LATITUDE (DEG)
0.1
0.5
2
10

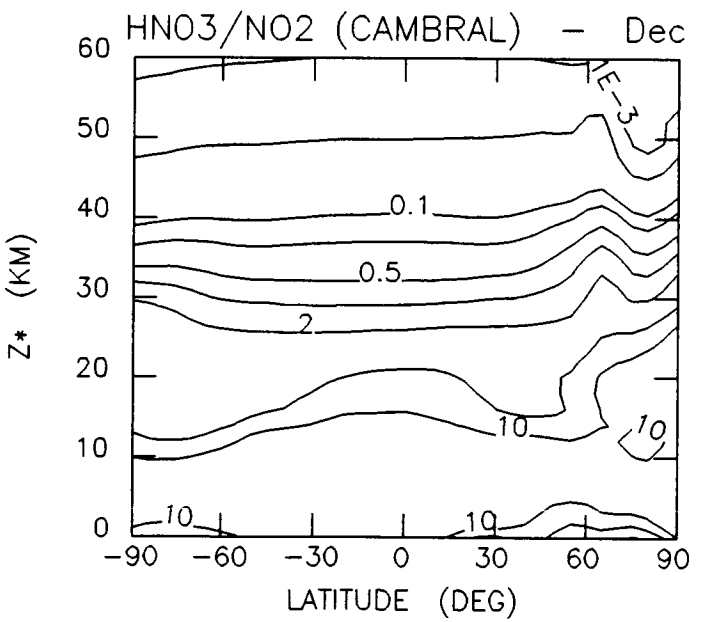
HNO3/NO2 (CAMBRAL) – Dec
Z* (KM)
LATITUDE (DEG)
1E-3
0.1
0.5
2
10

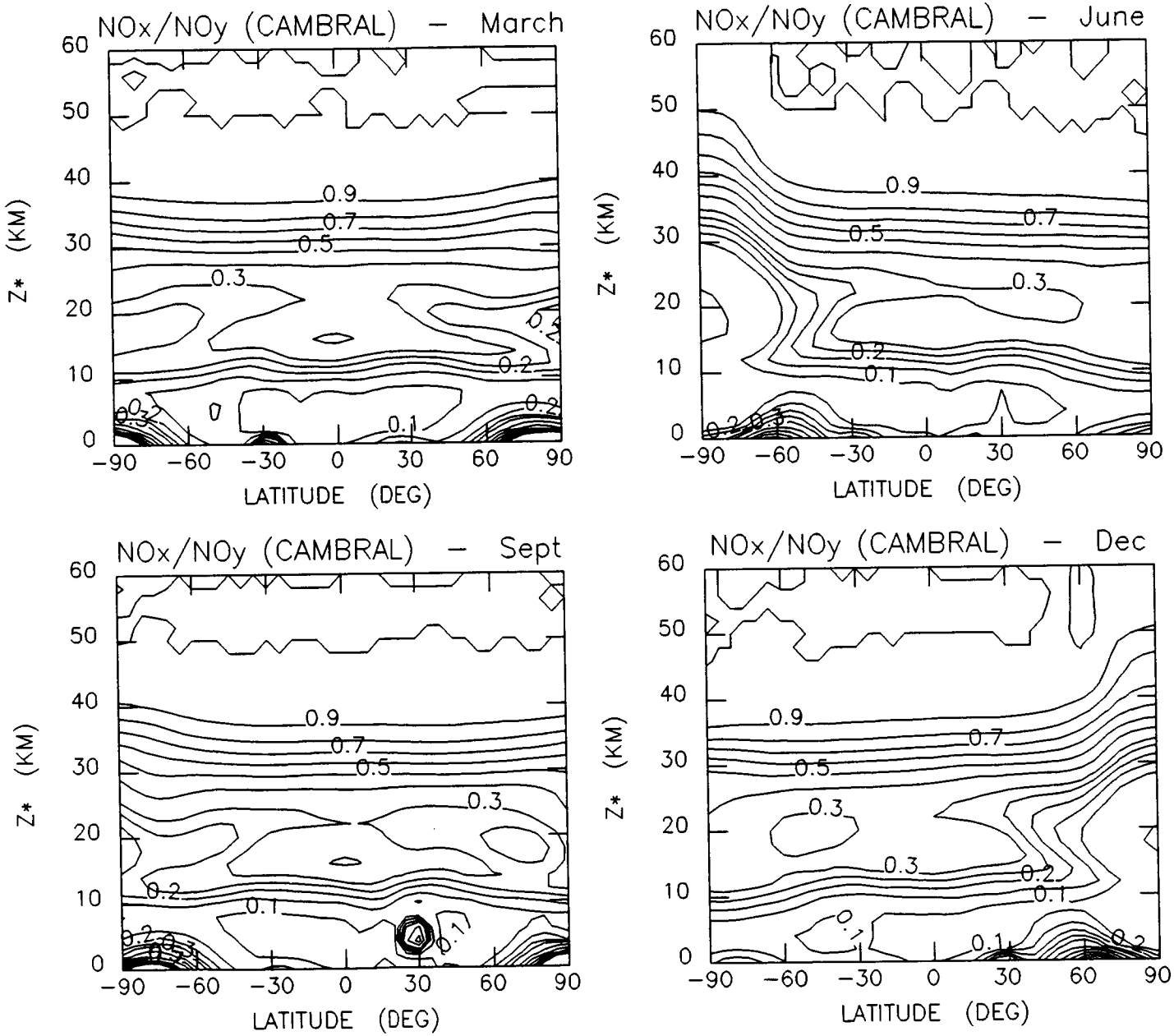
NOx/NOy (CAMBRAL) – March
NOx/NOy (CAMBRAL) – June
NOx/NOy (CAMBRAL) – Sept
NOx/NOy (CAMBRAL) – Dec
Z* (KM)
LATITUDE (DEG)
0
10
20
30
40
50
60
-90
-60
-30
0
30
60
90
0.9
0.7
0.5
0.3
0.2
0.1

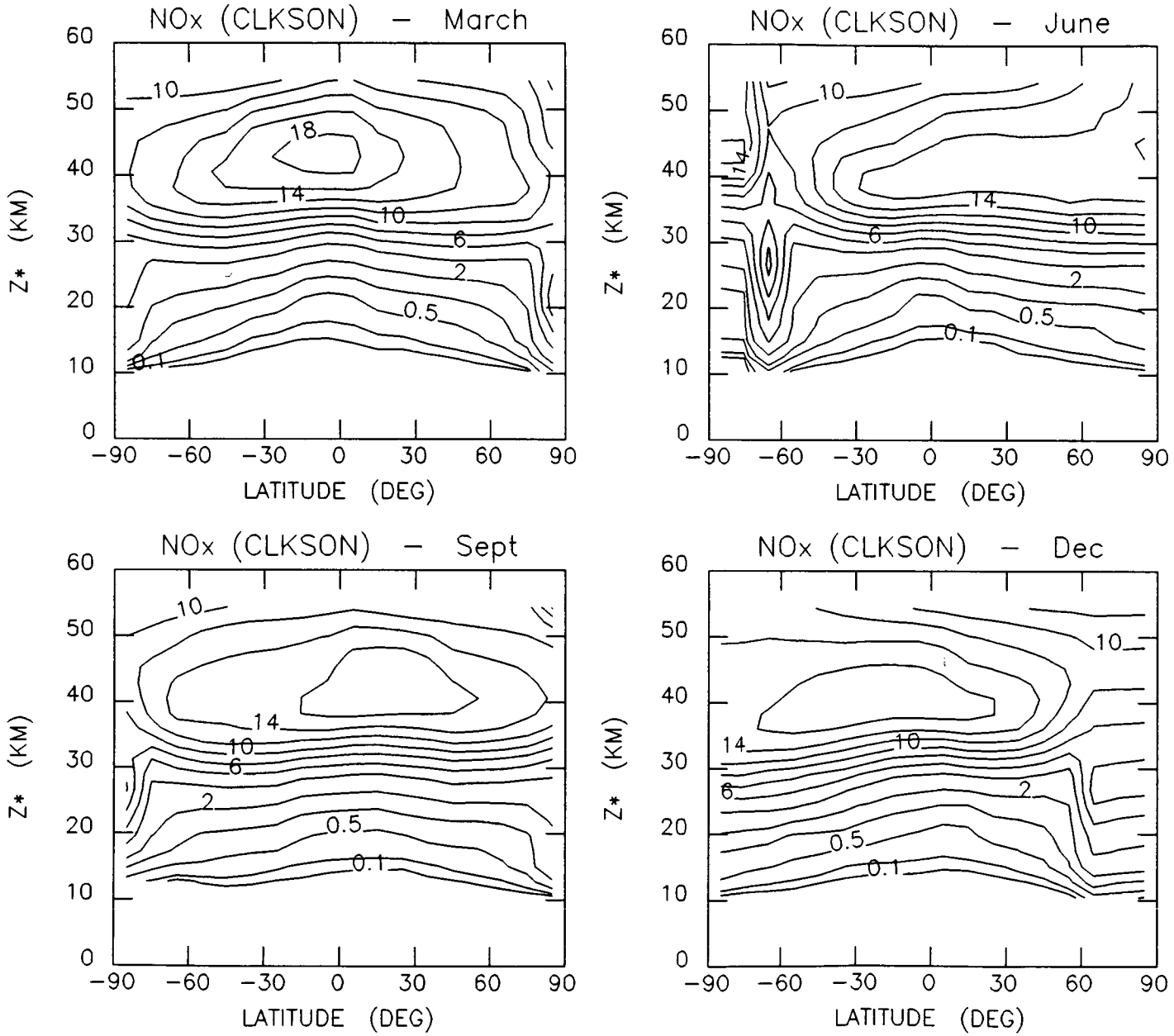
NOx (CLKSON) – March
NOx (CLKSON) – June
NOx (CLKSON) – Sept
NOx (CLKSON) – Dec
Z* (KM)
LATITUDE (DEG)
60
50
40
30
20
10
0
−90 −60 −30 0 30 60 90
10
18
14
6
2
0.5
0.1

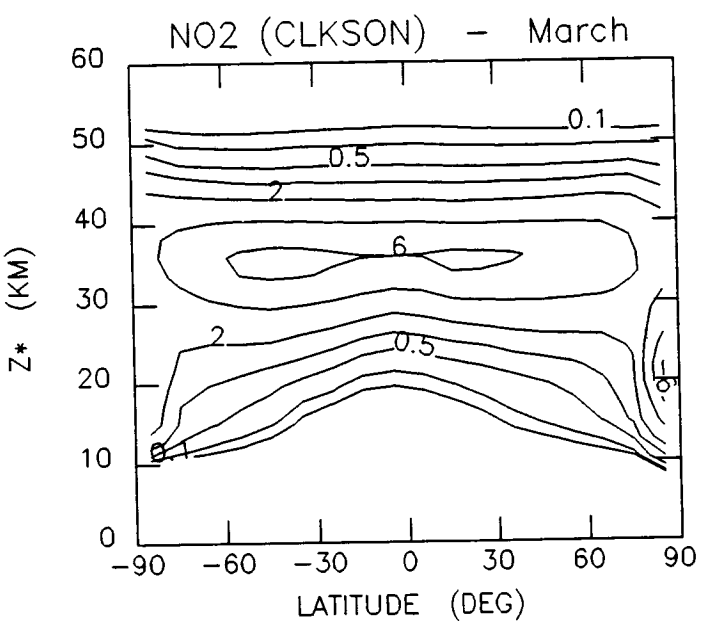
NO2 (CLKSON) – March
Z* (KM)
LATITUDE (DEG)
0.1
0.5
2
6

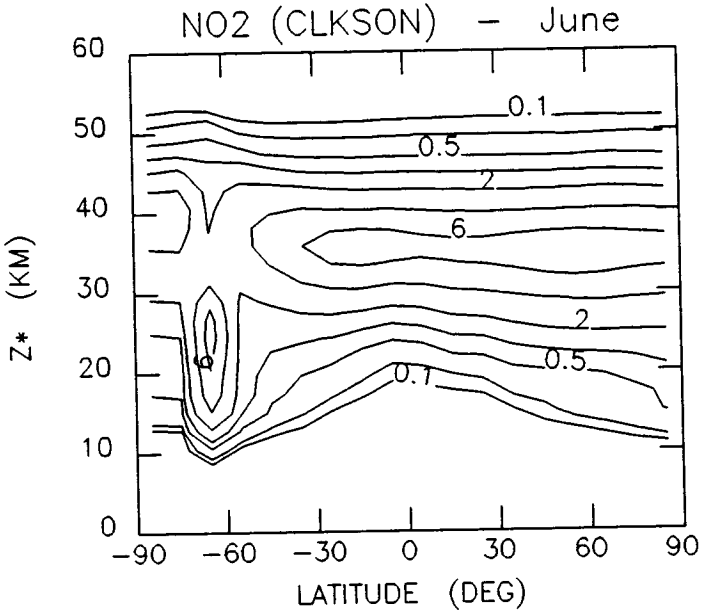
NO2 (CLKSON) – June
Z* (KM)
LATITUDE (DEG)
0.1
0.5
2
6

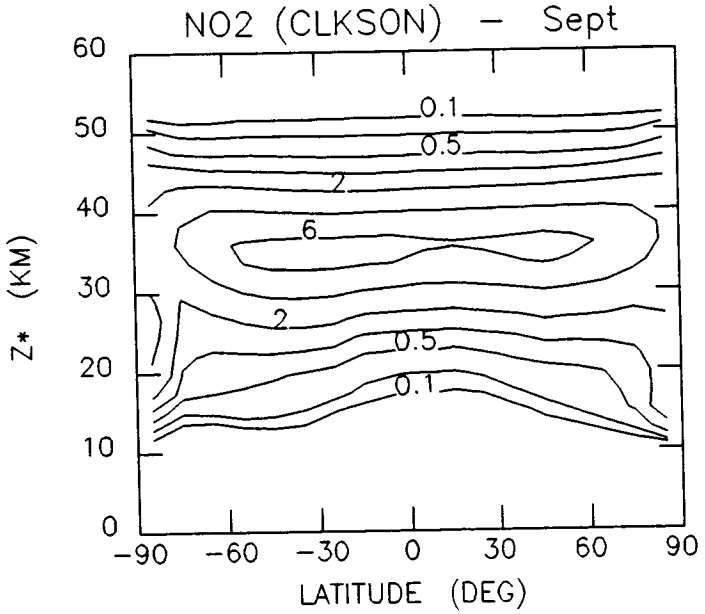
NO2 (CLKSON) – Sept
Z* (KM)
LATITUDE (DEG)
0.1
0.5
2
6

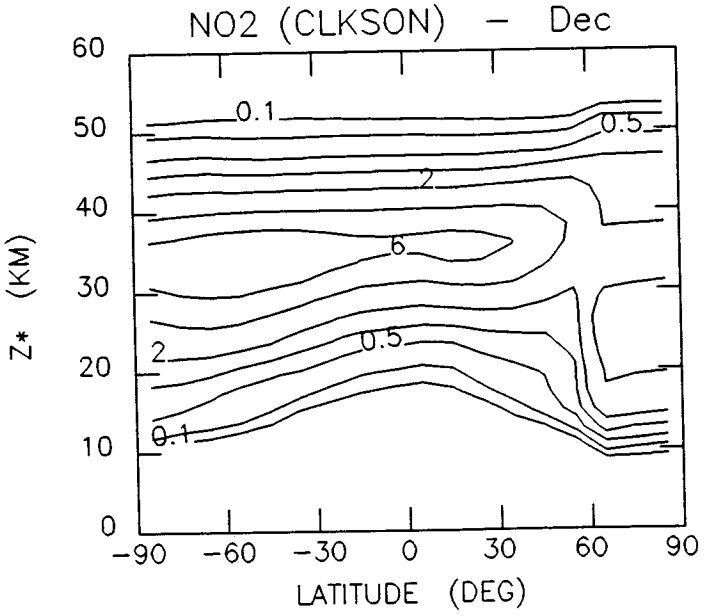
NO2 (CLKSON) – Dec
Z* (KM)
LATITUDE (DEG)
0.1
0.5
2
6

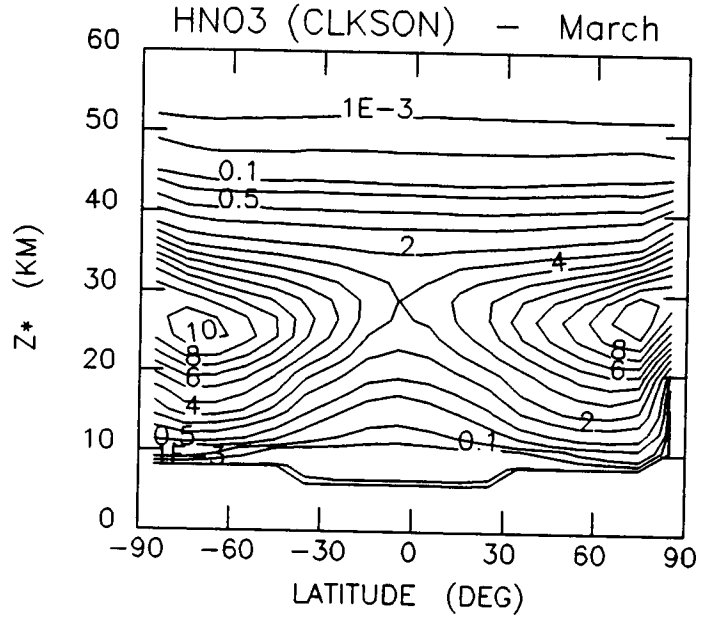
HNO3 (CLKSON) – March
Z* (KM)
LATITUDE (DEG)
1E-3
0.1
0.5
2
4
6
8
10

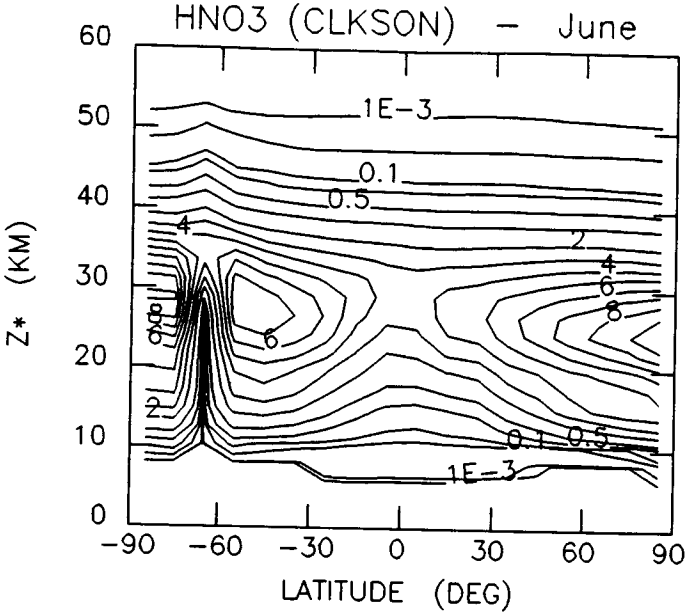
HNO3 (CLKSON) – June
Z* (KM)
LATITUDE (DEG)
1E-3
0.1
0.5
2
4
6
8

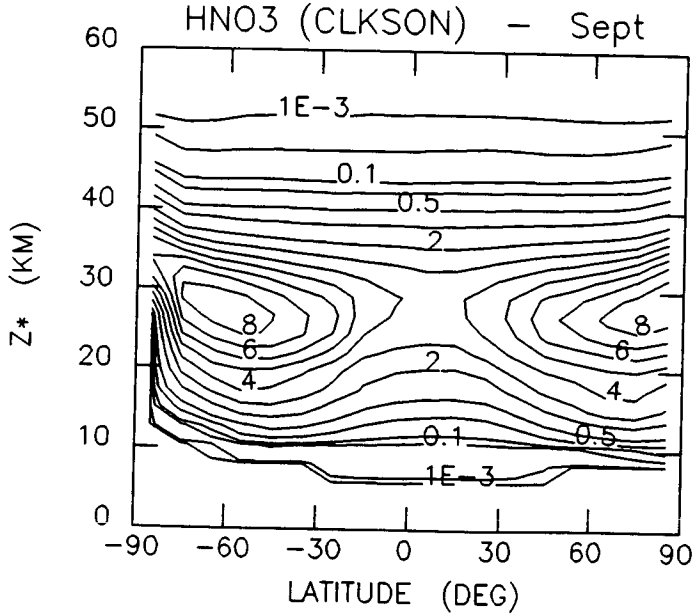
HNO3 (CLKSON) – Sept
Z* (KM)
LATITUDE (DEG)
1E-3
0.1
0.5
2
4
6
8

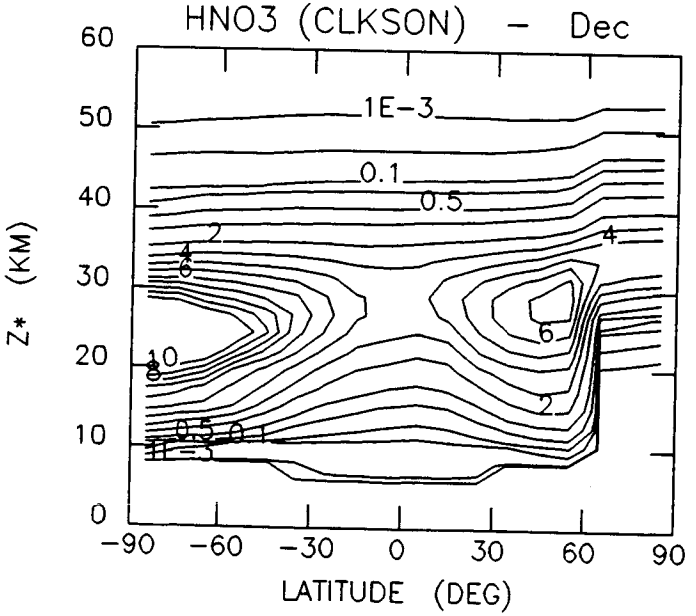
HNO3 (CLKSON) – Dec
Z* (KM)
LATITUDE (DEG)
1E-3
0.1
0.5
2
4
6
8
10

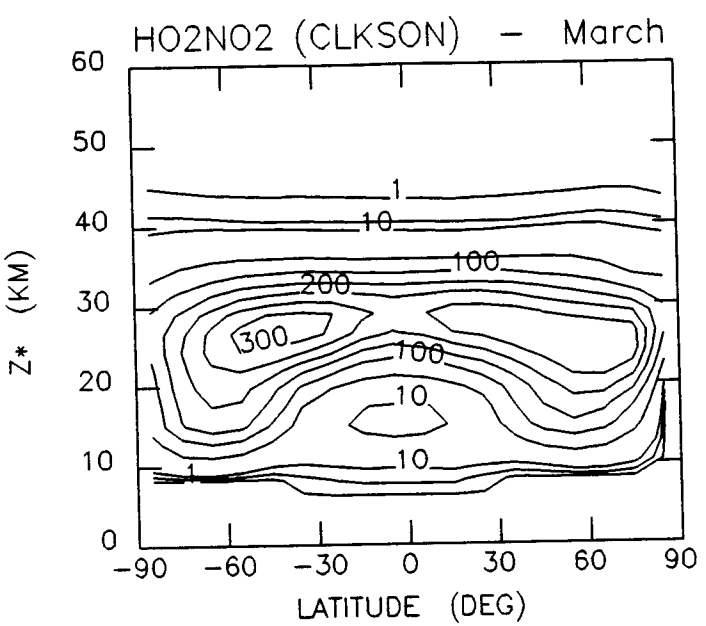
HO2NO2 (CLKSON) – March
Z* (KM)
LATITUDE (DEG)
1
10
100
200
300
100
10
10
1

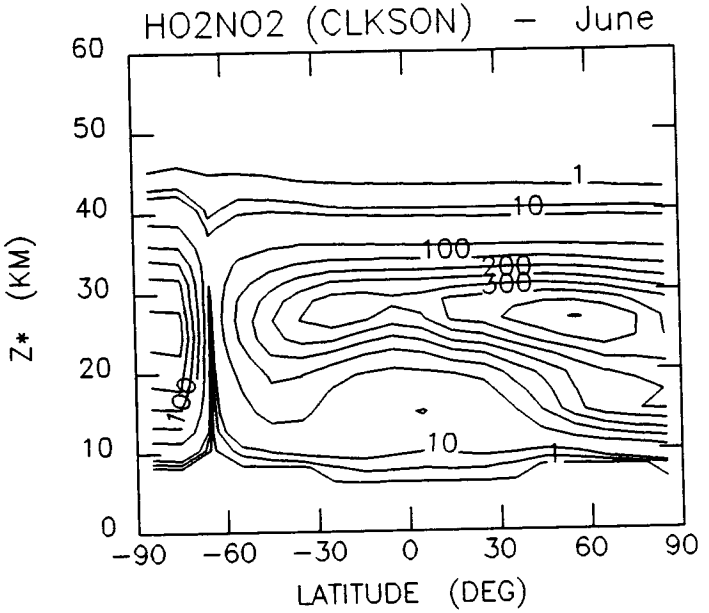
HO2NO2 (CLKSON) – June
Z* (KM)
LATITUDE (DEG)
1
10
100
200
300
100
10
1

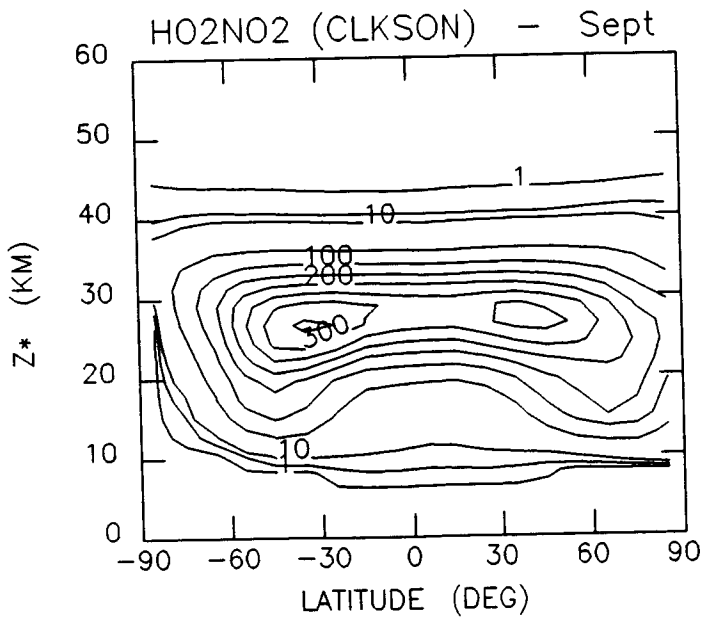
HO2NO2 (CLKSON) – Sept
Z* (KM)
LATITUDE (DEG)
1
10
100
200
300
10

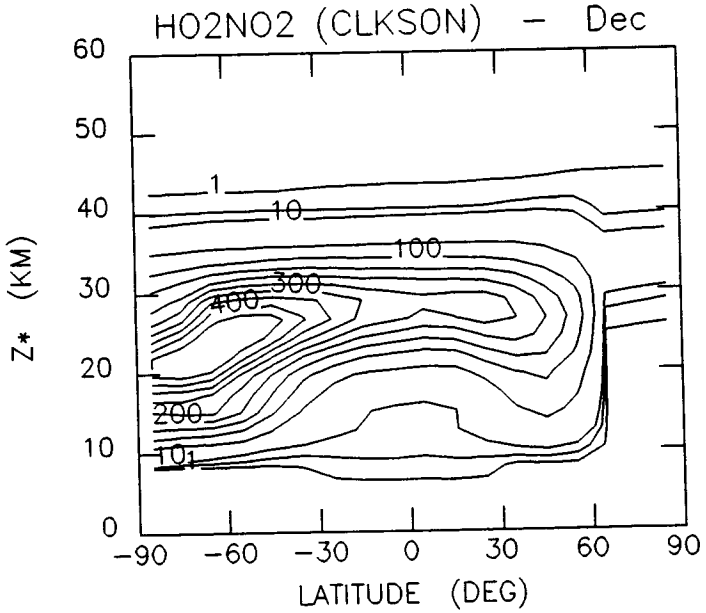
HO2NO2 (CLKSON) – Dec
Z* (KM)
LATITUDE (DEG)
1
10
100
300
400
200
10

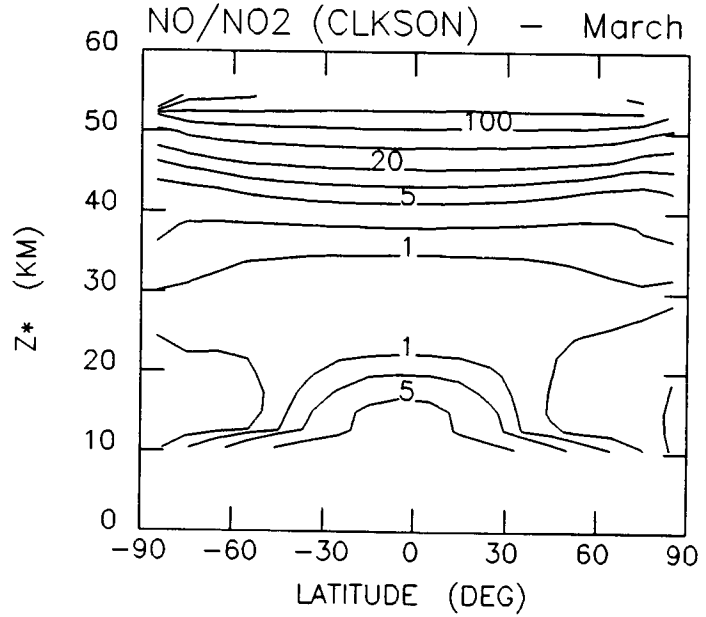
NO/NO2 (CLKSON) – March
Z* (KM)
LATITUDE (DEG)
100
20
5
1
1
5

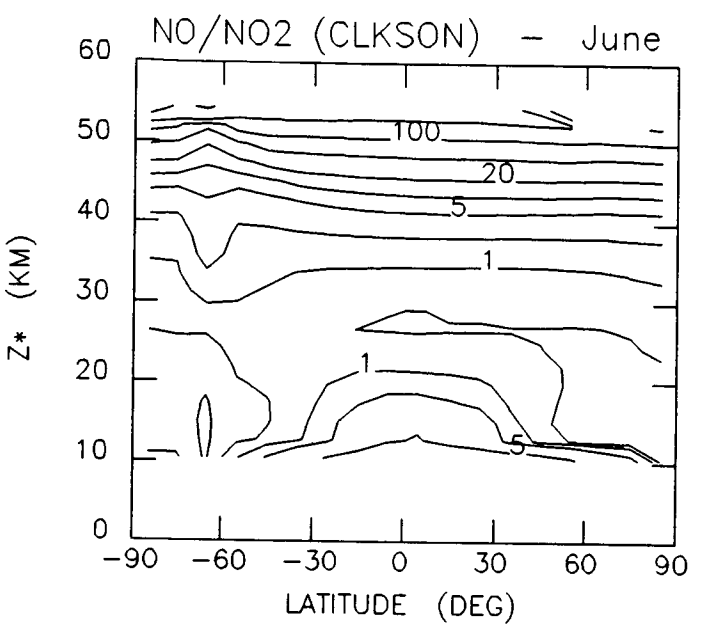
NO/NO2 (CLKSON) – June
Z* (KM)
LATITUDE (DEG)
100
20
5
1
1
5

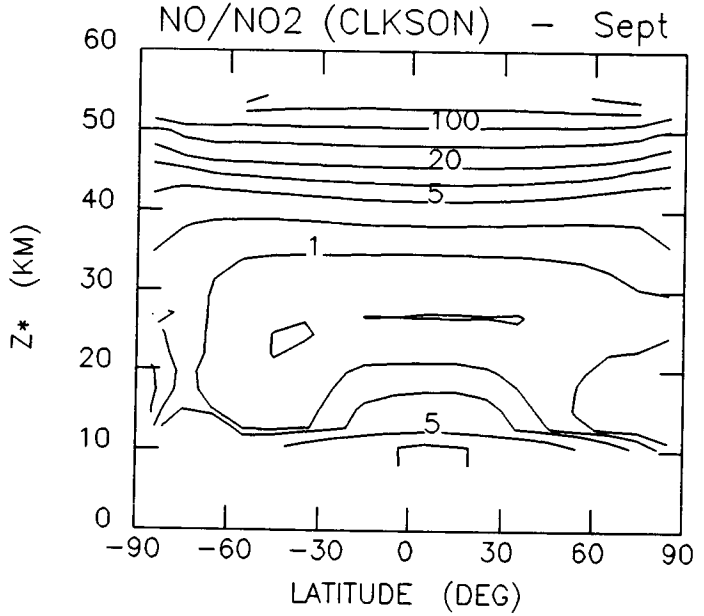
NO/NO2 (CLKSON) – Sept
Z* (KM)
LATITUDE (DEG)
100
20
5
1
5

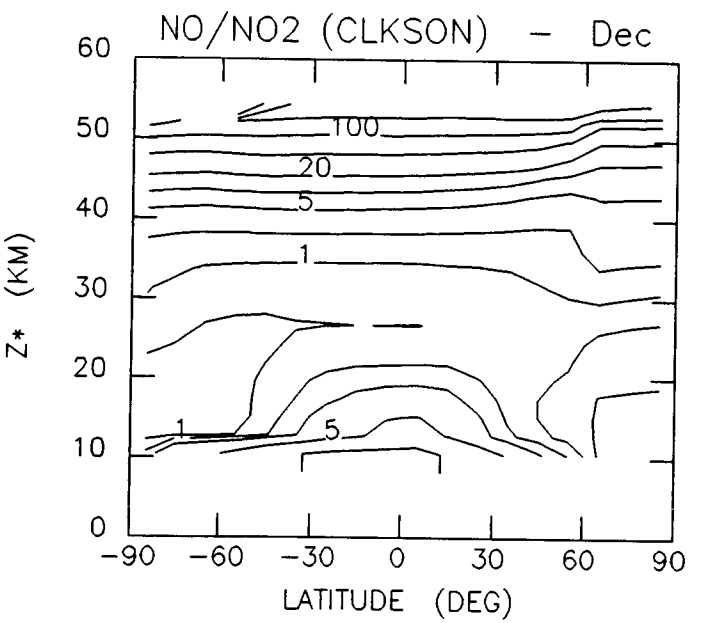
NO/NO2 (CLKSON) – Dec
Z* (KM)
LATITUDE (DEG)
100
20
5
1
1
5

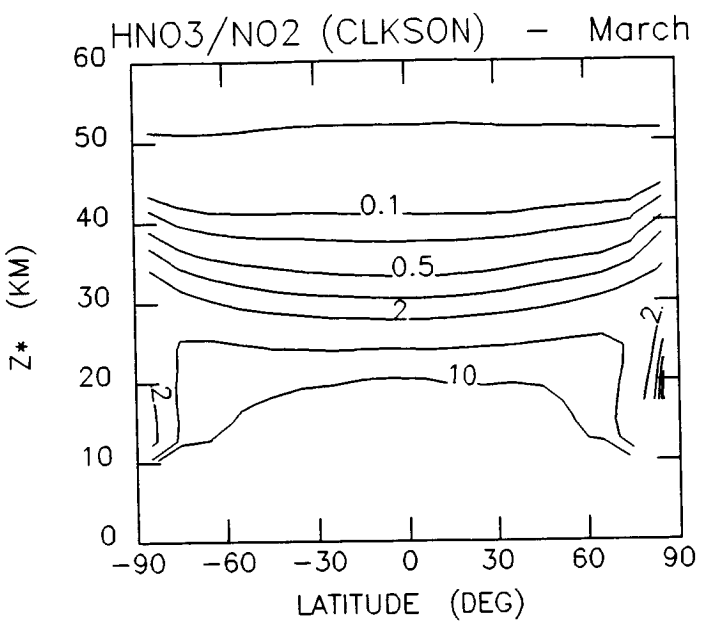
HNO3/NO2 (CLKSON) – March
Z* (KM)
LATITUDE (DEG)
0.1
0.5
2
10

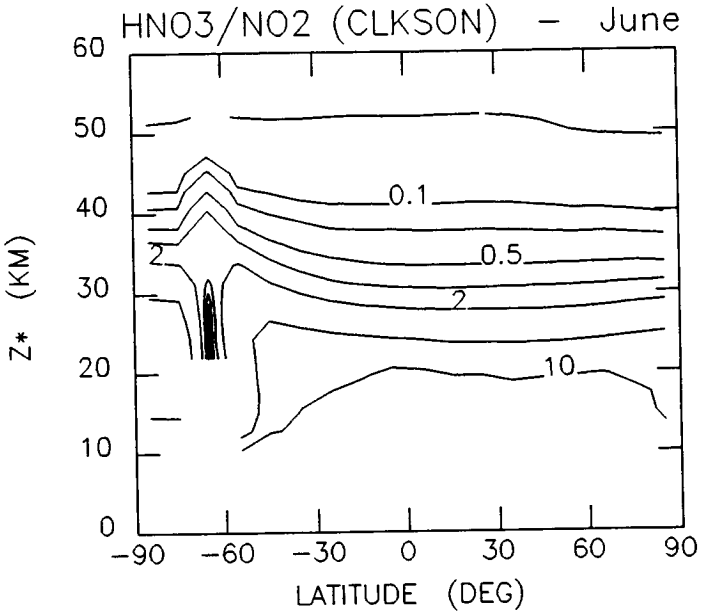
HNO3/NO2 (CLKSON) – June
Z* (KM)
LATITUDE (DEG)
0.1
0.5
2
10

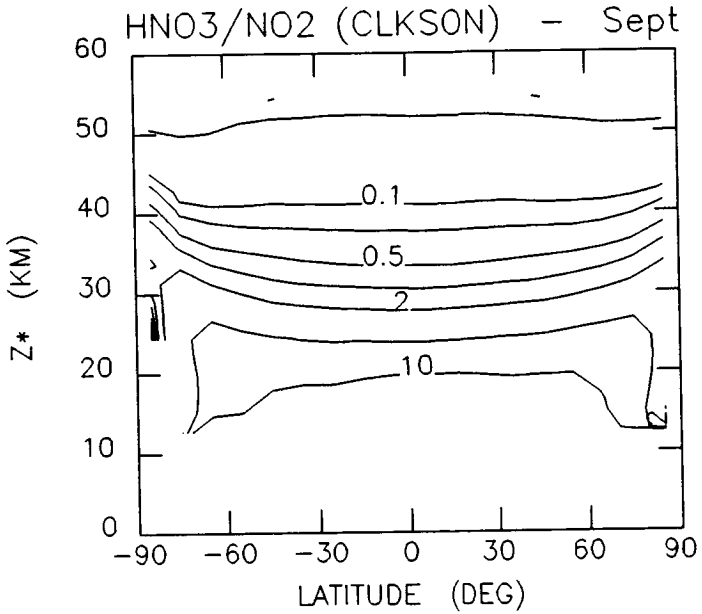
HNO3/NO2 (CLKSON) – Sept
Z* (KM)
LATITUDE (DEG)
0.1
0.5
2
10

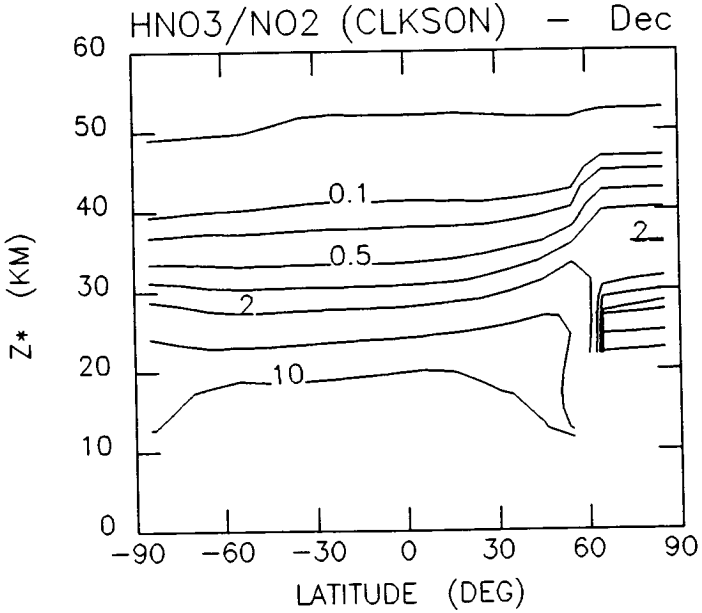
HNO3/NO2 (CLKSON) – Dec
Z* (KM)
LATITUDE (DEG)
0.1
0.5
2
10

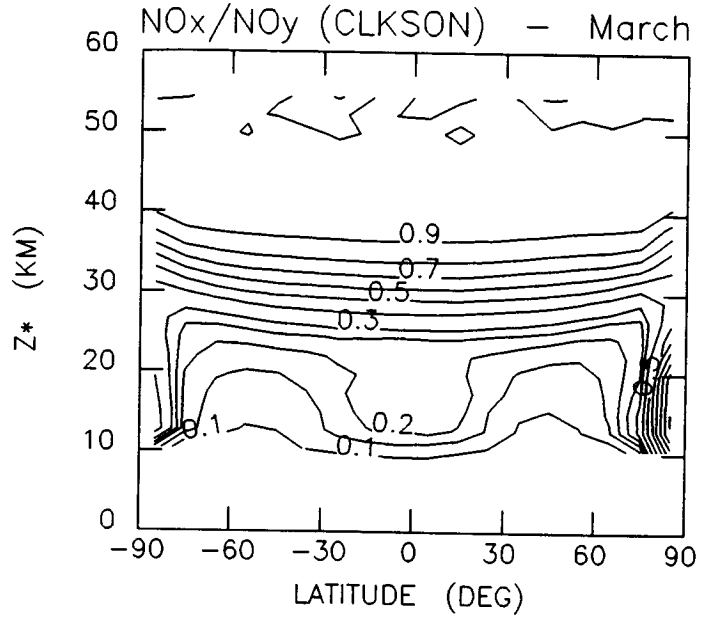
NOx/NOy (CLKSON) – March
Z* (KM)
LATITUDE (DEG)
0.9
0.7
0.5
0.3
0.2
0.1

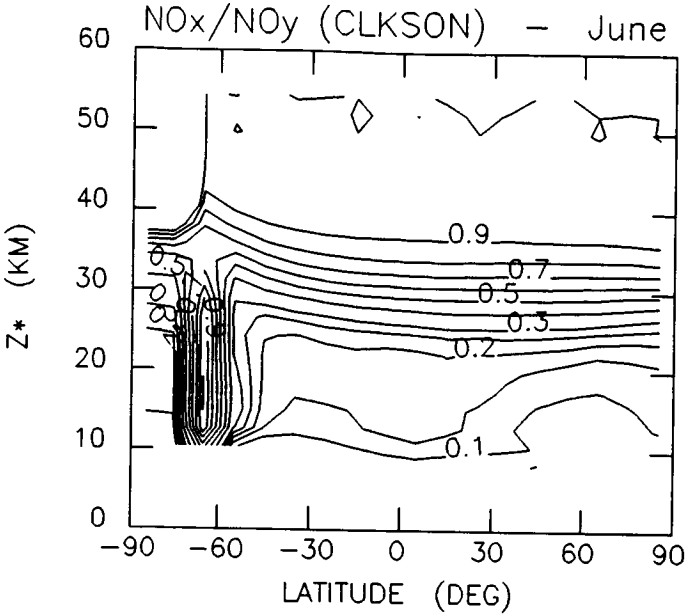
NOx/NOy (CLKSON) – June
Z* (KM)
LATITUDE (DEG)
0.9
0.7
0.5
0.3
0.2
0.1

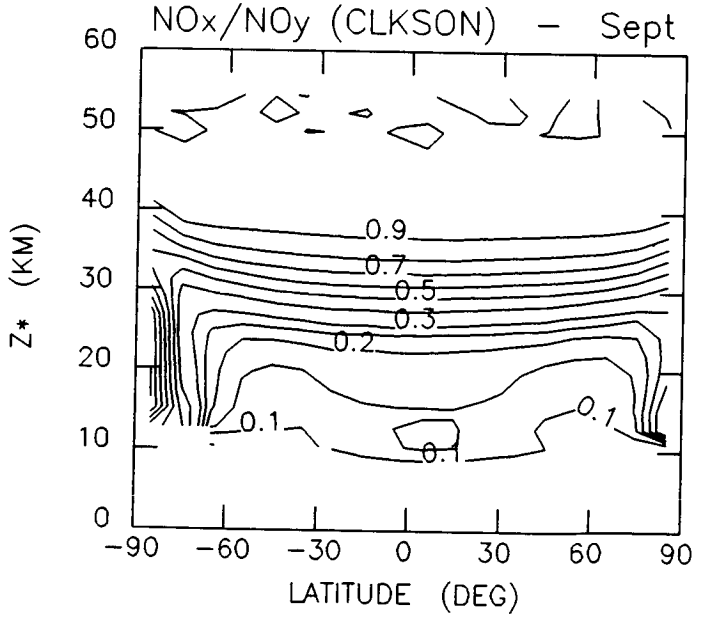
NOx/NOy (CLKSON) – Sept
Z* (KM)
LATITUDE (DEG)
0.9
0.7
0.5
0.3
0.2
0.1

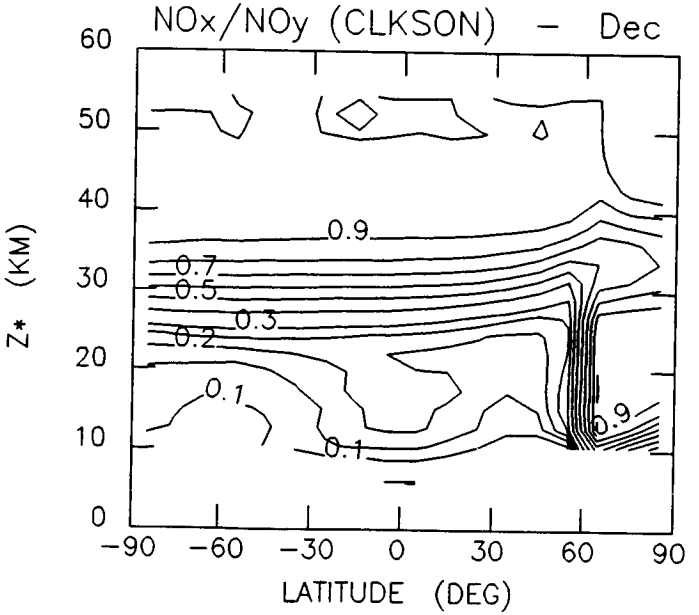
NOx/NOy (CLKSON) – Dec
Z* (KM)
LATITUDE (DEG)
0.9
0.7
0.5
0.3
0.2
0.1

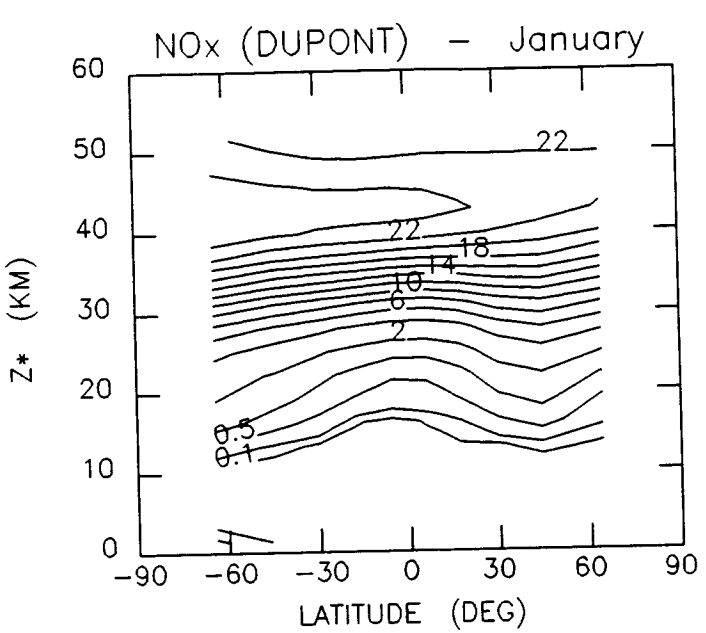
NOx (DUPONT) – January
Z* (KM)
LATITUDE (DEG)
22
18
14
10
6
2
0.5
0.1

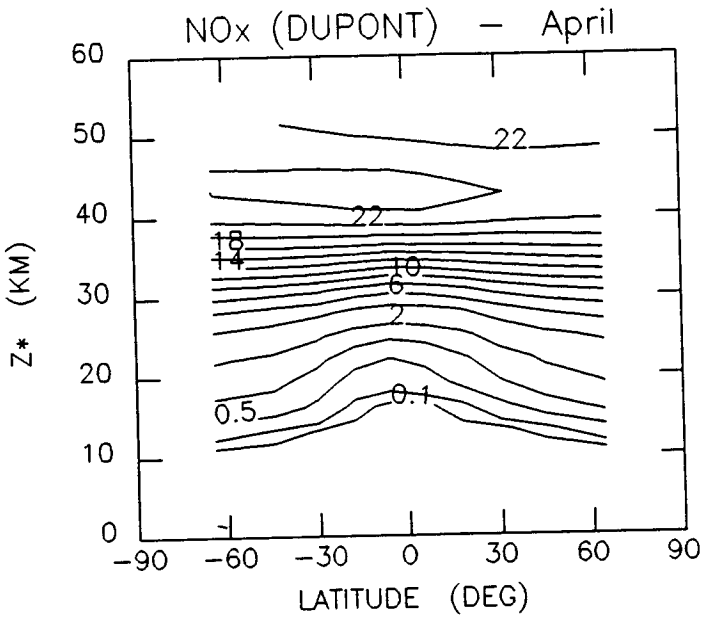
NOx (DUPONT) – April
Z* (KM)
LATITUDE (DEG)
22
18
14
10
6
2
0.5
0.1

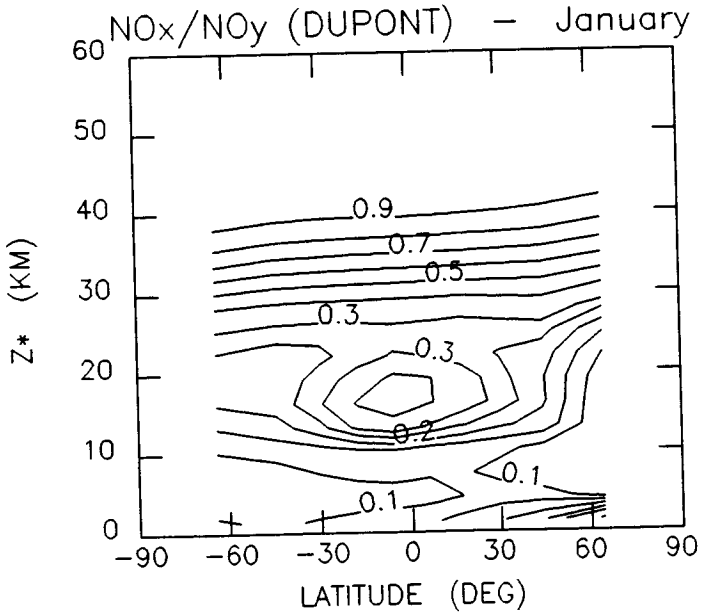
NOx/NOy (DUPONT) – January
Z* (KM)
LATITUDE (DEG)
0.9
0.7
0.5
0.3
0.3
0.2
0.1
0.1

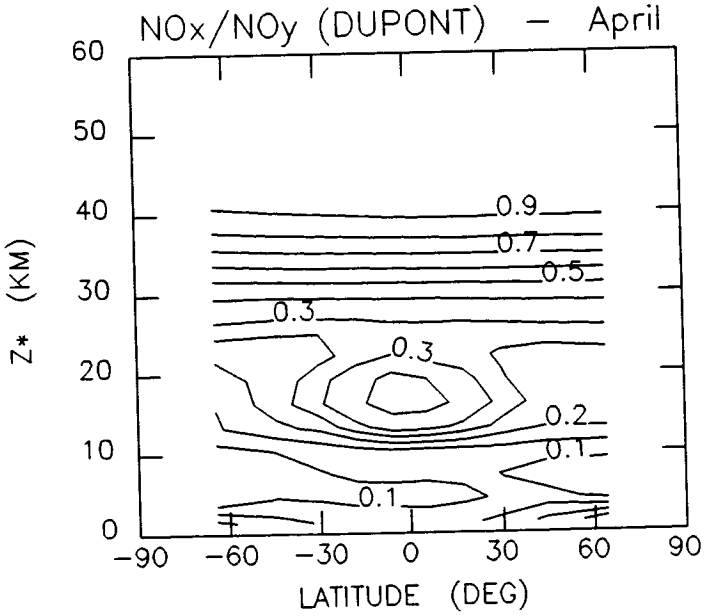
NOx/NOy (DUPONT) – April
Z* (KM)
LATITUDE (DEG)
0.9
0.7
0.5
0.3
0.3
0.2
0.1
0.1

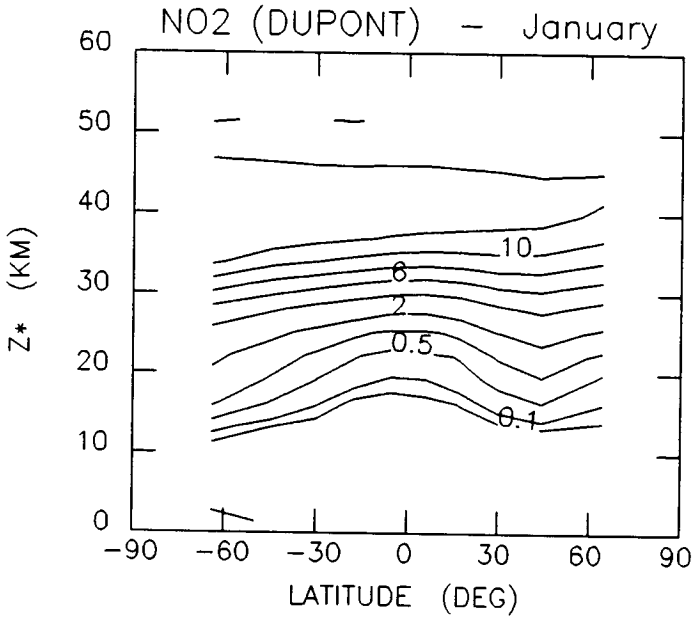
NO2 (DUPONT) – January
Z* (KM)
LATITUDE (DEG)
10
6
2
0.5
0.1

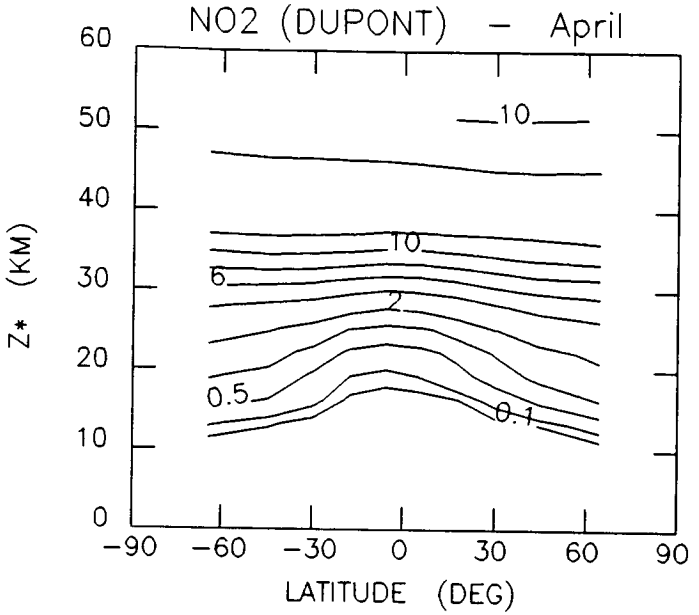
NO2 (DUPONT) – April
Z* (KM)
LATITUDE (DEG)
10
6
2
0.5
0.1

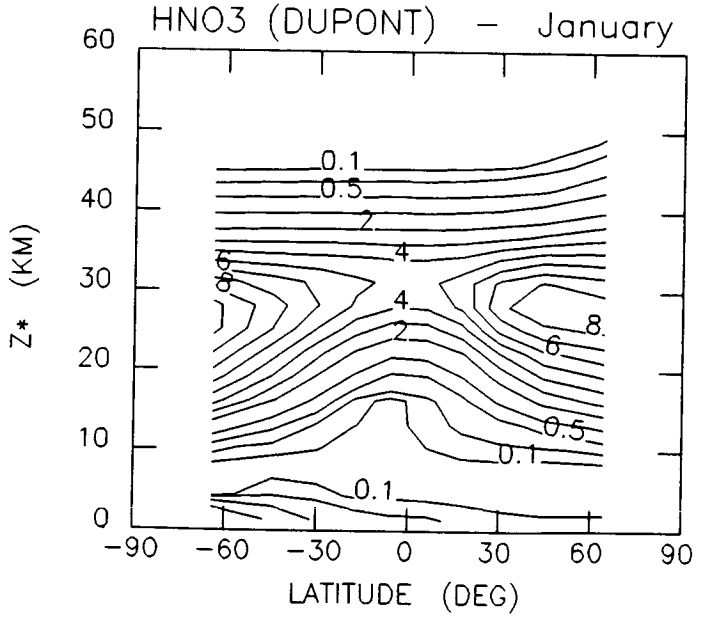
HNO3 (DUPONT) – January
Z* (KM)
LATITUDE (DEG)
0.1
0.5
2
4
6
8

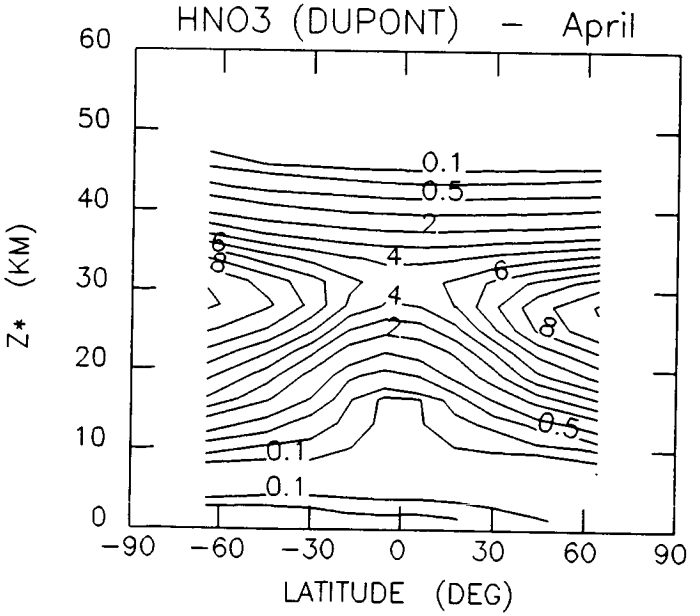
HNO3 (DUPONT) – April
Z* (KM)
LATITUDE (DEG)
0.1
0.5
2
4
6
8

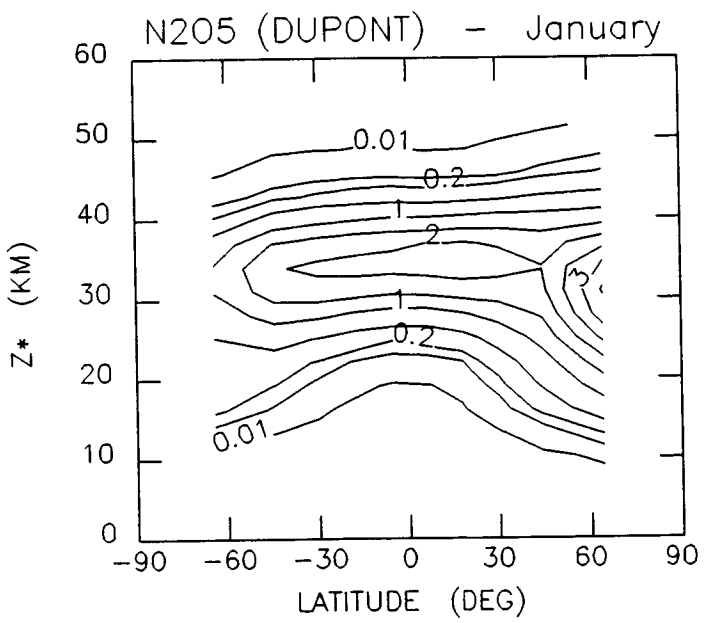
N2O5 (DUPONT) – January
Z* (KM)
LATITUDE (DEG)
0.01
0.2
1
2
3
0
10
20
30
40
50
60
-90
-60
-30
0
30
60
90

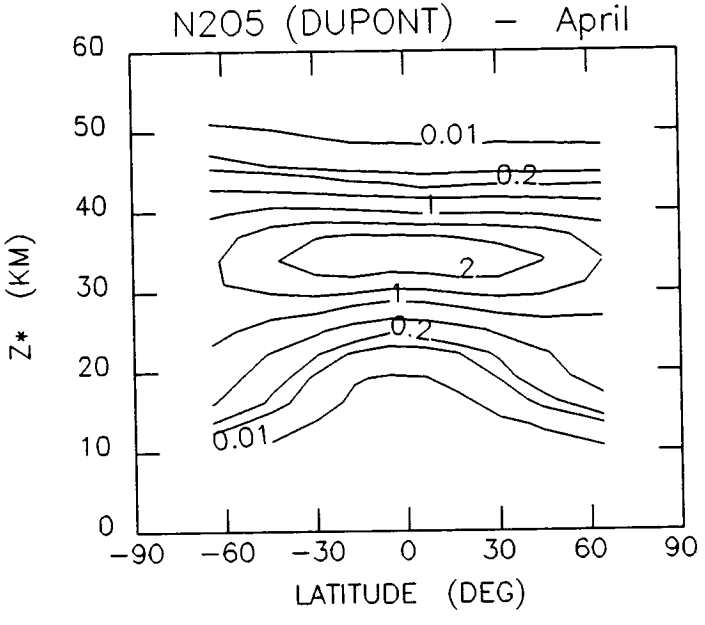
N2O5 (DUPONT) – April
Z* (KM)
LATITUDE (DEG)
0.01
0.2
1
2
0
10
20
30
40
50
60
-90
-60
-30
0
30
60
90

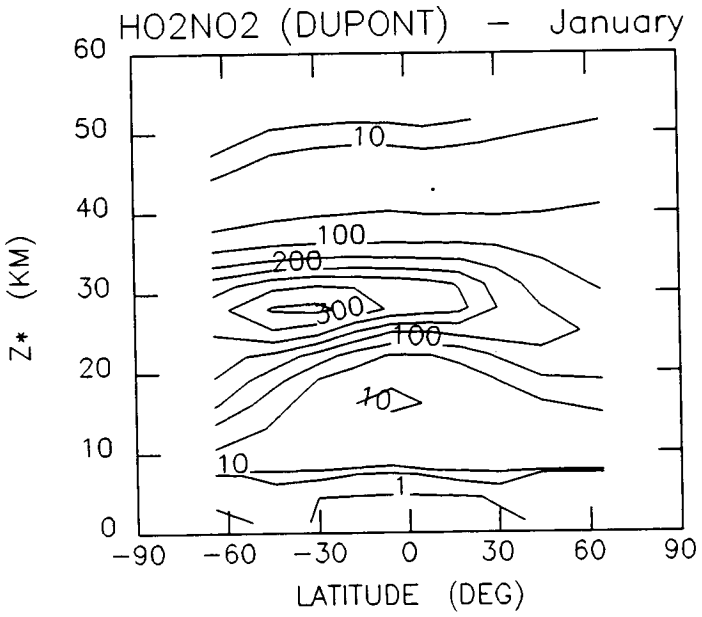
HO2NO2 (DUPONT) – January
Z* (KM)
LATITUDE (DEG)
10
100
200
300
1
0
10
20
30
40
50
60
-90
-60
-30
0
30
60
90

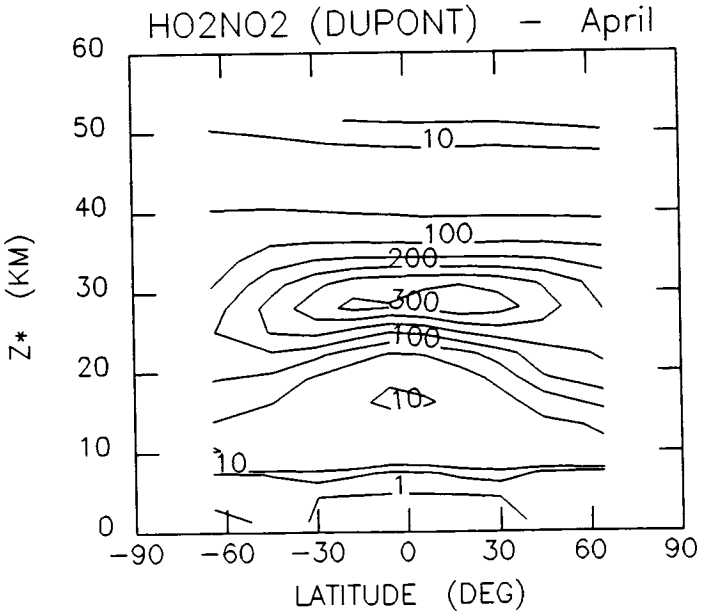
HO2NO2 (DUPONT) – April
Z* (KM)
LATITUDE (DEG)
10
100
200
300
1
0
10
20
30
40
50
60
-90
-60
-30
0
30
60
90

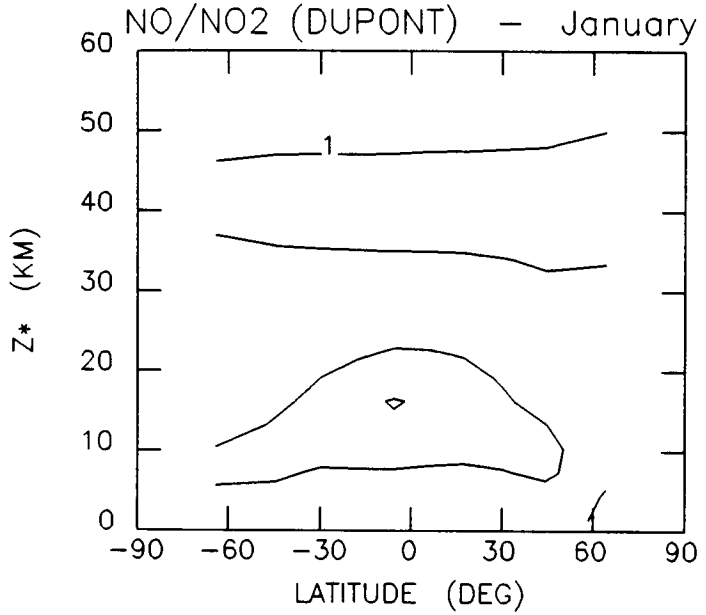
NO/NO2 (DUPONT) – January
Z* (KM)
LATITUDE (DEG)
1

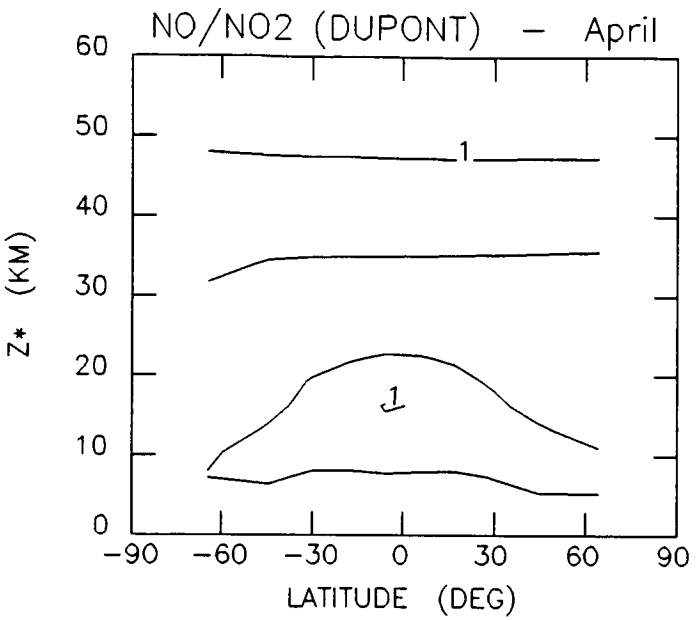
NO/NO2 (DUPONT) – April
Z* (KM)
LATITUDE (DEG)
1

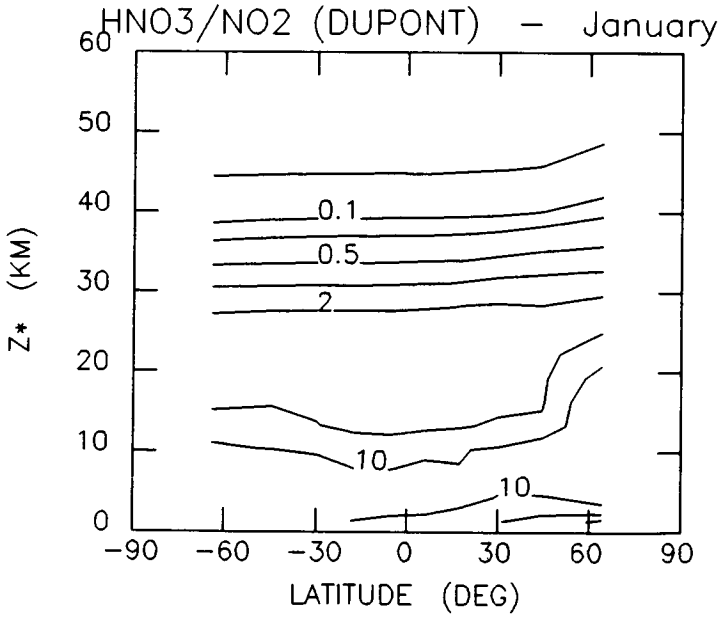
HNO3/NO2 (DUPONT) – January
Z* (KM)
LATITUDE (DEG)
0.1
0.5
2
10
10

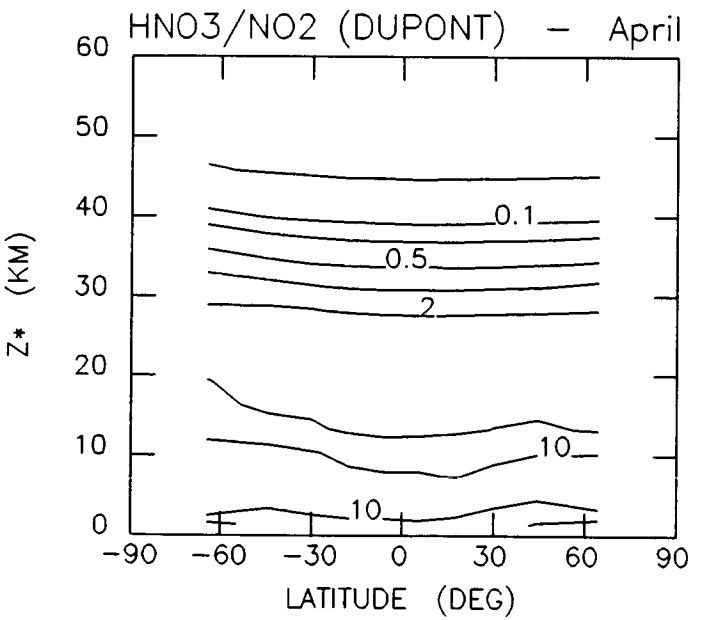
HNO3/NO2 (DUPONT) – April
Z* (KM)
LATITUDE (DEG)
0.1
0.5
2
10
10

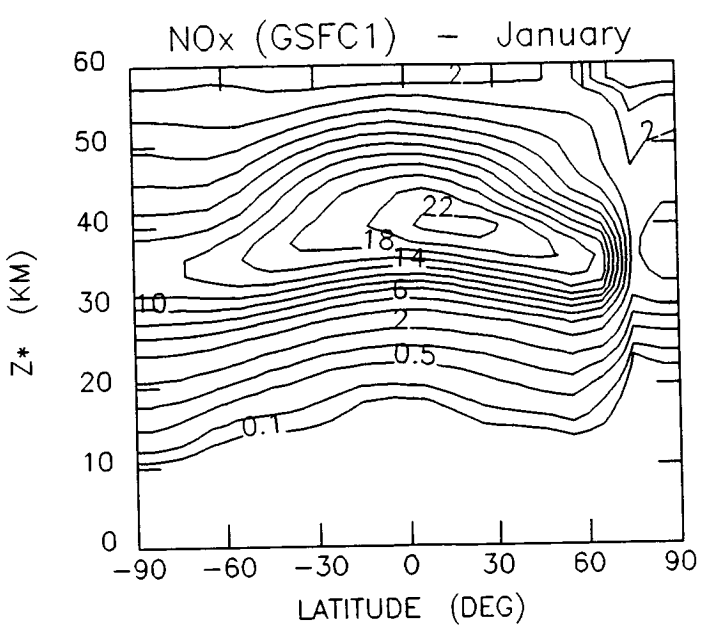
NOx (GSFC1) – January
Z* (KM)
LATITUDE (DEG)
22
18
14
10
6
2
0.5
0.1

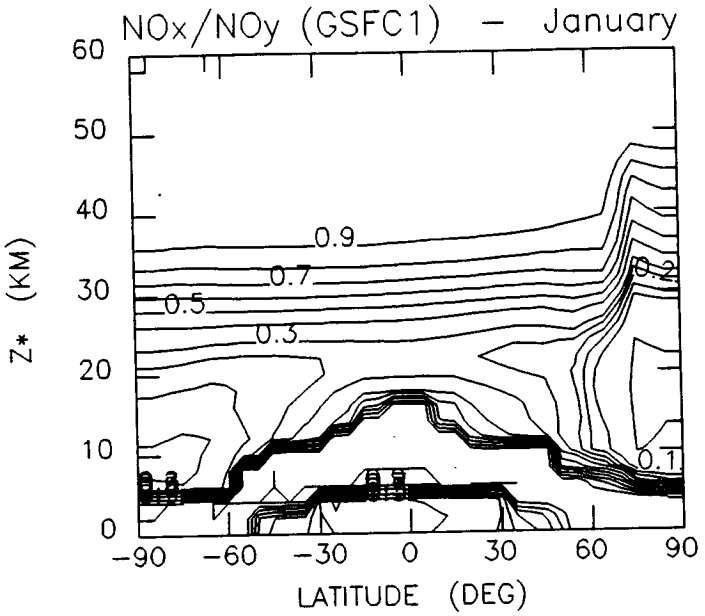
NOx/NOy (GSFC1) – January
Z* (KM)
LATITUDE (DEG)
0.9
0.7
0.5
0.3
0.1

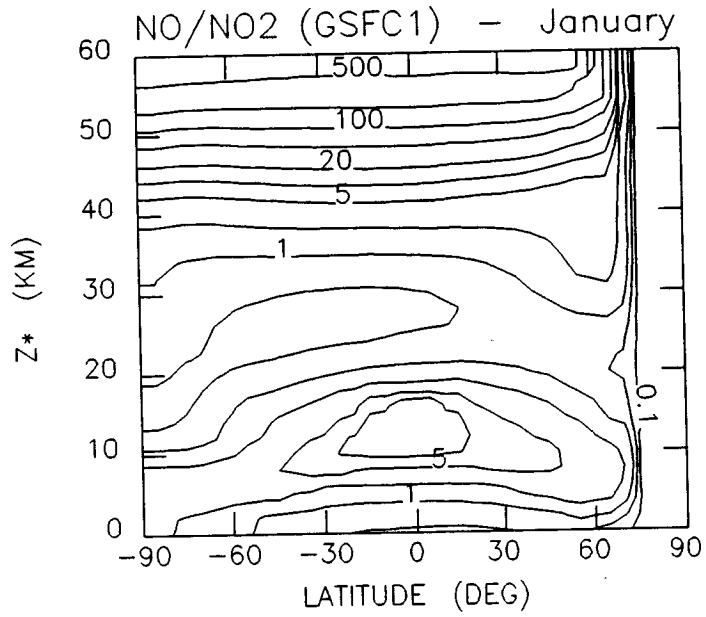
NO/NO2 (GSFC1) – January
Z* (KM)
LATITUDE (DEG)
500
100
20
5
1
0.1

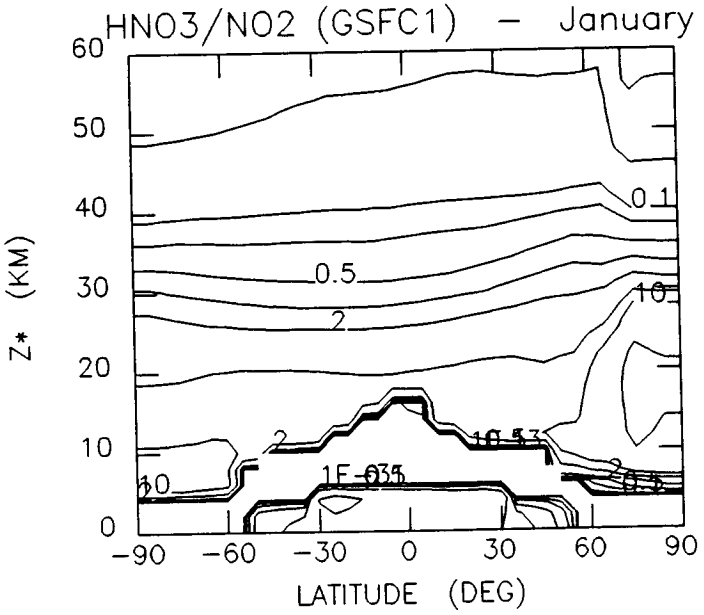
HNO3/NO2 (GSFC1) – January
Z* (KM)
LATITUDE (DEG)
0.1
0.5
2
10

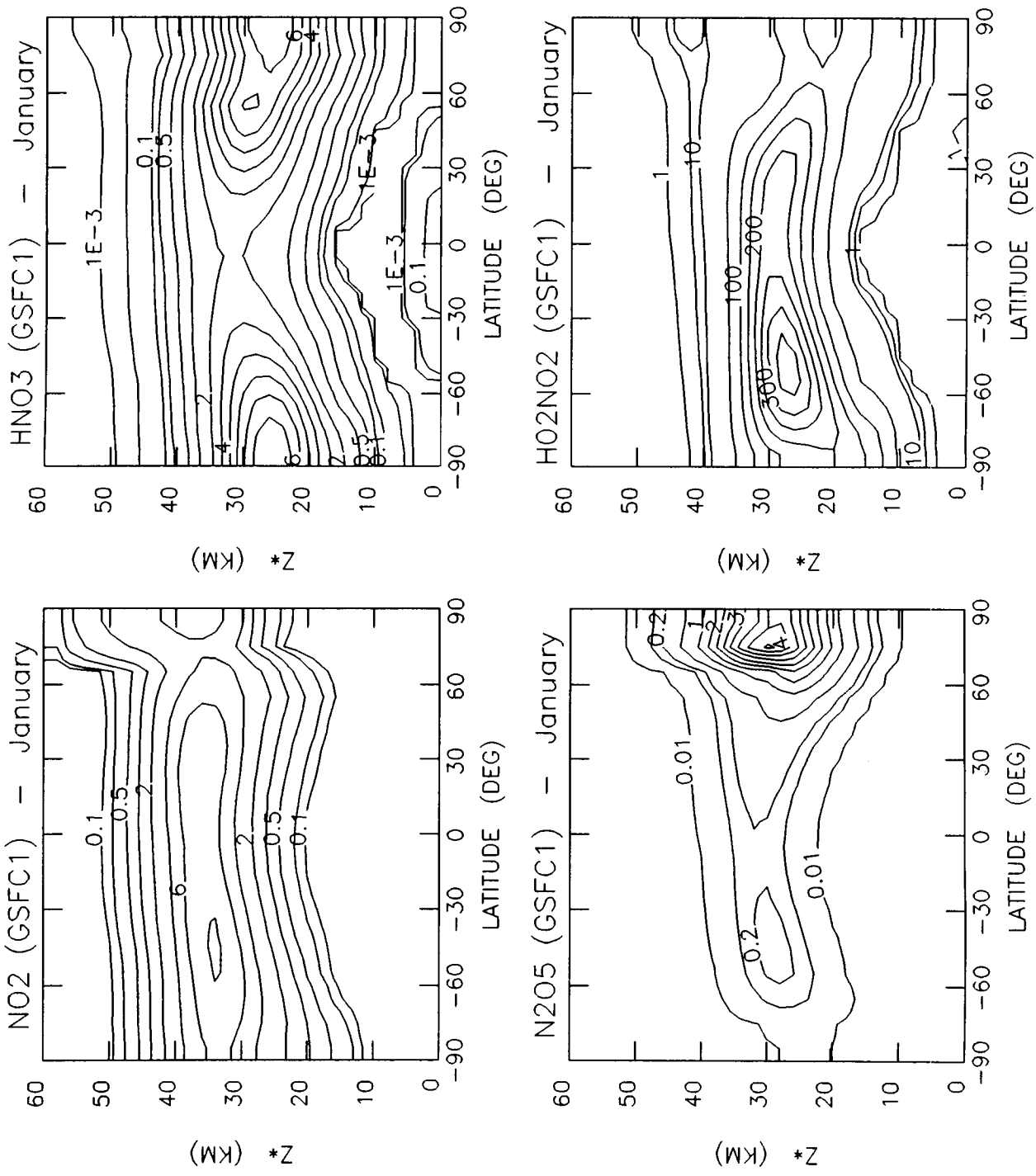
HNO3 (GSFC1) - January
H2O2 (GSFC1) - January
NO2 (GSFC1) - January
N2O5 (GSFC1) - January
Z* (KM)
LATITUDE (DEG)

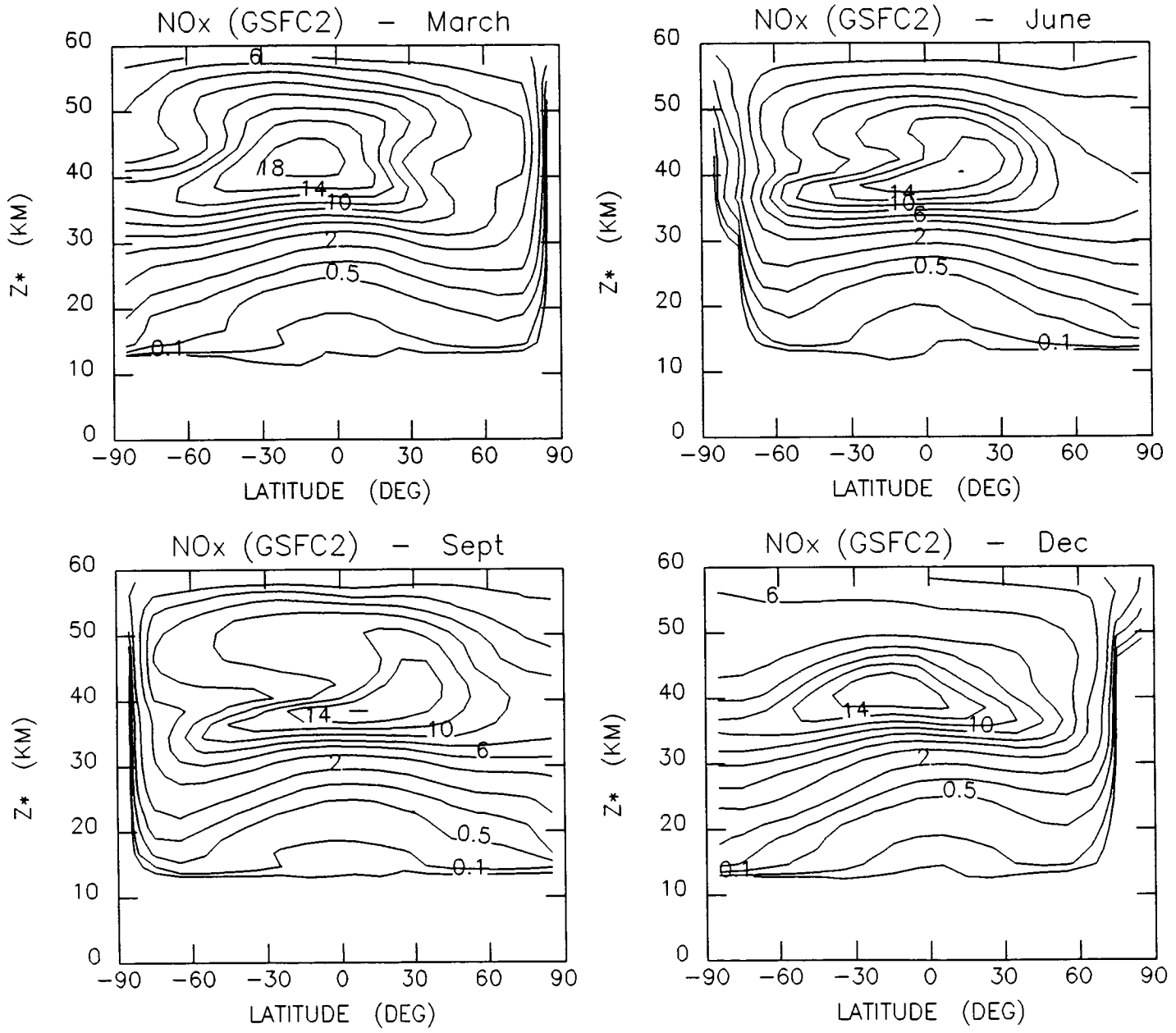
NOx (GSFC2) – March
NOx (GSFC2) – June
NOx (GSFC2) – Sept
NOx (GSFC2) – Dec
Z* (KM)
LATITUDE (DEG)
0
10
20
30
40
50
60
-90
-60
-30
0
30
60
90
18
14
10
6
2
0.5
0.1

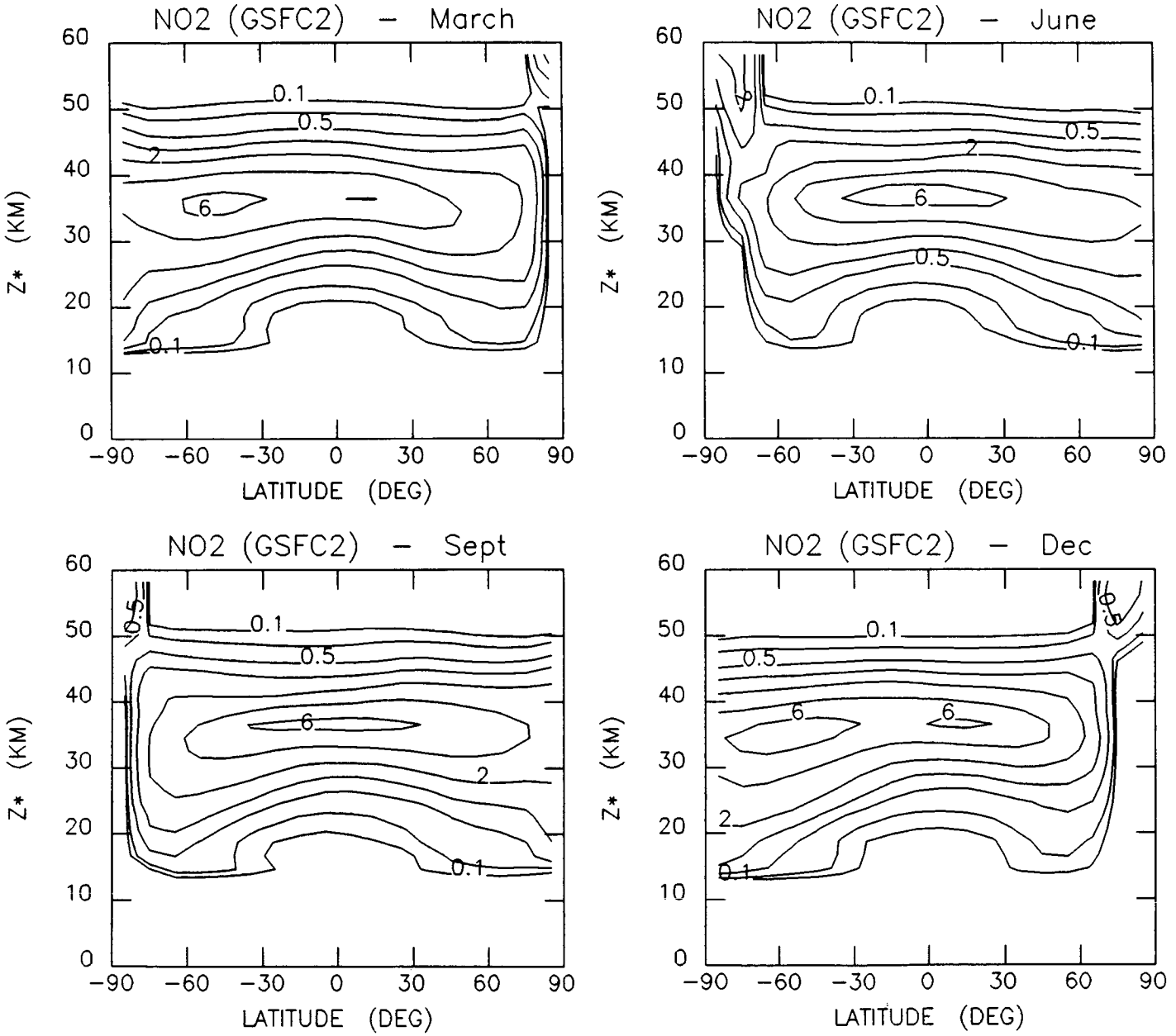
NO2 (GSFC2) – March
NO2 (GSFC2) – June
NO2 (GSFC2) – Sept
NO2 (GSFC2) – Dec
Z* (KM)
LATITUDE (DEG)
0
10
20
30
40
50
60
−90
−60
−30
0
30
60
90
0.1
0.5
2
6

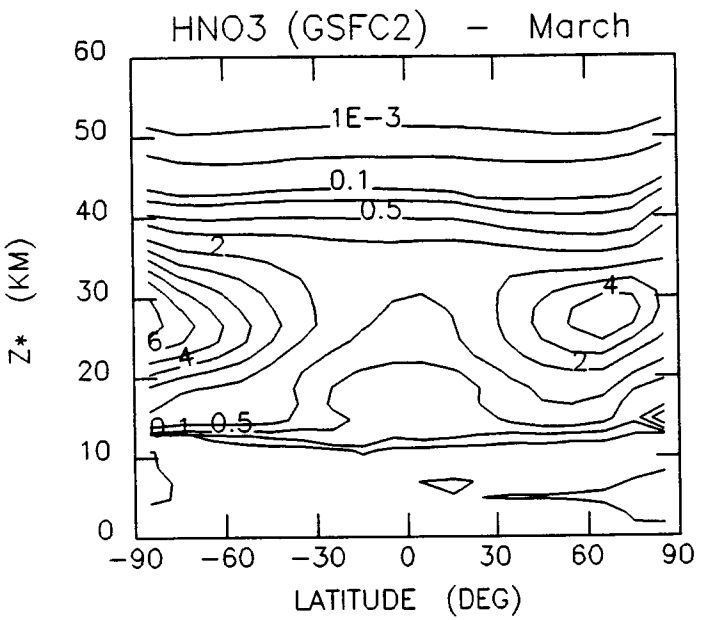
HNO3 (GSFC2) – March
Z* (KM)
LATITUDE (DEG)
1E-3
0.1
0.5
2
4
6

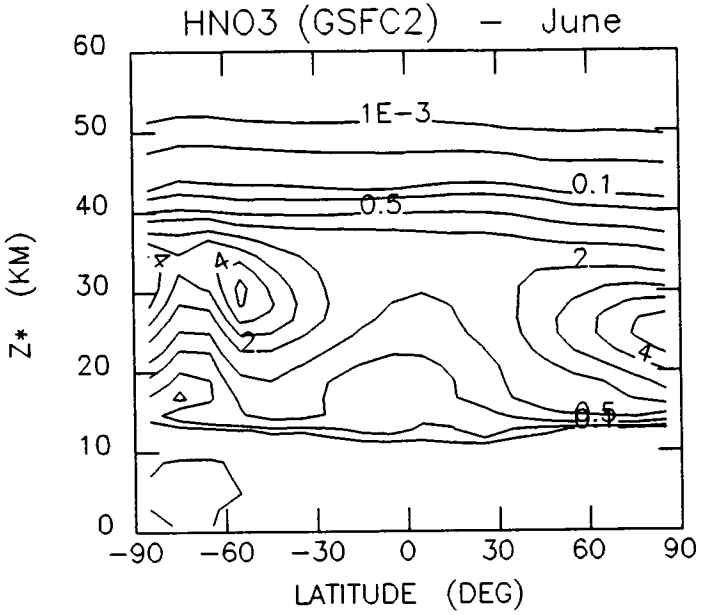
HNO3 (GSFC2) – June
Z* (KM)
LATITUDE (DEG)
1E-3
0.1
0.5
2
4

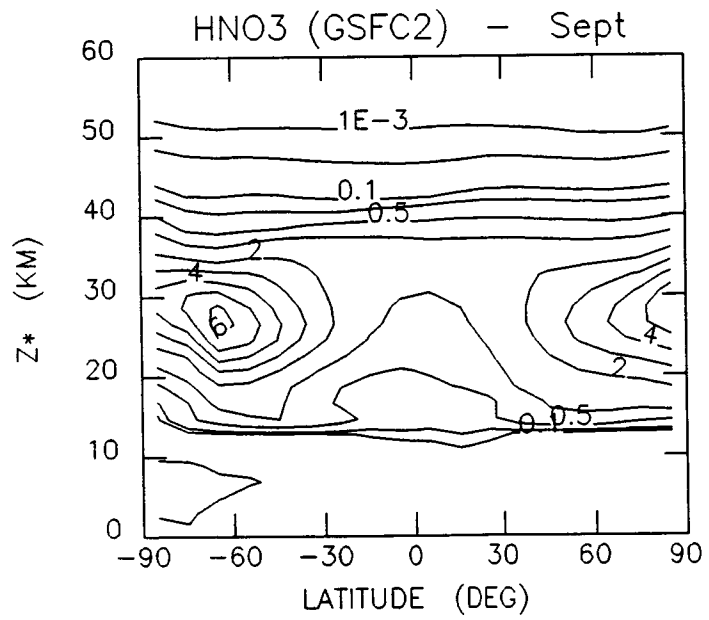
HNO3 (GSFC2) – Sept
Z* (KM)
LATITUDE (DEG)
1E-3
0.1
0.5
2
4
6

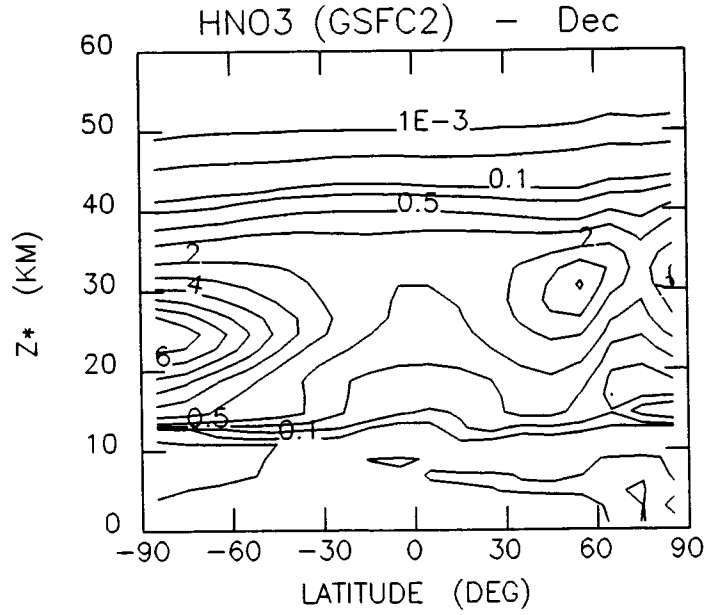
HNO3 (GSFC2) – Dec
Z* (KM)
LATITUDE (DEG)
1E-3
0.1
0.5
2
4
6

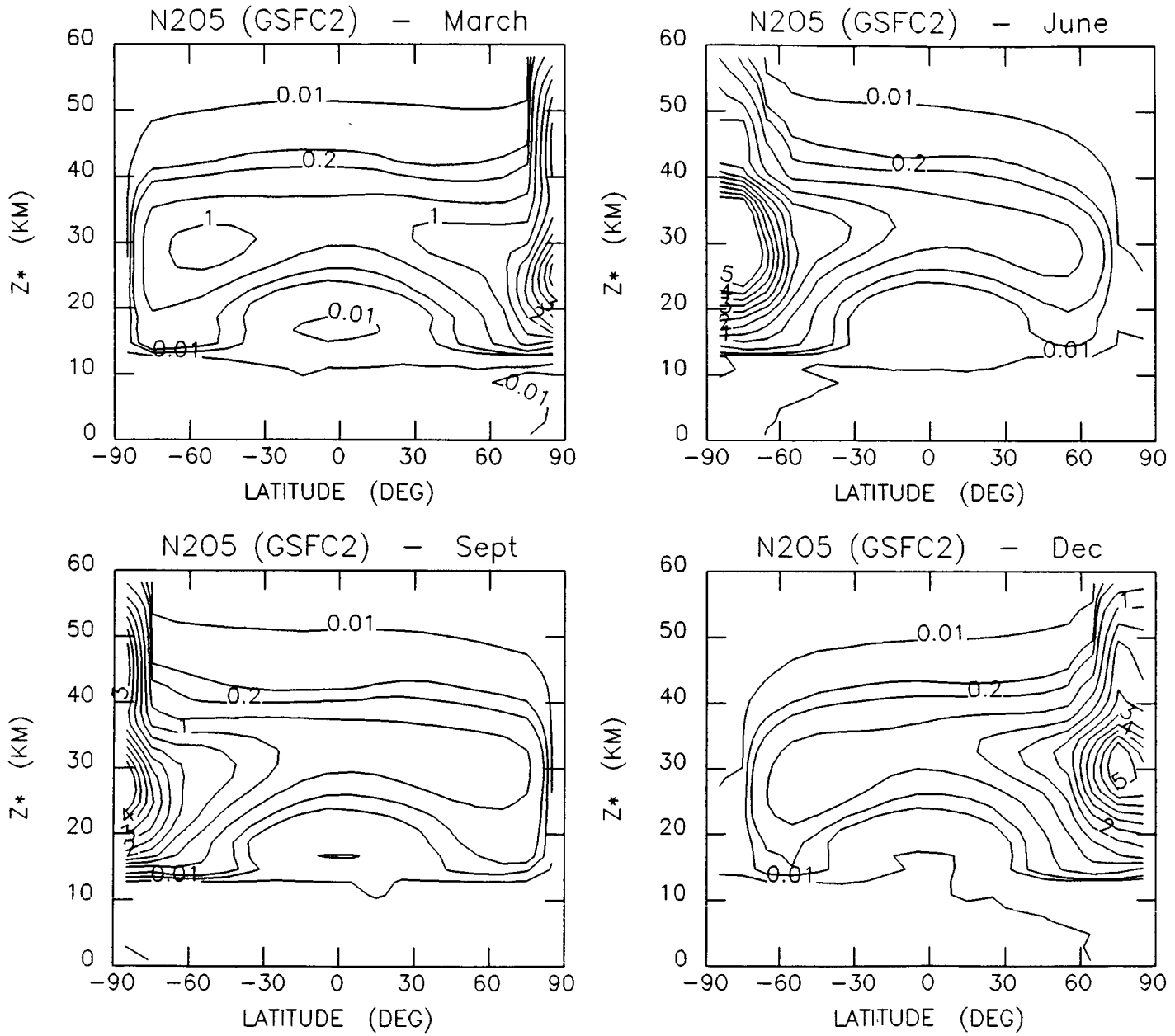
N2O5 (GSFC2) – March
N2O5 (GSFC2) – June
N2O5 (GSFC2) – Sept
N2O5 (GSFC2) – Dec
Z* (KM)
LATITUDE (DEG)
0.01
0.2
1
5

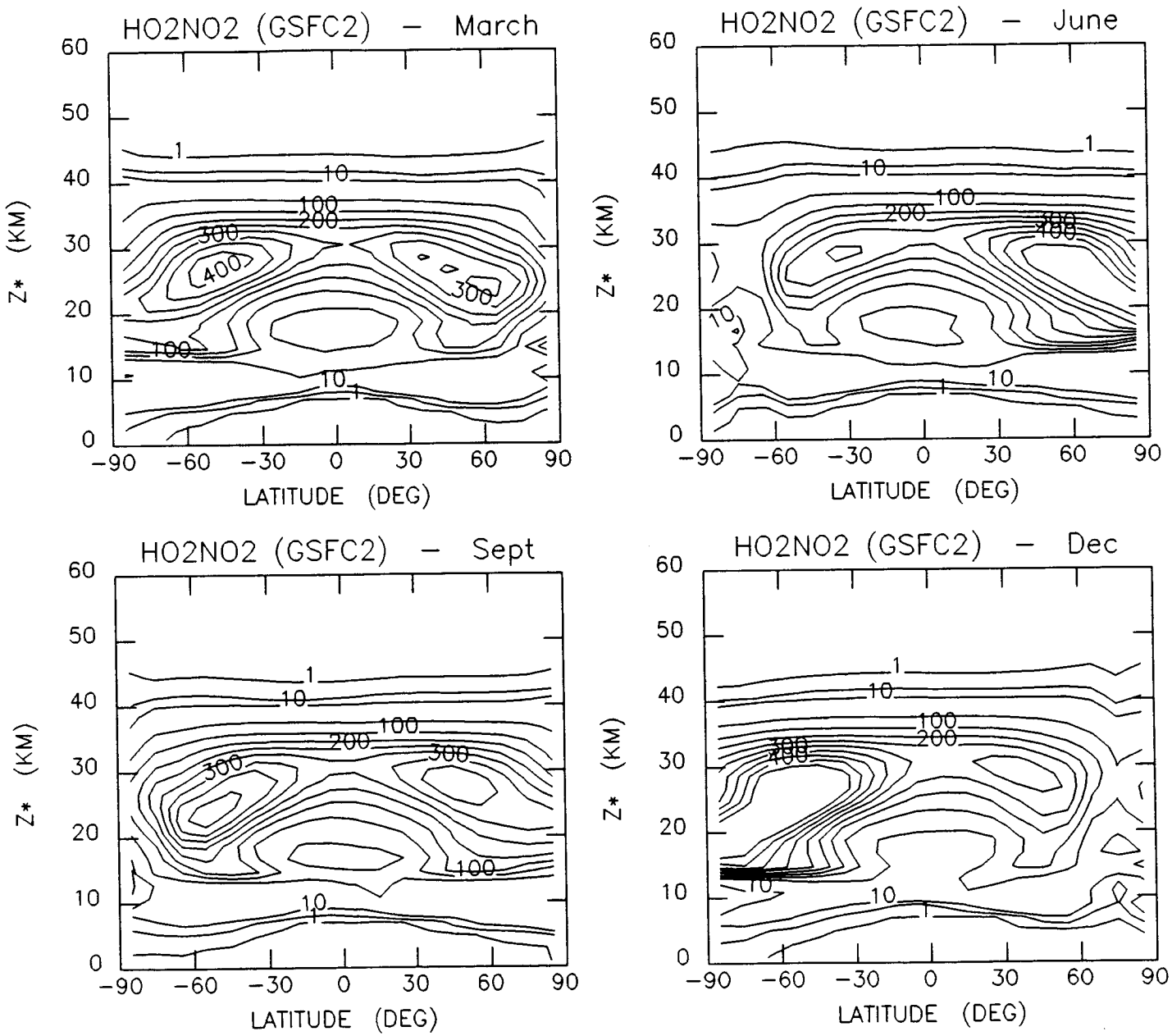
HO2NO2 (GSFC2) – March
HO2NO2 (GSFC2) – June
HO2NO2 (GSFC2) – Sept
HO2NO2 (GSFC2) – Dec
Z* (KM)
LATITUDE (DEG)
1
10
100
200
300
400

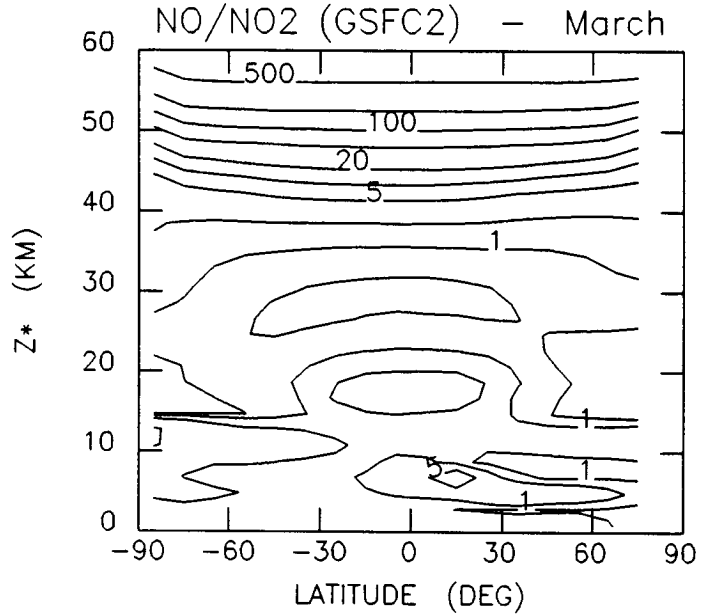
NO/NO2 (GSFC2) – March
Z* (KM)
LATITUDE (DEG)
500
100
20
5
1

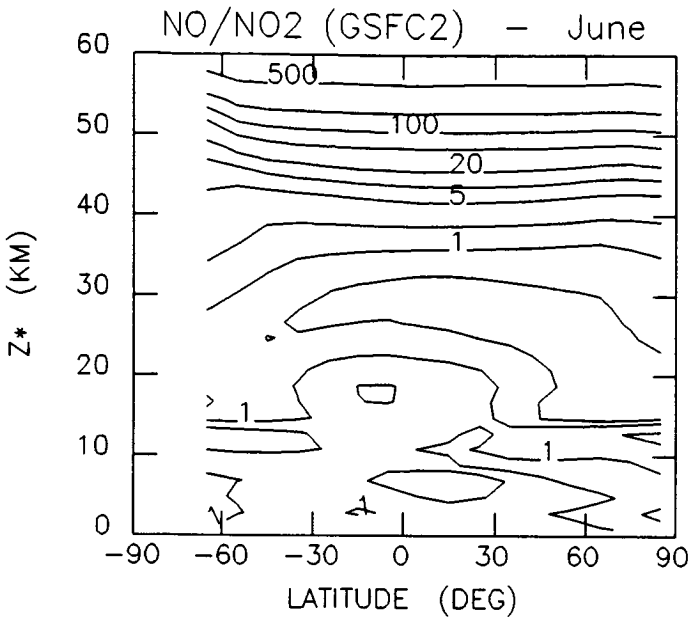
NO/NO2 (GSFC2) – June
Z* (KM)
LATITUDE (DEG)
500
100
20
5
1

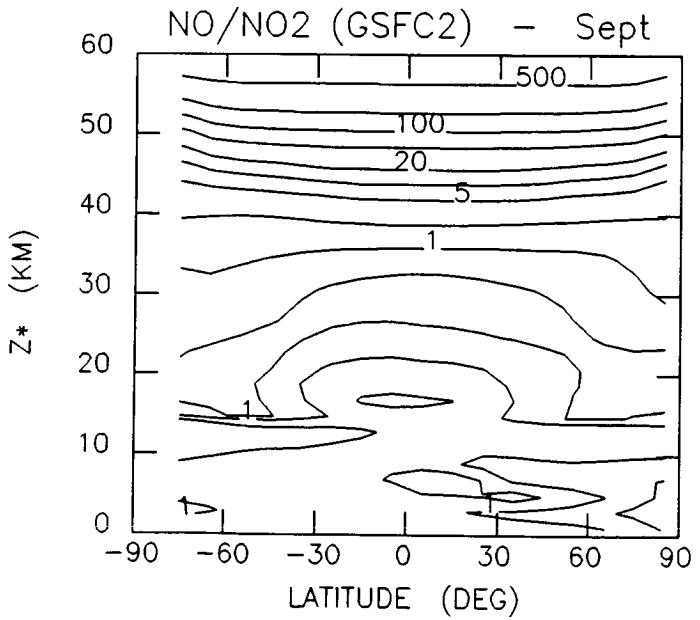
NO/NO2 (GSFC2) – Sept
Z* (KM)
LATITUDE (DEG)
500
100
20
5
1

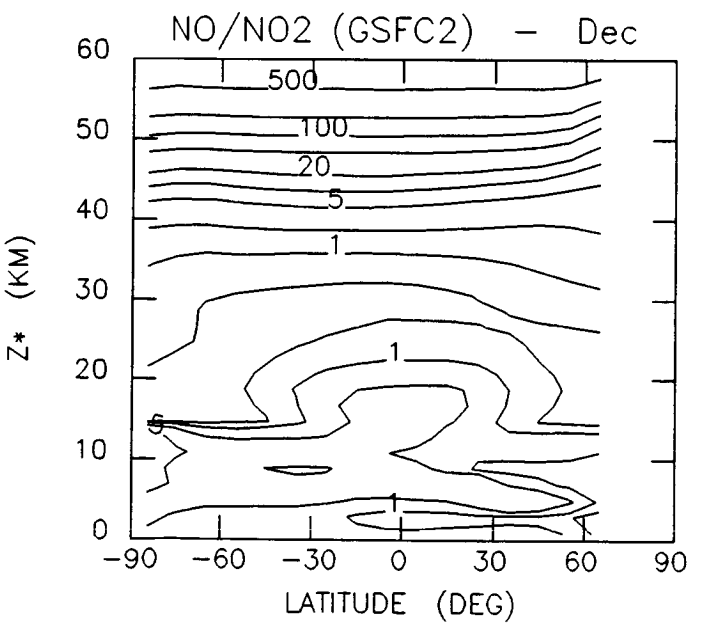
NO/NO2 (GSFC2) – Dec
Z* (KM)
LATITUDE (DEG)
500
100
20
5
1

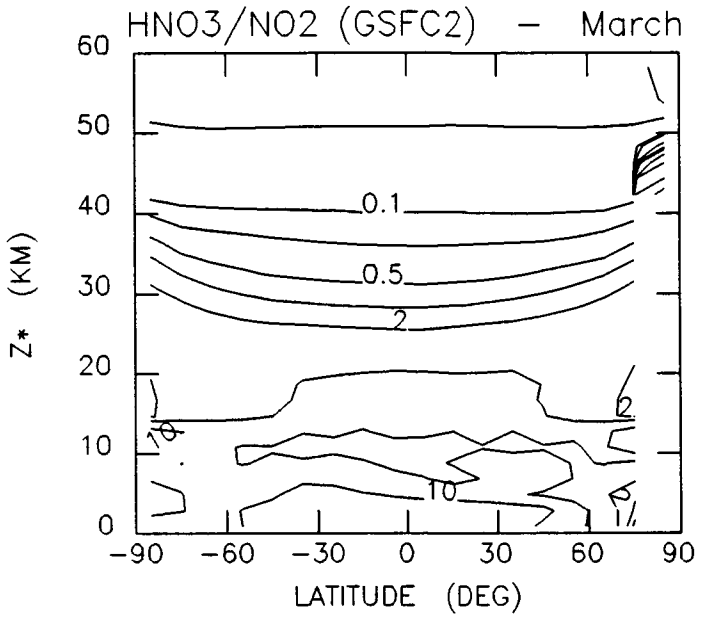
HNO3/NO2 (GSFC2) – March
Z* (KM)
LATITUDE (DEG)
0.1
0.5
2
10

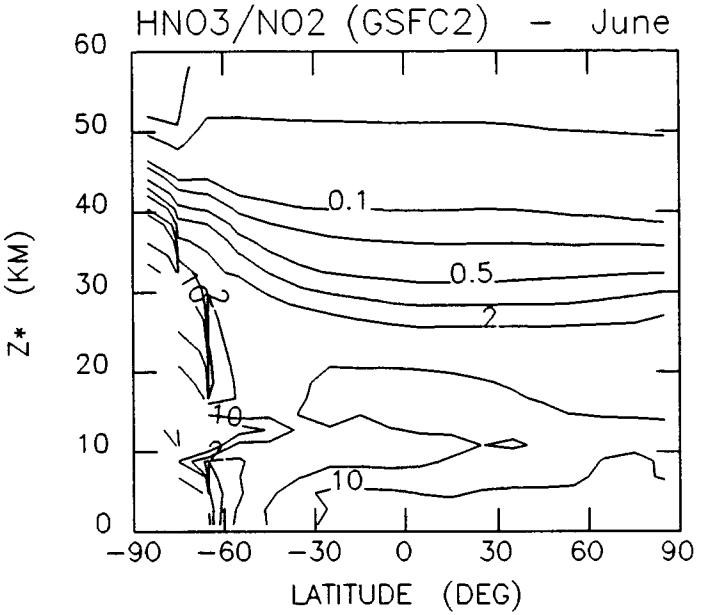
HNO3/NO2 (GSFC2) – June
Z* (KM)
LATITUDE (DEG)
0.1
0.5
2
10

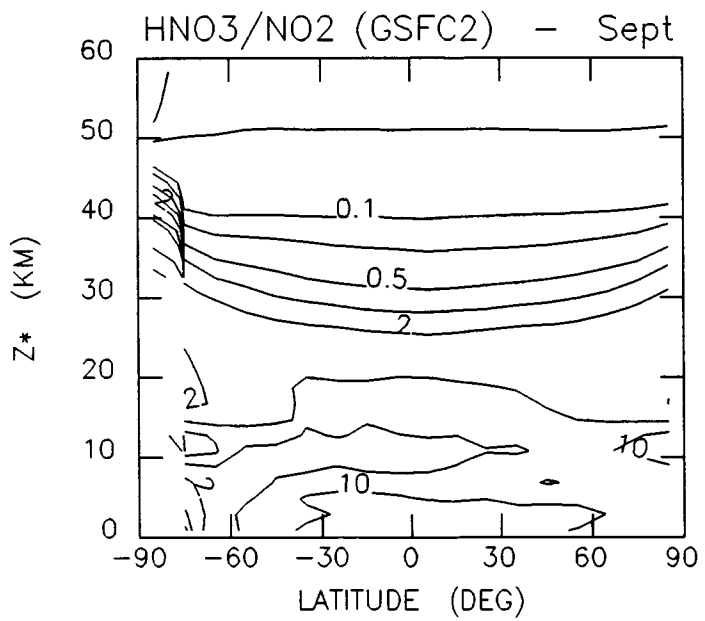
HNO3/NO2 (GSFC2) – Sept
Z* (KM)
LATITUDE (DEG)
0.1
0.5
2
10

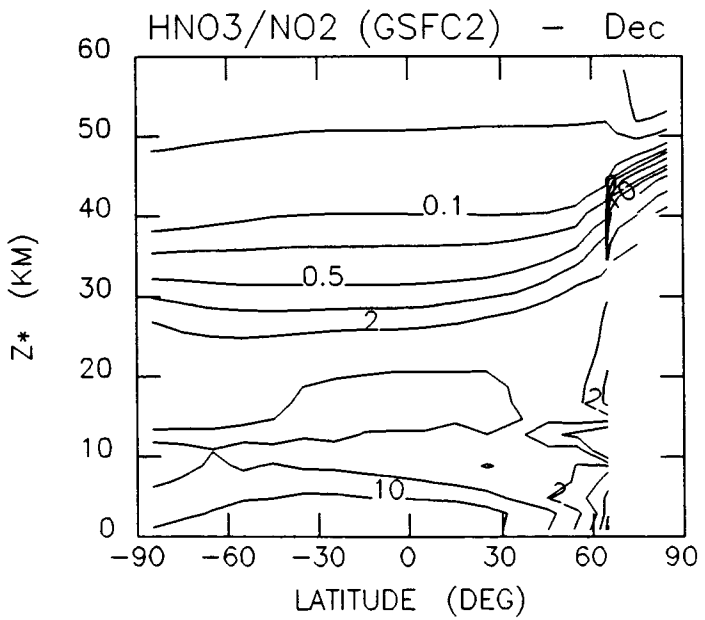
HNO3/NO2 (GSFC2) – Dec
Z* (KM)
LATITUDE (DEG)
0.1
0.5
2
10

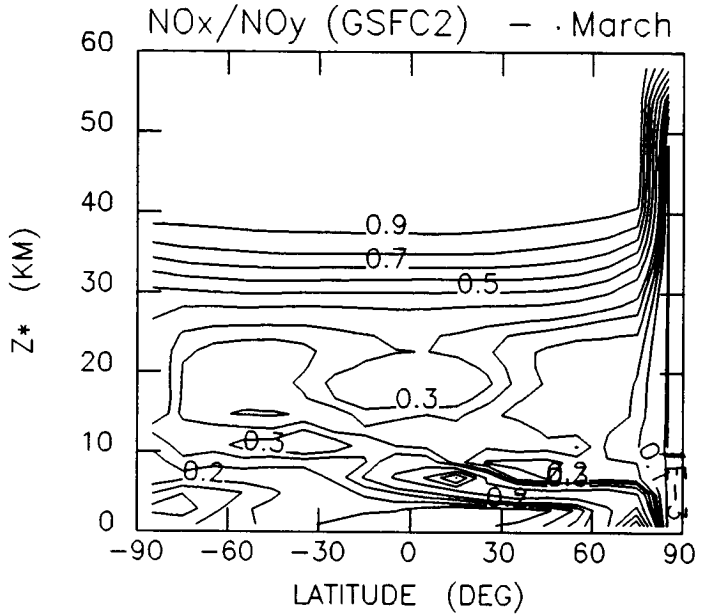
NOx/NOy (GSFC2) – March
Z* (KM)
LATITUDE (DEG)
0.9
0.7
0.5
0.3
0.2
0.1

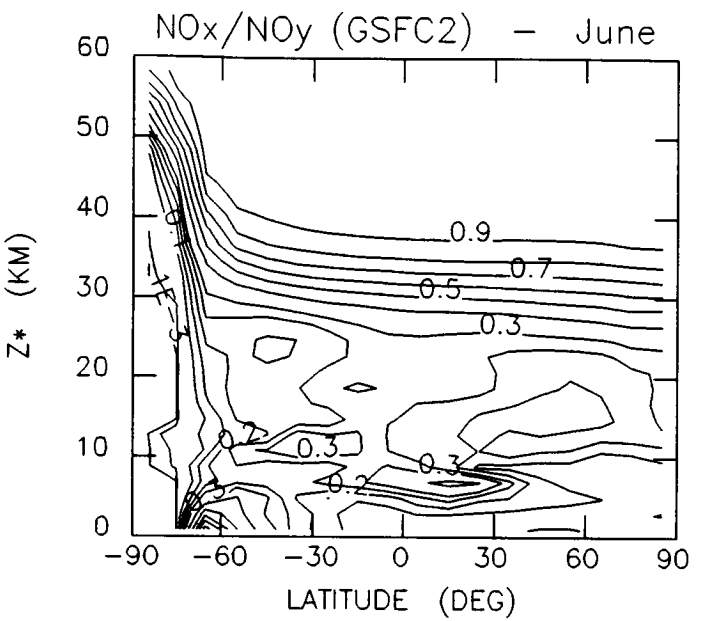
NOx/NOy (GSFC2) – June
Z* (KM)
LATITUDE (DEG)
0.9
0.7
0.5
0.3
0.2
0.1

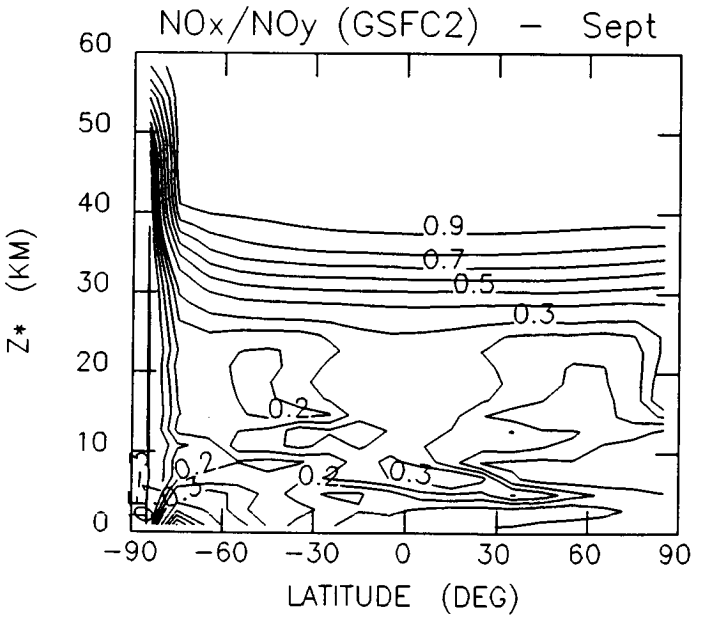
NOx/NOy (GSFC2) – Sept
Z* (KM)
LATITUDE (DEG)
0.9
0.7
0.5
0.3
0.2
0.1

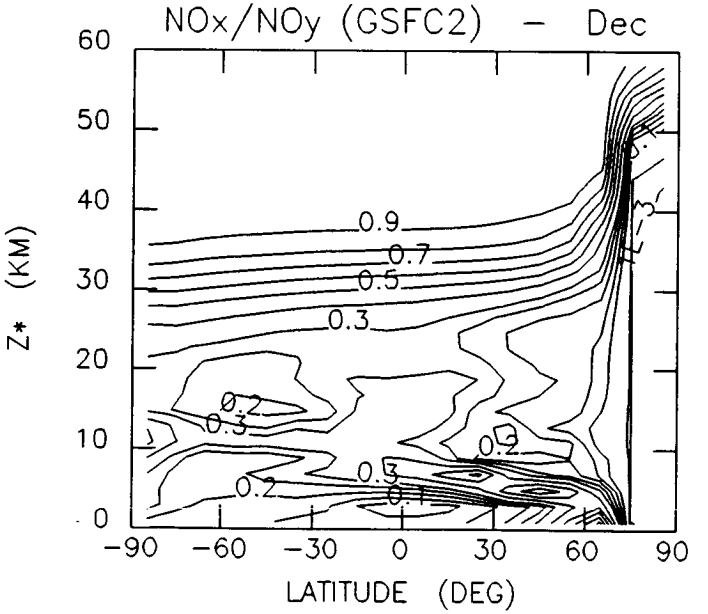
NOx/NOy (GSFC2) – Dec
Z* (KM)
LATITUDE (DEG)
0.9
0.7
0.5
0.3
0.2
0.1

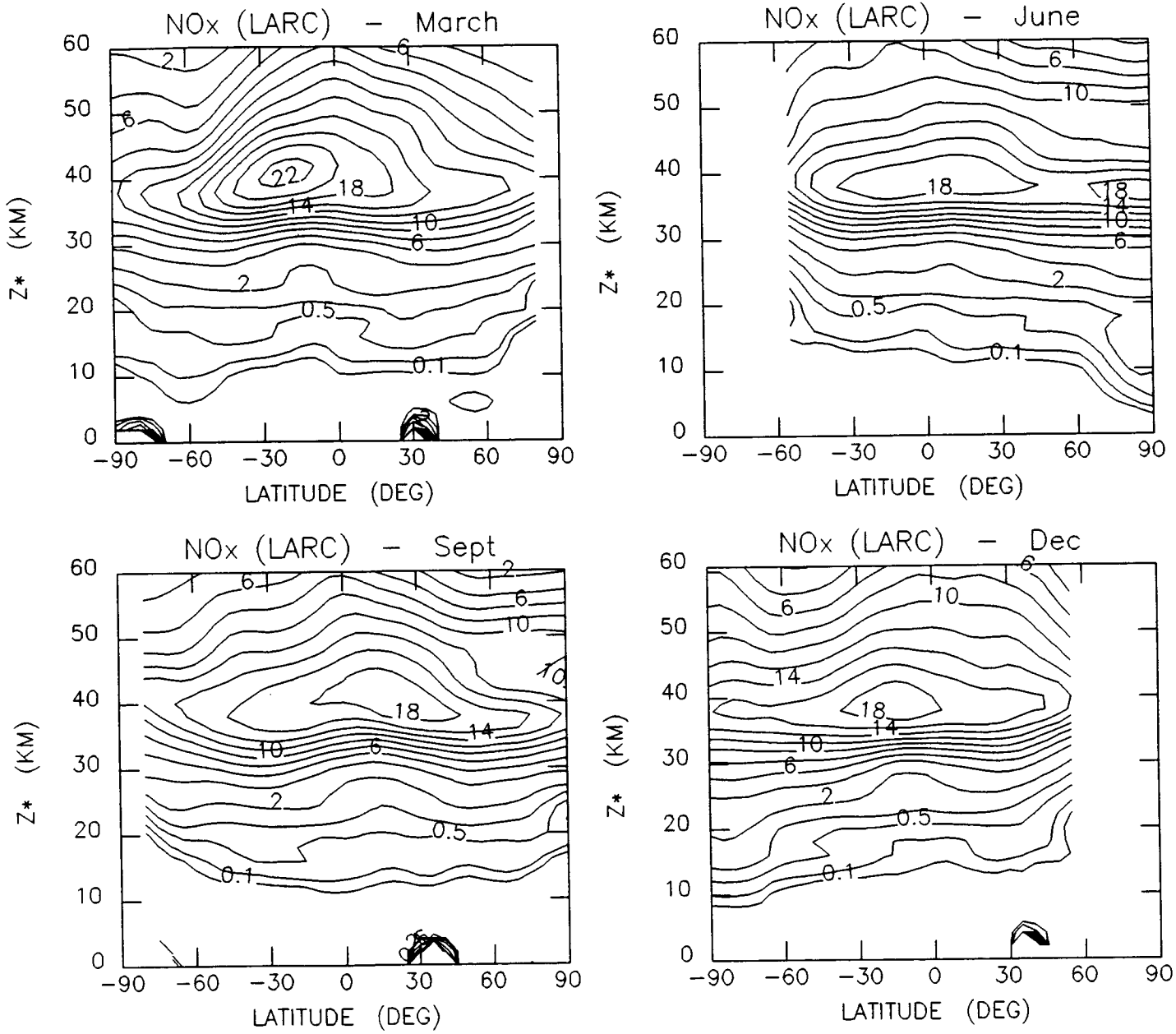
NOx (LARC) – March
NOx (LARC) – June
NOx (LARC) – Sept
NOx (LARC) – Dec
Z* (KM)
LATITUDE (DEG)
0
10
20
30
40
50
60
−90
−60
−30
0
30
60
90
22
18
14
10
6
2
0.5
0.1

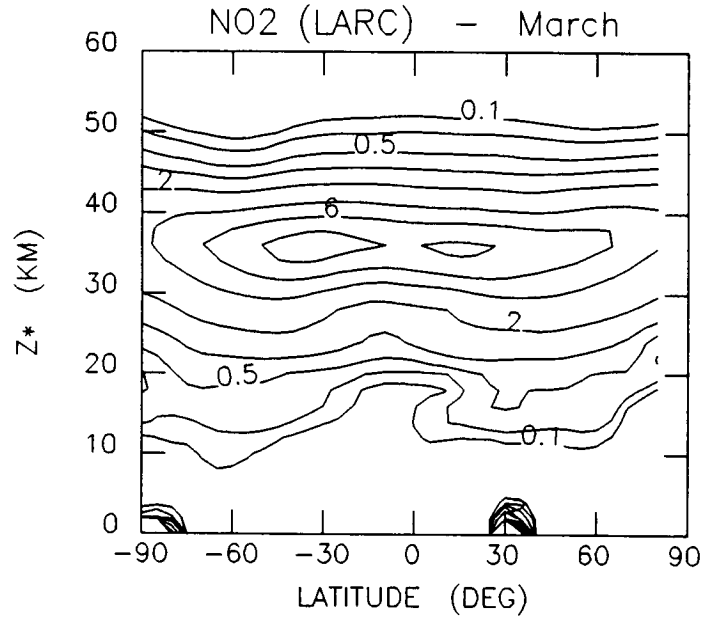
NO2 (LARC) – March
Z* (KM)
LATITUDE (DEG)
0.1
0.5
2
6
2
0.5
0.1

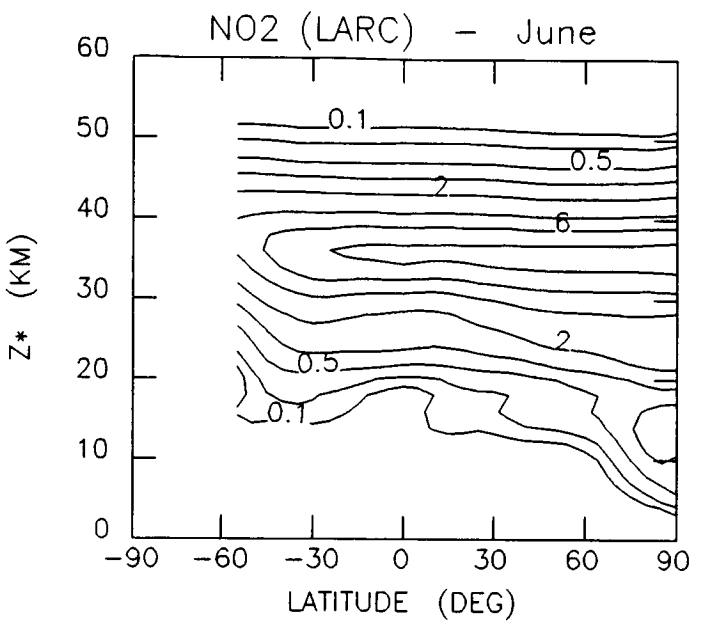
NO2 (LARC) – June
Z* (KM)
LATITUDE (DEG)
0.1
0.5
2
6
2
0.5
0.1

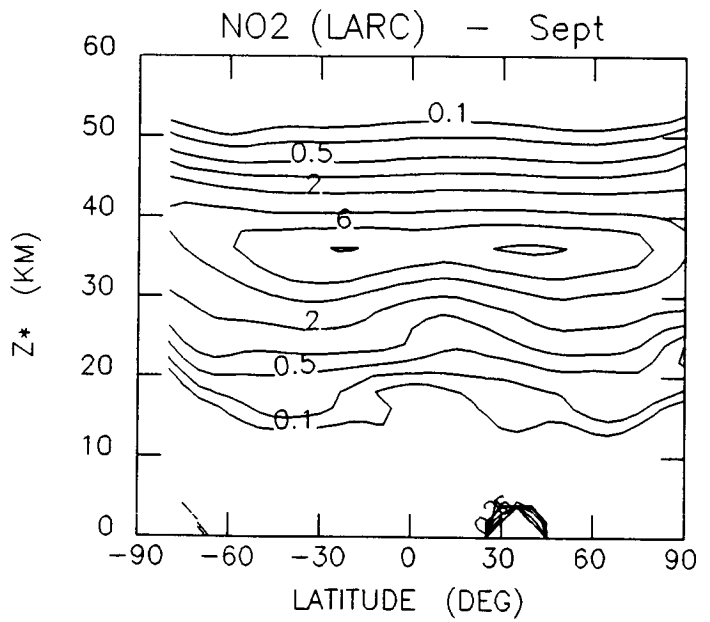
NO2 (LARC) – Sept
Z* (KM)
LATITUDE (DEG)
0.1
0.5
2
6
2
0.5
0.1

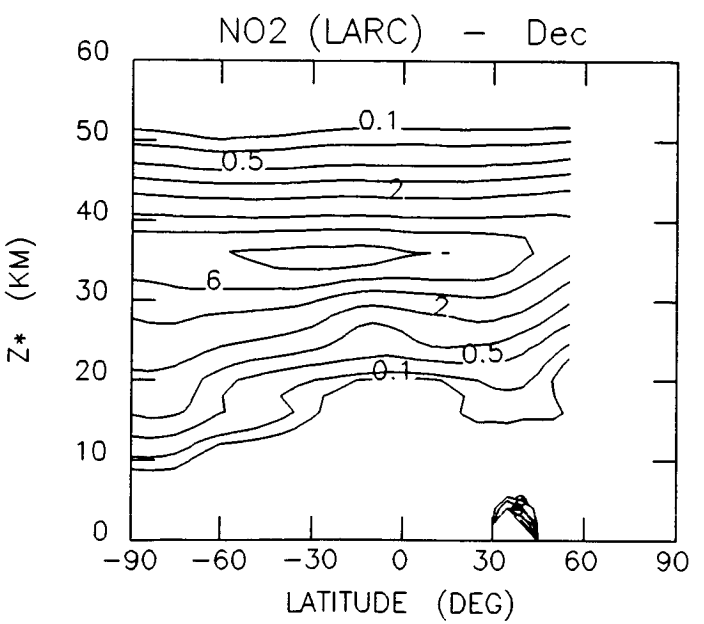
NO2 (LARC) – Dec
Z* (KM)
LATITUDE (DEG)
0.1
0.5
2
6
2
0.5
0.1

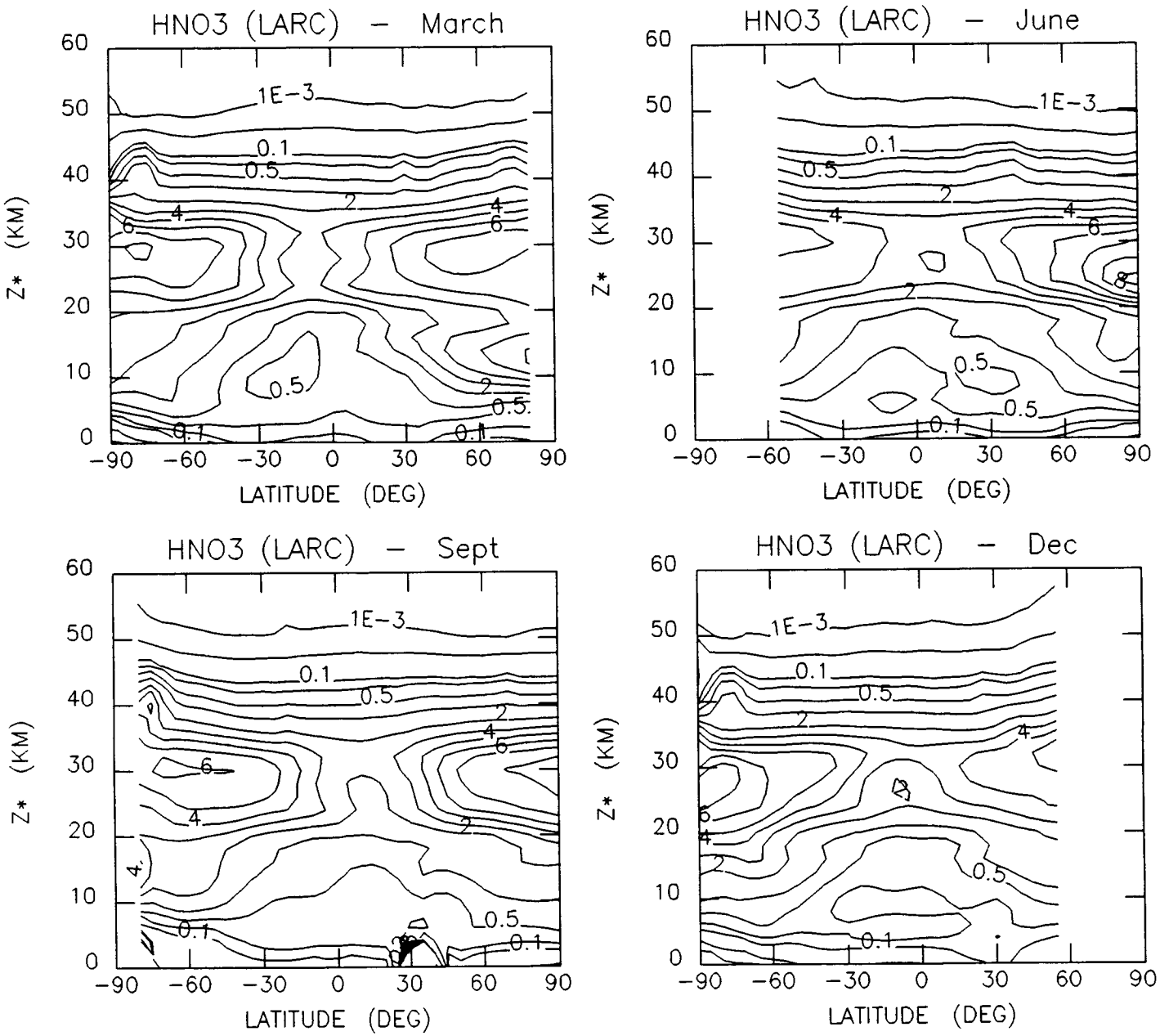
HNO3 (LARC) – March
HNO3 (LARC) – June
HNO3 (LARC) – Sept
HNO3 (LARC) – Dec
Z* (KM)
LATITUDE (DEG)
1E-3
0.1
0.5
2
4
6
8
0
10
20
30
40
50
60
-90
-60
-30
0
30
60
90

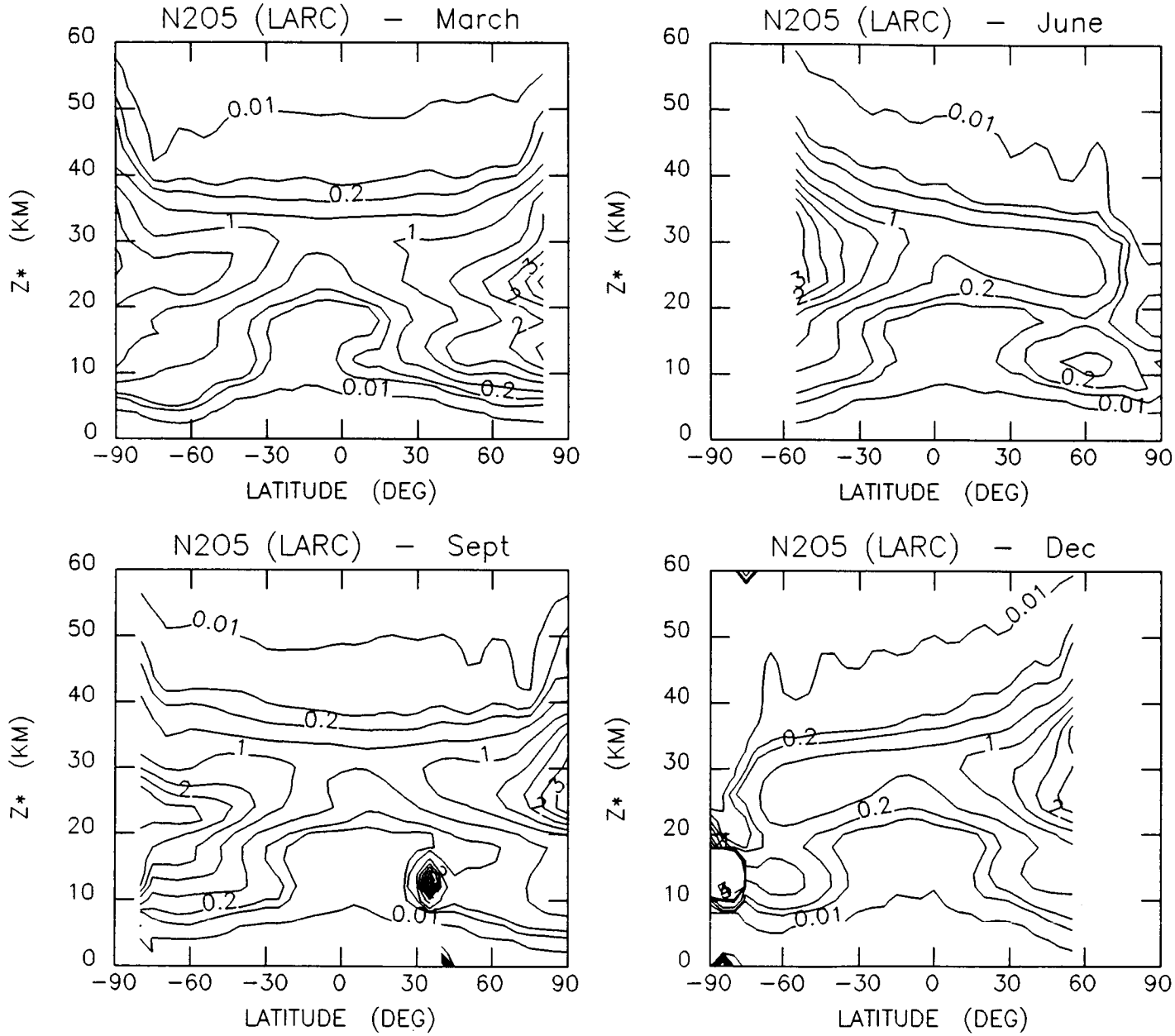
N2O5 (LARC) – March
N2O5 (LARC) – June
N2O5 (LARC) – Sept
N2O5 (LARC) – Dec
Z* (KM)
LATITUDE (DEG)
0
10
20
30
40
50
60
−90
−60
−30
0
30
60
90
0.01
0.2
1
2
3

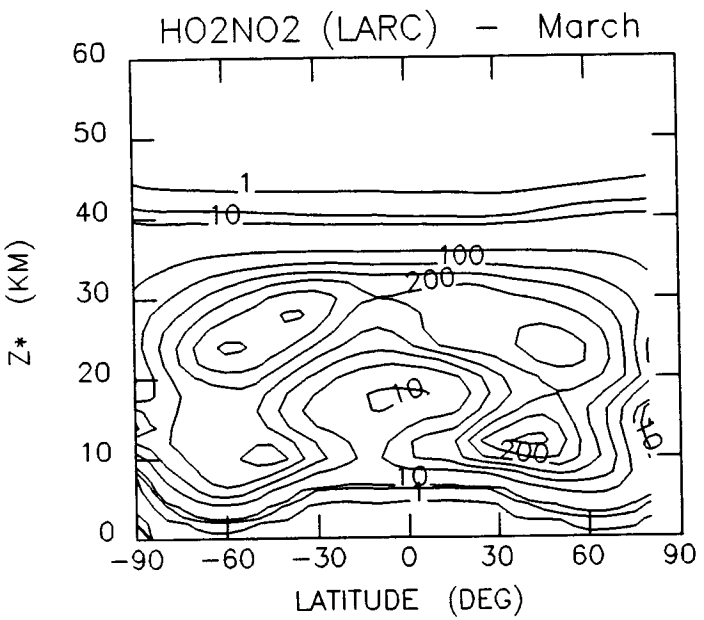
HO2NO2 (LARC) – March
Z* (KM)
LATITUDE (DEG)
60
50
40
30
20
10
0
-90 -60 -30 0 30 60 90
1
10
100
200
10
200
10
10

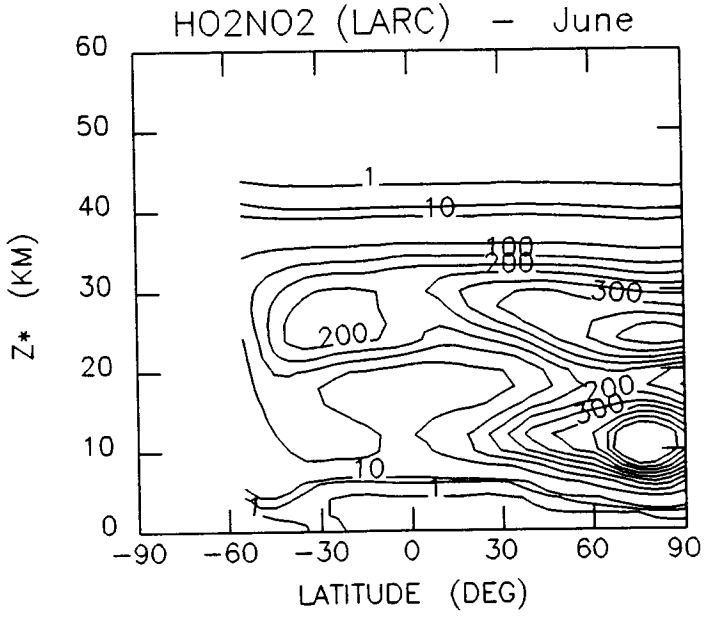
HO2NO2 (LARC) – June
Z* (KM)
LATITUDE (DEG)
60
50
40
30
20
10
0
-90 -60 -30 0 30 60 90
1
10
100
200
300
200
200
300
10
1

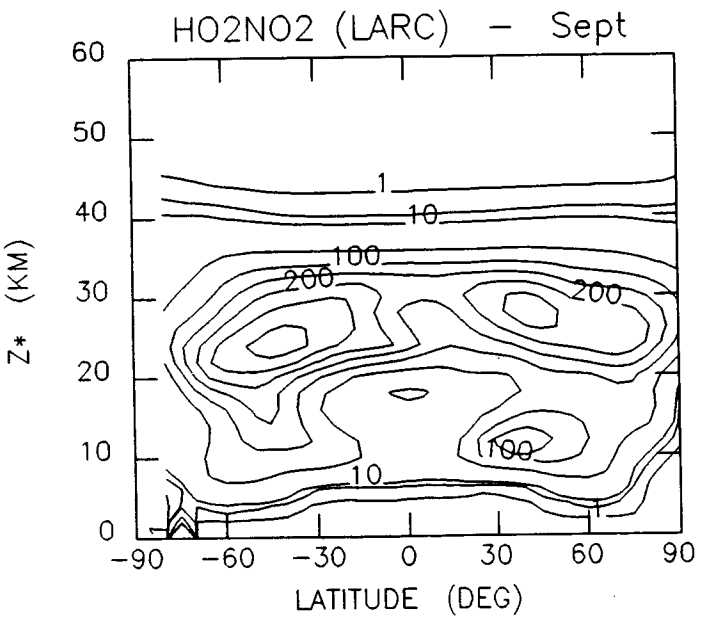
HO2NO2 (LARC) – Sept
Z* (KM)
LATITUDE (DEG)
60
50
40
30
20
10
0
-90 -60 -30 0 30 60 90
1
10
100
200
200
100
10

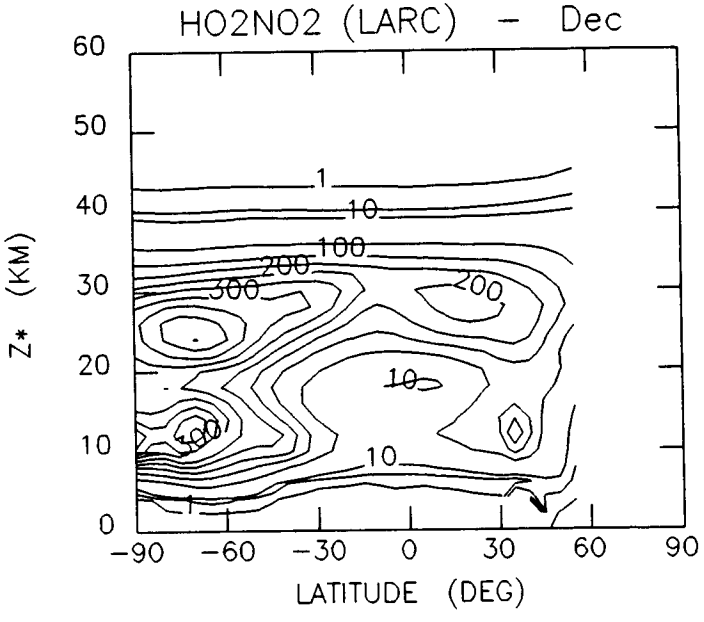
HO2NO2 (LARC) – Dec
Z* (KM)
LATITUDE (DEG)
60
50
40
30
20
10
0
-90 -60 -30 0 30 60 90
1
10
100
200
300
200
10
300
10
1

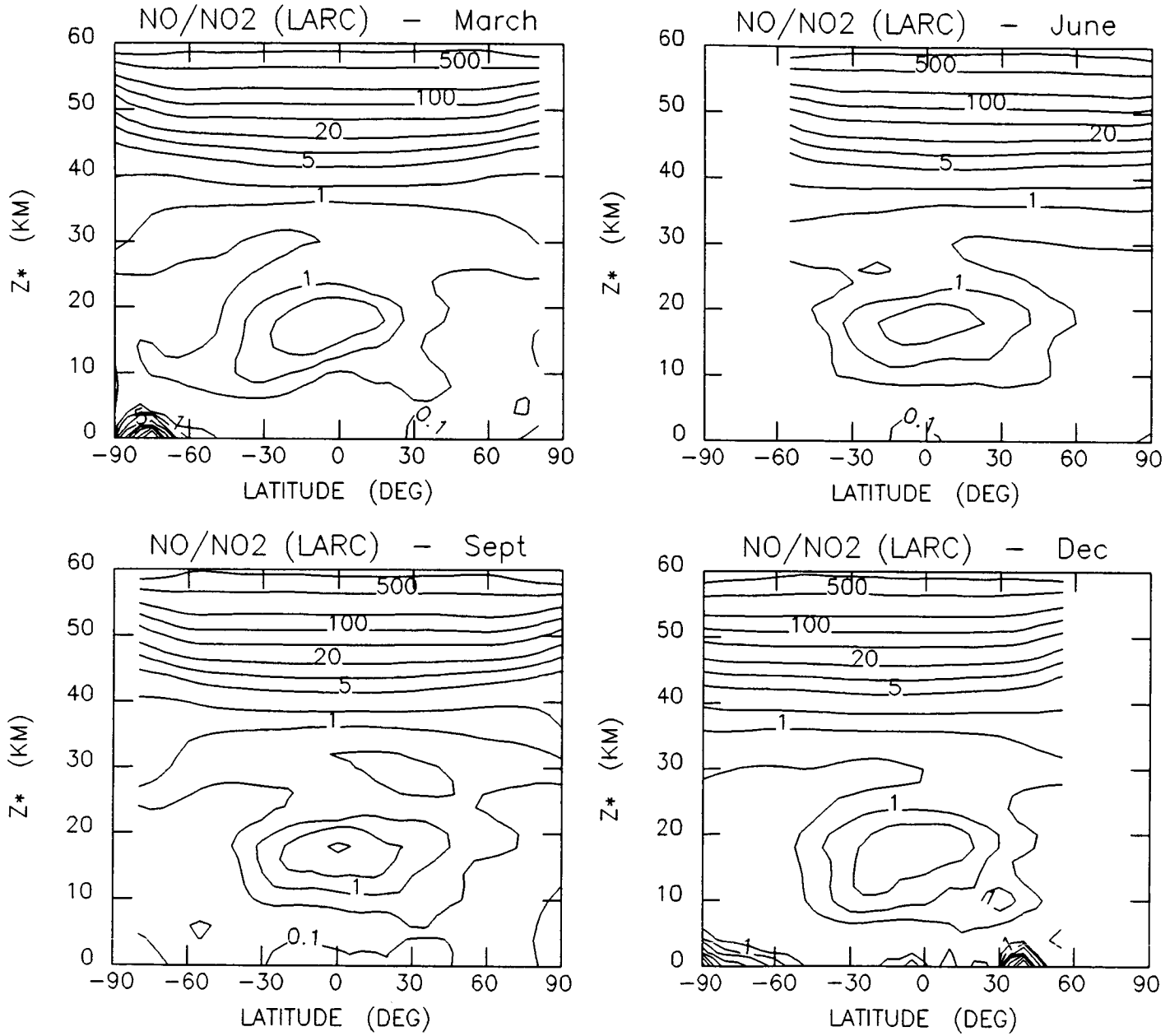
NO/NO2 (LARC) – March
NO/NO2 (LARC) – June
NO/NO2 (LARC) – Sept
NO/NO2 (LARC) – Dec
Z* (KM)
LATITUDE (DEG)
500
100
20
5
1
0.1
0
10
20
30
40
50
60
-90
-60
-30
0
30
60
90

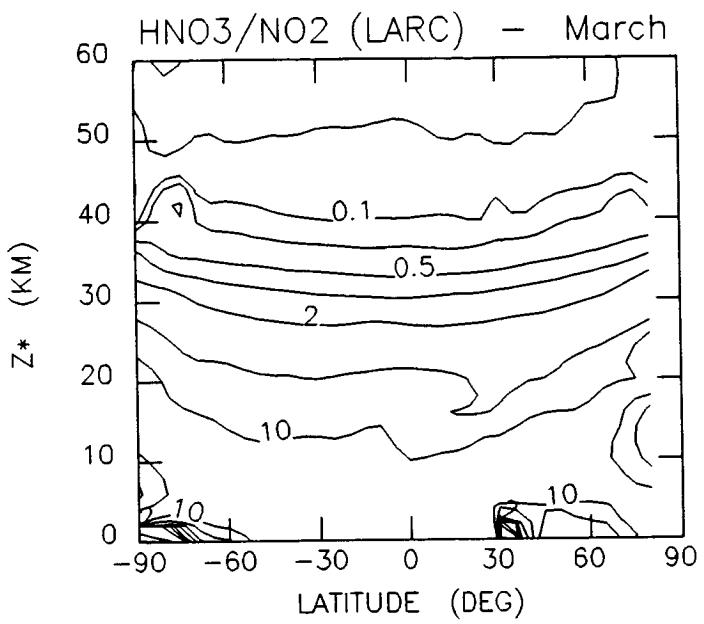
HNO3/NO2 (LARC) – March
Z* (KM)
LATITUDE (DEG)
0.1
0.5
2
10
10
10

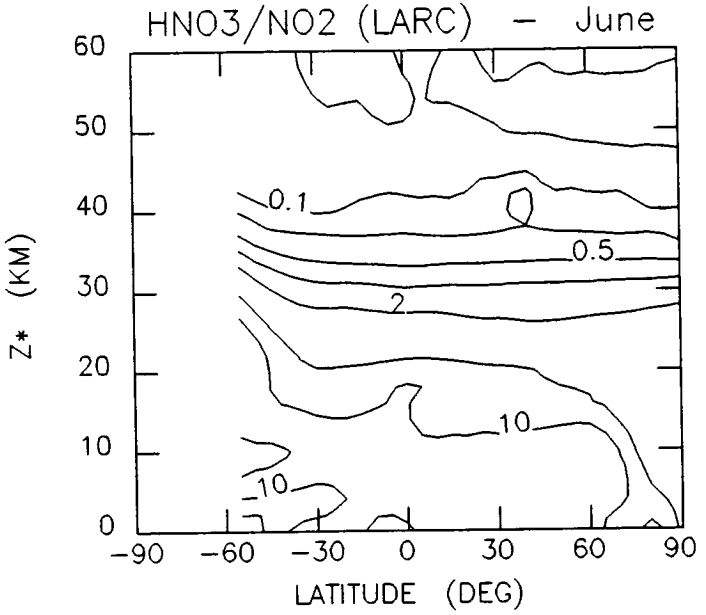
HNO3/NO2 (LARC) – June
Z* (KM)
LATITUDE (DEG)
0.1
0.5
2
10
10

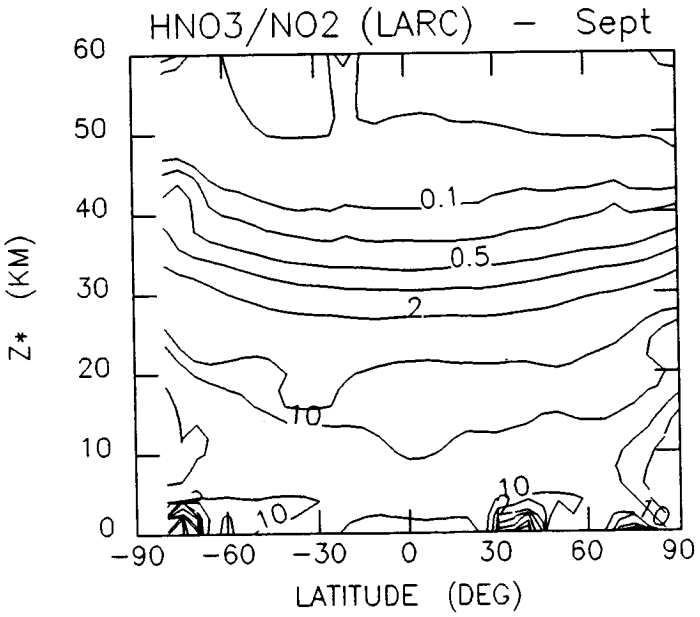
HNO3/NO2 (LARC) – Sept
Z* (KM)
LATITUDE (DEG)
0.1
0.5
2
10
10
10
10

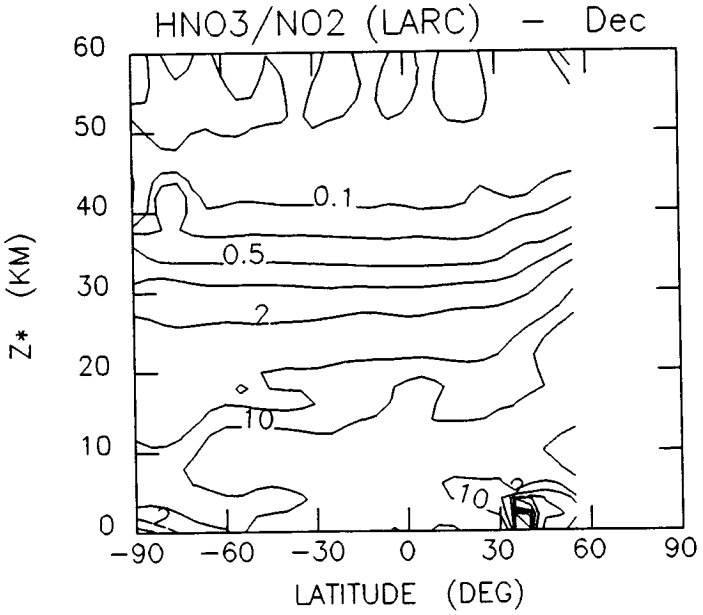
HNO3/NO2 (LARC) – Dec
Z* (KM)
LATITUDE (DEG)
0.1
0.5
2
10
10

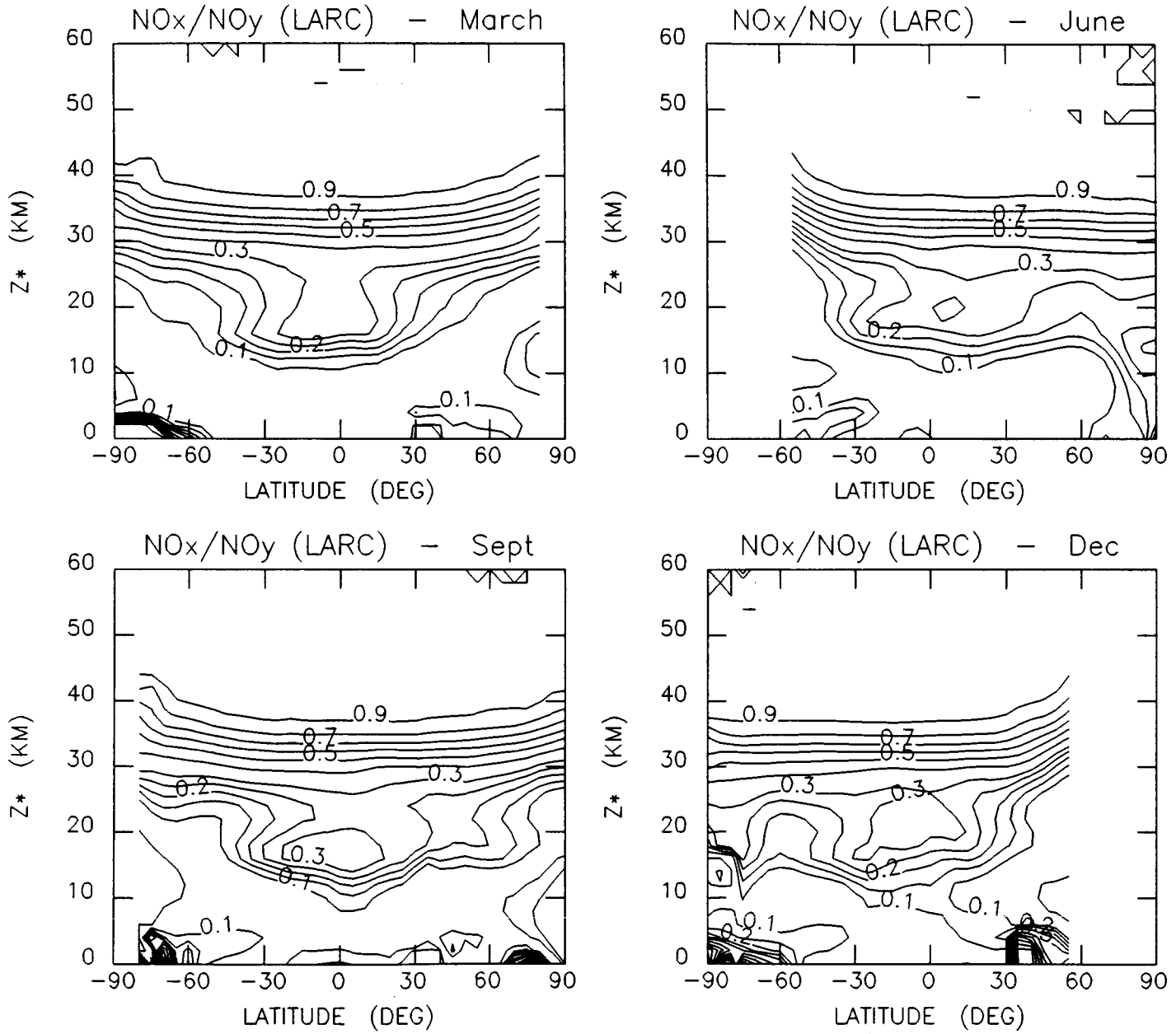
NOx/NOy (LARC) – March
NOx/NOy (LARC) – June
NOx/NOy (LARC) – Sept
NOx/NOy (LARC) – Dec
Z* (KM)
LATITUDE (DEG)
0
10
20
30
40
50
60
-90
-60
-30
0
30
60
90
0.9
0.7
0.5
0.3
0.2
0.1

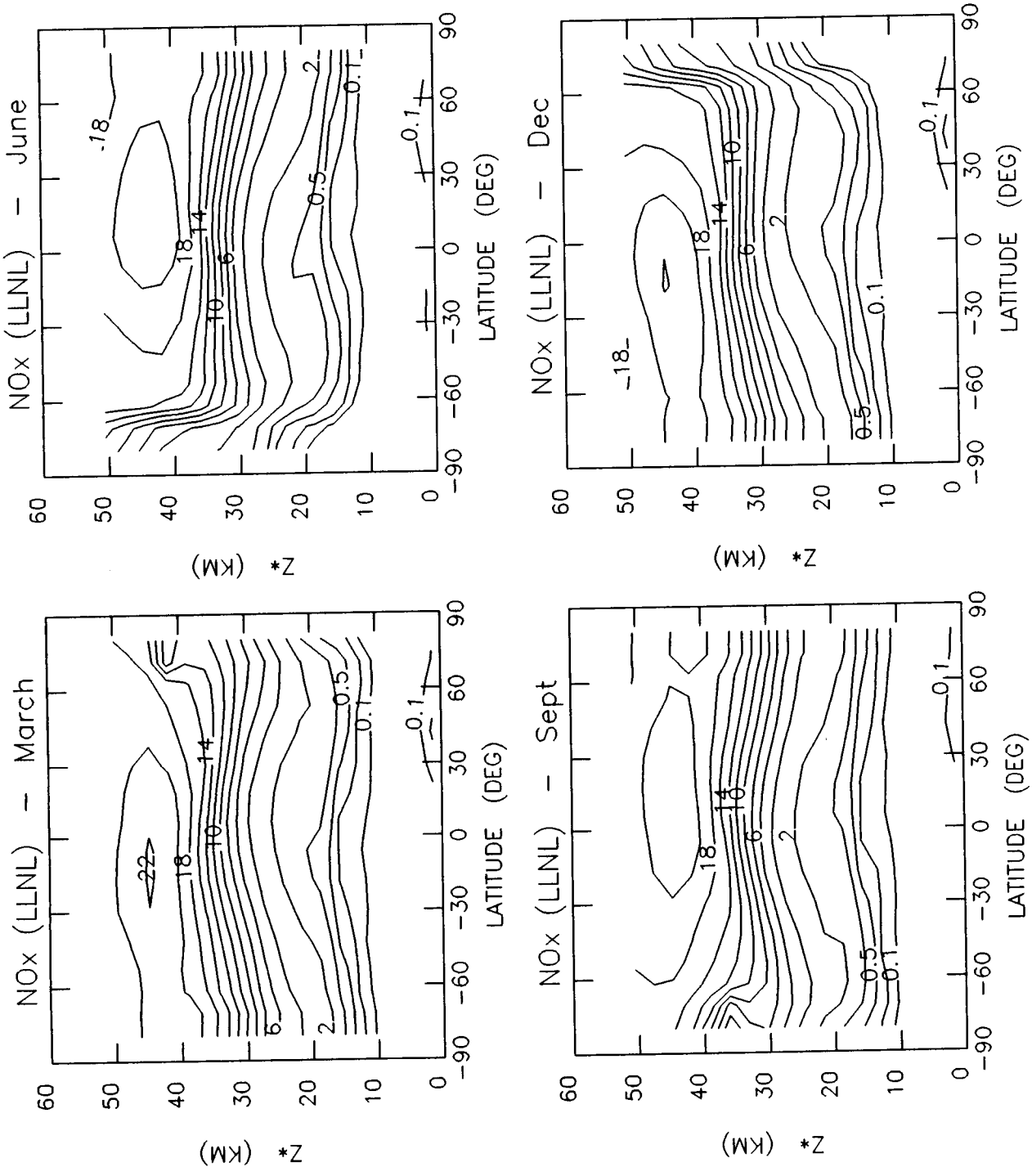
NOx (LLNL) - March
NOx (LLNL) - June
NOx (LLNL) - Sept
NOx (LLNL) - Dec
Z* (KM)
LATITUDE (DEG)
60
50
40
30
20
10
0
-90
-60
-30
0
30
60
90
22
18
14
10
6
2
0.5
0.1

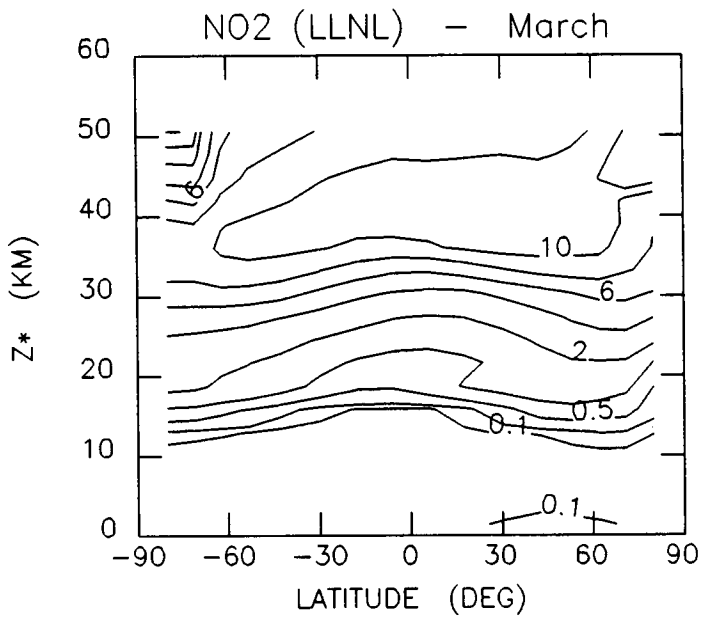
NO2 (LLNL) – March
Z* (KM)
LATITUDE (DEG)
60
50
40
30
20
10
0
-90 -60 -30 0 30 60 90
10
6
2
0.5
0.1

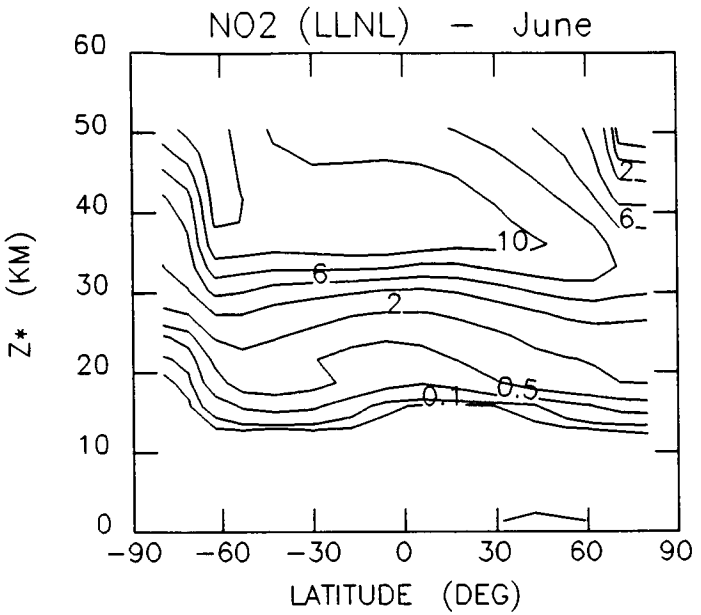
NO2 (LLNL) – June
Z* (KM)
LATITUDE (DEG)
60
50
40
30
20
10
0
-90 -60 -30 0 30 60 90
10
6
2
0.5
0.1

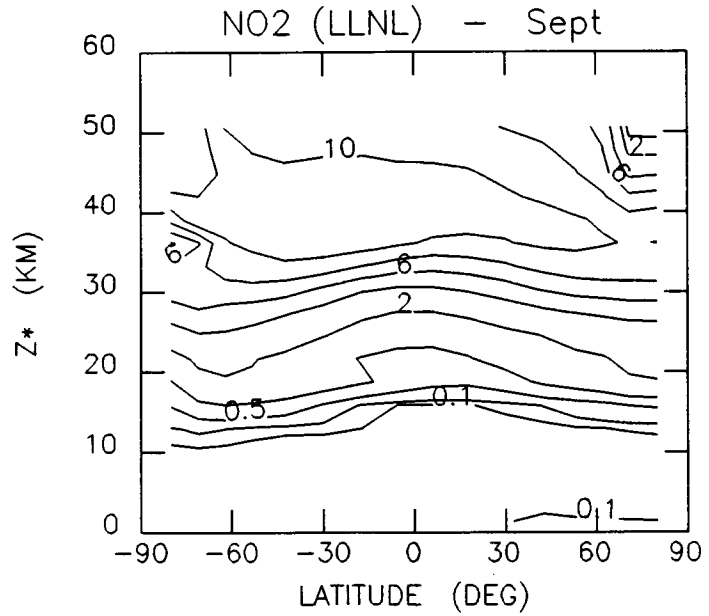
NO2 (LLNL) – Sept
Z* (KM)
LATITUDE (DEG)
60
50
40
30
20
10
0
-90 -60 -30 0 30 60 90
10
6
2
0.5
0.1

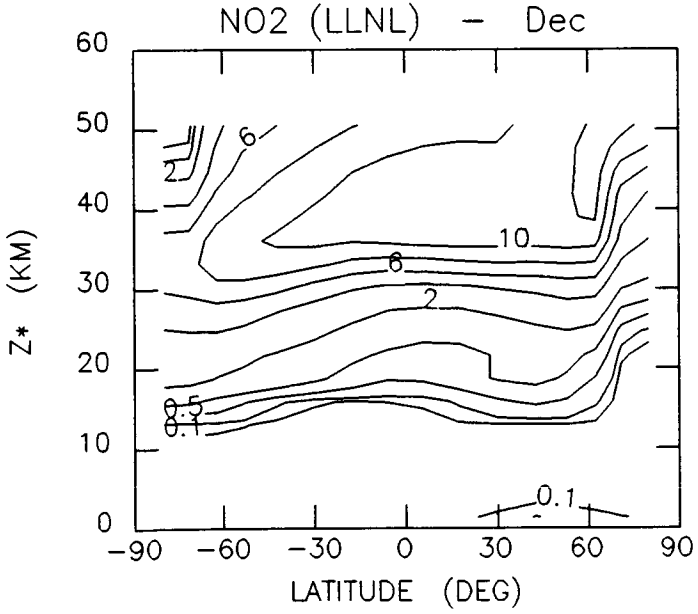
NO2 (LLNL) – Dec
Z* (KM)
LATITUDE (DEG)
60
50
40
30
20
10
0
-90 -60 -30 0 30 60 90
10
6
2
0.5
0.1

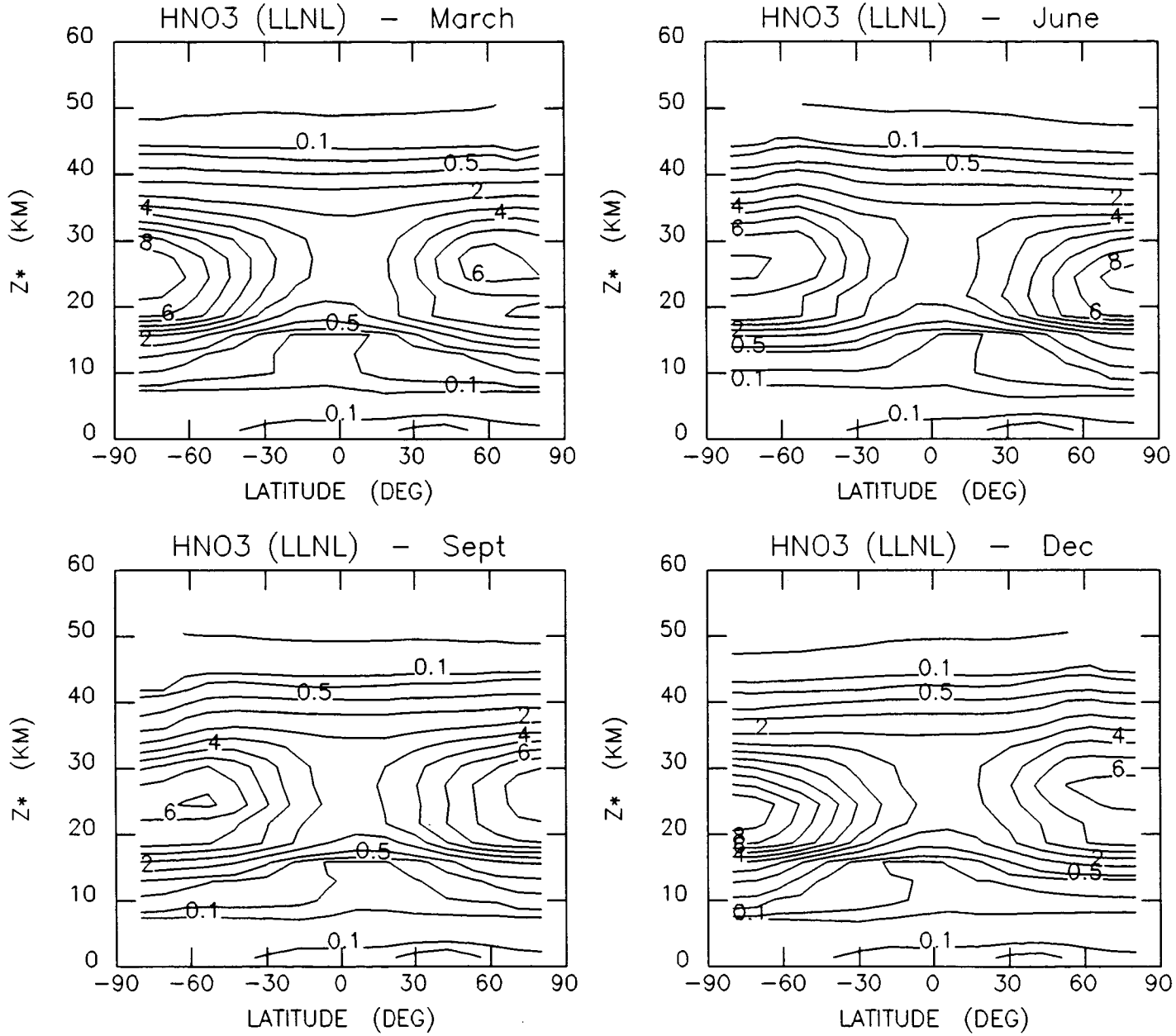
HNO3 (LLNL) – March
HNO3 (LLNL) – June
HNO3 (LLNL) – Sept
HNO3 (LLNL) – Dec
Z* (KM)
LATITUDE (DEG)
0
10
20
30
40
50
60
-90
-60
-30
0
30
60
90
0.1
0.5
2
4
6
8

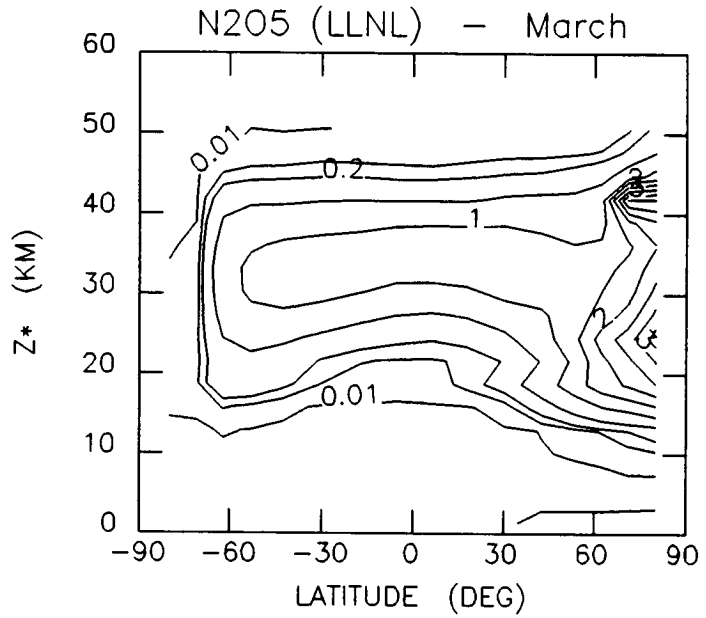
N2O5 (LLNL) – March
Z* (KM)
LATITUDE (DEG)
0.01
0.2
1
2
3
4
5
0.01
0
10
20
30
40
50
60
-90
-60
-30
0
30
60
90

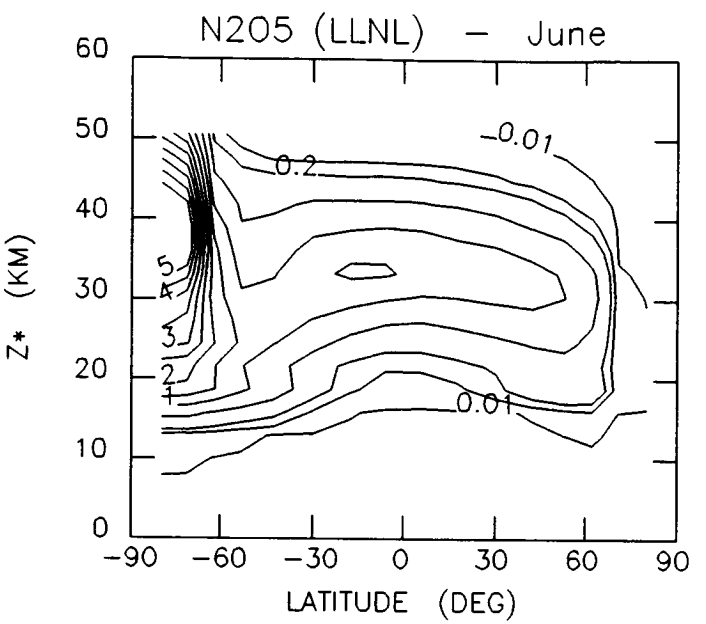
N2O5 (LLNL) – June
Z* (KM)
LATITUDE (DEG)
0.01
0.2
1
2
3
4
5
0.01
0
10
20
30
40
50
60
-90
-60
-30
0
30
60
90

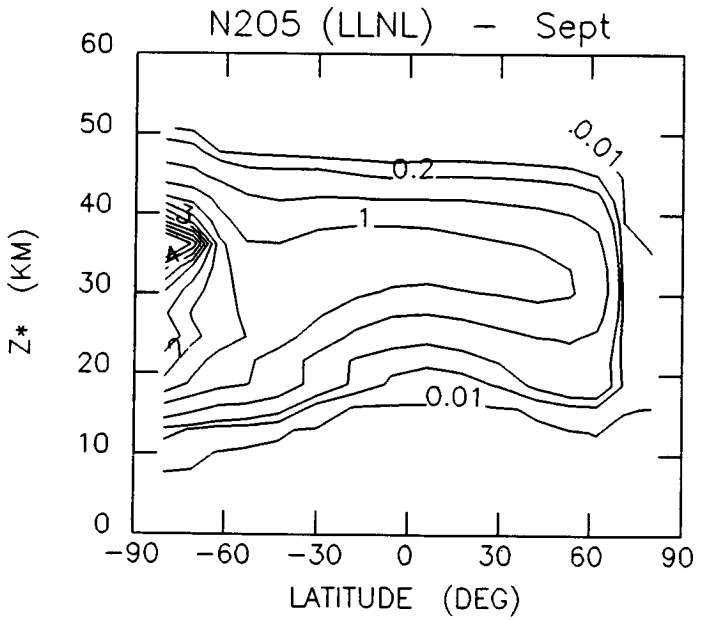
N2O5 (LLNL) – Sept
Z* (KM)
LATITUDE (DEG)
0.01
0.2
1
2
3
4
5
0.01
0
10
20
30
40
50
60
-90
-60
-30
0
30
60
90

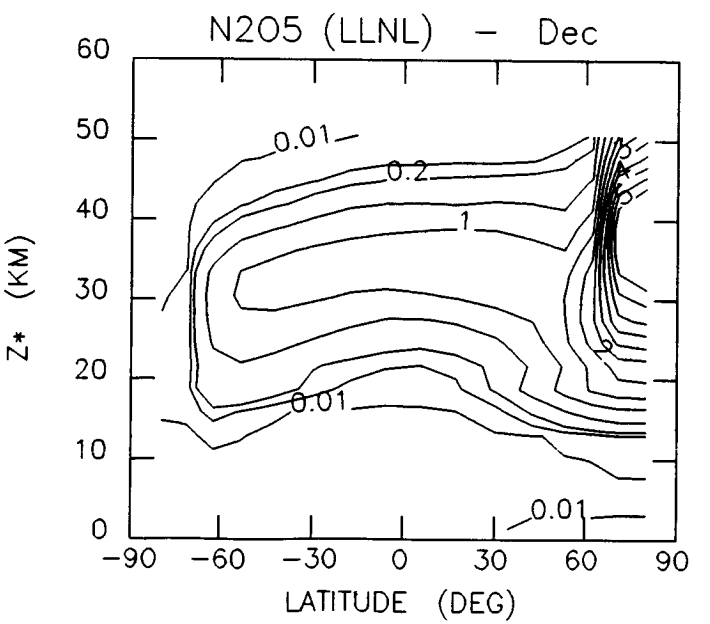
N2O5 (LLNL) – Dec
Z* (KM)
LATITUDE (DEG)
0.01
0.2
1
2
3
4
5
0.01
0
10
20
30
40
50
60
-90
-60
-30
0
30
60
90

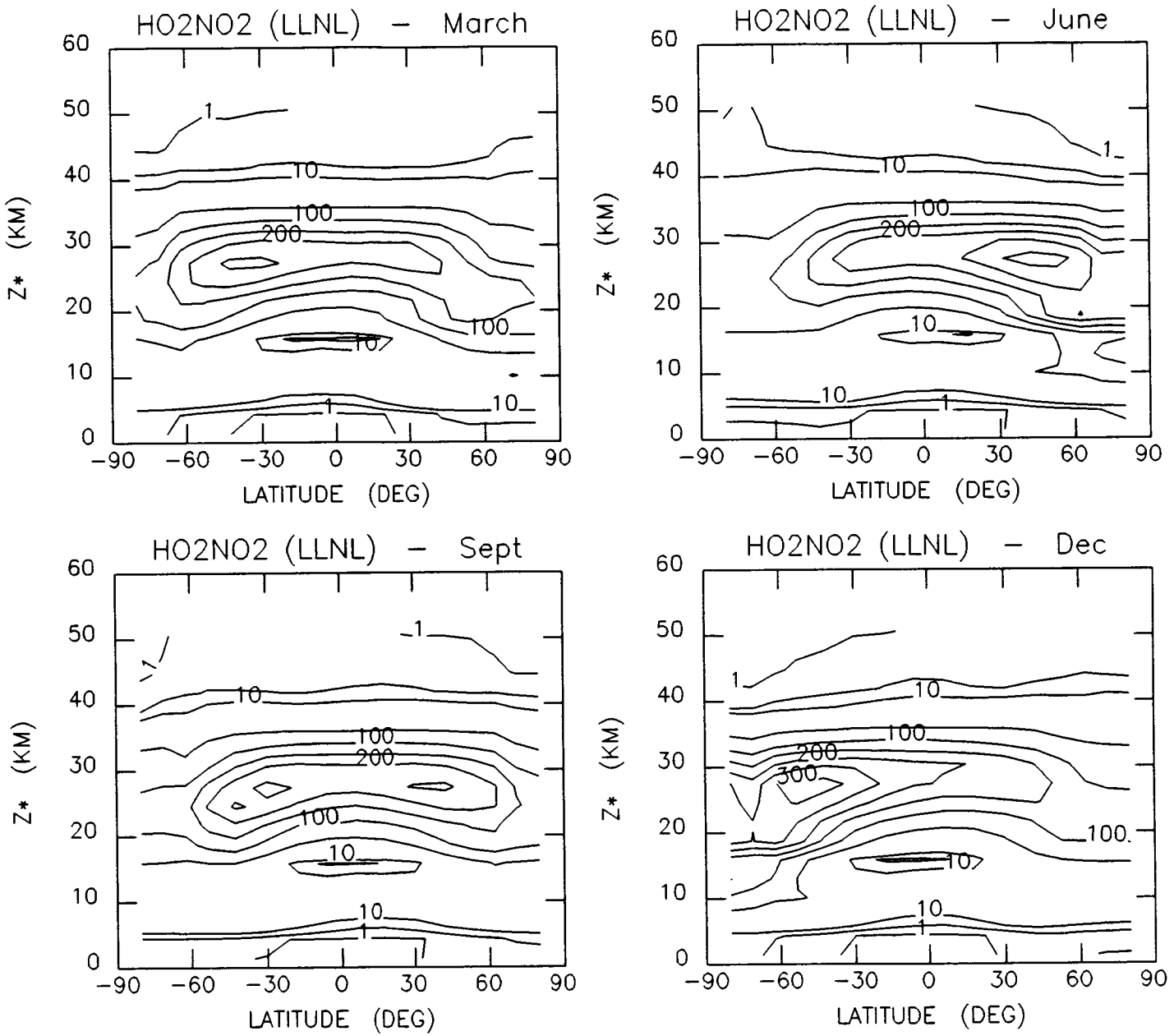
HO2NO2 (LLNL) – March
HO2NO2 (LLNL) – June
HO2NO2 (LLNL) – Sept
HO2NO2 (LLNL) – Dec
Z* (KM)
LATITUDE (DEG)
60
50
40
30
20
10
0
-90 -60 -30 0 30 60 90
1
10
100
200
300

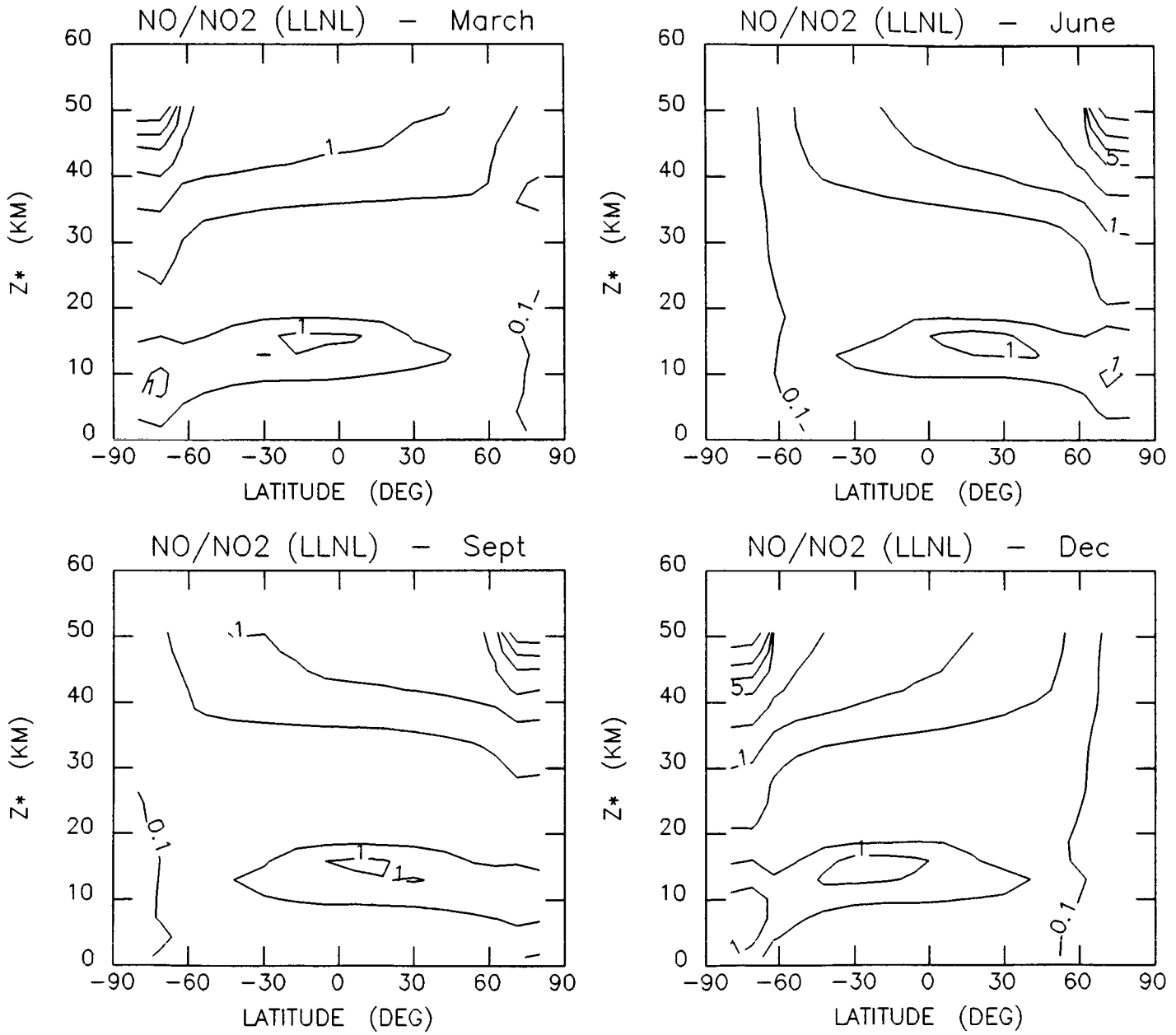
NO/NO2 (LLNL) – March
NO/NO2 (LLNL) – June
NO/NO2 (LLNL) – Sept
NO/NO2 (LLNL) – Dec
Z* (KM)
LATITUDE (DEG)
0
10
20
30
40
50
60
-90
-60
-30
0
30
60
90
1
0.1
5

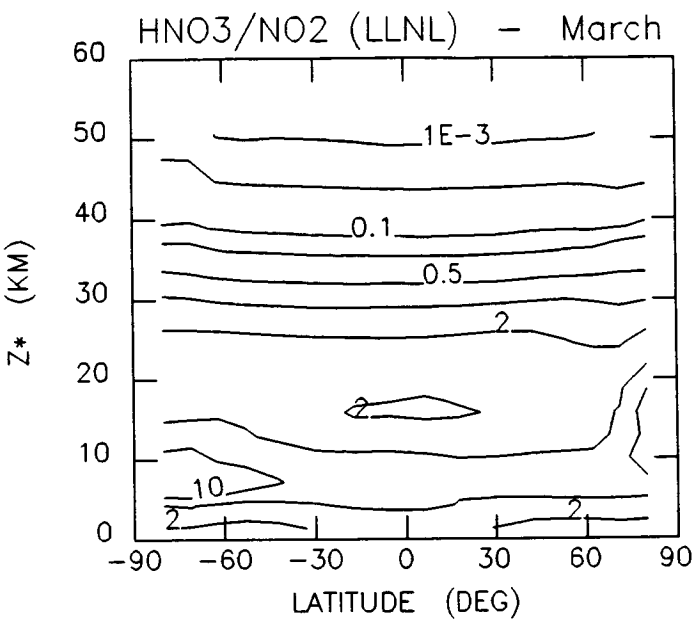
HNO3/NO2 (LLNL) – March
Z* (KM)
LATITUDE (DEG)
1E-3
0.1
0.5
2
10

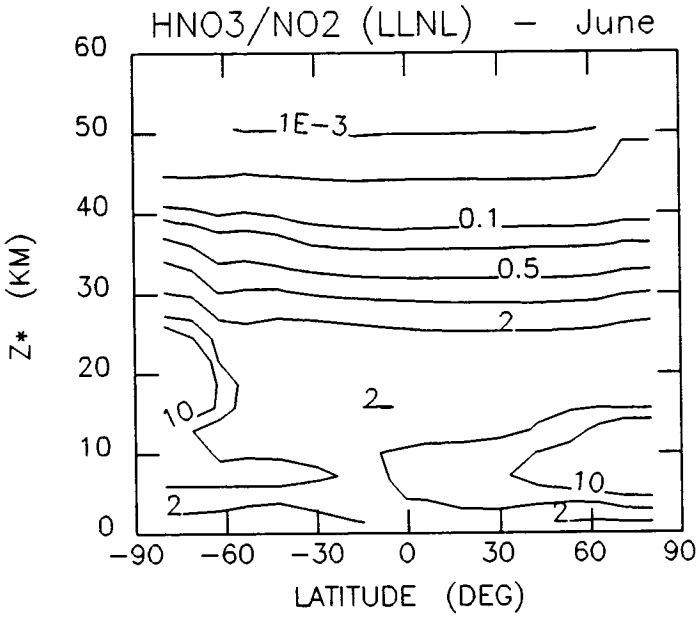
HNO3/NO2 (LLNL) – June
Z* (KM)
LATITUDE (DEG)
1E-3
0.1
0.5
2
10

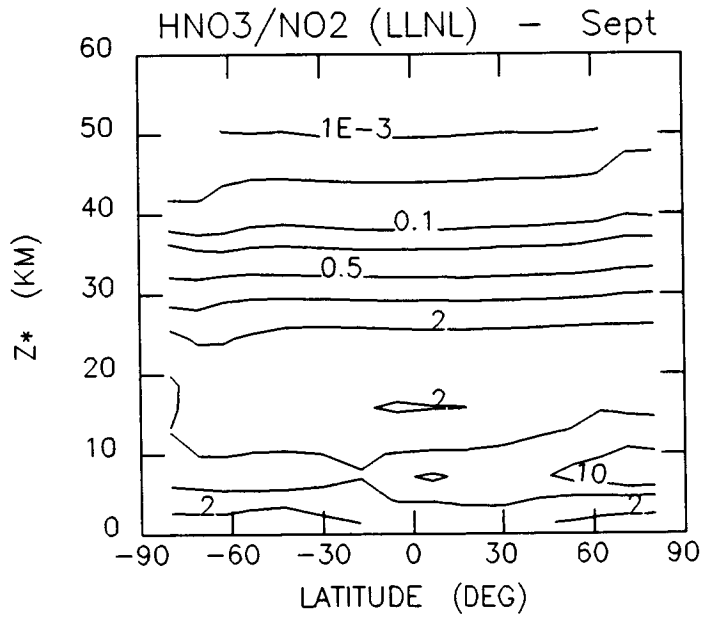
HNO3/NO2 (LLNL) – Sept
Z* (KM)
LATITUDE (DEG)
1E-3
0.1
0.5
2
10

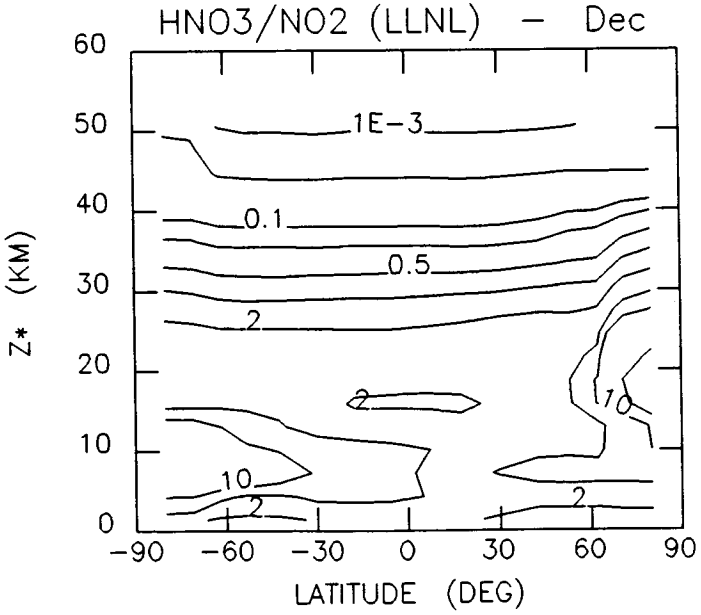
HNO3/NO2 (LLNL) – Dec
Z* (KM)
LATITUDE (DEG)
1E-3
0.1
0.5
2
10

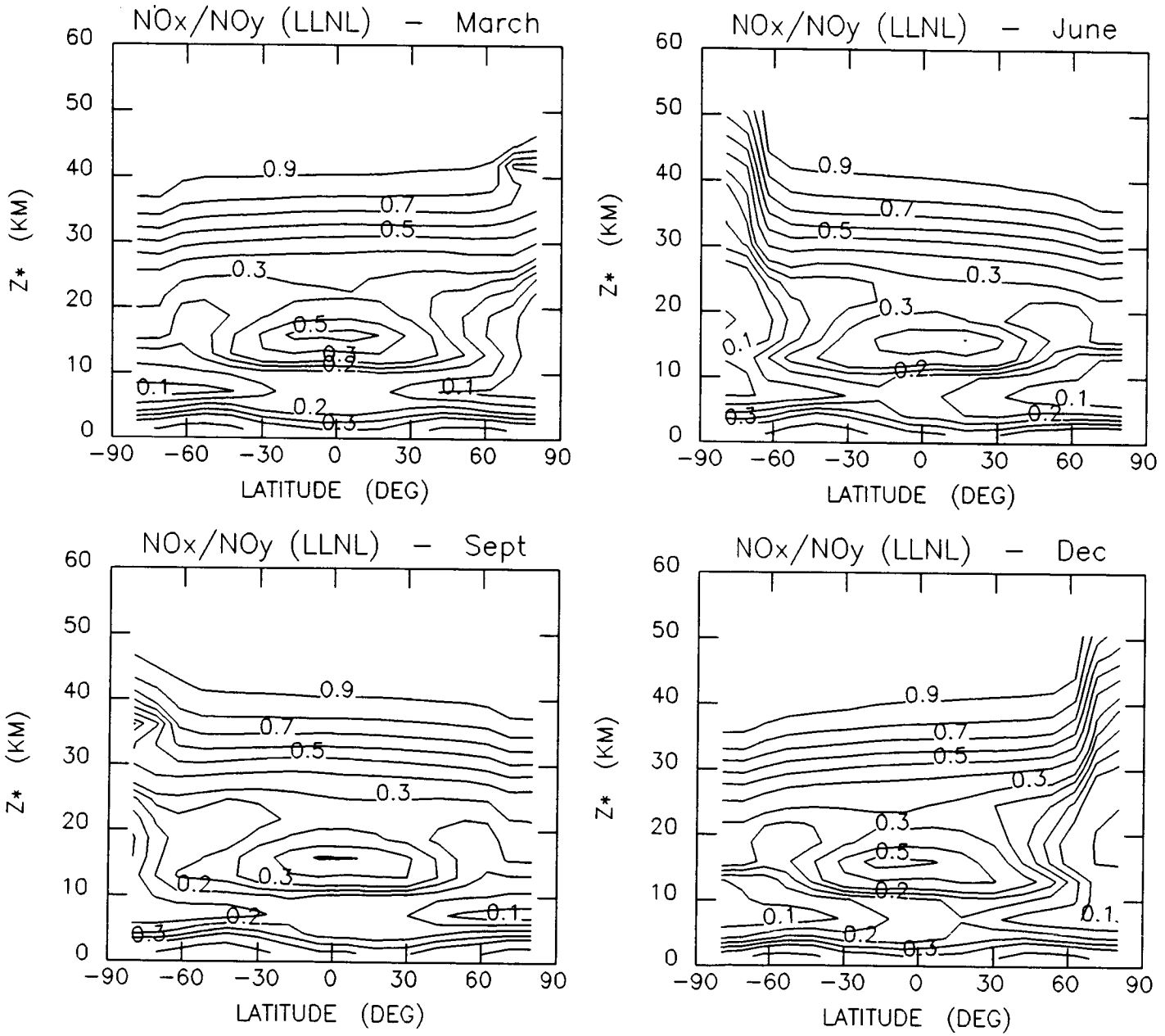
NOx/NOy (LLNL) – March
NOx/NOy (LLNL) – June
NOx/NOy (LLNL) – Sept
NOx/NOy (LLNL) – Dec
Z* (KM)
LATITUDE (DEG)
0
10
20
30
40
50
60
-90
-60
-30
0
30
60
90
0.9
0.7
0.5
0.3
0.2
0.1

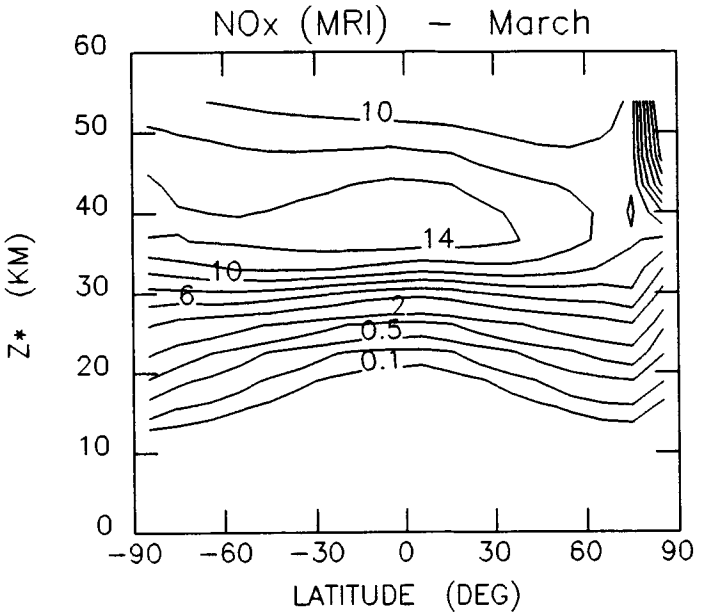
NOx (MRI) – March
Z* (KM)
LATITUDE (DEG)
10
14
10
6
2
0.5
0.1

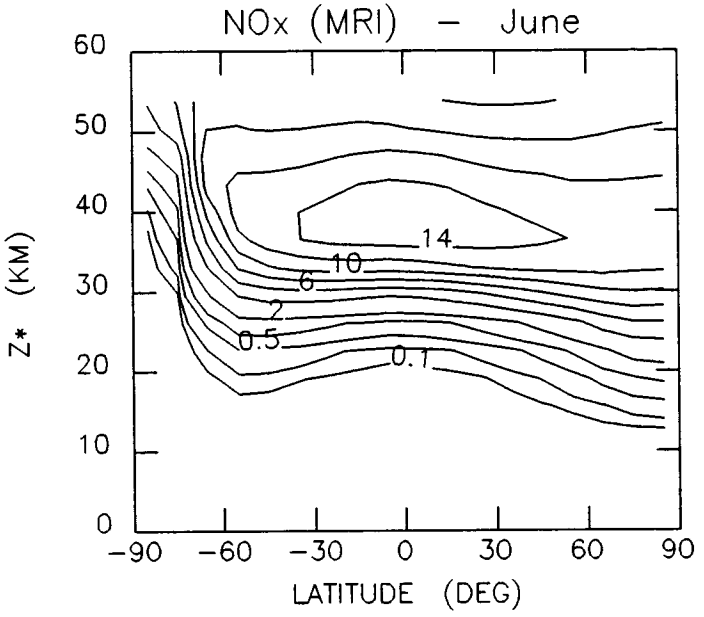
NOx (MRI) – June
Z* (KM)
LATITUDE (DEG)
14
10
6
2
0.5
0.1

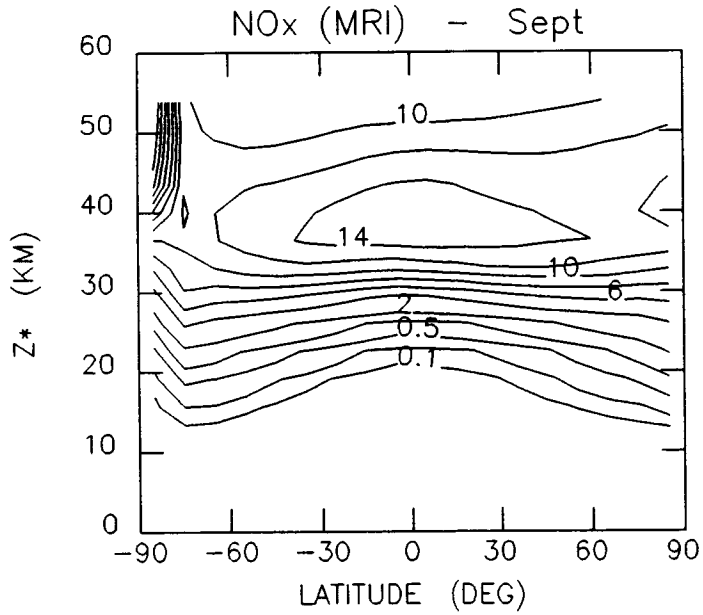
NOx (MRI) – Sept
Z* (KM)
LATITUDE (DEG)
10
14
10
6
2
0.5
0.1

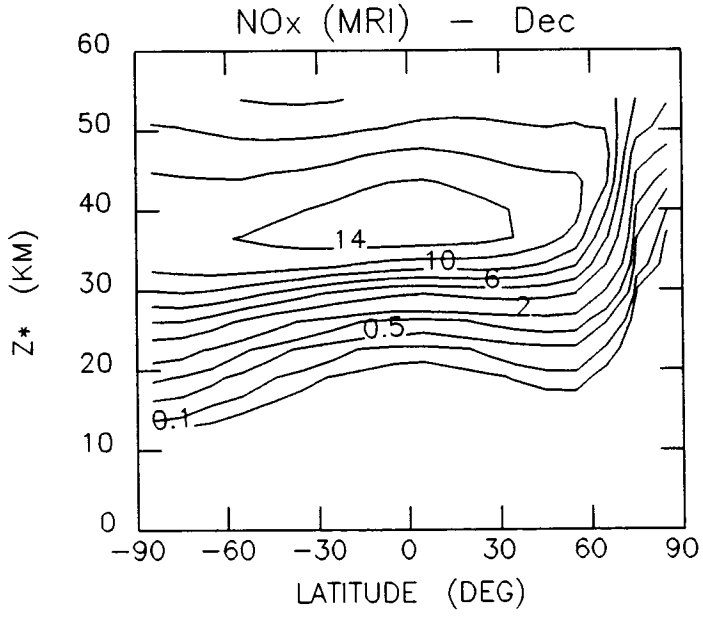
NOx (MRI) – Dec
Z* (KM)
LATITUDE (DEG)
14
10
6
2
0.5
0.1

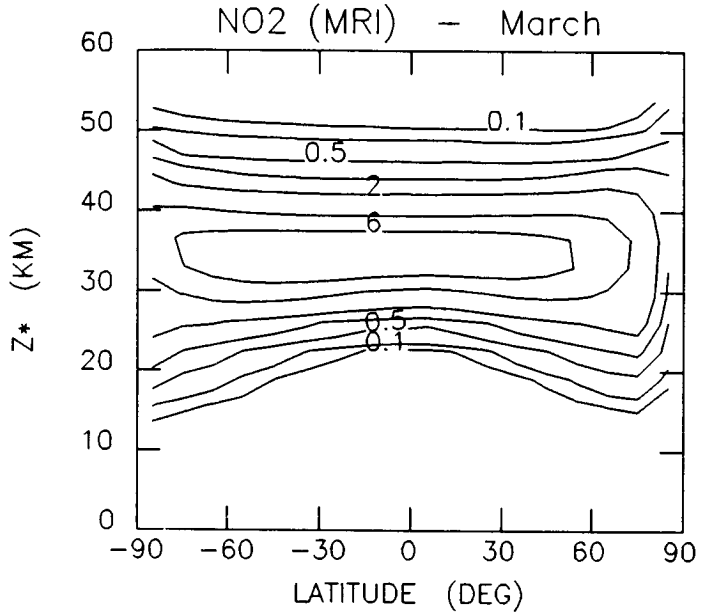
NO2 (MRI) – March
Z* (KM)
LATITUDE (DEG)
0.1
0.5
2
6
0.5
0.1

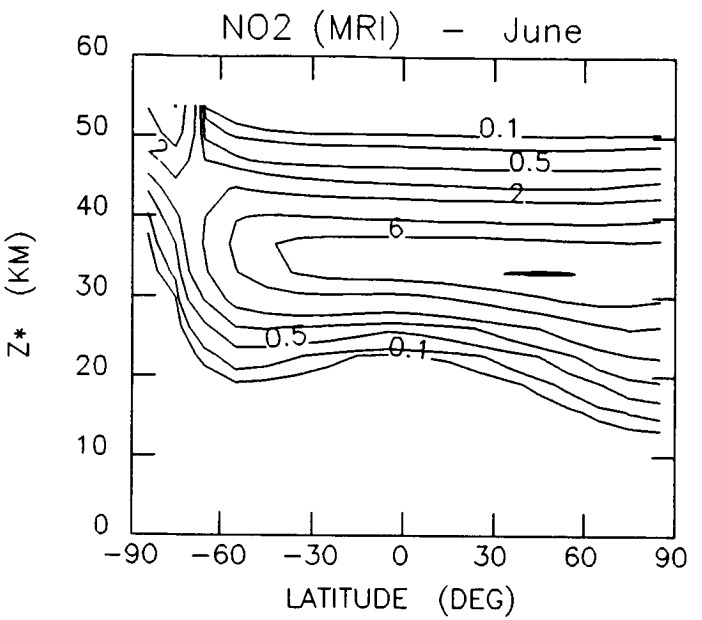
NO2 (MRI) – June
Z* (KM)
LATITUDE (DEG)
0.1
0.5
2
6
0.5
0.1

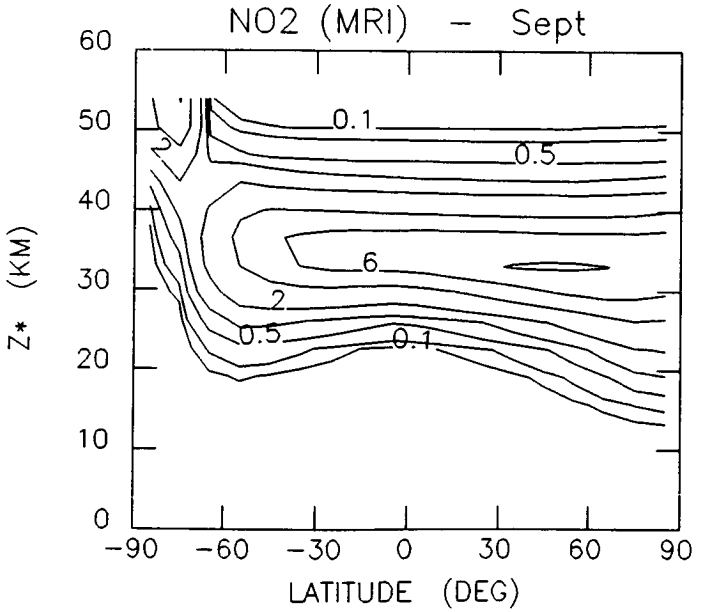
NO2 (MRI) – Sept
Z* (KM)
LATITUDE (DEG)
0.1
0.5
6
2
0.5
0.1

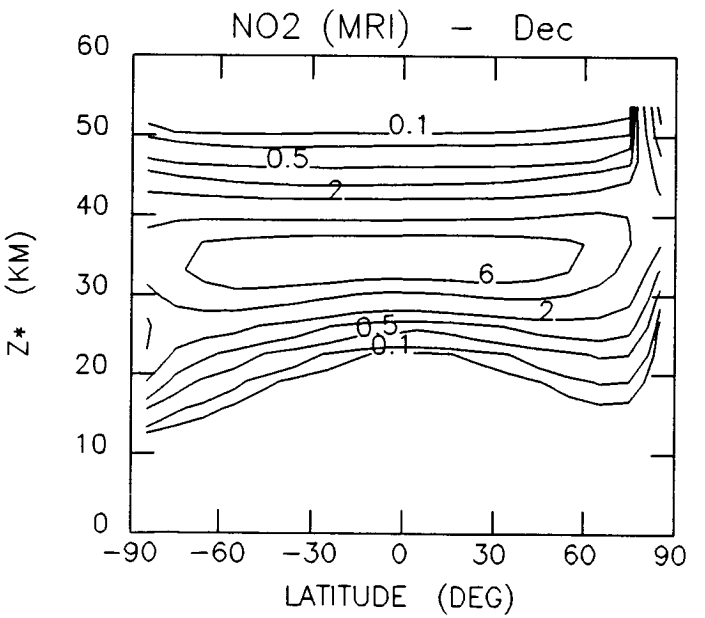
NO2 (MRI) – Dec
Z* (KM)
LATITUDE (DEG)
0.1
0.5
2
6
2
0.5
0.1

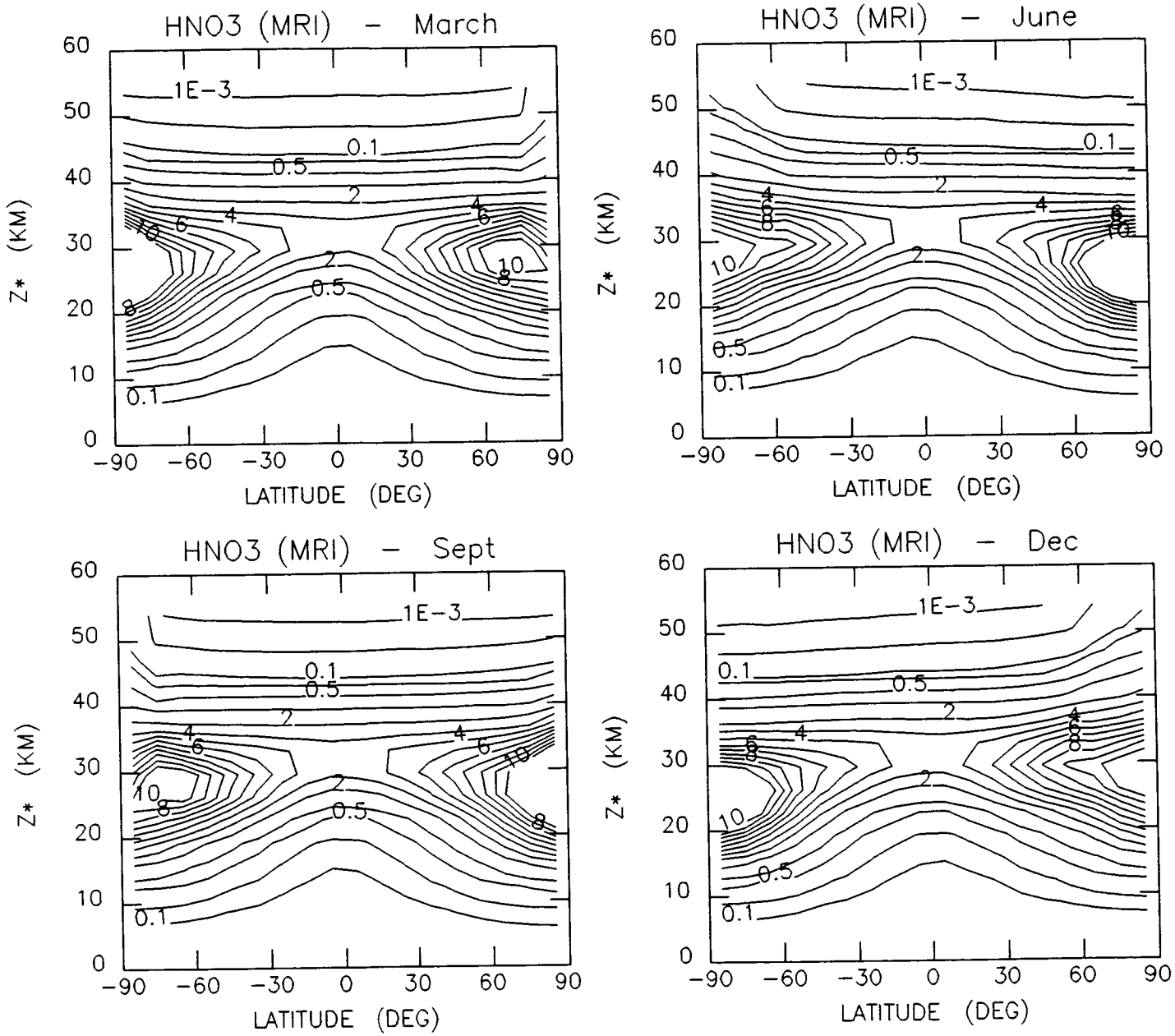
HNO3 (MRI) – March
HNO3 (MRI) – June
HNO3 (MRI) – Sept
HNO3 (MRI) – Dec
Z* (KM)
LATITUDE (DEG)
1E-3
0.1
0.5
2
4
6
8
10
0
10
20
30
40
50
60
-90
-60
-30
0
30
60
90

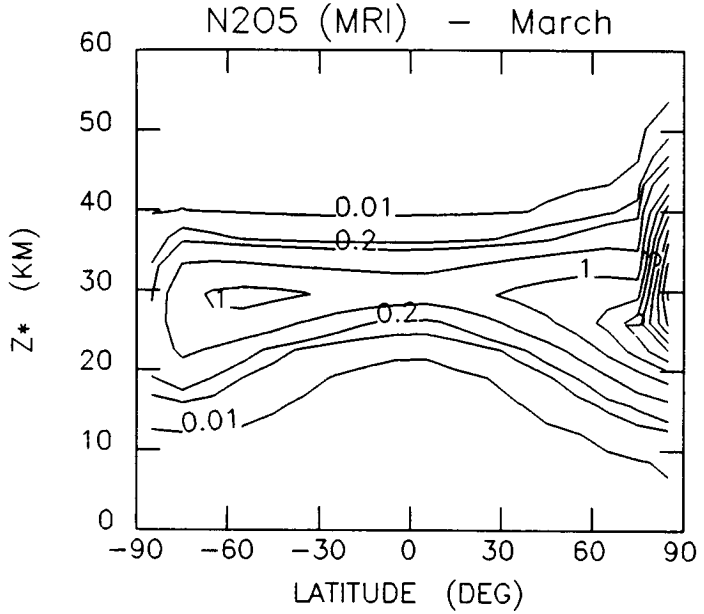
N205 (MRI) – March
Z* (KM)
LATITUDE (DEG)
0.01
0.2
1
0.2
0.01
1
0
10
20
30
40
50
60
−90
−60
−30
0
30
60
90

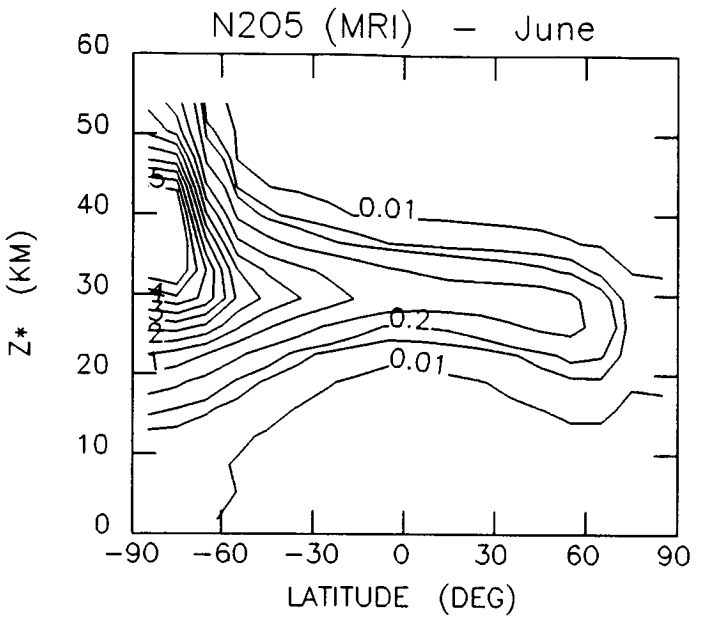
N205 (MRI) – June
Z* (KM)
LATITUDE (DEG)
0.01
0.2
0.01
1
0
10
20
30
40
50
60
−90
−60
−30
0
30
60
90

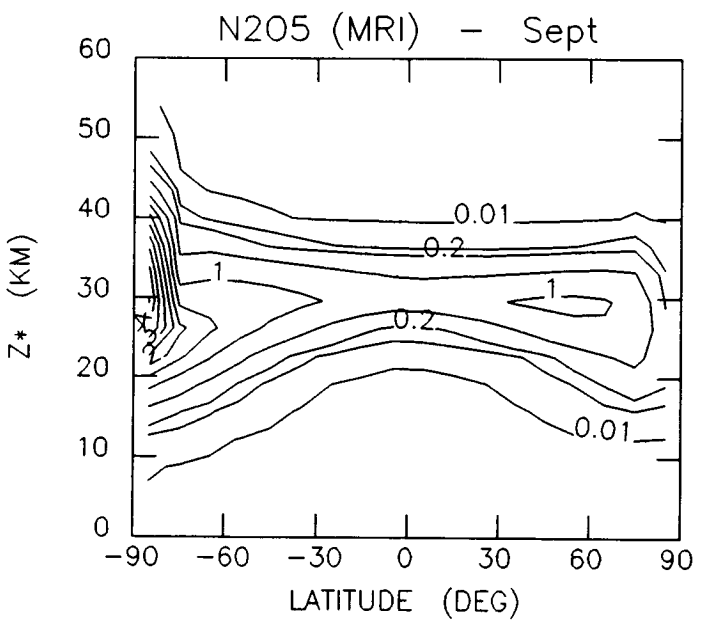
N205 (MRI) – Sept
Z* (KM)
LATITUDE (DEG)
0.01
0.2
1
1
0.2
0.01
0
10
20
30
40
50
60
−90
−60
−30
0
30
60
90

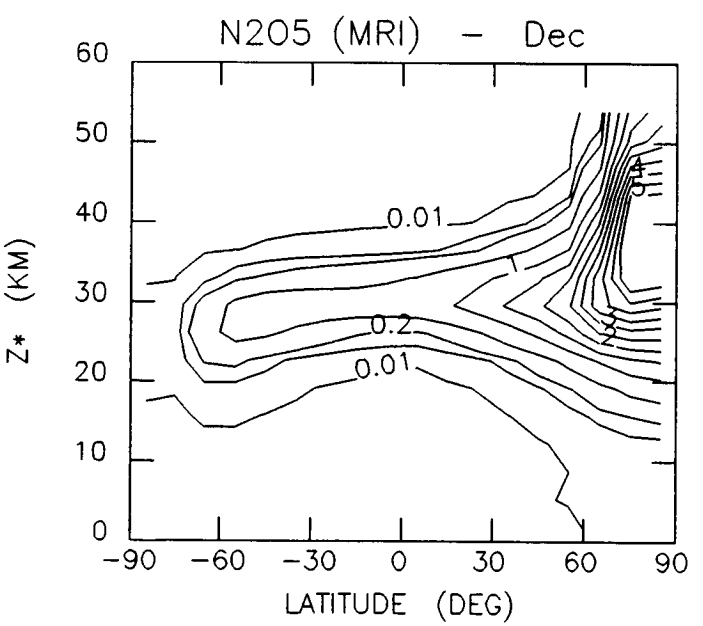
N205 (MRI) – Dec
Z* (KM)
LATITUDE (DEG)
0.01
0.2
0.01
1
0
10
20
30
40
50
60
−90
−60
−30
0
30
60
90

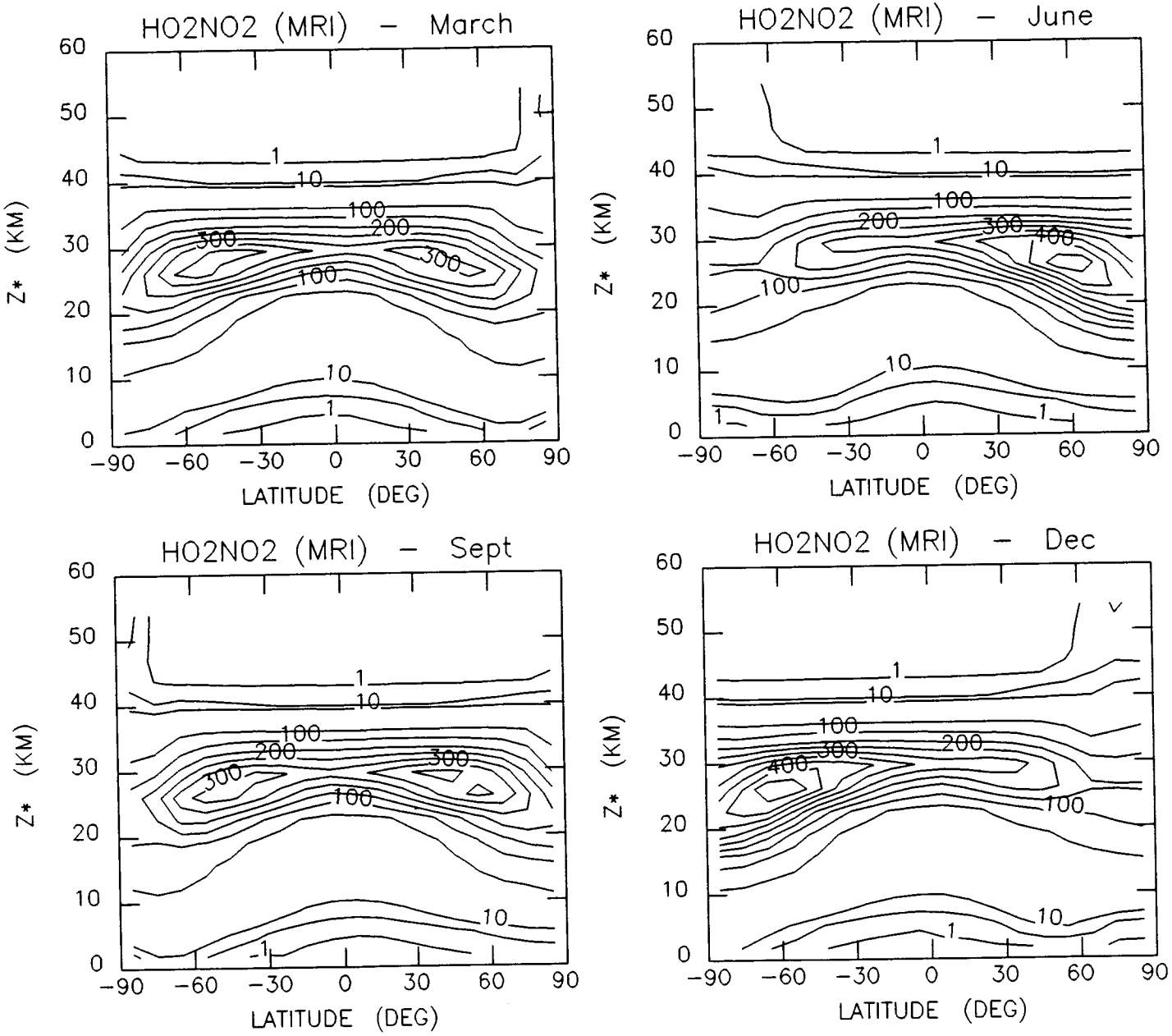
HO2NO2 (MRI) – March
HO2NO2 (MRI) – June
HO2NO2 (MRI) – Sept
HO2NO2 (MRI) – Dec
Z* (KM)
LATITUDE (DEG)
60
50
40
30
20
10
0
-90 -60 -30 0 30 60 90
1
10
100
200
300
400

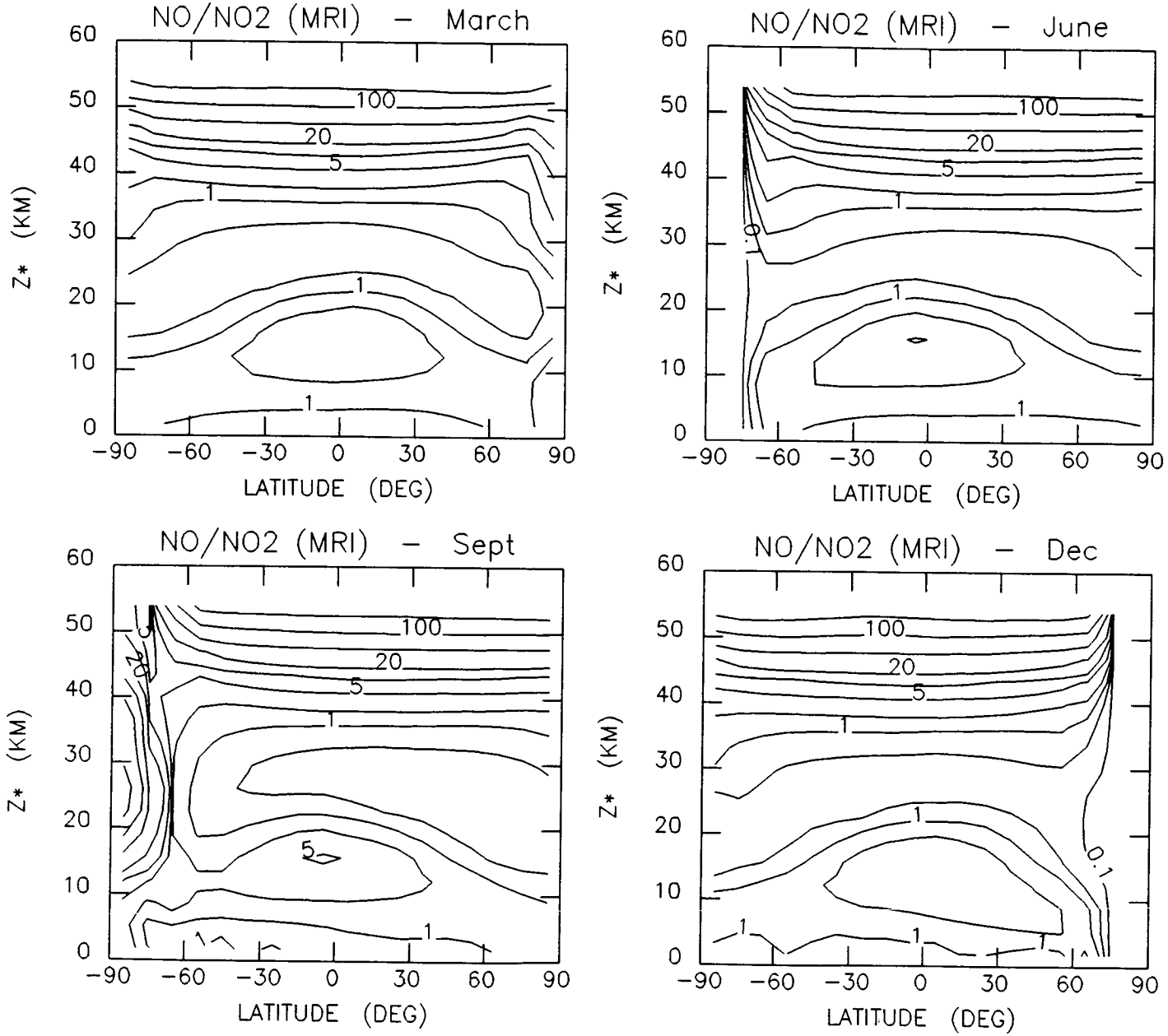
NO/NO2 (MRI) – March
NO/NO2 (MRI) – June
NO/NO2 (MRI) – Sept
NO/NO2 (MRI) – Dec
Z* (KM)
LATITUDE (DEG)
60
50
40
30
20
10
0
-90
-60
-30
0
30
60
90
100
20
5
1
0.1

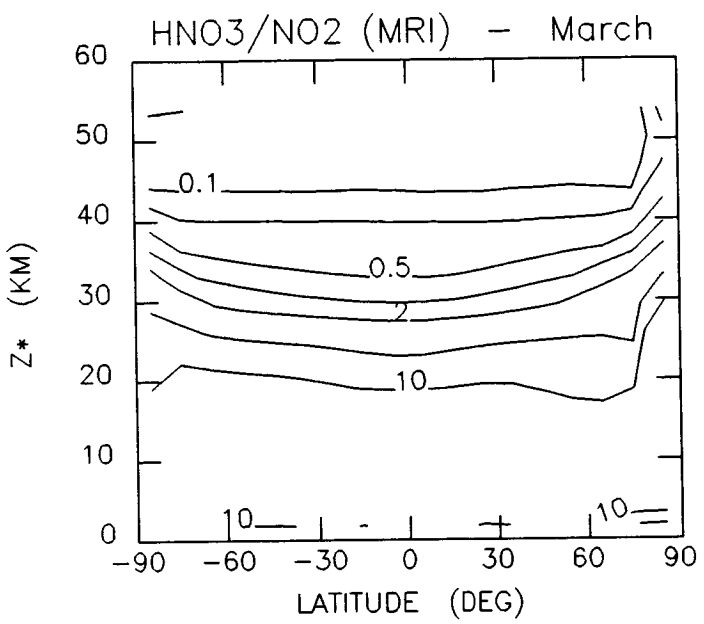
HNO3/NO2 (MRI) – March
Z* (KM)
LATITUDE (DEG)
0.1
0.5
2
10

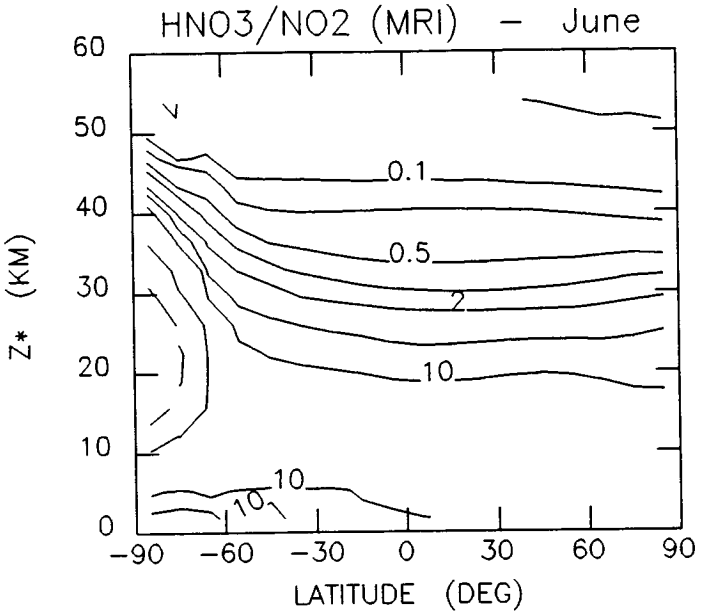
HNO3/NO2 (MRI) – June
Z* (KM)
LATITUDE (DEG)
0.1
0.5
2
10

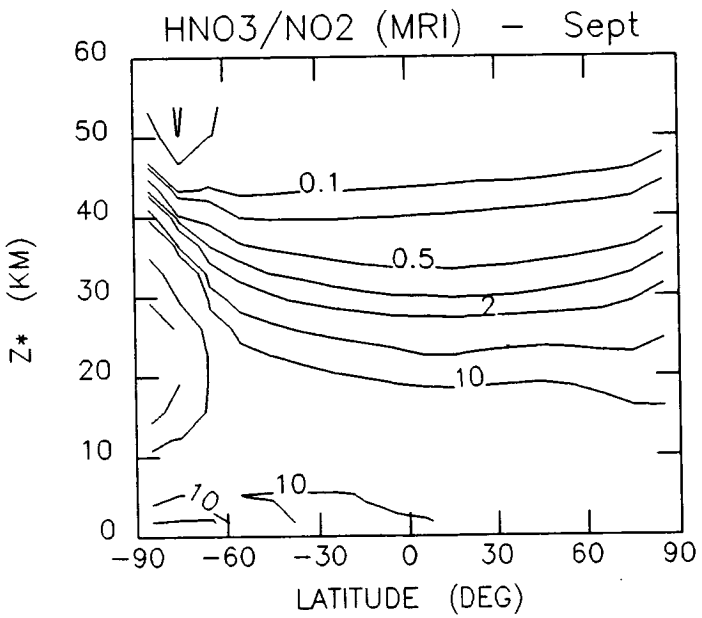
HNO3/NO2 (MRI) – Sept
Z* (KM)
LATITUDE (DEG)
0.1
0.5
2
10

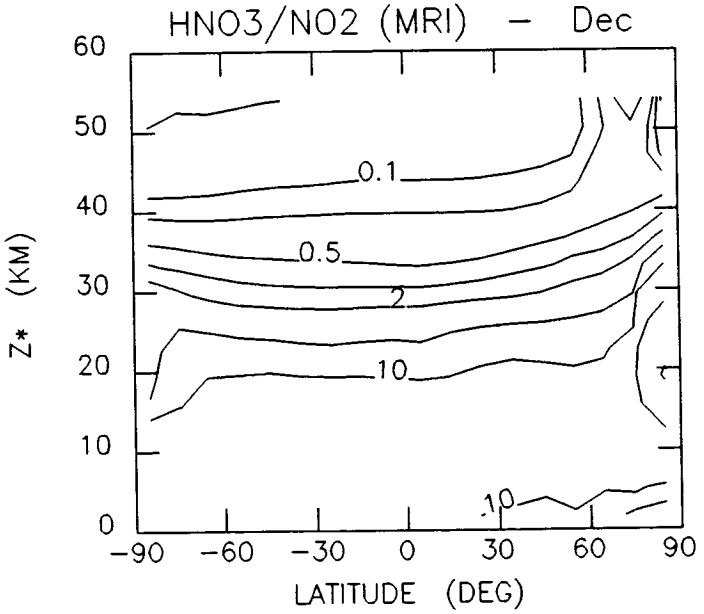
HNO3/NO2 (MRI) – Dec
Z* (KM)
LATITUDE (DEG)
0.1
0.5
2
10

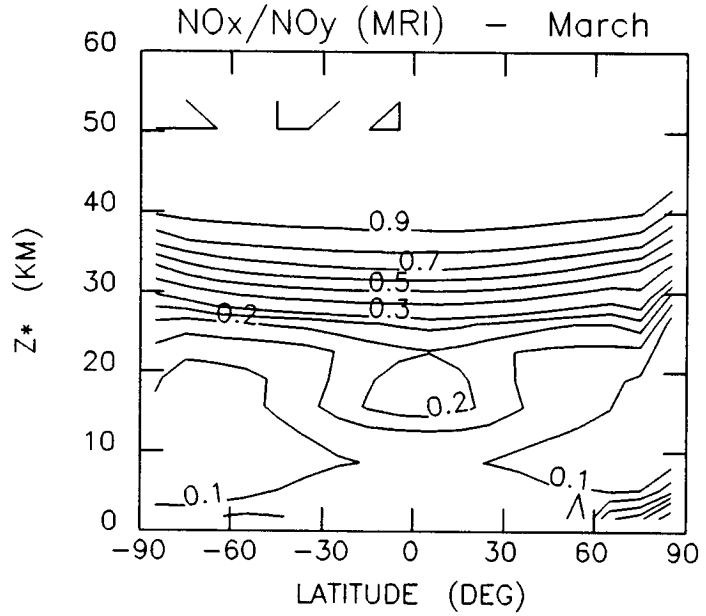
NOx/NOy (MRI) – March
Z* (KM)
LATITUDE (DEG)
0.9
0.7
0.5
0.3
0.2
0.1

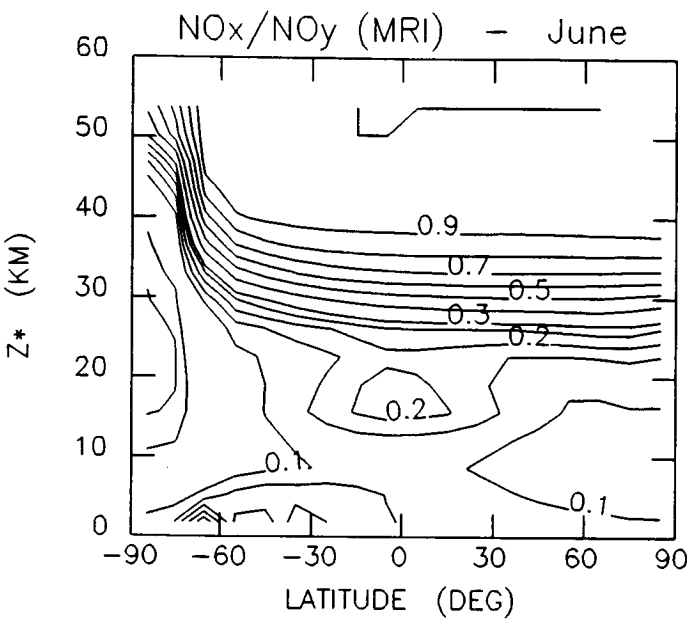
NOx/NOy (MRI) – June
Z* (KM)
LATITUDE (DEG)
0.9
0.7
0.5
0.3
0.2
0.1

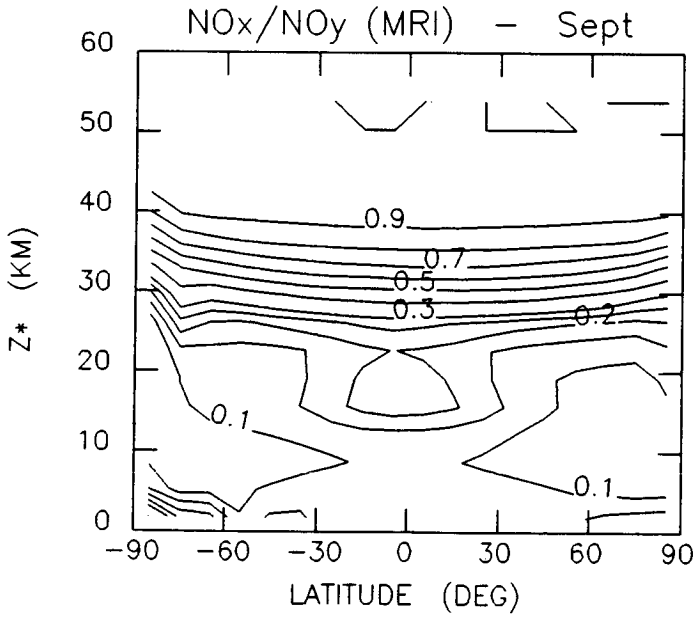
NOx/NOy (MRI) – Sept
Z* (KM)
LATITUDE (DEG)
0.9
0.7
0.5
0.3
0.2
0.1

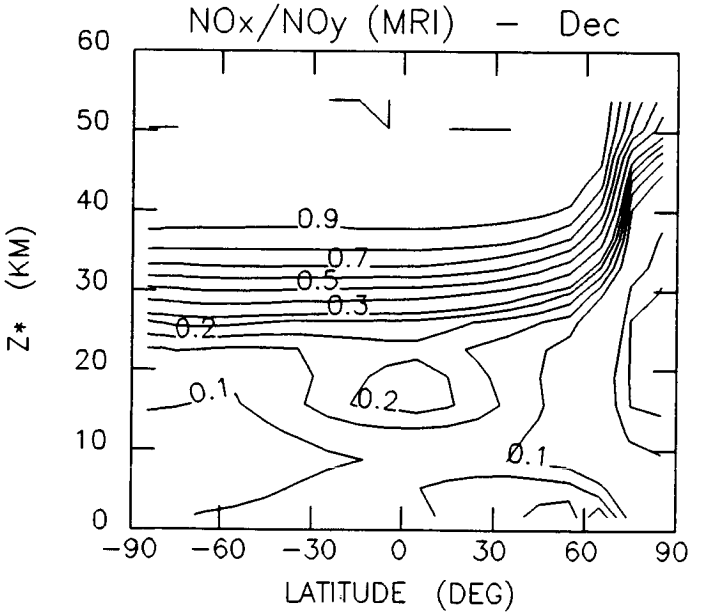
NOx/NOy (MRI) – Dec
Z* (KM)
LATITUDE (DEG)
0.9
0.7
0.5
0.3
0.2
0.1

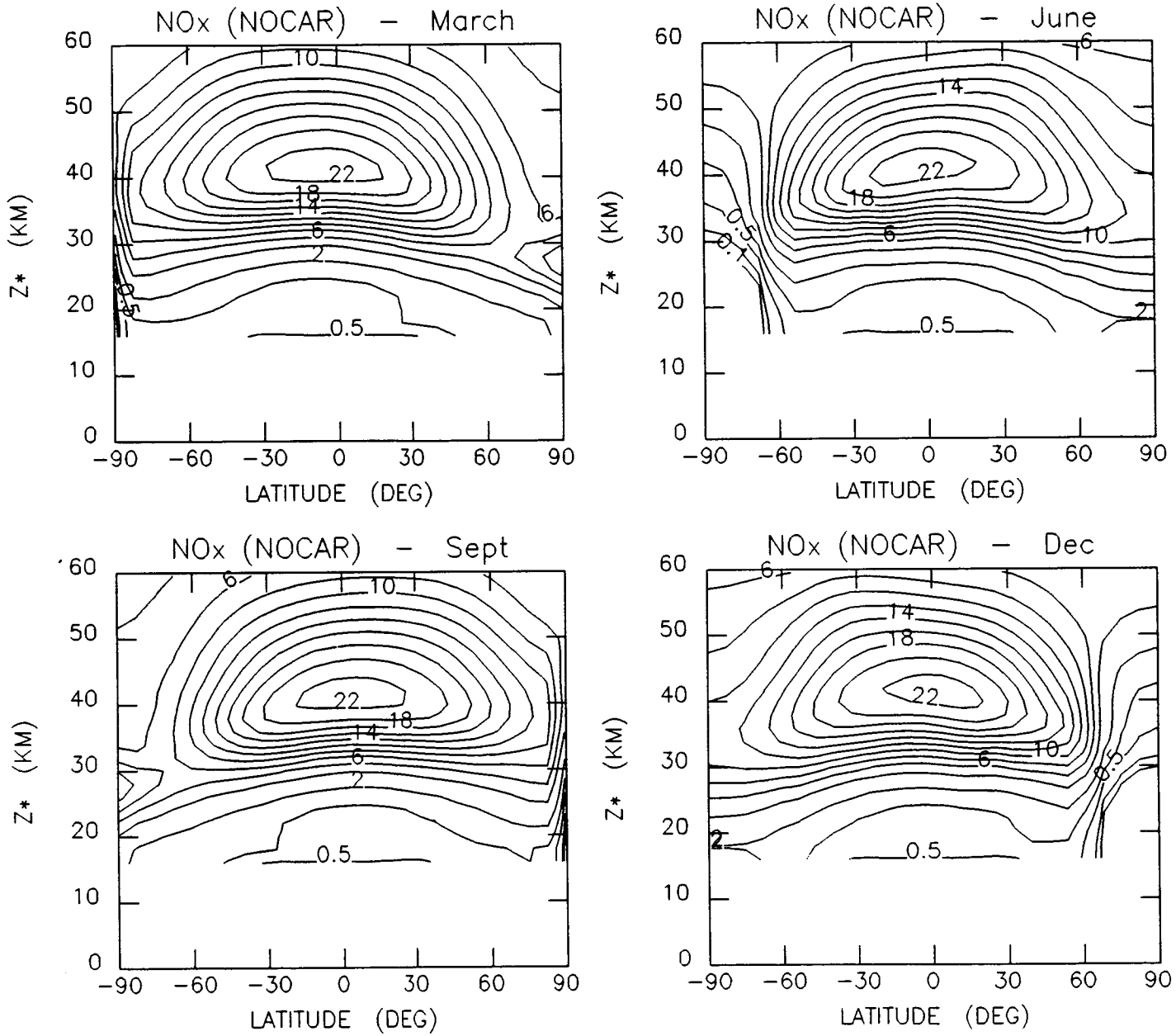
NOx (NOCAR) – March
NOx (NOCAR) – June
NOx (NOCAR) – Sept
NOx (NOCAR) – Dec
Z* (KM)
LATITUDE (DEG)
0
10
20
30
40
50
60
−90
−60
−30
0
30
60
90
0.1
0.5
2
6
10
14
18
22

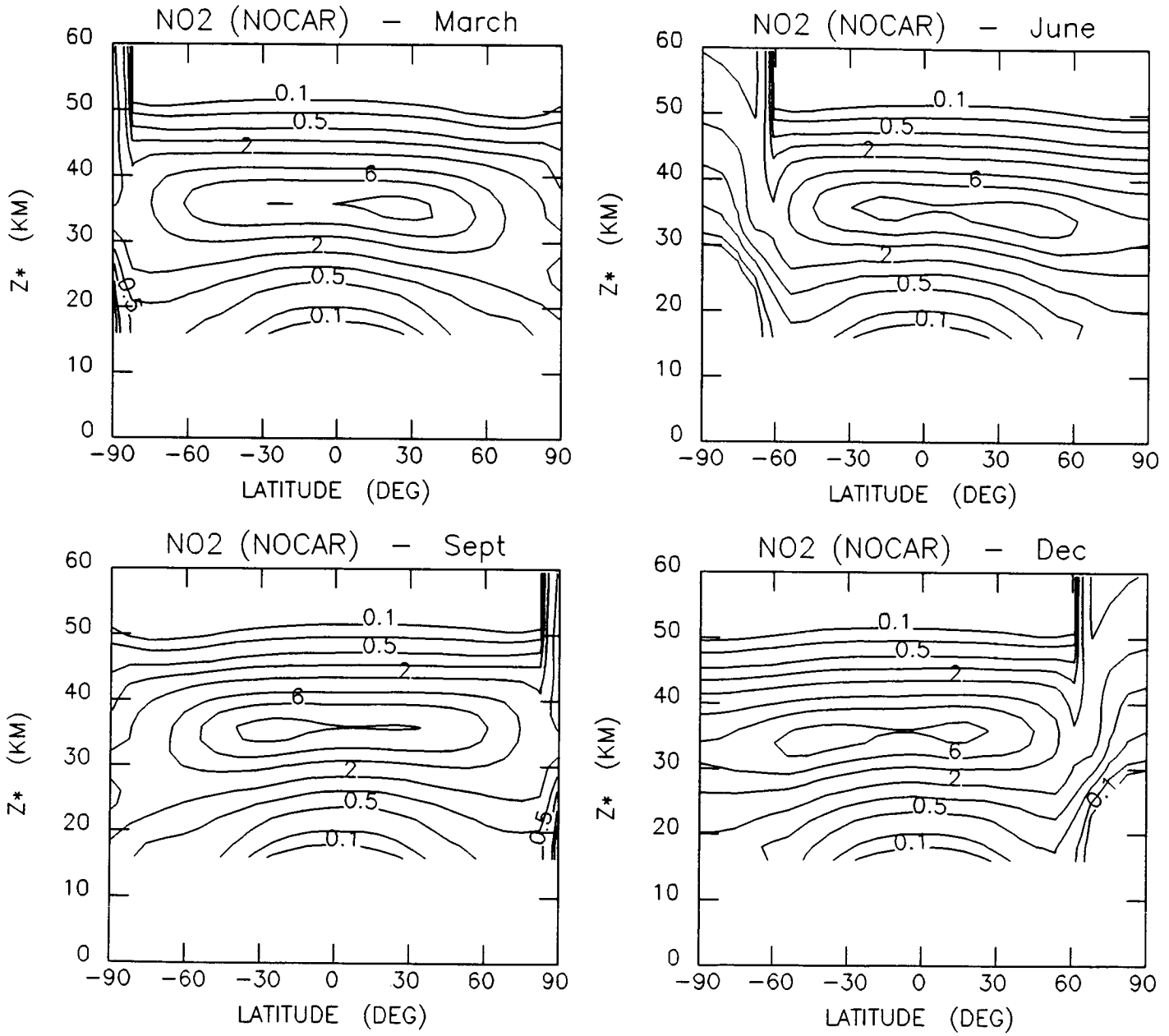
NO2 (NOCAR) – March
NO2 (NOCAR) – June
NO2 (NOCAR) – Sept
NO2 (NOCAR) – Dec
Z* (KM)
LATITUDE (DEG)
0.1
0.5
2
6
0
10
20
30
40
50
60
−90
−60
−30
0
30
60
90

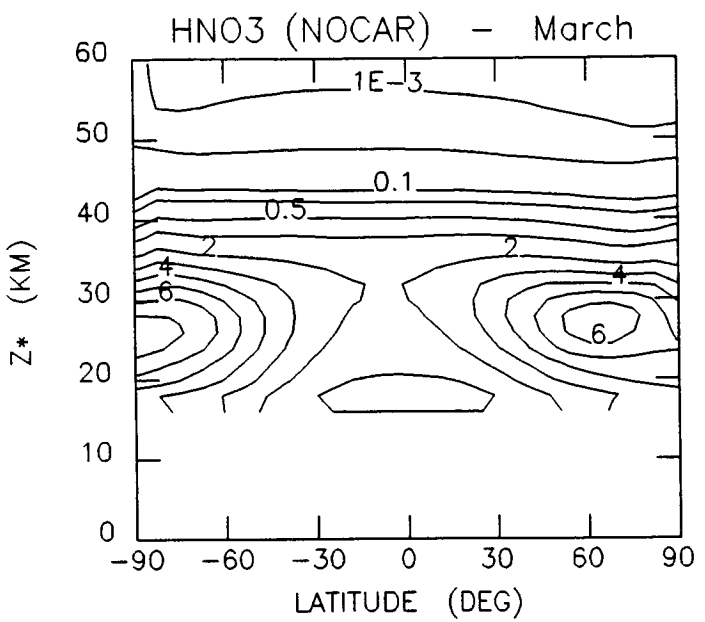
HNO3 (NOCAR) – March
1E-3
0.1
0.5
2
4
6
Z* (KM)
LATITUDE (DEG)

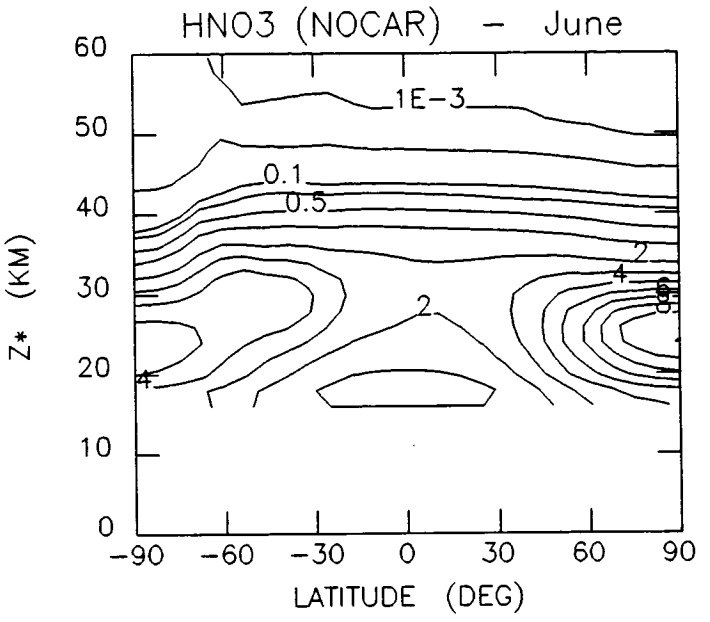
HNO3 (NOCAR) – June
1E-3
0.1
0.5
2
4
6
Z* (KM)
LATITUDE (DEG)

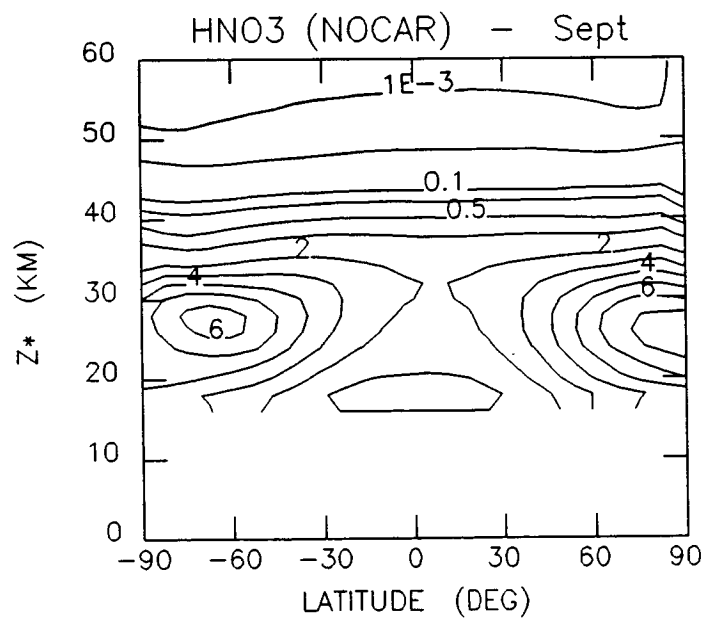
HNO3 (NOCAR) – Sept
1E-3
0.1
0.5
2
4
6
Z* (KM)
LATITUDE (DEG)

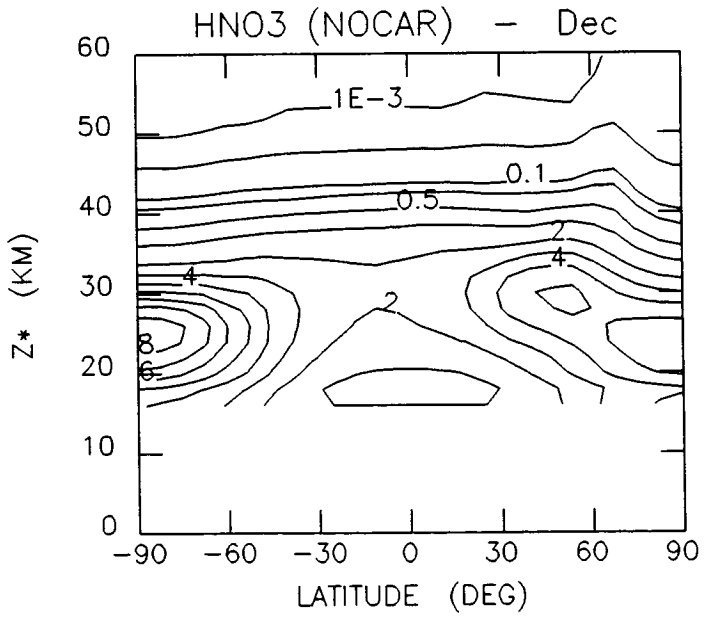
HNO3 (NOCAR) – Dec
1E-3
0.1
0.5
2
4
6
8
Z* (KM)
LATITUDE (DEG)

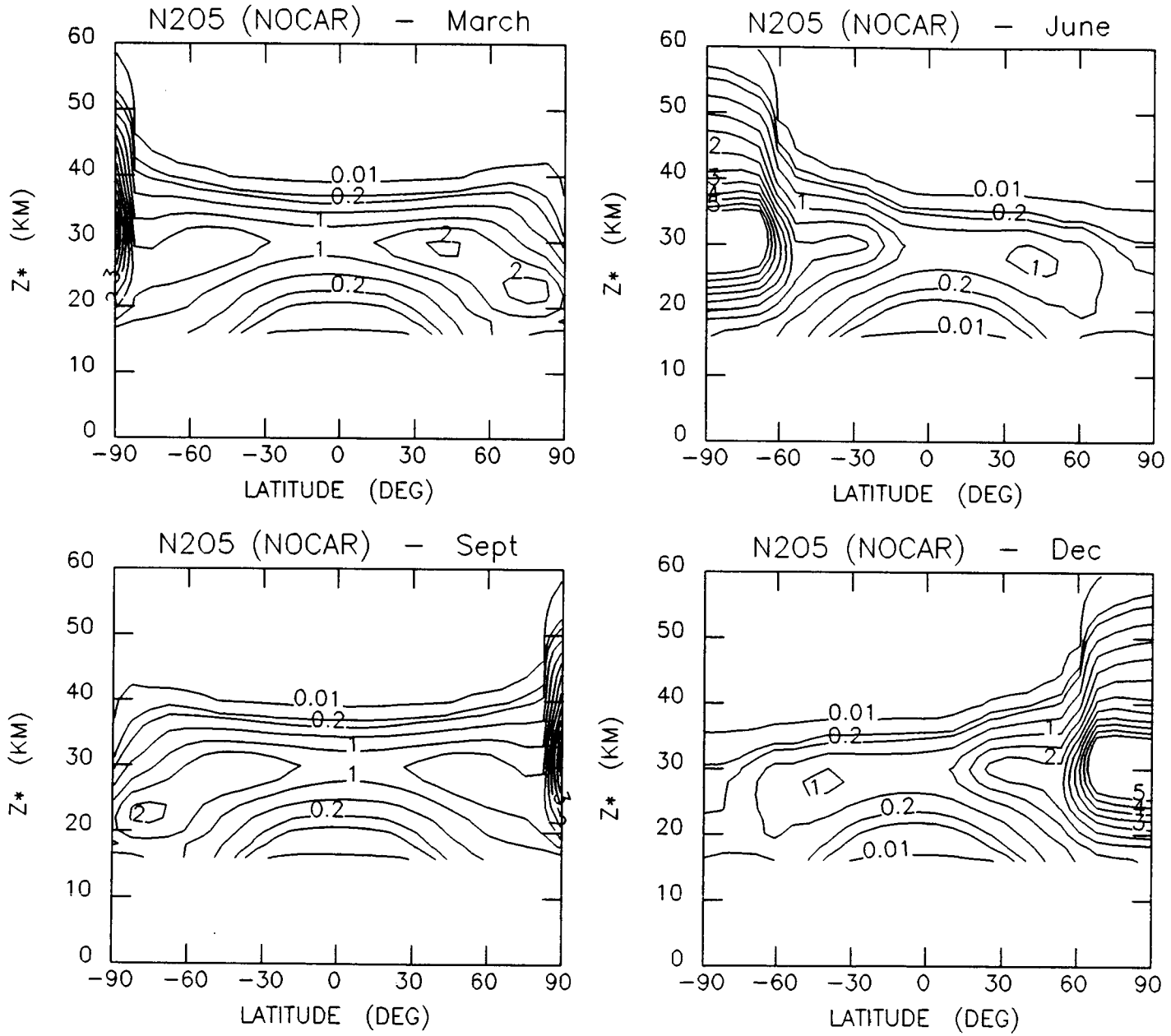
N205 (NOCAR) – March
N205 (NOCAR) – June
N205 (NOCAR) – Sept
N205 (NOCAR) – Dec
Z* (KM)
LATITUDE (DEG)
0
10
20
30
40
50
60
−90
−60
−30
0
30
60
90
0.01
0.2
1
2
5

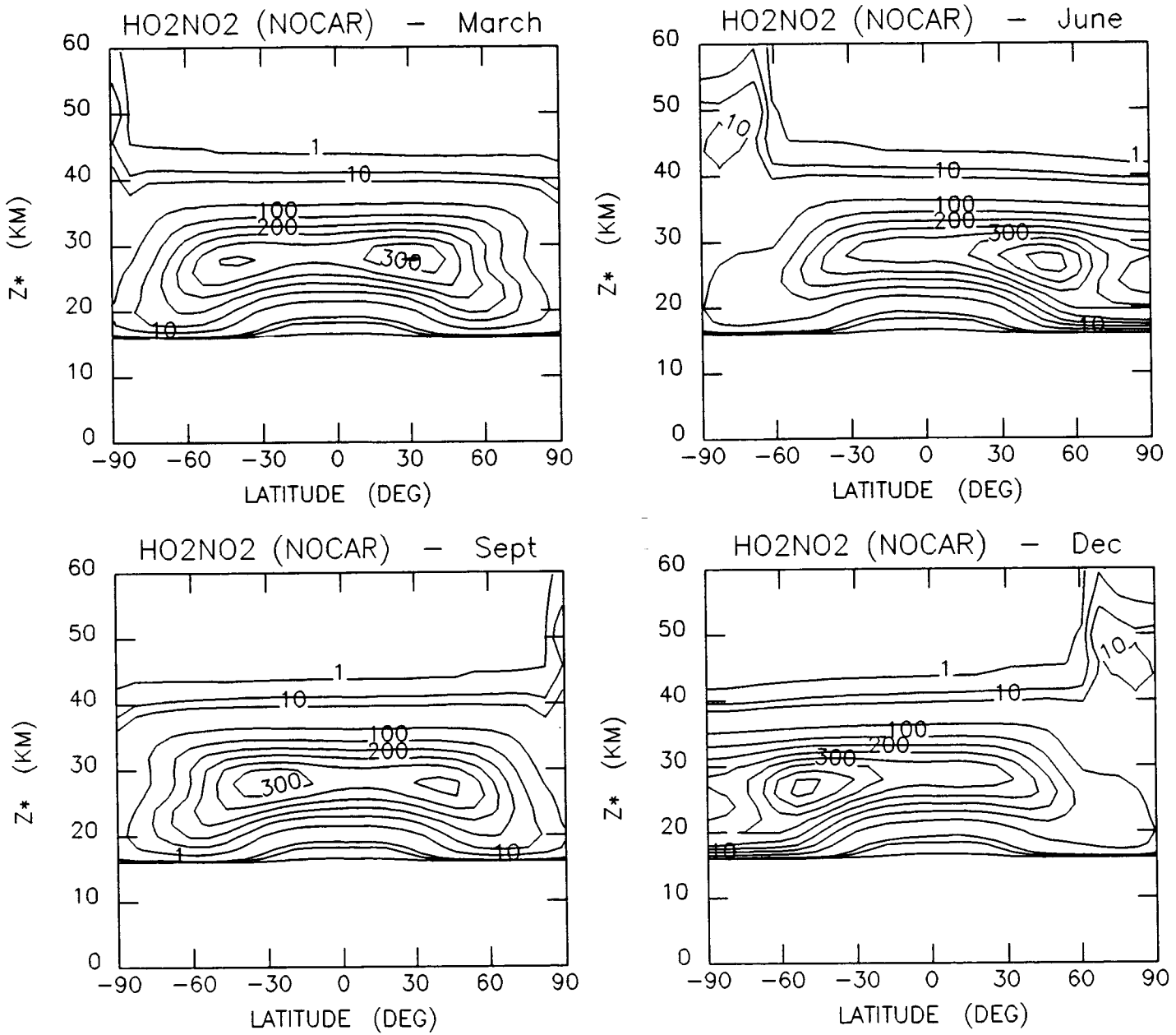
HO2NO2 (NOCAR) – March
HO2NO2 (NOCAR) – June
HO2NO2 (NOCAR) – Sept
HO2NO2 (NOCAR) – Dec
Z* (KM)
LATITUDE (DEG)
0
10
20
30
40
50
60
-90
-60
-30
0
30
60
90
1
10
100
200
300

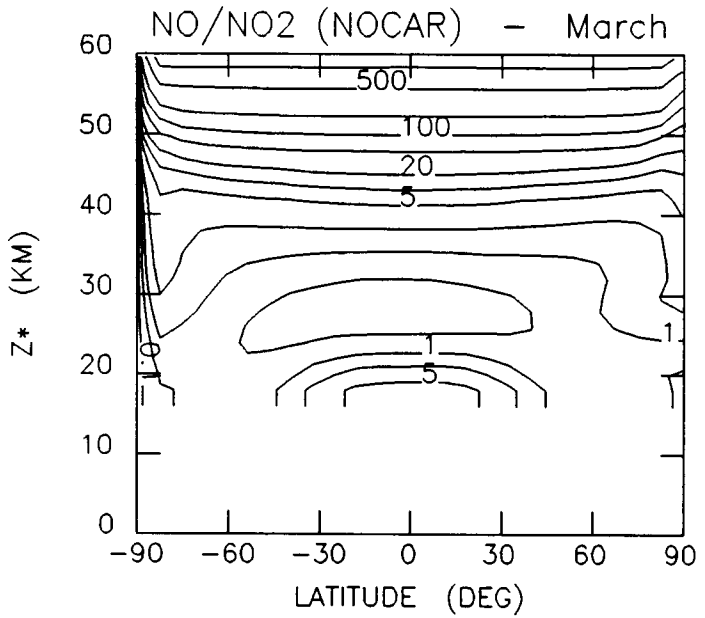
NO/NO2 (NOCAR) – March
Z* (KM)
LATITUDE (DEG)
500
100
20
5
1
0.1

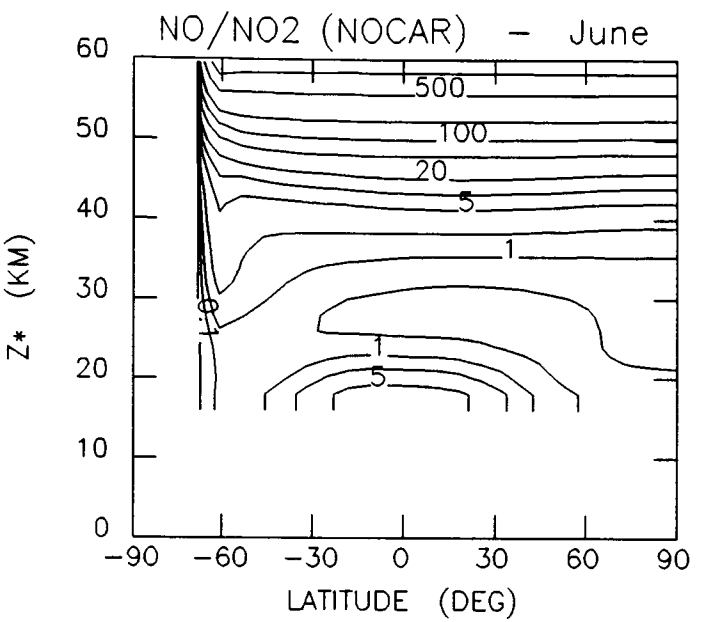
NO/NO2 (NOCAR) – June
Z* (KM)
LATITUDE (DEG)
500
100
20
5
1
0.1

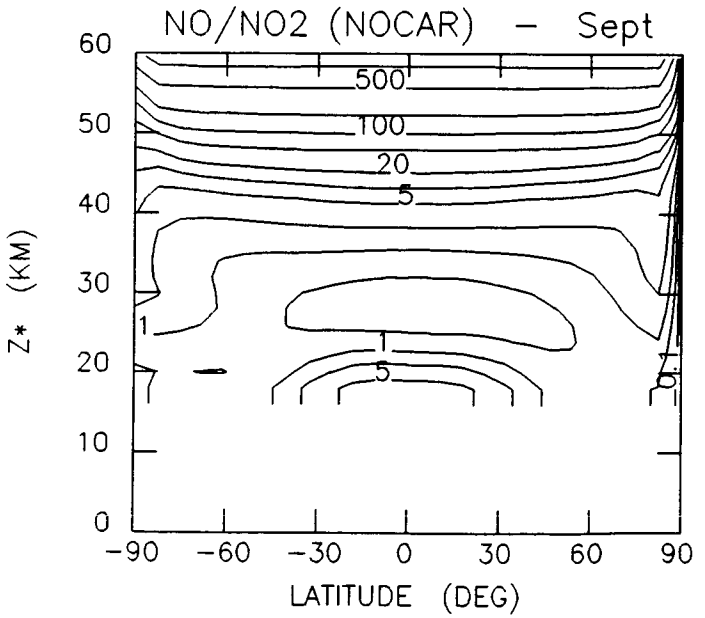
NO/NO2 (NOCAR) – Sept
Z* (KM)
LATITUDE (DEG)
500
100
20
5
1
0.1

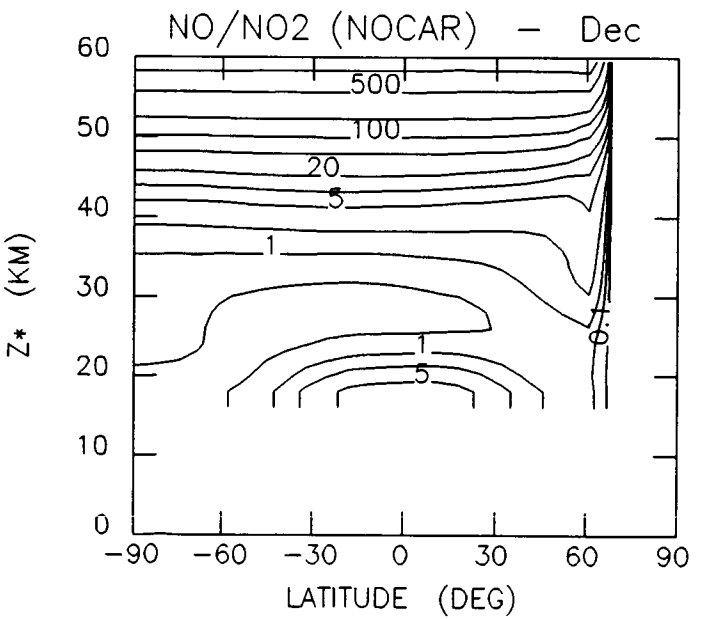
NO/NO2 (NOCAR) – Dec
Z* (KM)
LATITUDE (DEG)
500
100
20
5
1
0.1

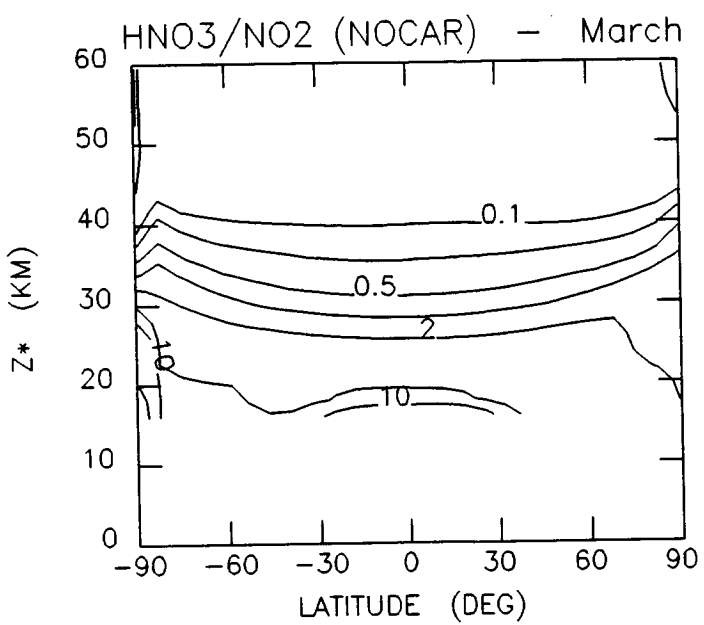
HNO3/NO2 (NOCAR) – March
Z* (KM)
LATITUDE (DEG)
0.1
0.5
2
10

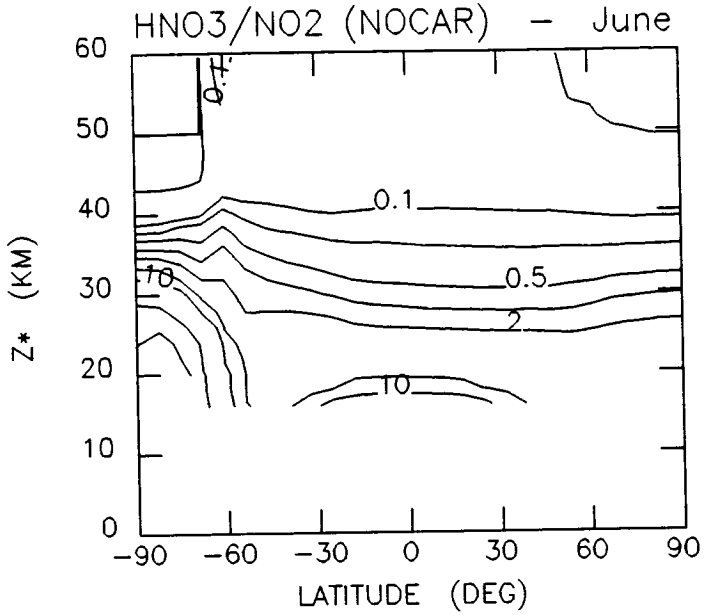
HNO3/NO2 (NOCAR) – June
Z* (KM)
LATITUDE (DEG)
0.1
0.5
2
10

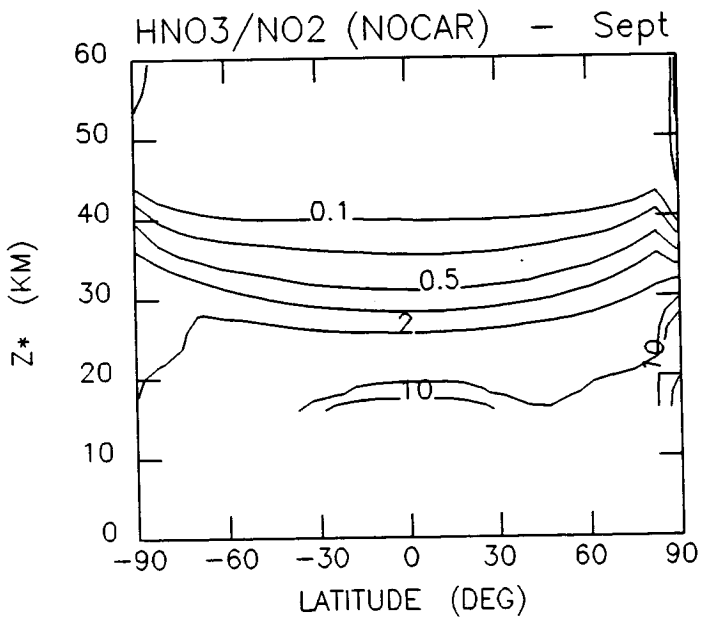
HNO3/NO2 (NOCAR) – Sept
Z* (KM)
LATITUDE (DEG)
0.1
0.5
2
10

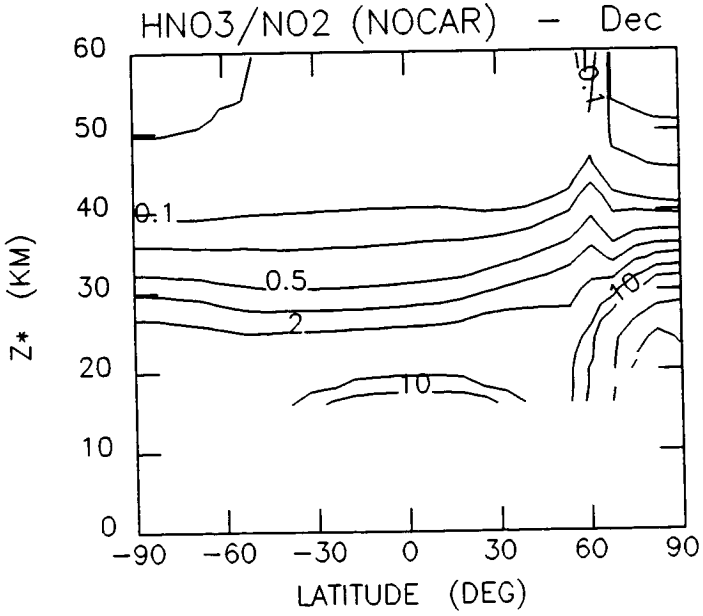
HNO3/NO2 (NOCAR) – Dec
Z* (KM)
LATITUDE (DEG)
0.1
0.5
2
10

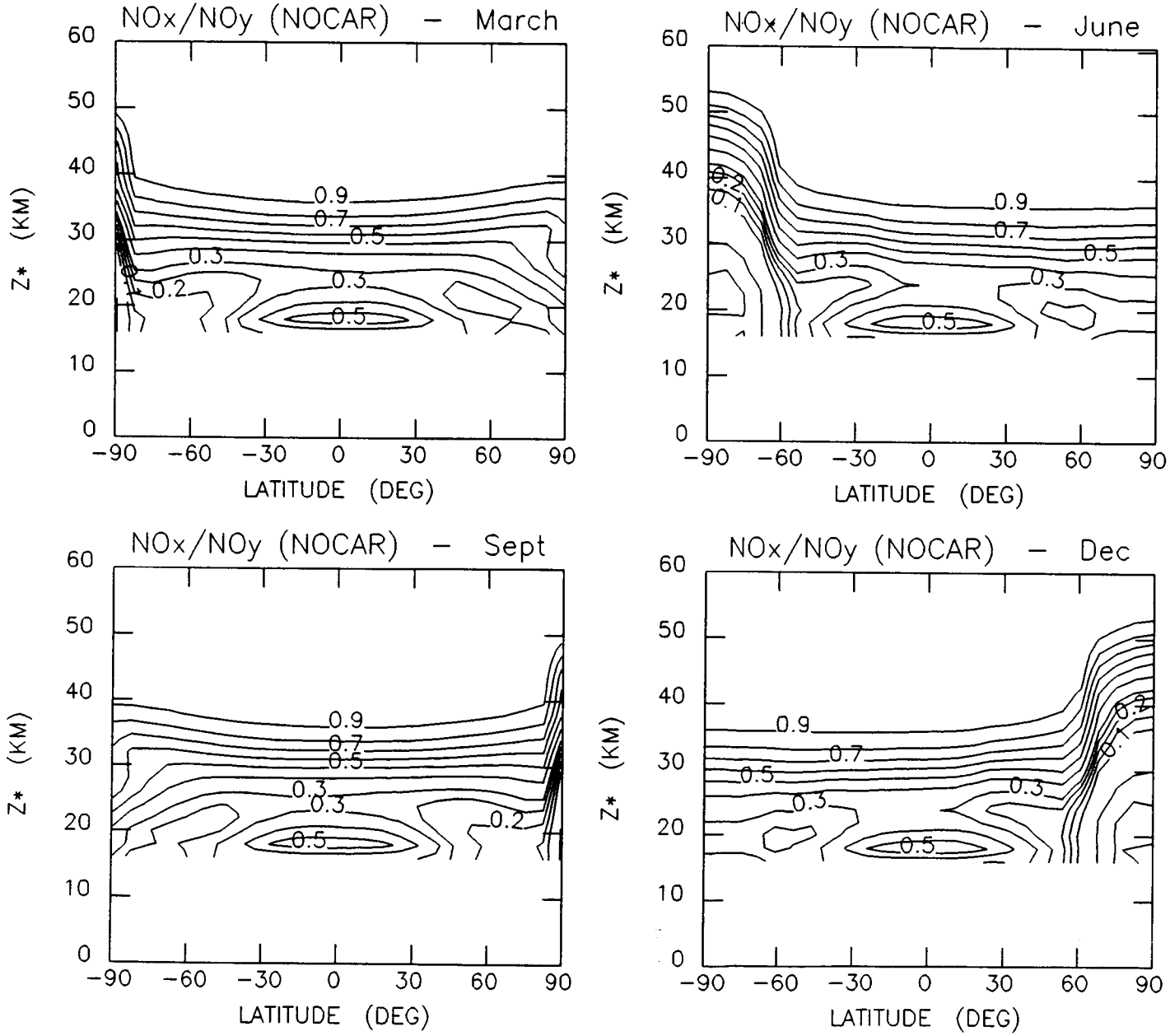
NOx/NOy (NOCAR) – March
NOx/NOy (NOCAR) – June
NOx/NOy (NOCAR) – Sept
NOx/NOy (NOCAR) – Dec
Z* (KM)
LATITUDE (DEG)
0
10
20
30
40
50
60
-90
-60
-30
0
30
60
90
0.9
0.7
0.5
0.3
0.2

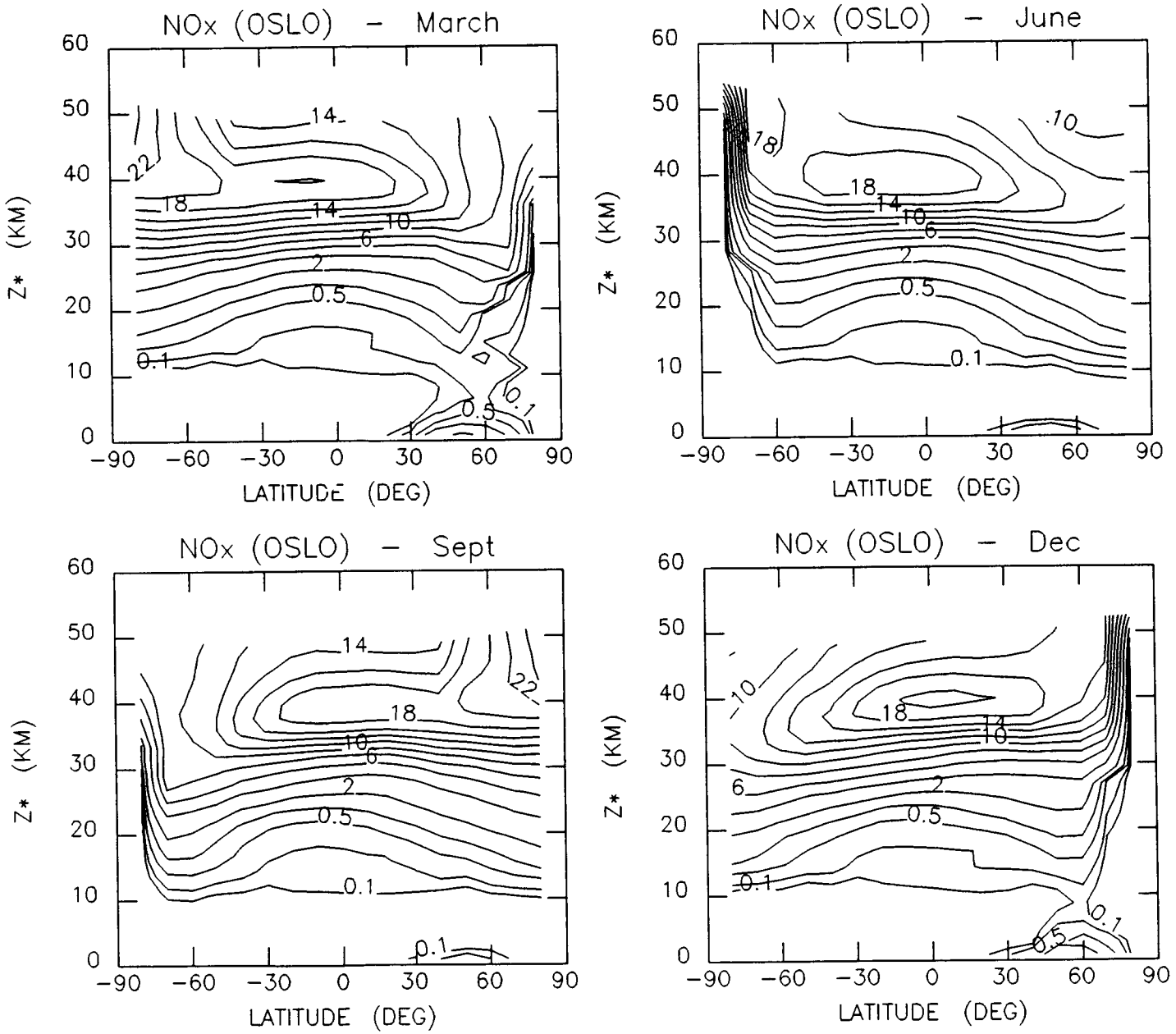
NOx (OSLO) - March
NOx (OSLO) - June
NOx (OSLO) - Sept
NOx (OSLO) - Dec
Z* (KM)
LATITUDE (DEG)
60
50
40
30
20
10
0
-90
-60
-30
0
30
60
90
22
18
14
10
6
2
0.5
0.1

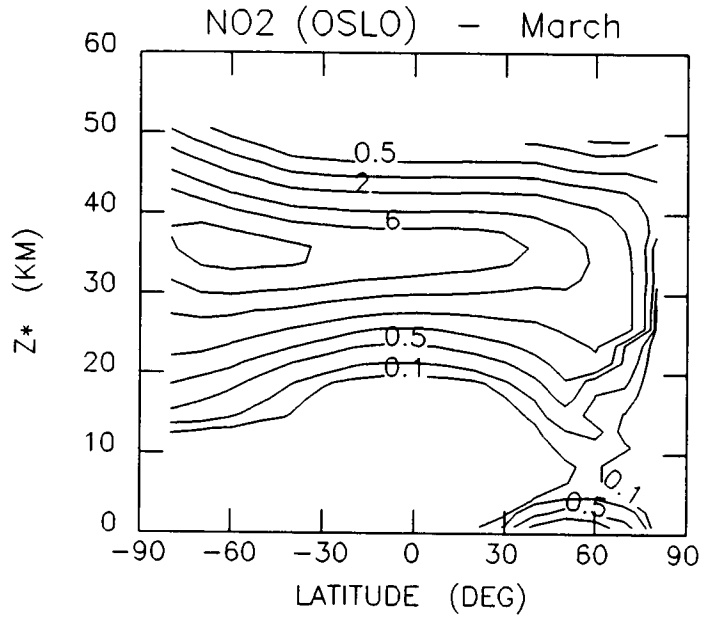
NO2 (OSLO) – March
Z* (KM)
LATITUDE (DEG)
0.5
2
6
0.5
0.1
0.1
0.5

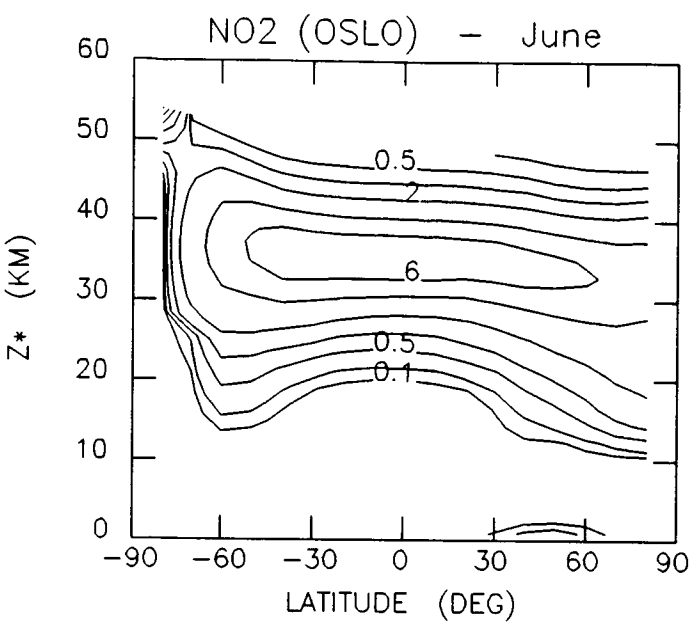
NO2 (OSLO) – June
Z* (KM)
LATITUDE (DEG)
0.5
2
6
0.5
0.1

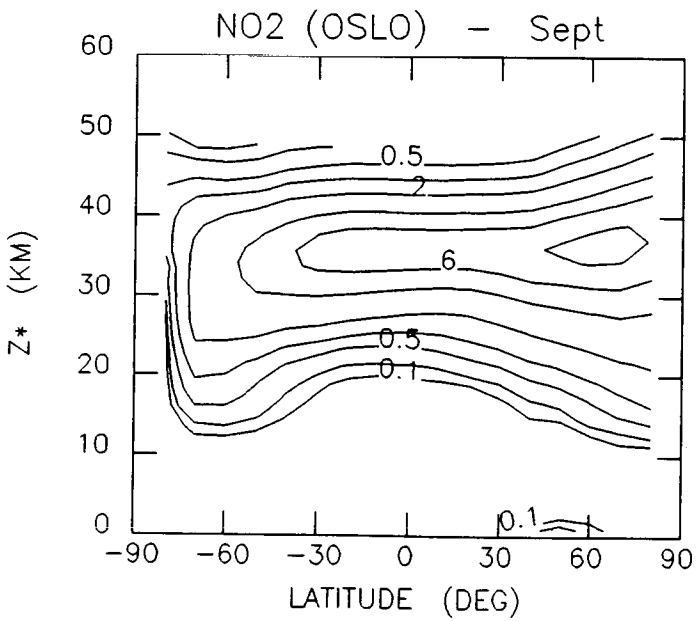
NO2 (OSLO) – Sept
Z* (KM)
LATITUDE (DEG)
0.5
2
6
0.5
0.1
0.1

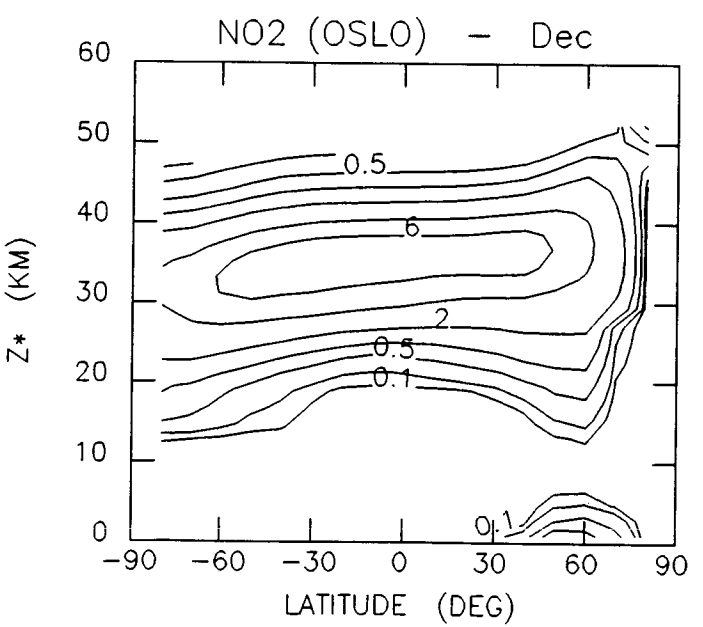
NO2 (OSLO) – Dec
Z* (KM)
LATITUDE (DEG)
0.5
6
2
0.5
0.1
0.1

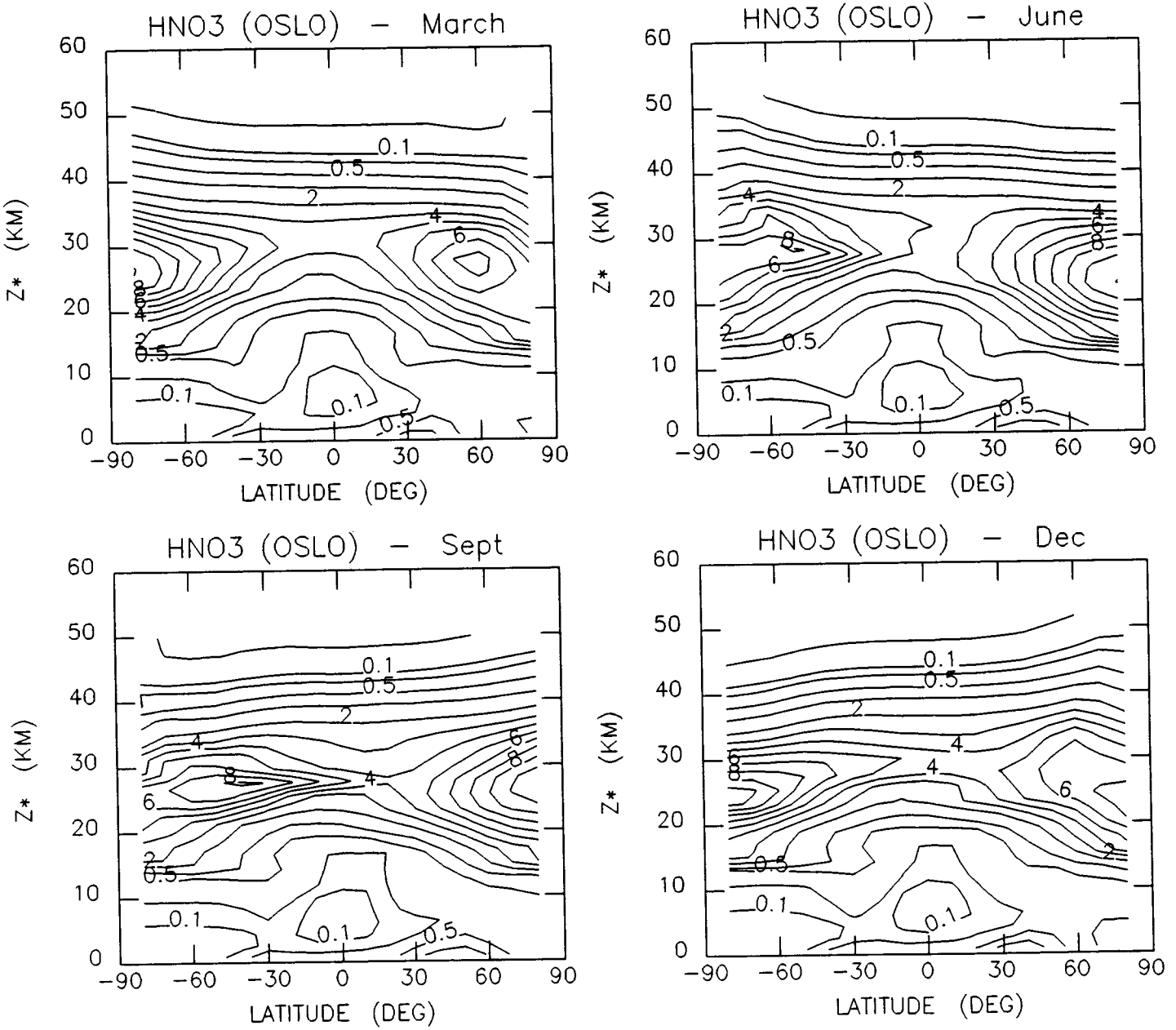
HNO3 (OSLO) – March
HNO3 (OSLO) – June
HNO3 (OSLO) – Sept
HNO3 (OSLO) – Dec
Z* (KM)
LATITUDE (DEG)
0
10
20
30
40
50
60
−90
−60
−30
0
30
60
90
0.1
0.5
2
4
6
8

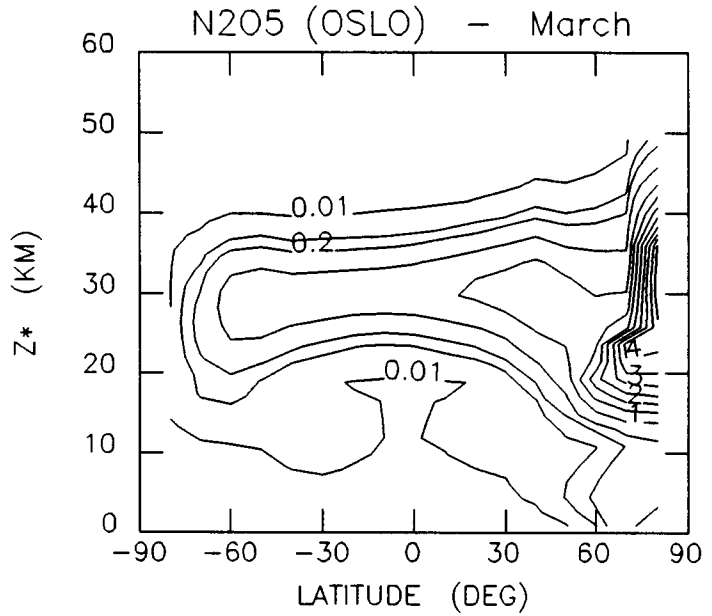
N205 (OSLO) – March
Z* (KM)
LATITUDE (DEG)
0.01
0.2
0.01

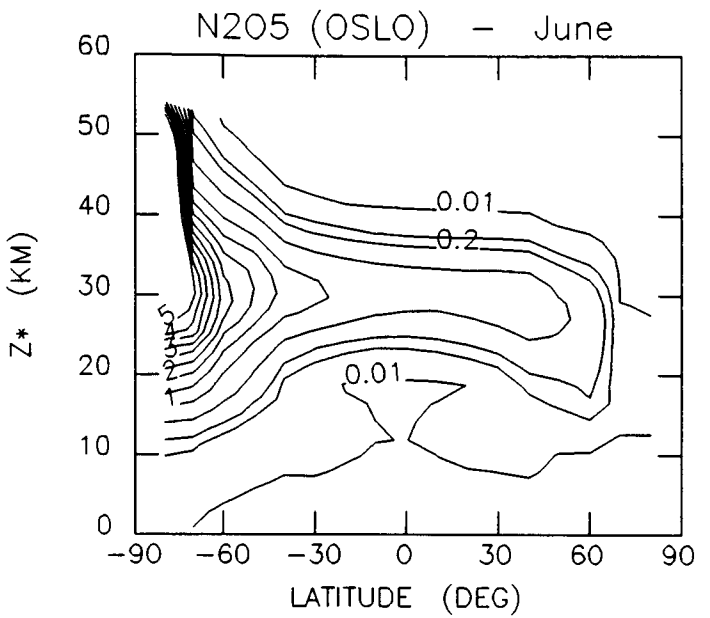
N205 (OSLO) – June
Z* (KM)
LATITUDE (DEG)
0.01
0.2
0.01

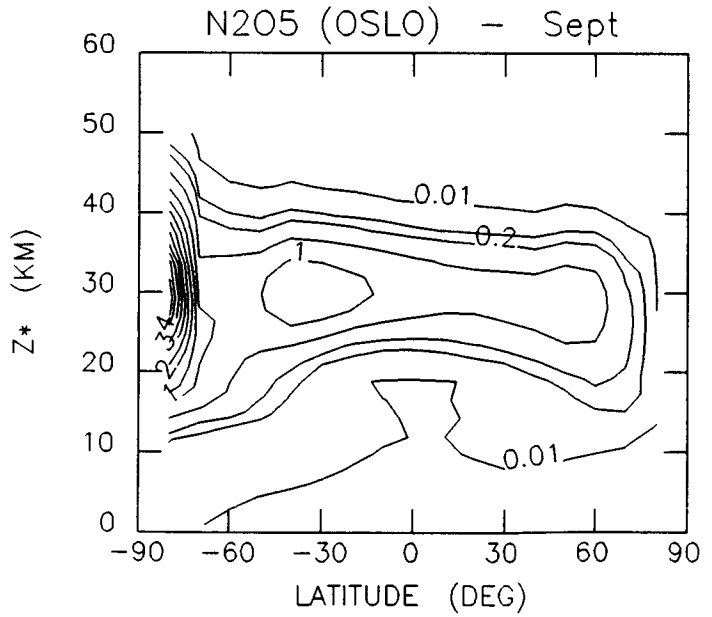
N205 (OSLO) – Sept
Z* (KM)
LATITUDE (DEG)
0.01
0.2
1
0.01

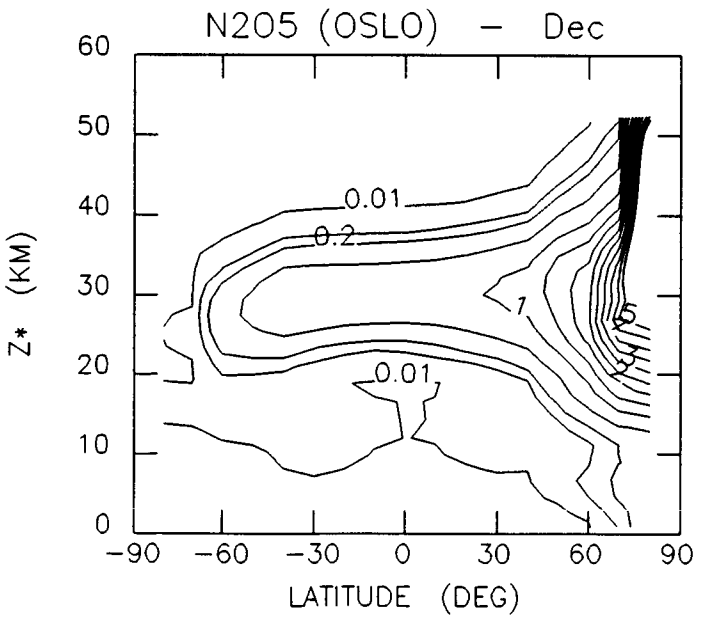
N205 (OSLO) – Dec
Z* (KM)
LATITUDE (DEG)
0.01
0.2
1
0.01

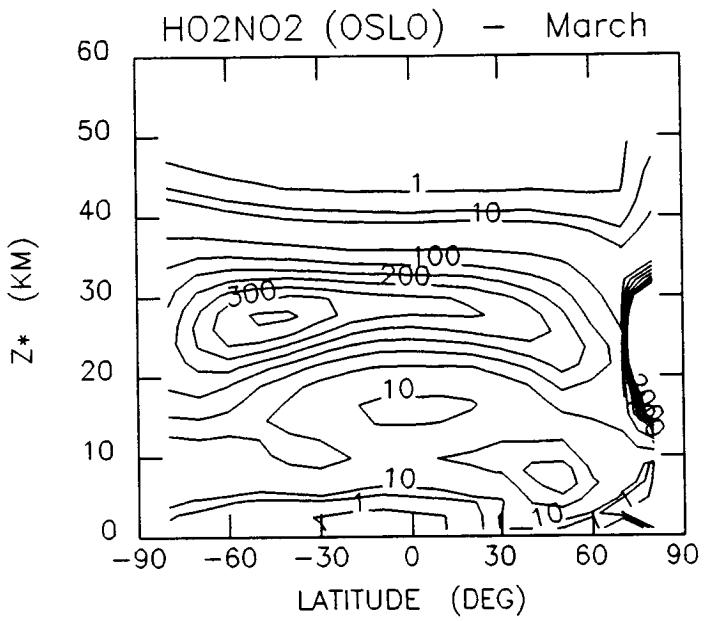
HO2NO2 (OSLO) – March
Z* (KM)
LATITUDE (DEG)
1
10
100
200
300

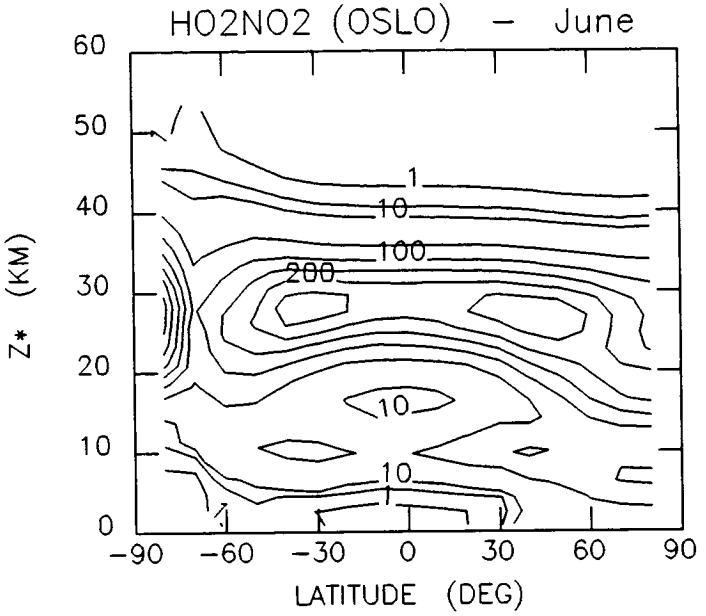
HO2NO2 (OSLO) – June
Z* (KM)
LATITUDE (DEG)
1
10
100
200

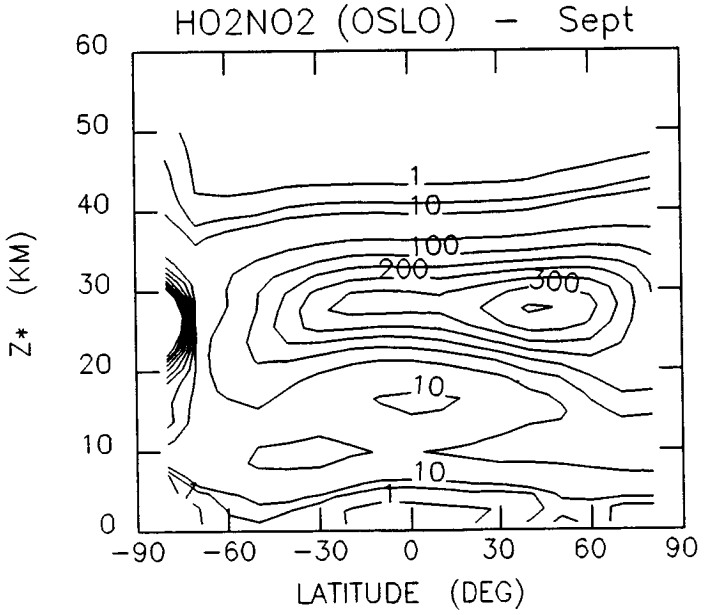
HO2NO2 (OSLO) – Sept
Z* (KM)
LATITUDE (DEG)
1
10
100
200
300

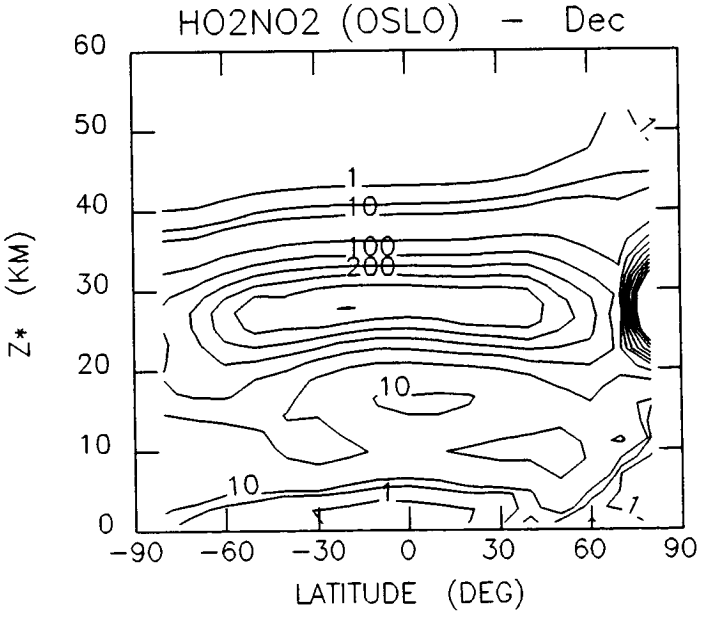
HO2NO2 (OSLO) – Dec
Z* (KM)
LATITUDE (DEG)
1
10
100
200

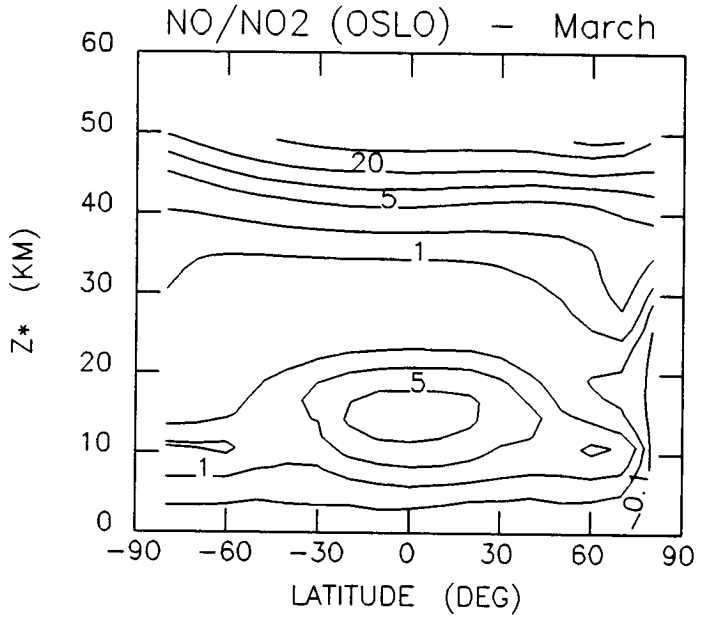
NO/NO2 (OSLO) – March
Z* (KM)
LATITUDE (DEG)
20
5
1
0.1

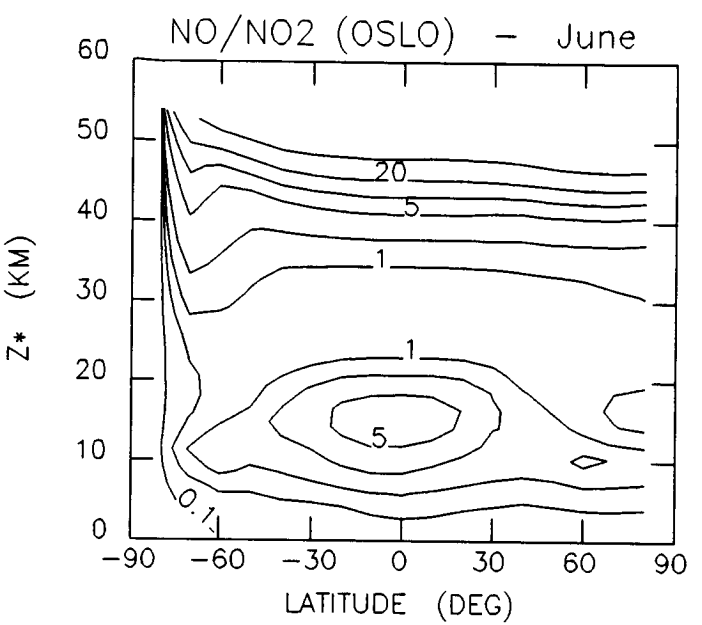
NO/NO2 (OSLO) – June
Z* (KM)
LATITUDE (DEG)
20
5
1
0.1

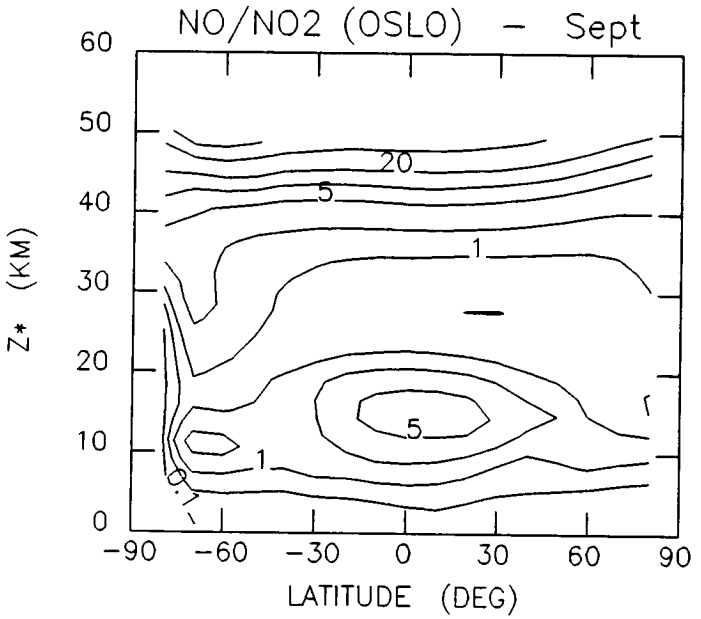
NO/NO2 (OSLO) – Sept
Z* (KM)
LATITUDE (DEG)
20
5
1
0.1

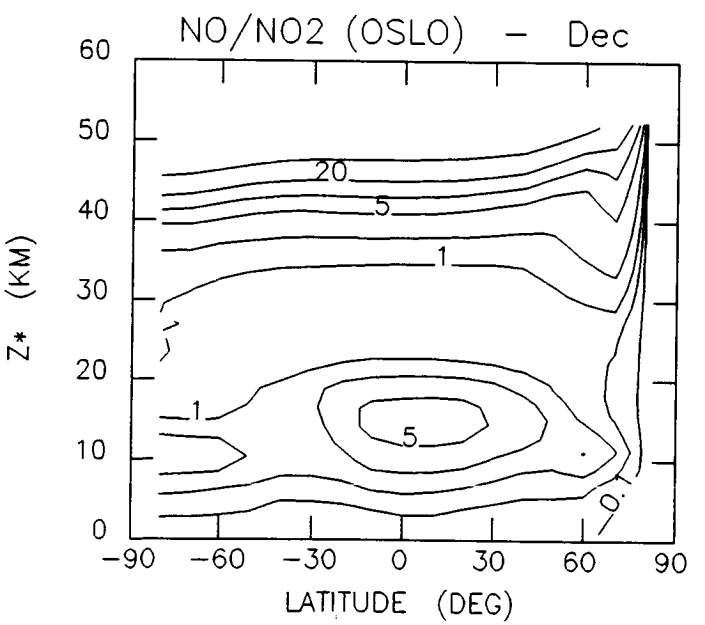
NO/NO2 (OSLO) – Dec
Z* (KM)
LATITUDE (DEG)
20
5
1
0.1

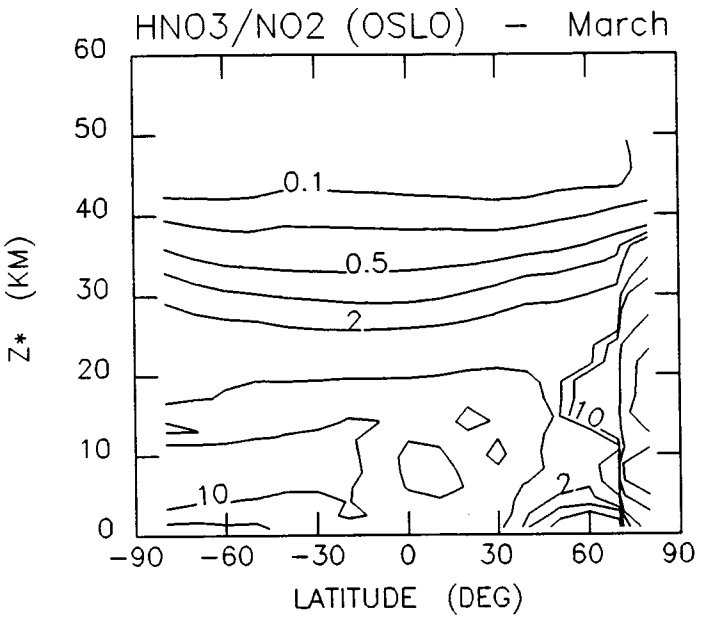
HNO3/NO2 (OSLO) – March
Z* (KM)
LATITUDE (DEG)
0.1
0.5
2
10
10
2
10

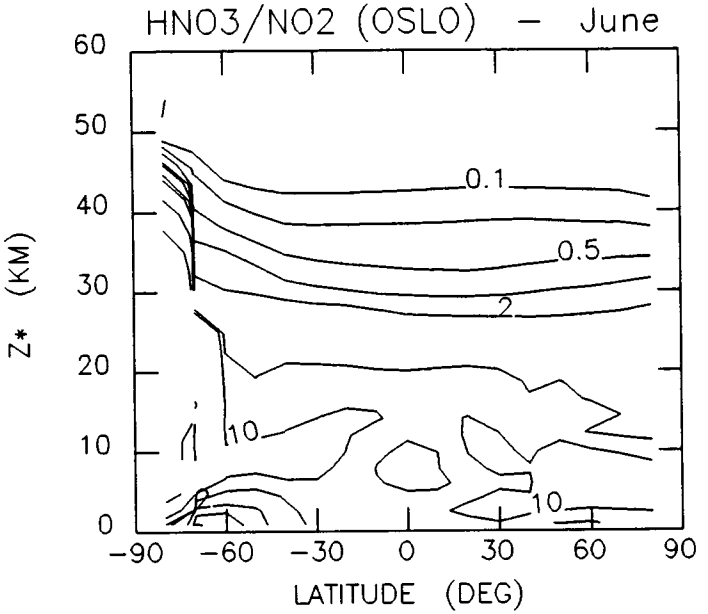
HNO3/NO2 (OSLO) – June
Z* (KM)
LATITUDE (DEG)
0.1
0.5
2
10
10

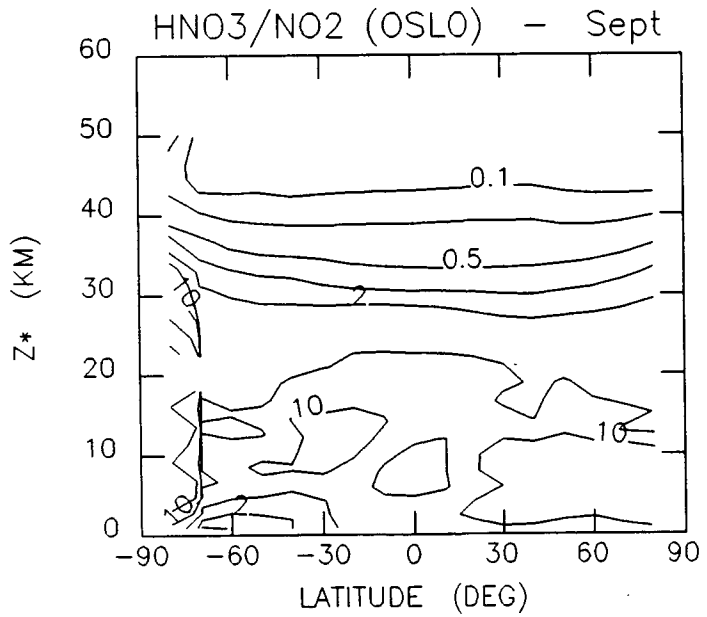
HNO3/NO2 (OSLO) – Sept
Z* (KM)
LATITUDE (DEG)
0.1
0.5
2
10
10
10
2

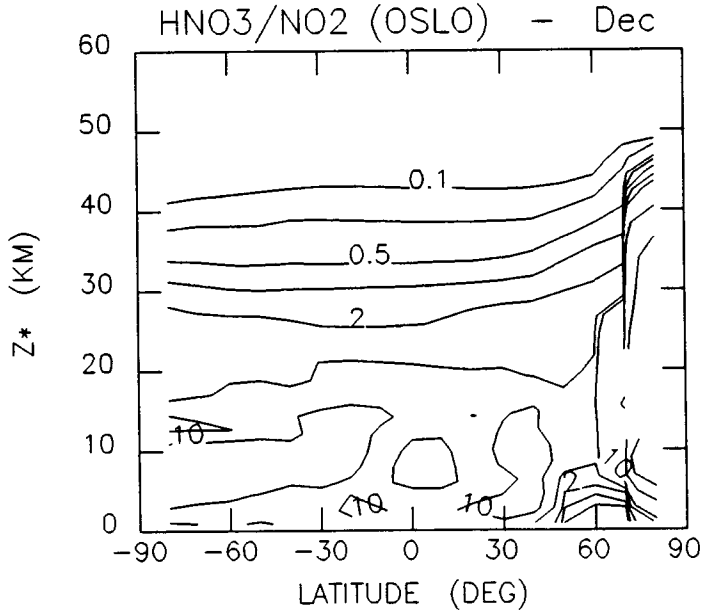
HNO3/NO2 (OSLO) – Dec
Z* (KM)
LATITUDE (DEG)
0.1
0.5
2
10
10
10
2

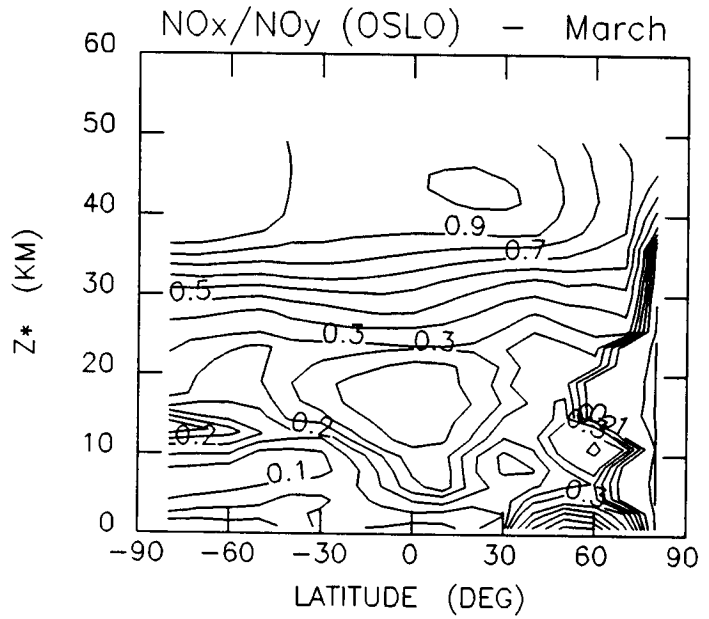
NOx/NOy (OSLO) – March
Z* (KM)
LATITUDE (DEG)
0.9
0.7
0.5
0.3
0.2
0.1

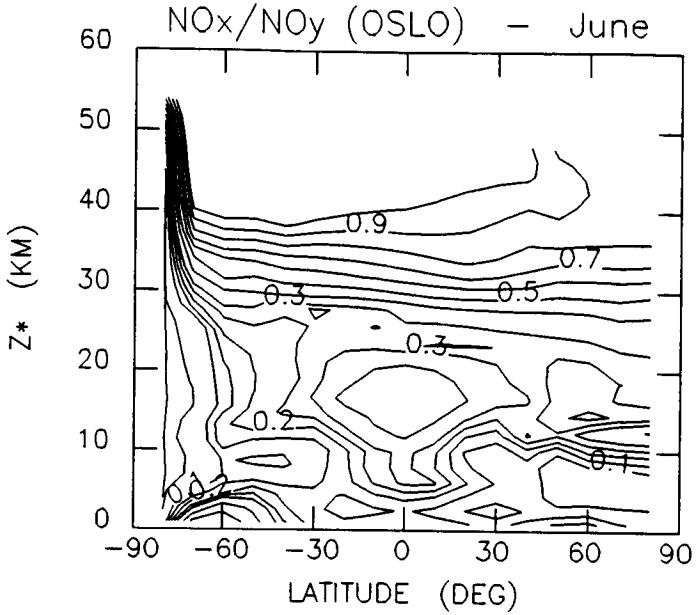
NOx/NOy (OSLO) – June
Z* (KM)
LATITUDE (DEG)
0.9
0.7
0.5
0.3
0.2
0.1

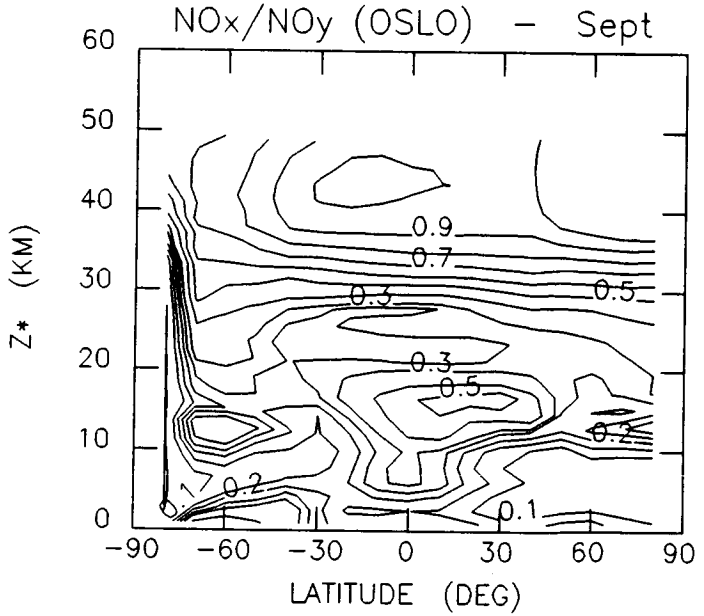
NOx/NOy (OSLO) – Sept
Z* (KM)
LATITUDE (DEG)
0.9
0.7
0.5
0.3
0.2
0.1

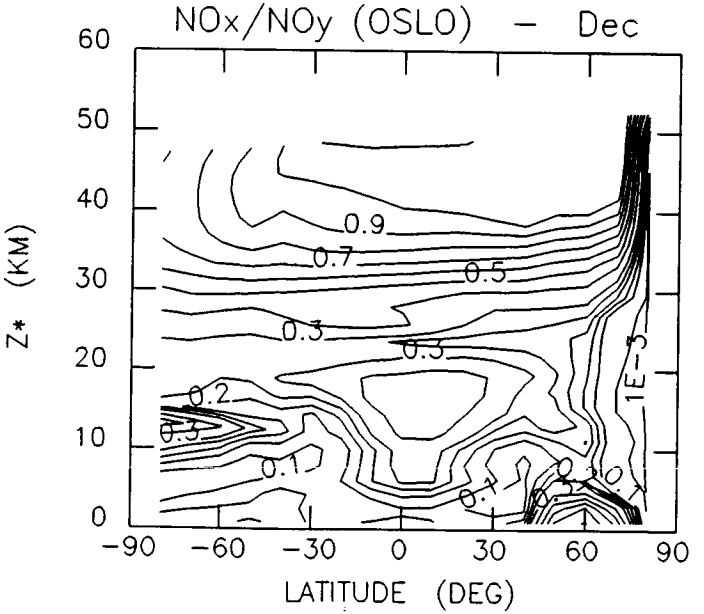
NOx/NOy (OSLO) – Dec
Z* (KM)
LATITUDE (DEG)
0.9
0.7
0.5
0.3
0.2
0.1
1E-3

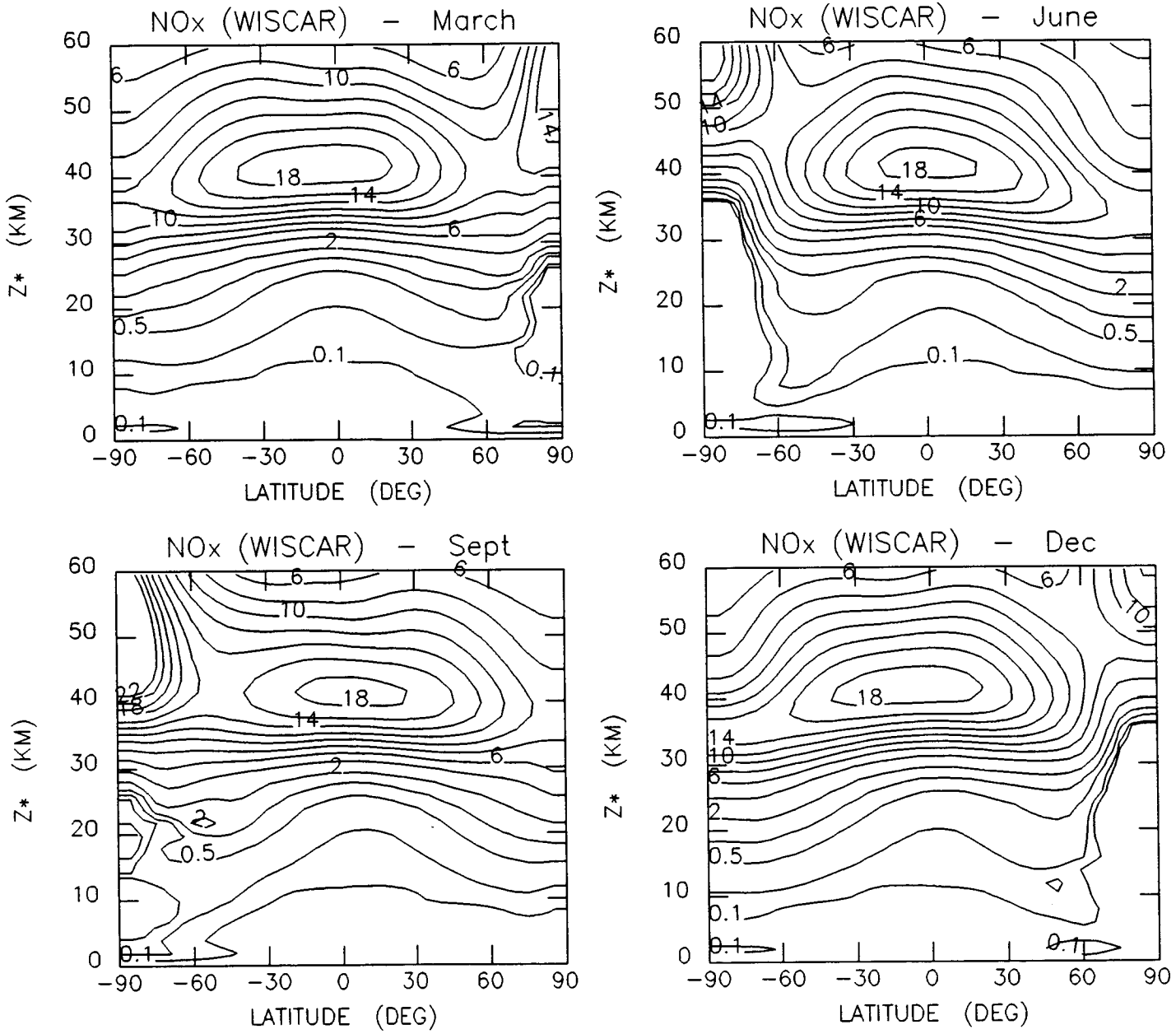
NOx (WISCAR) – March
NOx (WISCAR) – June
NOx (WISCAR) – Sept
NOx (WISCAR) – Dec
Z* (KM)
LATITUDE (DEG)
60
50
40
30
20
10
0
−90 −60 −30 0 30 60 90
6
10
14
18
2
0.5
0.1

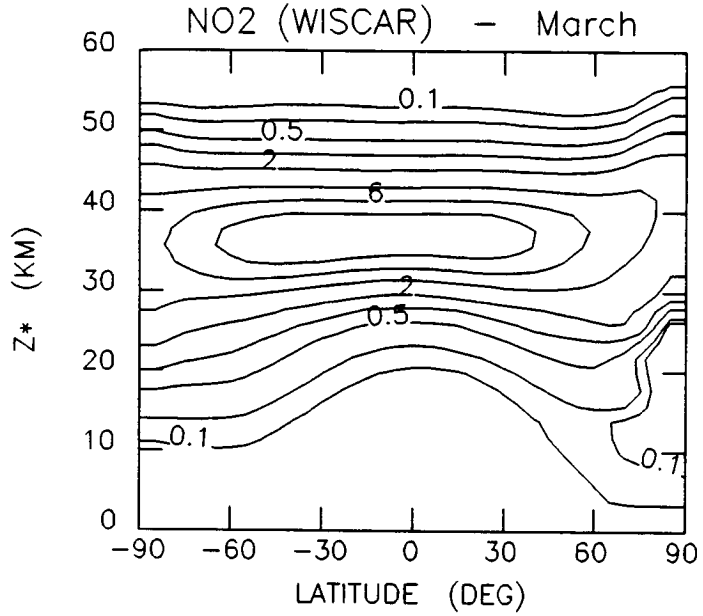
NO2 (WISCAR) – March
Z* (KM)
LATITUDE (DEG)
0.1
0.5
2
6
2
0.5
0.1
0.1
0
10
20
30
40
50
60
−90 −60 −30 0 30 60 90

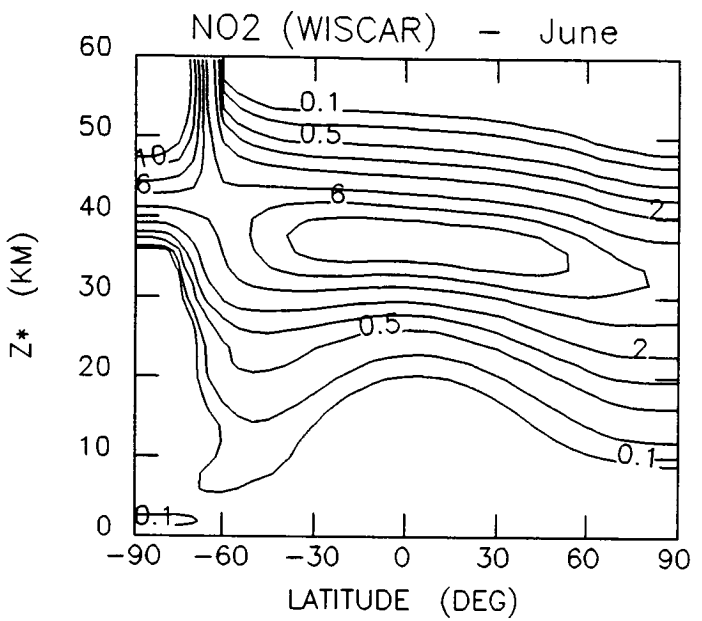
NO2 (WISCAR) – June
Z* (KM)
LATITUDE (DEG)
0.1
0.5
10
6
6
2
0.5
2
0.1
0.1
0
10
20
30
40
50
60
−90 −60 −30 0 30 60 90

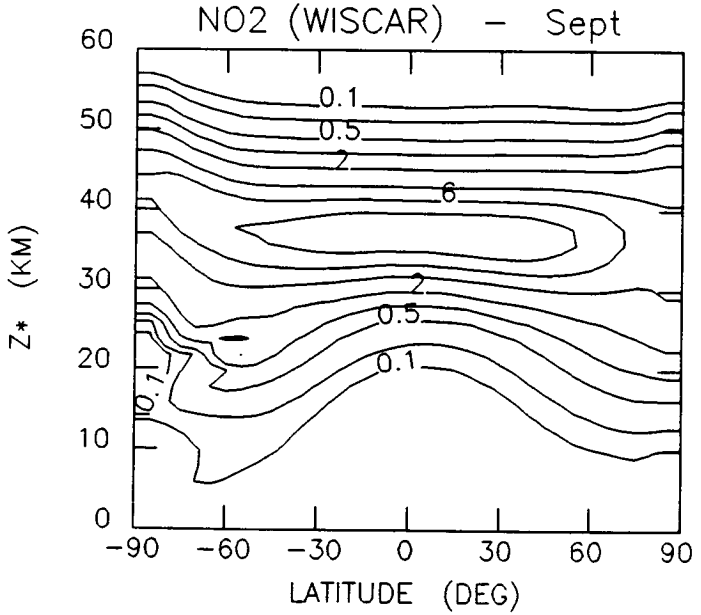
NO2 (WISCAR) – Sept
Z* (KM)
LATITUDE (DEG)
0.1
0.5
2
6
2
0.5
0.1
0.1
0
10
20
30
40
50
60
−90 −60 −30 0 30 60 90

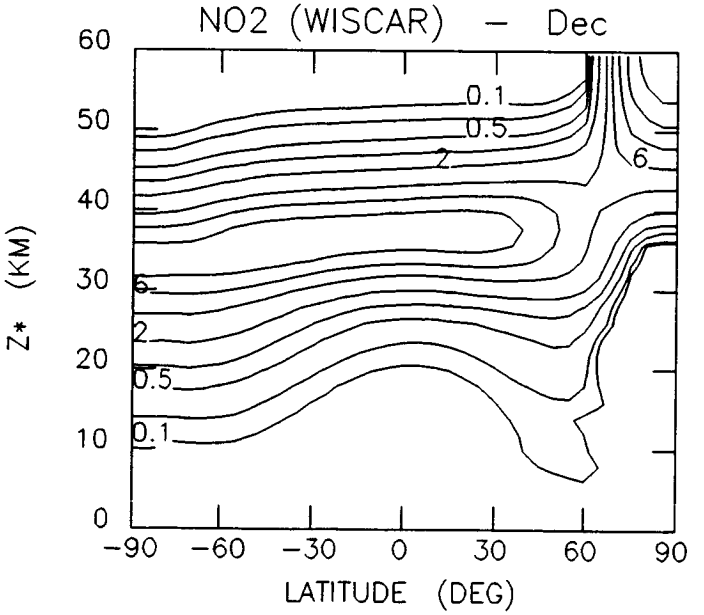
NO2 (WISCAR) – Dec
Z* (KM)
LATITUDE (DEG)
0.1
0.5
2
6
6
2
0.5
0.1
0
10
20
30
40
50
60
−90 −60 −30 0 30 60 90

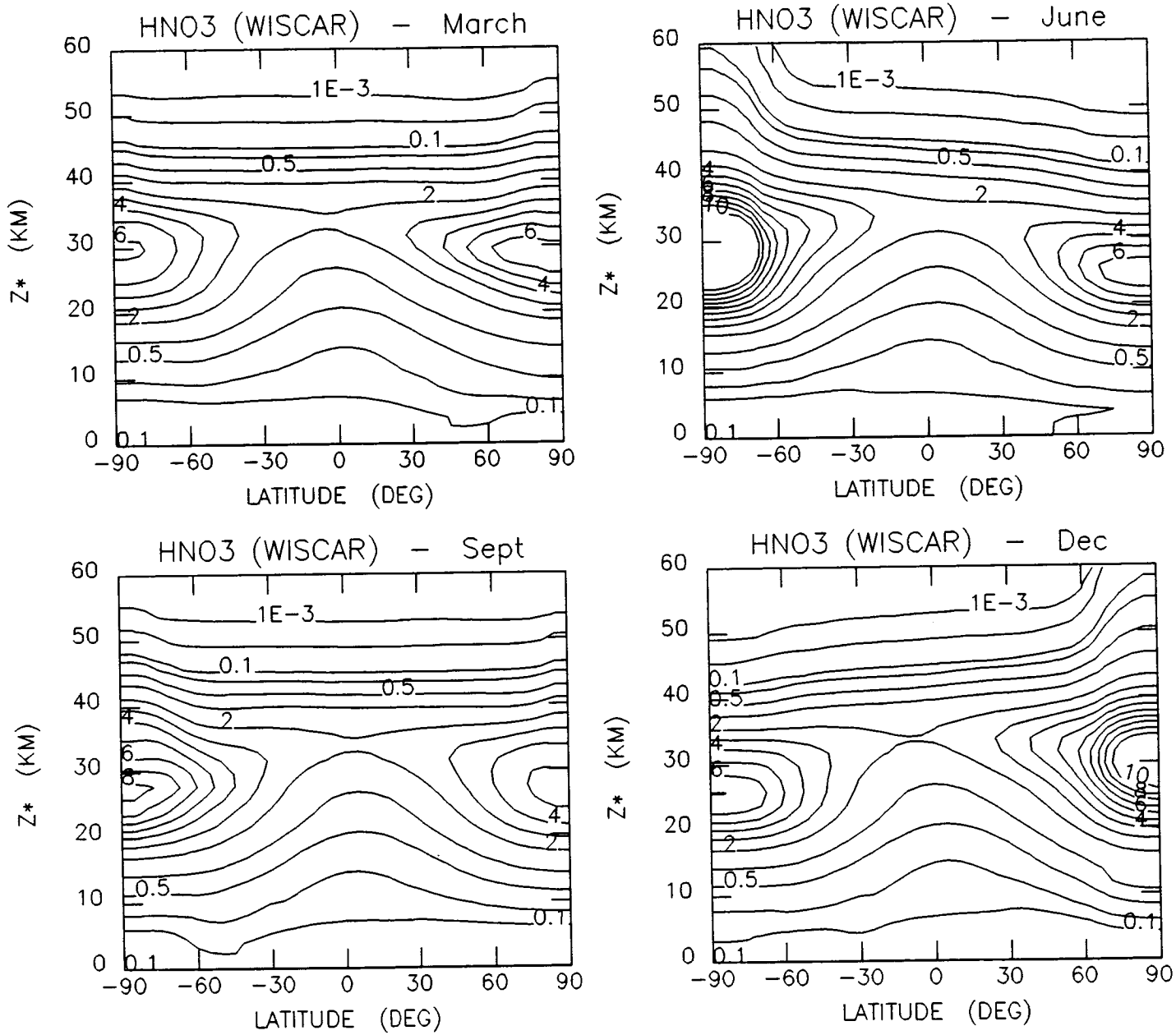
HNO3 (WISCAR) – March
HNO3 (WISCAR) – June
HNO3 (WISCAR) – Sept
HNO3 (WISCAR) – Dec
Z* (KM)
LATITUDE (DEG)
1E-3
0.1
0.5
2
4
6
10
0
10
20
30
40
50
60
-90
-60
-30
0
30
60
90

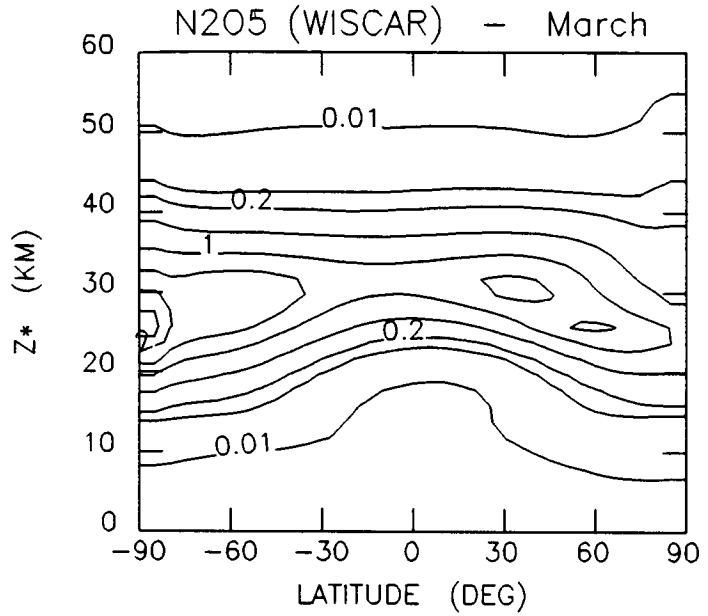
N2O5 (WISCAR) – March
Z* (KM)
LATITUDE (DEG)
0.01
0.2
1
2
60
50
40
30
20
10
0
−90 −60 −30 0 30 60 90

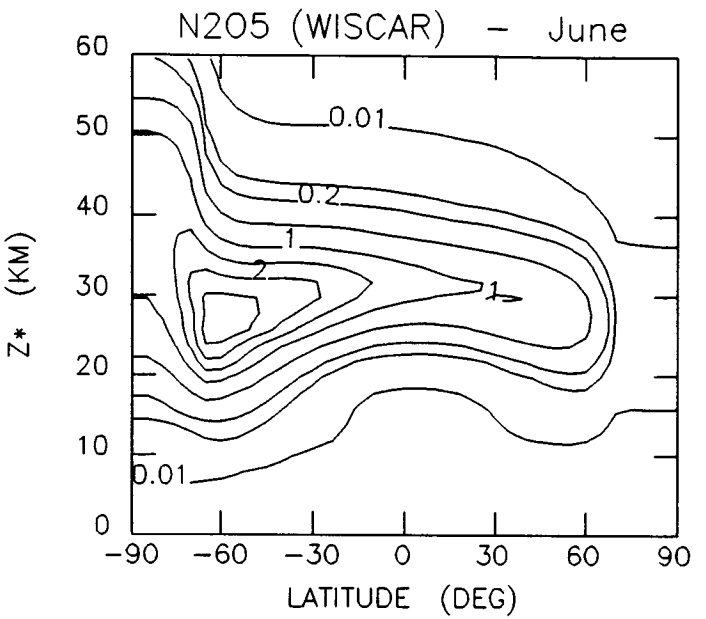
N2O5 (WISCAR) – June
Z* (KM)
LATITUDE (DEG)
0.01
0.2
1
2
60
50
40
30
20
10
0
−90 −60 −30 0 30 60 90

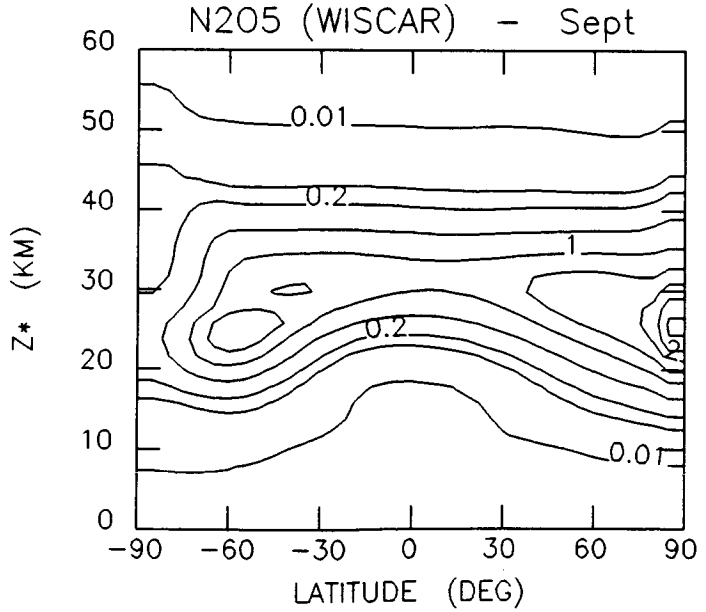
N2O5 (WISCAR) – Sept
Z* (KM)
LATITUDE (DEG)
0.01
0.2
1
60
50
40
30
20
10
0
−90 −60 −30 0 30 60 90

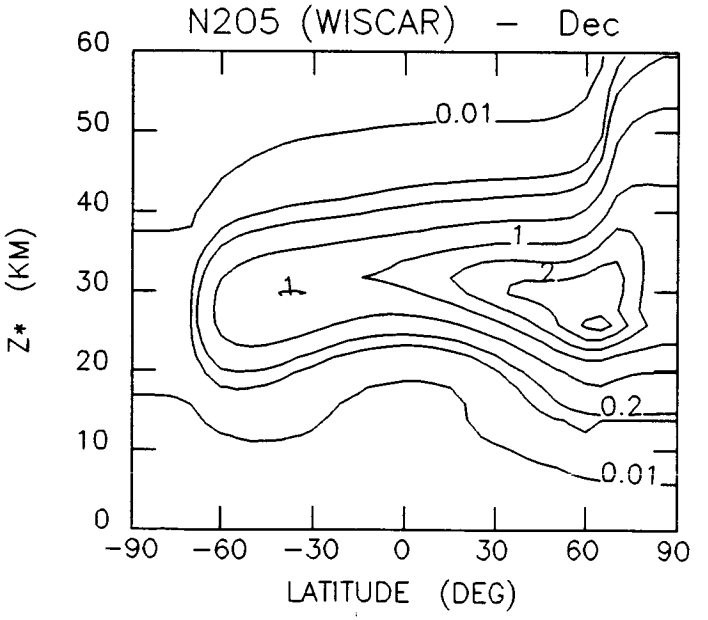
N2O5 (WISCAR) – Dec
Z* (KM)
LATITUDE (DEG)
0.01
0.2
1
2
60
50
40
30
20
10
0
−90 −60 −30 0 30 60 90

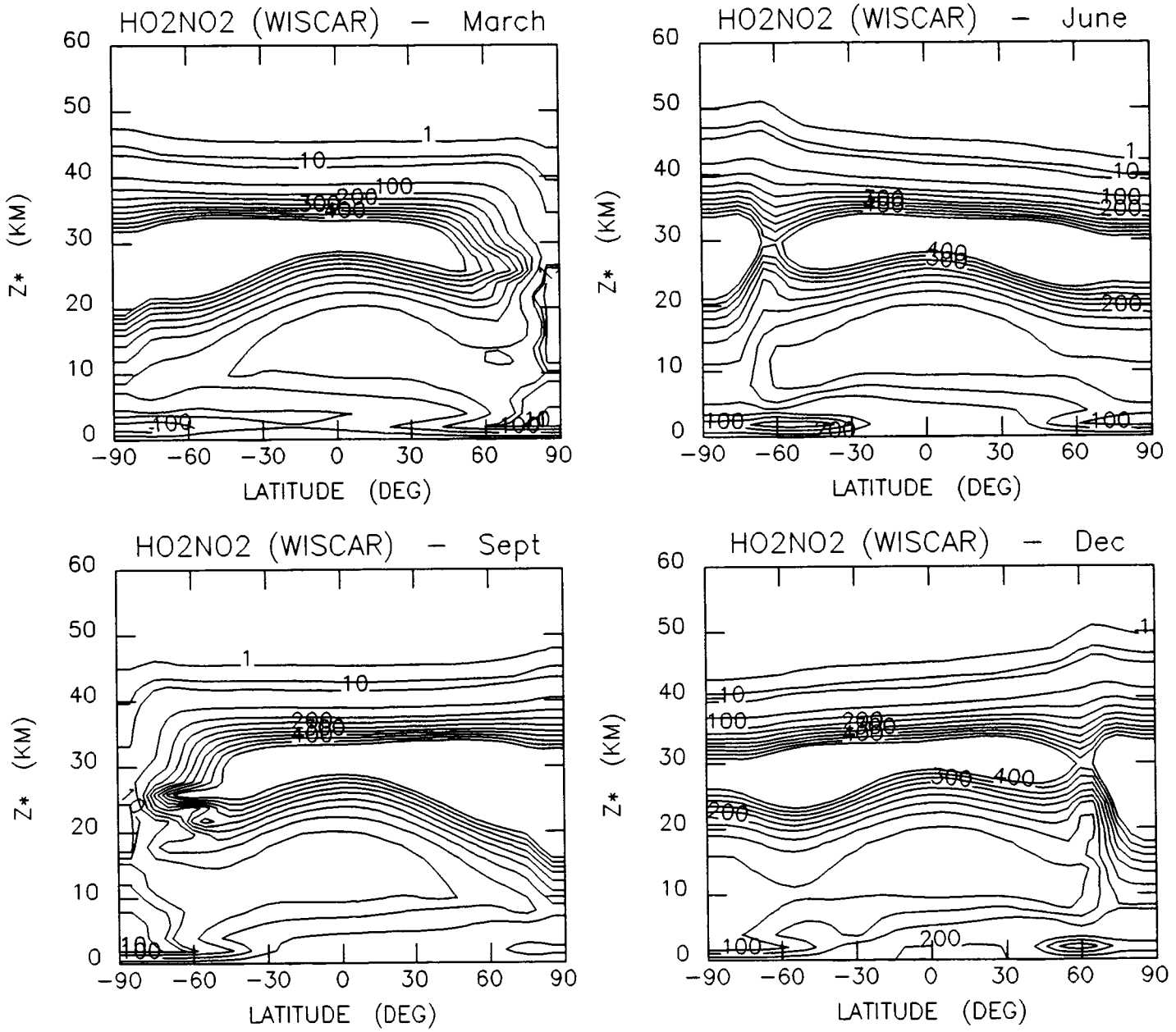
HO2NO2 (WISCAR) – March
HO2NO2 (WISCAR) – June
HO2NO2 (WISCAR) – Sept
HO2NO2 (WISCAR) – Dec
Z* (KM)
LATITUDE (DEG)
0
10
20
30
40
50
60
-90
-60
-30
0
30
60
90
1
10
100
200
300
400

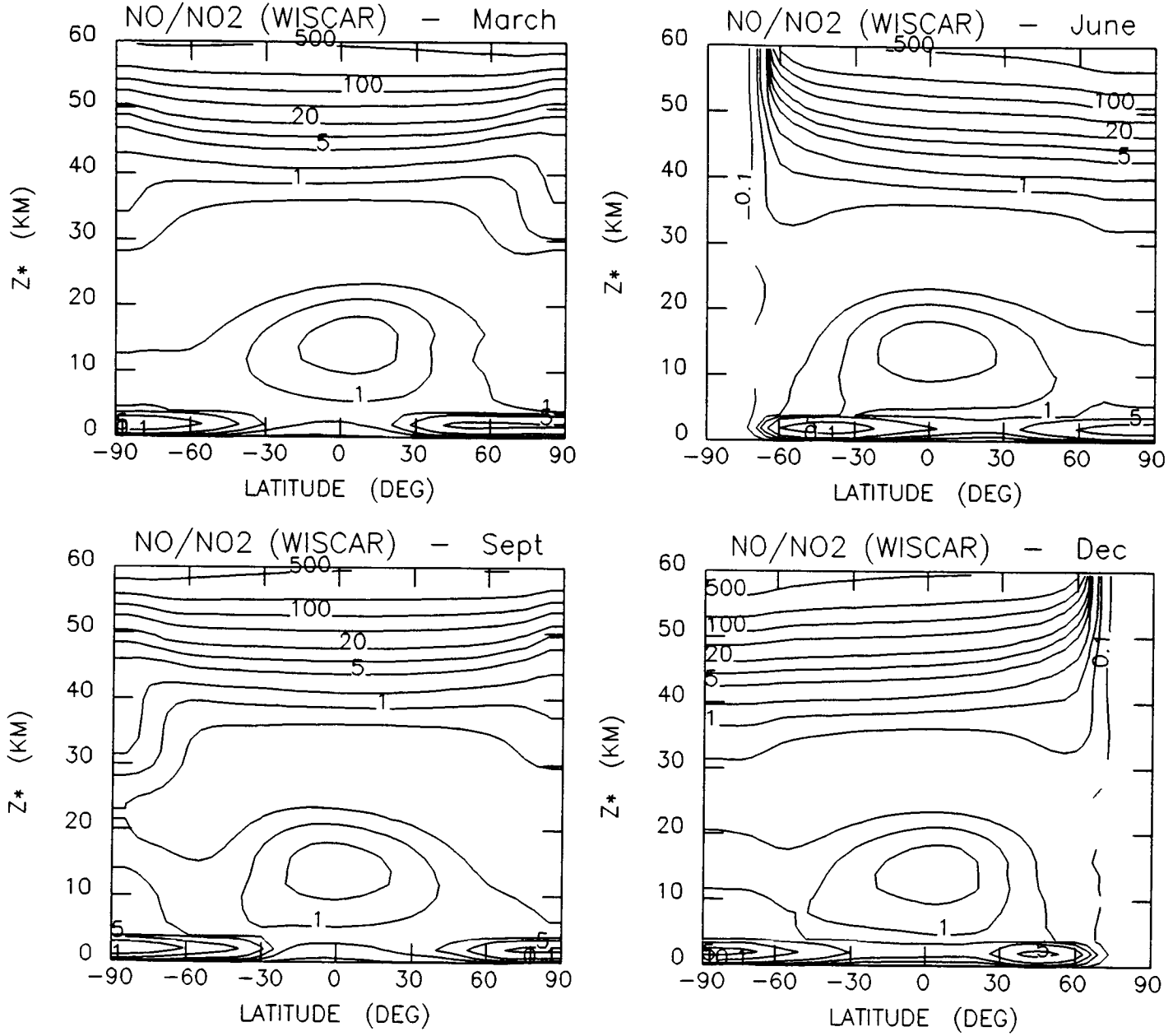
NO/NO2 (WISCAR) – March
NO/NO2 (WISCAR) – June
NO/NO2 (WISCAR) – Sept
NO/NO2 (WISCAR) – Dec
Z* (KM)
LATITUDE (DEG)
0
10
20
30
40
50
60
-90
-60
-30
0
30
60
90
500
100
20
5
1
0.1

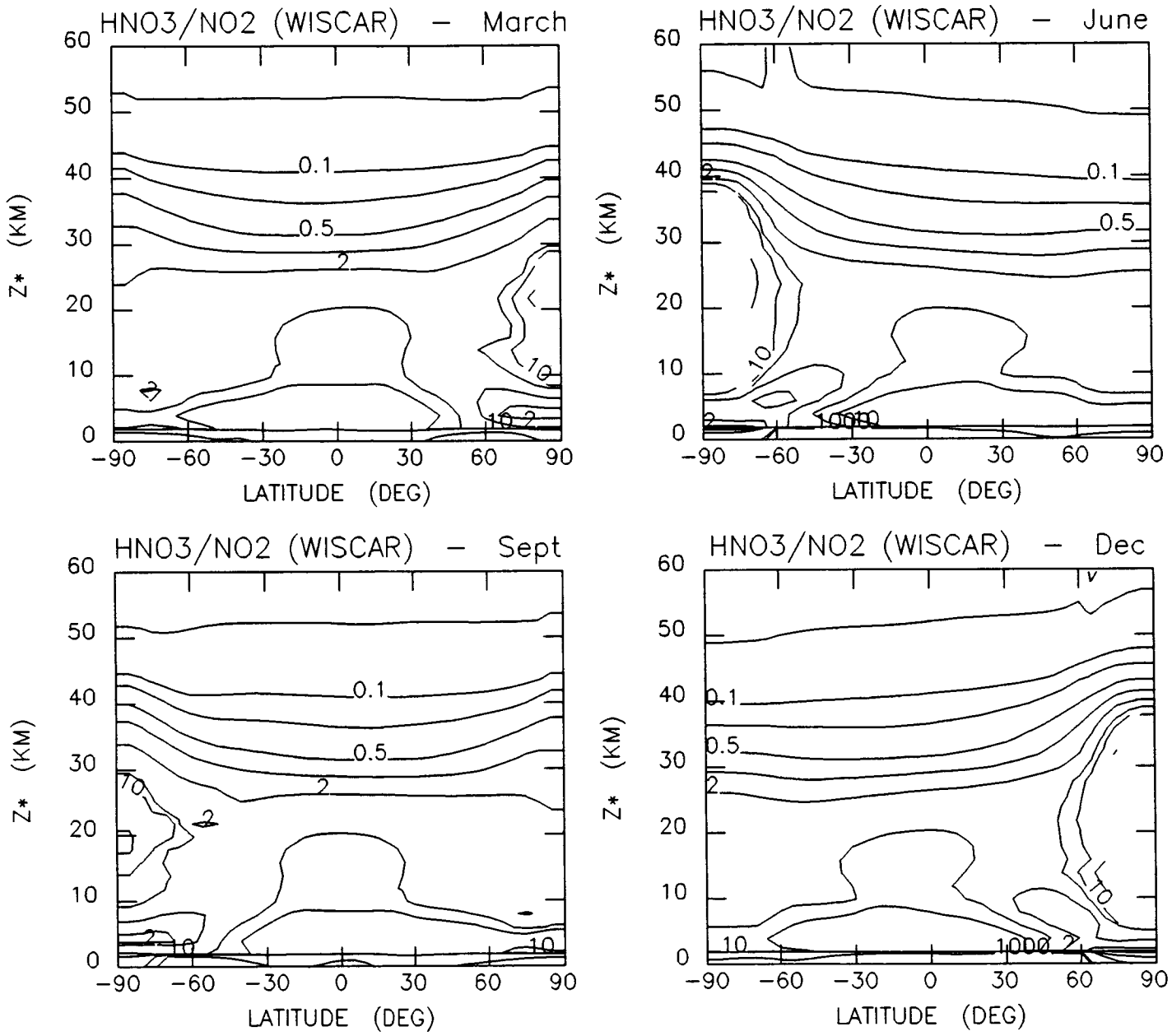
HNO3/NO2 (WISCAR) – March
HNO3/NO2 (WISCAR) – June
HNO3/NO2 (WISCAR) – Sept
HNO3/NO2 (WISCAR) – Dec
Z* (KM)
LATITUDE (DEG)
0
10
20
30
40
50
60
-90
-60
-30
0
30
60
90
0.1
0.5
2
10
1000

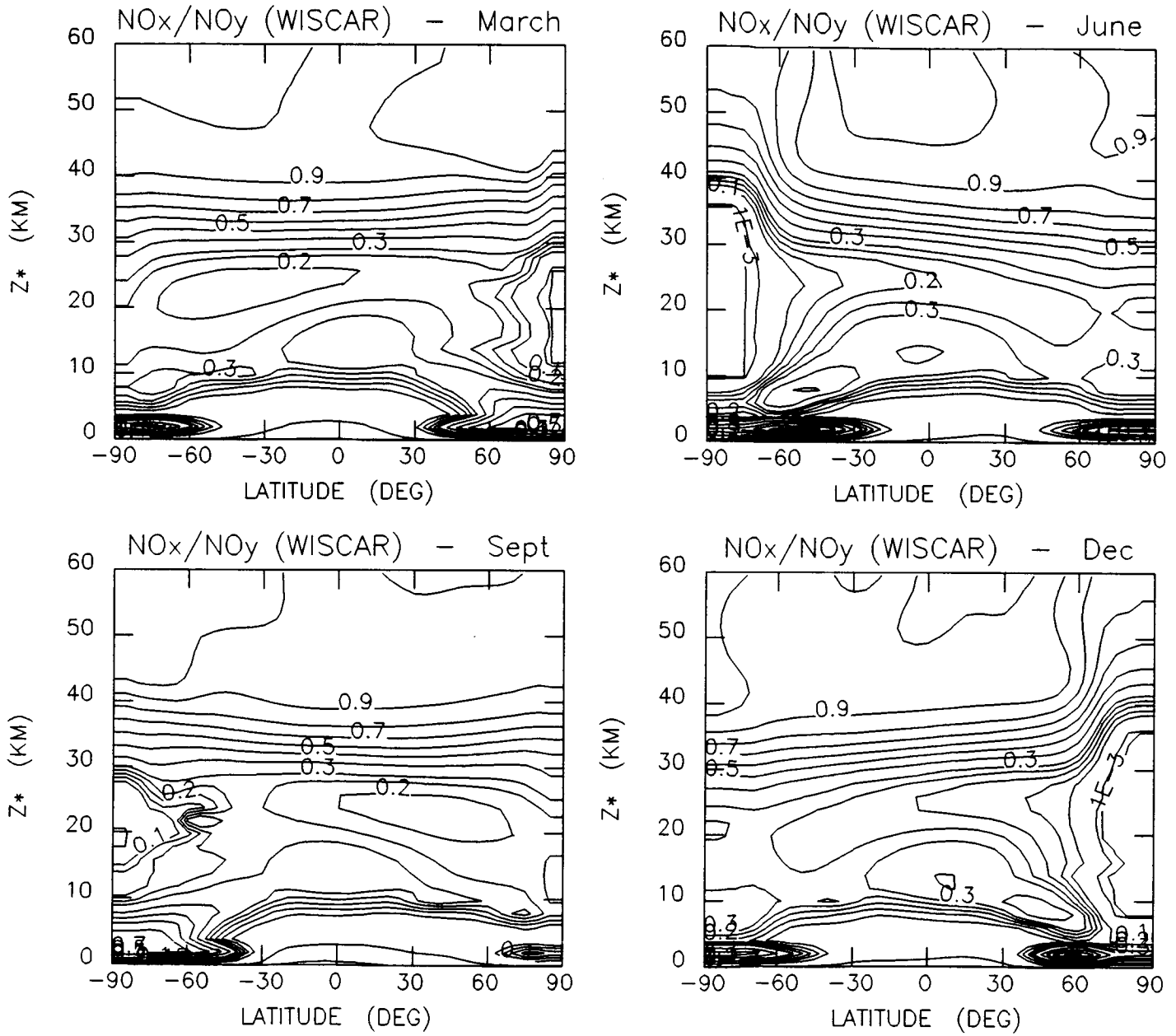
NOx/NOy (WISCAR) – March
NOx/NOy (WISCAR) – June
NOx/NOy (WISCAR) – Sept
NOx/NOy (WISCAR) – Dec
Z* (KM)
LATITUDE (DEG)
0
10
20
30
40
50
60
−90
−60
−30
0
30
60
90
0.9
0.7
0.5
0.3
0.2
0.1
1E-3

**Table 6-3d.** Current Atmosphere (1980): Chlorine Gases

March, June, September, and December
Models Represented - AER, CAMBRAL, CLKSON, DUPONT (Jan. & April), GSFC1 (Jan.), GSFC2, LARC, LLNL, MRI, NOCAR, OSLO, WISCAR

| Parameter | Description | Units | Contour Levels |
|---|---|---|---|
| ClO | ClO Mixing Ratio | ppbv | 0.05, 0.1, 0.2, 0.4, 0.6, 0.8, 1, 1.2, 1.4, 1.6, 1.8, 2 |
| HCl | HCl Mixing Ratio | ppbv | 0, 0.25, 0.5, 0.75, 1, 1.25, 1.5, 1.75, 2, 2.25, 2.5, 2.75, 3 |
| $ClNO_3$ | $ClNO_3$ ($ClONO_2$) Mixing Ratio | ppbv | 0.05, 0.1, 0.2, 0.4, 0.6, 0.8, 1, 1.2, 1.4, 1.6, 1.8, 2 |
| HOCl | HOCl Mixing Ratio | pptv | 1, 5, 10, 50, 100, 150, 200, 250, 300, 350, 400, 450, 500 |
| Cl/ClO | Ratio of Cl to ClO Mixing Ratios | --- | 1.0E-04, 2.0E-04, 5.0E-04, 1.0E-03, 2.0E-03, 5.0E-03, 0.01, 0.02, 0.05, 0.1, 0.2, 0.5, 1 |
| $ClO/Cl_y$ | Ratio of ClO to $Cl_y$ Mixing Ratios | --- | 1.0E-03, 2.0E-03, 5.0E-03, 0.01, 0.02, 0.05, 0.1, 0.2, 0.3, 0.4, 0.5, 0.6, 0.7, 0.8, 0.9, 1 |
| ClO/HCl | Ratio of ClO to HCl Mixing Ratios | --- | 1.0E-03, 2.0E-03, 5.0E-03, 0.01, 0.02, 0.05, 0.1, 0.2, 0.3, 0.4, 0.5, 0.6, 0.7, 0.8, 0.9, 1 |

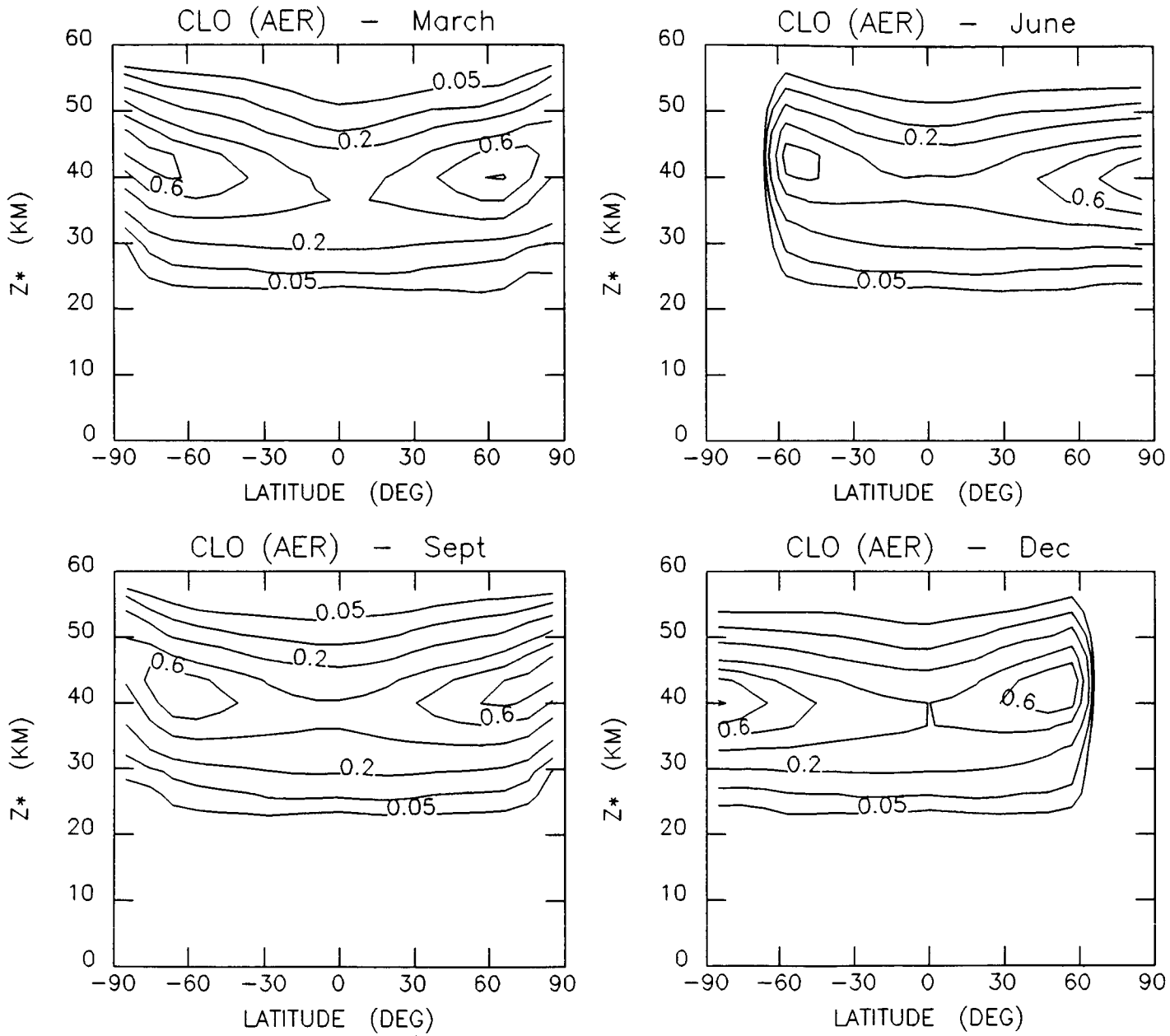
CLO (AER) – March
CLO (AER) – June
CLO (AER) – Sept
CLO (AER) – Dec
Z* (KM)
LATITUDE (DEG)
0
10
20
30
40
50
60
−90
−60
−30
0
30
60
90
0.05
0.2
0.6

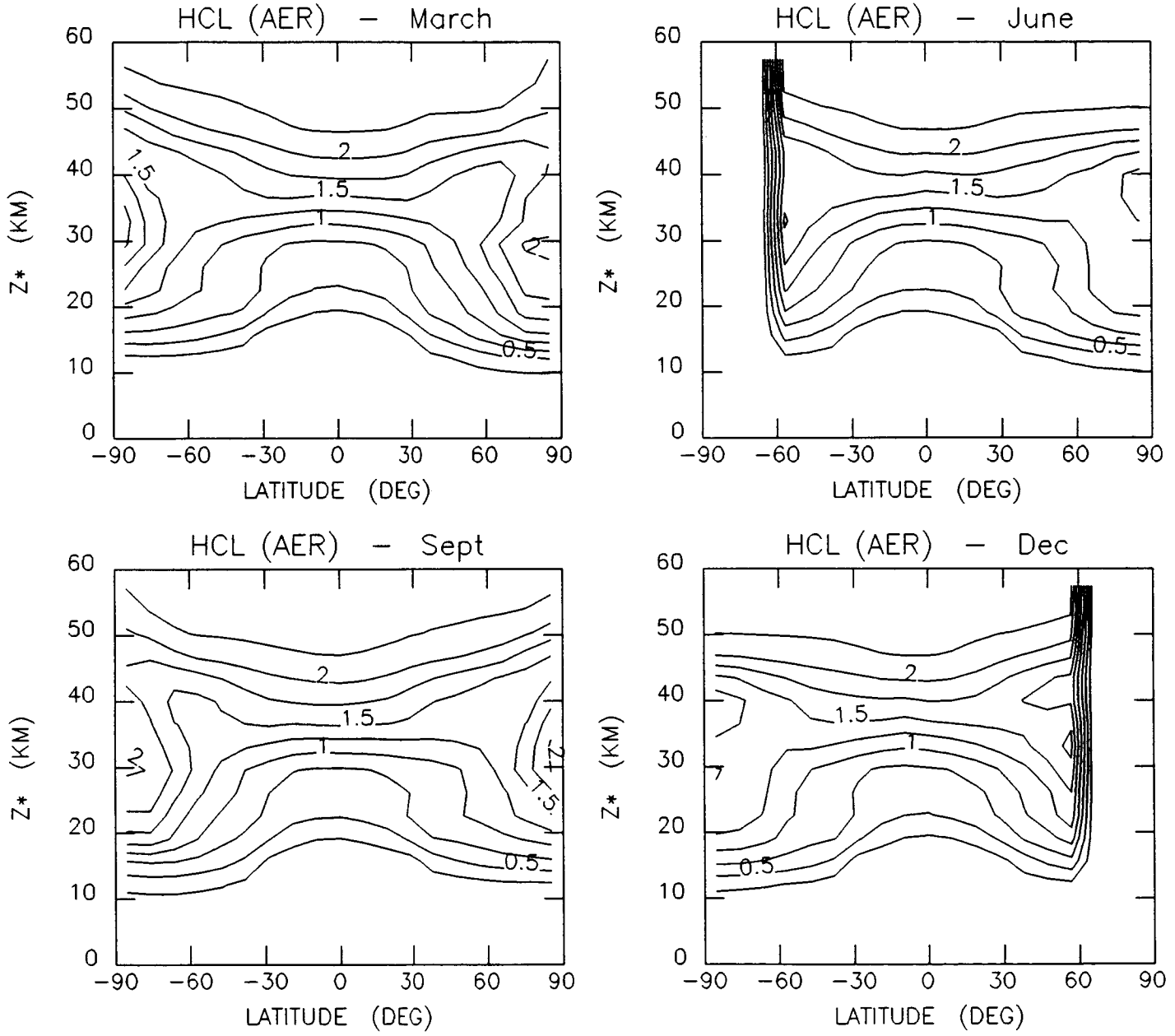
HCL (AER) – March
HCL (AER) – June
HCL (AER) – Sept
HCL (AER) – Dec
Z* (KM)
LATITUDE (DEG)
60
50
40
30
20
10
0
-90
-60
-30
0
30
60
90
2
1.5
1
0.5

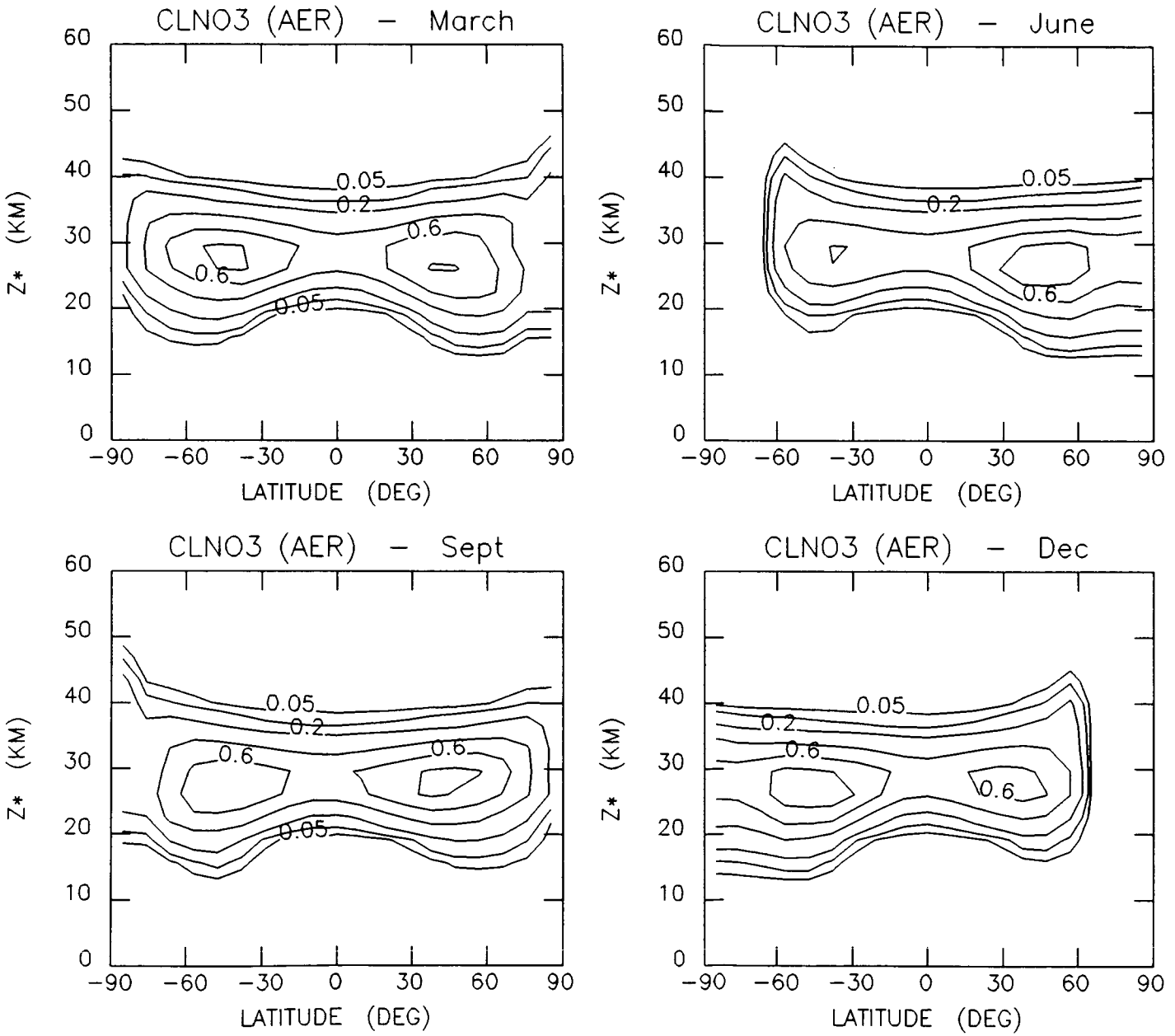
CLNO3 (AER) – March
CLNO3 (AER) – June
CLNO3 (AER) – Sept
CLNO3 (AER) – Dec
Z* (KM)
LATITUDE (DEG)
0.05
0.2
0.6
0
10
20
30
40
50
60
−90
−60
−30
0
30
60
90

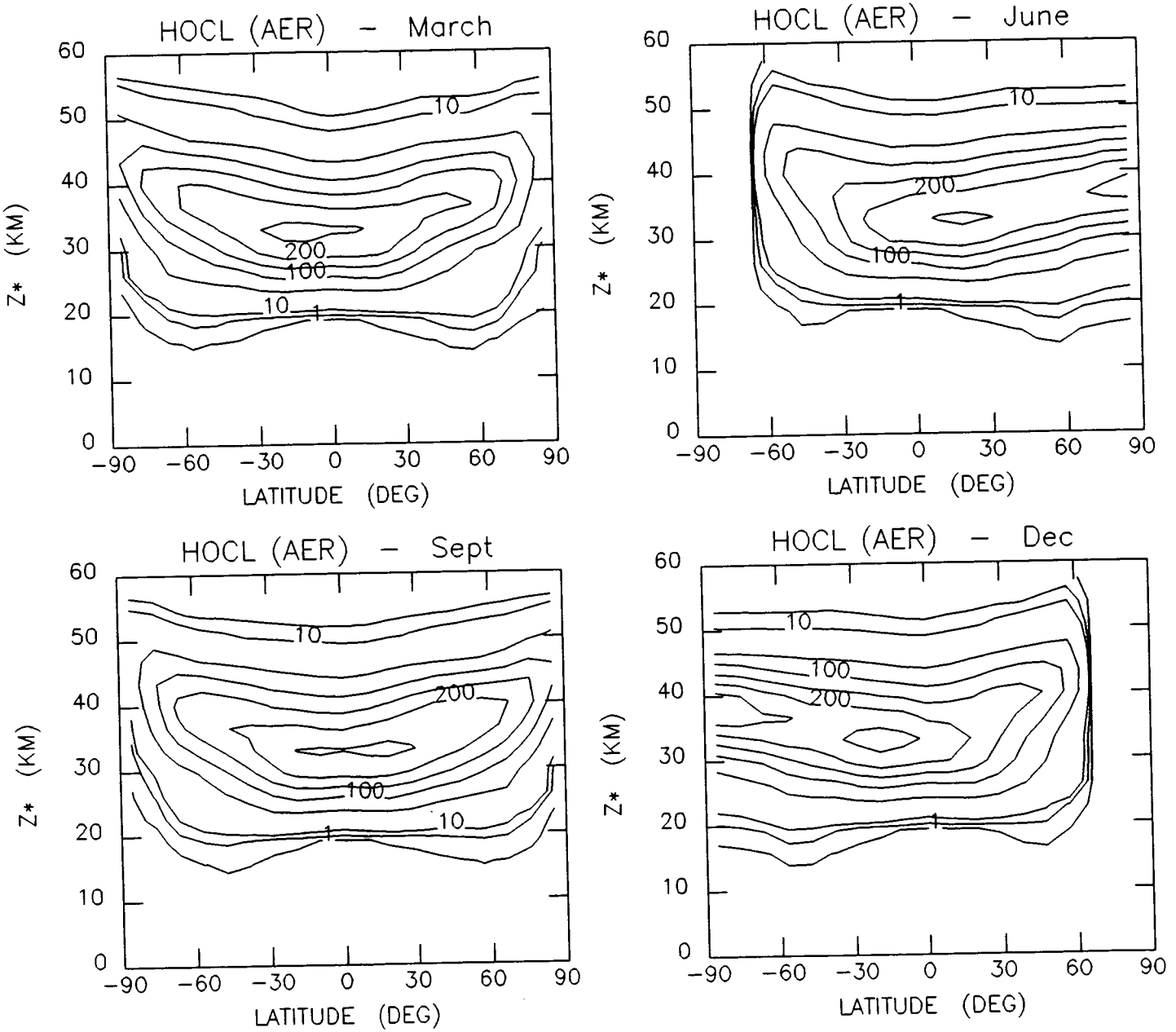
HOCL (AER) – March
HOCL (AER) – June
HOCL (AER) – Sept
HOCL (AER) – Dec
Z* (KM)
LATITUDE (DEG)
10
100
200
1
0
10
20
30
40
50
60
-90
-60
-30
0
30
60
90

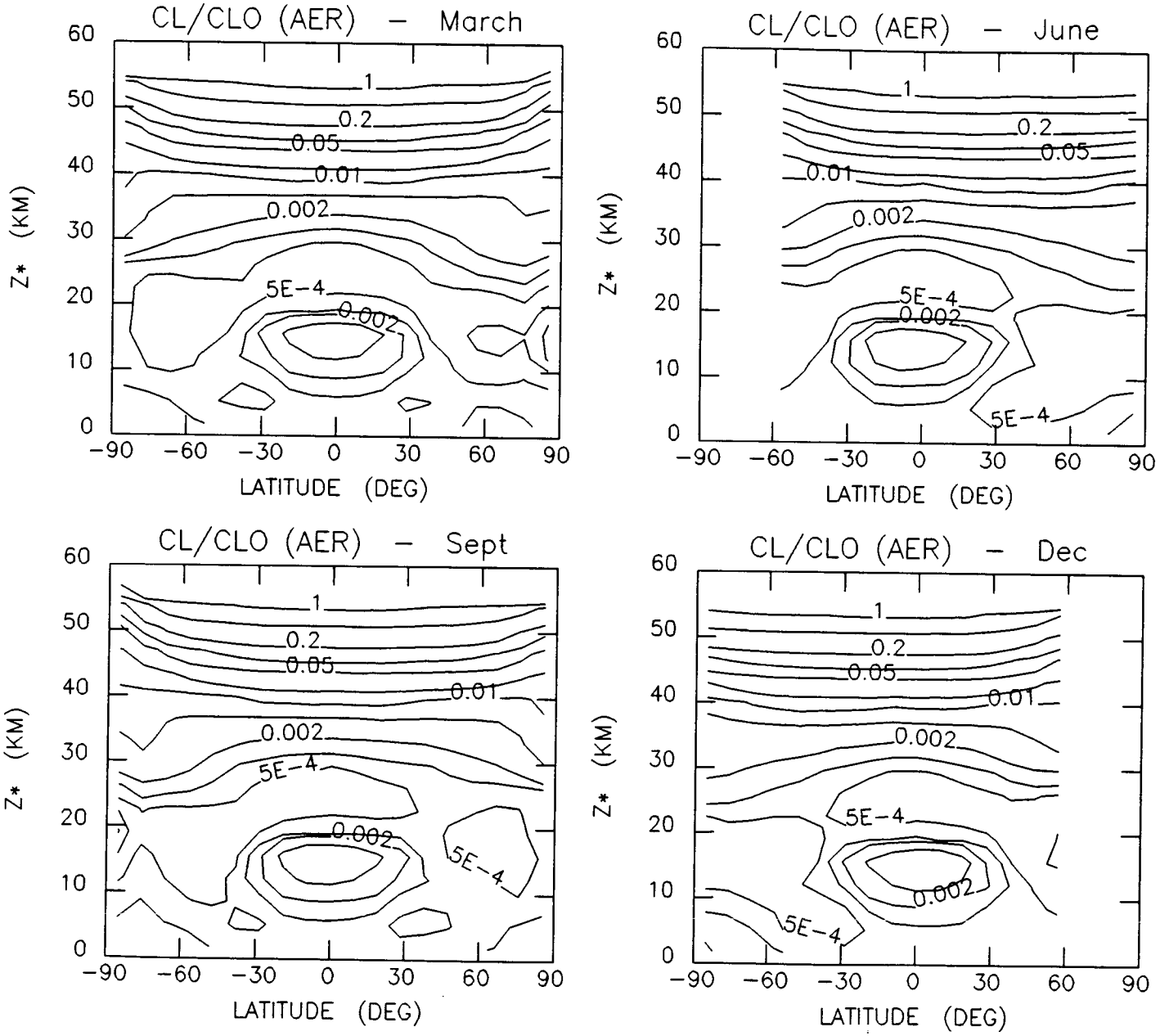
CL/CLO (AER) – March
CL/CLO (AER) – June
CL/CLO (AER) – Sept
CL/CLO (AER) – Dec
Z* (KM)
LATITUDE (DEG)
1
0.2
0.05
0.01
0.002
5E-4
0
10
20
30
40
50
60
-90
-60
-30
0
30
60
90

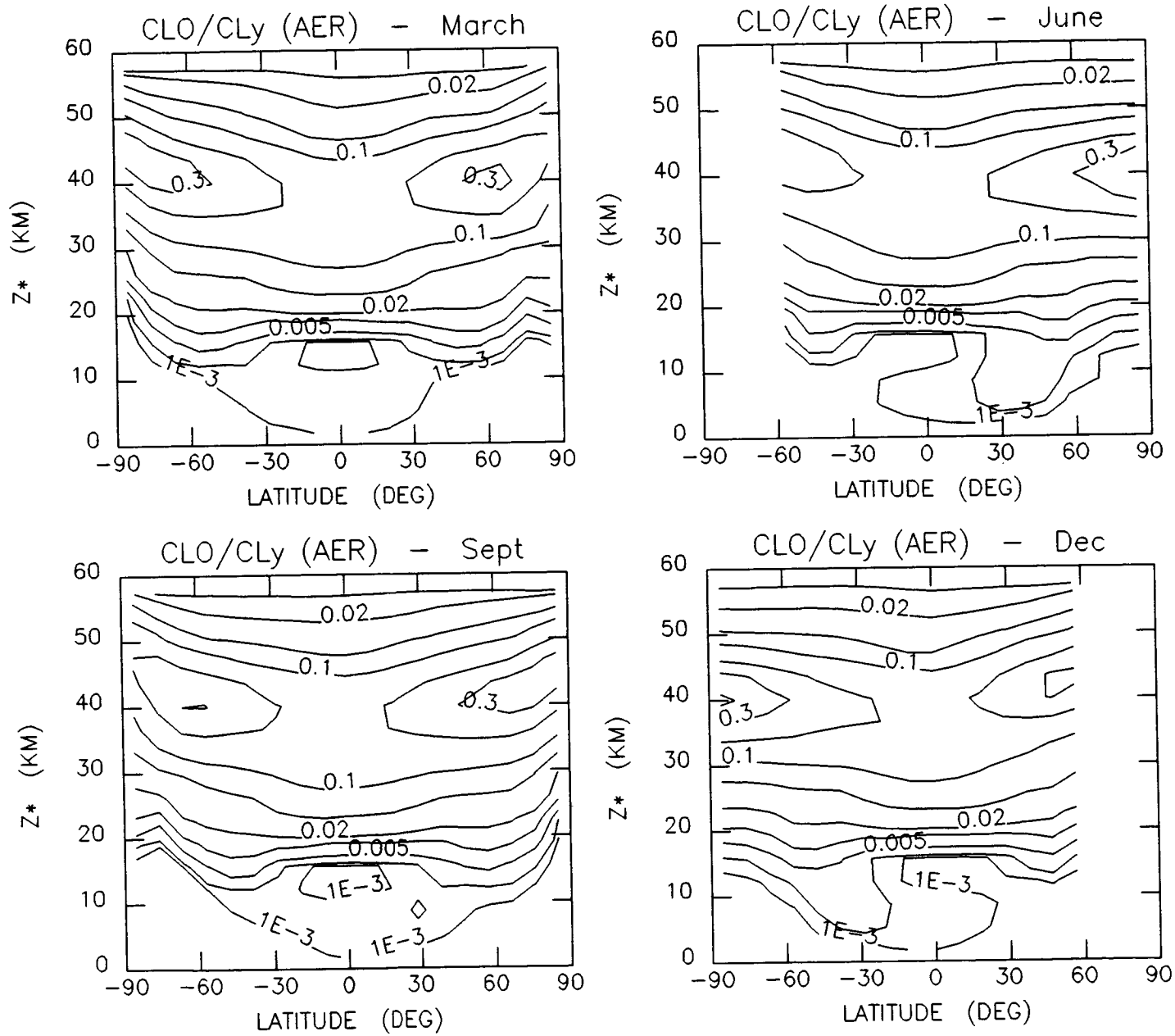
CLO/CLy (AER) – March
CLO/CLy (AER) – June
CLO/CLy (AER) – Sept
CLO/CLy (AER) – Dec
Z* (KM)
LATITUDE (DEG)
0.02
0.1
0.3
0.005
1E-3

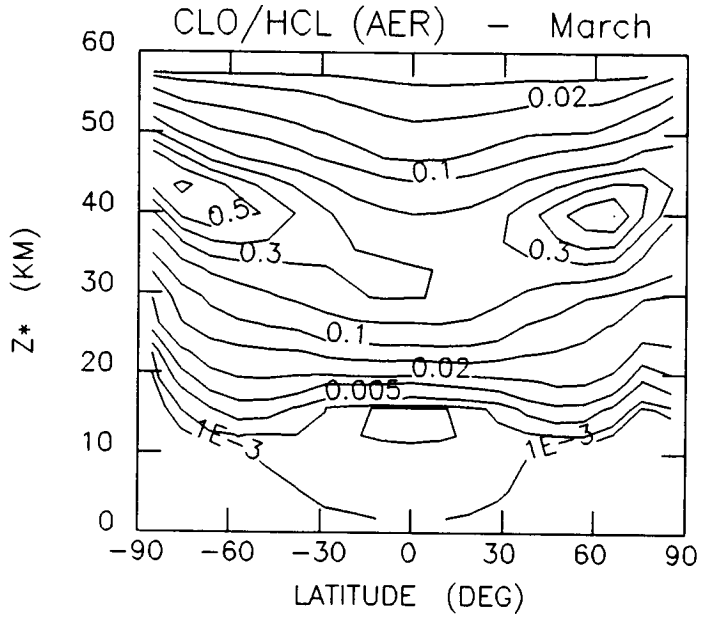
CLO/HCL (AER) – March
Z* (KM)
LATITUDE (DEG)
0.02
0.1
0.5
0.3
0.005
1E-3

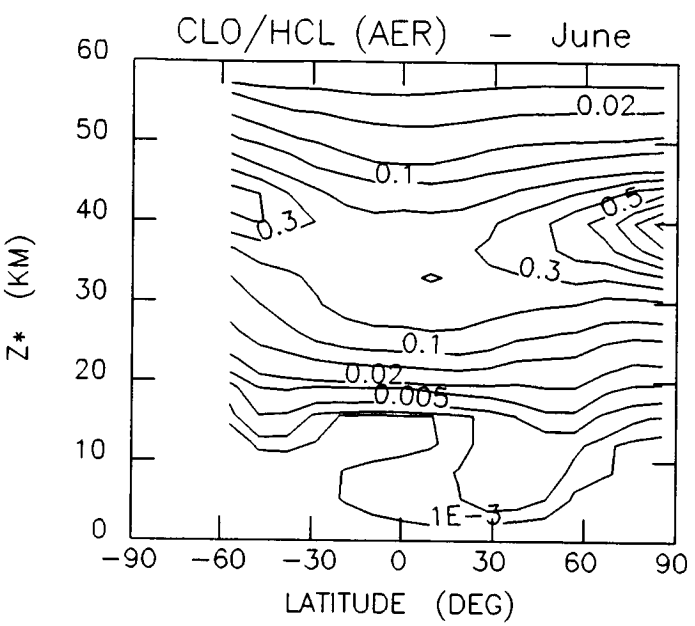
CLO/HCL (AER) – June
Z* (KM)
LATITUDE (DEG)
0.02
0.1
0.3
0.5
0.005
1E-3

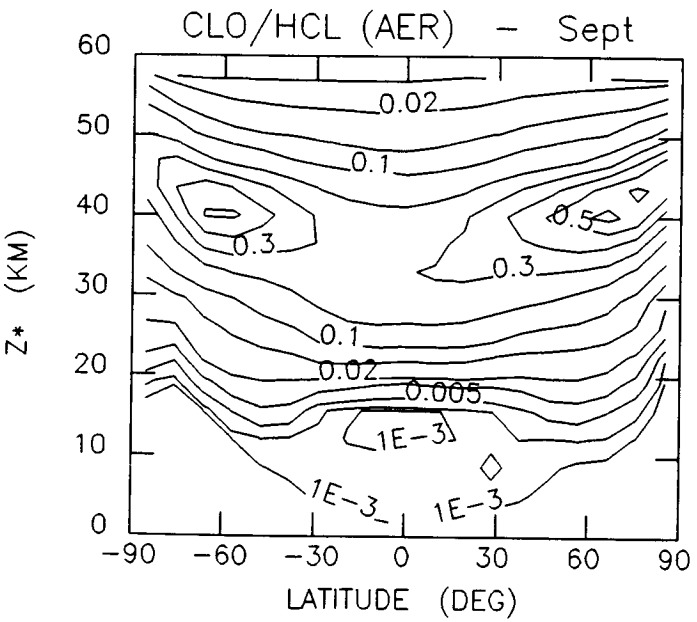
CLO/HCL (AER) – Sept
Z* (KM)
LATITUDE (DEG)
0.02
0.1
0.3
0.5
0.005
1E-3

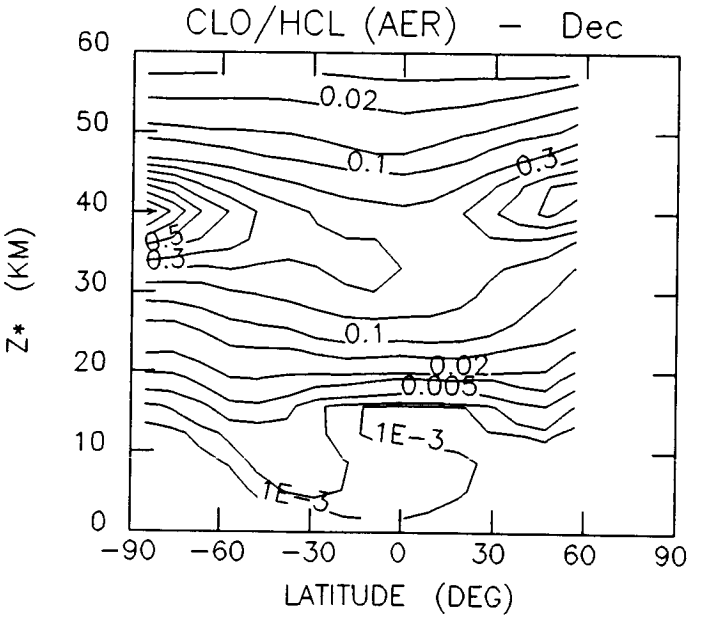
CLO/HCL (AER) – Dec
Z* (KM)
LATITUDE (DEG)
0.02
0.1
0.3
0.5
0.005
1E-3

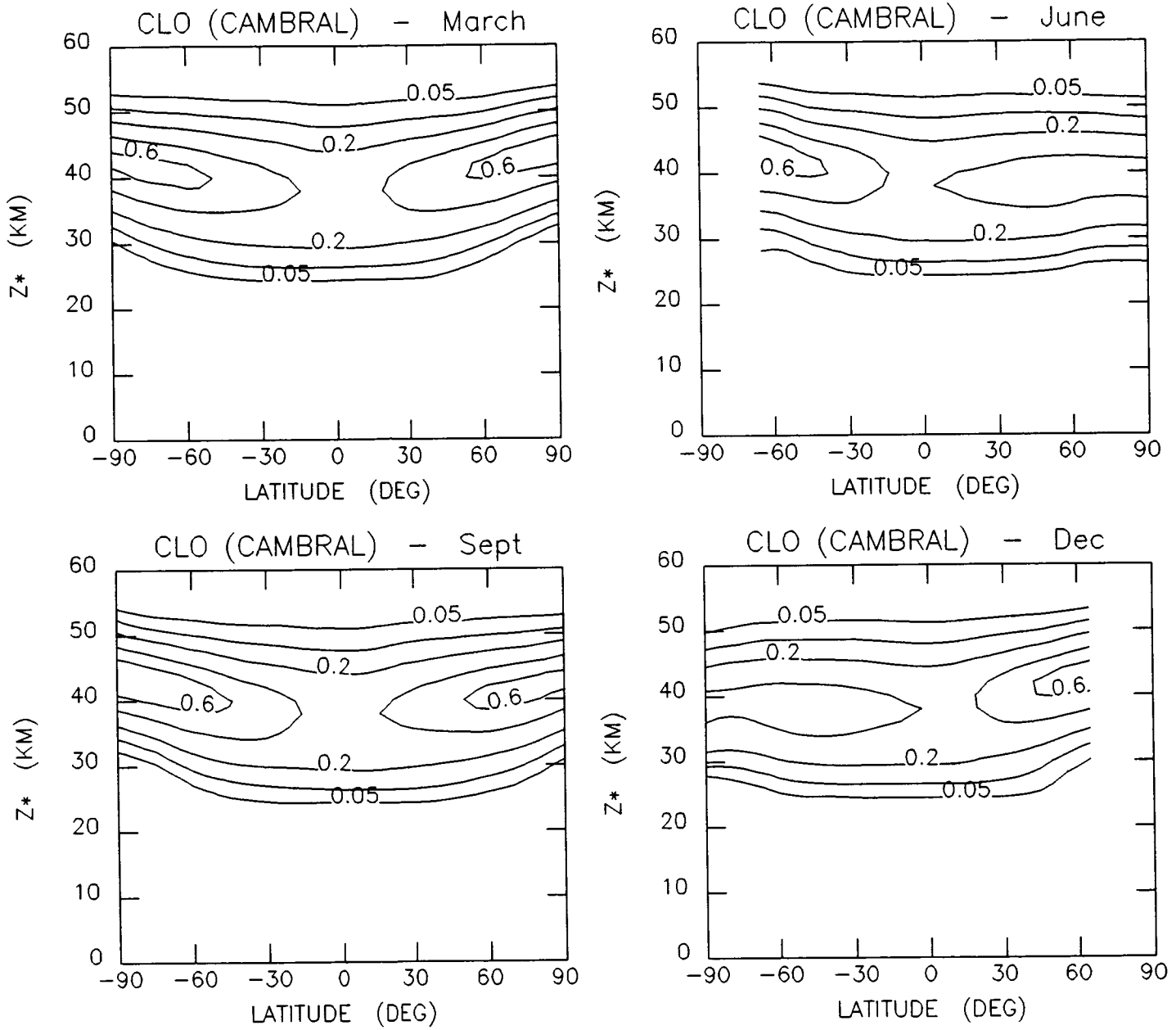
CLO (CAMBRAL) – March
CLO (CAMBRAL) – June
CLO (CAMBRAL) – Sept
CLO (CAMBRAL) – Dec
Z* (KM)
LATITUDE (DEG)
0.05
0.2
0.6
0 10 20 30 40 50 60
−90 −60 −30 0 30 60 90

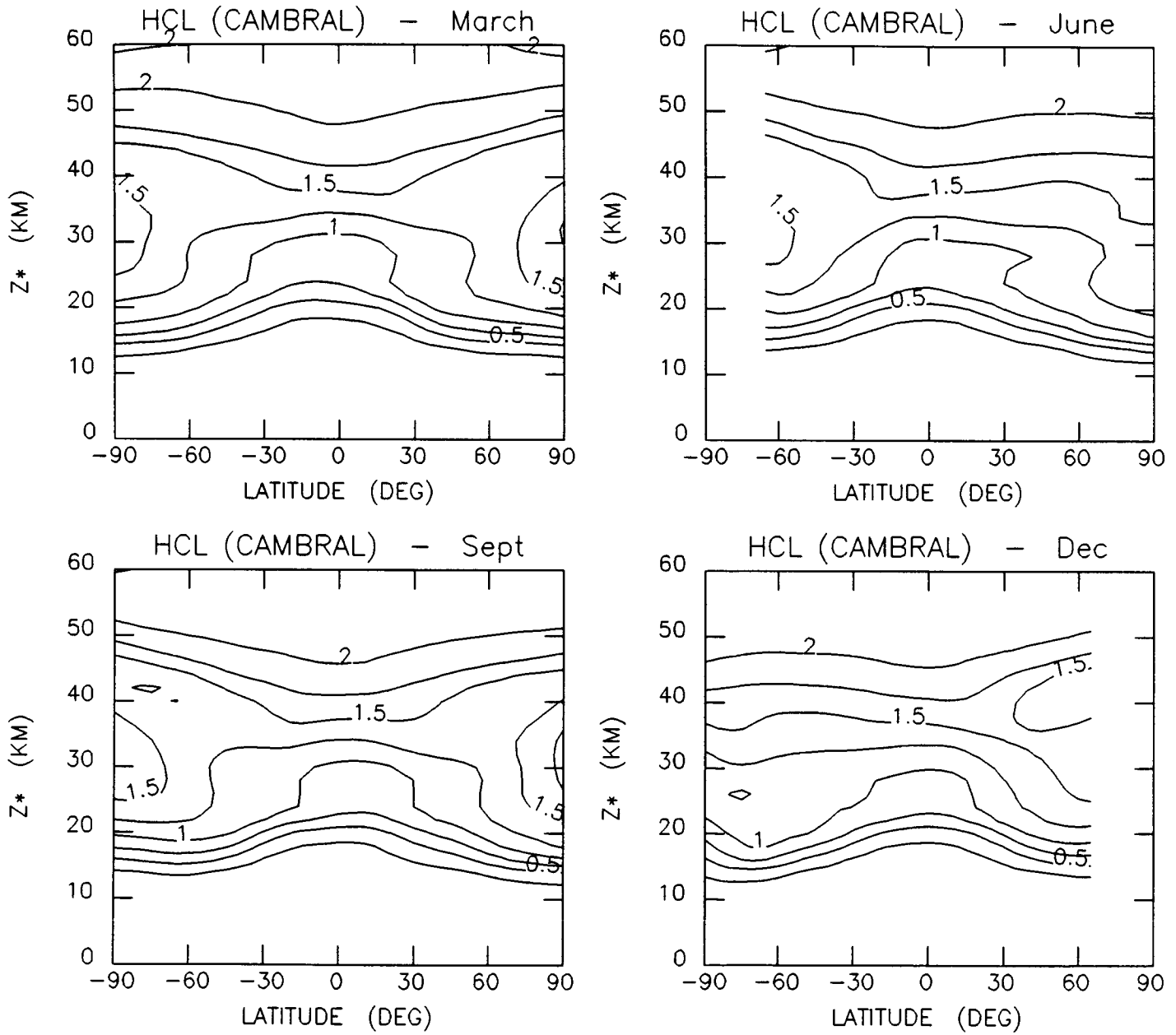
HCL (CAMBRAL) – March
HCL (CAMBRAL) – June
HCL (CAMBRAL) – Sept
HCL (CAMBRAL) – Dec
Z* (KM)
LATITUDE (DEG)
60
50
40
30
20
10
0
−90 −60 −30 0 30 60 90
2
1.5
1
0.5

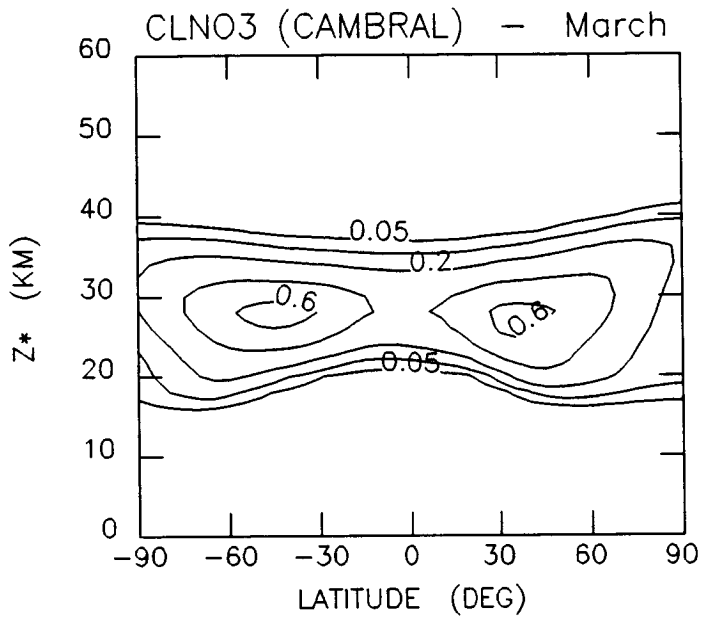
CLNO3 (CAMBRAL) – March
Z* (KM)
LATITUDE (DEG)
0.05
0.2
0.6
0.6
0.05

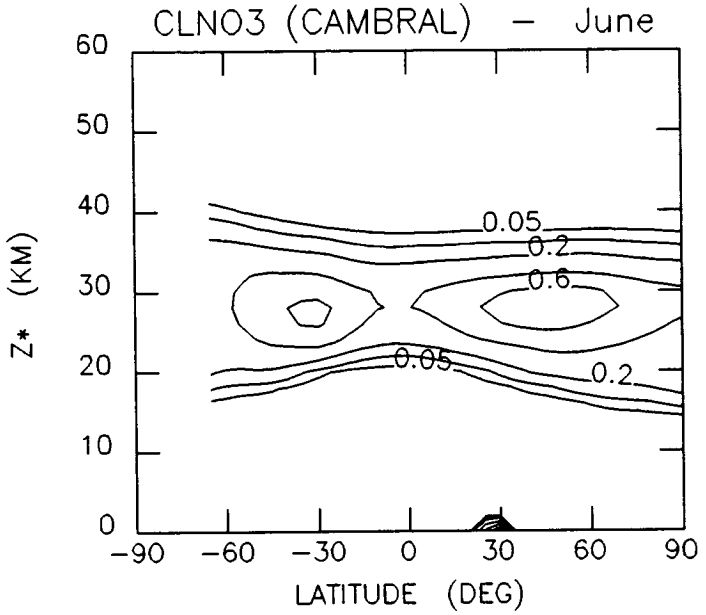
CLNO3 (CAMBRAL) – June
Z* (KM)
LATITUDE (DEG)
0.05
0.2
0.6
0.05
0.2

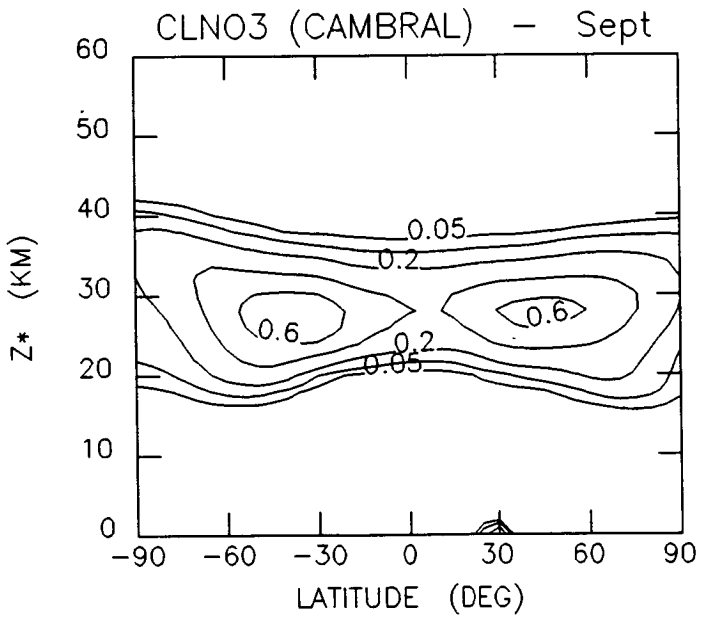
CLNO3 (CAMBRAL) – Sept
Z* (KM)
LATITUDE (DEG)
0.05
0.2
0.6
0.6
0.2
0.05

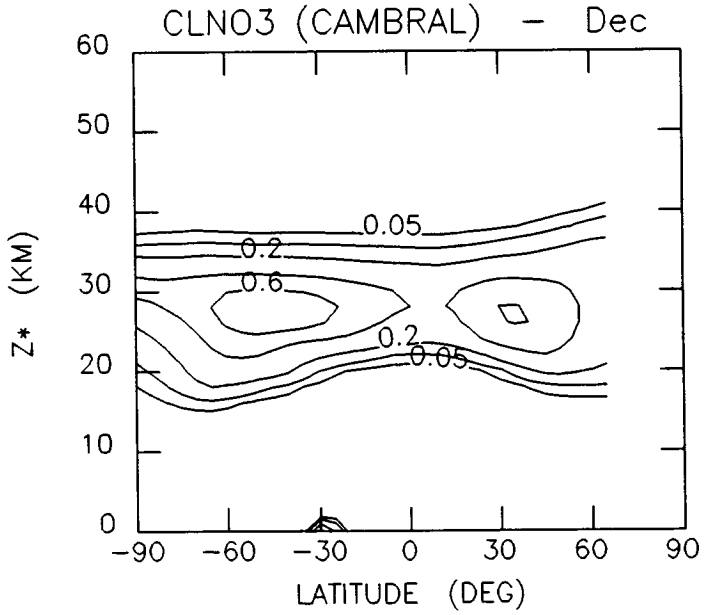
CLNO3 (CAMBRAL) – Dec
Z* (KM)
LATITUDE (DEG)
0.05
0.2
0.6
0.2
0.05

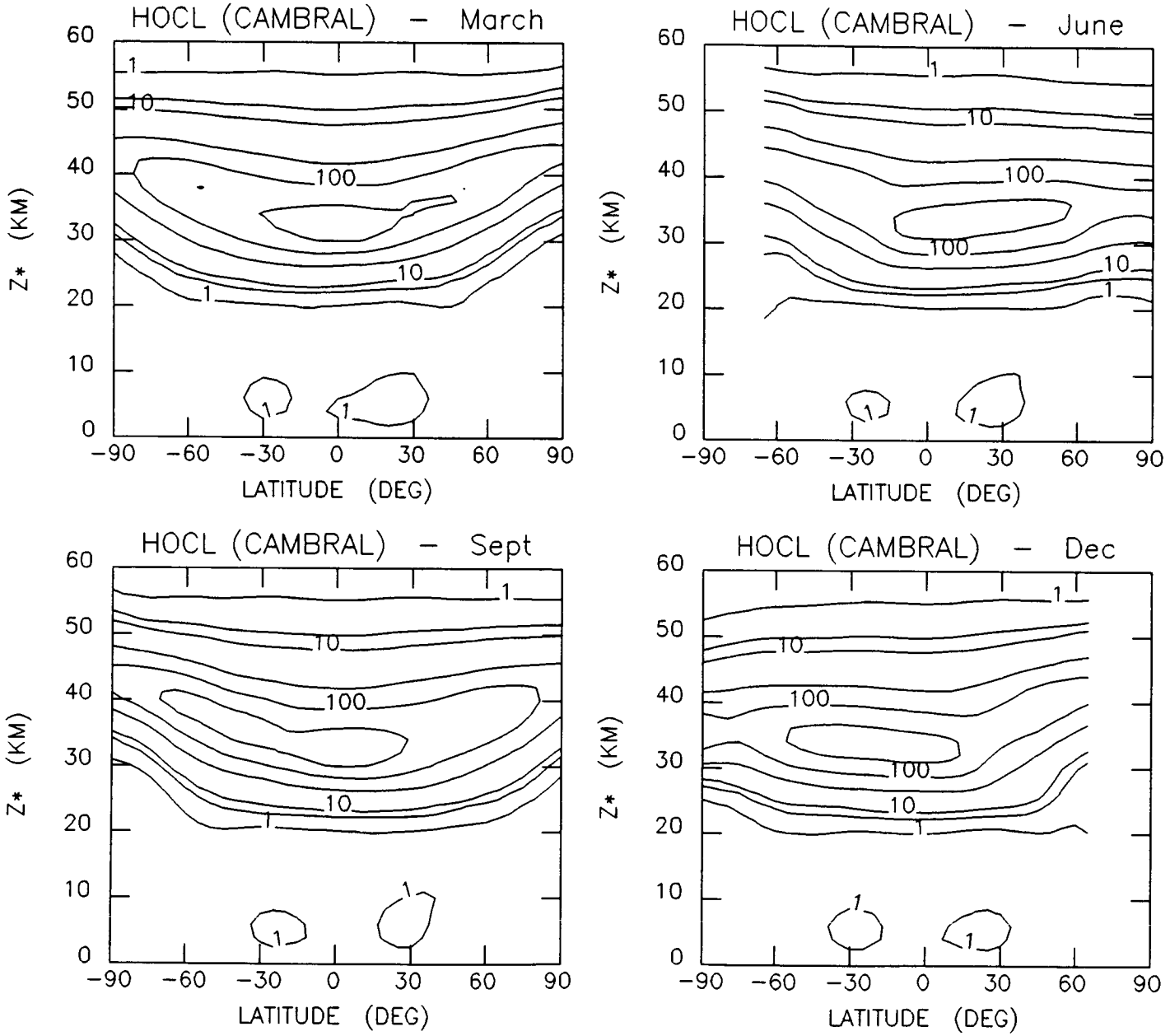
HOCL (CAMBRAL) – March
HOCL (CAMBRAL) – June
HOCL (CAMBRAL) – Sept
HOCL (CAMBRAL) – Dec
Z* (KM)
LATITUDE (DEG)
60
50
40
30
20
10
0
-90
-60
-30
0
30
60
90
1
10
100

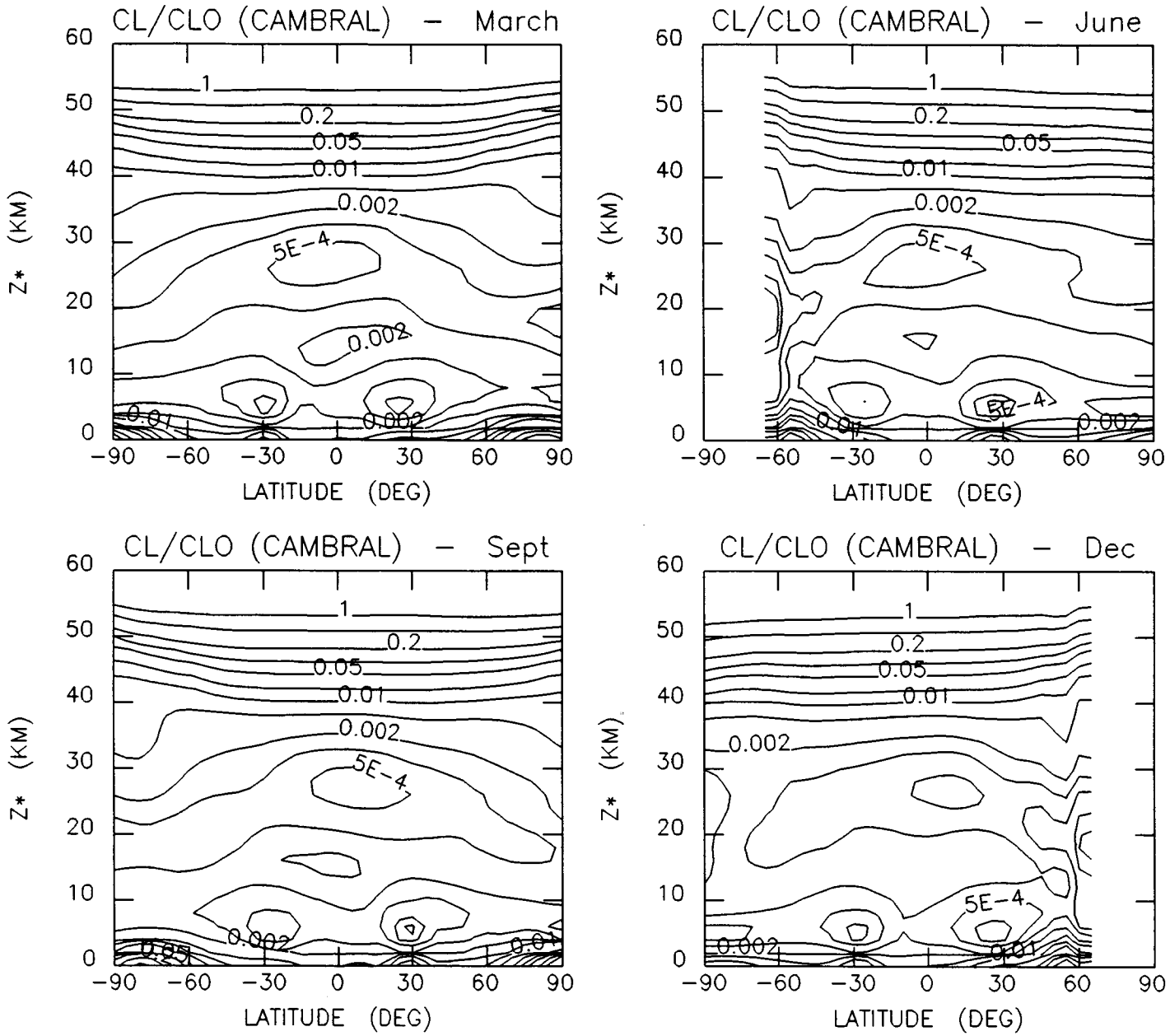
CL/CLO (CAMBRAL) – March
CL/CLO (CAMBRAL) – June
CL/CLO (CAMBRAL) – Sept
CL/CLO (CAMBRAL) – Dec
Z* (KM)
LATITUDE (DEG)
1
0.2
0.05
0.01
0.002
5E-4

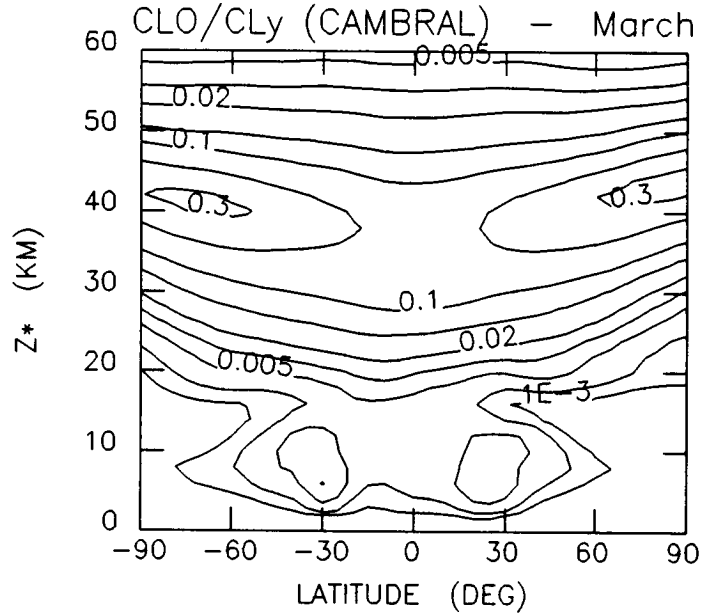
CLO/CLy (CAMBRAL) – March
Z* (KM)
LATITUDE (DEG)
0.005
0.02
0.1
0.3
1E-3

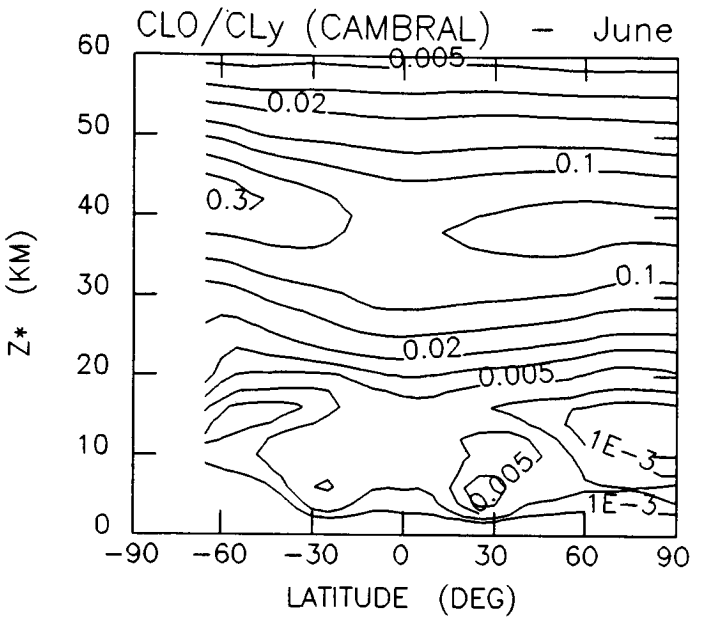
CLO/CLy (CAMBRAL) – June
Z* (KM)
LATITUDE (DEG)
0.005
0.02
0.1
0.3
1E-3

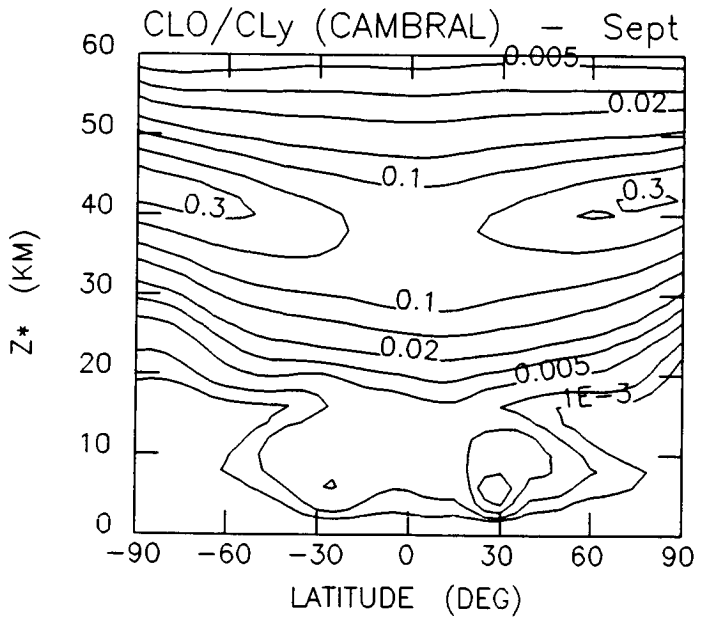
CLO/CLy (CAMBRAL) – Sept
Z* (KM)
LATITUDE (DEG)
0.005
0.02
0.1
0.3
1E-3

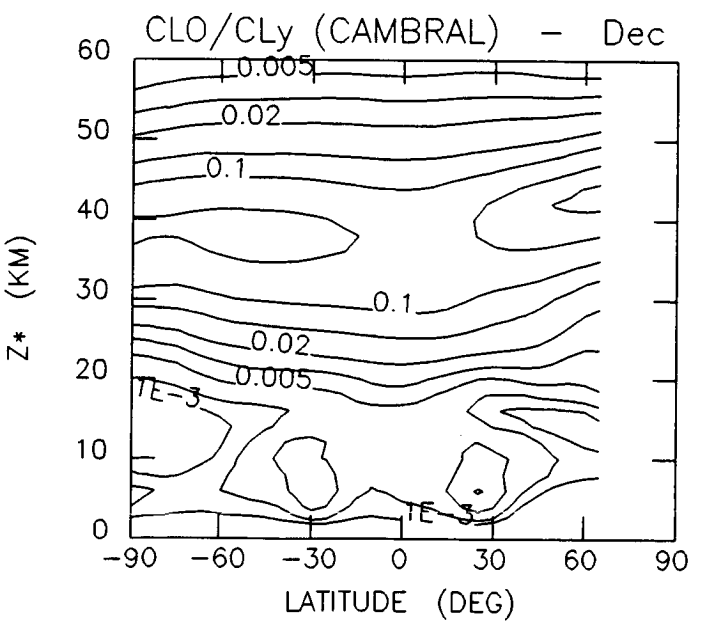
CLO/CLy (CAMBRAL) – Dec
Z* (KM)
LATITUDE (DEG)
0.005
0.02
0.1
1E-3

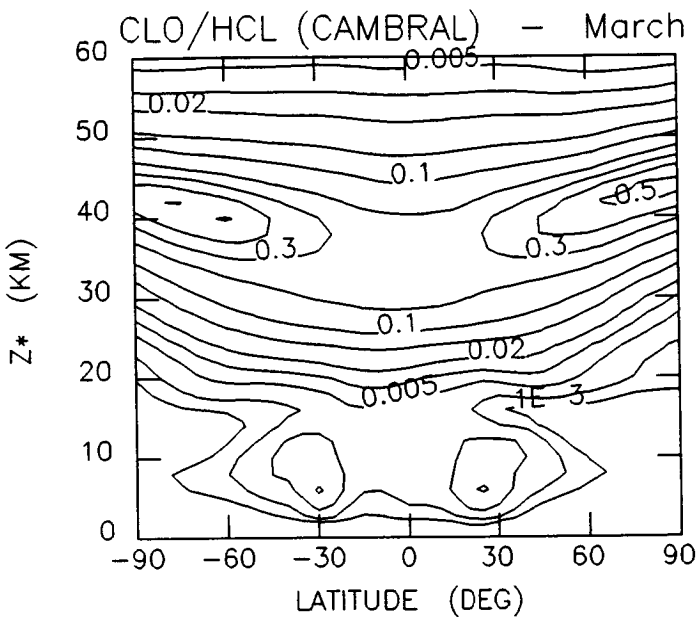
CLO/HCL (CAMBRAL) – March
Z* (KM)
LATITUDE (DEG)
0.005
0.02
0.1
0.5
0.3
0.02
0.005
1E-3

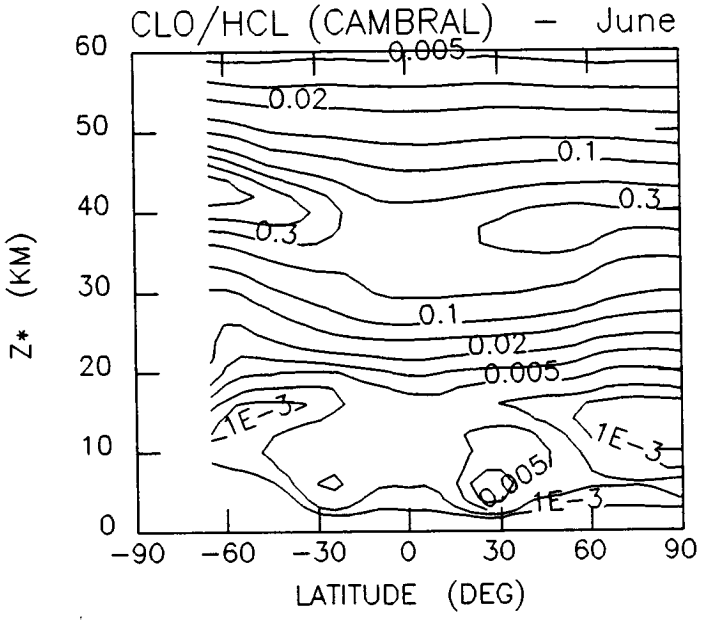
CLO/HCL (CAMBRAL) – June
Z* (KM)
LATITUDE (DEG)
0.005
0.02
0.1
0.3
0.3
0.1
0.02
0.005
1E-3
1E-3
0.005
1E-3

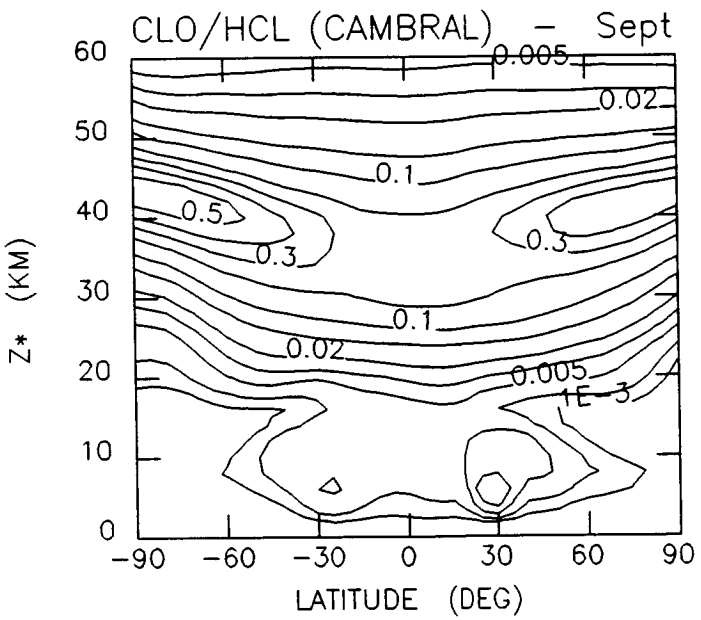
CLO/HCL (CAMBRAL) – Sept
Z* (KM)
LATITUDE (DEG)
0.005
0.02
0.1
0.5
0.3
0.3
0.1
0.02
0.005
1E-3

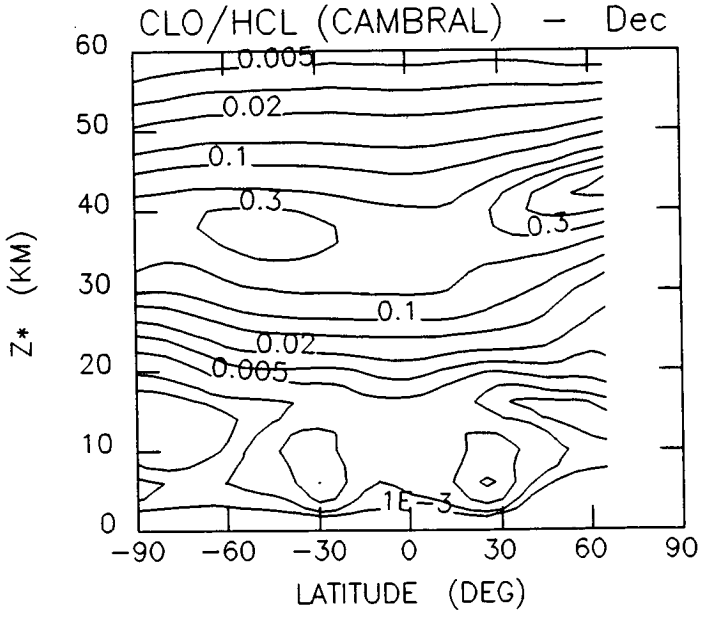
CLO/HCL (CAMBRAL) – Dec
Z* (KM)
LATITUDE (DEG)
0.005
0.02
0.1
0.3
0.3
0.1
0.02
0.005
1E-3

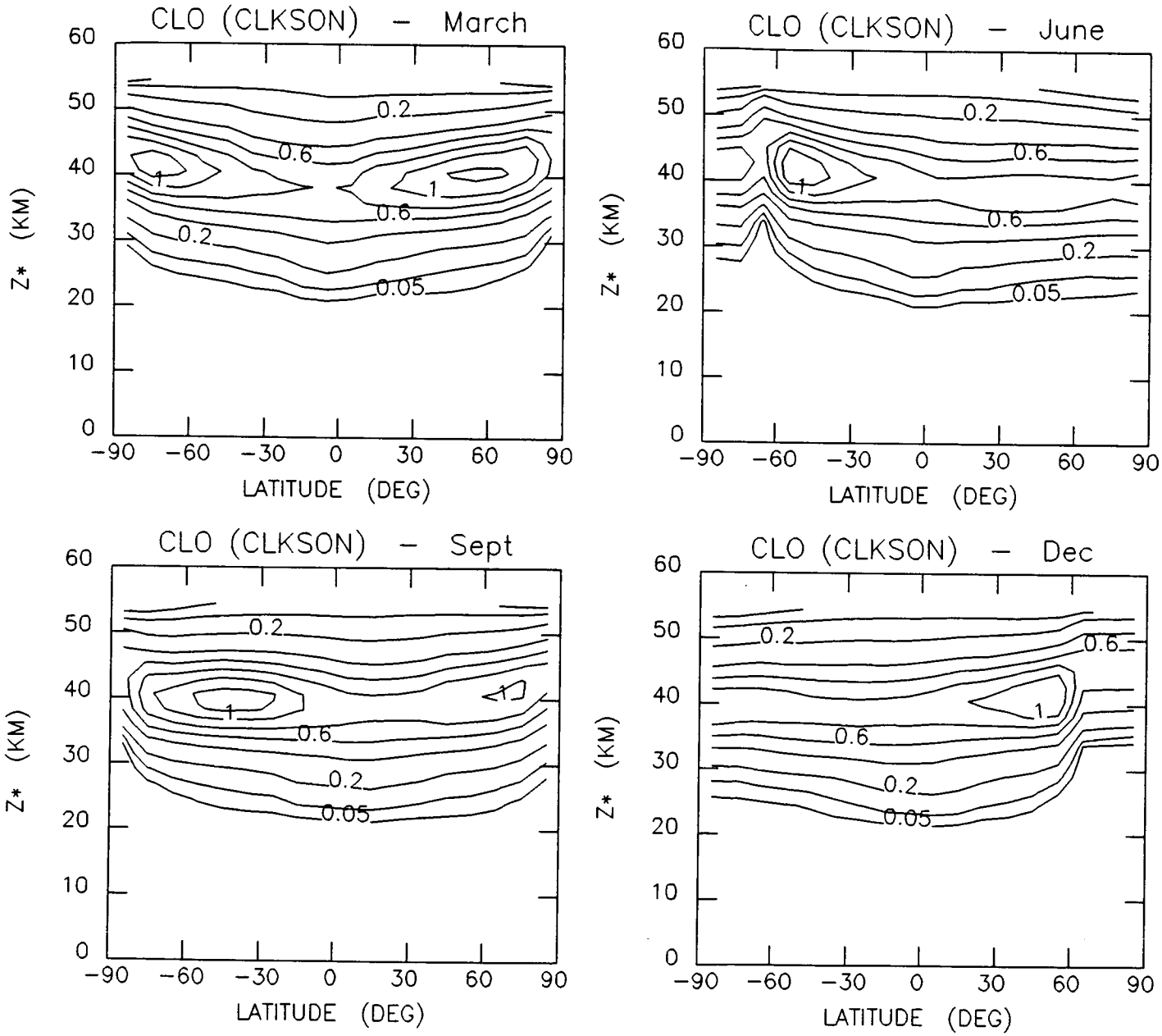
CLO (CLKSON) – March
CLO (CLKSON) – June
CLO (CLKSON) – Sept
CLO (CLKSON) – Dec
Z* (KM)
LATITUDE (DEG)
0
10
20
30
40
50
60
-90
-60
-30
0
30
60
90
0.2
0.6
1
0.05

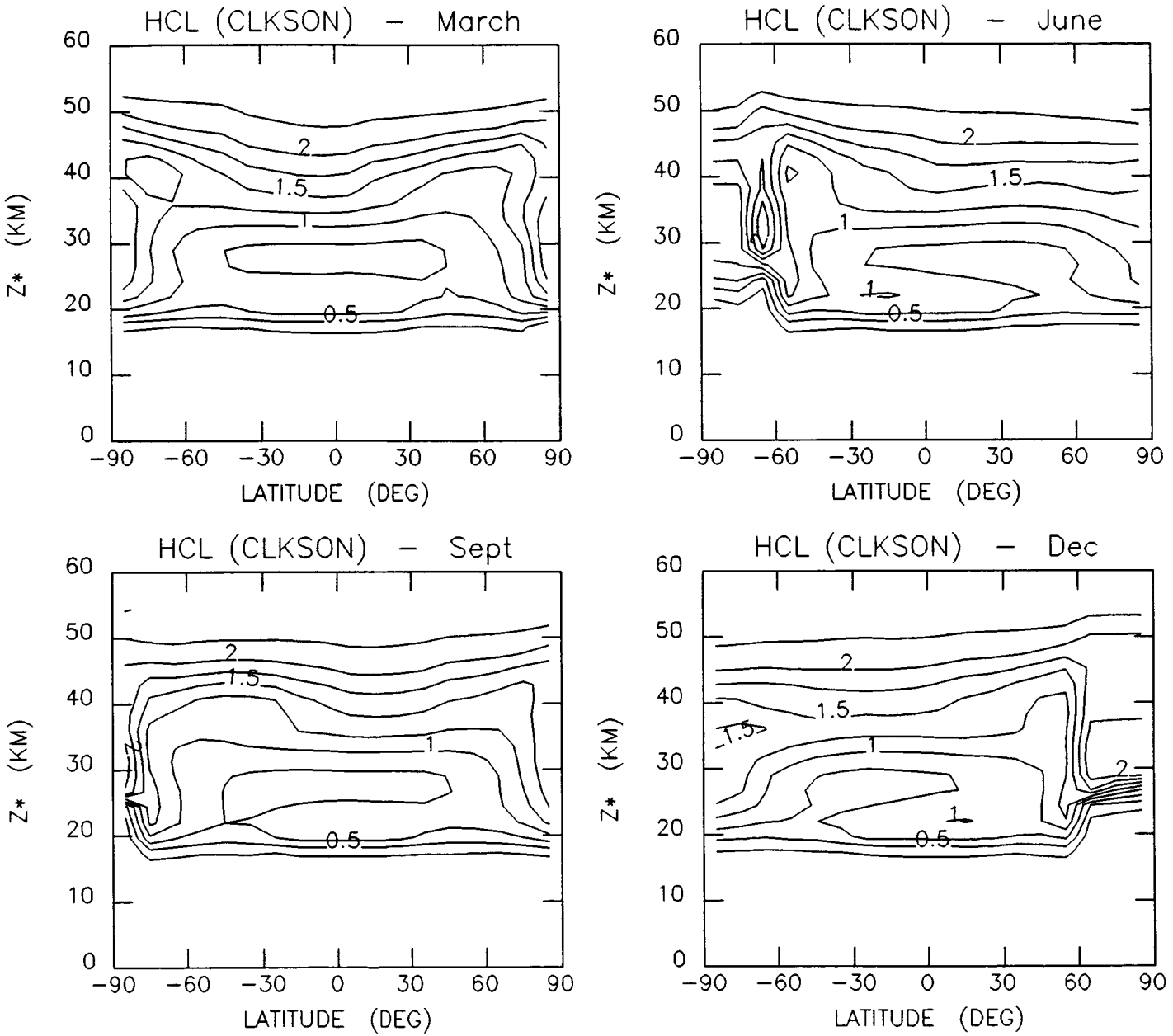
HCL (CLKSON) – March
HCL (CLKSON) – June
HCL (CLKSON) – Sept
HCL (CLKSON) – Dec
Z* (KM)
LATITUDE (DEG)
0
10
20
30
40
50
60
-90
-60
-30
0
30
60
90
0.5
1
1.5
2

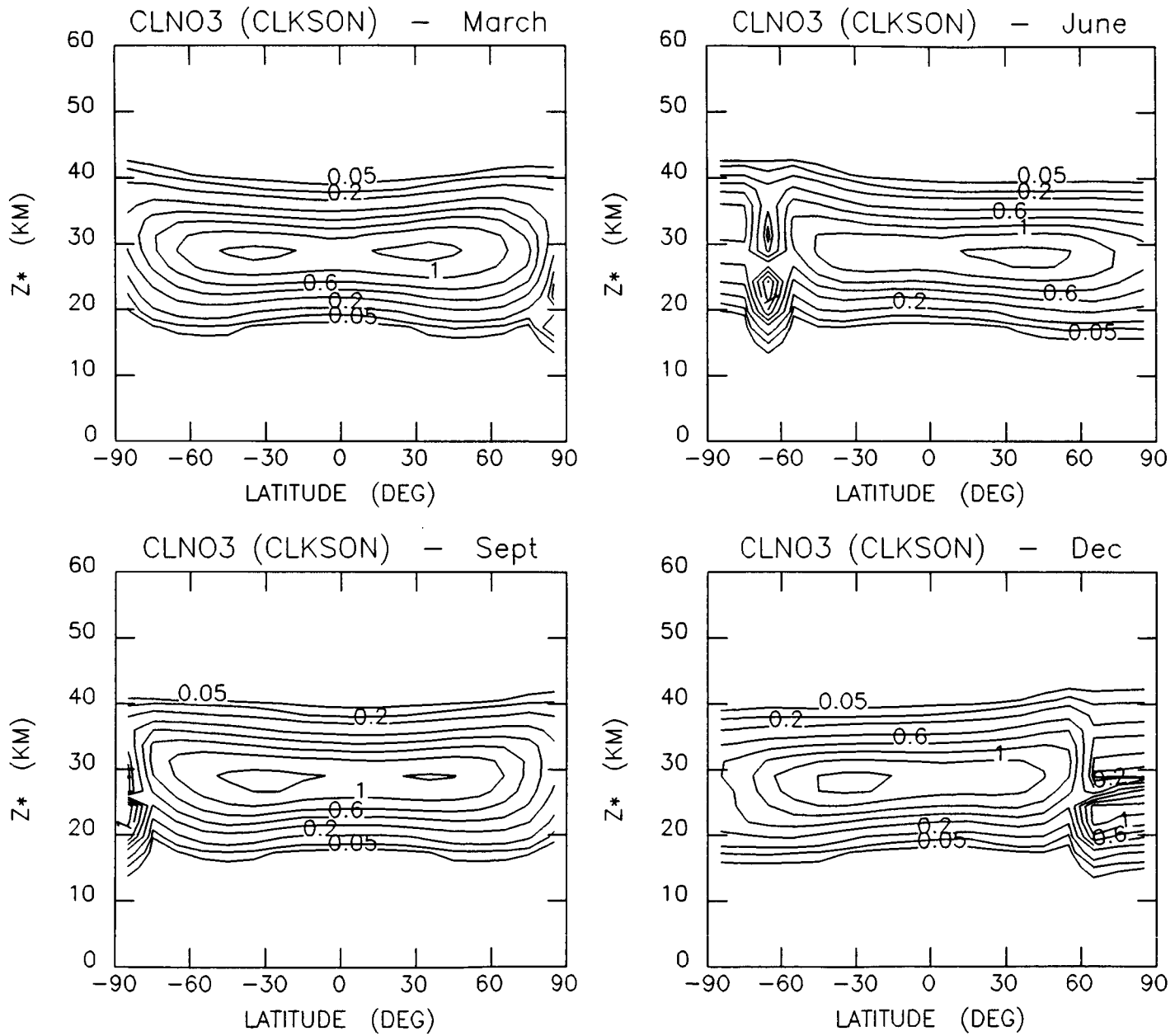
CLNO3 (CLKSON) – March
CLNO3 (CLKSON) – June
CLNO3 (CLKSON) – Sept
CLNO3 (CLKSON) – Dec
Z* (KM)
LATITUDE (DEG)
0
10
20
30
40
50
60
-90
-60
-30
0
30
60
90
0.05
0.2
0.6
1

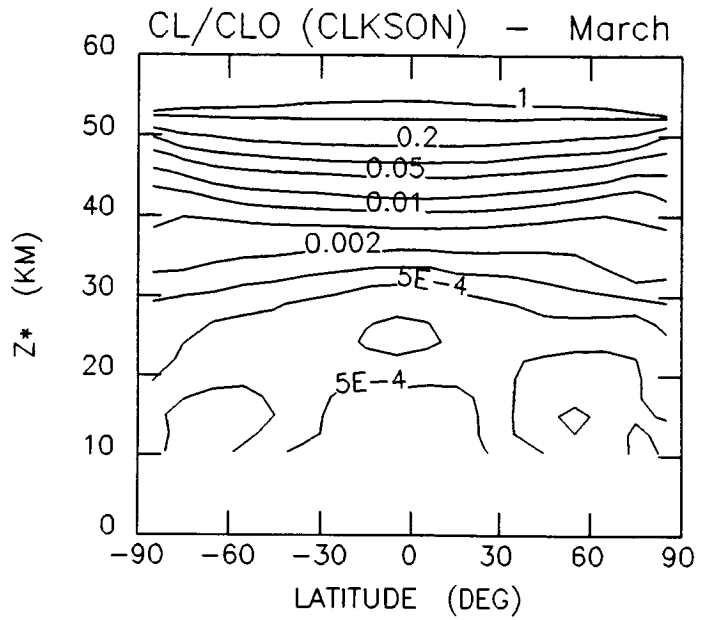
CL/CLO (CLKSON) – March
Z* (KM)
LATITUDE (DEG)
1
0.2
0.05
0.01
0.002
5E-4
5E-4

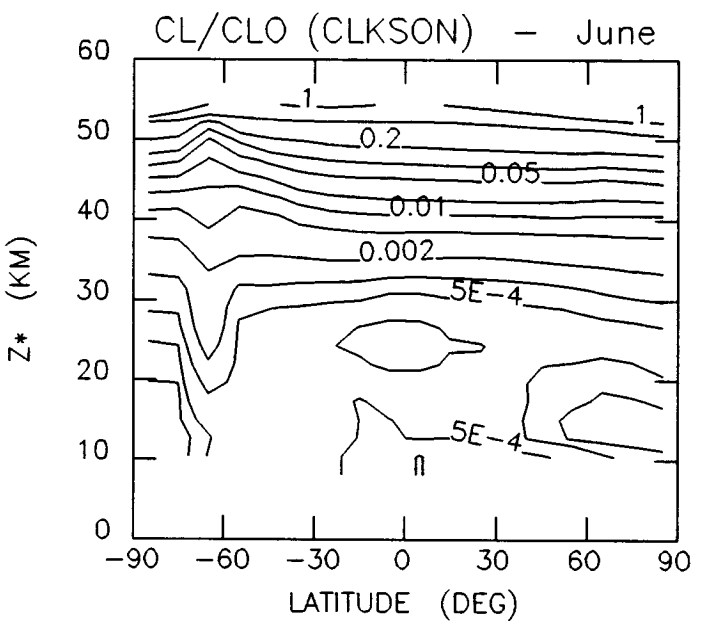
CL/CLO (CLKSON) – June
Z* (KM)
LATITUDE (DEG)
1
1
0.2
0.05
0.01
0.002
5E-4
5E-4

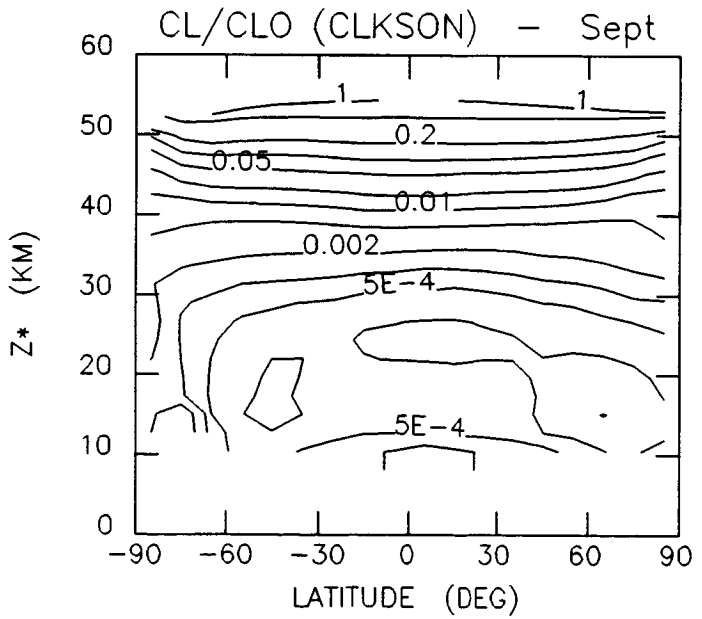
CL/CLO (CLKSON) – Sept
Z* (KM)
LATITUDE (DEG)
1
1
0.2
0.05
0.01
0.002
5E-4
5E-4

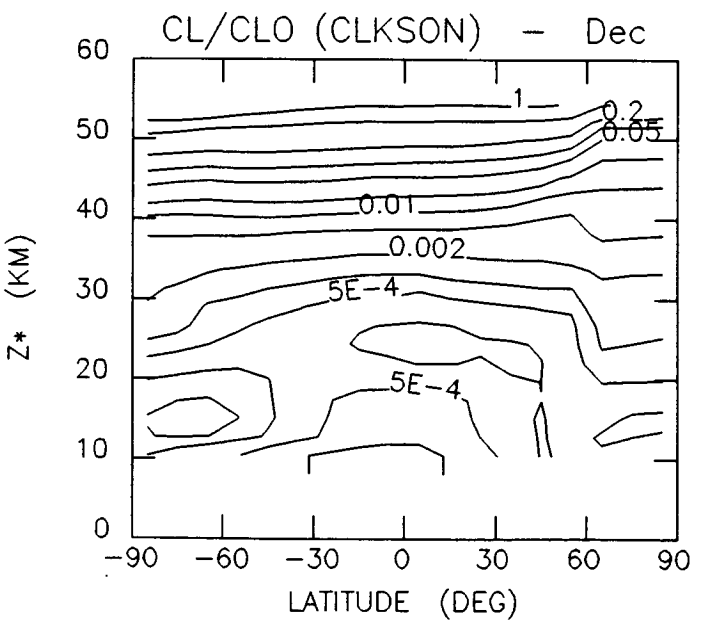
CL/CLO (CLKSON) – Dec
Z* (KM)
LATITUDE (DEG)
1
0.2
0.05
0.01
0.002
5E-4
5E-4

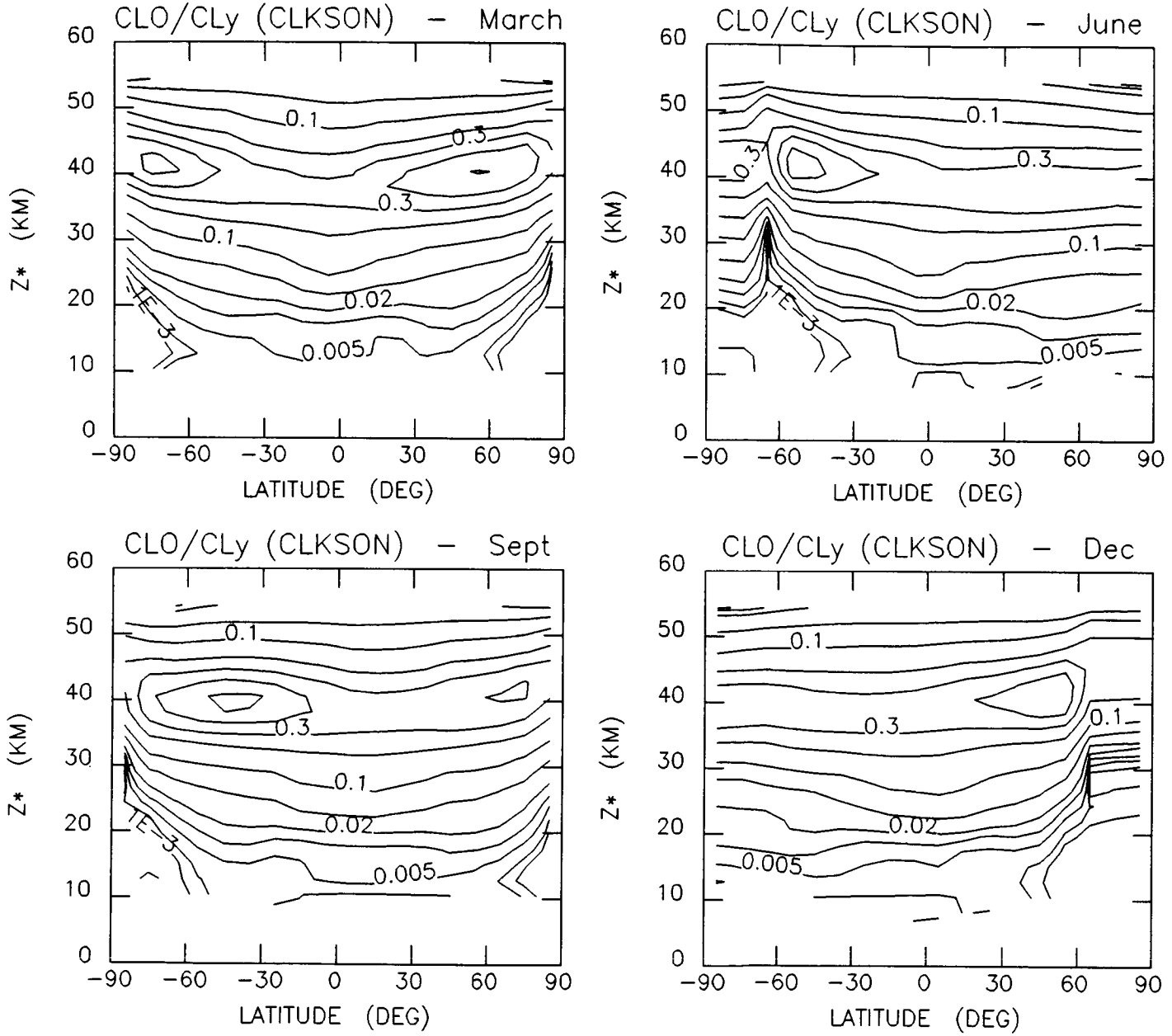
CLO/CLy (CLKSON) – March
CLO/CLy (CLKSON) – June
CLO/CLy (CLKSON) – Sept
CLO/CLy (CLKSON) – Dec
Z* (KM)
LATITUDE (DEG)
0.1
0.3
0.02
0.005
1E-3

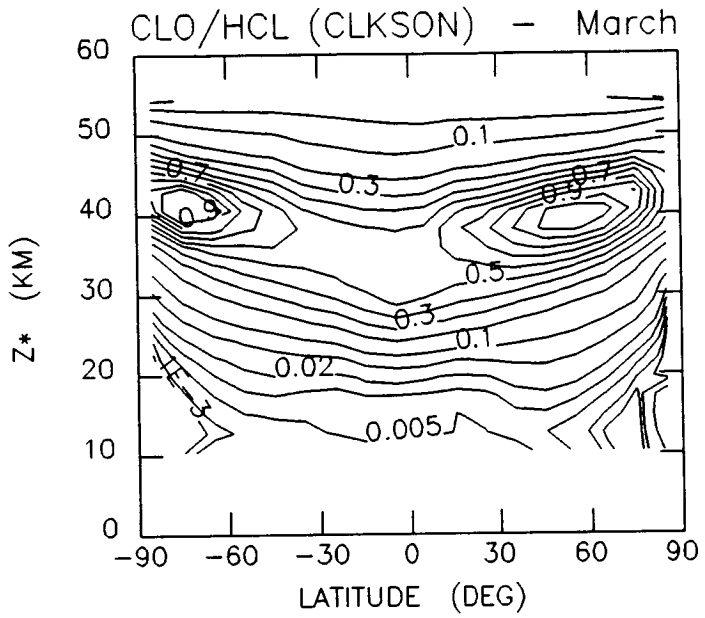
CLO/HCL (CLKSON) – March
Z* (KM)
LATITUDE (DEG)
0.1
0.3
0.5
0.7
0.9
0.02
0.005

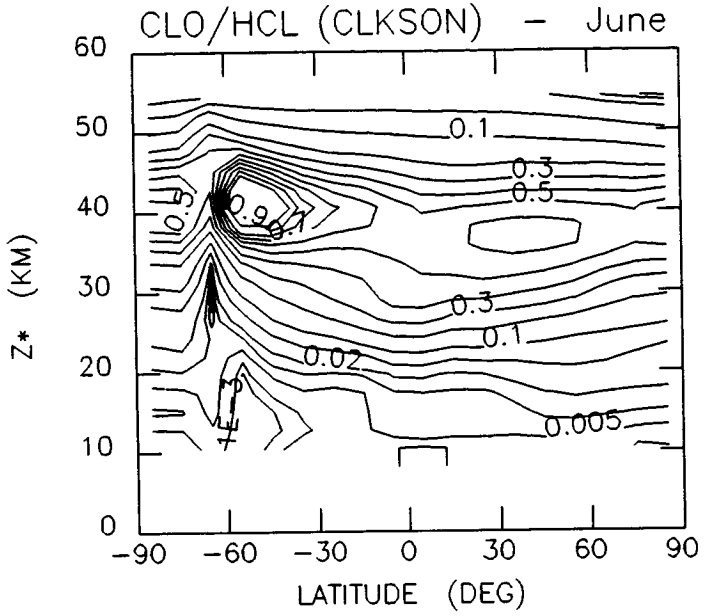
CLO/HCL (CLKSON) – June
Z* (KM)
LATITUDE (DEG)
0.1
0.3
0.5
0.9
0.02
0.005

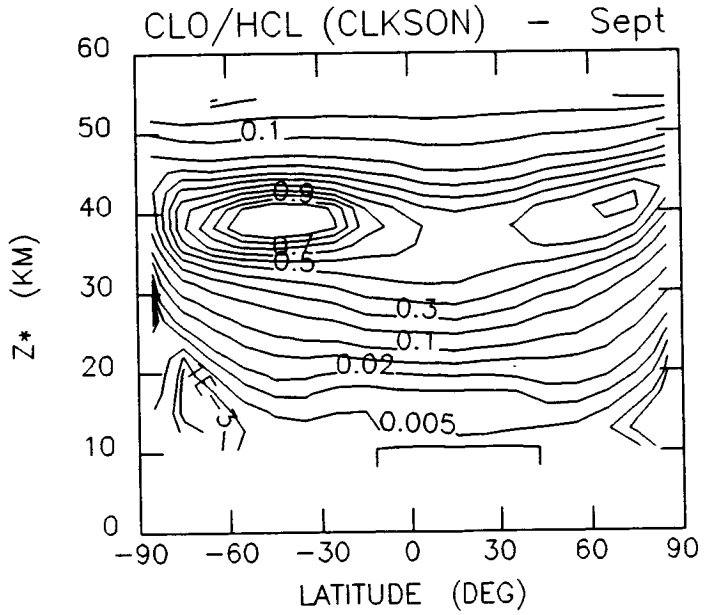
CLO/HCL (CLKSON) – Sept
Z* (KM)
LATITUDE (DEG)
0.1
0.3
0.5
0.7
0.9
0.02
0.005

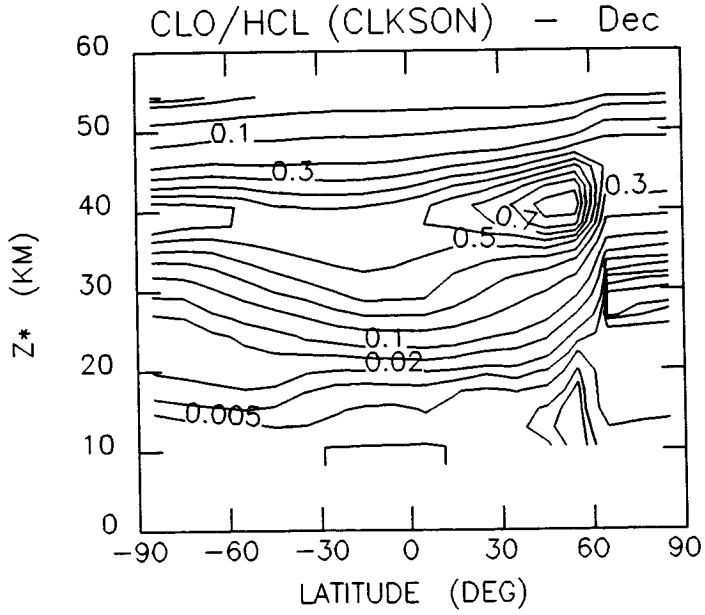
CLO/HCL (CLKSON) – Dec
Z* (KM)
LATITUDE (DEG)
0.1
0.3
0.5
0.7
0.02
0.005

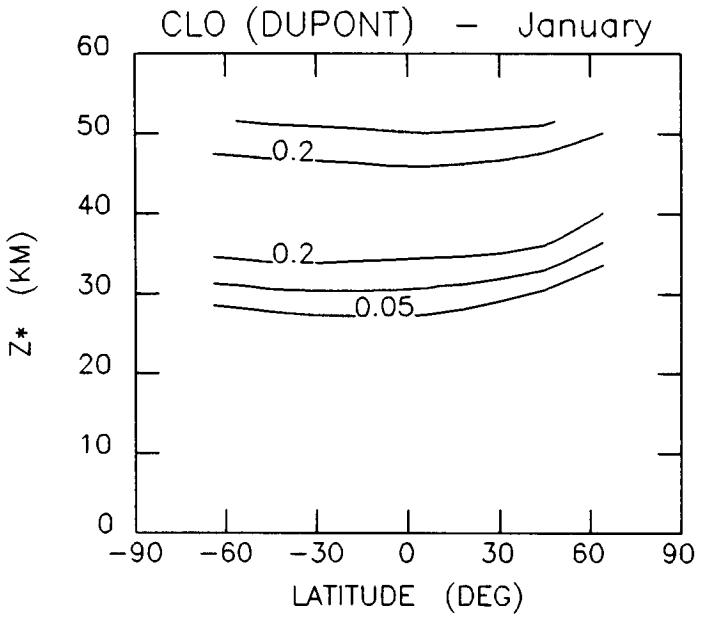
CLO (DUPONT) – January
Z* (KM)
LATITUDE (DEG)
0.2
0.2
0.05

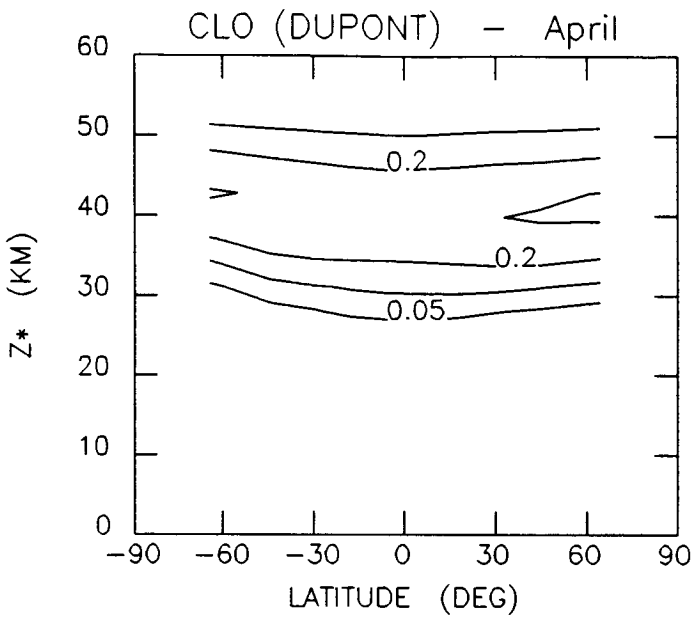
CLO (DUPONT) – April
Z* (KM)
LATITUDE (DEG)
0.2
0.2
0.05

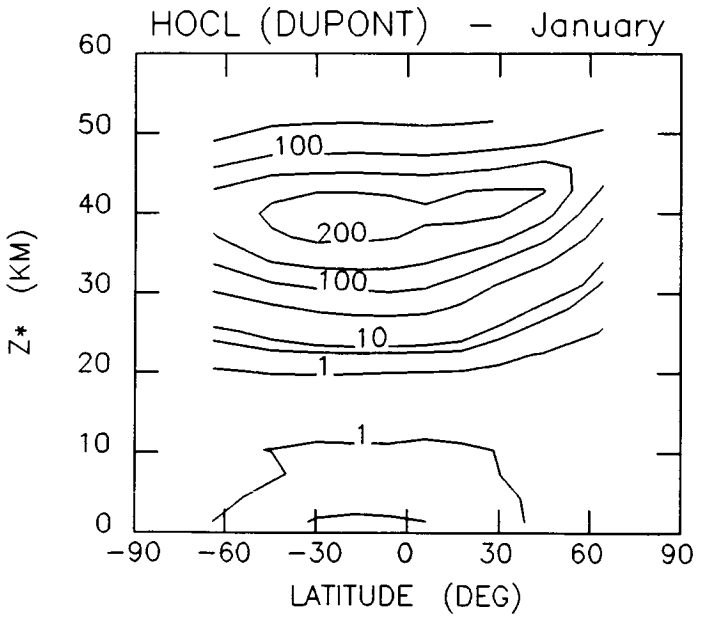
HOCL (DUPONT) – January
Z* (KM)
LATITUDE (DEG)
100
200
100
10
1
1

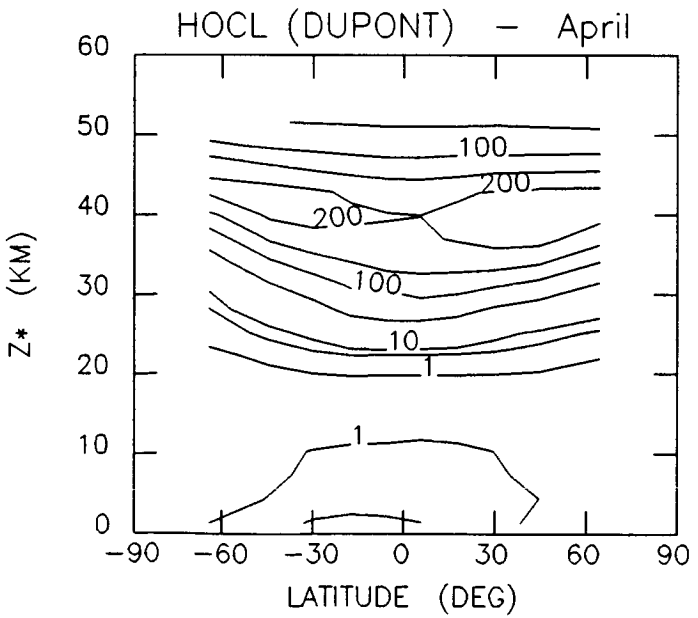
HOCL (DUPONT) – April
Z* (KM)
LATITUDE (DEG)
100
200
200
100
10
1
1

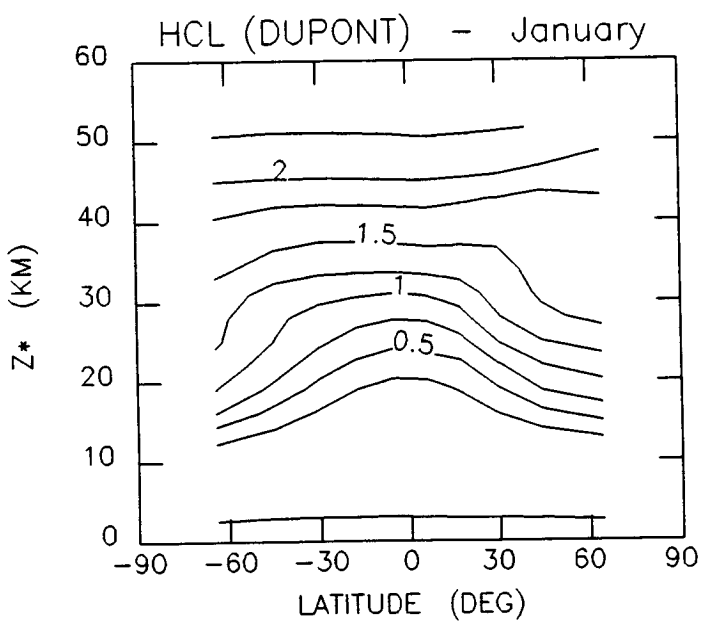
HCL (DUPONT) – January
Z* (KM)
LATITUDE (DEG)
2
1.5
1
0.5

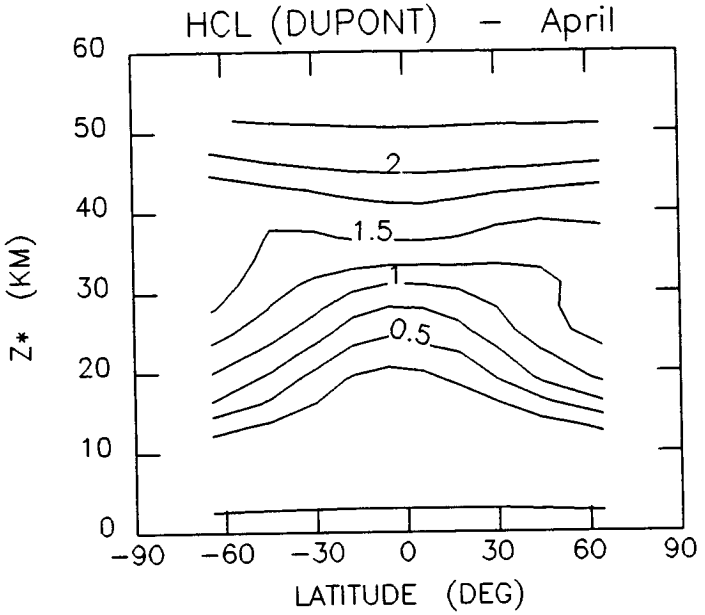
HCL (DUPONT) – April
Z* (KM)
LATITUDE (DEG)
2
1.5
1
0.5

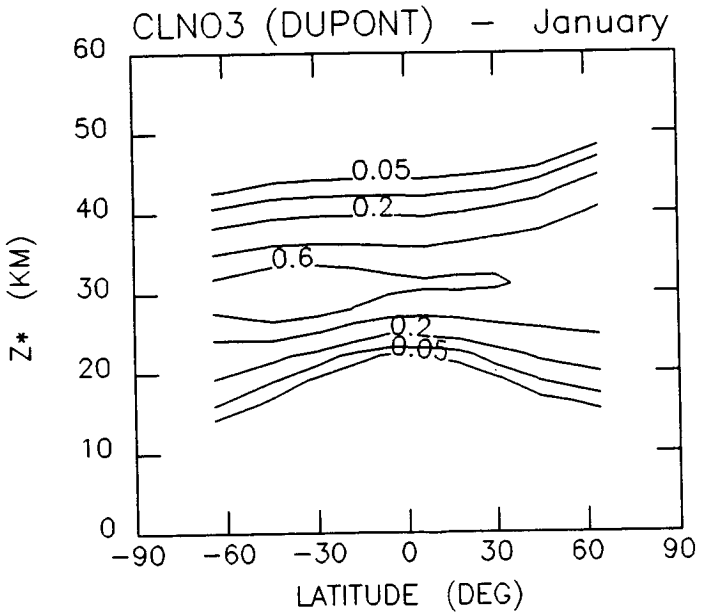
CLNO3 (DUPONT) – January
Z* (KM)
LATITUDE (DEG)
0.05
0.2
0.6
0.2
0.05

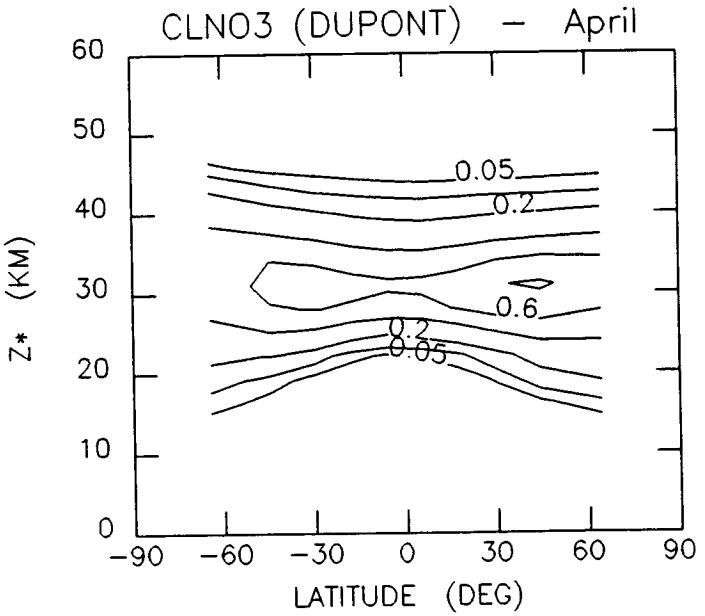
CLNO3 (DUPONT) – April
Z* (KM)
LATITUDE (DEG)
0.05
0.2
0.6
0.2
0.05

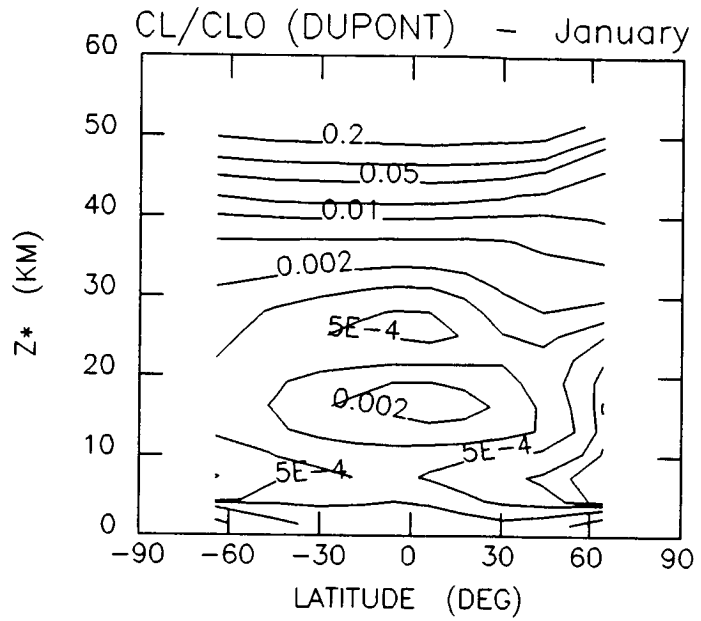
CL/CLO (DUPONT) – January
Z* (KM)
LATITUDE (DEG)
0.2
0.05
0.01
0.002
5E-4
0.002
5E-4
5E-4
60
50
40
30
20
10
0
-90
-60
-30
0
30
60
90

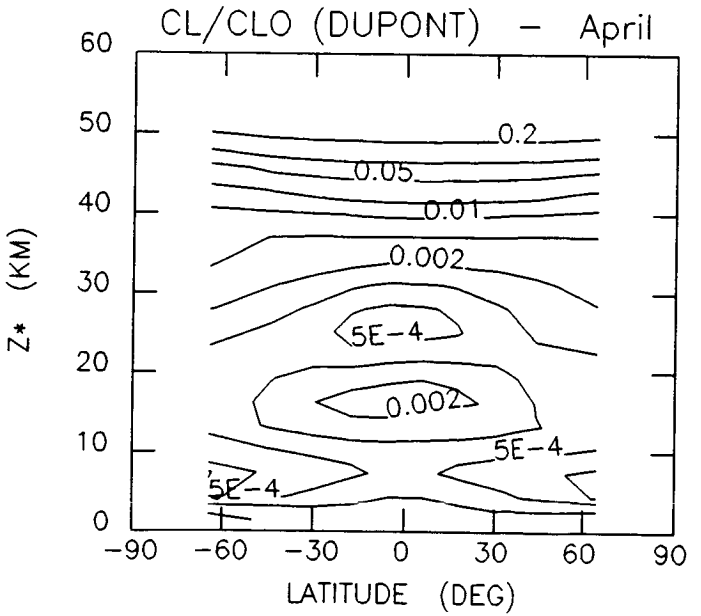
CL/CLO (DUPONT) – April
Z* (KM)
LATITUDE (DEG)
0.2
0.05
0.01
0.002
5E-4
0.002
5E-4
5E-4
60
50
40
30
20
10
0
-90
-60
-30
0
30
60
90

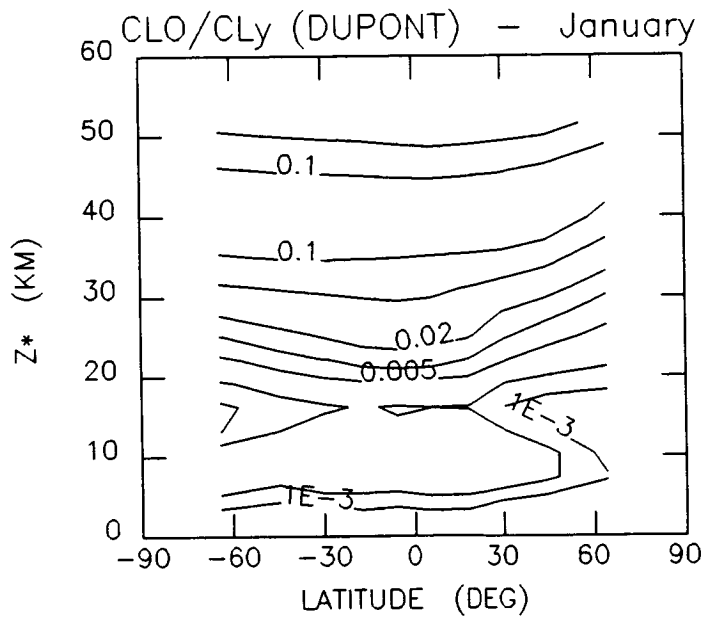
CLO/CLy (DUPONT) – January
Z* (KM)
LATITUDE (DEG)
0.1
0.1
0.02
0.005
1E-3
1E-3

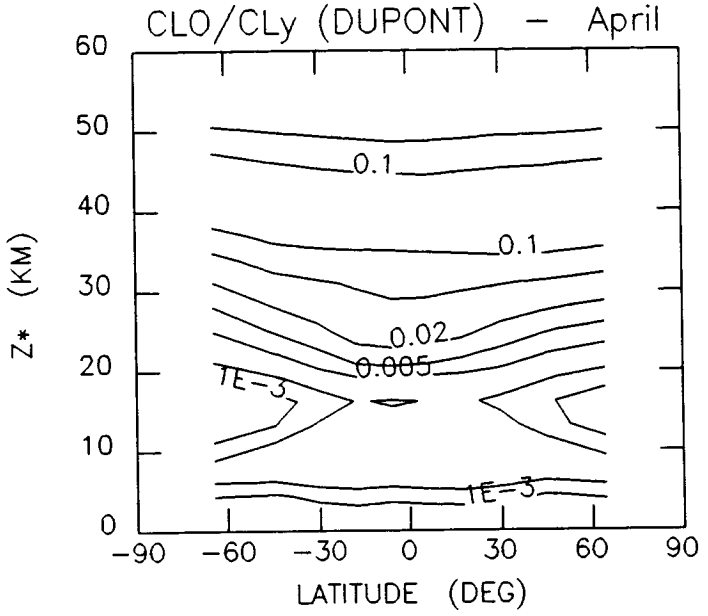
CLO/CLy (DUPONT) – April
Z* (KM)
LATITUDE (DEG)
0.1
0.1
0.02
0.005
1E-3
1E-3

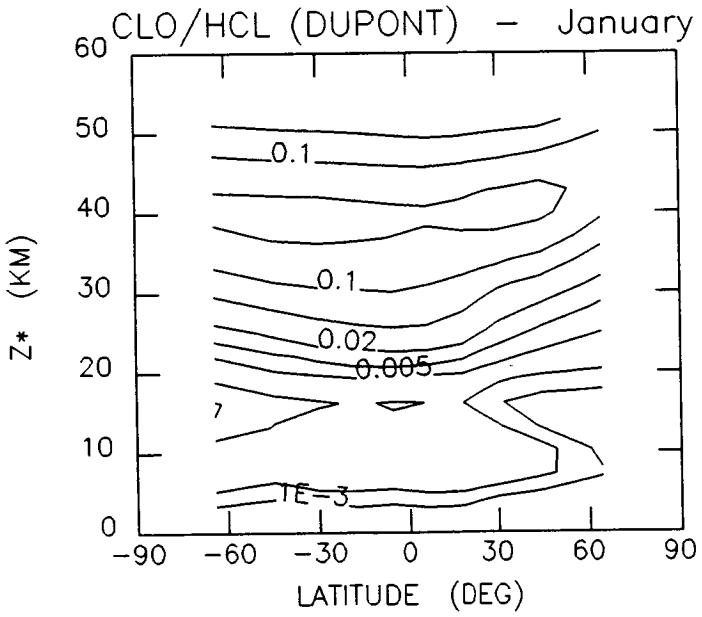
CLO/HCL (DUPONT) – January
Z* (KM)
LATITUDE (DEG)
0.1
0.1
0.02
0.005
1E-3

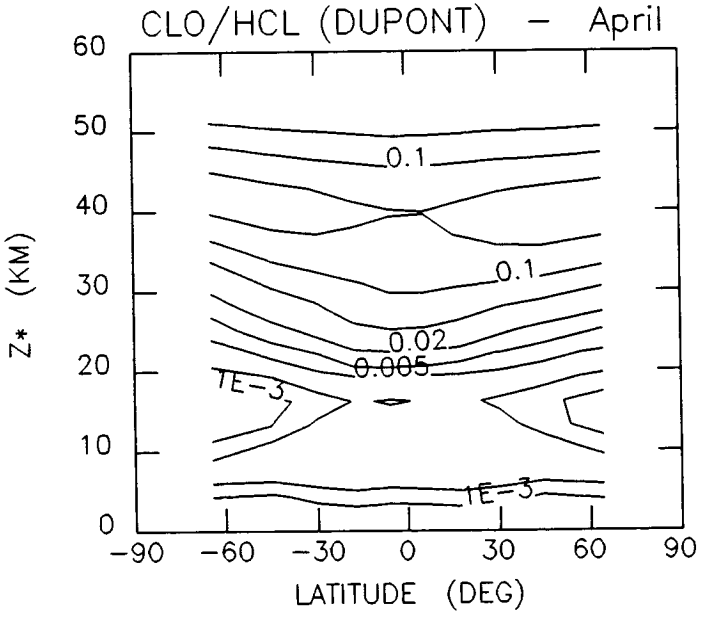
CLO/HCL (DUPONT) – April
Z* (KM)
LATITUDE (DEG)
0.1
0.1
0.02
0.005
1E-3
1E-3

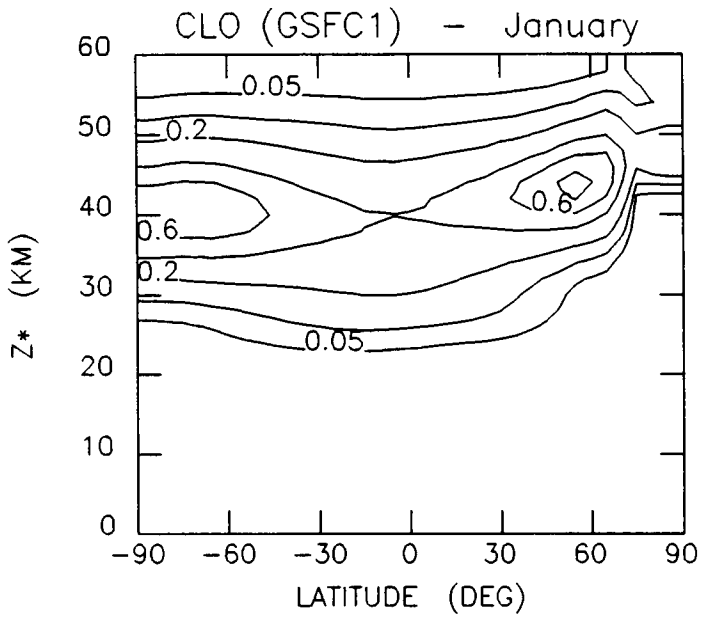
CLO (GSFC1) – January
Z* (KM)
LATITUDE (DEG)
0.05
0.2
0.6
0.6
0.2
0.05

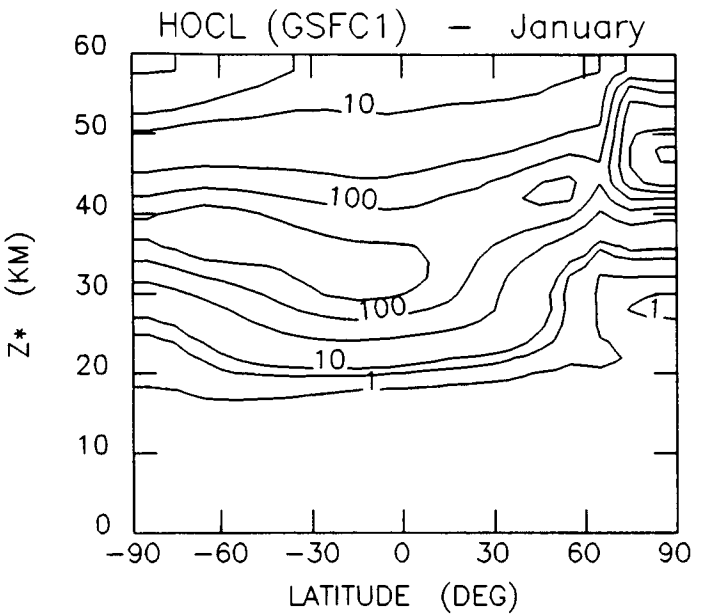
HOCL (GSFC1) – January
Z* (KM)
LATITUDE (DEG)
10
100
100
1
10
1

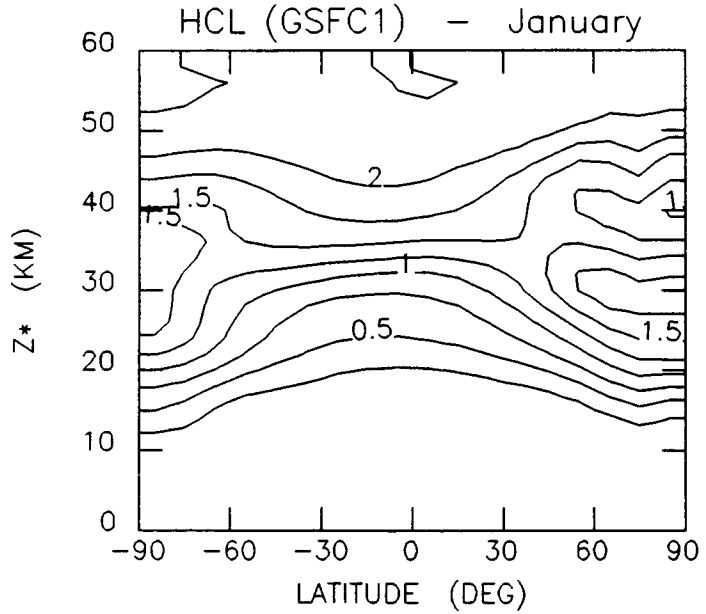
HCL (GSFC1) – January
Z* (KM)
LATITUDE (DEG)
2
1.5
1.5
1
1
0.5
1.5

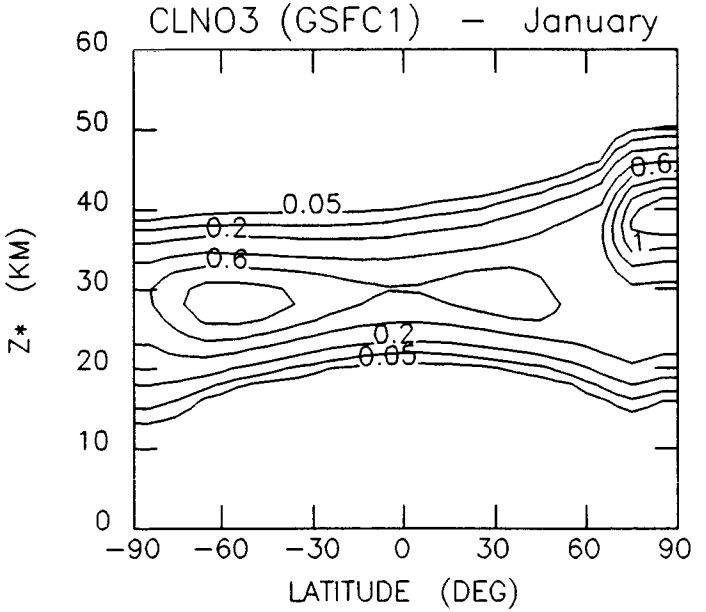
CLNO3 (GSFC1) – January
Z* (KM)
LATITUDE (DEG)
0.6
0.05
0.2
0.6
1
0.2
0.05

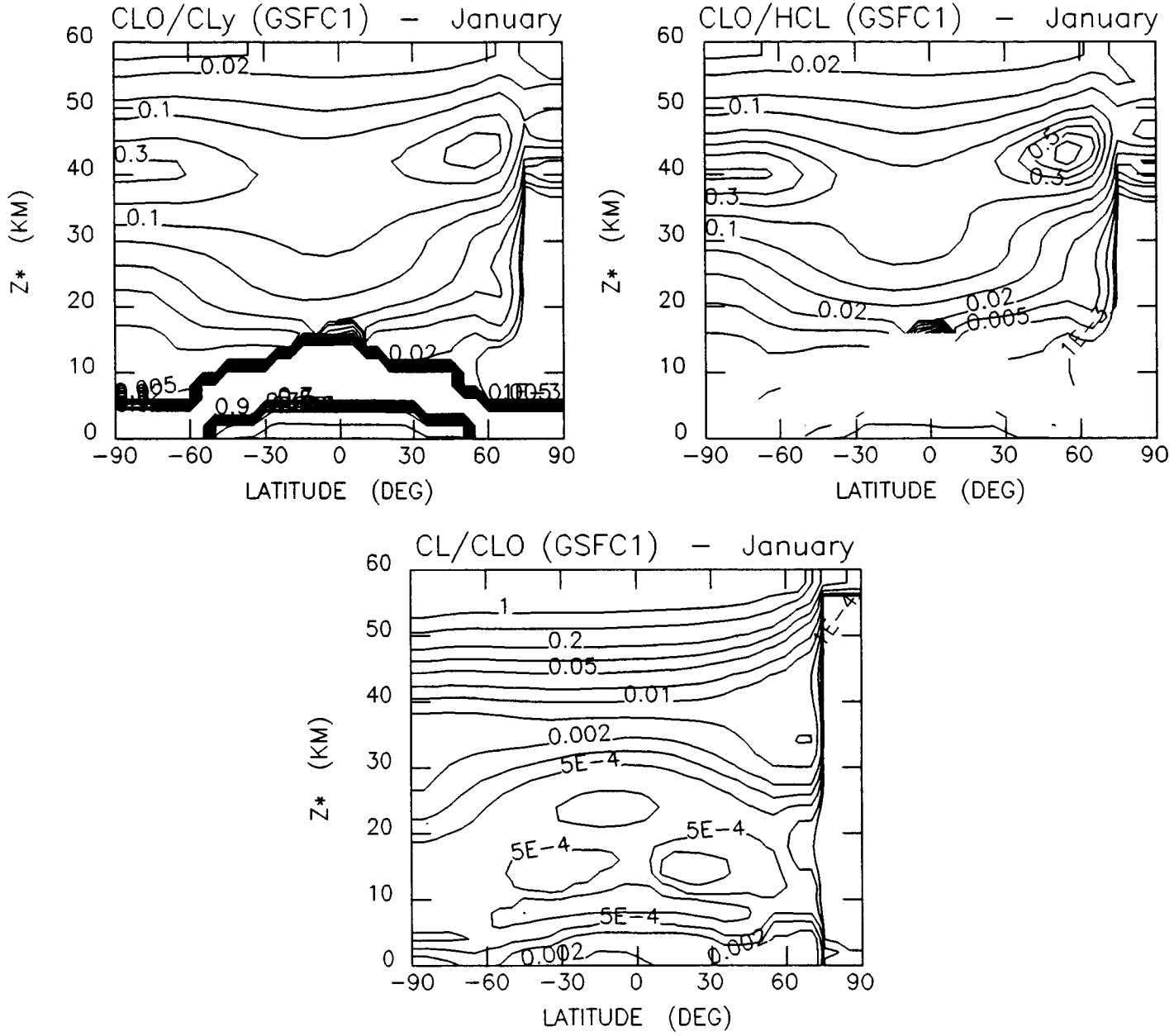
CLO/CLy (GSFC1) – January
Z* (KM)
LATITUDE (DEG)
0.02
0.1
0.3
0.1
0.02
0.9
CLO/HCL (GSFC1) – January
Z* (KM)
LATITUDE (DEG)
0.02
0.1
0.3
0.3
0.1
0.02
0.02
0.005
CL/CLO (GSFC1) – January
Z* (KM)
LATITUDE (DEG)
1
0.2
0.05
0.01
0.002
5E-4
0
5E-4
5E-4
5E-4
0.002
0.002

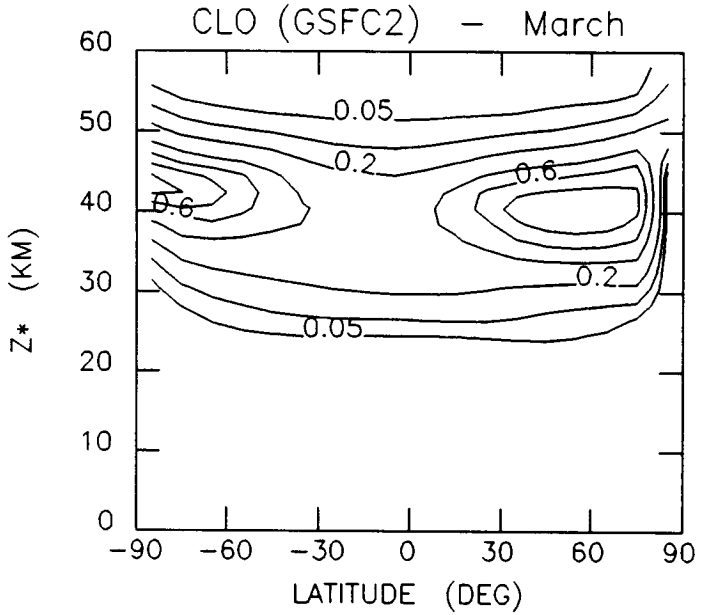
CLO (GSFC2) – March
Z* (KM)
LATITUDE (DEG)
0.05
0.2
0.6

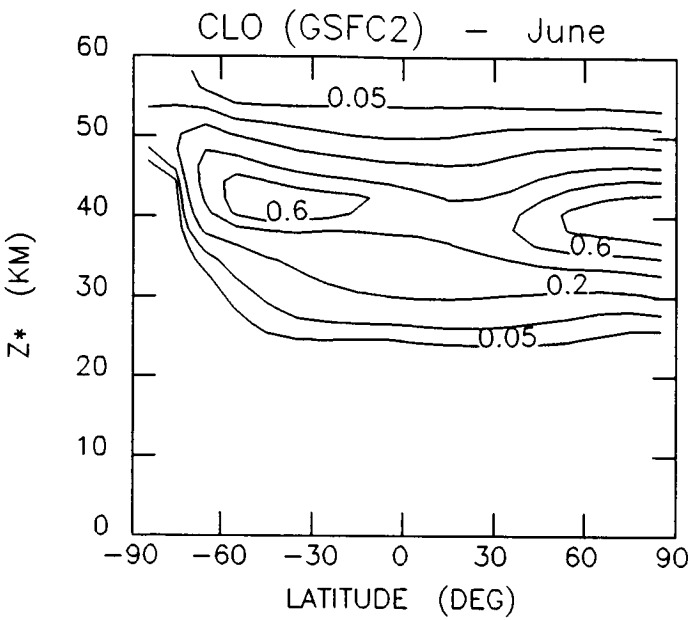
CLO (GSFC2) – June
Z* (KM)
LATITUDE (DEG)
0.05
0.6
0.2

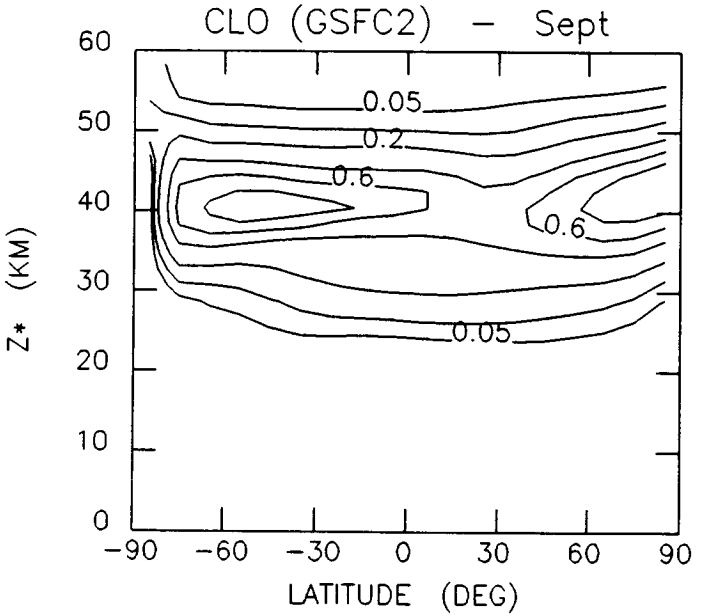
CLO (GSFC2) – Sept
Z* (KM)
LATITUDE (DEG)
0.05
0.2
0.6

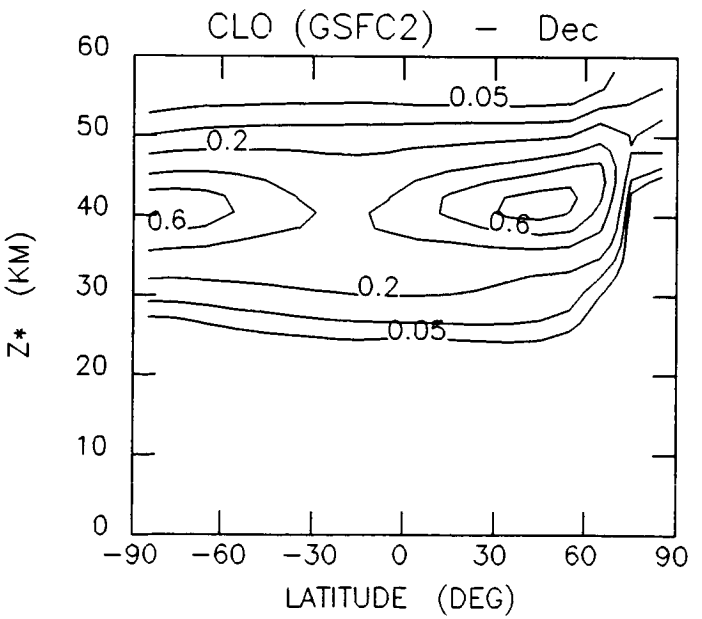
CLO (GSFC2) – Dec
Z* (KM)
LATITUDE (DEG)
0.05
0.2
0.6

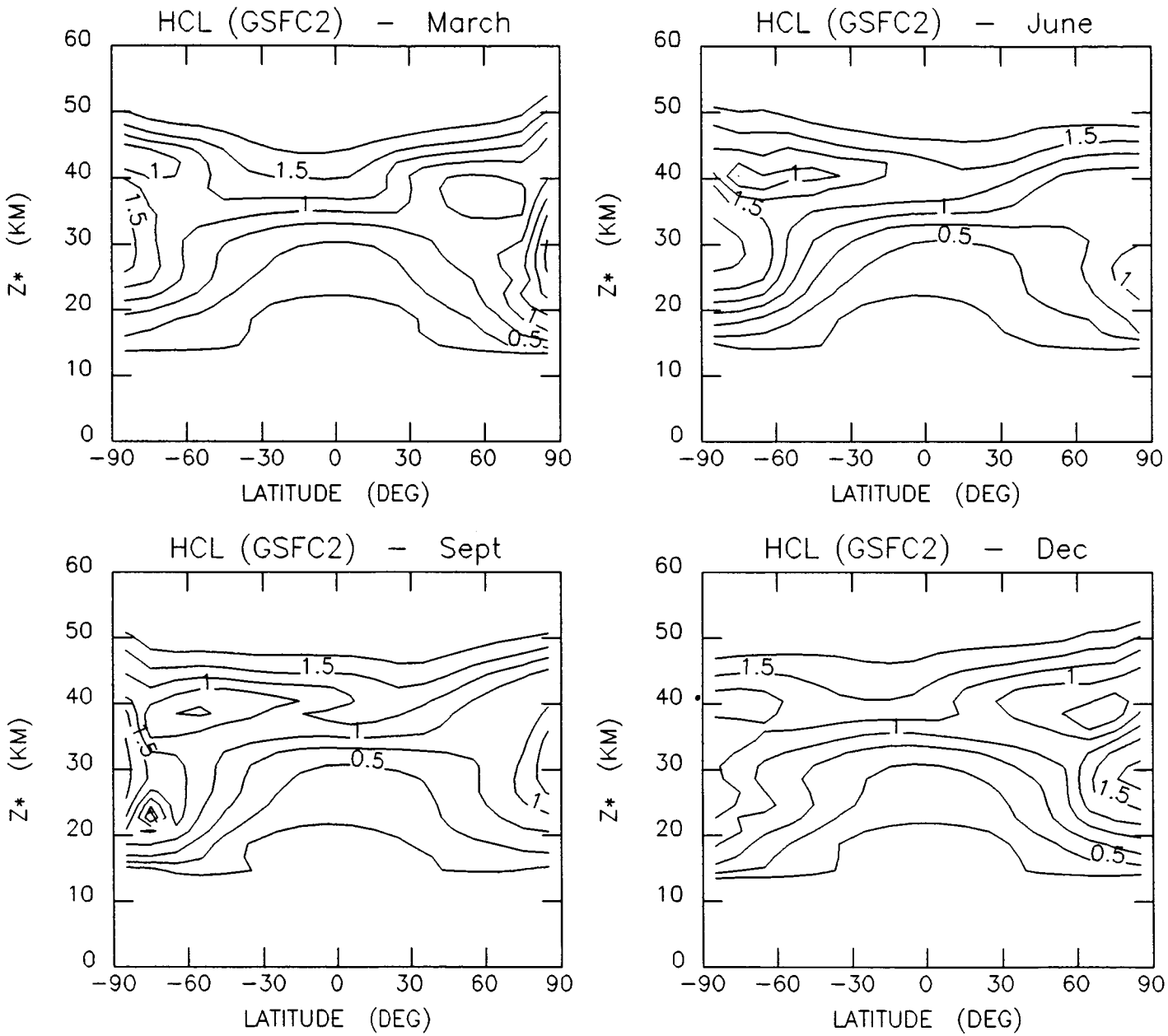
HCL (GSFC2) – March
HCL (GSFC2) – June
HCL (GSFC2) – Sept
HCL (GSFC2) – Dec
Z* (KM)
LATITUDE (DEG)
60
50
40
30
20
10
0
-90 -60 -30 0 30 60 90
1.5
1
0.5

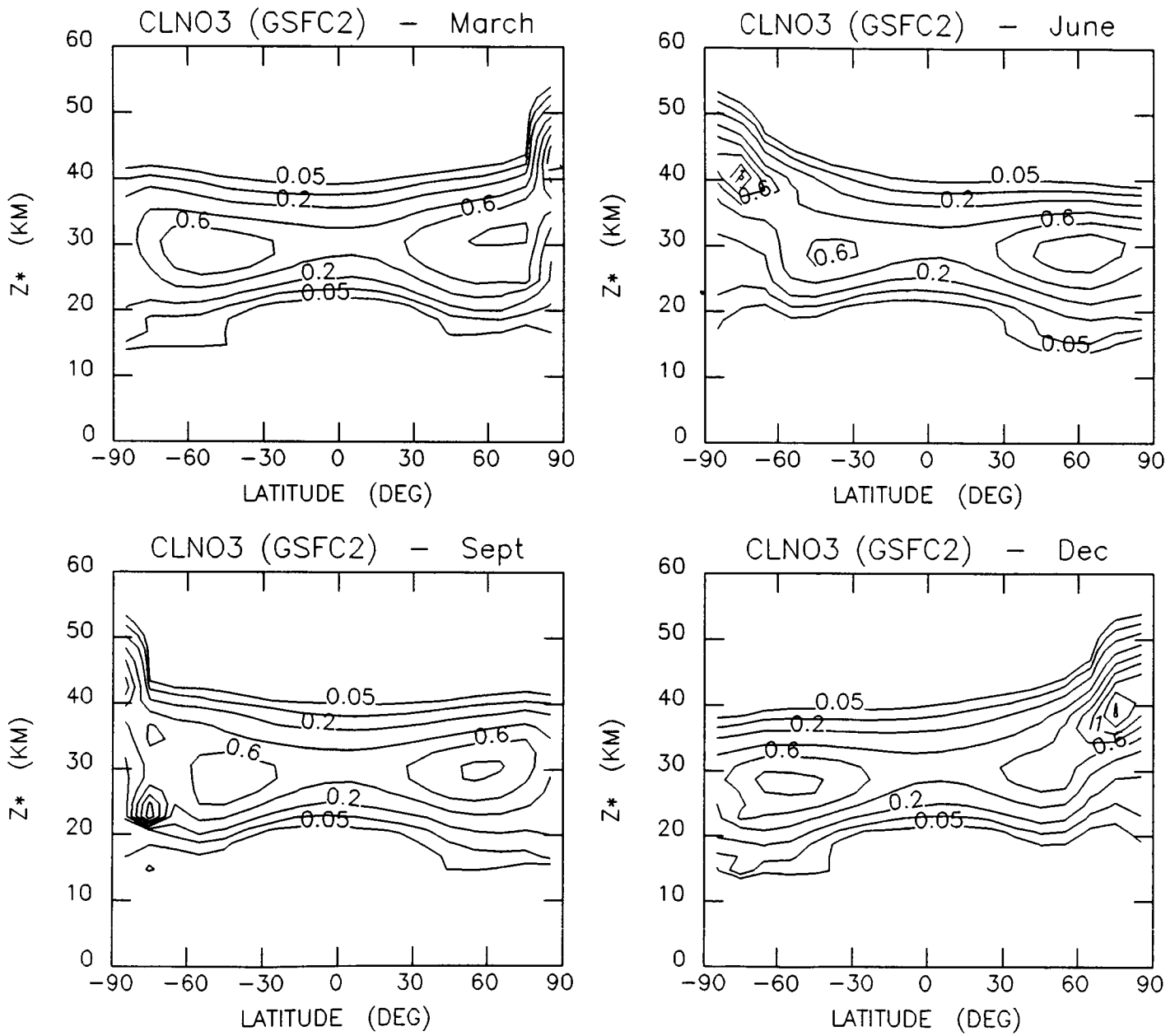
CLNO3 (GSFC2) – March
CLNO3 (GSFC2) – June
CLNO3 (GSFC2) – Sept
CLNO3 (GSFC2) – Dec
Z* (KM)
LATITUDE (DEG)
0
10
20
30
40
50
60
-90
-60
-30
0
30
60
90
0.05
0.2
0.6
1

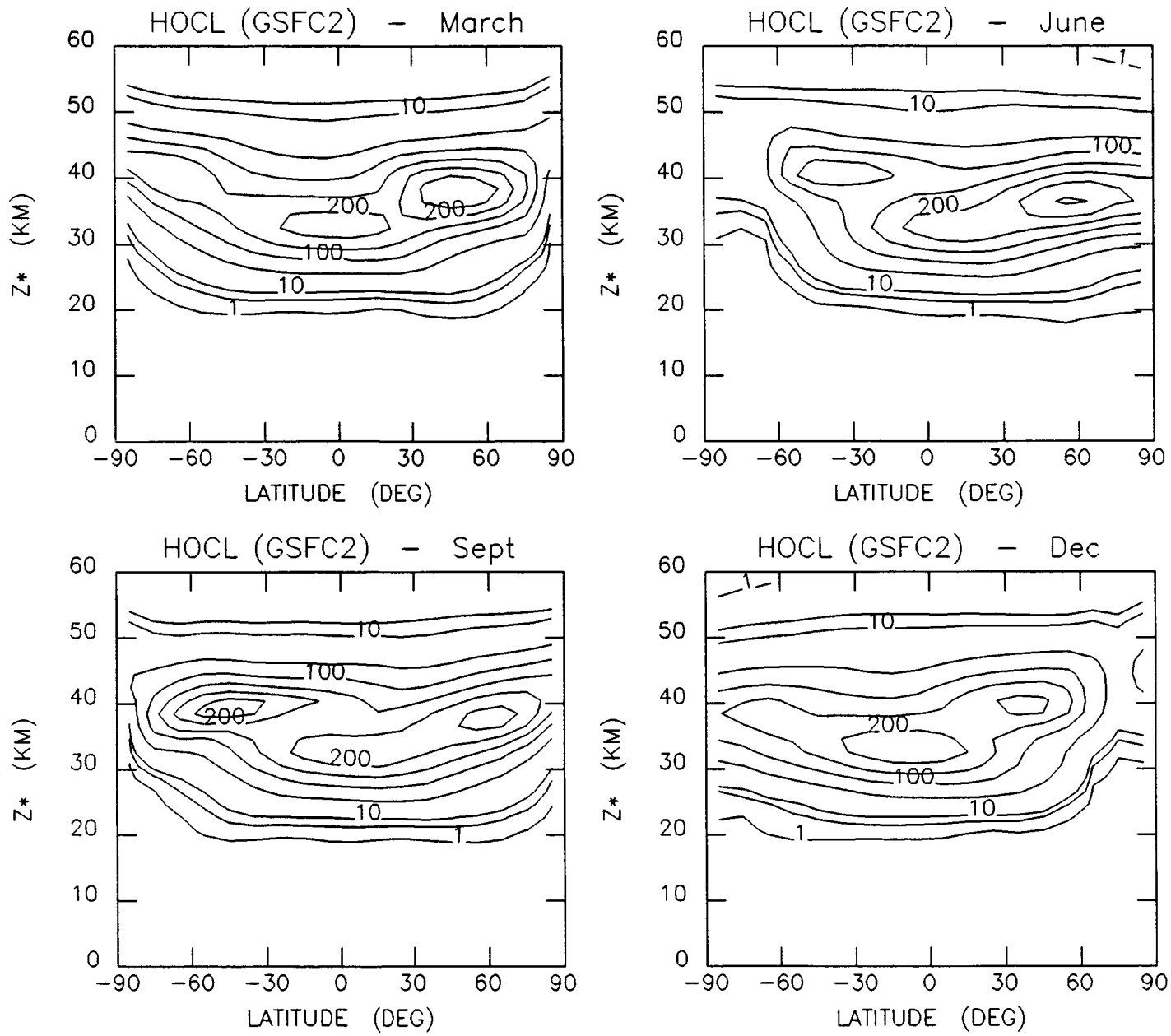
HOCL (GSFC2) – March
HOCL (GSFC2) – June
HOCL (GSFC2) – Sept
HOCL (GSFC2) – Dec
Z* (KM)
LATITUDE (DEG)
0
10
20
30
40
50
60
-90
-60
-30
0
30
60
90
1
10
100
200

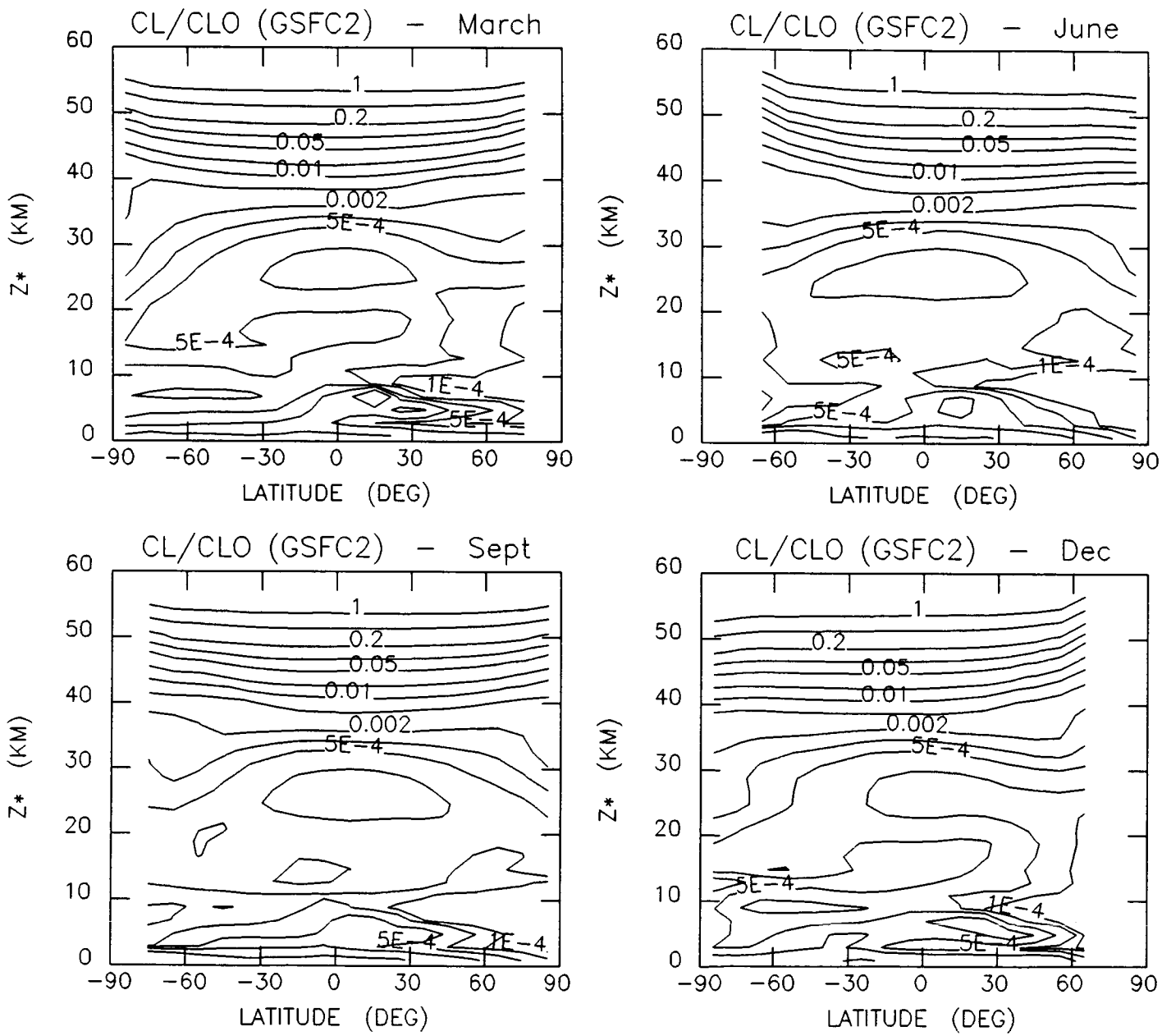
CL/CLO (GSFC2) – March
CL/CLO (GSFC2) – June
CL/CLO (GSFC2) – Sept
CL/CLO (GSFC2) – Dec
Z* (KM)
LATITUDE (DEG)
60
50
40
30
20
10
0
−90 −60 −30 0 30 60 90
1
0.2
0.05
0.01
0.002
5E−4
1E−4

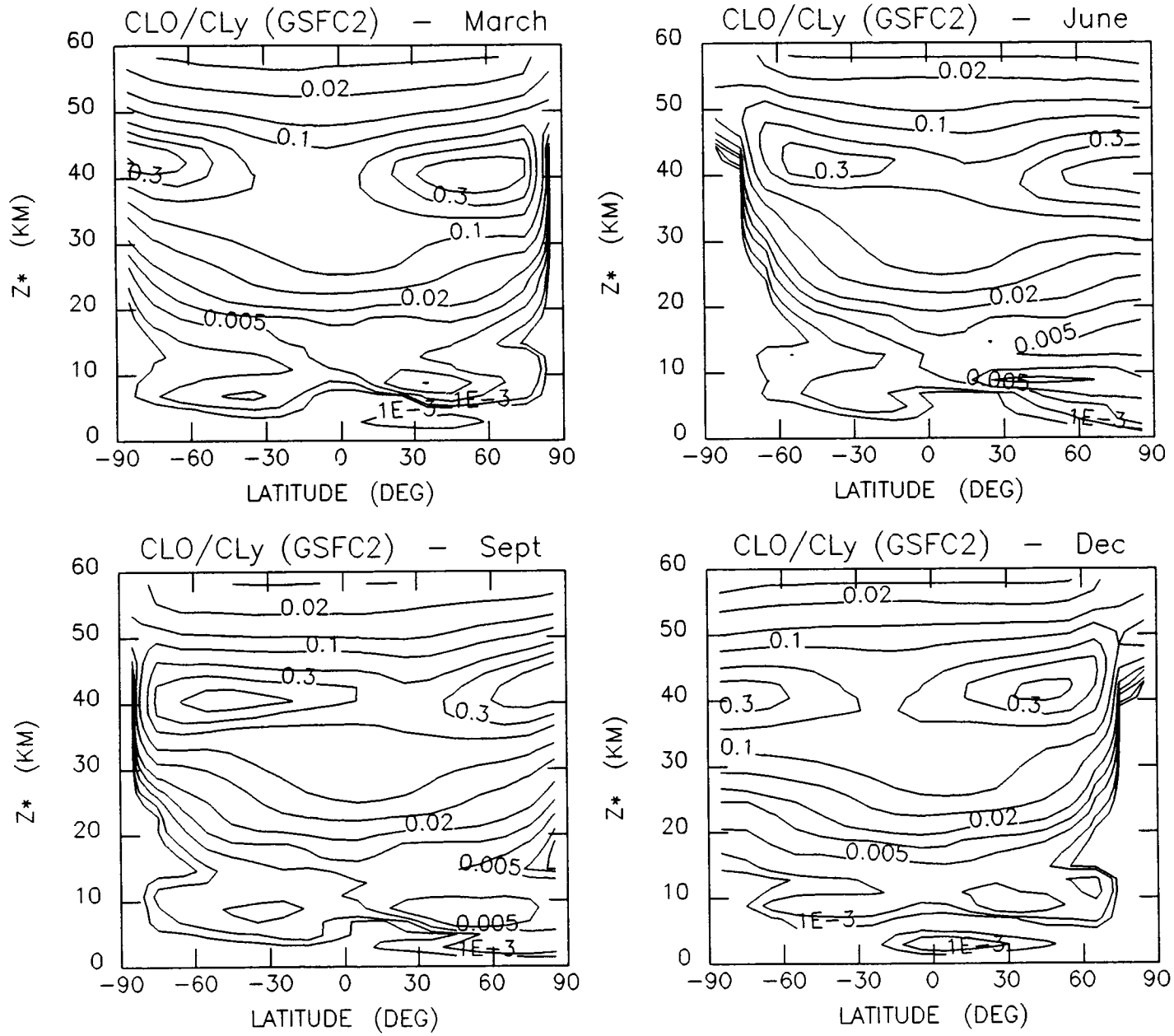
CLO/CLy (GSFC2) – March
CLO/CLy (GSFC2) – June
CLO/CLy (GSFC2) – Sept
CLO/CLy (GSFC2) – Dec
Z* (KM)
LATITUDE (DEG)
0.02
0.1
0.3
0.005
1E-3

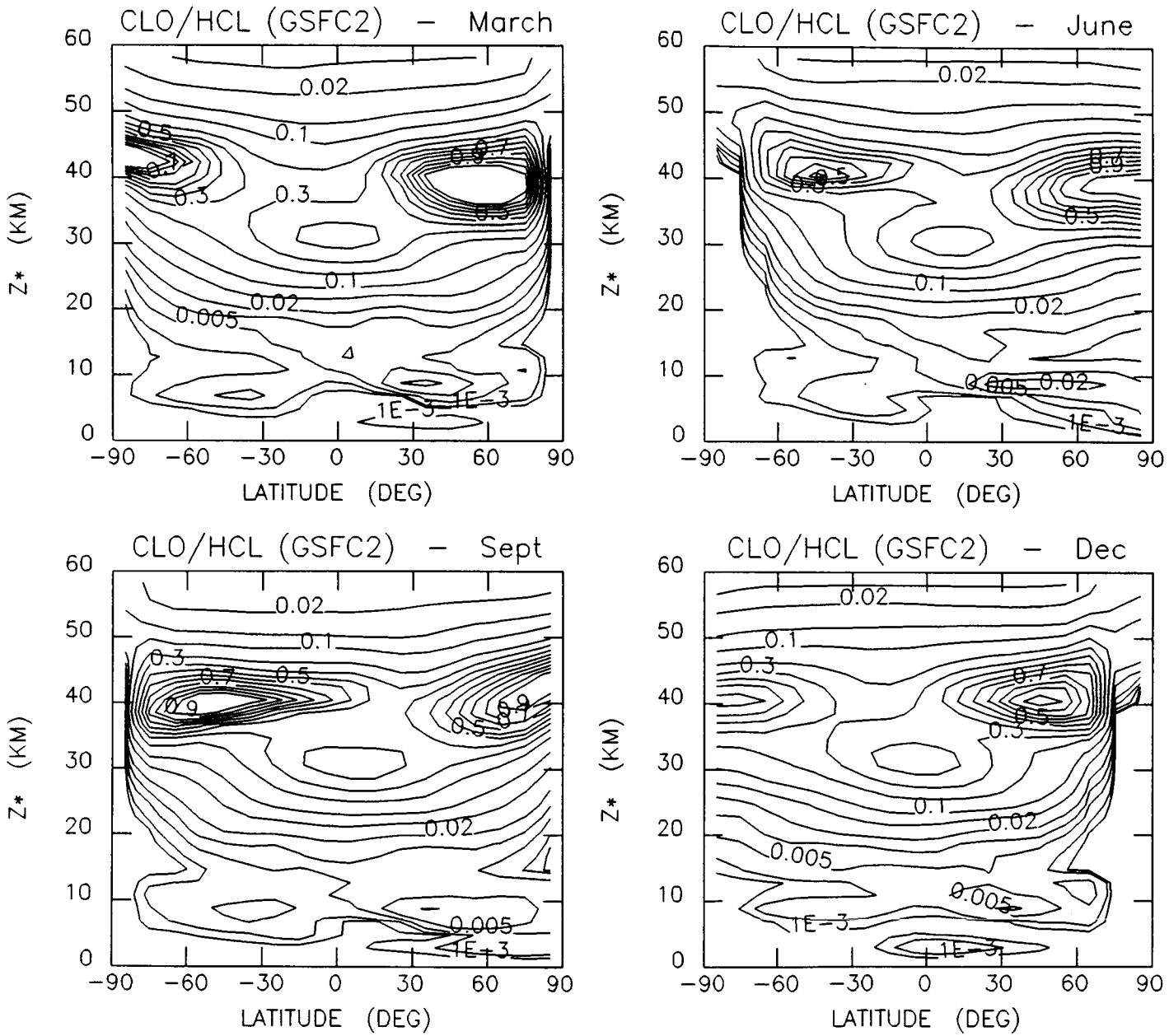
CLO/HCL (GSFC2) – March
CLO/HCL (GSFC2) – June
CLO/HCL (GSFC2) – Sept
CLO/HCL (GSFC2) – Dec
Z* (KM)
LATITUDE (DEG)
0
10
20
30
40
50
60
−90
−60
−30
0
30
60
90
0.02
0.1
0.3
0.5
0.7
0.9
0.005
1E−3

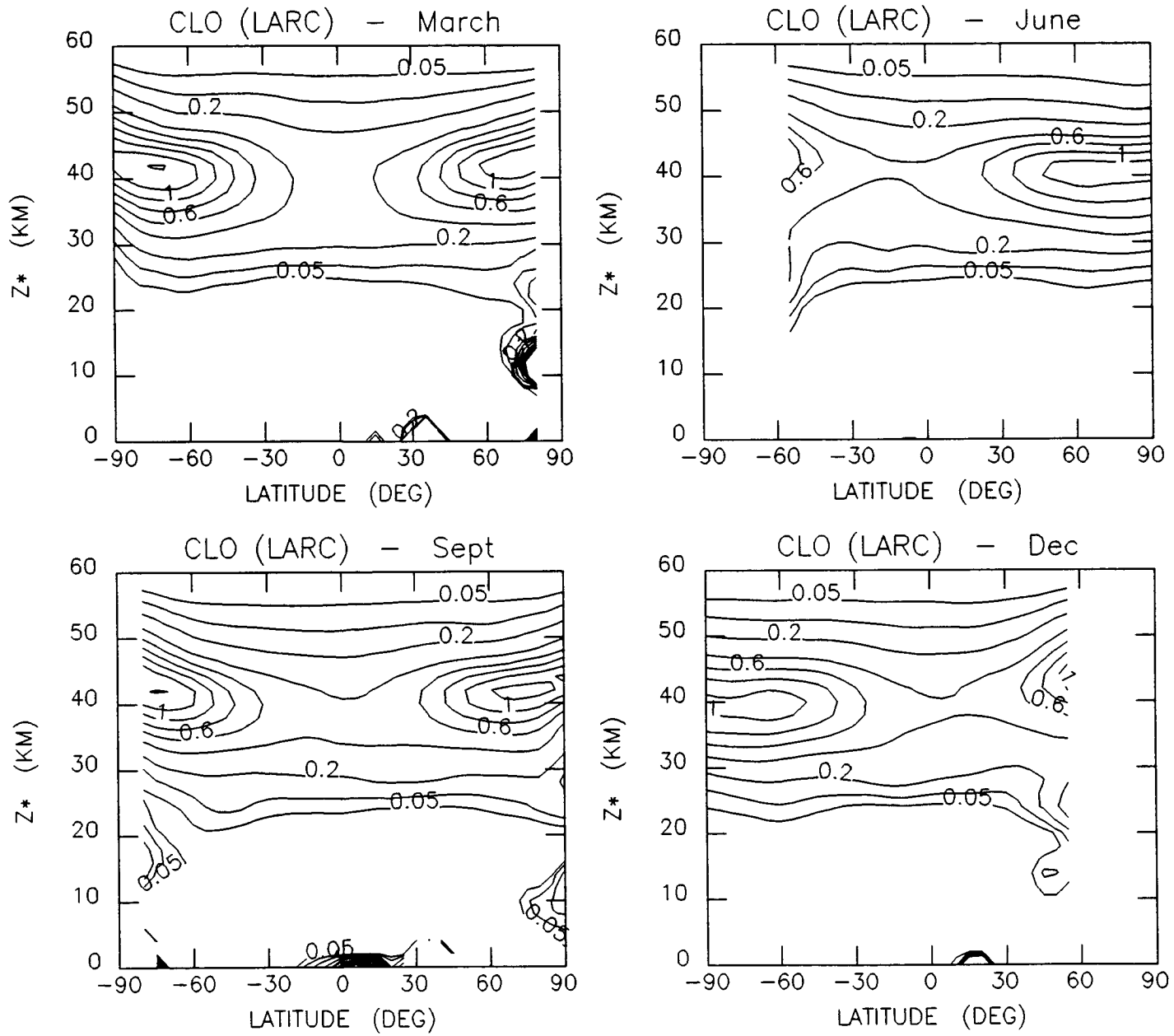
CLO (LARC) – March
CLO (LARC) – June
CLO (LARC) – Sept
CLO (LARC) – Dec
Z* (KM)
LATITUDE (DEG)
0
10
20
30
40
50
60
-90
-60
-30
0
30
60
90
0.05
0.2
0.6
1
2

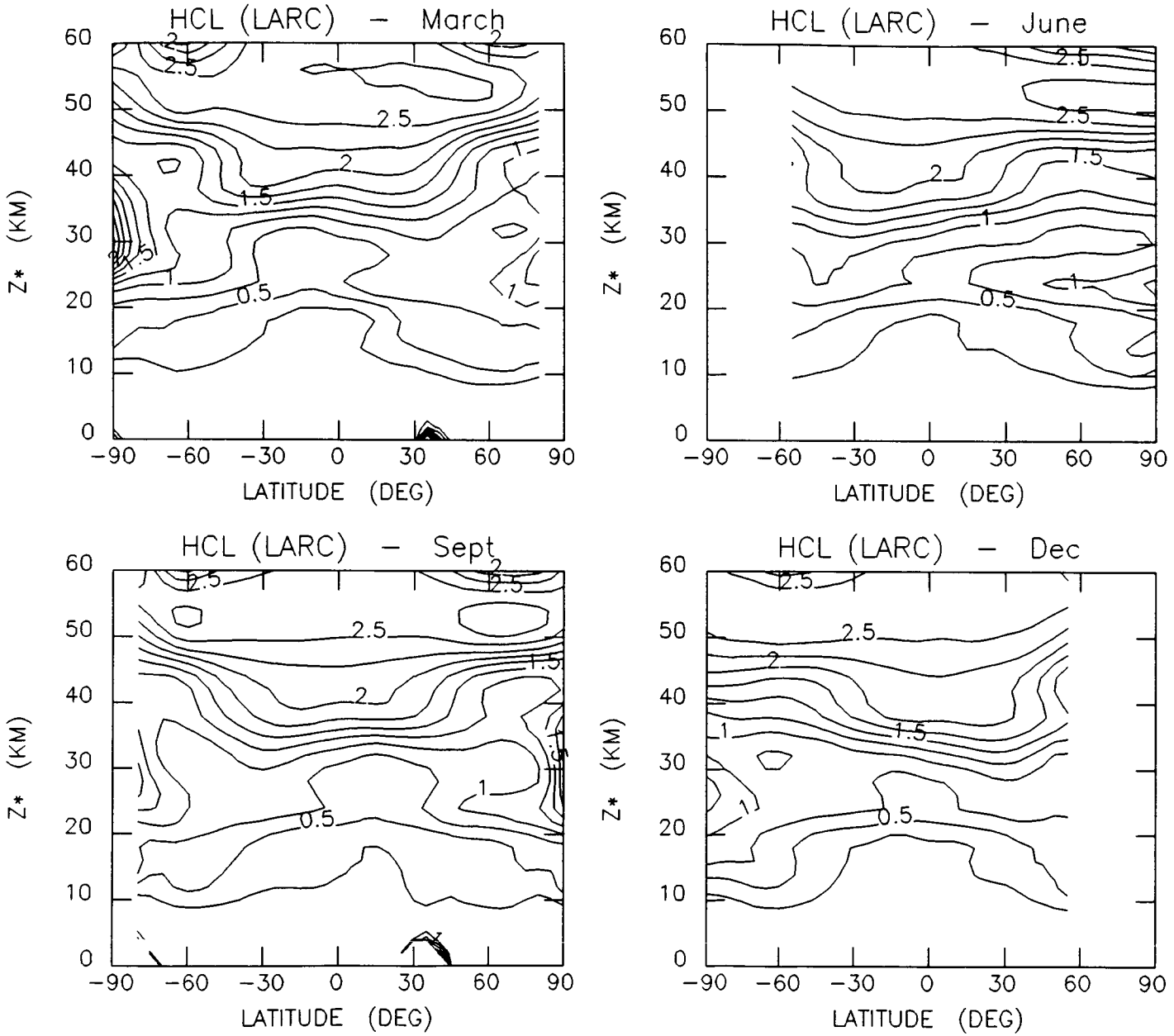
HCL (LARC) – March
HCL (LARC) – June
HCL (LARC) – Sept
HCL (LARC) – Dec
Z* (KM)
LATITUDE (DEG)
0
10
20
30
40
50
60
−90
−60
−30
0
30
60
90
0.5
1
1.5
2
2.5

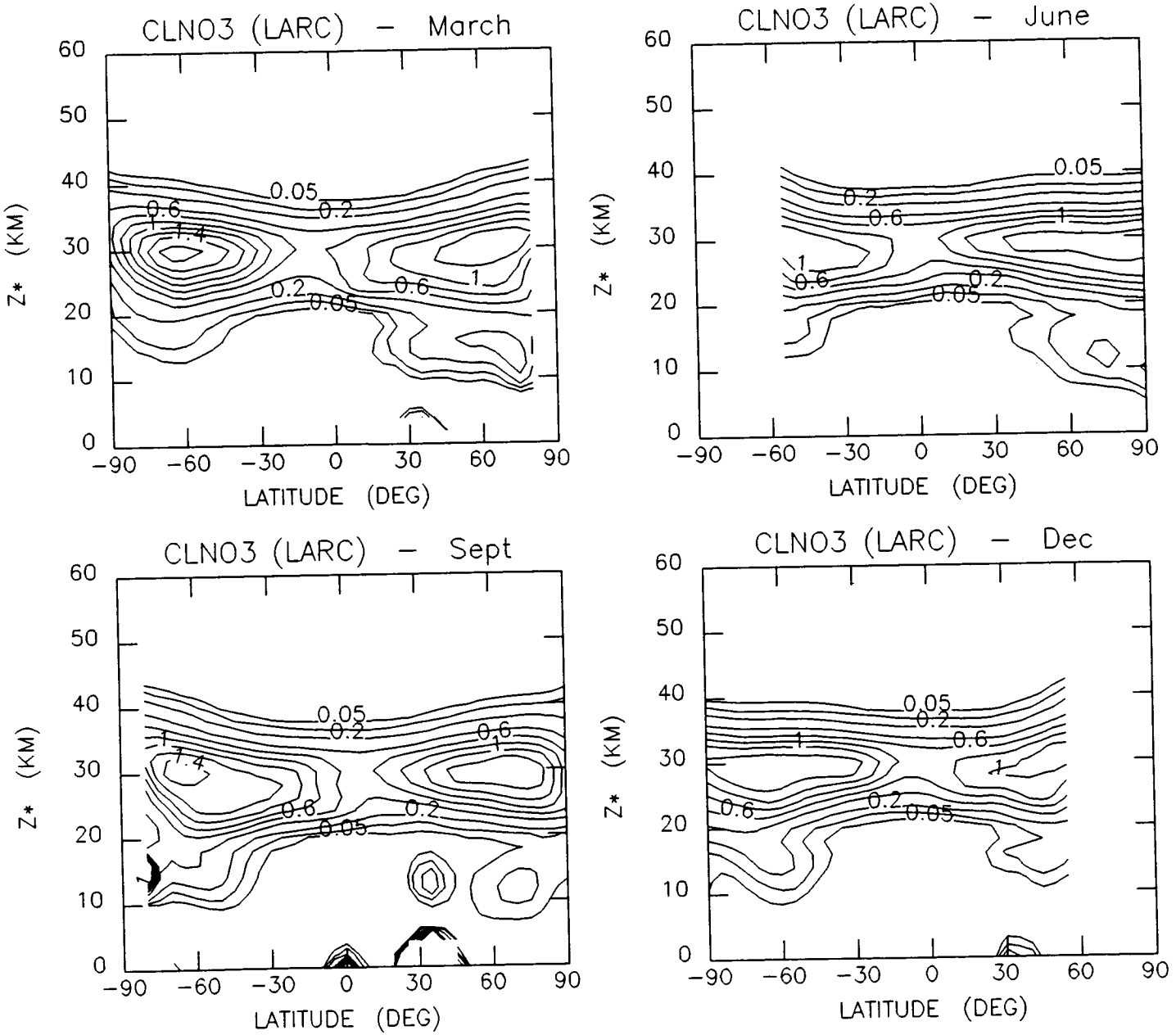
CLNO3 (LARC) – March
CLNO3 (LARC) – June
CLNO3 (LARC) – Sept
CLNO3 (LARC) – Dec
Z* (KM)
LATITUDE (DEG)
0
10
20
30
40
50
60
-90
-60
-30
0
30
60
90
0.05
0.2
0.6
1
1.4

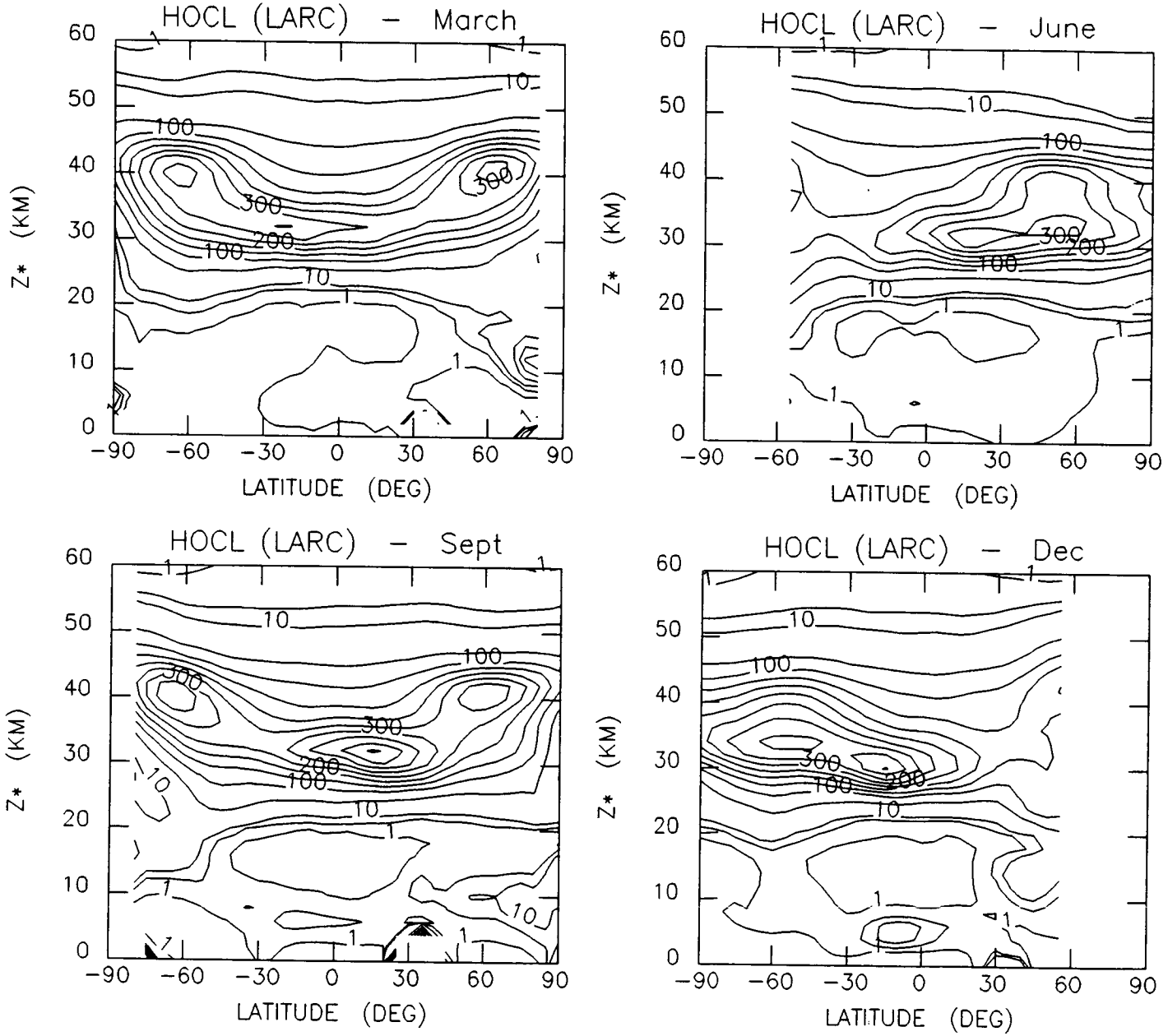
HOCL (LARC) – March
HOCL (LARC) – June
HOCL (LARC) – Sept
HOCL (LARC) – Dec
Z* (KM)
LATITUDE (DEG)
0
10
20
30
40
50
60
-90
-60
-30
0
30
60
90
1
10
100
200
300

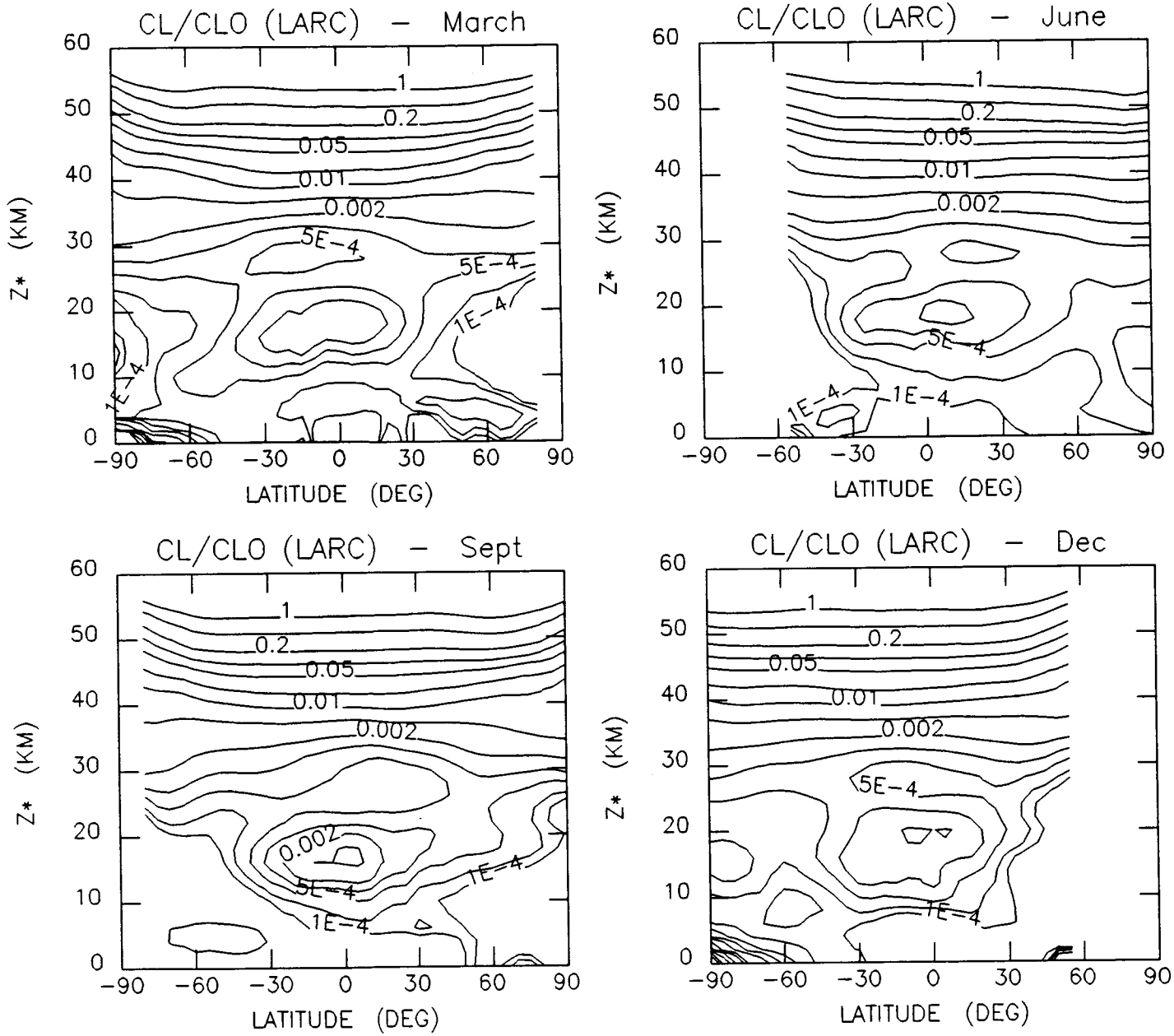
CL/CLO (LARC) – March
CL/CLO (LARC) – June
CL/CLO (LARC) – Sept
CL/CLO (LARC) – Dec
Z* (KM)
LATITUDE (DEG)
1
0.2
0.05
0.01
0.002
5E-4
1E-4
0
10
20
30
40
50
60
-90
-60
-30
0
30
60
90

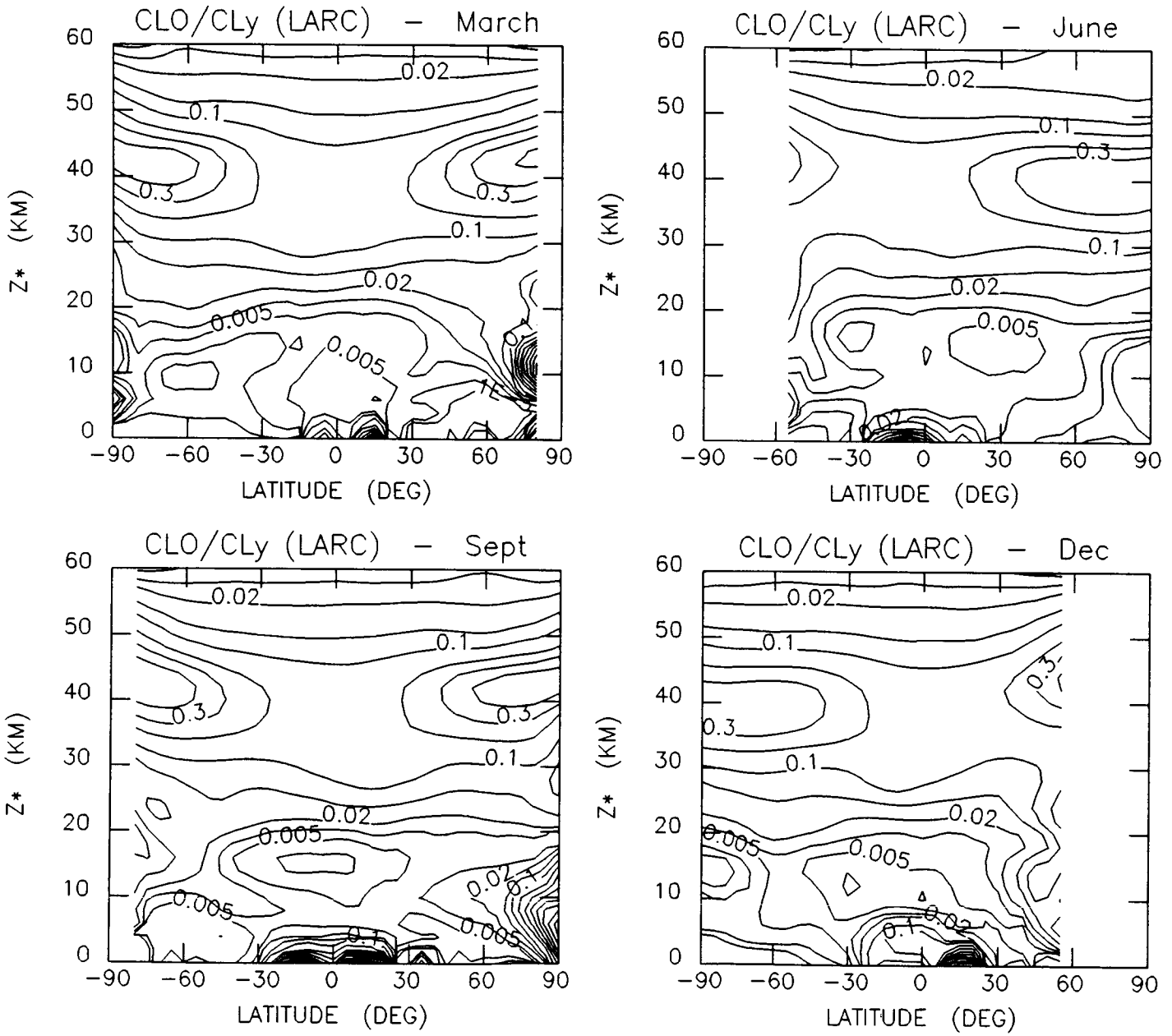
CLO/CLy (LARC) – March
CLO/CLy (LARC) – June
CLO/CLy (LARC) – Sept
CLO/CLy (LARC) – Dec
Z* (KM)
LATITUDE (DEG)
0
10
20
30
40
50
60
−90
−60
−30
0
30
60
90
0.02
0.1
0.3
0.005

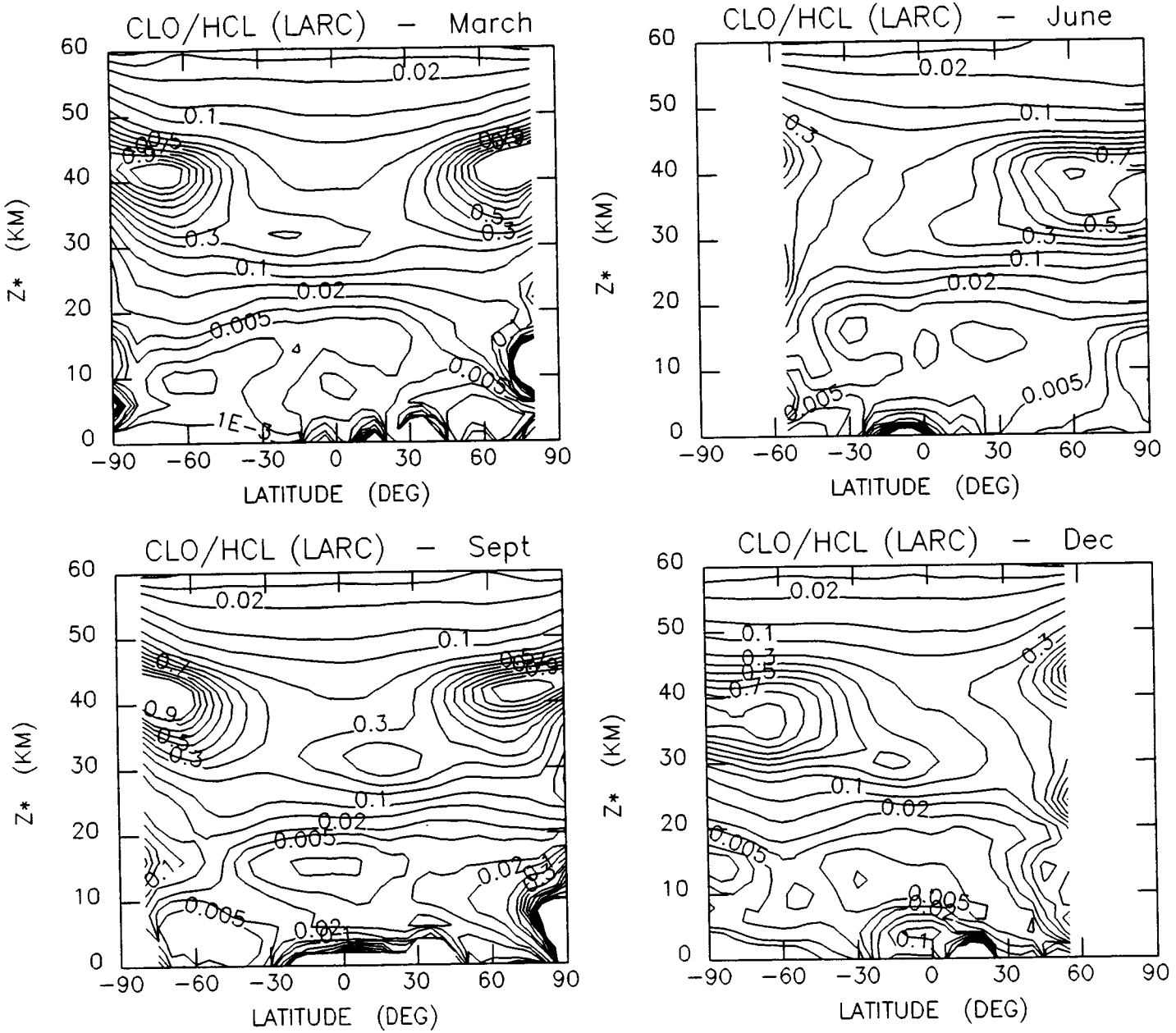
CLO/HCL (LARC) – March
CLO/HCL (LARC) – June
CLO/HCL (LARC) – Sept
CLO/HCL (LARC) – Dec
Z* (KM)
LATITUDE (DEG)
0
10
20
30
40
50
60
−90
−60
−30
0
30
60
90
0.02
0.1
0.3
0.5
0.7
0.9
0.005
1E-3

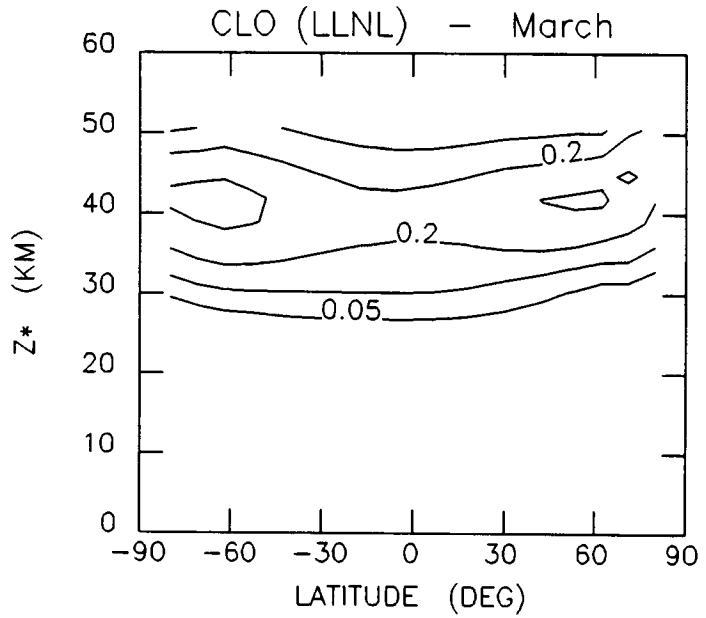
CLO (LLNL) – March
Z* (KM)
LATITUDE (DEG)
0.2
0.2
0.05
60
50
40
30
20
10
0
-90 -60 -30 0 30 60 90

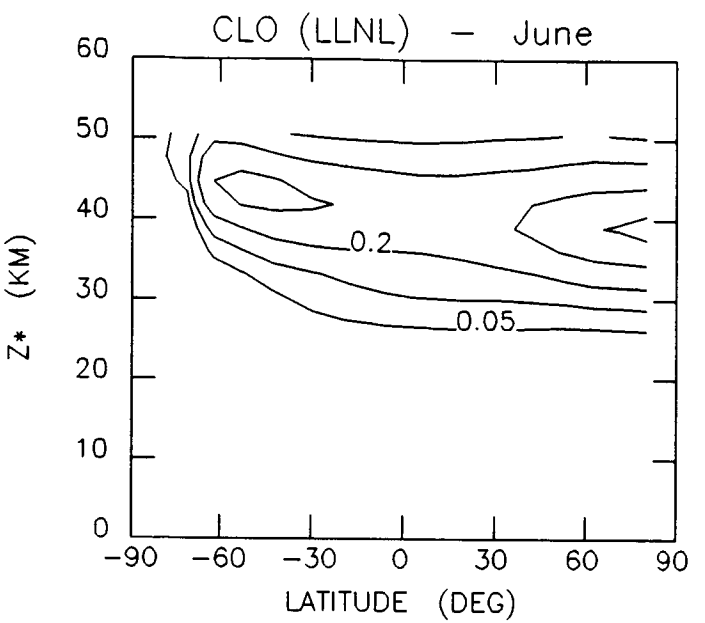
CLO (LLNL) – June
Z* (KM)
LATITUDE (DEG)
0.2
0.05
60
50
40
30
20
10
0
-90 -60 -30 0 30 60 90

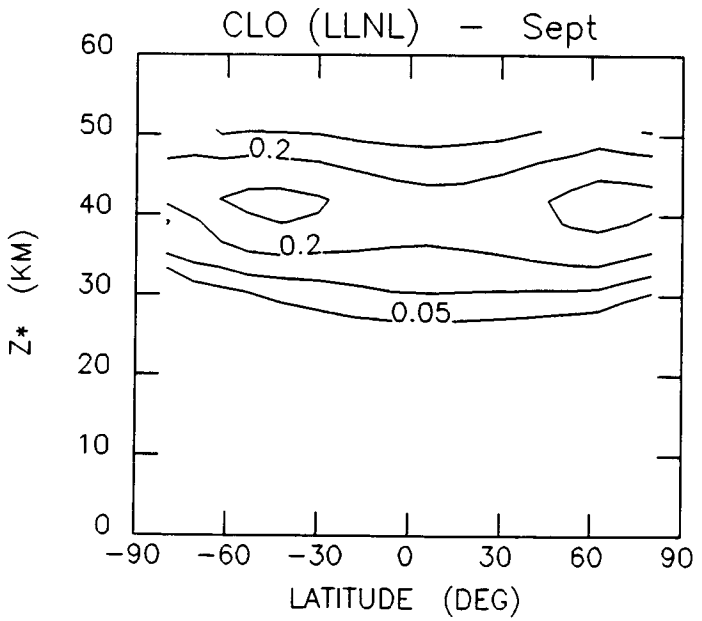
CLO (LLNL) – Sept
Z* (KM)
LATITUDE (DEG)
0.2
0.2
0.05
60
50
40
30
20
10
0
-90 -60 -30 0 30 60 90

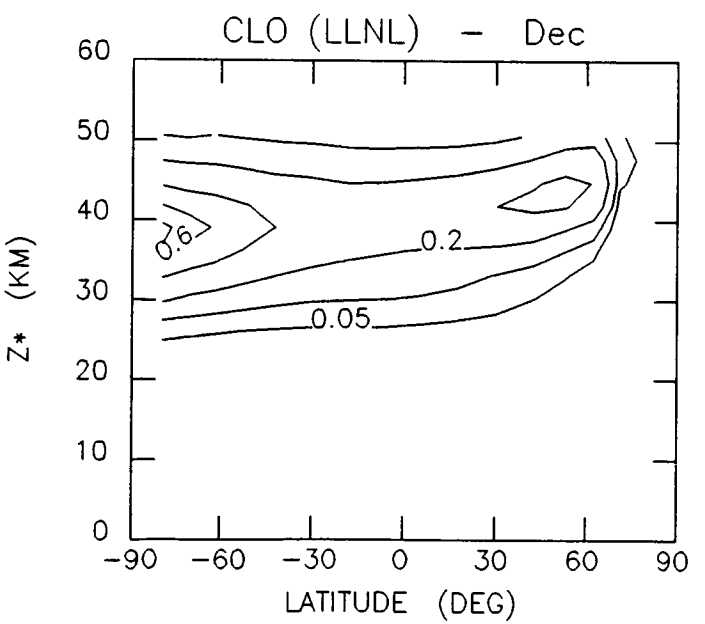
CLO (LLNL) – Dec
Z* (KM)
LATITUDE (DEG)
0.6
0.2
0.05
60
50
40
30
20
10
0
-90 -60 -30 0 30 60 90

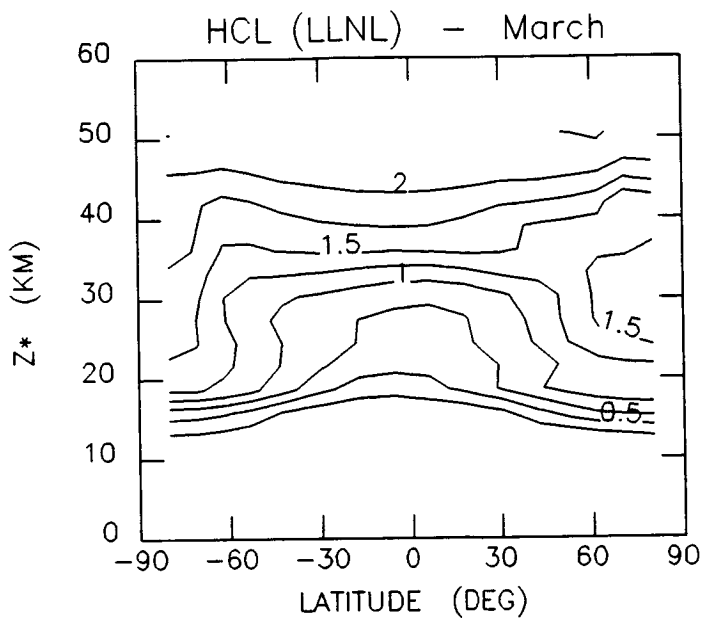
HCL (LLNL) – March
Z* (KM)
LATITUDE (DEG)
2
1.5
1.5
0.5

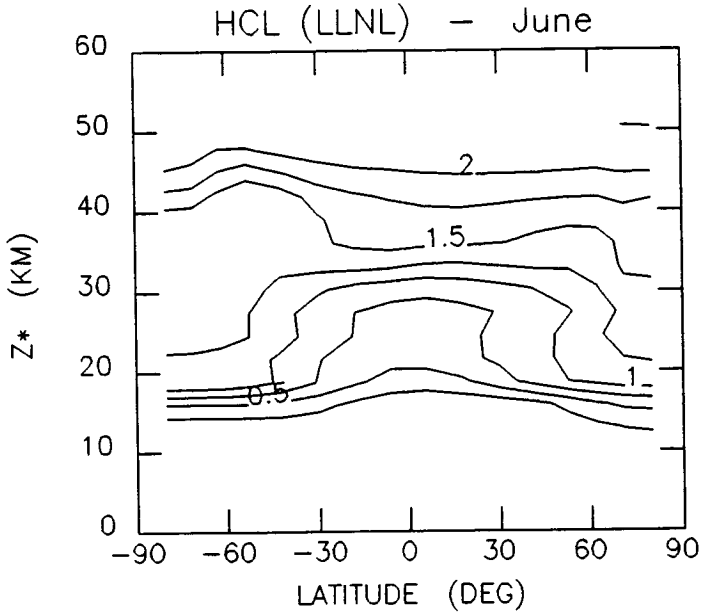
HCL (LLNL) – June
Z* (KM)
LATITUDE (DEG)
2
1.5
1
0.5

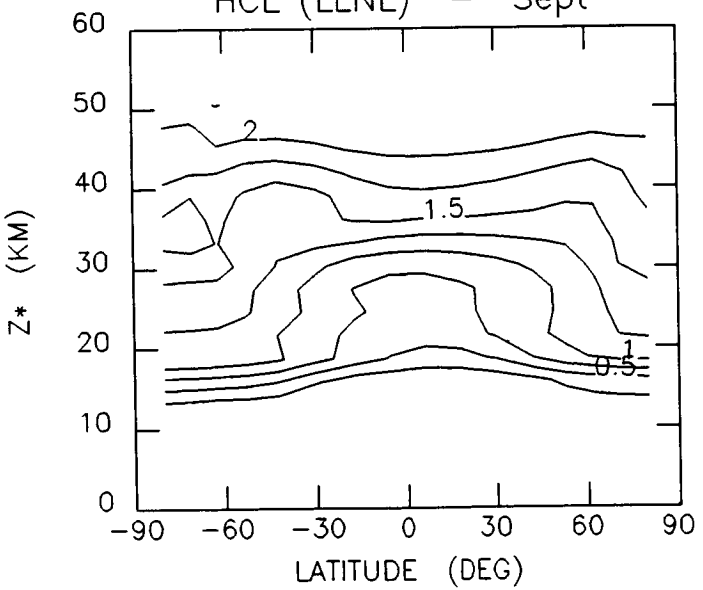
HCL (LLNL) – Sept
Z* (KM)
LATITUDE (DEG)
2
1.5
1
0.5

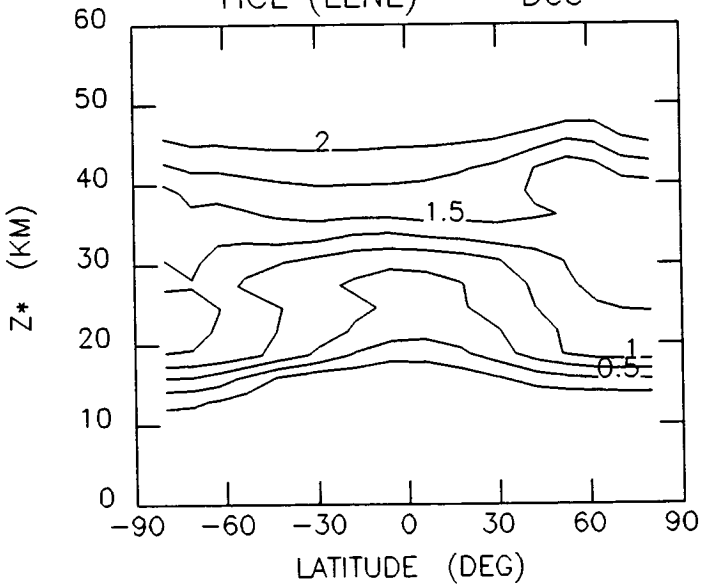
HCL (LLNL) – Dec
Z* (KM)
LATITUDE (DEG)
2
1.5
1
0.5

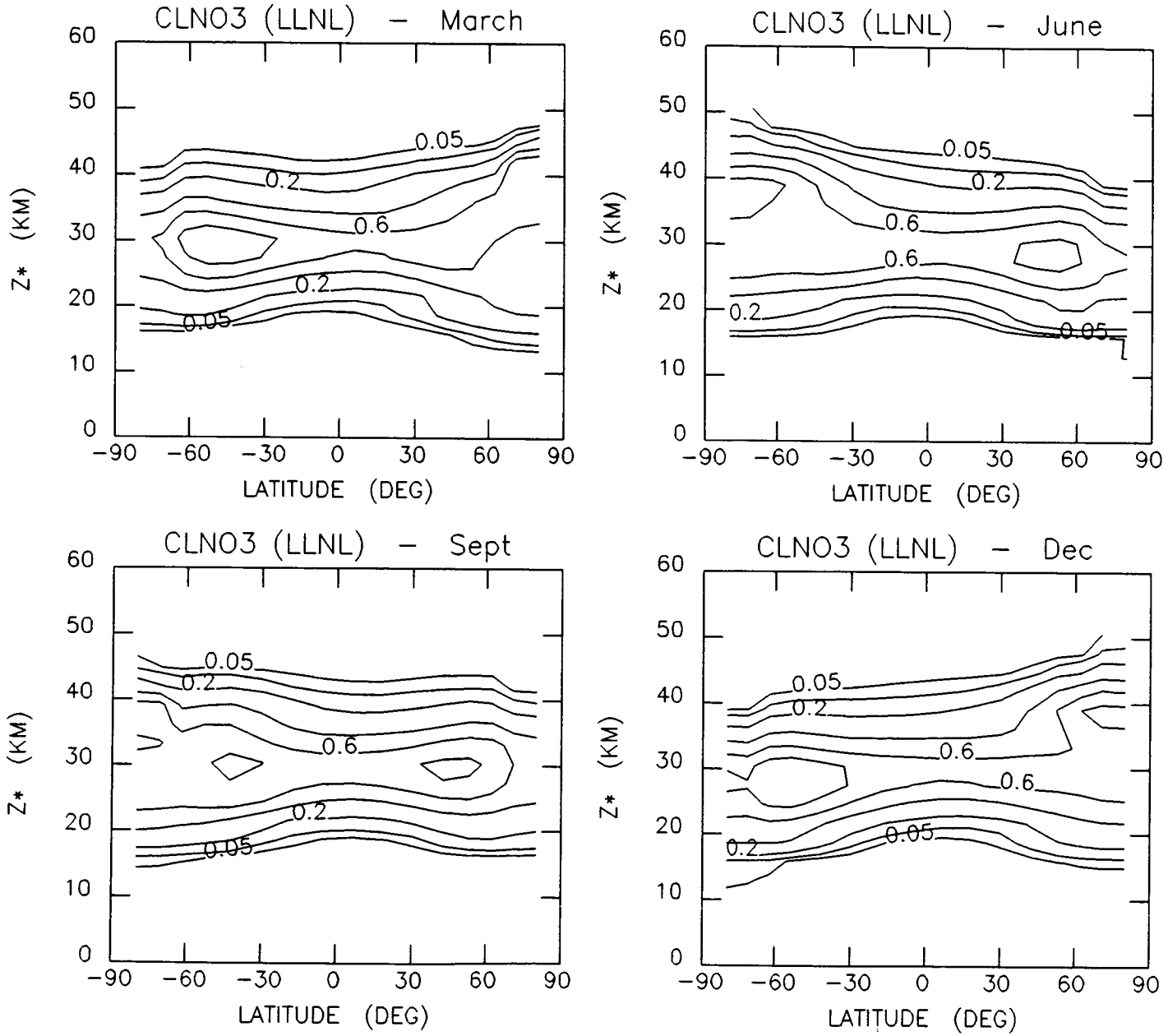
CLNO3 (LLNL) – March
CLNO3 (LLNL) – June
CLNO3 (LLNL) – Sept
CLNO3 (LLNL) – Dec
Z* (KM)
LATITUDE (DEG)
0.05
0.2
0.6
0
10
20
30
40
50
60
-90
-60
-30
0
30
60
90

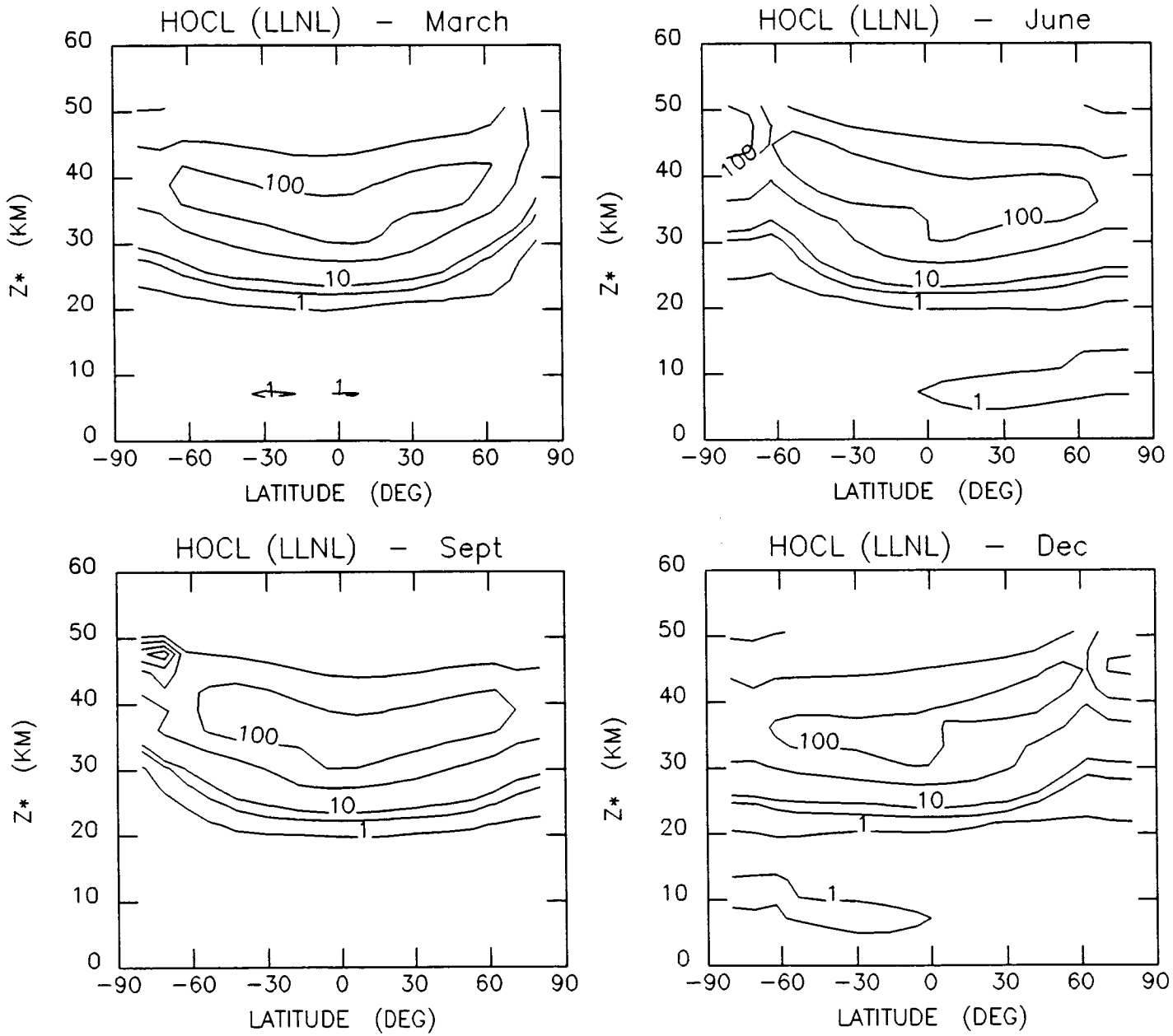
HOCL (LLNL) – March
HOCL (LLNL) – June
HOCL (LLNL) – Sept
HOCL (LLNL) – Dec
Z* (KM)
LATITUDE (DEG)
100
10
1
0
10
20
30
40
50
60
-90
-60
-30
0
30
60
90

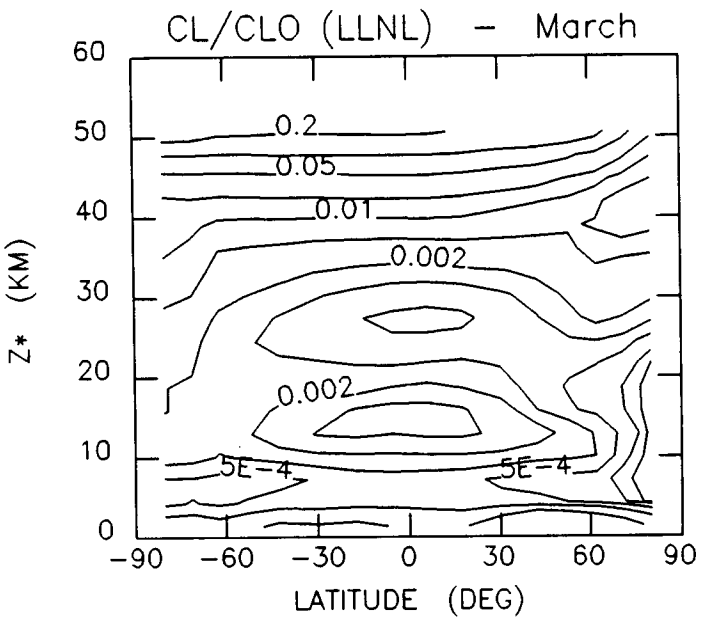
CL/CLO (LLNL) – March
Z* (KM)
LATITUDE (DEG)
0.2
0.05
0.01
0.002
5E-4

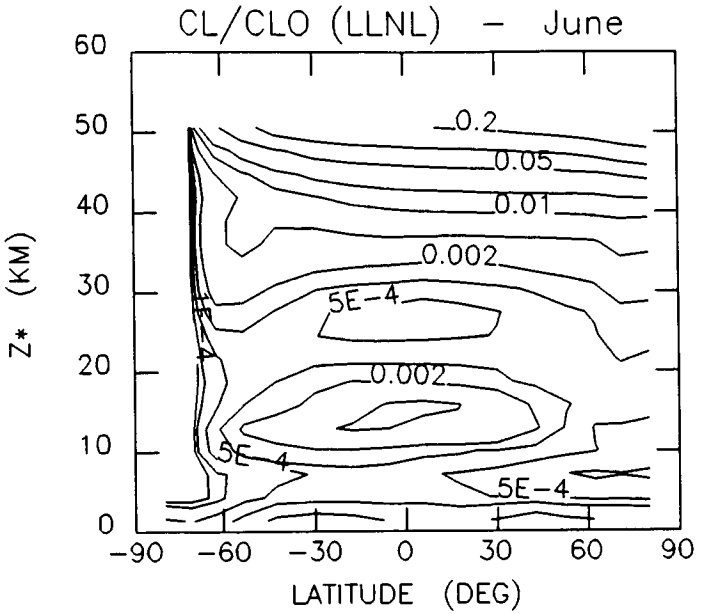
CL/CLO (LLNL) – June
Z* (KM)
LATITUDE (DEG)
0.2
0.05
0.01
0.002
5E-4

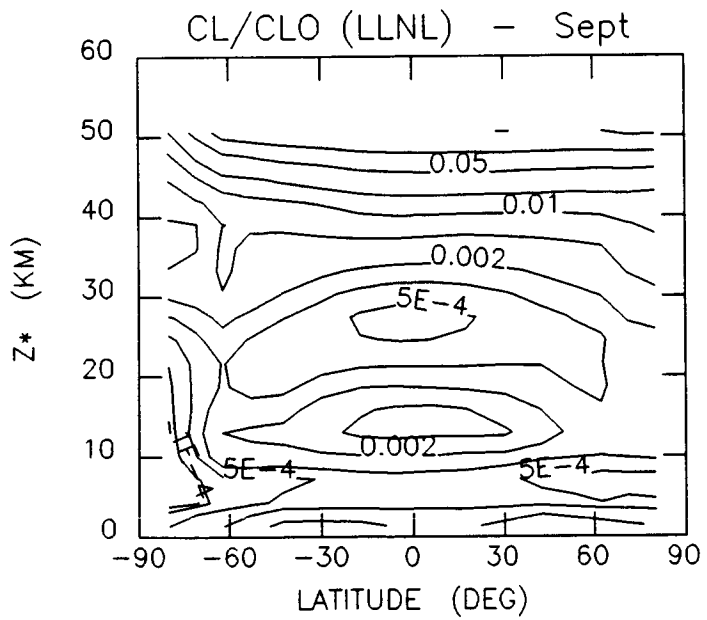
CL/CLO (LLNL) – Sept
Z* (KM)
LATITUDE (DEG)
0.05
0.01
0.002
5E-4

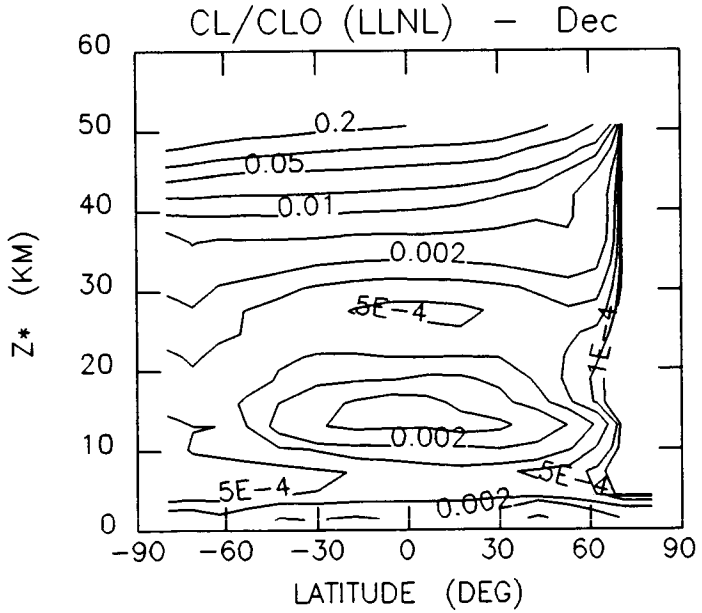
CL/CLO (LLNL) – Dec
Z* (KM)
LATITUDE (DEG)
0.2
0.05
0.01
0.002
5E-4

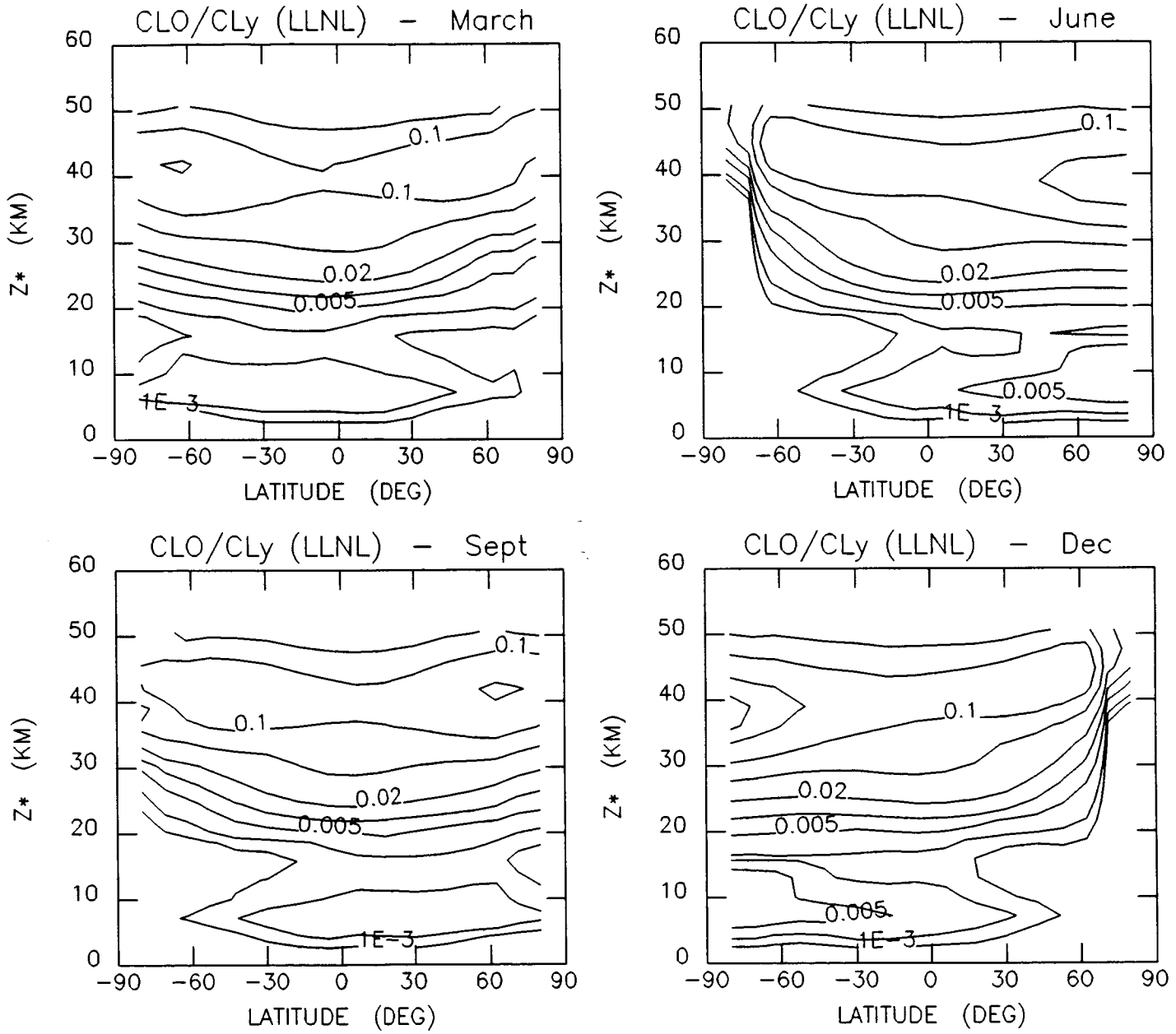
CLO/CLy (LLNL) – March
CLO/CLy (LLNL) – June
CLO/CLy (LLNL) – Sept
CLO/CLy (LLNL) – Dec
Z* (KM)
LATITUDE (DEG)
0.1
0.02
0.005
1E-3
0
10
20
30
40
50
60
-90
-60
-30
0
30
60
90

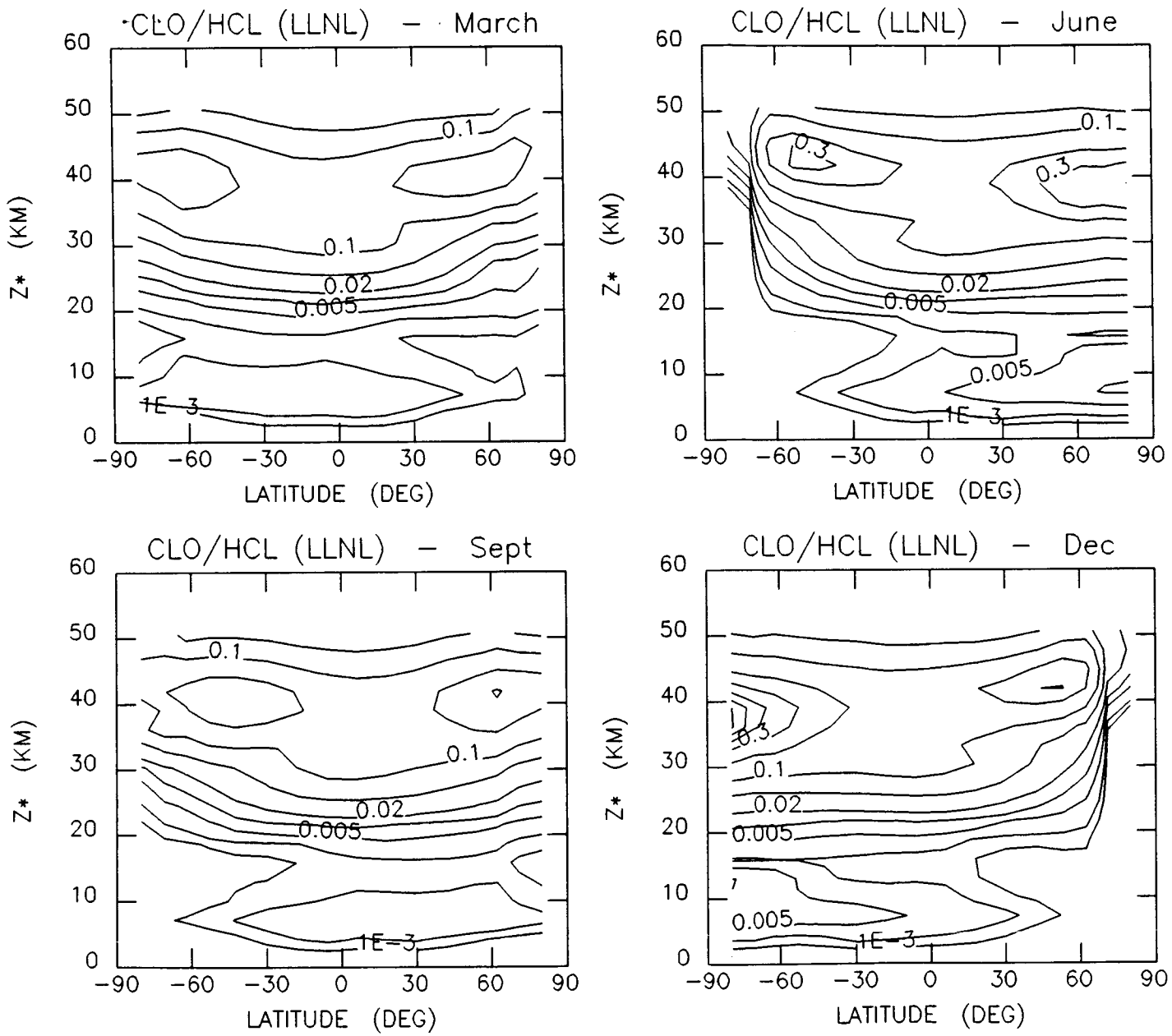
CLO/HCL (LLNL) – March
CLO/HCL (LLNL) – June
CLO/HCL (LLNL) – Sept
CLO/HCL (LLNL) – Dec
Z* (KM)
LATITUDE (DEG)
0.1
0.3
0.02
0.005
1E-3
0
10
20
30
40
50
60
-90
-60
-30
0
30
60
90

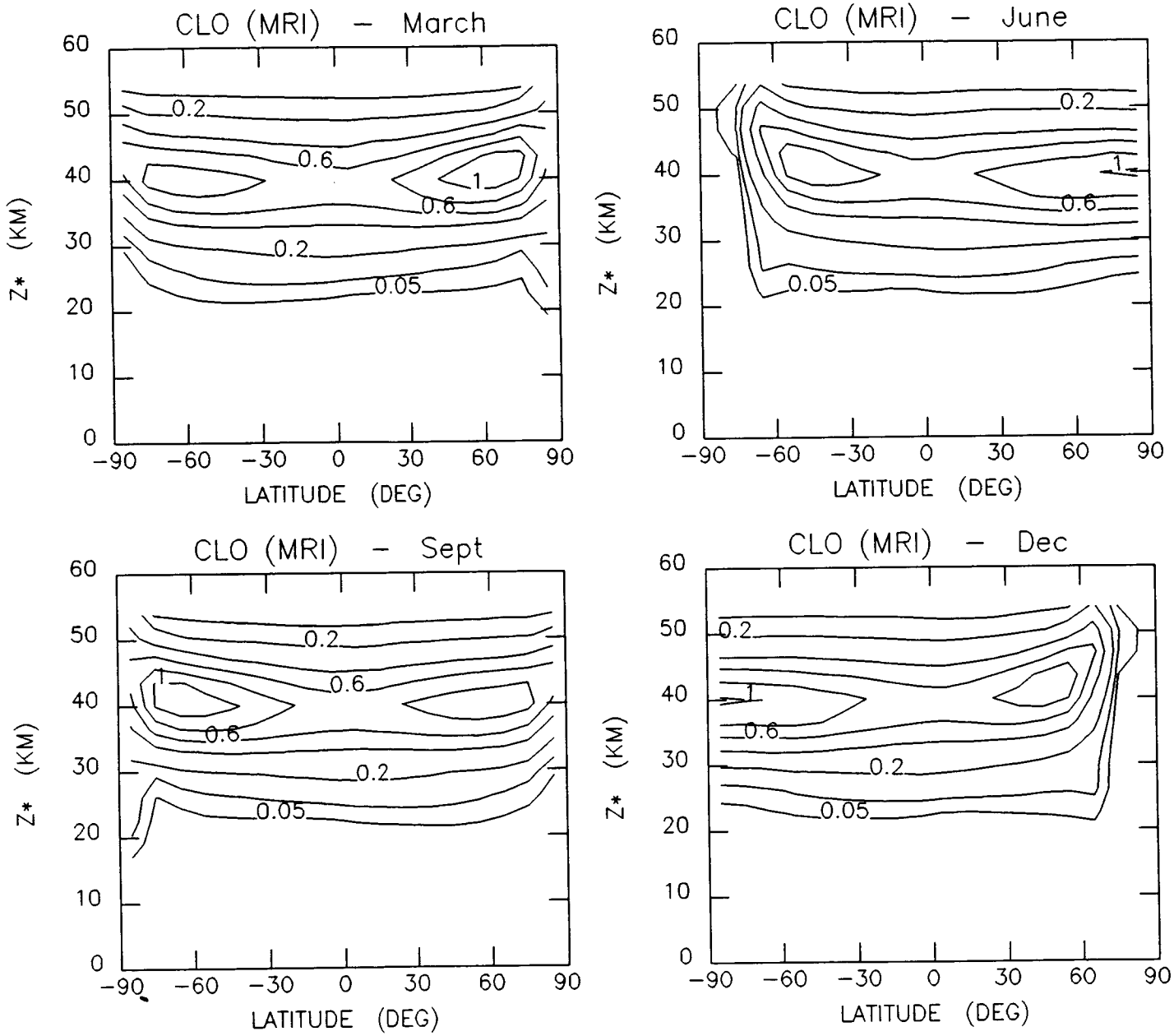
CLO (MRI) – March
CLO (MRI) – June
CLO (MRI) – Sept
CLO (MRI) – Dec
Z* (KM)
LATITUDE (DEG)
0.2
0.6
1
0.05
0
10
20
30
40
50
60
−90
−60
−30
0
30
60
90

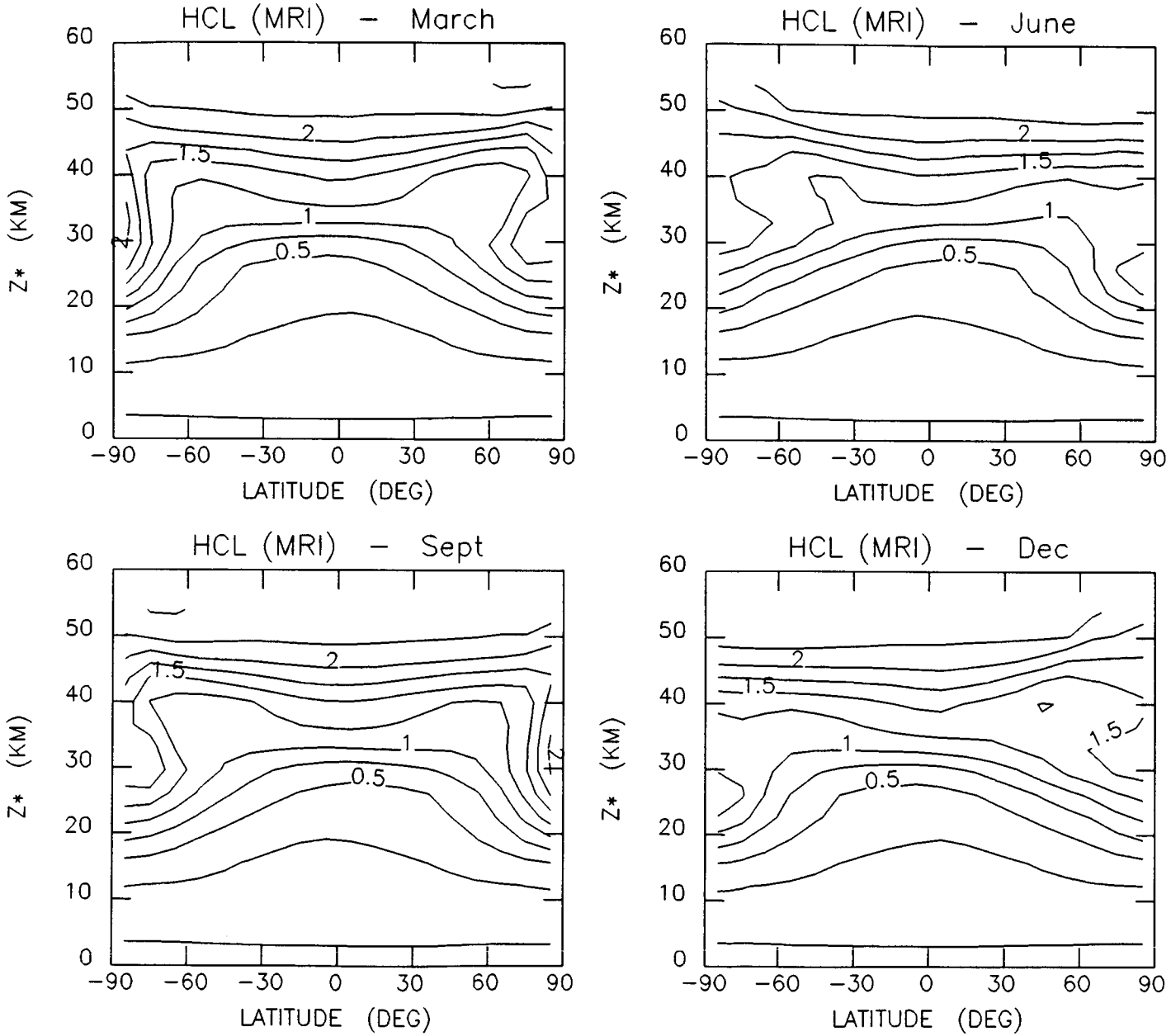
HCL (MRI) – March
HCL (MRI) – June
HCL (MRI) – Sept
HCL (MRI) – Dec
Z* (KM)
LATITUDE (DEG)
60
50
40
30
20
10
0
−90 −60 −30 0 30 60 90
2
1.5
1
0.5

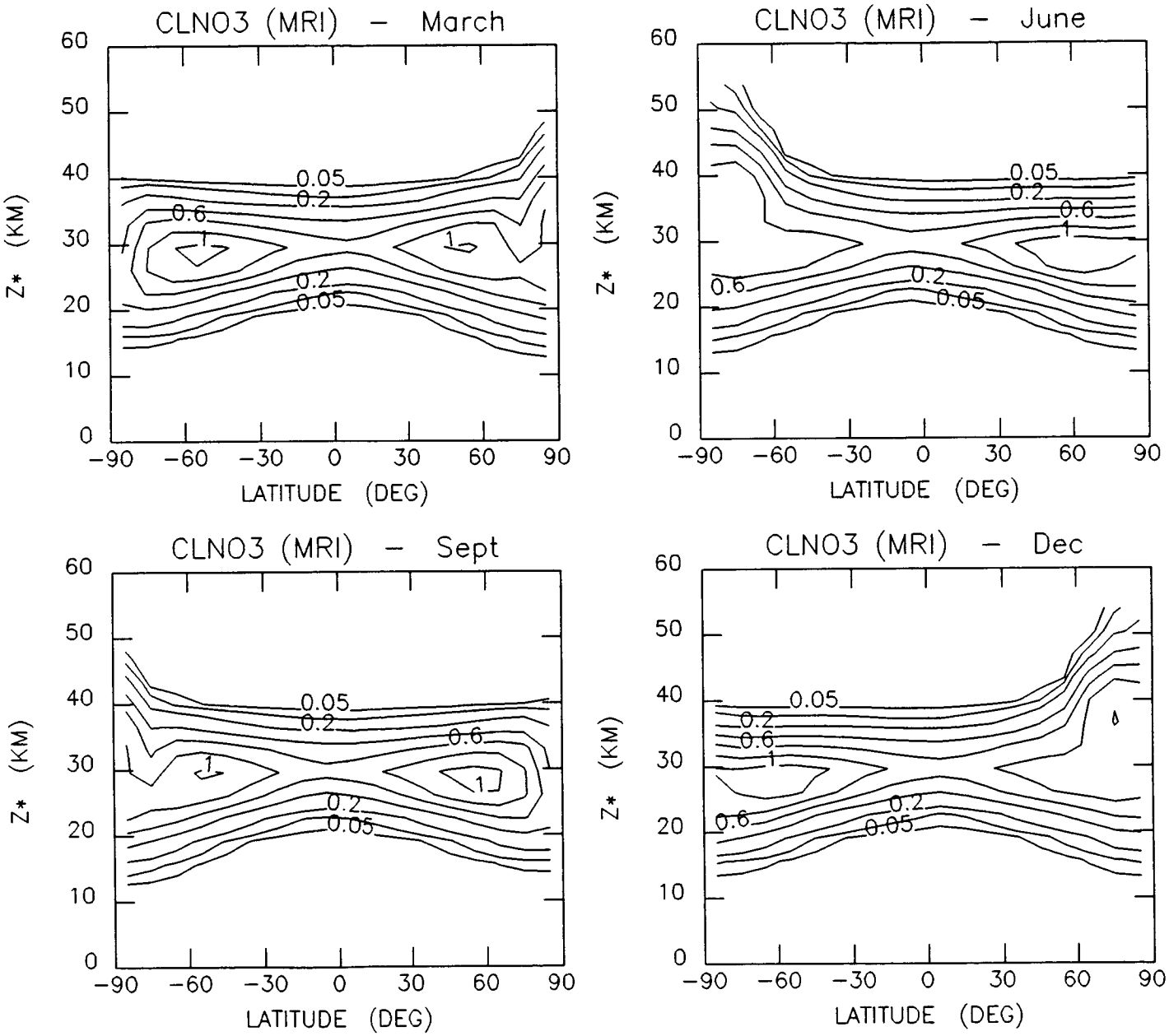
CLNO3 (MRI) – March
CLNO3 (MRI) – June
CLNO3 (MRI) – Sept
CLNO3 (MRI) – Dec
Z* (KM)
LATITUDE (DEG)
0
10
20
30
40
50
60
-90
-60
-30
0
30
60
90
0.05
0.2
0.6
1

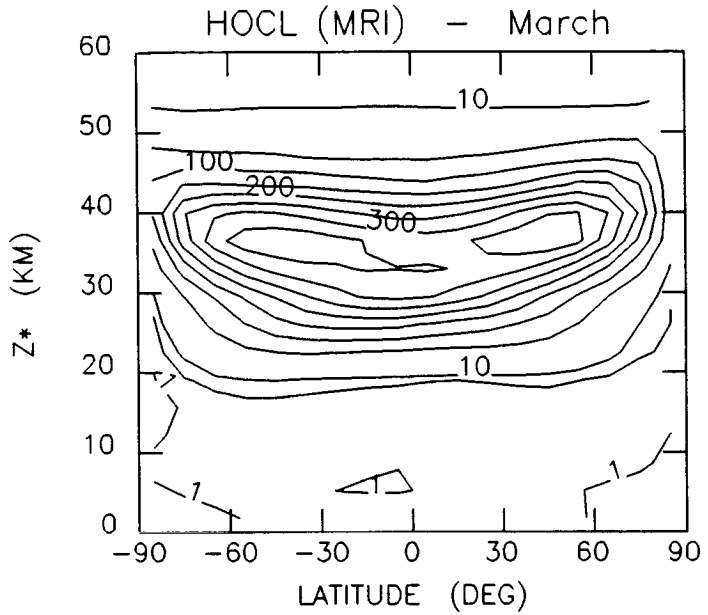
HOCL (MRI) – March
Z* (KM)
LATITUDE (DEG)
10
100
200
300
1

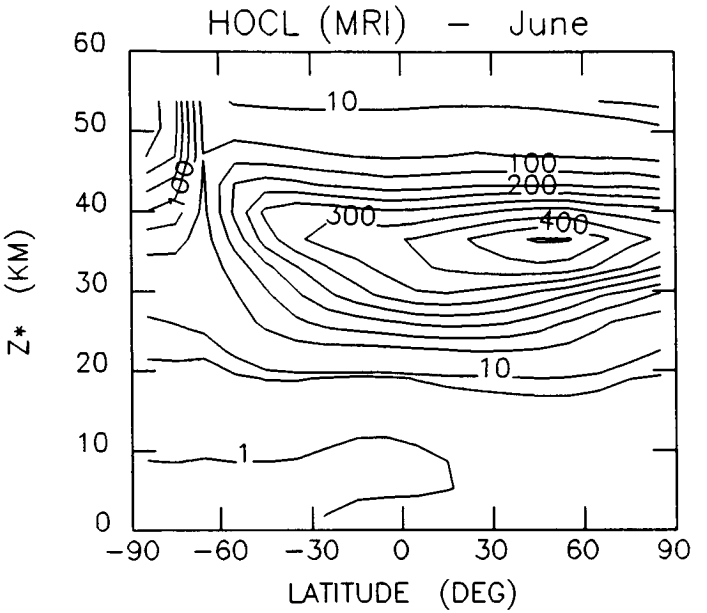
HOCL (MRI) – June
Z* (KM)
LATITUDE (DEG)
10
100
200
300
400
1

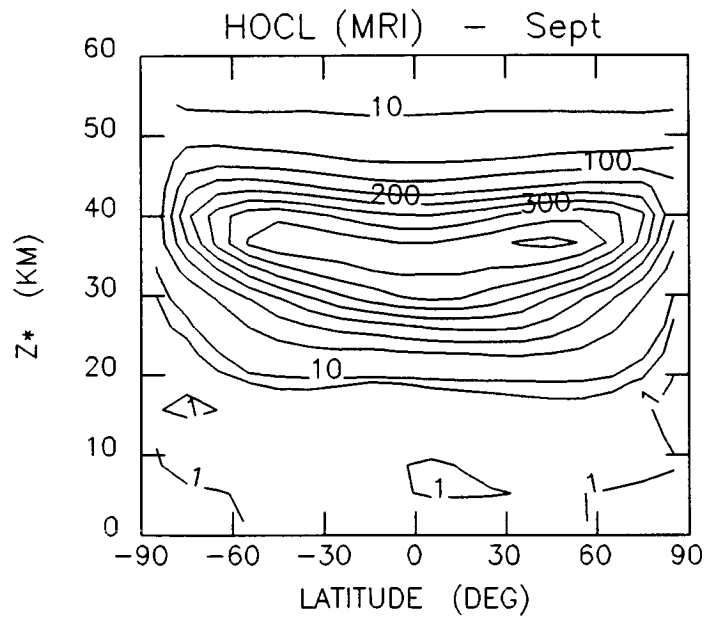
HOCL (MRI) – Sept
Z* (KM)
LATITUDE (DEG)
10
100
200
300
1

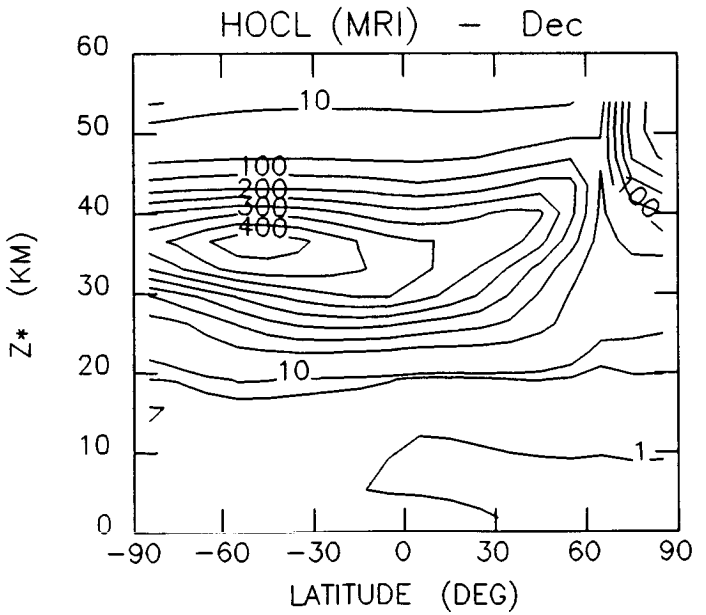
HOCL (MRI) – Dec
Z* (KM)
LATITUDE (DEG)
10
100
200
300
400
1

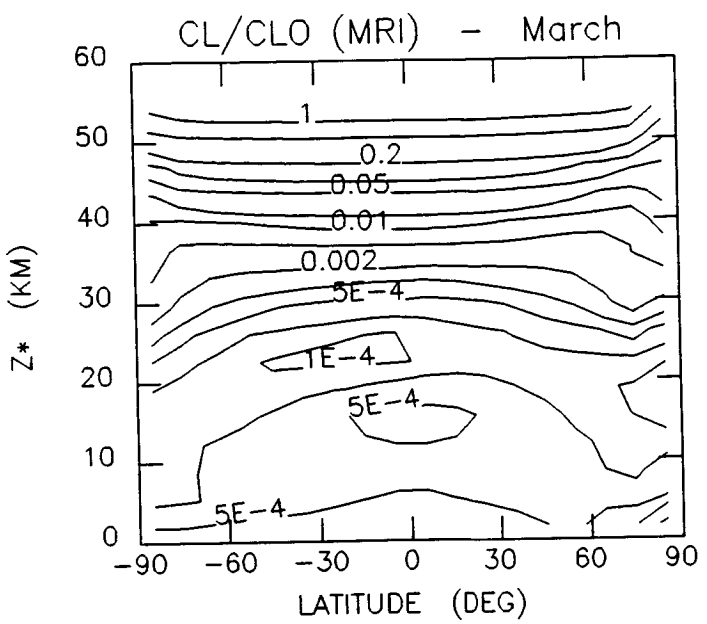
CL/CLO (MRI) – March
Z* (KM)
LATITUDE (DEG)
1
0.2
0.05
0.01
0.002
5E-4
1E-4
5E-4
5E-4

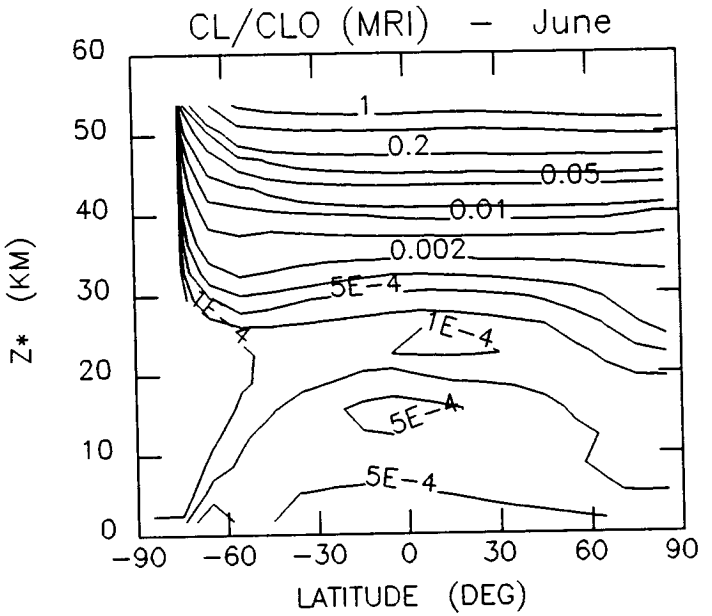
CL/CLO (MRI) – June
Z* (KM)
LATITUDE (DEG)
1
0.2
0.05
0.01
0.002
5E-4
1E-4
1E-4
5E-4
5E-4

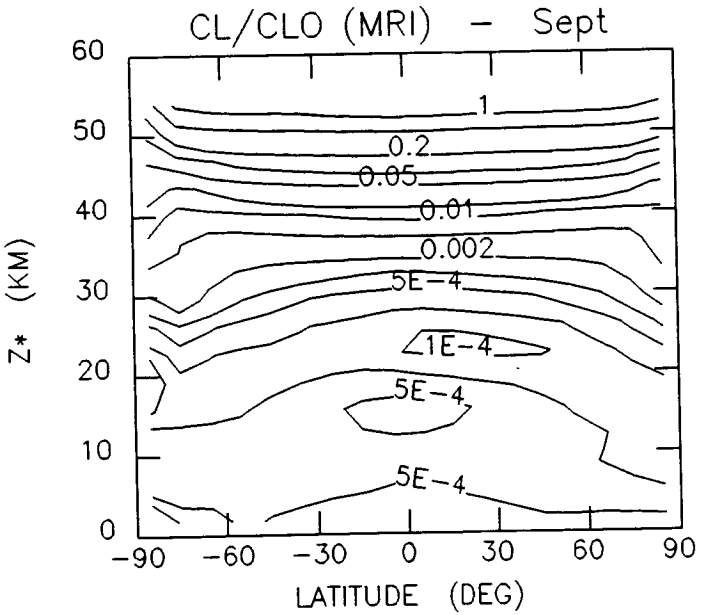
CL/CLO (MRI) – Sept
Z* (KM)
LATITUDE (DEG)
1
0.2
0.05
0.01
0.002
5E-4
1E-4
5E-4
5E-4

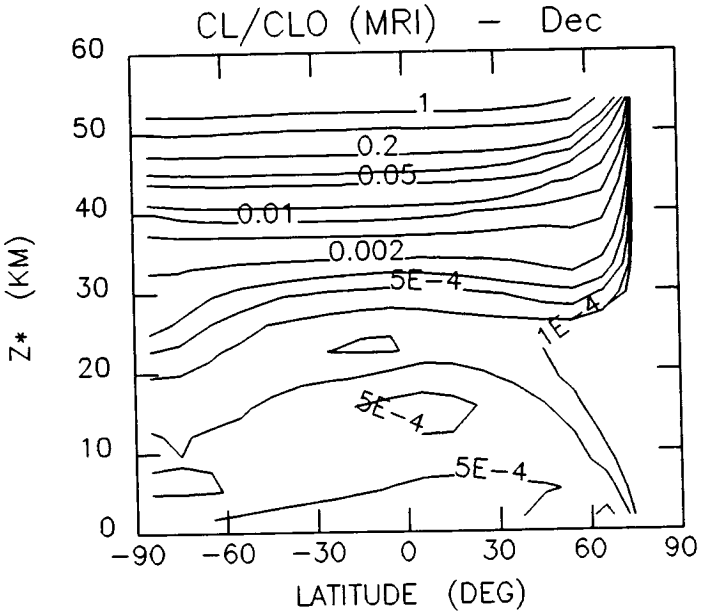
CL/CLO (MRI) – Dec
Z* (KM)
LATITUDE (DEG)
1
0.2
0.05
0.01
0.002
5E-4
1E-4
5E-4
5E-4

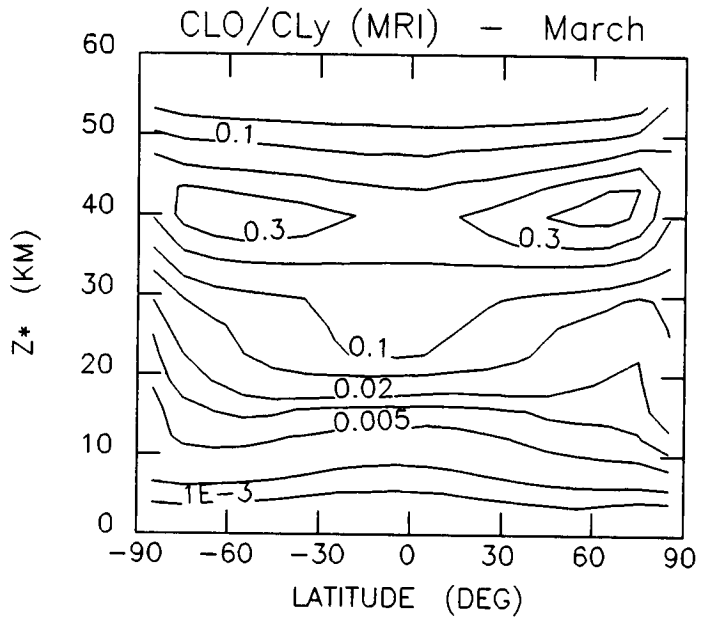
CLO/CLy (MRI) – March
Z* (KM)
LATITUDE (DEG)
0.1
0.3
0.02
0.005
1E-3

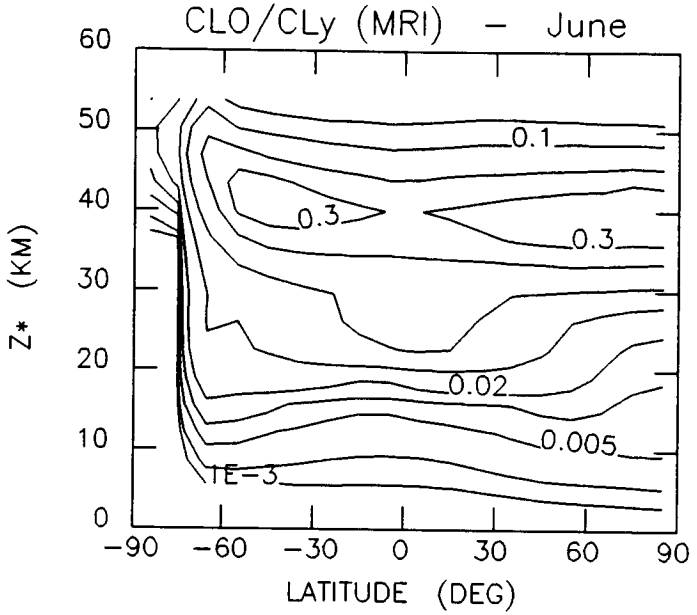
CLO/CLy (MRI) – June
Z* (KM)
LATITUDE (DEG)
0.1
0.3
0.02
0.005
1E-3

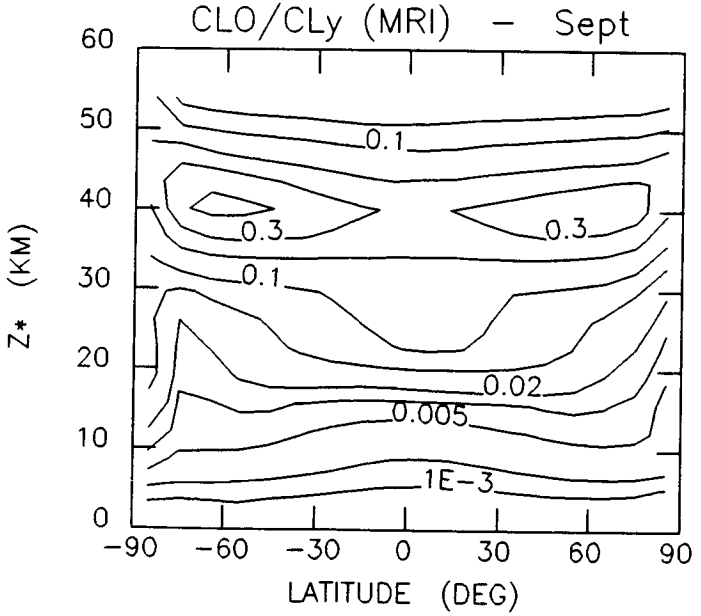
CLO/CLy (MRI) – Sept
Z* (KM)
LATITUDE (DEG)
0.1
0.3
0.02
0.005
1E-3

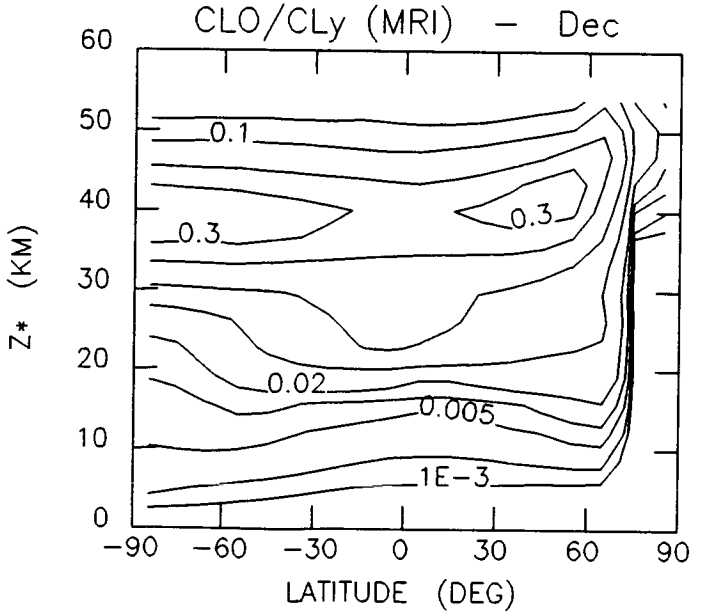
CLO/CLy (MRI) – Dec
Z* (KM)
LATITUDE (DEG)
0.1
0.3
0.02
0.005
1E-3

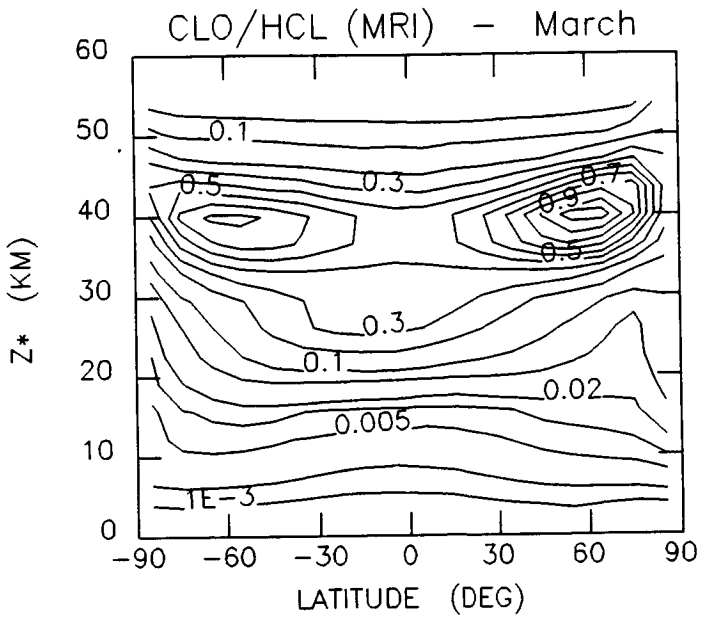
CLO/HCL (MRI) – March
Z* (KM)
LATITUDE (DEG)
0.1
0.3
0.5
0.7
0.9
0.02
0.005
1E-3

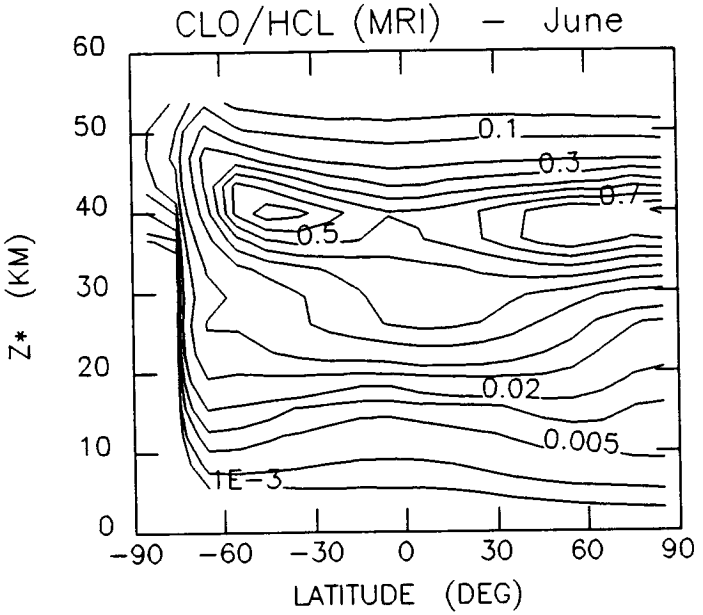
CLO/HCL (MRI) – June
Z* (KM)
LATITUDE (DEG)
0.1
0.3
0.5
0.7
0.02
0.005
1E-3

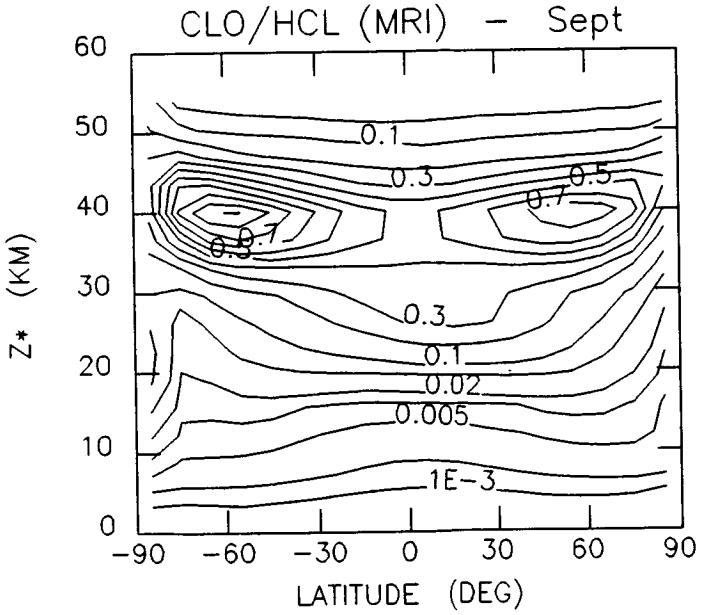
CLO/HCL (MRI) – Sept
Z* (KM)
LATITUDE (DEG)
0.1
0.3
0.5
0.7
0.9
0.02
0.005
1E-3

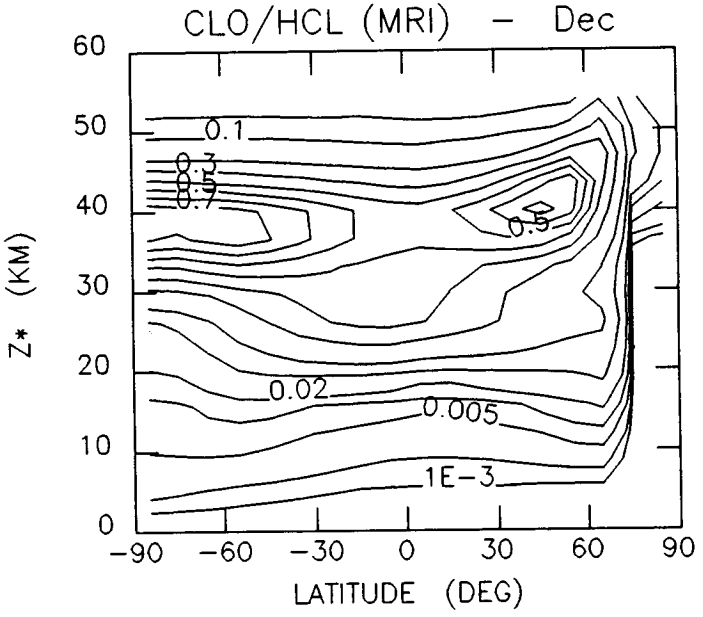
CLO/HCL (MRI) – Dec
Z* (KM)
LATITUDE (DEG)
0.1
0.3
0.5
0.7
0.02
0.005
1E-3

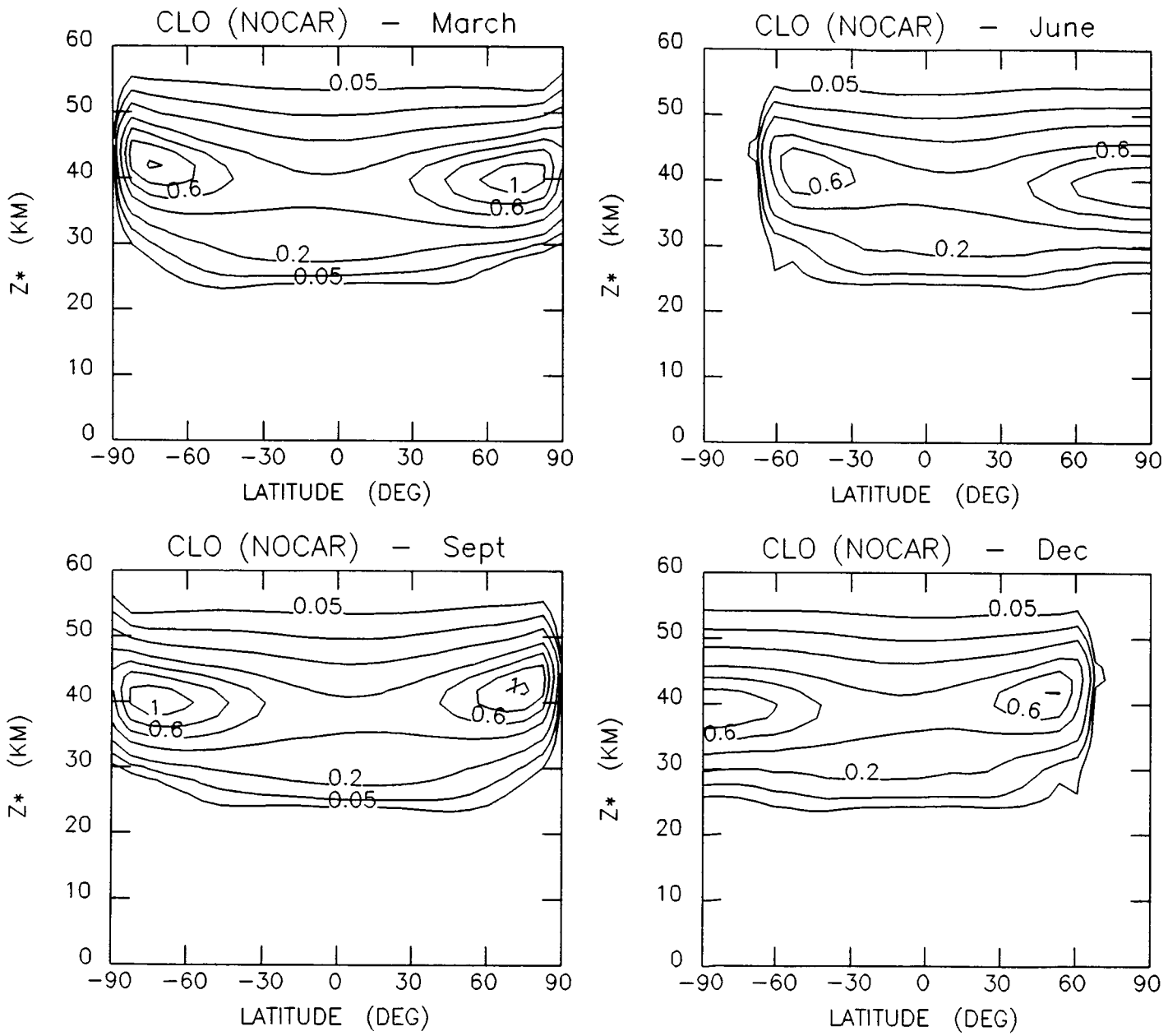
CLO (NOCAR) – March
CLO (NOCAR) – June
CLO (NOCAR) – Sept
CLO (NOCAR) – Dec
Z* (KM)
LATITUDE (DEG)
0
10
20
30
40
50
60
-90
-60
-30
0
30
60
90
0.05
0.2
0.6
1

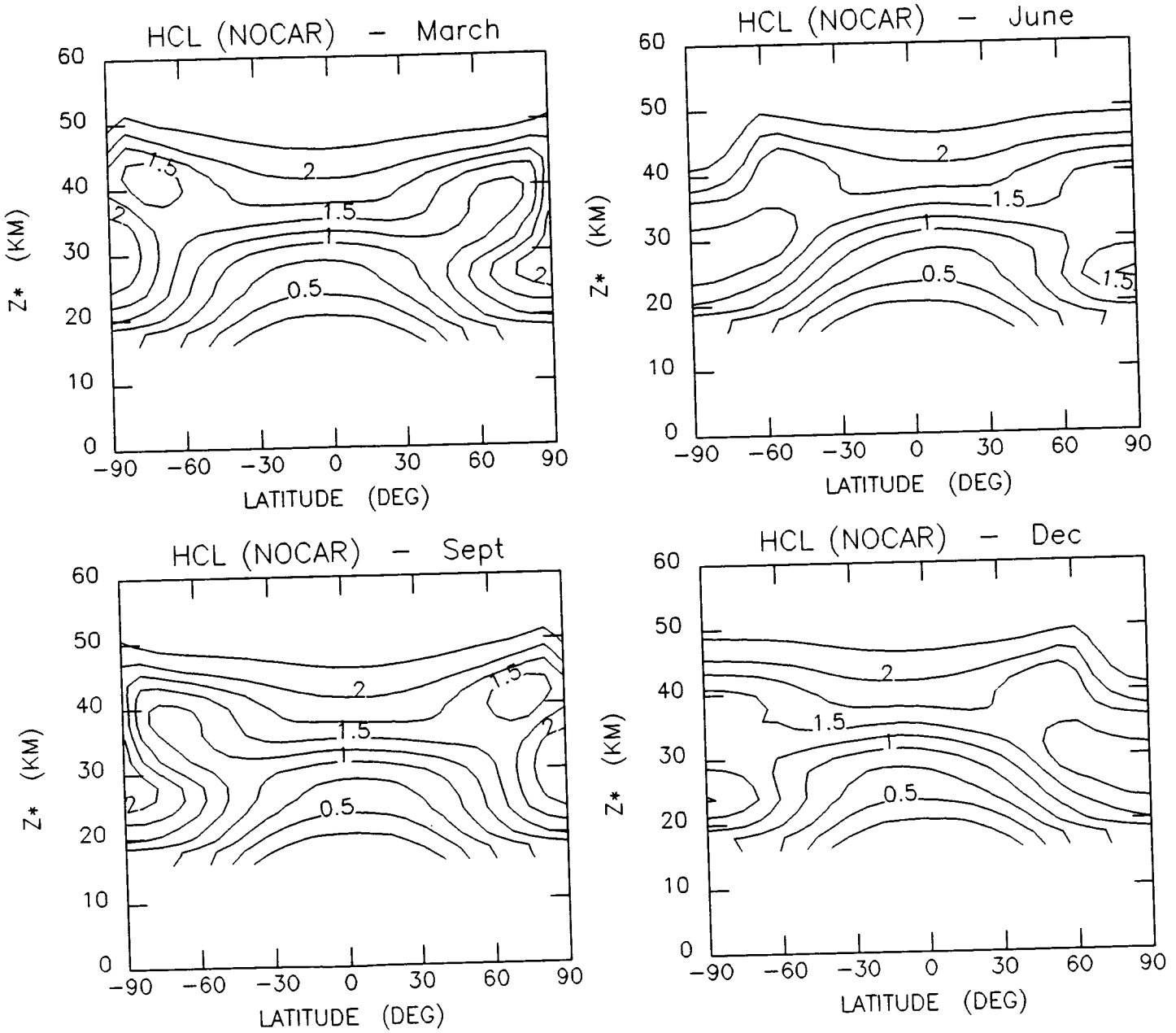
HCL (NOCAR) – March
HCL (NOCAR) – June
HCL (NOCAR) – Sept
HCL (NOCAR) – Dec
Z* (KM)
LATITUDE (DEG)
0
10
20
30
40
50
60
-90
-60
-30
0
30
60
90
0.5
1
1.5
2

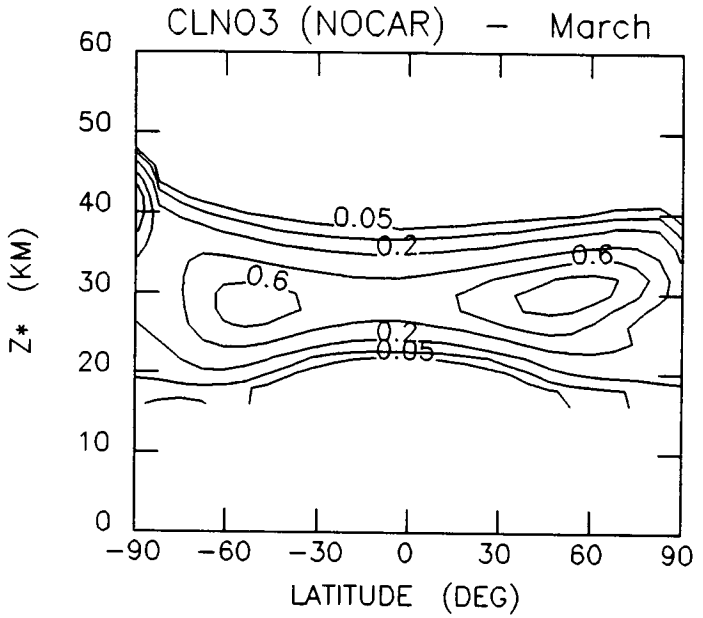
CLNO3 (NOCAR) – March
Z* (KM)
LATITUDE (DEG)
0.05
0.2
0.6
0.6
0.2
0.05

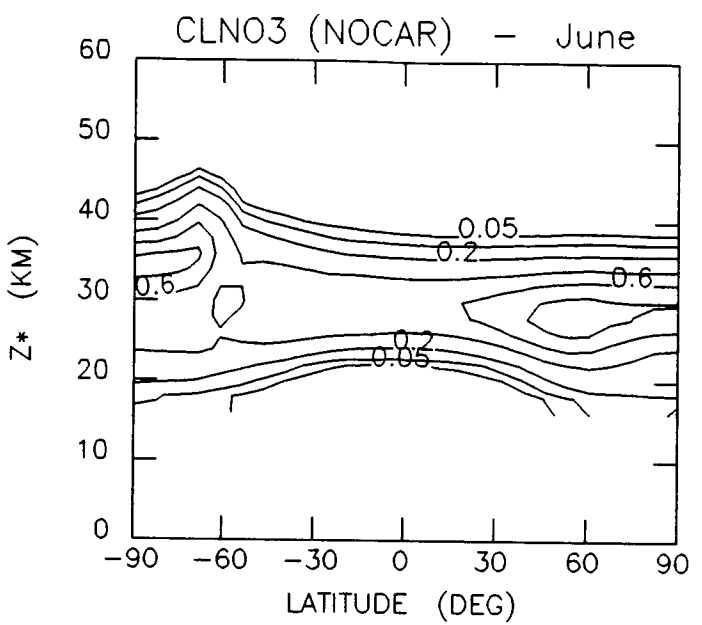
CLNO3 (NOCAR) – June
Z* (KM)
LATITUDE (DEG)
0.05
0.2
0.6
0.6
0.2
0.05

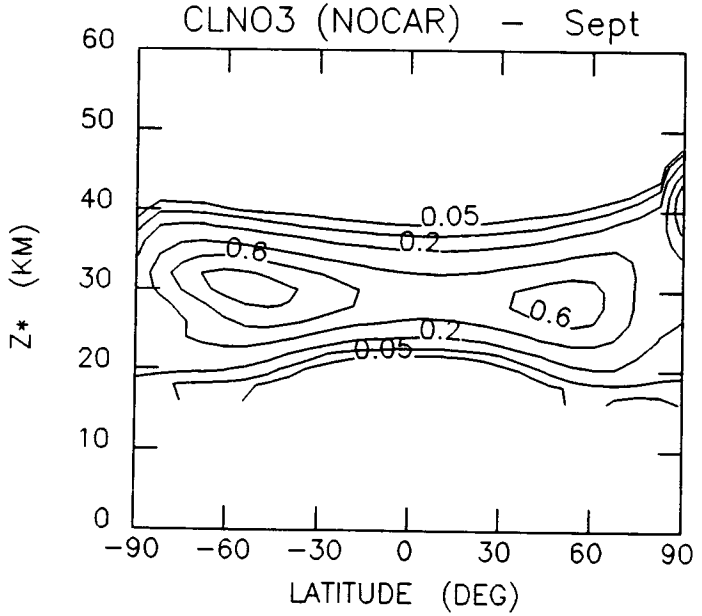
CLNO3 (NOCAR) – Sept
Z* (KM)
LATITUDE (DEG)
0.05
0.2
0.6
0.6
0.2
0.05

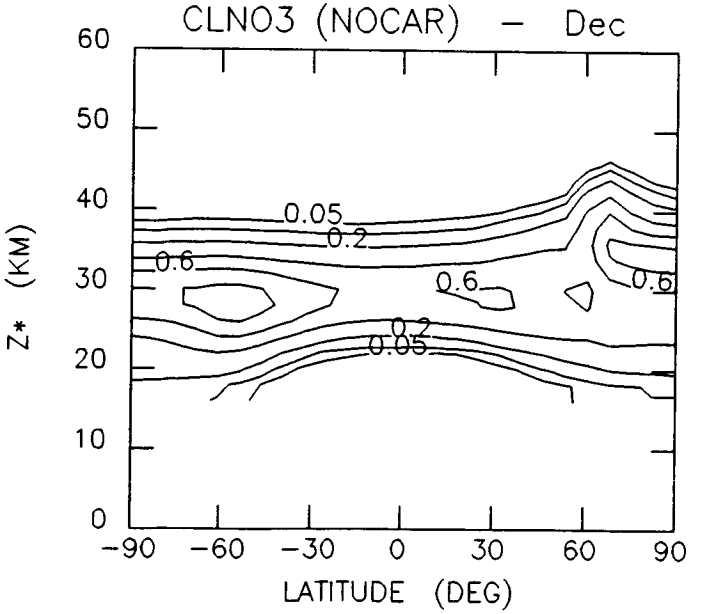
CLNO3 (NOCAR) – Dec
Z* (KM)
LATITUDE (DEG)
0.05
0.2
0.6
0.6
0.6
0.2
0.05

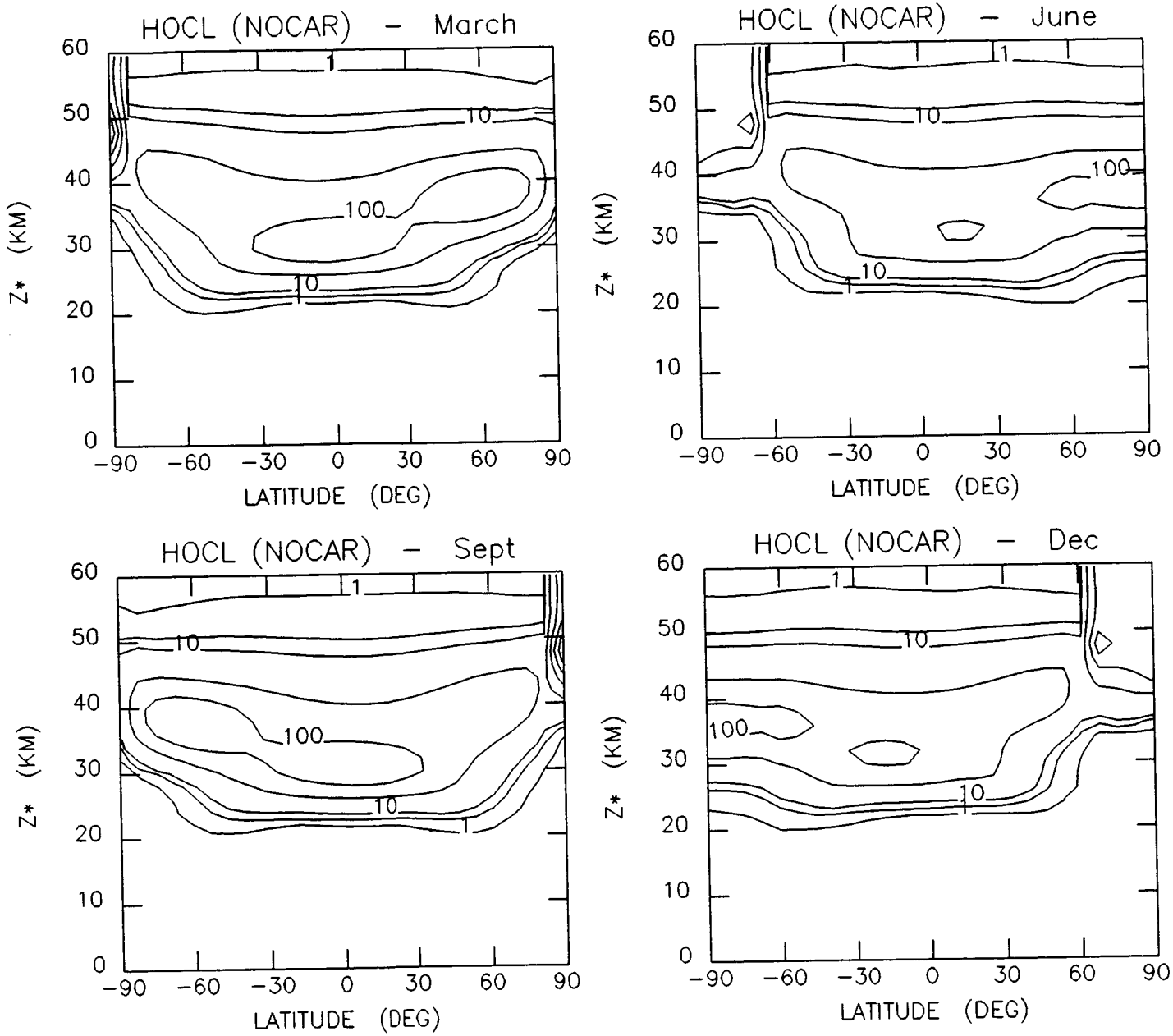
HOCL (NOCAR) – March
HOCL (NOCAR) – June
HOCL (NOCAR) – Sept
HOCL (NOCAR) – Dec
Z* (KM)
LATITUDE (DEG)
0
10
20
30
40
50
60
-90
-60
-30
0
30
60
90
1
10
100

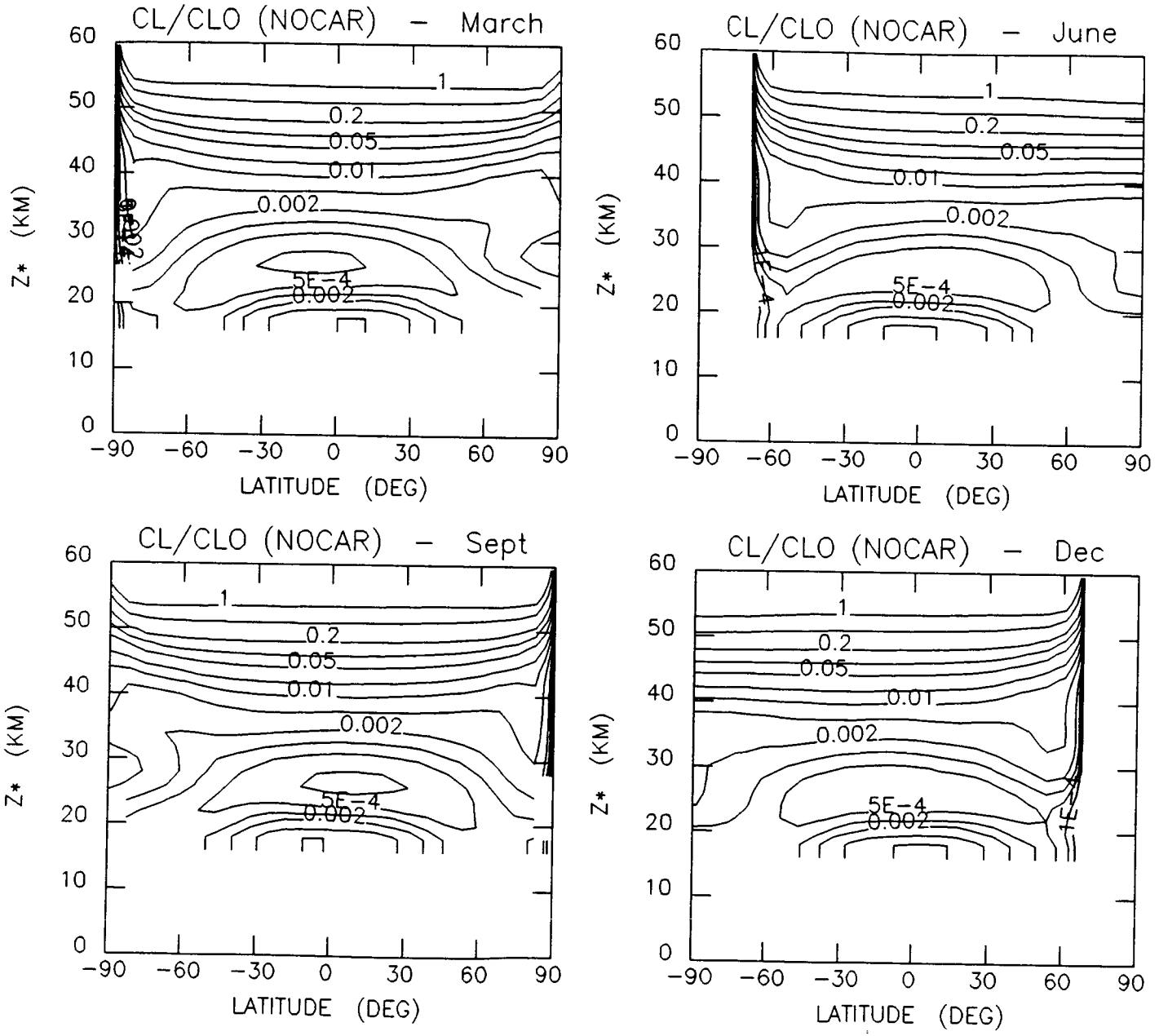
CL/CLO (NOCAR) – March
CL/CLO (NOCAR) – June
CL/CLO (NOCAR) – Sept
CL/CLO (NOCAR) – Dec
Z* (KM)
LATITUDE (DEG)
1
0.2
0.05
0.01
0.002
5E-4
0
10
20
30
40
50
60
-90
-60
-30
0
30
60
90

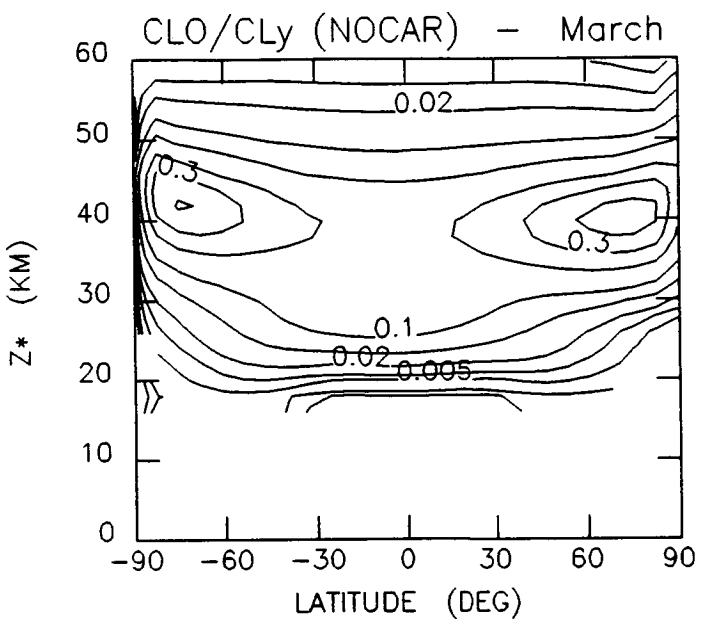
CLO/CLy (NOCAR) – March
Z* (KM)
LATITUDE (DEG)
0.02
0.3
0.3
0.1
0.02
0.005

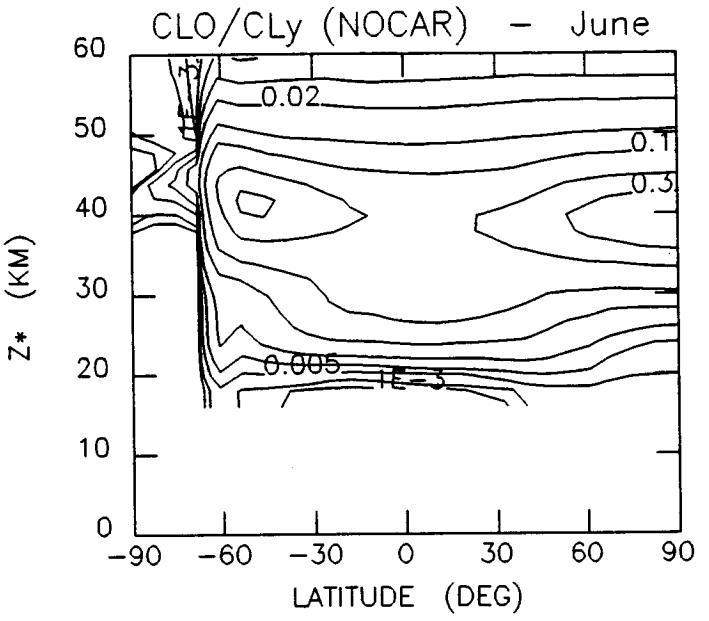
CLO/CLy (NOCAR) – June
Z* (KM)
LATITUDE (DEG)
0.02
0.1
0.3
0.005
1E-3

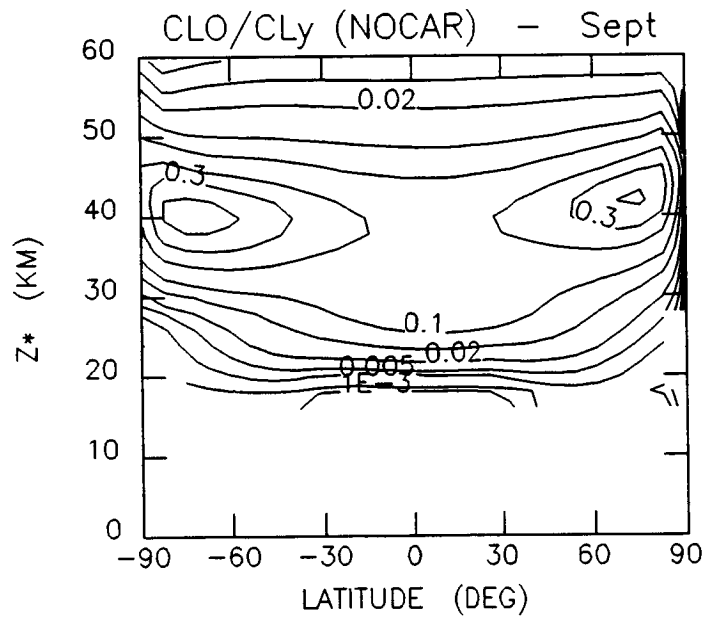
CLO/CLy (NOCAR) – Sept
Z* (KM)
LATITUDE (DEG)
0.02
0.3
0.3
0.1
0.02
0.005
1E-3

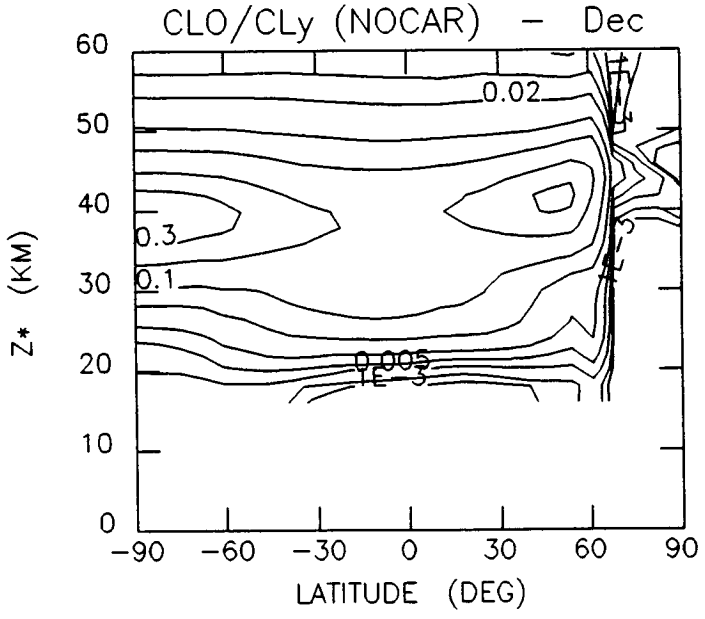
CLO/CLy (NOCAR) – Dec
Z* (KM)
LATITUDE (DEG)
0.02
0.3
0.1
0.005
1E-3

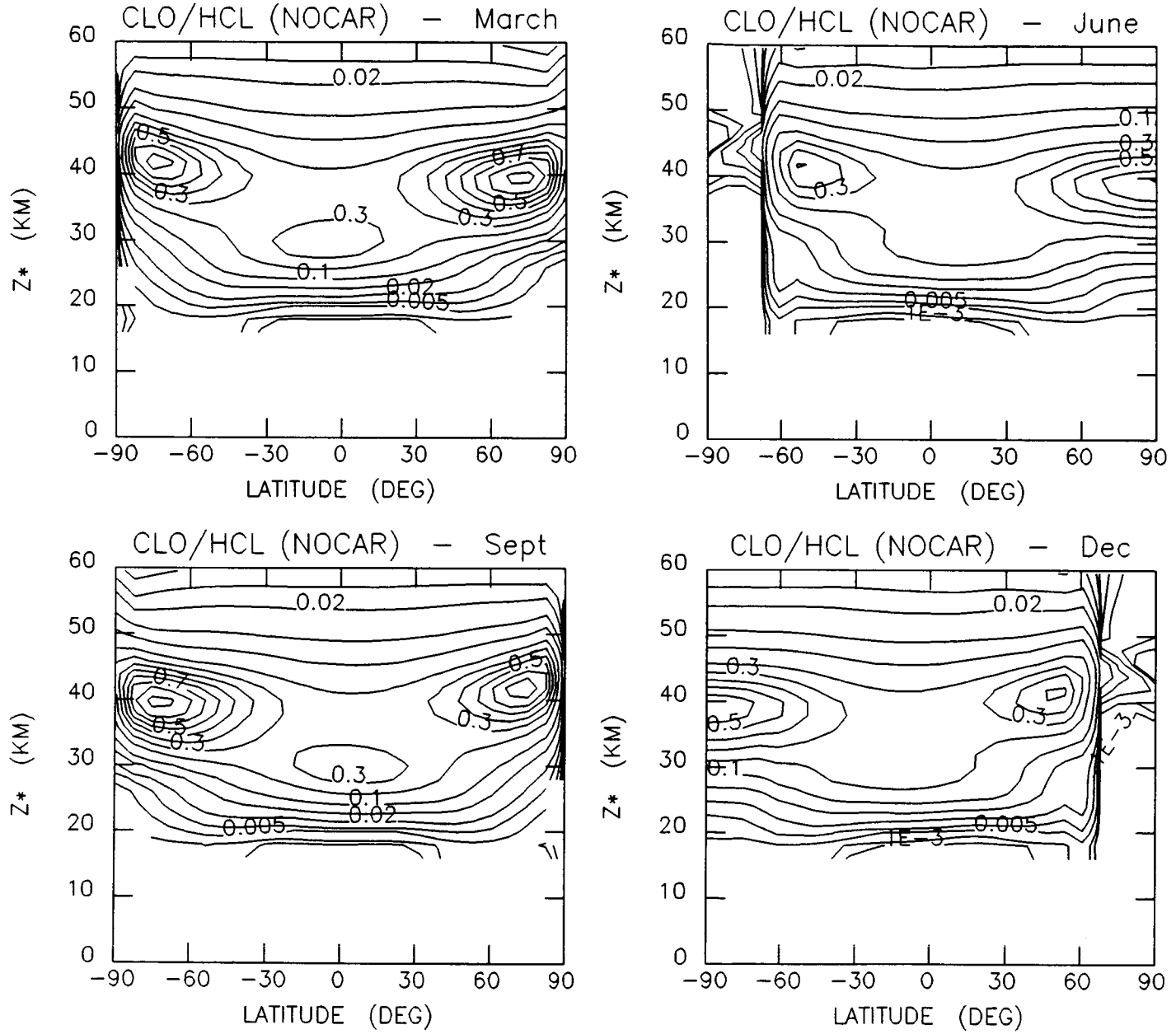
CLO/HCL (NOCAR) – March
CLO/HCL (NOCAR) – June
CLO/HCL (NOCAR) – Sept
CLO/HCL (NOCAR) – Dec
Z* (KM)
LATITUDE (DEG)
0
10
20
30
40
50
60
−90
−60
−30
0
30
60
90
0.02
0.5
0.7
0.3
0.1
0.005
1E−3

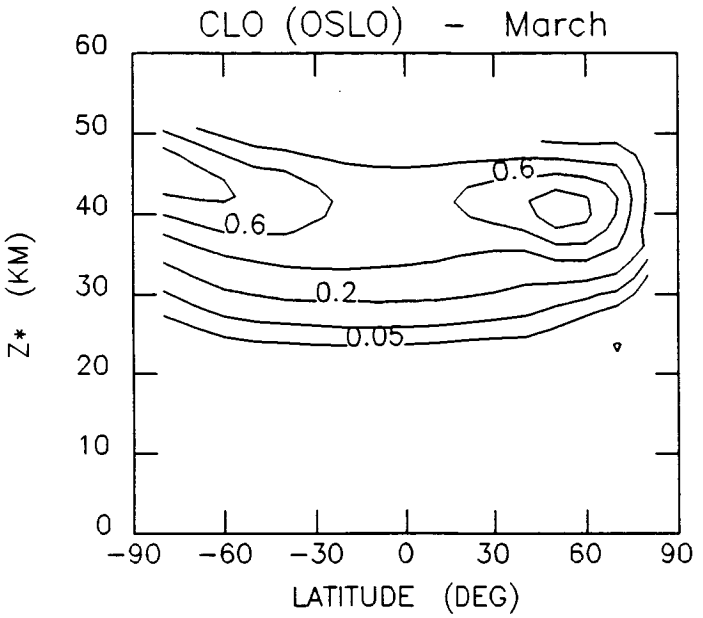
CLO (OSLO) - March
Z* (KM)
LATITUDE (DEG)
0.6
0.6
0.2
0.05

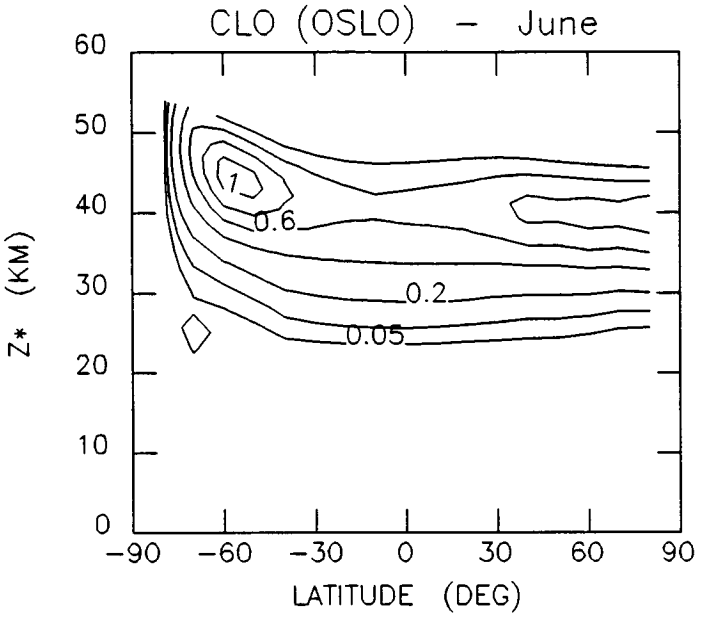
CLO (OSLO) - June
Z* (KM)
LATITUDE (DEG)
1
0.6
0.2
0.05

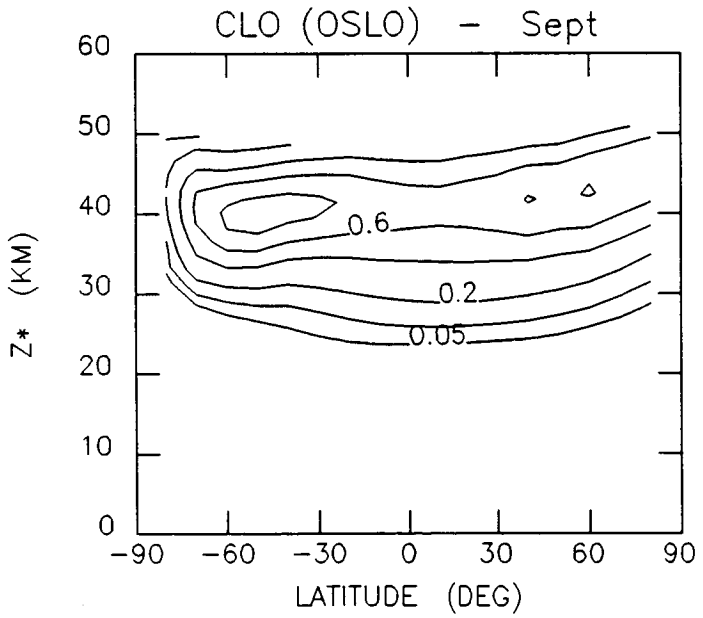
CLO (OSLO) - Sept
Z* (KM)
LATITUDE (DEG)
0.6
0.2
0.05

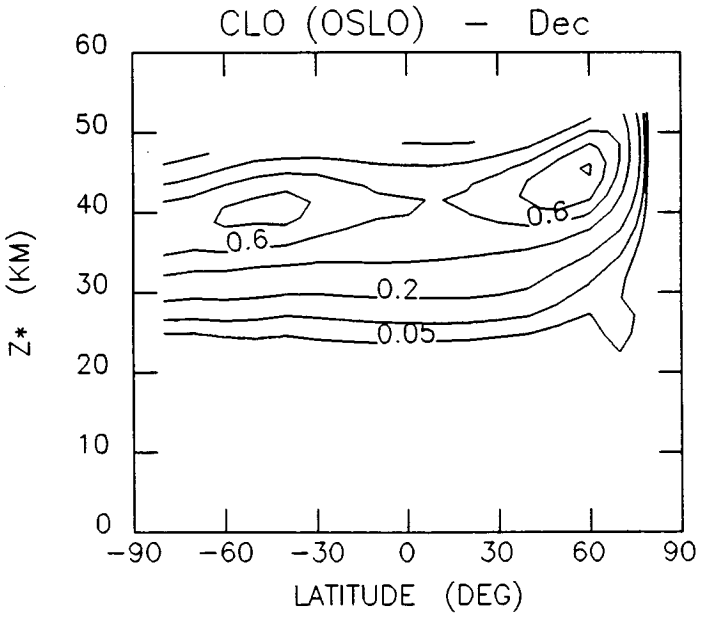
CLO (OSLO) - Dec
Z* (KM)
LATITUDE (DEG)
0.6
0.6
0.2
0.05

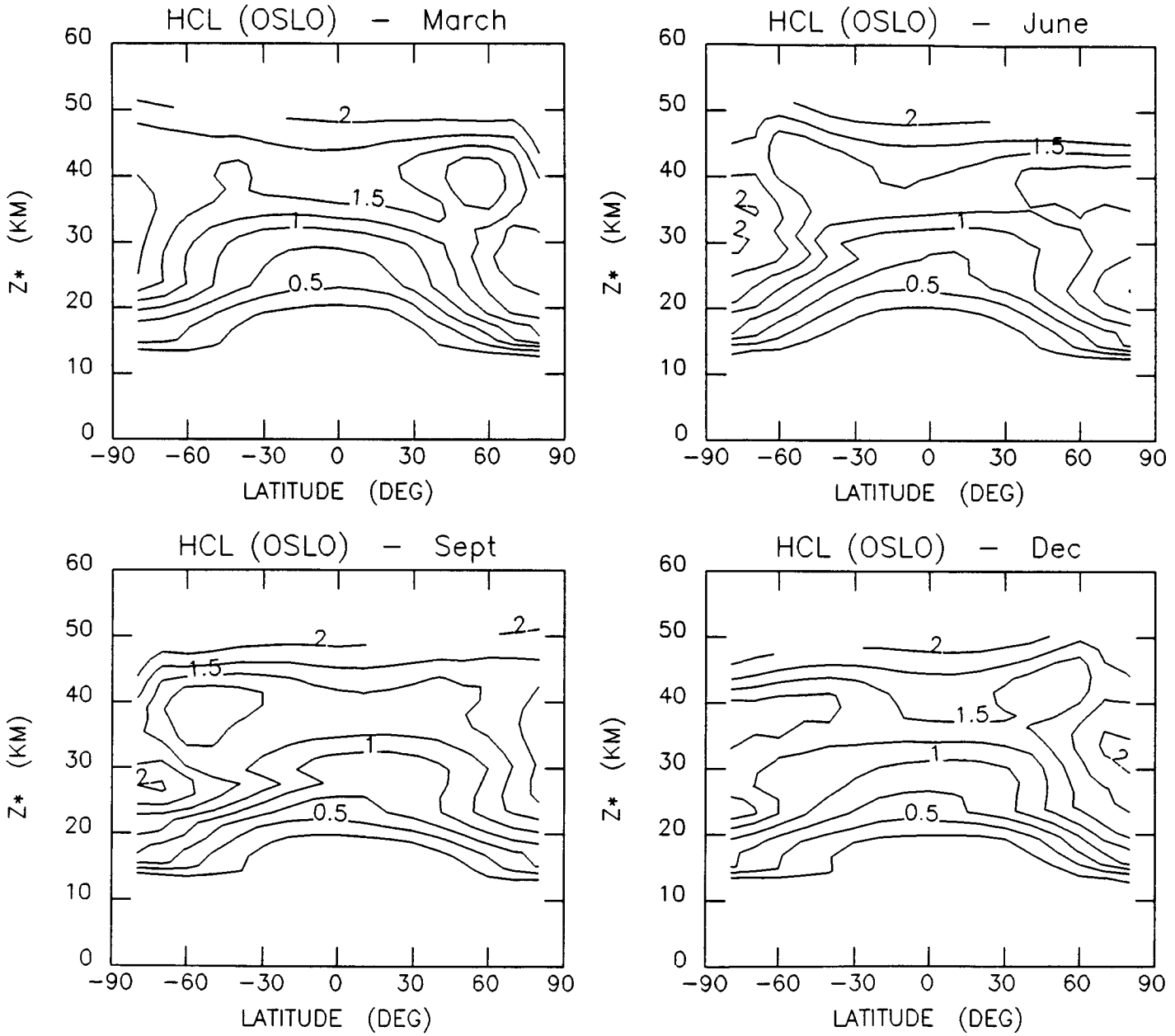
HCL (OSLO) – March
HCL (OSLO) – June
HCL (OSLO) – Sept
HCL (OSLO) – Dec
Z* (KM)
LATITUDE (DEG)
0
10
20
30
40
50
60
-90
-60
-30
0
30
60
90
0.5
1
1.5
2

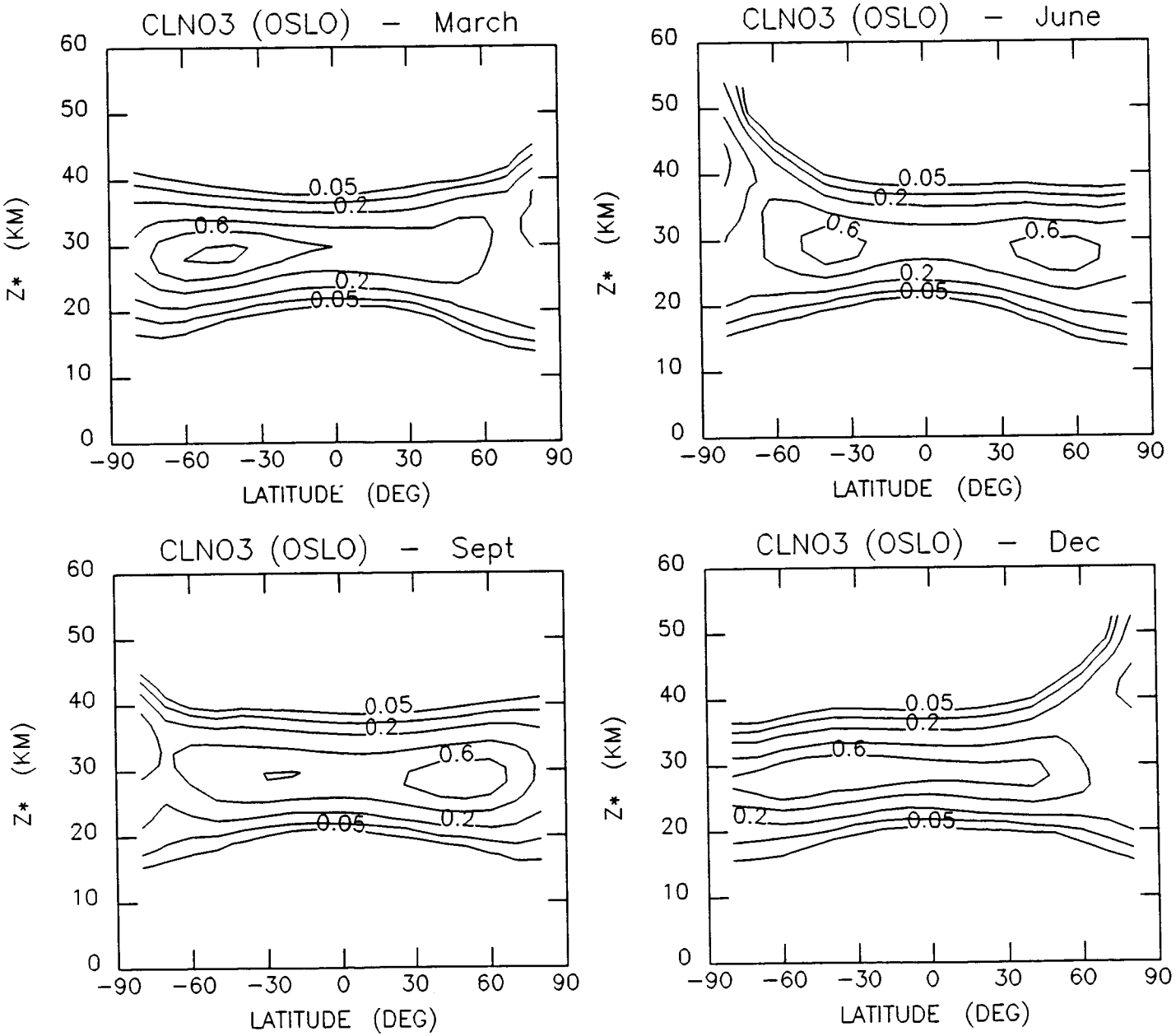
CLNO3 (OSLO) – March
CLNO3 (OSLO) – June
CLNO3 (OSLO) – Sept
CLNO3 (OSLO) – Dec
Z* (KM)
LATITUDE (DEG)
0.05
0.2
0.6
0
10
20
30
40
50
60
-90
-60
-30
0
30
60
90

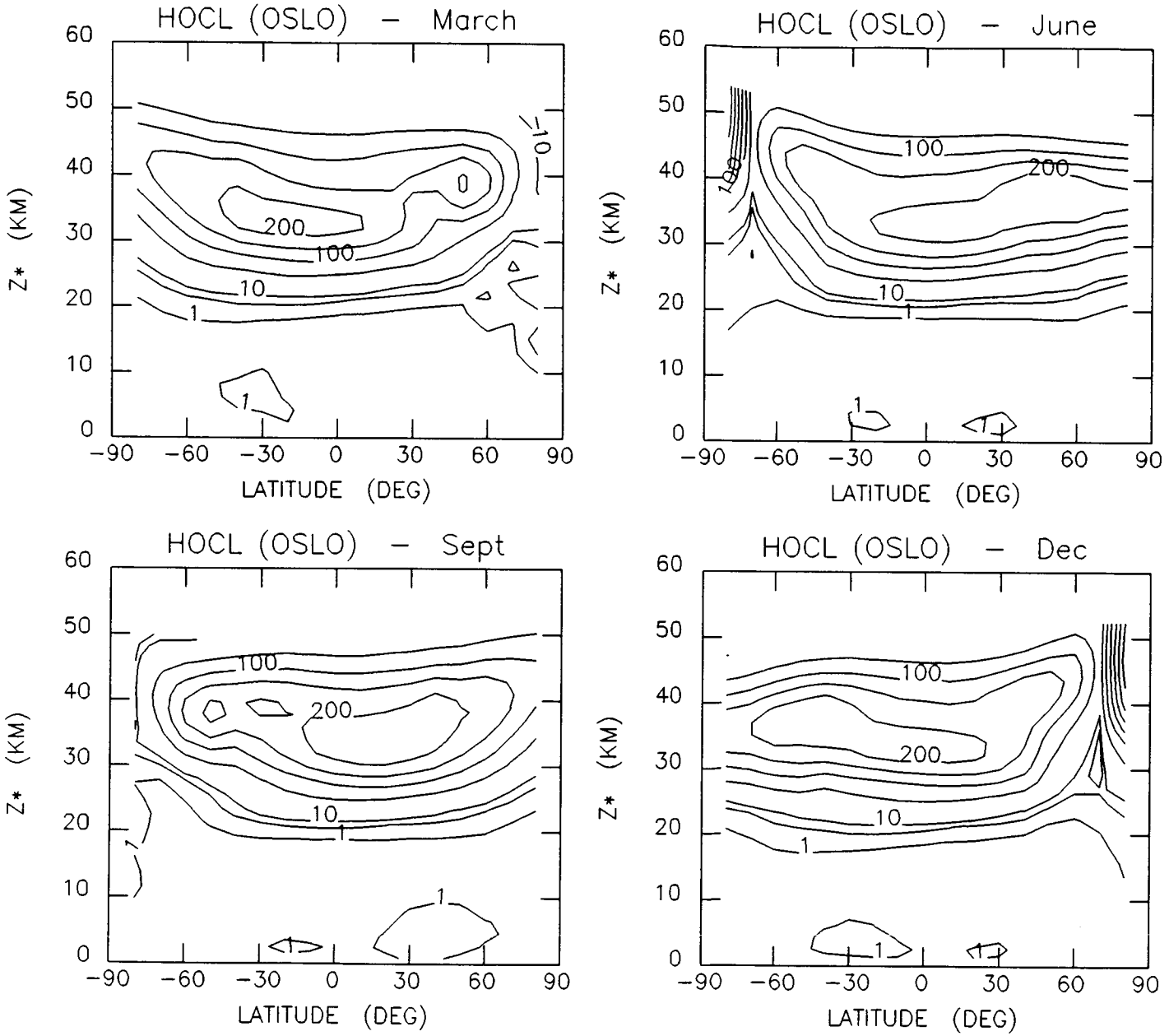
HOCL (OSLO) – March
HOCL (OSLO) – June
HOCL (OSLO) – Sept
HOCL (OSLO) – Dec
Z* (KM)
LATITUDE (DEG)
60
50
40
30
20
10
0
-90
-60
-30
0
30
60
90
200
100
10
1

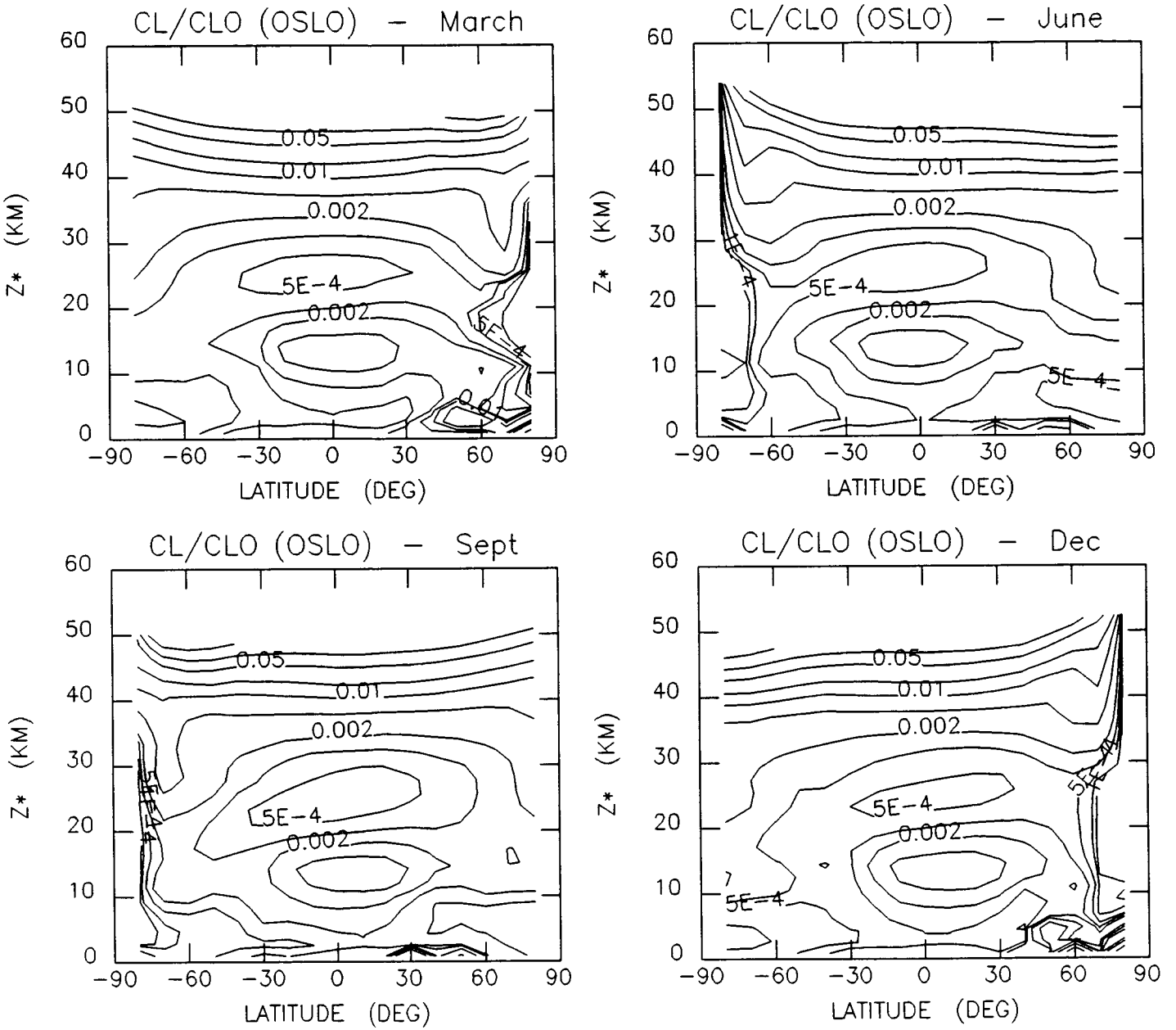
CL/CLO (OSLO) – March
CL/CLO (OSLO) – June
CL/CLO (OSLO) – Sept
CL/CLO (OSLO) – Dec
Z* (KM)
LATITUDE (DEG)
0.05
0.01
0.002
5E-4
60
50
40
30
20
10
0
-90
-60
-30
0
30
60
90

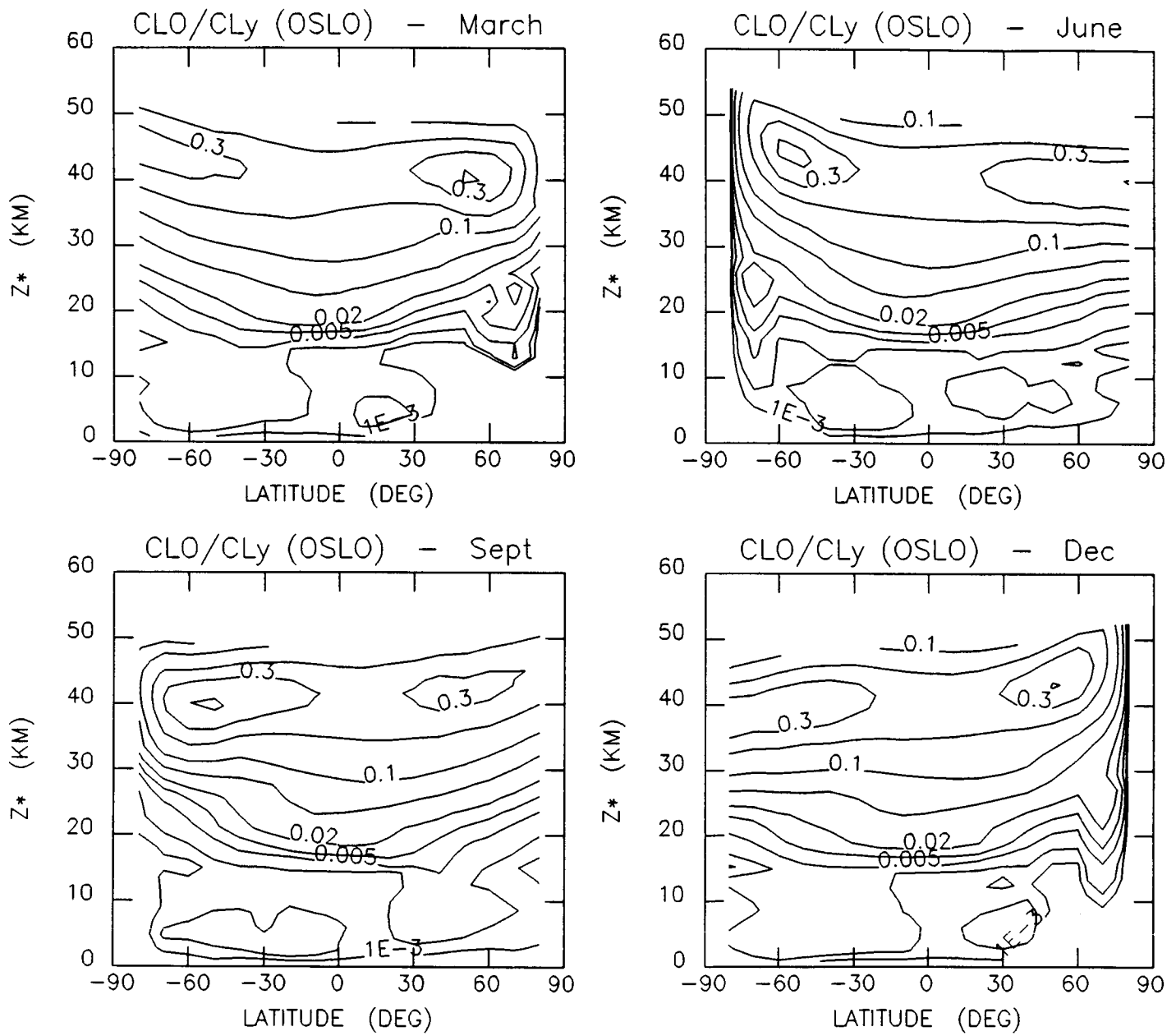
CLO/CLy (OSLO) – March
CLO/CLy (OSLO) – June
CLO/CLy (OSLO) – Sept
CLO/CLy (OSLO) – Dec
Z* (KM)
LATITUDE (DEG)
0
10
20
30
40
50
60
−90
−60
−30
0
30
60
90
0.3
0.1
0.02
0.005
1E−3

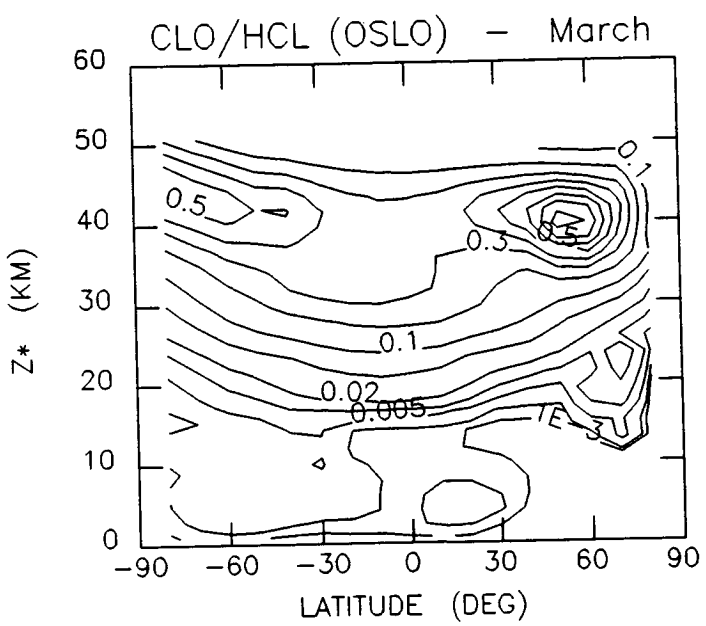
CLO/HCL (OSLO) – March
Z* (KM)
LATITUDE (DEG)
0.5
0.3
0.1
0.02
0.005
1E-3

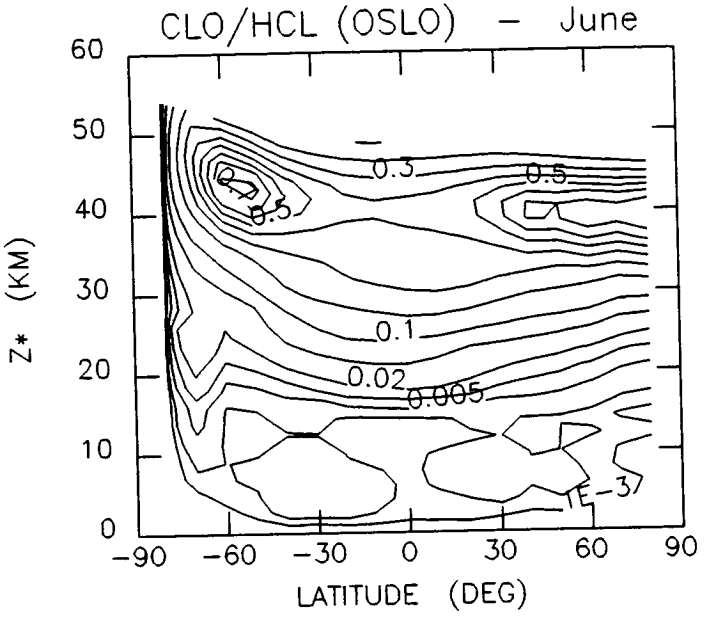
CLO/HCL (OSLO) – June
Z* (KM)
LATITUDE (DEG)
0.5
0.3
0.1
0.02
0.005
1E-3

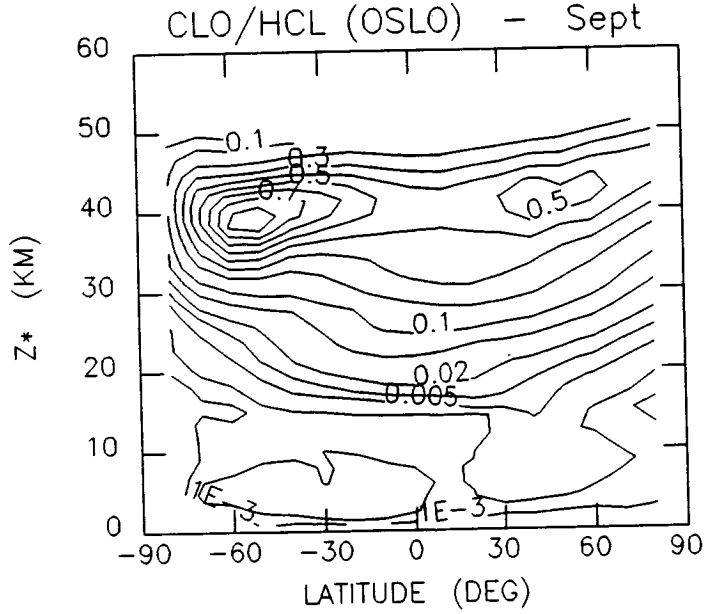
CLO/HCL (OSLO) – Sept
Z* (KM)
LATITUDE (DEG)
0.5
0.3
0.1
0.02
0.005
1E-3

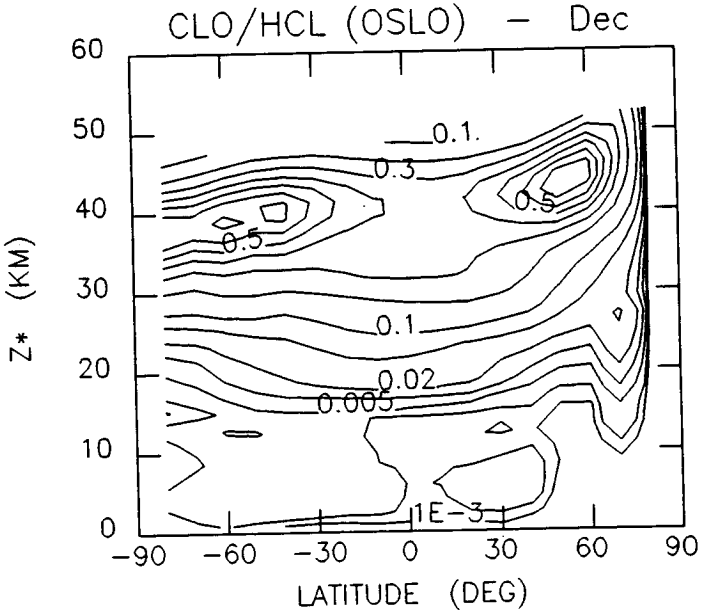
CLO/HCL (OSLO) – Dec
Z* (KM)
LATITUDE (DEG)
0.5
0.3
0.1
0.02
0.005
1E-3

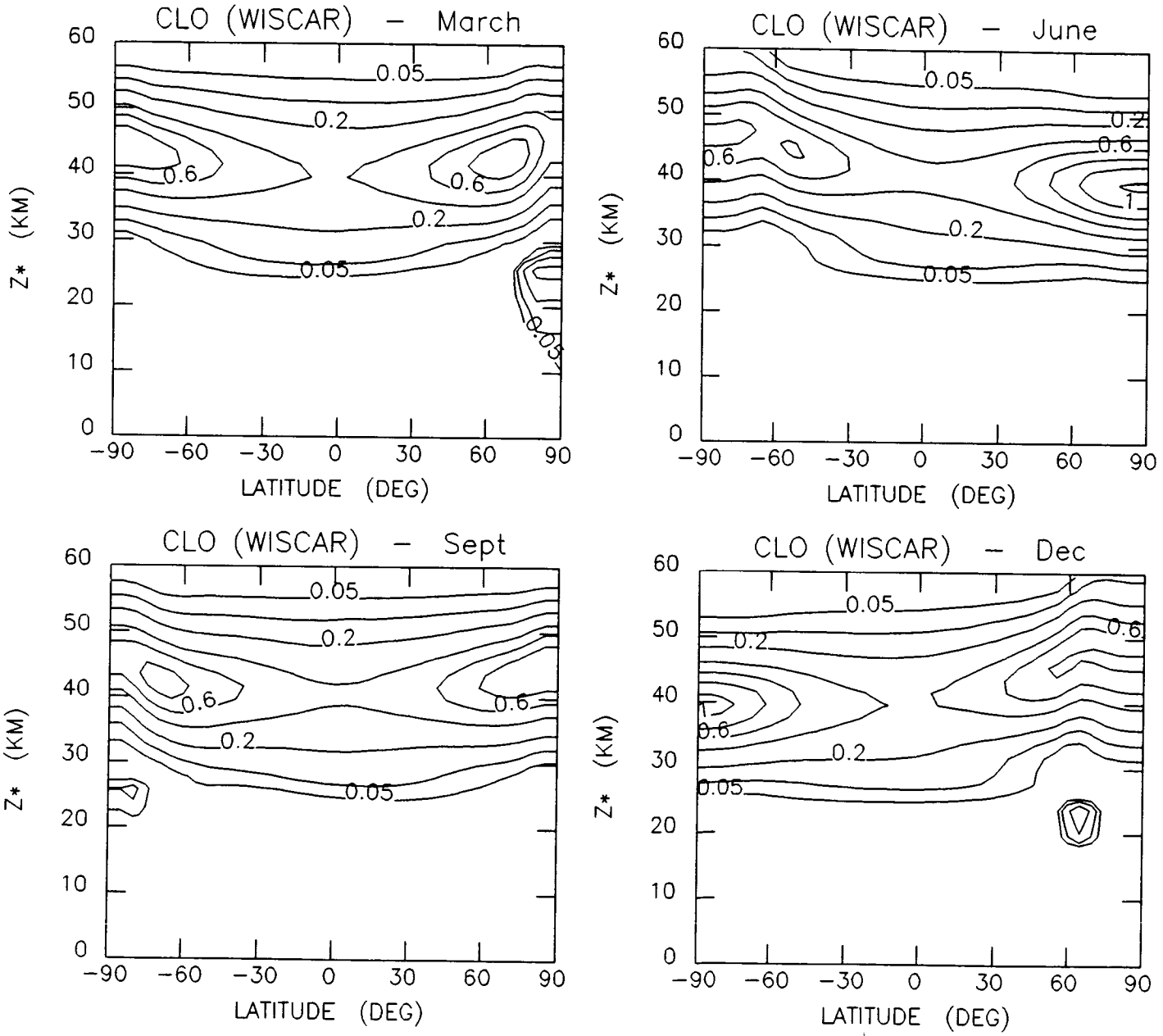
CLO (WISCAR) – March
CLO (WISCAR) – June
CLO (WISCAR) – Sept
CLO (WISCAR) – Dec
Z* (KM)
LATITUDE (DEG)
0.05
0.2
0.6
1
0
10
20
30
40
50
60
−90
−60
−30
0
30
60
90

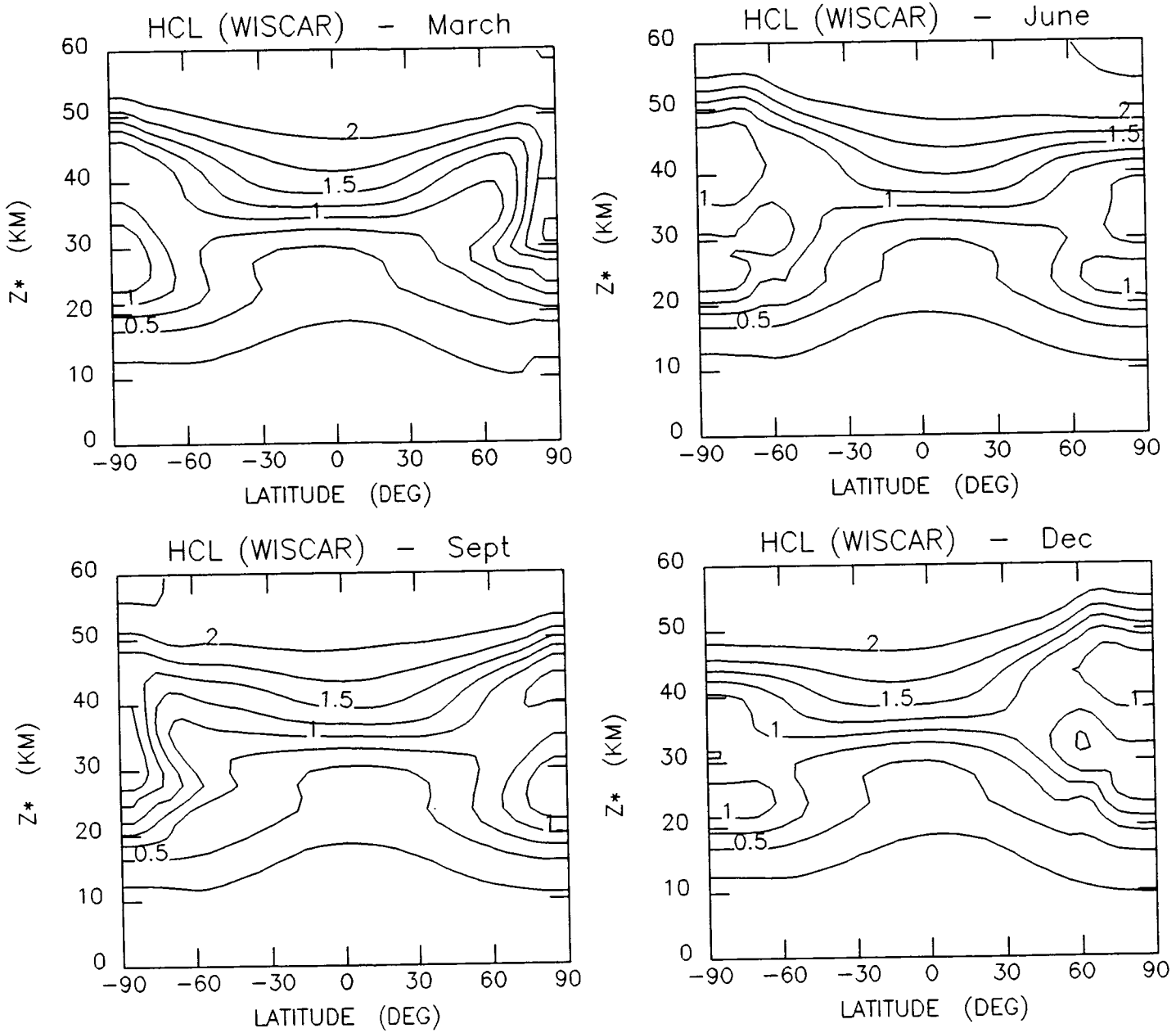
HCL (WISCAR) – March
HCL (WISCAR) – June
HCL (WISCAR) – Sept
HCL (WISCAR) – Dec
Z* (KM)
LATITUDE (DEG)
0
10
20
30
40
50
60
-90
-60
-30
0
30
60
90
0.5
1
1.5
2

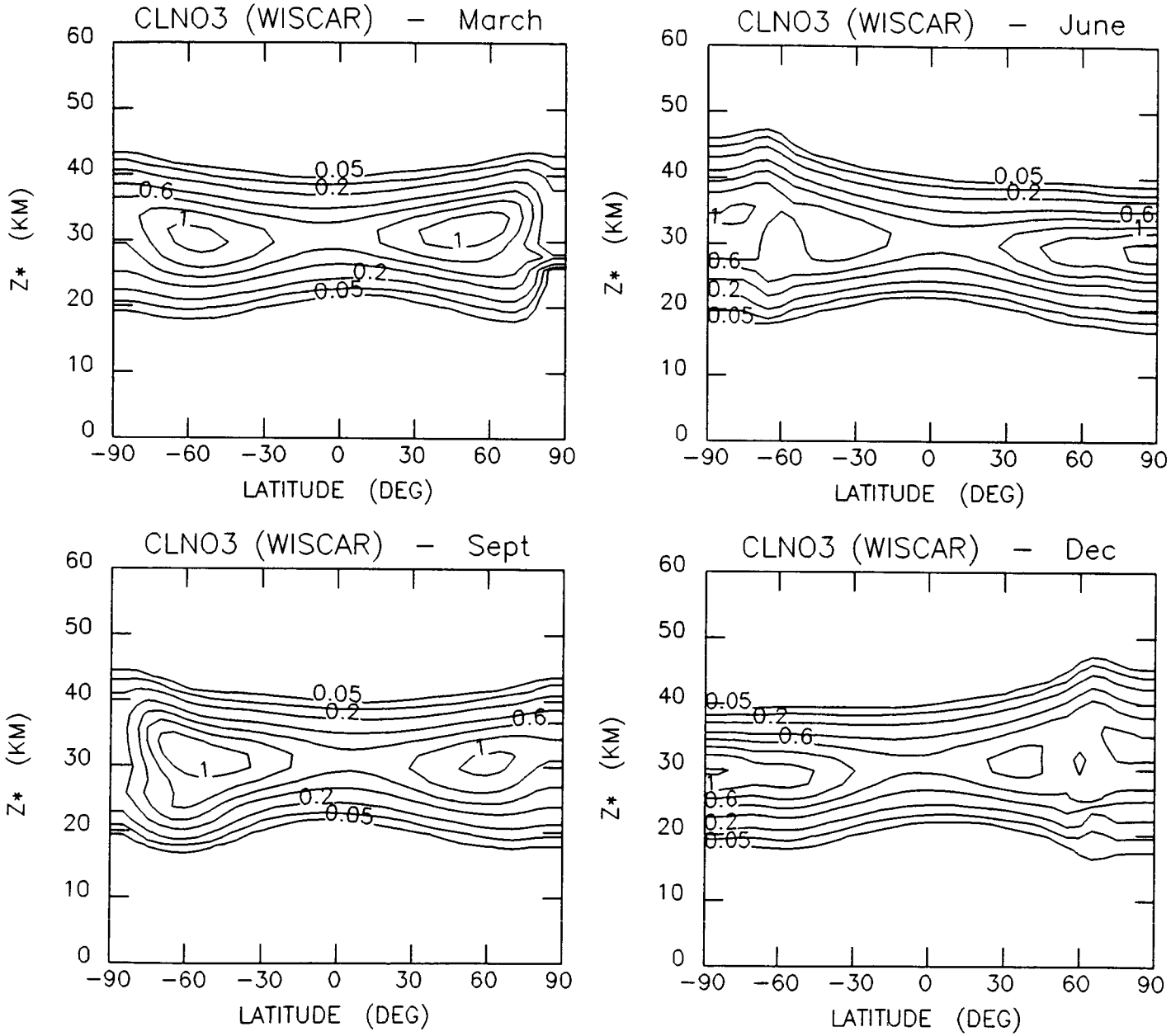
CLNO3 (WISCAR) – March
CLNO3 (WISCAR) – June
CLNO3 (WISCAR) – Sept
CLNO3 (WISCAR) – Dec
Z* (KM)
LATITUDE (DEG)
0
10
20
30
40
50
60
−90
−60
−30
0
30
60
90
0.05
0.2
0.6
1

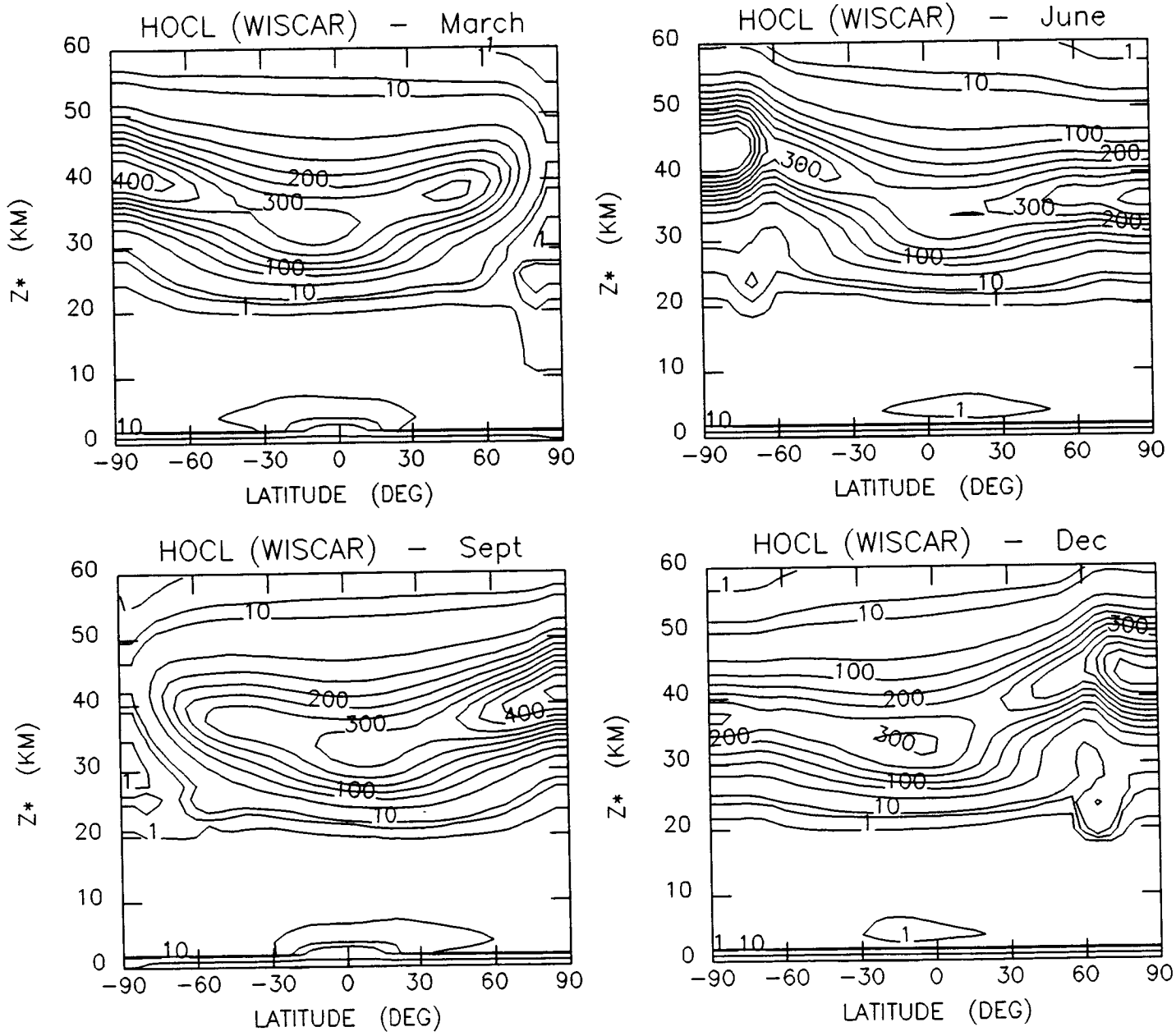
HOCL (WISCAR) – March
HOCL (WISCAR) – June
HOCL (WISCAR) – Sept
HOCL (WISCAR) – Dec
Z* (KM)
LATITUDE (DEG)
60
50
40
30
20
10
0
-90
-60
-30
0
30
60
90
1
10
100
200
300
400

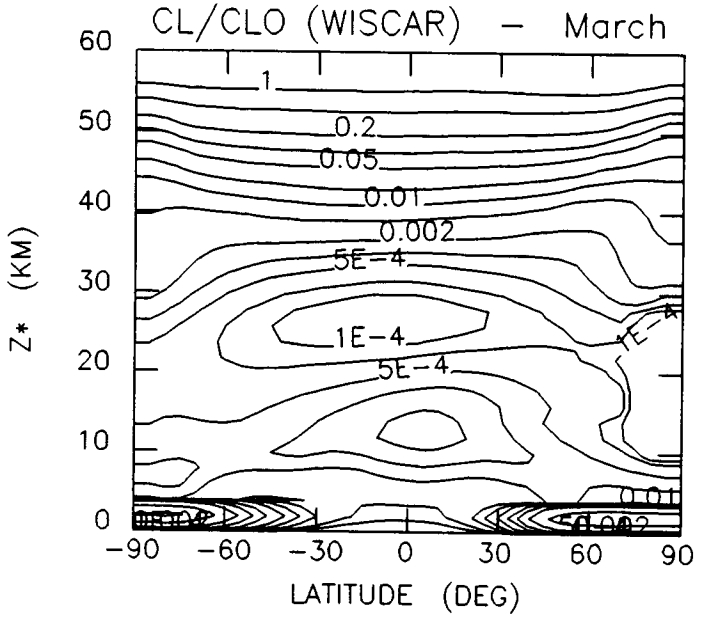
CL/CLO (WISCAR) – March
Z* (KM)
LATITUDE (DEG)
1
0.2
0.05
0.01
0.002
5E-4
1E-4

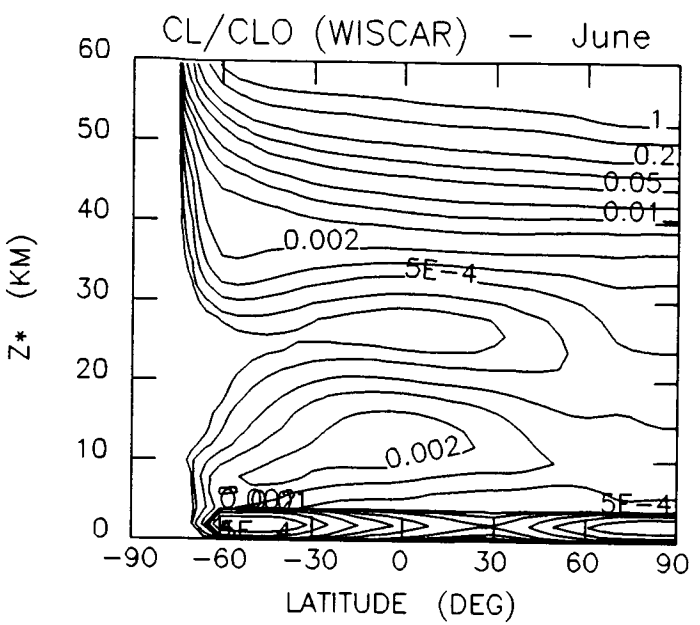
CL/CLO (WISCAR) – June
Z* (KM)
LATITUDE (DEG)
1
0.2
0.05
0.01
0.002
5E-4

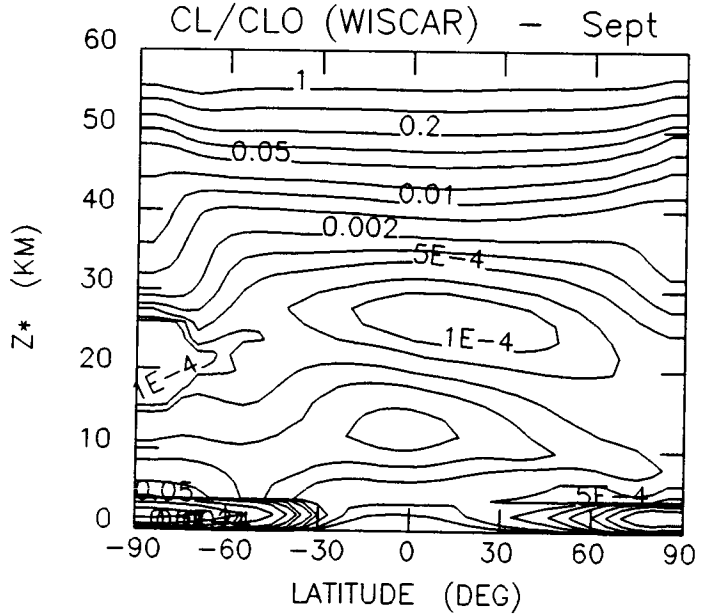
CL/CLO (WISCAR) – Sept
Z* (KM)
LATITUDE (DEG)
1
0.2
0.05
0.01
0.002
5E-4
1E-4

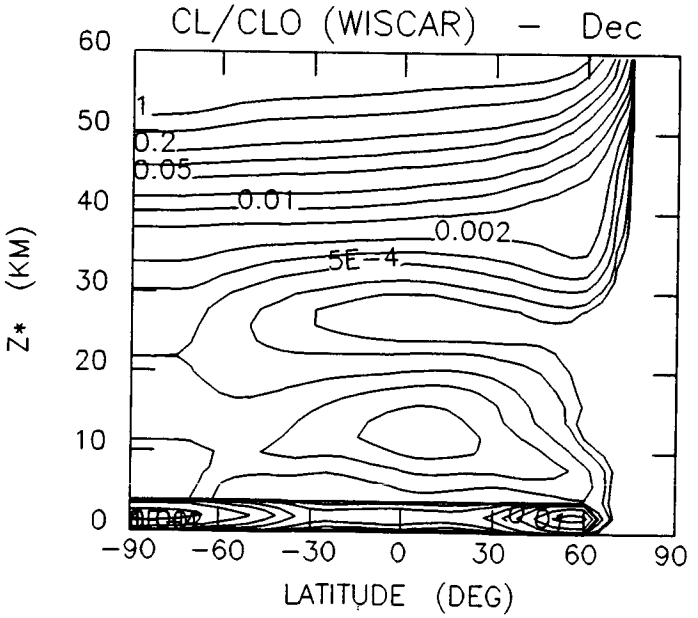
CL/CLO (WISCAR) – Dec
Z* (KM)
LATITUDE (DEG)
1
0.2
0.05
0.01
0.002
5E-4

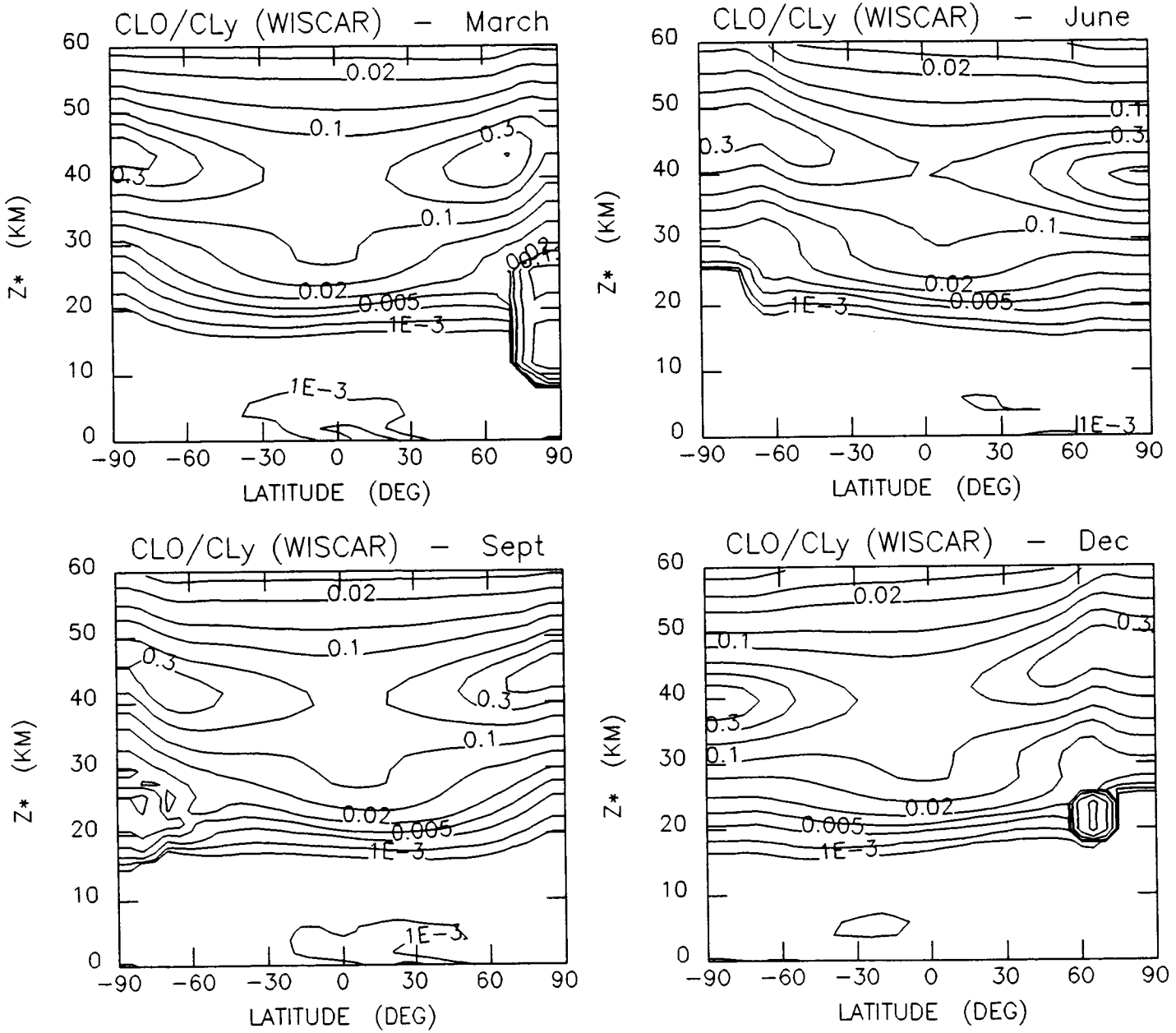
CLO/CLy (WISCAR) – March
CLO/CLy (WISCAR) – June
CLO/CLy (WISCAR) – Sept
CLO/CLy (WISCAR) – Dec
Z* (KM)
LATITUDE (DEG)
0.02
0.1
0.3
0.005
1E-3

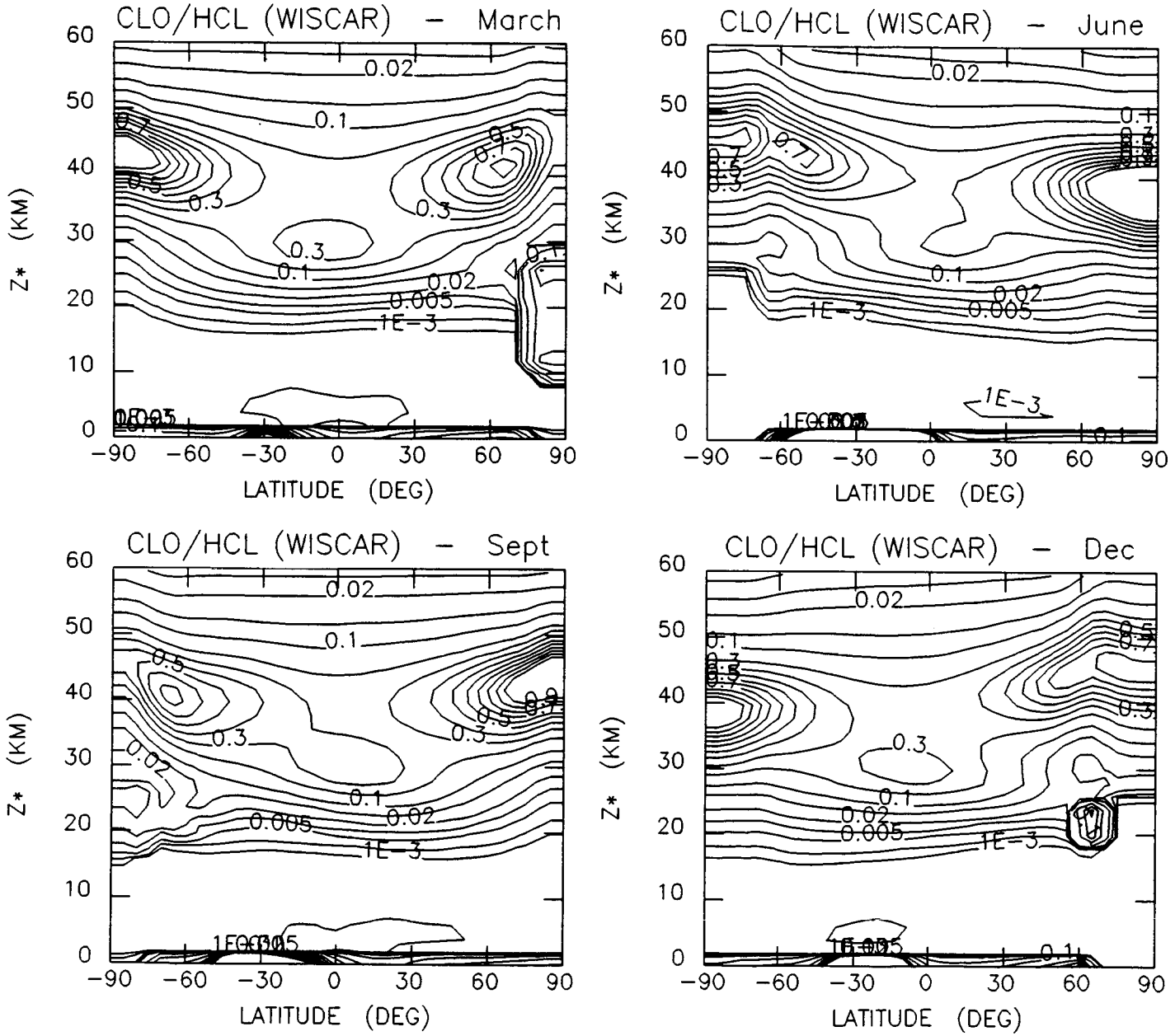
CLO/HCL (WISCAR) – March
CLO/HCL (WISCAR) – June
CLO/HCL (WISCAR) – Sept
CLO/HCL (WISCAR) – Dec
Z* (KM)
LATITUDE (DEG)
0.02
0.1
0.3
0.5
0.7
0.005
1E-3

**Table 6-3e.** Current Atmosphere (1980): $O_x$ and $HO_x$ Gases

March, June, September, and December
Models Represented - AER, CAMBRAL, CLKSON, DUPONT (Jan. & April), GSFC1 (Jan.), GSFC2, LARC, LLNL, MRI, NOCAR, OSLO, WISCAR

| Parameter | Description | Units | Contour Levels |
|---|---|---|---|
| $O_3$ | $O_3$ Mixing Ratio | ppmv | 0.1, 0.2, 0.5, 1, 2, 4, 6, 8, 10, 12, 14, 16, 18, 20 |
| $HO_2$ | $HO_2$ Mixing Ratio | pptv | 1, 5, 10, 20, 50, 100, 150, 200, 250, 300, 350, 400, 450, 500, 550, 600 |
| $H_2O_2$ | $H_2O_2$ Mixing Ratio | pptv | 1, 5, 10, 20, 50, 100, 150, 200, 250, 300, 350, 400, 450, 500 |
| $H_2CO$ | $H_2CO$ ($CH_2O$) Mixing Ratio | pptv | 1, 5, 10, 20, 50, 100, 150, 200, 250, 300, 350, 400 |
| O | O Number Density | 10E+9 Molecules/$cm^3$ | 1.0E-04, 1-0E-03, 0.01, 0.02, 0.05, 0.1, 0.2, 0.5, 1, 2, 3, 4, 5, 6, 7 |
| OH | OH Number Density | 10E+7 Molecules/$cm^3$ | 0.01, 0.05, 0.1, 0.2, 0.5, 0.75, 1, 1.25, 1.5, 1.75, 2, 2.25, 2.5, 2.75, 3 |
| $O/O_3$ | Ratio of O to $O_3$ Mixing Ratios | --- | 1.0E-07, 4.0E-07, 1.0E-06, 4.0E-06, 1.0E-05, 4.0E-05, 1.0E-04, 4.0E-04, 1.0E-03, 4.0E-03, 0.01, 0.04, 0.1, 0.4, 1 |
| $OH/HO_2$ | Ratio of OH to $HO_2$ Mixing Ratios | --- | 0.01, 0.05, 0.1, 0.2, 0.4, 0.6, 0.8, 1, 1.2, 1.4, 1.6, 1.8, 2, 2.2, 2.4 |

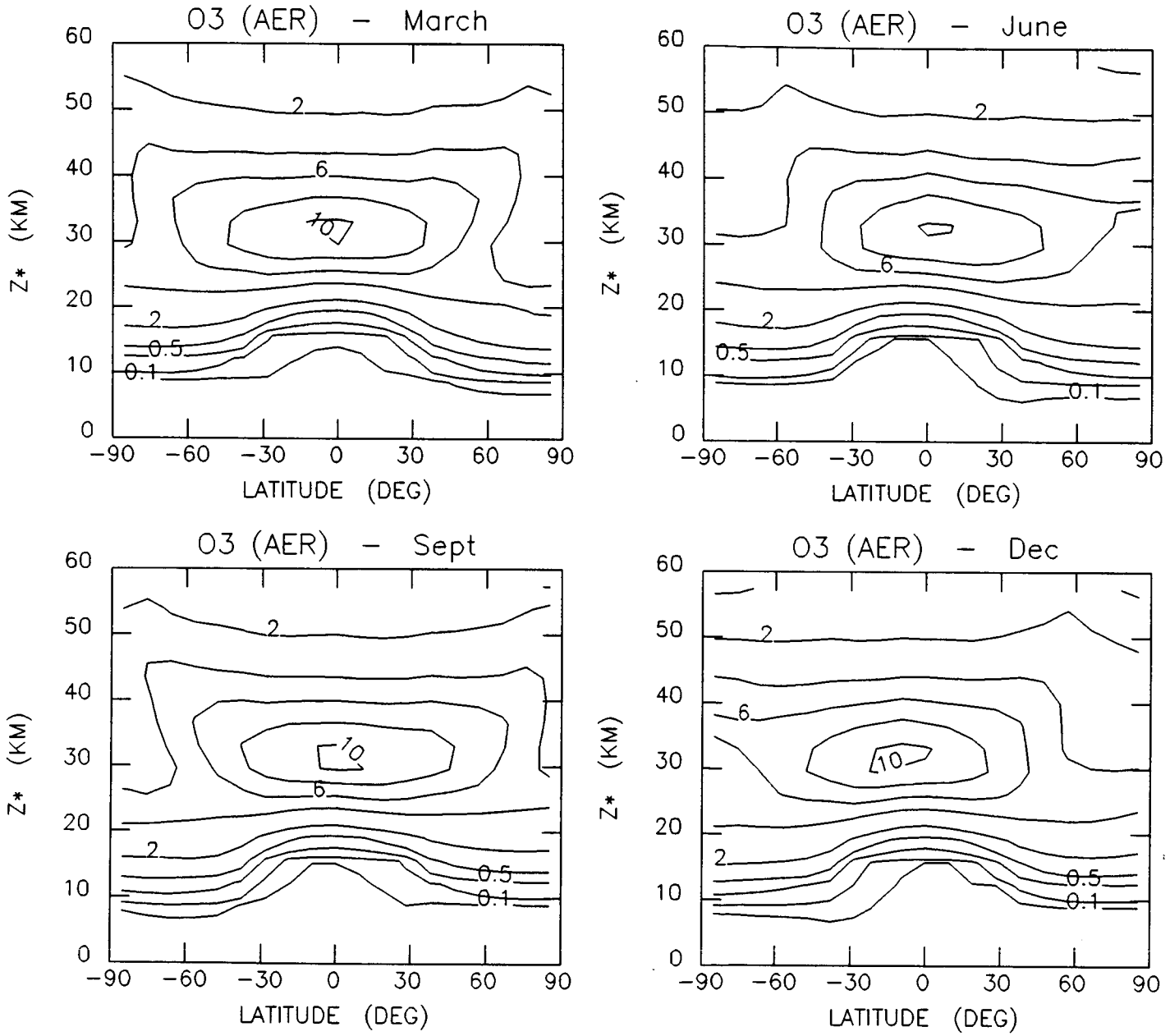
O3 (AER) – March
O3 (AER) – June
O3 (AER) – Sept
O3 (AER) – Dec
Z* (KM)
LATITUDE (DEG)
0
10
20
30
40
50
60
−90
−60
−30
0
30
60
90
2
6
10
0.5
0.1

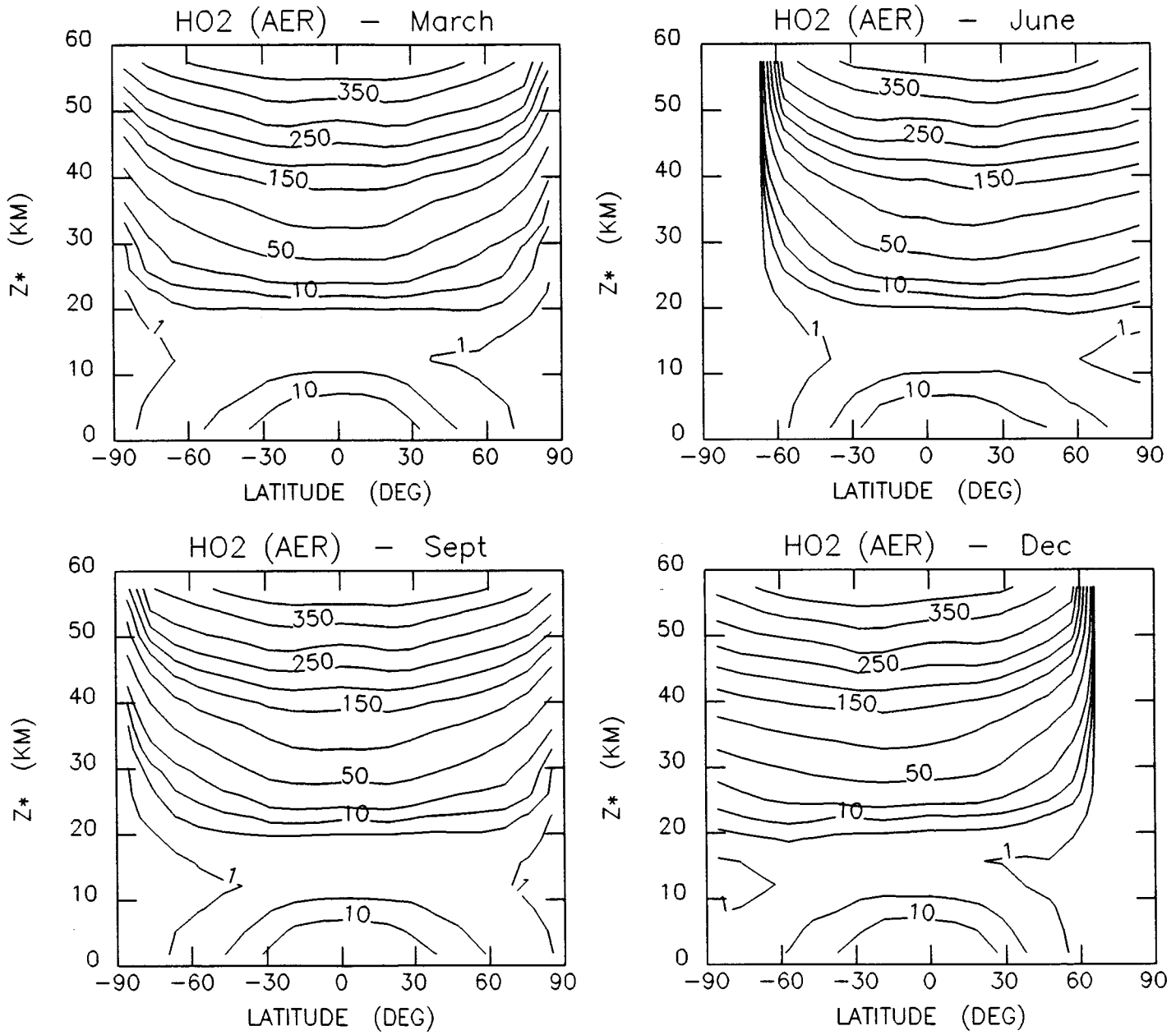
HO2 (AER) – March
HO2 (AER) – June
HO2 (AER) – Sept
HO2 (AER) – Dec
Z* (KM)
LATITUDE (DEG)
60
50
40
30
20
10
0
−90
−60
−30
0
30
60
90
350
250
150
50
10
1

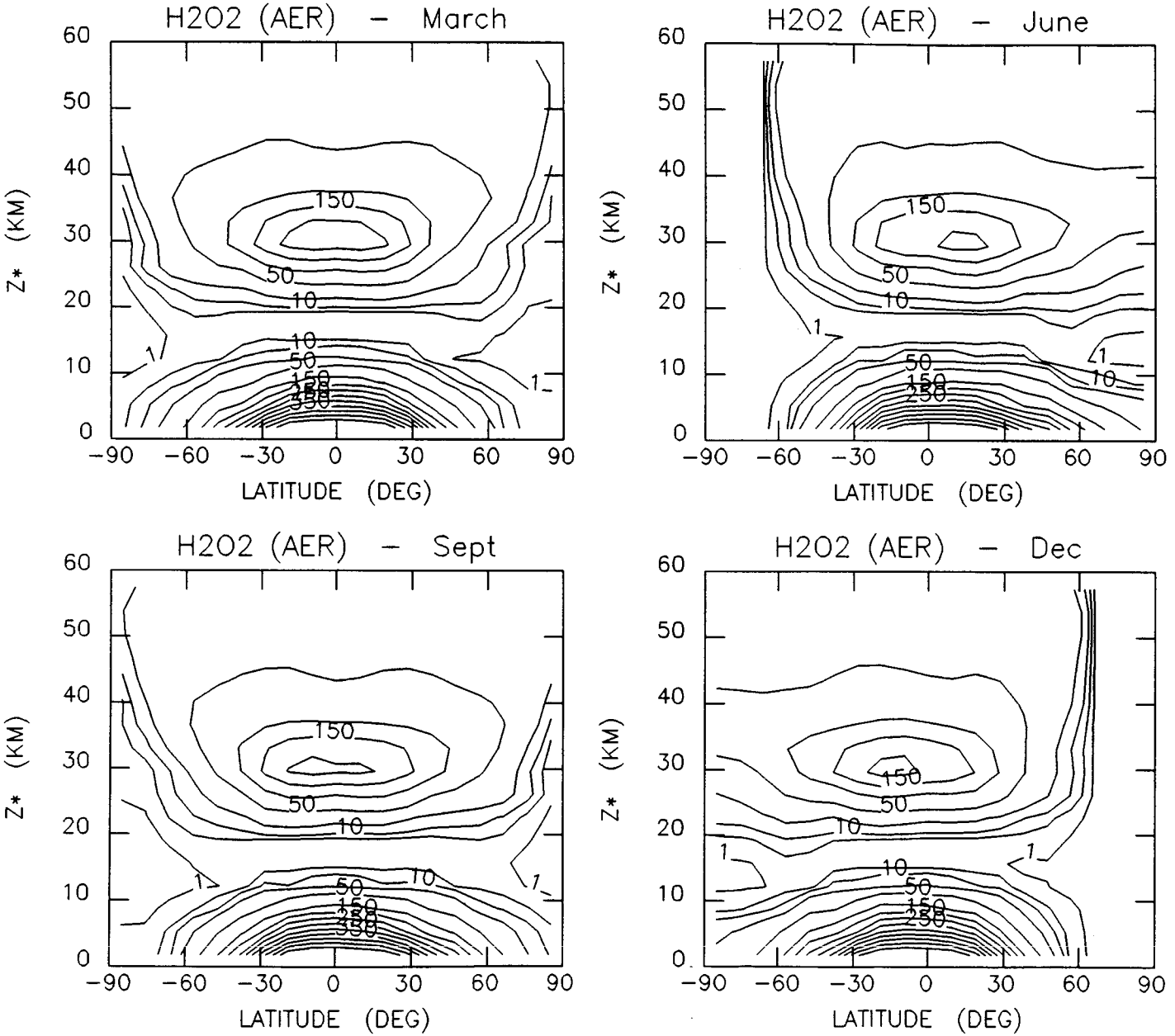
H2O2 (AER) – March
H2O2 (AER) – June
H2O2 (AER) – Sept
H2O2 (AER) – Dec
Z* (KM)
LATITUDE (DEG)
0
10
20
30
40
50
60
-90
-60
-30
0
30
60
90
1
10
50
150
250
350

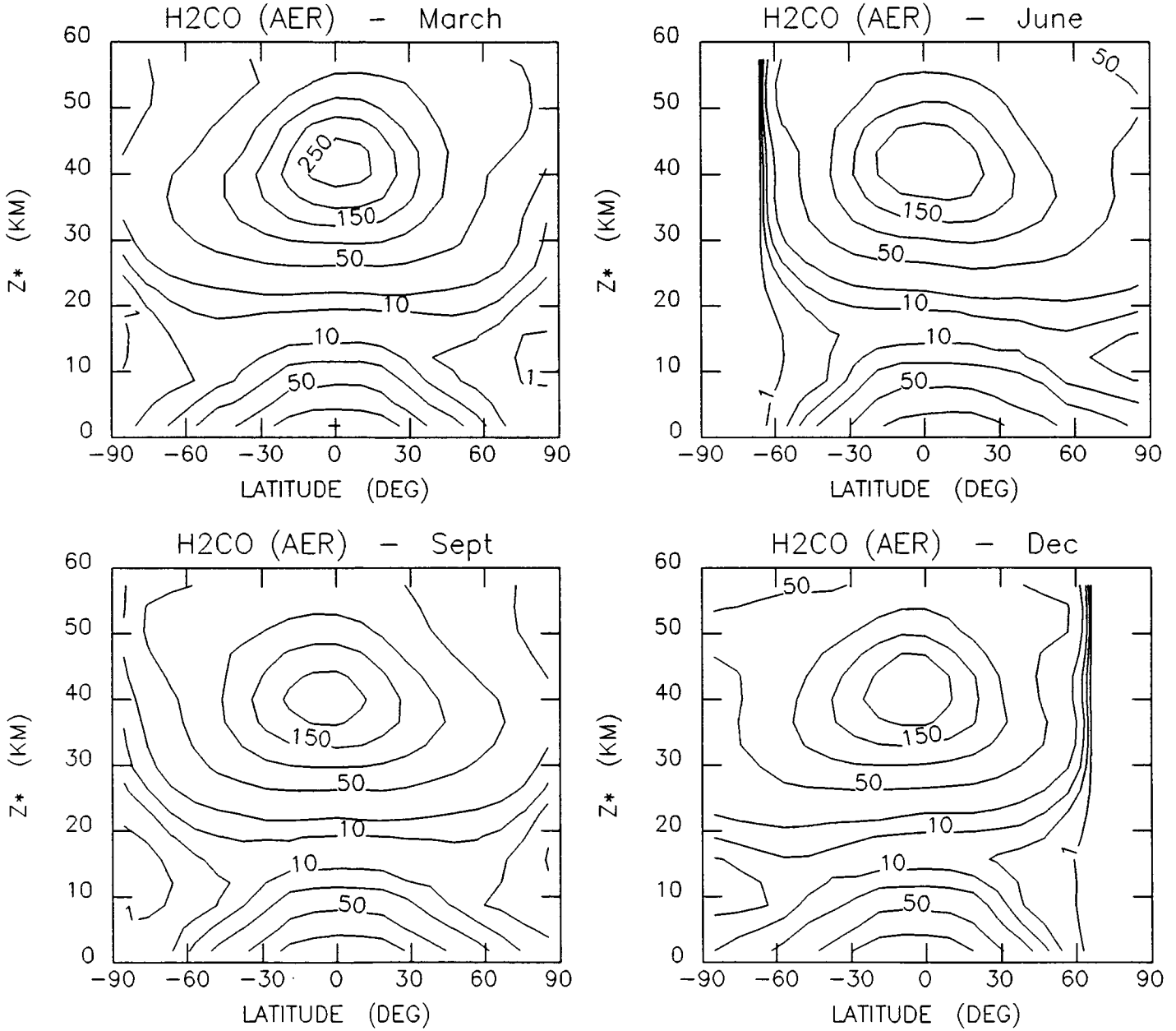
H2CO (AER) – March
H2CO (AER) – June
H2CO (AER) – Sept
H2CO (AER) – Dec
Z* (KM)
LATITUDE (DEG)
60
50
40
30
20
10
0
−90
−60
−30
0
30
60
90
250
150
50
10
1

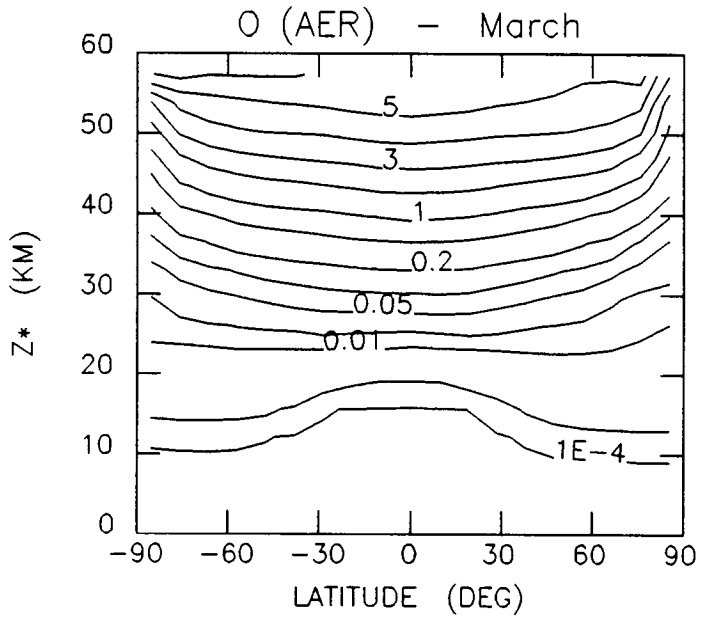
O (AER) – March
Z* (KM)
LATITUDE (DEG)
5
3
1
0.2
0.05
0.01
1E-4

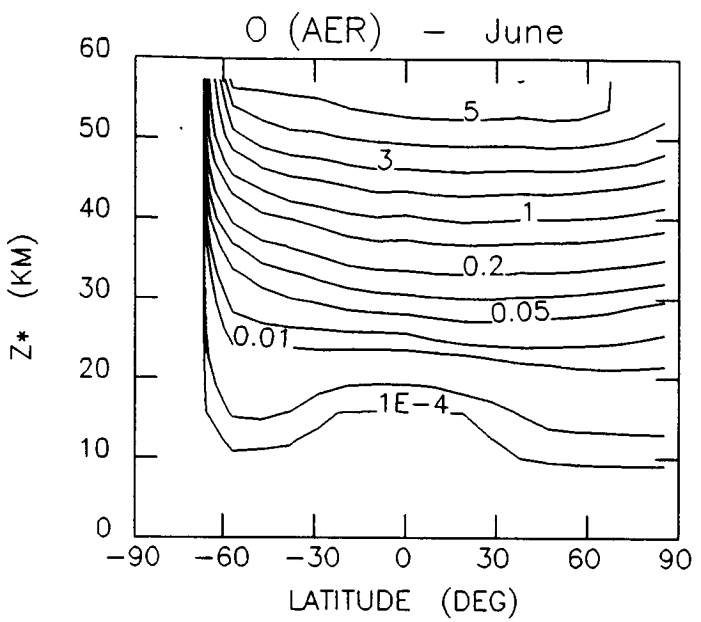
O (AER) – June
Z* (KM)
LATITUDE (DEG)
5
3
1
0.2
0.05
0.01
1E-4

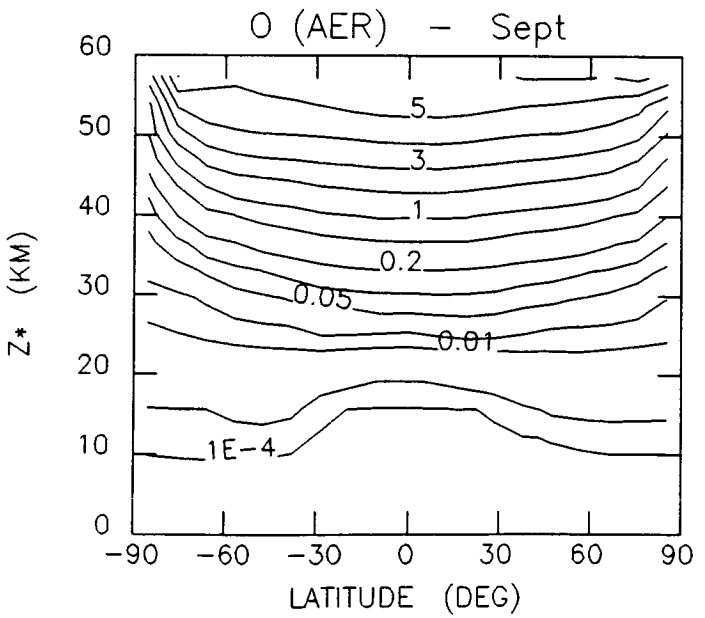
O (AER) – Sept
Z* (KM)
LATITUDE (DEG)
5
3
1
0.2
0.05
0.01
1E-4

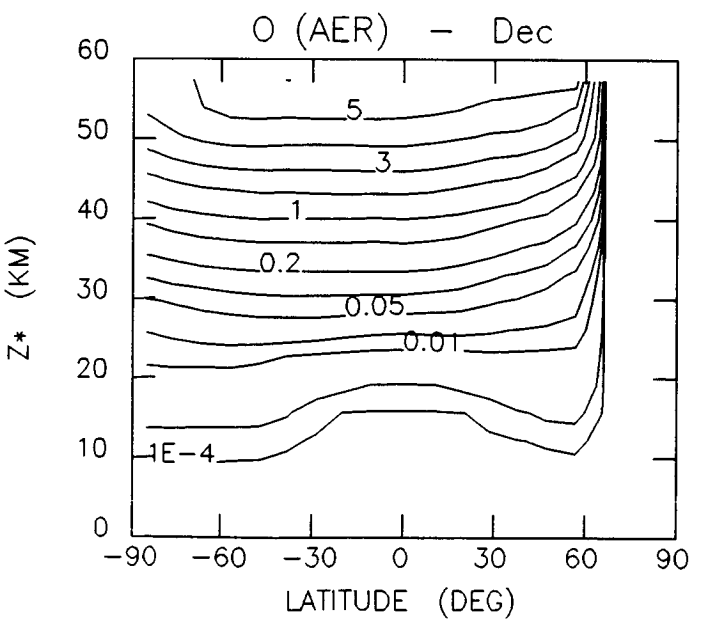
O (AER) – Dec
Z* (KM)
LATITUDE (DEG)
5
3
1
0.2
0.05
0.01
1E-4

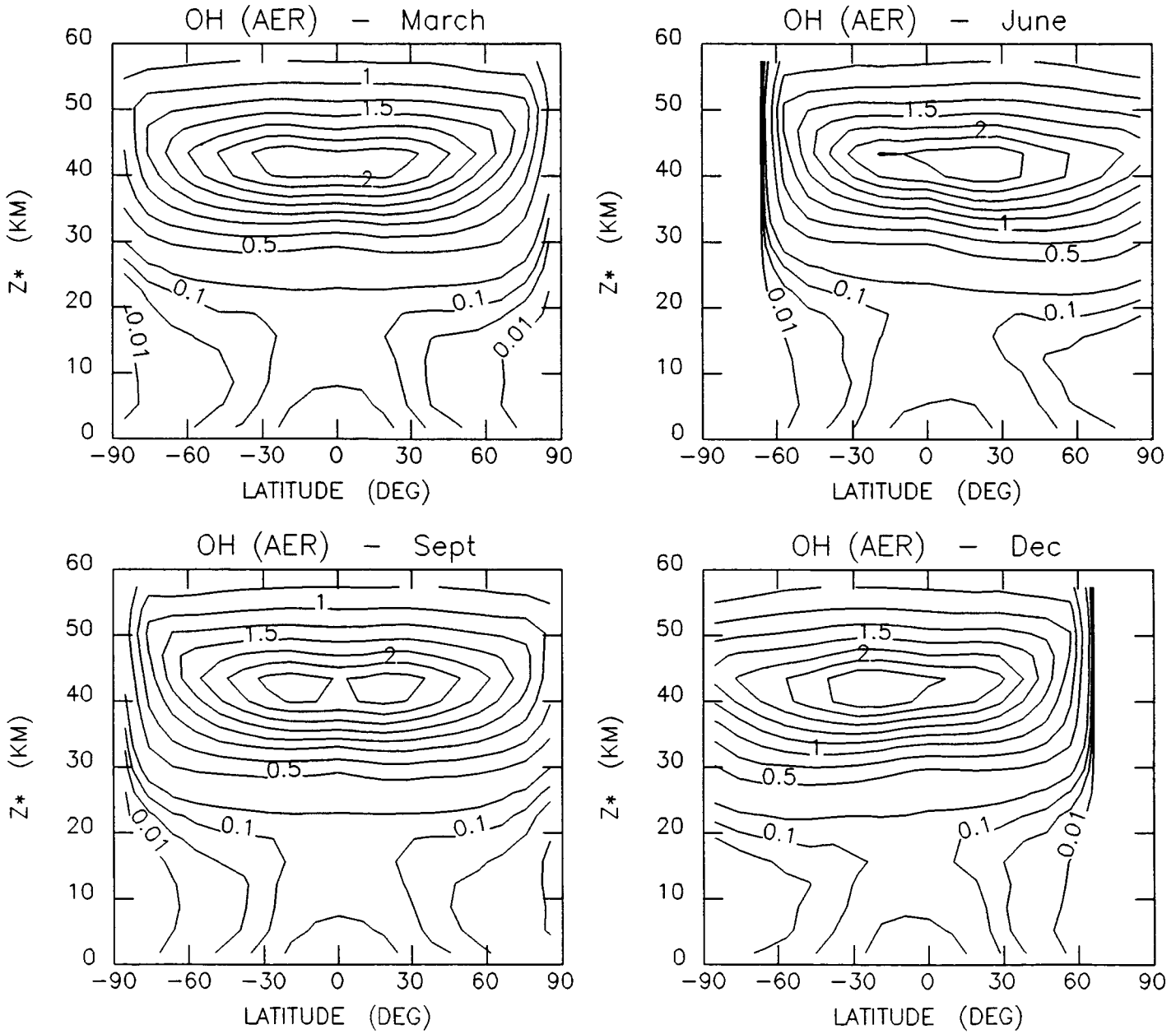
OH (AER) – March
OH (AER) – June
OH (AER) – Sept
OH (AER) – Dec
Z* (KM)
LATITUDE (DEG)
0
10
20
30
40
50
60
−90
−60
−30
0
30
60
90
1
1.5
2
0.5
0.1
0.01

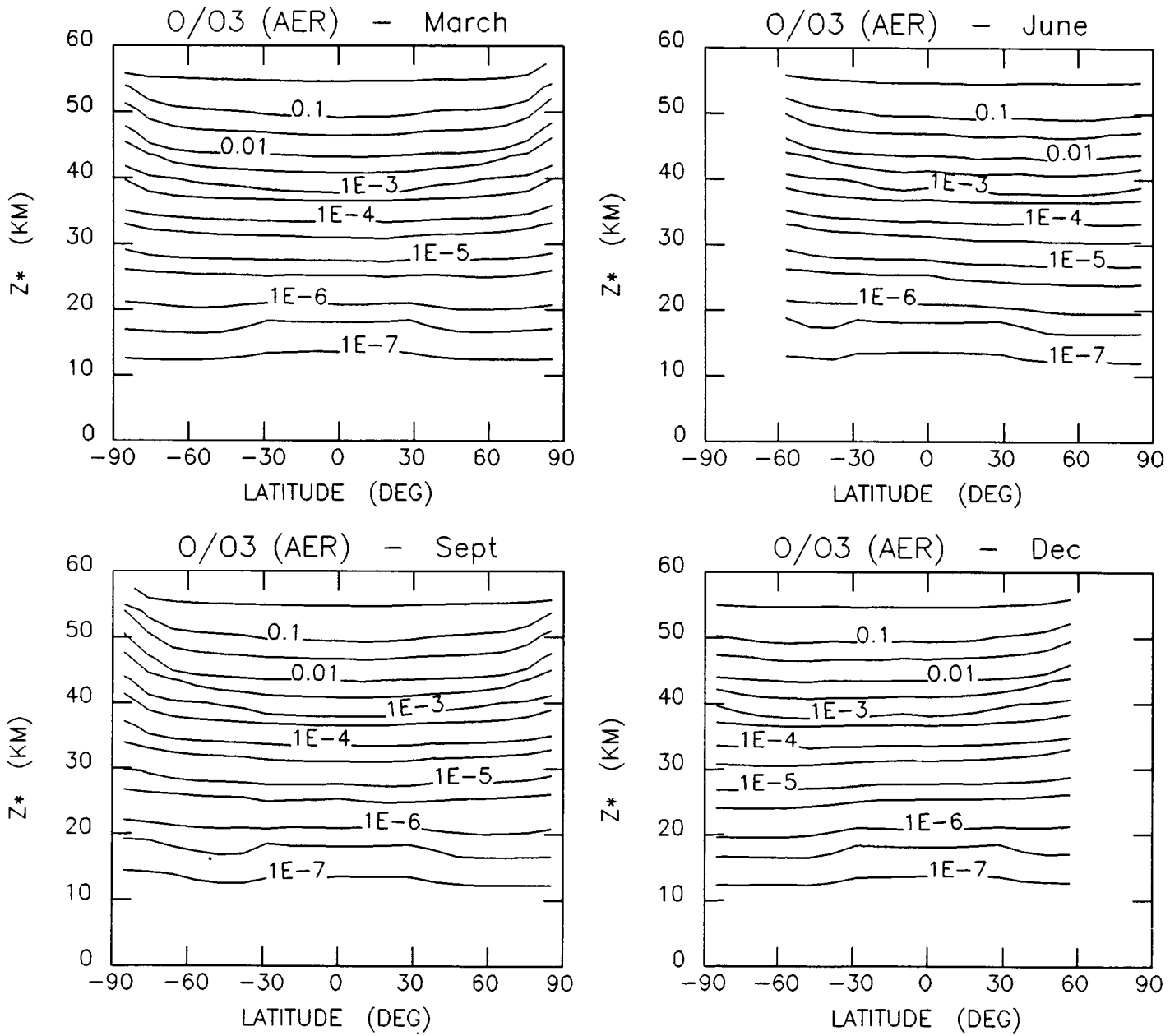
O/O3 (AER) – March
O/O3 (AER) – June
O/O3 (AER) – Sept
O/O3 (AER) – Dec
Z* (KM)
LATITUDE (DEG)
0.1
0.01
1E-3
1E-4
1E-5
1E-6
1E-7
0
10
20
30
40
50
60
−90
−60
−30
0
30
60
90

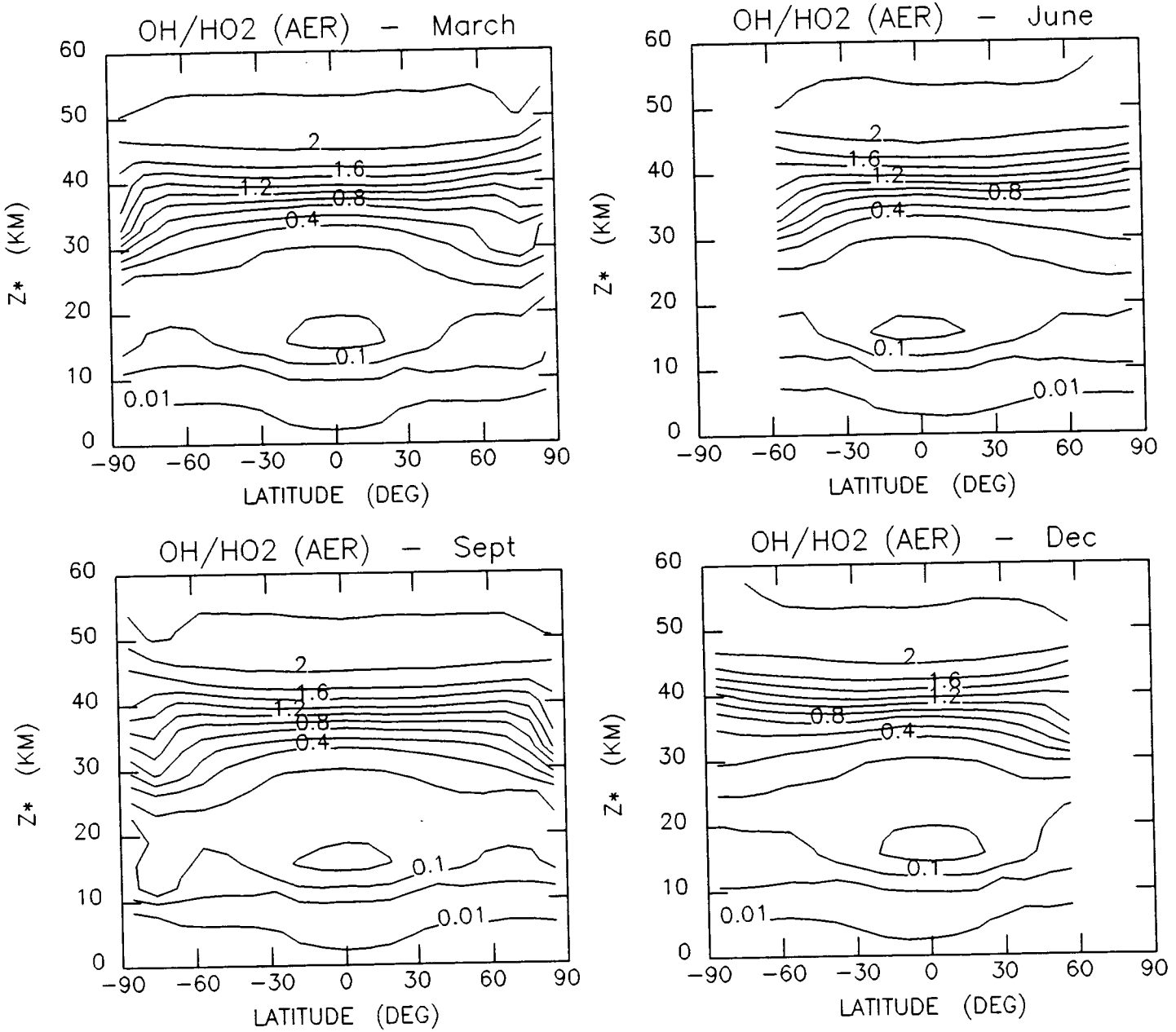
OH/HO2 (AER) – March
OH/HO2 (AER) – June
OH/HO2 (AER) – Sept
OH/HO2 (AER) – Dec
Z* (KM)
LATITUDE (DEG)
60
50
40
30
20
10
0
-90
-60
-30
0
30
60
90
2
1.6
1.2
0.8
0.4
0.1
0.01

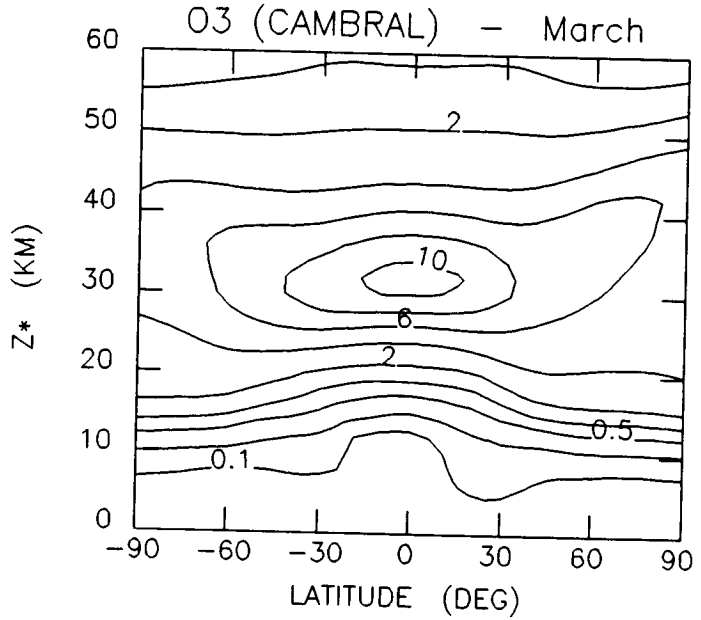
O3 (CAMBRAL) – March
Z* (KM)
LATITUDE (DEG)
60
50
40
30
20
10
0
-90 -60 -30 0 30 60 90
2
10
6
2
0.5
0.1

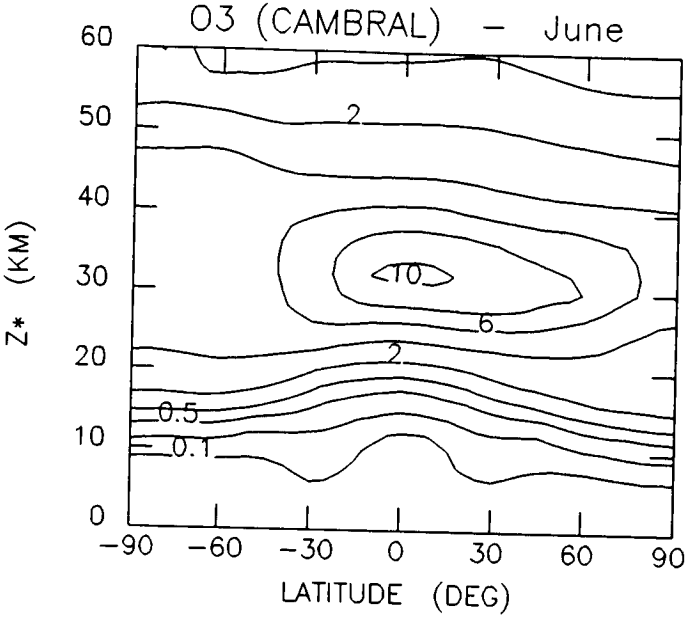
O3 (CAMBRAL) – June
Z* (KM)
LATITUDE (DEG)
60
50
40
30
20
10
0
-90 -60 -30 0 30 60 90
2
10
6
2
0.5
0.1

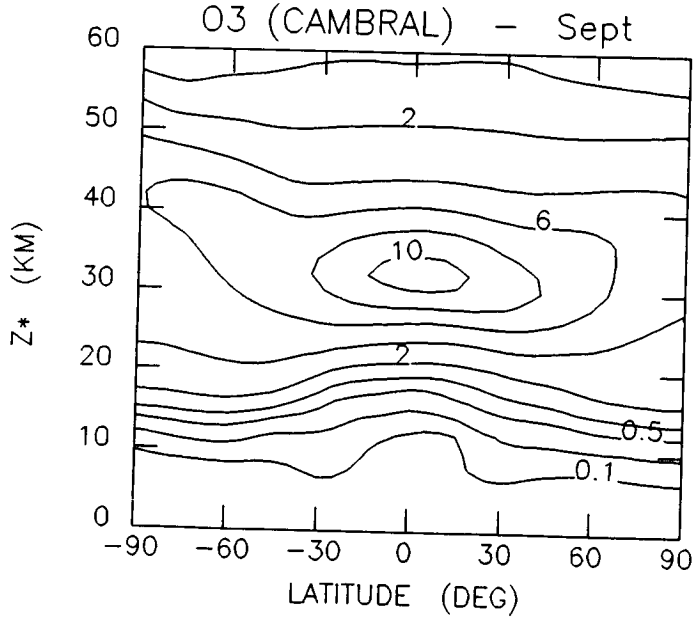
O3 (CAMBRAL) – Sept
Z* (KM)
LATITUDE (DEG)
60
50
40
30
20
10
0
-90 -60 -30 0 30 60 90
2
6
10
2
0.5
0.1

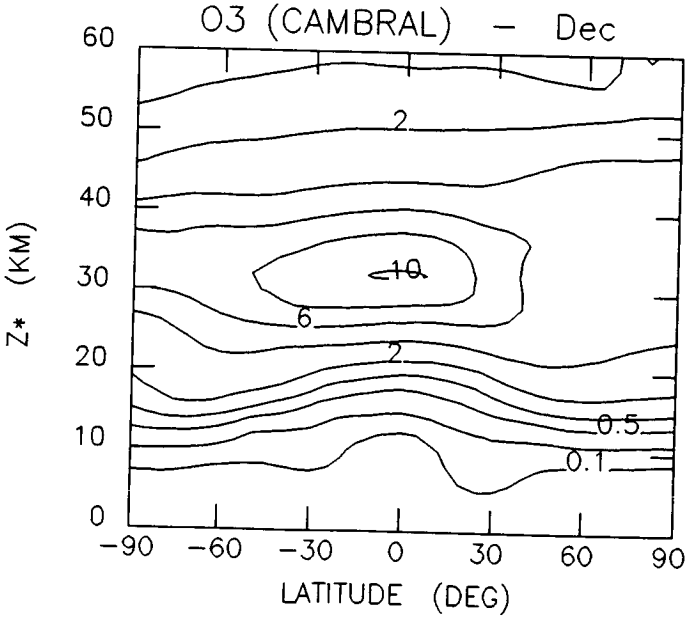
O3 (CAMBRAL) – Dec
Z* (KM)
LATITUDE (DEG)
60
50
40
30
20
10
0
-90 -60 -30 0 30 60 90
2
10
6
2
0.5
0.1

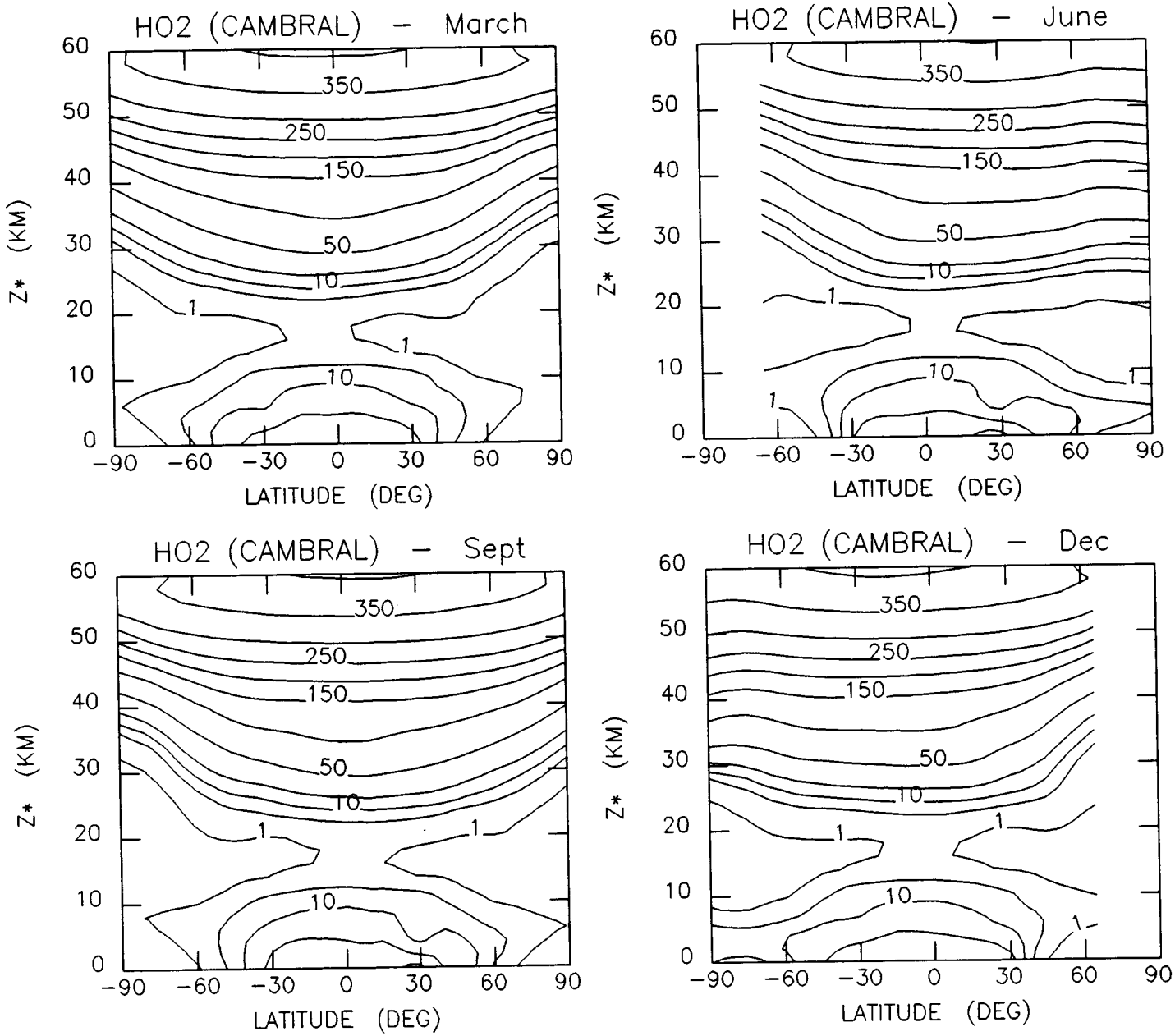
HO2 (CAMBRAL) – March
HO2 (CAMBRAL) – June
HO2 (CAMBRAL) – Sept
HO2 (CAMBRAL) – Dec
Z* (KM)
LATITUDE (DEG)
0
10
20
30
40
50
60
-90
-60
-30
0
30
60
90
350
250
150
50
10
1

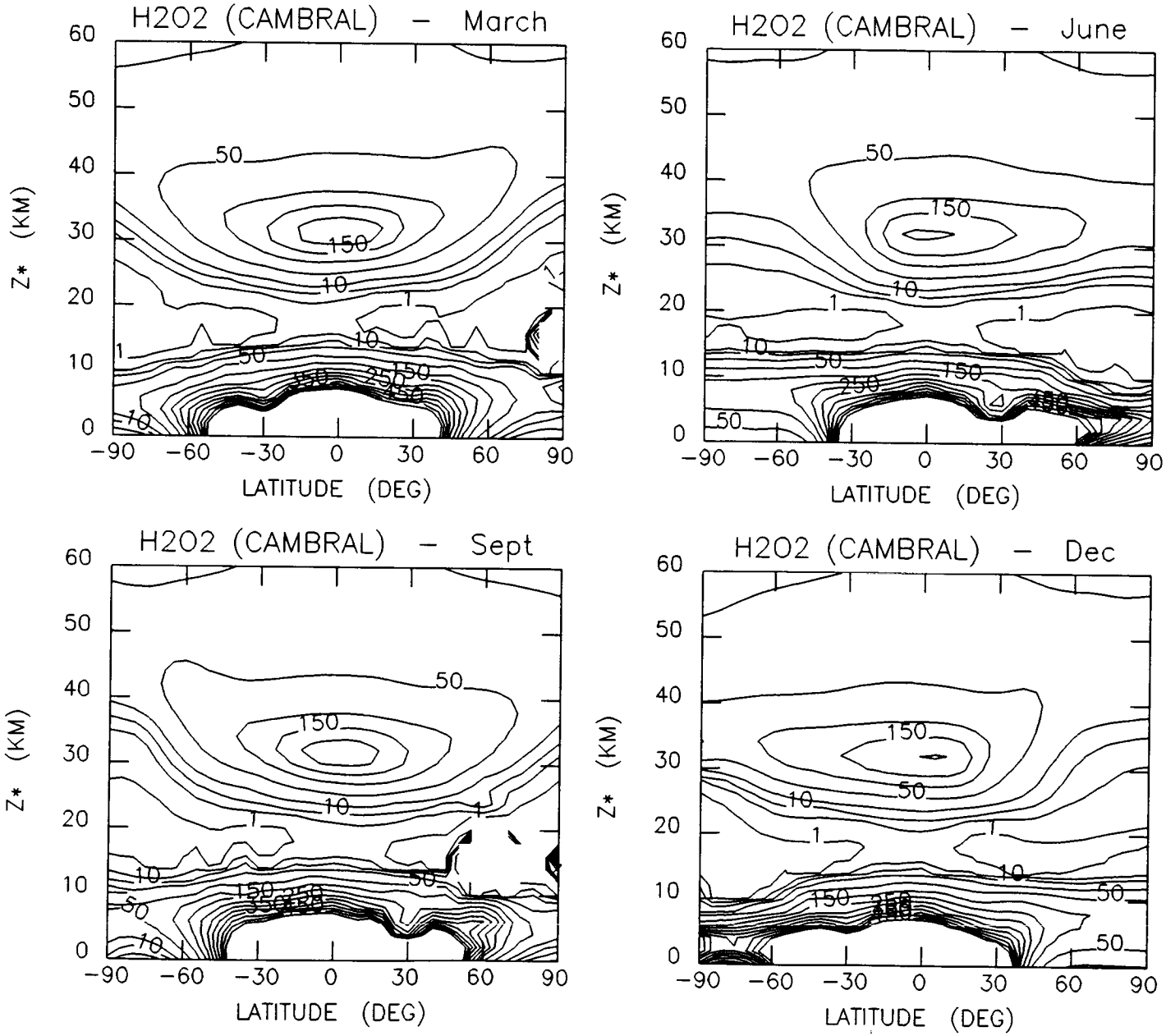
H2O2 (CAMBRAL) – March
H2O2 (CAMBRAL) – June
H2O2 (CAMBRAL) – Sept
H2O2 (CAMBRAL) – Dec
Z* (KM)
LATITUDE (DEG)
60
50
40
30
20
10
0
−90 −60 −30 0 30 60 90
50
150
10
1
250
350

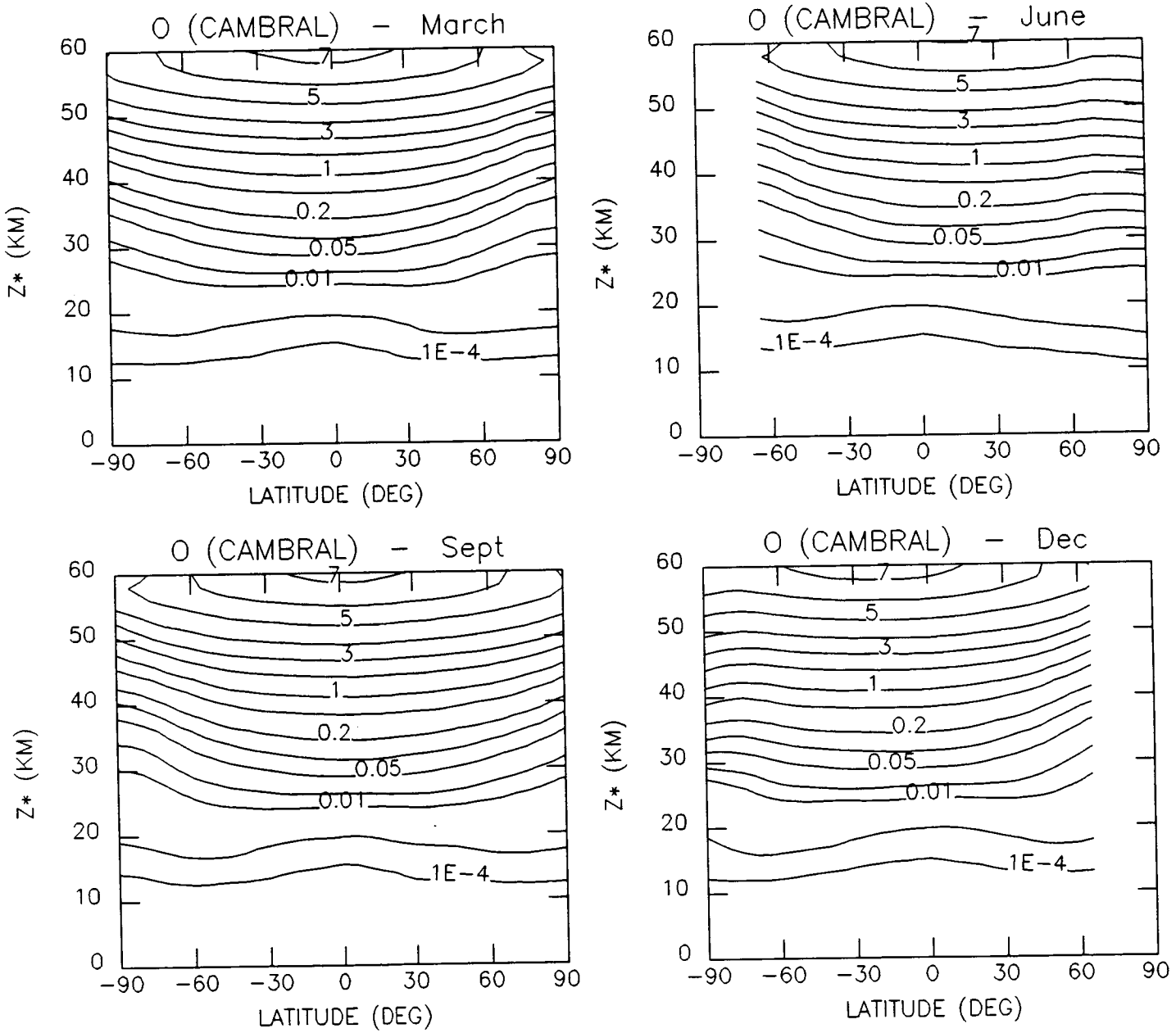
O (CAMBRAL) – March
O (CAMBRAL) – June
O (CAMBRAL) – Sept
O (CAMBRAL) – Dec
Z* (KM)
LATITUDE (DEG)
7
5
3
1
0.2
0.05
0.01
1E-4
0
10
20
30
40
50
60
-90
-60
-30
0
30
60
90

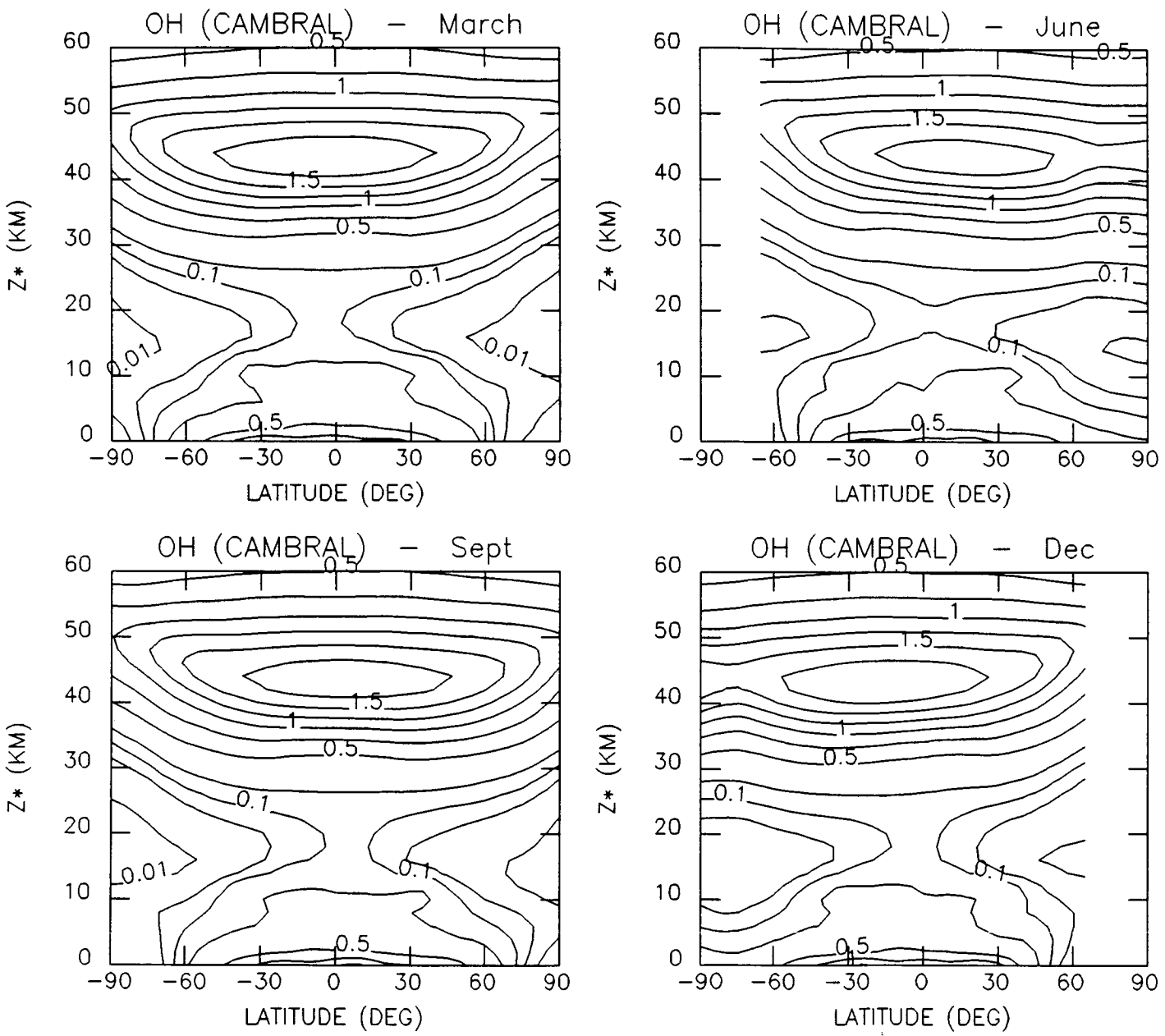
OH (CAMBRAL) – March
OH (CAMBRAL) – June
OH (CAMBRAL) – Sept
OH (CAMBRAL) – Dec
Z* (KM)
LATITUDE (DEG)
0
10
20
30
40
50
60
−90
−60
−30
0
30
60
90
0.5
1
1.5
0.1
0.01

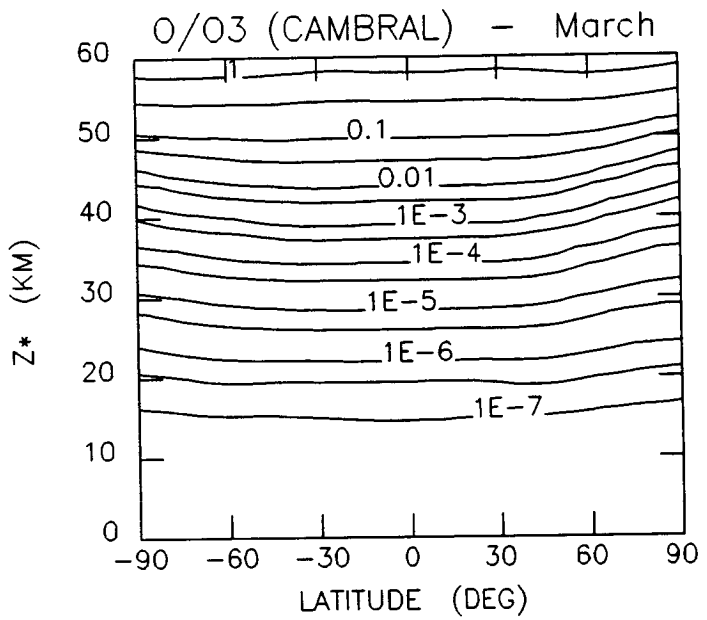
O/O3 (CAMBRAL) – March
Z* (KM)
LATITUDE (DEG)
1
0.1
0.01
1E-3
1E-4
1E-5
1E-6
1E-7
0
10
20
30
40
50
60
-90
-60
-30
0
30
60
90

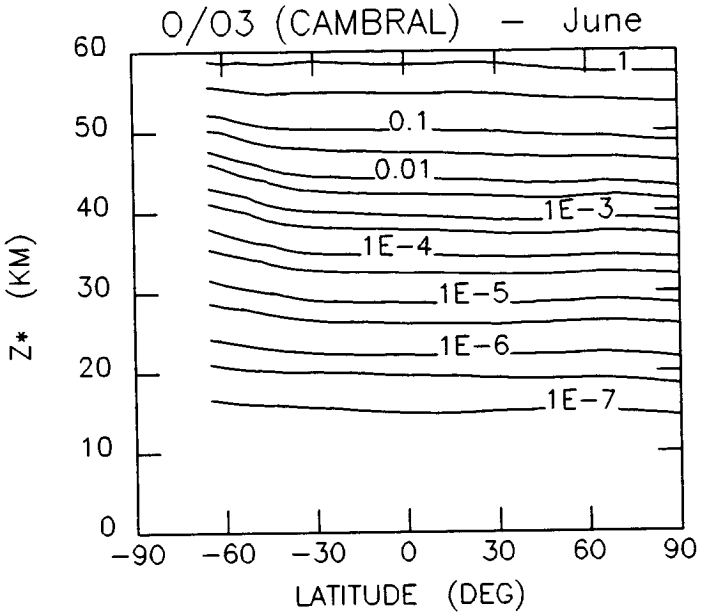
O/O3 (CAMBRAL) – June
Z* (KM)
LATITUDE (DEG)
1
0.1
0.01
1E-3
1E-4
1E-5
1E-6
1E-7
0
10
20
30
40
50
60
-90
-60
-30
0
30
60
90

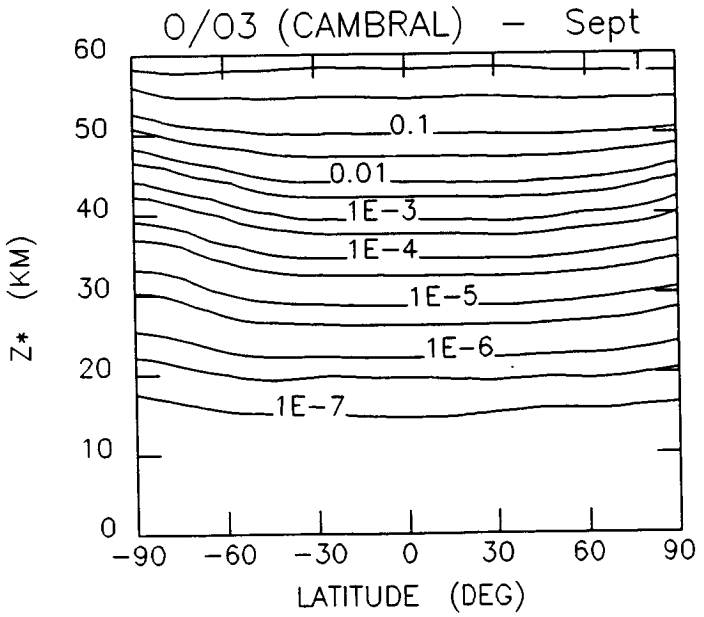
O/O3 (CAMBRAL) – Sept
Z* (KM)
LATITUDE (DEG)
1
0.1
0.01
1E-3
1E-4
1E-5
1E-6
1E-7
0
10
20
30
40
50
60
-90
-60
-30
0
30
60
90

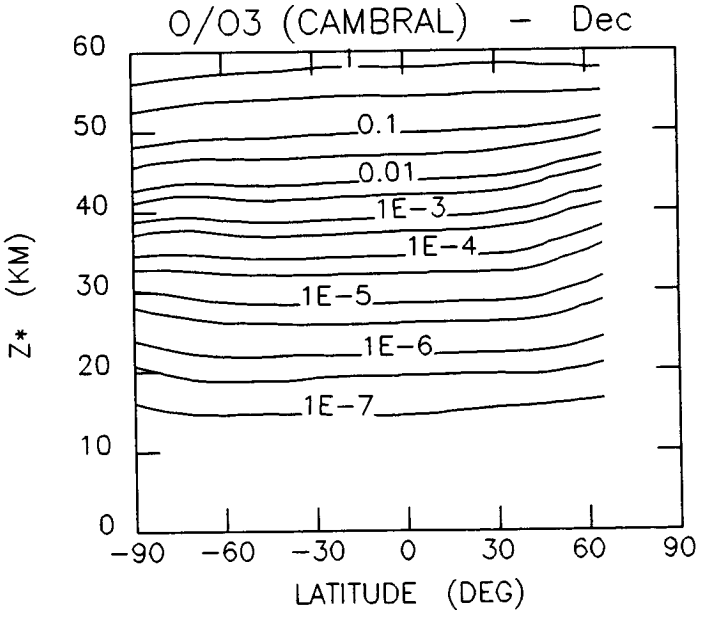
O/O3 (CAMBRAL) – Dec
Z* (KM)
LATITUDE (DEG)
1
0.1
0.01
1E-3
1E-4
1E-5
1E-6
1E-7
0
10
20
30
40
50
60
-90
-60
-30
0
30
60
90

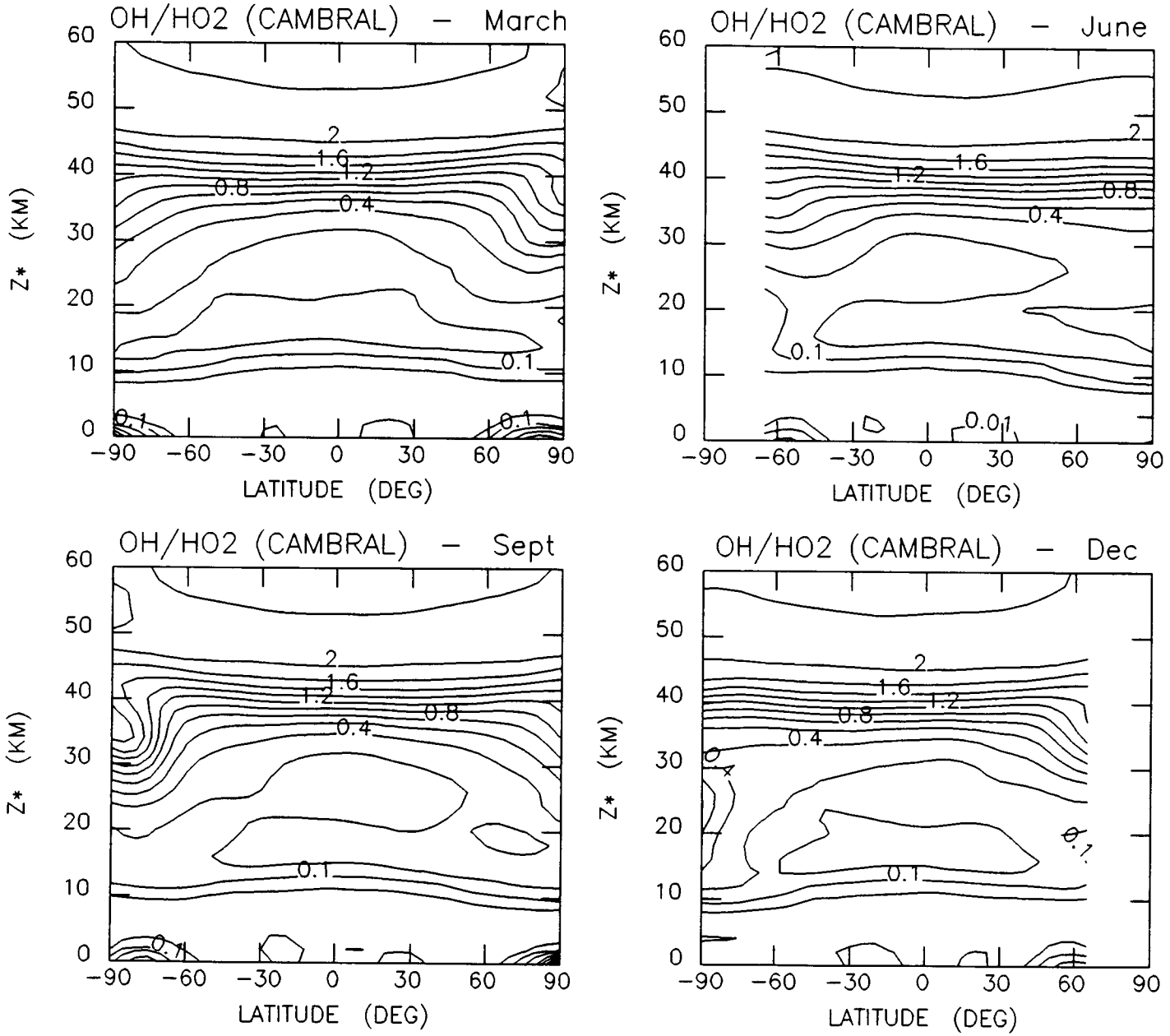
OH/HO2 (CAMBRAL) – March
OH/HO2 (CAMBRAL) – June
OH/HO2 (CAMBRAL) – Sept
OH/HO2 (CAMBRAL) – Dec
Z* (KM)
LATITUDE (DEG)
60
50
40
30
20
10
0
-90 -60 -30 0 30 60 90
2
1.6
1.2
0.8
0.4
0.1
0.01

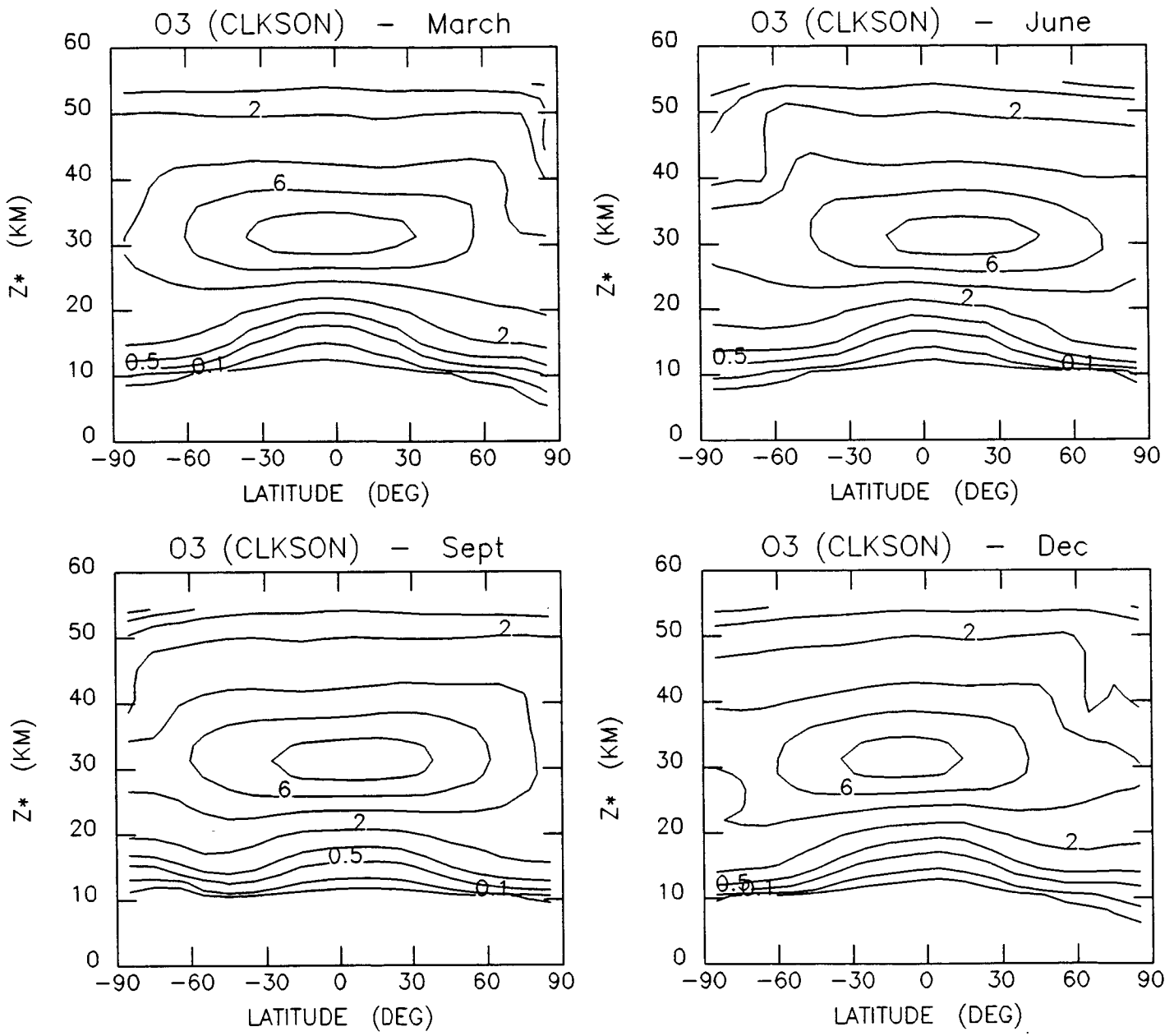
O3 (CLKSON) – March
O3 (CLKSON) – June
O3 (CLKSON) – Sept
O3 (CLKSON) – Dec
Z* (KM)
LATITUDE (DEG)
0
10
20
30
40
50
60
-90
-60
-30
0
30
60
90
2
6
0.5
0.1

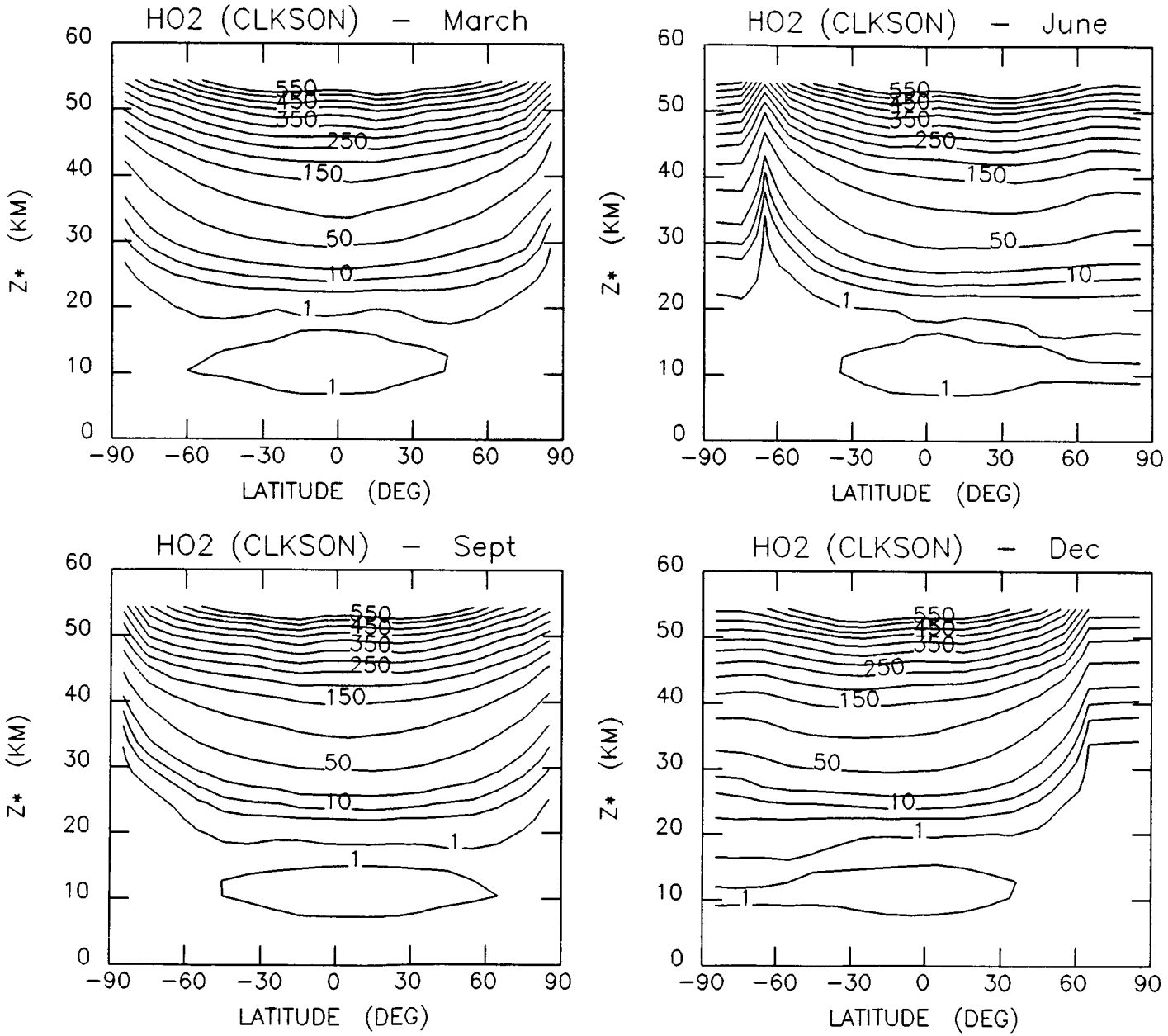
HO2 (CLKSON) – March
HO2 (CLKSON) – June
HO2 (CLKSON) – Sept
HO2 (CLKSON) – Dec
Z* (KM)
LATITUDE (DEG)
0
10
20
30
40
50
60
−90
−60
−30
0
30
60
90
550
450
350
250
150
50
10
1

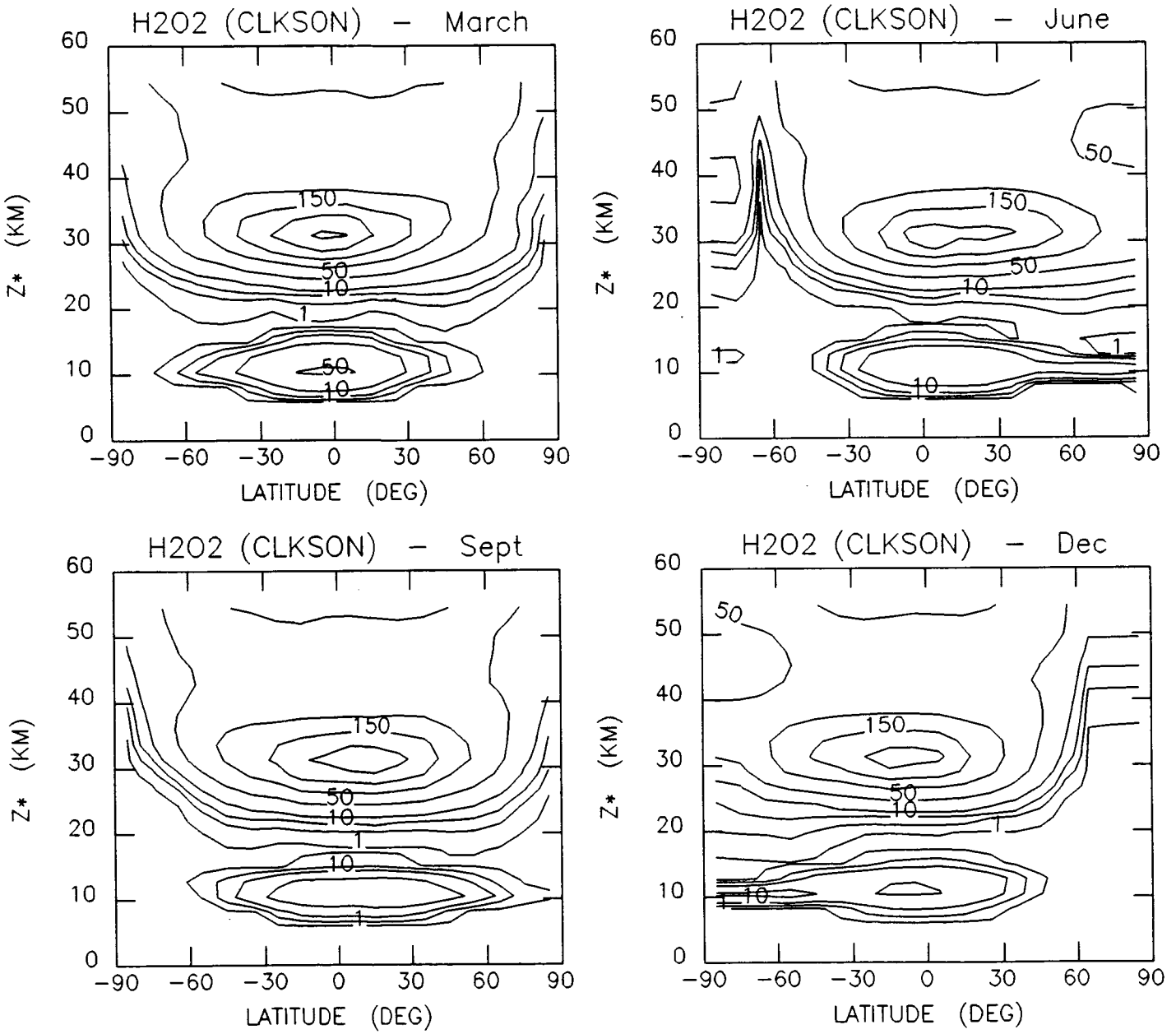
H2O2 (CLKSON) – March
H2O2 (CLKSON) – June
H2O2 (CLKSON) – Sept
H2O2 (CLKSON) – Dec
Z* (KM)
LATITUDE (DEG)
0
10
20
30
40
50
60
-90
-60
-30
0
30
60
90
150
50
10
1

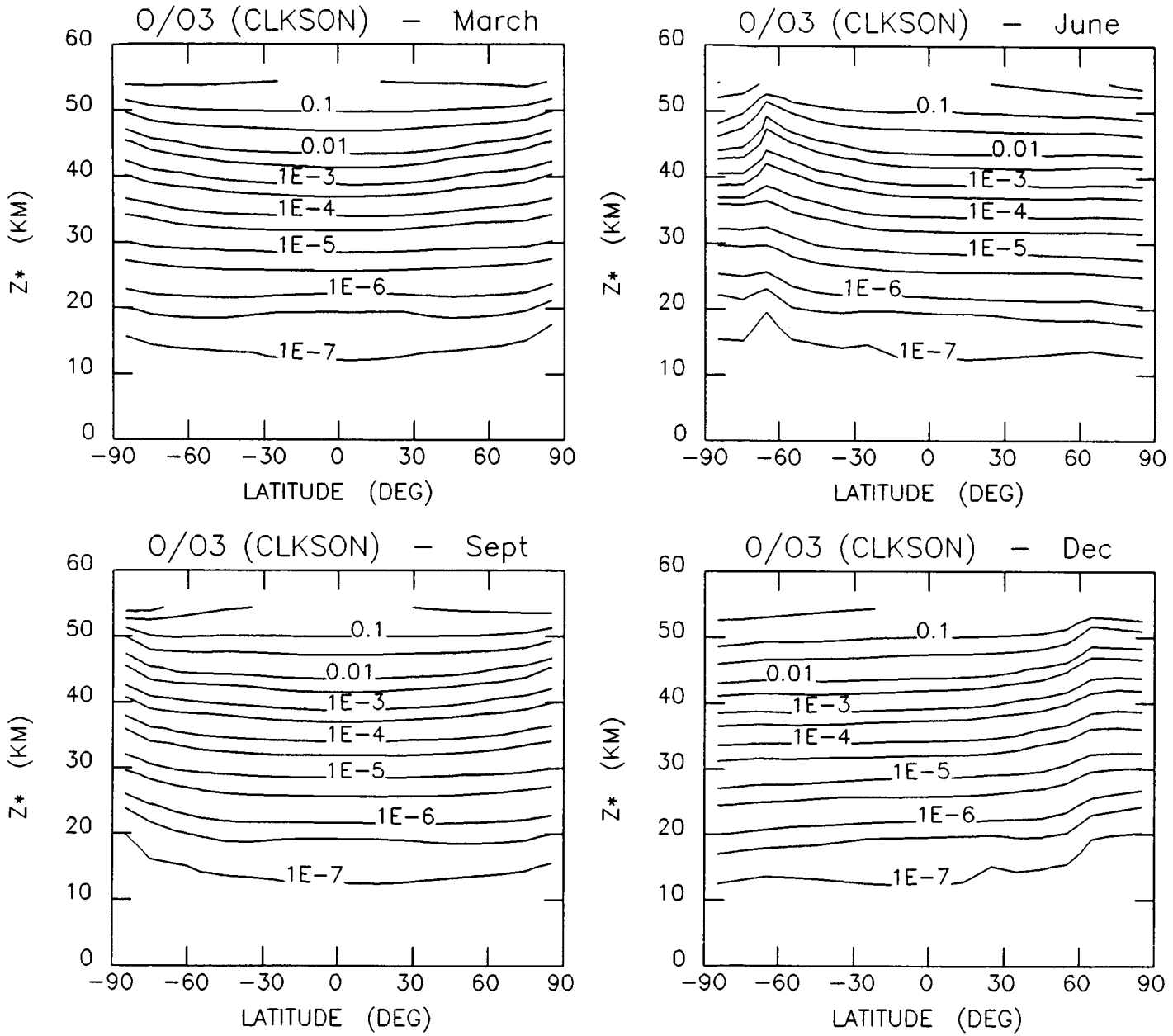
O/O3 (CLKSON) – March
O/O3 (CLKSON) – June
O/O3 (CLKSON) – Sept
O/O3 (CLKSON) – Dec
Z* (KM)
LATITUDE (DEG)
0.1
0.01
1E-3
1E-4
1E-5
1E-6
1E-7
0
10
20
30
40
50
60
-90
-60
-30
0
30
60
90

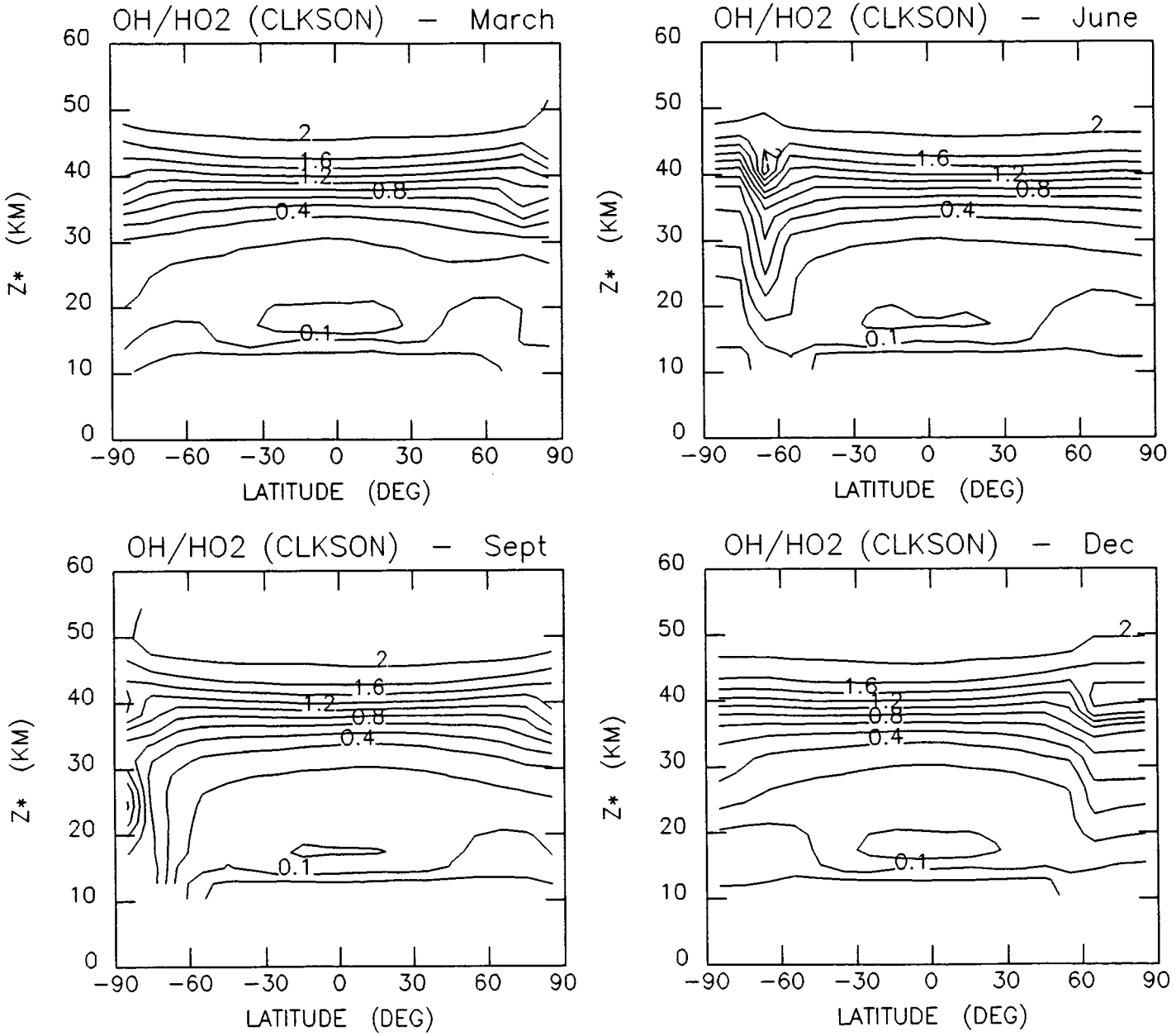
OH/HO2 (CLKSON) – March
OH/HO2 (CLKSON) – June
OH/HO2 (CLKSON) – Sept
OH/HO2 (CLKSON) – Dec
Z* (KM)
LATITUDE (DEG)
0
10
20
30
40
50
60
-90
-60
-30
0
30
60
90
2
1.6
1.2
0.8
0.4
0.1

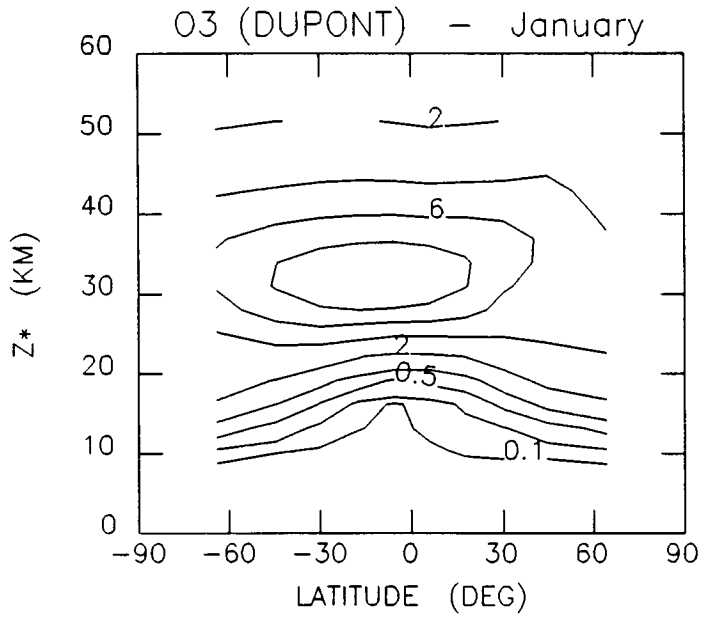
O3 (DUPONT) – January
Z* (KM)
LATITUDE (DEG)
2
6
2
0.5
0.1

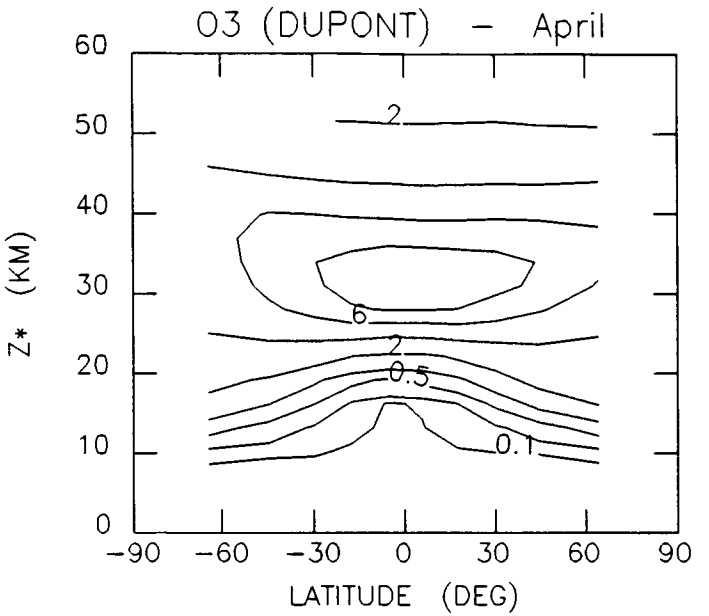
O3 (DUPONT) – April
Z* (KM)
LATITUDE (DEG)
2
6
2
0.5
0.1

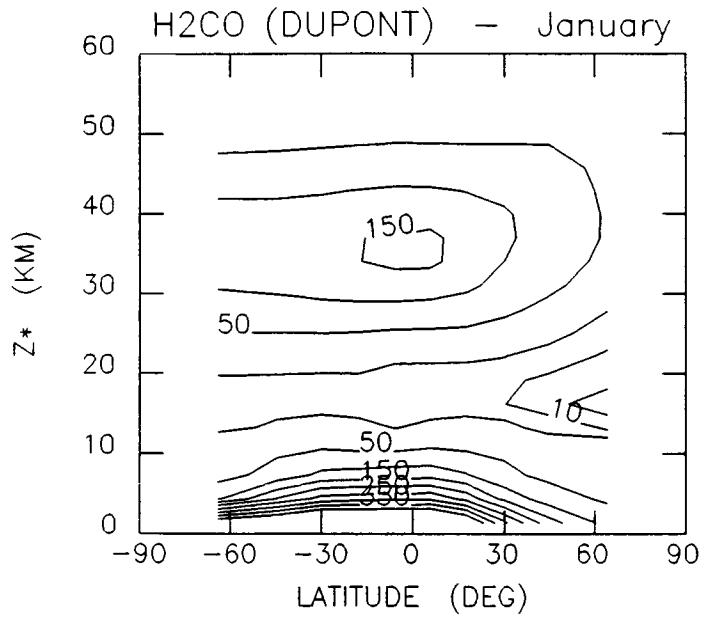
H2CO (DUPONT) – January
Z* (KM)
LATITUDE (DEG)
150
50
10
50
150
250

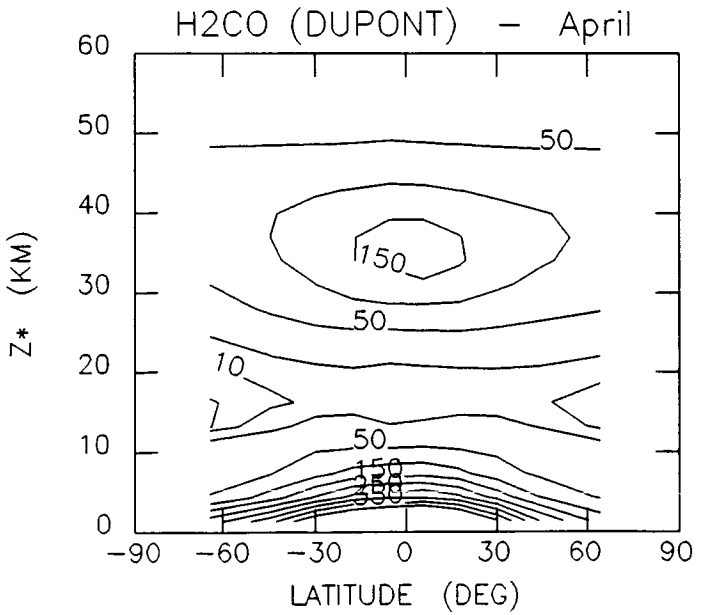
H2CO (DUPONT) – April
Z* (KM)
LATITUDE (DEG)
50
150
50
10
50
150
250

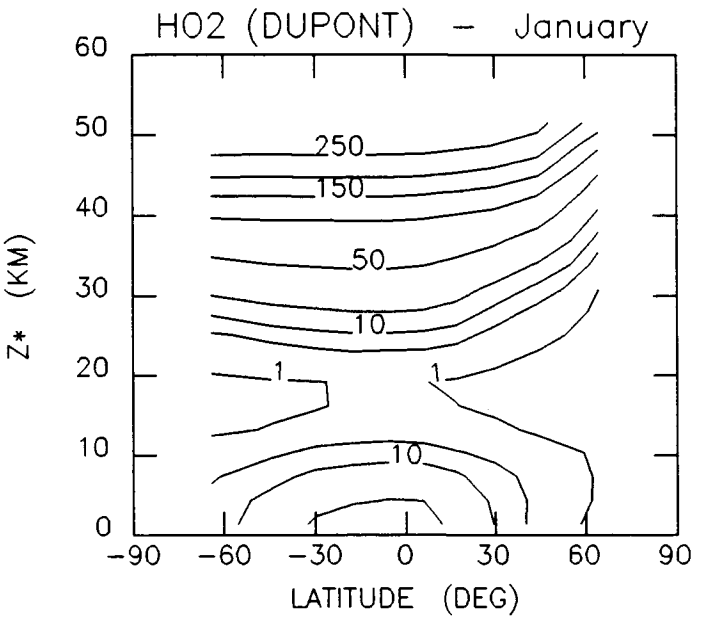
HO2 (DUPONT) – January
Z* (KM)
LATITUDE (DEG)
250
150
50
10
1
1
10

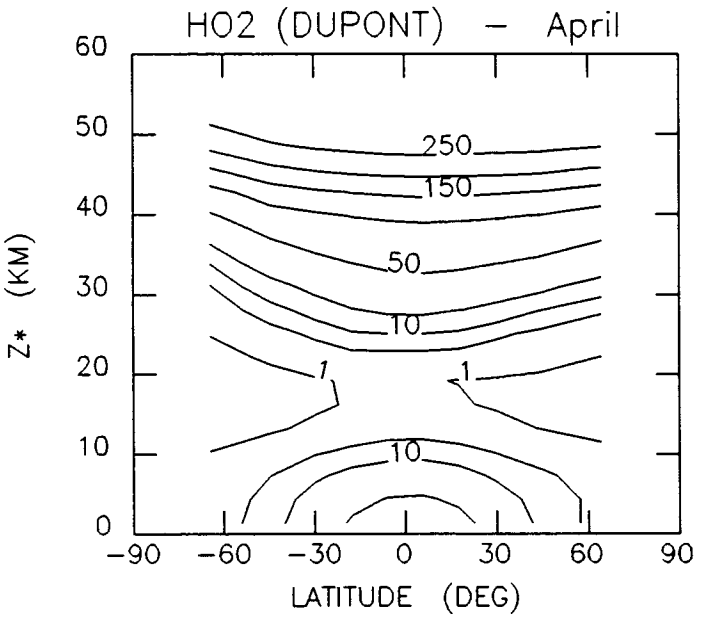
HO2 (DUPONT) – April
Z* (KM)
LATITUDE (DEG)
250
150
50
10
1
1
10

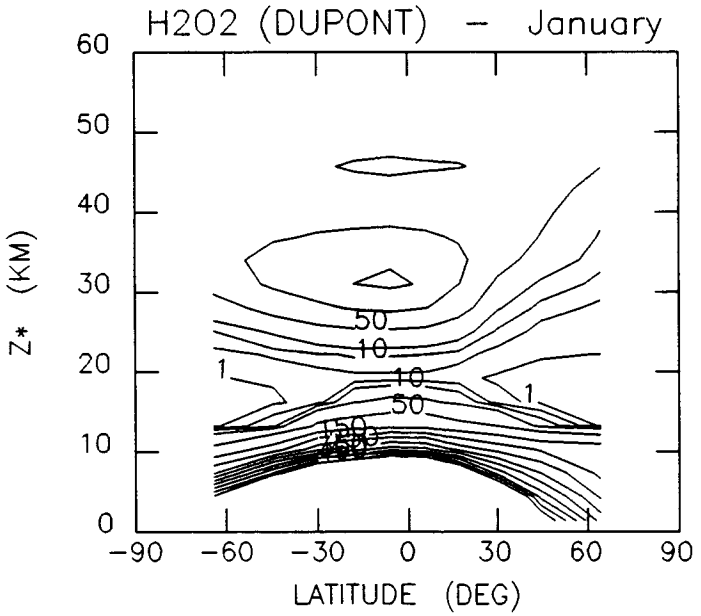
H2O2 (DUPONT) – January
Z* (KM)
LATITUDE (DEG)
50
10
1
10
50
1

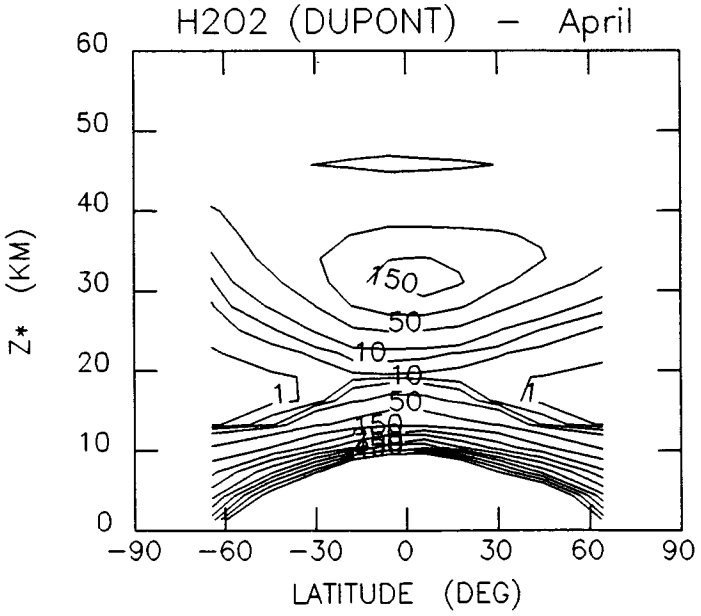
H2O2 (DUPONT) – April
Z* (KM)
LATITUDE (DEG)
150
50
10
10
50
1
1

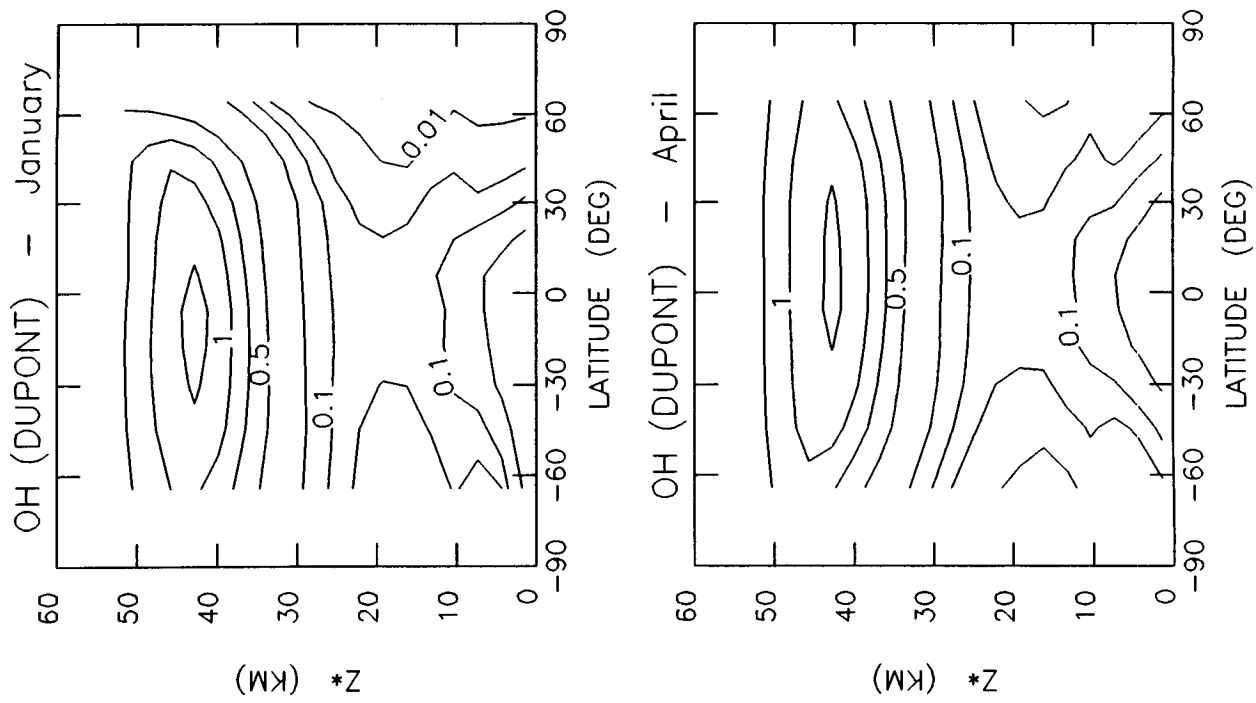
OH (DUPONT) - January
OH (DUPONT) - April
Z* (KM)
LATITUDE (DEG)
1
0.5
0.1
0.01
0
10
20
30
40
50
60
-90
-60
-30
0
30
60
90

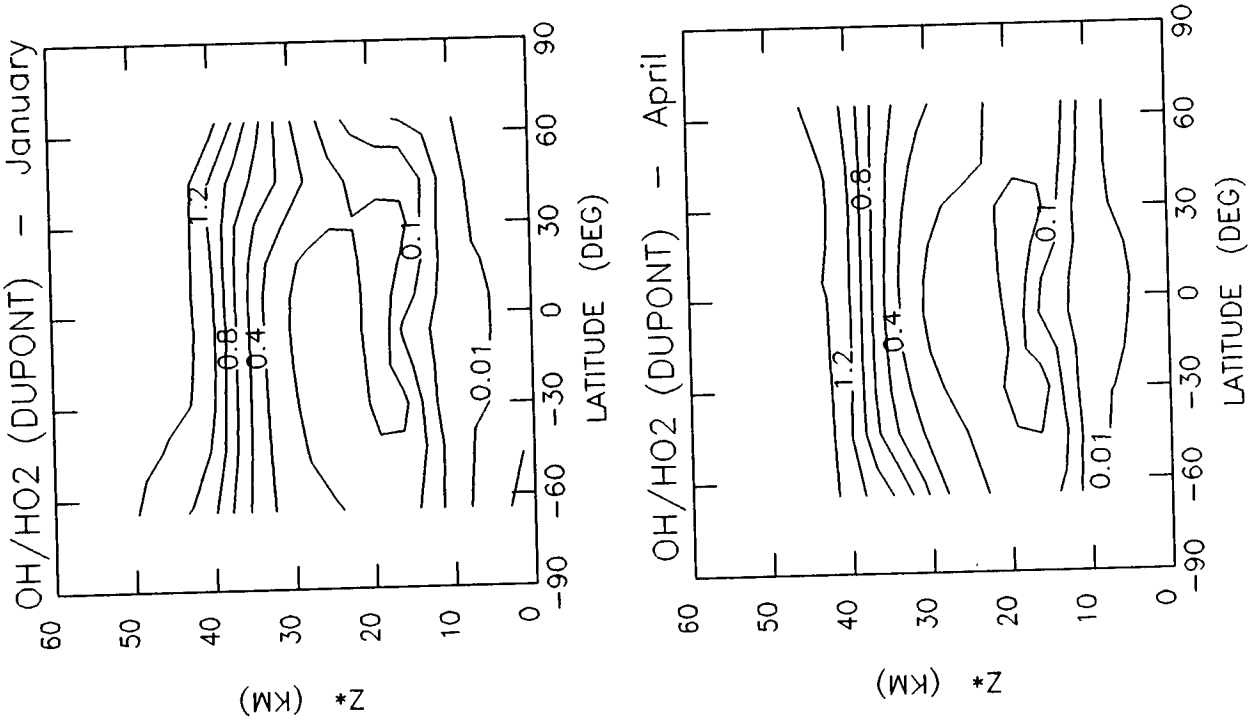
OH/HO2 (DUPONT) - January
OH/HO2 (DUPONT) - April
1.2
0.8
0.4
0.1
0.01
LATITUDE (DEG)
Z* (KM)
60
50
40
30
20
10
0
-90
-60
-30
0
30
60
90

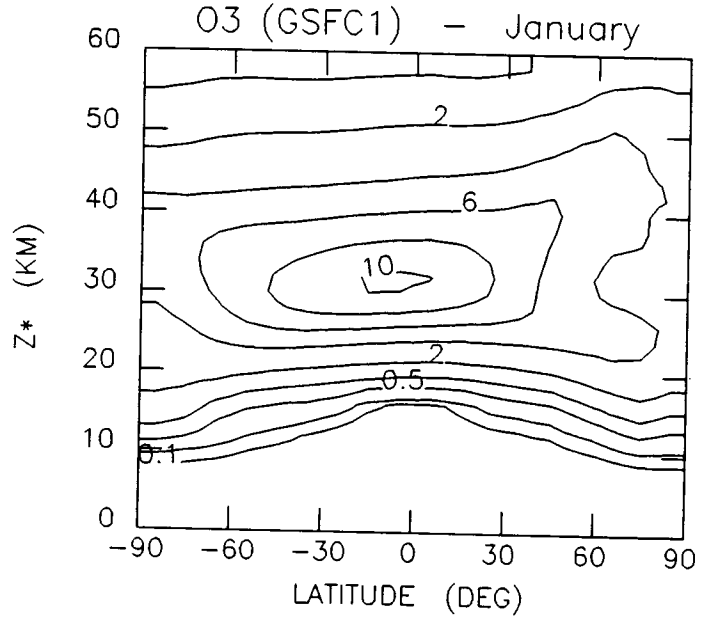
O3 (GSFC1) – January
Z* (KM)
LATITUDE (DEG)
2
6
10
2
0.5
0.1

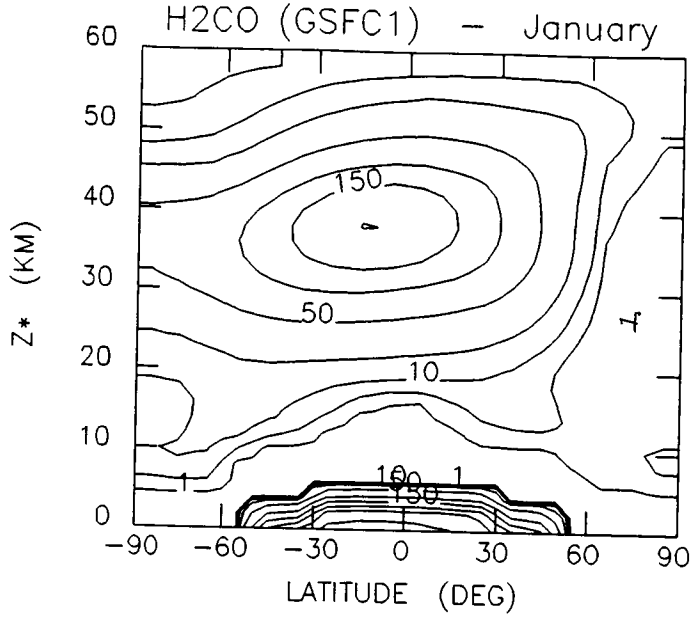
H2CO (GSFC1) – January
Z* (KM)
LATITUDE (DEG)
150
50
10
1

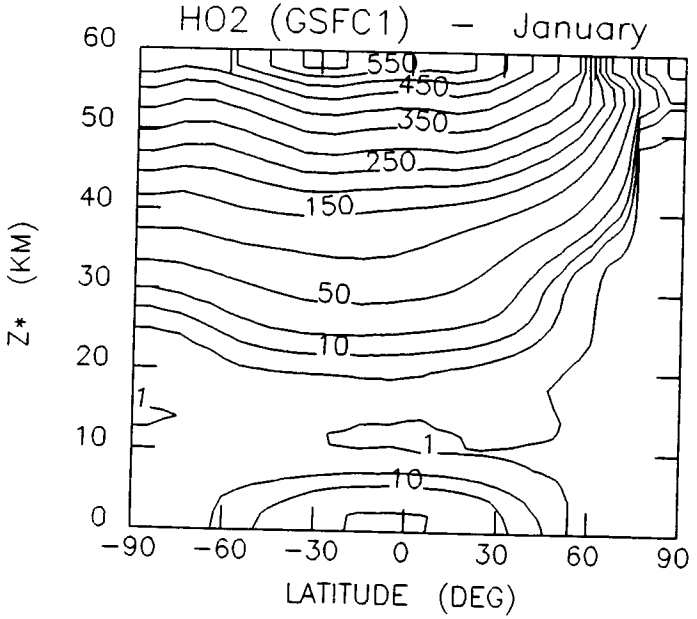
HO2 (GSFC1) – January
Z* (KM)
LATITUDE (DEG)
550
450
350
250
150
50
10
1

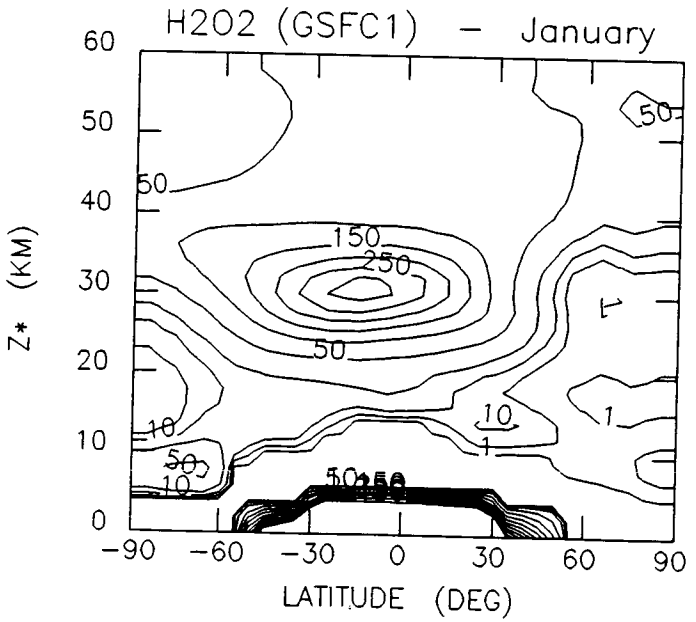
H2O2 (GSFC1) – January
Z* (KM)
LATITUDE (DEG)
50
150
250
10
1

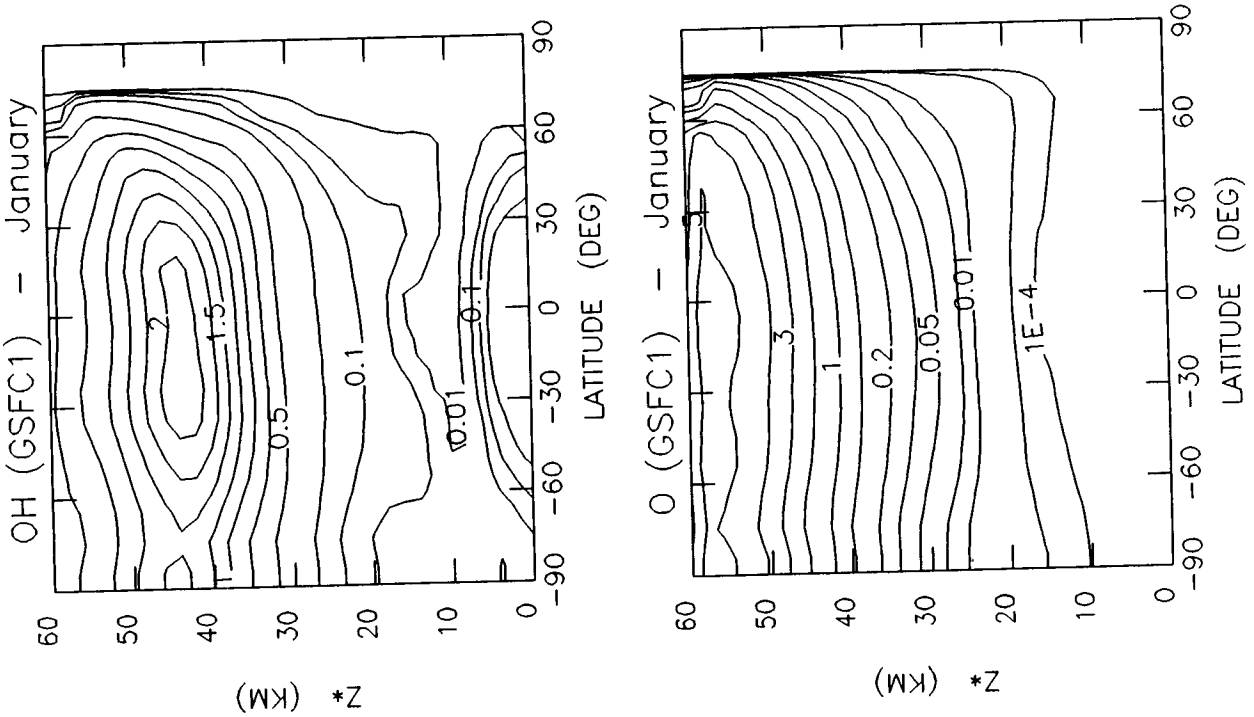
OH (GSFC1) - January
2
1.5
1
0.5
0.1
0.01
0.1
Z* (KM)
60
50
40
30
20
10
0
-90
-60
-30
0
30
60
90
LATITUDE (DEG)
O (GSFC1) - January
5
3
1
0.2
0.05
0.01
1E-4
Z* (KM)
60
50
40
30
20
10
0
-90
-60
-30
0
30
60
90
LATITUDE (DEG)

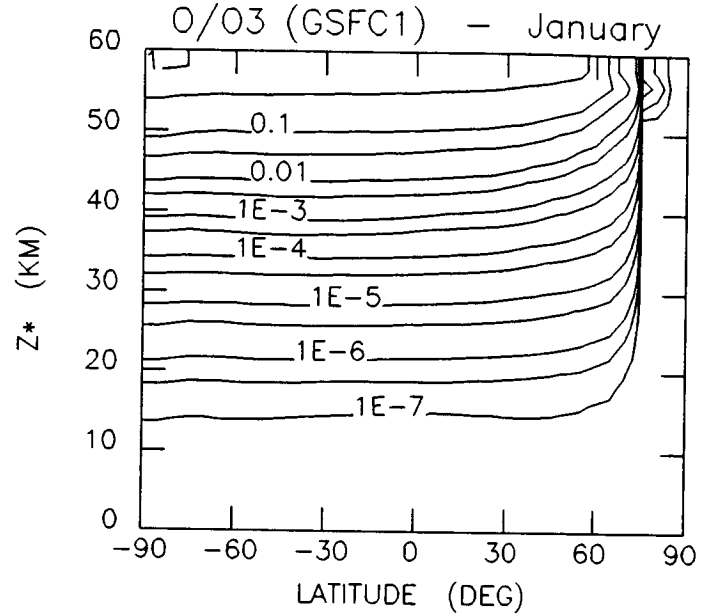
O/O3 (GSFC1) – January
Z* (KM)
60
50
40
30
20
10
0
1
0.1
0.01
1E-3
1E-4
1E-5
1E-6
1E-7
−90 −60 −30 0 30 60 90
LATITUDE (DEG)

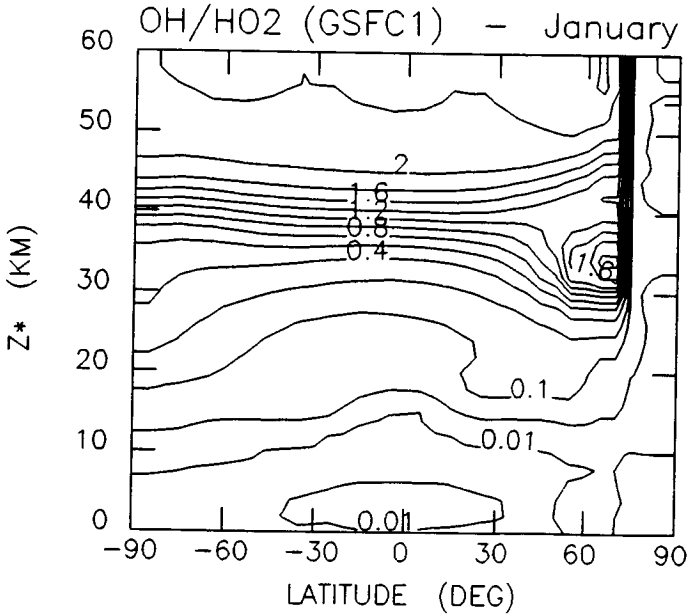
OH/HO2 (GSFC1) – January
Z* (KM)
60
50
40
30
20
10
0
2
1.6
0.8
0.4
1.6
0.1
0.01
0.01
−90 −60 −30 0 30 60 90
LATITUDE (DEG)

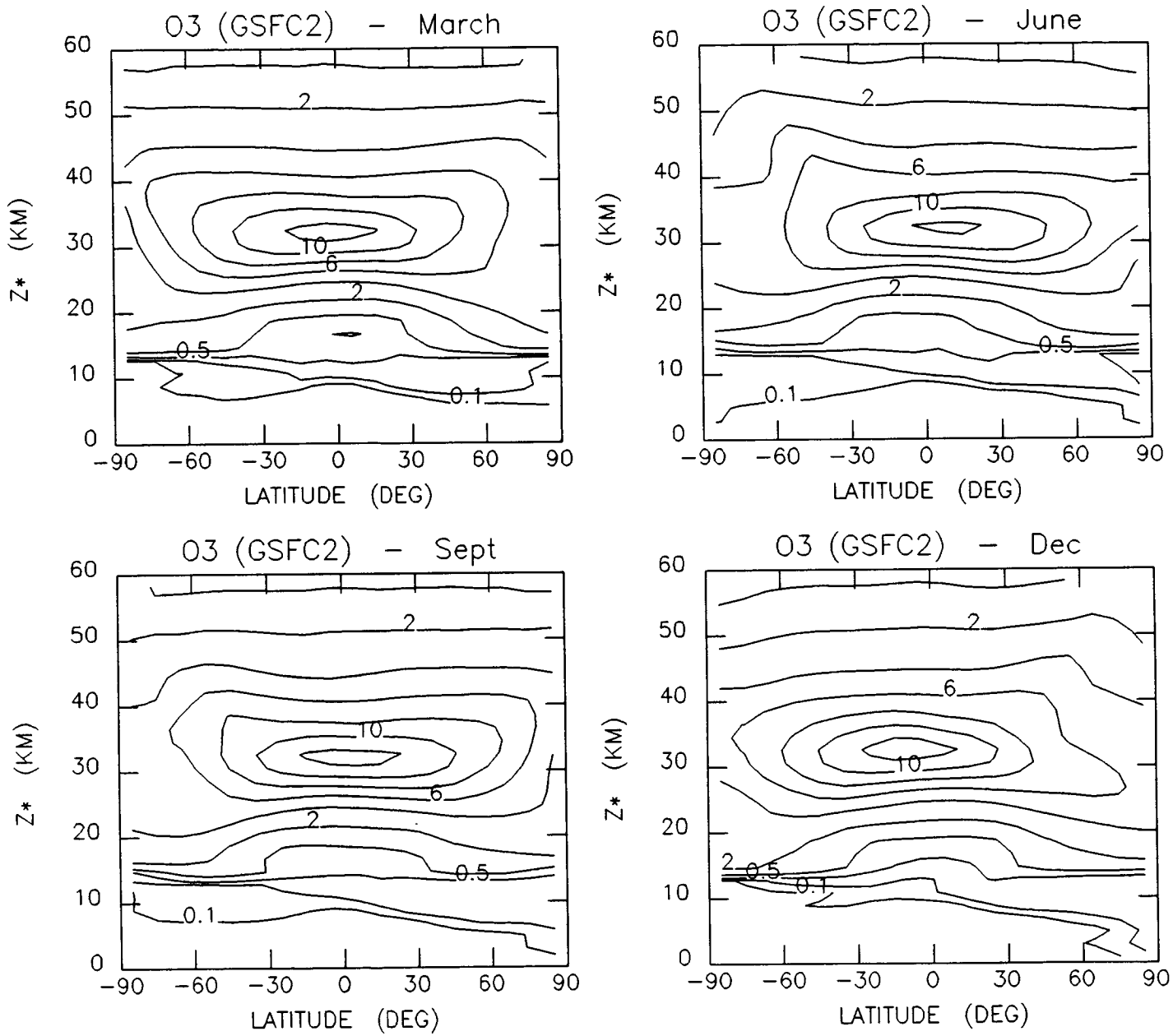
O3 (GSFC2) – March
O3 (GSFC2) – June
O3 (GSFC2) – Sept
O3 (GSFC2) – Dec
Z* (KM)
LATITUDE (DEG)
0
10
20
30
40
50
60
-90
-60
-30
0
30
60
90
2
6
10
0.5
0.1

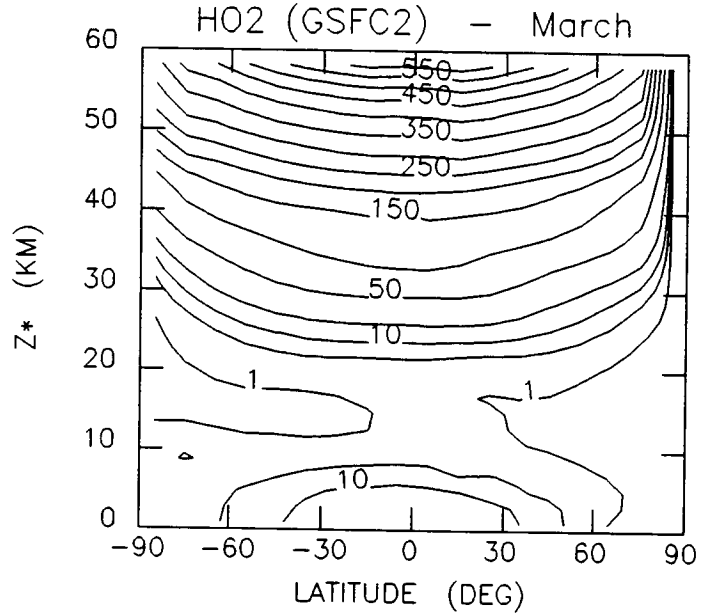
HO2 (GSFC2) – March
Z* (KM)
LATITUDE (DEG)
550
450
350
250
150
50
10
1
10
0
10
20
30
40
50
60
-90
-60
-30
0
30
60
90

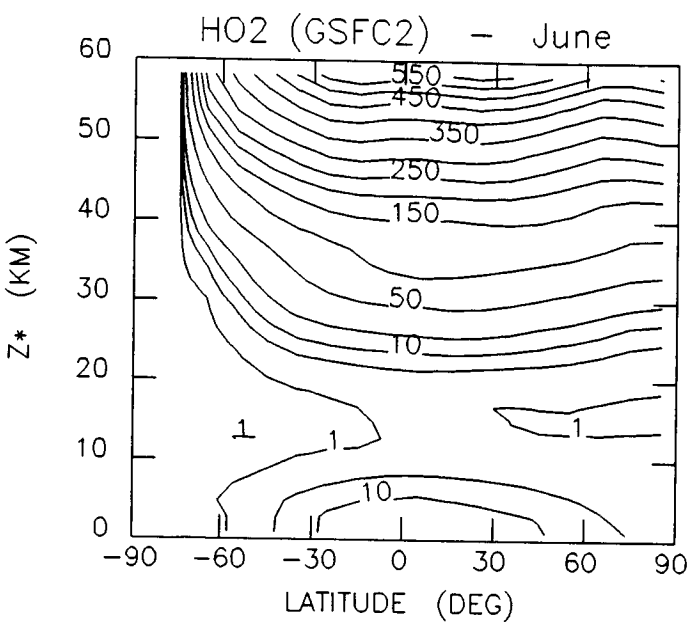
HO2 (GSFC2) – June
Z* (KM)
LATITUDE (DEG)
550
450
350
250
150
50
10
1
1
1
10
0
10
20
30
40
50
60
-90
-60
-30
0
30
60
90

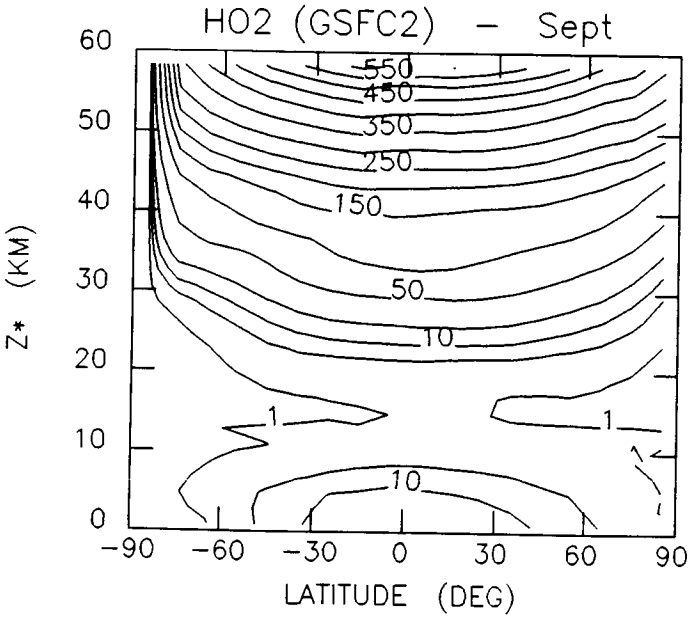
HO2 (GSFC2) – Sept
Z* (KM)
LATITUDE (DEG)
550
450
350
250
150
50
10
1
1
10
0
10
20
30
40
50
60
-90
-60
-30
0
30
60
90

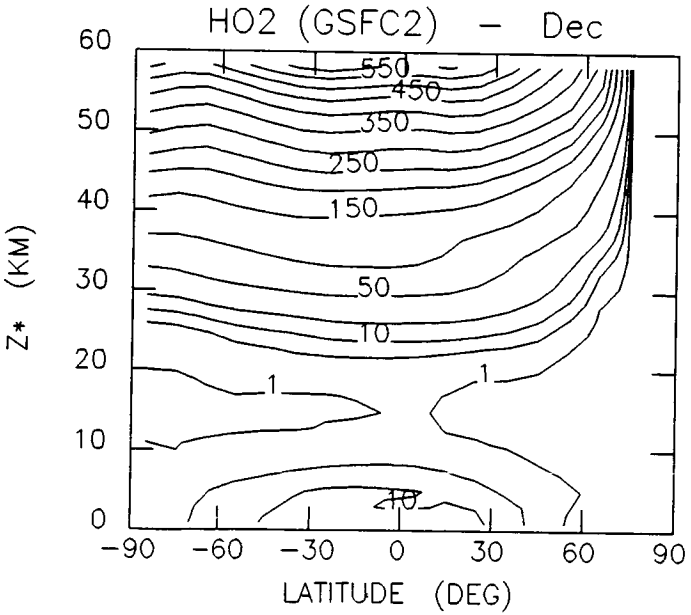
HO2 (GSFC2) – Dec
Z* (KM)
LATITUDE (DEG)
550
450
350
250
150
50
10
1
1
10
0
10
20
30
40
50
60
-90
-60
-30
0
30
60
90

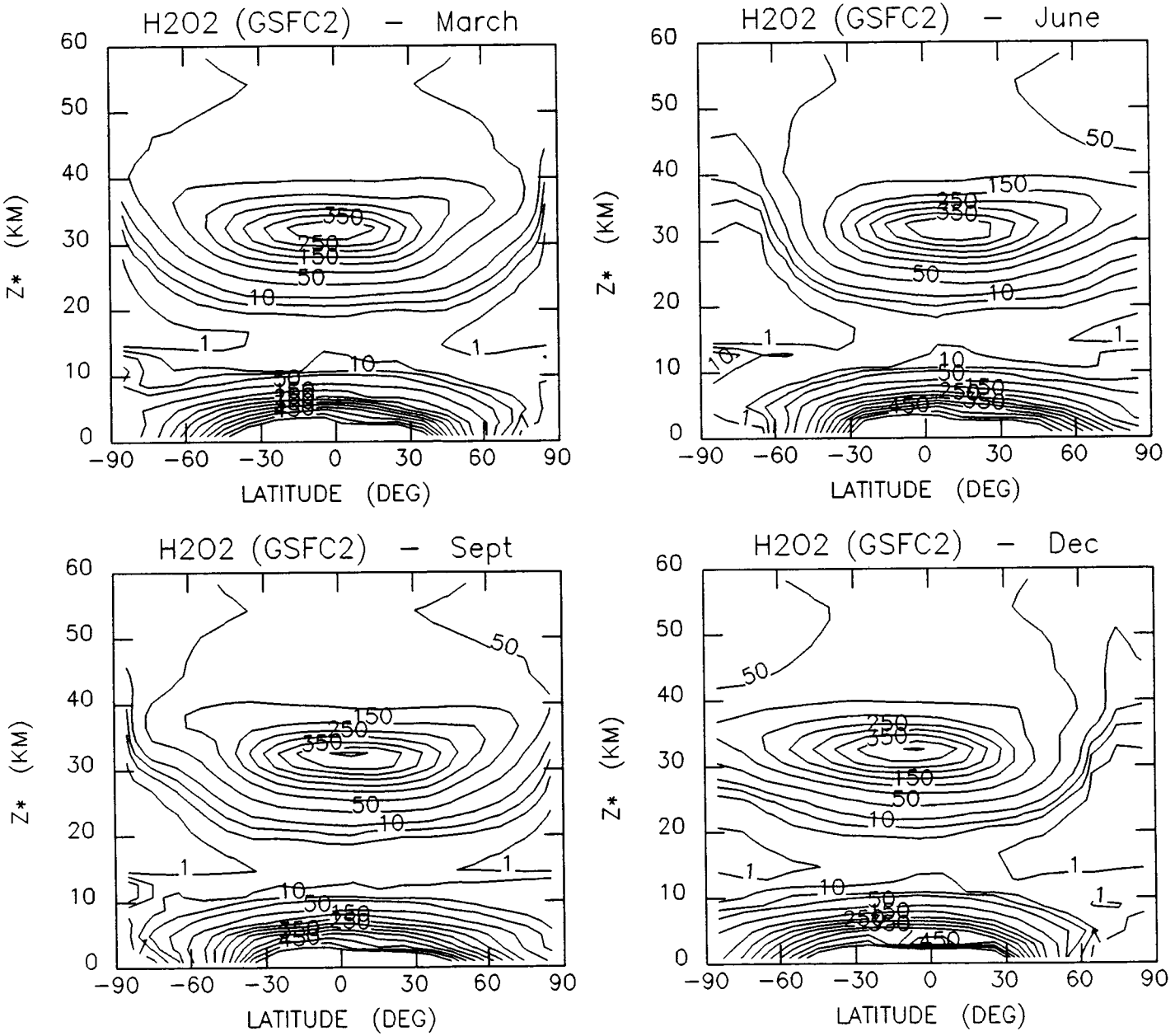
H2O2 (GSFC2) – March
H2O2 (GSFC2) – June
H2O2 (GSFC2) – Sept
H2O2 (GSFC2) – Dec
Z* (KM)
LATITUDE (DEG)
60
50
40
30
20
10
0
-90 -60 -30 0 30 60 90
350
250
150
50
10
1

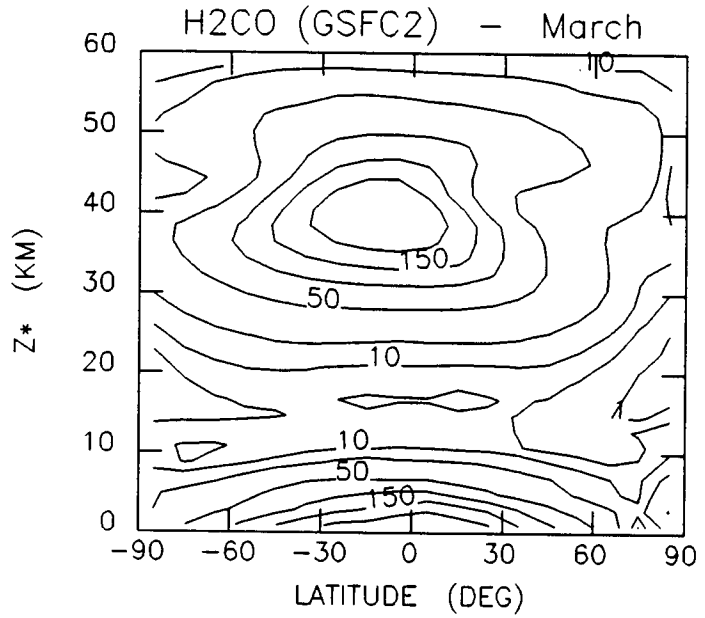
H2CO (GSFC2) – March
Z* (KM)
LATITUDE (DEG)
60
50
40
30
20
10
0
-90 -60 -30 0 30 60 90
10
150
50
10
10
50
150

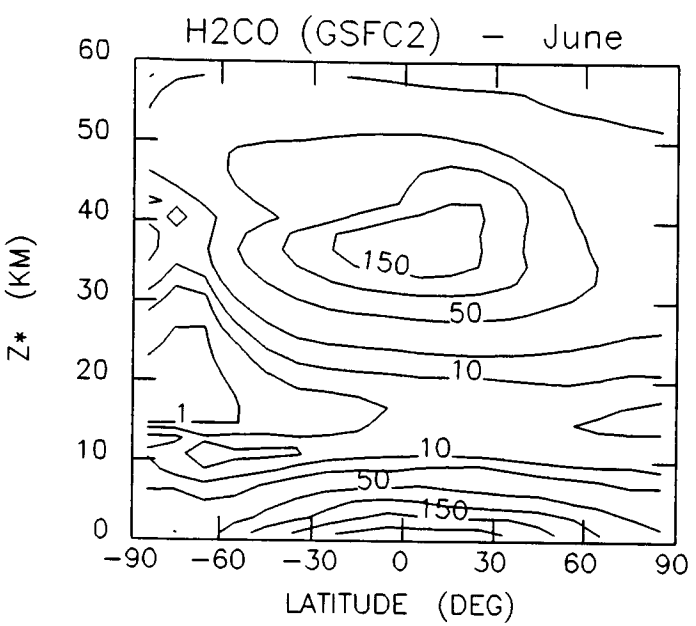
H2CO (GSFC2) – June
Z* (KM)
LATITUDE (DEG)
60
50
40
30
20
10
0
-90 -60 -30 0 30 60 90
150
50
10
1
10
50
150

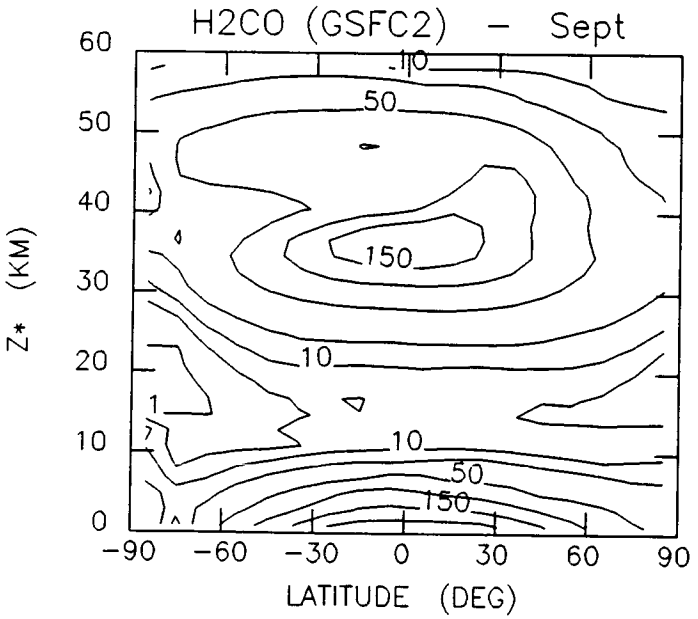
H2CO (GSFC2) – Sept
Z* (KM)
LATITUDE (DEG)
60
50
40
30
20
10
0
-90 -60 -30 0 30 60 90
10
50
150
10
1
10
50
150

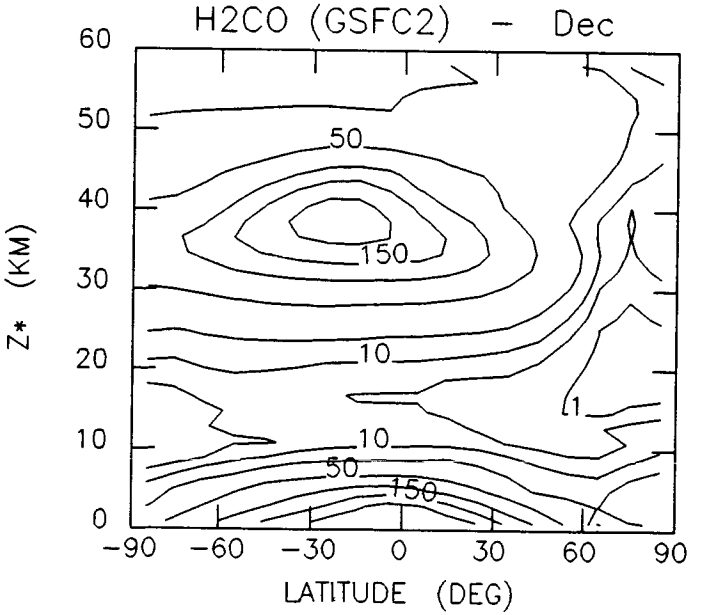
H2CO (GSFC2) – Dec
Z* (KM)
LATITUDE (DEG)
60
50
40
30
20
10
0
-90 -60 -30 0 30 60 90
50
150
10
1
10
50
150

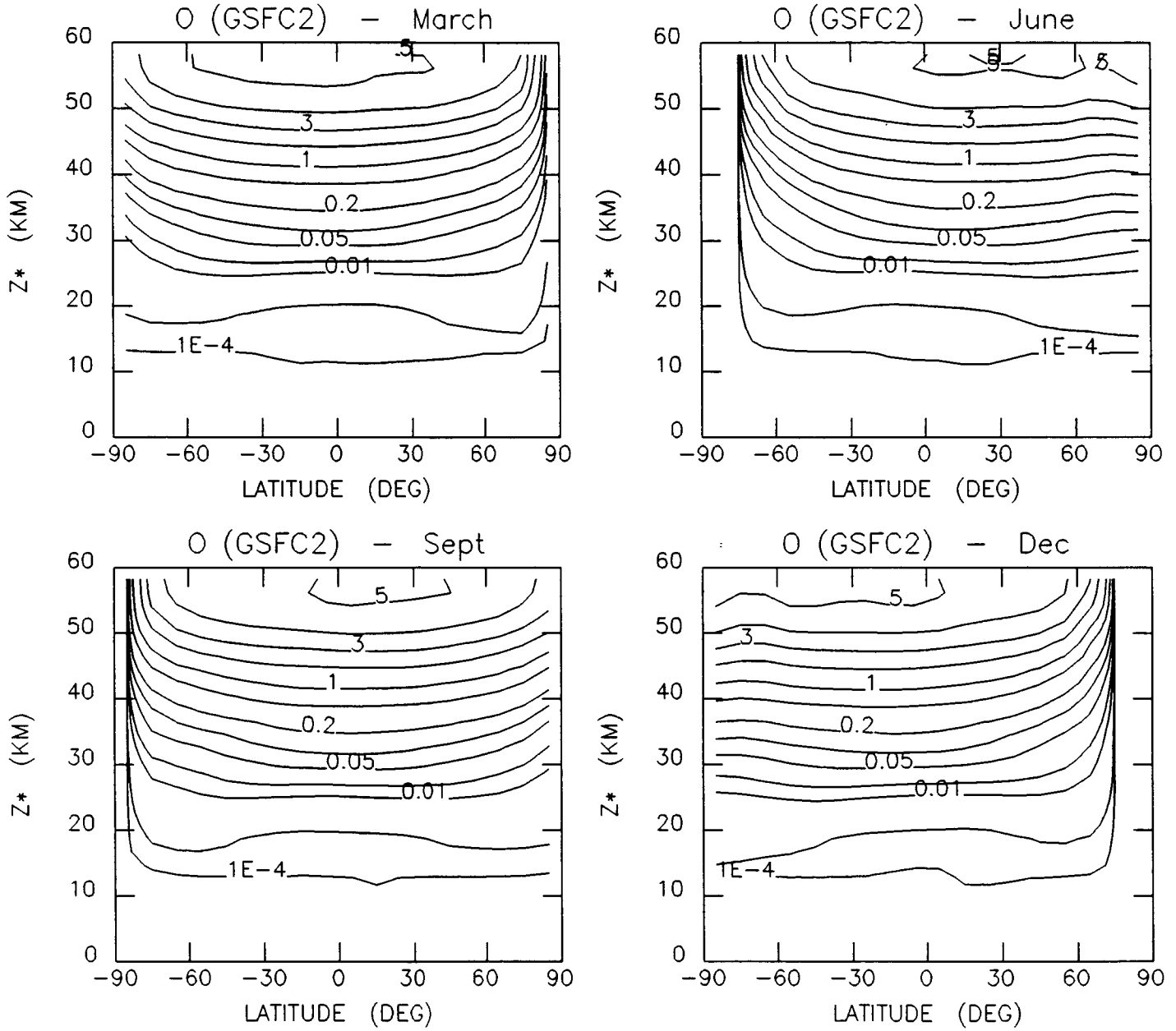
O (GSFC2) – March
O (GSFC2) – June
O (GSFC2) – Sept
O (GSFC2) – Dec
Z* (KM)
LATITUDE (DEG)
5
3
1
0.2
0.05
0.01
1E-4
0
10
20
30
40
50
60
-90
-60
-30
0
30
60
90

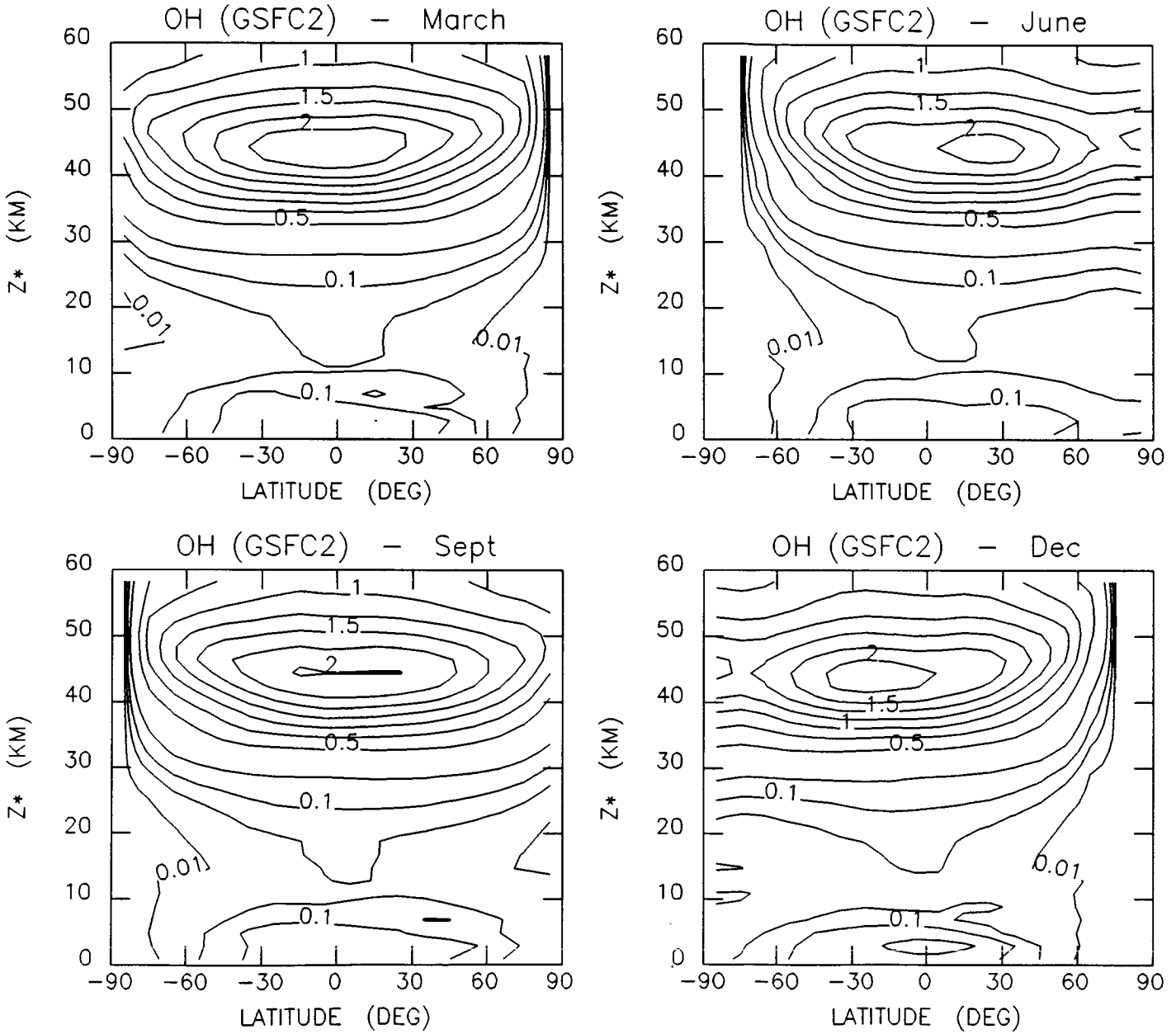
OH (GSFC2) – March
OH (GSFC2) – June
OH (GSFC2) – Sept
OH (GSFC2) – Dec
Z* (KM)
LATITUDE (DEG)
0
10
20
30
40
50
60
−90
−60
−30
0
30
60
90
1
1.5
2
0.5
0.1
0.01

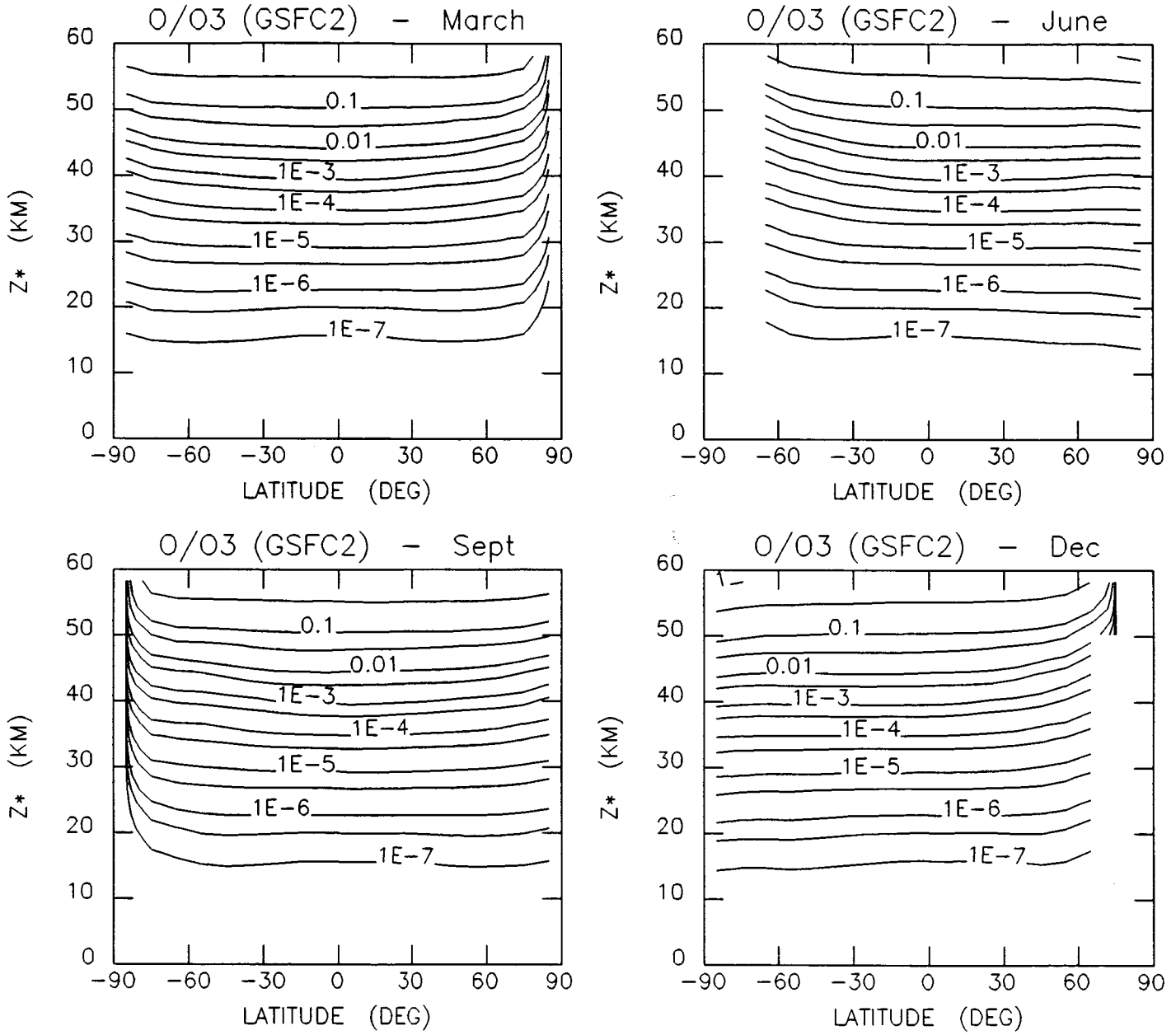
O/O3 (GSFC2) - March
O/O3 (GSFC2) - June
O/O3 (GSFC2) - Sept
O/O3 (GSFC2) - Dec
Z* (KM)
LATITUDE (DEG)
0.1
0.01
1E-3
1E-4
1E-5
1E-6
1E-7
0
10
20
30
40
50
60
-90
-60
-30
0
30
60
90

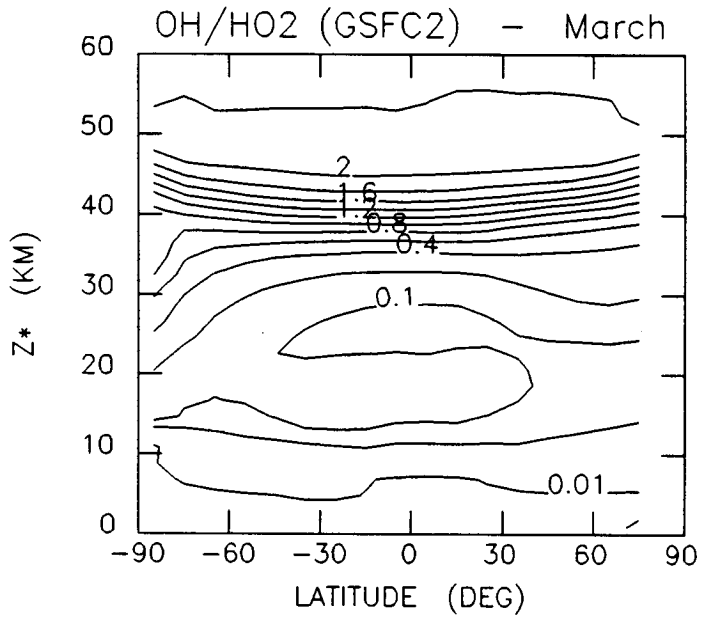
OH/HO2 (GSFC2) – March
Z* (KM)
LATITUDE (DEG)
2
1.6
1.2
0.8
0.4
0.1
0.01

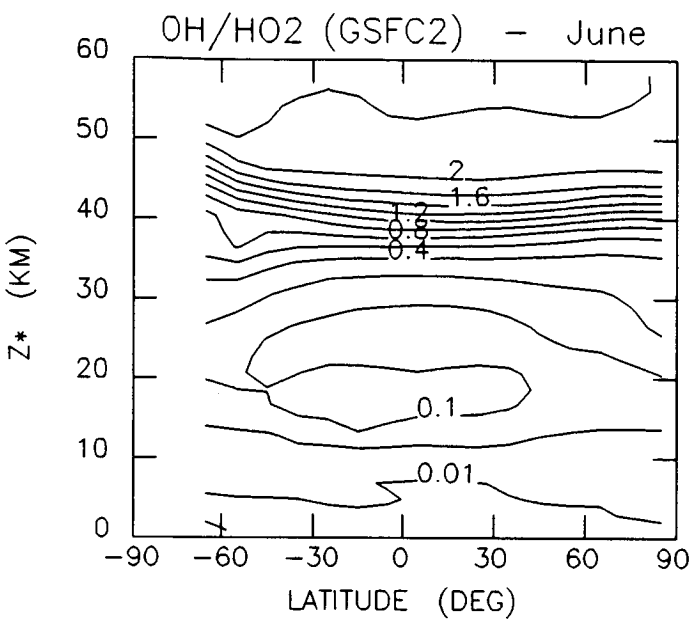
OH/HO2 (GSFC2) – June
Z* (KM)
LATITUDE (DEG)
2
1.6
1.2
0.8
0.4
0.1
0.01

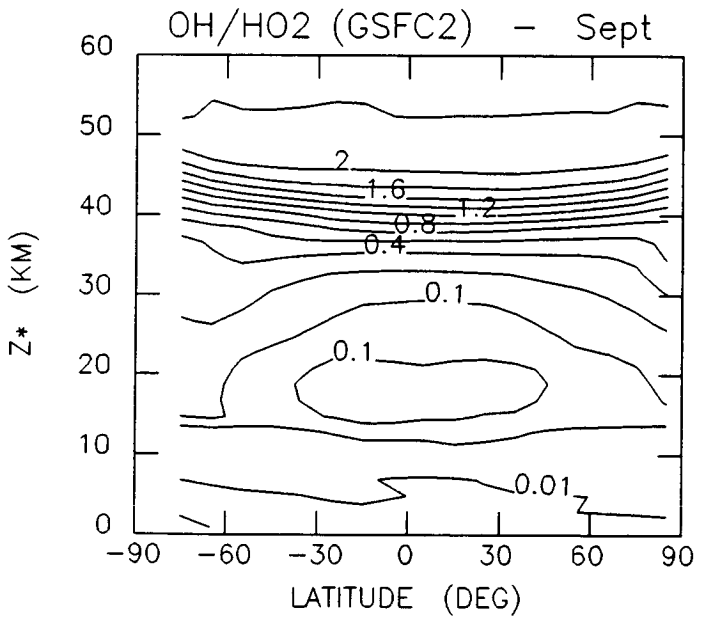
OH/HO2 (GSFC2) – Sept
Z* (KM)
LATITUDE (DEG)
2
1.6
1.2
0.8
0.4
0.1
0.1
0.01

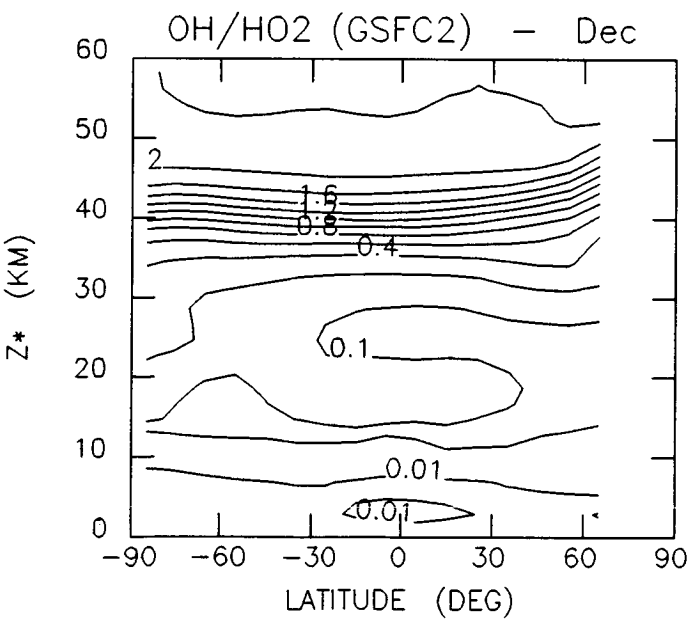
OH/HO2 (GSFC2) – Dec
Z* (KM)
LATITUDE (DEG)
2
1.6
0.8
0.4
0.1
0.01
<0.01

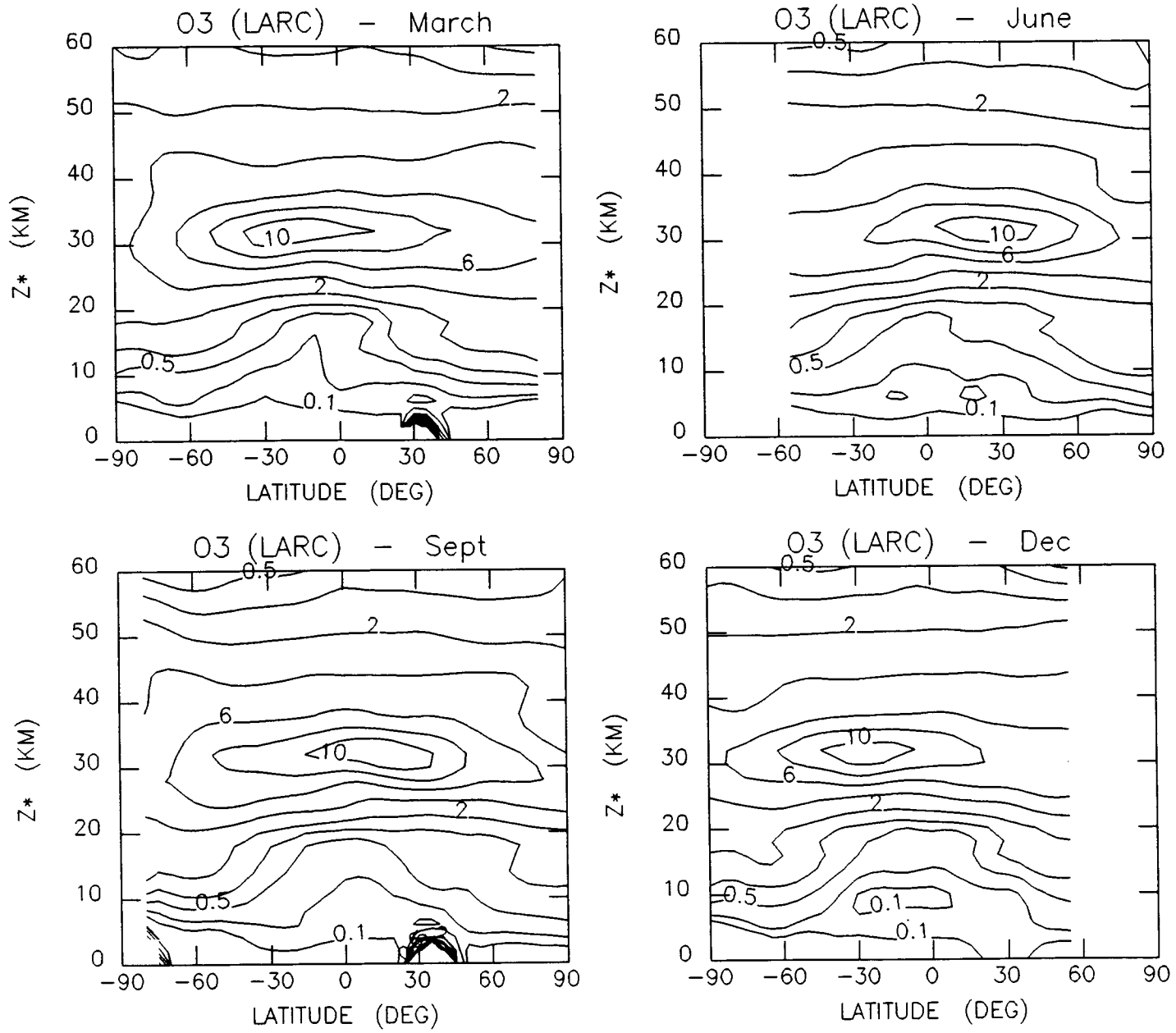
O3 (LARC) – March
O3 (LARC) – June
O3 (LARC) – Sept
O3 (LARC) – Dec
Z* (KM)
LATITUDE (DEG)
0
10
20
30
40
50
60
-90
-60
-30
0
30
60
90
0.1
0.5
2
6
10

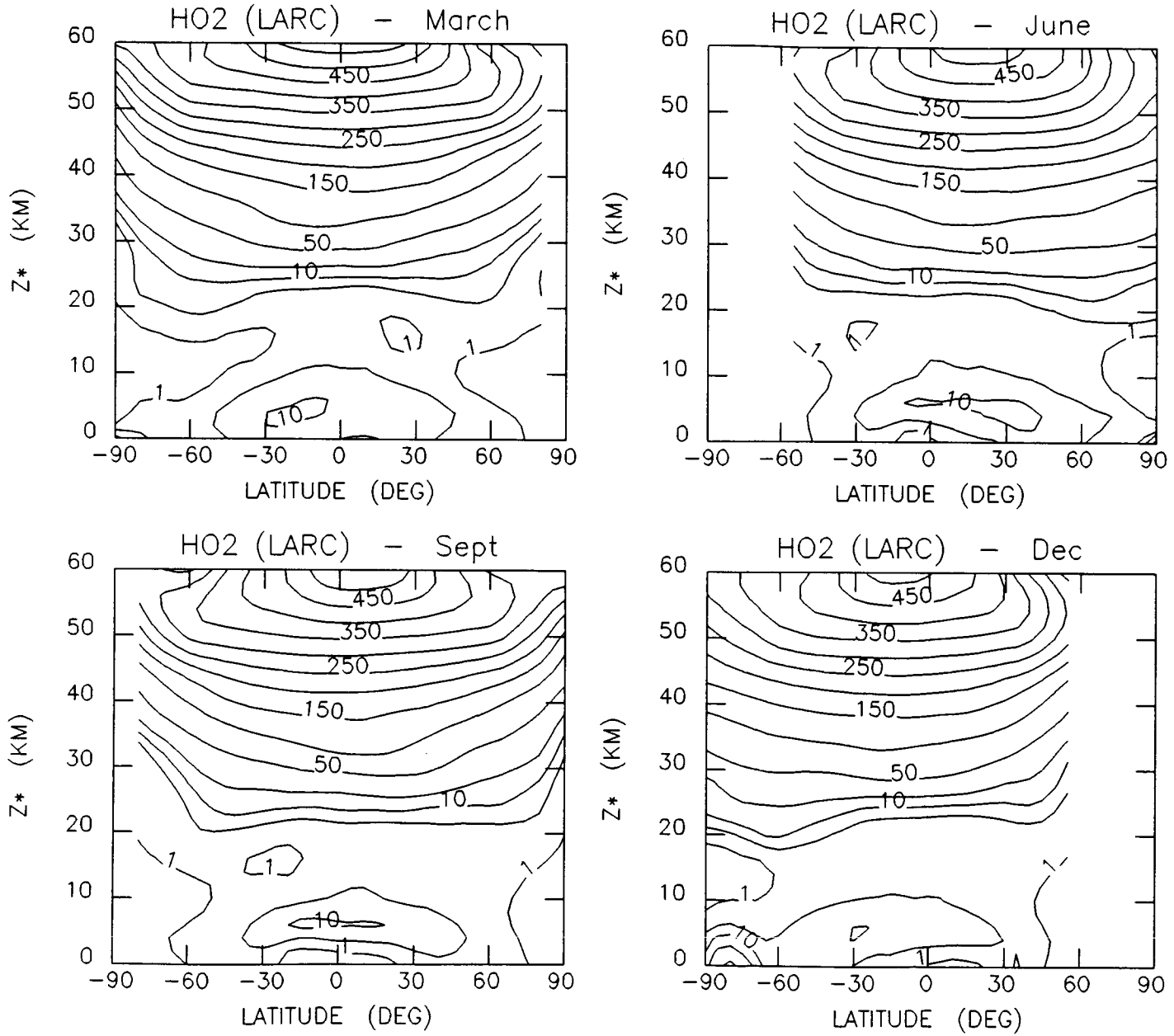
HO2 (LARC) – March
HO2 (LARC) – June
HO2 (LARC) – Sept
HO2 (LARC) – Dec
Z* (KM)
LATITUDE (DEG)
60
50
40
30
20
10
0
-90 -60 -30 0 30 60 90
450
350
250
150
50
10
1

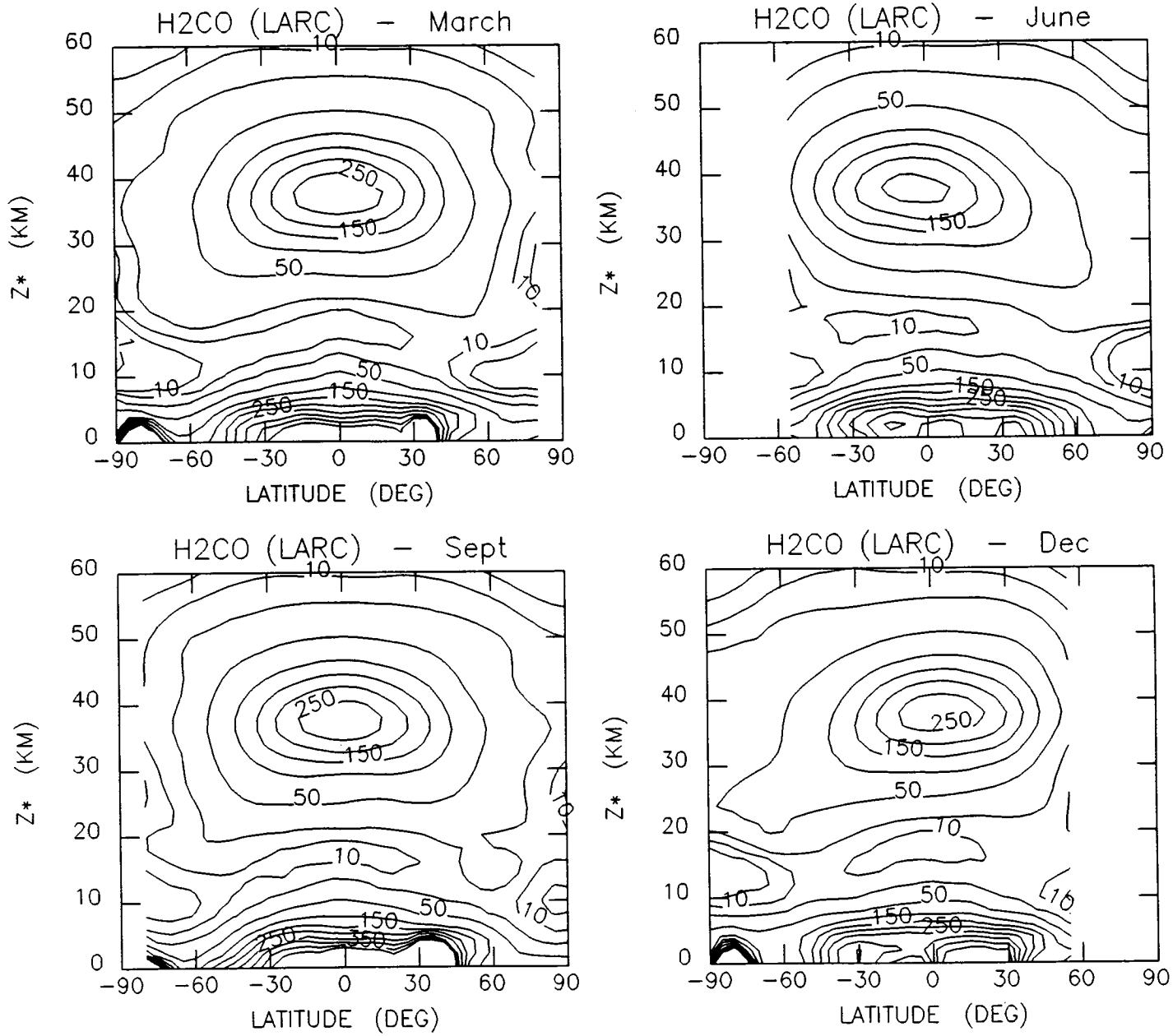
H2CO (LARC) – March
H2CO (LARC) – June
H2CO (LARC) – Sept
H2CO (LARC) – Dec
Z* (KM)
LATITUDE (DEG)
60
50
40
30
20
10
0
-90
-60
-30
0
30
60
90
10
50
150
250
350

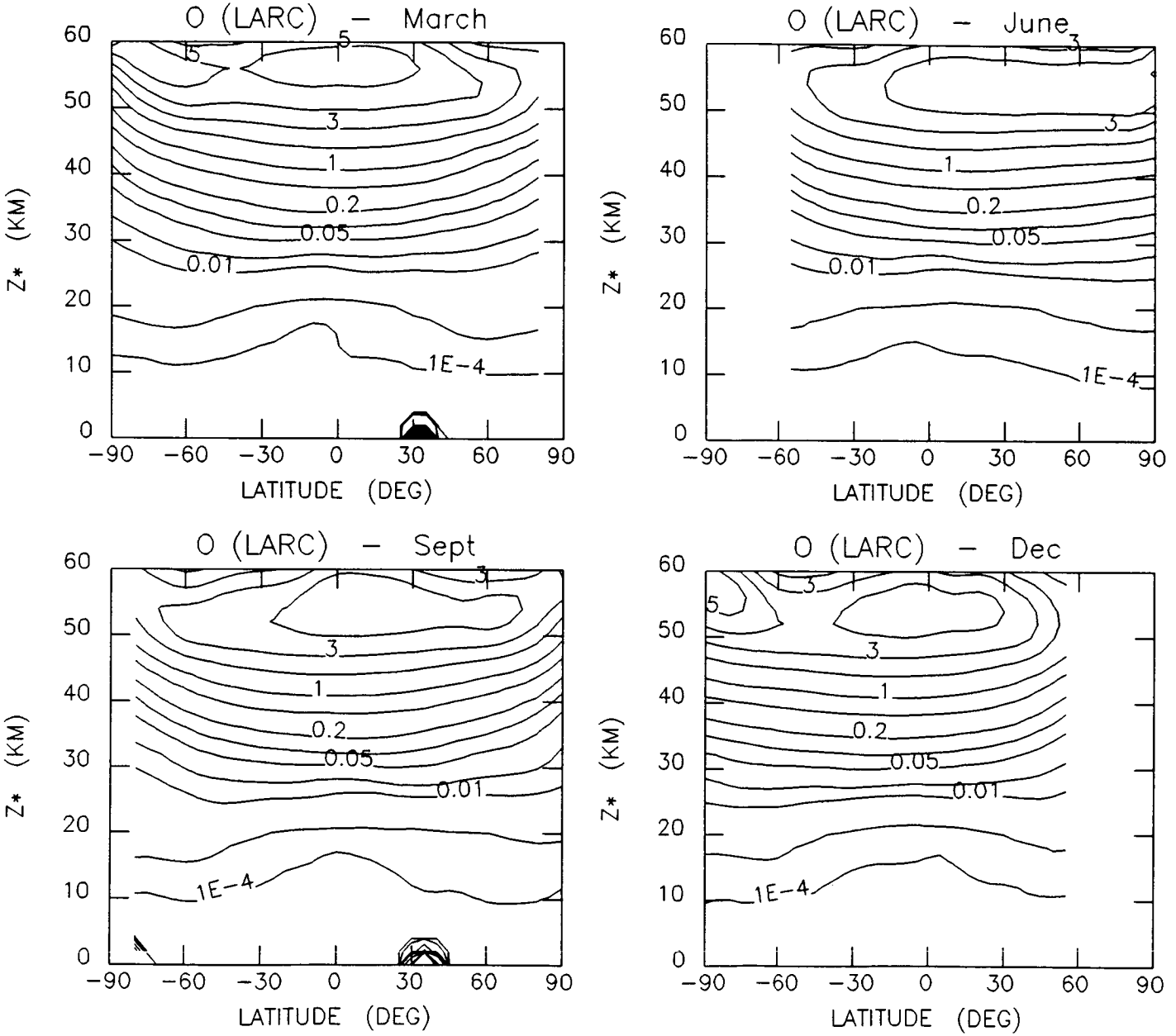
O (LARC) – March
O (LARC) – June
O (LARC) – Sept
O (LARC) – Dec
Z* (KM)
LATITUDE (DEG)
60
50
40
30
20
10
0
−90
−60
−30
0
30
60
90
5
3
1
0.2
0.05
0.01
1E−4

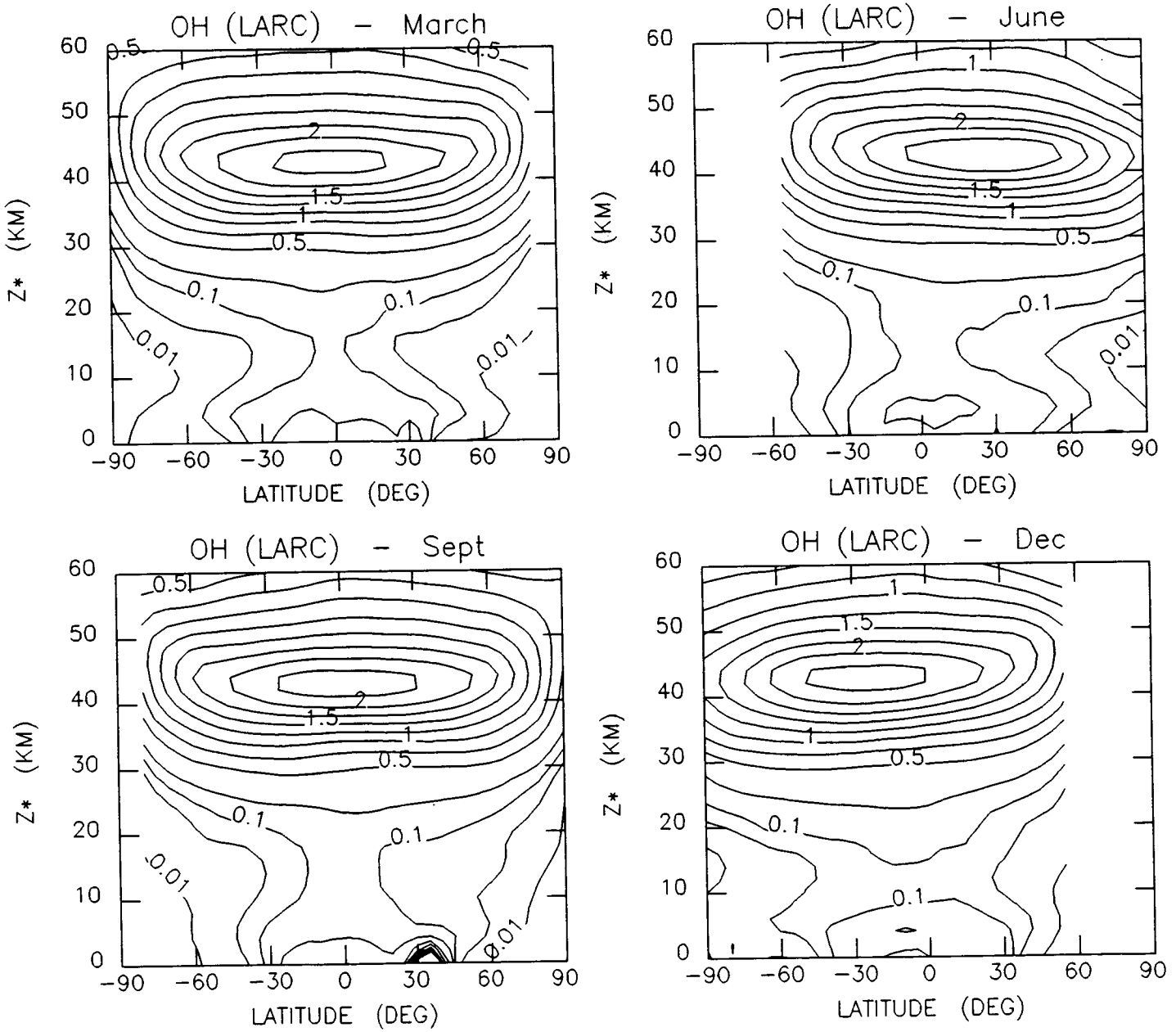
OH (LARC) – March
OH (LARC) – June
OH (LARC) – Sept
OH (LARC) – Dec
Z* (KM)
LATITUDE (DEG)
0
10
20
30
40
50
60
-90
-60
-30
0
30
60
90
0.5
1
1.5
2
0.1
0.01

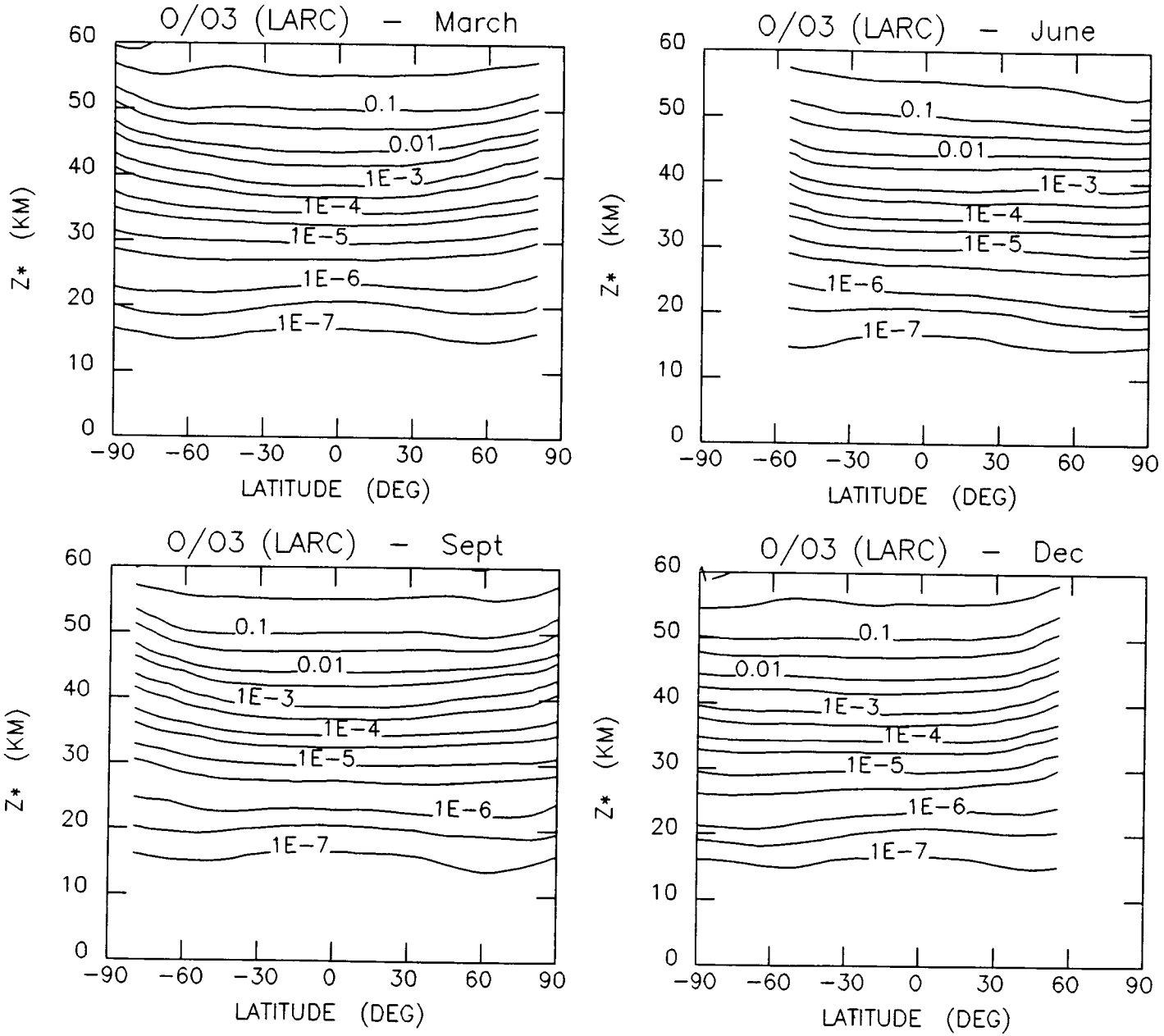
O/O3 (LARC) – March
O/O3 (LARC) – June
O/O3 (LARC) – Sept
O/O3 (LARC) – Dec
Z* (KM)
LATITUDE (DEG)
0.1
0.01
1E-3
1E-4
1E-5
1E-6
1E-7
0
10
20
30
40
50
60
-90
-60
-30
0
30
60
90

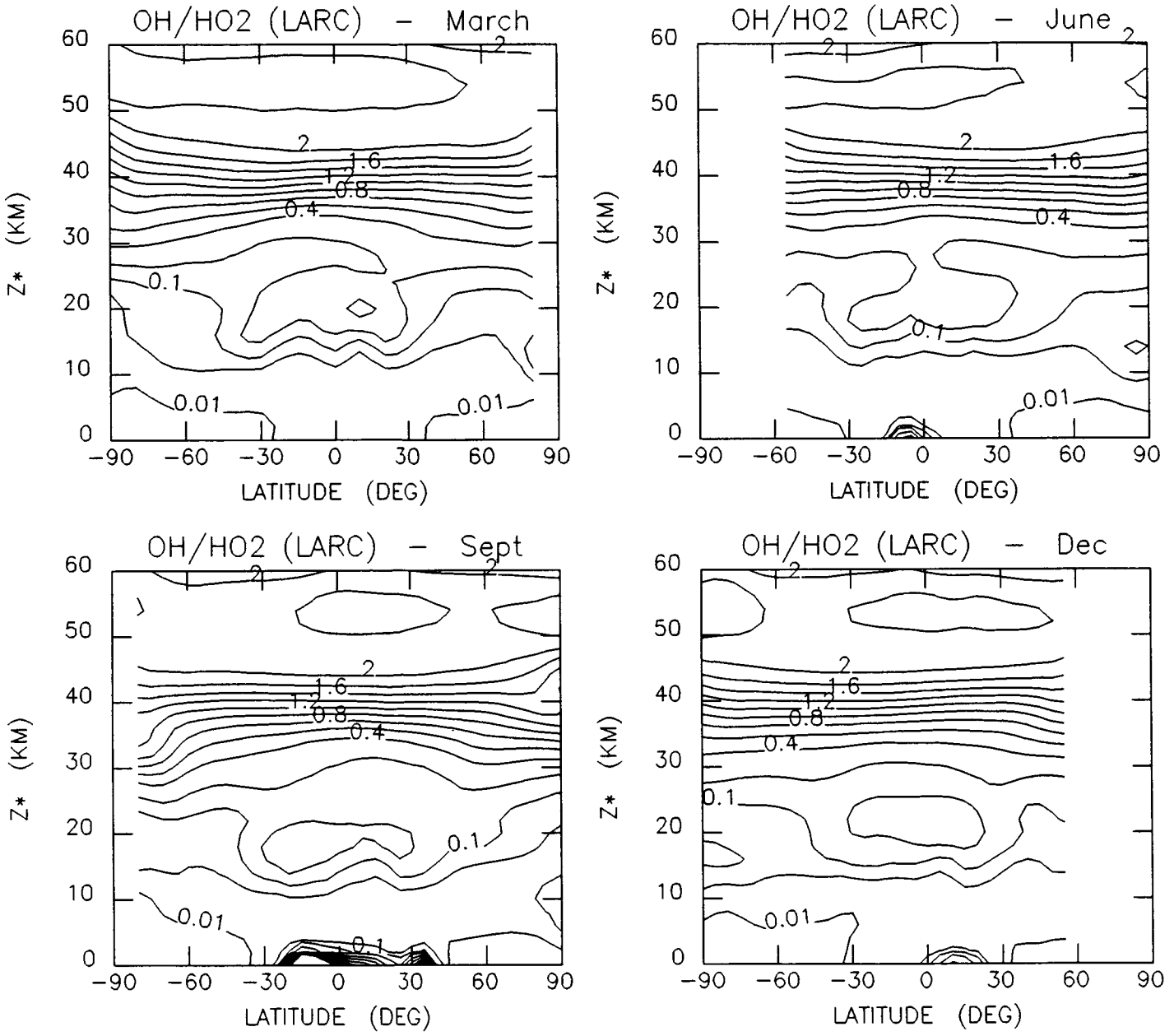
OH/HO2 (LARC) – March
OH/HO2 (LARC) – June
OH/HO2 (LARC) – Sept
OH/HO2 (LARC) – Dec
Z* (KM)
LATITUDE (DEG)
0
10
20
30
40
50
60
−90
−60
−30
0
30
60
90
2
1.6
1.2
0.8
0.4
0.1
0.01

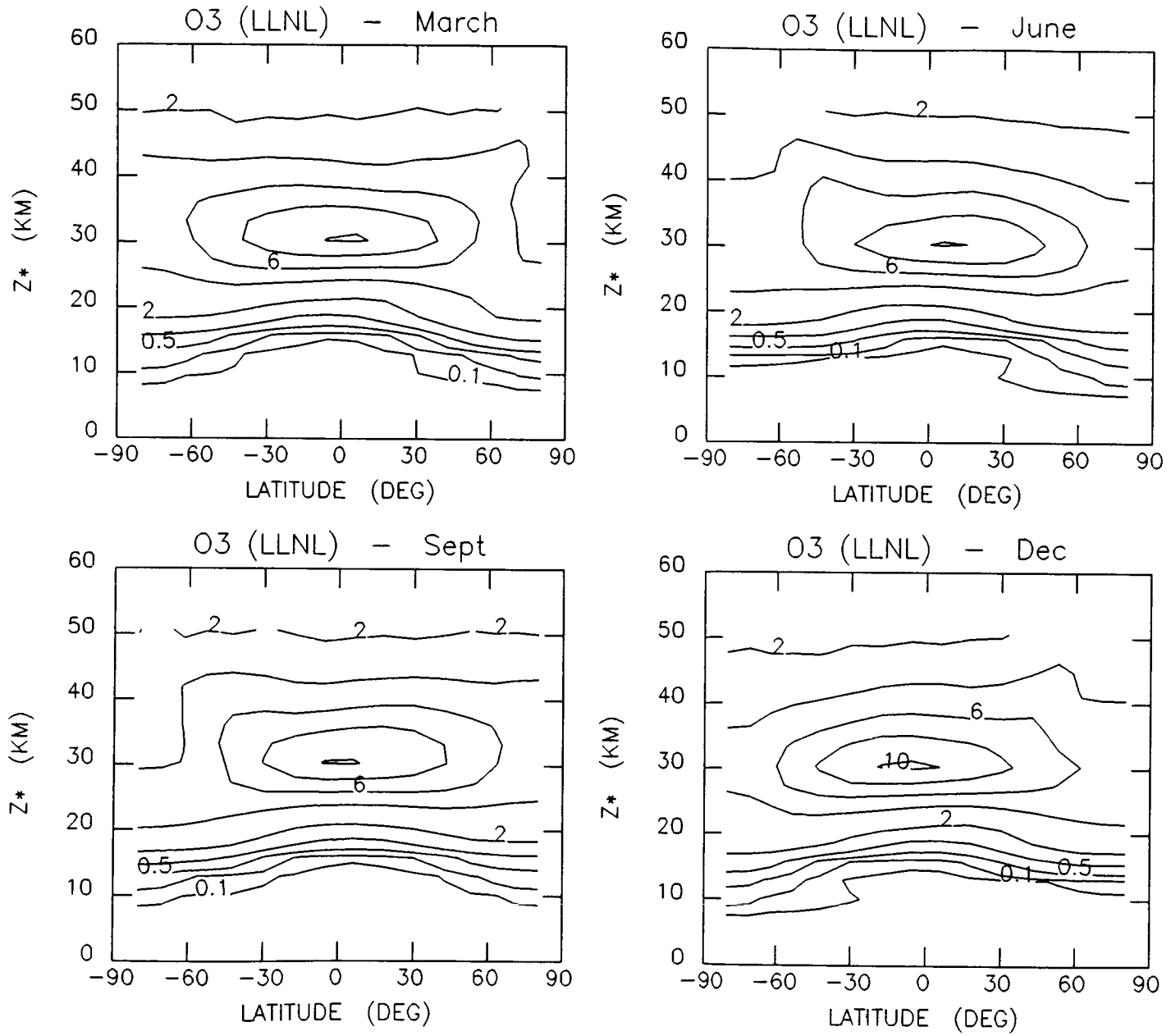
O3 (LLNL) – March
O3 (LLNL) – June
O3 (LLNL) – Sept
O3 (LLNL) – Dec
Z* (KM)
LATITUDE (DEG)
0
10
20
30
40
50
60
-90
-60
-30
0
30
60
90
2
6
10
0.5
0.1

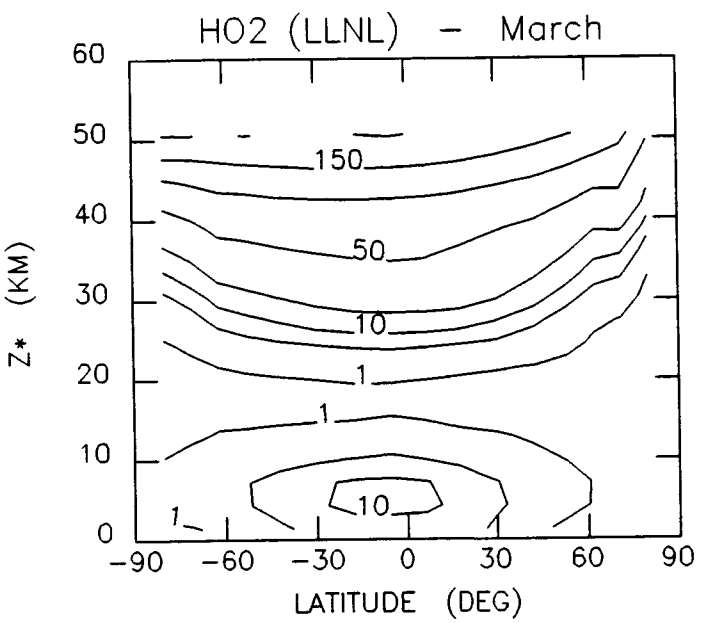
HO2 (LLNL) – March
Z* (KM)
LATITUDE (DEG)
150
50
10
1
1
10
1

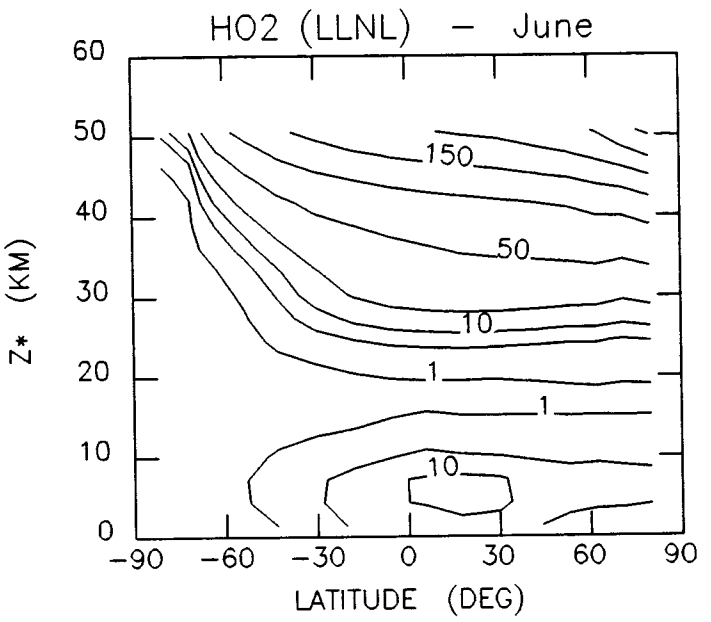
HO2 (LLNL) – June
Z* (KM)
LATITUDE (DEG)
150
50
10
1
1
10

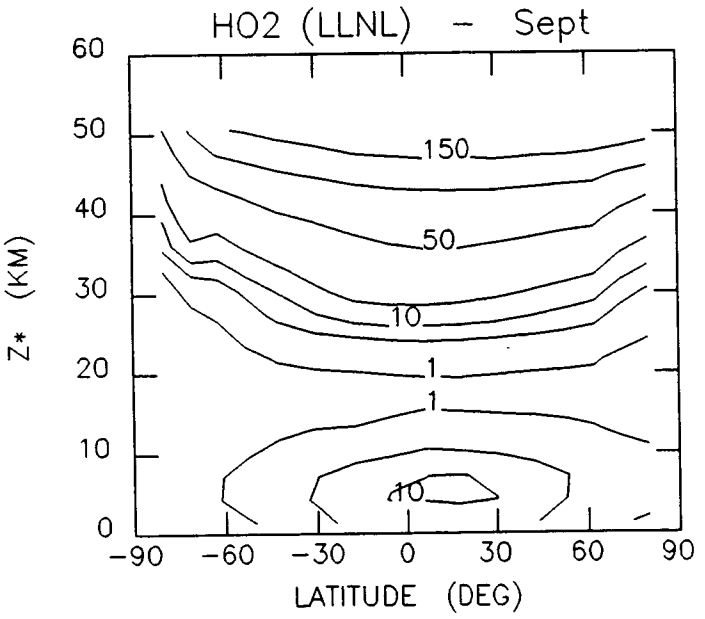
HO2 (LLNL) – Sept
Z* (KM)
LATITUDE (DEG)
150
50
10
1
1
10

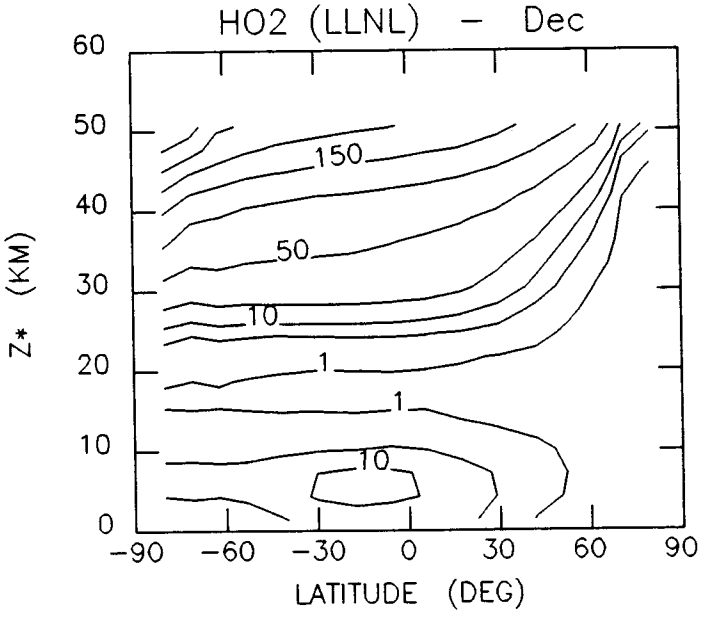
HO2 (LLNL) – Dec
Z* (KM)
LATITUDE (DEG)
150
50
10
1
1
10

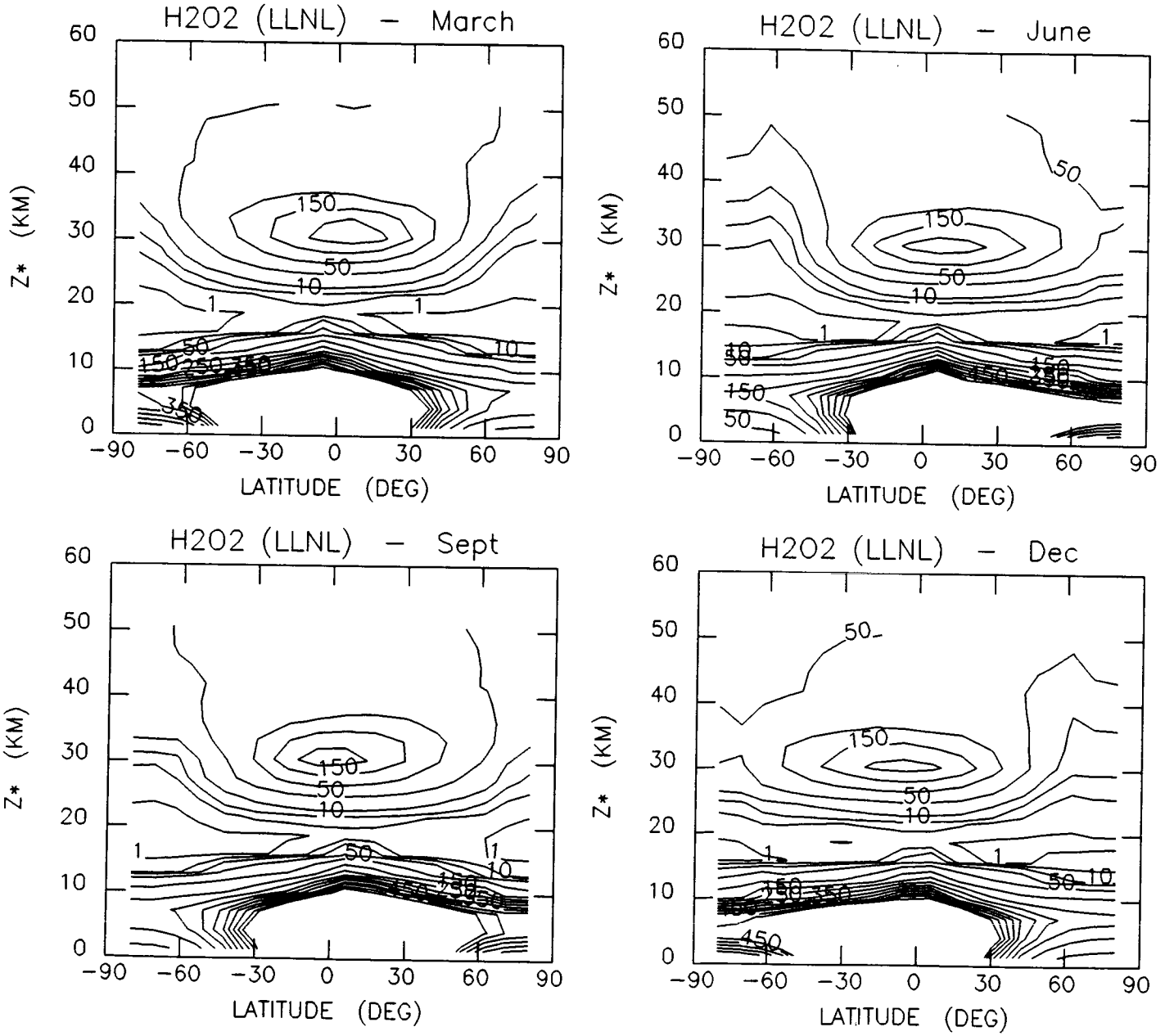
H2O2 (LLNL) – March
H2O2 (LLNL) – June
H2O2 (LLNL) – Sept
H2O2 (LLNL) – Dec
Z* (KM)
LATITUDE (DEG)
60
50
40
30
20
10
0
-90
-60
-30
0
30
60
90
150
50
10
1
450
350

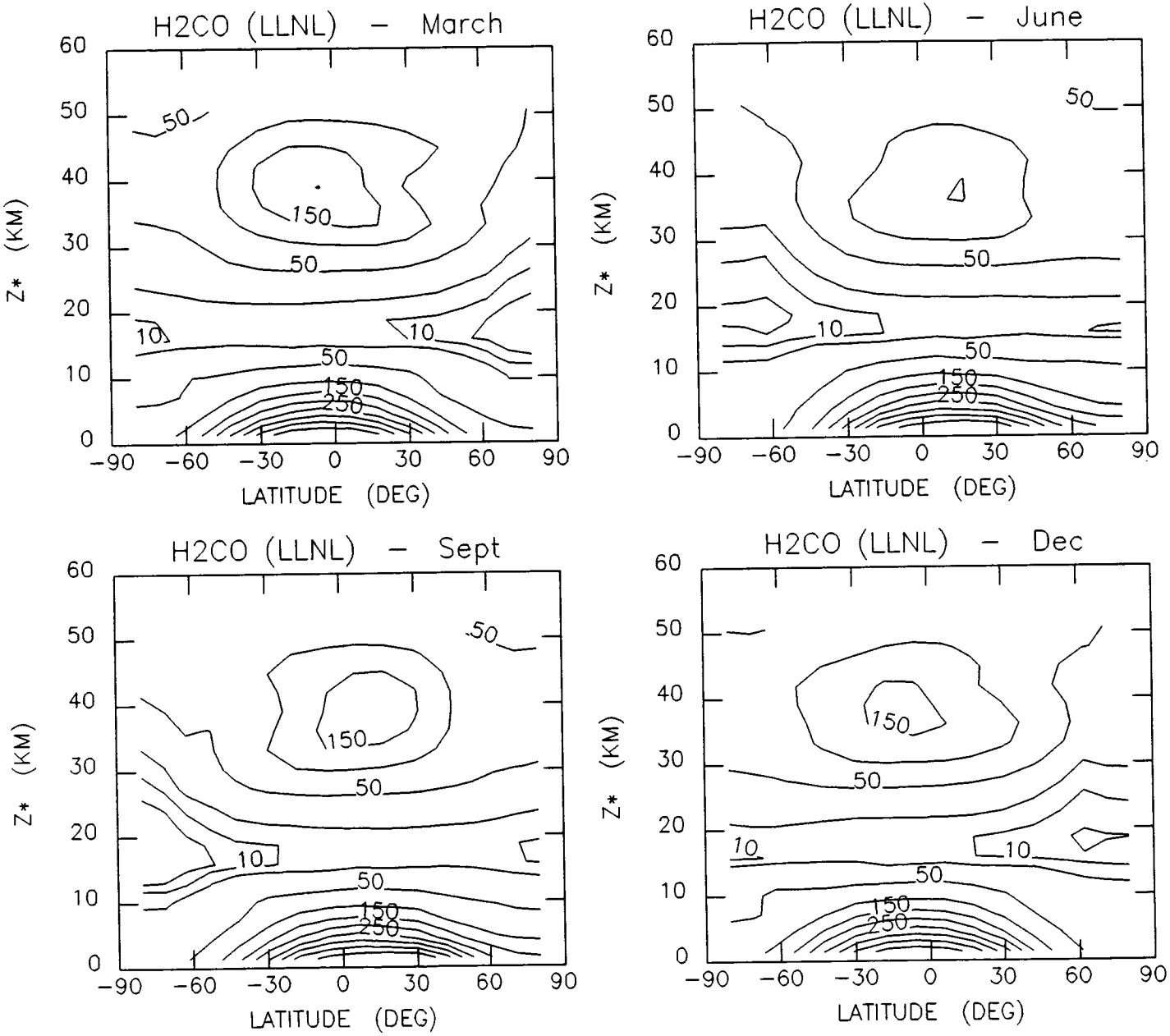
H2CO (LLNL) – March
H2CO (LLNL) – June
H2CO (LLNL) – Sept
H2CO (LLNL) – Dec
Z* (KM)
LATITUDE (DEG)
60
50
40
30
20
10
0
-90
-60
-30
0
30
60
90
50
150
250
10

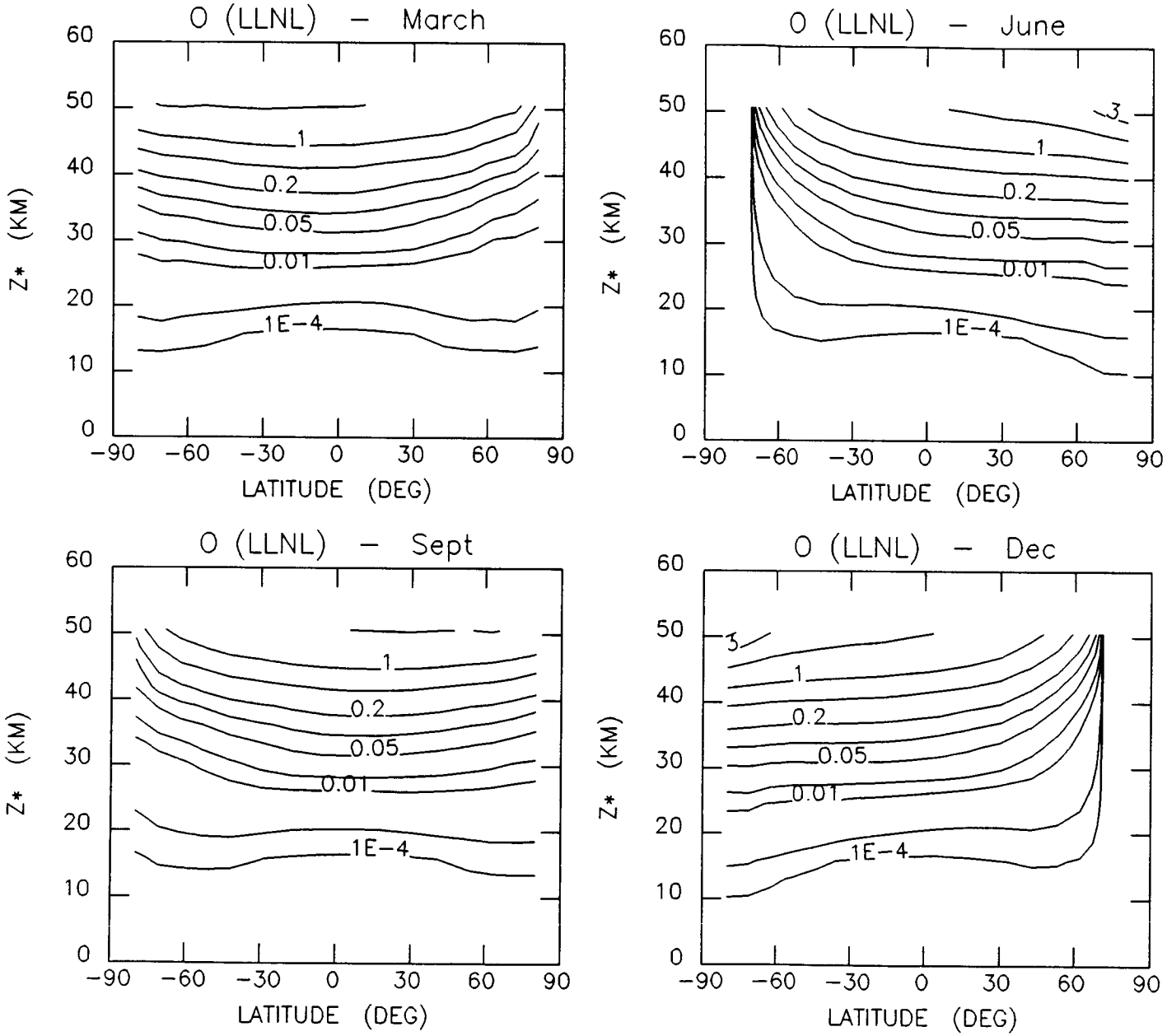
O (LLNL) – March
O (LLNL) – June
O (LLNL) – Sept
O (LLNL) – Dec
Z* (KM)
LATITUDE (DEG)
60
50
40
30
20
10
0
−90 −60 −30 0 30 60 90
3
1
0.2
0.05
0.01
1E−4

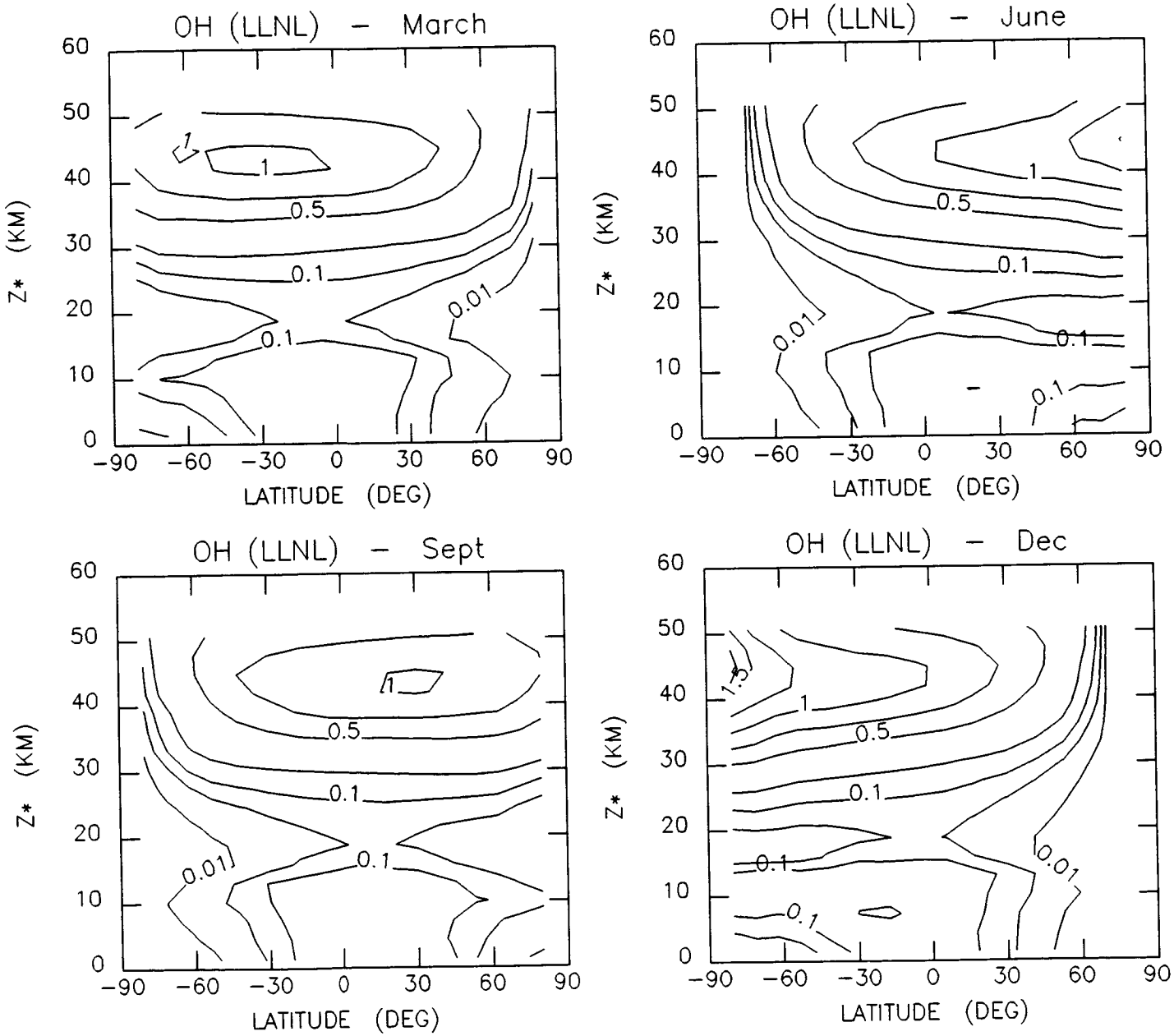
OH (LLNL) – March
OH (LLNL) – June
OH (LLNL) – Sept
OH (LLNL) – Dec
Z* (KM)
LATITUDE (DEG)
0
10
20
30
40
50
60
-90
-60
-30
0
30
60
90
1.5
1
0.5
0.1
0.01

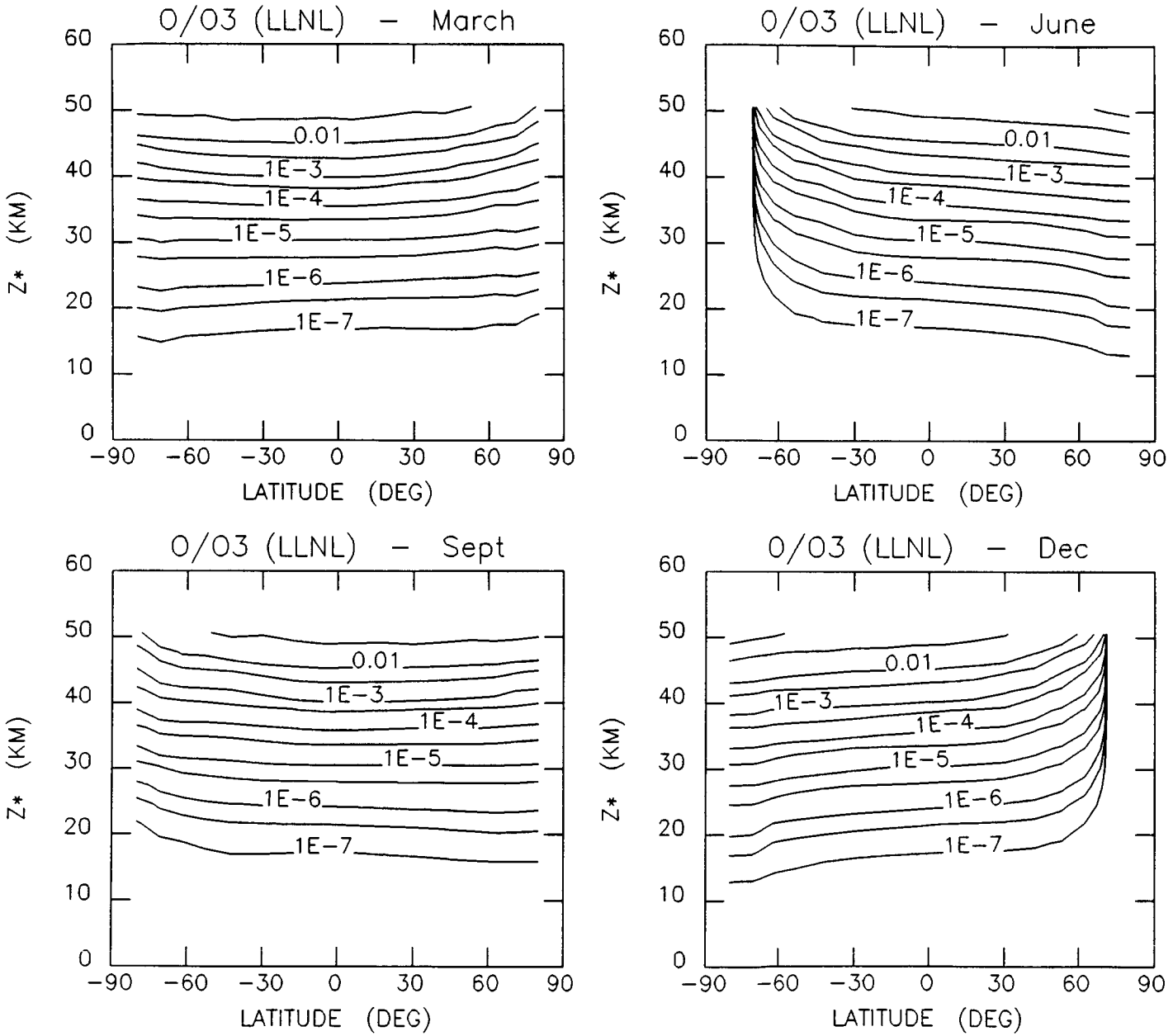
O/O3 (LLNL) – March
O/O3 (LLNL) – June
O/O3 (LLNL) – Sept
O/O3 (LLNL) – Dec
Z* (KM)
LATITUDE (DEG)
0.01
1E-3
1E-4
1E-5
1E-6
1E-7
0
10
20
30
40
50
60
-90
-60
-30
0
30
60
90

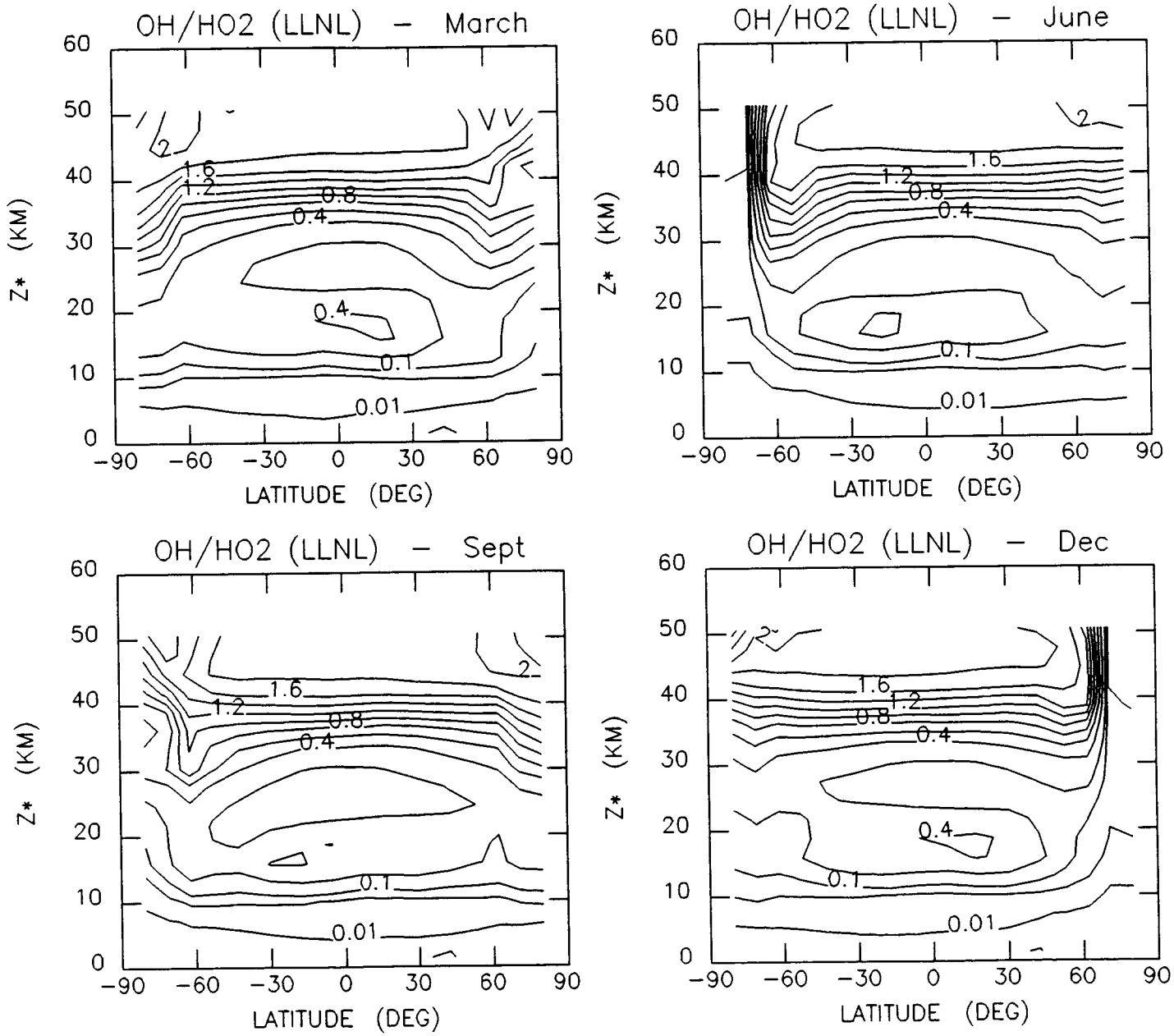
OH/HO2 (LLNL) – March
OH/HO2 (LLNL) – June
OH/HO2 (LLNL) – Sept
OH/HO2 (LLNL) – Dec
Z* (KM)
LATITUDE (DEG)
0
10
20
30
40
50
60
-90
-60
-30
0
30
60
90
2
1.6
1.2
0.8
0.4
0.1
0.01

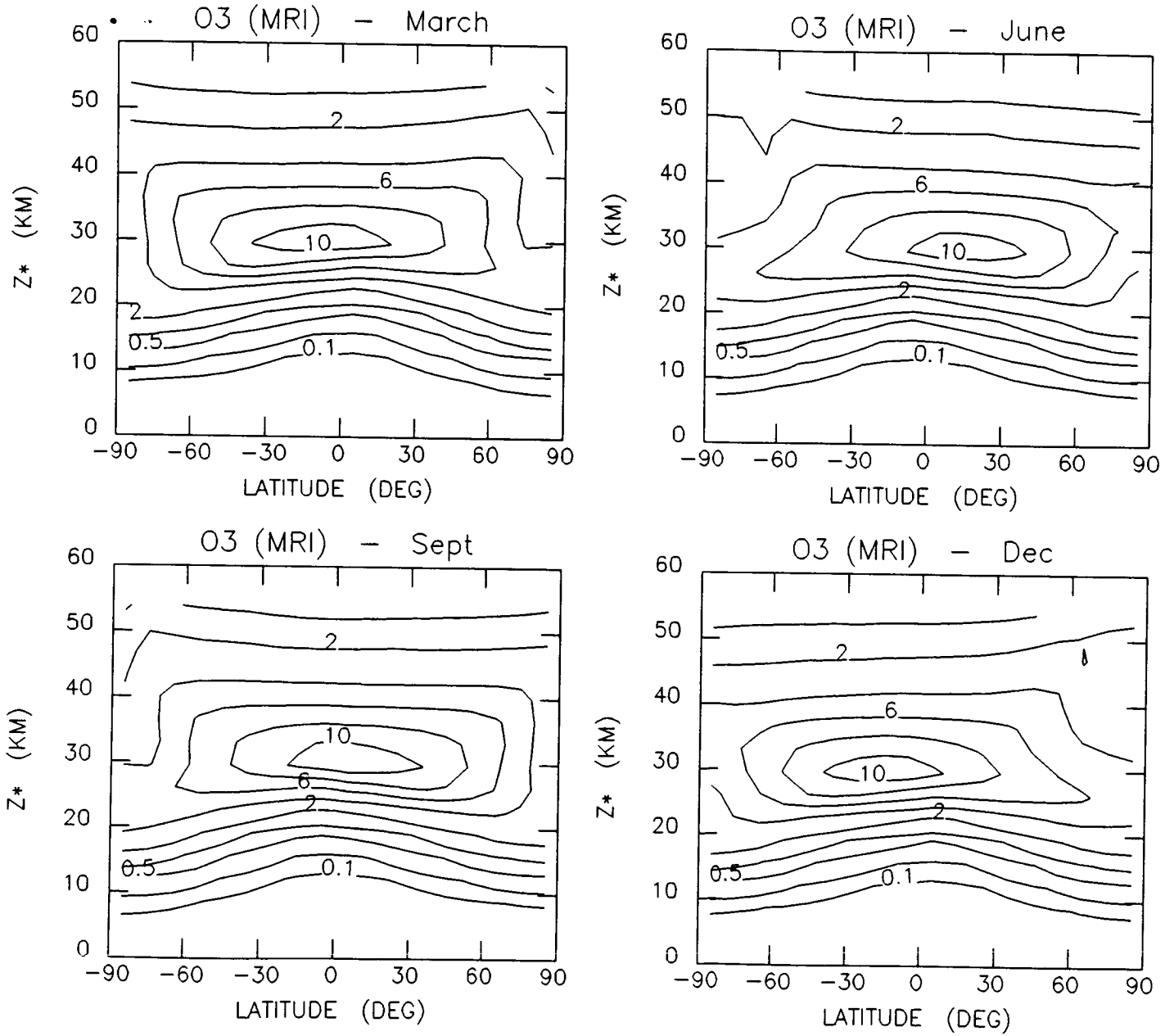
O3 (MRI) – March
O3 (MRI) – June
O3 (MRI) – Sept
O3 (MRI) – Dec
Z* (KM)
LATITUDE (DEG)
60
50
40
30
20
10
0
-90 -60 -30 0 30 60 90
2
6
10
0.5
0.1

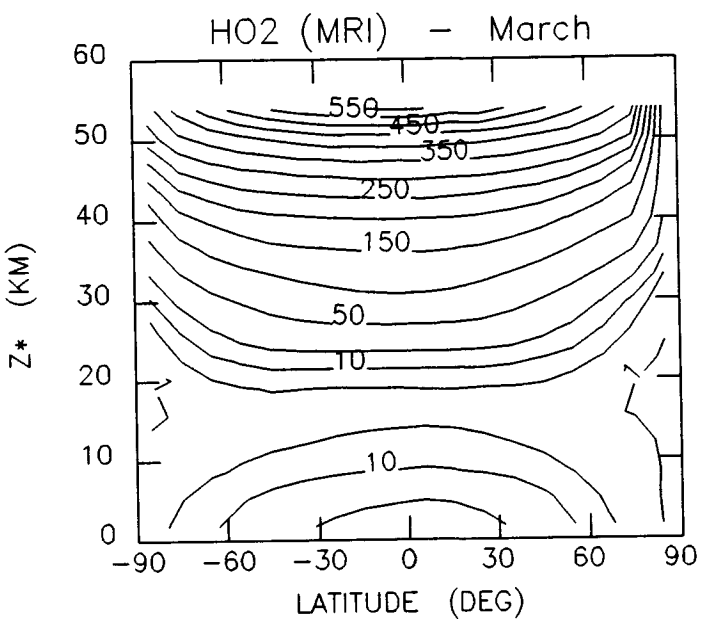
HO2 (MRI) - March
Z* (KM)
LATITUDE (DEG)
550
450
350
250
150
50
10
1

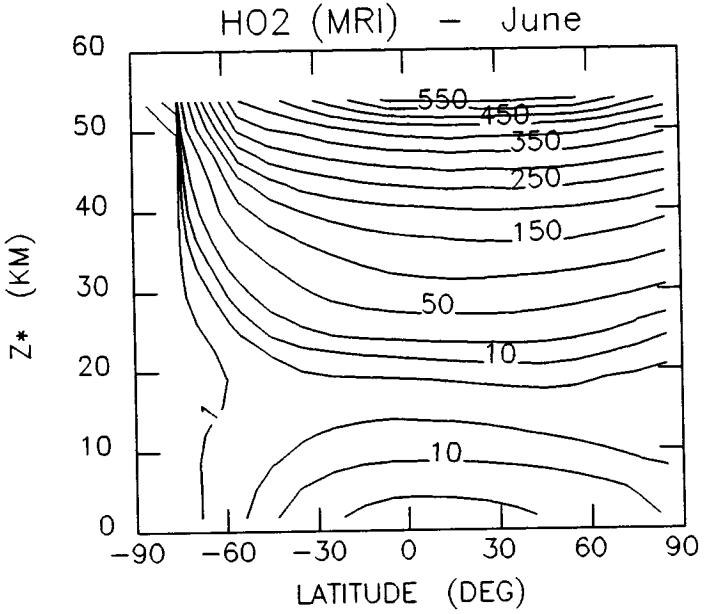
HO2 (MRI) - June
Z* (KM)
LATITUDE (DEG)
550
450
350
250
150
50
10
1

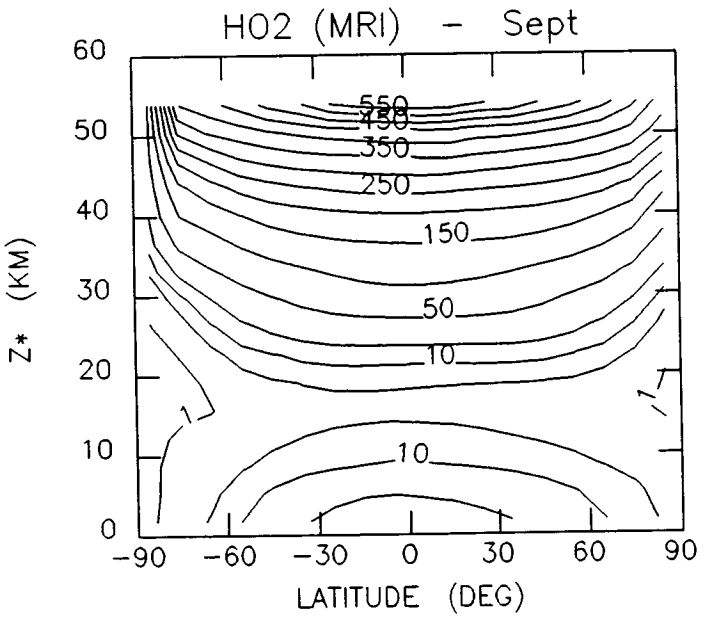
HO2 (MRI) - Sept
Z* (KM)
LATITUDE (DEG)
550
450
350
250
150
50
10
1

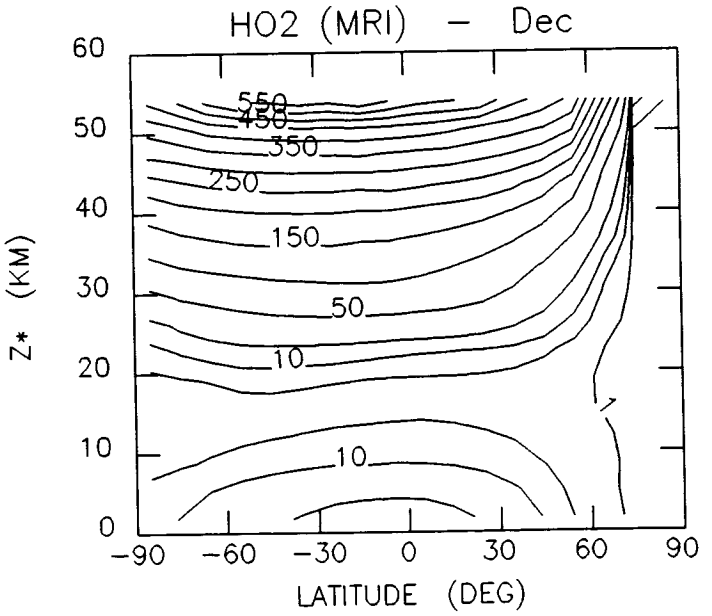
HO2 (MRI) - Dec
Z* (KM)
LATITUDE (DEG)
550
450
350
250
150
50
10
1

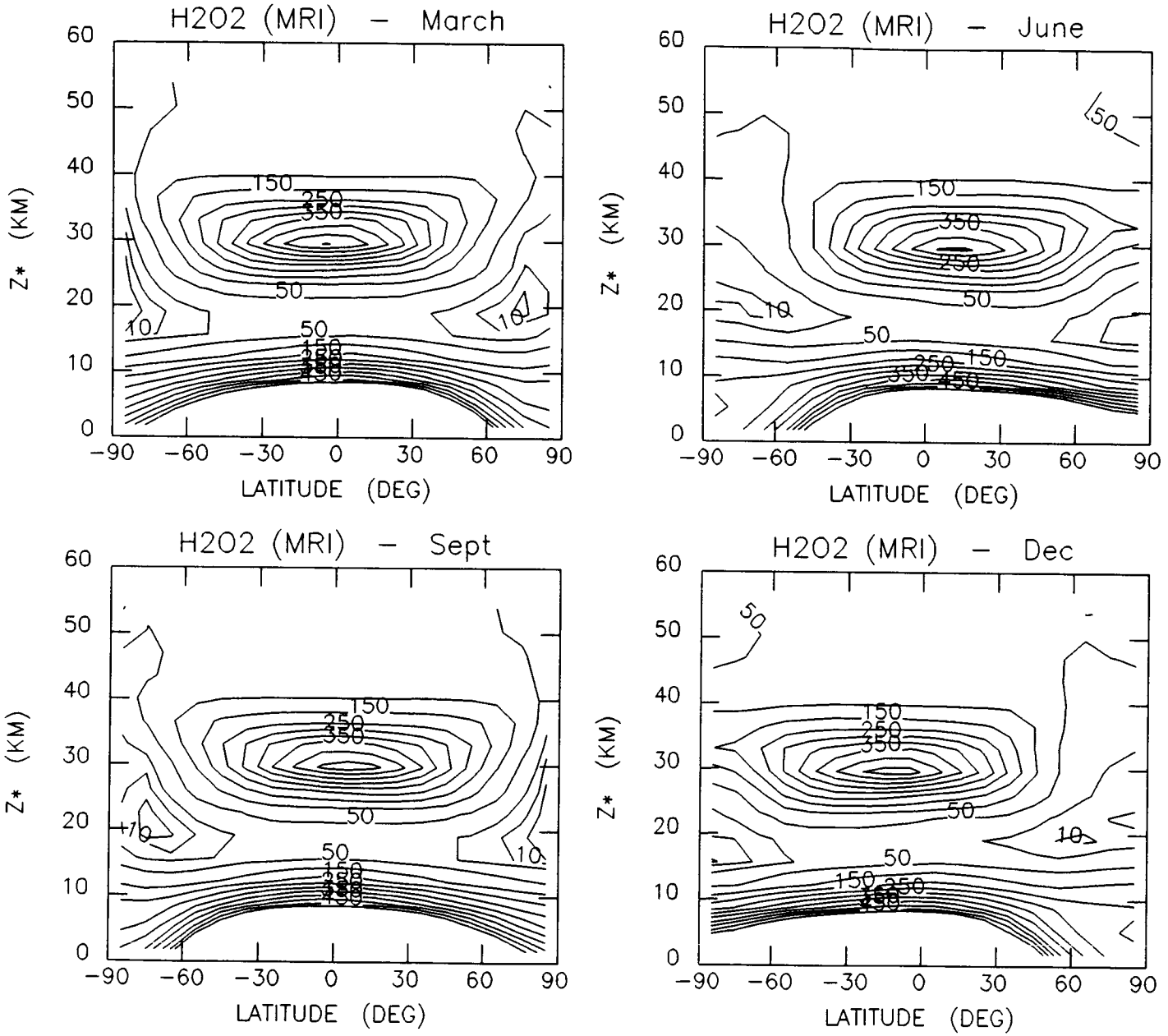
H2O2 (MRI) – March
H2O2 (MRI) – June
H2O2 (MRI) – Sept
H2O2 (MRI) – Dec
Z* (KM)
LATITUDE (DEG)
60
50
40
30
20
10
0
-90 -60 -30 0 30 60 90
150
250
350
50
10

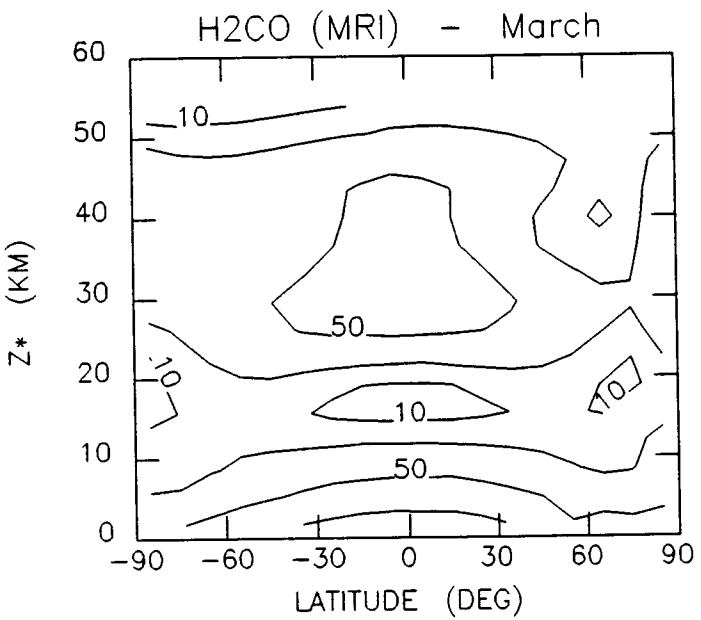
H2CO (MRI) – March
Z* (KM)
LATITUDE (DEG)
10
50

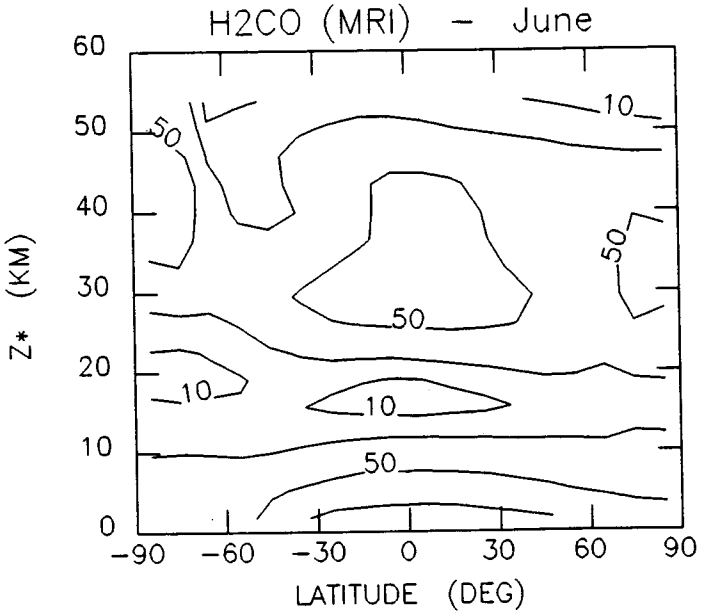
H2CO (MRI) – June
Z* (KM)
LATITUDE (DEG)
10
50

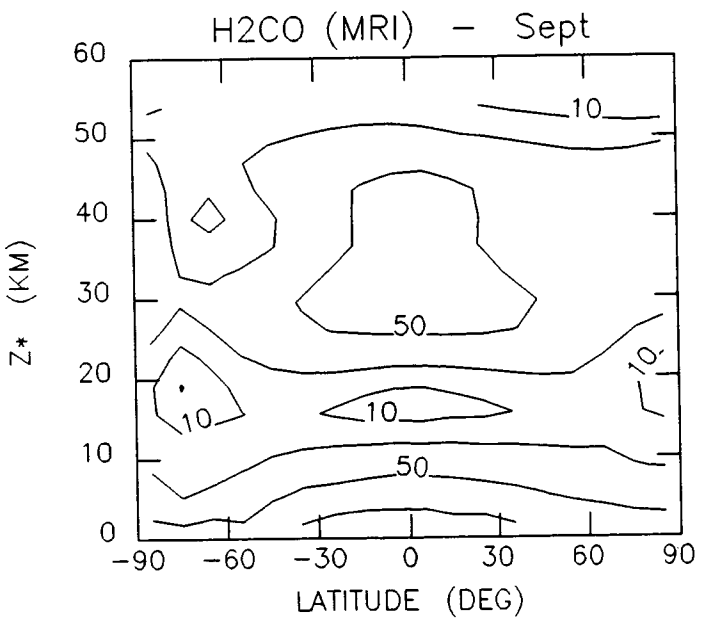
H2CO (MRI) – Sept
Z* (KM)
LATITUDE (DEG)
10
50

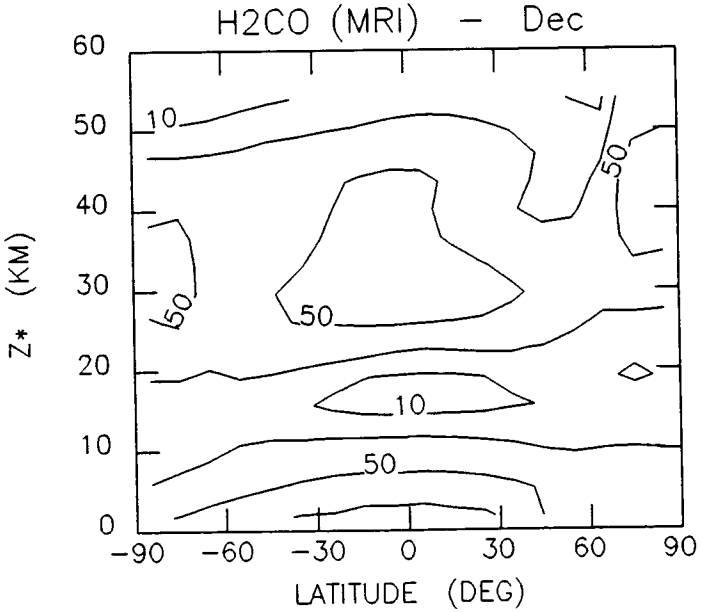
H2CO (MRI) – Dec
Z* (KM)
LATITUDE (DEG)
10
50
60

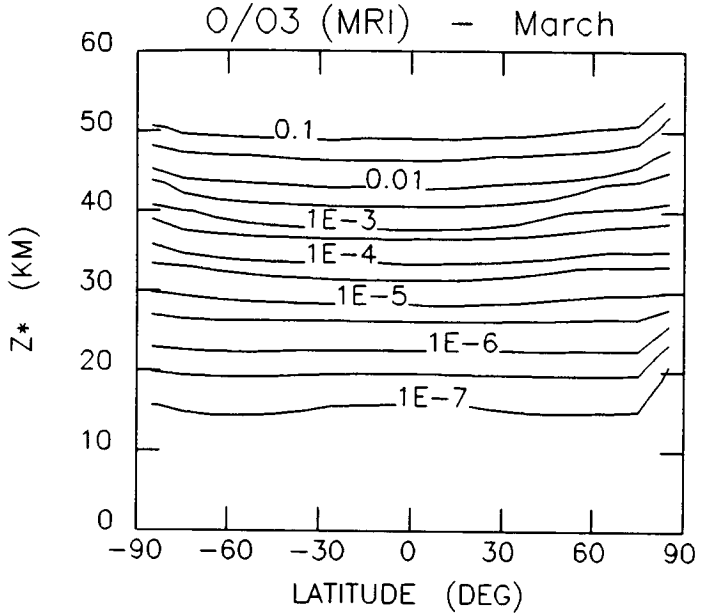
O/O3 (MRI) – March
Z* (KM)
LATITUDE (DEG)
0.1
0.01
1E-3
1E-4
1E-5
1E-6
1E-7

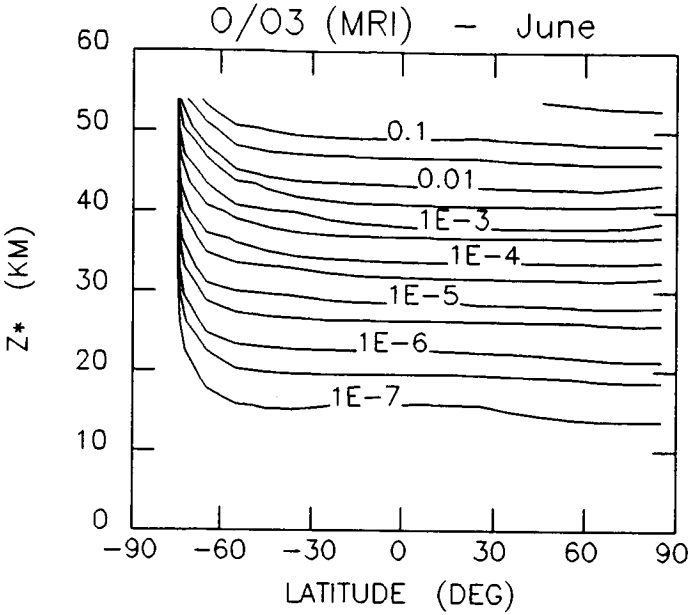
O/O3 (MRI) – June
Z* (KM)
LATITUDE (DEG)
0.1
0.01
1E-3
1E-4
1E-5
1E-6
1E-7

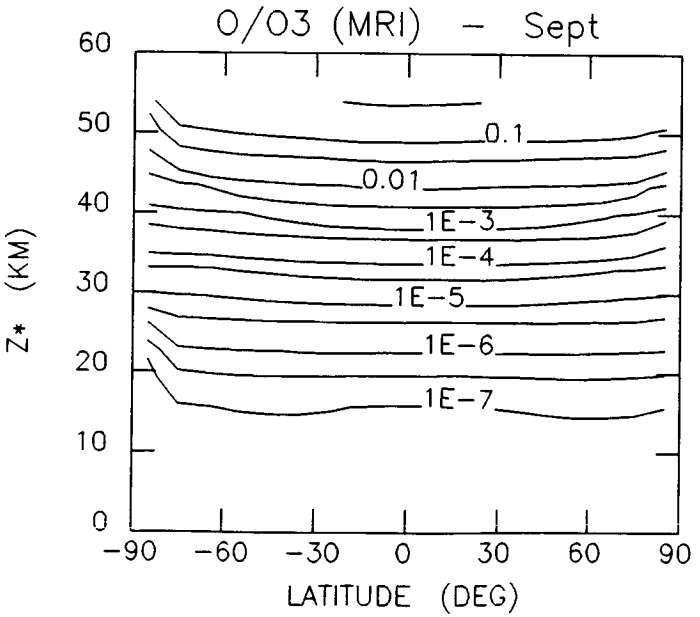
O/O3 (MRI) – Sept
Z* (KM)
LATITUDE (DEG)
0.1
0.01
1E-3
1E-4
1E-5
1E-6
1E-7

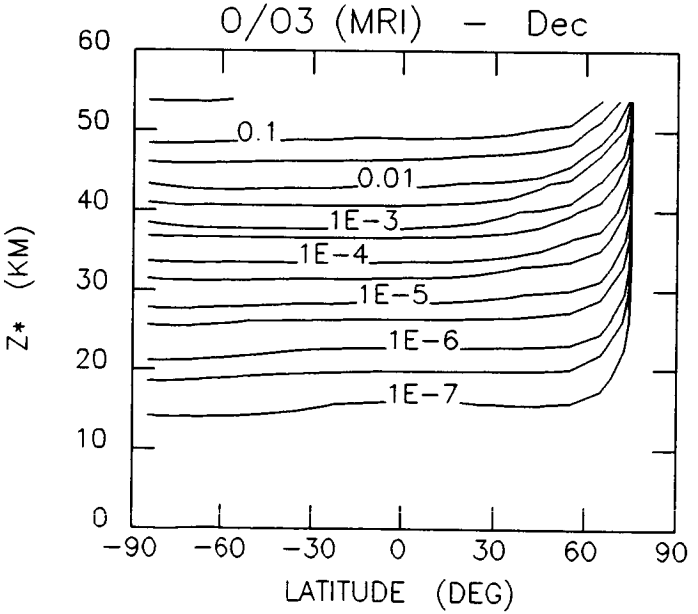
O/O3 (MRI) – Dec
Z* (KM)
LATITUDE (DEG)
0.1
0.01
1E-3
1E-4
1E-5
1E-6
1E-7

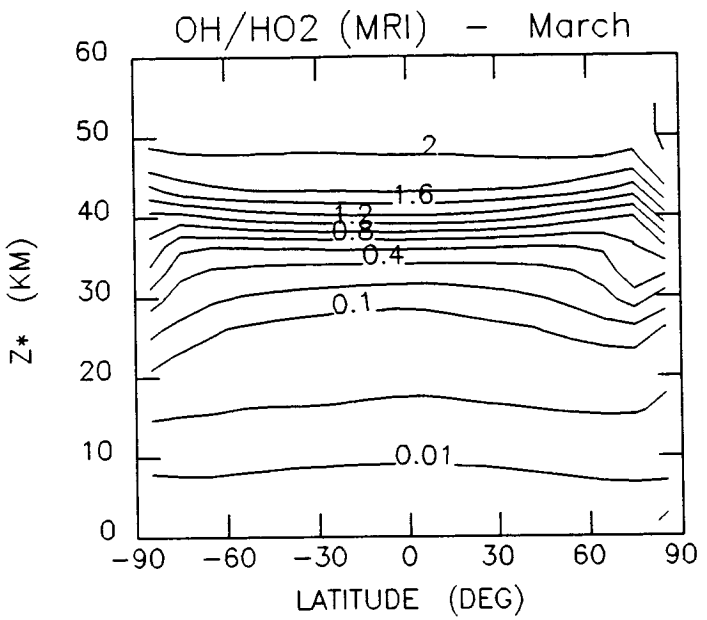
OH/HO2 (MRI) – March
Z* (KM)
LATITUDE (DEG)
2
1.6
1.2
0.8
0.4
0.1
0.01

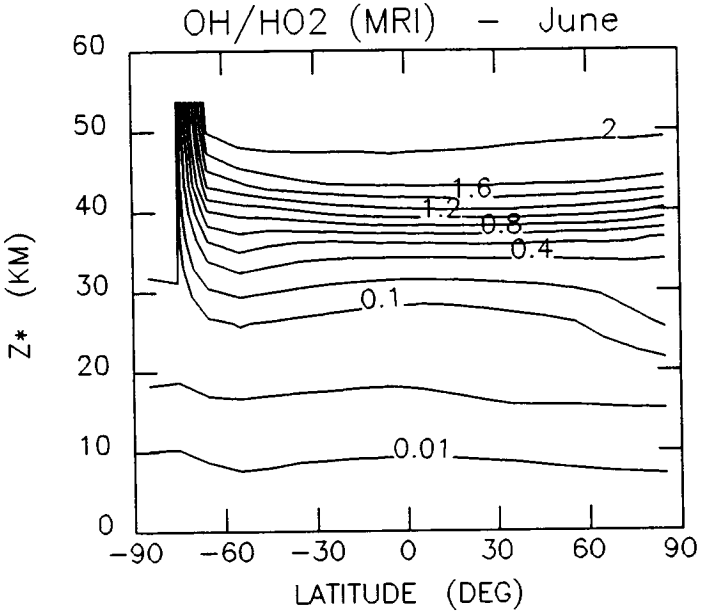
OH/HO2 (MRI) – June
Z* (KM)
LATITUDE (DEG)
2
1.6
1.2
0.8
0.4
0.1
0.01

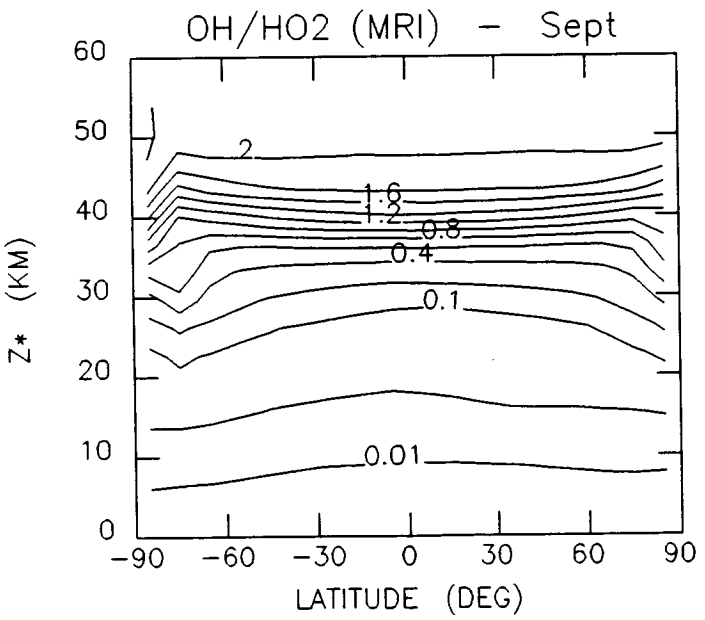
OH/HO2 (MRI) – Sept
Z* (KM)
LATITUDE (DEG)
2
1.6
1.2
0.8
0.4
0.1
0.01

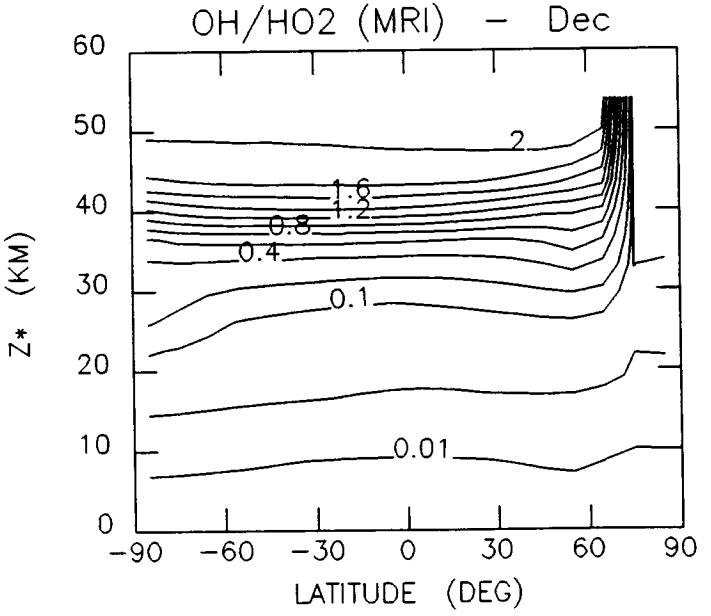
OH/HO2 (MRI) – Dec
Z* (KM)
LATITUDE (DEG)
2
1.6
1.2
0.8
0.4
0.1
0.01

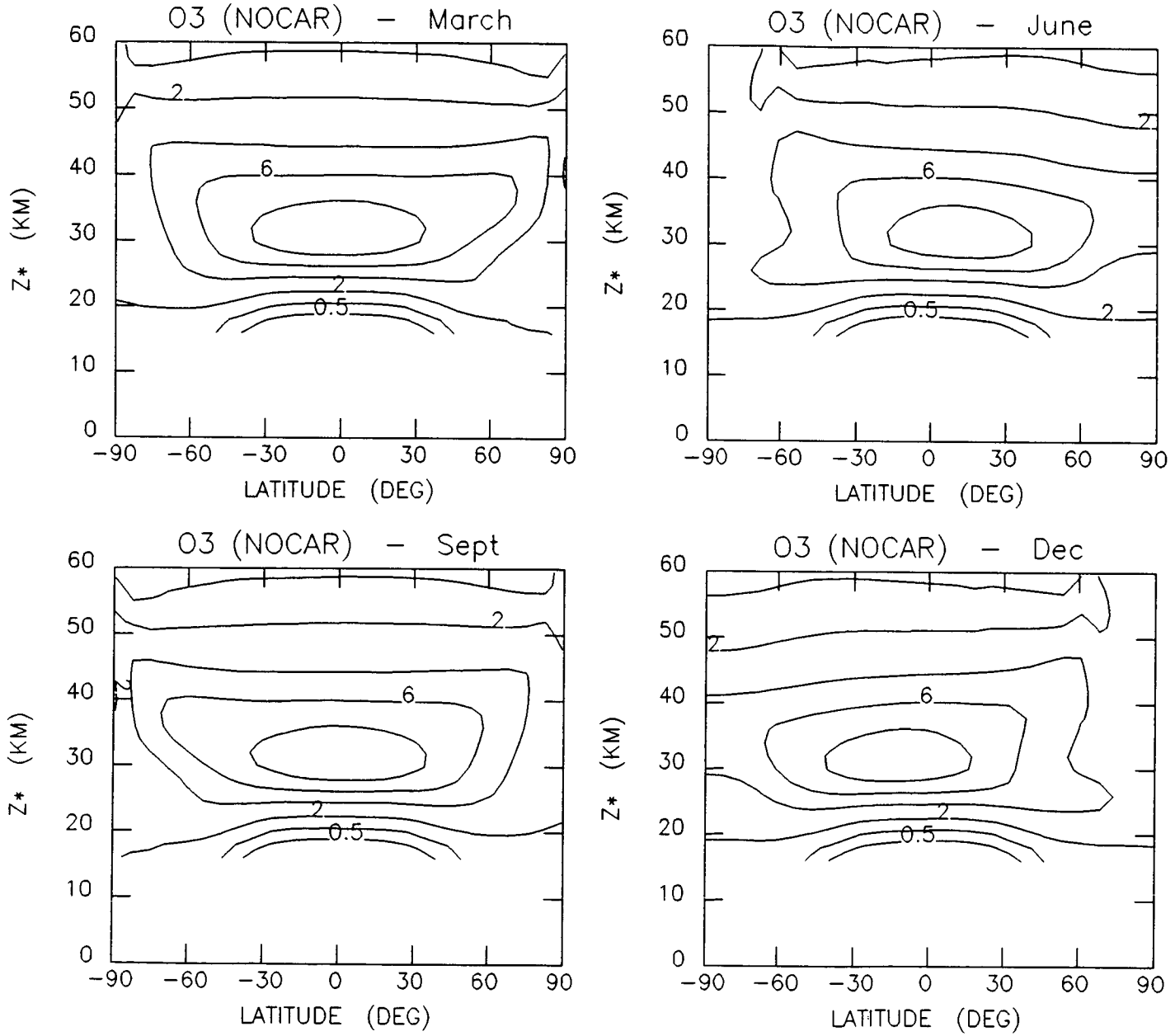
O3 (NOCAR) – March
O3 (NOCAR) – June
O3 (NOCAR) – Sept
O3 (NOCAR) – Dec
Z* (KM)
LATITUDE (DEG)
0
10
20
30
40
50
60
−90
−60
−30
0
30
60
90
2
6
0.5

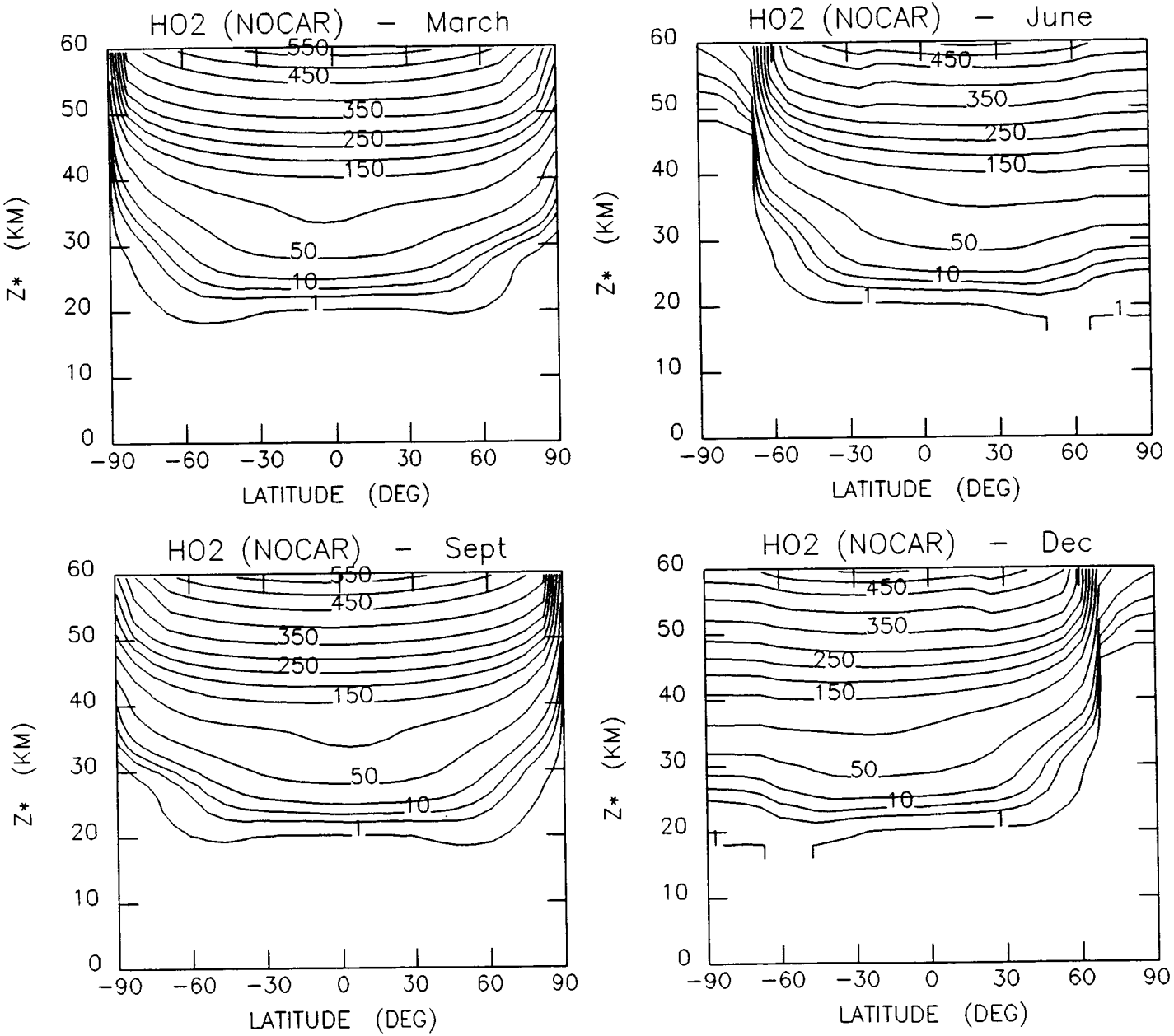
HO2 (NOCAR) – March
HO2 (NOCAR) – June
HO2 (NOCAR) – Sept
HO2 (NOCAR) – Dec
Z* (KM)
LATITUDE (DEG)
550
450
350
250
150
50
10
1
0
10
20
30
40
50
60
-90
-60
-30
0
30
60
90

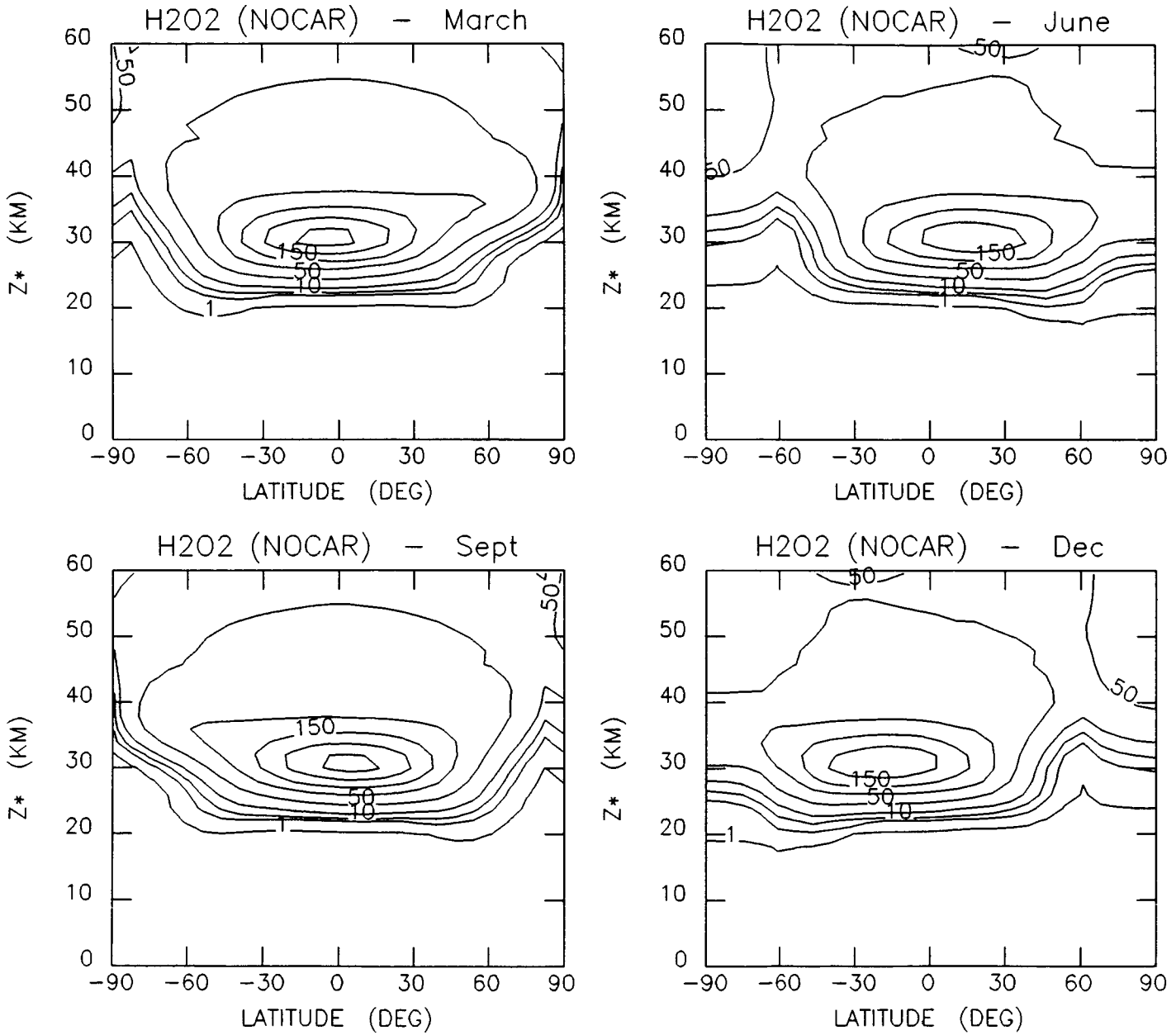
H2O2 (NOCAR) – March
H2O2 (NOCAR) – June
H2O2 (NOCAR) – Sept
H2O2 (NOCAR) – Dec
Z* (KM)
LATITUDE (DEG)
0
10
20
30
40
50
60
−90
−60
−30
0
30
60
90
150
50
10
1

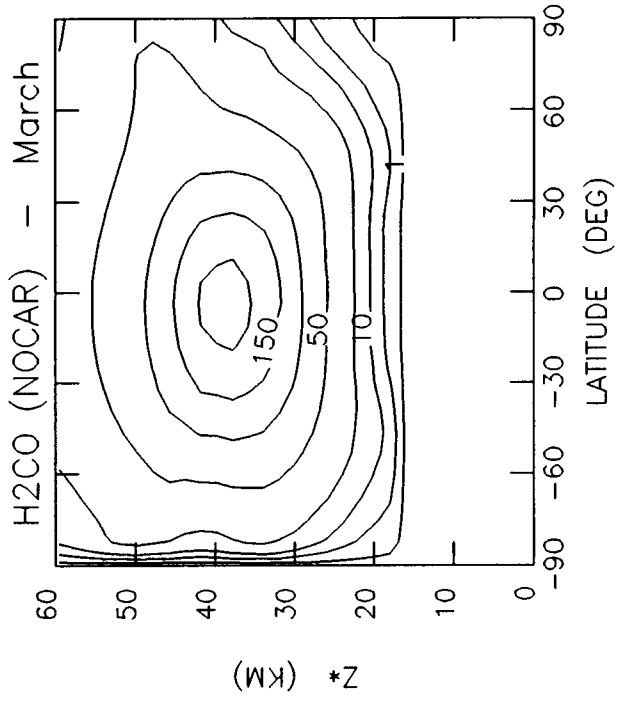
H2CO (NOCAR) – March
150
50
10
1
Z* (KM)
60
50
40
30
20
10
0
-90
-60
-30
0
30
60
90
LATITUDE (DEG)

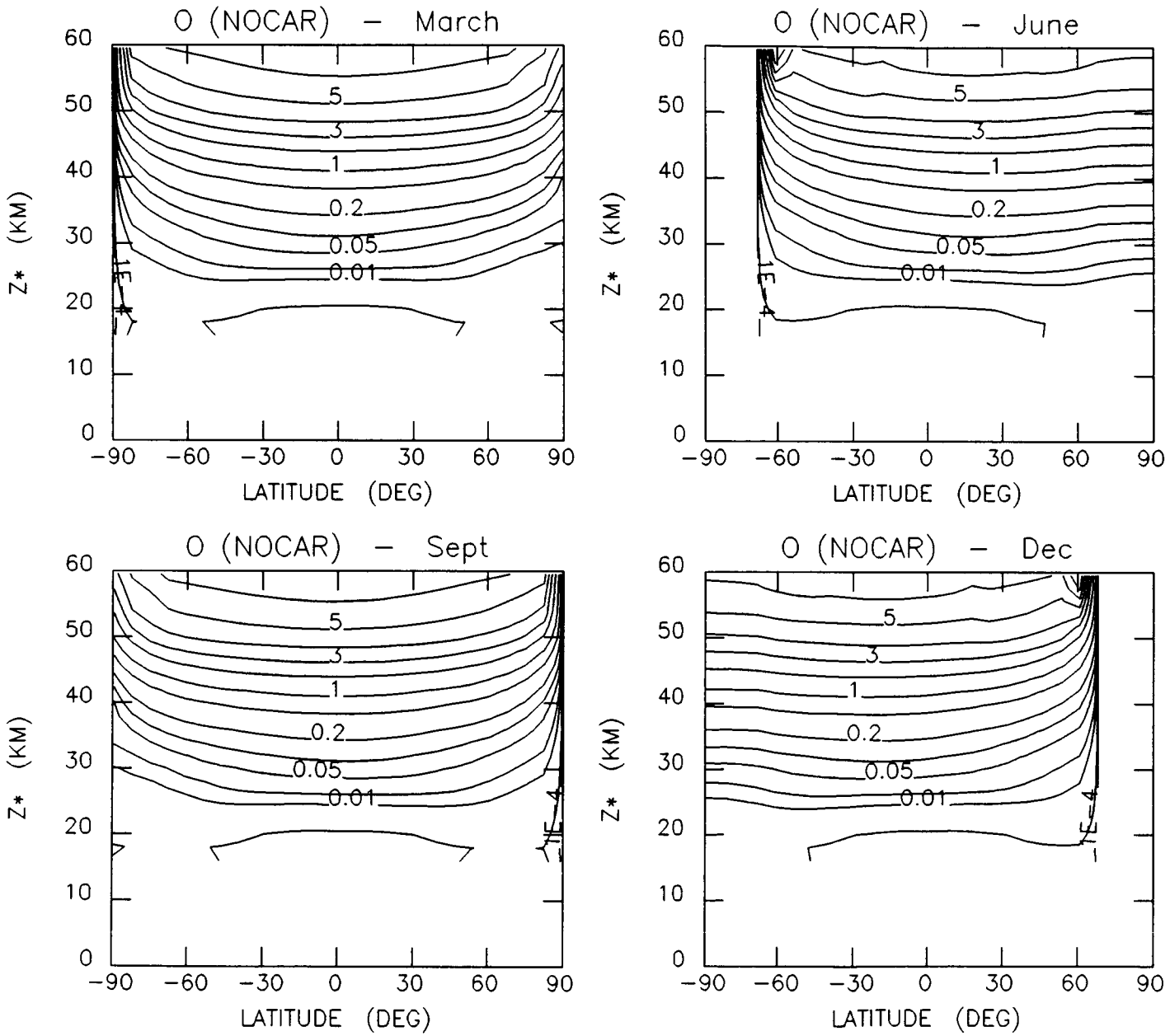
O (NOCAR) – March
O (NOCAR) – June
O (NOCAR) – Sept
O (NOCAR) – Dec
Z* (KM)
LATITUDE (DEG)
5
3
1
0.2
0.05
0.01
1E-4
0
10
20
30
40
50
60
−90
−60
−30
0
30
60
90

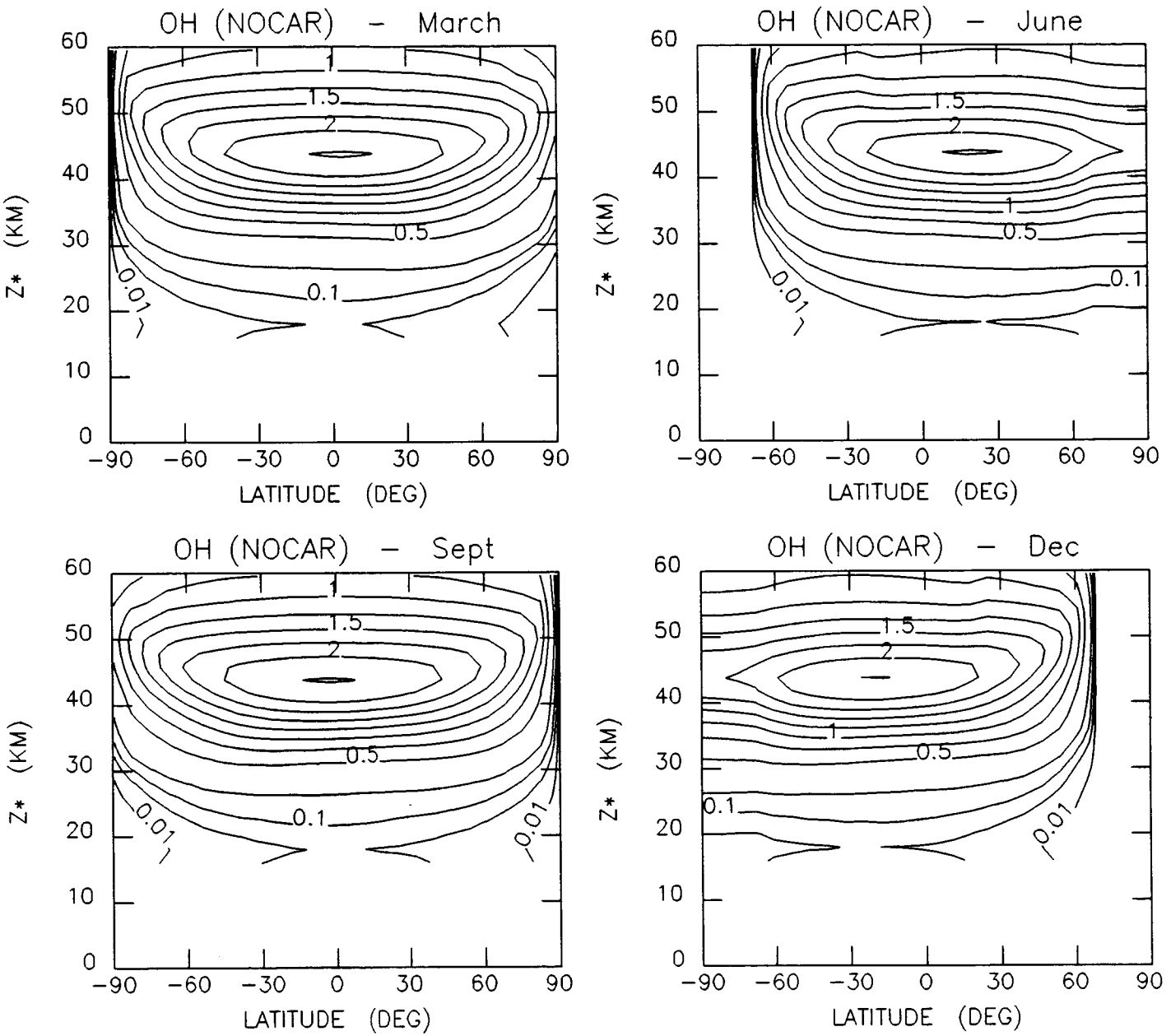
OH (NOCAR) – March
OH (NOCAR) – June
OH (NOCAR) – Sept
OH (NOCAR) – Dec
Z* (KM)
LATITUDE (DEG)
0
10
20
30
40
50
60
−90
−60
−30
0
30
60
90
1
1.5
2
0.5
0.1
0.01

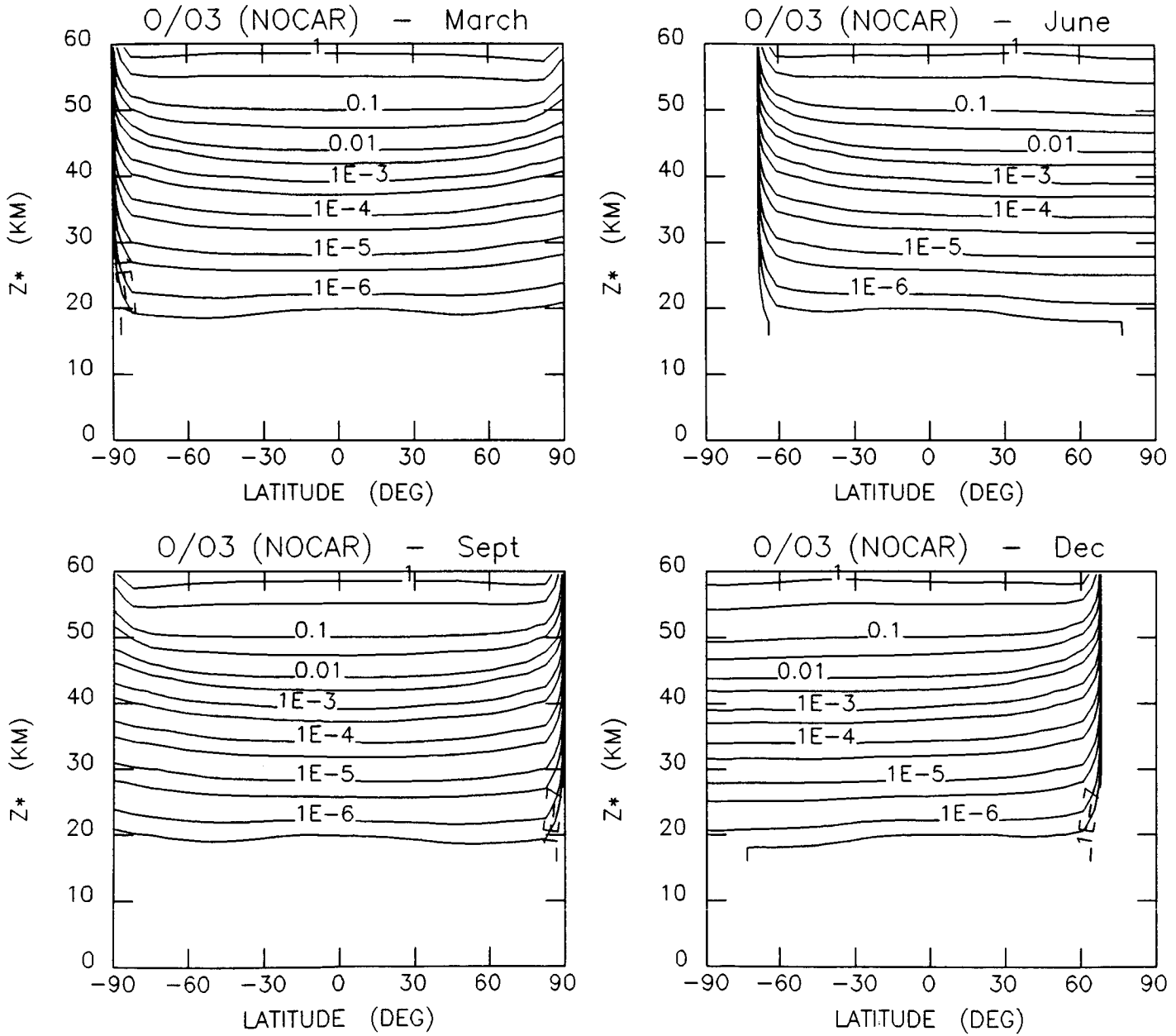
O/O3 (NOCAR) – March
O/O3 (NOCAR) – June
O/O3 (NOCAR) – Sept
O/O3 (NOCAR) – Dec
Z* (KM)
LATITUDE (DEG)
60
50
40
30
20
10
0
−90 −60 −30 0 30 60 90
1
0.1
0.01
1E−3
1E−4
1E−5
1E−6

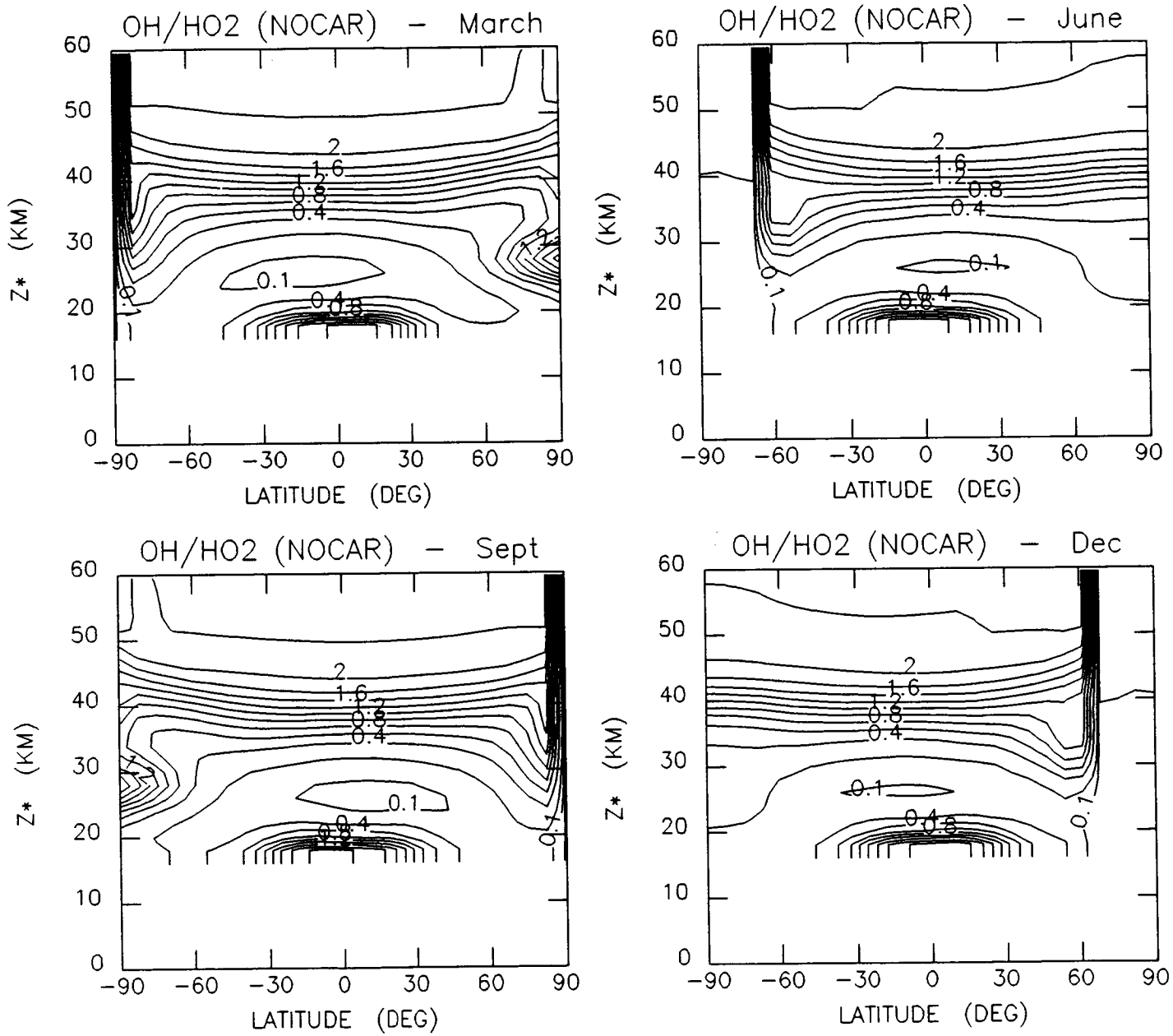
OH/HO2 (NOCAR) – March
OH/HO2 (NOCAR) – June
OH/HO2 (NOCAR) – Sept
OH/HO2 (NOCAR) – Dec
Z* (KM)
LATITUDE (DEG)
0
10
20
30
40
50
60
-90
-60
-30
0
30
60
90
2
1.6
1.2
0.8
0.4
0.1

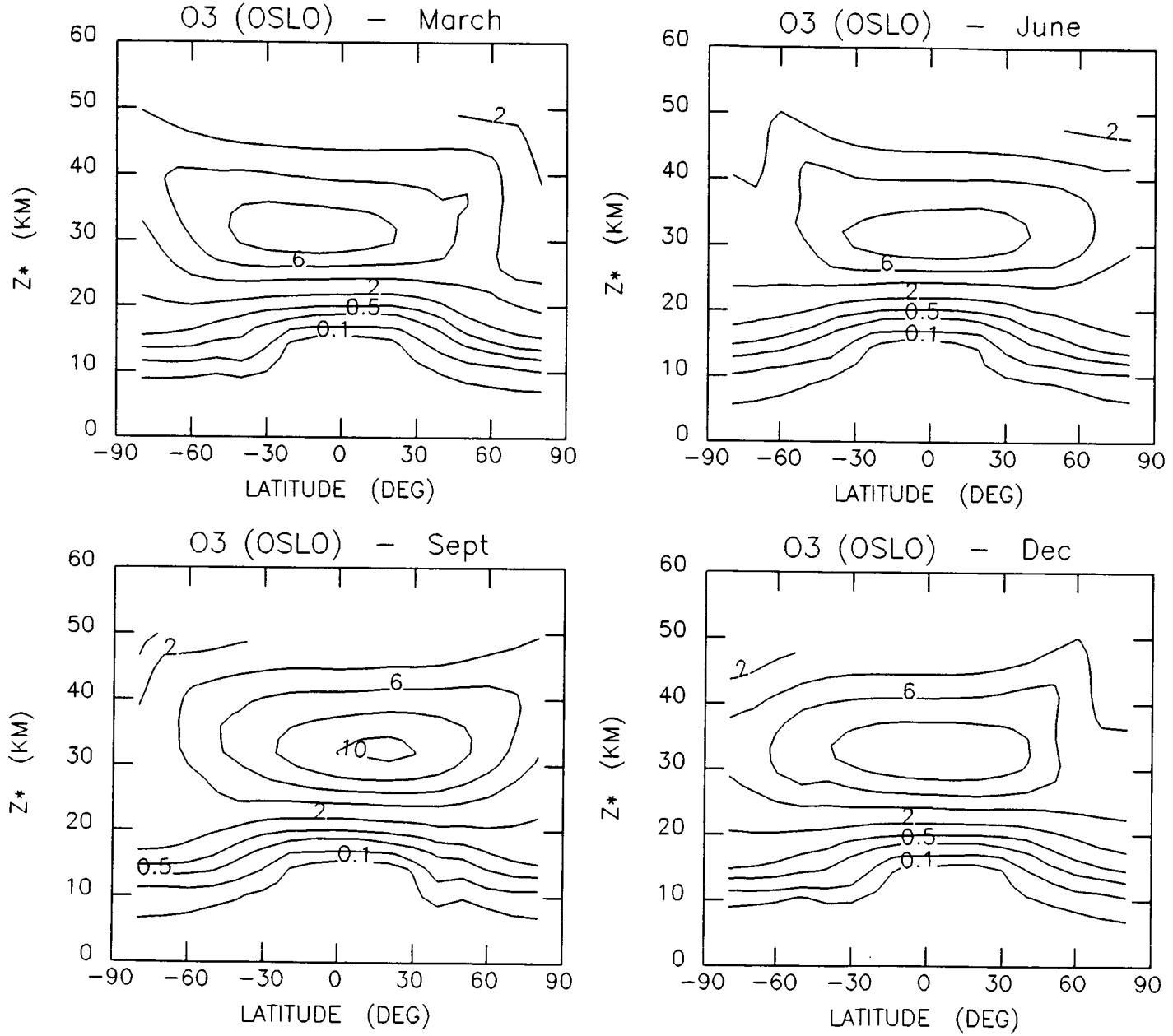
O3 (OSLO) – March
O3 (OSLO) – June
O3 (OSLO) – Sept
O3 (OSLO) – Dec
Z* (KM)
LATITUDE (DEG)
60
50
40
30
20
10
0
-90
-60
-30
0
30
60
90
2
6
10
0.5
0.1

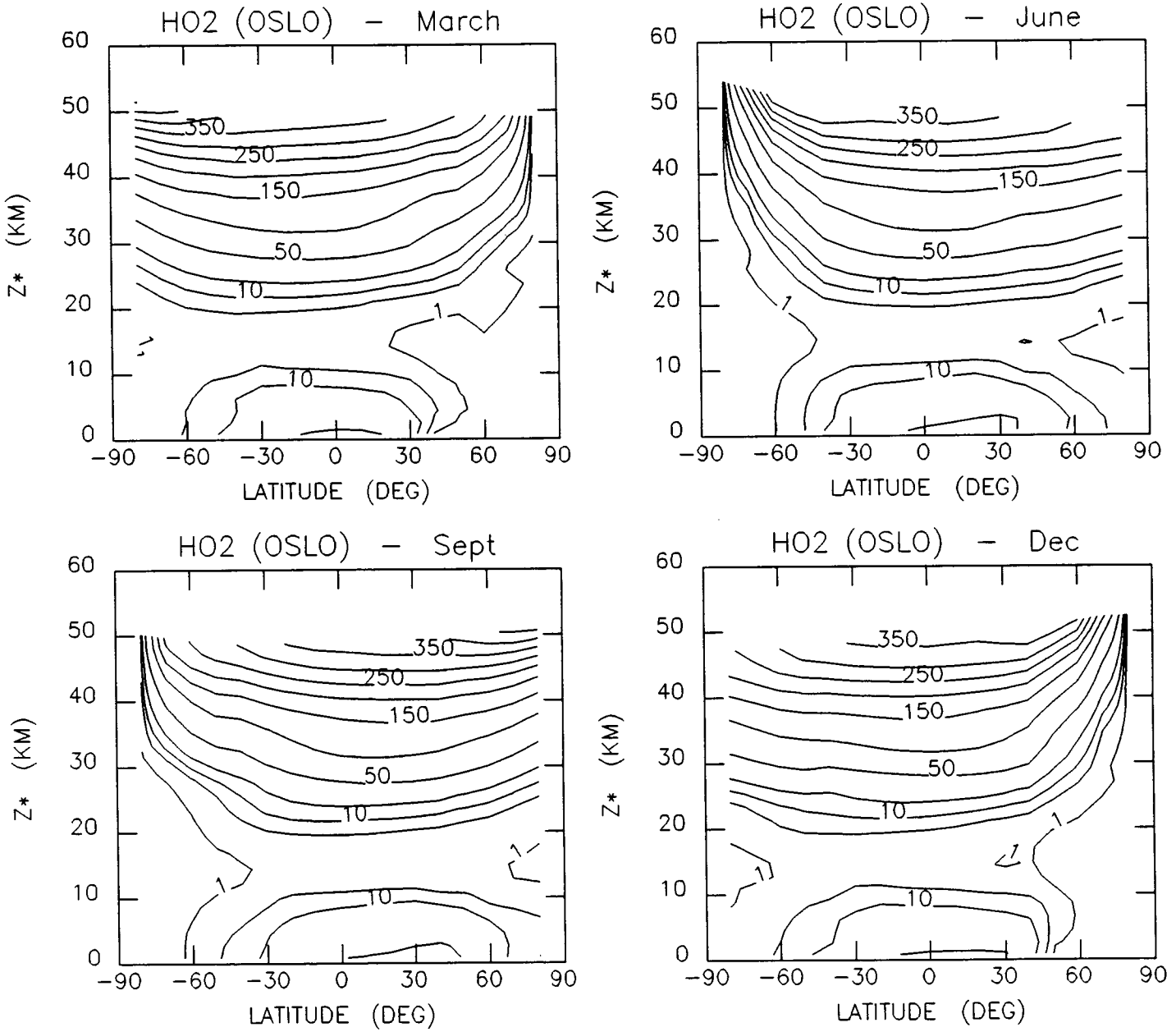
HO2 (OSLO) – March
HO2 (OSLO) – June
HO2 (OSLO) – Sept
HO2 (OSLO) – Dec
Z* (KM)
LATITUDE (DEG)
0
10
20
30
40
50
60
-90
-60
-30
0
30
60
90
350
250
150
50
10
1

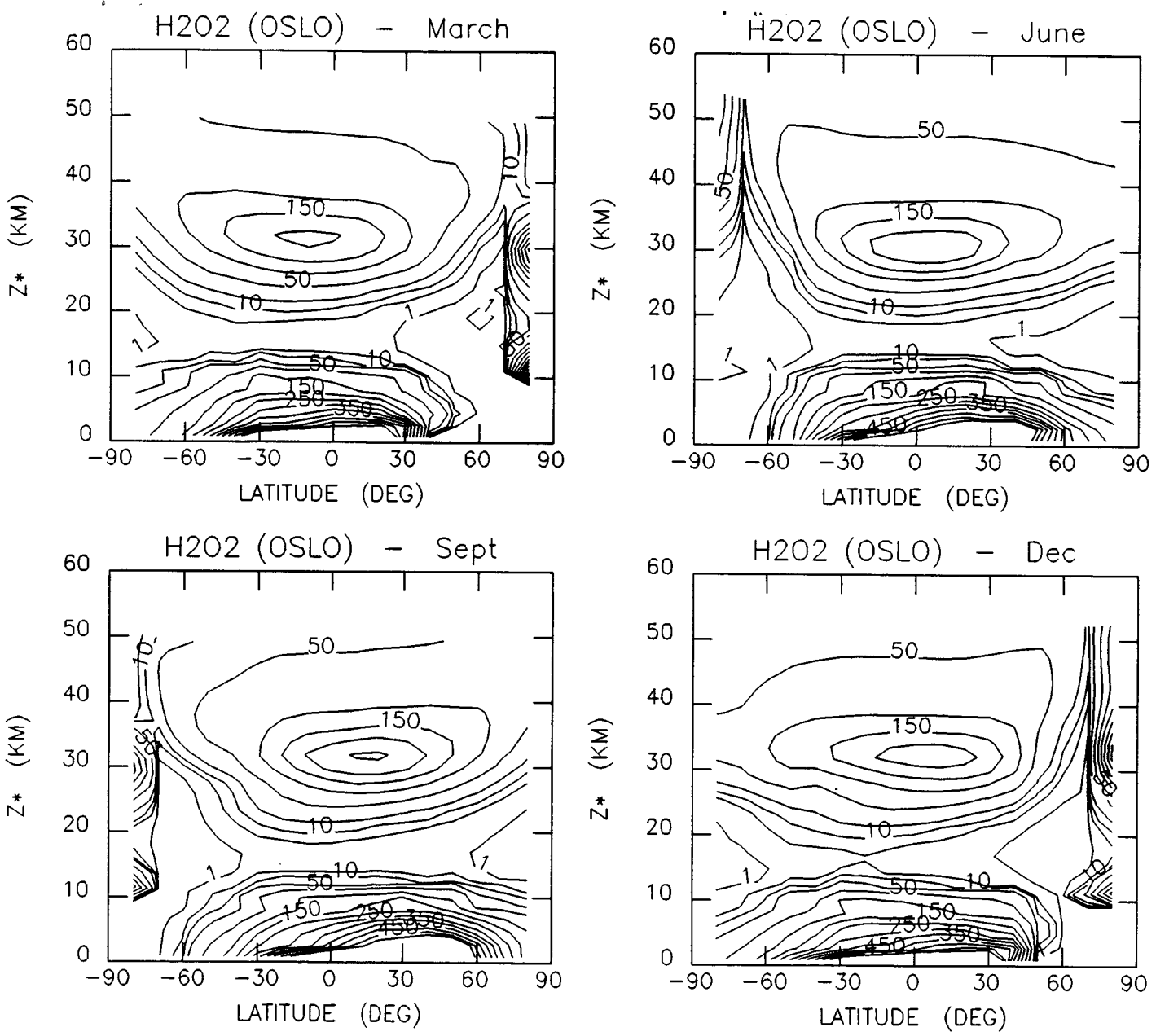
H202 (OSLO) – March
H202 (OSLO) – June
H202 (OSLO) – Sept
H202 (OSLO) – Dec
Z* (KM)
LATITUDE (DEG)
0
10
20
30
40
50
60
-90
-60
-30
0
30
60
90
1
10
50
150
250
350
450

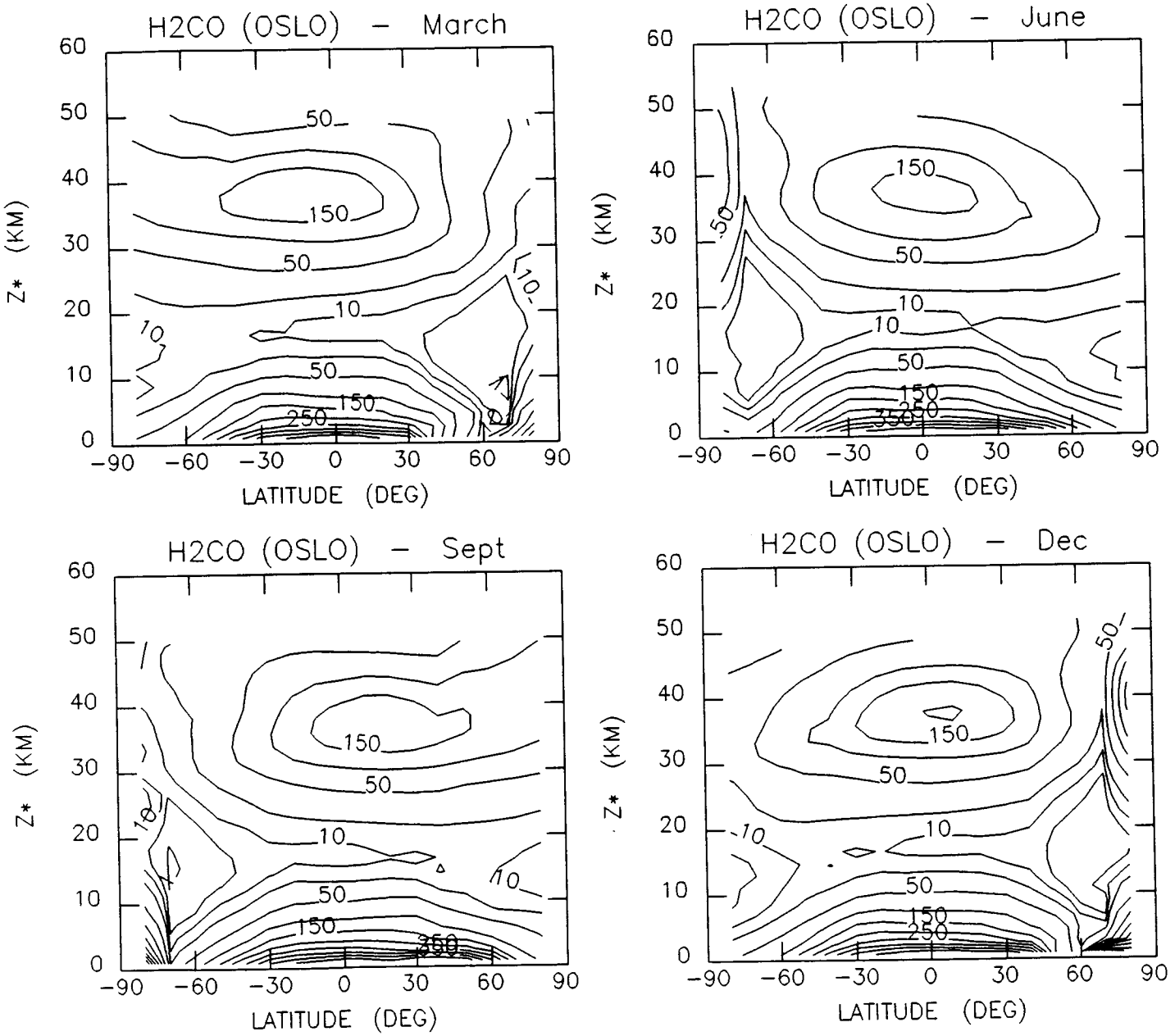
H2CO (OSLO) – March
H2CO (OSLO) – June
H2CO (OSLO) – Sept
H2CO (OSLO) – Dec
Z* (KM)
LATITUDE (DEG)
0
10
20
30
40
50
60
-90
-60
-30
0
30
60
90
10
50
150
250
350

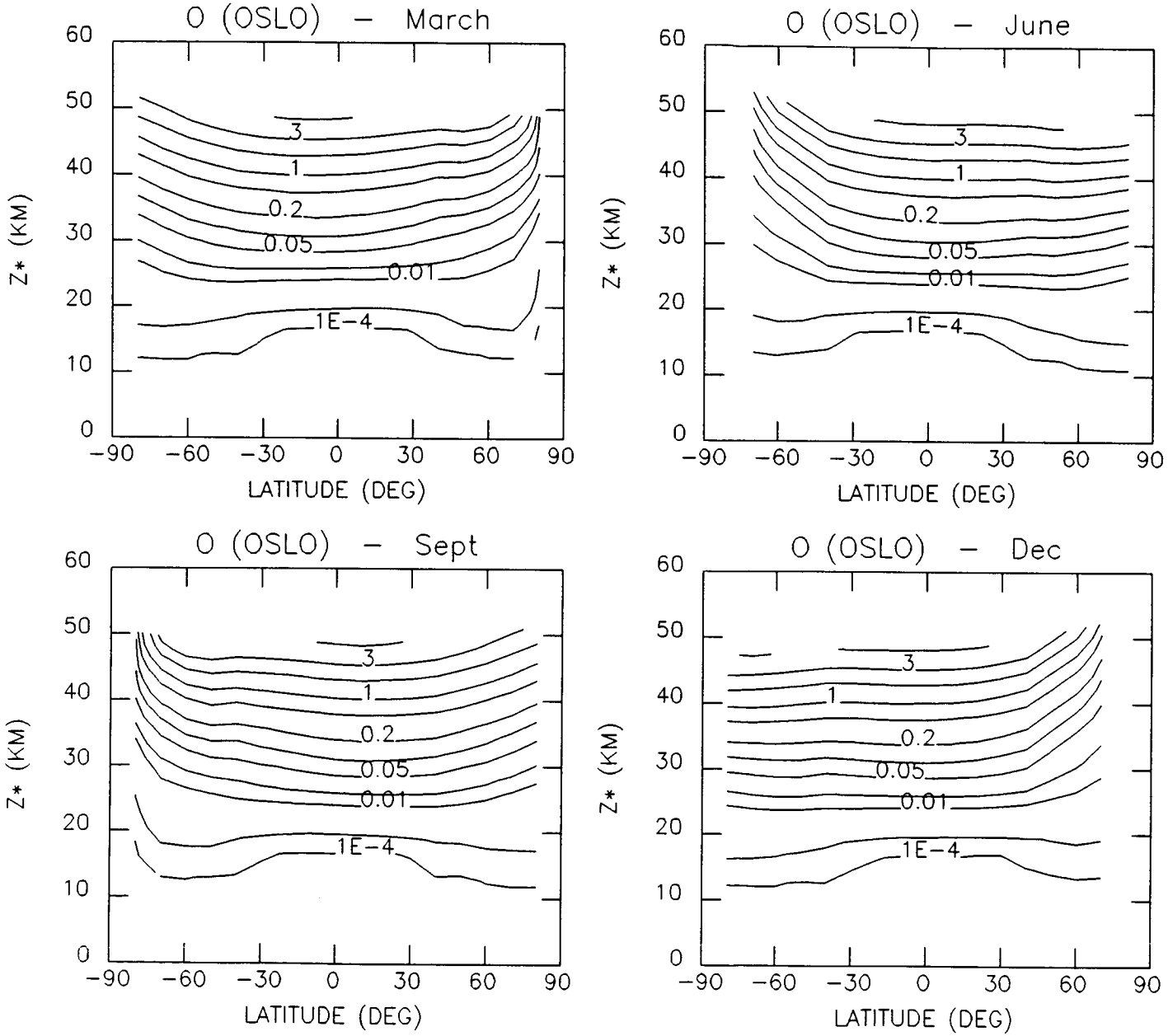
O (OSLO) – March
O (OSLO) – June
O (OSLO) – Sept
O (OSLO) – Dec
Z* (KM)
LATITUDE (DEG)
60
50
40
30
20
10
0
−90 −60 −30 0 30 60 90
3
1
0.2
0.05
0.01
1E−4

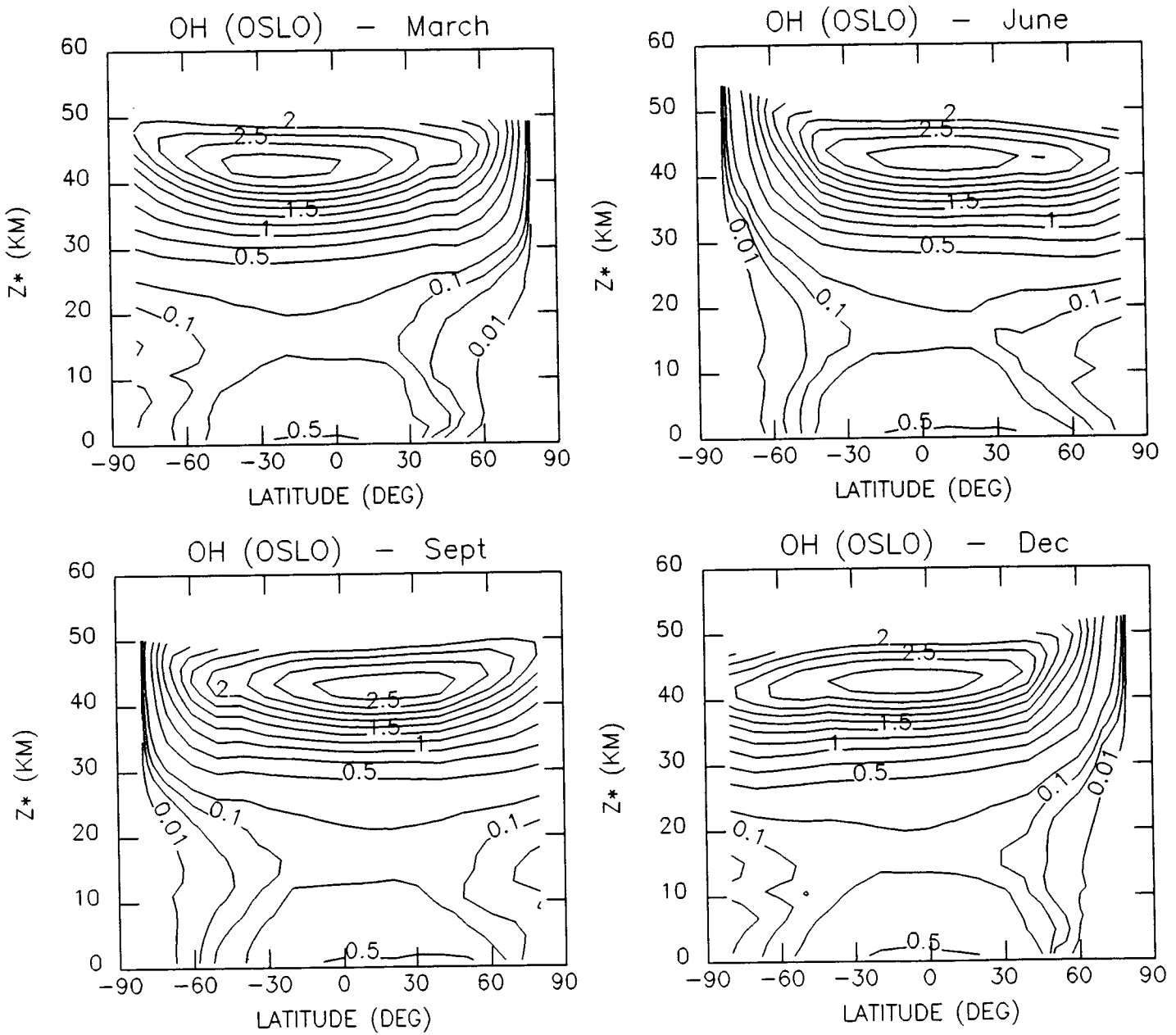
OH (OSLO) – March
OH (OSLO) – June
OH (OSLO) – Sept
OH (OSLO) – Dec
Z* (KM)
LATITUDE (DEG)
0
10
20
30
40
50
60
-90
-60
-30
0
30
60
90
2
2.5
1.5
1
0.5
0.1
0.01

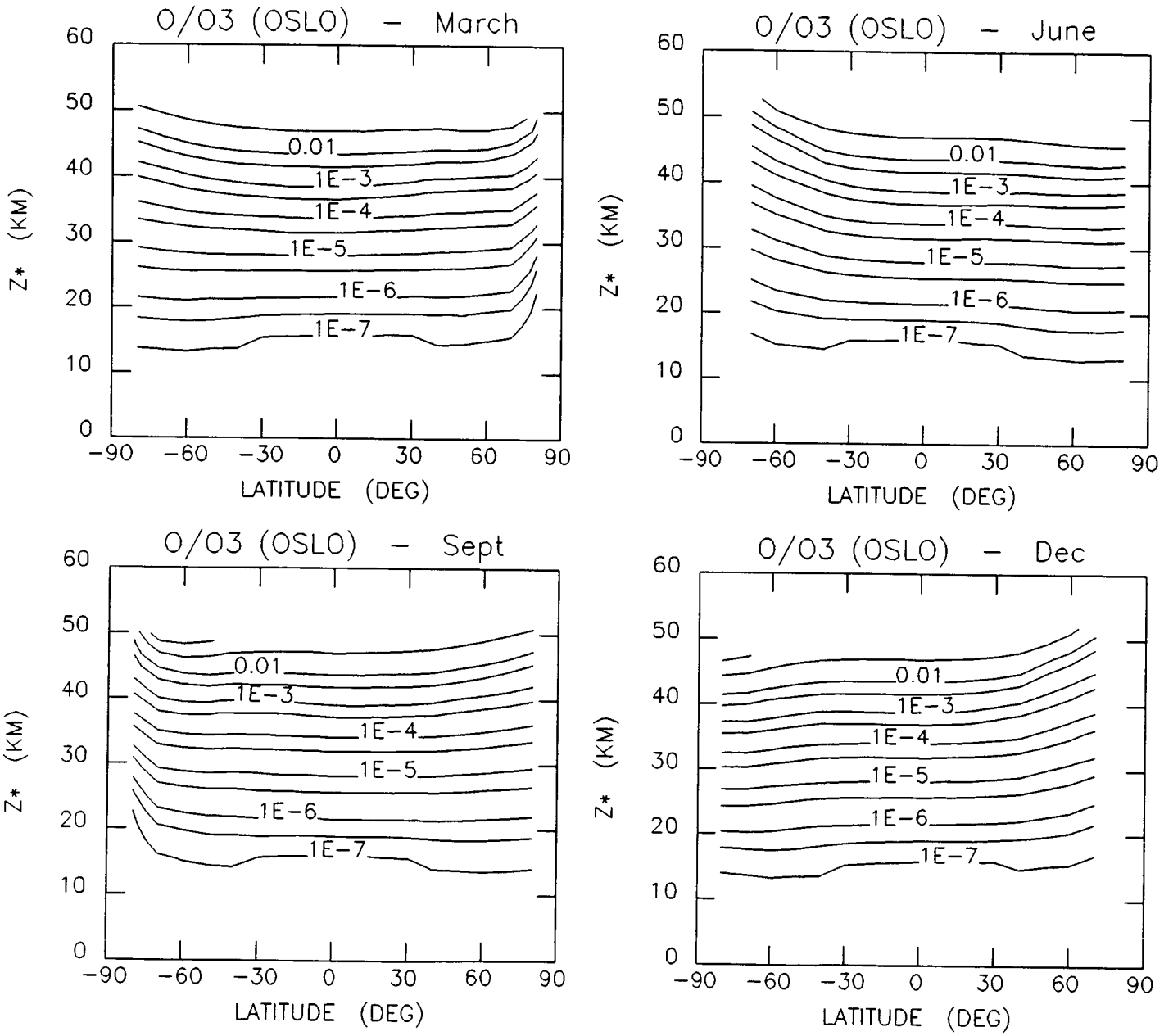
O/O3 (OSLO) – March
O/O3 (OSLO) – June
O/O3 (OSLO) – Sept
O/O3 (OSLO) – Dec
Z* (KM)
LATITUDE (DEG)
0.01
1E-3
1E-4
1E-5
1E-6
1E-7
0
10
20
30
40
50
60
-90
-60
-30
0
30
60
90

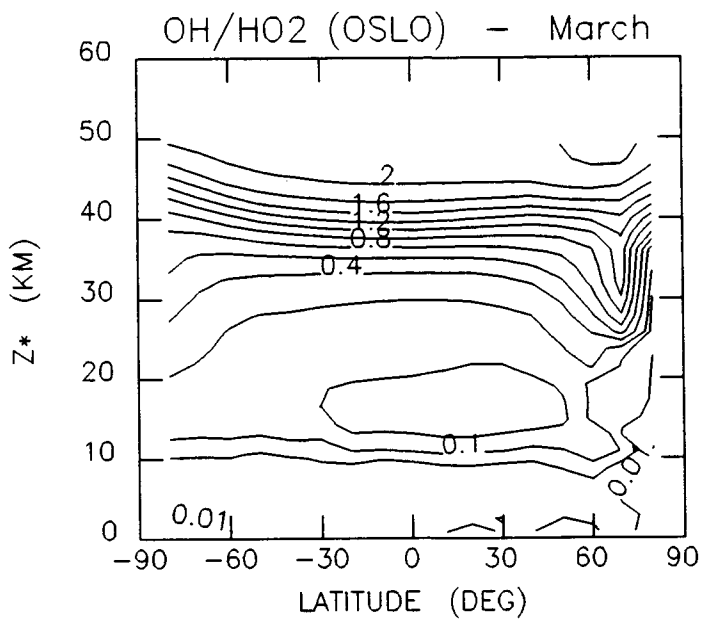
OH/HO2 (OSLO) – March
Z* (KM)
LATITUDE (DEG)
2
1.6
1.2
0.8
0.4
0.1
0.01
1

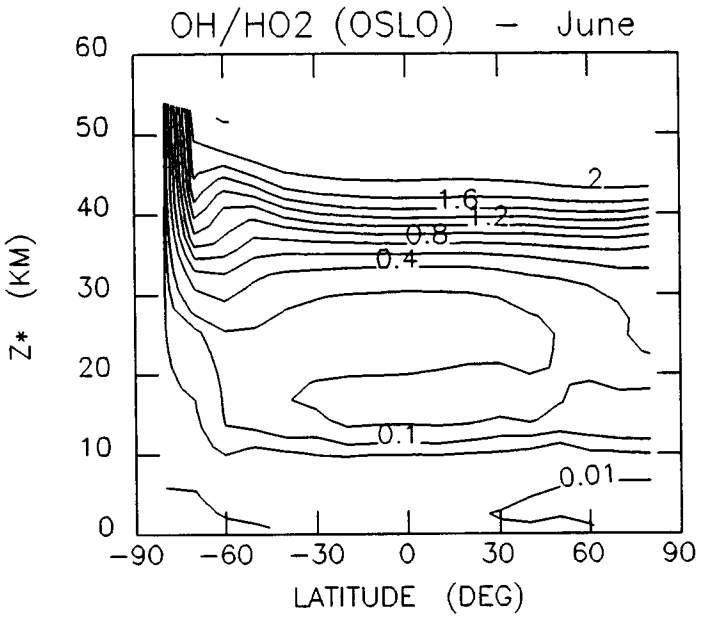
OH/HO2 (OSLO) – June
Z* (KM)
LATITUDE (DEG)
2
1.6
1.2
0.8
0.4
0.1
0.01

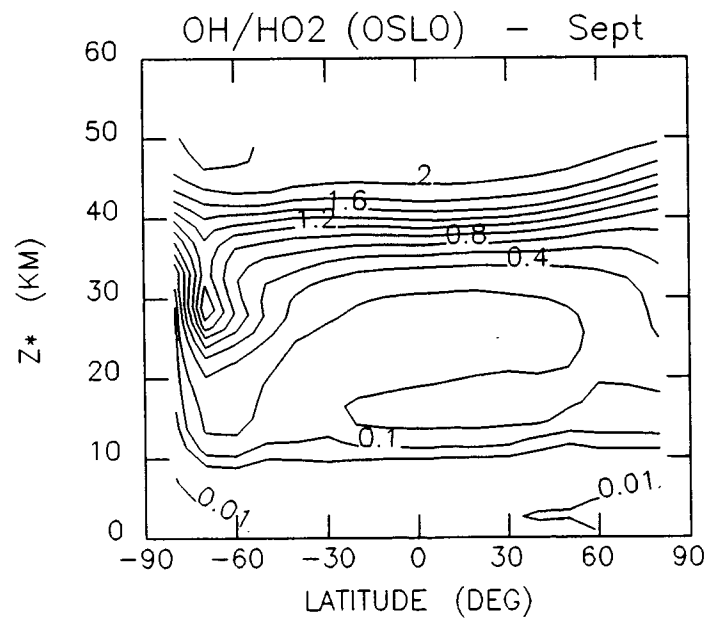
OH/HO2 (OSLO) – Sept
Z* (KM)
LATITUDE (DEG)
2
1.6
1.2
0.8
0.4
0.1
0.01

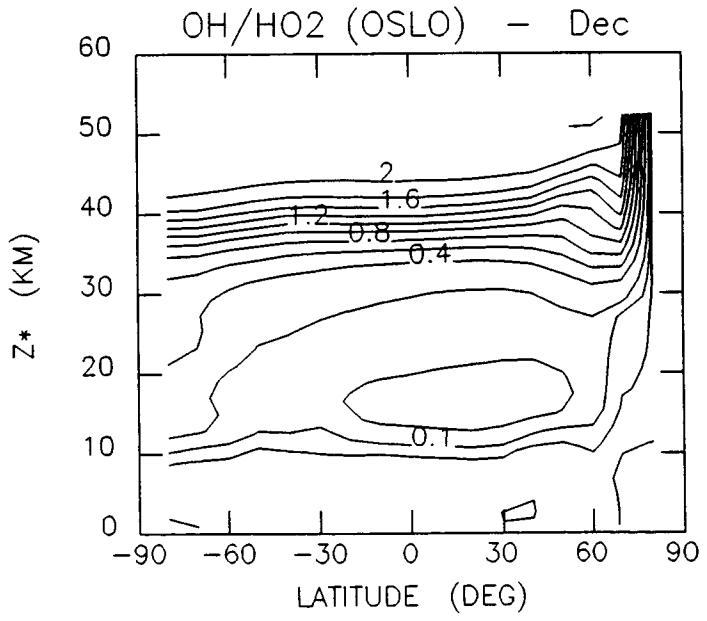
OH/HO2 (OSLO) – Dec
Z* (KM)
LATITUDE (DEG)
2
1.6
1.2
0.8
0.4
0.1

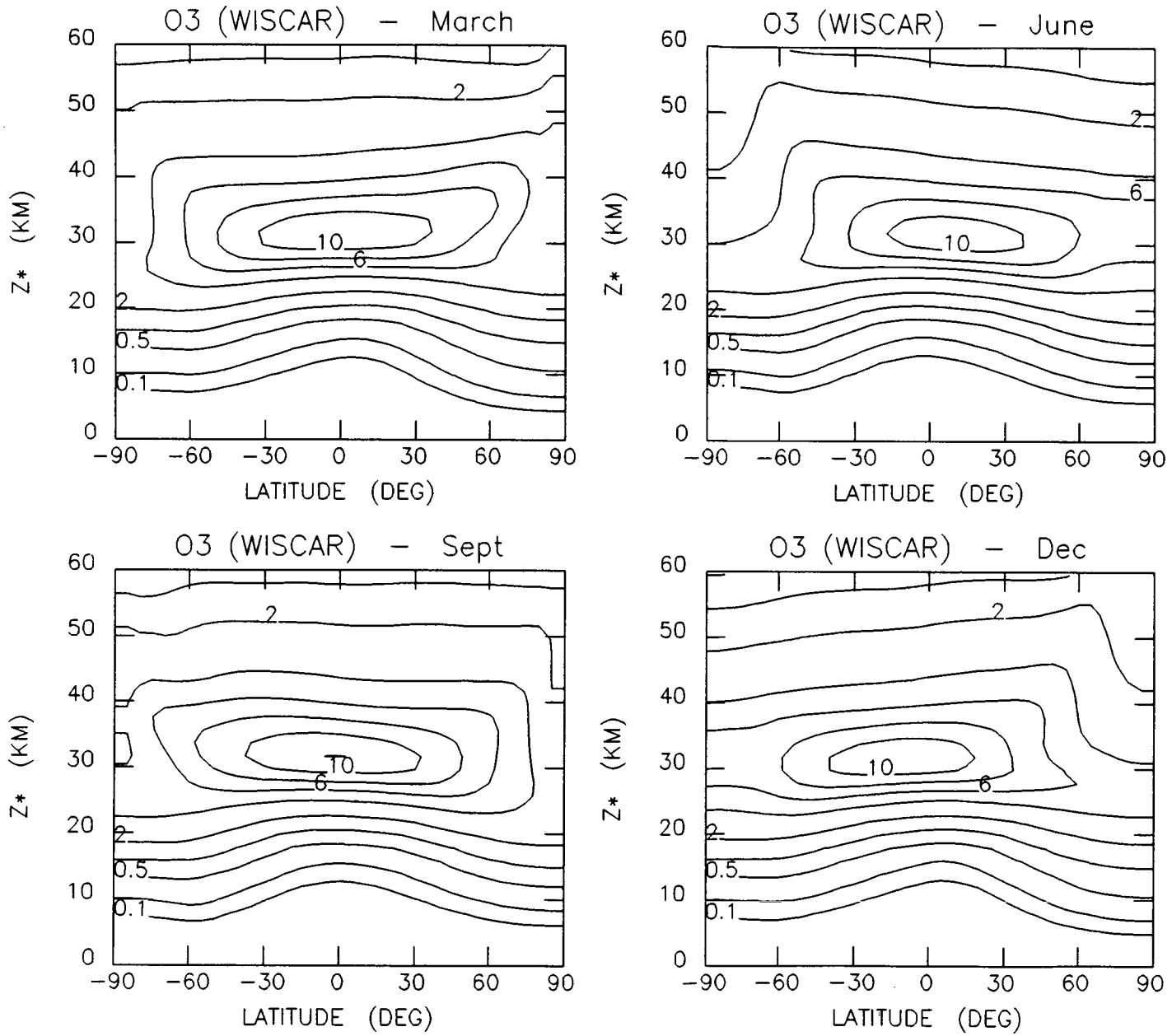
O3 (WISCAR) – March
O3 (WISCAR) – June
O3 (WISCAR) – Sept
O3 (WISCAR) – Dec
Z* (KM)
LATITUDE (DEG)
0
10
20
30
40
50
60
-90
-60
-30
0
30
60
90
2
6
10
0.5
0.1

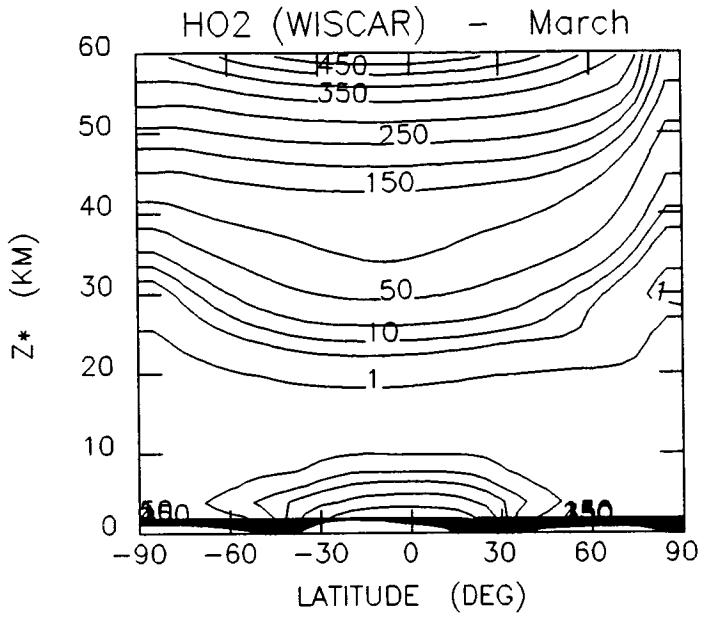
HO2 (WISCAR) – March
Z* (KM)
LATITUDE (DEG)
450
350
250
150
50
10
1

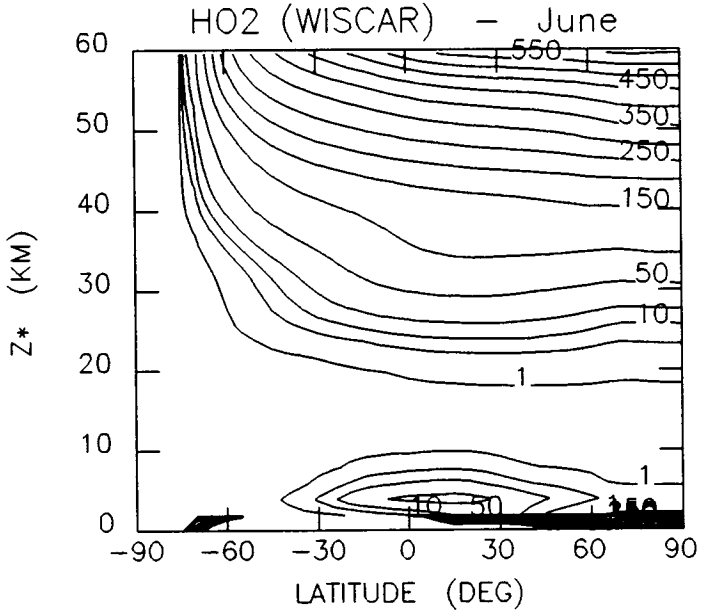
HO2 (WISCAR) – June
Z* (KM)
LATITUDE (DEG)
550
450
350
250
150
50
10
1

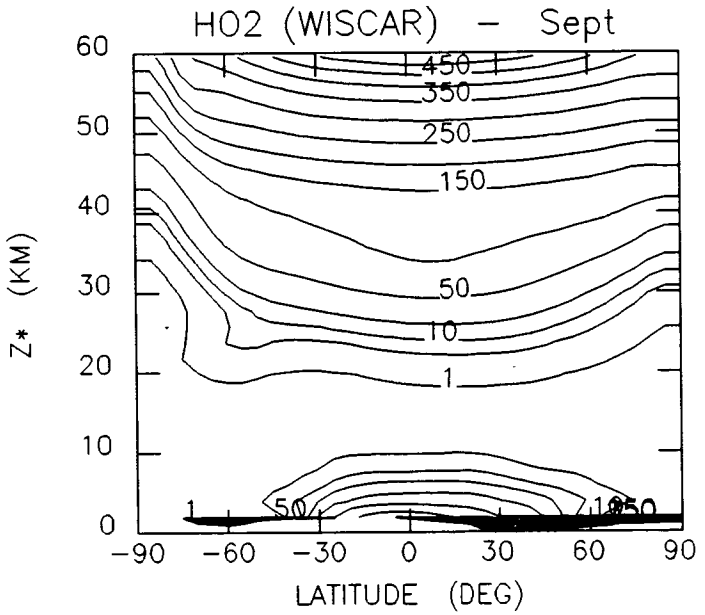
HO2 (WISCAR) – Sept
Z* (KM)
LATITUDE (DEG)
450
350
250
150
50
10
1

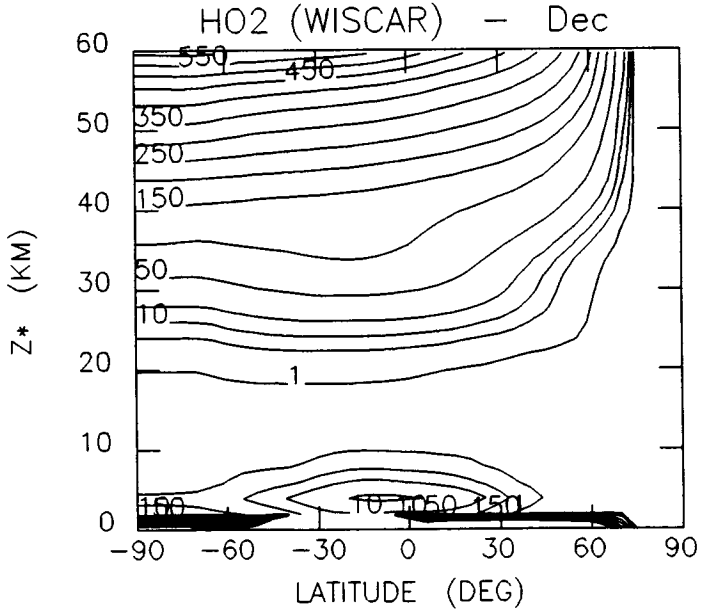
HO2 (WISCAR) – Dec
Z* (KM)
LATITUDE (DEG)
550
450
350
250
150
50
10
1

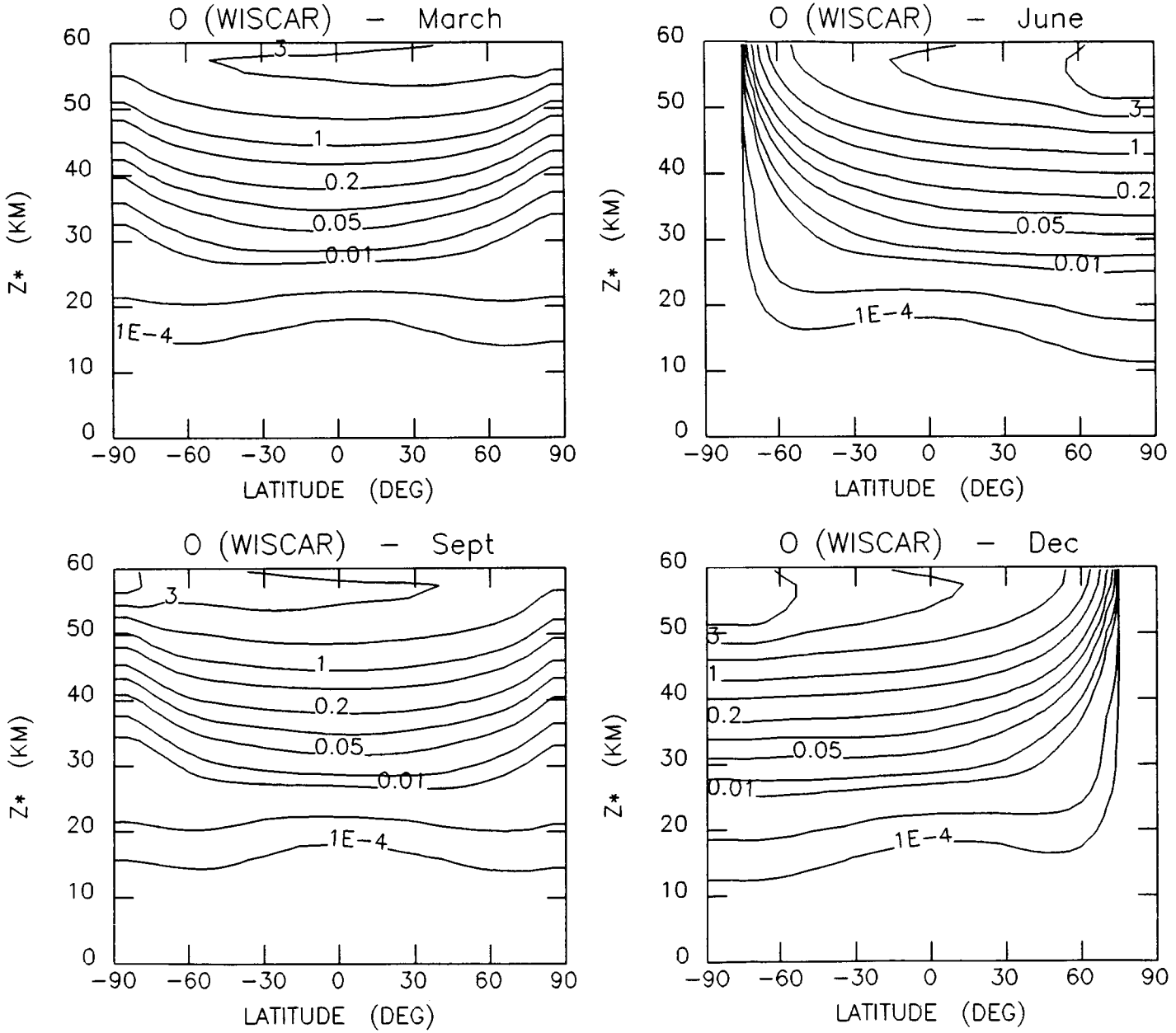
O (WISCAR) – March
O (WISCAR) – June
O (WISCAR) – Sept
O (WISCAR) – Dec
Z* (KM)
LATITUDE (DEG)
3
1
0.2
0.05
0.01
1E-4
0
10
20
30
40
50
60
-90
-60
-30
0
30
60
90

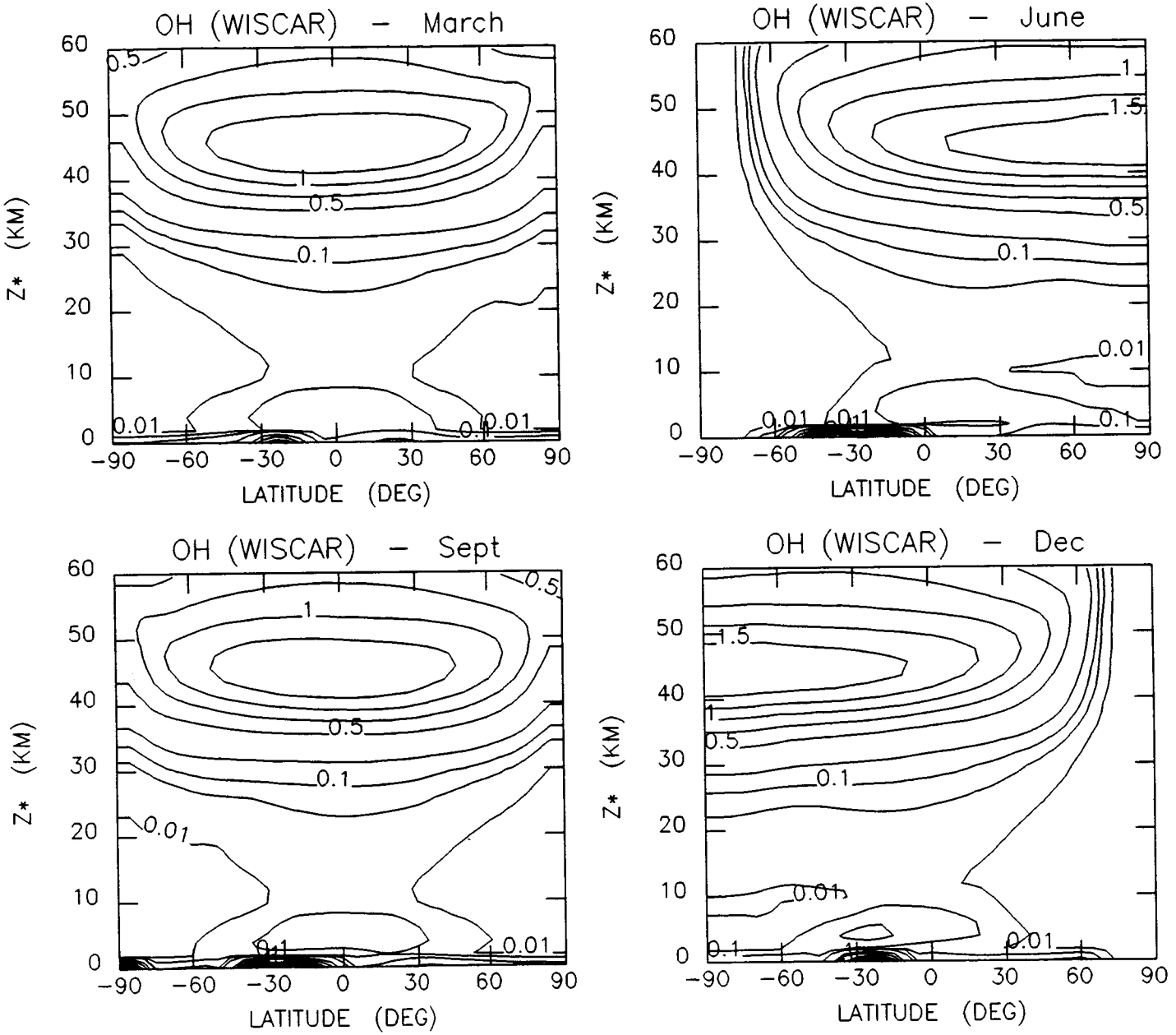
OH (WISCAR) – March
OH (WISCAR) – June
OH (WISCAR) – Sept
OH (WISCAR) – Dec
Z* (KM)
LATITUDE (DEG)
60
50
40
30
20
10
0
-90
-60
-30
0
30
60
90
0.5
1
0.1
0.01
1.5

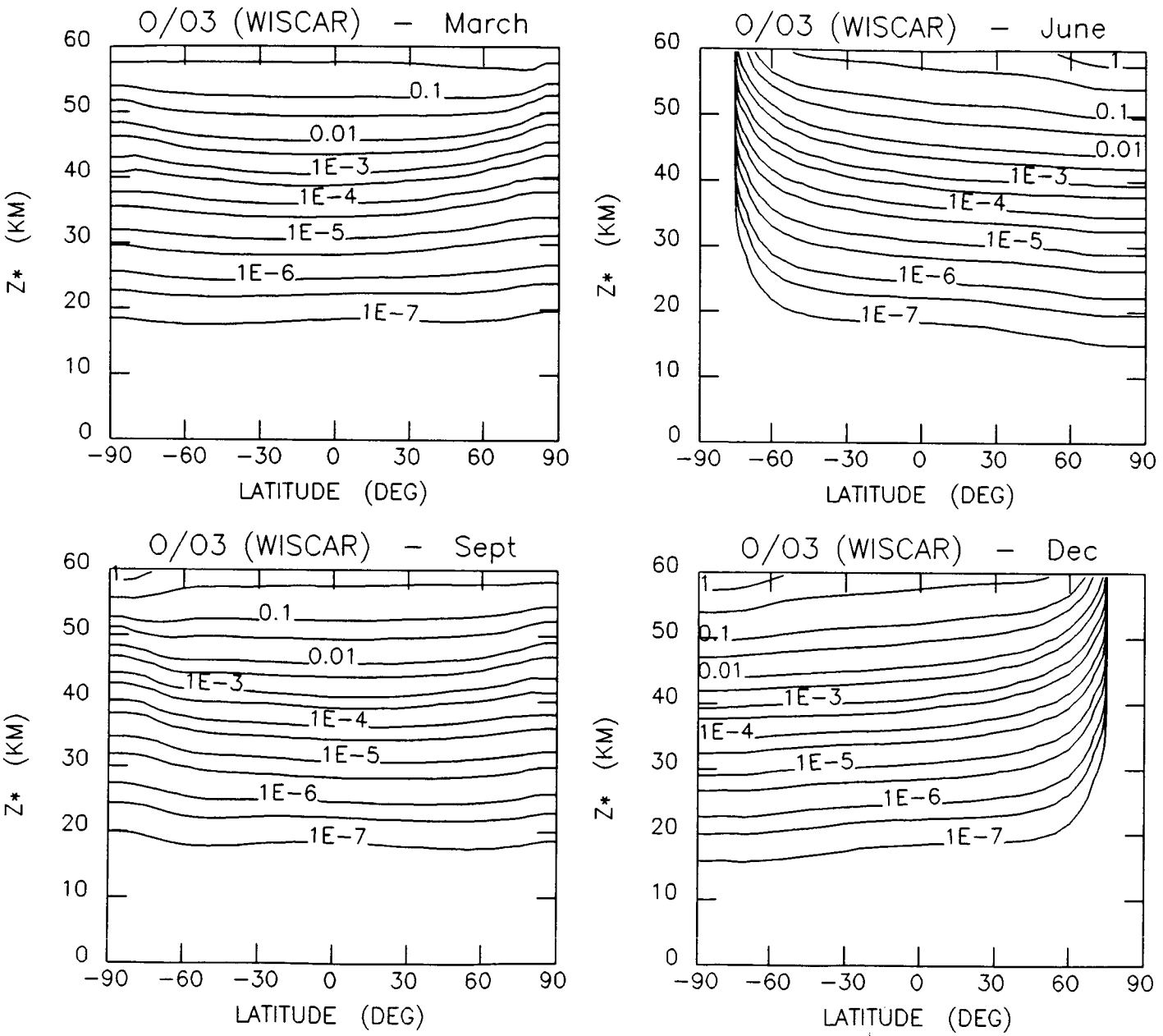
O/O3 (WISCAR) – March
O/O3 (WISCAR) – June
O/O3 (WISCAR) – Sept
O/O3 (WISCAR) – Dec
Z* (KM)
LATITUDE (DEG)
1
0.1
0.01
1E-3
1E-4
1E-5
1E-6
1E-7
0
10
20
30
40
50
60
-90
-60
-30
0
30
60
90

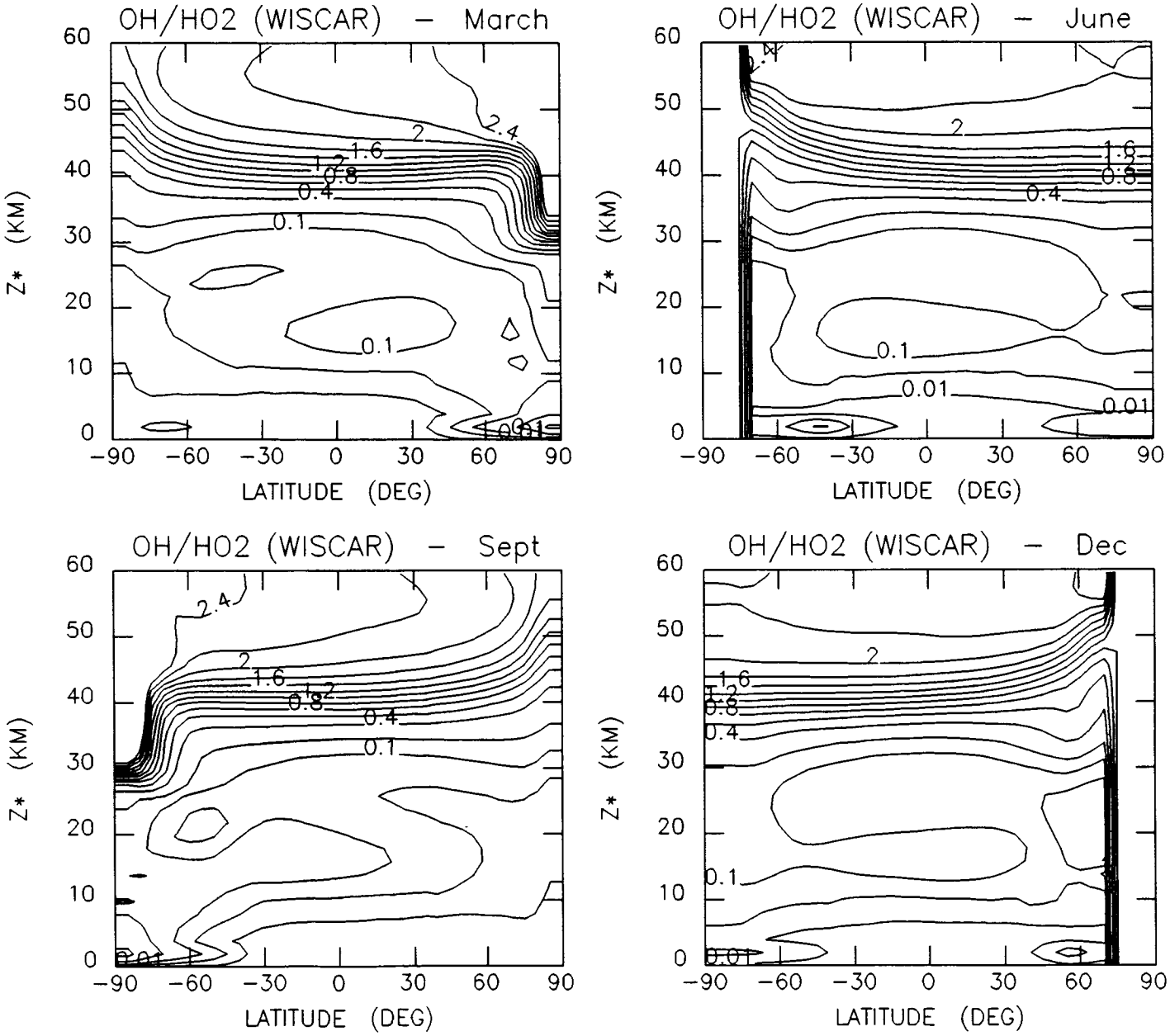
OH/HO2 (WISCAR) – March
OH/HO2 (WISCAR) – June
OH/HO2 (WISCAR) – Sept
OH/HO2 (WISCAR) – Dec
Z* (KM)
LATITUDE (DEG)
0
10
20
30
40
50
60
-90
-60
-30
0
30
60
90
2.4
2
1.6
1.2
0.8
0.4
0.1
0.01

**Table 6-3f.** Current Atmosphere (1980): Source Gases

March, June, September, and December
Models Represented - AER, CAMBRAL, CLKSON, DUPONT (Jan. & April), GSFC1 (Jan.), GSFC2, LLNL, MRI, NOCAR, OSLO, WISCAR

| Parameter | Description | Units | Contour Levels |
|---|---|---|---|
| $N_2O$ | $N_2O$ Mixing Ratio | ppbv | 0.1, 0.2, 0.5, 1, 2, 5, 10, 20, 50, 100, 150, 200, 240, 260, 280 |
| $CH_4$ | $CH_4$ Mixing Ratio | ppmv | 0.01, 0.05, 0.1, 0.2, 0.4, 0.6, 0.8, 1, 1.1, 1.2, 1.3, 1.4, 1.5 |
| $CFCl_3$ | $CFCl_3$ (F-11) Mixing Ratio | pptv | 1.0E-03, 0.01, 0.1, 1, 10, 20, 40, 60, 80, 100, 120, 140, 160, 180 |
| $CF_2Cl_2$ | $CF_2Cl_2$ (F-12) Mixing Ratio | pptv | 1.0E-03, 0.01, 0.1, 1, 10, 20, 50, 100, 150, 200, 250, 300 |
| $CCl_4$ | $CCl_4$ Mixing Ratio | pptv | 1.0E-03, 0.01, 0.1, 1, 5, 10, 20, 40, 60, 80 |
| $CH_3CCl_3$ | $CH_3CCl_3$ Mixing Ratio | pptv | 1.0E-03, 0.01, 0.1, 1, 5, 10, 20, 40, 60, 80 |

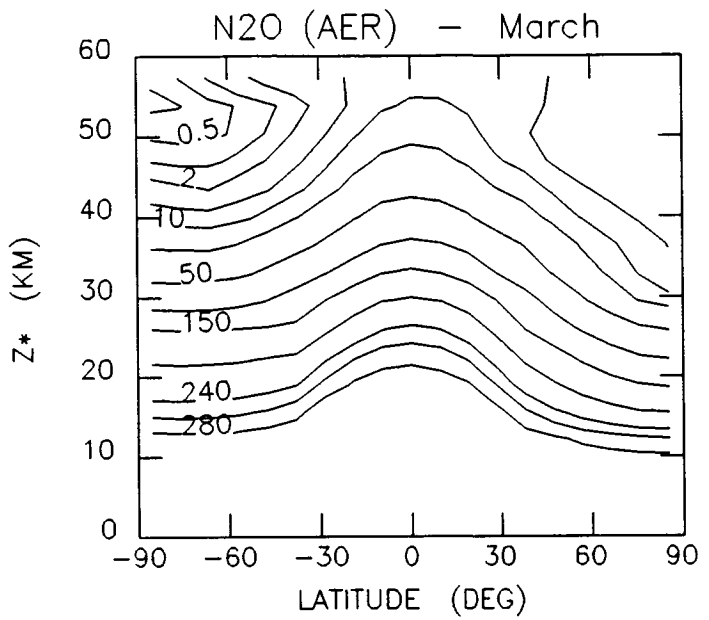
N2O (AER) – March
Z* (KM)
LATITUDE (DEG)
0.5
2
10
50
150
240
280

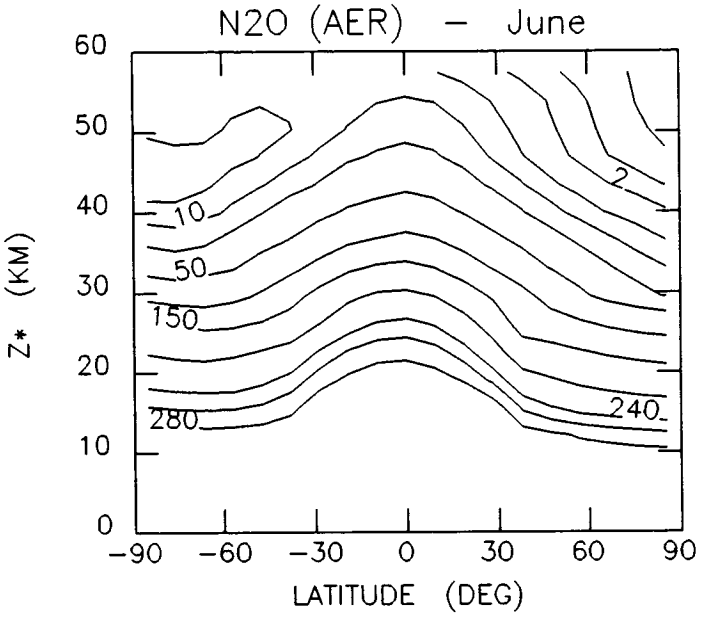
N2O (AER) – June
Z* (KM)
LATITUDE (DEG)
2
10
50
150
240
280

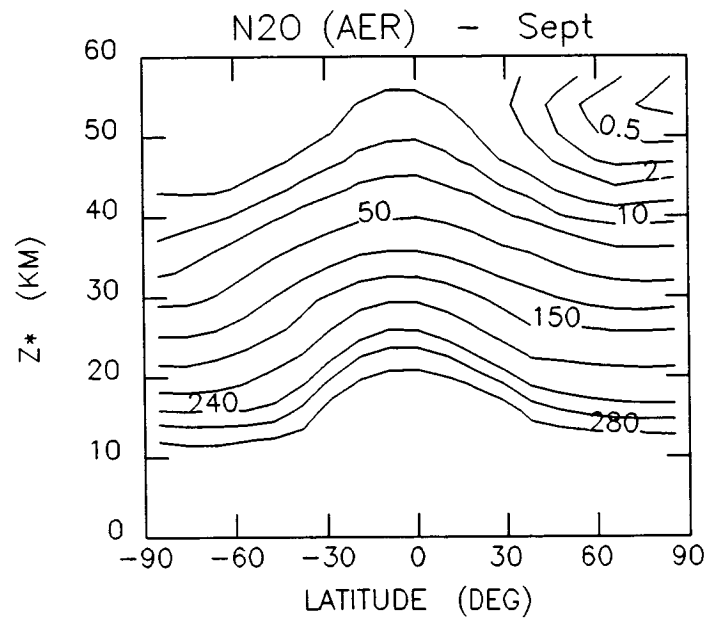
N2O (AER) – Sept
Z* (KM)
LATITUDE (DEG)
0.5
2
10
50
150
240
280

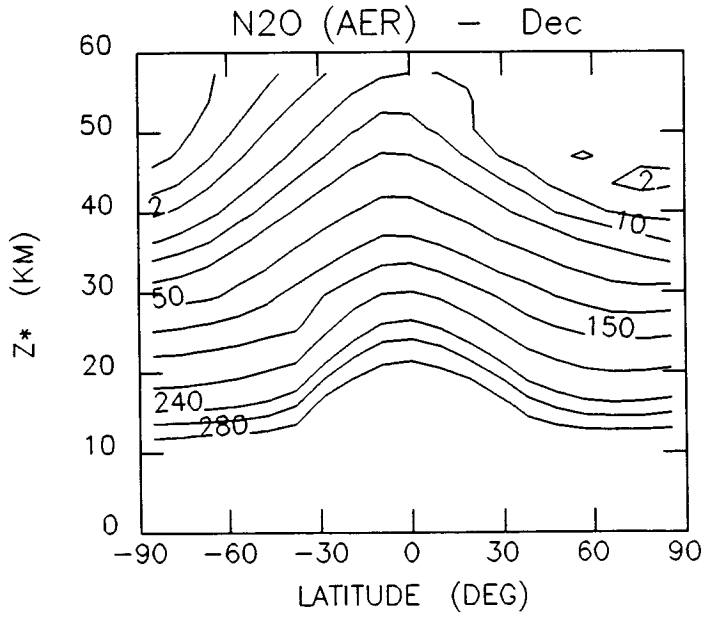
N2O (AER) – Dec
Z* (KM)
LATITUDE (DEG)
2
2
10
50
150
240
280

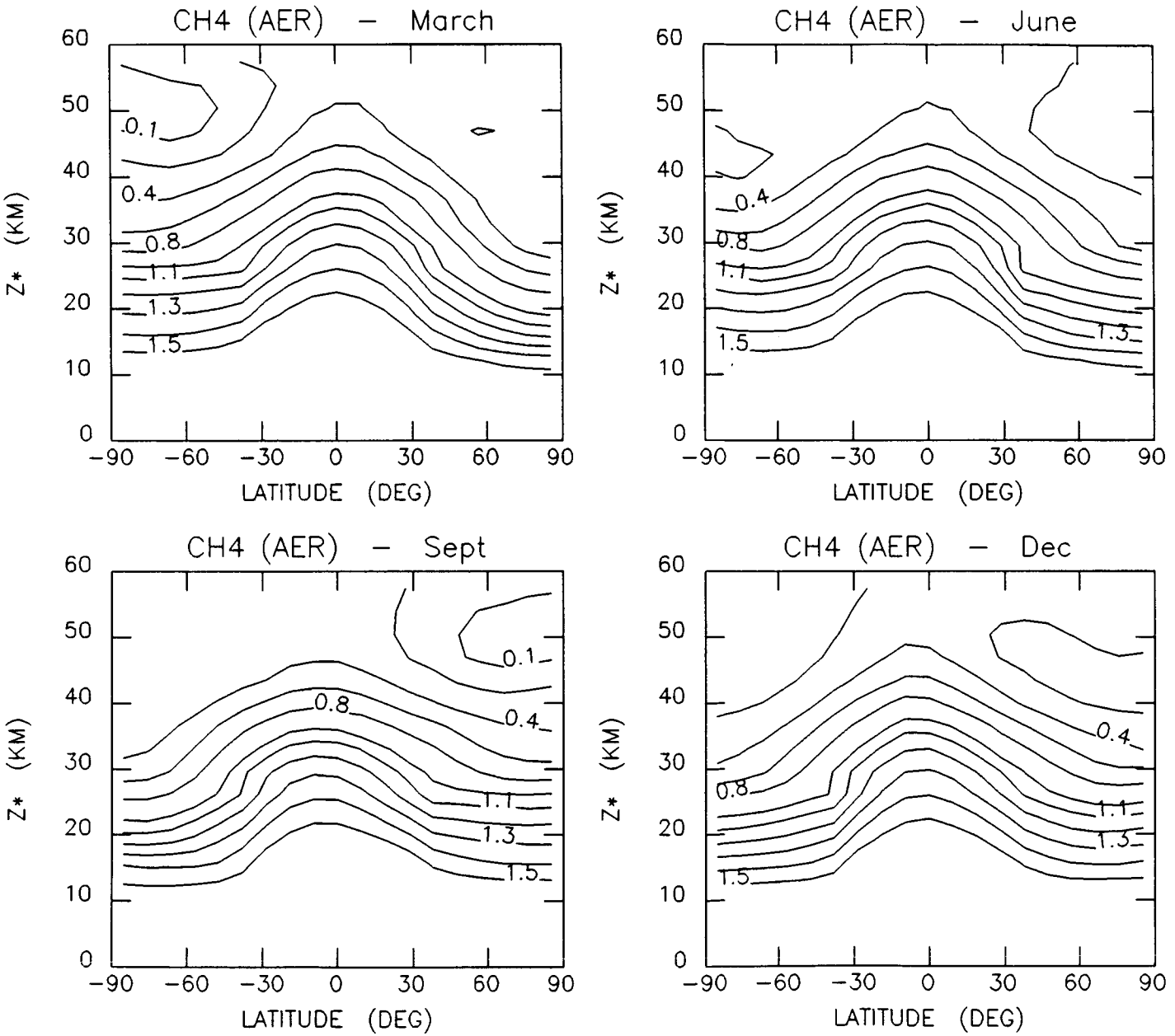
CH4 (AER) – March
CH4 (AER) – June
CH4 (AER) – Sept
CH4 (AER) – Dec
Z* (KM)
LATITUDE (DEG)
0
10
20
30
40
50
60
−90 −60 −30 0 30 60 90
0.1
0.4
0.8
1.1
1.3
1.5

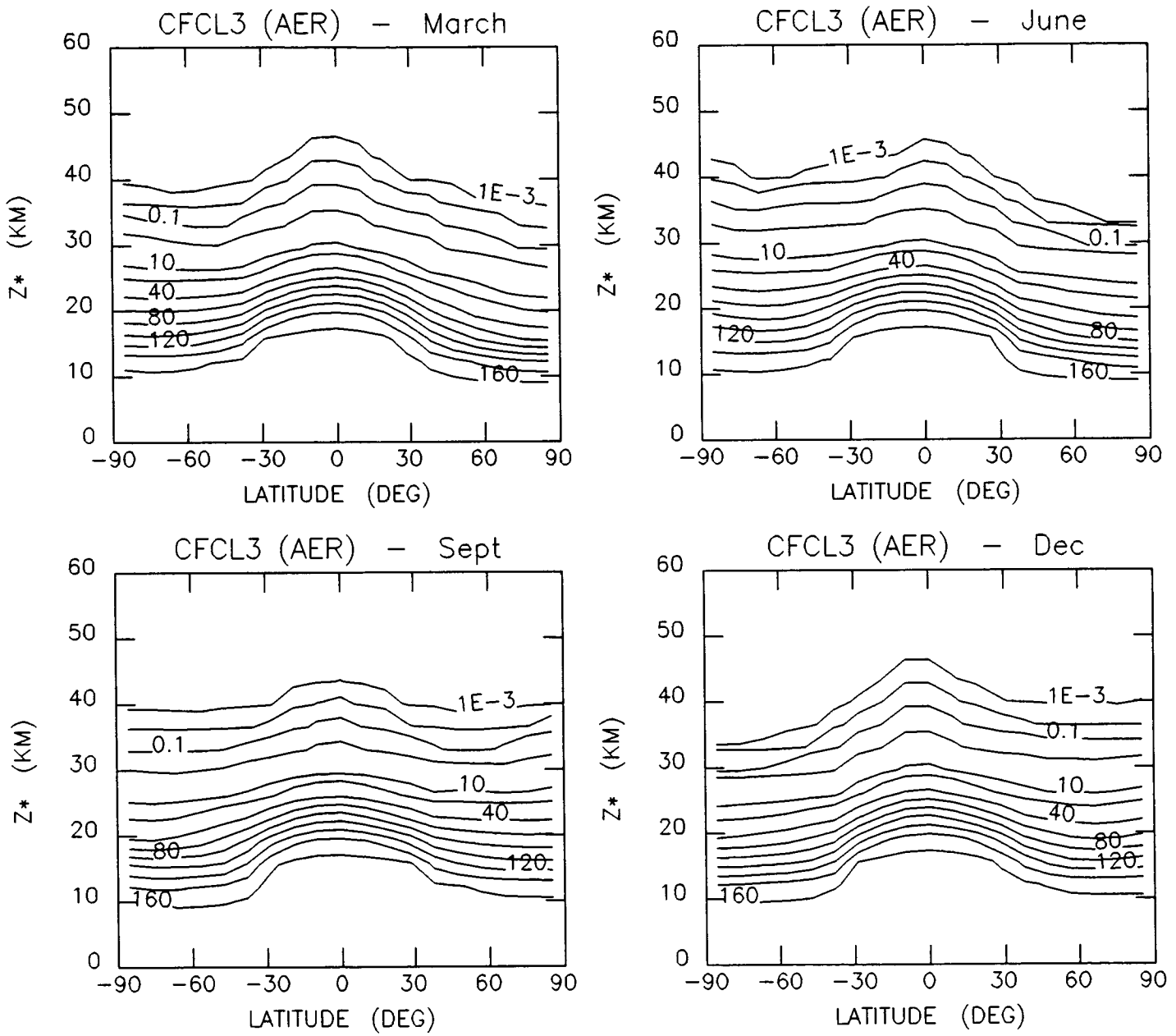
CFCL3 (AER) – March
CFCL3 (AER) – June
CFCL3 (AER) – Sept
CFCL3 (AER) – Dec
Z* (KM)
LATITUDE (DEG)
1E-3
0.1
10
40
80
120
160
0
10
20
30
40
50
60
-90
-60
-30
0
30
60
90

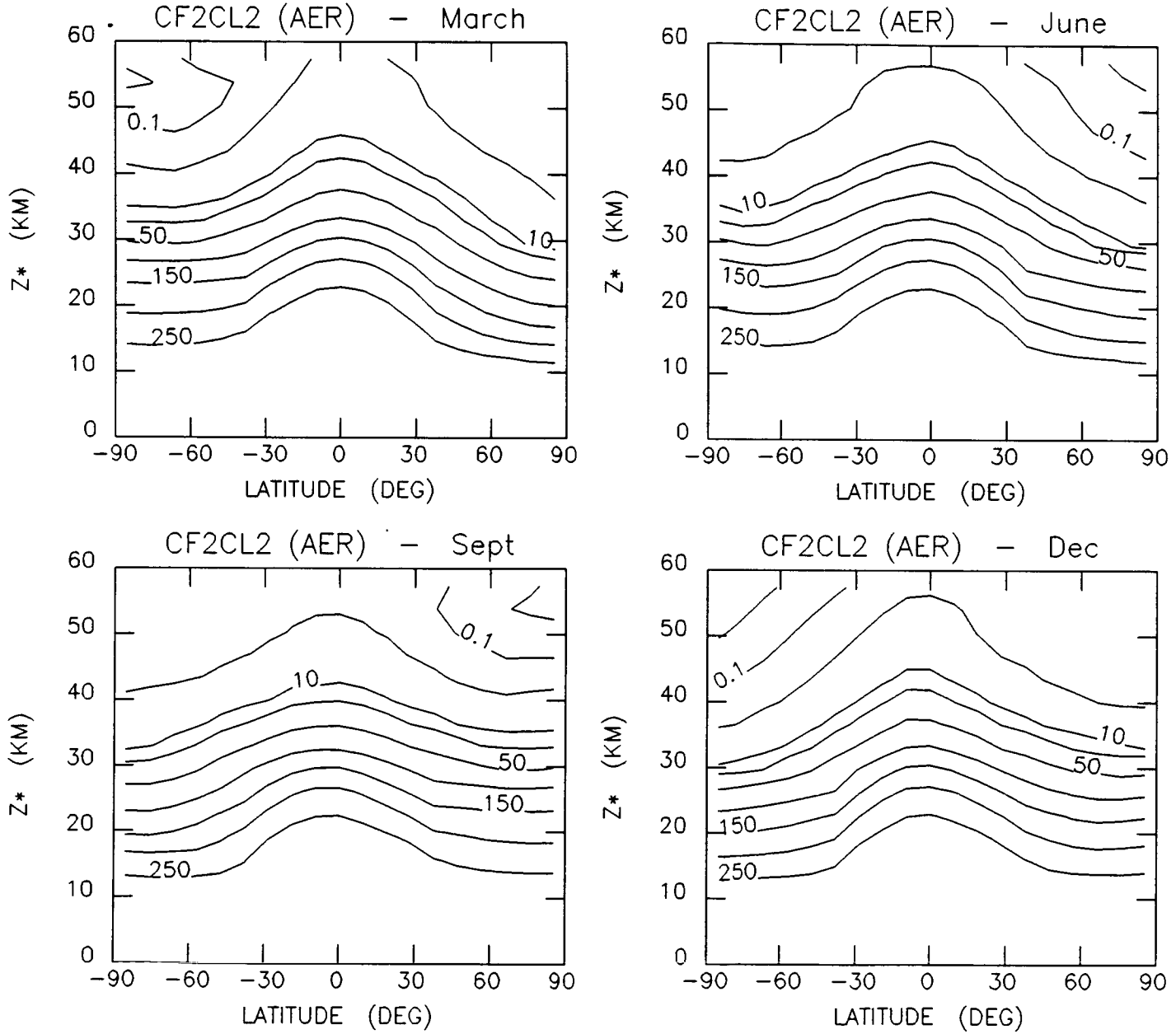
CF2CL2 (AER) – March
CF2CL2 (AER) – June
CF2CL2 (AER) – Sept
CF2CL2 (AER) – Dec
Z* (KM)
LATITUDE (DEG)
0.1
10
50
150
250
0
10
20
30
40
50
60
-90
-60
-30
0
30
60
90

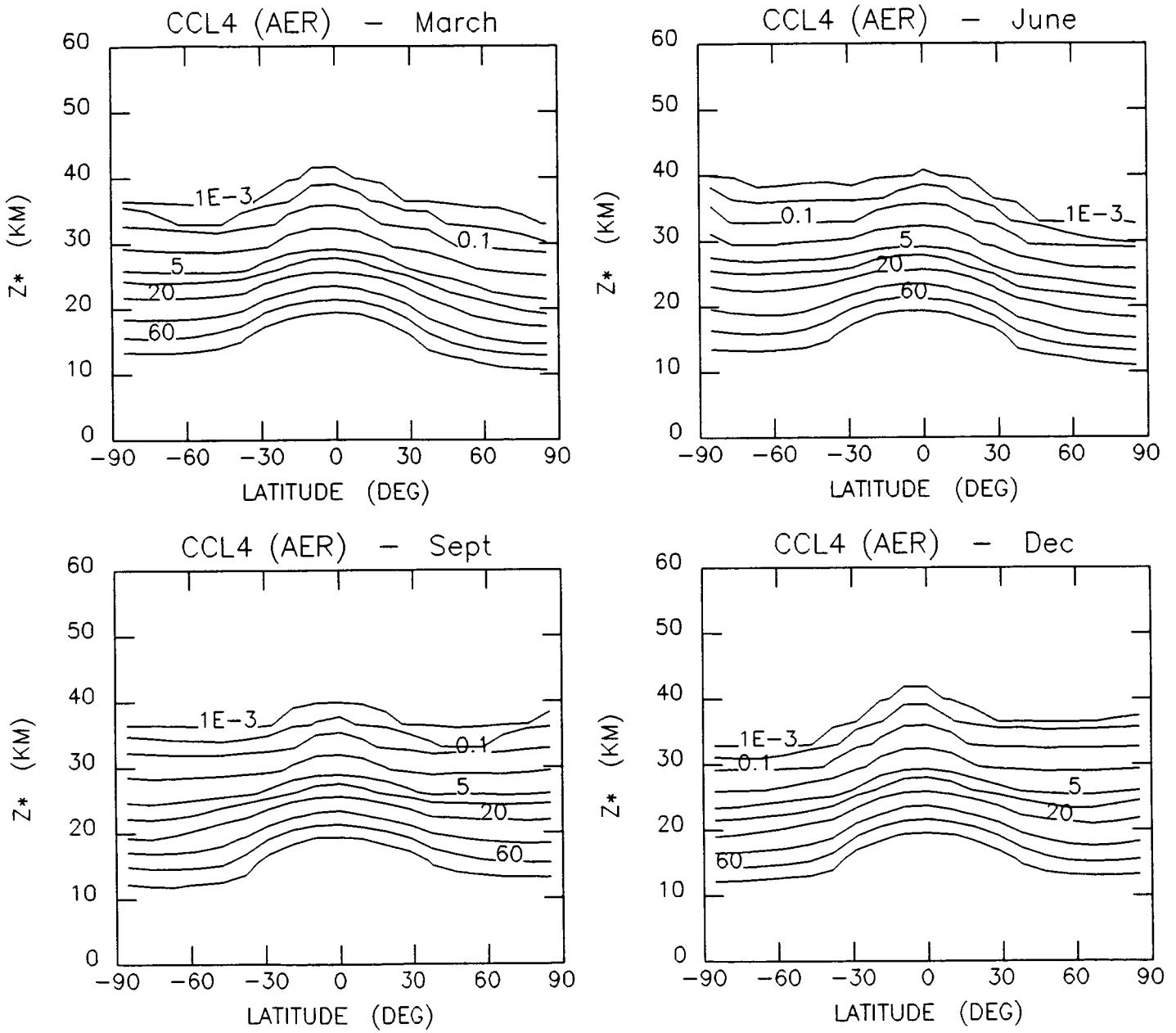
CCL4 (AER) – March
CCL4 (AER) – June
CCL4 (AER) – Sept
CCL4 (AER) – Dec
Z* (KM)
LATITUDE (DEG)
1E-3
0.1
5
20
60
0
10
20
30
40
50
60
-90
-60
-30
0
30
60
90

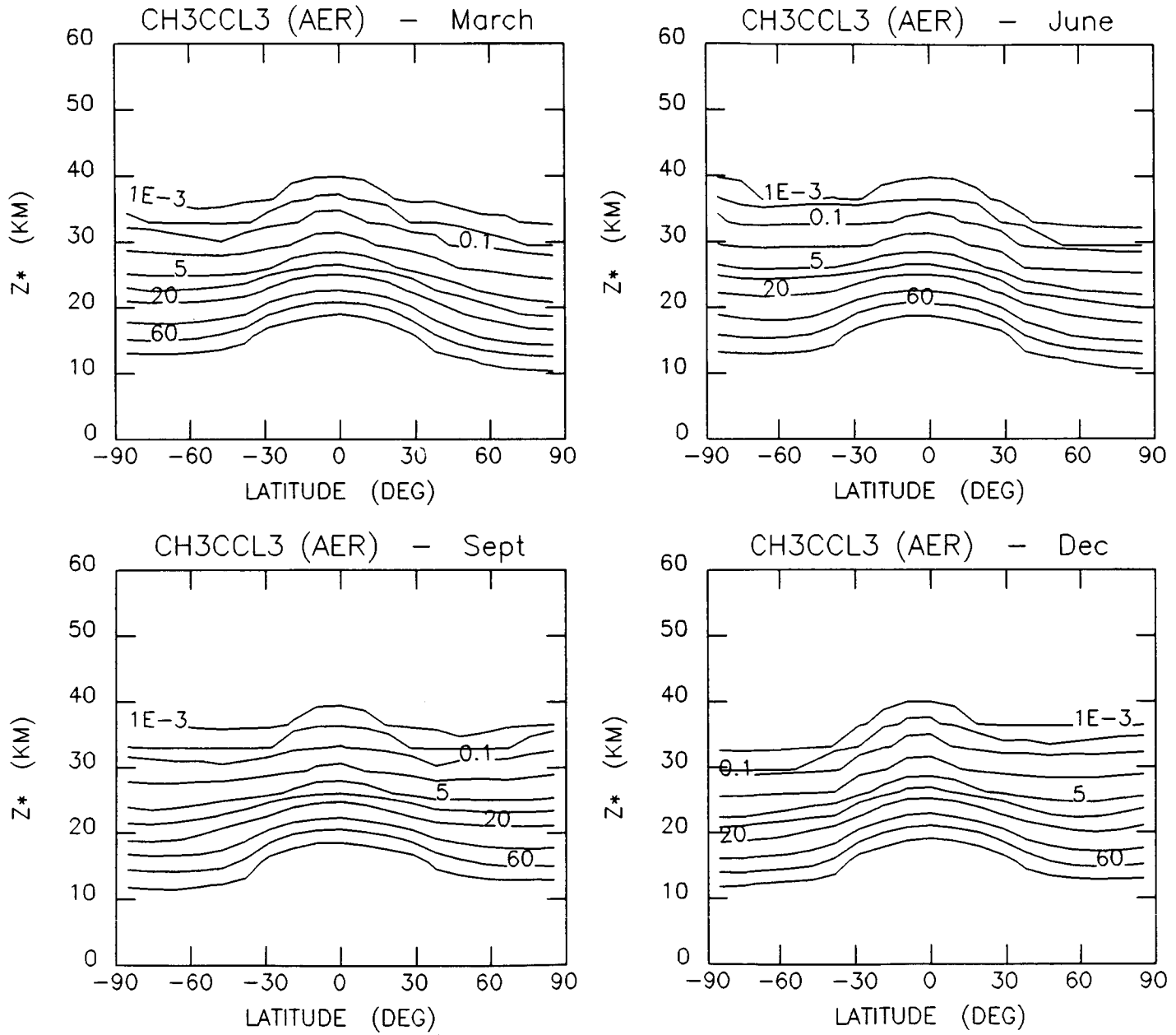
CH3CCL3 (AER) – March
CH3CCL3 (AER) – June
CH3CCL3 (AER) – Sept
CH3CCL3 (AER) – Dec
Z* (KM)
LATITUDE (DEG)
1E-3
0.1
5
20
60
0
10
20
30
40
50
60
-90
-60
-30
0
30
60
90

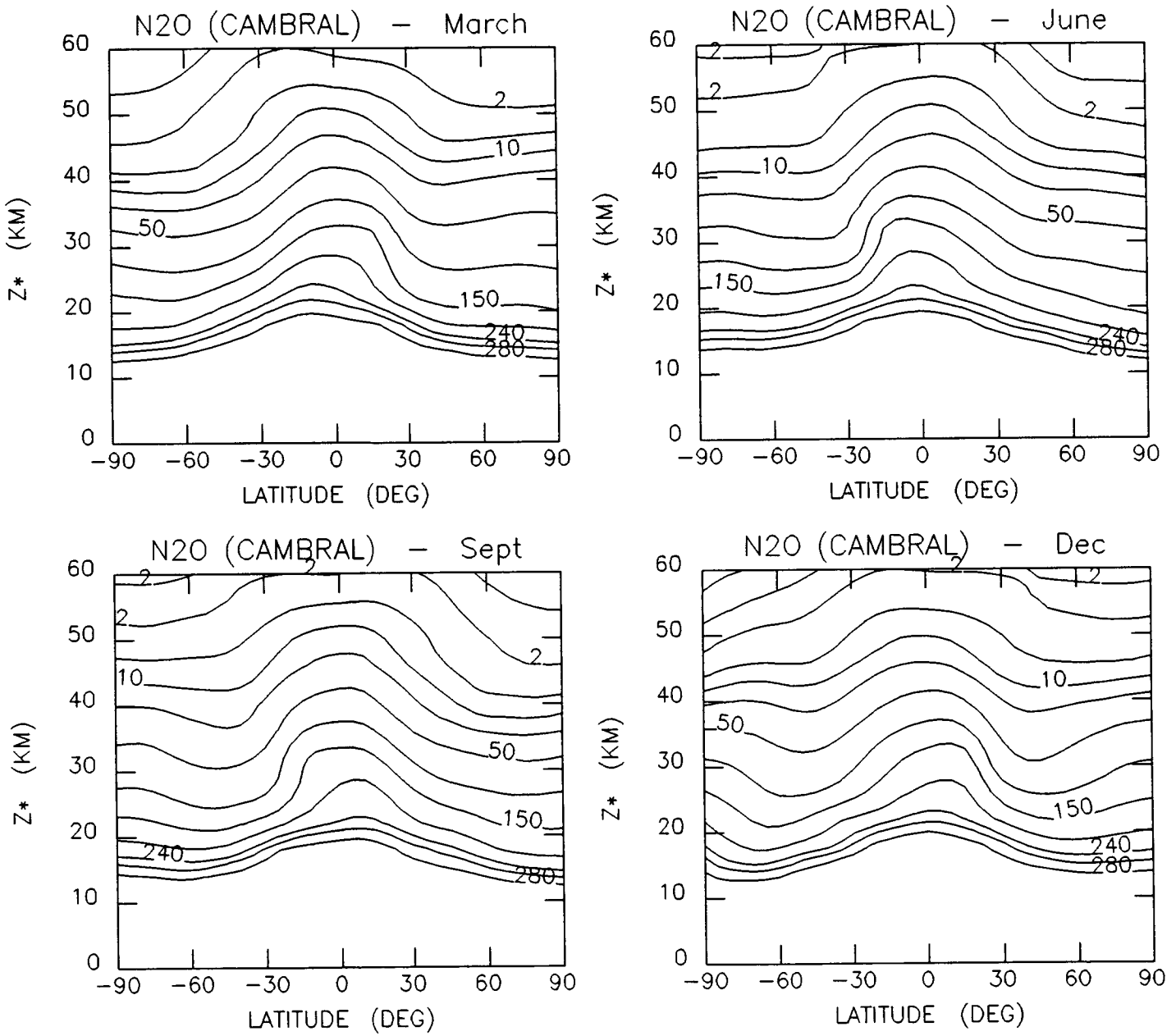
N2O (CAMBRAL) – March
N2O (CAMBRAL) – June
N2O (CAMBRAL) – Sept
N2O (CAMBRAL) – Dec
Z* (KM)
LATITUDE (DEG)
60
50
40
30
20
10
0
-90
-60
-30
0
30
60
90
2
10
50
150
240
280

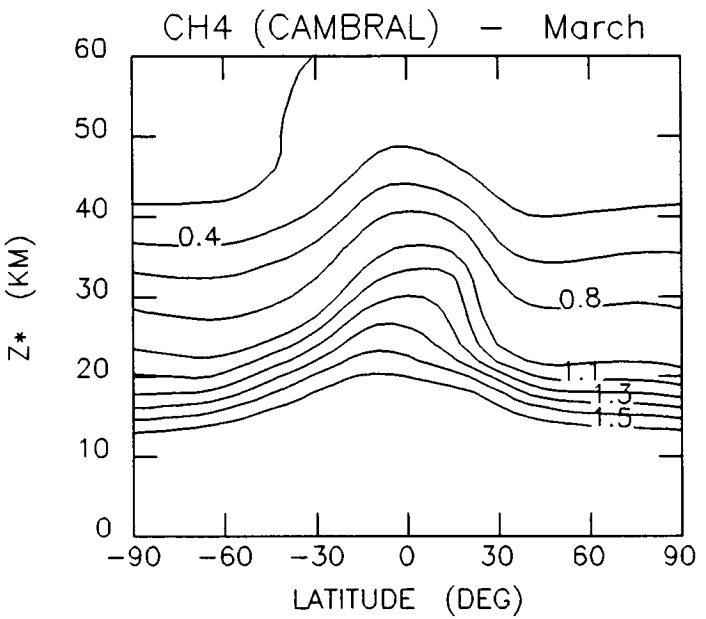
CH4 (CAMBRAL) – March
Z* (KM)
LATITUDE (DEG)
0.4
0.8
1.1
1.3
1.5

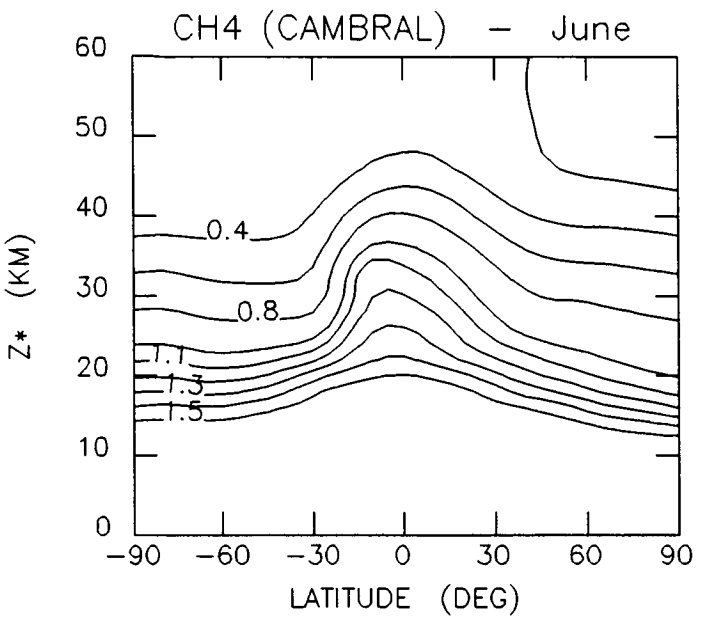
CH4 (CAMBRAL) – June
Z* (KM)
LATITUDE (DEG)
0.4
0.8
1.1
1.3
1.5

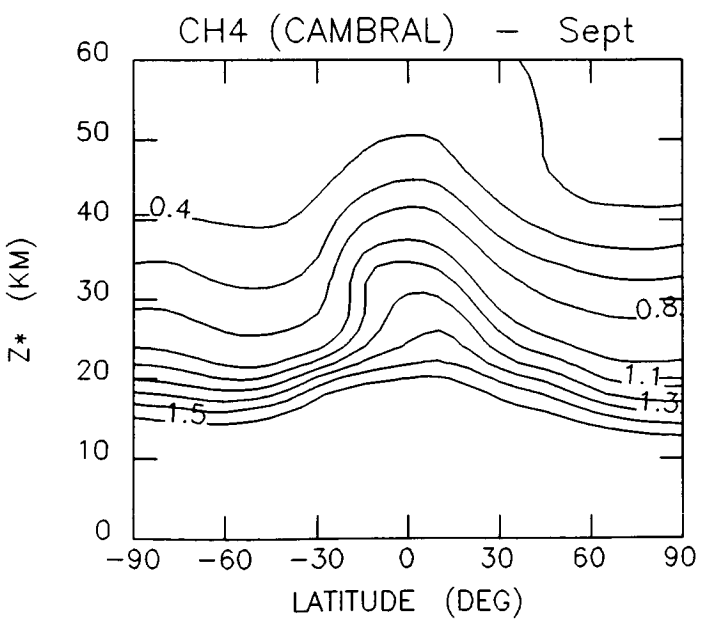
CH4 (CAMBRAL) – Sept
Z* (KM)
LATITUDE (DEG)
0.4
0.8
1.1
1.3
1.5

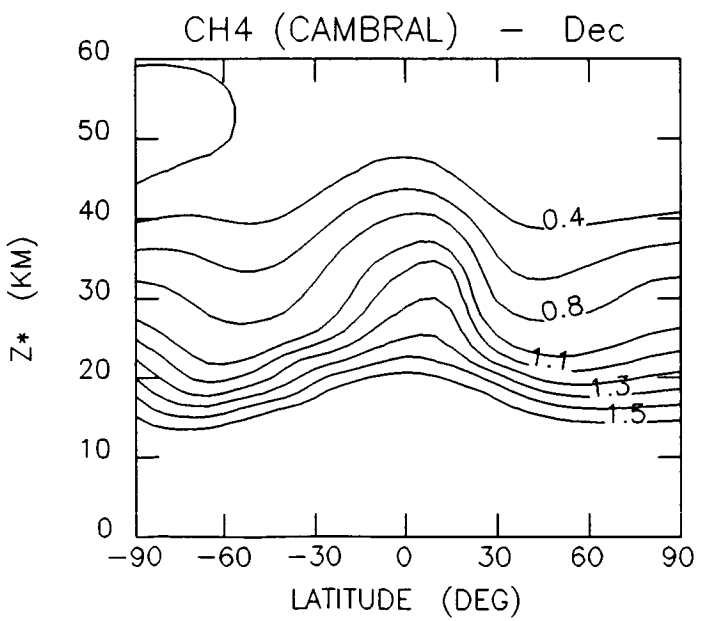
CH4 (CAMBRAL) – Dec
Z* (KM)
LATITUDE (DEG)
0.4
0.8
1.1
1.3
1.5

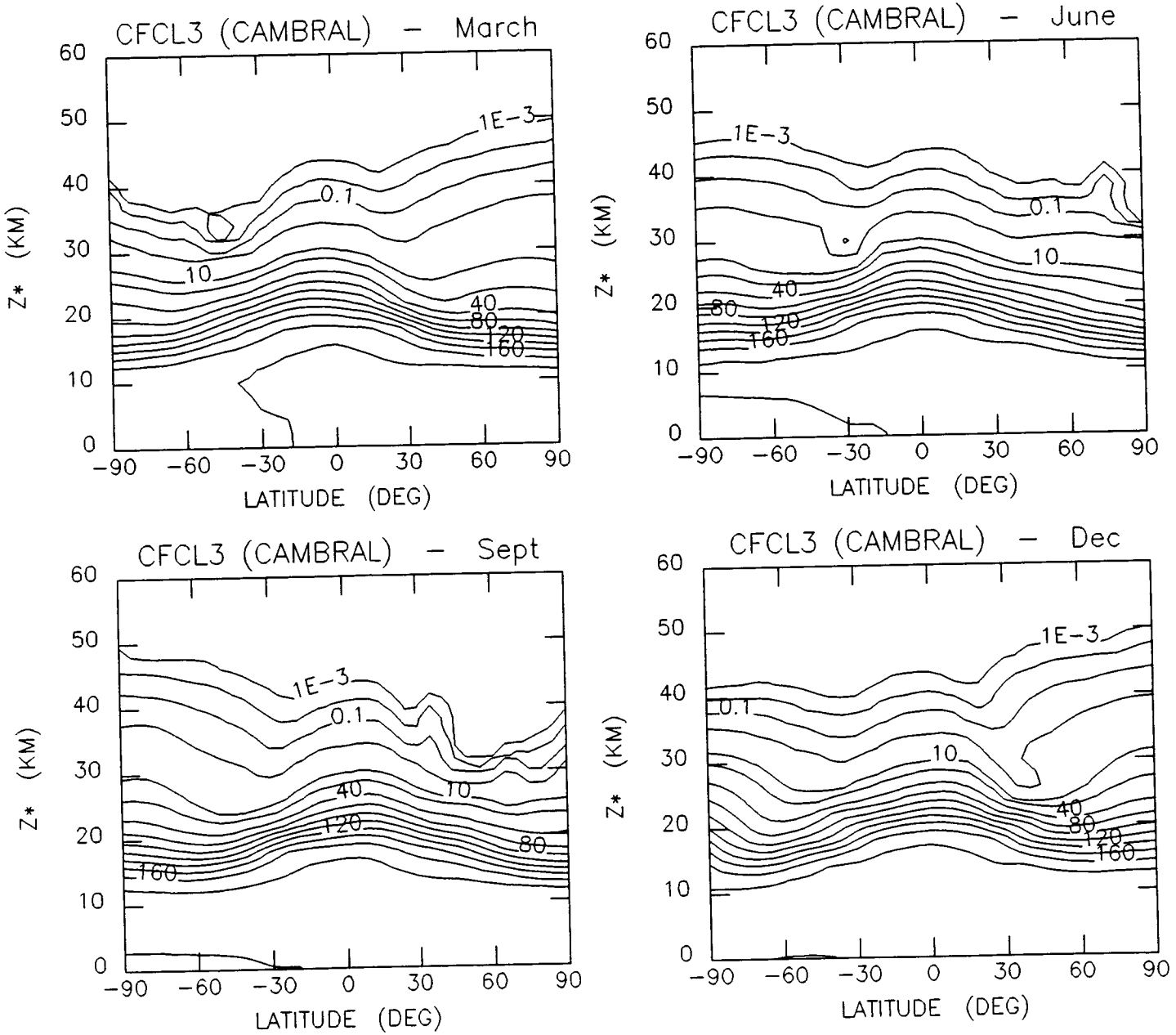
CFCL3 (CAMBRAL) – March
CFCL3 (CAMBRAL) – June
CFCL3 (CAMBRAL) – Sept
CFCL3 (CAMBRAL) – Dec
Z* (KM)
LATITUDE (DEG)
1E-3
0.1
10
40
80
120
160
0
10
20
30
40
50
60
-90
-60
-30
0
30
60
90

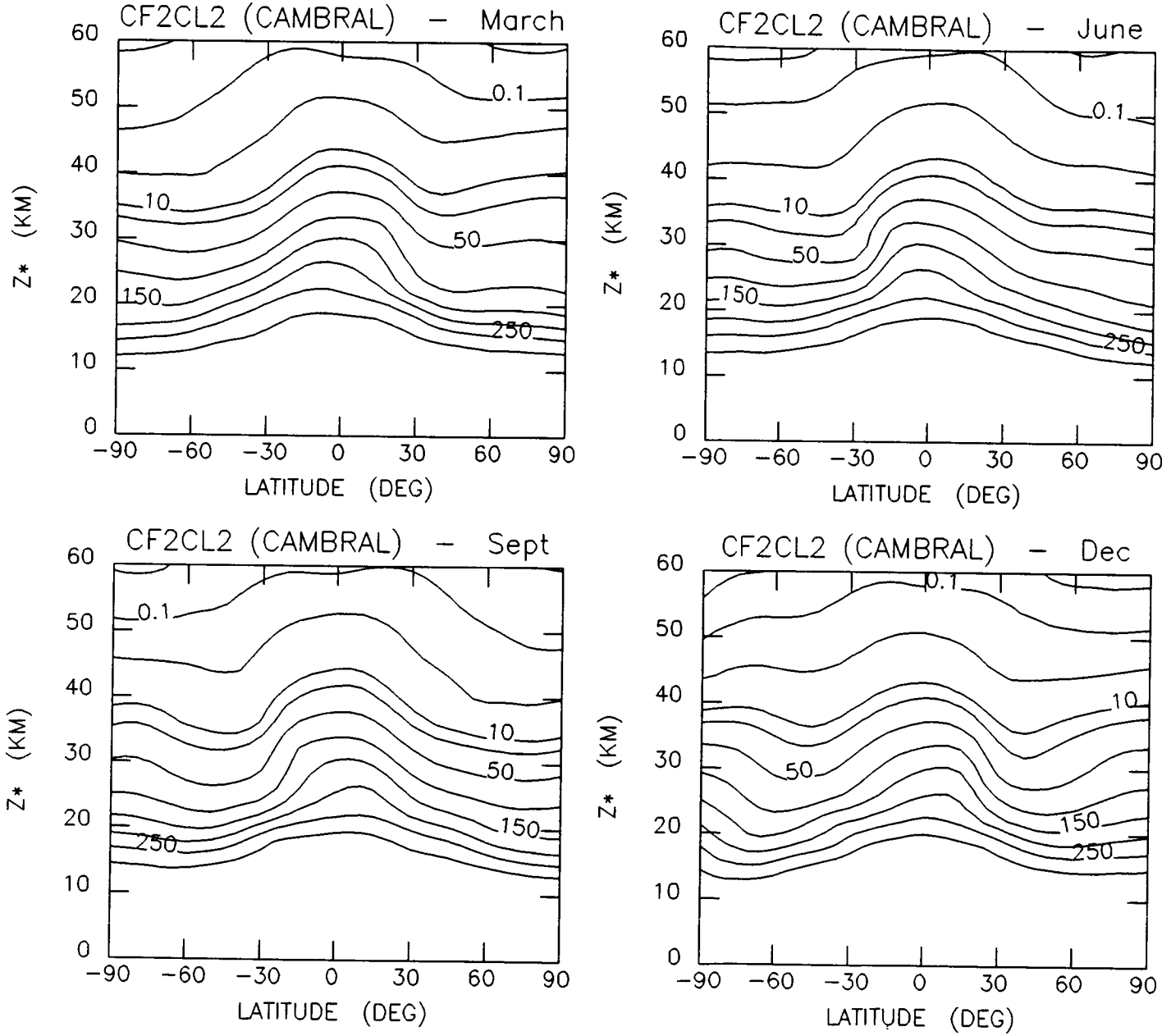
CF2CL2 (CAMBRAL) – March
CF2CL2 (CAMBRAL) – June
CF2CL2 (CAMBRAL) – Sept
CF2CL2 (CAMBRAL) – Dec
Z* (KM)
LATITUDE (DEG)
0.1
10
50
150
250
0
10
20
30
40
50
60
−90
−60
−30
0
30
60
90

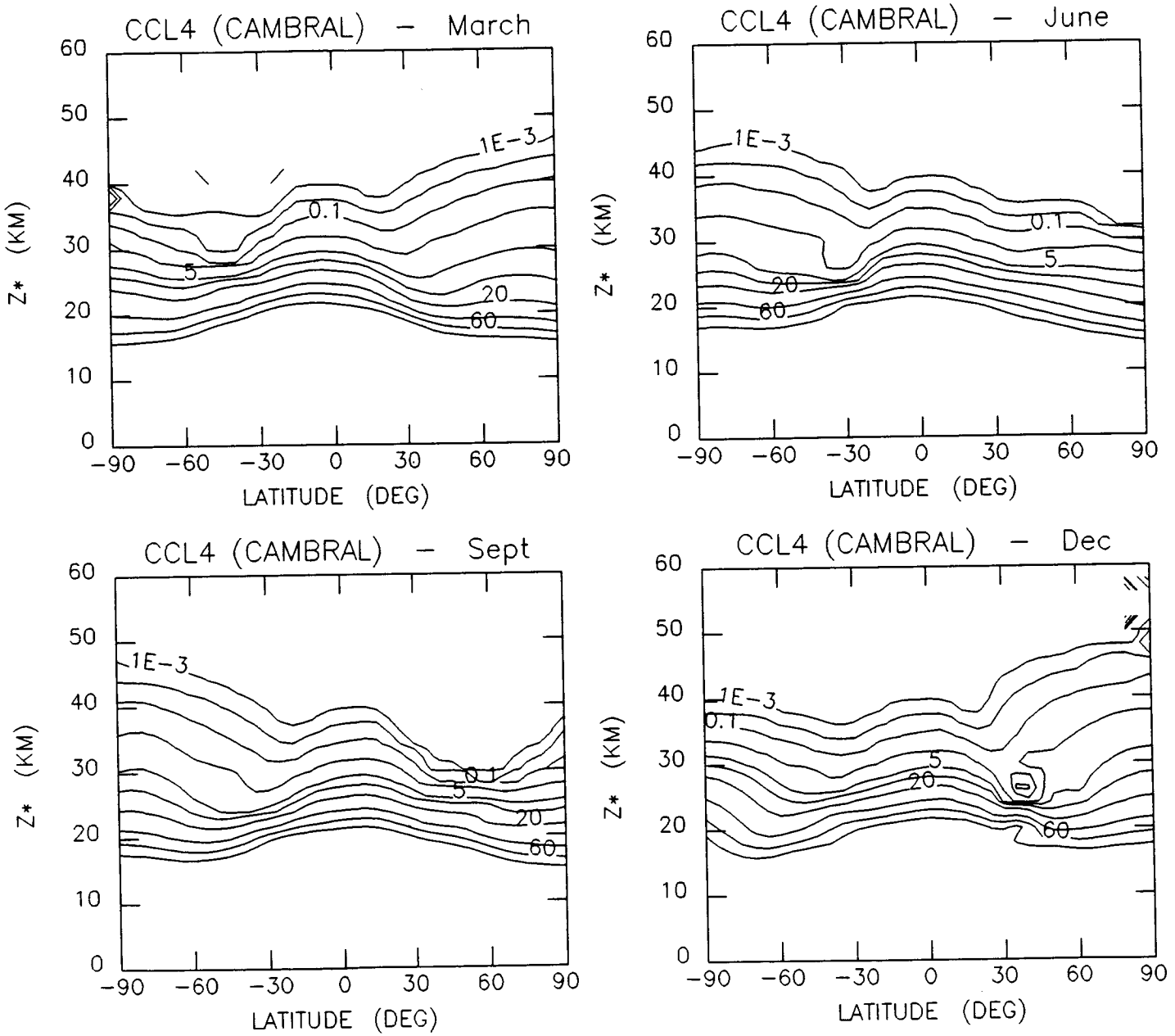
CCL4 (CAMBRAL) – March
CCL4 (CAMBRAL) – June
CCL4 (CAMBRAL) – Sept
CCL4 (CAMBRAL) – Dec
Z* (KM)
LATITUDE (DEG)
1E-3
0.1
5
20
60
0
10
30
40
50
-90
-60
-30
30
60
90

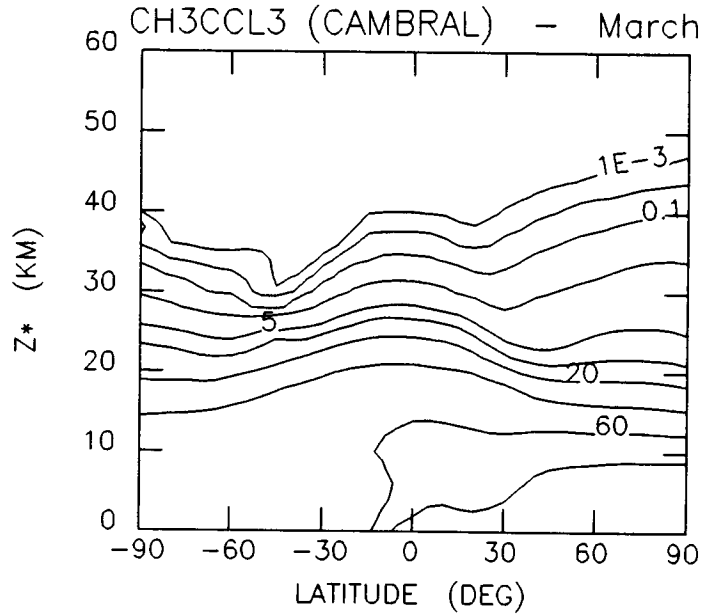
CH3CCL3 (CAMBRAL) – March
Z* (KM)
LATITUDE (DEG)
1E-3
0.1
5
20
60

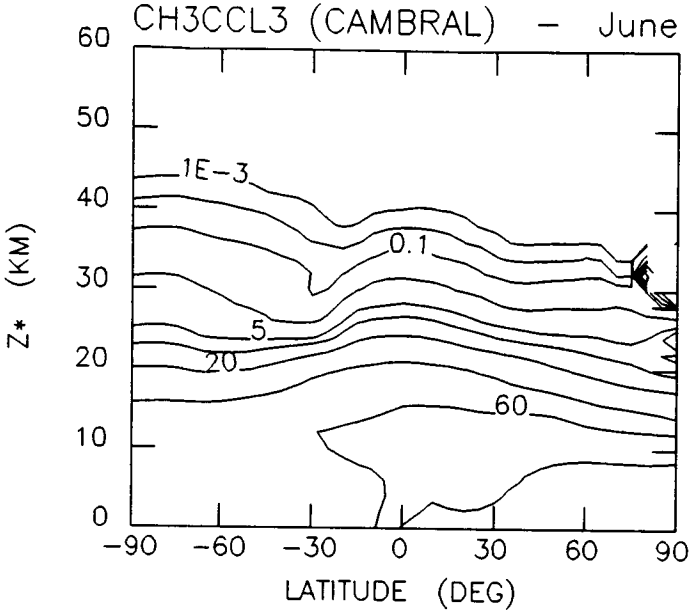
CH3CCL3 (CAMBRAL) – June
Z* (KM)
LATITUDE (DEG)
1E-3
0.1
5
20
60

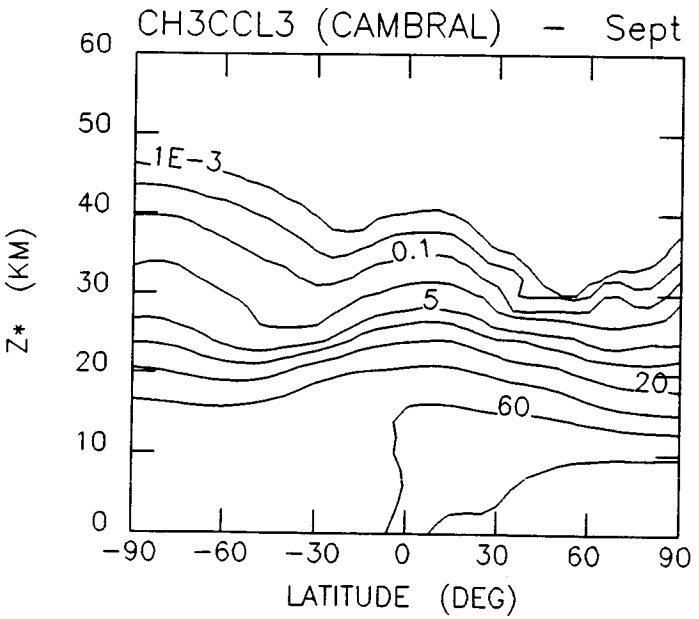
CH3CCL3 (CAMBRAL) – Sept
Z* (KM)
LATITUDE (DEG)
1E-3
0.1
5
20
60

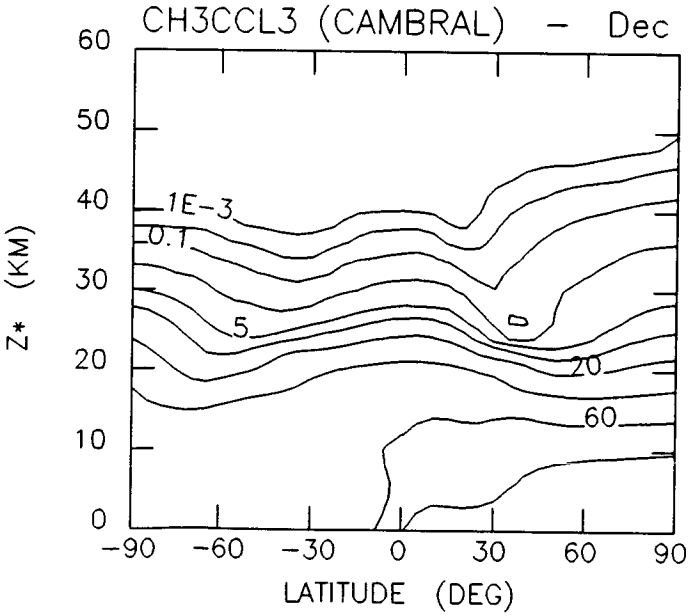
CH3CCL3 (CAMBRAL) – Dec
Z* (KM)
LATITUDE (DEG)
1E-3
0.1
5
20
60

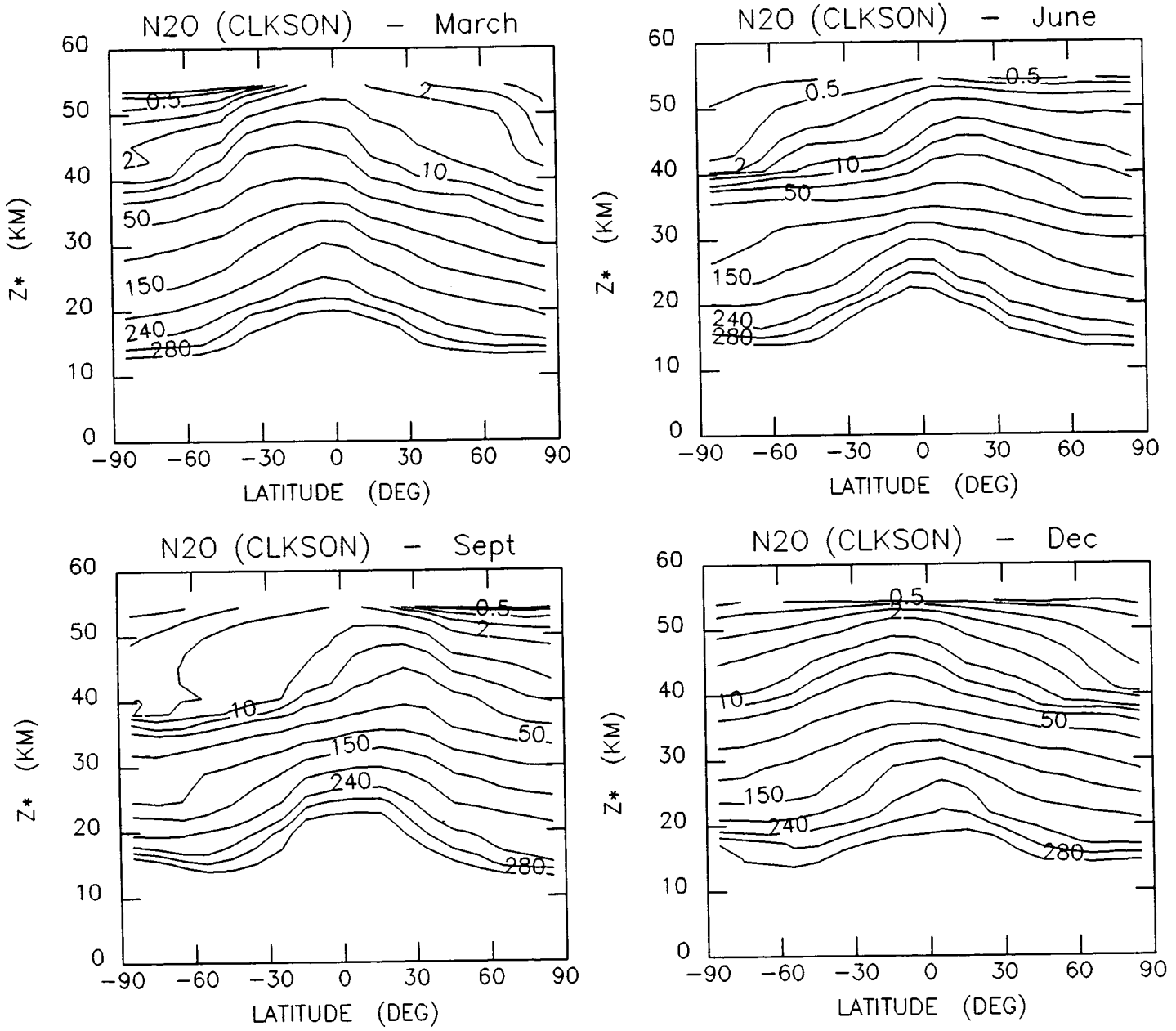
N2O (CLKSON) – March
N2O (CLKSON) – June
N2O (CLKSON) – Sept
N2O (CLKSON) – Dec
Z* (KM)
LATITUDE (DEG)
0.5
2
10
50
150
240
280
0
10
20
30
40
50
60
−90
−60
−30
0
30
60
90

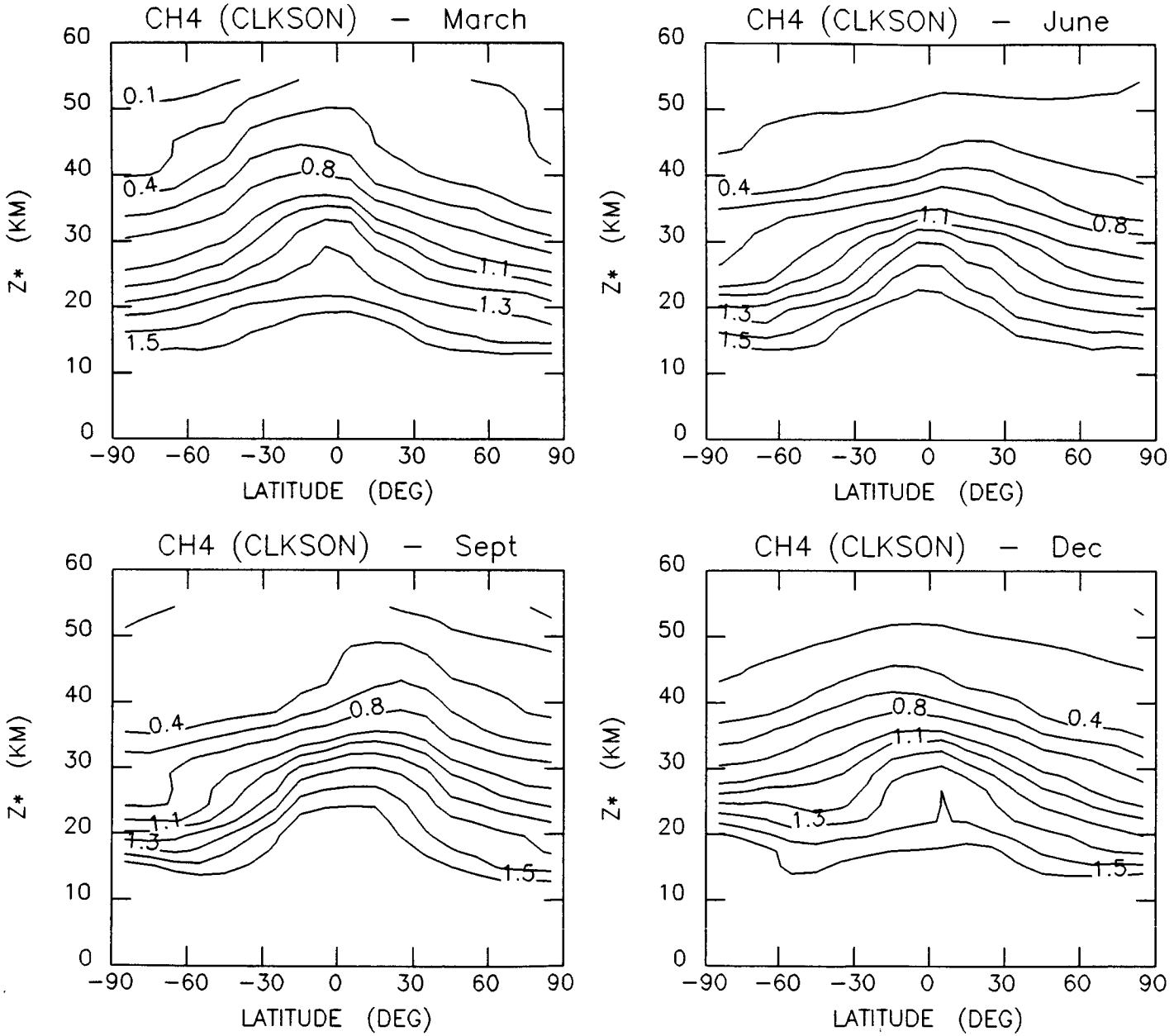
CH4 (CLKSON) – March
CH4 (CLKSON) – June
CH4 (CLKSON) – Sept
CH4 (CLKSON) – Dec
Z* (KM)
LATITUDE (DEG)
0
10
20
30
40
50
60
−90
−60
−30
0
30
60
90
0.1
0.4
0.8
1.1
1.3
1.5

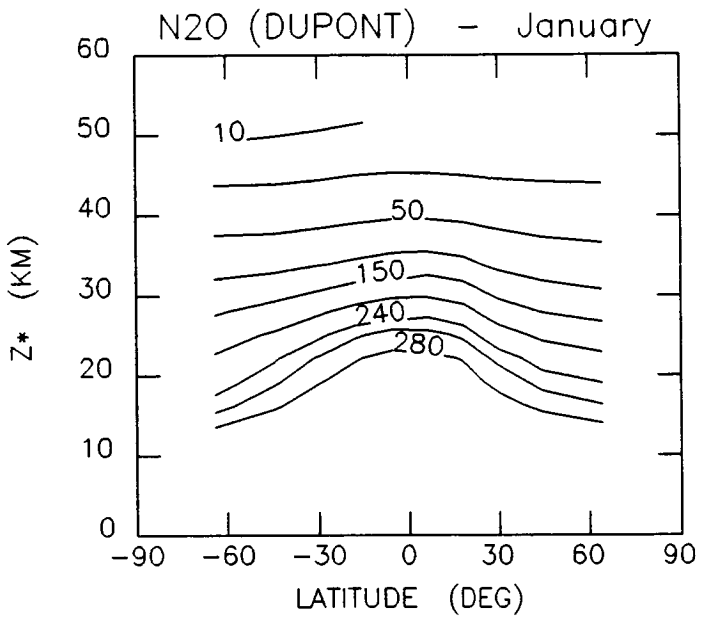
N2O (DUPONT) – January
Z* (KM)
LATITUDE (DEG)
10
50
150
240
280

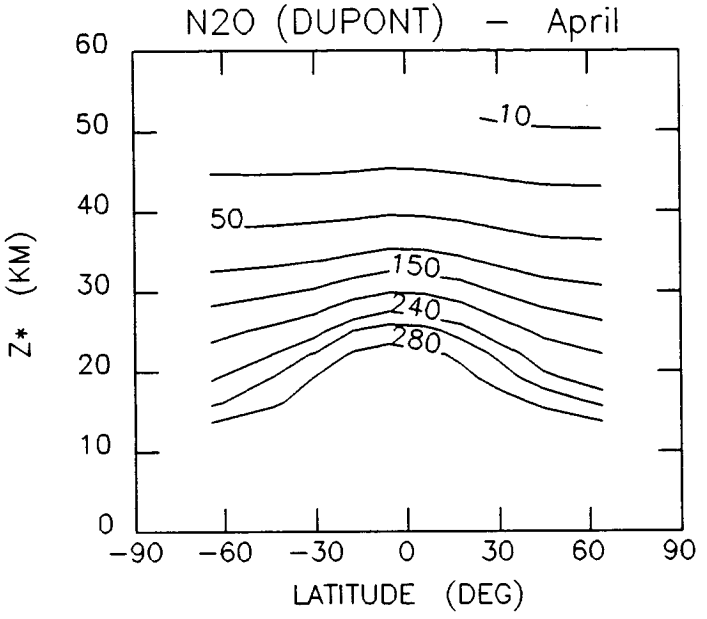
N2O (DUPONT) – April
Z* (KM)
LATITUDE (DEG)
10
50
150
240
280

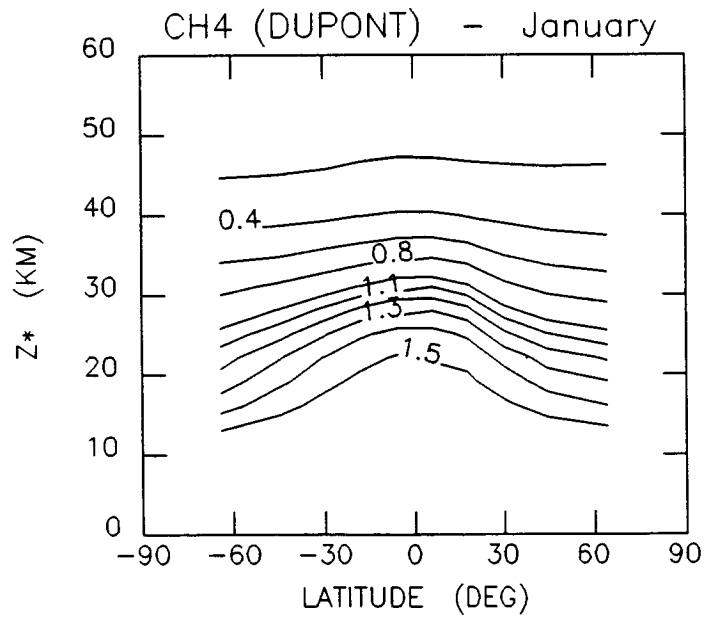
CH4 (DUPONT) – January
Z* (KM)
LATITUDE (DEG)
0.4
0.8
1.1
1.3
1.5

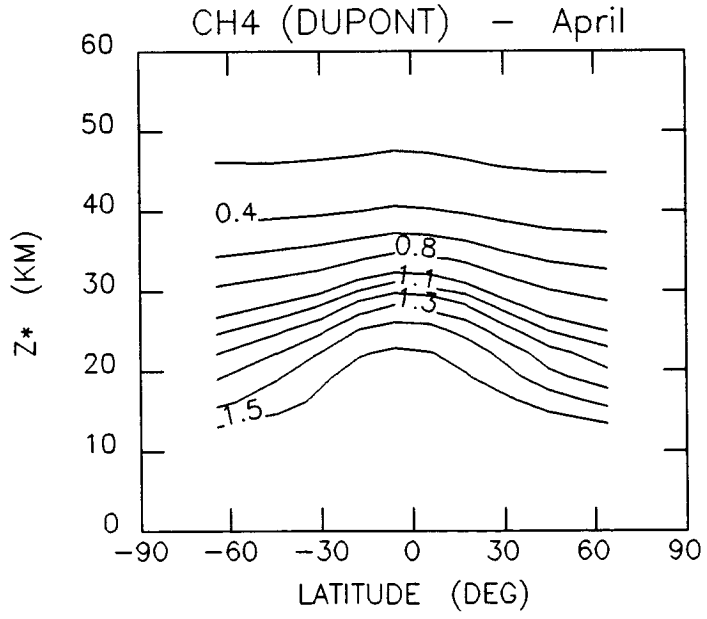
CH4 (DUPONT) – April
Z* (KM)
LATITUDE (DEG)
0.4
0.8
1.1
1.3
1.5

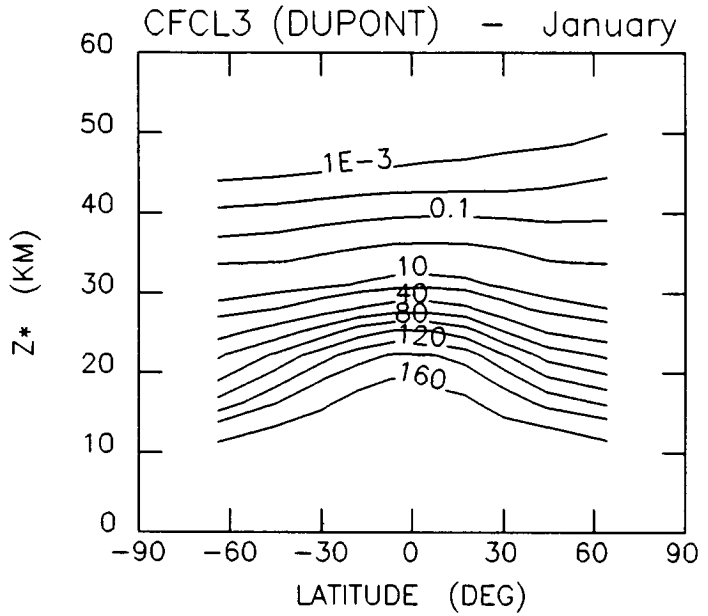
CFCL3 (DUPONT) – January
Z* (KM)
LATITUDE (DEG)
1E-3
0.1
10
40
80
120
160

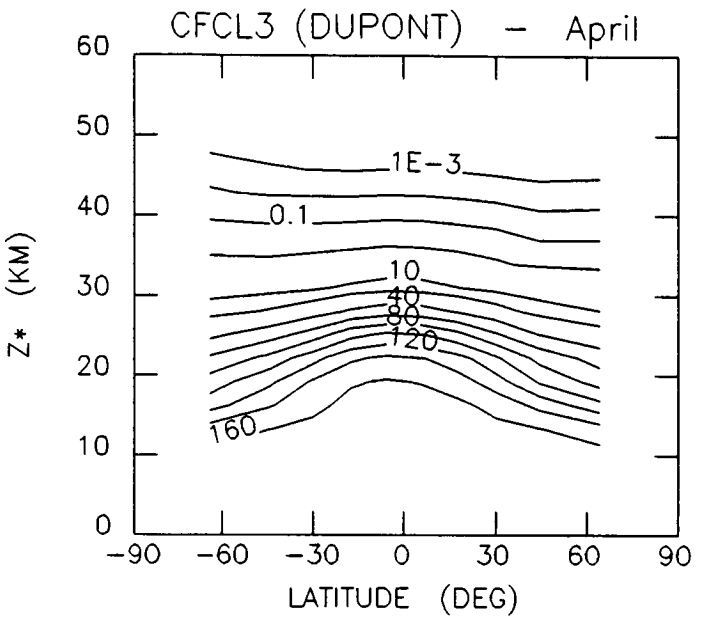
CFCL3 (DUPONT) – April
Z* (KM)
LATITUDE (DEG)
1E-3
0.1
10
40
80
120
160

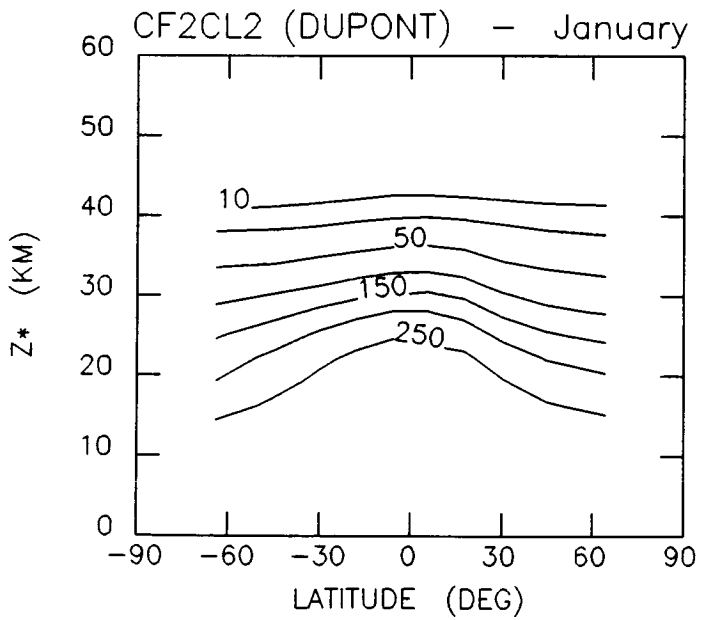
CF2CL2 (DUPONT) – January
Z* (KM)
LATITUDE (DEG)
10
50
150
250

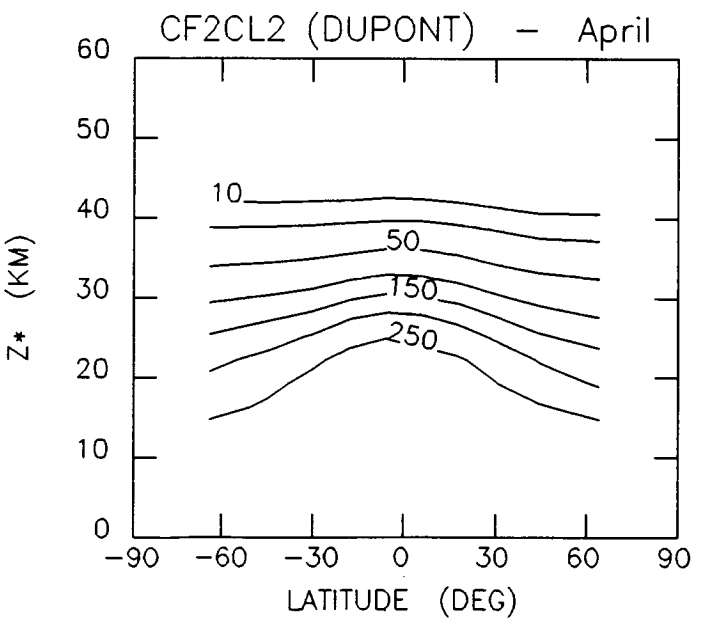
CF2CL2 (DUPONT) – April
Z* (KM)
LATITUDE (DEG)
10
50
150
250

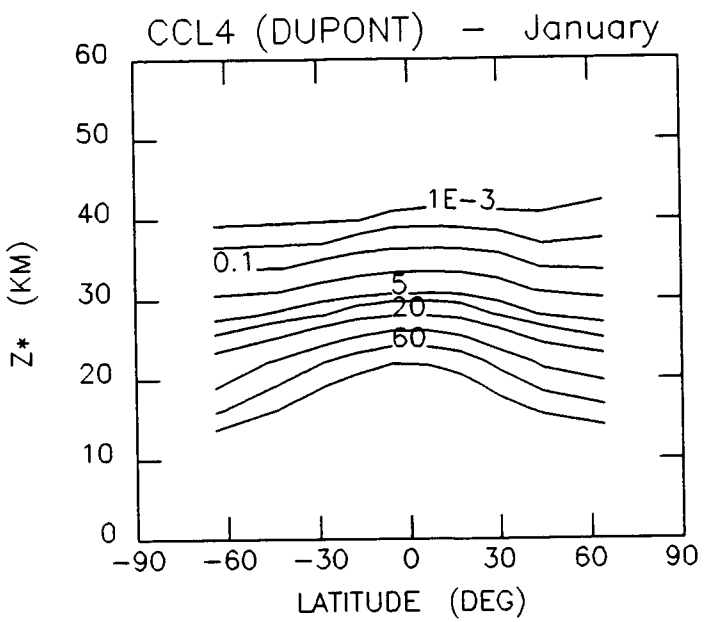
CCL4 (DUPONT) – January
Z* (KM)
LATITUDE (DEG)
1E-3
0.1
5
20
60

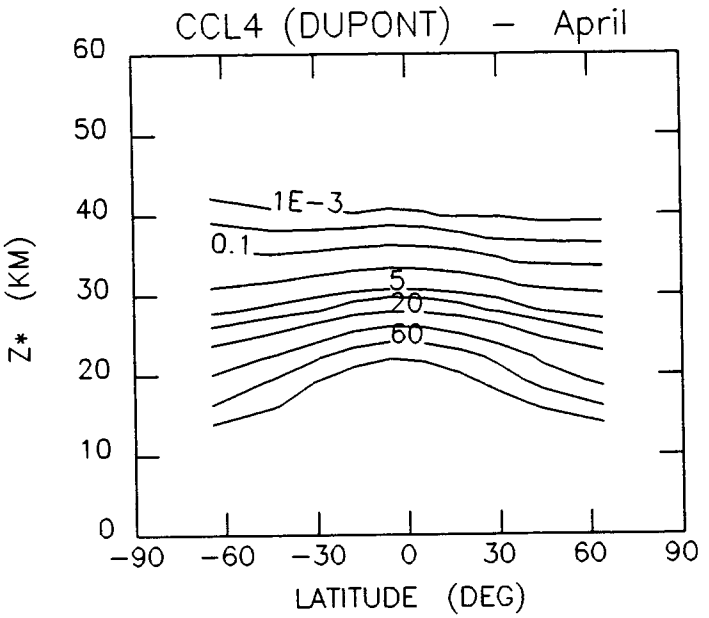
CCL4 (DUPONT) – April
Z* (KM)
LATITUDE (DEG)
1E-3
0.1
5
20
60

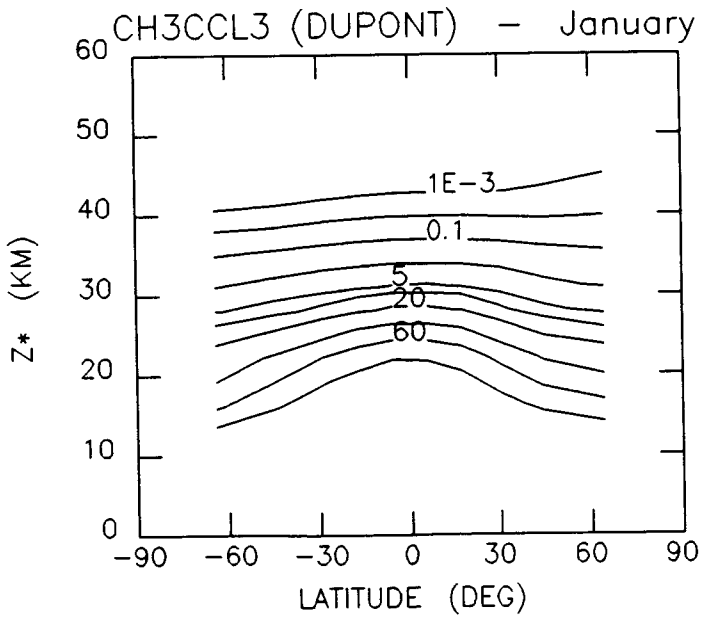
CH3CCL3 (DUPONT) – January
Z* (KM)
LATITUDE (DEG)
1E-3
0.1
5
20
60

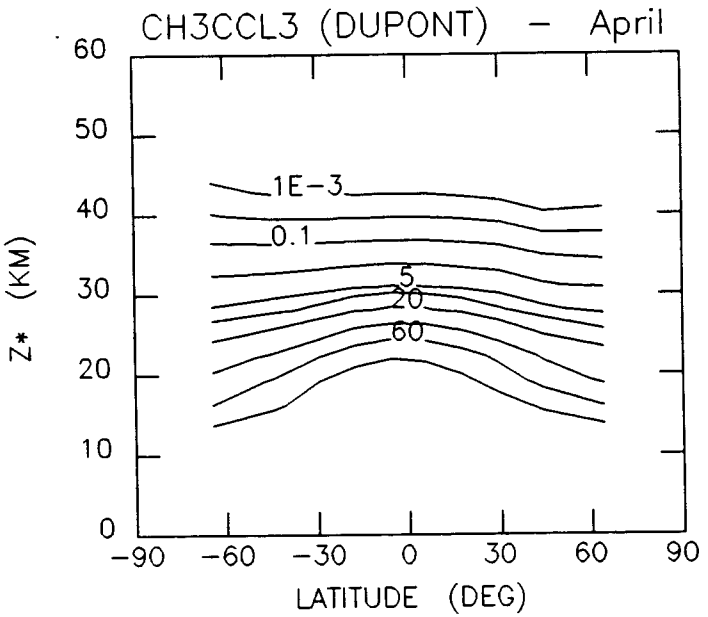
CH3CCL3 (DUPONT) – April
Z* (KM)
LATITUDE (DEG)
1E-3
0.1
5
20
60

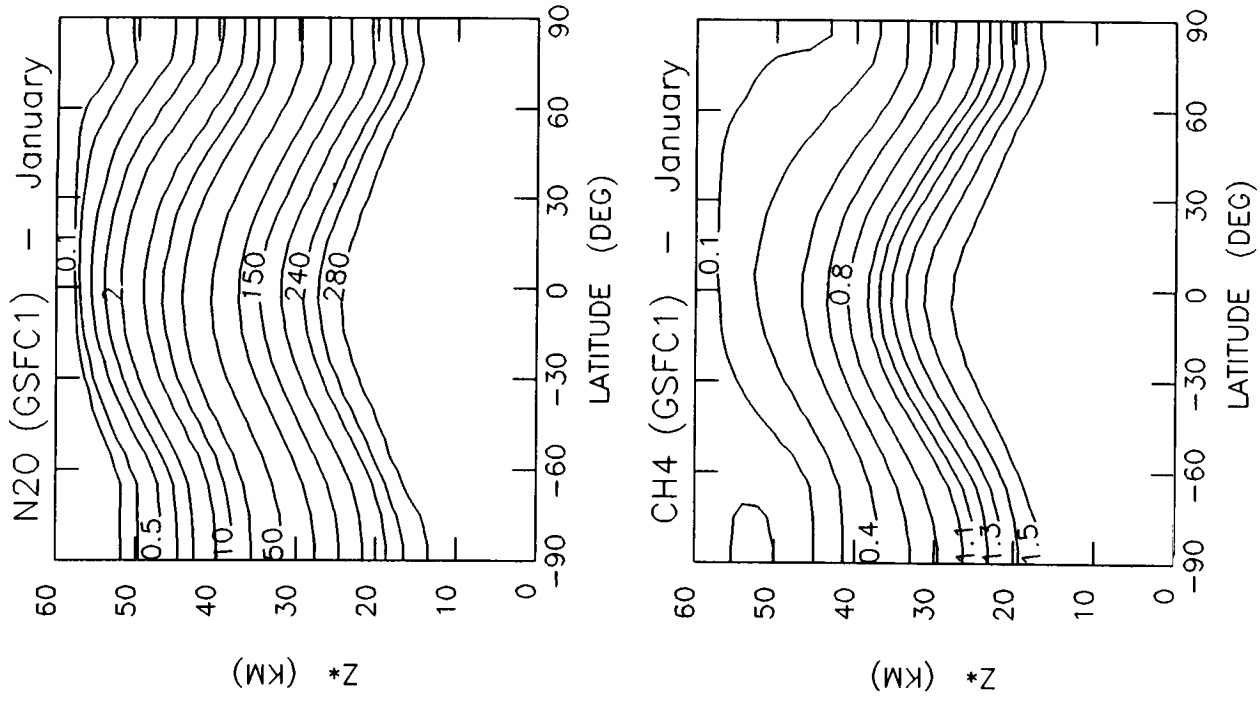
N2O (GSFC1) – January
0.1
2
0.5
10
50
150
240
280
60
50
40
30
20
10
0
Z* (KM)
-90
-60
-30
0
30
60
90
LATITUDE (DEG)
CH4 (GSFC1) – January
0.1
0.8
0.4
1.1
1.3
1.5
60
50
40
30
20
10
0
Z* (KM)
-90
-60
-30
0
30
60
90
LATITUDE (DEG)

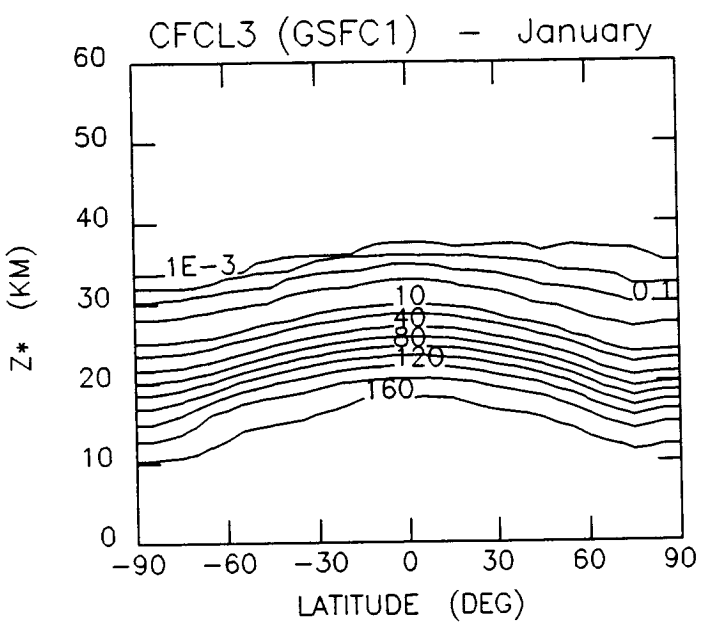
CFCL3 (GSFC1) – January
Z* (KM)
LATITUDE (DEG)
1E-3
0.1
10
40
80
120
160

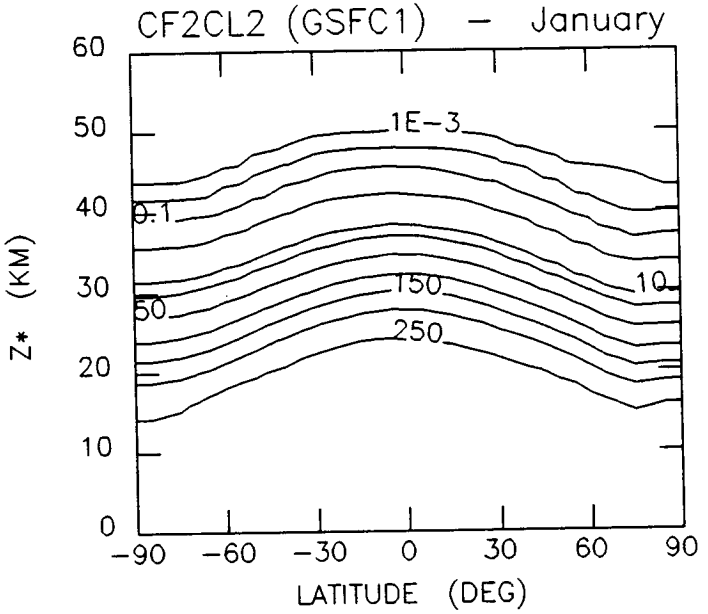
CF2CL2 (GSFC1) – January
Z* (KM)
LATITUDE (DEG)
1E-3
0.1
10
50
150
250

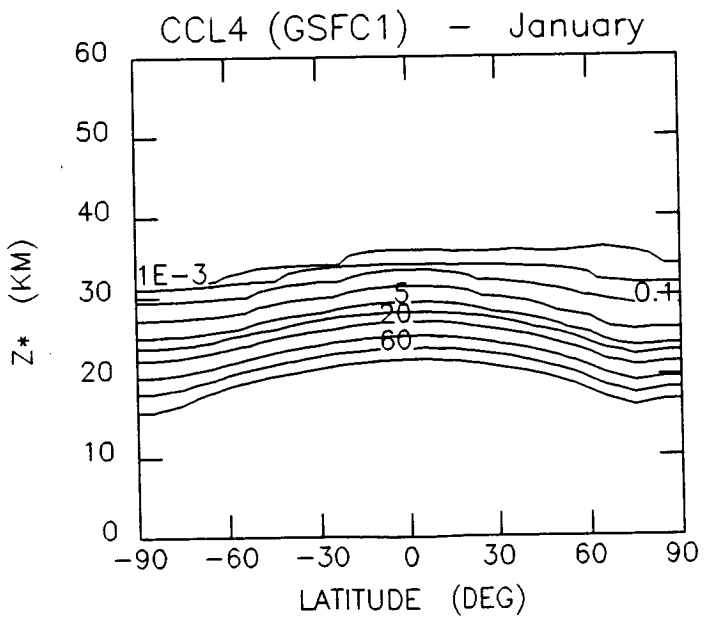
CCL4 (GSFC1) – January
Z* (KM)
LATITUDE (DEG)
1E-3
0.1
5
20
60

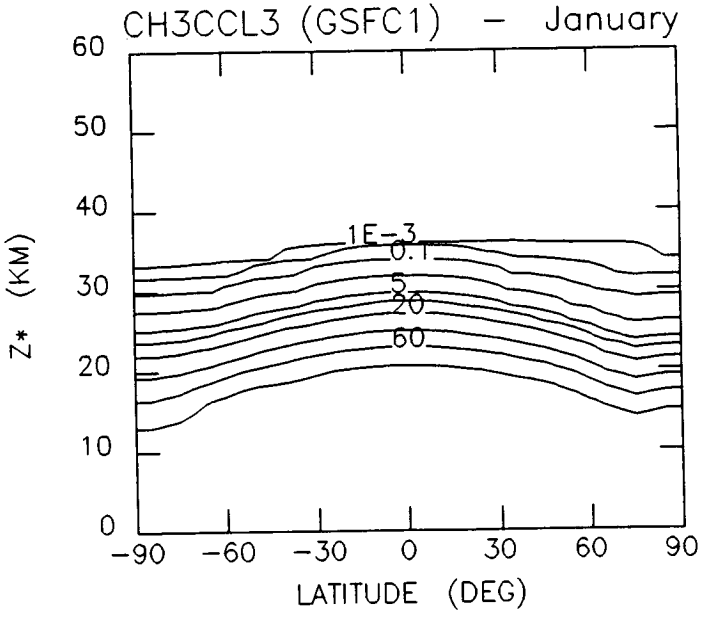
CH3CCL3 (GSFC1) – January
Z* (KM)
LATITUDE (DEG)
1E-3
0.1
5
20
60

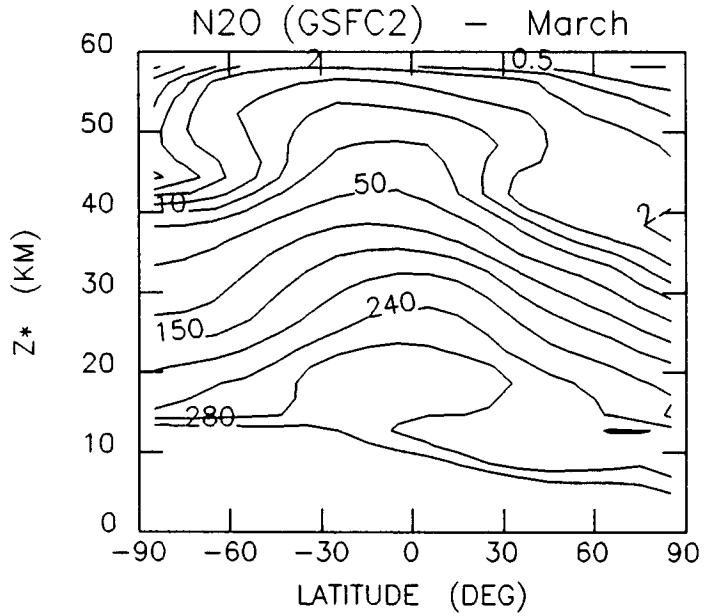
N2O (GSFC2) – March
Z* (KM)
LATITUDE (DEG)
0.5
2
10
50
150
240
280

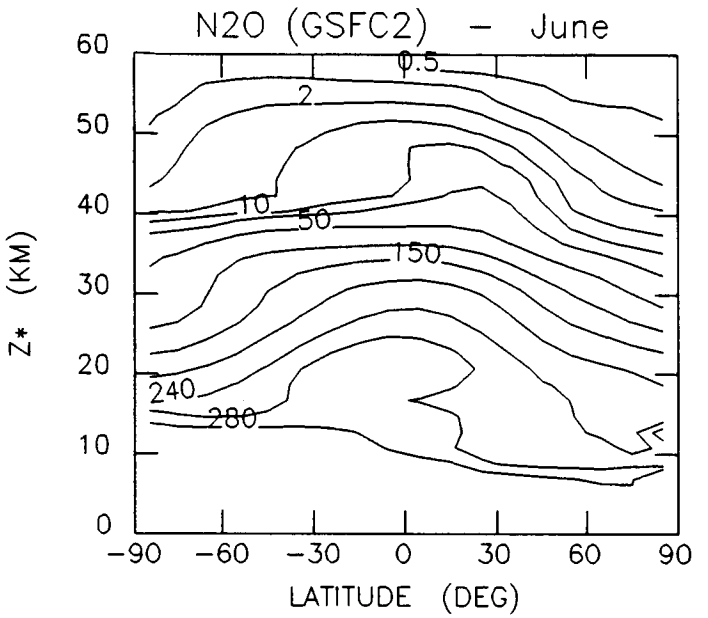
N2O (GSFC2) – June
Z* (KM)
LATITUDE (DEG)
0.5
2
10
50
150
240
280

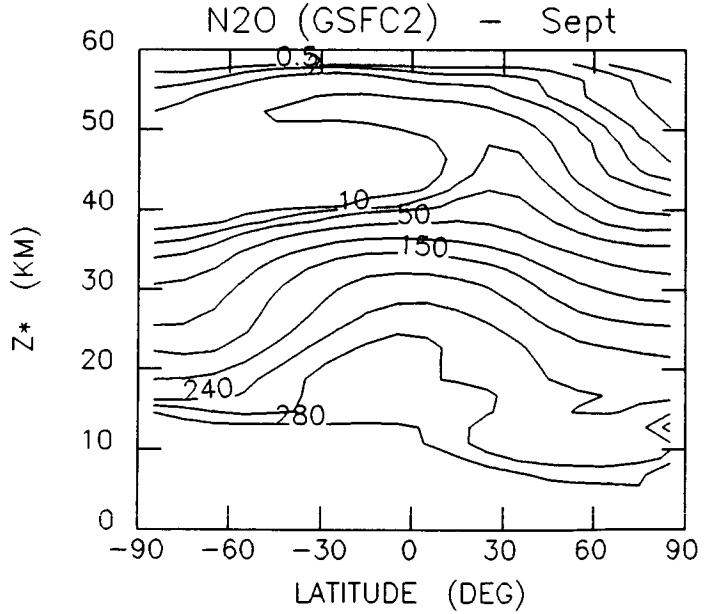
N2O (GSFC2) – Sept
Z* (KM)
LATITUDE (DEG)
0.5
10
50
150
240
280

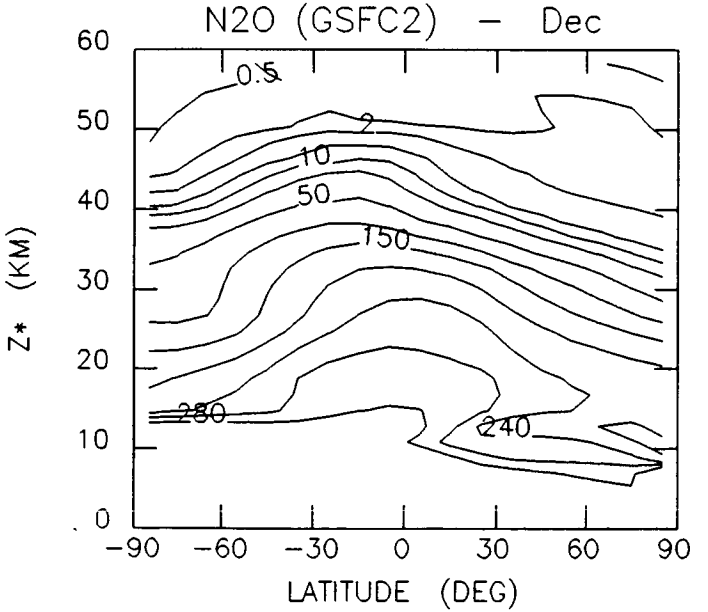
N2O (GSFC2) – Dec
Z* (KM)
LATITUDE (DEG)
0.5
2
10
50
150
240
280

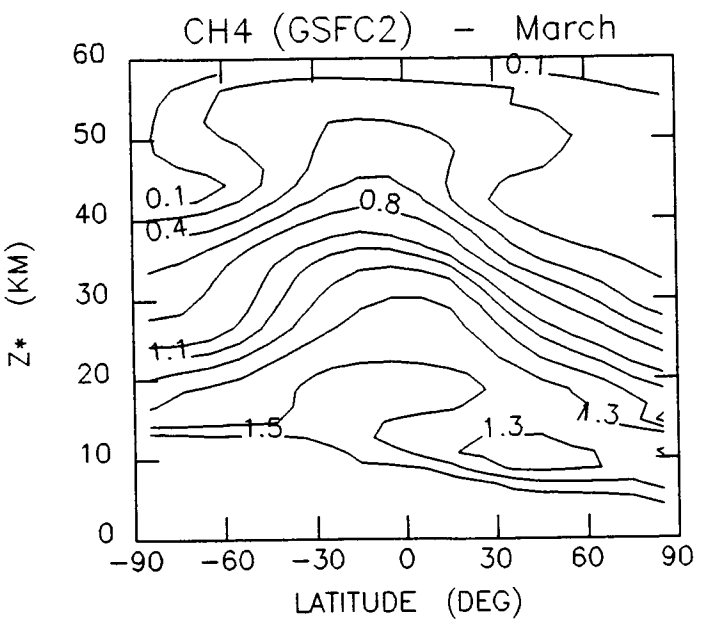
CH4 (GSFC2) – March
Z* (KM)
LATITUDE (DEG)
0.1
0.4
0.8
1.1
1.3
1.5

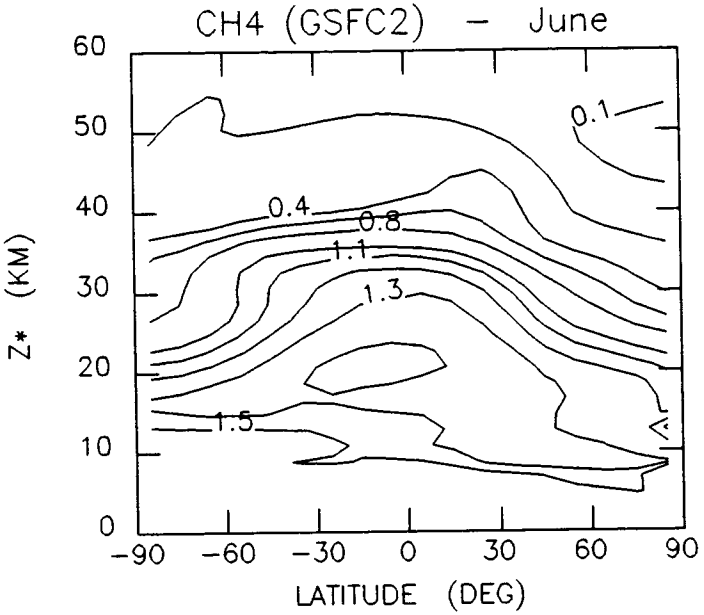
CH4 (GSFC2) – June
Z* (KM)
LATITUDE (DEG)
0.1
0.4
0.8
1.1
1.3
1.5

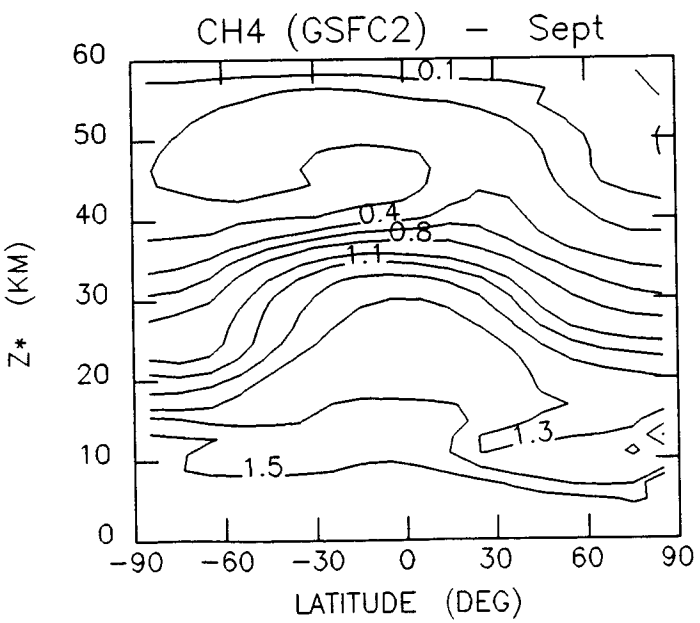
CH4 (GSFC2) – Sept
Z* (KM)
LATITUDE (DEG)
0.1
0.4
0.8
1.1
1.3
1.5

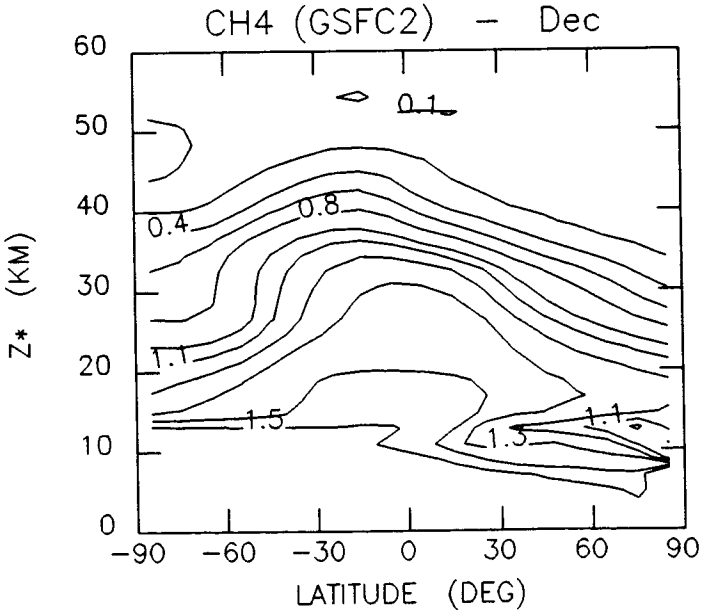
CH4 (GSFC2) – Dec
Z* (KM)
LATITUDE (DEG)
0.1
0.4
0.8
1.1
1.3
1.5

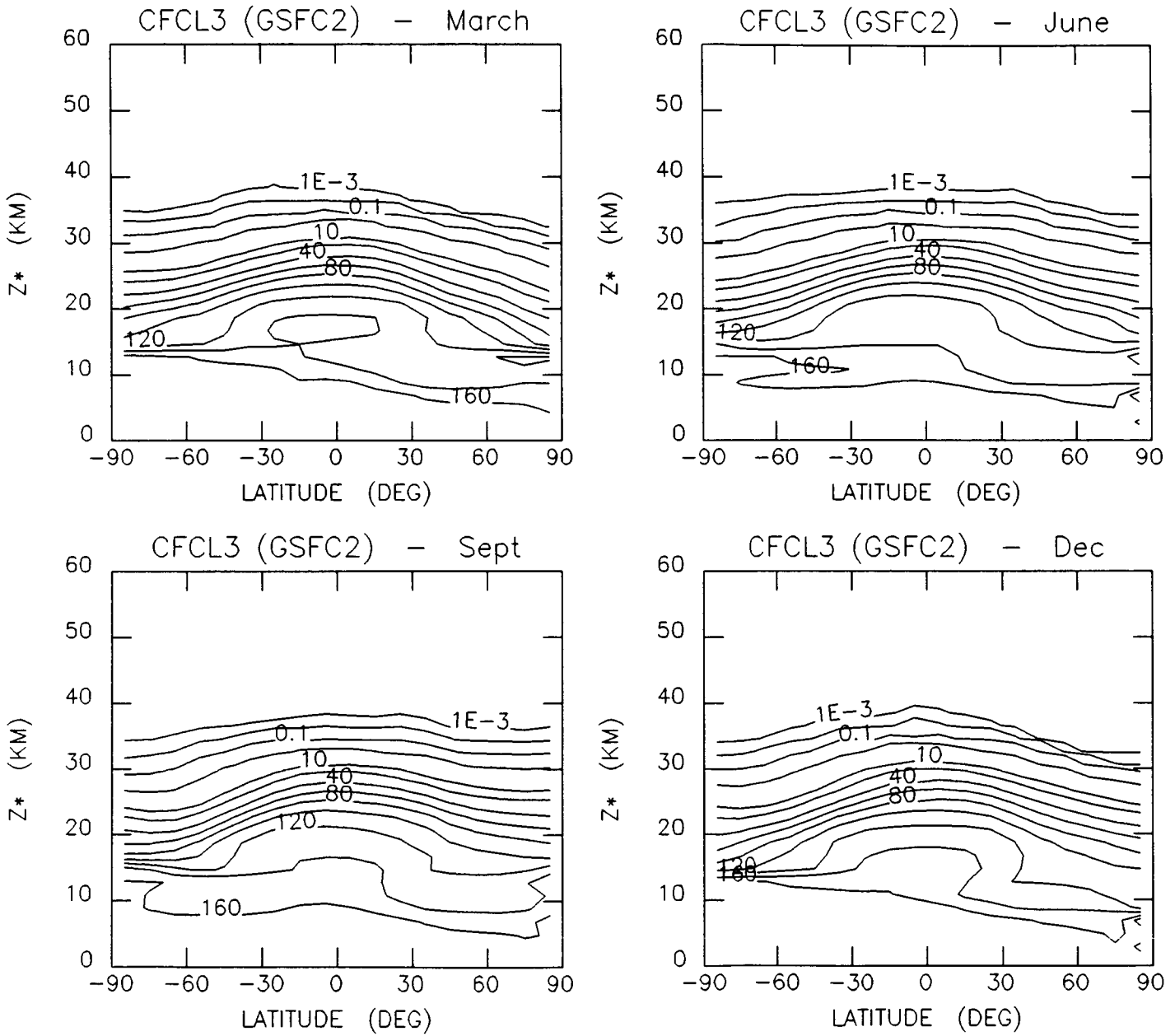
CFCL3 (GSFC2) – March
CFCL3 (GSFC2) – June
CFCL3 (GSFC2) – Sept
CFCL3 (GSFC2) – Dec
Z* (KM)
LATITUDE (DEG)
1E-3
0.1
10
40
80
120
160
0
10
20
30
40
50
60
-90
-60
-30
0
30
60
90

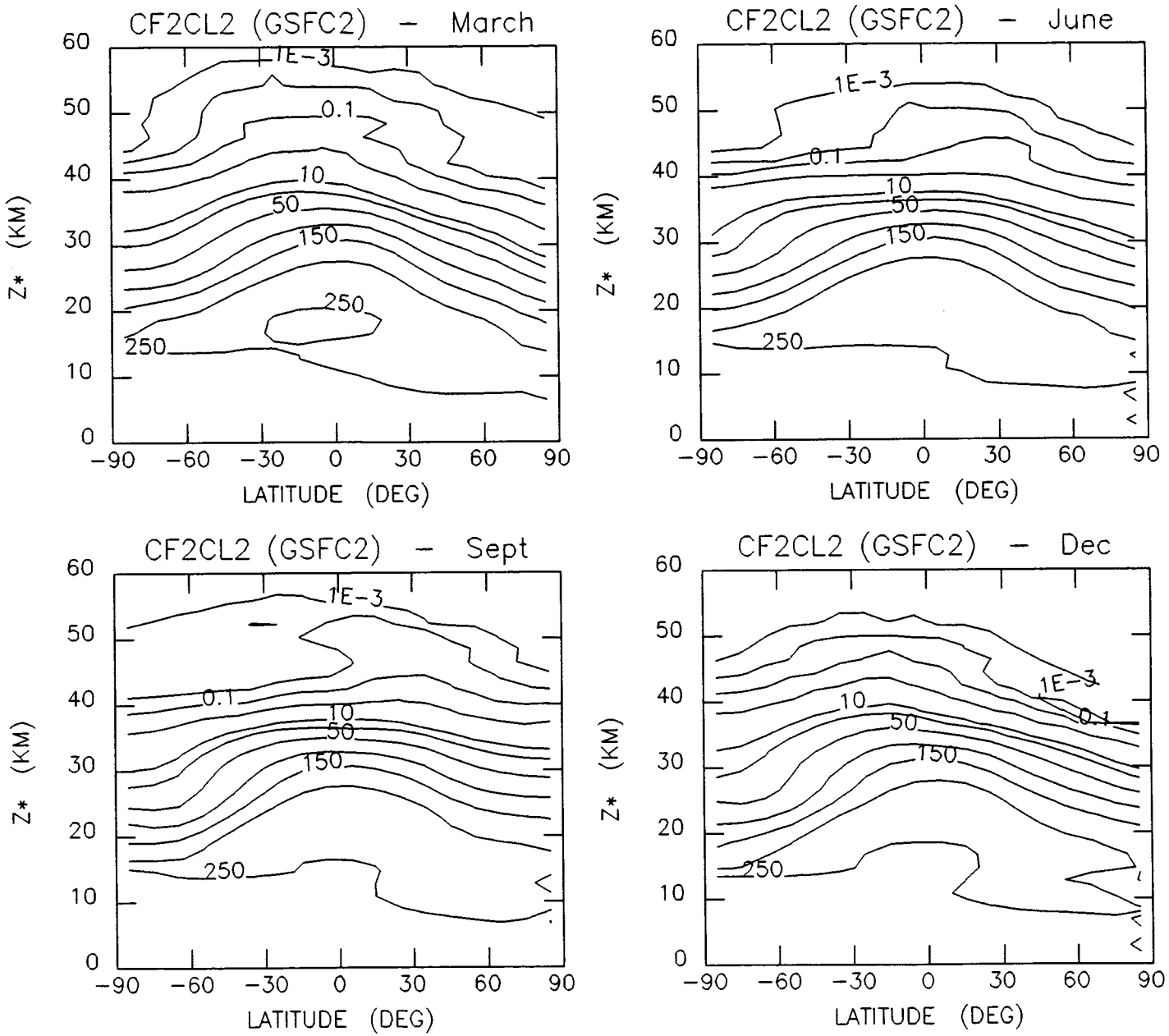
CF2CL2 (GSFC2) – March
CF2CL2 (GSFC2) – June
CF2CL2 (GSFC2) – Sept
CF2CL2 (GSFC2) – Dec
Z* (KM)
LATITUDE (DEG)
1E-3
0.1
10
50
150
250
0
10
20
30
40
50
60
-90
-60
-30
0
30
60
90

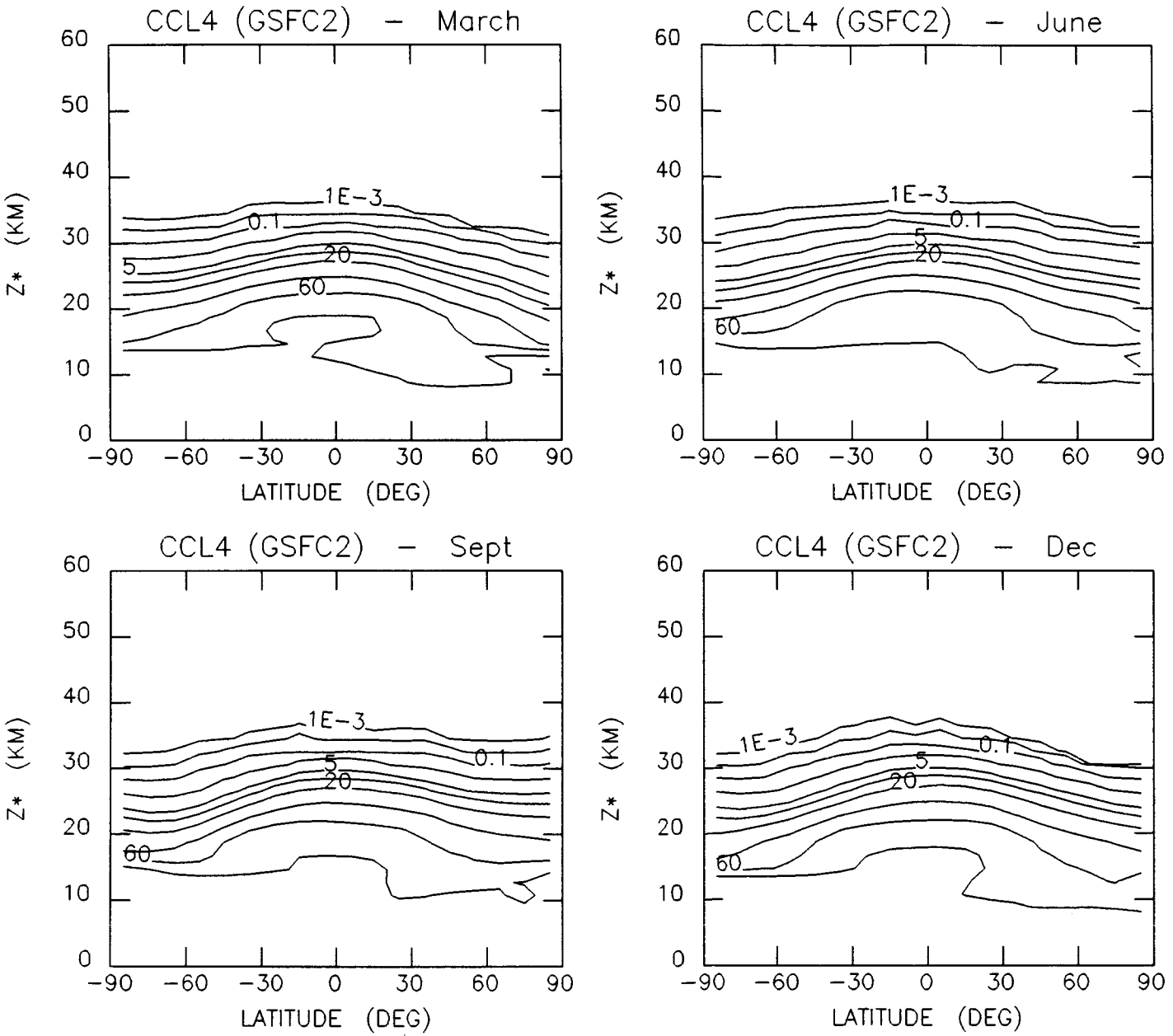
CCL4 (GSFC2) – March
CCL4 (GSFC2) – June
CCL4 (GSFC2) – Sept
CCL4 (GSFC2) – Dec
Z* (KM)
LATITUDE (DEG)
1E-3
0.1
5
20
60
0
10
20
30
40
50
60
-90
-60
-30
0
30
60
90

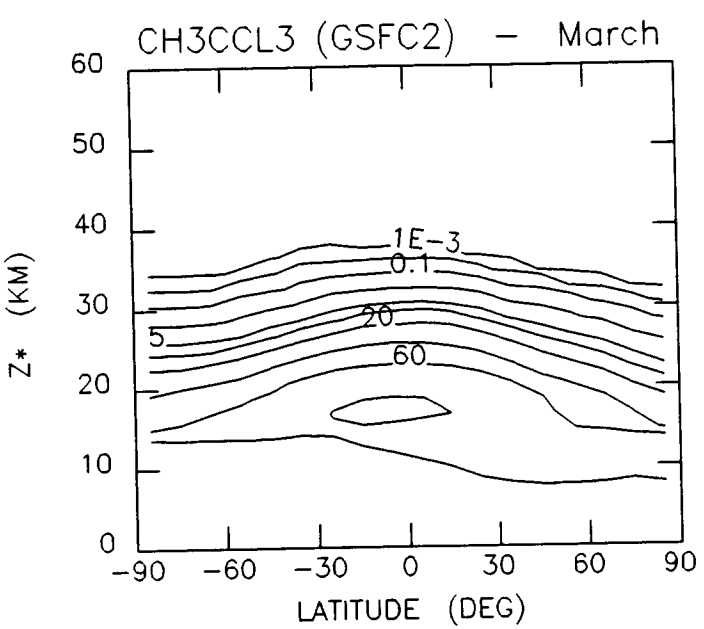
CH3CCL3 (GSFC2) – March
Z* (KM)
LATITUDE (DEG)
1E-3
0.1
5
20
60

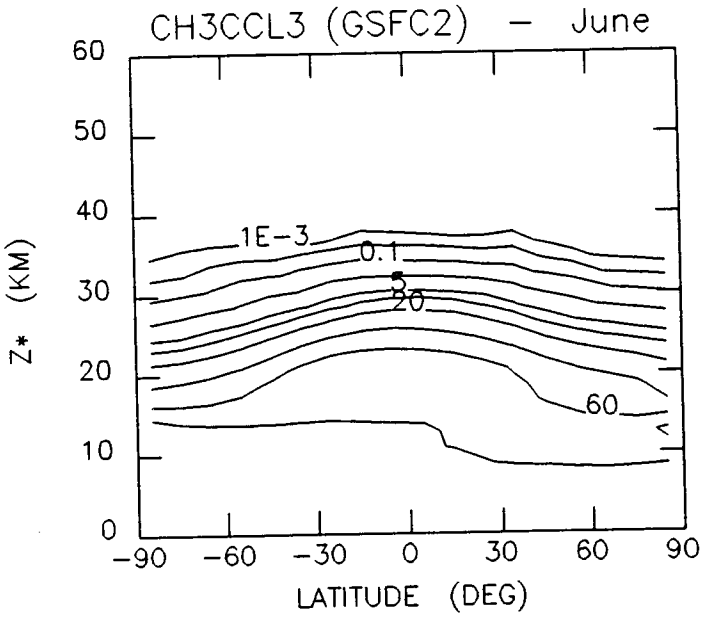
CH3CCL3 (GSFC2) – June
Z* (KM)
LATITUDE (DEG)
1E-3
0.1
5
20
60

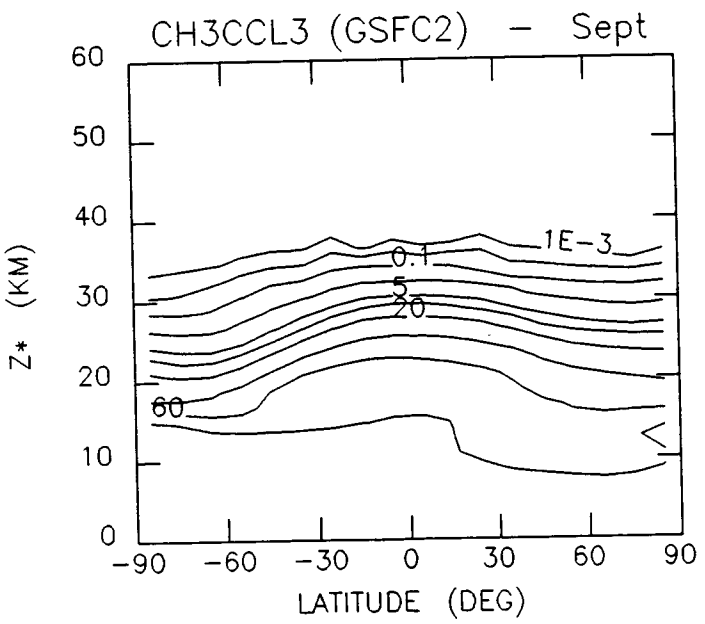
CH3CCL3 (GSFC2) – Sept
Z* (KM)
LATITUDE (DEG)
1E-3
0.1
5
20
60

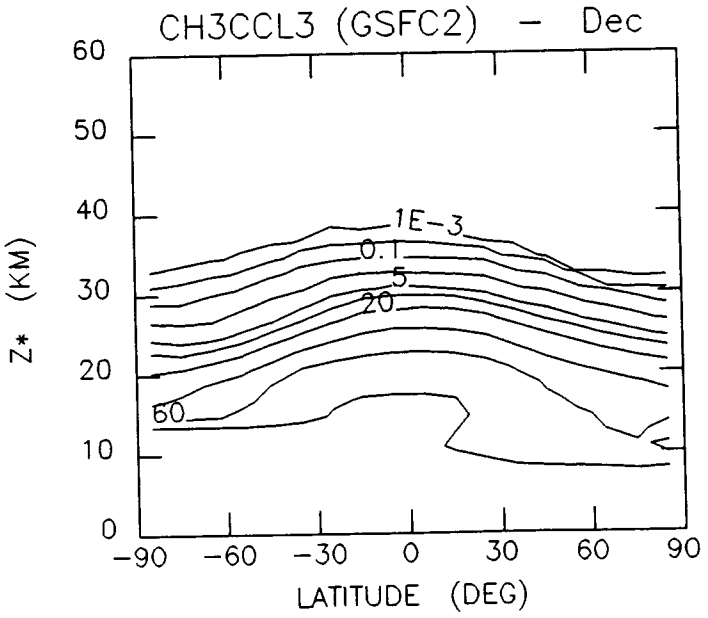
CH3CCL3 (GSFC2) – Dec
Z* (KM)
LATITUDE (DEG)
1E-3
0.1
5
20
60

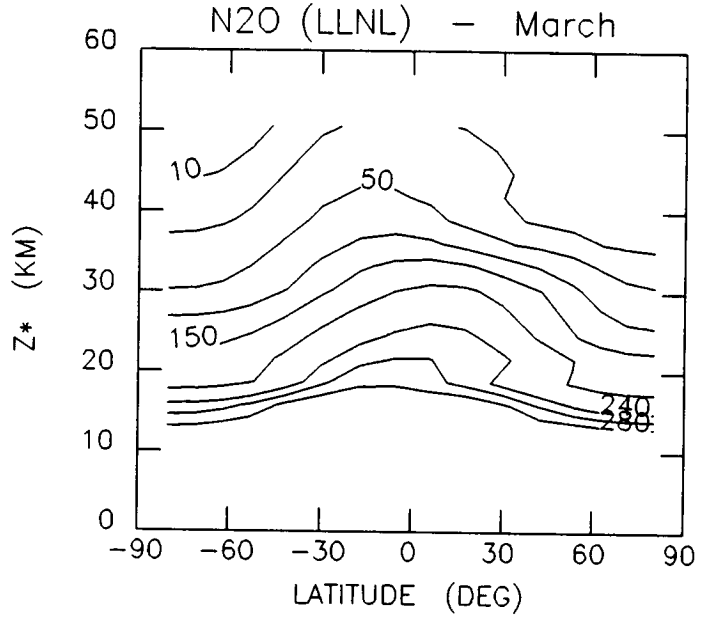
N2O (LLNL) – March
Z* (KM)
LATITUDE (DEG)
10
50
150
240
280

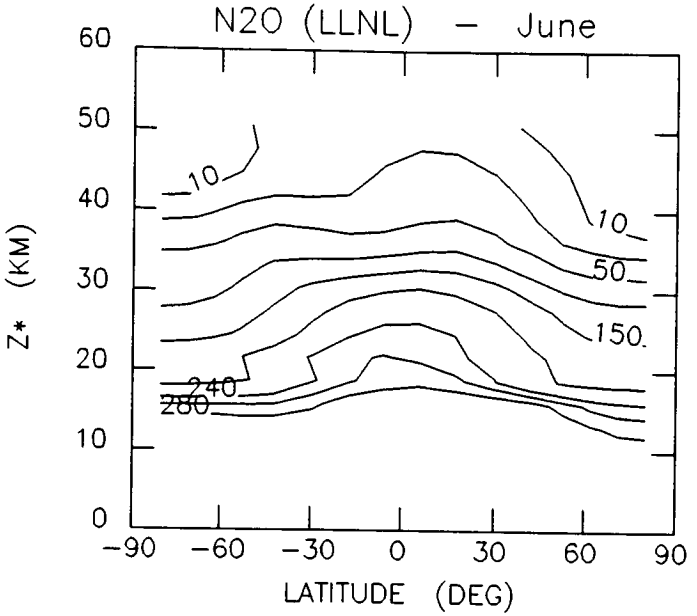
N2O (LLNL) – June
Z* (KM)
LATITUDE (DEG)
10
50
150
240
280

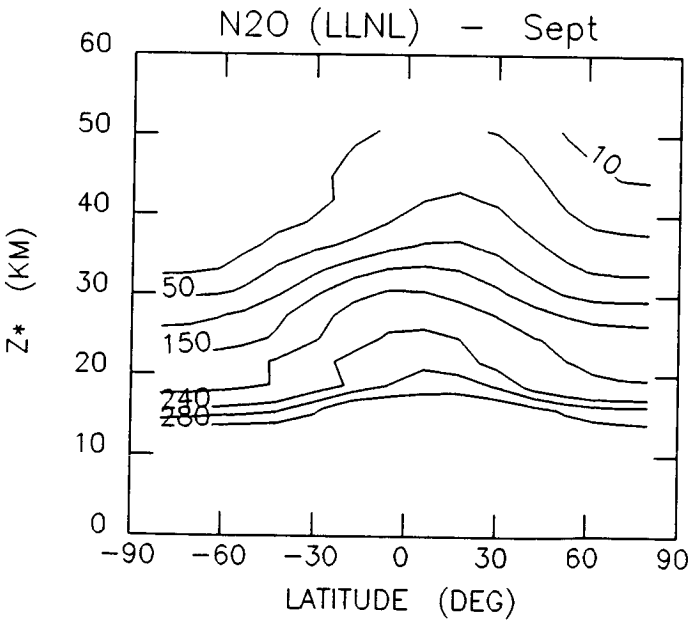
N2O (LLNL) – Sept
Z* (KM)
LATITUDE (DEG)
10
50
150
240
280

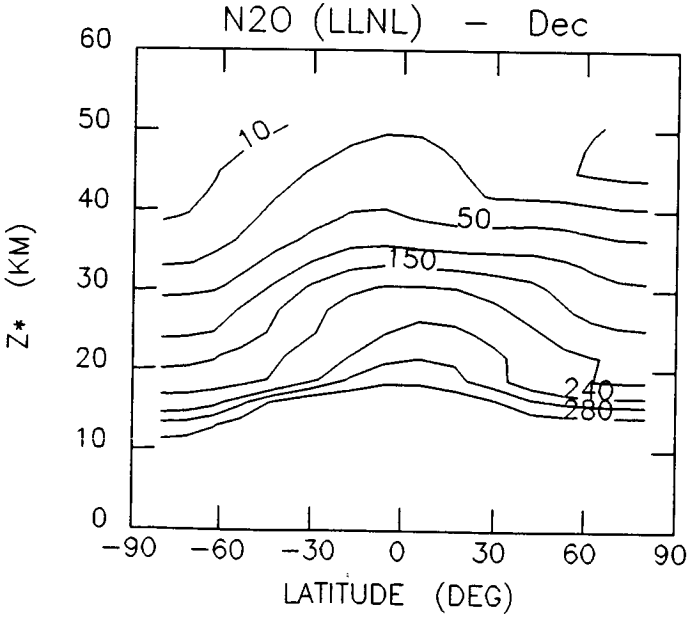
N2O (LLNL) – Dec
Z* (KM)
LATITUDE (DEG)
10
50
150
240
280

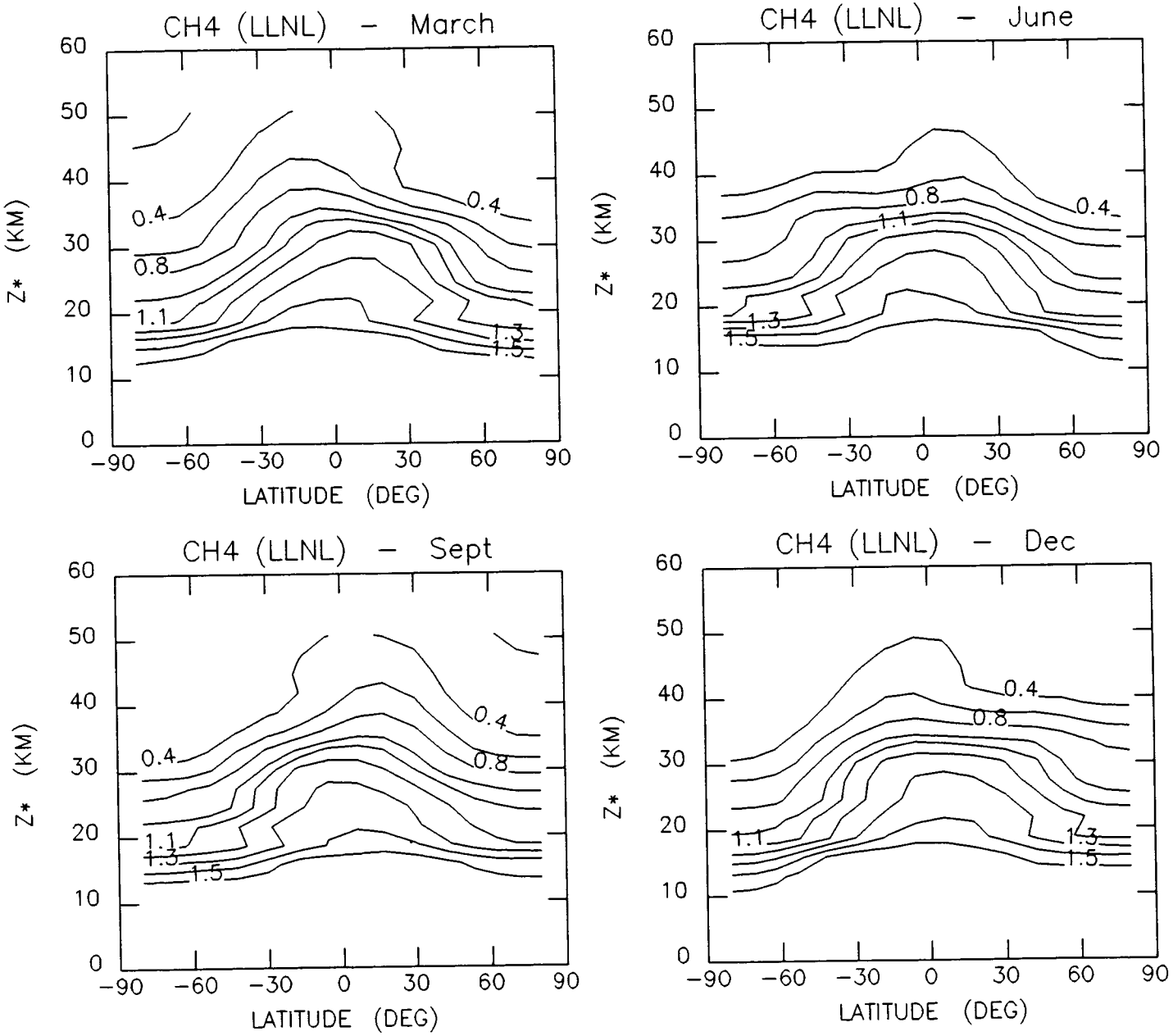
CH4 (LLNL) – March
CH4 (LLNL) – June
CH4 (LLNL) – Sept
CH4 (LLNL) – Dec
Z* (KM)
LATITUDE (DEG)
0
10
20
30
40
50
60
-90
-60
-30
0
30
60
90
0.4
0.8
1.1
1.3
1.5

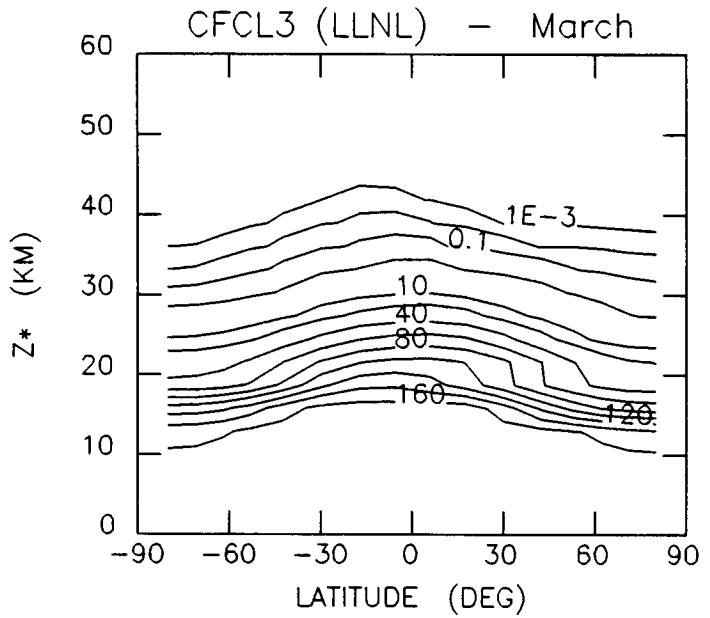
CFCL3 (LLNL) – March
Z* (KM)
LATITUDE (DEG)
1E-3
0.1
10
40
80
120
160

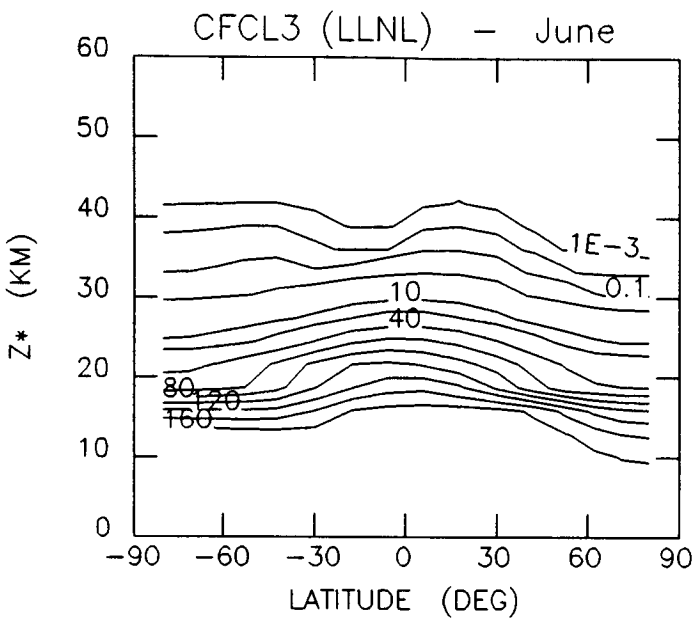
CFCL3 (LLNL) – June
Z* (KM)
LATITUDE (DEG)
1E-3
0.1
10
40
80
120
160

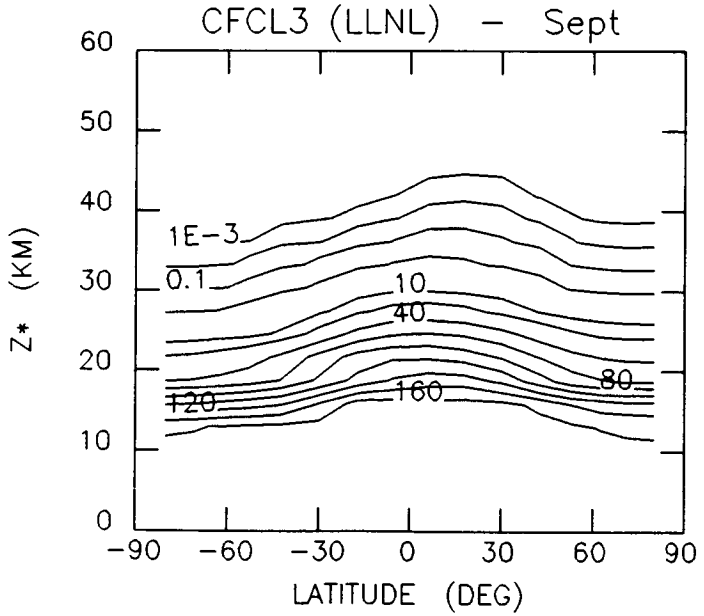
CFCL3 (LLNL) – Sept
Z* (KM)
LATITUDE (DEG)
1E-3
0.1
10
40
80
120
160

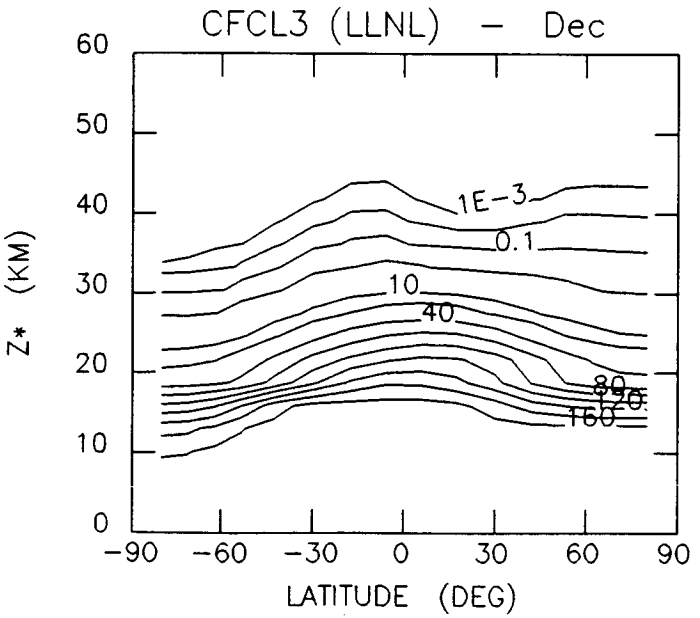
CFCL3 (LLNL) – Dec
Z* (KM)
LATITUDE (DEG)
1E-3
0.1
10
40
80
120
160

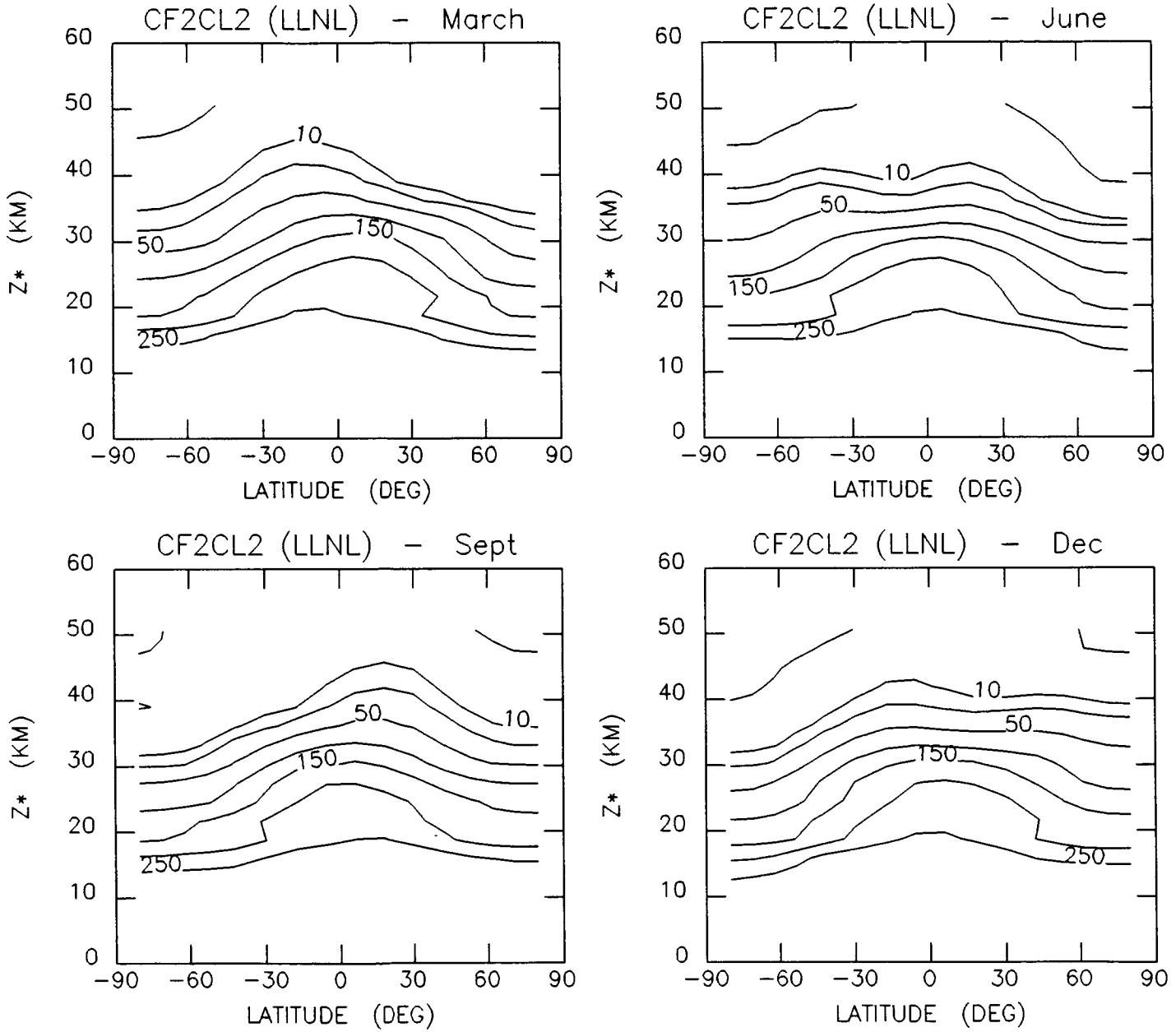
CF2CL2 (LLNL) – March
CF2CL2 (LLNL) – June
CF2CL2 (LLNL) – Sept
CF2CL2 (LLNL) – Dec
Z* (KM)
LATITUDE (DEG)
10
50
150
250
0
10
20
30
40
50
60
-90
-60
-30
0
30
60
90

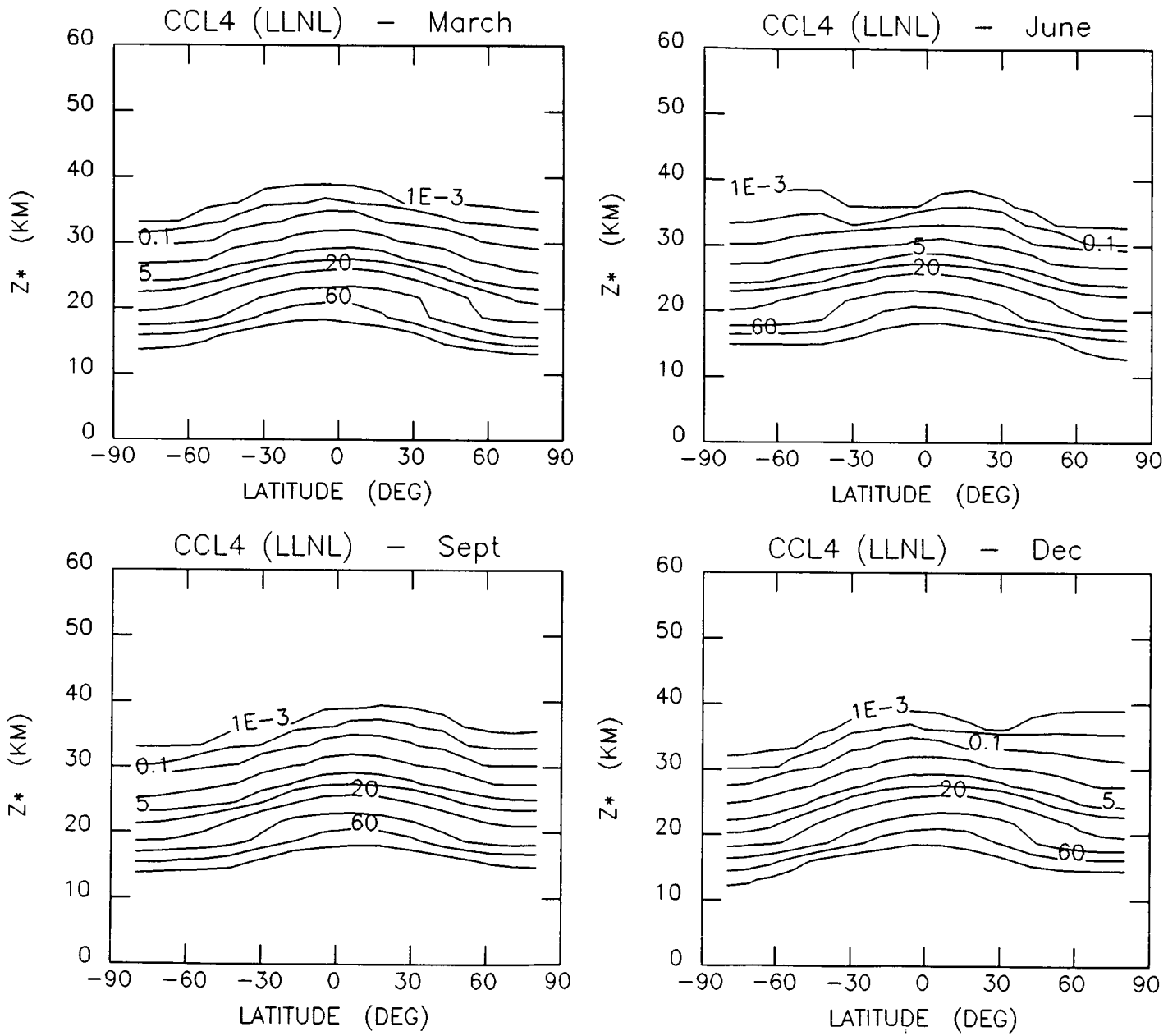
CCL4 (LLNL) – March
Z* (KM)
LATITUDE (DEG)
1E-3
0.1
5
20
60
CCL4 (LLNL) – June
CCL4 (LLNL) – Sept
CCL4 (LLNL) – Dec

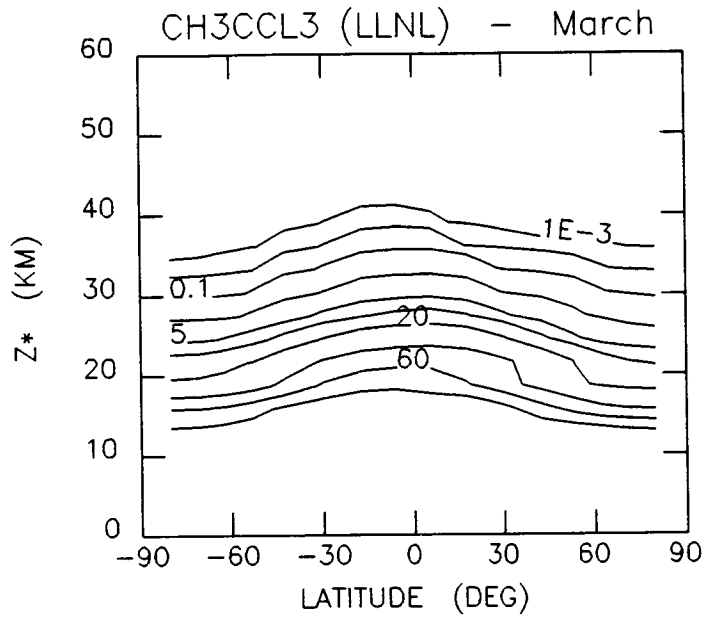
CH3CCL3 (LLNL) – March
Z* (KM)
LATITUDE (DEG)
1E-3
0.1
5
20
60

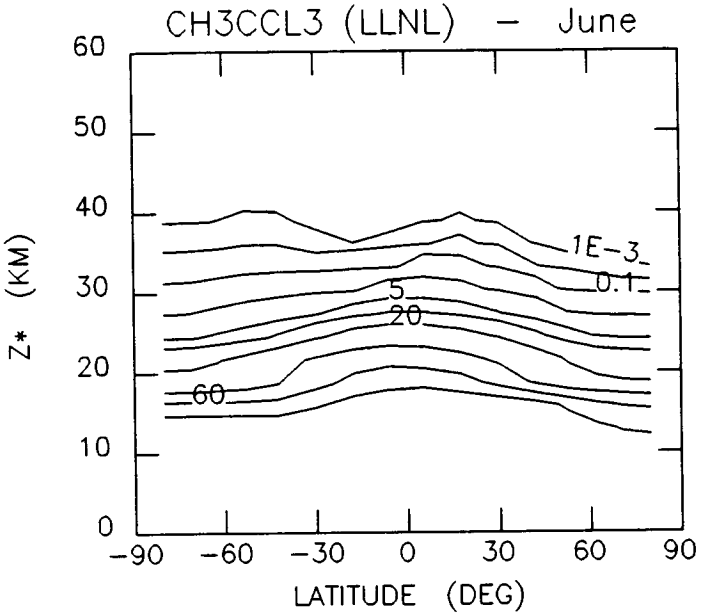
CH3CCL3 (LLNL) – June
Z* (KM)
LATITUDE (DEG)
1E-3
0.1
5
20
60

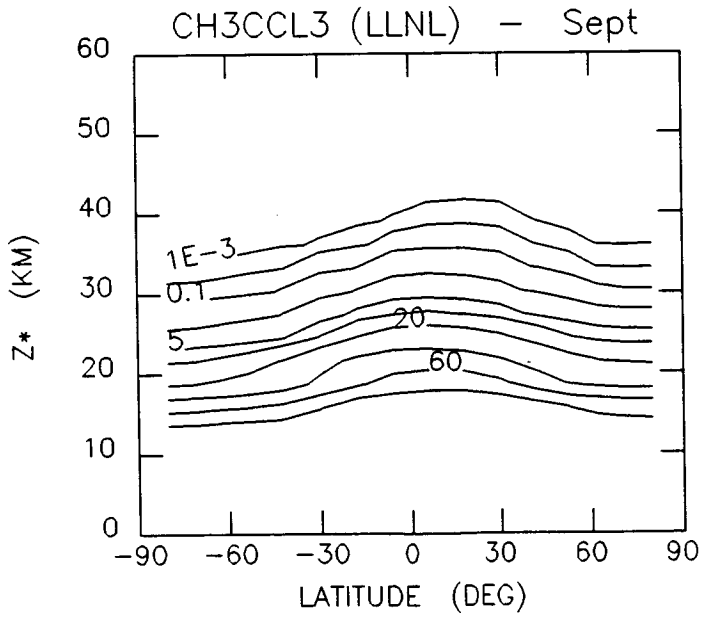
CH3CCL3 (LLNL) – Sept
Z* (KM)
LATITUDE (DEG)
1E-3
0.1
5
20
60

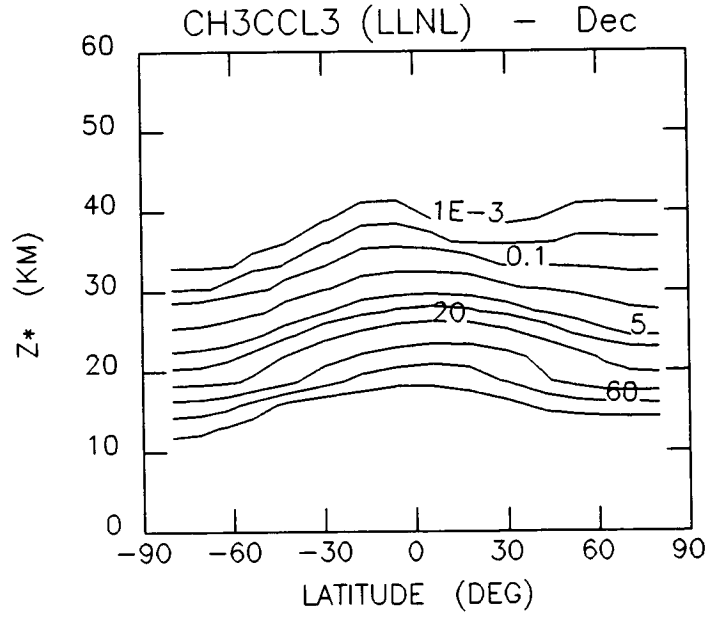
CH3CCL3 (LLNL) – Dec
Z* (KM)
LATITUDE (DEG)
1E-3
0.1
5
20
60

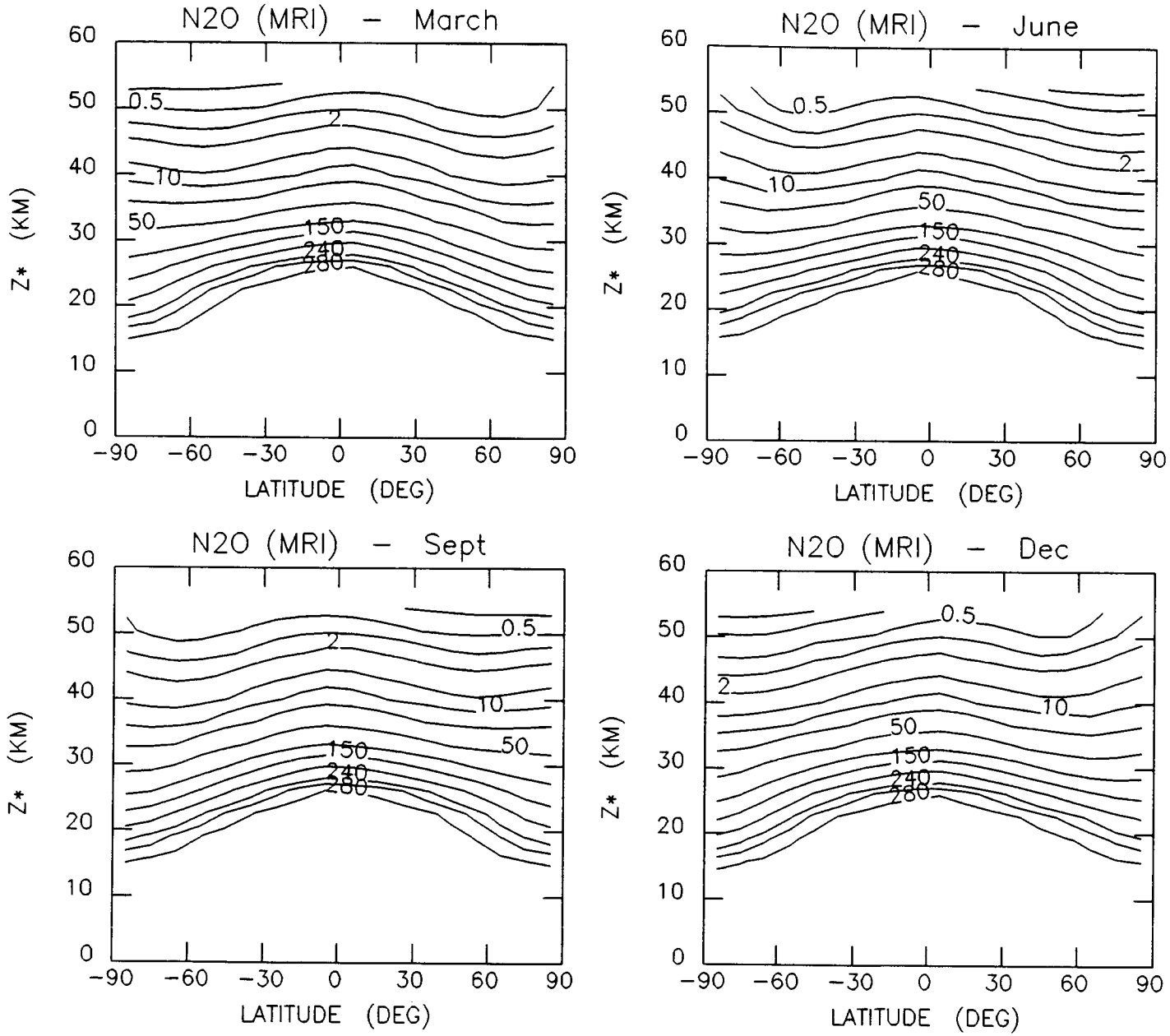
N2O (MRI) – March
N2O (MRI) – June
N2O (MRI) – Sept
N2O (MRI) – Dec
Z* (KM)
LATITUDE (DEG)
0.5
2
10
50
150
240
280
0
10
20
30
40
50
60
-90
-60
-30
0
30
60
90

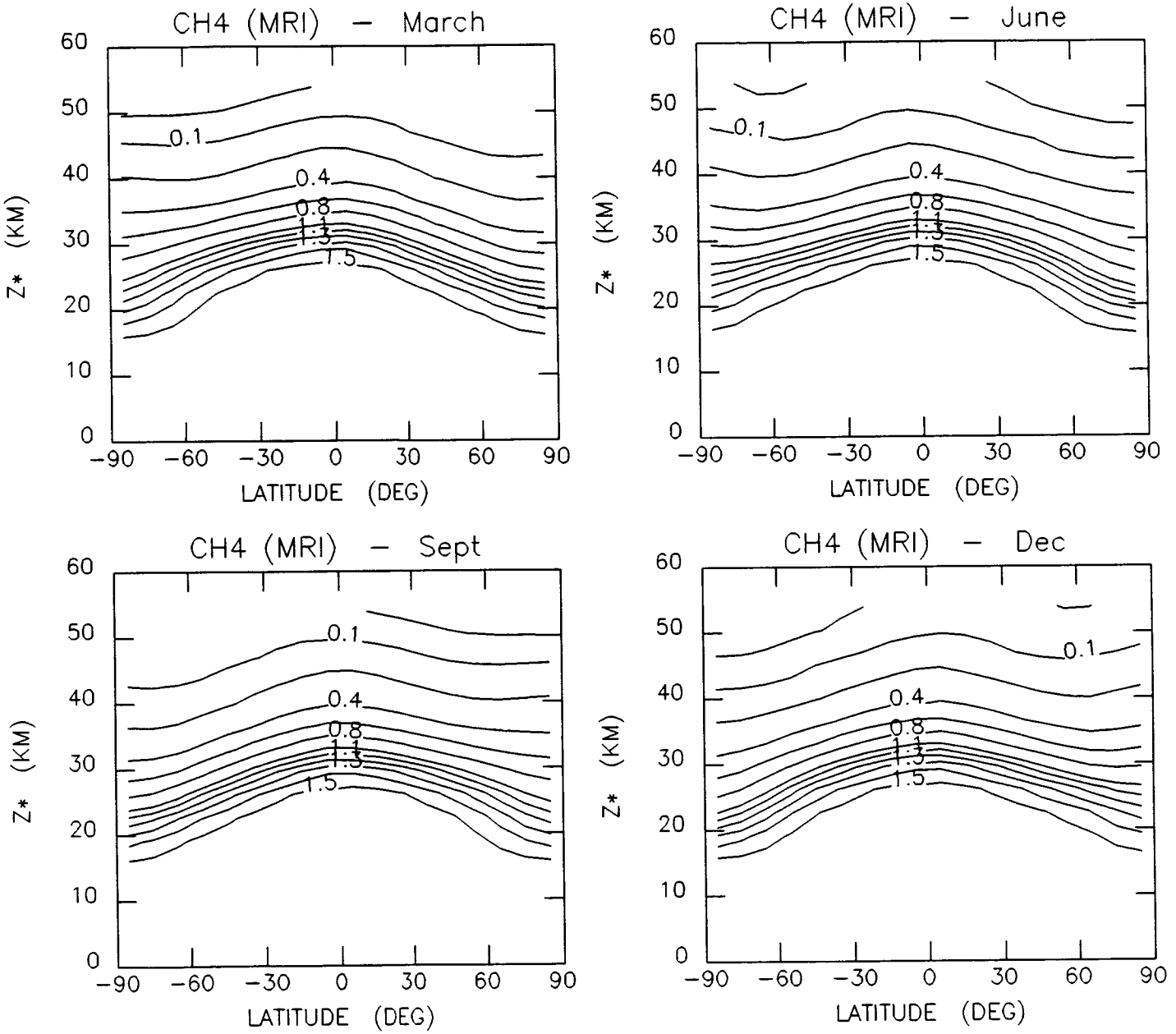
CH4 (MRI) – March
CH4 (MRI) – June
CH4 (MRI) – Sept
CH4 (MRI) – Dec
Z* (KM)
LATITUDE (DEG)
0.1
0.4
0.8
1.1
1.3
1.5
0
10
20
30
40
50
60
-90
-60
-30
0
30
60
90

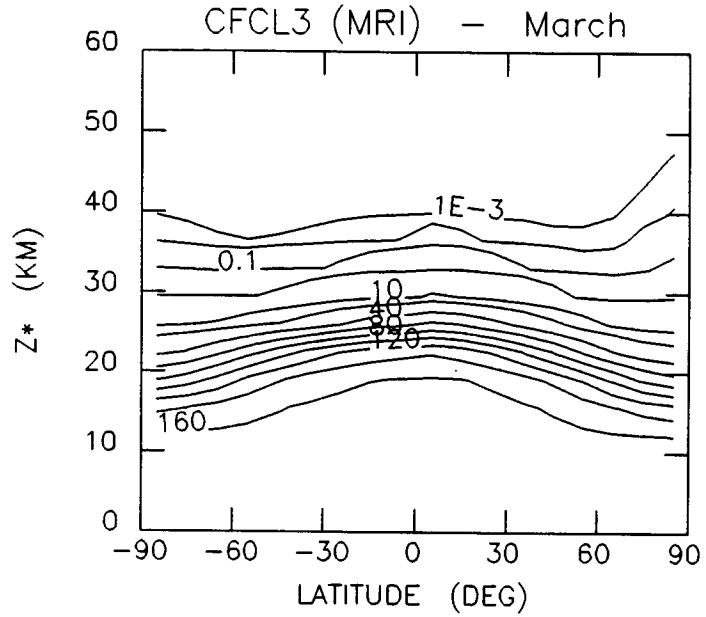
CFCL3 (MRI) – March
Z* (KM)
LATITUDE (DEG)
1E-3
0.1
10
40
80
120
160

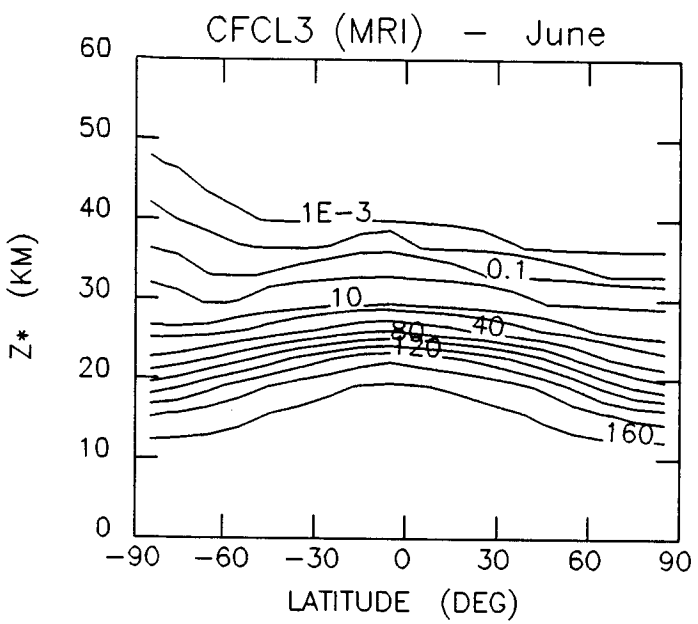
CFCL3 (MRI) – June
Z* (KM)
LATITUDE (DEG)
1E-3
0.1
10
40
80
120
160

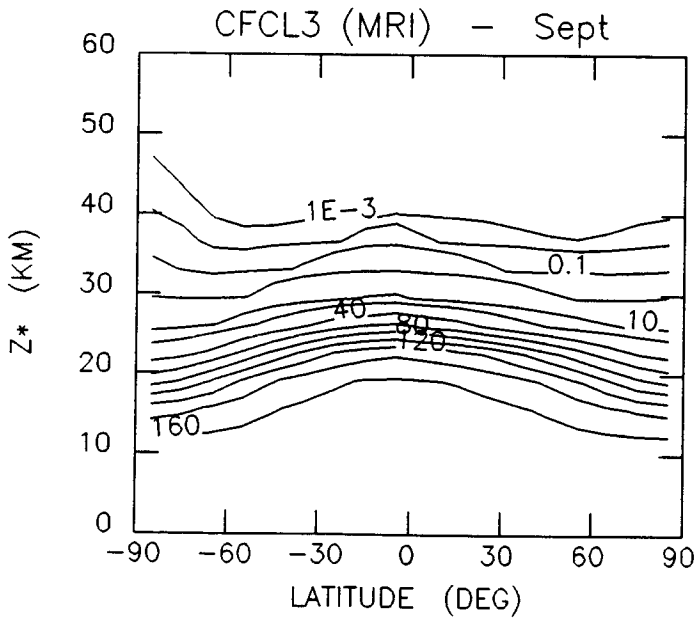
CFCL3 (MRI) – Sept
Z* (KM)
LATITUDE (DEG)
1E-3
0.1
10
40
80
120
160

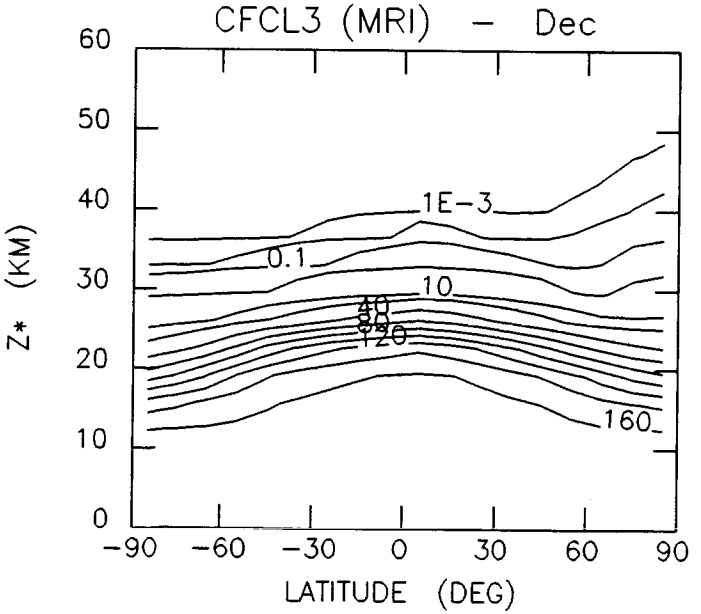
CFCL3 (MRI) – Dec
Z* (KM)
LATITUDE (DEG)
1E-3
0.1
10
40
80
120
160

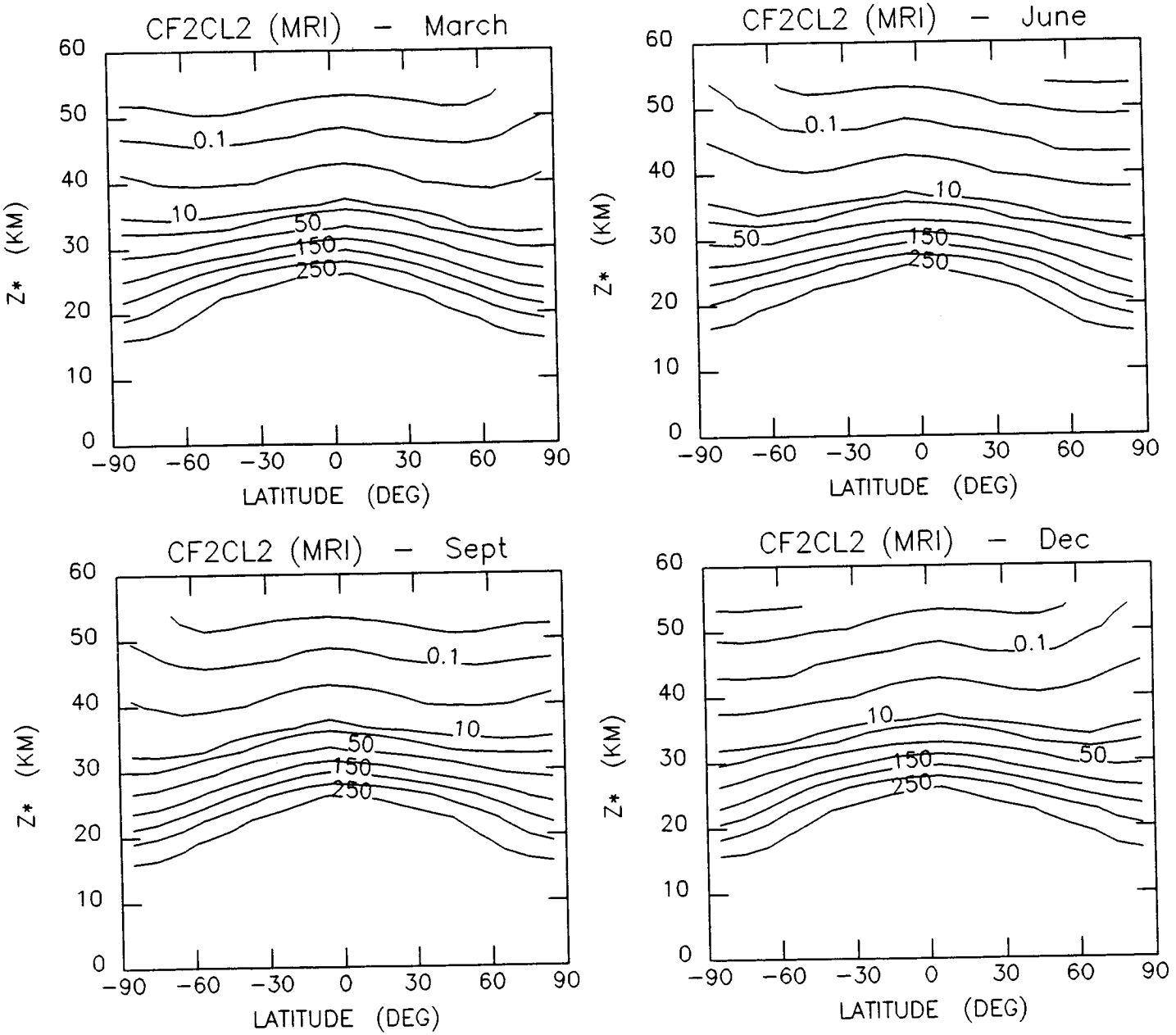
CF2CL2 (MRI) – March
CF2CL2 (MRI) – June
CF2CL2 (MRI) – Sept
CF2CL2 (MRI) – Dec
Z* (KM)
LATITUDE (DEG)
0.1
10
50
150
250
0
10
20
30
40
50
60
-90
-60
-30
0
30
60
90

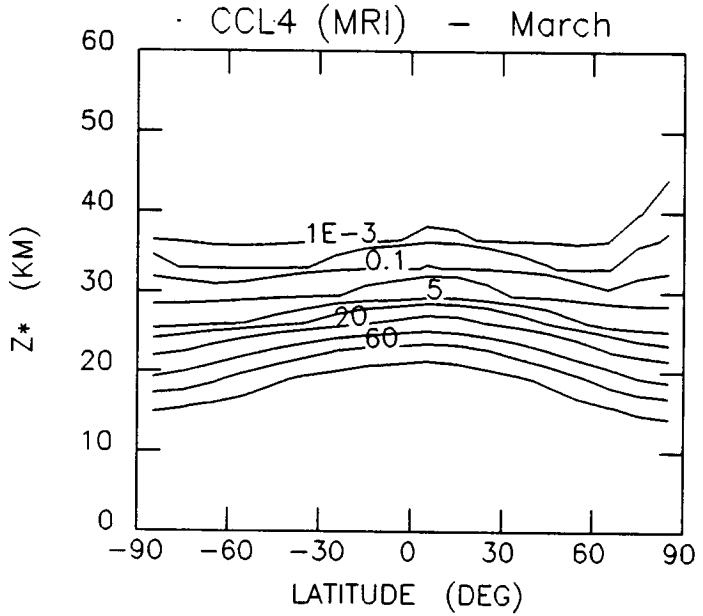
CCL4 (MRI) – March
Z* (KM)
LATITUDE (DEG)
1E-3
0.1
5
20
60

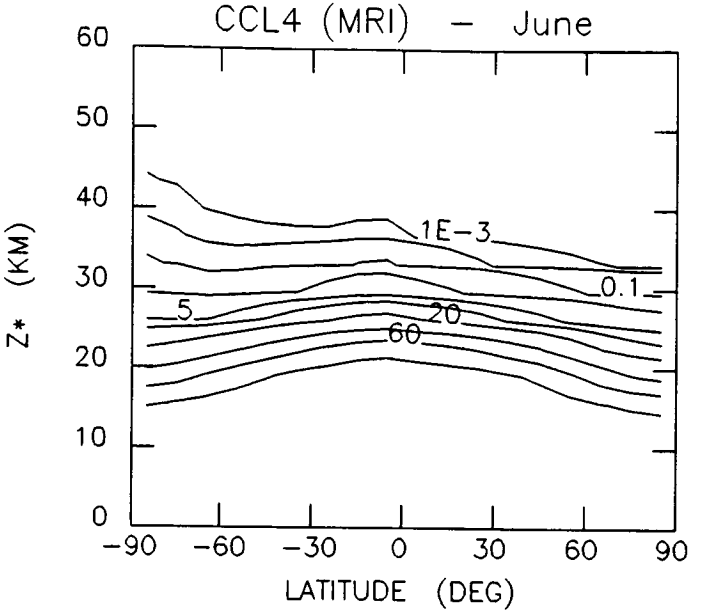
CCL4 (MRI) – June
Z* (KM)
LATITUDE (DEG)
1E-3
0.1
5
20
60

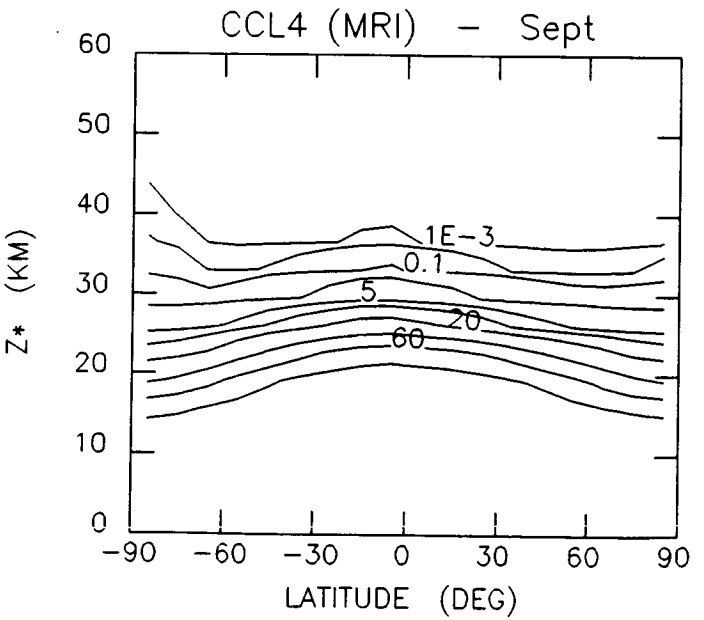
CCL4 (MRI) – Sept
Z* (KM)
LATITUDE (DEG)
1E-3
0.1
5
20
60

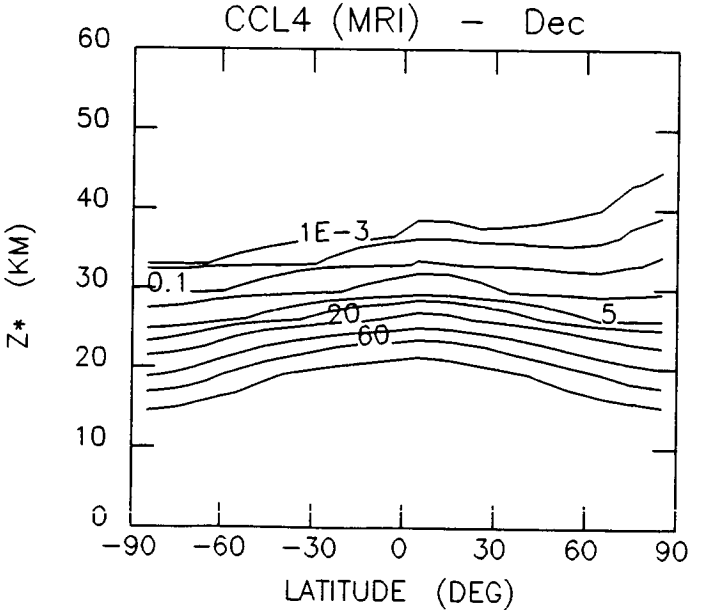
CCL4 (MRI) – Dec
Z* (KM)
LATITUDE (DEG)
1E-3
0.1
5
20
60

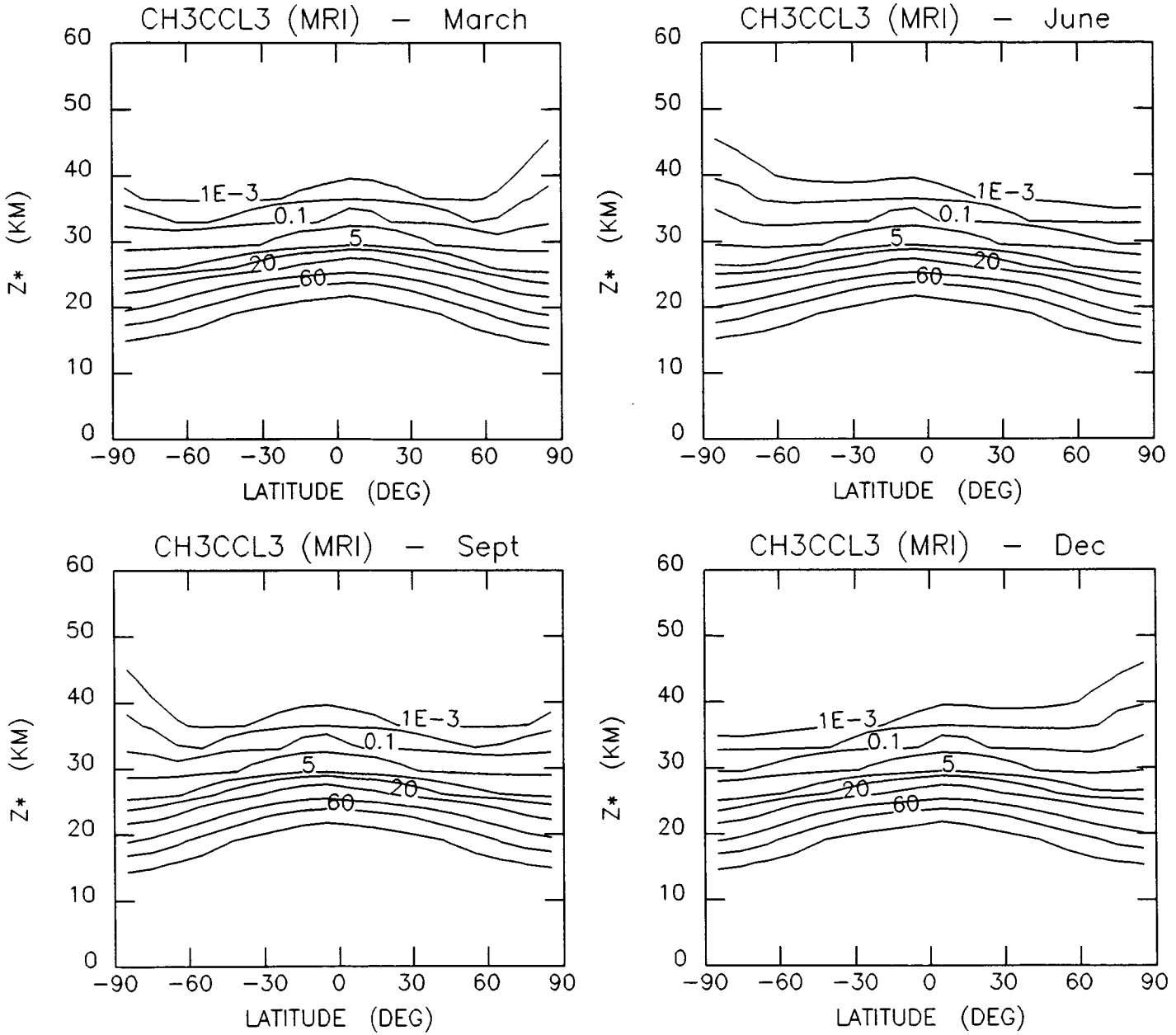
CH3CCL3 (MRI) – March
CH3CCL3 (MRI) – June
CH3CCL3 (MRI) – Sept
CH3CCL3 (MRI) – Dec
Z* (KM)
LATITUDE (DEG)
1E-3
0.1
5
20
60
0
10
20
30
40
50
60
-90
-60
-30
0
30
60
90

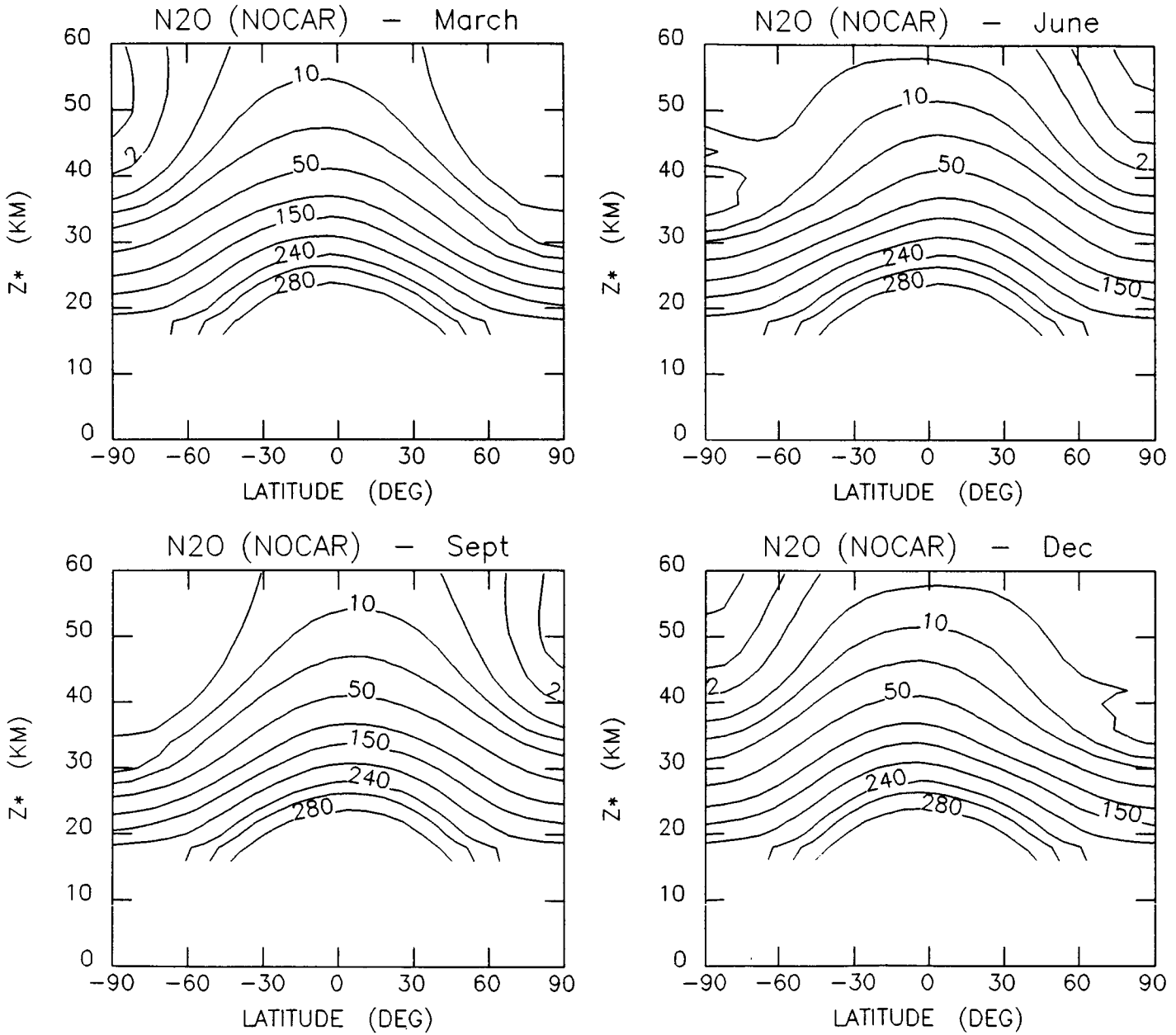
N2O (NOCAR) – March
N2O (NOCAR) – June
N2O (NOCAR) – Sept
N2O (NOCAR) – Dec
Z* (KM)
LATITUDE (DEG)
60
50
40
30
20
10
0
-90
-60
-30
0
30
60
90
2
10
50
150
240
280

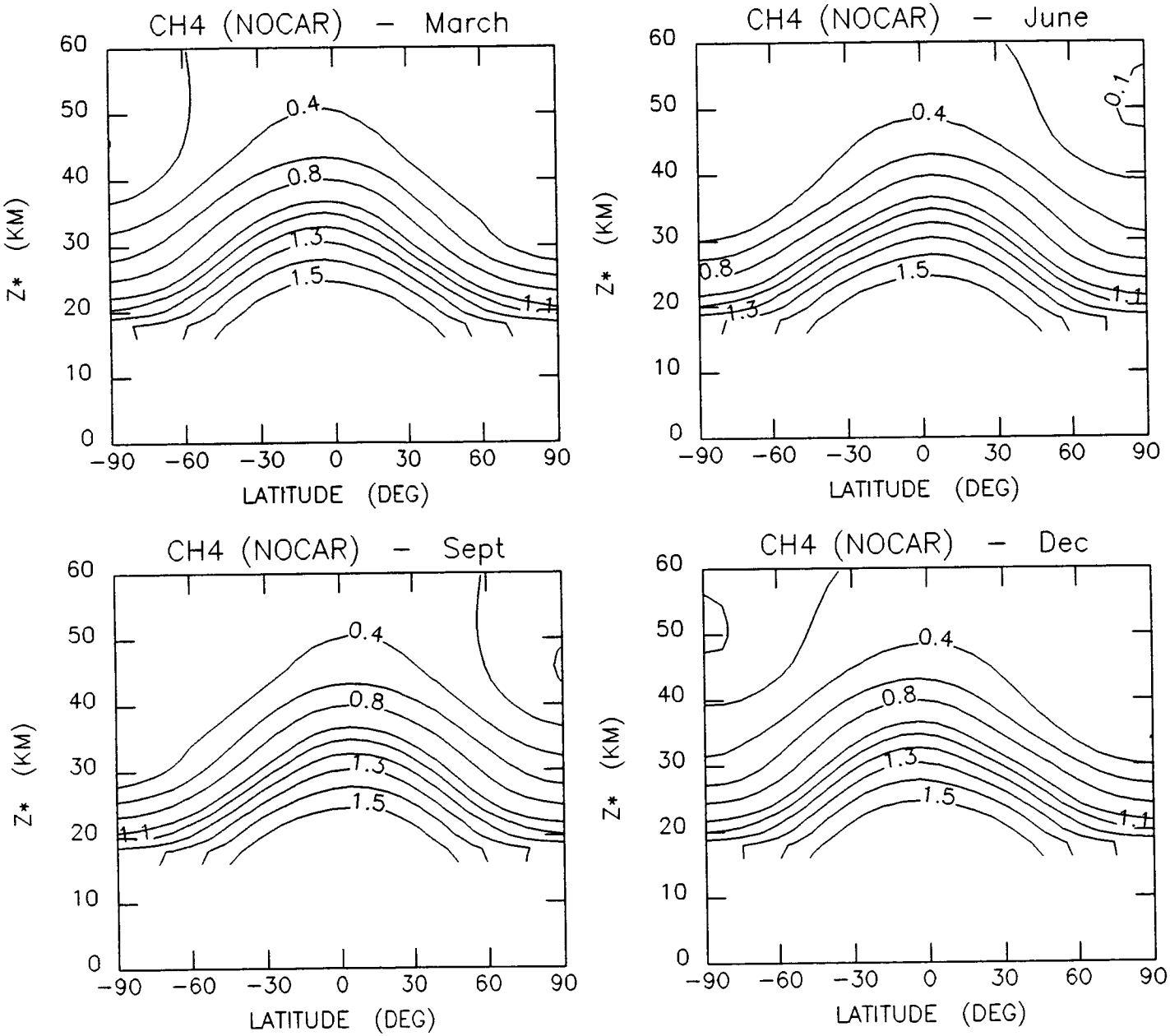
CH4 (NOCAR) – March
CH4 (NOCAR) – June
CH4 (NOCAR) – Sept
CH4 (NOCAR) – Dec
Z* (KM)
LATITUDE (DEG)
0.1
0.4
0.8
1.3
1.5
1.1
0
10
20
30
40
50
60
-90
-60
-30
0
30
60
90

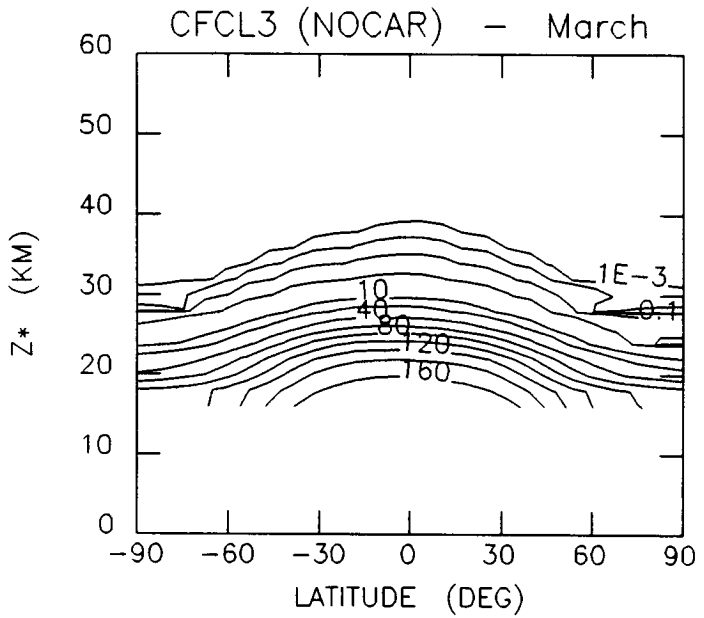
CFCL3 (NOCAR) – March
Z* (KM)
LATITUDE (DEG)
1E-3
0.1
10
40
80
120
160

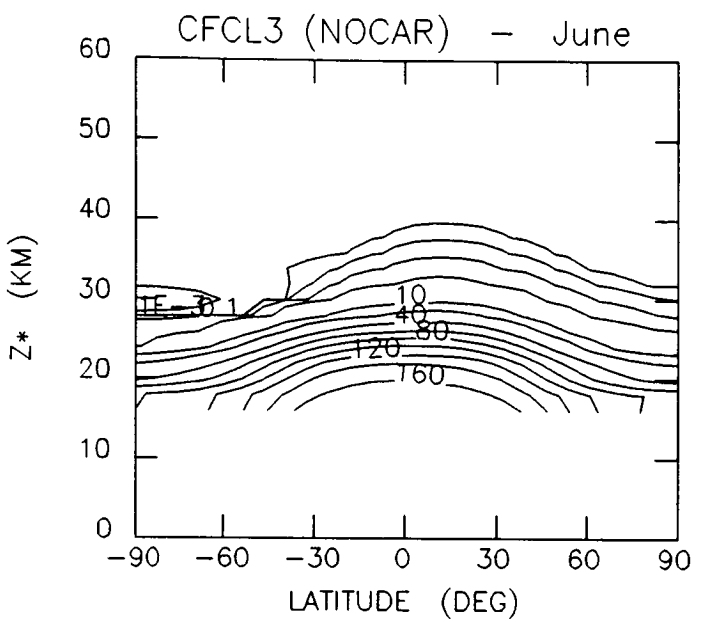
CFCL3 (NOCAR) – June
Z* (KM)
LATITUDE (DEG)
1E-3
0.1
10
40
80
120
160

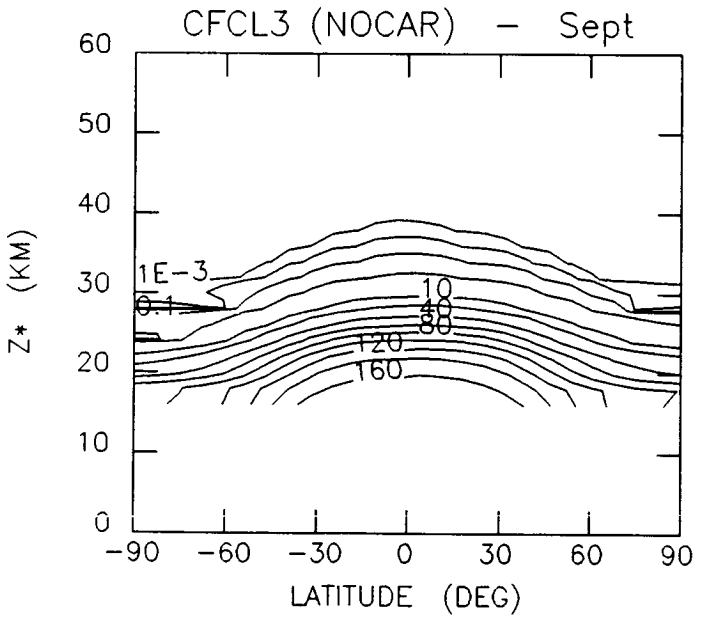
CFCL3 (NOCAR) – Sept
Z* (KM)
LATITUDE (DEG)
1E-3
0.1
10
40
80
120
160

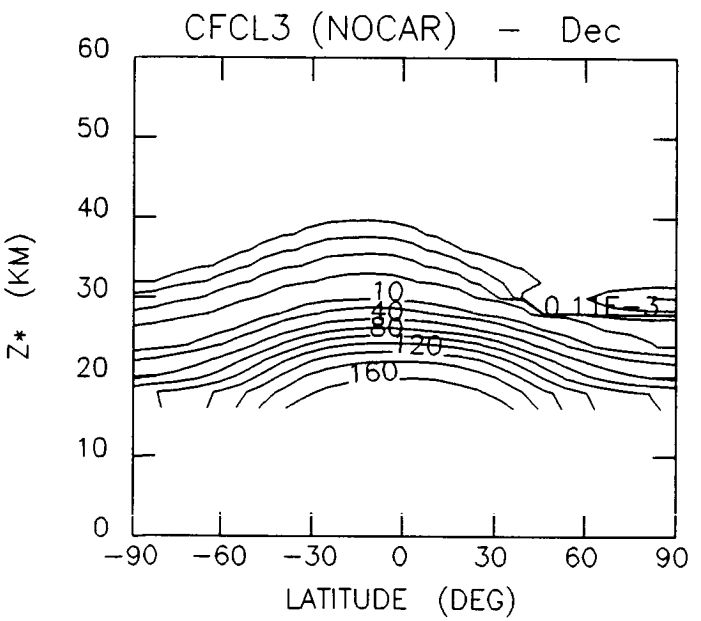
CFCL3 (NOCAR) – Dec
Z* (KM)
LATITUDE (DEG)
0.1
1E-3
10
40
80
120
160

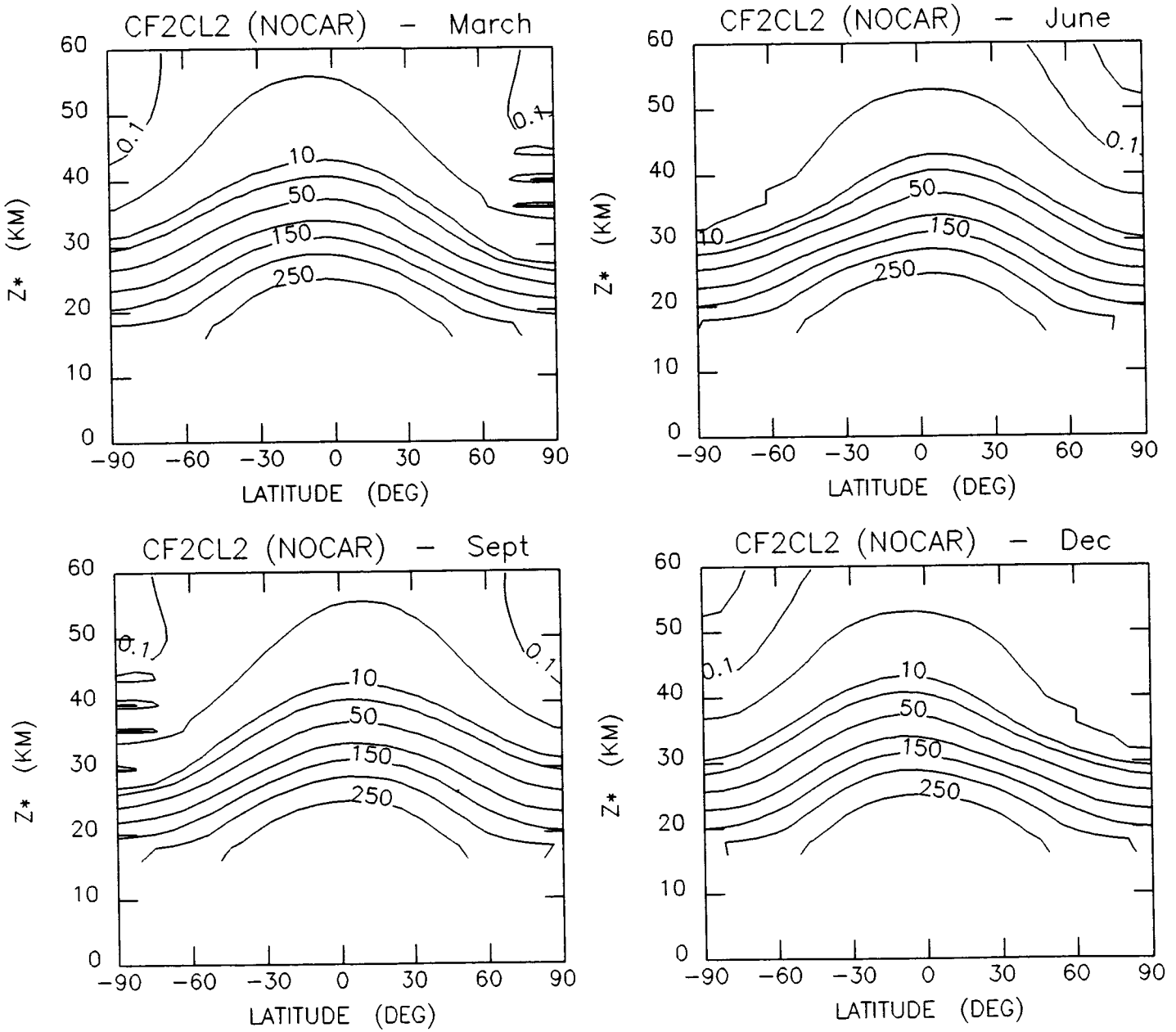
CF2CL2 (NOCAR) – March
CF2CL2 (NOCAR) – June
CF2CL2 (NOCAR) – Sept
CF2CL2 (NOCAR) – Dec
Z* (KM)
LATITUDE (DEG)
0.1
10
50
150
250
0
10
20
30
40
50
60
−90
−60
−30
0
30
60
90

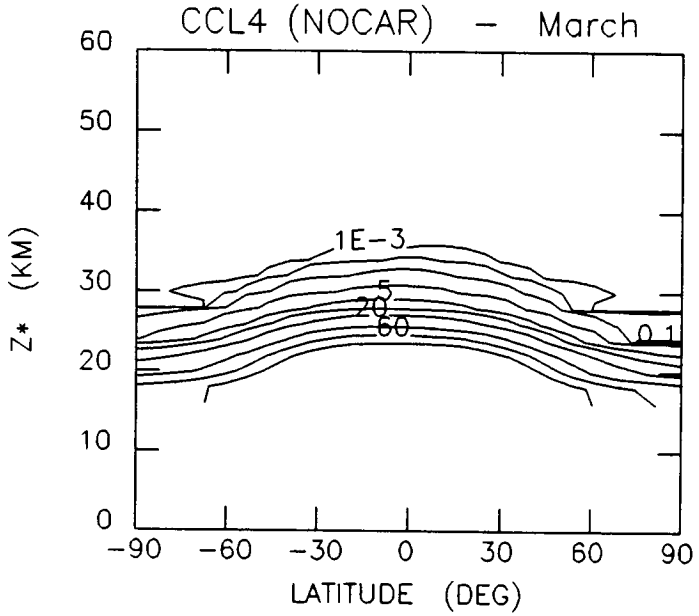
CCL4 (NOCAR) – March
Z* (KM)
LATITUDE (DEG)
1E-3
5
20
60
0.1

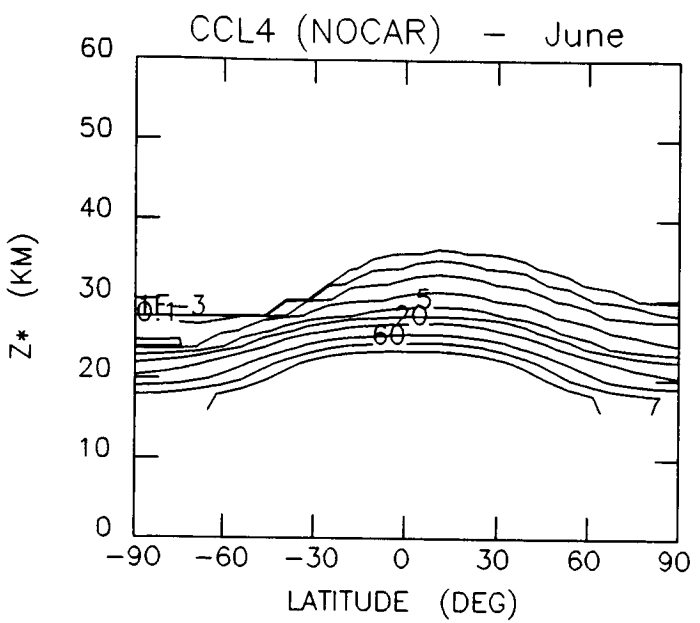
CCL4 (NOCAR) – June
Z* (KM)
LATITUDE (DEG)
1E-3
5
20
60
0.1

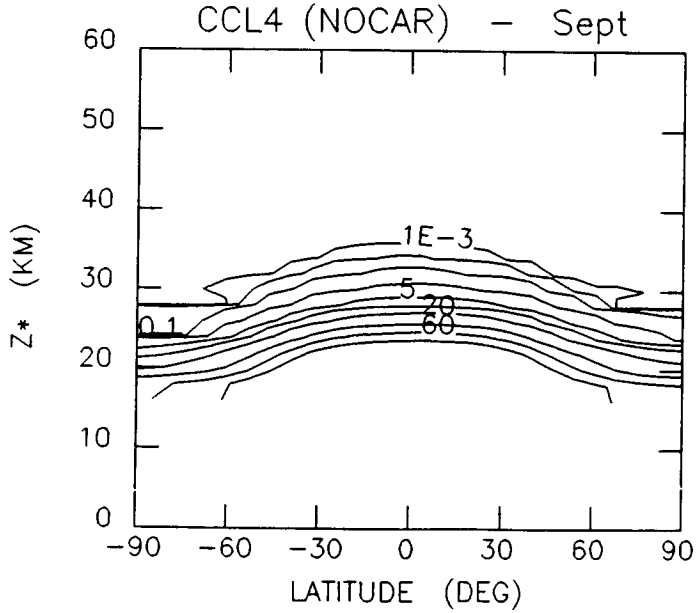
CCL4 (NOCAR) – Sept
Z* (KM)
LATITUDE (DEG)
1E-3
5
20
60
0.1

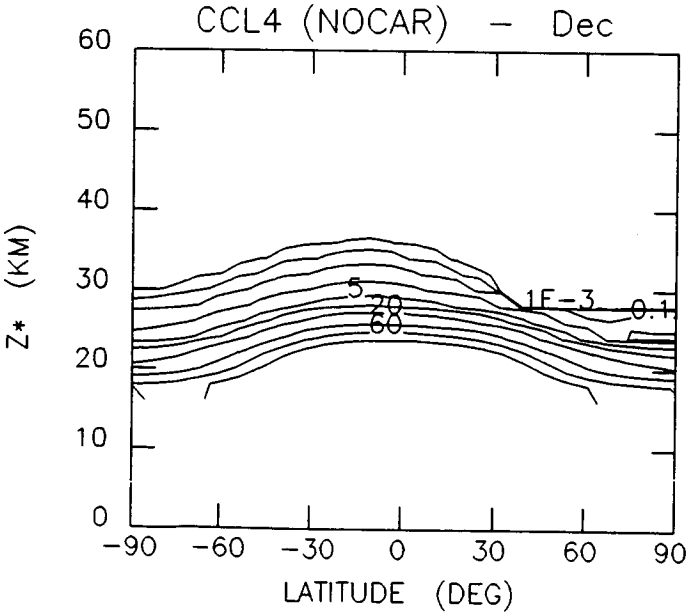
CCL4 (NOCAR) – Dec
Z* (KM)
LATITUDE (DEG)
5
20
60
1E-3
0.1

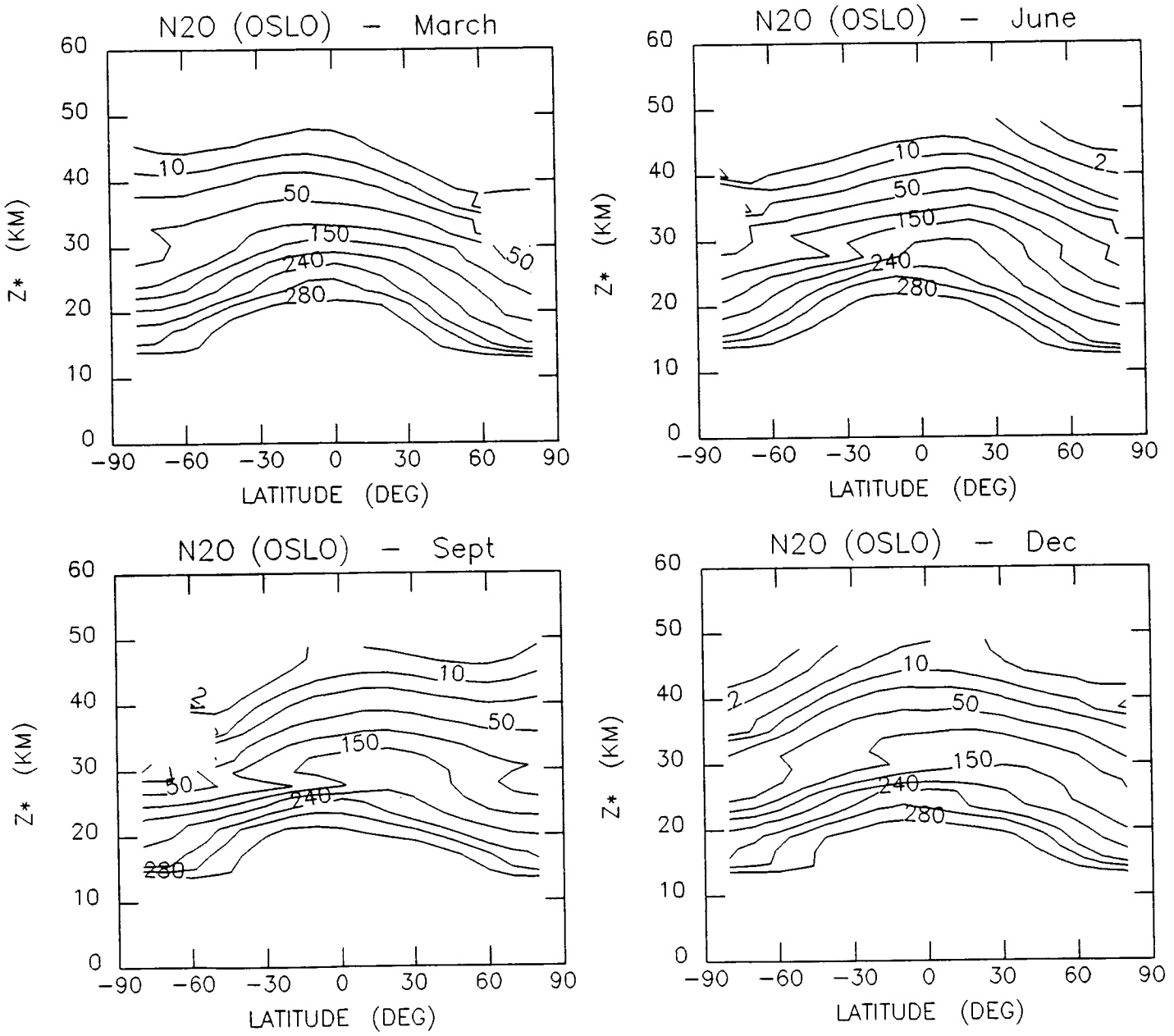
N2O (OSLO) – March
N2O (OSLO) – June
N2O (OSLO) – Sept
N2O (OSLO) – Dec
Z* (KM)
LATITUDE (DEG)
10
50
150
240
280
2

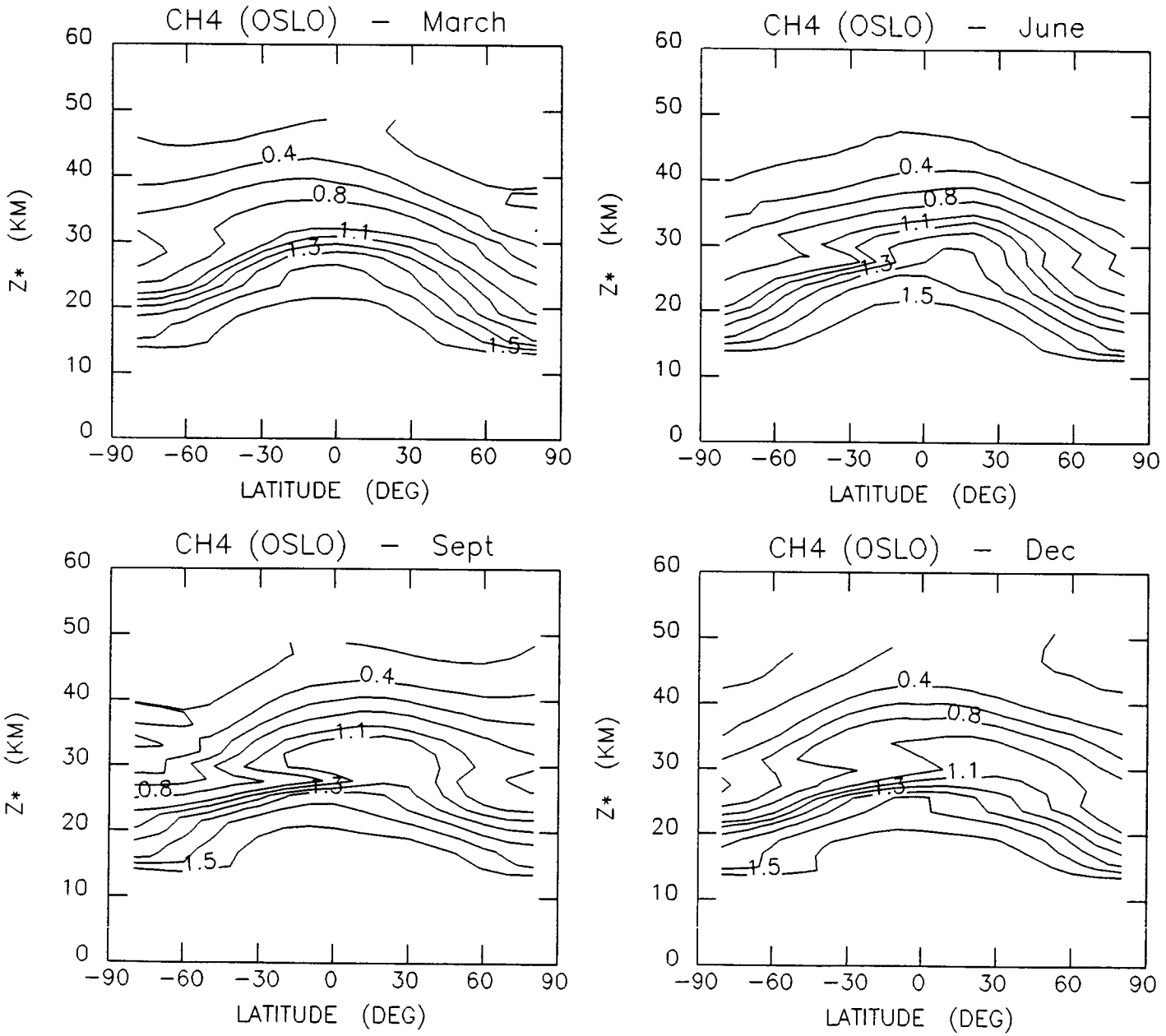
CH4 (OSLO) – March
CH4 (OSLO) – June
CH4 (OSLO) – Sept
CH4 (OSLO) – Dec
Z* (KM)
LATITUDE (DEG)
0
10
20
30
40
50
60
-90
-60
-30
0
30
60
90
0.4
0.8
1.1
1.3
1.5

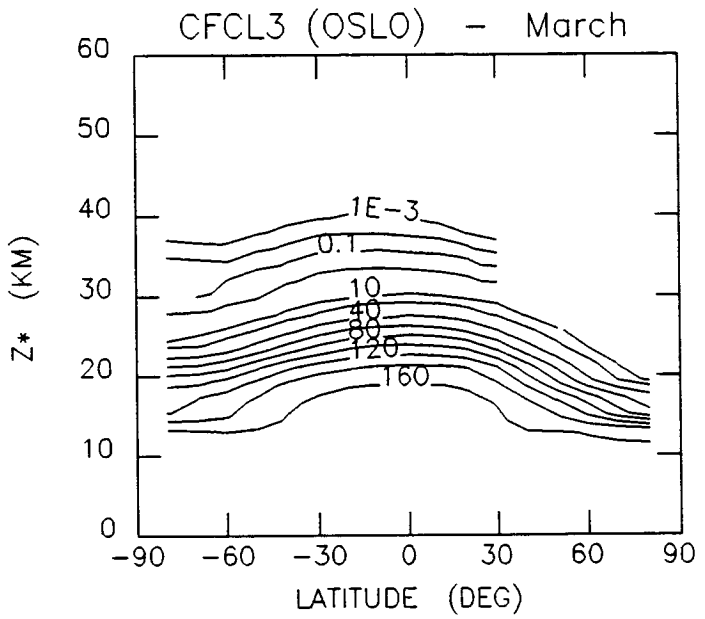
CFCL3 (OSLO) – March
Z* (KM)
LATITUDE (DEG)
1E-3
0.1
10
40
80
120
160

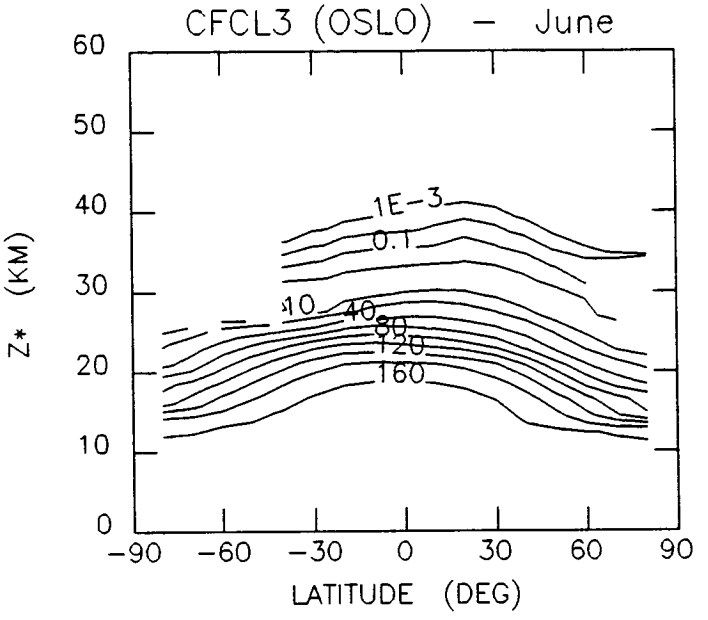
CFCL3 (OSLO) – June
Z* (KM)
LATITUDE (DEG)
1E-3
0.1
10
40
80
120
160

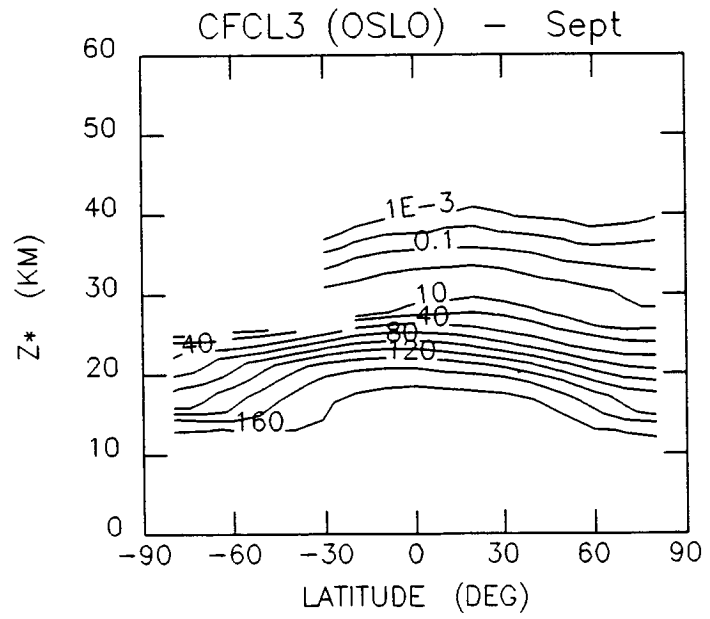
CFCL3 (OSLO) – Sept
Z* (KM)
LATITUDE (DEG)
1E-3
0.1
10
40
80
120
160

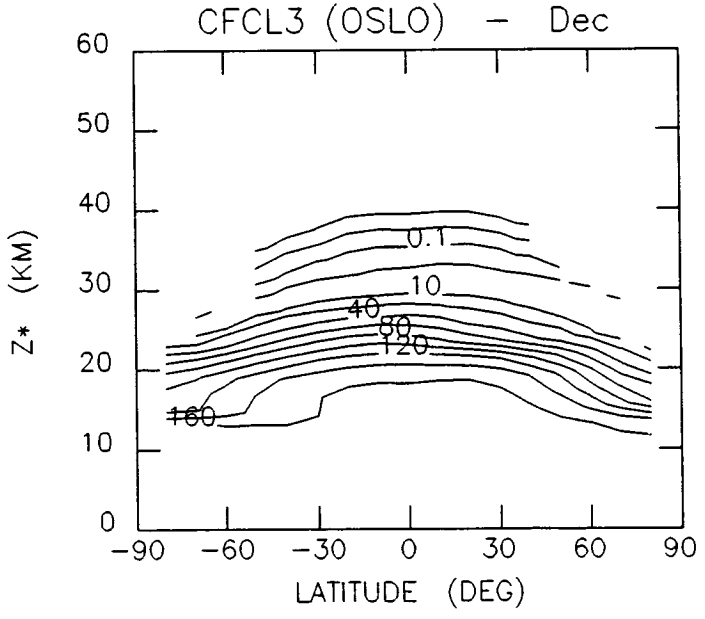
CFCL3 (OSLO) – Dec
Z* (KM)
LATITUDE (DEG)
0.1
10
40
80
120
160

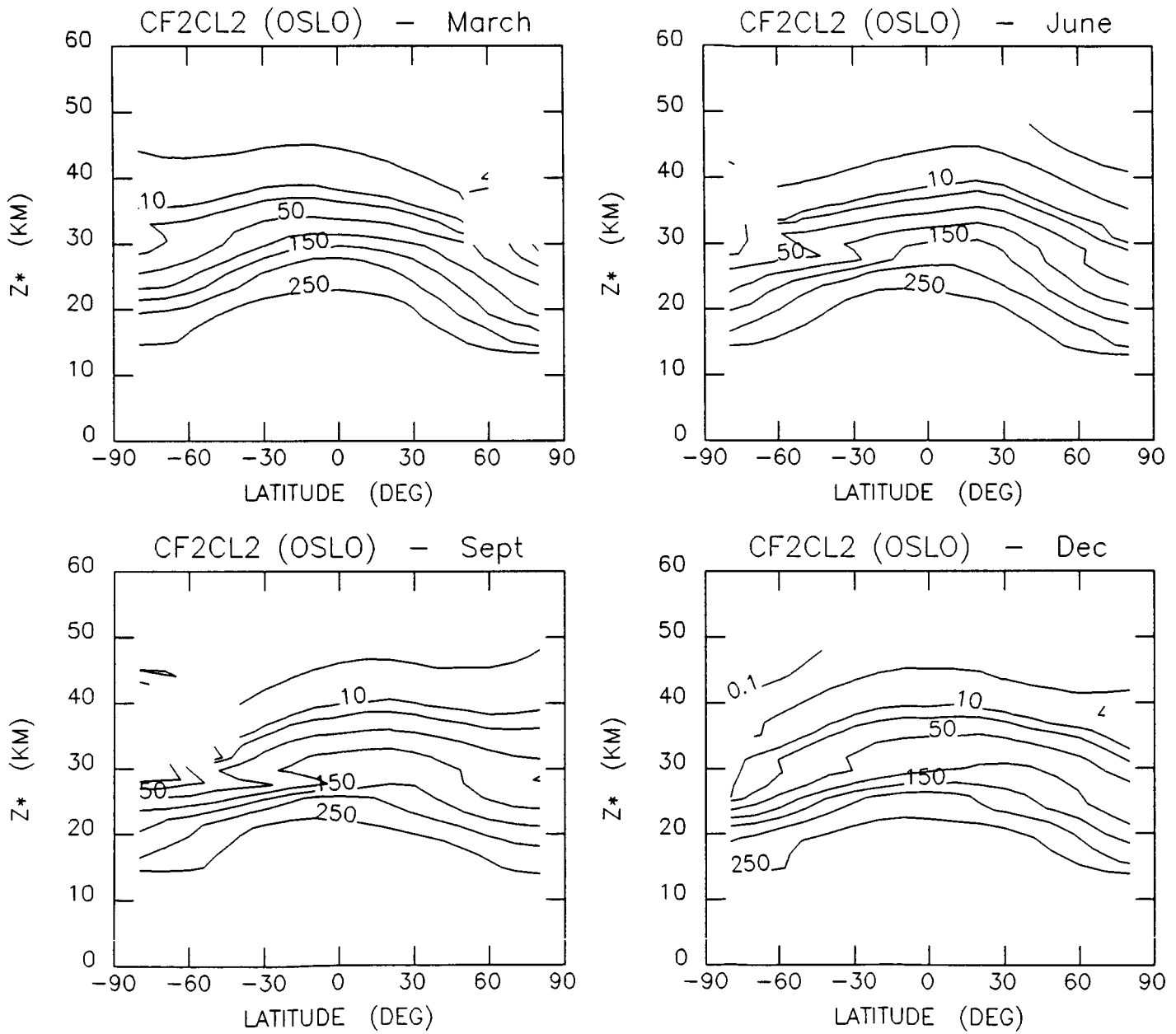
CF2CL2 (OSLO) – March
CF2CL2 (OSLO) – June
CF2CL2 (OSLO) – Sept
CF2CL2 (OSLO) – Dec
Z* (KM)
LATITUDE (DEG)
0.1
10
50
150
250
0
10
20
30
40
50
60
-90
-60
-30
0
30
60
90

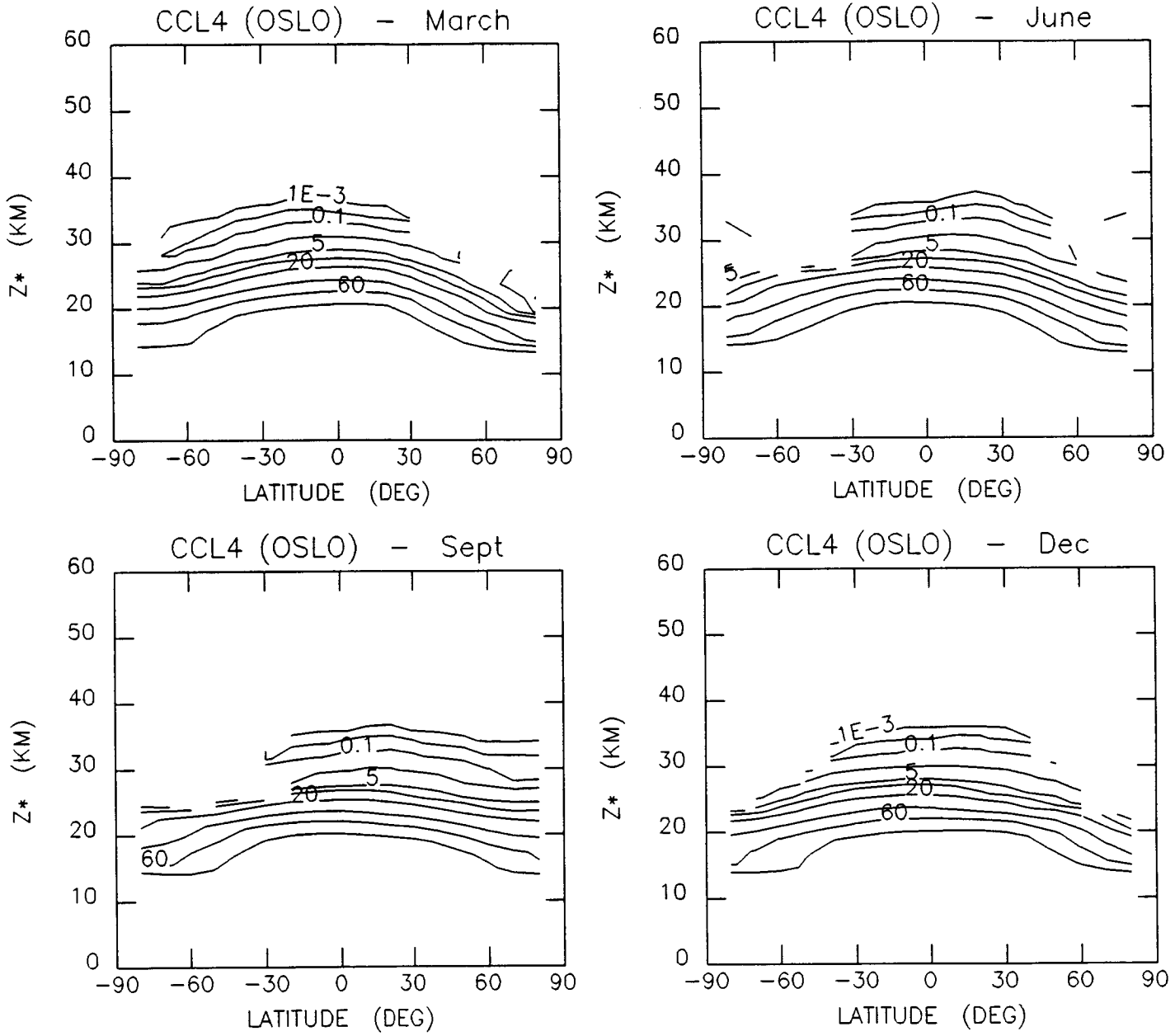
CCL4 (OSLO) – March
CCL4 (OSLO) – June
CCL4 (OSLO) – Sept
CCL4 (OSLO) – Dec
Z* (KM)
LATITUDE (DEG)
1E-3
0.1
5
20
60
0
10
20
30
40
50
60
-90
-60
-30
0
30
60
90

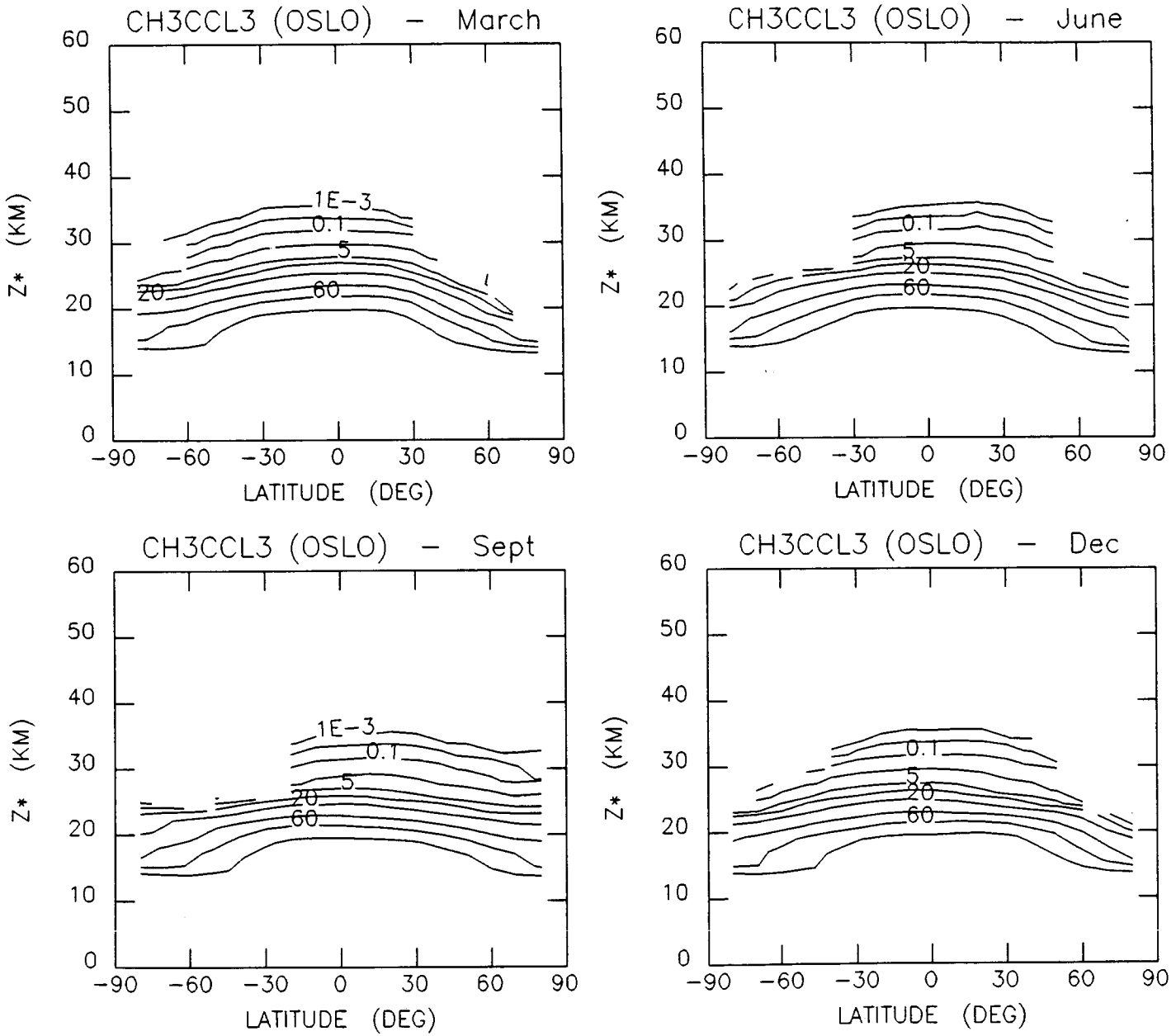
CH3CCL3 (OSLO) – March
CH3CCL3 (OSLO) – June
CH3CCL3 (OSLO) – Sept
CH3CCL3 (OSLO) – Dec
Z* (KM)
LATITUDE (DEG)
1E-3
0.1
5
20
60
0
10
20
30
40
50
60
-90
-60
-30
0
30
60
90

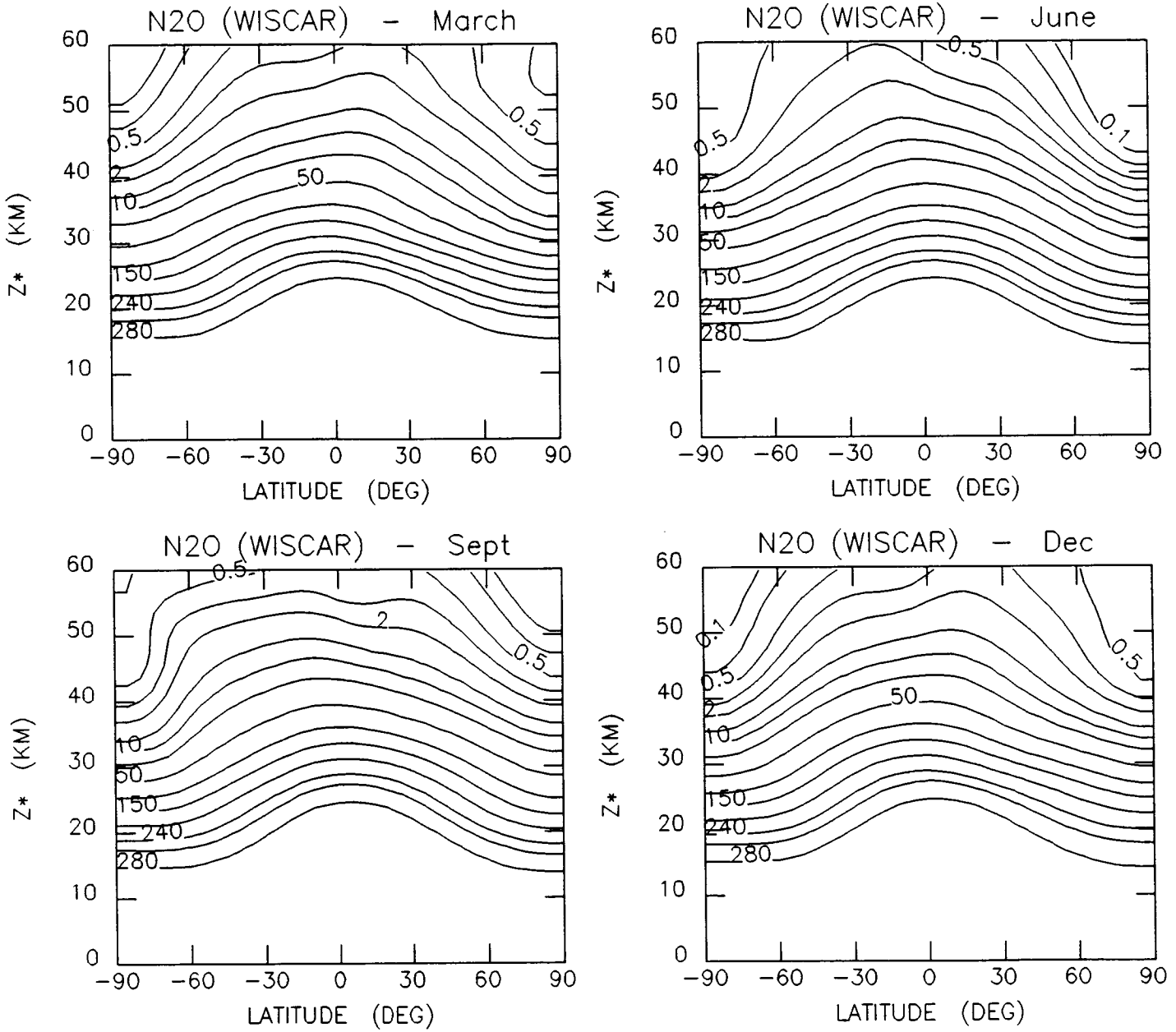
N2O (WISCAR) – March
N2O (WISCAR) – June
N2O (WISCAR) – Sept
N2O (WISCAR) – Dec
Z* (KM)
LATITUDE (DEG)
0
10
20
30
40
50
60
−90
−60
−30
0
30
60
90
0.5
2
10
50
150
240
280
0.1

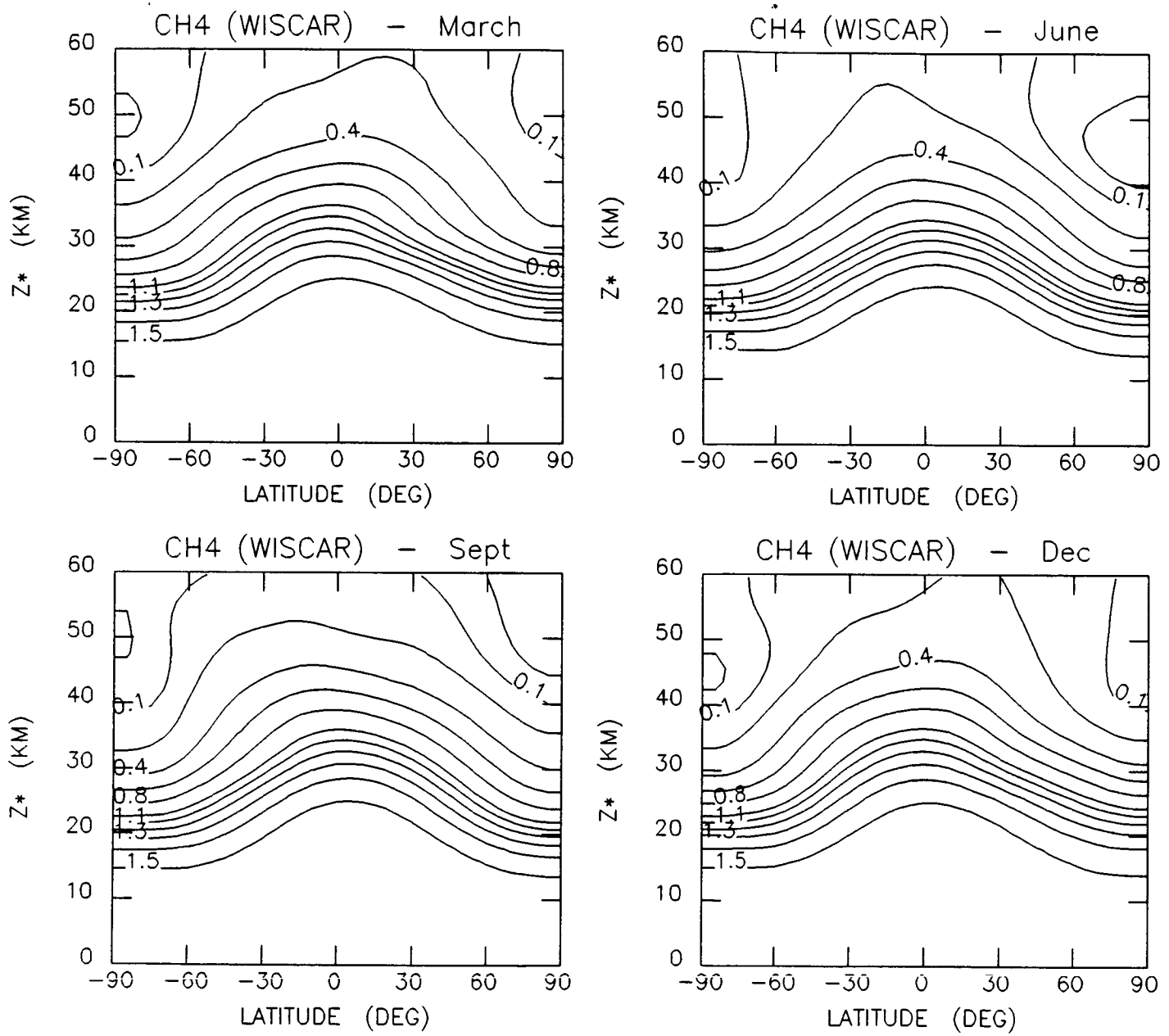
CH4 (WISCAR) – March
CH4 (WISCAR) – June
CH4 (WISCAR) – Sept
CH4 (WISCAR) – Dec
Z* (KM)
LATITUDE (DEG)
0
10
20
30
40
50
60
-90
-60
-30
0
30
60
90
0.1
0.4
0.8
1.1
1.3
1.5

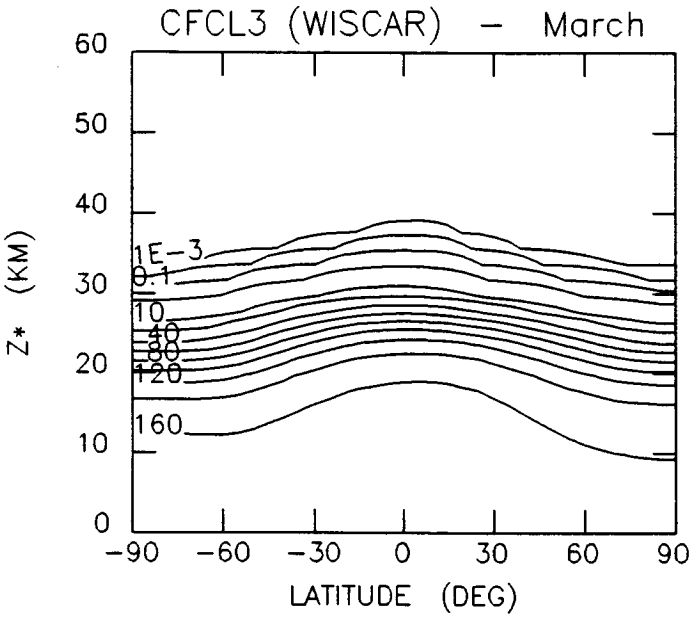
CFCL3 (WISCAR) – March
Z* (KM)
LATITUDE (DEG)
1E-3
0.1
10
40
80
120
160

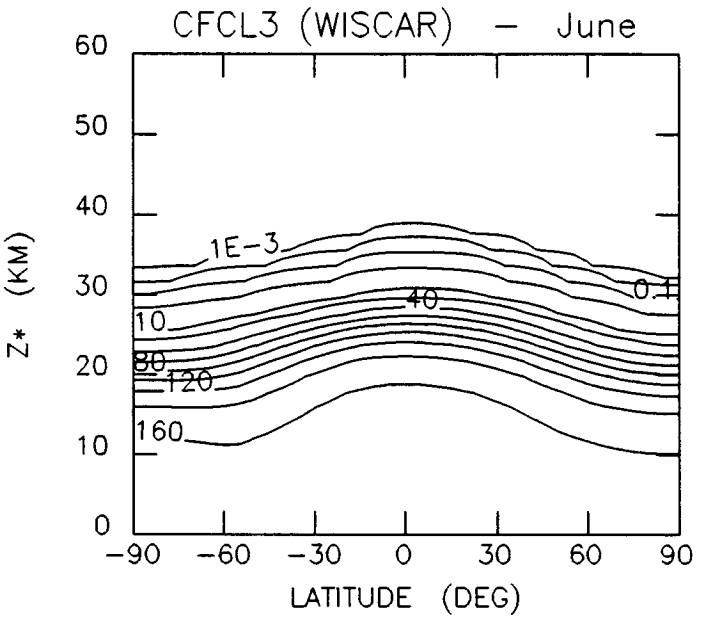
CFCL3 (WISCAR) – June
Z* (KM)
LATITUDE (DEG)
1E-3
0.1
40
10
80
120
160

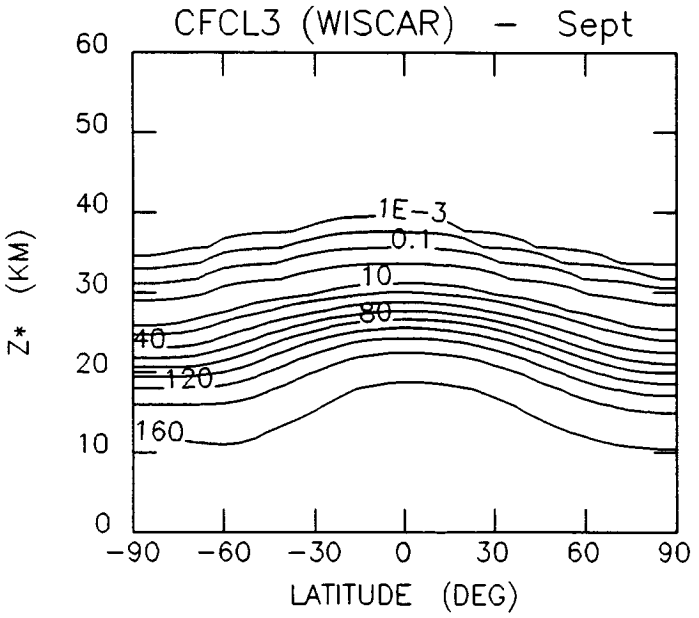
CFCL3 (WISCAR) – Sept
Z* (KM)
LATITUDE (DEG)
1E-3
0.1
10
80
40
120
160

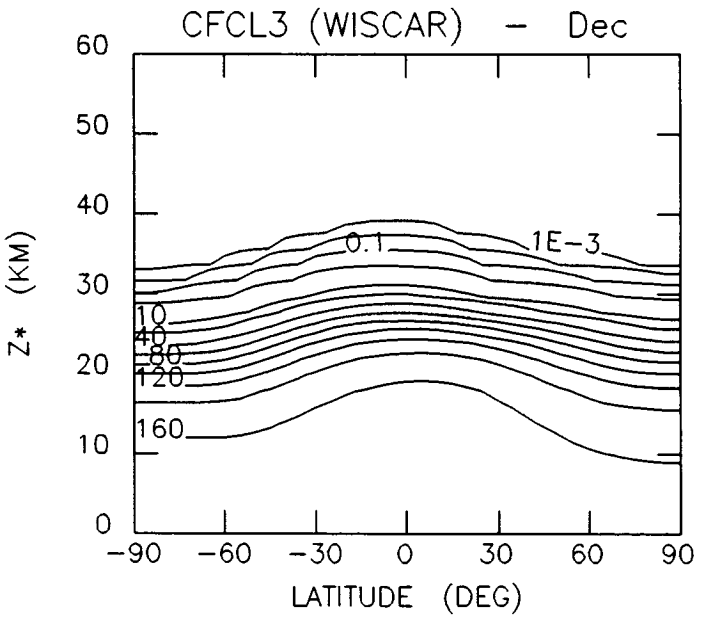
CFCL3 (WISCAR) – Dec
Z* (KM)
LATITUDE (DEG)
0.1
1E-3
10
40
80
120
160

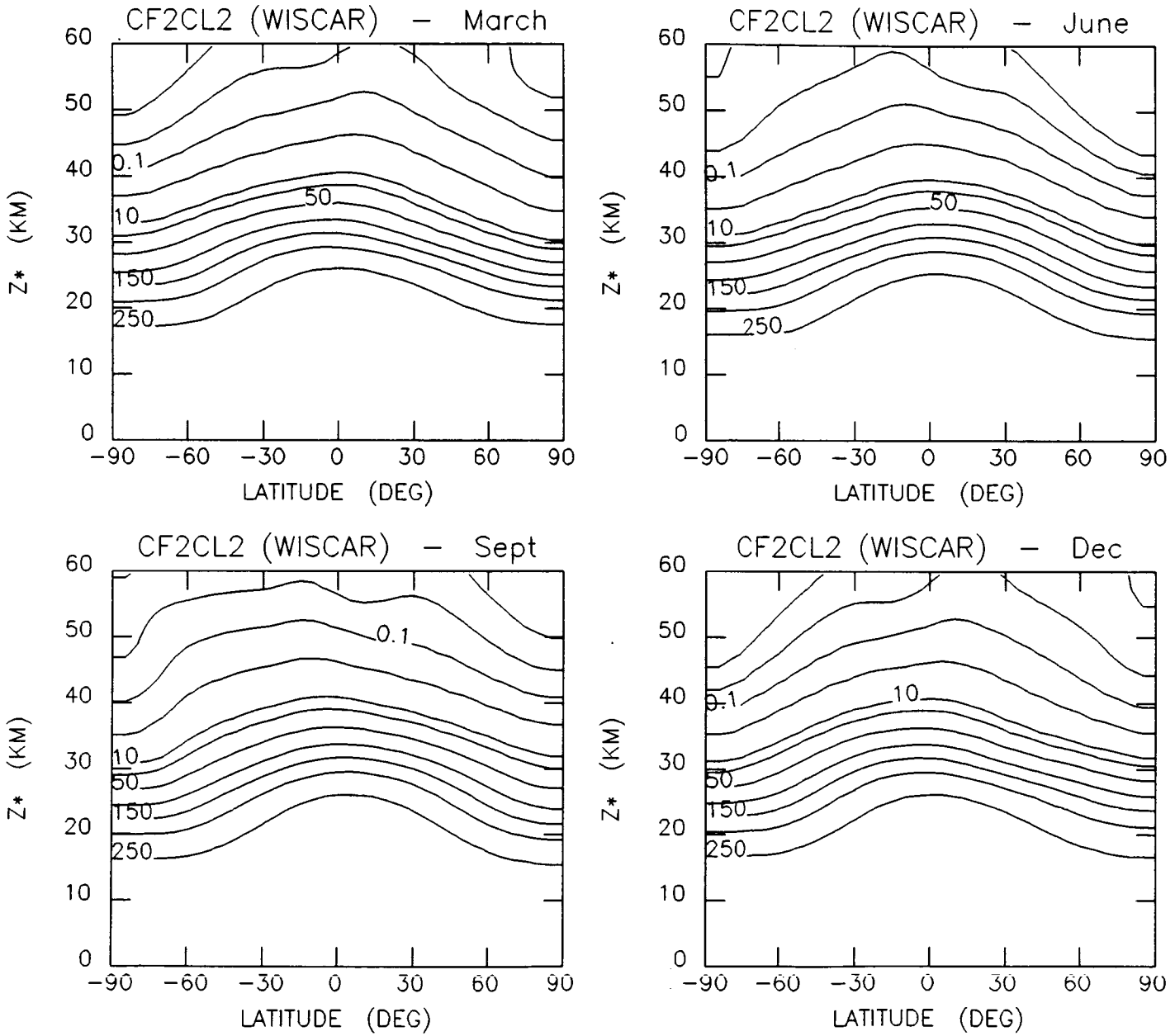
CF2CL2 (WISCAR) – March
CF2CL2 (WISCAR) – June
CF2CL2 (WISCAR) – Sept
CF2CL2 (WISCAR) – Dec
Z* (KM)
LATITUDE (DEG)
0.1
10
50
150
250
0
10
20
30
40
50
60
−90
−60
−30
0
30
60
90

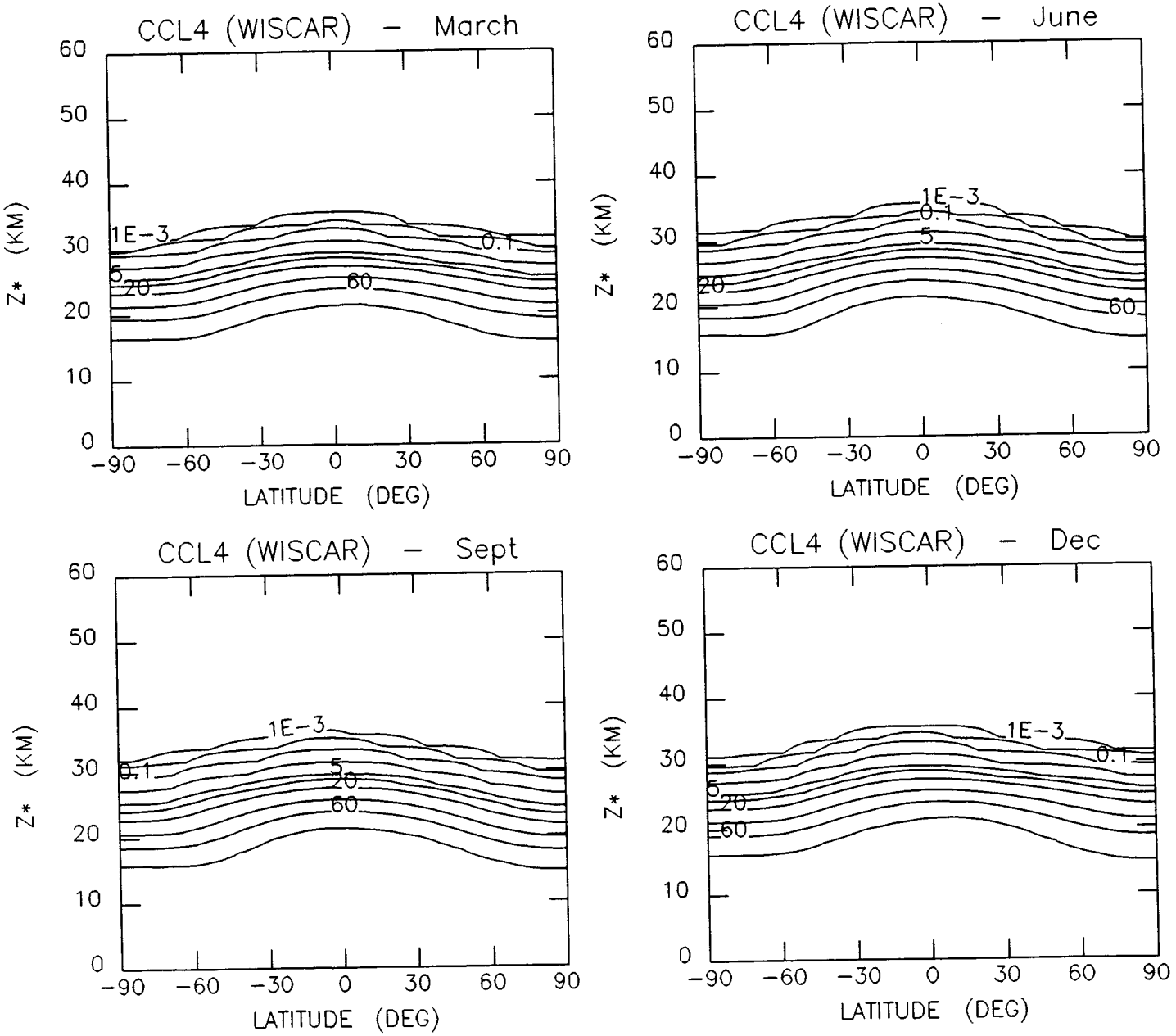
CCL4 (WISCAR) – March
CCL4 (WISCAR) – June
CCL4 (WISCAR) – Sept
CCL4 (WISCAR) – Dec
Z* (KM)
LATITUDE (DEG)
1E-3
0.1
5
20
60
0
10
20
30
40
50
60
-90
-60
-30
0
30
60
90

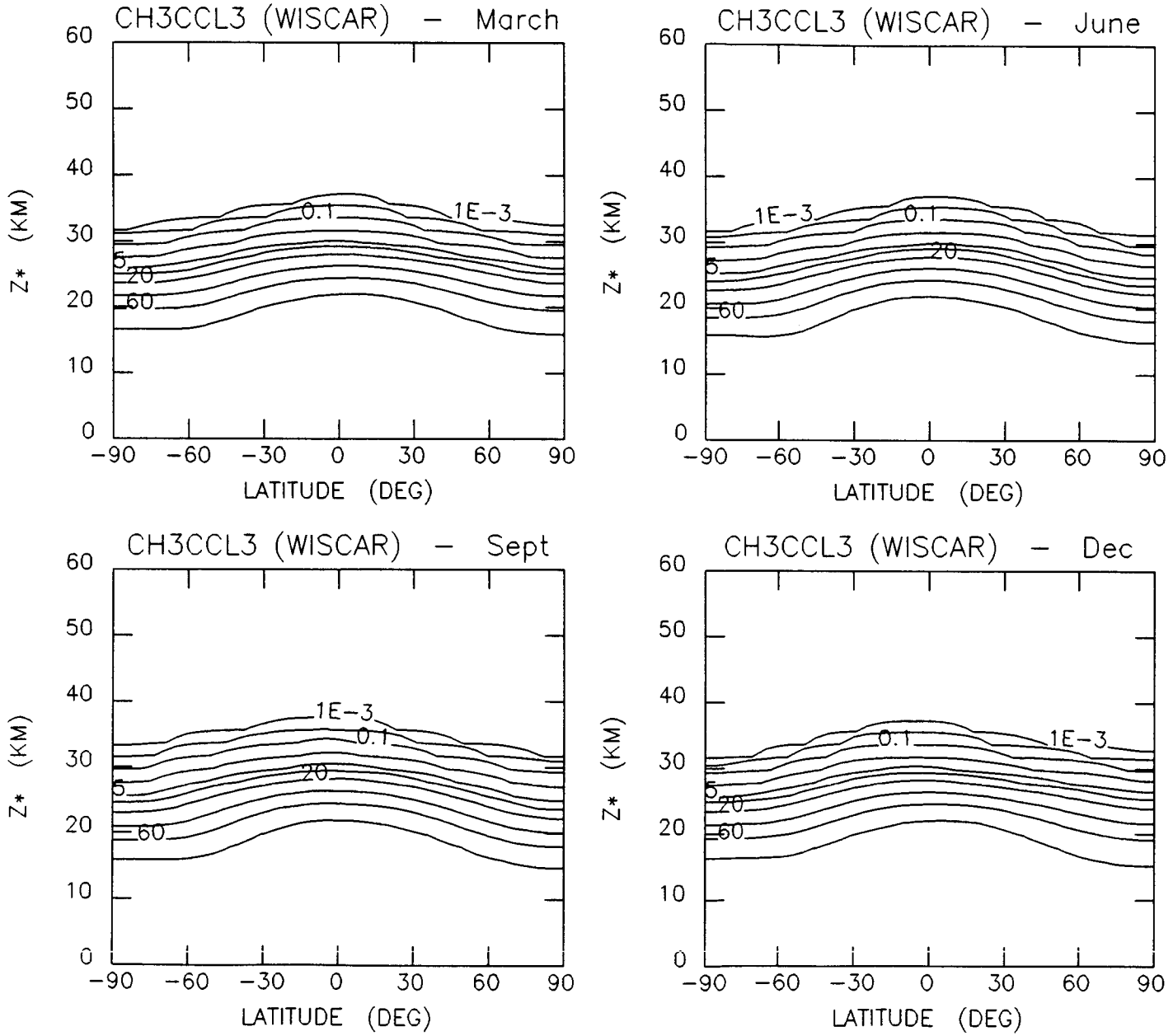
CH3CCL3 (WISCAR) – March
CH3CCL3 (WISCAR) – June
CH3CCL3 (WISCAR) – Sept
CH3CCL3 (WISCAR) – Dec
Z* (KM)
LATITUDE (DEG)
0
10
20
30
40
50
60
-90
-60
-30
0
30
60
90
1E-3
0.1
5
20
60

**Table 6-4.** Perturbed Circulations and Temperatures

Circulation (Q) and Temperature (T) Differences Between Perturbed
(Scenarios A, B, C, and D) and Current (1980) Atmospheres
March, June, September, and December
Models Represented - AERI (B, C, and D) and WISCAR (A, B, C, and D)

| Parameter | Description | Units | Contour Levels |
|---|---|---|---|
| DQ-X | Q for perturbed atmosphere X minus $Q_{net}$ for current atmosphere | K/day | -3, -2, -1.5, -1, -0.8, -0.6, -.04, -0.2, -0.1, -0.05, 0, 0.05, 0.1, 0.2, 0.3 |
| DT-X | T for perturbed atmosphere X minus T for current atmosphere | K | -28. -26., -24., -22., -20., -18., -16., -14., -12., -10, -8, -6, -4, -2, -1, -0.5, 0, 0.5, 1, 2, 4 |

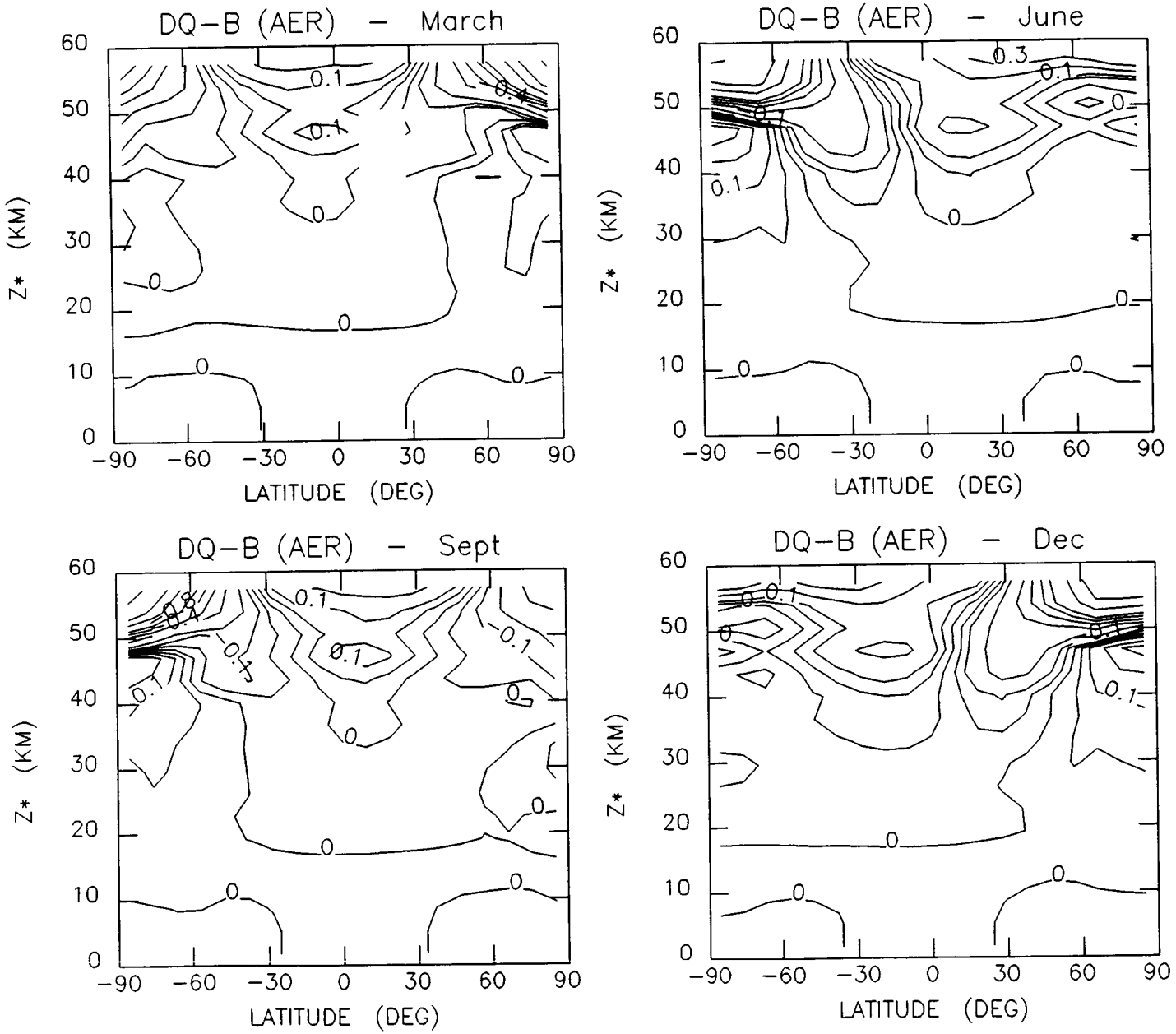
DQ-B (AER) - March
DQ-B (AER) - June
DQ-B (AER) - Sept
DQ-B (AER) - Dec
Z* (KM)
LATITUDE (DEG)
0
10
20
30
40
50
60
-90
-60
-30
0
30
60
90
0.1
0.3
0.4
-0.1

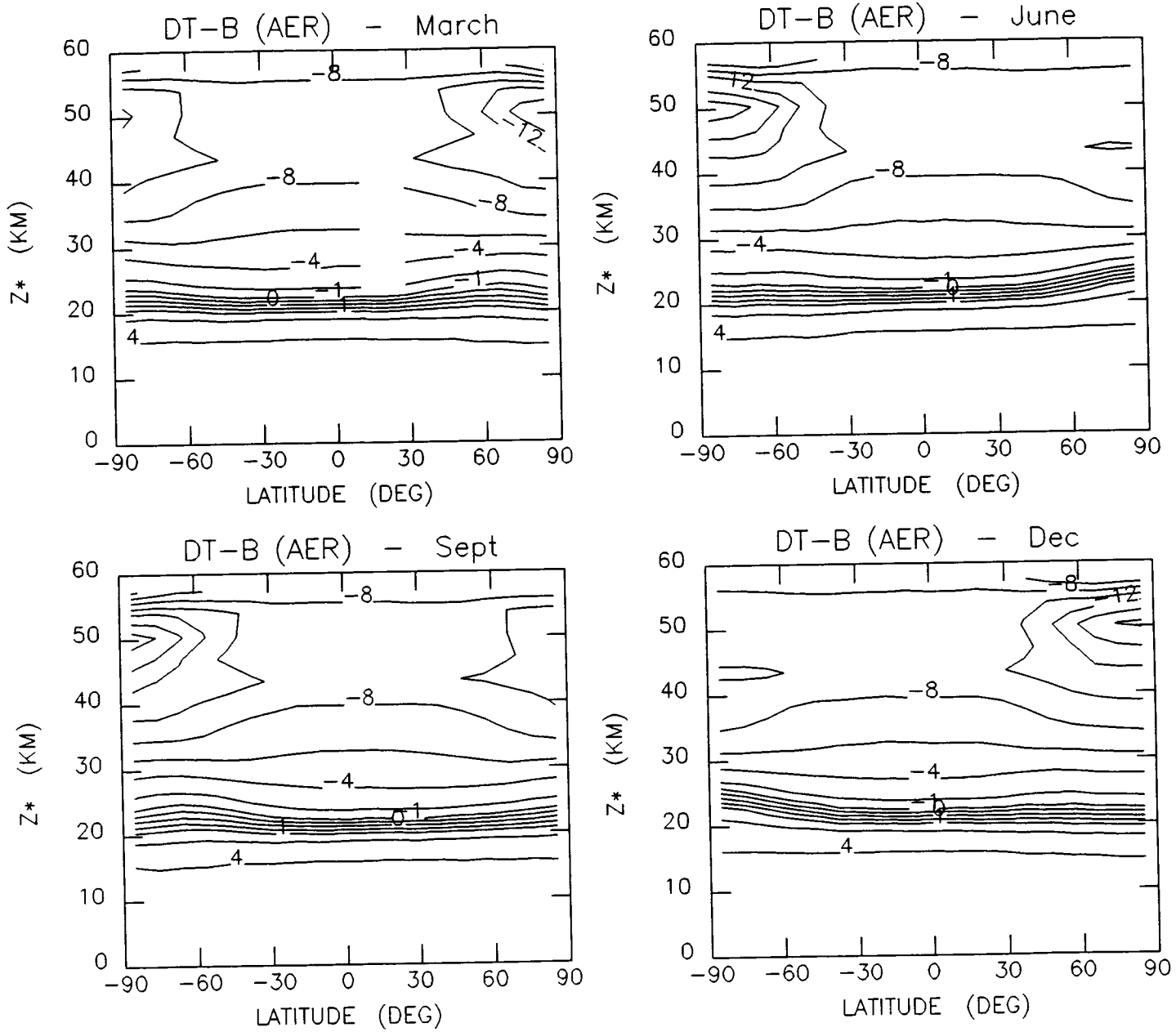
DT−B (AER) − March
DT−B (AER) − June
DT−B (AER) − Sept
DT−B (AER) − Dec
Z* (KM)
LATITUDE (DEG)
60
50
40
30
20
10
0
−90 −60 −30 0 30 60 90
−12
−8
−4
−1
0
1
4

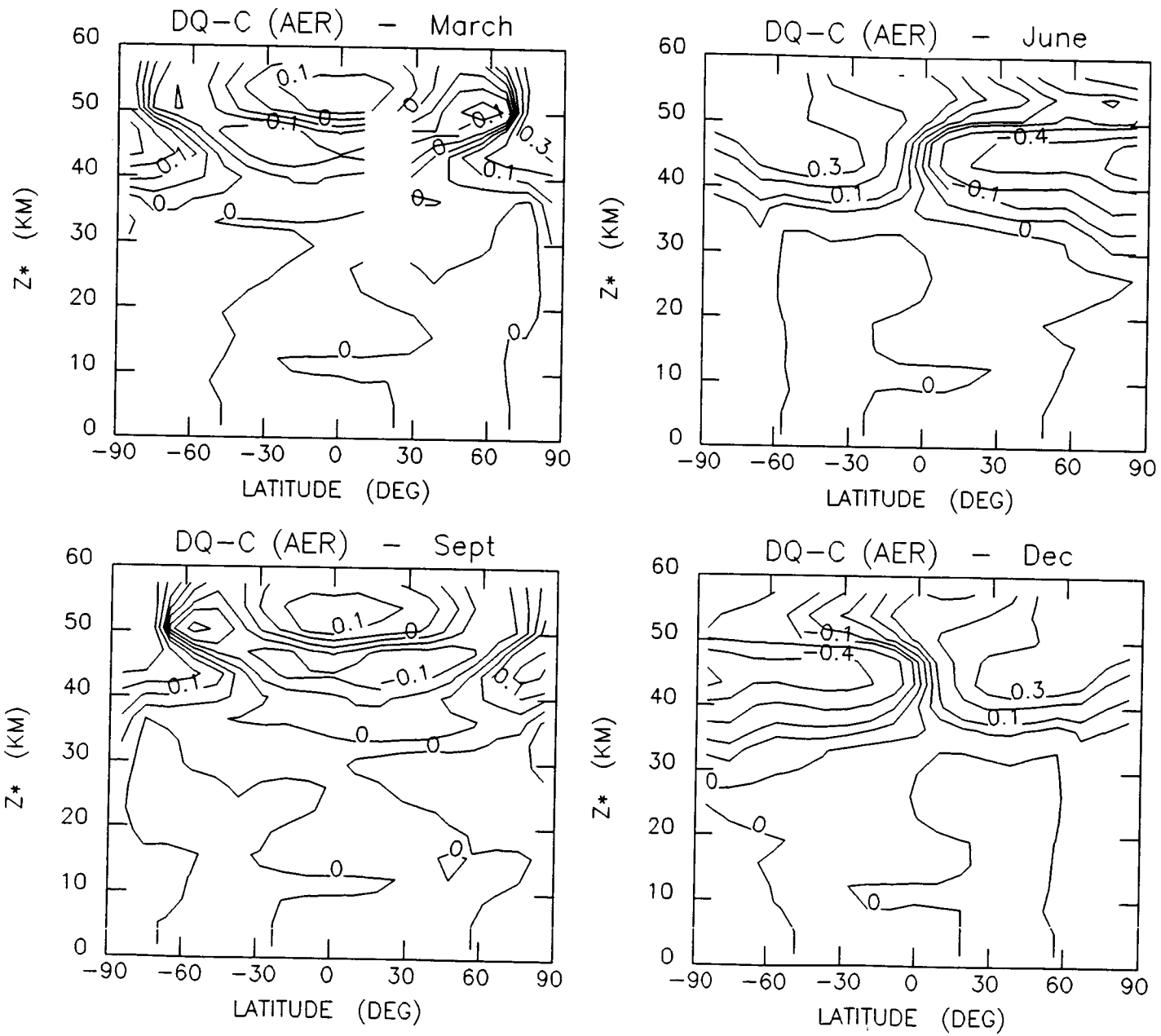
DQ-C (AER) - March
DQ-C (AER) - June
DQ-C (AER) - Sept
DQ-C (AER) - Dec
Z* (KM)
LATITUDE (DEG)
60
50
40
30
20
10
0
-90
-60
-30
0
30
60
90
0.1
0
-0.1
0.3
-0.4

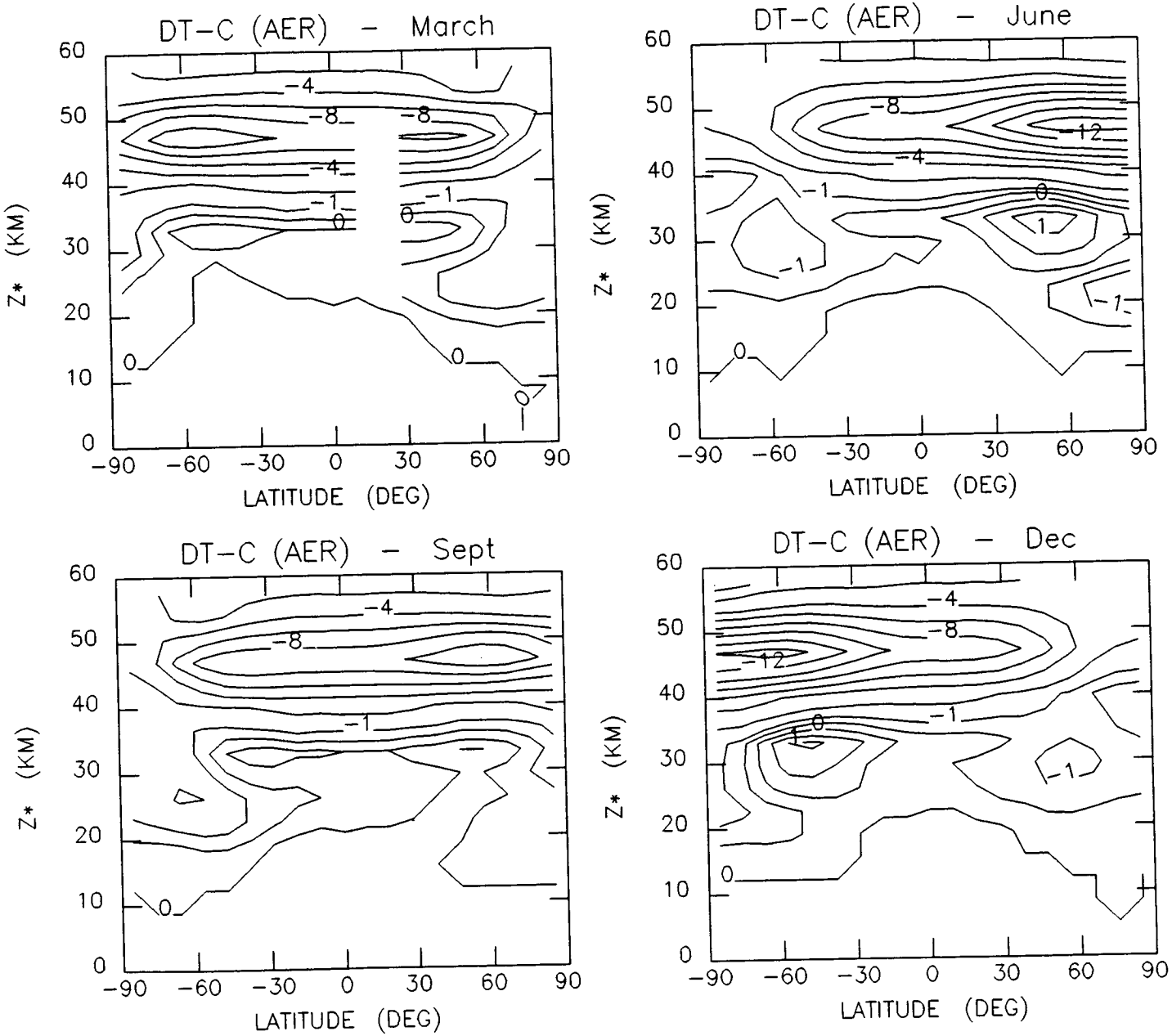
DT−C (AER) − March
DT−C (AER) − June
DT−C (AER) − Sept
DT−C (AER) − Dec
Z* (KM)
LATITUDE (DEG)
0
10
20
30
40
50
60
−90
−60
−30
0
30
60
90
−4
−8
−1
0
1
−12

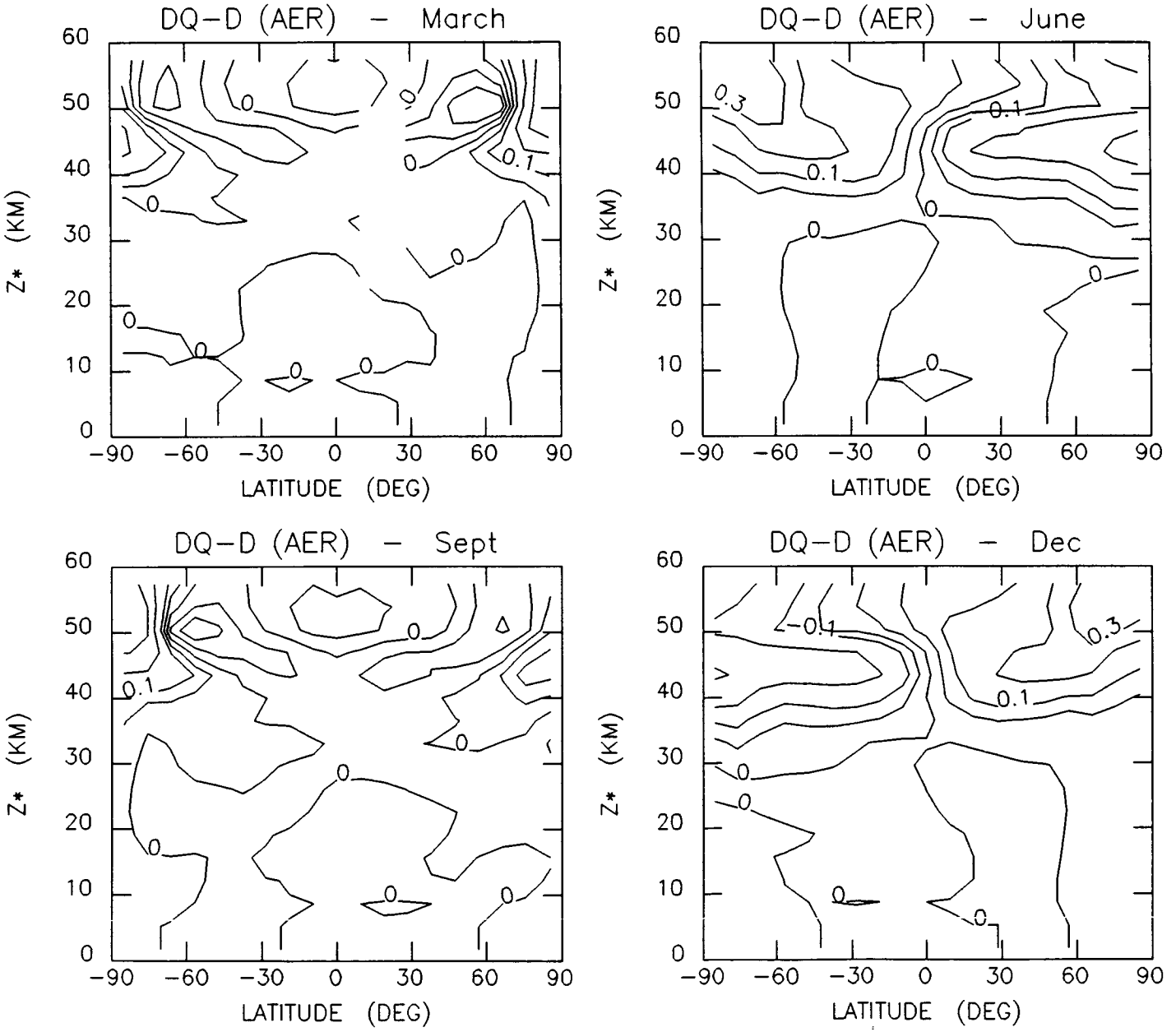
DQ-D (AER) - March
DQ-D (AER) - June
DQ-D (AER) - Sept
DQ-D (AER) - Dec
Z* (KM)
LATITUDE (DEG)
0
10
20
30
40
50
60
-90
-60
-30
0
30
60
90
0
0.1
0.3
-0.1

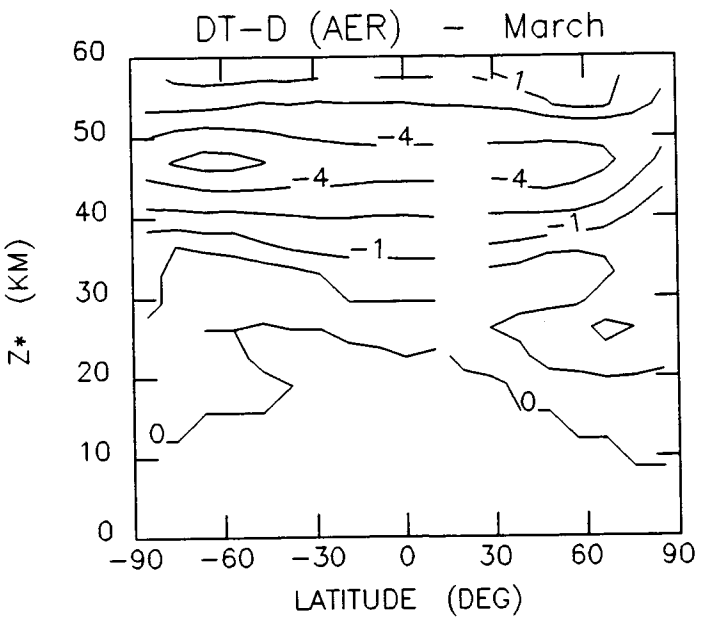
DT−D (AER) − March
Z* (KM)
LATITUDE (DEG)
60
50
40
30
20
10
0
−90 −60 −30 0 30 60 90
1
−4
−4
−4
−1
−1
0
0

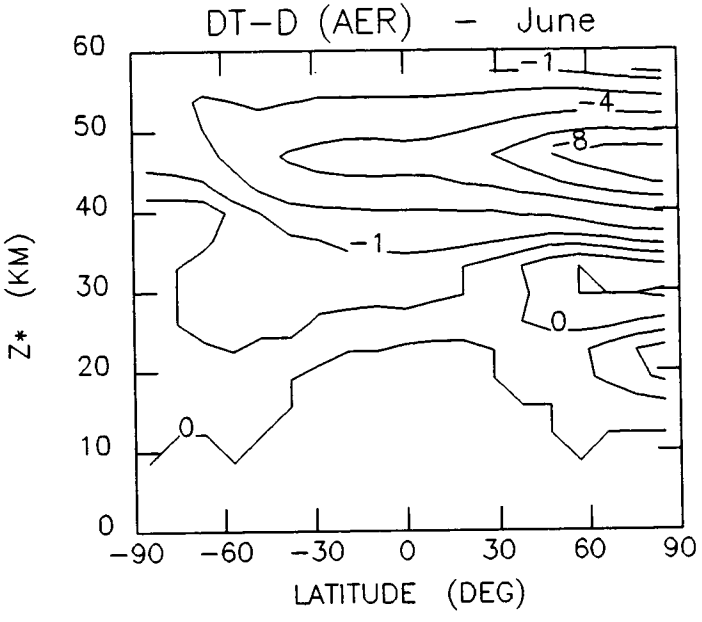
DT−D (AER) − June
Z* (KM)
LATITUDE (DEG)
60
50
40
30
20
10
0
−90 −60 −30 0 30 60 90
−1
−4
−8
−1
0
0

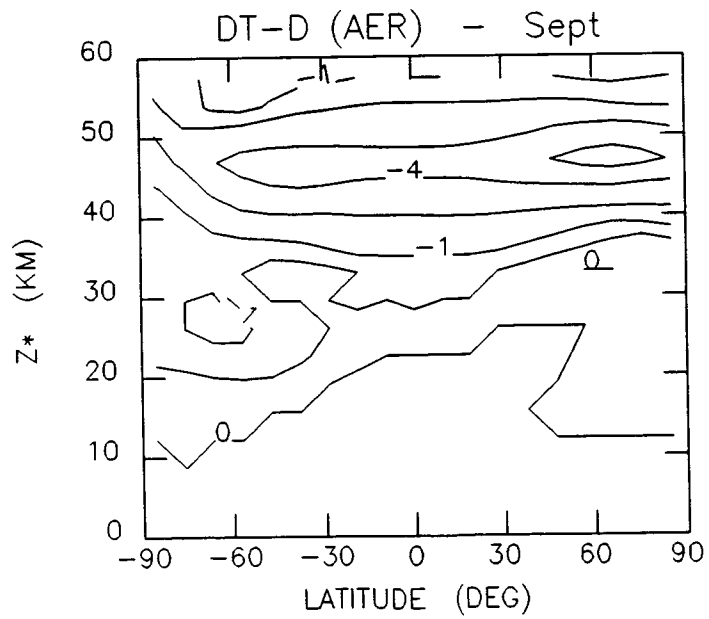
DT−D (AER) − Sept
Z* (KM)
LATITUDE (DEG)
60
50
40
30
20
10
0
−90 −60 −30 0 30 60 90
−1
−4
−1
0
0

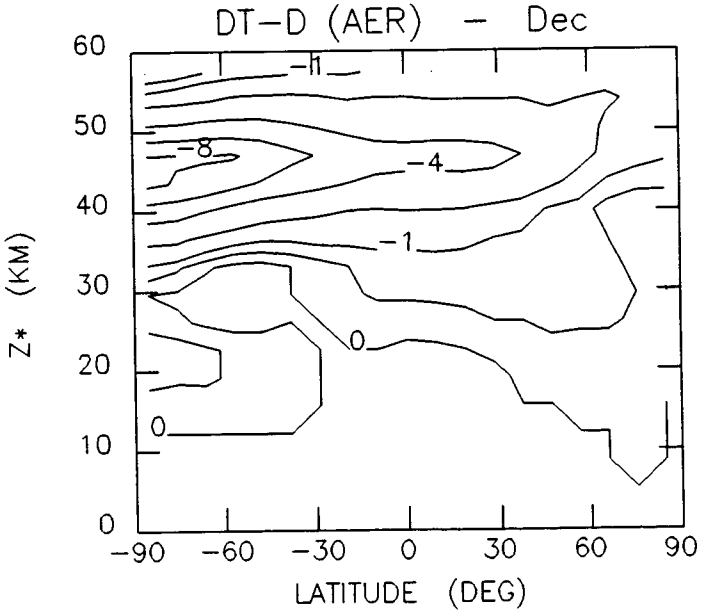
DT−D (AER) − Dec
Z* (KM)
LATITUDE (DEG)
60
50
40
30
20
10
0
−90 −60 −30 0 30 60 90
−1
−8
−4
−1
0
0

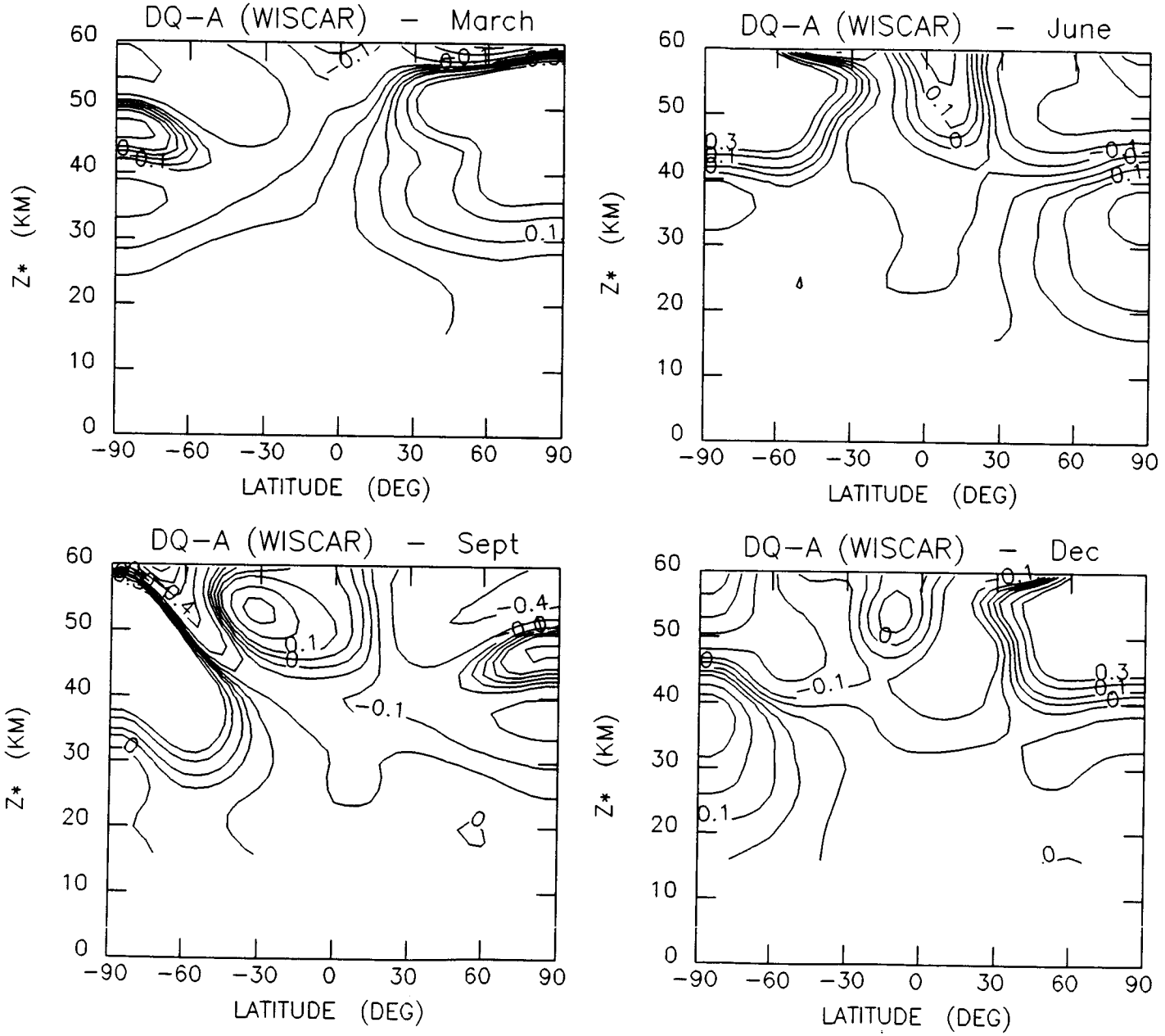
DQ–A (WISCAR) – March
DQ–A (WISCAR) – June
DQ–A (WISCAR) – Sept
DQ–A (WISCAR) – Dec
Z* (KM)
LATITUDE (DEG)
0
10
20
30
40
50
60
−90
−60
−30
0
30
60
90

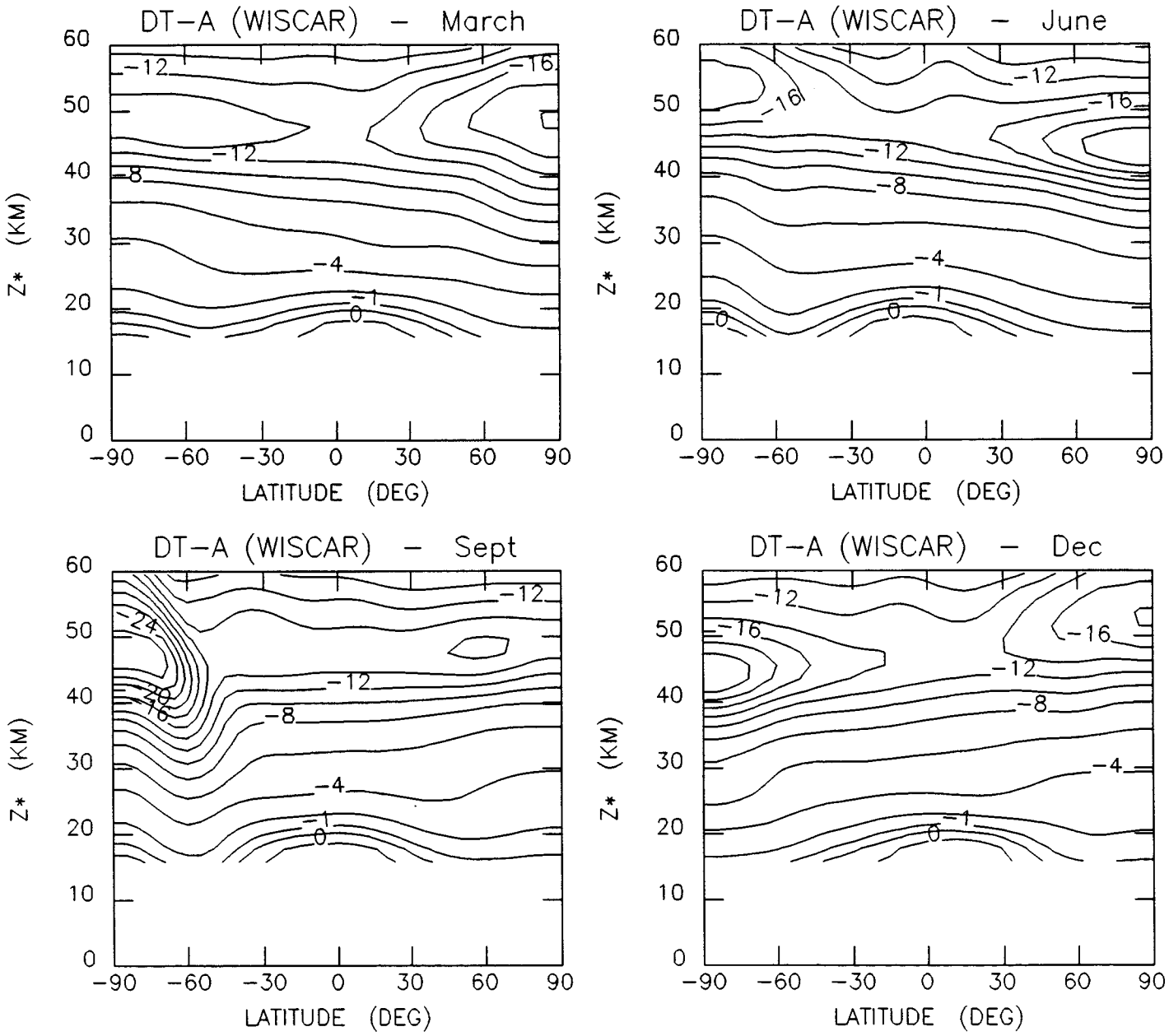
DT−A (WISCAR) − March
DT−A (WISCAR) − June
DT−A (WISCAR) − Sept
DT−A (WISCAR) − Dec
Z* (KM)
LATITUDE (DEG)
60
50
40
30
20
10
0
−90 −60 −30 0 30 60 90
−12
−16
−8
−4
−1
0
−24
−20

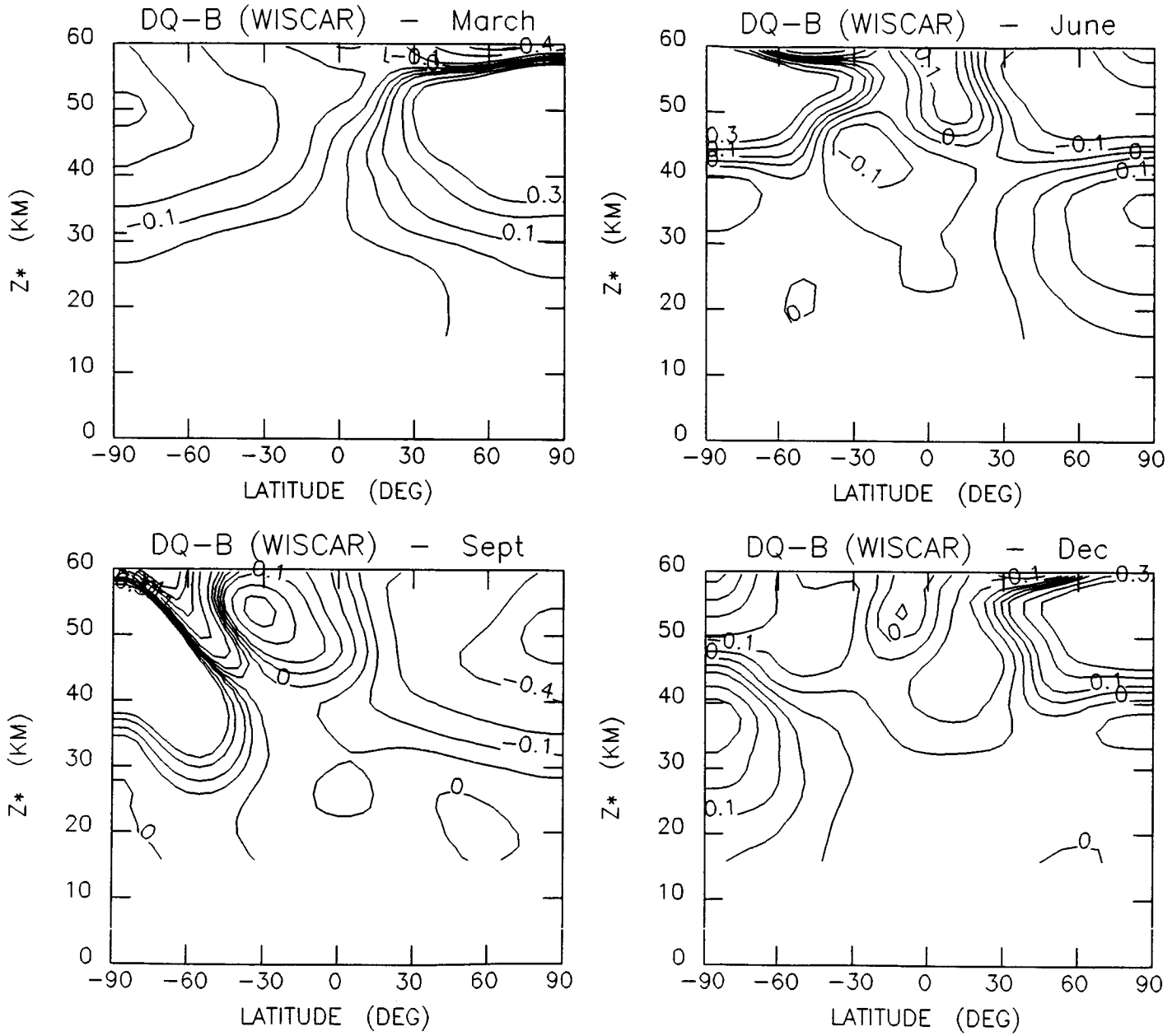
DQ–B (WISCAR) – March
DQ–B (WISCAR) – June
DQ–B (WISCAR) – Sept
DQ–B (WISCAR) – Dec
Z* (KM)
LATITUDE (DEG)
0
10
20
30
40
50
60
−90
−60
−30
0
30
60
90
0.4
0.3
0.1
0
−0.1
−0.4

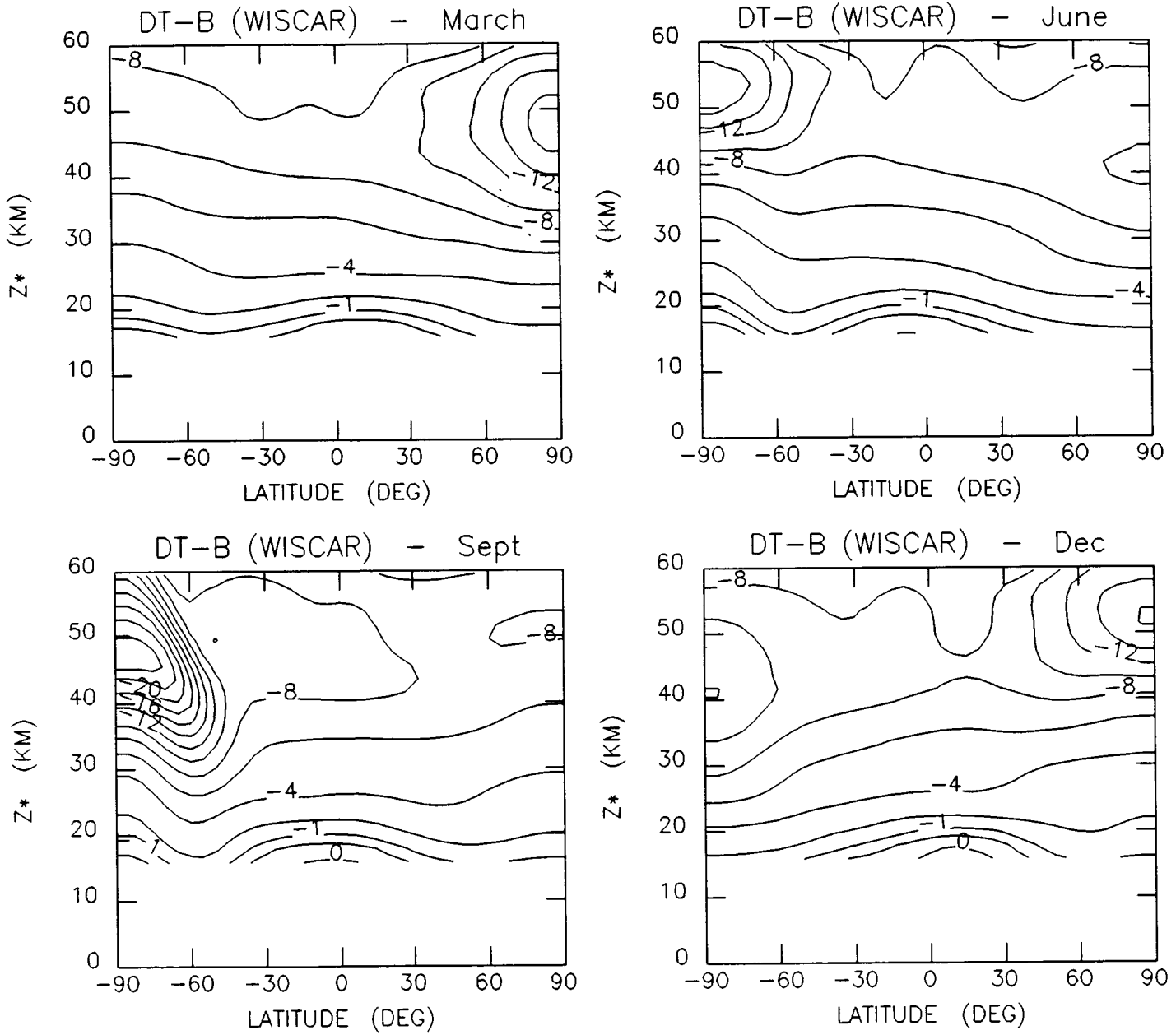
DT−B (WISCAR) − March
DT−B (WISCAR) − June
DT−B (WISCAR) − Sept
DT−B (WISCAR) − Dec
Z* (KM)
LATITUDE (DEG)
0
10
20
30
40
50
60
−90
−60
−30
0
30
60
90
−8
−12
−4
−1
1
16
20

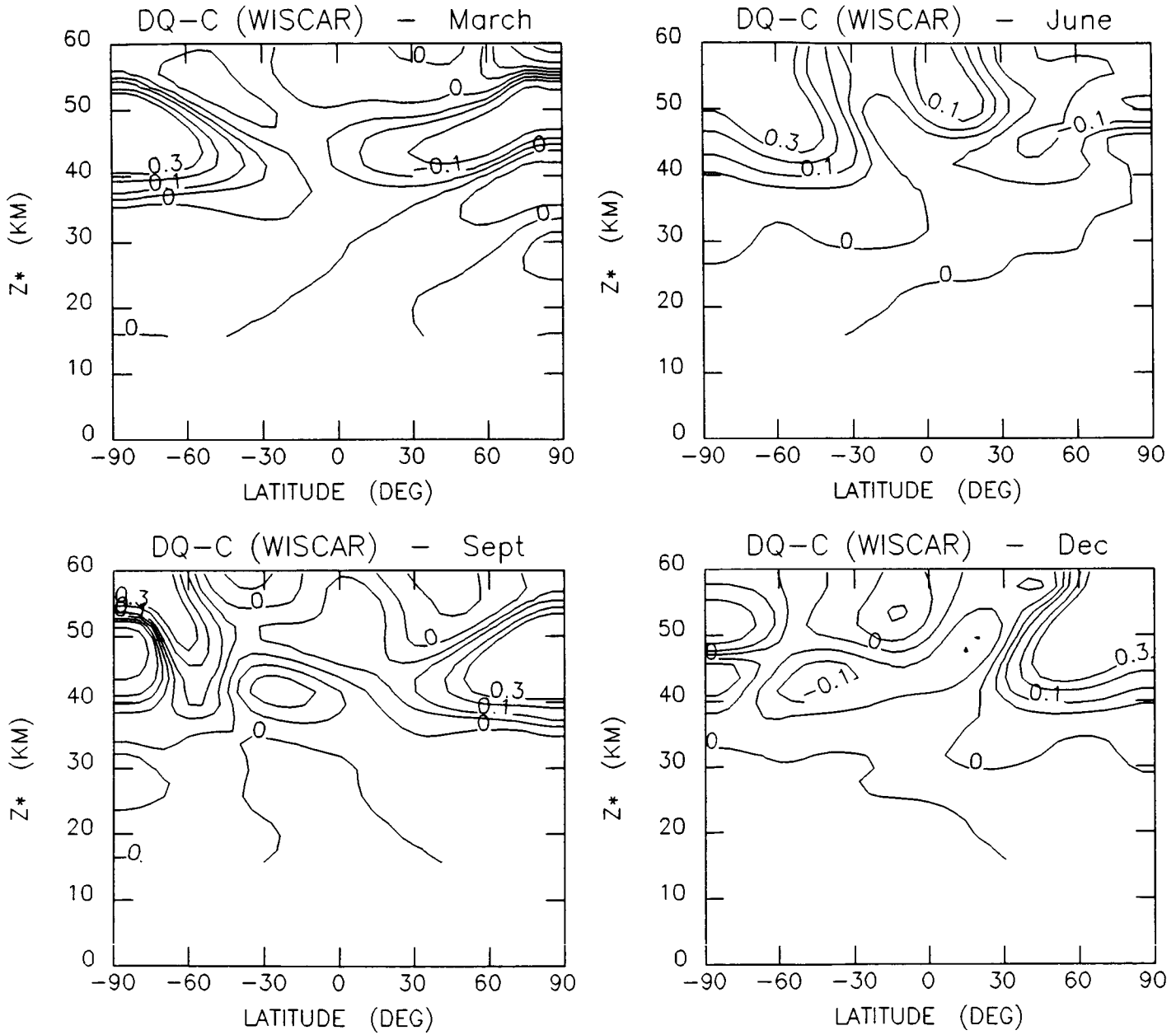
DQ-C (WISCAR) - March
DQ-C (WISCAR) - June
DQ-C (WISCAR) - Sept
DQ-C (WISCAR) - Dec
Z* (KM)
LATITUDE (DEG)
0
10
20
30
40
50
60
-90
-60
-30
0
30
60
90
0.3
0.1
-0.1

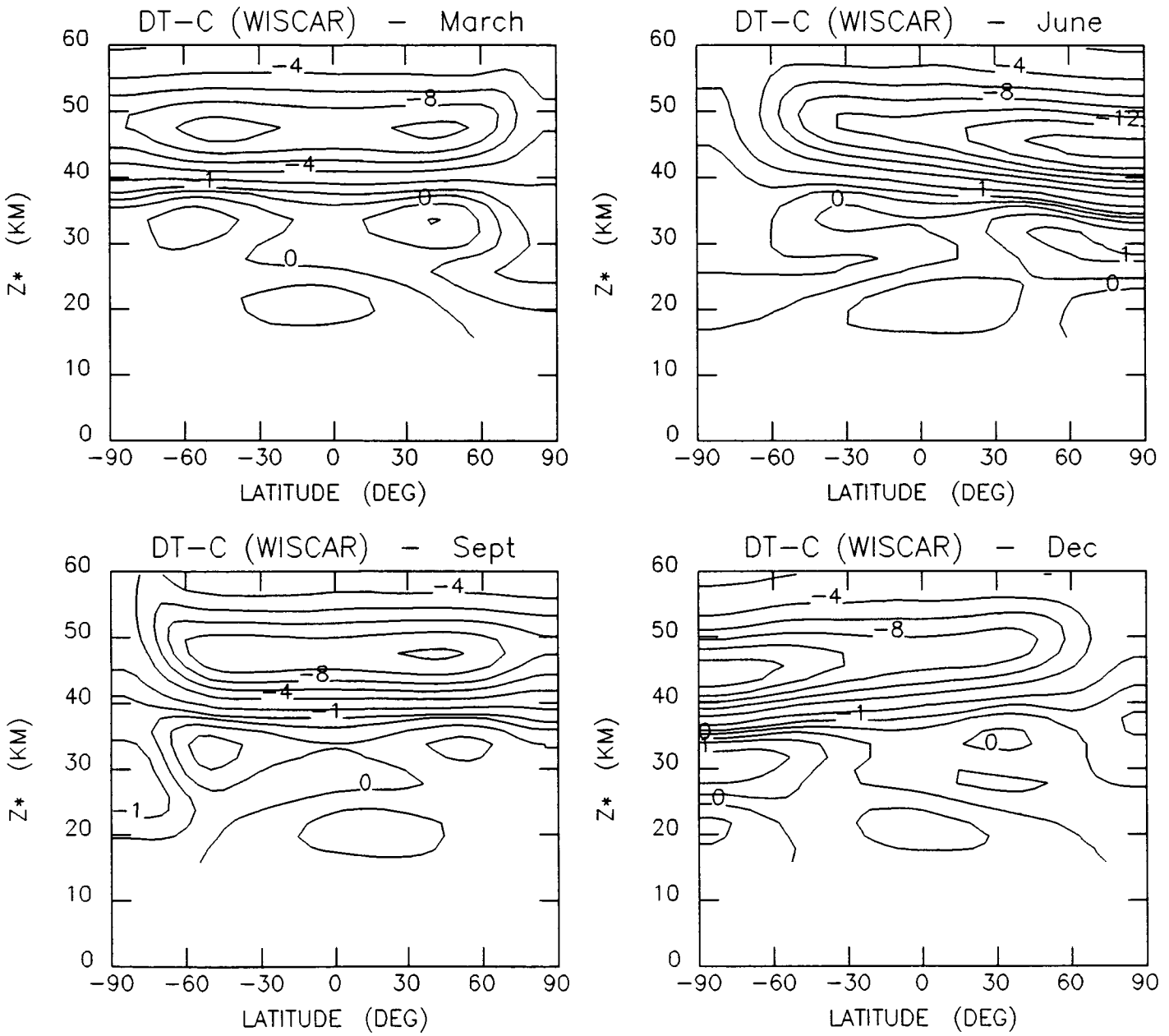
DT−C (WISCAR) − March
DT−C (WISCAR) − June
DT−C (WISCAR) − Sept
DT−C (WISCAR) − Dec
Z* (KM)
LATITUDE (DEG)
0
10
20
30
40
50
60
−90
−60
−30
0
30
60
90
−4
−8
−12
−1
1

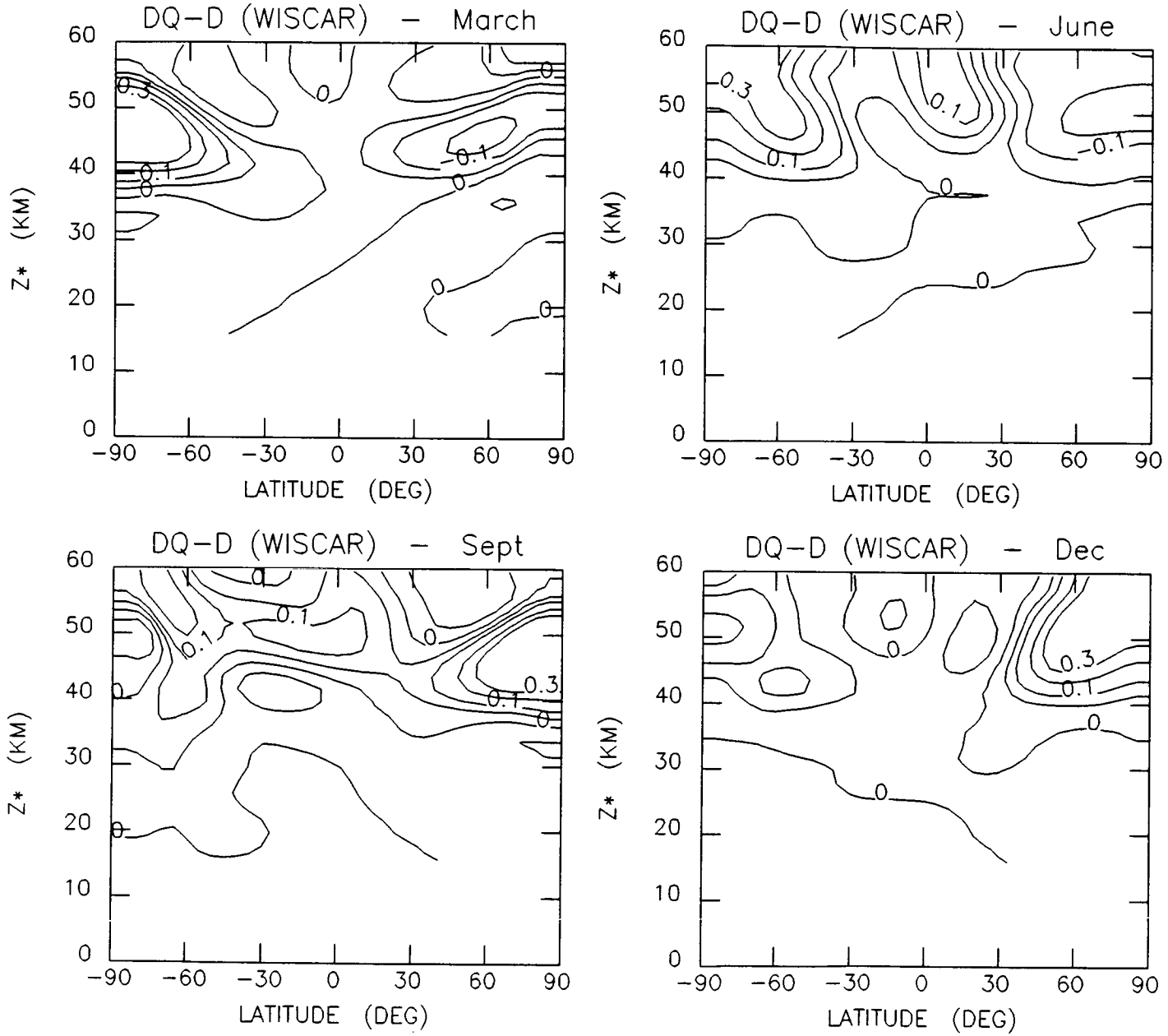
DQ−D (WISCAR) − March
DQ−D (WISCAR) − June
DQ−D (WISCAR) − Sept
DQ−D (WISCAR) − Dec
Z* (KM)
LATITUDE (DEG)
0
10
20
30
40
50
60
−90
−60
−30
0
30
60
90
0.3
0.1
0
−0.1

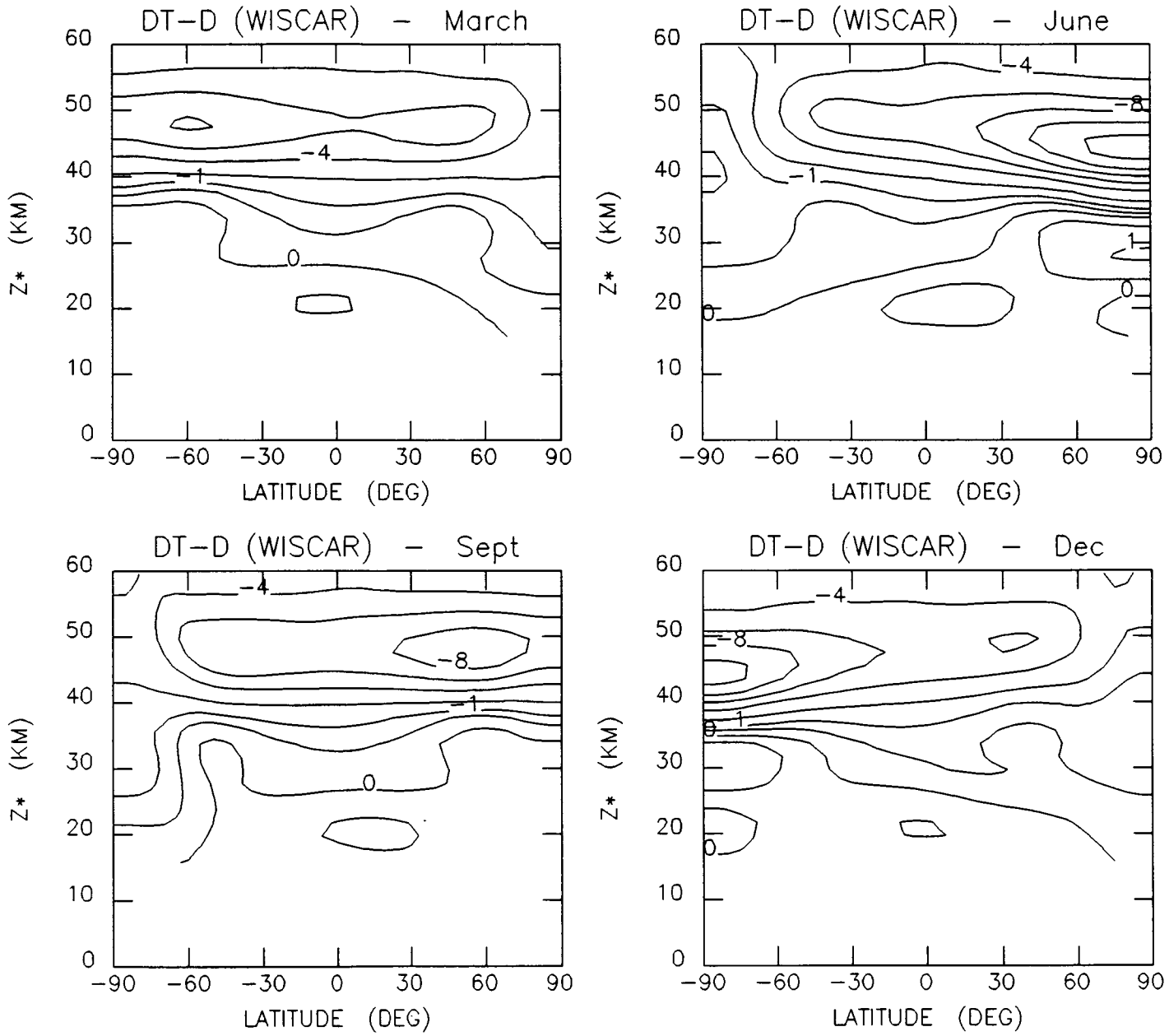
DT−D (WISCAR) − March
DT−D (WISCAR) − June
DT−D (WISCAR) − Sept
DT−D (WISCAR) − Dec
Z* (KM)
LATITUDE (DEG)
0
10
20
30
40
50
60
−90
−60
−30
0
30
60
90
−4
−1
0
−8
1

NASA
National Aeronautics and Space Administration

# Report Documentation Page

| 1. Report No. | 2. Government Accession No. | 3. Recipient's Catalog No. |
|---|---|---|
| NASA CP-3042 | | |

| 4. Title and Subtitle | 5. Report Date |
|---|---|
| Two-Dimensional Intercomparison of Stratospheric Models | August 1989 |
| | 6. Performing Organization Code: 616 |

| 7. Author(s) | 8. Performing Organization Report No. |
|---|---|
| Charles H. Jackman, Robert K. Seals, Jr., and Michael J. Prather, Editors | 89B00192 |
| | 10. Work Unit No.: 673-6212 |

| 9. Performing Organization Name and Address | 11. Contract or Grant No. |
|---|---|
| Goddard Space Flight Center<br>Atmospheric Chemistry and Dynamics Branch<br>Greenbelt, MD 20771 | |

| 12. Sponsoring Agency Name and Address | 13. Type of Report and Period Covered |
|---|---|
| National Aeronautics and Space Administration<br>Washington, D. C. 20546 | Conference Publication<br>September 11-16, 1988 |
| | 14. Sponsoring Agency Code |

15. Supplementary Notes

C. Jackman, Goddard Space Flight Center, Greenbelt, Maryland;
R. Seals, Jr., Langley Research Center, Hampton, Virginia;
M. Prather, Goddard Institute for Space Studies, New York, New York.

16. Abstract

This publication provides a complete account of the proceedings of the Two-Dimensional Intercomparison of Stratospheric Models Workshop, sponsored by the NASA Upper Atmosphere Theory and Data Analysis Program, held at Virginia Beach, Virginia, September 11-16, 1988. The purpose of the workshop was to provide a detailed record for the examination of fundamental differences in photochemistry and transport among stratospheric models. Approximately 35 scientists from universities, governments, and laboratories around the world were involved in presenting the results of 16 different modeling groups for several model experiments.

| 17. Key Words (Suggested by Author(s)) | 18. Distribution Statement |
|---|---|
| 2-D, Ozone, Radiative Model Documentation, Perturbation, Transport, Eddy Diffusion, Net Heating Rate | Unclassified - Unlimited<br>Subject Category 46 |

| 19. Security Classif. (of this report) | 20. Security Classif. (of this page) | 21. No. of pages | 22. Price |
|---|---|---|---|
| Unclassified | Unclassified | 608 | A99 |



NASA-Langley, 1989